



ایران مواد

Iran-mavad.com



@iranmavad



شبکه آزمایشگاهی ایران مواد

FESEM, SEM, TEM, XRD

XRF, SPS, TGA, DTA, DSC, FTIR, BET

www.IMlabsnet.ir

مرکز آموزش تخصصی ایران مواد

Iran Mavad Education Professional Center

آموزش های تخصصی و نرم افزاری مهندسی مواد و متالورژی

www.IMpec.ir

گروه فنی پژوهش ایران مواد

ویراستاری، ترجمه تخصصی مقالات و کتب مهندسی مواد

مشاوره پژوهشی تا چاپ مقاله ISI

www.IMpaper.ir

The Minerals, Metals & Materials Series

D.R. Poirier
G.H. Geiger

Transport Phenomena in Materials Processing

TMS
The Minerals, Metals & Materials Society

 Springer

www.iran-mavad.com

ایران مواد

TRANSPORT
PHENOMENA
in
MATERIALS
PROCESSING

T R A N S P O R T
P H E N O M E N A
in
M A T E R I A L S
P R O C E S S I N G

D.R. Poirier
G.H. Geiger

A Publication of

TMS
Minerals • Metals • Materials

Authors

D.R. Poirier

G.H. Geiger

ISBN 978-3-319-48565-2

ISBN 978-3-319-48090-9 (eBook)

DOI 10.1007/978-3-319-48090-9

Library of Congress Control Number: 94-76335

Chemistry and Materials Science: Professional

© 2016 by The Minerals, Metals & Materials Society

Published by Springer International Publishers, Switzerland, 2016

Reprint of the original edition published by The Minerals, Metals & Materials Society, 1994, 978-0-87339-272-3

This work is subject to copyright. All rights are reserved by the Publisher, whether the whole or part of the material is concerned, specifically the rights of translation, reprinting, reuse of illustrations, recitation, broadcasting, reproduction on microfilms or in any other physical way, and transmission or information storage and retrieval, electronic adaptation, computer software, or by similar or dissimilar methodology now known or hereafter developed.

The use of general descriptive names, registered names, trademarks, service marks, etc. in this publication does not imply, even in the absence of a specific statement, that such names are exempt from the relevant protective laws and regulations and therefore free for general use.

The publisher, the authors and the editors are safe to assume that the advice and information in this book are believed to be true and accurate at the date of publication. Neither the publisher nor the authors or the editors give a warranty, express or implied, with respect to the material contained herein or for any errors or omissions that may have been made.

Printed on acid-free paper

This Springer imprint is published by Springer Nature

The registered company is Springer International Publishing AG

The registered company address is: Gewerbestrasse 11, 6330 Cham, Switzerland

PREFACE

Transport Phenomena in Metallurgy was published more than twenty years ago. The need then was to provide a textbook on transport phenomena (momentum, heat, and mass transport) with metallurgical pedagogy. Many academic programs in metallurgy and metallurgical engineering have since evolved to programs in materials science and engineering, but the need to include transport phenomena in the curricula still remains. Indeed, the importance of transport phenomena in curricula is probably greater today than it was in the early seventies for two reasons: (1) the recognition of the importance of materials processing and synthesis, and (2) the increasing use of sophisticated softwares to simulate materials processes. We hope, therefore, that this textbook provides a teachable and readable approach to transport phenomena and then goes further by providing numerous examples and applications, which are particularly important to metallurgical, ceramic, and materials engineers.

Like its predecessor, this textbook has been designed to utilize the mathematical abilities of upper-class engineering students. In particular, students in materials related programs have studied integral and differential calculus, but often make little use of it again, except in rather trivial applications. Since one can proceed quite a way into the field of transport phenomena without resorting to higher-level mathematics, and because we think that it is important for students and practicing engineers to visualize the physical situations, we have attempted to lead the readers through the development and solution of the relevant differential equations by applying the familiar principles of conservation to numerous situations and by including many worked examples in each chapter. We hope that readers with good mathematical abilities will not feel that we are being condescending but will realize that we have tried to make transport phenomena understandable to a group as large as possible. Also, because of the increased availability of computing power and software utilizing numerical methods to solve the differential equations with more realistic boundary conditions, we believe that it is even more important to be able to recognize and define the problem than to analytically solve a specific equation with the usual attendant limitations on boundary conditions.

The book is organized in a manner characteristic of other texts in transport phenomena. Section I deals with the properties and mechanics of fluid motion; Section II with thermal properties and heat transfer; and Section III with diffusion and mass transfer. We depart from the tradition, however, in that we build on a presumed understanding of the

vi Preface

relationships between the structure and properties of matter, particularly in the chapters devoted to the transport properties (viscosity, thermal conductivity, and diffusion coefficients). In addition, generous portions of the text, numerous examples, and many problems at the ends of the chapters apply transport phenomena to materials processing.

Those familiar with *Transport Phenomena in Metallurgy* will see a large carry-over to this textbook. The major and perhaps most welcome change is the use of S.I. units. In a few instances, there are compelling reasons to maintain non-S.I. units, but lest the modern student lose heart we explain our reasons and present the relevant unit conversions. The problem sets have been greatly expanded, which should provide a more than an adequate supply of instructional fodder to build on the reading in the individual chapters. We added a concluding chapter entitled Numerical Methods and Models to serve as a bridge between this textbook and books intended for advanced study and, indeed, for the practice of materials engineering. One chapter from *Transport Phenomena in Metallurgy* was completely eliminated, and all other chapters and the Appendices have been extensively revised to make this textbook an introduction to *materials processing*.

We emphasize that the book is not intended to be a comprehensive review of all the applications and current research in the field. Its aim is rather to present the basic equations and show how they can be applied to a variety of topics, thereby preparing the readers to make use of transport phenomena and to understand and interpret the current literature in the field. We also hope that the book will be useful to those who are already active in seeking better ways to engineer materials processes.

February 1994

David R. Poirier
Gordon H. Geiger

ACKNOWLEDGMENTS

We express our sincere thanks to Merton Flemings and Morris Cohen of M.I.T. for always rising as champions of materials processing within the materials science and engineering community and for their encouragement to redo *Transport Phenomena in Metallurgy* into the present book. Publication of the manuscript by The Minerals, Metals and Materials Society (TMS) was recommended by the Publication Committee of TMS, under the Chairmanship of Gary Warren of the University of Alabama-Tuscaloosa. We thank the Committee for its endorsement, and Robert Makowski, Wendy McCalip, and the entire publications staff of TMS for working with us on this project.

The text for the manuscript was typed by Patricia Broyles and the illustrations were done by Alison Habel, James Abbot, Patricia Broyles, and Robert Erdmann, all at the University of Arizona. As a "fill-in," one of the authors (DRP) made some of the illustrations with help from Mary Cromwell. We are very grateful that these good people shared their talents with us.

The manuscript readers were Kathryn Sole of the Council of Mineral Technology in South Africa (formerly of the University of Arizona) and Ernest Poirier, a consultant to the metals casting industry and brother of DRP from Gales Ferry, Connecticut. They pointed out many computational errors and typos, and provided ways of improving both the text and problem statements. We are very grateful that they participated so diligently in our undertaking. It was wonderful working with them and knowing that at least two other people have read this book.

CONTENTS

PART 1 FLUID DYNAMICS

Chapter 1 Viscous Properties of Fluids

1.1 Types of fluid flow	3
1.2 Newtonian fluids	4
1.3 Viscosity of gases	7
1.4 Viscosity of liquids	13
1.5 Non-Newtonian fluids	29

Chapter 2 Laminar Flow and the Momentum Equation

2.1 Momentum balance	39
2.2 Flow of a falling film	40
2.3 Fully developed flow between parallel plates	44
2.4 Fully developed flow through a circular tube	46
2.5 Equation of continuity and the momentum equation	50
2.6 The momentum equation in rectangular and curvilinear coordinates	56
2.7 Application of Navier-Stokes' equation	62

Chapter 3 Turbulent Flow and Complex Flows

3.1 Friction factors for flow in tubes	76
3.2 Flow in noncircular conduits	81
3.3 Flow past submerged bodies	82
3.4 Flow through porous media	90
3.5 Fluidized beds	101

Chapter 4 Energy Balance Applications in Fluid Flow

4.1 Conservation of energy	113
4.2 Friction losses in straight conduits	117
4.3 Enlargement and contraction	119
4.4 Flow through valves and fittings	122
4.5 Flow through smooth bends and coils	123
4.6 Flow measurement	124
4.7 Flow from ladles	131
4.8 Flow through piping networks	135

Chapter 5 Flow and Vacuum Production

5.1 Pumps	145
5.2 Fans and blowers	151
5.3 Interactions between fans or pumps and systems	154
5.4 Supersonic nozzles and jet behavior	158
5.5 Vacuum production	166

PART 2 ENERGY TRANSPORT

Chapter 6 Fourier's Law and Thermal Conductivity of Materials

6.1 Fourier's law and thermal conductivity	187
6.2 Thermal conductivity of gases	190
6.3 Thermal conductivity of solids	191
6.4 Thermal conductivity of liquids	203
6.5 Thermal conductivity of bulk materials	208

Chapter 7 Heat Transfer and the Energy Equation

7.1 Heat transfer with forced convection in a tube	219
7.2 Heat transfer with laminar forced convection over a flat plate	224
7.3 Heat transfer with natural convection	228
7.4 Heat conduction	233
7.5 The general energy equation	236
7.6 The energy equation in rectangular and curvilinear coordinates	240

Chapter 8 Correlations and Data for Heat Transfer Coefficients

8.1 Heat transfer coefficients for forced convection in tubes	248
8.2 Heat transfer coefficients for forced convection past submerged objects	254
8.3 Heat transfer coefficients for natural convection	258
8.4 Quenching heat transfer coefficients	262
8.5 Heat transfer coefficients in fluidized beds	268
8.6 Heat transfer coefficients in packed beds	272
8.7 Heat transfer coefficients in forging	274

Chapter 9 Conduction of Heat in Solids

9.1	The energy equation for conduction	281
9.2	Steady-state one-dimensional systems	282
9.3	Transient systems, finite dimensions	288
9.4	Transient conditions, infinite and semi-infinite solids	304
9.5	Simple multidimensional problems	312
9.6	Moving sources	315

Chapter 10 Solidification of Metals

10.1	Solidification in sand molds	329
10.2	Solidification in metal molds	334
10.3	Continuous casting	350
10.4	Crystal growth	355

Chapter 11 Radiation Heat Transfer

11.1	Basic characteristics	369
11.2	The black radiator and emissivity	370
11.3	The energy distribution and the emissive power	372
11.4	Gray bodies and absorptivity	378
11.5	Exchange between infinite parallel plates	378
11.6	View factors	381
11.7	Electric circuit analog	386
11.8	Furnace enclosures	390
11.9	Radiation combined with convection	395
11.10	Radiation from gases	398
11.11	Enclosures filled with radiating gas	402
11.12	Radiation in transparent solids	404
11.13	Transient conduction with radiation at the surface	407
11.14	Transient heating with thermal stresses	409

PART III MASS TRANSPORT**Chapter 12 Interphase Mass Transfer**

12.1	Definition of fluxes—Fick's first law	419
12.2	Diffusion in solids	420
12.3	Diffusion in ceramic materials	435
12.4	Diffusion in elemental semiconductors	442
12.5	Diffusion in liquids	444
12.6	Diffusion in gases	453
12.7	Diffusion through porous media	457

Chapter 13 Diffusion in Solids

13.1	Steady-state diffusion experiments	463
13.2	Transient diffusion experiments	468
13.3	Finite system solutions	476
13.4	Microelectronic diffusion processing	480
13.5	Homogenization of alloys	485
13.6	Formation of surface layers	491

Chapter 14 Mass Transfer in Fluid Systems

14.1	Diffusion through a stagnant gas film	510
14.2	Diffusion in a moving gas stream	513
14.3	Diffusion into a falling liquid film	516
14.4	The mass transfer coefficient	519
14.5	General equation of diffusion with convection	523
14.6	Mass transfer with forced convection over a flat plate	526
14.7	Correlations of mass transfer coefficients for turbulent flow	529
14.8	Models of the mass transfer coefficient	535
14.9	Mass transfer in chemical vapor deposition	537

Chapter 15 Interphase Mass Transfer

15.1	Two-resistance mass transfer theory	547
15.2	Mixed control in gas-solid reactions	551
15.3	Mass transfer with vaporization	560

Chapter 16 Numerical Methods and Models

16.1	Finite difference approximations	571
16.2	Turbulent flow	598
16.3	Discretization in convective flows	606

Appendix A	Physical Constants	611
Appendix B	Thermal Properties	613
Appendix C	Conversion Factors	621
Appendix D	Description of Particulate Materials	631
Appendix E	Flow Measurement Instruments	637
Appendix F	Derivation of Eq. (9.62) for Semi-infinite Solids	641
Appendix G	Derivation of Eq. (13.53) for Drive-in Diffusion	643
Index		645

PART ONE

FLUID DYNAMICS

The first part of this text deals with fluids, their intrinsic properties, their behavior under various conditions, and the methods by which we can manipulate and utilize them to produce desired results. Most materials processing deals with fluids at one point or another, and although the materials engineer is usually not required to be an "expert" on fluids, he should understand the fundamentals of fluid dynamics as presented in the following chapters, and be able to make intelligent use of the properties of fluids and characteristics of equipment used to manipulate and control fluids.

The behavior of fluids is also intimately related to heat and mass transport processes. For example, if a gas is hotter than a solid past which it is flowing, the solid naturally is heated. The rate at which heat is transferred to the solid's surface is dependent on the fluid's properties and its flow pattern. Similarly, if a piece of graphite is to be dissolved in a bath of molten iron, the rate of dissolution depends on the motion of the liquid iron adjacent to the graphite. Thus, to appreciate transfer of heat and/or mass, an understanding of fluid dynamics is important.

These are just two simple examples which illustrate the necessity for the student to become acquainted with the means of examining and expressing the flow of fluids and to eventually recognize the role of fluid flow in rate processes involving heat and mass transfer. Actually, if we take a fundamental approach to the study of fluid flow, then the subject matter is appropriately designated *momentum transport*. Momentum transport with *energy transport* and *mass transport* make up the subject of *transport phenomena*, which Bird, Stewart, and Lightfoot* rank as a "key engineering science," along with thermodynamics and mechanics. Transport phenomena as a key engineering science has been well received in both the academic and industrial communities of engineering.

*R. B. Bird, W. E. Stewart, and E. N. Lightfoot, *Transport Phenomena*, Wiley, New York, 1960.

VISCOUS PROPERTIES OF FLUIDS

1.1 TYPES OF FLUID FLOW

When fluids move through a system, either one of two different types of fluid flow may occur. We can most easily visualize the fact that there are two distinctly different types of fluid flow by referring to an experiment performed by Reynolds in 1883. Imagine a transparent pipe with water flowing through it; several threadlike streams of dye are injected parallel to the path of the water's flow. At sufficiently small velocities of water, the dye will flow in parallel, straight lines. When the velocity is increased, a point is reached at which the entire mass of water becomes colored. In other words, hypothetical individual particles of liquid, instead of flowing in an orderly manner parallel to the long axis of the pipe, flow in an erratic manner so as to cause complete mixing of the dye and water.

The first type of dye flow is called *laminar* or *streamline* flow. The significance of these terms is that the fluid's motion seems to be the sliding of laminations of infinitesimal thickness relative to adjacent layers, and that the hypothetical particles in the layers move in predictable paths or streamlines, as depicted in Fig. 1.1.

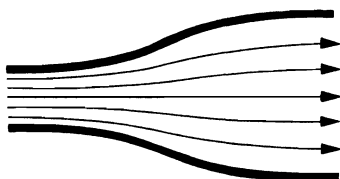


Fig. 1.1 Laminar flow.

The second (erratic) type of flow is described as *turbulent* flow. In turbulent flow, the motion of the fluid particles is irregular, and accompanied by fluctuations in velocity. This type of flow is illustrated in Fig. 1.2, in which part (a) shows the erratic path of a single

4 Viscous Properties of Fluids

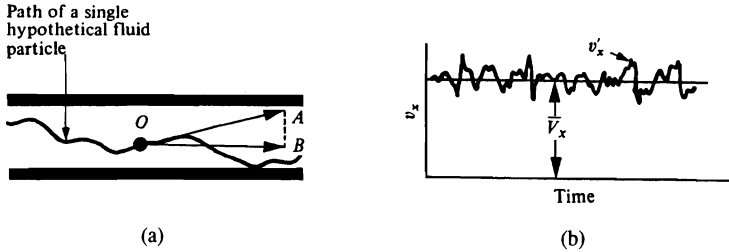


Fig. 1.2 Turbulent flow. (a) The instantaneous velocity OA varies continually in direction and magnitude. The velocity OB is the x -directed component and is designated v_x in (b). (b) Variation at point O of v_x about the temporal mean velocity \bar{V}_x .

particle during some time interval and part (b) demonstrates that the velocity at a fixed point in the fluid fluctuates randomly about some mean value, which is called the *temporal mean* or *time averaged* velocity, and which is given the symbol \bar{V}_x .

One of the earliest systematic investigations of turbulent flow was conducted by Reynolds, who suggested the parameter $\bar{V}D/\nu$ as the criterion for predicting the type of flow in round tubes, where \bar{V} is the average fluid velocity, D is the pipe diameter, and ν is the kinematic viscosity, which is a property of the fluid to be described in the following section. In a consistent set of units, the parameter is dimensionless, and is called the *Reynolds number* (Re). The value of Re at which transition from laminar to turbulent flow occurs is approximately 2100 in the usual engineering applications of flow in pipes. In general, however, the transition Reynolds number varies with different systems, and even for a given system it may vary according to such external factors as surface roughness and initial disturbances in the fluid.

Figure 1.3 shows the distribution of velocity across the radius of a tube, for laminar and turbulent flow. The temporal mean velocity is plotted for turbulent flow. When dealing with turbulent flow, we are usually interested in the temporal mean value, so that, unless otherwise stated, the temporal mean value will be implied. Note that for both cases the velocity is zero at the fluid-wall interface; this is known as the no-slip boundary condition. For laminar flow the velocity profile is parabolic; in turbulent flow, the curve is somewhat flattened in the middle.

1.2 NEWTONIAN FLUIDS

Consider a fluid between two parallel plates (Fig. 1.4). The upper plate is stationary and the lower one is set in motion with a velocity V at time zero. From experience we know that the fluid adjacent to the plates will have the same velocity as the plates themselves. Hence the fluid adjacent to the lower plate moves with a velocity V , while that adjacent to the upper plate has null velocity. As time proceeds, the fluid gains momentum, and after sufficient time has elapsed a steady state is reached, in which, in order to keep the lower plate in motion with the velocity V , a force F must be maintained, and an equal but opposite force is exerted on the stationary plate.

At steady state, for plates of area A , and laminar flow, the force is expressed by

$$\frac{F}{A} = \eta \frac{V}{Y}, \quad (1.1)$$

where Y = distance between plates and η = constant of proportionality.

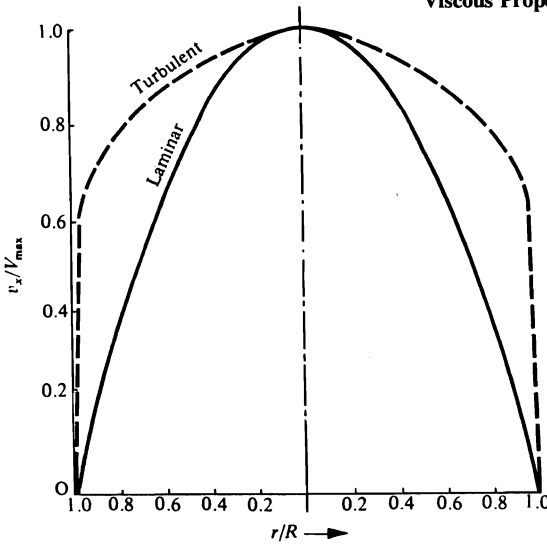


Fig. 1.3 Qualitative distribution of laminar and turbulent velocities in a tube.

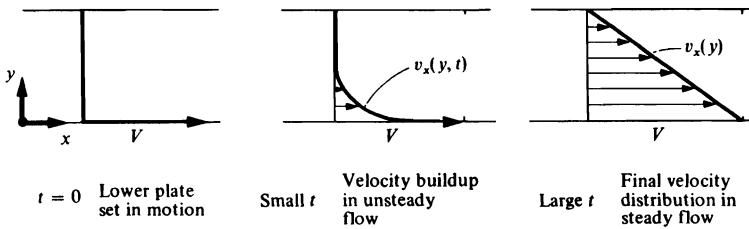


Fig. 1.4 Laminar flow of fluid between parallel plates.

The force system as described is pure shear, and the force per unit area (F/A) is the shear stress. At steady state, when the velocity profile is linear, V/Y exactly equals the constant velocity gradient dv_x/dy and the shear stress τ_{yx} between any two thin layers of fluid may be expressed as

$$\tau_{yx} = -\eta \frac{dv_x}{dy} \tag{1.2}$$

Equation (1.2) may alternatively be interpreted in terms of momentum transport. Picture the fluid as a series of thin layers parallel to the plates. By the shearing action each layer causes the layer directly above it to move. Thus momentum is transported in the y -direction. The subscripts of τ_{yx} refer to this direction of momentum transport (y) and the velocity component being considered (x -direction). The minus sign in Eq. (1.2) reflects the fact that momentum is transferred from the lower layers of fluid to the upper layers, that is, in the positive y -direction. In this case, dv_x/dy is negative, so that the minus sign makes τ_{yx} positive. This follows the generally accepted convention for heat transfer, in that momentum flows in the direction of decreasing velocity, just as heat flows from hot to cold.

6 Viscous Properties of Fluids

The period between $t = 0$, when the lower plate is set into motion, and large t , when steady state is reached, is called the *transient period*. During the transient period, v_x is a function of both time and position, so that a more general relationship for τ_{yx} is used:

$$\tau_{yx} = -\eta \frac{\partial v_x}{\partial y}. \quad (1.3)$$

This empirical relationship is known as *Newton's law of viscosity*, and defines the constant of proportionality, η , as the *viscosity*.

The dimensions of viscosity are found by referring to Eq. (1.3):

$$\eta = -\frac{\tau_{yx}}{(\partial v_x / \partial y)}.$$

Units of η are:

$$\eta = \frac{\text{N m}^{-2}}{(\text{m s}^{-1})(\text{m}^{-1})} = \text{N s m}^{-2}.$$

In keeping with the trend to using SI units, the units used in examples will be SI. However, since data are still available in cgs units and English units, the ability to convert back and forth between systems remains important, and some data will also be presented in units other than SI. Accordingly, the English system yields the following units for η :

$$\eta = \frac{(\text{lb}_m \text{ ft hr}^{-2})(\text{ft}^{-2})}{(\text{ft hr}^{-1})(\text{ft}^{-1})} = \text{lb}_m \text{ hr}^{-1} \text{ ft}^{-1}.$$

In the cgs system of units, the *poise* (P) is used, in which

$$1 \text{ poise (P)} = 1 \text{ dyn s cm}^{-2}.$$

The *centipoise* (cP) is probably the most common unit tabulated for viscosity. It equals 0.01 poise. The viscosity of water at 68.4°F (20.2°C) is 1 cP. Thus the value of the viscosity in centipoises is an indication of the viscosity of the fluid relative to that of water at 68.4°F. Viscosity in N s m^{-2} is 10^3 times viscosity in cP. (See Table C.8 in the Appendix for these and other conversion factors.)

In many problems involving viscosity, it is useful to have a value of a fluid's viscosity divided by its density ρ . Hence we define the *kinematic viscosity* ν at this point as

$$\nu \equiv \frac{\eta}{\rho}.$$

The kinematic viscosity is a fundamental quantity, in that it is a measure of *momentum diffusivity*, analogous to thermal and mass diffusivities, which will be presented in later chapters.

In SI units, the kinematic viscosity is measured in $\text{m}^2 \text{ s}^{-1}$, while in the cgs system the units are commonly $\text{cm}^2 \text{ s}^{-1}$, sometimes called the *stoke*.

Example 1.1 Two parallel plates are 1 mm apart. The lower plate is stationary and the upper plate moves with a velocity of 2 m s^{-1} . A stress of 5 N m^{-2} is needed to maintain the

upper plate in motion. Find the viscosity of the fluid contained between the plates in (a) N s m^{-2} and (b) cP.

Solution. From Eq. (1.1) and referring to Fig. 1.4, we have

$$\eta = \frac{F/A}{V/Y}$$

$$V/Y = \frac{2 \text{ m}}{\text{s}} \bigg| \frac{1 \times 10^{-3} \text{ m}}{1 \times 10^{-3} \text{ m}} = 2 \times 10^3 \text{ s}^{-1}.$$

F/A is the stress; then

$$\eta = \frac{5 \text{ N}}{\text{m}^2} \bigg| \frac{\text{s}}{2 \times 10^3} = 2.50 \times 10^{-3} \text{ N s m}^{-2} = 2.5 \text{ cP}.$$

1.3 VISCOSITY OF GASES

For the purpose of explaining momentum transport in gases, we resort to the simplest treatment of the kinetic theory of gases. We utilize the concept of the mean free path, in which the molecules are idealized as billiard balls, and postulate a hypothetical "ideal" gas possessing the following features:

1. The molecules are hard spheres resembling billiard balls, having diameter d and mass m .
2. The molecules exert no force on one another except when they collide.
3. The collisions are perfectly elastic and obey the classical laws of conservation of momentum and energy.
4. The molecules are uniformly distributed in a concentration of n per unit volume throughout the gas. They are in a state of continuous motion and are separated by distances which are large compared to their diameter.
5. All directions of molecular velocities are equally probable. The speed (magnitude of velocity) of a molecule can have any value between zero and infinity.

If we assume that the molecules possess a Maxwellian speed distribution, then the average speed \bar{V} is given by

$$\bar{V} = \left[\frac{8\kappa_B T}{\pi m} \right]^{1/2}, \quad (1.4)$$

where κ_B is the Boltzmann constant and T is absolute temperature.

In addition, for such a collection of molecules, a significant parameter that governs the momentum transfer in gases is the free path, defined as the distance traveled by a molecule between two successive collisions. At the instant of collision, the center-to-center distance of two molecules is d . Intuitively we know that the *mean free path* λ should be inversely proportional to the collision cross section πd^2 , and also inversely proportional to the concentration n of the molecules. The rigorous analysis for determining λ includes these

8 Viscous Properties of Fluids

terms, along with a coefficient whose numerical value is developed by considering the random fluctuations of the colliding molecules. The final result gives

$$\lambda = \left[\frac{1}{\sqrt{2}} \right] \left[\frac{1}{\pi d^2 n} \right]. \quad (1.5)$$

Now consider an imaginary plane at $y = y_1$, which is being crossed by molecules in either direction. If we examine the condition of no bulk motion (no macroscopic flow) of the gas in the y -direction, then the molecules cross the y_1 plane from both sides with equal frequency. This frequency per unit area at which molecules cross the plane at y_1 from one side is given by

$$Z = n\bar{v}/4. \quad (1.6)$$

We may picture the molecules crossing the y_1 -plane as carrying momentum characteristic of an average distance \bar{y} above and below the y_1 -plane at which they made this last collision. Numerically, \bar{y} is not exactly equal to λ , but rather is given by

$$\bar{y} = 2/3\lambda. \quad (1.7)$$

Up to this point, no macroscopic flow of the gas has been considered, so that, as stated above, the number of molecules arriving from above and below y_1 is equal, and on the average no net momentum is transferred across the plane y_1 .

To determine the viscosity of the gas, consider the gas under the influence of macroscopic flow in the x -direction, with a velocity gradient, dv_x/dy , as depicted in Fig. 1.5.

Now if all the molecules have velocities characteristic of the plane in which they last collided, we may write the x -momentum above y_1 as

$$mv_x \Big|_{y_1+\bar{y}} = mv_x \Big|_{y_1} + \frac{2}{3}\lambda m \frac{dv_x}{dy}. \quad (1.8)$$

Similarly, for below y_1

$$mv_x \Big|_{y_1-\bar{y}} = mv_x \Big|_{y_1} - \frac{2}{3}\lambda m \frac{dv_x}{dy}. \quad (1.9)$$

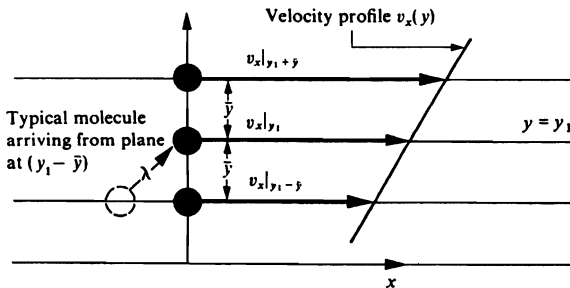


Fig. 1.5 Relation between the macroscopic velocity profile and the plane of interest at y_1 .

We find the net rate of x -momentum crossing the plane y_1 by summing the x -momentum of molecules that cross from below and subtracting the x -momentum of those that cross from above. In this manner, we write

$$\tau_{yx} = Zm \left[v_x \Big|_{y, -\bar{y}} - v_x \Big|_{y, +\bar{y}} \right]. \quad (1.10)$$

By combining Eqs. (1.6), (1.8), and (1.9), we arrive at

$$\tau_{yx} = -\frac{1}{3}nm\bar{V}\lambda \frac{dv_x}{dy}. \quad (1.11)$$

In addition, by utilizing the expressions for \bar{V} and λ , Eqs. (1.4) and (1.5), respectively, we write

$$\tau_{yx} = -\frac{2}{3\pi^{3/2}} \frac{(m\kappa_B T)^{1/2}}{d^2} \frac{dv_x}{dy}. \quad (1.12)$$

This result corresponds to Newton's law of viscosity (Eq. 1.2), with the viscosity given by

$$\eta = \frac{2}{3\pi^{3/2}} \frac{(m\kappa_B T)^{1/2}}{d^2}. \quad (1.13)$$

A significant conclusion from the above argument is that the viscosity of a gas is independent of pressure and depends only on temperature. This conclusion is in good agreement with experimental data up to about ten atmospheres.¹ However, the temperature dependency is only qualitatively correct, in that η does increase with increasing temperatures; but, quantitatively, the temperature dependency is not satisfactory. Data for real gases indicate that η varies with T^n , with n between 0.6 and unity, rather than 0.5, as in Eq. (1.13).

The more up-to-date kinetic theories replace the billiard-ball model with a more realistic molecular force field by considering the force of attraction and repulsion between molecules. These theories, reviewed by Hirschfelder, Curtiss, and Bird,² make use of the potential energy of interaction between a pair of molecules in the gas. This function—often referred to as the *Lennard-Jones potential*—displays the behavior of molecular interactions by exhibiting weak attraction at large separation distances and strong repulsion at small separations, as shown in Fig. 1.6.

Where the position of the molecules is δ , the potential energy is a minimum at $-\epsilon$; ϵ is called the *characteristic energy parameter*. Using the Lennard-Jones potential, Chapman and Enskog have developed the following equation for the viscosity of nonpolar gases at low pressures:

$$\eta = 2.67 \times 10^{-5} \frac{\sqrt{MT}}{\sigma^2 \Omega_\eta}. \quad (1.14)$$

¹1 standard atmosphere (atm) = $1.0133 \times 10^5 \text{ N m}^{-2}$.

²J. O. Hirschfelder, C. F. Curtiss, and R. B. Bird, *Molecular Theory of Gases and Liquids*, Wiley, New York, 1954.

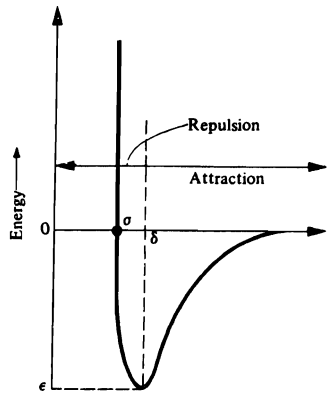


Fig. 1.6 Lennard-Jones potential function describing the interaction of two nonpolar molecules.

Here M is the gram-molecular weight, η is in poises, T in K, and σ is a characteristic diameter of the molecule in Å (see Fig. 1.6). The quantity Ω_η is the *collision integral* of the Chapman-Enskog theory, which is a function of a dimensionless temperature parameter $\kappa_B T/\epsilon$. In order to use Eq. (1.14), we need values of σ and ϵ/κ_B ; these parameters are known for many substances. A partial list of them is given in Table 1.1. We can then determine the collision integral by using Table 1.2.

Example 1.2 Compute the viscosity of hydrogen at 1 atm and 1364 K.

Solution. From Table 1.1, we find that

$$\epsilon/\kappa_B = 59.7 \text{ K}, \quad \sigma = 2.827 \text{ \AA}.$$

From Table 1.2,

$$\Omega_\eta \cong 0.733.$$

Substituting appropriate values into Eq. (1.14), we have

$$\eta = 2.67 \times 10^{-5} \frac{\sqrt{(2)(1364)}}{(2.827)^2(0.733)} = 2.38 \times 10^{-4} \text{ poise.}$$

(Observed viscosity is 2.44×10^{-4} poise.)

Using Eq. (1.14) to calculate η requires knowing σ and ϵ/κ_B . When values of σ are not available, one may use a modified form of Eq. (1.14), as presented by Bromley and Wilke³:

$$\eta = 3.33 \times 10^{-5} \frac{\sqrt{MT_c}}{\hat{V}_c^{2/3}} f \left[\frac{\kappa_B T}{\epsilon} \right]. \quad (1.15)$$

³L. R. Bromley and C. R. Wilke, *Ind. Eng. Chem.* **43**, 1641 (1951).

Table 1.1 Intermolecular force parameters and critical properties

Substance	Molecular weight, M	Lennard-Jones parameters*		Critical constants*	
		σ , Å	ϵ/κ_B , K	T_c , K	\hat{V}_c , cm ³ /mol
<i>Light elements</i>					
H ₂	2.016	2.827	59.7	33.2	65.1
He	4.003	2.551	10.22	5.19	57.4
<i>Noble gases</i>					
Ne	20.183	2.820	32.8	44.4	41.6
Ar	39.948	3.542	93.3	150.8	74.9
Kr	83.80	3.655	178.9	209.4	91.2
Xe	131.3	4.047	231.0	289.7	118.4
<i>Polyatomic gases</i>					
Air	28.97	3.711	78.6	-	-
N ₂	28.013	3.798	71.4	126.2	89.8
O ₂	32.00	3.467	106.7	154.6	50.4
CO	28.01	3.690	91.7	132.9	93.2
CO ₂	44.01	3.941	195.2	304.1	93.9
H ₂ O	18.02	2.641	809.1	647.3	57.1
SO ₂	64.06	4.112	335.4	430.8	122.2
F ₂	38.00	3.357	112.6	144.3	66.3
Cl ₂	70.91	4.217	316.0	416.9	123.8
Br ₂	159.81	4.296	507.9	588	127.2
CH ₄	16.04	3.758	148.6	190.4	99.2

Note: The Angstrom, Å, equals 0.1 nm or 10⁻⁸ cm.

*R. C. Reid, J. M. Pausnitz, and B. E. Poling, *The Properties of Gases and Liquids*, 4th edition, McGraw-Hill Book Co., New York, NY, 1987, Appendices A and B.

Table 1.2 Values of Ω -integral for viscosity and of the viscosity function $f(\kappa_B T/\epsilon)$, based on the Lennard-Jones potential*

$\kappa_B T/\epsilon$	Ω_η	$f(\kappa_B T/\epsilon)$	$\kappa_B T/\epsilon$	Ω_η	$f(\kappa_B T/\epsilon)$
0.3	2.785	0.1969	6.0	0.8963	2.751
0.4	2.492	0.2540	8.0	0.8538	3.337
0.5	2.257	0.3134	10	0.8242	3.866
0.6	2.065	0.3751	20	0.7432	6.063
0.7	1.908	0.4384	40	0.6718	9.488
0.8	1.780	0.5025	60	0.6335	12.324
0.9	1.675	0.5666	80	0.6076	14.839
1.0	1.587	0.6302	100	0.5882	17.137
2.0	1.175	1.2048	200	0.5320	26.80
4.0	0.9700	2.0719	400	0.4811	41.90

*J. O. Hirschfelder, C. F. Curtiss, and R. B. Bird, *Molecular Theory of Gases and Liquids*, Wiley, New York, 1954.

12 Viscous Properties of Fluids

where η is in poises, T_c (K) and \hat{V}_c (cm^3/mol) are the critical temperature and volume, respectively, and $f(\kappa_p T/\varepsilon)$ is an empirical function also to be found in Table 1.2.

The Chapman-Enskog theory has been extended to include multicomponent gas mixtures at low density. For most purposes, the semiempirical formula of Wilke⁴ is quite adequate:

$$\eta_{\text{mix}} = \sum_{i=1}^n \frac{x_i \eta_i}{\sum_{j=1}^n x_j \Phi_{ij}}, \quad (1.16)$$

in which

$$\Phi_{ij} = \frac{1}{\sqrt{8}} \left[1 + \frac{M_i}{M_j} \right]^{-1/2} \left[1 + \left(\frac{\eta_i}{\eta_j} \right)^{1/2} \left(\frac{M_j}{M_i} \right)^{1/4} \right]^2.$$

Here n is the number of chemical species in the mixture; x_i and x_j are the mole fractions of species i and j ; η_i and η_j are the viscosities of species i and j at the system temperature and pressure; and M_i and M_j are the corresponding molecular weights. Note that Φ_{ij} is dimensionless, and, when $i = j$, $\Phi_{ij} = 1$.

Example 1.3 Estimate the viscosity of a gas comprising 20% CO_2 , 50% CO and 30% He at 800 K and 10^5 N m^{-2} (approx. 1 atm), given the viscosities of the pure components.

i	x_i	M_i g mol ⁻¹	η_i N s m ⁻²
1 (CO_2)	0.2	44.011	3.37×10^{-5}
2 (CO)	0.5	28.011	3.43×10^{-5}
3 (He)	0.3	4.003	3.82×10^{-5}

Solution. Calculate values of Φ_{ij} first and collect the denominators for Eq. (1.16).

i	j	M_i/M_j	η_i/η_j	Φ_{ij}	$\sum_{j=1}^3 x_j \Phi_{ij}$
1	1	1.000	1.000	1.000	} 0.404 ($j = 1, x_j = 0.2$)
	2	1.571	0.982	0.784	
	3	10.994	0.882	0.235	
2	1	0.636	1.018	1.254	} 1.284 ($j = 2, x_j = 0.5$)
	2	1.000	1.000	1.000	
	3	6.998	0.898	0.313	
3	1	0.091	1.133	2.921	} 1.908 ($j = 3, x_j = 0.3$)
	2	0.143	1.114	2.440	
	3	1.000	1.000	1.000	

⁴C. R. Wilke, *J. Chem. Phys.* **18**, 517 (1950).

Then

$$\eta_{\text{mix}} = \frac{(0.2)(3.37 \times 10^{-5})}{0.404} + \frac{(0.5)(3.43 \times 10^{-5})}{1.284} + \frac{(0.3)(3.82 \times 10^{-5})}{1.980}$$

$$\eta_{\text{mix}} = 3.60 \times 10^{-5} \text{ N s m}^{-2}.$$

To summarize, Eqs. (1.14), (1.15), and (1.16) are useful equations for computing viscosities of nonpolar gases and gas mixtures at low density from tabulated values of the intermolecular force parameters σ and ϵ . They cannot, however, be applied with confidence to gases consisting of polar or highly elongated molecules such as H_2O , NH_3 , CH_3OH , and NOCl . A further limitation is that for the most part these equations have been tested only over the temperature range 100 K to 1500 K.

The data on viscosity of several gases as a function of temperature are given in Fig. 1.7. Keep in mind that the data are valid for pressures up to about 10 atmospheres. Note that (1) the viscosity of all gases increases with temperature, and (2) the magnitude of viscosity does not solely depend on the molecular weight of the gas. For example, the data for helium fall in the range of much heavier gases than hydrogen. Sports commentators in particular should heed some of the data and stop propagating the myth that baseballs can be hit farther in dry air than under humid weather conditions. Not only is the viscosity of humid air less than that of dry air, the density is too.

1.4 VISCOSITY OF LIQUIDS

In dealing with transport processes in liquids, we are always faced with the problem that much less is known about the structure of liquids than about the structures of solids or gases. However, there is more similarity between liquids and solids than between liquids and gases. This similarity is based on the small fractional increase in volume on melting (3 to 5% for metals), and the fact that the heat of fusion is quite a bit less than the heat of vaporization. Furthermore, x-ray data tell us that there is at least some degree of short-range order in a liquid. That is, at a short distance from a central atom, the arrangement of nearest neighbors is reasonably predictable. However, as the distance increases, the predictability of atom positions decreases rapidly, unlike in solids.

Several theories have been postulated to account for the observed properties of liquids, none without some serious deficiencies. The oldest, in terms of the structural picture involved, is the *hole theory*, which postulates that a liquid contains many holes or vacant areas, distributed throughout the liquid, with these holes having some distribution of sizes about an average. Although this theory does not explain all observations of the changes of properties of materials upon fusion, it has been useful in deriving a relatively simple approach to predicting the temperature dependence of the viscosity of liquids. Other models, based on differing assumptions of where the extra volume associated with a liquid is assumed to reside, are discussed in Chapter 12.

Because liquids near their melting points still represent a dense phase, the concept of transfer of momentum from atom to atom, as utilized in the kinetic theory approach to gas-phase viscosity, is invalid, since the momentum of each atom varies rapidly with the vibration of the atoms within the pseudo-lattice of the liquid. As Frenkel⁵ points out, the fact to be explained in the case of liquids is not their resistance to shearing stress, but rather their capability of yielding to stress.

⁵J. Frenkel, *Kinetic Theory of Liquids*, Dover, New York, 1955.

14 Viscous Properties of Fluids

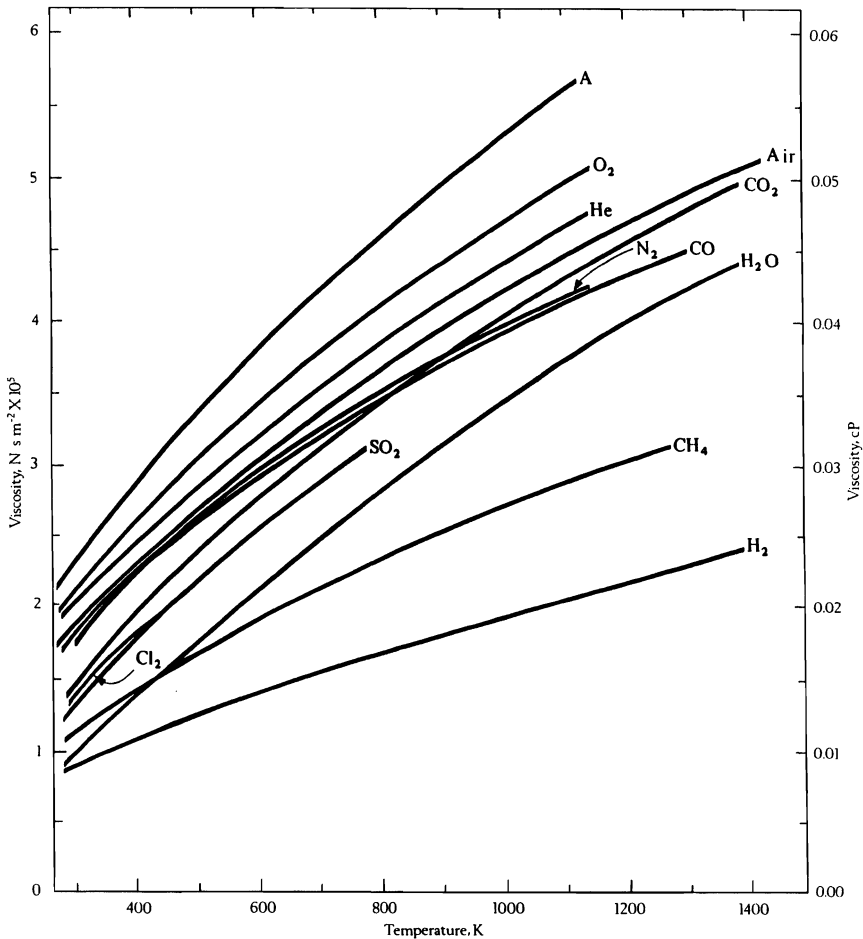


Fig. 1.7 The viscosity of common gases at 1 atm. (Curves drawn from data given in A. Schack, *Industrial Heat Transfer*, sixth edition, Wiley, New York, 1965, and *Handbook of Chemistry and Physics*, 52nd edition, The Chemical Rubber Co., Cleveland, 1971.)

Without recourse to any specific model of a liquid, but assuming only that viscous flow takes place by movement of particles past other particles, we can start by considering the mobility of an individual particle. Einstein has shown that the mobility B of a particle under the influence of an external force is related to the diffusion coefficient D by the relationship

$$D = B\kappa_B T; \quad (1.17)$$

B is the mean velocity divided by the force acting on the particle. Since diffusion appears to be an activated process, i.e., a minimum activation energy ΔG^\ddagger must be supplied to the particle to move it from one stable position to the next, then the fluidity, which is proportional to the capability of atoms to move, just as diffusion is, must also be thermally activated.

However, fluidity is the inverse of viscosity, so that, although D is proportional to $\exp [-\Delta G^\ddagger/RT]$, η must be proportional to $\exp [+ \Delta G^\ddagger/RT]$. That is, the viscosity of *liquids decreases* with increasing temperature. Recall that the viscosity of *gases increases* with temperature. The temperature dependence of η may then be described by an equation of the form

$$\eta = A \exp \left[\frac{\Delta G_{\text{vis}}^\ddagger}{RT} \right], \quad (1.18)$$

where η = viscosity, A = constant, T = absolute temperature, K, R = gas constant, and $\Delta G_{\text{vis}}^\ddagger$ = activation energy of viscosity.

The constant A is the object of much of the theoretical work done on the structure of liquids. None of the theories to date gives satisfactory equations, based on fundamental parameters, which can be used to accurately predict values of A . The closest is *Eyring's theory*, which predicts A according to the equation

$$A \cong \frac{N_0 h}{\hat{V}}, \quad (1.19)$$

in which N_0 = Avogadro's number, \hat{V} = molar volume, and h = Planck's constant.

For *molecular liquids* in which the bonding force is of a van der Waals type, we can predict the activation energy of viscosity from the vaporization energy ΔE_{vap} :

$$\Delta G^\ddagger \cong 0.41 \Delta E_{\text{vap}}. \quad (1.20)$$

Equations (1.19) and (1.20) are *not valid* for liquid metals, which are not molecular, nor are they valid for polymers or other chainlike molecules, and should not be used except as a last resort.

It is surprising that the viscosities of many diverse liquids, in terms of bonding nature in the solid state, are very similar. To illustrate this point, Table 1.3 lists groups of various materials under general ranges of viscosity. The viscosities used are those of the material in the normal temperature range of interest.

Table 1.3 Viscosity ranges for various liquids

Viscosity range, poise	Materials
1-100	<ul style="list-style-type: none"> CaO-Al₂O₃-SiO₂ slags 50% NaOH, 50% H₂O Linseed oil Liquid polymer melts
0.1-1.0	H ₂ SO ₄
0.01-0.1	<ul style="list-style-type: none"> Molten salts Heavy metals (Pb, Au, Zn, etc.) Alkaline earth metals (Ca, Mg) Transition metals (Fe, Ni, Co, etc.) Water (22°C) Kerosene (22°C)
0.001-0.01	<ul style="list-style-type: none"> Acetone Alkali metals

Figure 1.8 gives a nomograph for the viscosity of common liquids. More specific aspects of several classes of liquids of particular interest in materials processing are taken up in the following sections.

1.4.1 Viscosity of liquid metals and alloys

As you are undoubtedly aware, metals are not molecular in nature and neither the constants A nor $\Delta G_{\text{vis}}^{\ddagger}$ can be predicted by using the simplified equations presented above. Metals do, however, show activated behavior. Figure 1.9 plots the viscosities for many of the common metals as $\log \eta$ versus $1/T$.

Chapman⁶ analyzed these data in the light of the theory of liquids developed by Kirkwood⁷ and by Born and Green.⁸ He arrived at a generalized model for the viscosity of liquid metals which involves no assumptions of the structure other than that the atoms are spherical and that the potential between atoms can be expressed by some function $\phi(r)$ of the distance between atoms and an energy parameter, such as is done in the Lennard-Jones picture of the potential energy well between atoms, in which

$$\phi(r) = 4\epsilon \left[\left(\frac{\delta}{r} \right)^{12} - \left(\frac{\delta}{r} \right)^6 \right].$$

By obtaining a suitable expression for the time average of the interactions between atoms, when their normal molecular motion is disturbed by imposing a velocity gradient on the liquid, and by attributing virtually all the momentum flux to intermolecular forces (that is, neglecting the very small contribution from the kinetic motion of the atoms), Chapman deduced a relationship between the viscosity, an energy parameter ϵ , and a separation distance δ . Then, by further assuming that all liquid metals obey the same function $\phi(r)$ he concluded that all substances with this $\phi(r)$ should have a reduced viscosity η^* , which is a function of the reduced temperature T^* and volume V^* , where the functional relationship is given by

$$\eta^* (V^*)^2 = f(T^*), \quad (1.21)$$

and

$$\eta^* = \frac{\eta \delta^2 N_0}{\sqrt{MRT}}, \quad (1.22)$$

$$T^* = \frac{\kappa_B T}{\epsilon}, \quad (1.23)$$

and

$$V^* = \frac{1}{n\delta^3}. \quad (1.24)$$

⁶T. Chapman, *AIChE J.* **12**, 395 (1966).

⁷J. G. Kirkwood, *J. Chem. Phys.* **14**, 180 (1946).

⁸M. Born and H. S. Green, *A General Kinetic Theory of Liquids*, University Press, Cambridge, 1949.

Viscosities of liquids (coordinates for use with Fig. 1.8)

Liquid	x	y	Liquid	x	y
Acetone	14.5	7.2	Nitric acid, 95%	12.8	13.8
Brine, 25% NaCl	10.2	16.6	Nitric acid, 60%	10.8	17.0
Carbon tetrachloride	12.7	13.1	Sodium hydroxide, 50%	3.2	25.8
Fuel oil	6.0	33.7	Sulfuric acid, 100%	8.0	25.1
Hydrochloric acid, 31.5%	13.0	16.6	Titanium tetrachloride	14.4	12.3
Kerosene	10.2	16.9	Water	10.2	13.0
Linseed oil, raw	7.5	27.2			

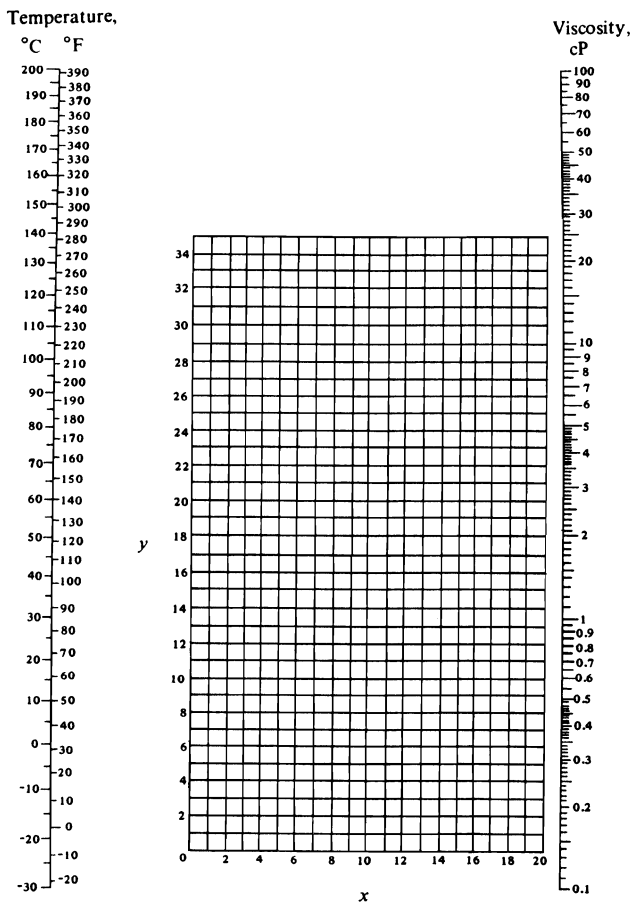


Fig. 1.8 Viscosities of liquids at 1 atm. For coordinates see the table above. (From J. H. Perry (editor), *Chemical Engineers' Handbook*, fourth edition, McGraw-Hill, New York, 1963.)

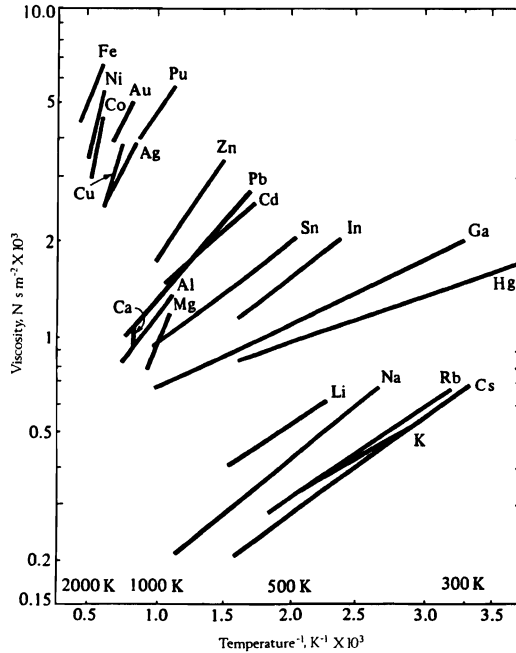


Fig. 1.9 The viscosities of liquid metals and their dependence on temperature. (From Chapman, *ibid.*)

The variables used are:

- δ = interatomic distance in the close-packed crystal at 0 K, Å,
- ε = energy parameter characteristic of specific metal,
- N_0 = Avogadro's number,
- M = atomic weight,
- R = gas constant,
- T = absolute temperature, K,
- κ_B = Boltzmann's constant, and
- n = number of atoms per unit volume.

The parameter δ is taken as the interatomic spacing for the close-packed crystal at 0 K. The energy parameters present the largest difficulty, and have been derived in the following manner. The effective Lennard-Jones parameters for sodium and potassium have been determined.⁹ Using these two values, one can plot the reduced viscosity data for sodium and potassium as a function of reduced temperature. The data points fall on a smooth curve, as predicted by Eq. (1.21). Then, assuming that all the rest of the metals in Fig. 1.9 obey the same functional relationship, the viscosity-temperature data for the remainder of the pure metals are correlated by empirically adjusting the parameter ε/κ_B until all the data for a given metal fall on one point on the curve, given in Fig. 1.10. Table 1.4 shows the resulting values of ε/κ_B starting with the known (measured) values for sodium and potassium.

⁹R. C. Ling, *J. Chem. Phys.* **25**, 609 (1956).

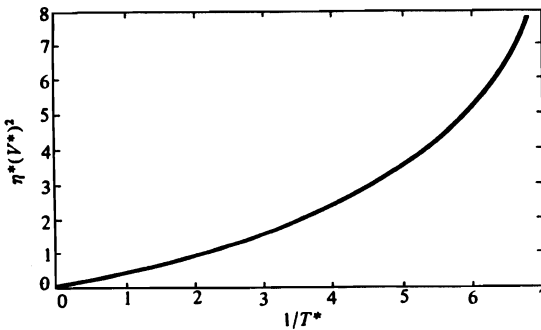


Fig. 1.10 Correlation curve for viscosities of liquid metals. (From Chapman, *ibid.*)

Table 1.4 Empirically determined values of ε/κ_B (from Chapman, *ibid.*)

Metals	δ , Å	ε/κ_B , K	Metals	δ , Å	ε/κ_B , K
Na	3.84	1970	Rb	5.04	1600
K	4.76	1760	Ag	2.88	6400
Li	3.14	2350	Cd	3.04	3300
Mg	3.20	4300	In	3.14	2500
Al	2.86	4250	Sn	3.16	2650
Ca	4.02	5250	Cs	5.40	1550
Fe	2.52	10 900	Au	2.88	6750
Co	2.32	9550	Hg	3.10	1250
Ni	2.50	9750	Pb	3.50	2800
Cu	2.56	6600	Pu	3.10	5550
Zn	2.74	4700			

The fact that, by adjusting an unmeasured parameter, it is possible to correlate all these liquid-metal viscosities on a single curve, might not be taken as significant, except for the fact that one theory of melting indicates that the melting point should be proportional to ε , and that this relationship has been observed for other classes of materials. The empirically determined values of ε/κ_B from Table 1.4 have been plotted as a function of the absolute melting temperature, and an excellent correlation has been observed, leading to the equation

$$\frac{\varepsilon}{\kappa_B} = 5.20T_m, \text{ K.} \quad (1.25)$$

For metals with high melting points, this may be used to predict viscosities, as no further data are available.

Example 1.4 Estimate the viscosity of liquid titanium at 2120 K. The following data are available: $T_m = 1943$ K (1670°C), $M = 47.9$ g mol⁻¹, ρ (density) = 4.5×10^3 kg m⁻³, and $\delta = 0.289$ nm.

Solution. Using Eq. (1.25), one can estimate ε/κ_B to be

$$\varepsilon/\kappa_B = (5.20)(1943) = 10\,100 \text{ K.}$$

20 Viscous Properties of Fluids

Then T^* is given by Eq. (1.23), and $\eta^*(V^*)^2$ is found from Fig. 1.10:

$$T^* = \frac{2120}{10,100} = 0.210,$$

and

$$\eta^* (V^*)^2 = 3.1.$$

From the given data, one can calculate V^* :

$$V^* = \frac{1}{\left[\frac{6.023 \times 10^{23} \text{ atoms}}{47.9 \text{ g}} \right] \left[\frac{4.5 \text{ g}}{\text{cm}^3} \right] (2.89 \times 10^{-8} \text{ cm})^3} = 0.733.$$

Then

$$\eta^* = \frac{3.1}{(0.733)^2} = 5.77.$$

Solving for η , we first obtain

$$(MRT)^{1/2} = \left[\frac{47.9 \text{ g}}{\text{mol}} \mid \frac{8.3144 \text{ J}}{\text{mol K}} \mid \frac{2120 \text{ K}}{\text{mol}} \right]^{1/2} = 918.9 \text{ (J g)}^{1/2} \text{ mol}^{-1};$$

then

$$\begin{aligned} \eta &= \frac{\eta^* (MRT)^{1/2}}{\delta^2 N_0} = \frac{5.77 \mid 918.9 \text{ J}^{1/2} \text{ g}^{1/2}}{\text{mol} \mid (0.289 \times 10^{-9})^2 \text{ m}^2 \mid 6.023 \times 10^{23}} \\ &= \frac{0.1054 \text{ J}^{1/2} \text{ g}^{1/2}}{\text{m}^2} \mid \frac{1 \text{ kg}^{1/2}}{10^{3/2} \text{ g}^{1/2}} \mid \frac{1 \text{ kg}^{1/2} \text{ m}}{1 \text{ J}^{1/2} \text{ s}} = 3.33 \times 10^{-3} \text{ kg m}^{-1} \text{ s}^{-1}, \end{aligned}$$

or

$$\eta = 3.33 \times 10^{-3} \text{ N s m}^{-2} \text{ (3.33 cP)}.$$

Other theories on the viscosity of liquid metals are reviewed in Iida and Guthrie,¹⁰ who estimate the preexponential constant in Eq. (1.18) by

$$A \approx \frac{5.7 \times 10^{-5} (MT_m^{1/2})}{V_m^{2/3} \exp(\Delta G_{vis}^\ddagger / RT_m)}. \quad (1.26)$$

¹⁰T. Iida and R. I. L. Guthrie, *The Physical Properties of Liquid Metals*, Clarendon Press, Oxford, 1988, p. 196.

where A is in N s m^{-2} , M is the atomic weight, T_m is the absolute melting point, V_m is the atomic volume at T_m , R is the gas constant and $\Delta G_{\text{vis}}^\ddagger$ is the activation energy of viscosity. For metals:

$$\Delta G_{\text{vis}}^\ddagger = 5.06T_m^{1.2}, \quad (1.27)$$

and for semi-metals (Hg, Ga, K, In, Sn, Bi and Pb)

$$\Delta G_{\text{vis}}^\ddagger \approx 3.14T_m^{1.2}, \quad (1.28)$$

where $\Delta G_{\text{vis}}^\ddagger$ is in kJ mol^{-1} .

Experimental data for the viscosity of binary liquid alloys sometimes show anomalous viscosity changes at compositions corresponding to eutectics and limits of solid solubility. Data that show discontinuous viscosities with respect to composition should be doubted, although there may be some mild indications of structure related to the phase diagram. Iida and Guthrie¹¹ give a phenomenological equation to estimate viscosity, but it is too lengthy to repeat here. Kucharski¹² put forth a model to relate the viscosity of binary alloys to their structure. Kucharski's predictive equation is

$$\eta = \sum_{i=1}^2 x_i (V_i/V) (\beta/\beta_i)^2 \gamma_i^\alpha \eta_i, \quad (1.29)$$

where i denotes species 1 and 2, V_i is molar volume of i , V is molar volume of the alloy, γ_i is the thermodynamic activity coefficient of i and α is a constant, that varies slightly with temperature. Also

$$\beta_i = x_i V_i^{1/3} + x_j V_j^{4/3}/V_i$$

and

$$\beta = \sum_{i=1}^2 x_i V_i^{1/3}.$$

The use of Eq. (1.29) requires activity coefficients and molar volumes so it cannot be readily applied without first gathering thermodynamic data. At least for the Al-Cu system, the parameter α was found to vary with both temperature and composition,¹³ so in applying Eq. (1.29) this should be carefully checked.

In Fig. 1.11, the viscosities in an important binary system, Fe-C, are superimposed on the phase diagram to illustrate the effect an alloying element may have on viscosity. Viscosity data for many alloys can be found in Elliott *et al.*¹⁴

¹¹T. Iida and R. I. L. Guthrie, *ibid.*, p. 196.

¹²M. Kucharski, *Z. Metallk.* **77**, 393 (1986).

¹³S. Ganesan, R. Speiser and D. R. Poirier, *Metall. Trans. B* **18B**, 421 (1987).

¹⁴J. F. Elliott, M. Gleiser and V. Ramakrishna, *Thermochemistry for Steelmaking*, Vol. II, Addison-Wesley, Reading, MA, 1963, Section 9.

22 Viscous Properties of Fluids

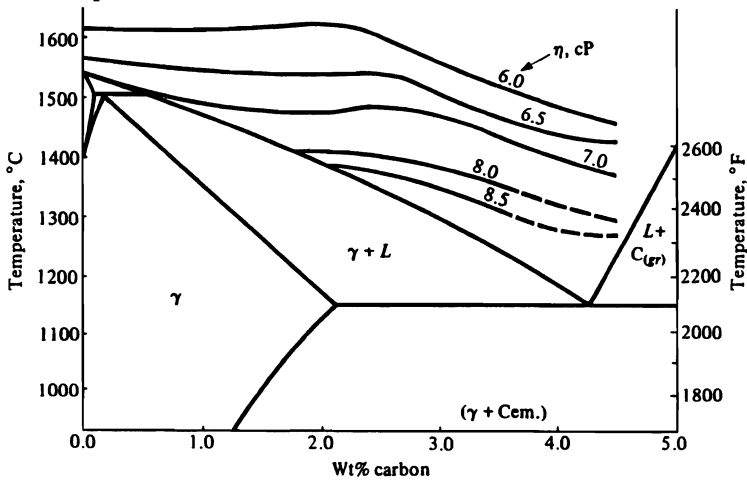


Fig. 1.11 Viscosities of iron-carbon alloys. (From R. N. Barfield and J. A. Kitchener, *J. Iron and Steel Inst.* **180**, 324 (1955).)

1.4.2 Viscosity of molten slags, silicates, and salts

The structures of molten slag systems have been studied from many aspects. At this point we will not go into the detail of the various structures, but rather discuss briefly their basic aspects which affect viscosity.

In general, slags consist of cations and anions resulting from ionization of basic and acidic constituents in molten oxide solution. We may consider an acidic component to be an oxide which, when dissolved in the slag, acquires additional oxygen ions to form a complex anion, while a basic oxide contributes an oxygen ion to the melt; the cation then remains dissociated from any other ions, and moves about freely. The most common acidic component is SiO_2 , and Al_2O_3 behaves in a similar manner. Starting with pure SiO_2 , in which the bonding is both strong and highly directional, and in which viscous flow occurs only by breaking bonds, let us examine what happens if we add a basic oxide, such as CaO , to it.

We presume that the structure of pure liquid silica is quite similar to that of solid silica, in which each Si^{4+} ion shares one electron with each of four O^{2-} ions which form a tetrahedron about the Si^{4+} ion. In the solid state, electroneutrality is maintained by each oxygen ion sharing its other electron between two tetrahedra, or Si^{4+} ions, and the structure built up is a regular crystalline array of SiO_4^{4-} groups. This is illustrated in Fig. 1.12(a). When this substance is melted, the arrangement presumably continues, but the long-range order is destroyed, as indicated in Fig. 1.12(b). However, the same Si-O bonds are present and these high energy bonds need to be broken so that viscous flow could take place. The activation energy for this process is quite high (135 kcal) and the viscosity of pure liquid SiO_2 at 1940°C is 1.5×10^5 poises ($1.5 \times 10^4 \text{ N s m}^{-2}$).

When CaO , or another similar divalent basic oxide, is added to the melt, the Ca^{2+} ions are accommodated in the interstices of the silicate structure and the O^{2-} ions enter into the network (Fig. 1.13). The O^{2-} ions cause two of the tetrahedra to separate since each corner of these two can now have an oxygen ion of its own. Increasing additions of base results in a progressive breakdown of the original three-dimensional network.

Table 1.5 shows this progression as a function of total oxygen atoms to silicon atoms. As the breakdown progresses, we may consider the silicate network to be made up of

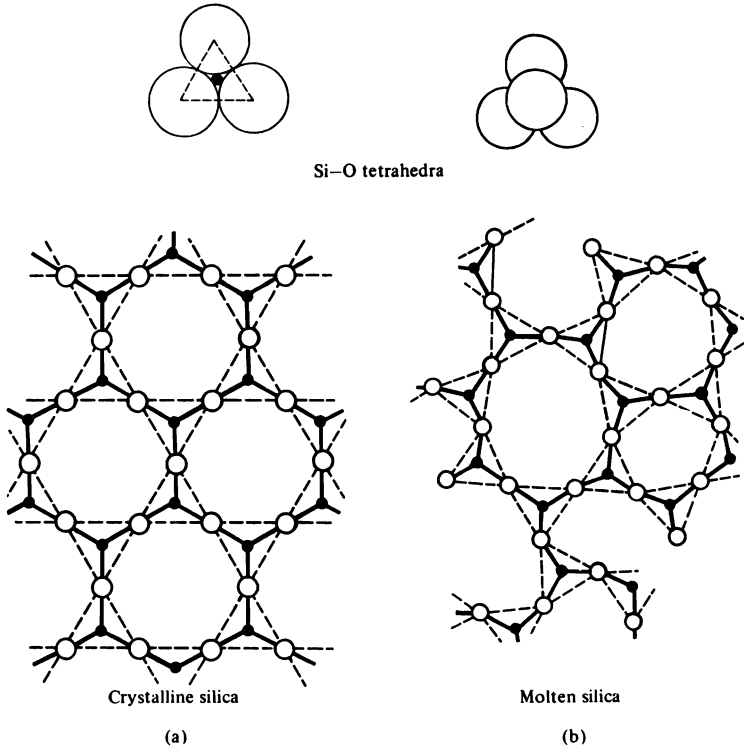


Fig. 1.12 Silicate tetrahedron and the structure of silica.

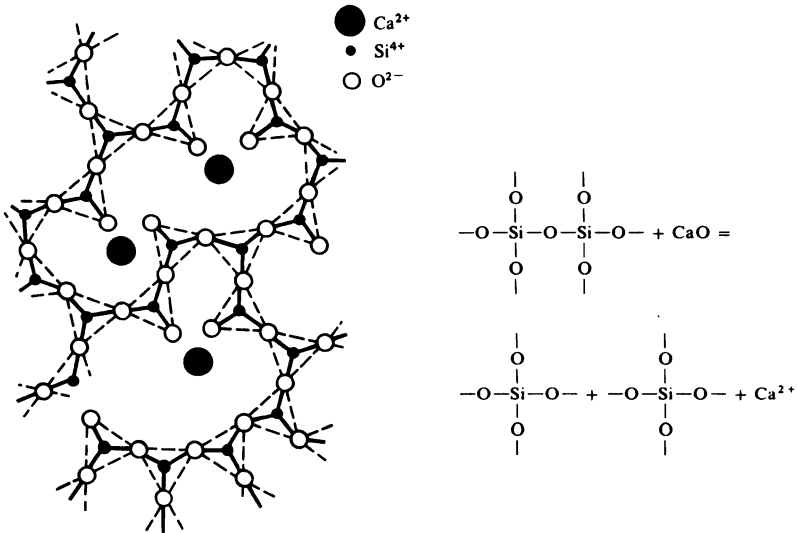


Fig. 1.13 The solution of a divalent metal oxide in molten silica.

Table 1.5 Structural relationships in basic oxide-silicate melts

$\frac{\text{Total oxygen atoms}}{\text{Silicon atoms}}$	Corresponding binary molecular formula	Structure	Equivalent silicate ion
2:1	SiO ₂	All corners of tetrahedra shared	Infinite network
5:2	MO·2SiO ₂	One broken link per tetrahedron	(Si ₆ O ₁₅) ⁶⁻ or (Si ₈ O ₂₀) ⁸⁻
3:1	MO·SiO ₂	Two broken links per tetrahedron (ring)	(Si ₃ O ₉) ⁶⁻ or (Si ₄ O ₁₂) ⁸⁻
7:2	3MO·SiO ₂	Three broken links per tetrahedron (chain)	(Si ₂ O ₇) ⁶⁻
4:1	2MO·SiO ₂ (orthosilicate)	All links broken	Discrete (SiO ₄) ⁴⁻ tetrahedra

progressively smaller discrete ions. From the original three-dimensional network, we progress to discrete molecules, such as (Si₆O₁₅)⁶⁻ and (Si₃O₉)⁶⁻, as more and more oxygen ions are contributed by the basic oxide. Actually, it is more probable that rather than only one type of silicate ion existing at any given ratio of base to acid, there exists a statistical distribution of sizes about the average one, as indicated by the number of links broken per tetrahedron.

As the three-dimensional network breaks down, the number of Si-O bonds that need to be broken during viscous flow decreases. The shear process becomes easier as the size of the anions decreases (Fig. 1.14), so that the activation energy ΔG_{vis}^\ddagger falls off continuously as basic oxide is added (Fig. 1.14), up to the orthosilicate composition, beyond which no further significant decrease is expected. At that point the network of (SiO₄)⁴⁻ tetrahedra is completely broken down. For compositions more basic than the orthosilicate, the viscosity changes that do occur are more likely due to changes in the liquidus temperature.

Alumina, which appears to exist in molten oxide solutions as (AlO₃)³⁻ anions, behaves in much the same way as silica. However, silica and alumina are not equivalent on a molar basis, since the basic building block of alumina is (AlO₃)³⁻, and two Al³⁺ ions can replace two Si⁴⁺ ions only if one Ca²⁺ ion is available to maintain electrical neutrality. Thus, as far as its effect on viscosity is concerned, alumina has a *silica equivalence* X_a , which depends on the Al₂O₃/CaO ratio and on the total Al₂O₃ content, as shown in Fig. 1.15. Turkdogan and Bills,¹⁵ using these data in correlating the viscosity and composition of CaO-MgO-Al₂O₃-SiO₂ slags, have found that, for a given temperature, a smooth curve correlates all compositions in the studied range (Fig. 1.16). To utilize this fact, we convert the slag analysis to mole fractions, and determine X_a from Fig. 1.15. Magnesium oxide (MgO) is equivalent to CaO, up to about 10 mole percent MgO, and their mole fractions are added together to obtain X_{CaO} . Thus, when we add X_{SiO_2} and X_a , and know the temperature, we can find the viscosity from Fig. 1.16. Up to a concentration of 16 mole percent, we may consider FeO to be identical to CaO, as far as their effect on viscosity is concerned. Above 16%, FeO decreases viscosity more than CaO or MgO, except at lower temperatures.

¹⁵E. T. Turkdogan and P. M. Bills, *Amer. Ceram. Soc. Bull.* **39**, 682 (1960).

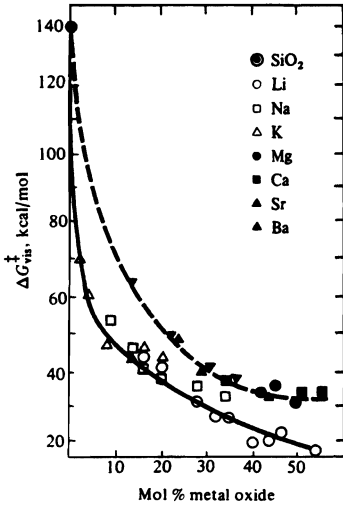


Fig. 1.14 Decrease of the activation energy of viscosity for silica as basic oxides are added. (From P. M. Bills, *J. Iron and Steel Inst.* **201**, 133 (1963).)

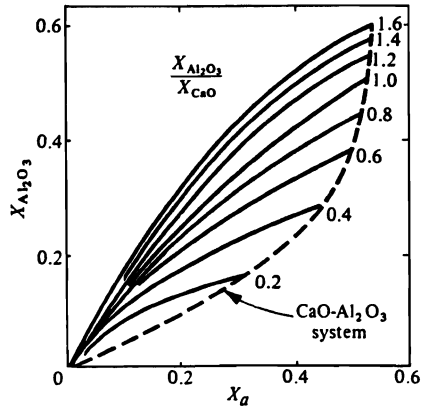


Fig. 1.15 Silica equivalence of alumina related to alumina molar concentrations and alumina: lime molar ratios. (From Bills, *J. Iron and Steel Inst.* **201**, 133 (1963).)

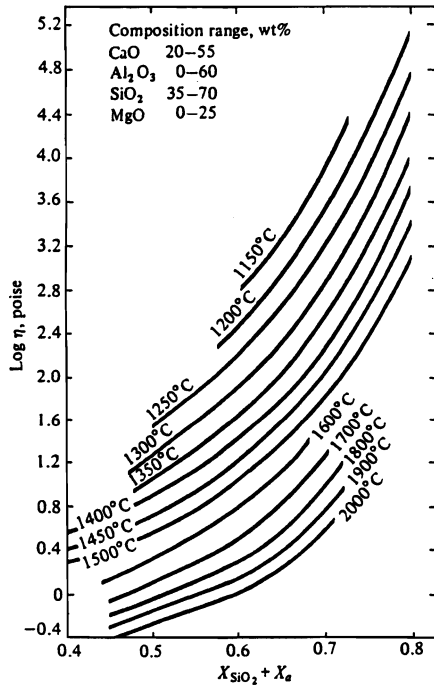


Fig. 1.16 Viscosity of CaO-Al₂O₃-SiO₂-MgO melts. Viscosity is expressed in poises. (From E. T. Turkdogan and P. M. Bills, *Amer. Cer. Soc. Bull.* **39**, 682 (1960).)

26 Viscous Properties of Fluids

Finally, we should note the ability of the well-known flux CaF_2 (fluorspar) to decrease the viscosity of oxide slags. Although we do not quite understand the reason, it may be due to the ability of CaF^+ cations to move between silicate anions that are electrostatically bound together, by mutual attraction to a Ca^{2+} cation, thereby decreasing the electrostatic bond and thus lowering the viscosity. The effect is much more pronounced at low rather than at elevated temperatures, and in acidic slags more than in basic slags. Viscosity data for an important class of fluxes used in the continuous casting of steel are available in McCauley and Apelian.¹⁶

Example 1.5 Calculate the viscosity of a slag with composition 40% CaO , 40% SiO_2 , 8% MgO , 12% Al_2O_3 at 1600°C and at 1500°C.

Solution. Converting to mole fractions, we have $X_{\text{CaO}} = 0.422$, $X_{\text{MgO}} = 0.117$, $X_{\text{SiO}_2} = 0.390$, $X_{\text{Al}_2\text{O}_3} = 0.069$.

For our purposes, we lump X_{CaO} and X_{MgO} together, so the effective $X_{\text{CaO}} = 0.539$.

Calculating the ratio $X_{\text{Al}_2\text{O}_3}/X_{\text{CaO}} (=0.128)$, enter Fig. 1.15 at $X_{\text{Al}_2\text{O}_3} = 0.069$, move slightly to the right of $X_{\text{Al}_2\text{O}_3}/X_{\text{CaO}} = 0.2$, and go down to find $X_a \approx 0.10$. After calculating $X_{\text{SiO}_2} + X_a = 0.490$, move to Fig. 1.16, and go up to the curves for 1600°C and 1500°C. The viscosity values are approximately 2.1 and 3.6 poises, respectively.

Urbain and Boiret¹⁷ have a model of viscosity for a variety of liquid systems, including silicates. They derived a theoretical equation that suggests viscosity varies with temperature as

$$\eta = AT \exp(1000 B/T), \quad (1.30)$$

where η is in poise, T is in K and A and B are empirical constants (Table 1.6). If values of A and B are not known, then one may estimate values of A and B , depending on the type of liquid and other parameters given in their paper.

The simplest molten salts are those in which we take the bonding to be essentially electrostatic; for example, we consider that molten NaCl consists entirely of Na^+ and Cl^- ions. Since there appear to be no large anion or cation complexes analogous to the $(\text{SiO}_4)^{4-}$ or $(\text{AlO}_3)^{3-}$ ions in molten oxide systems, and since there is a relatively large fraction of nondirectional electrostatic bonding, flow takes place relatively easily in these materials. Figure 1.17 shows viscosities of many molten salts. Note that their viscosities are about 1/100th of those of the molten oxides.

Because of the nondirectionality of the bond forces, the activation energies of viscosity for salts are also lower than those of the slags and silicates. We can also use Eq. (1.30) to estimate viscosities of molten salts. Values of A and B can be found in Table 1.7.

¹⁶W. L. McCauley and D. Apelian, *Can. Met. Quart.* **20**, 247 (1981).

¹⁷G. Urbain and M. Boiret, *Ironmkg. and Steelmkg.* **17**, 255, 1990.

Table 1.6 Values of A and B for inorganic melts including silicates (from G. Urbain and M. Boiret, *Ironmkg. and Steelmkg.* 17, 255 (1990)).

Type of Melt	Melt	$-\ln A$	B
Network Liquid	SiO ₂	23.1	64.1
	GeO ₂	18.3	32.9
Ionic Liquids	'FeO'	12.5	6.1
	Al ₂ O ₃	14.2	13.2
	B ₂ O ₃	12.3	13.2
	P ₂ O ₅	16.6	21.7
	Fe ₂ SiO ₄	13.6	9.2
	Mg ₂ SiO ₄	14.8	13.3
	MgCaSiO ₄	16.9	19.1
	MgSiO ₃	17.7	18.8
	(Mg/Ca)SiO ₃	17.5	20.8
	CaSiO ₃	17.3	19.6
	MnSiO ₃	19.6	24
	SrSiO ₃	17.4	20.6
	BaSiO ₃	17.7	21.1
	LiAlSiO ₄	19.8	28.1
	NaAlSiO ₄	25.6	43.9
	KAlSiO ₄	25.3	50.2
	Ca(AlSiO ₄) ₂	20.7	30.6
	Sr(AlSiO ₄) ₂	21.3	33.2
	Ba(AlSiO ₄) ₂	22.6	37.2
	LiAlSi ₂ O ₆	21.2	34.7
	LiAlSi ₃ O ₈	21.4	38
	NaAlSi ₃ O ₈	26	51.5
	KAlSi ₃ O ₈	27.4	55.6
LiAlSi ₄ O ₁₀	23.2	42.5	
Binary Silicate B ₂ O ₃ -SiO ₂	Mole Fraction B ₂ O ₃		
	0.062	21.9	55.1
	0.100	20.1	48.5
	0.147	19.5	44
	0.252	15.5	35
	0.446	12.3	21.9
	0.516	12.04	19.8
	0.777	12.4	15.02
	0.893	13.1	14.2
0.940	13.1	13.7	
Binary Silicate Al ₂ O ₃ -SiO ₂	Mole Fraction Al ₂ O ₃		
	0.202	21.67	39.21
	0.500	18.54	25.85
	0.700	17.12	21.01

Table 1.6 (continued)

Type of Melt	Melt	$-\ln A$	B
Binary Silicate PbO-SiO ₂	Mole Fraction PbO		
	0.429	21.1	20.6
	0.474	18.9	17.8
	0.512	19.2	17.8
	0.603	17.4	12.6
	0.606	17.3	12.6
	0.633	16.7	11.3
	0.641	17.7	12.7
	0.651	17.5	11.9
	0.670	17.1	12
	0.815	15.4	8.6

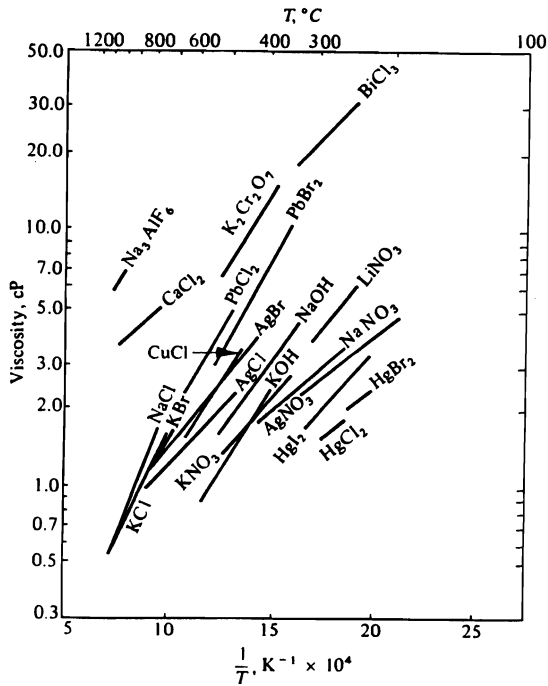


Fig. 1.17 Viscosities of molten salts. (From C. J. Smithells, *Metals Reference Book*, fourth edition, Vol. 1, Plenum Press, New York, 1967.)

Table 1.7 Values of A and B for molten salts (from Urbain and Boiret, *ibid.*)

Melt	$-\ln A$	B	Melt	$-\ln A$	B
LiCl	15.91	4.52	KI	14.9	3.75
NaCl	16.65	5.85	LiNO ₃	14.9	3.18
KCl	15.63	4.44	NaNO ₃	14.36	2.61
LiBr	15.14	3.65	KNO ₃	14.66	2.88
NaBr	14.84	3.71	Li ₂ CO ₃	19.16	9.59
KBr	15.01	3.7	Na ₂ CO ₃	22.86	14.41
Lil	14.48	3.04	K ₂ CO ₃	24.08	16.06
Nal	15.17	3.88			

1.5 NON-NEWTONIAN FLUIDS

According to Newton's law of viscosity (Eq. 1.3) the shear stress τ_{yx} , plotted versus the velocity gradient $-dv_x/dy$, should yield a straight line running through the origin. Experimentally, this has been proved true for all gases and for all single-phase nonpolymeric liquids. Fluids that behave in this manner—and most fluids do—are termed *Newtonian fluids*. However, Eq. (1.3) does not describe the behavior of a large number of fluids which are called *non-Newtonian fluids* and include substances such as molten plastics, slurries, and certain slags.

The study of Newtonian flow is part of a larger discipline of science known as *rheology*. Rheology encompasses the mechanical behavior of gases, liquids, and solids, including Newtonian gases and liquids on the one hand and elastic stress-strain behavior of solids on the other.

A large number of non-Newtonian fluids follow one of the behavioral patterns represented in Fig. 1.18, where the shear stress τ_{yx} is plotted versus the rate of strain $\dot{\gamma}$ ($\dot{\gamma}$ equals $-dv_x/dy$ at steady state). The curve of stress-strain rate is also plotted for Newtonian fluids, demonstrating the obvious fact that $\tau_{yx}/\dot{\gamma}$ is independent of $\dot{\gamma}$, i.e., the slope of the Newtonian curve is η . On the other hand, non-Newtonian fluids are those in which $\tau_{yx}/\dot{\gamma}$ is a function of $\dot{\gamma}$.

The fluids classified as *Bingham plastics* require a finite shear stress τ_0 (yield stress) to initiate flow. In other words, the fluid remains rigid when the shear stress is less than τ_0 , but flows when the shear stress exceeds τ_0 . An example of a fluid exhibiting Bingham plastic behavior is an aqueous slurry of fine, powdered coal. The following relationship gives the rate of shear stress and shear strain:

$$\tau_{yx} = \pm \tau_0 + \eta_p \dot{\gamma}, \quad \tau_{yx} > \tau_0. \quad (1.31)$$

Here η_p is a plastic viscosity or coefficient of rigidity. We use the plus sign when $\dot{\gamma}$ is positive, and the minus sign when $\dot{\gamma}$ is negative.

Pseudoplastic fluids, which are characterized by a decreasing slope of the τ_{yx} versus $\dot{\gamma}$ curve as the stress increases, need, like Newtonian fluids, no yield stress for flow, but, unlike Newtonian fluids, $\tau_{yx}/\dot{\gamma}$ does depend on τ_{yx} . *Dilatant fluids* differ from pseudoplastics in that the τ_{yx} versus $\dot{\gamma}$ curve has an increasing slope as stress increases. For both pseudoplastic and dilatant fluids we can sometimes use the *Ostwald power law* to describe the relationship of the stress-strain rate:

$$\tau_{yx} = k\dot{\gamma}^n. \quad (1.32)$$

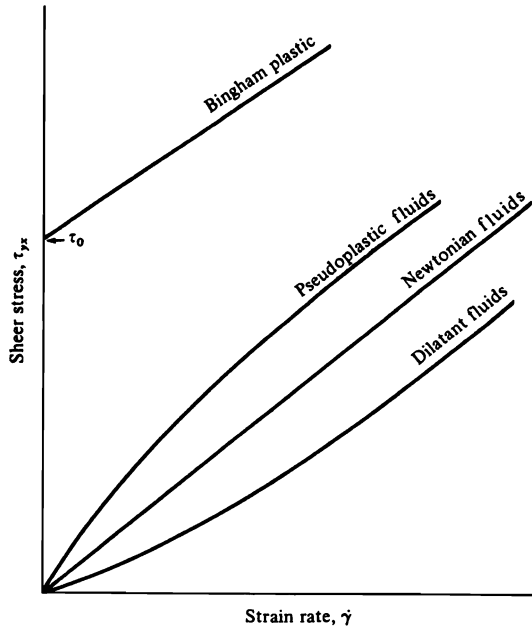


Fig. 1.18 Stress-strain rate curves for time-independent fluids.

Here, k is a measure of the fluid's consistency, and n is a measure of the fluid's departure from Newtonian behavior. For $n = 1$, Eq. (1.32) reduces to Newton's law of viscosity with $k = \eta$. For $n < 1$, the behavior is pseudoplastic, whereas if $n > 1$ it is dilatant. Aqueous suspensions of clay, lime, and cement rock are examples of various fluids described by the power law.

Since the Ostwald power law is the simplest model to describe dilatant and pseudoplastic fluids, it is often applied. However, when using it, we should keep in mind that this model does not give an accurate portrayal of the low-shear-rate region (i.e., low flow rates).¹⁸

In addition to these models, numerous other empirical equations have been proposed to express the relationship between shear stress and strain rate. The models we have been discussing are called *generalized Newtonian fluids* (GNF). They should not be applied to those fluids or conditions in which viscoelastic effects are present and play an important role, or to the fluids which exhibit *time-dependent properties*. The fluids in which viscoelastic effects are of great importance under certain conditions are *high polymers*.

Viscoelastic fluids are fluids which exhibit elastic recovery from deformation, that is, they *recoil*. This is in contrast with the behavior of GNF's which do not recoil. This difference is illustrated by the experiment depicted in Fig. 1.19. We observe the behavior of a black line made by injecting a charcoal slurry into a transparent tube. In part (a), the line has just been introduced into the tube with the fluid at rest. The fluid starts flowing when the pressure is lowered at the right end of the tube; both fluids flow in the direction of the lower

¹⁸R. B. Bird, *Can. J. of Chem. Eng.* **43**, 161 (Aug. 1965).

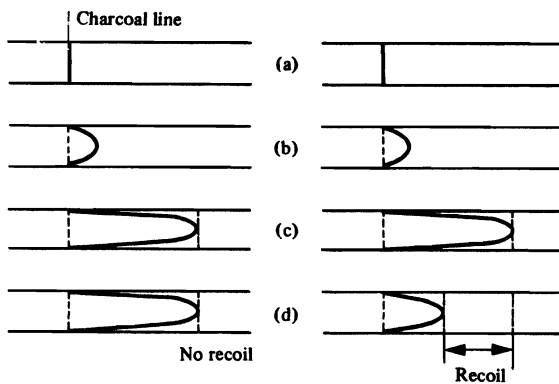


Fig. 1.19 Recoil effect in a viscoelastic fluid. Fluid on the left is a GNF; that on the right is a viscoelastic fluid.

pressure, as shown in parts (b) and (c). An instant after part (c) is reached, the pressure difference is removed and we can see that the GNF moves no further while the viscoelastic fluid goes backward. It does not, however, return to its original position, recoiling only partly.

Different conditions create different types of time-dependent fluid behavior. For example, *thixotropic fluids* have a structure that breaks down with time under shear. At a constant shear-strain rate, the viscosity decreases with time and approaches an asymptotic value. Under steady-state flow conditions, when the asymptotic value is maintained, thixotropic fluids may be treated as GNF's. *Rheopectic fluids*, in which viscosity increases with time, behave again quite differently from thixotropic fluids.

The purpose of this brief introduction to non-Newtonian fluids has been to make the reader aware of the fact that there are many fluids that do not necessarily obey Newton's law of viscosity, and that a direct application to such fluids of data and concepts in fluid mechanics dealing with Newtonian fluids could lead to serious engineering blunders. In the remainder of the text, we deal usually with Newtonian fluids.

The rheology of polymers, in itself, is a complex science. The viscosity of a polymer is a function of shear stress (or strain rate), temperature and molecular weight. The shear stress dependence at a given temperature is usually given by the power law of Eq. (1.32). The temperature dependence of viscosity can be represented by the exponential function, given by Eq. (1.18), provided there is no transition in the temperature range being considered and the temperature is at least $1.5 T_g$ (T_g is the glass transition temperature). Equation (1.20) indicates that ΔG^\ddagger increases with the vaporization energy, so we could expect that ΔG^\ddagger would increase with molecular weight. This is true, but at very high degrees of polymerization, the activation energy is independent of molecular weight.

Based on the above, therefore, we represent the viscosity of a particular polymer as a function of degree of polymerization (N), temperature (T), and strain rate ($\dot{\gamma}$). Generally, the functional dependence of $\dot{\gamma}$ is separated from the other two so that

$$\eta(N, T, \dot{\gamma}) = f(N, T) g(\dot{\gamma}). \quad (1.33)$$

32 Viscous Properties of Fluids

Many polymers follow the power law given by Eq. (1.32), where k can be interpreted as the Newtonian viscosity or zero strain rate viscosity, η_0 . In the absence of data, the viscosity can be approximated¹⁹ by

$$\frac{\eta}{\eta_0} = 1 + A_1(\dot{\gamma}\eta_0)^\alpha + A_2(\dot{\gamma}\eta_0)^{2\alpha}, \quad (1.34)$$

with $A_1 = 6.12 \times 10^{-2.645}$, $A_2 = 2.85 \times 10^{-3.645}$, $\alpha = 0.355$ and η and η_0 in N s m^{-2} and $\dot{\gamma}$ in s^{-1} .

The dependence of the Newtonian viscosity on molecular weight and temperature for many high molecular weight polymers show

$$\log \eta_0 = 3.4 \log N + k(T), \quad (1.35)$$

where N is the weight-average degree of polymerization and $k(T)$ is given in Table 1.8. The weight-average degree of polymerization is based on the so-called weight-average molecular weight:

$$\bar{M}_w = \frac{\sum x_i M_i^2}{\sum x_i M_i},$$

Table 1.8 Temperature dependence of k in Eq. (1.35) for long-chain polymers (from A. T. DiBenedetto, *The Structure and Properties of Materials*, McGraw-Hill, New York, 1967, p. 364).

Polymer	$k(T, K)$	k	T, K	N greater than
<u>Linear nonpolar polymers</u>				
Polyisobutylene	$5.5 \times 10^5/T^2 - 10.93$	—	—	610
Polystyrene	$2.7 \times 10^{16}/T^6 - 9.51$	—	—	730
<u>Linear polar polymers</u>				
Polymethyl methacrylate	$4.5 \times 10^{34}/T^{13} - 7.4$	—	—	208
Polyvinyl acetate	$9.77 \times 10^{10}/T^4 - 10.05$	—	—	—
Decamethylene sebacate	—	-8.2	382	290
Decamethylene adipate	$3.4 \times 10^5/T^2 - 11.2$	—	—	280
Decamethylene succinate	—	-8.0	382	290
Diethyl adipate	$2.1 \times 10^{10}/T^4 - 9.1$	—	—	290
<u>Effect of branching</u>				
Poly(ϵ -caprolactam):				
Linear	—	-8.0	526	340
Tetrachain	—	-8.1	526	390
Octachain	—	-8.7	526	550

¹⁹J. R. A. Pearson, *Mechanics of Polymer Processing*, Elsevier Applied Science Publ., London, 1985, p. 82.

where x_i is the mole fraction of molecules with molecular weight M_i . After \bar{M}_w is found, then N is simply

$$N = \frac{\bar{M}_w}{M_m},$$

where M_m is the molecular weight of a mer.

When $k(T)$ is not available, then an empirical equation for temperature dependence is recommended. It is

$$\log \frac{\eta_0}{\eta_r} = - \frac{8.86(T - T_r)}{101.6 + T - T_r}, \quad (1.36)$$

where the subscript r refers to a reference state. Values of T_r and T_g for several polymers are in Table 1.9. Equation (1.36) works best in the range $T_g \leq T < T_g + 100$ K. Since most thermoplastics are formed in the range of 1.3 to 1.5 T_g , Eq. (1.36) is often used for temperature extrapolations. For temperatures above the limit of Eq. (1.36), $T > 1.5 T_g$, we can use Eq. (1.18) for extrapolations.

Table 1.9 Reference Temperature, T_r , and Glass Transition Temperature, T_g , for Selected Polymers (from DiBenedetto, *ibid.*, p. 362)

Polymer	T_r , K	T_g , K
Polyisobutylene	243	202
Polymethylacrylate	378	324
Polyvinylacetate	349	301
Polystyrene	408	373
Polymethylmethacrylate	433	378
Polyvinylacetal	380	
Butadiene-styrene:		
75-25	268	216
60-40	283	235
50-50	296	252
30-70	328	291

Example 1.6 Polystyrene has an average molecular weight (\bar{M}_w) of 10^6 g mol⁻¹. The mer is C₈H₈. Estimate its Newtonian viscosity at 450 K.

Solution. We can make use of Eq. (1.35) and Table 1.8. To do so we first calculate the mer weight and the degree of polymerization.

$$M_m = (8)(12.01) + (8)(1) = 104.08 \text{ g mol}^{-1}$$

$$N = \frac{\bar{M}_w}{M_m} = \frac{10^6}{104.08} = 9608$$

34 Viscous Properties of Fluids

Then

$$\log \eta = 3.4 \log 9608 + \frac{2.7 \times 10^{16}}{450^6} - 9.51 = 7.28$$

$$\eta = 1.92 \times 10^7 \text{ poise} = 1.92 \times 10^6 \text{ N s m}^{-2}.$$

Example 1.7 At 50 K above T_g , the Newtonian viscosity of a polymer is 10^4 N s m^{-2} . Estimate the viscosity at 25 K above T_g .

Solution. The given data can be used to represent the reference state in Eq. (1.36). Then

$$\log \frac{\eta_0}{10^4} = -\frac{8.86(-25)}{101.6 - 25} = 2.892$$

$$\eta_0 = 7.80 \times 10^6 \text{ N s m}^{-2}.$$

This illustrates very clearly the rapid increase in viscosity as T_g is approached.

Before we leave this chapter, we must make it abundantly clear that the relationships used to estimate the viscosities of polymers are just that--only estimates. We have not considered situations in which polymers are in solvents and in polymer systems undergoing polymerization. Students of polymers, desirous of more information, should consult the references already presented. In addition, other useful starting sources are Biesenberger and Sebastian,²⁰ Rodriguez,²¹ and Crawford.²² Viscosities of polymers are used to characterize degree of polymerization and, indeed, as part of specifications in purchasing polymers and in quality control. Practitioners tell us that viscosity can vary from batch to batch, and so it is always better to measure viscosity than it is to rely on an estimate.

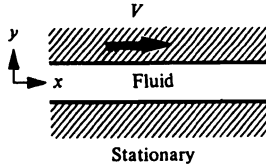
²⁰J. A. Biesenberger and D. H. Sebastian, *Principles of Polymerization Engineering*, John Wiley & Sons, New York, NY, 1983.

²¹F. Rodriguez, *Principles of Polymer Systems*, 2nd ed., Hemisphere Publ. Corp., Washington, DC, 1982.

²²R. J. Crawford, *Plastics Engineering*, 2nd ed., Pergamon Press, Oxford, England, 1987.

PROBLEMS

1.1 Compute the steady-state momentum flux (N m^{-2}) in a lubricating oil, viscosity equal to $2 \times 10^{-2} \text{ N s m}^{-2}$, that is contained between a stationary plate and one that is moving with a velocity of 61.0 cm s^{-1} . The distance between the plates is 2 mm . Next, show the direction of the momentum flux and the shear stress with respect to the x - y axis system in the diagram below.

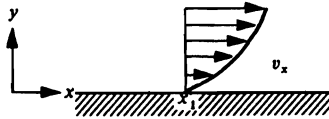


1.2 Near the surface of a flat plate, water has a velocity profile given by

$$v_x = 3y - y^3$$

with y in mm , v_x in cm s^{-1} , and $0 \leq y \leq 1 \text{ mm}$. The density and the kinematic viscosity of water are 10^3 kg m^{-3} and $7 \times 10^{-7} \text{ m}^2 \text{ s}^{-1}$, respectively.

- a) What is the shear stress at x_1 on the plate?
- b) What is the momentum flux at $y = 0.8 \text{ mm}$ and $x = x_1$ in the y -direction?
- c) Is there momentum flux in the x -direction at $y = 0.8 \text{ mm}$ and $x = x_1$ in the x -direction? If so, evaluate.



1.3 In fluidized bed processes, operating temperatures can vary from process to process or within the beds itself. Therefore, it is necessary to know how these temperature variations affect the properties, such as viscosity of the fluidizing gas in the reactor. Taking air as the fluidizing gas, estimate its viscosity at 313 K and 1073 K when considered as a one component gas with the parameters given in Table 1.1. Repeat the estimates, only now consider the air to be $79\% \text{ N}_2$, $21\% \text{ O}_2$. Compare these results to the experimental values of 0.019 cP and 0.0438 cP at 313 K and 1073 K , respectively.

1.4 Consider that the binary gas A-B is such that at a given temperature $\eta_A = \eta_B$. Plot the ratio of η_{mix}/η_A versus x_B if the ratio of the molecular weights of the two species, M_A/M_B , is: a) 100; b) 10; c) 1.

1.5 A quick estimate of the viscosity of a binary gas A-B is

$$\eta_{mix} = x_A \eta_A + x_B \eta_B.$$

What are the maximum errors in the viscosities estimated by the above equation when compared to the results calculated for a), b) and c) in problem 1.4? Briefly discuss the errors.

36 Viscous Properties of Fluids

1.6 At 920 K the viscosity of methane (CH_4) is $2.6 \times 10^{-5} \text{ N s m}^{-2}$, and the viscosity of nitrogen is $3.8 \times 10^{-5} \text{ N s m}^{-2}$. Plot the viscosity of methane-nitrogen mixtures versus mole fraction methane at 920 K.

1.7 Estimate the viscosity of liquid beryllium at 1575 K. The following data are available: atomic weight, 9.01 g mol^{-1} ; melting point, 1550 K; density at 293 K, 1850 kg m^{-3} ; crystal structure, hcp; atomic radius, 0.114 nm.

1.8 Chromium melts at approximately 2148 K. Estimate its viscosity at 2273 K given the following data: atomic weight, 52 g mol^{-1} ; density, 7100 kg m^{-3} ; interatomic distance, 0.272 nm.

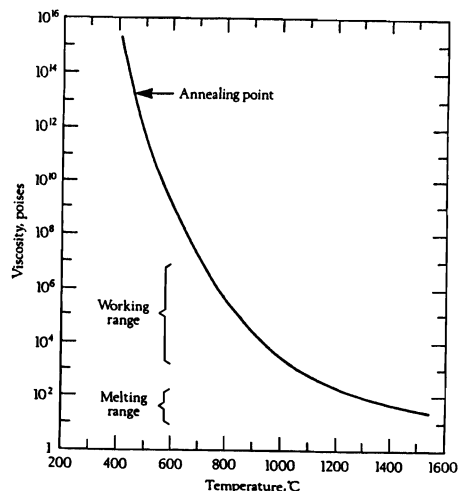
1.9 At 1273 K a melt of Cu-40% Zn has a viscosity of 5 cP and at 1223 K this same alloy has a viscosity of 6 cP. Using this information, estimate the viscosity of the alloy at 1373 K.

1.10 Many metal processing operations, such as steelmaking, employ a slag as a means by which impurities are removed from the processing operation. Thus, it becomes necessary to characterize certain properties of the slag, such as viscosity, at temperatures it will encounter in the processing operation. Using Bills' method, estimate the viscosity of a 50 wt. % SiO_2 , 30 wt. % CaO , 20 wt. % Al_2O_3 slag at 1773 K.

1.11 Assume that the viscosity of a glass varies with temperature according to Eq. (1.18). At 1700 K it has a viscosity of 20 N s m^{-2} ; at 1500 K it is 100 N s m^{-2} . What is the viscosity at 1450 K?

1.12 When oxides such as MgO and CaO are added to molten silica, the activation energy of viscosity is reduced from 135 kcal/mol for pure SiO_2 to approximately 39 kcal/mol for 0.5 mole fraction of SiO_2 . We can observe even more dramatic effects when oxides such as Li_2O and Na_2O are added to silica. For example, for 0.5 mol fraction SiO_2 , the activation energy is only 23 kcal/mol. Explain with the aid of any appropriate sketches, why this phenomenon occurs.

1.13 The glass transition temperature for the soda-lime-silicate glass shown to the right is approximately 720 K. Test the applicability of Eq. (1.18). Does it apply? Explain why or why not.



1.14 Equation (1.30) differs in form from Eq. (1.18). Based on Eq. (1.30) and Table 1.6, calculate the viscosity of 0.5 Al₂O₃-0.5 SiO₂ (mol fraction) in the temperature range of 2100 to 2500 K. Plot your results as $\ln \eta$ vs. T^{-1} . Does Eq. (1.18) adequately represent your results?

1.15 Estimate the viscosities of LiCl and LiBr at 1000 K. Which is greater? Can you explain your results on the basis of ionic bonding?

1.16 Estimate the percent change in viscosity of polymer melts on changing the shear strain rate from 10^4 s^{-1} to 10^1 s^{-1} .

1.17 Estimate the viscosity of poly(ϵ -caprolactam) at 526 K (see Table 1.8). Compare its viscosity to that of a branched form (octachain). On the basis of the structure of polymers, explain the effect of branching on the viscosity.

1.18 Refer to Example 1.6. Estimate the viscosities at the glass transition temperature (T_g) and 10 K above T_g . Comment on the sensitivity of the viscosity with temperature near the glass transition temperature.

2

LAMINAR FLOW AND THE MOMENTUM EQUATION

In discussing Newton's law of viscosity, we have described fluid motion as flowing parallel layers which, because of viscosity, establish a velocity gradient dependent upon the shear stress applied to the fluid. This velocity gradient has been regarded as a potential or a "reason" for momentum transport from layer to layer.

In this chapter, we shall first derive simple differential equations of momentum for special cases of flow, for example, flow of a falling film, flow between two parallel plates, and flow through tubes. To make it possible for the student to participate in developing complex formulas, these derivations make use of the concept of a momentum balance and the definition of viscosity. These classic examples of viscous flow patterns certainly apply to rather simplified and idealized conditions. You may be tempted, therefore, to disregard the importance of thoroughly understanding these examples; however, we should point out that despite the simplicity of the following calculations, you will gain an appreciation of the variables involved. Also, you will obtain a basic tool for analyzing engineering problems: the ability to arrive at pertinent differential equations.

2.1 MOMENTUM BALANCE*

A momentum balance is applied to a small control volume of fluid to develop a differential equation. The differential equations, when their solutions comply with the physical restrictions (boundary conditions), yield the algebraic relationships which can be used to determine the engineering characteristics of the system. The solutions give the velocity distributions from which other characteristics, including the shear stress at the fluid-solid interface, are developed. As we shall see in Chapter 3, the shear stress at the fluid-solid

*The general aspects of the developments in Sections 2.1-2.6 are similar to those found in Chapters 2-3 in R. B. Bird, W. E. Stewart, and E. N. Lightfoot, *Transport Phenomena*, Wiley, New York, 1960.

40 Laminar Flow and the Momentum Equation

interface is very important in analyzing the disposition of energy flowing through a system. For steady state flow, the momentum balance is

$$\left(\begin{array}{c} \text{rate of} \\ \text{momentum in} \end{array} \right) - \left(\begin{array}{c} \text{rate of} \\ \text{momentum out} \end{array} \right) + \left(\begin{array}{c} \text{sum of forces} \\ \text{acting on system} \end{array} \right) = 0. \quad (2.1)$$

Momentum in (or out) may enter a system by momentum transfer according to Newton's equation of viscosity (if the fluid is Newtonian; otherwise various equations for non-Newtonian fluids are used), or it may enter due to the overall fluid motion. The forces applied to the balance are pressure forces and/or gravity forces.

The momentum balance is actually a force balance because we are concerned with the *rate of momentum* that enters and leaves the unit volume. Units of momentum are MLT^{-1} ($M = \text{mass}$, $L = \text{length}$, $T = \text{time}$), whereas a rate of momentum is MLT^{-2} . Classical physics states clearly that forces ($F = ma$) are involved when we consider momentum rates. Thus, if the term momentum balance confuses the reader, he or she is reassured that a force balance is being applied.

2.2 FLOW OF A FALLING FILM

Consider the flow of a liquid at steady state along an inclined plane (Fig. 2.1). The liquid is at a constant temperature, and therefore its density and viscosity are constant. Furthermore, we consider only that portion of the plane where the entrance and exit of the liquid to the plane are sufficiently remote so as not to influence the velocity v_z . In this situation, v_z is not a function of z but obviously a function of x .^{*} Figure 2.1 also depicts the unit volume as a "shell" with a thickness Δx and length L ; the width of the shell extends a distance W , perpendicular to the page. The terms used in Eq. (2.1) are as follows:

Rate of momentum in across surface at x (moment transport due to viscosity)	$(LW)(\tau_{xz}) _x$
Rate of momentum out across surface at $x + \Delta x$ (due to viscosity)	$(LW)(\tau_{xz}) _{x + \Delta x}$
Rate of momentum in across surface at $z = 0$ (due to fluid motion)	$(W\Delta xv_z)(\rho v_z) _{z = 0}$
Rate of momentum out across surface at $z = L$ (due to fluid motion)	$(W\Delta xv_z)(\rho v_z) _{z = L}$
Gravity force acting on fluid	$(LW\Delta x)(\rho g \cos \beta)$

In this particular problem, the pressure forces are irrelevant because the pressure does not vary with z . Also note that all terms in the list, including the first two, are z -directed forces. Figure 2.1 shows that momentum in by viscous transport is x -directed, but if we think of

^{*}In the region where $v_z = f(x)$ and $v_z \neq f(z)$, we say that the flow is *fully developed*.

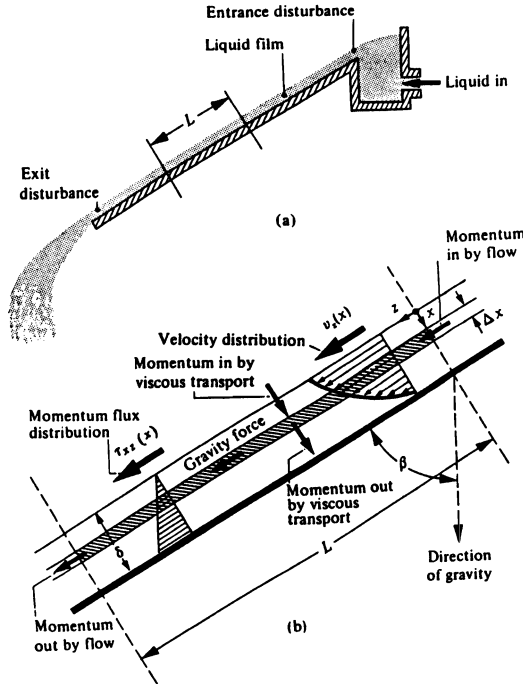


Fig. 2.1 Flow of a falling film.

interpreting τ_{xz} in an alternative way—namely, as a shear stress—we certainly realize that we are dealing with a z -directed force.

When all these terms are substituted into the momentum balance, we get

$$LW\tau_{xz}|_x - LW\tau_{xz}|_{x+\Delta x} + W\Delta x\rho v_z^2|_{z=0} - W\Delta x\rho v_z^2|_{z=L} + LW\Delta x\rho g \cos \beta = 0. \quad (2.2)$$

Because we are restricted to that part of the inclined plane which does not feel the effects of the exit and entrance, v_z is independent of z . Therefore, the third and fourth terms cancel one another out. Equation (2.2) is now divided by $LW\Delta x$ and, if Δx is allowed to be infinitely small, we obtain

$$\lim_{\Delta x \rightarrow 0} \frac{\tau_{xz}|_{x+\Delta x} - \tau_{xz}|_x}{\Delta x} = \rho g \cos \beta. \quad (2.3)$$

We have now recognized the definition of the first derivative of τ_{xz} with respect to x , and have thus developed the differential equation pertinent to our system:

$$\frac{d\tau_{xz}}{dx} = \rho g \cos \beta. \quad (2.4)$$

This equation is integrated to yield

$$\tau_{xz} = \rho g x \cos \beta + C_1. \quad (2.5)$$

42 Laminar Flow and the Momentum Equation

Equation (2.5) describes the momentum flux (or alternatively the shear-stress distribution), but contains an integration constant C_1 . This constant is evaluated by recognizing that the shear stress in the liquid is very nearly zero at a liquid-gas interface. In other words, the gas phase, in this instance, offers little resistance to liquid flow, which results in a realistic *boundary condition*:

$$\text{B.C.1} \quad \text{at } x = 0, \quad \tau_{xz} = 0. \quad (2.6)$$

Substitution of this boundary condition into Eq. (2.5) requires that $C_1 = 0$; hence the momentum flux is

$$\tau_{xz} = \rho g x \cos \beta. \quad (2.7)$$

If the fluid is Newtonian, then we know that the momentum flux is related to the velocity gradient according to

$$\tau_{xz} = -\eta \frac{dv_z}{dx}. \quad (2.8)$$

Substituting this expression for τ_{xz} in Eq. (2.7) gives the distribution of the velocity gradient:

$$\frac{dv_z}{dx} = -\frac{\rho g \cos \beta}{\eta} x. \quad (2.9)$$

Integrating Eq. (2.9), we have

$$v_z = -\left[\frac{\rho g \cos \beta}{2\eta}\right] x^2 + C_2. \quad (2.10)$$

Another integration constant has evolved which is evaluated by examining the other boundary condition, namely, that at the fluid-solid interface the fluid clings to the wall; that is,

$$\text{B.C.2} \quad \text{at } x = \delta, \quad v_z = 0. \quad (2.11)$$

Substituting this into Eq. (2.10), we determine the constant of integration; $C_2 = (\rho g \cos \beta / 2\eta)\delta^2$. Therefore the velocity distribution is

$$v_z = \frac{\rho g \delta^2 \cos \beta}{2\eta} \left[1 - \left(\frac{x}{\delta}\right)^2\right]. \quad (2.12)$$

and is parabolic. Once the velocity profile has been found, a number of quantities may be calculated.

i) The *maximum velocity*, V_z^{\max} , is that velocity at $x = 0$:

$$V_z^{\max} = \frac{\rho g \delta^2 \cos \beta}{2\eta}. \quad (2.13)$$

ii) The *average velocity*, \bar{v}_z , is simply

$$\bar{v}_z = \frac{1}{\delta} \int_0^\delta v_z dx = \frac{\rho g \delta \cos \beta}{2\eta} \int_0^\delta \left[1 - \left(\frac{x}{\delta}\right)^2\right] dx = \frac{\rho g \delta^2 \cos \beta}{3\eta}. \quad (2.14)$$

iii) The *volume flow rate*, Q , is given by the product of the average velocity and the cross-section of flow:

$$Q = \bar{v}_z(W\delta) = \frac{\rho g W \delta^3 \cos \beta}{3\eta}. \quad (2.15)$$

The foregoing analytical results are valid only when the film is falling in laminar flow (straight streamlines). This condition can easily be satisfied for the slow flow of viscous films, but experimentally, it has been found that as the film velocity increases, the film thickness increases (according to Eq. (2.14)) to a critical value, depending on the liquid's kinematic viscosity, where turbulence replaces laminar flow. Of course, when turbulent flow develops, Eqs. (2.12)-(2.15) are no longer valid.

Example 2.1 A viscous molten glass covers a molten metal, and together they flow slowly down an inclined plane that makes an angle β with the vertical. The thickness of the glass is δ_1 , and the combined thickness of both layers is δ_2 . Of course, each layer has its own viscosity. For a plane of length L , assume laminar flow that is fully developed and derive an equation for the velocity distribution in each layer.

Solution. We should recognize that Eq. (2.4) applies to both layers. In the glass (i.e., the top layer), $\tau_{xz} = 0$ at $x = 0$. Therefore, after integrating Eq. (2.4) the shear stress in the glass is

$$\tau_{xz} = \rho_g x g \cos \beta$$

or

$$\frac{dv_z}{dx} = - \frac{x g \cos \beta}{\nu_g}$$

where the subscript g is for glass. Another integration gives:

$$v_z = - \frac{x^2 g \cos \beta}{2\nu_g} + c_1, \quad \delta_1 \leq x \leq 0.$$

In the metal, we rewrite Eq. (2.4) as

$$\frac{d^2 v_z}{dx^2} = - \frac{g \cos \beta}{\nu_m}$$

and integrate twice. The result is

$$v_z = - \frac{x^2 g \cos \beta}{2\nu_m} - c_2 x + c_3, \quad \delta_1 \leq x \leq \delta_2$$

where the subscript m is for metal.

In order to evaluate the three constants, c_1 , c_2 and c_3 , we apply the following conditions:

- B.C. 1: $v_z = 0$ at $x = \delta_2$,
- B.C. 2: v_z (metal) = v_z (glass) at $x = \delta_1$,
- B.C. 3: τ_{xz} (metal) = τ_{xz} (glass) at $x = \delta_1$.

44 Laminar Flow and the Momentum Equation

From these three conditions (and lines and lines of algebra), the three constants can be determined so that the velocity distribution in both layers can be found. The results are

$$c_2 = \frac{(\rho_g - \rho_m) \delta_1 g \cos \beta}{\eta_m},$$

$$c_3 = \frac{\delta_2^2 g \cos \beta}{2\nu_m} + c_2 \delta_2,$$

and

$$c_1 = \left[\frac{\delta_2^2 - \delta_1^2}{\nu_m} + \frac{\delta_1^2}{\nu_g} \right] \frac{g \cos \beta}{2} + c_2(\delta_2 - \delta_1).$$

2.3 FULLY DEVELOPED FLOW BETWEEN PARALLEL PLATES

Consider the flow of fluid between parallel plates in Fig. 2.2. The velocity at the entrance is uniform and, as the flow progresses, velocity gradients must form because the fluid clings to the wall. At some distance downstream from the entrance, the velocity profile becomes independent of the distance from the entrance, and the flow is then fully developed. Let this region of fully developed flow start at $x = 0$ and consider the unit volume in Fig. 2.2 with a thickness Δy , width W , and length L .

Rate of momentum in
across surface at y
(momentum transport due to viscosity)

$$(LW)(\tau_{yx})|_y$$

Rate of momentum out
across surface at $y + \Delta y$
(due to viscosity)

$$(LW)(\tau_{yx})|_{y + \Delta y}$$

Rate of momentum in
across surface at $x = 0$
(due to fluid motion)

$$(W\Delta y v_x)(\rho v_x)|_{x=0}$$

Rate of momentum out
across surface at $x = L$
(due to fluid motion)

$$(W\Delta y v_x)(\rho v_x)|_{x=L}$$

Pressure force on liquid at $x = 0$

$$\Delta y W [P(x = 0)] = P_0 \Delta y W$$

Pressure force on liquid at $x = L$

$$-\Delta y W [P(x = L)] = -P_L \Delta y W$$

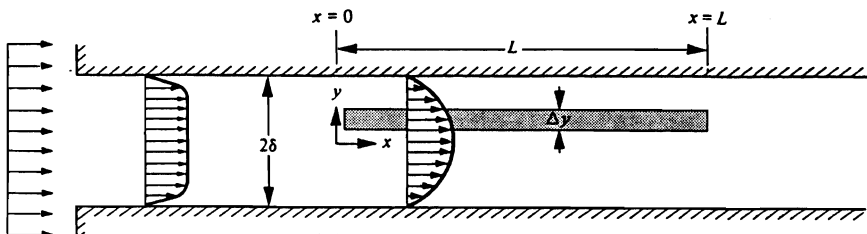


Fig. 2.2 Flow between parallel plates.

Again, the momentum in and out of the system due to the fluid motion are equal. We are left with

$$(LW)(\tau_{yx})|_y - (LW)(\tau_{yx})|_{y + \Delta y} + (P_0 - P_L)\Delta y W = 0. \quad (2.16)$$

Dividing through by $LW\Delta y$ and letting Δy approach zero, we develop the differential equation

$$\frac{d\tau_{yx}}{dy} = \frac{(P_0 - P_L)}{L}. \quad (2.17)$$

The boundary conditions are described at the centerline ($y = 0$) and at the solid wall ($y = \delta$) as follows:

$$\text{B.C. 1} \quad \text{at } y = 0, \quad \tau_{yx} = 0; \quad (2.18)$$

$$\text{B.C. 2} \quad \text{at } y = \delta, \quad v_x = 0.$$

It is left as an exercise for the reader to show that the shear stress distribution is given by

$$\tau_{yx} = \frac{(P_0 - P_L)}{L} y, \quad (2.19)$$

and the velocity distribution (for a Newtonian fluid) by

$$v_x = \frac{1}{2\eta} (\delta^2 - y^2) \frac{(P_0 - P_L)}{L}. \quad (2.20)$$

We determine other characteristics of the system by the method shown in Section 2.2. These are:

i) The maximum velocity

$$v_x^{\max} = \frac{1}{2\eta} \delta^2 \frac{(P_0 - P_L)}{L}. \quad (2.21)$$

ii) The average velocity

$$\bar{v}_x = \frac{1}{\delta} \int_0^\delta v_x dy = \frac{\delta^2}{3\eta} \frac{(P_0 - P_L)}{L}. \quad (2.22)$$

iii) The volume flow rate

$$Q = \frac{2}{3} \frac{W\delta^3}{\eta} \frac{(P_0 - P_L)}{L}. \quad (2.23)$$

On looking back through this example, we note that in this instance the fluid flows because of the pressure drop ($P_0 - P_L$). For horizontal flow, such a pressure drop would be necessary to make the fluid flow, in contrast to the flow down an inclined plane (Section 2.2) on which gravity exerts the necessary force for fluid motion.

2.4 FULLY DEVELOPED FLOW THROUGH A CIRCULAR TUBE

In this section we derive the momentum balance for steady flow through a long cylindrical tube for a Newtonian fluid and then for a non-Newtonian fluid, using an empirical equation that is often applied to polymeric melts.

2.4.1 Newtonian Fluids

Consider the fully developed flow of a fluid in a long tube of length L and radius R ; we specify fully developed flow so that end effects are negligible. Since we are dealing with a pipe, it is convenient to work with cylindrical coordinates. Therefore the shell in Fig. 2.3 is cylindrical, of thickness Δr and length L .

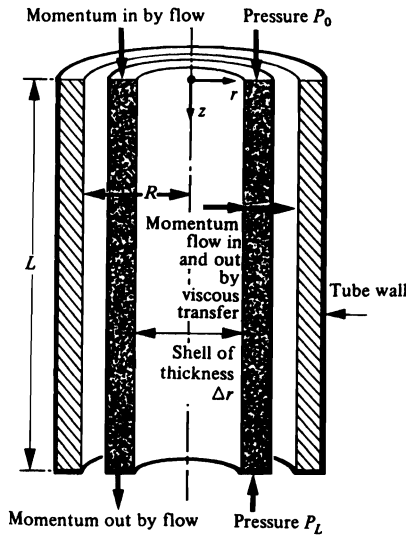


Fig. 2.3 Cylindrical shell chosen for momentum balance in tubes.

Rate of momentum in
across surface at r
(due to viscosity)

$$(2\pi r L \tau_{rz})|_r$$

Note that here we include the area factor $(2\pi r L)$ in parentheses. This is because the area as well as the shear stress is a function of r .

Rate of momentum out
across surface at $r + \Delta r$
(due to viscosity)

$$(2\pi r L \tau_{rz})|_{r + \Delta r}$$

Since we are considering fully developed flow, the momentum fluxes due to flow are equal; hence these terms are omitted.

Gravity force acting on the cylindrical shell

$$(2\pi r \Delta r L) \rho g$$

Pressure force acting on surface at $z = 0$ $(2\pi r\Delta r)P_0$

Pressure force acting on surface at $z = L$ $-(2\pi r\Delta r)P_L$

We now add up the contributions to the momentum balance:

$$(2\pi rL\tau_{rz})|_r - (2\pi rL\tau_{rz})|_{r+\Delta r} + 2\pi r\Delta rL\rho g + 2\pi r\Delta r(P_0 - P_L) = 0. \quad (2.24)$$

Note that all terms contain the factor r ; however, since r is a variable, it should not be used as a common divisor. By dividing through by $2\pi L\Delta r$ and taking the limit as Δr goes to zero, we develop the differential equation

$$\frac{d}{dr} (r\tau_{rz}) = \left[\frac{P_0 - P_L}{L} + \rho g \right] r. \quad (2.25)$$

Integration yields

$$\tau_{rz} = \left[\frac{P_0 - P_L}{L} + \rho g \right] \frac{r}{2} + \frac{C_1}{r}. \quad (2.26)$$

At $r = 0$, the velocity gradient (hence, the shear stress) equals zero; this can be realized because of the symmetry of flow.

Thus for this case,

$$\text{B.C. 1} \quad \text{at } r = 0, \quad \tau_{rz} = 0. \quad (2.27)$$

Therefore, $C_1 = 0$, and the momentum flux is given by

$$\tau_{rz} = \left[\frac{P_0 - P_L}{L} + \rho g \right] \frac{r}{2}. \quad (2.28)$$

Substituting Newton's law of viscosity

$$\tau_{rz} = -\eta \frac{dv_z}{dr}, \quad (2.29)$$

and noting

$$\text{B.C. 2} \quad \text{at } r = R, \quad v_z = 0, \quad (2.30)$$

we obtain the solution for the velocity distribution:

$$v_z = \left[\frac{P_0 - P_L}{L} + \rho g \right] \left[\frac{R^2}{4\eta} \right] \left[1 - \left[\frac{r}{R} \right]^2 \right]. \quad (2.31)$$

As before:

i) The maximum velocity is at $r = 0$, and is given by

$$V_z^{\max} = \left[\frac{P_0 - P_L}{L} + \rho g \right] \frac{R^2}{4\eta}. \quad (2.32)$$

48 Laminar Flow and the Momentum Equation

ii) The average velocity is

$$\bar{v}_z = \frac{1}{\pi R^2} \int_0^{2\pi} \int_0^R v_z r \, dr \, d\theta = \left[\frac{P_0 - P_L}{L} + \rho g \right] \frac{R^2}{8\eta}. \quad (2.33)$$

iii) The volume flow rate is

$$Q = \left[\frac{P_0 - P_L}{L} + \rho g \right] \left[\frac{\pi R^4}{8\eta} \right]. \quad (2.34)$$

This latter result, which is commonly referred to as the *Hagen-Poiseuille law*, is valid for laminar steady-state flow of incompressible fluids in tubes having sufficient length to make end effects negligible. An entrance length given by $L_e = 0.035 DRe$ is required before we can establish fully developed parabolic velocity distribution.

Example 2.2 Water at 290 K flows through a horizontal tube of diameter 1.6 mm with a pressure drop of 900 N m⁻³. Find the mass flow rate through the tube.

Solution. In this situation, the force of gravity does not act on the fluid in the direction of flow, so according to Eq. (2.34) the volume flow rate is

$$Q = \left[\frac{P_0 - P_L}{L} \right] \frac{\pi R^4}{8\eta}.$$

The viscosity and density of water at 290 K are 1.080×10^{-3} N s m⁻² and 10^3 kg m⁻³, respectively. Substituting in values, we obtain:

$$Q = \frac{900 \text{ N}}{\text{m}^3} \left| \frac{\pi}{8} \right| \frac{(0.8 \times 10^{-3})^4 \text{ m}^4}{1.080 \times 10^{-3} \text{ N s}} = 1.34 \times 10^{-7} \text{ m}^3 \text{ s}^{-1}$$

Thus we see that the mass flow rate is

$$\rho Q = (10^3)(1.34 \times 10^{-7}) = 1.34 \times 10^{-4} \text{ kg s}^{-1}$$

We should then check if the flow is laminar, by evaluating the Reynolds number. As mentioned in Chapter 1, the criterion is $Re < 2100$:

$$Re = \frac{D\bar{V}}{\nu} = \frac{D\bar{V}\rho}{\eta}.$$

Also

$$\rho\bar{V} = \frac{\rho Q}{\pi D^2/4}.$$

so that the Reynolds number may be written in the alternative form

$$Re = \frac{D\rho Q}{(\pi D^2/4)\eta} = \frac{4\rho Q}{\pi D\eta}$$

Therefore,

$$Re = \frac{4}{\pi} \left| \frac{1.34 \times 10^{-4} \text{ kg}}{\text{s}} \right| \left| \frac{1.6 \times 10^{-3} \text{ m}}{1.080 \times 10^{-3} \text{ N s}} \right| \left| \frac{\text{m}^2}{1 \text{ kg m}} \right| \left| \frac{1 \text{ N s}^2}{1 \text{ kg m}} \right|$$

$$= 77.6$$

Because $Re < 2100$, the flow is laminar.

2.4.2 Power law non-Newtonian fluids

Now we consider the isothermal flow of a non-Newtonian fluid through the circular tube of Fig. 2.3. The momentum balance is precisely the same as in Section 2.4.1 up to Eq. (2.28). We assume that the relationship between the shear stress and the shear rate is given by a power law, Eq. (1.32), as is often used for polymeric melts. Then

$$\tau_{rz} = -\eta \frac{\partial v_z}{\partial r} = -\eta_0 \left[\frac{\partial v_z}{\partial r} \right]^n \tag{2.35}$$

and by combining Eqs. (2.28) and (2.35), we obtain

$$\left[\frac{\partial v_z}{\partial r} \right] = - \left[\frac{1}{2\eta_0} \left[\frac{P_0 - P_L}{L} + \rho g \right] \right]^{1/n} r^{1/n} \tag{2.36}$$

Integrating with $v_z = 0$ at $r = R$, the velocity distribution is obtained:

$$v_z = \left[\frac{1}{2\eta_0} \left[\frac{P_0 - P_L}{L} + \rho g \right] \right]^{1/n} \left[\frac{n}{n+1} \right] \left[R^{(n+1)/n} - r^{(n+1)/n} \right] \tag{2.37}$$

The maximum velocity is at $r = 0$ and is given by

$$V_z^{\max} = \left[\frac{1}{2\eta_0} \left[\frac{P_0 - P_L}{L} + \rho g \right] \right]^{1/n} \left[\frac{n}{n+1} \right] R^{(n+1)/n} \tag{2.38}$$

so that Eq. (2.37) can be written in a simpler form:

$$v_z = V_z^{\max} \left[1 - \left(\frac{r}{R} \right)^{(n+1)/n} \right] \tag{2.39}$$

50 Laminar Flow and the Momentum Equation

The volume flow rate is

$$Q = \int_0^R 2\pi r v_z dr = 2\pi V_z^{\max} \int_0^R r \left[1 - \left(\frac{r}{R} \right)^{(n+1)/n} \right] dr$$

or

$$Q = \left[\frac{n+1}{3n+1} \right] \pi R^2 V_z^{\max}. \quad (2.40)$$

The average velocity is simply

$$\bar{v}_z = \frac{Q}{\pi R^2}$$

or

$$\bar{v}_z = \left[\frac{n+1}{3n+1} \right] V_z^{\max}. \quad (2.41)$$

2.5 EQUATION OF CONTINUITY AND THE MOMENTUM EQUATION

In the previous sections of this chapter, we determined velocity distributions for some simple flow systems by applying differential momentum balances. The balances for these systems served to illustrate the application of the momentum equation. In general, when dealing with isothermal fluid systems which do not involve changes in compositions, we can solve problems by starting with general expressions. This method is better than developing formulations peculiar to the specific problem at hand. The general momentum equation is also called the *equation of motion* or the *Navier-Stokes' equation*; in addition the *equation of continuity* is frequently used in conjunction with the momentum equation.

The continuity equation is developed simply by applying the law of conservation of mass to a small volume element within a flowing fluid. The principle of conservation of mass is quite simple to apply and we assume that the reader has used it in developing material balances. We develop the momentum equation by applying the momentum balance which, in its general form, is an extension of Eq. (2.1). With the aid of these two equations, we can mathematically describe the problems encountered in the previous section, as well as more complicated problems. However, as we shall see, these expressions are rather cumbersome, and exact solutions can be found only in very limited cases. Hence these equations are used primarily as starting points for solving problems. The equations of continuity and motion are simplified to fit the problem at hand. Although theoretically these equations are valid for both laminar and turbulent flows, in practice they are applied only to laminar flow.

2.5.1 Equation of continuity

Consider the stationary volume element within a fluid moving with a velocity having the components v_x , v_y , and v_z , as shown in Fig. 2.4. We begin with the basic representation of the conservation of mass:

$$\left(\begin{array}{c} \text{rate of mass} \\ \text{accumulation} \end{array} \right) = \left(\begin{array}{c} \text{rate of} \\ \text{mass in} \end{array} \right) - \left(\begin{array}{c} \text{rate of} \\ \text{mass out} \end{array} \right). \quad (2.42)$$

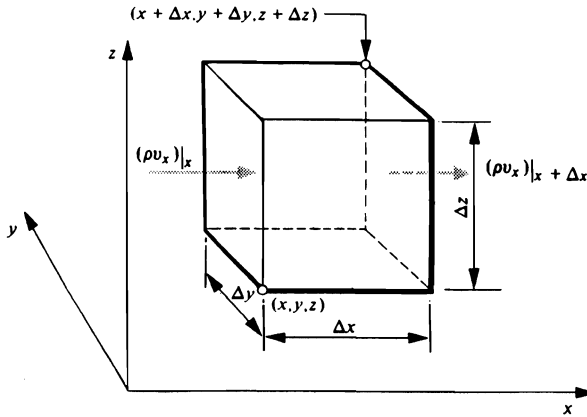


Fig. 2.4 Volume element fixed in space with fluid flowing through it.

First, look at the faces perpendicular to the x -axis. The volume flow rate of fluid in across the face at x is simply the product of the velocity (x -component) and the cross-sectional area, yielding $\Delta y \Delta z v_x|_x$. The rate of mass in through the face at x is then $\Delta y \Delta z (\rho v_x)|_x$. Similarly, the rate of mass out through the face at $x + \Delta x$ is $\Delta y \Delta z (\rho v_x)|_{x + \Delta x}$. We may write analogous expressions for the other two pairs of faces, and then enter all the terms that account for the fluid entering and leaving the system into the mass balance, and leave the accumulation term to be developed.

The *accumulation* is the rate of change of mass within the control volume

$$\Delta x \Delta y \Delta z \frac{\partial \rho}{\partial t}$$

The mass balance thus becomes

$$\begin{aligned} \Delta x \Delta y \Delta z \frac{\partial \rho}{\partial t} = & \Delta y \Delta z [\rho v_x|_x - \rho v_x|_{x + \Delta x}] + \Delta x \Delta z [\rho v_y|_y - \rho v_y|_{y + \Delta y}] \\ & + \Delta x \Delta y [\rho v_z|_z - \rho v_z|_{z + \Delta z}]. \end{aligned} \quad (2.43)$$

Then, dividing through by $\Delta x \Delta y \Delta z$, and taking the limit as these dimensions approach zero, we get the *equation of continuity*:

$$\frac{\partial \rho}{\partial t} = - \left[\frac{\partial}{\partial x} \rho v_x + \frac{\partial}{\partial y} \rho v_y + \frac{\partial}{\partial z} \rho v_z \right]. \quad (2.44)$$

A very important form of Eq. (2.44) is the form that applies to a fluid of constant density. For this case, which frequently occurs in engineering problems, the continuity equation reduces to

$$\frac{\partial v_x}{\partial x} + \frac{\partial v_y}{\partial y} + \frac{\partial v_z}{\partial z} = 0$$

or in vector notation

$$\nabla \cdot \mathbf{v} = 0. \quad (2.45)$$

2.5.2 The momentum equation

When Eq. (2.1) is extended to include unsteady-state systems, the momentum balance takes the form:

$$\left[\begin{array}{c} \text{rate of} \\ \text{momentum} \\ \text{accumulation} \end{array} \right] = \left[\begin{array}{c} \text{rate of} \\ \text{momentum} \\ \text{in} \end{array} \right] - \left[\begin{array}{c} \text{rate of} \\ \text{momentum} \\ \text{out} \end{array} \right] + \left[\begin{array}{c} \text{sum of} \\ \text{forces acting} \\ \text{on system} \end{array} \right]. \quad (2.46)$$

For simplicity, we begin by considering only the x -component of each term in Eq. (2.46); the y - and z -components may be handled in the same manner.

Figure 2.5(a) shows the x -components of τ as if they were made up of viscous momentum fluxes rather than shear stresses. On the other hand Fig. 2.5(b) shows the x -component of τ as stresses. Note the appearance of τ_{xx} , which by the scheme of subscripts represents the transport of x -momentum in the x -direction. Alternatively, we view τ_{xx} as the x -directed normal stress on the x -face, in contrast to τ_{yx} which we view as the x -directed shear stress on the y -face.

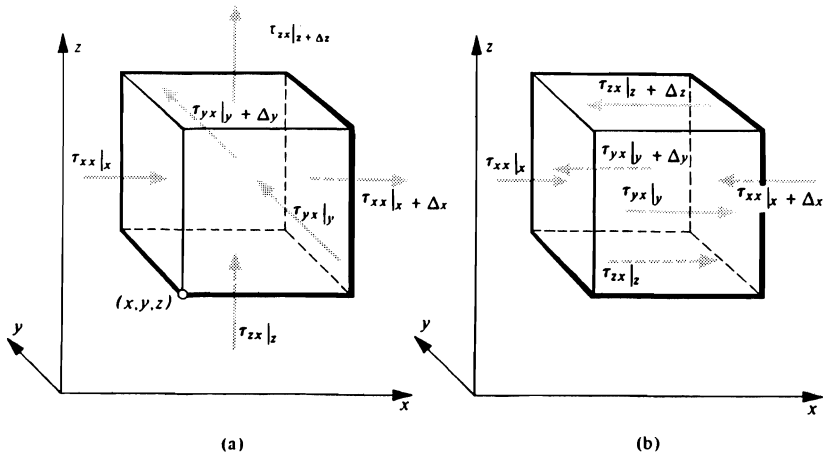


Fig. 2.5 Momentum transport (x -component) due to viscosity into the volume element. (a) Directions of viscous momentum transport. (b) Directions of stresses.

Let us now develop the terms that enter into Eq. (2.46). First, the net rate at which the x -component of the convective momentum enters the unit volume, is

$$\begin{aligned} \Delta y \Delta z (\rho v_x v_x|_x - \rho v_x v_x|_{x + \Delta x}) + \Delta x \Delta z (\rho v_y v_x|_y - \rho v_y v_x|_{y + \Delta y}) \\ + \Delta x \Delta y (\rho v_z v_x|_z - \rho v_z v_x|_{z + \Delta z}). \end{aligned} \quad (2.47)$$

Similarly, the net rate of *viscous* momentum flow into the unit volume across the six faces is

$$\begin{aligned} \Delta y \Delta z (\tau_{xx}|_x - \tau_{xx}|_{x+\Delta x}) + \Delta x \Delta z (\tau_{yx}|_y - \tau_{yx}|_{y+\Delta y}) \\ + \Delta x \Delta y (\tau_{zx}|_z - \tau_{zx}|_{z+\Delta z}). \end{aligned} \quad (2.48)$$

The reader who has not come in contact with this development before might find a brief explanation of the meaning of $\rho v_x v_x$ and $\rho v_y v_x$ useful. Remember that we are applying the law of conservation of momentum to the x -component of momentum. Thus v_x represents the x -velocity, and the rate at which mass enters the system through the y -face is given by $\Delta x \Delta z \rho v_y|_y$. Hence the rate at which x -momentum enters through the y -face is simply the product of mass-flow rate and velocity:

$$\Delta x \Delta z \rho v_y v_x|_y.$$

In most cases, the forces acting on the system are those arising from the pressure P and the gravitational force per unit mass g . In the x -direction, these forces are

$$\Delta y \Delta z (P|_x - P|_{x+\Delta x}), \quad (2.49)$$

and

$$\rho g_x \Delta x \Delta y \Delta z, \quad (2.50)$$

respectively. Here g_x is the x -component of g . Finally, the rate of accumulation of x -momentum within the element is

$$\Delta x \Delta y \Delta z \left[\frac{\partial}{\partial t} \rho v_x \right]. \quad (2.51)$$

Entering Eqs. (2.47)-(2.51) into the momentum balance, dividing through by $\Delta x \Delta y \Delta z$, and taking the limit as all three approach zero, we obtain the x -component of the momentum equation:

$$\begin{aligned} \frac{\partial}{\partial t} \rho v_x = - \left[\frac{\partial}{\partial x} \rho v_x v_x + \frac{\partial}{\partial y} \rho v_y v_x + \frac{\partial}{\partial z} \rho v_z v_x \right] \\ - \left[\frac{\partial}{\partial x} \tau_{xx} + \frac{\partial}{\partial y} \tau_{yx} + \frac{\partial}{\partial z} \tau_{zx} \right] - \frac{\partial P}{\partial x} + \rho g_x. \end{aligned} \quad (2.52)$$

The y - and z -components, which we obtain in a similar manner, are

$$\begin{aligned} \frac{\partial}{\partial t} \rho v_y = - \left[\frac{\partial}{\partial x} \rho v_x v_y + \frac{\partial}{\partial y} \rho v_y v_y + \frac{\partial}{\partial z} \rho v_z v_y \right] \\ - \left[\frac{\partial}{\partial x} \tau_{xy} + \frac{\partial}{\partial y} \tau_{yy} + \frac{\partial}{\partial z} \tau_{zy} \right] - \frac{\partial P}{\partial y} + \rho g_y, \end{aligned} \quad (2.53)$$

54 Laminar Flow and the Momentum Equation

and

$$\begin{aligned} \frac{\partial}{\partial t} \rho v_z = & - \left[\frac{\partial}{\partial x} \rho v_x v_z + \frac{\partial}{\partial y} \rho v_y v_z + \frac{\partial}{\partial z} \rho v_z v_z \right] \\ & - \left[\frac{\partial}{\partial x} \tau_{xz} + \frac{\partial}{\partial y} \tau_{yz} + \frac{\partial}{\partial z} \tau_{zz} \right] - \frac{\partial P}{\partial z} + \rho g_z. \end{aligned} \quad (2.54)$$

To describe the general case, all three Equations (2.52), (2.53), and (2.54) are needed. Vector notation can reduce these to one equation which is just as meaningful as all three. The quantities ρv_x , ρv_y , and ρv_z are the components of the mass velocity $\rho \mathbf{v}$; similarly g_x , g_y , and g_z are the components of \mathbf{g} . Vectorial representation of a velocity and an acceleration is familiar to most readers. However, the terms $\partial P/\partial x$, $\partial P/\partial y$, and $\partial P/\partial z$ all represent pressure *gradients*. By itself, pressure is a scalar quantity, but the gradient of pressure is a vector denoted, in general, by ∇P (sometimes written $\text{grad } P$). Therefore

$$\nabla P = \frac{\partial}{\partial x} P + \frac{\partial}{\partial y} P + \frac{\partial}{\partial z} P,$$

and ∇ can be thought to be an operator, such that

$$\nabla = \frac{\partial}{\partial x} + \frac{\partial}{\partial y} + \frac{\partial}{\partial z}.$$

The terms $\rho v_x v_x$, $\rho v_x v_y$, $\rho v_x v_z$, $\rho v_y v_x$, etc., are the nine components of the convective momentum flux $\rho \mathbf{v} \mathbf{v}$, which is the *dyadic product* of $\rho \mathbf{v}$ and \mathbf{v} . Also, τ_{xx} , τ_{xy} , etc., are the nine components of τ .

The vector equation representing Eqs. (2.52)-(2.54) is finally written:

$$\frac{\partial}{\partial t} \rho \mathbf{v} = -[\nabla \cdot \rho \mathbf{v} \mathbf{v}] - \nabla P - [\nabla \cdot \tau] + \rho \mathbf{g}. \quad (2.55)$$

To interpret the mathematical nature of $\nabla \cdot \rho \mathbf{v} \mathbf{v}$ and $\nabla \cdot \tau$ in physical terms is difficult. However, for sufficient understanding of this text it is enough if the reader accepts them as mathematical shorthands of the appropriate terms in Eqs. (2.52)-(2.54).

So far we have developed a general expression, namely, Eq. (2.55) for the law of conservation of momentum. However, in order to use this equation for the determination of velocity distributions, it is necessary to insert expressions for the various stresses in terms of velocity gradients and fluid properties. The following equations are presented without proof because the arguments involved are quite lengthy. For *Newtonian fluids*, the nine components of τ are written as follows.¹

$$\begin{cases} \tau_{xx} = -2\eta \frac{\partial v_x}{\partial x} + \frac{2}{3} \eta(\nabla \cdot \mathbf{v}) & (2.56) \\ \tau_{yy} = -2\eta \frac{\partial v_y}{\partial y} + \frac{2}{3} \eta(\nabla \cdot \mathbf{v}) & (2.57) \\ \tau_{zz} = -2\eta \frac{\partial v_z}{\partial z} + \frac{2}{3} \eta(\nabla \cdot \mathbf{v}) & (2.58) \end{cases}$$

¹V. L. Streeter, *Fluid Dynamics*, McGraw-Hill, New York, 1948, Chapter 10.

$$\text{Shear stresses} \left\{ \begin{array}{l} \tau_{xy} = \tau_{yx} = -\eta \left[\frac{\partial v_x}{\partial y} + \frac{\partial v_y}{\partial x} \right] \\ \tau_{yz} = \tau_{zy} = -\eta \left[\frac{\partial v_y}{\partial z} + \frac{\partial v_z}{\partial y} \right] \\ \tau_{zx} = \tau_{xz} = -\eta \left[\frac{\partial v_z}{\partial x} + \frac{\partial v_x}{\partial z} \right] \end{array} \right. \quad \begin{array}{l} (2.59) \\ (2.60) \\ (2.61) \end{array}$$

These equations constitute a more general statement of Newton’s law of viscosity than that given in Eq. (1.2), and apply to complex flow situations. When the fluid flows between two parallel plates in the x -direction so that v_x is a function of y alone, where the y -direction is perpendicular to the plates’ surfaces (Fig. 1.4), then Eqs.(2.56)-(2.61) yield

$$\tau_{xx} = \tau_{yy} = \tau_{zz} = \tau_{yz} = \tau_{zx} = 0 \quad \text{and} \quad \tau_{yx} = -\eta \left[\frac{\partial v_x}{\partial y} \right],$$

which is the same as the simple relationship previously used to describe Newton’s law of viscosity. Also in many other problems of physical significance in which v_x is recognized as a function of both y and x , we find that $\partial v_x/\partial y \gg \partial v_x/\partial x$, and the simple rate Eq. (1.2) can be used for τ_{yx} as an example with a high degree of accuracy rather than Eq. (2.59).

2.5.3 Navier-Stokes’ equation, constant ρ and η

The continuity equation for constant density is given by Eq. (2.45) or in vector notation,

$$\nabla \cdot \mathbf{v} = 0. \quad (2.62)$$

Regarding the momentum equation, we can write Eqs. (2.52)-(2.54) with constant ρ and η .*

$$\rho \left[\frac{\partial v_x}{\partial t} + v_x \frac{\partial v_x}{\partial x} + v_y \frac{\partial v_x}{\partial y} + v_z \frac{\partial v_x}{\partial z} \right] = -\frac{\partial P}{\partial x} + \eta \left[\frac{\partial^2 v_x}{\partial x^2} + \frac{\partial^2 v_x}{\partial y^2} + \frac{\partial^2 v_x}{\partial z^2} \right] + \rho g_x, \quad (2.63)$$

$$\rho \left[\frac{\partial v_y}{\partial t} + v_x \frac{\partial v_y}{\partial x} + v_y \frac{\partial v_y}{\partial y} + v_z \frac{\partial v_y}{\partial z} \right] = -\frac{\partial P}{\partial y} + \eta \left[\frac{\partial^2 v_y}{\partial x^2} + \frac{\partial^2 v_y}{\partial y^2} + \frac{\partial^2 v_y}{\partial z^2} \right] + \rho g_y, \quad (2.64)$$

$$\rho \left[\frac{\partial v_z}{\partial t} + v_x \frac{\partial v_z}{\partial x} + v_y \frac{\partial v_z}{\partial y} + v_z \frac{\partial v_z}{\partial z} \right] = -\frac{\partial P}{\partial z} + \eta \left[\frac{\partial^2 v_z}{\partial x^2} + \frac{\partial^2 v_z}{\partial y^2} + \frac{\partial^2 v_z}{\partial z^2} \right] + \rho g_z. \quad (2.65)$$

*This development is the subject of Problem 2.11.

56 Laminar Flow and the Momentum Equation

The bracketed terms on the left side of these equations merit attention. Consider a control volume of fluid moving in space with no mass flow across its surface. The change in the x -component of its velocity with time and position is given by

$$\Delta v_x = \frac{\partial v_x}{\partial t} \Delta t + \frac{\partial v_x}{\partial x} \Delta x + \frac{\partial v_x}{\partial y} \Delta y + \frac{\partial v_x}{\partial z} \Delta z, \quad (2.66)$$

and since the x -component of acceleration is defined as

$$a_x = \lim_{\Delta t \rightarrow 0} \frac{\Delta v_x}{\Delta t} = \lim_{\Delta t \rightarrow 0} \left\{ \frac{\partial v_x}{\partial t} \frac{\Delta t}{\Delta t} + \frac{\partial v_x}{\partial x} \frac{\Delta x}{\Delta t} + \frac{\partial v_x}{\partial y} \frac{\Delta y}{\Delta t} + \frac{\partial v_x}{\partial z} \frac{\Delta z}{\Delta t} \right\}, \quad (2.67)$$

then we obtain

$$a_x = \frac{\partial v_x}{\partial t} + v_x \frac{\partial v_x}{\partial x} + v_y \frac{\partial v_x}{\partial y} + v_z \frac{\partial v_x}{\partial z} = \frac{Dv_x}{Dt}. \quad (2.68)$$

This is the acceleration one would feel if riding with the control volume of fluid. We also refer to this time derivative of velocity, Dv_x/Dt , as the *substantial derivative*. Analogous expressions exist for the y - and z -directions. In general, one notation can represent all three substantial derivatives, so that Eqs. (2.63)-(2.65) become

$$\rho \frac{Dv}{Dt} = -\nabla P + \eta \nabla^2 v + \rho g. \quad (2.69)$$

Equation (2.69), or Eqs. (2.63)-(2.65) which taken together represent the expansion of Eq. (2.69), is often referred to as the *Navier-Stokes' equation*. In the form of Eq. (2.69), we can recognize it as a statement of Newton's law in the form *mass* (ρ) \times *acceleration* (Dv/Dt) equals the *sum of forces*, namely, the pressure force ($-\nabla P$), the viscous force ($\eta \nabla^2 v$), and the gravity or body force ρg .

2.6 THE MOMENTUM EQUATION IN RECTANGULAR AND CURVILINEAR COORDINATES

In many instances rectangular coordinates are not useful for analyzing problems. For example, in the Hagen-Poiseuille problem discussed in Section 2.4, we described the axial velocity v_z as a function of only a single variable r by employing cylindrical coordinates. If rectangular coordinates had been used instead, v_z would have been a very complicated function of x and y . Similarly, it would have been difficult to describe and apply the boundary condition at the tube wall.

The equations of continuity and motion in Section 2.5 were given in rectangular coordinates and are repeated here, along with spherical or cylindrical coordinates in Tables 2.1-2.7.

Table 2.1 The continuity equation in different coordinates systems

Rectangular coordinates (x, y, z) :

$$\frac{\partial \rho}{\partial t} + \frac{\partial}{\partial x}(\rho v_x) + \frac{\partial}{\partial y}(\rho v_y) + \frac{\partial}{\partial z}(\rho v_z) = 0 \quad (\text{A})$$

Cylindrical coordinates (r, θ, z) :

$$\frac{\partial \rho}{\partial t} + \frac{1}{r} \frac{\partial}{\partial r}(\rho r v_r) + \frac{1}{r} \frac{\partial}{\partial \theta}(\rho v_\theta) + \frac{\partial}{\partial z}(\rho v_z) = 0 \quad (\text{B})$$

Spherical coordinates (r, θ, ϕ) :

$$\frac{\partial \rho}{\partial t} + \frac{1}{r^2} \frac{\partial}{\partial r}(\rho r^2 v_r) + \frac{1}{r \sin \theta} \frac{\partial}{\partial \theta}(\rho v_\theta \sin \theta) + \frac{1}{r \sin \theta} \frac{\partial}{\partial \phi}(\rho v_\phi) = 0 \quad (\text{C})$$

*Tables 2.1-2.7 are from R. B. Bird, W. E. Stewart, and E. N. Lightfoot, *Transport Phenomena*, Wiley, New York, 1960, pages 83-91. Reprinted by permission.

Table 2.2 The momentum equation in rectangular coordinates (x, y, z)In terms of τ :

$$\begin{aligned} \text{x-component} \quad \rho \left(\frac{\partial v_x}{\partial t} + v_x \frac{\partial v_x}{\partial x} + v_y \frac{\partial v_x}{\partial y} + v_z \frac{\partial v_x}{\partial z} \right) &= -\frac{\partial P}{\partial x} \\ &\quad - \left(\frac{\partial \tau_{xx}}{\partial x} + \frac{\partial \tau_{yx}}{\partial y} + \frac{\partial \tau_{zx}}{\partial z} \right) + \rho g_x \quad (\text{A}) \end{aligned}$$

$$\begin{aligned} \text{y-component} \quad \rho \left(\frac{\partial v_y}{\partial t} + v_x \frac{\partial v_y}{\partial x} + v_y \frac{\partial v_y}{\partial y} + v_z \frac{\partial v_y}{\partial z} \right) &= -\frac{\partial P}{\partial y} \\ &\quad - \left(\frac{\partial \tau_{xy}}{\partial x} + \frac{\partial \tau_{yy}}{\partial y} + \frac{\partial \tau_{zy}}{\partial z} \right) + \rho g_y \quad (\text{B}) \end{aligned}$$

$$\begin{aligned} \text{z-component} \quad \rho \left(\frac{\partial v_z}{\partial t} + v_x \frac{\partial v_z}{\partial x} + v_y \frac{\partial v_z}{\partial y} + v_z \frac{\partial v_z}{\partial z} \right) &= -\frac{\partial P}{\partial z} \\ &\quad - \left(\frac{\partial \tau_{xz}}{\partial x} + \frac{\partial \tau_{yz}}{\partial y} + \frac{\partial \tau_{zz}}{\partial z} \right) + \rho g_z \quad (\text{C}) \end{aligned}$$

In terms of velocity gradients for a Newtonian fluid with constant ρ and η :

$$\begin{aligned} \text{x-component} \quad \rho \left(\frac{\partial v_x}{\partial t} + v_x \frac{\partial v_x}{\partial x} + v_y \frac{\partial v_x}{\partial y} + v_z \frac{\partial v_x}{\partial z} \right) &= -\frac{\partial P}{\partial x} \\ &\quad + \eta \left(\frac{\partial^2 v_x}{\partial x^2} + \frac{\partial^2 v_x}{\partial y^2} + \frac{\partial^2 v_x}{\partial z^2} \right) + \rho g_x \quad (\text{D}) \end{aligned}$$

$$\begin{aligned} \text{y-component} \quad \rho \left(\frac{\partial v_y}{\partial t} + v_x \frac{\partial v_y}{\partial x} + v_y \frac{\partial v_y}{\partial y} + v_z \frac{\partial v_y}{\partial z} \right) &= -\frac{\partial P}{\partial y} \\ &\quad + \eta \left(\frac{\partial^2 v_y}{\partial x^2} + \frac{\partial^2 v_y}{\partial y^2} + \frac{\partial^2 v_y}{\partial z^2} \right) + \rho g_y \quad (\text{E}) \end{aligned}$$

$$\begin{aligned} \text{z-component} \quad \rho \left(\frac{\partial v_z}{\partial t} + v_x \frac{\partial v_z}{\partial x} + v_y \frac{\partial v_z}{\partial y} + v_z \frac{\partial v_z}{\partial z} \right) &= -\frac{\partial P}{\partial z} \\ &\quad + \eta \left(\frac{\partial^2 v_z}{\partial x^2} + \frac{\partial^2 v_z}{\partial y^2} + \frac{\partial^2 v_z}{\partial z^2} \right) + \rho g_z \quad (\text{F}) \end{aligned}$$

Table 2.3 The momentum equation in cylindrical coordinates (r, θ, z)

 In terms of τ :

$$\begin{aligned}
 \text{r-component*} \quad \rho \left(\frac{\partial v_r}{\partial t} + v_r \frac{\partial v_r}{\partial r} + \frac{v_\theta}{r} \frac{\partial v_r}{\partial \theta} - \frac{v_\theta^2}{r} + v_z \frac{\partial v_r}{\partial z} \right) &= -\frac{\partial P}{\partial r} \\
 &- \left(\frac{1}{r} \frac{\partial}{\partial r} (r\tau_{rr}) + \frac{1}{r} \frac{\partial \tau_{r\theta}}{\partial \theta} - \frac{\tau_{\theta\theta}}{r} + \frac{\partial \tau_{rz}}{\partial z} \right) + \rho g_r \quad (\text{A})
 \end{aligned}$$

$$\begin{aligned}
 \text{\theta-component} \quad \rho \left(\frac{\partial v_\theta}{\partial t} + v_r \frac{\partial v_\theta}{\partial r} + \frac{v_\theta}{r} \frac{\partial v_\theta}{\partial \theta} + \frac{v_r v_\theta}{r} + v_z \frac{\partial v_\theta}{\partial z} \right) &= -\frac{1}{r} \frac{\partial P}{\partial \theta} \\
 &- \left(\frac{1}{r^2} \frac{\partial}{\partial r} (r^2 \tau_{r\theta}) + \frac{1}{r} \frac{\partial \tau_{\theta\theta}}{\partial \theta} + \frac{\partial \tau_{\theta z}}{\partial z} \right) + \rho g_\theta \quad (\text{B})
 \end{aligned}$$

$$\begin{aligned}
 \text{z-component} \quad \rho \left(\frac{\partial v_z}{\partial t} + v_r \frac{\partial v_z}{\partial r} + \frac{v_\theta}{r} \frac{\partial v_z}{\partial \theta} + v_z \frac{\partial v_z}{\partial z} \right) &= -\frac{\partial P}{\partial z} \\
 &- \left(\frac{1}{r} \frac{\partial}{\partial r} (r\tau_{rz}) + \frac{1}{r} \frac{\partial \tau_{\theta z}}{\partial \theta} + \frac{\partial \tau_{zz}}{\partial z} \right) + \rho g_z \quad (\text{C})
 \end{aligned}$$

 In terms of velocity gradients for a Newtonian fluid with constant ρ and η :

$$\begin{aligned}
 \text{r-component*} \quad \rho \left(\frac{\partial v_r}{\partial t} + v_r \frac{\partial v_r}{\partial r} + \frac{v_\theta}{r} \frac{\partial v_r}{\partial \theta} - \frac{v_\theta^2}{r} + v_z \frac{\partial v_r}{\partial z} \right) &= -\frac{\partial P}{\partial r} \\
 &+ \eta \left[\frac{\partial}{\partial r} \left(\frac{1}{r} \frac{\partial}{\partial r} (rv_r) \right) + \frac{1}{r^2} \frac{\partial^2 v_r}{\partial \theta^2} - \frac{2}{r^2} \frac{\partial v_\theta}{\partial \theta} + \frac{\partial^2 v_r}{\partial z^2} \right] + \rho g_r \quad (\text{D})
 \end{aligned}$$

$$\begin{aligned}
 \text{\theta-component} \quad \rho \left(\frac{\partial v_\theta}{\partial t} + v_r \frac{\partial v_\theta}{\partial r} + \frac{v_\theta}{r} \frac{\partial v_\theta}{\partial \theta} + \frac{v_r v_\theta}{r} + v_z \frac{\partial v_\theta}{\partial z} \right) &= -\frac{1}{r} \frac{\partial P}{\partial \theta} \\
 &+ \eta \left[\frac{\partial}{\partial r} \left(\frac{1}{r} \frac{\partial}{\partial r} (rv_\theta) \right) + \frac{1}{r^2} \frac{\partial^2 v_\theta}{\partial \theta^2} + \frac{2}{r^2} \frac{\partial v_r}{\partial \theta} + \frac{\partial^2 v_\theta}{\partial z^2} \right] + \rho g_\theta \quad (\text{E})
 \end{aligned}$$

$$\begin{aligned}
 \text{z-component} \quad \rho \left(\frac{\partial v_z}{\partial t} + v_r \frac{\partial v_z}{\partial r} + \frac{v_\theta}{r} \frac{\partial v_z}{\partial \theta} + v_z \frac{\partial v_z}{\partial z} \right) &= -\frac{\partial P}{\partial z} \\
 &+ \eta \left[\frac{1}{r} \frac{\partial}{\partial r} \left(r \frac{\partial v_z}{\partial r} \right) + \frac{1}{r^2} \frac{\partial^2 v_z}{\partial \theta^2} + \frac{\partial^2 v_z}{\partial z^2} \right] + \rho g_z \quad (\text{F})
 \end{aligned}$$

*The term $\rho v_\theta^2 / r$ is the *centrifugal force*. It gives the effective force in the r -direction resulting from fluid motion in the θ -direction. This term arises automatically on transformation from rectangular to cylindrical coordinates; it does not have to be added on physical grounds.

Table 2.4 The momentum equation in spherical coordinates (r, θ, ϕ)In terms of τ :

$$\begin{aligned}
 r\text{-component} \quad & \rho \left(\frac{\partial v_r}{\partial t} + v_r \frac{\partial v_r}{\partial r} + \frac{v_\theta}{r} \frac{\partial v_r}{\partial \theta} + \frac{v_\phi}{r \sin \theta} \frac{\partial v_r}{\partial \phi} - \frac{v_\theta^2 + v_\phi^2}{r} \right) \\
 & = -\frac{\partial P}{\partial r} - \left(\frac{1}{r^2} \frac{\partial}{\partial r} (r^2 \tau_{rr}) + \frac{1}{r \sin \theta} \frac{\partial}{\partial \theta} (\tau_{r\theta} \sin \theta) \right. \\
 & \quad \left. + \frac{1}{r \sin \theta} \frac{\partial \tau_{r\phi}}{\partial \phi} - \frac{\tau_{\theta\theta} + \tau_{\phi\phi}}{r} \right) + \rho g_r
 \end{aligned} \tag{A}$$

$$\begin{aligned}
 \theta\text{-component} \quad & \rho \left(\frac{\partial v_\theta}{\partial t} + v_r \frac{\partial v_\theta}{\partial r} + \frac{v_\theta}{r} \frac{\partial v_\theta}{\partial \theta} + \frac{v_\phi}{r \sin \theta} \frac{\partial v_\theta}{\partial \phi} + \frac{v_r v_\theta}{r} - \frac{v_\phi^2 \cot \theta}{r} \right) \\
 & = -\frac{1}{r} \frac{\partial P}{\partial \theta} - \left(\frac{1}{r^2} \frac{\partial}{\partial r} (r^2 \tau_{r\theta}) + \frac{1}{r \sin \theta} \frac{\partial}{\partial \theta} (\tau_{\theta\theta} \sin \theta) + \frac{1}{r \sin \theta} \frac{\partial \tau_{\theta\phi}}{\partial \phi} \right. \\
 & \quad \left. + \frac{\tau_{r\theta}}{r} - \frac{\cot \theta}{r} \tau_{\phi\phi} \right) + \rho g_\theta
 \end{aligned} \tag{B}$$

$$\begin{aligned}
 \phi\text{-component} \quad & \rho \left(\frac{\partial v_\phi}{\partial t} + v_r \frac{\partial v_\phi}{\partial r} + \frac{v_\theta}{r} \frac{\partial v_\phi}{\partial \theta} + \frac{v_\phi}{r \sin \theta} \frac{\partial v_\phi}{\partial \phi} + \frac{v_\phi v_r}{r} + \frac{v_\theta v_\phi}{r} \cot \theta \right) \\
 & = -\frac{1}{r \sin \theta} \frac{\partial P}{\partial \phi} - \left(\frac{1}{r^2} \frac{\partial}{\partial r} (r^2 \tau_{r\phi}) + \frac{1}{r} \frac{\partial \tau_{\theta\phi}}{\partial \theta} + \frac{1}{r \sin \theta} \frac{\partial \tau_{\phi\phi}}{\partial \phi} \right. \\
 & \quad \left. + \frac{\tau_{r\phi}}{r} + \frac{2 \cot \theta}{r} \tau_{\theta\phi} \right) + \rho g_\phi
 \end{aligned} \tag{C}$$

In terms of velocity gradients for a Newtonian fluid with constant ρ and η :

$$\begin{aligned}
 r\text{-component} \quad & \rho \left(\frac{\partial v_r}{\partial t} + v_r \frac{\partial v_r}{\partial r} + \frac{v_\theta}{r} \frac{\partial v_r}{\partial \theta} + \frac{v_\phi}{r \sin \theta} \frac{\partial v_r}{\partial \phi} - \frac{v_\theta^2 + v_\phi^2}{r} \right) \\
 & = -\frac{\partial P}{\partial r} + \eta \left(\nabla^2 v_r - \frac{2}{r^2} v_r - \frac{2}{r^2} \frac{\partial v_\theta}{\partial \theta} - \frac{2}{r^2} v_\theta \cot \theta \right. \\
 & \quad \left. - \frac{2}{r^2 \sin \theta} \frac{\partial v_\phi}{\partial \phi} \right) + \rho g_r
 \end{aligned} \tag{D}$$

$$\begin{aligned}
 \theta\text{-component} \quad & \rho \left(\frac{\partial v_\theta}{\partial t} + v_r \frac{\partial v_\theta}{\partial r} + \frac{v_\theta}{r} \frac{\partial v_\theta}{\partial \theta} + \frac{v_\phi}{r \sin \theta} \frac{\partial v_\theta}{\partial \phi} + \frac{v_r v_\theta}{r} - \frac{v_\phi^2 \cot \theta}{r} \right) \\
 & = -\frac{1}{r} \frac{\partial P}{\partial \theta} + \eta \left(\nabla^2 v_\theta + \frac{2}{r^2} \frac{\partial v_r}{\partial \theta} - \frac{v_\theta}{r^2 \sin^2 \theta} - \frac{2 \cos \theta}{r^2 \sin^2 \theta} \frac{\partial v_\phi}{\partial \phi} \right) + \rho g_\theta
 \end{aligned} \tag{E}$$

$$\begin{aligned}
 \phi\text{-component} \quad & \rho \left(\frac{\partial v_\phi}{\partial t} + v_r \frac{\partial v_\phi}{\partial r} + \frac{v_\theta}{r} \frac{\partial v_\phi}{\partial \theta} + \frac{v_\phi}{r \sin \theta} \frac{\partial v_\phi}{\partial \phi} + \frac{v_\phi v_r}{r} + \frac{v_\theta v_\phi}{r} \cot \theta \right) \\
 & = -\frac{1}{r \sin \theta} \frac{\partial P}{\partial \phi} + \eta \left(\nabla^2 v_\phi - \frac{v_\phi}{r^2 \sin^2 \theta} + \frac{2}{r^2 \sin \theta} \frac{\partial v_r}{\partial \phi} \right. \\
 & \quad \left. + \frac{2 \cos \theta}{r^2 \sin^2 \theta} \frac{\partial v_\theta}{\partial \phi} \right) + \rho g_\phi
 \end{aligned} \tag{F}$$

Table 2.5 Components of the stress tensor in rectangular coordinates (x, y, z)

$$\tau_{xx} = -\eta \left[2 \frac{\partial v_x}{\partial x} - \frac{2}{3}(\nabla \cdot \mathbf{v}) \right] \quad (\text{A})$$

$$\tau_{yy} = -\eta \left[2 \frac{\partial v_y}{\partial y} - \frac{2}{3}(\nabla \cdot \mathbf{v}) \right] \quad (\text{B})$$

$$\tau_{zz} = -\eta \left[2 \frac{\partial v_z}{\partial z} - \frac{2}{3}(\nabla \cdot \mathbf{v}) \right] \quad (\text{C})$$

$$\tau_{xy} = \tau_{yx} = -\eta \left[\frac{\partial v_x}{\partial y} + \frac{\partial v_y}{\partial x} \right] \quad (\text{D})$$

$$\tau_{yz} = \tau_{zy} = -\eta \left[\frac{\partial v_y}{\partial z} + \frac{\partial v_z}{\partial y} \right] \quad (\text{E})$$

$$\tau_{zx} = \tau_{xz} = -\eta \left[\frac{\partial v_z}{\partial x} + \frac{\partial v_x}{\partial z} \right] \quad (\text{F})$$

$$(\nabla \cdot \mathbf{v}) = \frac{\partial v_x}{\partial x} + \frac{\partial v_y}{\partial y} + \frac{\partial v_z}{\partial z} \quad (\text{G})$$

Table 2.6 Components of the stress tensor in cylindrical coordinates (r, θ, z)

$$\tau_{rr} = -\eta \left[2 \frac{\partial v_r}{\partial r} - \frac{2}{3}(\nabla \cdot \mathbf{v}) \right] \quad (\text{A})$$

$$\tau_{\theta\theta} = -\eta \left[2 \left(\frac{1}{r} \frac{\partial v_\theta}{\partial \theta} + \frac{v_r}{r} \right) - \frac{2}{3}(\nabla \cdot \mathbf{v}) \right] \quad (\text{B})$$

$$\tau_{zz} = -\eta \left[2 \frac{\partial v_z}{\partial z} - \frac{2}{3}(\nabla \cdot \mathbf{v}) \right] \quad (\text{C})$$

$$\tau_{r\theta} = \tau_{\theta r} = -\eta \left[r \frac{\partial}{\partial r} \left(\frac{v_\theta}{r} \right) + \frac{1}{r} \frac{\partial v_r}{\partial \theta} \right] \quad (\text{D})$$

$$\tau_{\theta z} = \tau_{z\theta} = -\eta \left[\frac{\partial v_\theta}{\partial z} + \frac{1}{r} \frac{\partial v_z}{\partial \theta} \right] \quad (\text{E})$$

$$\tau_{rz} = \tau_{rz} = -\eta \left[\frac{\partial v_z}{\partial r} + \frac{\partial v_r}{\partial z} \right] \quad (\text{F})$$

$$(\nabla \cdot \mathbf{v}) = \frac{1}{r} \frac{\partial}{\partial r} (rv_r) + \frac{1}{r} \frac{\partial v_\theta}{\partial \theta} + \frac{\partial v_z}{\partial z} \quad (\text{G})$$

Table 2.7 Components of the stress tensor in spherical coordinates (r, θ, ϕ)

$$\tau_{rr} = -\eta \left[2 \frac{\partial v_r}{\partial r} - \frac{2}{3}(\nabla \cdot \mathbf{v}) \right] \quad (\text{A})$$

$$\tau_{\theta\theta} = -\eta \left[2 \left(\frac{1}{r} \frac{\partial v_\theta}{\partial \theta} + \frac{v_r}{r} \right) - \frac{2}{3}(\nabla \cdot \mathbf{v}) \right] \quad (\text{B})$$

$$\tau_{\phi\phi} = -\eta \left[2 \left(\frac{1}{r \sin \theta} \frac{\partial v_\phi}{\partial \phi} + \frac{v_r}{r} + \frac{v_\theta \cot \theta}{r} \right) - \frac{2}{3}(\nabla \cdot \mathbf{v}) \right] \quad (\text{C})$$

$$\tau_{r\theta} = \tau_{\theta r} = -\eta \left[r \frac{\partial}{\partial r} \left(\frac{v_\theta}{r} \right) + \frac{1}{r} \frac{\partial v_r}{\partial \theta} \right] \quad (\text{D})$$

$$\tau_{\theta\phi} = \tau_{\phi\theta} = -\eta \left[\frac{\sin \theta}{r} \frac{\partial}{\partial \theta} \left(\frac{v_\phi}{\sin \theta} \right) + \frac{1}{r \sin \theta} \frac{\partial v_\theta}{\partial \phi} \right] \quad (\text{E})$$

$$\tau_{r\phi} = \tau_{\phi r} = -\eta \left[\frac{1}{r \sin \theta} \frac{\partial v_r}{\partial \phi} + r \frac{\partial}{\partial r} \left(\frac{v_\phi}{r} \right) \right] \quad (\text{F})$$

$$(\nabla \cdot \mathbf{v}) = \frac{1}{r^2} \frac{\partial}{\partial r} (r^2 v_r) + \frac{1}{r \sin \theta} \frac{\partial}{\partial \theta} (v_\theta \sin \theta) + \frac{1}{r \sin \theta} \frac{\partial v_\phi}{\partial \phi} \quad (\text{G})$$

2.7 APPLICATION OF NAVIER-STOKES' EQUATION

In this section, we show how to set up problems of viscous flow, by selecting the appropriate equation of motion that applies to the problem at hand and by simplifying it to manageable proportions so that it still relates to the given problem, and yet is not oversimplified. We do so by discarding those terms which are zero, and then recognizing those terms which can be neglected. To decide this, is, to a certain extent, a matter of experience, but in most instances even the novice can make intelligent decisions by making an order-of-magnitude estimate. For this purpose, we shall discuss below an order-of-magnitude technique that can be used to arrive at a more simplified, but still relevant, equation of motion. We also introduce other topics, such as the *boundary layer* and *drag forces* exerted by fluids on solids.

2.7.1 Flow over a flat plate

Figure 2.6 depicts the velocity profile of a fluid flowing parallel to a flat plate. Before it meets the leading edge of the plate, we assume that the fluid has a uniform velocity V_∞ . At any point x downstream from the leading edge of the plate, we observe that the velocity increases from zero at the wall to very near V_∞ at a very short distance δ from the plate. The loci of positions where $v_x/V_\infty = 0.99$, is δ , and it is defined as the *boundary layer*. At the leading edge of the plate ($x = 0$), δ is zero, and it progressively grows as flow proceeds down the plate.

Whenever problems of this type are encountered, namely, in the flow of fluid past a stationary solid, the viscous effects are felt only within the fluid near the solid, that is, $y < \delta$. Of course, this is exactly where the behavior of the fluid should be analyzed, because for $y > \delta$, the happenings from the point of view of this discussion are essentially uneventful,

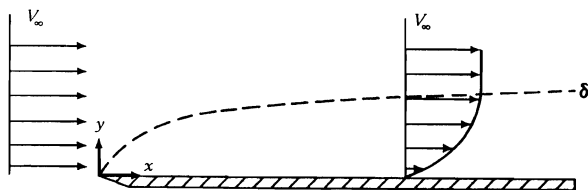


Fig. 2.6 Velocity profile and momentum boundary layer of flow parallel to a flat plate.

due to the fact that in this region v_x is essentially uniform and constant, being equal to V_∞ . Since v_x is uniform and constant for $y > \delta$, Eq. (D) in Table 2.2 reveals that the pressure gradient $\partial P/\partial x$ is zero or, stated differently, pressure everywhere in the bulk stream is uniform. In turn, the pressure within the boundary layer is equal to the pressure in the bulk stream, so that $\partial P/\partial x$ is also zero within the boundary layer. We are now almost ready to pick out the appropriate equation of motion for the flow pattern in Fig. 2.6, but before we do so, let us examine which velocity components are relevant.

As discussed above, v_x is a function of y , and the determination of this functional relationship is indeed a major part of describing the flow and how the fluid and the solid surface interact. Also note that v_x depends on x . This results from the fact that, as the fluid progresses down the plate, it is retarded more and more by the drag at the plate's surface. Thus $\partial v_x/\partial x$ is not zero, and the equation of continuity for steady two-dimensional flow of fluid with constant ρ and η is

$$\frac{\partial v_x}{\partial x} + \frac{\partial v_y}{\partial y} = 0. \quad (2.70)$$

Thus v_y exists and we should consider both the x - and y -components in Table 2.2.

For the steady-state case with constant density and viscosity, Eqs. (D) and (E) in Table 2.2 reduce to

$$v_x \frac{\partial v_x}{\partial x} + v_y \frac{\partial v_x}{\partial y} = \nu \left[\frac{\partial^2 v_x}{\partial x^2} + \frac{\partial^2 v_x}{\partial y^2} \right], \quad (2.71)$$

and

$$v_x \frac{\partial v_y}{\partial x} + v_y \frac{\partial v_y}{\partial y} = \nu \left[\frac{\partial^2 v_y}{\partial x^2} + \frac{\partial^2 v_y}{\partial y^2} \right] + g_y. \quad (2.72)$$

When we remember that we are primarily interested in the region $y \leq \delta$, at this point it is convenient to define some dimensionless parameters:[†]

$$u^* = \frac{v_x}{V_\infty}, \quad x^* = \frac{x}{L}, \quad \delta^* = \frac{\delta}{L},$$

[†]The *Reynolds number* Re_L , which was briefly introduced in Chapter 1 reappears here again. Also the *Froude number* Fr_L , is introduced. These two dimensionless numbers, which so often occur in engineering studies, have been given names in honor of those two early workers in fluid mechanics.

64 Laminar Flow and the Momentum Equation

$$v^* = \frac{v_y}{V_\infty}, \quad y^* = \frac{y}{L}, \quad \text{Re}_L = \frac{V_\infty L}{\nu},$$

$$\text{Fr}_L = \frac{V_\infty^2}{g_y L}.$$

Substituting these parameters into Eqs. (2.71), (2.72), and the continuity equation, we get

Continuity:

$$\frac{\partial u^*}{\partial x^*} + \frac{\partial v^*}{\partial y^*} = 0. \quad (2.73)$$

Momentum:

$$u^* \frac{\partial u^*}{\partial x^*} + v^* \frac{\partial u^*}{\partial y^*} = \frac{1}{\text{Re}_L} \left[\frac{\partial^2 u^*}{\partial (x^*)^2} + \frac{\partial^2 u^*}{\partial (y^*)^2} \right]; \quad (2.74)$$

$$u^* \frac{\partial v^*}{\partial x^*} + v^* \frac{\partial v^*}{\partial y^*} = \frac{1}{\text{Re}_L} \left[\frac{\partial^2 v^*}{\partial (x^*)^2} + \frac{\partial^2 v^*}{\partial (y^*)^2} \right] + \frac{1}{\text{Fr}_L}. \quad (2.75)$$

The next step is to make order-of-magnitude estimates of the terms in Eqs. (2.74) and (2.75), realizing that we are interested only in the happenings within the boundary layer.

Order of magnitudes:

$$\Delta x^* \cong 0 \text{ to } 1. \quad (2.76)$$

$$\Delta y^* \cong \delta^*. \quad (2.77)$$

$$\Delta u^* \cong 1. \quad (2.78)$$

From (2.76) and (2.78), we get

$$\frac{\partial u^*}{\partial x^*} \cong \frac{1}{1} = 1, \quad (2.79)$$

and from continuity,

$$\frac{\partial v^*}{\partial y^*} \cong 1. \quad (2.80)$$

From (2.77) and (2.78), we obtain

$$\frac{\partial u^*}{\partial y^*} \cong \frac{1}{\delta^*}, \quad (2.81)$$

and from (2.79) and (2.80),

$$\frac{\partial v^*}{\partial x^*} \cong \frac{\delta^*}{1} = \delta^* . \quad (2.82)$$

Now we can estimate all the second derivatives:

$$\frac{\partial^2 u^*}{\partial (x^*)^2} = \frac{\partial}{\partial x^*} \left(\frac{\partial u^*}{\partial x^*} \right) \cong \frac{1}{1} = 1 . \quad (2.83)$$

$$\frac{\partial^2 u^*}{\partial (y^*)^2} = \frac{\partial}{\partial y^*} \left(\frac{\partial u^*}{\partial y^*} \right) \cong \frac{1}{\delta^*} \left[\frac{1}{\delta^*} \right] = \frac{1}{\delta^{*2}} . \quad (2.84)$$

$$\frac{\partial^2 v^*}{\partial (x^*)^2} \cong \delta^* . \quad (2.85)$$

$$\frac{\partial^2 v^*}{\partial (y^*)^2} \cong \frac{1}{\delta^{*2}} . \quad (2.86)$$

Insertion of the various magnitudes into Eqs. (2.74) and (2.75) reveals two important facts: $\partial^2 u^*/\partial (y^*)^2 \gg \partial^2 u^*/\partial (x^*)^2$, and the equation involving the x -component of the velocity has much larger terms than that for v_x . Hence we deal only with

$$v_x \frac{\partial v_x}{\partial x} + v_y \frac{\partial v_x}{\partial y} = \nu \frac{\partial^2 v_x}{\partial y^2} , \quad (2.87)$$

which is the *boundary layer* equation for a flat plate with zero pressure gradient. We now proceed to solve Eq. (2.87) for the boundary conditions

$$\text{B.C. 1} \quad \text{at } y = 0, \quad v_x = 0, \quad v_y = 0; \quad (2.88)$$

$$\text{B.C. 2} \quad \text{at } y = \infty, \quad v_x = V_\infty . \quad (2.89)$$

In order to simplify Eq. (2.87), we define the *stream function* ψ as

$$v_x \equiv \frac{\partial \psi}{\partial y} \quad \text{and} \quad v_y \equiv - \frac{\partial \psi}{\partial x} . \quad (2.90)$$

The use of the stream functions simplifies Eq. (2.87) and automatically satisfies continuity (Eq. (2.70)). Substituting Eq. (2.90) into Eq. (2.87) yields:

$$\frac{\partial \psi}{\partial y} \frac{\partial^2 \psi}{\partial x \partial y} - \frac{\partial \psi}{\partial x} \frac{\partial^2 \psi}{\partial y^2} = \nu \frac{\partial^3 \psi}{\partial y^3} . \quad (2.91)$$

A *similarity argument*[†] shows that the stream function may be expressed as

$$\psi \equiv \sqrt{V_\infty \nu x} f(\beta) , \quad (2.92)$$

[†]Blasius showed that Eq. (2.91) could be solved in this manner. (See H. Blasius, *NACA Tech. Mem.*, 1949, page 1217.)

66 Laminar Flow and the Momentum Equation

where

$$\beta = \frac{y}{\sqrt{x}} (V_\infty/\nu)^{1/2}, \quad (2.93)$$

From Eqs. (2.90), (2.92), and (2.93),

$$v_x = \frac{\partial \psi}{\partial y} = \frac{\partial \psi}{\partial \beta} \frac{\partial \beta}{\partial y} = V_\infty \frac{df}{d\beta}, \quad (2.94)$$

$$v_y = -\frac{\partial \psi}{\partial x} = \frac{1}{2} \left[\frac{\nu V_\infty}{x} \right]^{1/2} \left[\beta \frac{df}{d\beta} - f \right]. \quad (2.95)$$

Then Eq. (2.91) becomes

$$2 \frac{d^3 f}{d\beta^3} + f \frac{d^2 f}{d\beta^2} = 0. \quad (2.96)$$

Mathematically, the use of ψ and β has reduced a partial differential equation to an ordinary differential equation with the boundary conditions also taking equivalent forms:

$$\text{B.C. 1} \quad \text{at } \beta = 0, \quad f = 0, \quad \frac{df}{d\beta} = 0; \quad (2.97)$$

$$\text{B.C. 2} \quad \text{at } \beta = \infty, \quad \frac{df}{d\beta} = 1. \quad (2.98)$$

Equation (2.96) may be solved by expressing $f(\beta)$ in a power series, that is, $f = \sum_0^\infty a_k \beta^k$.

The technique is too involved to develop here, but the solution conforming to the boundary conditions becomes

$$f = \frac{\alpha \beta^2}{2!} - \frac{1}{2} \frac{\alpha^2 \beta^5}{5!} + \frac{11}{4} \frac{\alpha^3 \beta^8}{8!} + \dots \quad (2.99)$$

where $\alpha = 0.332$. Then Eqs. (2.94) and (2.95) give expressions for v_x and v_y ; the solution for v_x is shown graphically in Fig. 2.7. The position, where $v_x/V_\infty = 0.99$, is located at $\beta = 5.0$; thus the boundary-layer thickness δ is

$$\delta = 5.0 \left[\frac{\nu x}{V_\infty} \right]^{1/2}. \quad (2.100)$$

Note that if we divide Eq. (2.100) by x , both sides become dimensionless:

$$\frac{\delta}{x} = 5.0 \left[\frac{\nu}{x V_\infty} \right]^{1/2} = \frac{5.0}{\sqrt{\text{Re}_x}}. \quad (2.101)$$

Note also that as a result of the analysis, the Reynolds number ($\text{Re}_x = xV_\infty/\nu$) has evolved; in this instance we give Re the subscript x in order to emphasize that it is a local value with

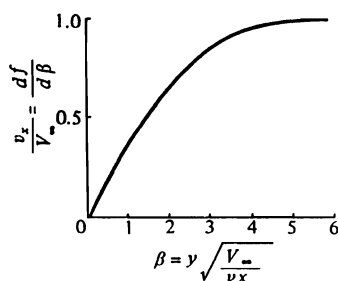


Fig. 2.7 Solution for the velocity distribution in the boundary layer over a flat plate. (From L. Howarth, *Proc. Roy. Soc.*, London A164, 547 (1938).)

the *characteristic dimension* x . We can also calculate the *drag force*, which is exerted by the fluid on the plate's surface. If the plate has a length L and width W , the drag force F_K is

$$F_K = \int_0^w \int_0^L \left[\eta \frac{\partial v_x}{\partial y} \right]_{y=0} dx dz. \quad (2.102)$$

In other words, the shear stress at the solid surface is integrated over the entire surface. From Fig. 2.7 we find that

$$\left[\frac{\partial(v_x/V_\infty)}{\partial\beta} \right]_{\beta=0} = 0.332. \quad (2.103)$$

Knowing the integrand in Eq. (2.102), we can now perform the integration. The result is

$$F_K = 0.664 \sqrt{\rho\eta L W^2 V_\infty^3}. \quad (2.104)$$

This is the drag force exerted by the fluid on one surface only.

2.7.2 Flow in inlet of circular tubes

In Section 2.4, we considered the flow of fluid in a long tube so that end effects were negligible. Now we wish to study the flow conditions at the inlet where the flow is not fully developed. The fluid enters the tube with a uniform velocity V_0 in the z -direction. The important component for this system is the z -component, just as the x -component is most important for the flow past a flat plate. According to Eq. (F) in Table 2.3, the momentum equation with $v_\theta = 0$, $\partial v_z/\partial t = 0$, and $g_z = 0$, reduces to

$$v_r \frac{\partial v_z}{\partial r} + v_z \frac{\partial v_z}{\partial z} = -\frac{1}{\rho} \frac{\partial P}{\partial z} + \nu \left[\frac{1}{r} \frac{\partial}{\partial r} \left(r \frac{\partial v_z}{\partial r} \right) + \frac{\partial^2 v_z}{\partial z^2} \right]$$

Again, the viscous effect in the direction parallel to flow is negligible, so that $\partial^2 v_z / \partial z^2 \cong 0$, and we are left with

$$v_r \frac{\partial v_z}{\partial r} + v_z \frac{\partial v_z}{\partial z} = -\frac{1}{\rho} \frac{\partial P}{\partial z} + \frac{\nu}{r} \frac{\partial}{\partial r} \left[r \frac{\partial v_z}{\partial r} \right] \quad (2.105)$$

We can deduce the equation of continuity from Eq. (B) in Table 2.1:

$$\frac{1}{r} \frac{\partial}{\partial r} (rv_r) + \frac{\partial v_z}{\partial z} = 0. \quad (2.106)$$

The method for the solution of Eq. (2.105) is not given here, but one should understand why Eq. (2.105) is the starting point. Langhaar² has developed the solution for this problem, as described in Fig. 2.8. His analysis shows that a fully developed flow is not established until $v_z/R^2 V_0 \cong 0.07$. Thus an entrance length ($z = L_e$) of approximately $0.035 (D^2 V_0 \rho) / \eta$ is required for buildup to the parabolic profile of the fully developed flow.

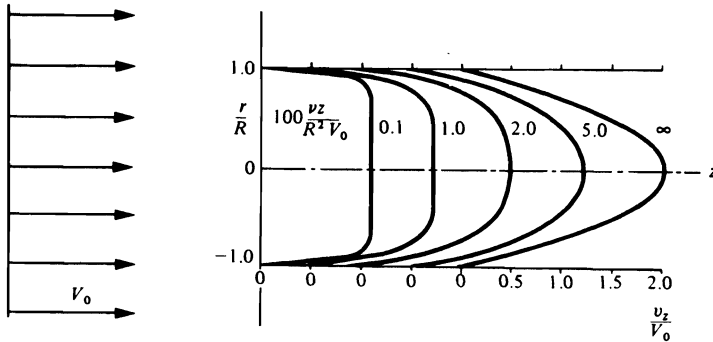


Fig. 2.8 Velocity distribution for laminar flow in the inlet section of a tube.

2.7.3 Creeping flow around a solid sphere

Consider the flow of an incompressible fluid about a solid sphere (Fig. 2.9). The fluid approaches the sphere upward along the z -axis with a uniform velocity V_∞ . Clearly, the momentum equation for this situation does not involve the ϕ -component. In addition, if the flow is slow enough, the acceleration terms in Navier-Stokes' equation can be ignored. Therefore, in spherical coordinates, from Eqs. (D) and (E) in Table 2.4, we obtain for the r -component:

$$-\frac{\partial P}{\partial r} + \eta \left[\nabla^2 v_r - \frac{2}{r^2} v_r - \frac{2}{r^2} \frac{\partial v_\theta}{\partial \theta} - \frac{2}{r^2} v_\theta \cot \theta \right] + \rho g_r = 0, \quad (2.107)$$

²H. L. Langhaar, *J. Appl. Mech.* **9**, A55-58 (1942).

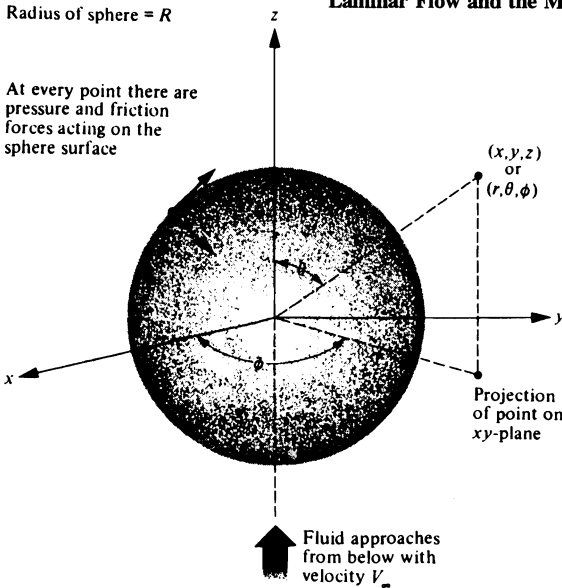


Fig. 2.9 Coordinate system used in describing the flow of a fluid about a rigid sphere.

and for the θ -component:

$$-\frac{1}{r} \frac{\partial P}{\partial \theta} + \eta \left[\nabla^2 v_\theta + \frac{2}{r^2} \frac{\partial v_r}{\partial \theta} - \frac{v_\theta}{r^2 \sin^2 \theta} \right] + \rho g_\theta = 0. \quad (2.108)$$

The continuity equation (Eq. (C) in Table 2.1) is

$$\frac{1}{r^2} \frac{\partial}{\partial r} (r^2 v_r) + \frac{1}{r \sin \theta} \frac{\partial}{\partial \theta} (v_\theta \sin \theta) = 0. \quad (2.109)$$

The momentum flux-distribution, pressure distribution, and velocity components have been found analytically:³

$$\tau_{r\theta} = \frac{3}{2} \frac{\eta V_\infty}{R} \left[\frac{R}{r} \right]^4 \sin \theta, \quad (2.110)$$

$$P = P_0 - \rho g z - \frac{3}{2} \frac{\eta V_\infty}{R} \left[\frac{R}{r} \right]^2 \cos \theta, \quad (2.111)$$

$$v_r = V_\infty \left[1 - \frac{3}{2} \left[\frac{R}{r} \right] + \frac{1}{2} \left[\frac{R}{r} \right]^3 \right] \cos \theta. \quad (2.112)$$

³V. L. Streeter, *Fluid Dynamics*, McGraw-Hill, New York, 1948, pages 235-240.

$$v_\theta = -V_\infty \left[1 - \frac{3}{4} \left(\frac{R}{r} \right) - \frac{1}{4} \left(\frac{R}{r} \right)^3 \right] \sin \theta. \quad (2.113)$$

We can check the validity of the results by showing that Eqs. (2.107)-(2.109) and the following conditions are satisfied:

$$\text{B.C. 1} \quad \text{at } r = R, \quad v_r = 0 = v_\theta;$$

$$\text{B.C. 2} \quad \text{at } r = \infty, \quad v_z = V_\infty.$$

In Eq. (2.111), the quantity P_0 is the pressure in the plane $z = 0$ far away from the sphere, $-\rho gz$ is simply the hydrostatic effect, and the term containing V_∞ results from the fluid flow around the sphere. These equations are valid for a Reynolds number (DV_∞/ν) less than approximately unity.

With these results, we can calculate the net force which is exerted by the fluid on the sphere. This force is computed by integrating the normal force and tangential force over the sphere surface as follows.

The *normal force* acting on the solid surface is due to the pressure given by Eq. (2.111) with $r = R$ and $z = R \cos \theta$. Thus

$$P(r = R) = P_0 - \rho g R \cos \theta - \frac{3}{2} \frac{\eta V_\infty}{R} \cos \theta.$$

The z -component of this pressure multiplied by the surface area on which it acts, $R^2 \sin \theta d\theta d\phi$, is integrated over the surface of the sphere to yield the net force due to the pressure difference:

$$F_n = \int_0^{2\pi} \int_0^\pi \left[P_0 - \rho g R \cos \theta - \frac{3}{2} \frac{\eta V_\infty}{R} \cos \theta \right] R^2 \sin \theta d\theta d\phi. \quad (2.114)$$

Equation (2.114), integrated, yields two terms:

$$F_n = \frac{4}{3} \pi R^3 \rho g + 2\pi \eta R V_\infty, \quad (2.115)$$

the *buoyant force* and *form drag*, respectively.

At each point on the surface, there is also a shear stress acting tangentially, $-\tau_{r\theta}$, which is the force acting on a unit surface area. The z -component of this force is $(-\tau_{r\theta})(-\sin \theta)R^2 \sin \theta d\theta d\phi$; again, integration over the sphere's surface yields

$$F_t = \int_0^{2\pi} \int_0^\pi (\tau_{r\theta}|_{r=R} \sin \theta) R^2 \sin \theta d\theta d\phi.$$

From Eq. (2.110), we get

$$\tau_{r\theta}|_{r=R} = \frac{3}{2} \frac{\eta V_\infty}{R} \sin \theta,$$

so that the *friction drag* results:

$$F_t = 4\pi \eta R V_\infty. \quad (2.116)$$

The total force F of the fluid on the sphere is given by the sum of Eqs. (2.115) and (2.116):

$$F = \frac{4}{3} \pi R^3 \rho g + 6\pi\eta R V_\infty. \quad (2.117)$$

These two terms are designated as F_s (the force exerted even if the fluid is stationary) and F_K (the force associated with fluid movement). Thus these forces are

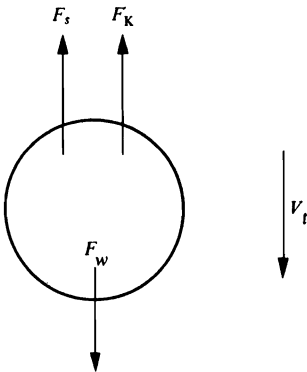
$$F_s = \frac{4}{3} \pi R^3 \rho g, \quad (2.118)$$

$$F_K = 6\pi\eta R V_\infty. \quad (2.119)$$

We use Eq. (2.119), known as *Stokes' law*, primarily for determining the terminal velocity, V_t of small spherical particles moving through fluid media. The fluid media are stagnant; the spherical particle moves through the fluid, and V_∞ is viewed as V_t . With this in mind, we may use Stokes' law as the basis of a *falling-sphere* viscometer, in which the liquid is placed in a tall transparent cylinder and a sphere of known mass and diameter is dropped into it. The terminal velocity of the falling sphere can be measured, and this in turn relates to the fluid's viscosity.

Example 2.3 Apply Stokes' law to the falling sphere viscometer and write an expression for the viscosity of the liquid in the viscometer.

Solution. A force balance on the sphere, as it falls through the liquid, is made according to the diagram:



Here F_s is the buoyant force exerted by the liquid and is therefore directed upward; F_K is often called the *drag force* and as such always acts in the opposite direction to that of motion and is therefore directed upward. The only force in the downward direction is the weight of the sphere. The terminal velocity is reached when the force system is in equilibrium. Therefore $F_s + F_K = F_w$, and by substituting in expressions for each of these forces, we have

$$\frac{4}{3} \pi R^3 \rho g + 6\pi\eta R V_t = \frac{4}{3} \pi R^3 \rho_s g. \quad (2.120)$$

where ρ_s is the sphere's density.

By solving Eq. (2.120) for η , we arrive at

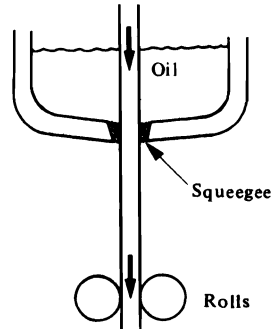
$$\eta = \frac{2R^2(\rho_s - \rho)g}{9V_t}. \quad (2.121)$$

The result is valid only if $2RV_t/\nu$ is less than approximately unity.

PROBLEMS

2.1 Refer to the results of Example 2.1. The viscosity of the glass is 1 N s m^{-2} , and the viscosity of the metal is $3 \times 10^{-3} \text{ N s m}^{-2}$. The densities of the glass and the metal are 3.2 kg m^{-3} and 7.0 kg m^{-3} , respectively. For $\beta = \pi/8$ and $\delta_1 = 1 \text{ mm}$ and $\delta_2 = 2 \text{ mm}$, calculate the maximum velocities and average velocities of the glass and the metal.

2.2 A continuous sheet of metal is cold-rolled by passing vertically between rolls. Before entering the rolls, the sheet passes through a tank of lubricating oil equipped with a squeegee device that coats both sides of the sheet uniformly as it exits. The amount of oil that is carried through can be controlled by adjusting the squeegee device. Prepare a control chart that can be used to determine the thickness of oil (in mm) on the plate just before it enters the roll as a function of the mass rate of oil (in kg per hour). Values of interest for the thickness of the oil film range from 0-0.6 mm. *Data:* Oil density, 962 kg m^{-3} ; oil viscosity, $4.1 \times 10^{-3} \text{ N s m}^{-2}$; width of sheet, 1.5 m ; velocity of sheet, 0.3 m s^{-1} .



2.3 A Newtonian liquid flows simultaneously through two parallel and vertical channels of different geometries. Channel "A" is circular with a radius R , and "B" is a slit of thickness 2δ and width W ; $2\delta \ll W$. Assume fully developed flow in both channels and derive an equation which gives the ratio of the volume flow rate through A to that through B.

2.4 Develop expressions for the flow of a fluid between vertical parallel plates. The plates are separated by a distance of 2δ . Consider fully developed flow and determine

- the velocity distribution,
- the volume flow rate.

Compare your expressions with Eqs. (2.20) and (2.23).

2.5 Repeat Problem 2.4 but now orient the plates at an angle β to the direction of gravity and obtain expressions for

- the velocity distribution,
- the volume flow rate.

Compare your expressions with the results of Problem 2.4 and Eqs. (2.20) and (2.23).

2.6 A liquid is flowing through a vertical tube 0.3 m long and 2.5 mm in I.D. The density of the liquid is 1260 kg m^{-3} and the mass flow rate is $3.8 \times 10^{-5} \text{ kg s}^{-1}$.

- What is the viscosity in N s m^{-2} ?
- Check on the validity of your results.

2.7 Water (viscosity $10^{-3} \text{ N s m}^{-2}$) flows parallel to a flat horizontal surface. The velocity profile at $x = x_1$ is given by

$$v_x = 6 \sin \left[\frac{\pi}{2} \right] y$$

with v_x in m s^{-1} and y as distance from surface in mm.

- a) Find the shear stress at the wall at x_1 . Express results in N m^{-2} .
 b) Farther downstream, at $x = x_2$, the velocity profile is given by

$$v_x = 4 \sin \left[\frac{\pi}{2} \right] y$$

Is the flow "fully developed"? Explain.

- c) Is there a y -component to flow (i.e., v_y)? Explain with the aid of the continuity equation.

2.8 For a polymeric melt that follows a power law for shear stress versus shear strain rate, derive an equation for the velocity profile and volume flow rate for flow between parallel plates.

2.9 The power law polymer of Problem 2.8 has constants $\eta_0 = 1.2 \times 10^4 \text{ N s m}^{-2}$ and $n = 0.35$. It is injected through a gate into a thin cavity, which has a thickness of 2 mm, a width of 10 mm and a length of 20 mm. If the injection rate is constant at $200 \text{ mm}^3 \text{ s}^{-1}$, estimate the time to fill the cavity and the injection pressure at the gate.

2.10 A wire is cooled after a heat treating operation by being pulled through the center of an open-ended, oil-filled tube which is immersed in a tank. In a region in the tube where end effects are negligible, obtain an expression for the velocity profile assuming steady state and all physical properties constant.

Tube inner radius: R

Wire radius: KR

Wire velocity: U



2.11 Starting with the x -component of the momentum equation (Eq. (2.52)), develop the x -component for the Navier-Stokes' equation (constant ρ and η , (Eq. 2.63)).

2.12 Air at 289 K flows over a flat plate with a velocity of 9.75 m s^{-1} . Assume laminar flow and a) calculate the boundary-layer thickness 50 mm from the leading edge; b) calculate the rate of growth of the boundary layer at that point; i.e., what is db/dx at that point? *Properties of air at 289 K:* density: 1.22 kg m^{-3} ; viscosity: $1.78 \times 10^{-5} \text{ N s m}^{-2}$.

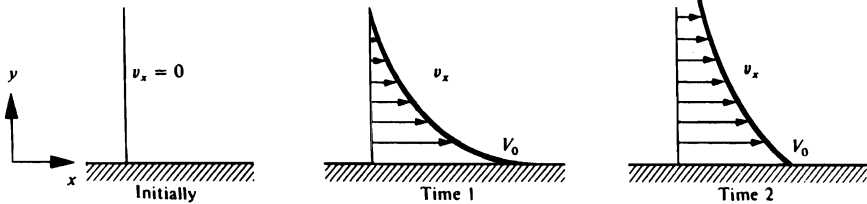
2.13 A fluid flows upward through a vertical cylindrical annulus of length L . Assume that the flow is fully developed. The inner radius of the annulus is κR , and the outer radius is R . a) Write the momentum equation in terms of velocity. b) Solve for the velocity profile. c) Solve for the maximum velocity.

2.14 In steelmaking, deoxidation of the melt is accomplished by the addition of aluminum, which combines with the free oxygen to form alumina, Al_2O_3 . It is then hoped that most of these alumina particles will float up to the slag layer for easy removal from the process, because their presence in steel can be detrimental to mechanical properties. Determine the size of the smallest alumina particles that will reach the slag layer from the bottom of the steel two minutes after the steel is deoxidized. It may be assumed that the alumina particles are spherical in nature. For the purpose of estimating the steel's viscosity use the data for Fe-0.5 wt pct C in Fig. 1.11. *Data:* Temperature of steel melt: 1873 K; steel melt depth: 1.5 m; density of steel: 7600 kg m^{-3} ; density of alumina: 3320 kg m^{-3} .

74 Laminar Flow and the Momentum Equation

2.15

- a) Consider a very large flat plate bounding a liquid that extends to $y = +\infty$. Initially, the liquid and the plate are at rest; then suddenly the plate is set into motion with velocity V_0 as shown in the figure below. Write (1) the pertinent differential equation in terms of velocity, for constant properties, that applies from the instant the plate moves, and (2) the appropriate boundary and initial conditions. The solution to these equations will be discussed in Chapter 9.



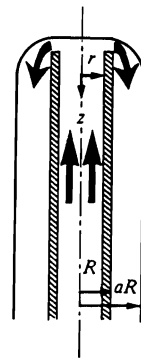
- b) A liquid flows upward through a long vertical conduit with a square cross section. With the aid of a clearly labeled sketch, write (1) a pertinent differential equation that describes the flow for constant properties, and (2) the appropriate boundary conditions. Consider only that portion of the conduit where flow is fully developed and be sure that your sketch and equations correspond to one another.

2.16 Molten aluminum is degassed by gently bubbling a 75%N₂-25%Cl₂ gas through the melt. The gas passes through a graphite tube at a volumetric flow rate of $6.6 \times 10^{-5} \text{ m}^3 \text{ s}^{-1}$. Calculate the pressure that should be maintained at the tube entrance if the pressure over the bath is $1.014 \times 10^5 \text{ N m}^{-2}$ (1 atm). Data: Tube dimensions: $L = 0.9 \text{ m}$; inside diameter = 2 mm. Temperature of aluminum melt is 973 K; density of aluminum is 2500 kg m^{-3} .

2.17 Glass flows through a small orifice by gravity to form a fiber. The free-falling fiber does not have a uniform diameter; furthermore as it falls through the air it cools so that its viscosity changes. a) Write the momentum equation for this situation. b) Write appropriate boundary conditions.

2.18 A liquid flows upward through a tube, overflows, and then flows downward as a film on the outside.

- a) Develop the pertinent momentum balance that applies to the falling film, for steady-state laminar flow, neglecting end effects.
 b) Develop an expression for the velocity distribution.



3

TURBULENT AND COMPLEX FLOWS

In Chapter 2 we discussed only laminar flow problems where we knew differential equations describing the flow, and could calculate the velocity distribution for simple systems. But more often than not, the flow is turbulent, and then experimental information must be sought. For example, it is practically impossible for laminar flow to persist in a pipe at values of Re greater than about 2100. This value of Re is subject to variations in that laminar flow has been maintained up to values of Re as high as 50 000. However, in such cases, the flow is extremely unstable, and the least disturbance transforms it instantly into turbulent flow. Also, the transition Re is higher in a converging pipe and lower in a diverging pipe than in a straight pipe, and even depends to some degree on the inside-surface roughness of the pipe.

If we accept 2100 as the normal transition value of Re for turbulent flow in pipes with normal roughness, we can easily show that turbulent flow is the usual case. Consider water at 289 K (60°F) which has a kinematic viscosity of $1.13 \times 10^{-6} \text{ m}^2 \text{ s}^{-1}$. In a pipe of 25.4 mm diam. the average velocity that still corresponds to laminar flow is

$$\begin{aligned} V_{\text{crit}} &= \frac{v}{D} Re_D = \frac{1.13 \times 10^{-6} \text{ m}^2 \text{ s}^{-1}}{25.4 \times 10^{-3} \text{ m}} \times 2100 \\ &= 9.34 \times 10^{-2} \text{ m s}^{-1}. \end{aligned}$$

Velocities as small as these (in 25 mm pipes) are not often encountered in practical engineering; most problems of engineering importance occur in the region of turbulent flow. Notwithstanding, many instances in engineering involve laminar flow.

In this chapter we examine some empirical information available for various systems. We may classify the flow systems into two groups: flow through closed conduits and flow past submerged bodies. We also introduce the readers to flow through porous media and in fluidized beds.

The fluctuating nature of turbulence and an introduction to turbulence models are reserved for Chapter 16. These models are being increasingly used in commercial software packages that are used for solving industrial flow problems.

3.1 FRICTION FACTORS FOR FLOW IN TUBES

As an example of a flow system, consider a length of horizontal pipe between $z = 0$ and $z = L$. We presume that in this length of pipe the fluid is flowing with an average velocity independent of time, and that the flow is fully developed. For flow in such a system, we may write the kinetic force of the fluid on the inner wall as

$$F_K = 2\pi RL\tau_0. \quad (3.1)$$

Here τ_0 is defined as the shear stress at the wall, or, in terms of previous notation $\tau_0 \equiv \tau_{rz}(r = R)$. According to Eq. (2.28), we can express τ_0 in terms of the pressure drop:

$$\tau_0 = \left[\frac{P_0 - P_L}{L} \right] \frac{R}{2}. \quad (3.2)$$

Equation (3.2) is also valid for turbulent flow as it specifies conditions only at the wall. Using Eq. (3.2), we may write F_K in an alternative form:

$$F_K = \pi R^2(P_0 - P_L). \quad (3.3)$$

Equation (3.3) focuses our attention on what should be considered if we ask the following question: What pressure drop is necessary to deliver a given volume of fluid through a tube? Thus we learn from Eq. (3.3) that F_K must be determined; for laminar flow, this can be calculated because the velocity distribution is amenable to analysis, and pressure drops can be determined *a priori*. For turbulent flow, the uncertainties involved in parallel analysis have led engineers to take an experimental approach to the problem.

In turbulent flow we may think that the flow pattern starts with a *laminar boundary layer*, in which the flow can be described by Newton's law of viscosity, followed by a transition region in which the degree of turbulence steadily increases and laminar effects diminish, until finally the region of fully developed turbulence is reached. These regions are illustrated in Fig. 3.1. In turbulent flow, therefore, the fluid still clings to the solid wall. Thus Eq. (3.1) is applicable, but, in general, the value of τ_0 is not determined by analytical means. More often we employ an empirical technique and express the force F_K as the product of a *characteristic area* A , a *characteristic kinetic energy* K (per unit volume), and a dimensionless quantity f , known as the *friction factor*:

$$F_K = AKf. \quad (3.4)$$

This is a useful definition because f is a function only of the dimensionless Reynolds number for a given geometrical shape. This is shown in a following discussion, but first let us present how f is related to τ_0 .

For flow in conduits, A is taken to be the wetted surface $2\pi RL$, and K is taken to be the kinetic energy based on the average velocity, that is, $\frac{1}{2}\rho\bar{V}^2$. Thus for flow in a filled pipe of length L , we have

$$F_K = f(2\pi RL)\left(\frac{1}{2}\rho\bar{V}^2\right). \quad (3.5)$$

Combining Eqs. (3.1) and (3.5), we see that

$$f = \frac{\tau_0}{\left(\frac{1}{2}\rho\bar{V}^2\right)}. \quad (3.6)$$

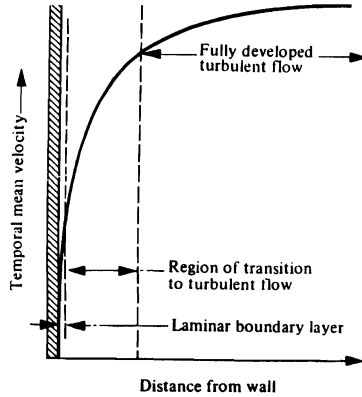


Fig. 3.1 Velocity distribution for turbulent flow in tubes in the region near the wall.

3.1.1 Dimensional analysis for friction factor

Now we resort to *dimensional analysis* which is a method of deducing logical groupings of the variables involved in a process. One of these methods, called the *similarity technique*, is applied to systems which are geometrically similar. For example, in two circular tubes, all comparable lengths have identical ratios. Thus we write

$$K_D = \frac{z_1}{z_2} = \frac{r_1}{r_2} = \frac{D_1}{D_2}, \quad (3.7)$$

where z_1 and z_2 are comparable distances along the lengths of tube; r_1 and r_2 are comparable radii in tubes 1 and 2, respectively.

For the flow system in either tube, the differential equation for the conservation of momentum that applies in the steady state is

$$\eta \left[\frac{1}{r} \frac{d}{dr} \left[r \frac{dv_z}{dr} \right] \right] - \frac{dP}{dz} = 0, \quad (3.8)$$

and a boundary condition is

$$\tau_{rz} \Big|_{r=R} \equiv \tau_0 = -\eta \left[\frac{dv_z}{dr} \right]_{r=R}. \quad (3.9)$$

The differential equation and the boundary condition require certain relationships among velocities, dP/dz , and fluid properties, at corresponding points in the two systems. Thus, in addition to the ratios of Eq. (3.7), we define the ratios for kinematic and dynamic similarity:

$$\begin{aligned} K_v &\equiv \frac{v_{z1}}{v_{z2}} = \frac{\bar{V}_1}{\bar{V}_2}, & K_p &\equiv \frac{dP_1/dz_1}{dP_2/dz_2}, \\ K_\eta &\equiv \frac{\eta_1}{\eta_2}, & K_\rho &\equiv \frac{\rho_1}{\rho_2}. \end{aligned} \quad (3.10)$$

78 Turbulent and Complex Flows

To investigate the conditions which must be satisfied by these ratios, we write Eq. (3.8) specifically for system 1:

$$\eta_1 \left[\frac{1}{r_1} \frac{d}{dr_1} \left[r_1 \frac{dv_{z1}}{dr_1} \right] \right] - \frac{dP_1}{dz_1} = 0. \quad (3.11)$$

Now if we replace r_1 , v_{r1} , etc., by their equivalents in Eqs. (3.7) and (3.10), then we can write Eq. (3.11) for system 2:

$$\left[\frac{K_\eta K_v}{K_D^2} \right] \eta_2 \left[\frac{1}{r_2} \frac{d}{dr_2} \left[r_2 \frac{dv_{z2}}{dr_2} \right] \right] - K_p \frac{dP_2}{dz_2} = 0. \quad (3.12)$$

Multiplying Eq. (3.12) by $K_D/K_v^2 K_p$, we finally obtain:

$$\left[\frac{K_\eta}{K_D K_v K_p} \right] \eta_2 \left[\frac{1}{r_2} \frac{d}{dr_2} \left[r_2 \frac{dv_{z2}}{dr_2} \right] \right] - \left[\frac{K_p K_D}{K_p K_v^2} \right] \frac{dP_2}{dz_2} = 0. \quad (3.13)$$

It is apparent that Eq. (3.13) written with subscripts 1 would also be valid, and because both systems must obey the original differential equation, then

$$\frac{K_\eta}{K_D K_v K_p} = 1 \quad \text{and} \quad \frac{K_p K_D}{K_p K_v^2} = 1,$$

or

$$\frac{D_1 \bar{V}_1 \rho_1}{\eta_1} = \frac{D_2 \bar{V}_2 \rho_2}{\eta_2}, \quad (3.14)$$

and

$$\frac{D_1 (dP_1/dz_1)}{\rho_1 \bar{V}_1^2} = \frac{D_2 (dP_2/dz_2)}{\rho_2 \bar{V}_2^2}. \quad (3.15)$$

The group in Eq. (3.14) is the Reynolds number which, of course, is dimensionless. Once again it appears—in fact, in all cases of forced convection, the Reynolds number is a significant dimensionless group. The group in Eq. (3.15) is another dimensionless group and, as shown in the following paragraph, is actually twice the friction factor.

If we define a new ratio as

$$K_\tau = \tau_{01}/\tau_{02},$$

then the boundary condition, (Eq. 3.9), applied to both systems, yields

$$\frac{K_\tau K_D}{K_\eta K_v} = 1 \quad \text{or} \quad \frac{\tau_{01} D_1}{\eta_1 \bar{V}_1} = \frac{\tau_{02} D_2}{\eta_2 \bar{V}_2}.$$

Dividing by the Reynolds number, we obtain

$$\frac{\tau_{01}}{\rho_1 \bar{V}_1^2} = \frac{\tau_{02}}{\rho_2 \bar{V}_2^2}, \quad (3.16)$$

which are equivalent to half the friction factor (Eq. 3.6). Now the dimensional analysis is complete; it has been shown that for flow in the two arbitrary systems having geometric similarity, the friction factors are equal when the Reynolds numbers are equal. Thus for flow in tubes, the friction factor f may be correlated as a function of the Reynolds number.

3.1.2 Experimental results for friction factor

Experimentally, f can be measured by noting that if F_K is eliminated between Eqs. (3.3) and (3.5), then

$$f = \frac{1}{4} \left[\frac{D}{L} \right] \left[\frac{P_0 - P_L}{\frac{1}{2} \rho \bar{V}^2} \right], \quad (3.17)$$

and the connection with Eq. (3.15) is made apparent. Also, as we have shown, the friction factor is only a function of the Reynolds number: $f = f(\text{Re}_D)$. In most designs the pressure drop is not usually known *a priori*; we therefore use Re_D to evaluate the friction factor and then the pressure drop developed due to friction. Since f is only a function of Re_D , it is sufficient to plot only a single curve of f against $D\bar{V}/\nu$ rather than determine how f varies for separate values of D , \bar{V} , ρ , and η . The lower curve in Fig. 3.2 gives a plot of f versus Re_D for smooth tubes. This curve reflects the laminar and turbulent behavior of fluids in long, smooth, circular tubes. For the laminar region,

$$f = \frac{16}{\text{Re}}, \quad (3.18)$$

which can be derived by using the Hagen-Poiseuille law developed in Chapter 2.

The turbulent region has been established solely by experimental data. The entire turbulent curve closely approximates

$$1/\sqrt{f} = 4.0 \log (\text{Re}\sqrt{f}) - 0.40, \quad (3.19)$$

and a simpler expression exists for $2.1 \times 10^3 < \text{Re} < 10^5$, namely,

$$f = 0.0791 \text{Re}^{-1/4}. \quad (3.20)$$

If the tubes are rough, then in turbulent flow the friction factor is higher than that indicated for smooth tubes. The *relative roughness*, ε/D , enters the correlation where ε is the height of protuberances on the tube wall. For use with Fig. 3.2, we can obtain values of ε from Table 3.1. However, the reader should note that these values apply for new, clean pipes, and even then the values may vary. For old pipes, they may be much higher and certainly ε varies greatly with age, depending on the fluid being transported. In addition, in small pipes, deposits may substantially reduce the inside diameter. Therefore we must carefully use our judgment in estimating a value of ε and consequently of f .

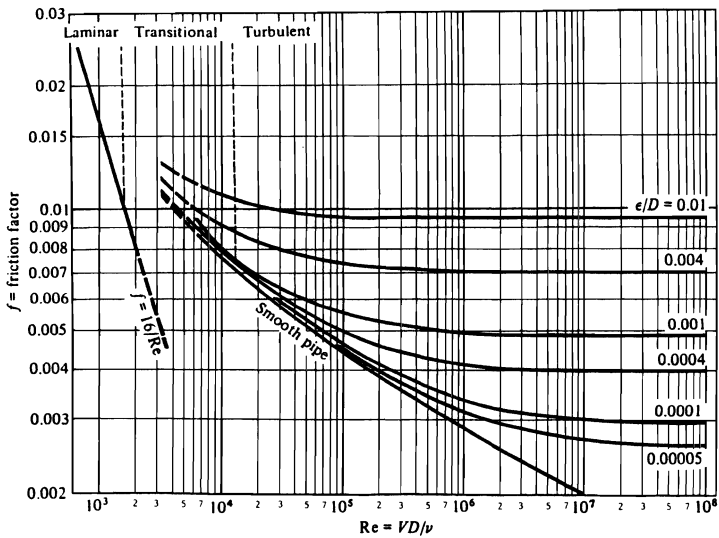


Fig. 3.2 Friction factors for flow in tubes. (Adapted from L. F. Moody, *Trans. ASME* **66**, 671 (1944), and *Mech. Eng.* **69**, 1005 (1947).)

Table 3.1 Values of absolute roughness ϵ for new pipes

	ϵ , mm
Drawn tubing, brass, lead, glass, centrifugally spun cement, bituminous lining, transite	0.0015
Commercial steel or wrought iron	0.046
Welded-steel pipe	0.046
Asphalt-dipped cast iron	0.12
Galvanized iron	0.15
Cast iron, average	0.26

Example 3.1 Determine the mass flow rate (kg s^{-1}) of water at 300 K through 180 m of horizontal pipe, having I.D. of 125 mm, under a pressure drop of $3.5 \times 10^4 \text{ N m}^{-2}$. The relative roughness ϵ/D of the pipe is estimated as 0.001.

Solution. The solution to this problem can be found by using Eq. (3.17) and solving for the average velocity \bar{V} . However, \bar{V} cannot be determined unless f is known and, because $f = f(\text{Re}_D)$, a trial and error solution is in order.

First approximation. In Fig. 3.2, $f = 0.005$ when $\epsilon/D = 0.001$ and $Re = 9 \times 10^5$. For this friction factor, the velocity is

$$\bar{V} = \left\{ \left[\frac{1}{2f} \right] \left[\frac{D}{L} \right] \left[\frac{\Delta P}{\rho} \right] \right\}^{1/2};$$

$$\begin{aligned} \left[\frac{D}{L} \right] \left[\frac{\Delta P}{\rho} \right] &= \frac{0.125 \text{ m}}{180 \text{ m}} \left| \frac{3.5 \times 10^4 \text{ N}}{\text{m}^2} \right| \frac{\text{m}^3}{1,000 \text{ kg}} \left| \frac{1 \text{ kg m}}{1 \text{ N s}^2} \right| \\ &= 2.43 \times 10^{-2} \text{ m}^2 \text{ s}^{-2}. \end{aligned}$$

Therefore

$$\bar{V} = \left\{ \left[\frac{1}{0.01} \right] (2.43 \times 10^{-2}) \right\}^{1/2} = 1.56 \text{ m s}^{-1}.$$

Now we make a second estimate of the Reynolds number and the friction factor. The estimated velocity gives the following Reynolds number:

$$\begin{aligned} Re_D = \frac{D\bar{V}\rho}{\eta} &= \frac{0.124 \text{ m}}{\eta} \left| \frac{1.56 \text{ m}}{\text{s}} \right| \frac{1000 \text{ kg}}{\text{m}^3} \left| \frac{\text{m}^2}{8.55 \times 10^{-4} \text{ N s}} \right| \frac{1 \text{ N s}^2}{1 \text{ kg m}} \\ &= 2.28 \times 10^5. \end{aligned}$$

Second approximation. This Reynolds number gives $f = 0.0052$. Thus, with this f , \bar{V} is corrected slightly.

$$\bar{V} = \left[\frac{0.0050}{0.0052} \right]^{1/2} (1.56) = 1.53 \text{ m s}^{-1}.$$

Therefore, the mass flow rate W is

$$W = \left[\frac{\pi D^2}{4} \right] \rho \bar{V} = \left[\frac{\pi}{4} \right] (0.125)^2 (1000) (1.53) = 18.8 \text{ kg s}^{-1}.$$

3.2 FLOW IN NONCIRCULAR CONDUITS

If the pipes are not circular and turbulent flow exists, then an *equivalent diameter* D_e^* replaces D in the Reynolds number:

$$D_e^* = \frac{4 \times \text{flow area}}{\text{wetted perimeter}} = \frac{4A}{P_w}. \quad (3.21)$$

*Many other texts refer to the hydraulic radius R_h rather than equivalent diameter. In such instances, D is replaced by $4R_h$, where $R_h = A/P_w$; the end result is the same whether D_e or R_h is employed.

82 Turbulent and Complex Flows

With this modification, we can determine the friction factor from Fig. 3.2 where ε/D is replaced by ε/D_e . Similarly in Eq. (3.17), we replace D by D_e , and calculate the pressure drop due to friction in noncircular conduits. This approach gives good results for turbulent flow, but for laminar flow the results are poor. For example, in a thin annulus in which the spacing z is very much less than the width, laminar flow has a parabolic distribution perpendicular to the walls. This situation closely approximates flow between parallel flat plates, and we can show the friction factor to be

$$f = \frac{24}{\text{Re}}. \quad (3.22)$$

This expression, of course, differs from Eq. (3.18) which applies to laminar flow in circular pipes.

For laminar flow in a rectangular duct of dimensions, $z_1 \times z_2$, the friction factor is

$$f = \frac{16}{\phi \text{Re}}. \quad (3.23)$$

Here we evaluate the Reynolds number using D_e , which for rectangular ducts is

$$D_e = \frac{2(z_1 z_2)}{(z_1 + z_2)},$$

and ϕ is given by Fig. 3.3. The laminar-to-turbulent transition for noncircular conduits is still normally taken at a Reynolds number of approximately 2100.

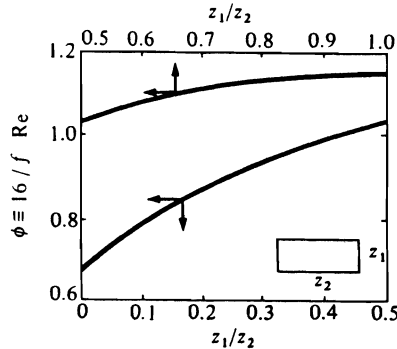


Fig 3.3 Values of ϕ for laminar flow in rectangular ducts. (From W. M. Rohsenow and H. Y. Choi, *Heat, Mass, and Momentum Transfer*, Prentice-Hall, Englewood Cliffs, New Jersey, 1961, page 63.)

3.3 FLOW PAST SUBMERGED BODIES

3.3.1 Turbulent boundary layer on flat plate

In Chapter 2, laminar flow over a flat plate was analyzed. The force exerted by the fluid on one side of the plate (drag force F_K) was calculated for laminar flow as

$$F_K = 0.664 \sqrt{\rho \eta L W^2 V_\infty^3}. \quad (2.104)$$

From Eq. (3.4),

$$f = \frac{F_k}{AK}, \tag{3.4a}$$

where, for this case, the characteristic area is conveniently defined $A = LW$ and the characteristic kinetic energy $K = \frac{1}{2}\rho V_\infty^2$. The friction factor for laminar flow is evaluated by combining Eqs. (2.104) and (3.4a) for laminar flow:

$$f = 1.328 (V_\infty L/\nu)^{-1/2} = 1.328 \text{Re}_L^{-1/2} \tag{3.24}$$

We again see that the friction factor is a function only of a Reynolds number.* These results hold so long as the boundary layer itself remains laminar. However, at a value of Re_∞ , between 300 000 and 500 000 the layer becomes turbulent, increasing significantly in thickness, and displaying a marked change in velocity distribution. We depict this transition in Fig. 3.4 which shows a much steeper gradient near the wall and flatter gradient throughout the remainder of the boundary layer for the turbulent zone. As a result, the shear stress at the wall is greater in the turbulent layer than in the laminar layer.

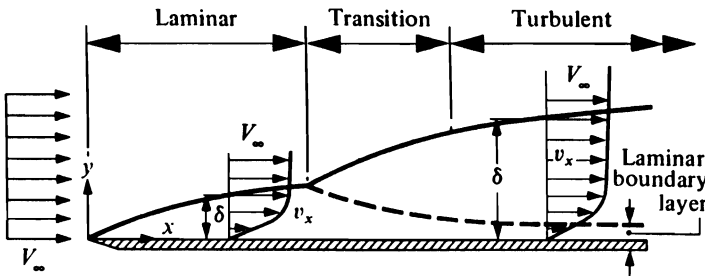


Fig. 3.4 Laminar and turbulent boundary-layers next to a flat plate (the vertical scale is greatly exaggerated).

Using the applicable differential equation, the geometric similarity argument would again indicate that the friction factor is a function of the same dimensionless group, Re . Again, experimental data have been gathered to correlate the friction factor and the Reynolds number. The results in Fig. 3.5 show that the laminar region may extend up to a Reynolds number of about 10^6 . However, this condition is only achieved on smooth surfaces, and if the system is protected against minute external vibrations caused by automobiles equipped with those highly amplified sound systems with special woofers that make the silly "boom-boom" sound or by passing trucks. The results for turbulent flow can be represented as

$$f = \frac{0.455}{(\log \text{Re}_L)^{2.58}}. \tag{3.25}$$

These equations are valid for a flat plate at zero incidence to the flow, providing separation does not occur.

*Most texts on fluid mechanics use the term *drag coefficient* C_D rather than friction factor f , when considering flow past submerged bodies. When the form drag is entirely friction drag, an even more specific term, *skin friction coefficient* C_f is sometimes used.

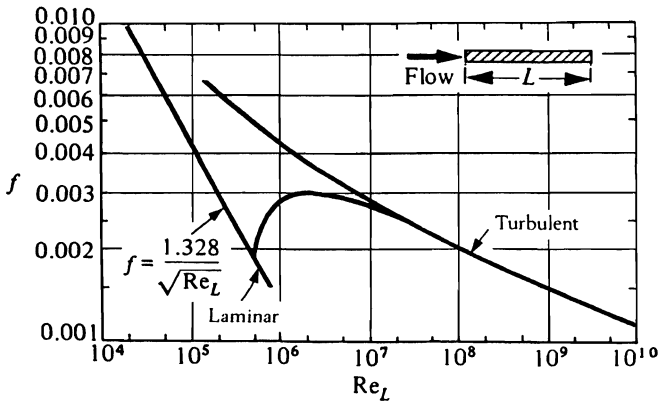
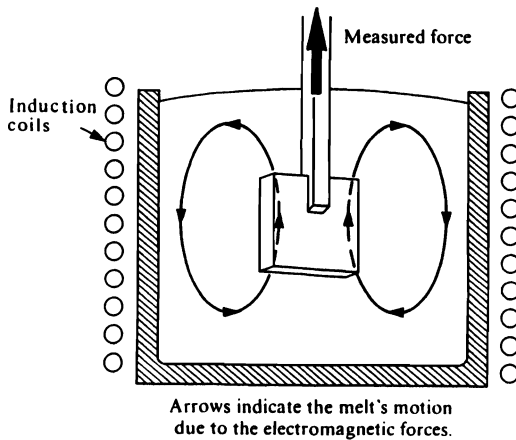


Fig. 3.5 Friction factor for flow parallel to flat plates. (From J. K. Vennard, *Elementary Fluid Mechanics*, Wiley, New York, 1954, page 384.)

Example 3.2 In order to study the mixing action in a molten bath of aluminum contained in an induction furnace, we use a steel *flag*. The flag is held in a vertical position, and placed in the central part of the furnace where the metal flows upward, as depicted in the figure below.



If provisions are made to measure the added force exerted on the flag due to fluid motion, prepare a control chart that relates this force to the velocity of the molten aluminum in the central portion of the furnace. Assume that turbulent flow encompasses the conditions of interest.

- Data:* Viscosity of aluminum, $1.1 \times 10^{-3} \text{ N s m}^{-2}$,
 Density of aluminum, $2.5 \times 10^3 \text{ kg m}^{-3}$,
 Flag dimensions, $0.3 \text{ m} \times 0.3 \text{ m} \times 5 \text{ mm}$ thickness.

Solution. In this problem it is convenient to choose values of Re_L and then calculate the corresponding sets of F_K and V_∞ . The velocity of the aluminum is found by:

$$V_\infty = \frac{\eta}{L\rho} Re_L,$$

and then we can write the corresponding force exerted by the moving aluminum on both sides of the flag:

$$F_K = 2f(LW)\left(\frac{1}{2}\rho V_\infty^2\right) = fLW\rho \left[\frac{\eta^2}{L^2\rho^2} Re_L^2 \right] = f \left[\frac{W}{L} \right] \left[\frac{1}{\rho} \right] (\eta^2 Re_L^2).$$

For $Re_L = 10^6$, Fig. 3.5 gives $f = 0.0045$.

$$V_\infty = \frac{1.1 \times 10^{-3} \text{ N s}}{\text{m}^2} \Big| \frac{0.3 \text{ m}}{0.3 \text{ m}} \Big| \frac{\text{m}^3}{2.5 \times 10^3 \text{ kg}} \Big| \frac{10^6}{10^6} \Big| \frac{1 \text{ kg m}}{1 \text{ N s}^2}$$

$$= 1.46 \text{ m s}^{-1},$$

and

$$F_K = \frac{0.0045}{0.0045} \Big| \frac{0.3 \text{ m}}{0.3 \text{ m}} \Big| \frac{1 \text{ m}^3}{2.5 \times 10^3 \text{ kg}} \Big| \frac{(1.1 \times 10^{-3})^2 \text{ N}^2 \text{ s}^2}{\text{m}^4} \Big| \frac{10^{12}}{10^{12}} \Big| \frac{1 \text{ kg m}}{1 \text{ N s}^2}$$

$$= 2.18 \text{ N}.$$

In a similar manner, the corresponding values of V_∞ and F_K can be found for other values of Re_L .

Re_L	f	$V_\infty, \text{ m s}^{-1}$	$F_K, \text{ N}$
10^5	0.0072	0.146	0.035
5×10^5	0.0051	0.73	0.62
10^6	0.0045	1.46	2.18
2×10^6	0.0039	2.92	7.56
5×10^6	0.0034	7.30	41.2

3.3.2 Flow past a sphere and other submerged objects

In Chapter 2, we analyzed laminar flow past a sphere, and gave the kinetic force of the fluid exerted on the sphere:

$$F_K = 6\pi\eta RV_\infty. \tag{2.119}$$

We have found that this force, often termed the *drag force*, is composed of two parts: the *friction drag* and the *form drag*. In a well-streamlined body (flow parallel to a flat plate, airplane wing, hull of a boat, etc.), the friction drag not only forms the major part of the total drag, but may even comprise it entirely. In the case of a body with sharp corners, or a sphere, or a cylinder oriented normally to flow, separation occurs, and a turbulent wake forms.

86 Turbulent and Complex Flows

With a plate oriented perpendicularly to flow, the separation always occurs at the same point, and the wake extends across the full projected width of the body, as shown in Fig. 3.6; this results in almost all form drag comprising the drag force. If the body has curved sides, the location of the separation point is determined according to whether the leading boundary layer is laminar or turbulent, as depicted in Fig. 3.7. In turn, this location determines the size of the wake and the amount of the form drag. After this brief introduction, let us now consider some of the available data.

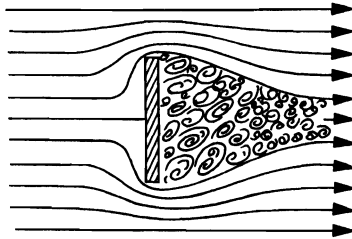


Fig. 3.6 Wake formation for flow normal to flat plate.

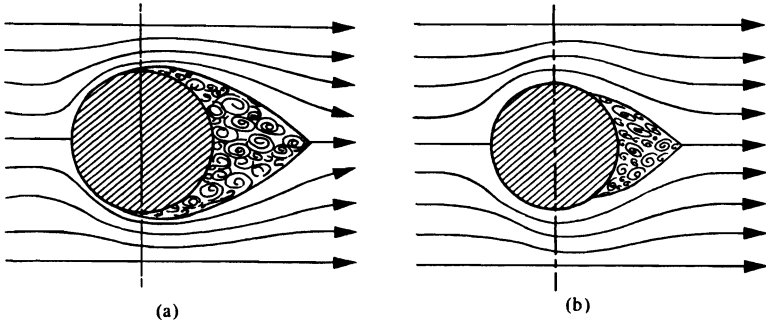


Fig. 3.7 Separation of boundary layer and wake formation with a cylinder or sphere immersed in a flowing fluid when (a) the leading boundary layer is laminar, and (b) the leading boundary layer is turbulent.

For the presentation of data, we use Eq. (3.4). As we come across the friction factor again, let us repeat the expression

$$F_K = fAK; \quad (3.4)$$

K still remains $\frac{1}{2}\rho V_\infty^2$, but for shapes such as spheres, cylinders, ellipsoids, etc., we choose the area A as the projected area normal to the flow. For example, for flow past a sphere, F_K takes the form

$$F_K = (\pi R^2) \left(\frac{1}{2} \rho V_\infty^2 \right) f. \quad (3.26)$$

From Stokes' law, which is the result of an analytical solution for creeping flow around a sphere, we can write the following equation by rearranging Eq. (2.119):

$$F_K = (\pi R^2) \left(\frac{1}{2} \rho V_\infty^2 \right) \left[\frac{24}{DV_\infty/\nu} \right]. \quad (3.27)$$

By comparing Eqs. (3.26) and (3.27), we obtain the friction factor (drag coefficient) for laminar flow past a sphere:

$$f = \frac{24}{Re} \tag{3.28}$$

Once again, the friction factor is a function of the Reynolds number. This is also true for turbulent flow but, as you may suspect, Eq. (3.28) does not apply for all velocities, and experimental correlation is sought in the form of $f = f(Re)$. Figure 3.8 shows such a correlation for spheres, as well as for some other geometrical shapes. We also include Fig. 3.9 to indicate other possibilities. Note that Stokes' law applies up to $Re \cong 1$ for spheres.

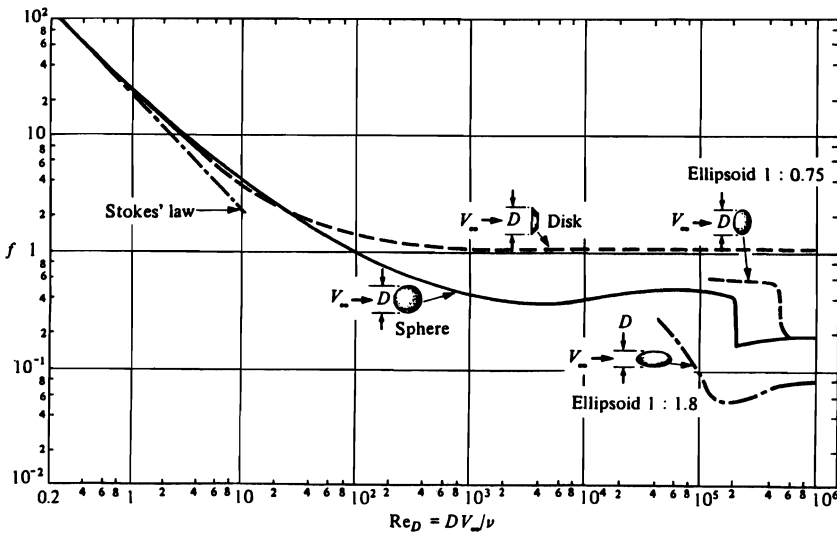


Fig. 3.8 Friction factors for submerged bodies. (Adapted from F. Eisner, *Proc. 3rd Intern. Congr. Appl. Mech.*, 1930, page 32.)

The phenomenon of boundary-layer separation has a major effect on the form drag. This effect is noticeable at large Re where the form drag comprises most of the total drag. At this high Re , the transition to turbulent flow occurs before separation, and the separation point is moved farther downstream, as illustrated in Fig. 3.7, thereby reducing the friction factor.

In materials processing, the discussed principles of flow past submerged bodies mostly apply to situations in which the body moves in a fluid. The friction factors are determined experimentally, and it makes no difference whether the body moves in a still fluid or is held stationary while the fluid flows past it. However, when the body is irregularly shaped, friction factors which are measured while the body is stationary may not be applicable when the body moves, because during free motion the orientation of the body may change rapidly and repeatedly.

It is often desirable to separate particulate mixtures of solids. These mixtures may consist of particles of the same material which have different sizes (homogeneous mixtures), or they may consist of particles of different materials and various sizes (heterogeneous mixtures).

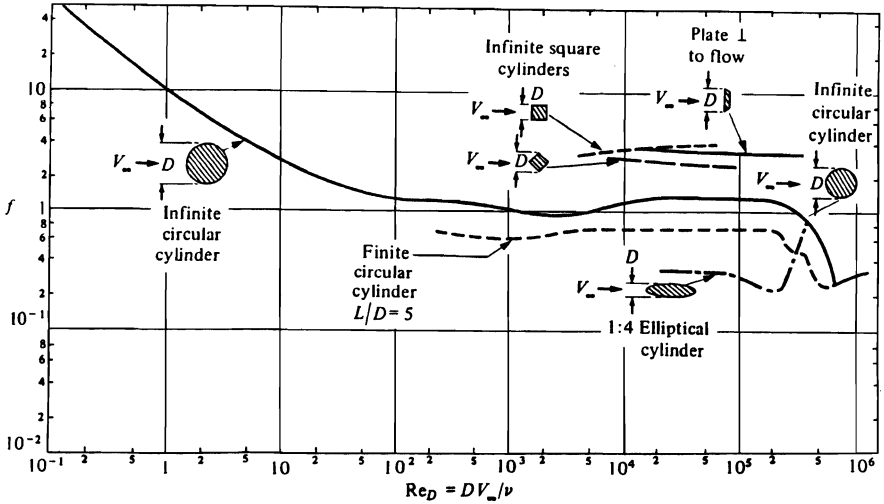
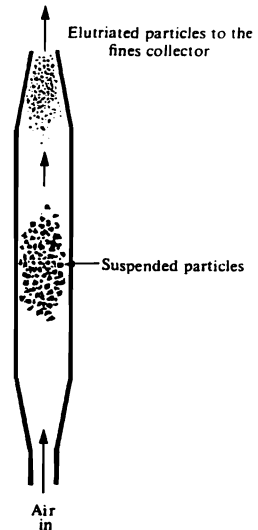


Fig. 3.9 Friction factors for submerged bodies. (Adapted from F. Eisner, *Proc. 3rd Intern. Congr. Appl. Mech.*, 1930, page 32.)

Homogeneous mixtures can be separated by screening, but for separating mixtures of fine sizes, free settling or centrifugal methods are preferred. In general, screening does not work for heterogeneous mixtures, and therefore separation is gained by free settling or centrifugal methods.

Example 3.3 With either metallic or ceramic powders, it is important to separate homogeneous mixtures in the range of particles sizes from 10 to 250 μm . For this purpose we apply the principle of air elutriation, which is illustrated by the device shown to the right. The force exerted by the air stream is great enough to suspend particles of a given diameter, and all particles of smaller diameter are carried upward and to the collector of fines. Larger particles fall back against the air stream and down into a settling chamber. For the effective operation of this device it is necessary to know the size of particles suspended at a given flow rate.

Assuming that a spherical particle, with a density of 4000 kg m^{-3} , applies to a homogeneous mixture of iron powder, draw a graph that relates the diameter of suspended particles to the velocity of the air in the expanded portion of the tube.



Solution. To obtain the solution, recognize that particles which have terminal velocities equal to the upward air velocities are those which remain suspended. Further, examine the criterion that Stokes' law applies for $Re_D < 1$ and that a simple expression for the diameter may be appropriate.

For air at 300 K, the fluid properties are $\eta = 1.80 \times 10^{-5} \text{ kg m}^{-1} \text{ s}^{-1}$ and $\rho = 1.18 \text{ kg m}^{-3}$. The largest particle that can be supported by the flow of air can be determined with the aid of a force balance. For upward flowing air:

$$F_K + \frac{4}{3}\pi R^3 \rho g = \frac{4}{3}\pi R^3 \rho_s g,$$

with ρ = density of the air and ρ_s = density of the solid. We substitute Eq. (3.26) for F_K and solve for V_∞ ; the result is

$$V_\infty = \left[\frac{8Rg(\rho_s - \rho)}{3f\rho} \right]^{1/2}.$$

Therefore, we determine V_∞ by trial and error as a function of R , because f depends upon V_∞ and R through the Reynolds number.

We can start with the smallest particles, $D = 2R = 10^{-5} \text{ m}$, and assume that Stokes' law applies; therefore

$$f = \frac{24\eta}{DV_\infty\rho} = \frac{12\eta}{RV_\infty\rho},$$

and

$$V_\infty = \frac{2R^2(\rho_s - \rho)g}{9\eta}.$$

Notice that this is just a rearrangement of Eq. (2.121).

$$V_\infty = \frac{(2)(0.5 \times 10^{-5})^2(4000)(9.8)}{(9)(1.80 \times 10^{-5})} = 1.21 \times 10^{-2} \text{ m s}^{-1}.$$

The corresponding value of Re_D is

$$Re_D = \frac{DV_\infty\rho}{\eta} = \frac{(10^{-5})(1.21 \times 10^{-2})(1.18)}{(1.80 \times 10^{-5})} \approx 0.008,$$

so that Stokes' law applies, at least for the smallest particles. Similar calculations can be repeated for all particles with diameters up to $50 \mu\text{m}$; Stokes' law is not valid for larger particles.

For larger particles, a trial and error method is used. Starting with $R = 7 \times 10^{-5} \text{ m}$, and the *first approximation* for V_∞ as 1 m s^{-1} , we get $Re_D = 9.2$. From Fig. 3.8, $f \approx 4.5$ and we calculate V_∞

$$V_\infty = \left[\frac{(8)(7 \times 10^{-5})(9.8)(4000)}{(3)(4.5)(1.18)} \right]^{1/2} = 1.17 \text{ m s}^{-1}.$$

90 Turbulent and Complex Flows

We see that a *second approximation*, at least, is needed. With $V_\infty = 1.35 \text{ m s}^{-1}$, $\text{Re}_D = 12.4$ and $f \approx 3.5$. Another recalculation for V_∞ yields

$$V_\infty = (1.17) \left[\frac{4.5}{3.5} \right]^{1/2} = 1.33 \text{ m s}^{-1}$$

which is very close to our assumed velocity of 1.35 m s^{-1} . The procedure is repeated for particle diameters up to $250 \mu\text{m}$. The results are tabulated below.

Particle diameter, μm	Velocity, m s^{-1}
10	0.012
20	0.048
40	0.19
70	0.62
140	1.33
200	2.05
250	2.65

3.4 FLOW THROUGH POROUS MEDIA

Granular solids or agglomerates of fine particles occur in many materials processing systems, ranging from sinter plants for agglomerating iron ores to the production of intricate parts via alloy powders or ceramic powders. In solidifying castings, there are regions in which solid and liquid coexist, and at least for a significant fraction of the solidification period the intermingled liquid (i.e., the interdendritic liquid) can convect through the stationary solid network (i.e., the dendritic solid). Convection of this type is a major cause of macrosegregation in cast products. Other applications in materials processing include the production of metal matrix composites by infiltration of alloy melts through ceramic fiber preforms and the use of reticulated ceramic foams as filter media for the refinement of molten metal.

The flow of fluids through porous media is not simple, especially because of the effect of the complex geometry of the solids on the flow. Therefore, we rely largely on empirical measurements of a system parameter, known as the *permeability*, or on measurements of friction factors.

3.4.1 Darcy's Law

If the flow occurs under low pressure gradients, that is it is slow enough, then the rate of flow is proportional to a pressure drop per unit length of the porous medium, $\Delta P'/L$:

$$Q = \frac{k_D A \Delta P'}{L}, \quad (3.29)$$

$\Delta P'$ is $\Delta P \pm \rho g L$, depending on the direction of flow.

where Q = volume flow rate, $\text{m}^3 \text{s}^{-1}$, A = cross-sectional area, m^2 , and k_D = permeability coefficient, a constant that depends on the fluid, temperature, and packing characteristics with units of $\text{m}^4 \text{N}^{-1} \text{s}^{-1}$. Equation (3.29), which is known as Darcy's law, is based on the experiments of Darcy in the middle of the nineteenth century.¹

The k_D in Eq. (3.29) is sometimes called the *permeability*, which is satisfactory provided we carry out the test with the same fluid at the same temperature, but it is more common and better to define a *specific permeability* \mathcal{P} by means of

$$k_D = \frac{\mathcal{P}}{\eta}, \quad (3.30)$$

where η is the viscosity of the fluid. This makes \mathcal{P} specific to the geometry of the solid phase only; therefore we can make predictions of the flows of other fluids, regardless of temperature. Actually \mathcal{P} is almost always used, rather than k_D , and it is commonly called the permeability instead of the specific permeability.

The units of permeability are m^2 , but some of the older data are in the unit called *Darcy*, defined as

$$1 \text{ Darcy} = 1 \times 10^{-12} \text{ m}^2.$$

Unfortunately the reader might even encounter a different Darcy in the British Standard Specification (BSS), which is

$$1 \text{ Darcy (BSS)} = 0.987 \times 10^{-12} \text{ m}^2.$$

As a starting point for analyzing unidirectional flow in porous media, Eq. (3.29) is usually written in terms of a pressure gradient and a *superficial velocity*, which is defined as $v_x = Q/A$; then

$$v_x = -\frac{\mathcal{P}}{\eta} \left[\frac{\partial P}{\partial x} - \rho g_x \right]. \quad (3.31)$$

If the flow is not unidirectional, then the superficial velocity has components v_x , v_y and v_z , the pressure gradient has components $\partial P/\partial x$, $\partial P/\partial y$ and $\partial P/\partial z$, and the body force has components ρg_x , ρg_y and ρg_z . With vector notation, therefore,

$$\mathbf{V} = -\frac{\mathcal{P}}{\eta} (\nabla P - \rho \mathbf{g}). \quad (3.32)$$

Example 3.4 An important characteristic of foundry molding sands is the allowance for the permeation of gases. Accordingly, the permeability of molding sands is routinely measured for process quality control purposes. Calculate the permeability of a sample of molding sand, 30 mm dia. by 60 mm length, through which 10^3 m^3 of air flows in 15 s under a pressure drop of 600 N m^{-2} .

¹The original paper by Darcy is not readily available, but a reproduction is in M. K. Hubbert, *The Theory of Ground-Water Motion and Related Papers*, Hefner Publishing, New York, NY, 1969, pp. 303-311.

92 Turbulent and Complex Flows

Solution. The flow through the sample is unidirectional so we can start with Eq. (3.31). The flow is steady, and $g_x = -g$; therefore

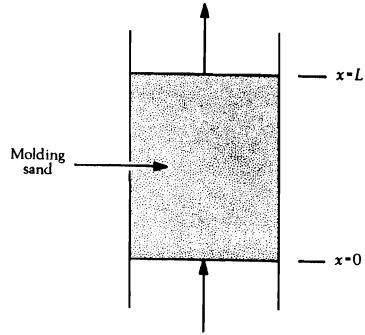
$$v_x = -\frac{\mathcal{P}}{\eta} \left[\frac{dP}{dx} + \rho g \right],$$

or

$$\frac{dP}{dx} = - \left[\rho g + \frac{v_x \eta}{\mathcal{P}} \right].$$

This is integrated with ρ constant, $P = P_0$ at $x = 0$ and $P = P_L$ at $x = L$. The result is

$$v_x = \frac{\mathcal{P}}{\eta} \left[\frac{P_0 - P_L}{L} - \rho g \right].$$



The minus sign results because the flow is antiparallel to gravity; if it is parallel then $+\rho g$ appears. Recall our goal is to calculate \mathcal{P} , so let's gather all of the terms:

$$v_x = \frac{Q}{A} = \frac{(4)(10^{-3}) \text{ m}^3}{(\pi)(0.03)^2 \text{ m}^2} \Bigg| \frac{1}{15 \text{ s}} = 9.43 \times 10^{-2} \text{ m s}^{-1}$$

$$\frac{P_0 - P_L}{L} = \frac{600 \text{ N}}{\text{m}^2} \Bigg| \frac{1}{0.06 \text{ m}} \Bigg| \frac{1 \text{ kg m}}{1 \text{ N s}^2} = 10^4 \text{ kg m}^{-2} \text{ s}^{-2}$$

$$\rho g = \frac{1.223 \text{ kg}}{\text{m}^3} \Bigg| \frac{9.8 \text{ m}}{\text{s}^2} = 12 \text{ kg m}^{-2} \text{ s}^{-2}$$

$$\eta = 1.90 \times 10^{-5} \text{ N s m}^{-2} = 1.90 \times 10^{-5} \text{ kg m}^{-1} \text{ s}^{-1}$$

Therefore,

$$\begin{aligned} \mathcal{P} &= \frac{\eta v_x}{\left[\frac{P_0 - P_L}{L} - \rho g \right]} = \frac{1.90 \times 10^{-5} \text{ kg}}{\text{m s}} \Bigg| \frac{9.43 \times 10^{-2} \text{ m}}{\text{s}} \Bigg| \frac{\text{m}^2 \text{s}^2}{10^4 \text{ kg}} \\ &= 17.9 \times 10^{-11} \text{ m}^2. \end{aligned}$$

This permeability is considered to be high for molding sands; a typical value would be 2×10^{-11} to $4 \times 10^{-11} \text{ m}^2$.

3.4.2 Tube-bundle theory and Ergun's equation

Darcy's law is an empirically observed law. However, a semitheoretical approach to the problem yields Darcy's law with more insight into the effect of the packing on \mathcal{P} . The theory, which is known as the *tube-bundle theory*, regards the porous medium as a bundle of tangled tubes with weird cross-sections. It is assumed that the packing is uniform without isolated porosity, that there is no *channeling* of flow, and that the diameter of the column is much greater than that of the particles. To start with, we look to the Hagen-Poiseuille formula for laminar flow in Chapter 2 (Eq. 2.33). By analogy, we say that

$$\bar{V} = K_1 \frac{\Delta P' R_h^2}{L\eta}, \quad (3.33)$$

where K_1 = constant of proportionality, and \bar{V} = average velocity in the interstices of the porous medium. If flow is unidirectional and in the x -direction, then let $V_0 = v_x$, the superficial velocity.

Engineers usually know V_0 rather than \bar{V} ; it is defined by

$$V_0 = Q/A,$$

where A is the cross-sectional area of the column and Q is the volume flow rate. Since,

$$V_0 = \bar{V}\omega, \quad (3.34)$$

then

$$V_0 = K_1 \frac{\Delta P' R_h^2 \omega}{L\eta}. \quad (3.35)$$

where ω = void fraction (also called voidage or porosity). The concept of the *hydraulic radius* R_h was introduced with the equivalent diameter (Eq. 3.21).

For porous media, R_h is defined as

$$R_h = \frac{\text{average cross section available for flow}}{\text{average wetted perimeter}} = \frac{A_h}{P_w}. \quad (3.36)$$

By the average wetted perimeter, we mean the average total boundary line between the fluid and the packing, viewed by a slice through the column normal to the axis of the column. Thus, in a column of length L ,

$$R_h = \frac{\text{volume available for flow}}{\text{total wetted perimeter}} = \frac{A_h L}{P_w L}. \quad (3.37)$$

Here $A_h L$ is also the volume of fluid in the packing, and if both the numerator and denominator of Eq. (3.37) are normalized by the column volume, we obtain

$$R_h = \frac{A_h L/V}{P_w L/V} = \frac{\omega}{S}, \quad (3.38)$$

where $S = S_0(1 - \omega)$.

94 Turbulent and Complex Flows

The factor S_0 is the total surface area of solid per unit volume of solid, while S is the total surface area per unit volume of the column. From this,

$$R_h = \frac{\omega}{S_0(1 - \omega)}. \quad (3.39)$$

We may substitute Eq. (3.39) into Eq. (3.35) and obtain

$$V_0 = K_1 \frac{\Delta P'}{L\eta S_0^2} \frac{\omega^3}{(1 - \omega)^2}. \quad (3.40)$$

Equation (3.40), which is the form of the pressure-drop relationship for flow through packed columns, is valid for the lower range of Reynolds numbers (creeping flow region), where K_1^{-1} has been found to equal 4.2.² Insertation of this value into Eq. (3.40) gives

$$V_0 = \frac{1}{4.2} \frac{\Delta P'}{L\eta S_0^2} \frac{\omega^3}{(1 - \omega)^2}, \quad (3.41)$$

which is the *Blake-Kozeny* equation. Note that this is the same as the Darcy equation, where

$$k_D = \frac{\omega^3}{4.2\eta S_0^2(1 - \omega)^2}, \quad (3.42)$$

or

$$\mathcal{P} = \frac{\omega^3}{4.2S_0^2(1 - \omega)^2}. \quad (3.43)$$

These equations emphasize the fact that k_D depends on the properties of both the fluid and solid, while \mathcal{P} depends only on the properties of the solid phase.

According to the flow behavior in all forced convection systems, a fluid velocity is eventually reached beyond which laminar flow no longer prevails. Under these conditions, we again resort to the use of a friction factor which can be correlated solely as a function of a Reynolds number. For packed beds, the modified friction factor may be measured by

$$f_c = \frac{\Delta P' \omega^3}{LS_0 \rho V_0^2 (1 - \omega)}. \quad (3.44)$$

This is analogous to Eq. (3.17). We utilize a modified Reynolds number for packed beds in the correlation

$$\text{Re}_c = \frac{\rho V_0}{\eta(1 - \omega)S_0}. \quad (3.45)$$

²S. Ergun, *Chem. Eng. Prog.* **48**, 93 (1952). The constant 4.2 is not universally selected; some believe the value to be as high as 5.0, based on a paper by P. C. Carman, *Trans. Inst. Chem. Eng.* **15**, 150 (1937). These are reasonable values for granular materials and spherical particles but are certainly not valid for other solid morphologies or for higher values of ω . For example, these factors are substantially different for packings that comprise fibers or even for uniform size spheres that are not consolidated.

When the flow exceeds that for $Re_c \cong 2$, then Eq. (3.41) no longer applies and we use Fig. 3.10. The equation

$$\frac{\Delta P}{L} = \frac{4.2\eta V_0 S_0^2 (1 - \omega)^2}{\omega^3} + \frac{0.292\rho V_0^2 S_0 (1 - \omega)}{\omega^3} \quad (3.46)$$

describes the entire curve analytically; the second term on the right describes the pressure drop under highly turbulent flow conditions. In dimensionless groups,

$$f_c = \frac{4.2}{Re_c} + 0.292. \quad (3.47)$$

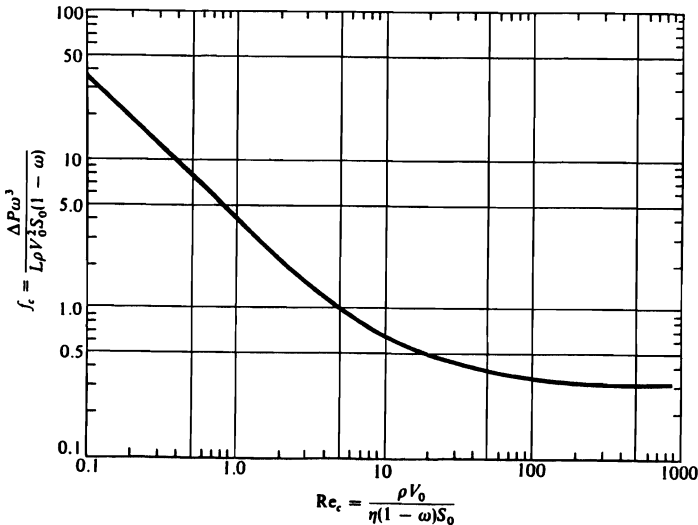


Fig. 3.10 Pressure-drop correlation for flow through packed beds. (Based on S. Ergun, *Chem. Eng. Prog.* 48, 93 (1952).)

When applying this expression to gases, we take the density of the gas as the arithmetic average of the end densities. For large pressure drops, however, it is better to apply Eq. (3.46), to express pressure gradient in the differential form, and to integrate over the bed thickness, taking into account the variations in density, viscosity, and superficial velocity.

Thus far, we have defined the modified Reynolds number and friction factor in terms of S_0 , the particle surface area per unit particle volume. If the particles in the bed are spheres of uniform size, S_0 may be easily related to the diameter, D_p , by

$$S_0 = \frac{\pi D_p^2}{(\pi D_p^3/6)} = \frac{6}{D_p}. \quad (3.48)$$

Then Eq. (3.46) becomes

$$\frac{\Delta P}{L} = \frac{150\eta V_0 (1 - \omega)^2}{D_p^2 \omega^3} + \frac{1.75\rho V_0^2 (1 - \omega)}{D_p \omega^3}, \quad (3.49)$$

96 Turbulent and Complex Flows

which is known as *Ergun's equation*. It is then useful to define a new friction factor which is often associated with Ergun's work:

$$f_E = 6f_c = \frac{D_p \Delta P \omega^3}{L \rho V_0^2 (1 - \omega)}, \quad (3.50)$$

and a new Reynolds number

$$\text{Re}_E = 6 \text{Re}_c = \frac{D_p \rho V_0}{\eta (1 - \omega)}. \quad (3.51)$$

Now, in dimensionless form, Eq. (3.49) becomes

$$f_E = \frac{150}{\text{Re}_E} + 1.75. \quad (3.52)$$

When a bed contains a mixture of different-size particles, the question arises as to what should be used for D_p in Eqs. (3.49)-(3.51). To this day, the question is still unanswered, but a suggestion commonly put forward (although not adequately tested) is to use the *volume-surface mean diameter*, \bar{D}_{vs} . This parameter is discussed in the following paragraph.

For a bed containing a mixture of different-size *spherical particles*, S_0 may be determined from the specific surface of the mixture, S_w (surface area per mass of particles). If the material is screened, and the diameter of each size fraction, \bar{D}_{p_i} , is taken as the arithmetic mean of the openings of the two screens defining the corresponding mass fraction, $\Delta\phi_i$, collected between them, then

$$S_w = \frac{6}{\rho_p} \sum_{i=1}^n \frac{\Delta\phi_i}{\bar{D}_{p_i}}, \quad (3.53)$$

where n is the number of screens used, and ρ_p is the density of the particulate material. The average particle diameter for this mixture is called the *volume-surface mean diameter*, defined as

$$\bar{D}_{vs} = \frac{6}{S_w \rho_p}. \quad (3.54)$$

Noting that $S_0 = S_w \rho_p$, then

$$S_0 = \frac{6}{\bar{D}_{vs}}, \quad (3.55)$$

and, by comparing Eq. (3.55) with Eq. (3.48), the proper value of D_p to use is \bar{D}_{vs} .

Finally, the situation arises that we have a bed of nonspherical particles. In this case, we define a shape factor λ , which does not depend on particle size and which is a function of the shape of the particles only, by:

$$S_0 = \frac{6\lambda}{D_p}. \quad (3.56)$$

Here D_p is a characteristic dimension of the particle, and thus serves to define λ .^{*} For a cube or a sphere, the simplest choice for D_p is the edge length or the diameter, respectively, and for both, λ is then unity. For screened irregular particles, D_p corresponds to \bar{D}_{vs} , in which \bar{D}_p is still the arithmetic mean of the screen openings. With this definition of D_p , corresponding values of λ for screened materials are given in Table 3.2.

Table 3.2 Shape factors for screened particles

Substance	Type of measurement	Shape factor, λ
Sand (jagged)	Permeability	1.68 ¹
Sand (nearly spherical)	Permeability	1.15 ¹
Sand (angular)	Permeability	1.49 ¹
Sand (flakes)	Permeability	2.54 ¹
Sand (rounded)	Metallographic	1.24 ¹
Crushed glass (jagged)	Metallographic	1.54 ¹
Coal (pulverized)	Metallographic	1.37 ¹
Coal dust (up to 10 mm)	Metallographic	1.54 ¹
Tungsten powder	Metallographic	1.12 ¹
Cu hot	Settling techniques	1.00 ²
Sand	Settling techniques	1.59 ²
Coal	Settling techniques	1.72 ²
Silimanite	Settling techniques	1.72 ²
Limestone	Settling techniques	2.20 ²
Flake graphite	Settling techniques	7.96 ²
Crushed and screened ores		1.75 ³

¹Values calculated from data presented by P. C. Carman, *Trans. Inst. Chem. Eng.* **15**, 155 (1937).

²Derived from data in F. A. Zenz and D. F. Othmer, *Fluidization and Fluid Particle Systems*, Reinhold, New York, 1960, pages 184, 213.

³Typical value suggested by A. M. Gaudin, *Principles of Mineral Dressing*, McGraw-Hill, New York, 1939, page 132.

Now, replace D_p in Eq. (3.49) by D_p/λ or \bar{D}_{vs}/λ , and other forms of Ergun's equation evolve:

Uniform size particles

$$\frac{\Delta P}{L} = \frac{150\eta V_0 \lambda^2}{D_p^2} \frac{(1 - \omega)^2}{\omega^3} + \frac{1.75\rho V_0^2 \lambda}{D_p} \frac{(1 - \omega)}{\omega^3} \tag{3.57a}$$

Nonuniform size particles

$$\frac{\Delta P}{L} = \frac{150\eta V_0 \lambda^2}{\bar{D}_{vs}^2} \frac{(1 - \omega)^2}{\omega^3} + \frac{1.75\rho V_0^2 \lambda}{\bar{D}_{vs}} \frac{(1 - \omega)}{\omega^3} \tag{3.57b}$$

^{*}We alert the reader that there are other shape factors used in particle technology. Another often used one is defined as the surface area divided by the surface area of a sphere with the same volume.

98 Turbulent and Complex Flows

We should caution the reader that the literature in this field abounds with confusion concerning the definition of D_p for nonspherical particles, and the shape factor λ . In general, values of λ are very difficult to obtain, and therefore pressure drop equations utilizing D_p , such as Eq. (3.49), are not of much use unless the particles are spherical. It is usually more satisfactory to use Eq. (3.46), determining S_0 by means of permeability tests and Eq. (3.43).

Example 3.5 Sintering of iron ore is an important metallurgical process in which gases must penetrate through a bed of solids. In this process, loosely packed fine particles of ore are sintered into larger particles by passing air through the bed, which in turn reacts with admixed coal to develop very high temperatures in the sinter. It is necessary that large amounts of air can pass through the bed without creating large pressure drops, which would require unduly large fans.

Calculate the pressure drop, prior to ignition, across a bed of sinter 0.305 m deep ($\omega = 0.39$) for air flowing at 289 K and with $V_0 = 0.25 \text{ m s}^{-1}$. The surface area S measures 8100 m^2 . For air: $\rho = 1.23 \text{ kg m}^{-3}$ and $\eta = 1.78 \times 10^{-5} \text{ N s m}^{-2}$.

Solution.

$$\text{Re}_c = \frac{\rho V_0}{\eta S} = \frac{(1.23)(0.25)}{(1.78 \times 10^{-5})(8100)} = 2.13.$$

Using Eq. (3.46), we get

$$\frac{\Delta P}{L} = \frac{\rho V_0^2 S}{\omega^3} \left[\frac{4.2}{\text{Re}_c} + 0.292 \right] = 2.38 \times 10^4 \text{ N m}^{-3}.$$

$$\Delta P = (2.38 \times 10^4)(0.305) = 7.25 \times 10^3 \text{ N m}^{-2}.$$

3.4.3 Wall effect

It is probably obvious to the reader that the container diameter must be a good deal larger than the mean particle diameter of the packing, in order for the above equations to be valid, since the void fraction at the wall will be larger than the bulk value of ω . This *wall effect* is demonstrated in Fig. 3.11, which shows that the container diameter should be approximately 20 times the particle diameter in order for Eq. (3.46) to predict the pressure drop to within 10% for Re_c between 2 and 150. If necessary, we may first compute the pressure drop using Eq. (3.46), and then use Fig. 3.11 for correction.

3.4.4 Applications

With Examples 3.4 and 3.5, we pointed out the application of relationships for flow through porous media to the testing and control of permeability in foundry molding sand and in estimating pressure drop requirements for flow in a sinter bed of iron ore.

In powder metallurgy, the permeability of a sintered metal compact is of importance because it is a measure of the relationship between processing variables and the pore structure developed during sintering, and because, in some instances, the flow of a fluid through a

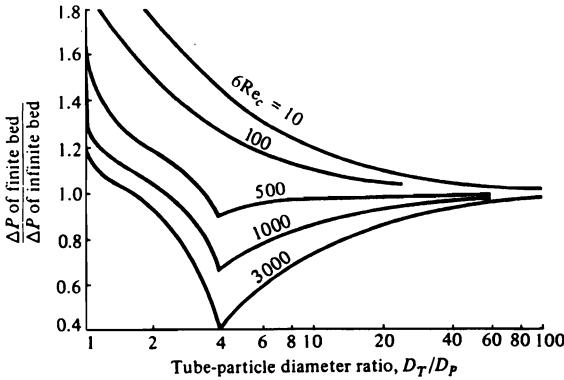


Fig. 3.11 Correction factor for wall effect. (Derived by H. E. Rose and A. M. Rizk, *Proc. Inst. Mech. Engrs.*, London, **60**, 493 (1950).)

porous sintered metal part is important. Self-lubricating bearings and porous metal filters for air, water, etc., can serve as examples.

Morgan³ used the following form of the Ergun equation for steady flow conditions through porous sintered metal:

$$\frac{\Delta P}{L} = \frac{\eta V_0}{\phi} + \frac{\rho V_0^2}{\Phi}, \tag{3.58}$$

where ϕ is called the viscous permeability, and Φ the inertial permeability; V_0 , η , and ρ are defined as before. We should compare this equation with Eq. (3.46), from which it appears that

$$\phi = \frac{\omega^3}{4.2S_0^2(1 - \omega)^2} \equiv \mathcal{P} \quad \text{and} \quad \Phi = \frac{\omega^3}{0.292S_0(1 - \omega)}.$$

Now, at low values of ω , S_0 is the surface area *seen* by the fluid, and there may be internal porosity which is not connected to any flow channels, and which contributes to the ω determined *in situ*. Because the total ω is then too large, S_0 measured in this manner will be larger than the true value of S_0 . The ω used when the isolated pore volume becomes significant should only be the interconnected void volume fraction.

Another complication in the use of the above relationships to estimate ϕ and Φ is the use of the constants 4.2 and 0.292, which are only valid for granular type packings with $0.3 < \omega < 0.6$. For a variety of particle sizes of partially sintered metal powders, German⁴ gives empirical results as

$$\phi = 4.6 \times 10^{-11} \bar{D}_{vs}^{0.73} \omega^{6.8}, \tag{3.59}$$

³V. T. Morgan, *Symposium sur la Metallurgie des Poudres*, Editions Metaux (sponsored by Société Française de Metallurgie), Paris, June, 1964, page 419.

⁴R. M. German, *Powder Technol.* **30**, 81 (1981).

and

$$\Phi = 3.9 \times 10^{-6} \bar{D}_{vs}^{0.92} \omega^{6.4}. \quad (3.60)$$

Equations (3.59) and (3.60) require that the unit of \bar{D}_{vs} is μm , with $59 \leq \bar{D}_{vs} \leq 715 \mu\text{m}$ (measured before sintering) and $0.25 \leq \omega \leq 0.56$.

As mentioned above the compressibility of a gas, with flow accompanied by a large pressure drop, should be taken into account. That effect and also the effect of a large mean free path of the gas relative to the pore size can be included with the equations given here. German⁵ has presented an excellent exposition of flow of gases through porous materials that includes these added factors.

During the solidification of dendritic alloys, there is a *mushy zone* comprising dendritic solid and interdendritic liquid. In general the liquid convects, and it is desirable to analyze this convection because it is a major cause of macrosegregation in cast products. The analysis is very complex with one complexity being the fact that ω (the volume fraction of liquid) varies spatially and temporally as solidification proceeds.

Because $\omega \rightarrow 1$ in some parts of the mushy zone, Darcy's law by itself is not a sufficient representation of the momentum equation. Ganesan and Poirier⁶ derived the momentum equation and then Nandapurkar et al.⁷ used it to analyze convection during solidification. For illustrative purposes, we give only the x -component of the momentum equation for the mushy zone with a fixed solid and convecting liquid:

$$\begin{aligned} \omega \frac{\partial(v_x/\omega)}{\partial t} + \frac{1}{\omega} \left[v_x \frac{\partial v_x}{\partial x} + v_y \frac{\partial v_x}{\partial y} + v_z \frac{\partial v_x}{\partial z} \right] \\ + v_x \left[v_x \frac{\partial}{\partial x} (1/\omega) + v_y \frac{\partial}{\partial y} (1/\omega) + v_z \frac{\partial}{\partial z} (1/\omega) \right] = +\omega g_x \\ - \frac{\omega}{\rho} \frac{\partial P}{\partial x} + \nu \left[\frac{\partial^2 v_x}{\partial x^2} + \frac{\partial^2 v_x}{\partial y^2} + \frac{\partial^2 v_x}{\partial z^2} \right] - \frac{\nu \omega}{\mathcal{P}} v_x, \end{aligned} \quad (3.61)$$

where v_x , v_y and v_z are the components of the superficial velocity. The last term on the right-hand-side of Eq. (3.61) is the Darcy term. The reader can deduce the y - and z -components of the momentum equation.

The utility of Eq. (3.61) is that it allows for a transition in the convection in the interior of the mushy zone to the region where there is only liquid remaining in the solidifying mass ($\omega = 1$). In the interior of the mushy zone where $\omega < 0.6$, the Darcy term dominates to the extent that it, along with the body force term and the pressure gradient term, comprise the momentum equation; therefore

$$0 = +\omega g_x - \frac{\omega}{\rho} \frac{\partial P}{\partial x} - \frac{\nu \omega}{\mathcal{P}} v_x.$$

⁵R. M. German, *Int. J. Powd. Metall. Powd. Tech.* **15**, 23 (1979).

⁶S. Ganesan and D. R. Poirier, *Metall. Trans.* **B 21B**, 173 (1990).

⁷P. J. Nandapurkar, D. R. Poirier and J. C. Heinrich, *Numerical Heat Transfer*, Part A **19**, 101 (1991).

This can be rearranged and put into the exact form of Eq. (3.31). Hence, Darcy's law is certainly adequate when ω is small enough. On the other hand, when $\omega \rightarrow 1$, $\mathcal{P} \rightarrow \infty$ and Eq. (3.61) reduces to the x -component of the Navier-Stokes' equation (see Eq. (D)) in Table 2.2), as it should.

Permeability data for flow through dendritic networks are presented in Poirier.⁸ Darcy's law has also been applied to study the infiltration of metal through both particulates⁹ and fiber preforms for the production of metal matrix composites.¹⁰ In the latter, the authors gave two useful relationships of permeability for flow through fibrous preforms. In both it is assumed that the fibers are continuous, with parallel axes located on a square grid. The first is

$$\mathcal{P} = \frac{0.427 a^2}{(1 - \omega)} [1 - f(\omega)]^4 [1 + 0.473 (f^{-1}(\omega) - 1)] \quad (3.62)$$

for flow parallel to the fiber axes, where a is the radius of the fiber and $f(\omega)$ is a function of the porosity given by

$$f(\omega) = \left[\frac{2(1 - \omega)}{\pi} \right]^{1/2}$$

Equation (3.62) is valid for $0.21 \leq \omega \leq 0.5$. The second equation is

$$\mathcal{P} = \frac{2\sqrt{2} a^2}{9(1 - \omega)} [1 - \sqrt{2}f(\omega)]^{5/2} \quad (3.63)$$

for flow perpendicular to the fiber axes. Equation (3.63) is applicable when $0.21 \leq \omega \leq 0.8$. An exhaustive review of permeability data for flow through fibrous porous media, particularly highly porous structures, is given by Jackson and James.¹¹

3.5 FLUIDIZED BEDS

For an up-draft packed column, an upper limit exists for the fluid flow rate. Let us consider what happens if the flow rate through a *static* bed steadily increases. The pressure drop across the bed increases steadily with increasing flow rate until, at a certain point, the bed expands slightly, and the individual particles become supported in the fluid stream with freedom to move relative to each other. At this point, the bed is no longer static, and is said to be *fluidized*. The void fraction at this point, ω_{mf} , corresponds to the loosest possible packing of the material in a fixed-bed configuration, and this is usually greater than the initial fixed-bed voidage, so that some internal rearrangement of the bed takes place prior to the onset of fluidization, as shown in Fig. 3.12. With increasing velocity, the bed expands, or ω increases. If this expansion is uniform, with the interparticle spacing increasing uniformly, then we speak of *particulate fluidization*. Bed expansion continues until the velocity required to balance or support a single particle acting alone is reached, which is the terminal or free-

⁸D. R. Poirier, *Metall. Trans. B* **18B**, 245 (1987).

⁹P. B. Maxwell, G. P. Martins, D. L. Olson and G. R. Edwards, *Metall. Trans. B* **21B**, 475 (1990).

¹⁰A. Mortensen, L. J. Masur, J. A. Cornie and M. C. Flemings, *Metall. Trans. A* **20A**, 2535 (1989).

¹¹G. W. Jackson and D. F. James, *Can. J. Chem. Eng.* **64**, 364 (1986).

fall velocity, V_f . This point is reached when ω approaches 1, and from that point on, the pressure drop is determined by the equation for flow through an empty tube. At velocities above V_f , the particles are entrained and blow out of the reactor. Figure 3.12 shows the various stages of fluidization schematically.

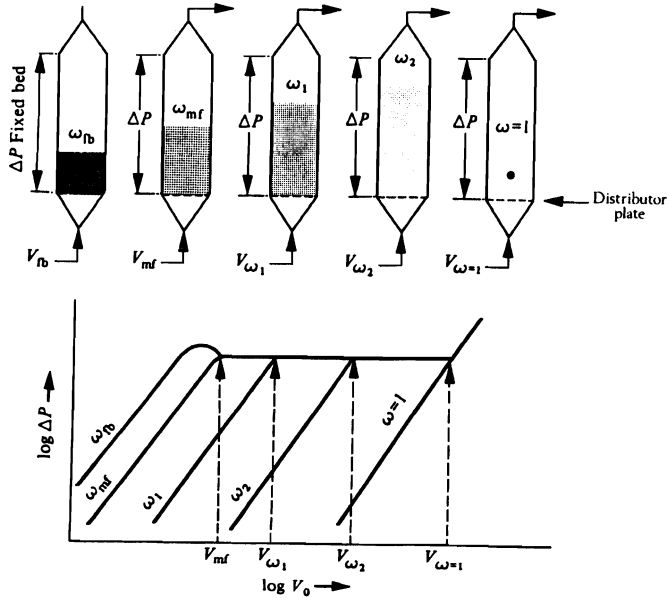


Fig. 3.12 Schematic representation of the relationship between the void fraction in the fluidized bed, the superficial velocity, and the pressure drop across the entire reactor, for particulate fluidization.

In Section 3.3.2 we discussed friction factors for flow past individual particles. In a fluidized bed, the particles, although suspended by the gas stream, exhibit a varying friction factor as the voidage varies, until finally at $\omega = 1$ the friction factor is the same as that for the suspended condition. When Eq. (3.26) is equated to the gravity force exerted on the particle less the buoyancy force, it can be shown that

$$f = \frac{4}{3} \frac{D_p(\rho_p - \rho_f)g}{\rho_f V_0^2}, \tag{3.64}$$

where the subscripts p and f represent the particles and fluid, respectively, and V_0 is the velocity of the fluid. In a fluidized bed, V_0 is taken as the superficial velocity which is defined as the volume flow rate of fluid through the bed divided by the cross-sectional area of the bed.

Zenz¹² proposed that for a fluid-solid system there are two operating characteristics that can be established: (1) the velocity-particle size relation at the condition of minimum fluidization (a fluidized bed's minimum possible fixed-bed configuration with ω_{mf}) and (2) the terminal velocity of the largest significant particle in the bed, where $\omega = 1$. He then pointed out that since the data of Fig. 3.8 were correlated by a plot of f versus Re , it is possible to

¹²F. A. Zenz, *Petrol. Refiner.* **36**, 147 (1957).

form new dimensionless parameters that contain D_p and V_0 separately and express the same data. These new dimensionless parameters are

$$\left[\frac{\text{Re}}{f} \right]^{1/3} = \frac{V_0}{\left[\frac{4g\eta_f(\rho_p - \rho_f)}{3\rho_f^2} \right]^{1/3}}, \quad (3.65)$$

and

$$(f\text{Re}^2)^{1/3} = \frac{D_p}{\left[\frac{3\eta_f^2}{4g\rho_f(\rho_p - \rho_f)} \right]^{1/3}}. \quad (3.66)$$

In Eqs. (3.65) and (3.66), f is given by Eq. (3.64) and the Reynolds number is defined with V_0 as the characteristic velocity. When the data of Fig. 3.8 are plotted in this way, a single curve corresponding to the terminal velocity at $\omega = 1$ is found.

Applying this same methodology to the experimental data of Wilhelm and Kwauk¹³ and other investigators who determined V_{mf} , the superficial velocity at minimum fluidization when particulate fluidization occurred, Zenz found a generalized empirical graph that describes the other boundary of the particulate fluid bed regime. For void fractions as the bed expands from ω_{mf} to $\omega = 1$, other experimental data also can be explained by the same correlation. The resulting set of curves is given in Fig. 3.13 with lines of constant void fraction and Re given.

Leva et al.¹⁴ give a relation for calculating V_{mf} :

$$V_{mf} = \frac{0.0007 g(\rho_p - \rho_f) D_p^2}{\eta_f} \text{Re}^{-0.063} \quad (3.67)$$

This can be rearranged to

$$\left[\frac{\text{Re}}{f} \right]^{1/3} = \frac{\text{Re}^{0.645}}{12.4}, \quad (3.68)$$

which falls essentially on the line for $\omega = 0.4$ on Fig. 3.13. Their data are for $0.35 \leq \omega \leq 0.45$ and $\text{Re} \leq 5$. The data of Frantz¹⁵ can similarly be shown to fit

$$\left[\frac{\text{Re}}{f} \right]^{1/3} = \frac{\text{Re}^{2/3}}{9.8}, \quad (3.69)$$

¹³R. H. Wilhelm and M. Kwauk, *Chem. Engr. Prog.* **44**, 201 (1948).

¹⁴M. Leva, T. Shirai and C. Y. Werr, *Genie Chim.* **75**, 33 (1956).

¹⁵J. F. Frantz, *Chem. Engr.* **69**, 161 (1962).

104 Turbulent and Complex Flows

which differs only slightly from that of Leva et al. Wen and Yu¹⁶ use a Galileo number, which is simply (fRe^2) and again falls in place on Fig. 3.13. Davison and Harrison¹⁷ worked the void fraction into their correlation:

$$V_{mf} = \frac{0.0055 \omega_{mf}^3}{(1 - \omega_{mf})} \cdot \frac{g D_p (\rho_p - \rho_f)}{\nu}, \quad (3.70)$$

which can be rearranged to

$$\left[\frac{Re}{f} \right]^{1/3} = \left[\frac{\omega^3}{1 - \omega} \right]^{1/3} \frac{Re^{2/3}}{5.67}. \quad (3.71)$$

When $\omega = 0.4687$, Eq. (3.71) reduces to Eq. (3.69).

There is another mode of fluidization besides *particulate fluidization* (in which the bed is assumed to expand essentially uniformly). The other mode is known as *aggregative fluidization*, in which the fluid tends to rise through the bed in discrete bubbles, and aggregates of particles circulate in the bed. Usually, gas-solid beds exhibit aggregative fluidization, and liquid-solid beds exhibit particulate fluidization.

The expansion of the bed in aggregative fluidization may be estimated using

$$\frac{H}{H_0} = 1 + \frac{V_0 - V_{mf}}{2.21 \sqrt{D_B}}, \quad (3.72)$$

where H_0 = height of bed (m) at minimum fluidization velocity, V_{mf} , $m\ s^{-1}$,
 H = height of bed (m) at superficial velocity, V_0 , $m\ s^{-1}$

and

$2.21 \sqrt{D_B}$ = the terminal rate of rise ($m\ s^{-1}$) of bubbles of diameter, D_B (m),
 through a freely bubbling bed.

More accurately, D_B should be expressed as a function of position in the bed, since as a gas bubble rises it expands as the pressure of the bed above it decreases. This relationship can be expressed as

$$\frac{D_B}{D_{Bi}} = 0.15 \frac{L_B}{D_{Bi}} + 0.85, \quad (3.73)$$

where D_B is the bubble diameter at height L_B above the distributor, and

D_{Bi} = the initial bubble diameter at the distributor
 = $P/2$ where P is the penetration of the gas into the bed from the orifice
 with diameter D_0 in the distributor, from Fig. 3.14.

In Fig. 3.14, V_{OR} is the average velocity of the gas through the orifice (m) and ρ_g is the density of the gas ($kg\ m^{-3}$).

¹⁶C. Y. Wen, and Y. H. Yu, *Fluid Particle Technology*, Chem. Engr. Prog. Symp. Ser., No. 62, AIChE, New York, 1966.

¹⁷J. F. Davison and D. Harrison, *Fluidized Particles*, Cambridge University Press, 1963.

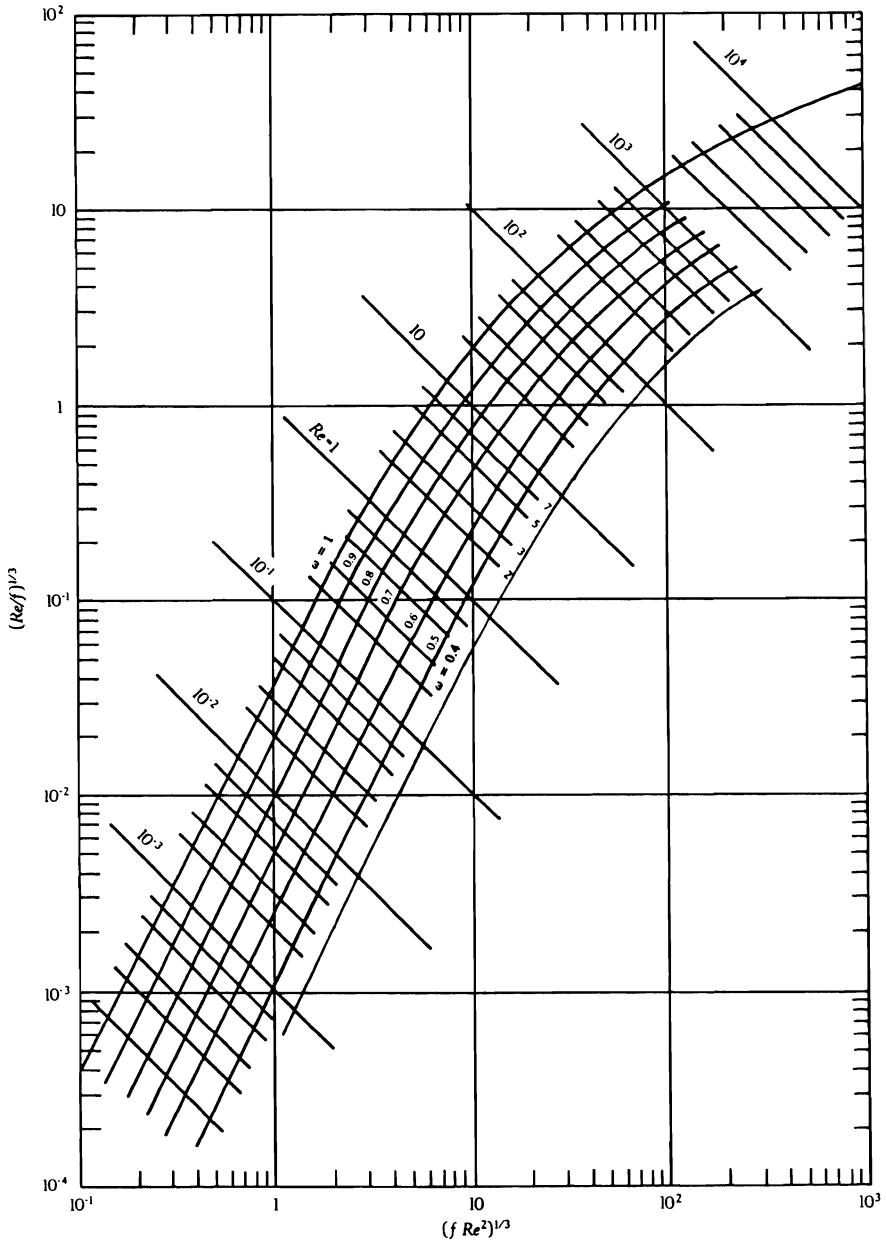


Fig 3.13 Smoothed correlation of particulate fluidization. (From F. A. Zenz and D. F. Othmer, *Fluidization and Fluid Particle Systems*, Reinhold Publ. Corp., New York, NY, 1960, page 236.)

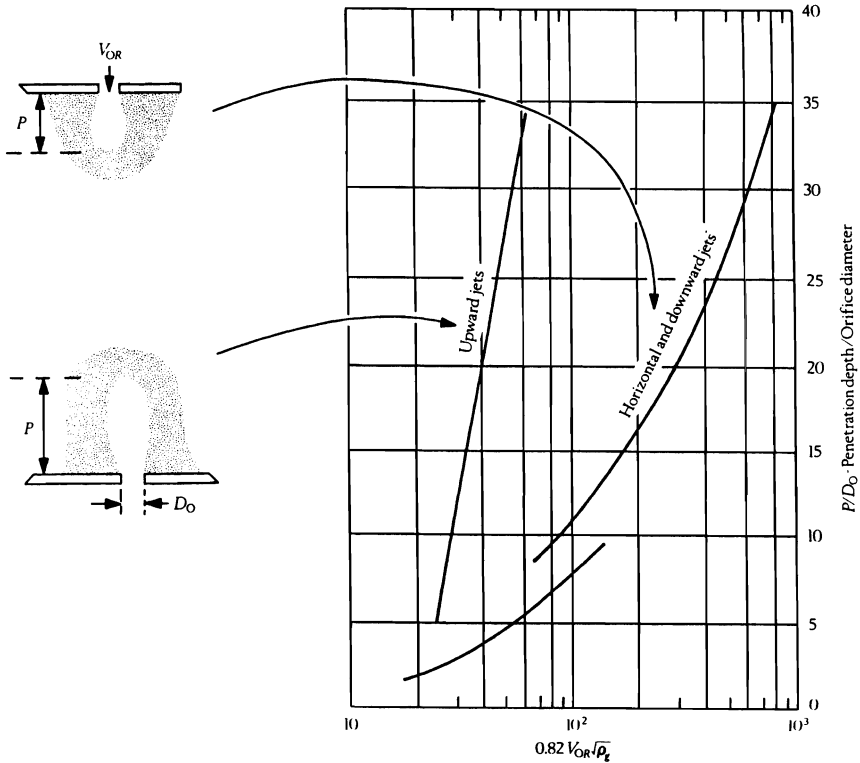


Fig 3.14 Jet penetration into fluid-particle media. (From F. A. Zenz, *Fluidization and Fluid-Particle Systems, Vol. II*, Pemm-Corp. Publ., Nelsonville, NY, 1989, page 114.)

There are many practical problems associated with the design of fluidized beds, particularly the design of distributor plates and tuyeres. For an excellent discussion of this entire topic and much practical advice, the reader is referred to Zenz,¹⁸ to Cheremisinoff and Gupta,¹⁹ and to Kunii and Levenspiel.²⁰

Fluidized beds are utilized in materials processing with increasing frequency. They have the ability to provide good gas-solid contact and therefore to carry out gas-solid reactions efficiently. Examples include the roasting of sulfide ores (e.g., ZnS) to oxides; the conversion of oxide particles, such as TiO₂, to gaseous products, such as TiCl₄; and the reduction of oxides to metal, such as Fe₂O₃ to Fe, or to carbides, such as Fe₃C. They have the additional capability to transfer heat to parts immersed in them more efficiently than

¹⁸F. A. Zenz, *Fluidization and Fluid-Particle Systems, Vol. II*, Pemm-Corp. Publ., Nelsonville, NY, 1989.

¹⁹N. P. Cheremisinoff and R. Gupta (editors), *Handbook of Fluids in Motion*, Butterworths, Boston, 1983, Chaps. 23-26.

²⁰D. Kunii and O. Levenspiel, *Fluidization Engineering*, Second Edition, Butterworths-Heinemann, Boston, 1991.

would gas alone, so they are used as heat transfer devices (see Chapter 8). And they make it possible to contact powdered solids evenly onto surfaces of parts immersed in them, so they are used to produce polymeric coatings on unusually shaped parts, and in a similar operation to build up ceramic shell molds for investment castings.

Example 3.6 Consider the design of a fluid bed to recover uranium from U_3O_8 nuclear fuel elements by fluorinating it to UF_6 . The U_3O_8 is fed into a fluidized bed of Al_2O_3 particles (90% by weight), fluidized with N_2 at 750 K to which a small amount of F_2 has been added. The properties of the materials involved are:

	ρ (kg m ⁻³)	η (N s m ⁻²)	D_p (m)
U_3O_8	8.3×10^3	—	?
Al_2O_3	3.9×10^3	—	1.2×10^{-4}
N_2 (750 K)	0.48	3.4×10^{-5}	—

Since the bed is primarily Al_2O_3 , the gas flow must be enough to exceed minimum fluidization velocity for the Al_2O_3 , yet not be so high as to carry out the U_3O_8 particles. The question is: What size U_3O_8 particles will stay in the bed?

Solution. Since the Al_2O_3 particles are uniformly sized, the void fraction at minimum fluidization will be just above that of the bed at rest, which would be about 0.4. Assume $\omega_{mf} = 0.45$.

Calculate

$$(fRe^2)^{1/3} = \frac{D_p}{\left[\frac{3\eta^2}{4g\rho_f(\rho_s - \rho_f)} \right]^{1/3}} = \frac{1.2 \times 10^{-4}}{\left[\frac{(3)(3.4 \times 10^{-5})^2}{(4)(9.8)(0.48)(3900 - 0.48)} \right]^{1/3}} = 3.32.$$

Entering Fig. 3.13 at $(fRe^2)^{1/3} = 3.32$ and $\omega = 0.45$, obtain a value of $(Re/f)^{1/3} = 0.0095$ from which V_{mf} can be calculated:

$$(Re/f)^{1/3} = \frac{V_{mf}}{\left[\frac{4g\eta_f(\rho_p - \rho_f)}{3\rho_f^2} \right]^{1/3}}.$$

$$V_{mf} = (0.0095) \left[\frac{(4)(9.8)(3.4 \times 10^{-5})(3900)}{(3)(0.48)^2} \right]^{1/3} = 0.019 \text{ m s}^{-1}.$$

Now calculate the entrainment velocity of the Al_2O_3 . $(fRe^2)^{1/3}$ is still 3.32, but now enter Fig. 3.13 and, for $\omega = 1.0$, obtain $(Re/f)^{1/3} = 0.41$. The corresponding velocity is now 0.82 m s^{-1} . Therefore, the operating velocity of the bed will be between 0.019 and 0.82 m s^{-1} . For a void fraction of 0.8 , V_0 will be 0.26 m s^{-1} .

The entrainment velocity of the reacted U_3O_8 particles must be calculated to see if it will stay in the reactor. At a bed operating velocity of 0.26 m s^{-1} , for the U_3O_8 ,

$$(Re/f)^{1/3} = \frac{0.26}{\left[\frac{(4)(9.8)(3.4 \times 10^{-5})(8300)}{(3)(0.48)^2} \right]^{1/3}} = 0.103.$$

108 Turbulent and Complex Flows

For $\omega = 1.0$ (elutriation), this gives $(fRe^2)^{1/3} = 1.5$. Therefore, the smallest particle of U_3O_8 that will remain in the bed will be

$$D_p = (1.5) \left[\frac{(3)(3.4 \times 10^{-5})^2}{(4)(9.8)(0.48)(8300 - 0.48)} \right]^{1/3} = 4.2 \times 10^{-5} \text{ m.}$$

Any particles of U_3O_8 smaller than this will be carried out of the bed when they reach the top.

PROBLEMS

3.1 Water at 300 K is flowing through a brass tube that is 30.0 m long and 13 mm in diameter (inner). The water is moving through the tube at a rate of $3.2 \times 10^{-3} \text{ m}^3 \text{ s}^{-1}$. The density of water is 1000 kg m^{-3} , and its viscosity is $8.55 \times 10^{-4} \text{ N s m}^{-2}$. Calculate the pressure drop in Pa that accompanies this flow.

3.2 Evaluate the pressure drop in a horizontal 30 m length of galvanized rectangular duct (30.0 mm x 75.0 mm) for the following conditions:

- An average air flow velocity of 0.46 m s^{-1} at 300 K and atmospheric pressure.
- An average air flow velocity of 4.6 m s^{-1} at 300 K and atmospheric pressure. The density and viscosity are 1.16 kg m^{-3} and $1.85 \times 10^{-5} \text{ N s m}^{-2}$.

3.3 For flow in tubes (smooth wall) the friction factor is given by Eq. (3.20) for $2.1 \times 10^3 < Re < 10^5$. What is the percent change in the pressure drop if the tube diameter is doubled for the same volume flow rate, same fluid and the same tube length? Assume that Eq. (3.20) for the friction factor applies.

3.4 Show that for flow through a slit with a spacing that is much less than the width, Eq. (3.22) gives the friction factor for laminar flow.

3.5 Determine the size of the largest alumina particle in Problem 2.14 that would be expected to obey Stokes' law, remembering that for spheres this law is valid for $Re \leq 1$.

3.6 A falling-sphere viscometer was used to determine the viscosity of a slag intended for the production of copper. The viscosity of the slag was determined to be 441.2 Poise, using a steel ball as the falling sphere. Is this a valid viscosity? Why or why not? If not, determine the real value of the viscosity and then calculate its kinematic viscosity. The density of the slag may be taken as one-half that of the steel ball.

Data: Radius of steel ball, 88.7 mm; terminal velocity of steel ball, 1.52 m s^{-1} .

3.7 Two spheres of equal density and different diameters fall through a liquid with an unknown density and an unknown viscosity. The diameter of the larger sphere is twice the diameter of the smaller sphere.

- With an appropriate force balance, derive an equation for the terminal velocity of either sphere. Your equation should be valid for any Reynolds number.
- Assume that $10^3 < Re_p < 2 \times 10^5$ for both spheres and calculate the ratio of the terminal velocity of the larger to that of the smaller.
- Assume that $Re_p < 1$ for both spheres, and calculate the ratio of terminal velocities.

3.8 Bubbles that rise through liquids may be treated as rigid spheres provided they are small enough. Assume that a spherical bubble of air has a diameter of 1 mm at the bottom of a glass melt that is 1 m deep.

- Calculate the pressure in the bubble as a function of the distance below the top surface of the glass. Neglect added pressure within the bubble because of the surface tension.
- Calculate the diameter of the bubble as a function of the distance below the top surface of the glass.
- Neglecting acceleration effects, calculate the velocity of the bubble as a function of distance below the top surface of the glass. *Data for melt:* Temperature is 1700 K; viscosity is 2.0 N s m^{-2} ; density is 3000 kg m^{-3} . Assume that air behaves as an ideal gas with a molecular weight of $28.8 \text{ kg kmol}^{-1}$.

3.9 A thermocouple tube lies in a melt that is flowing perpendicular to the axis of the tube. Calculate the force per unit length of tube exerted by the flowing metal. *Data:* Velocity of the melt is 3 m s^{-1} ; viscosity is $2 \times 10^{-3} \text{ N s m}^{-2}$; density of the melt is 8000 kg m^{-3} ; diameter of thermocouple tube is 61 mm.

3.10 A packed bed reduction-reactor, 15.0 m high and 6.0 m in diameter, is packed with spherical metal oxide pellets ($D_p = 3 \text{ mm}$). A reducing gas enters the top of the bed at 800 K and at a rate of 95 kg s^{-1} and exits the reactor at the same temperature. What should the pressure at the top of the reactor be if the pressure at the bottom of the reactor is maintained at $1.4 \times 10^5 \text{ Pa}$. *Data:* Bed porosity, ω is 0.40; viscosity of the reducing gas at 800 K is $4.13 \times 10^{-5} \text{ N s m}^{-2}$; density of the gas at atmospheric pressure and 800 K is 0.5 kg m^{-3} .

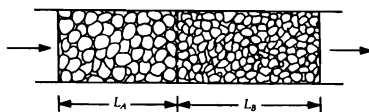
3.11 In a packed bed reactor (diameter = 4.5 m and height = 18 m), metal oxide *A* forms a central column within the reactor, having a diameter of 3.0 m, while pellets of metal oxide *B* fill the annulus between metal oxide *A* and the wall of the reactor. The pressure at the top of the bed is maintained at $6.9 \times 10^4 \text{ Pa}$, while the pressure at the bottom is kept at $1.72 \times 10^5 \text{ Pa}$. Calculate the fraction of reducing gas that passes through metal oxide *A*. It may be assumed that the temperature and reducing gas density are uniform throughout the reactor. Furthermore, turbulent flow conditions prevail.

Data for A: $\omega = 0.40$, $D_p = 76 \text{ mm}$.

Data for B: $\omega = 0.25$, $D_p = 19 \text{ mm}$.

3.12 Preliminary experimental studies have shown that the porosity in a newly developed packed bed reactor is $\omega < 0.6$. The pellets have a diameter of 30.0 mm and the reducing gas flows through the bed at a rate of 0.025 kg s^{-1} . The reactor has $3.0 \text{ m} \times 3.0 \text{ m}$ square cross section and is 15 m in height. A constant pressure difference of 690 Pa is maintained between the inlet and outlet nozzles, and it may be assumed that the temperature is uniform throughout the reactor. You are required to evaluate the bed porosity. The properties of the gas are $\eta = 2.07 \times 10^{-5} \text{ N s m}^{-2}$ and $\rho = 1.2 \text{ kg m}^{-3}$ (average).

3.13 Molten aluminum is passed through a horizontal filter bed of Al_2O_3 spheres in order to remove drossy oxides from the aluminum. The filter bed comprises two different packings arranged in series.



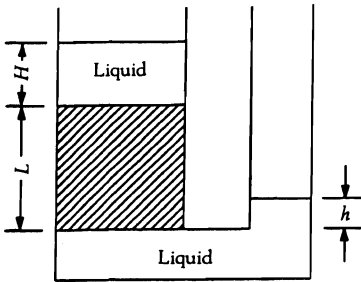
110 Turbulent and Complex Flows

The first packing encountered by the flow captures large drossy particles, and the second packing captures the smaller drossy particles. Given $L_A = 0.7 L_B$, $\omega_A = \omega_B$, $D_{p,A} = 2D_{p,B}$, compute the ratio of the pressure drop through A to the pressure through B for a) very low Reynolds numbers, and b) very high Reynolds numbers.

3.14 Derive an equation for the pressure drop through an isothermal column of a porous medium, that accompanies the flow of a compressible gas. Assume that the gas follows ideal behavior.

3.15 For unidirectional flow through a column of a porous medium, show that Eq. (3.61) reduces to Eq. (3.31).

3.16 In a *falling head permeameter*, the permeability is determined by measuring the difference in height between two liquid columns. In the apparatus depicted below, H decreases and h increases as liquid flows by gravity through the porous medium of length L . Derive an equation that gives h as a function of time t , assuming that \mathcal{P} is uniform and constant.



Cross-sectional areas of the larger and smaller columns of liquid are A and a , respectively.

3.17 The tube bundle theory for permeability predicts

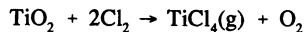
$$\mathcal{P} = \frac{\omega^3}{K S_0^2 (1 - \omega)^2}$$

where K is a constant. Assuming that Eq. (3.55) applies, does the tube bundle theory compare to the empirical result given by Eq. (3.59)?

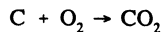
3.18 Consider Eqs. (3.62) and (3.63) and assume that the aspect ratio of the fibers is sufficiently large that the fibers can be assumed to have infinite lengths.

- Derive an equation for the relationship between S_0 and a .
- Does the equation for permeability given in Problem 3.17 predict the permeabilities for flow through fibrous media?

3.19 In the production of titanium (Ti), rutile ore (TiO_2) is fluidized with gaseous chlorine and the following reaction occurs:



The rate of this reaction is controlled by the removal of the oxygen by reaction with coke particles in the reactor, according to



The rutile ore, prior to being placed in the reactor, was analyzed according to size. The following ranges of particle diameters, D_p , were found:

$180 \leq D_p < 250 \mu\text{m}$	5%
$150 \leq D_p < 180 \mu\text{m}$	6.2%
$106 \leq D_p < 150 \mu\text{m}$	77.4%
$75 \leq D_p < 106 \mu\text{m}$	11.4%

Using the above data, calculate the possible chlorine mass flow rates (at 1223 K) that are needed to fluidize the ore in a reduction reactor that is 1.2 m in diameter and 10 m in height.

3.20 A bed of particles of uniform size is fluidized such that the bed voidage is 0.6 when the Reynolds number is 10. A second bed, similar to the first, contains particles with a diameter equal to one-half of the diameter of particles in the first bed. Both beds operate with the same superficial velocity. What is the bed voidage in the bed filled with the smaller particles?

3.21 A fan delivers air to two fluidized beds, *A* and *B*. Bed *A* is operating at a minimum volume (i.e., at minimum fluidization) and bed *B* is fluidized to a volume equal to twice its fixed bed volume.

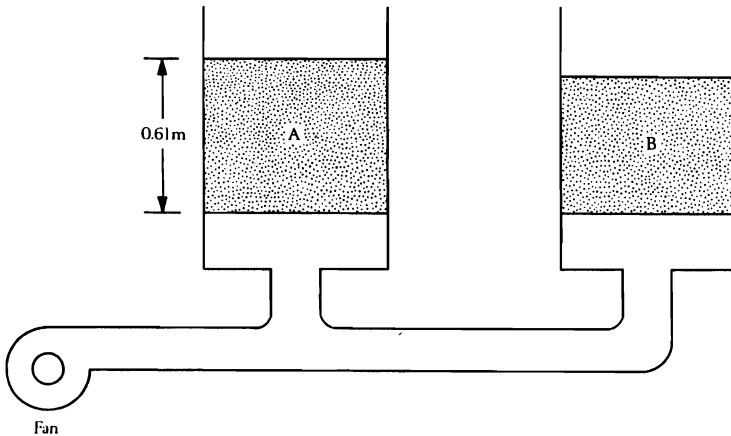
- Calculate the superficial velocity through bed *A*.
- Calculate the superficial velocity through bed *B*.
- Calculate ΔP across bed *A*.
- For bed *B*, prove that $\omega = 0.7$ when it is fluidized to twice the fixed bed volume.

Bed *A*: $D_p = 91.4 \mu\text{m}$ (uniform); ρ (solid) = 4808 kg m⁻³; $\lambda = 1$.

Bed *B*: $D_p = 61.0 \mu\text{m}$ (uniform); ρ (solid) = 4006 kg m⁻³; $\lambda = 1$;

ω (fixed bed) = 0.4; ω (fluidized) = 0.7.

Air: $\rho = 1.28 \text{ kg m}^{-3}$; $\eta = 2.07 \times 10^{-5} \text{ N s m}^{-2}$.



3.22 Metal parts are to be annealed at 800 K in a bed of silica sand fluidized by products of combustion of natural gas with 100% excess air. If the sand has a U.S. Standard screen analysis of 20% -30M+50M, 30% -50M+70M, 40%-70M+100M, and 10% -100M+140M, what superficial velocity of gas is required through the bed? (Hint: Think about at what void volume you want to operate.) What is the minimum superficial velocity that you can operate at?

112 Turbulent and Complex Flows

3.23 Pellets of polyethylene are to be fluidized in a column 1 meter in diameter and 10 meters high with air at 300 K. A hot steel pipe is lowered into the fluidized bed to bring it into contact with the pellets, which melt onto its surface to form a protective anticorrosion coating. Calculate the total flow of air required, if the pellets are 5 mm in diameter and the desired void fraction of the bed is 0.7. The density of the polyethylene is 920 kg m^{-3} .

3.24 During the compaction of metal powders into sheet material (powder rolling), as shown in the figure below, the entrapped air is expelled from the loose powder. This expulsion occurs at the line AB . Below AB , the powder is coherent, that is, the particles are locked together, but above AB , the powder is loose, i.e., a normal packed bed.

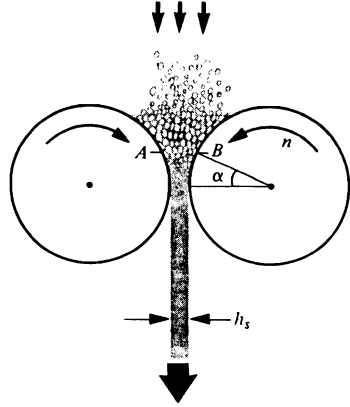
If the velocity of expulsion exceeds the minimum fluidization velocity, the powder does not feed properly into the roll gap and the sheet product is not satisfactory. This, in fact, limits the production rate of the process.

The following equation gives the superficial velocity V_0 (cm s^{-1}) of gas expulsion from the coherent zone:

$$V_0 = \frac{2\pi R^2 n (\alpha - \sin \alpha \cos \alpha)}{\alpha [2R(1 - \cos \alpha) + h_s]}$$

where R = roll radius, cm, n = rolling speed, rev s^{-1} , α = roll-coherent powder contact angle, rad, and h_s = roll gap, cm. For copper powder, α has been found to be 6° (0.1047 radians).

- Calculate the rolling speed at which copper powder, with properties given below, will just begin to be fluidized at the plane AB , for strip thickness 0.5 mm and roll diameter 200 mm.
- Calculate the corresponding speed of the emerging coherent strip.
- Discuss the effect that order-of-magnitude changes in particle size and roll radius would have on production rates. Data are given as follows: $\eta = 1.8 \times 10^{-6} \text{ N s m}^{-2}$, $\rho_{\text{air}} = 1.30 \text{ kg m}^{-3}$, $D_{p_{\text{Cu}}} = 40 \text{ }\mu\text{m}$, $\rho_{\text{Cu}} = 6700 \text{ kg m}^{-3}$.



4

ENERGY BALANCE APPLICATIONS IN FLUID FLOW

One of the most powerful analytical tools available for quantitative problems in engineering is the principle of the conservation of energy. In fluid flow, this principle is most often applied to open systems in the form of the *mechanical energy equation*, which is also commonly called *Bernoulli's equation*. The approach is macroscopic, since we examine the entire flow system with an entrance and an exit. This method is different from the one presented in Chapter 2, where we analyzed the microscopic volume element through which fluid flows as the starting point for solving problems.

4.1 CONSERVATION OF ENERGY

The *mechanical energy equation* is the starting point for analyzing many problems involving fluid flow. It can be derived from the first law of thermodynamics, which is usually written for a system (or control volume) with a fixed mass and no mass entering or leaving the system. For an *open system*, however, mass may enter or leave the system, and it is convenient to write the first law of thermodynamics for a control volume that allows for mass flow across its boundaries. Our goal is to apply the first law to engineering systems, in which there can be significant changes in both kinetic energy and potential energy as the fluid flows through the system. Furthermore, the fluid flow may be mechanically forced or assisted through the system by the power of a pump, fan, or blower.*

When presented the first law of thermodynamics for the first time, most readers were probably given

$$\Delta U = Q - M$$

where U is the internal energy, ΔU is the change in internal energy in going from "state 1" to "state 2" in a closed system, Q is the heat added to the system, and M is the work done

*In other engineering scenarios, the fluid provides power (e.g., a water-wheel, a steam turbine or a gas turbine).

114 Energy Balance Applications in Fluid Flow

by the system. This statement of the first law is usually adequate because our interest in applying thermodynamics to materials is usually based on principles of chemical thermodynamics. Changes in kinetic energy and potential energy of a substance are not important when our goal is to use thermodynamics to understand the structure and properties of materials. More generally, however, the first law of thermodynamics has far-reaching applications to devices and systems for producing electrical or mechanical power, and for effecting heating or cooling. In this broader context, the *total energy*, which comprises the sum of internal, potential and kinetic energies, and not the internal energy by itself, must be used in the first law of thermodynamics.

In materials processing, fluid flows are often driven through systems by pumps, fans or blowers, so we start with the first law of thermodynamics written for an open system. A derivation of the equation can be found in many engineering textbooks on thermodynamics.¹

With the aid of the symbols in Table 4.1, the conservation of energy can be written

$$\frac{d\Sigma}{dt} = -\Delta[(H + E_p + E_k)W] + Q - M + S_R. \quad (4.1)$$

In this form, the macroscopic energy balance is written for unsteady-state conditions in which the left side of the equation represents the accumulation of total energy in the system. The total energy, Σ , is defined as the sum of internal, potential, and kinetic energy. The operator Δ signifies exit minus entrance quantities, and note that the expression $\Delta H = \Delta U + \Delta(P/\rho)$ has been employed in the usual manner for open systems.

Table 4.1 Symbols used in the general energy balance

	Entering the system	Leaving the system
Mass flow rate	W_1	W_2
Pressure	P_1	P_2
Volume per unit mass	$1/\rho_1$	$1/\rho_2$
Energy per unit mass		
Potential	E_{p1}	E_{p2}
Kinetic	E_{k1}	E_{k2}
Internal	U_1	U_2
Enthalpy	$H_1 = U_1 + P_1(1/\rho_1)$	$H_2 = U_2 + P_2(1/\rho_2)$
Mechanical power done by the system, M		
Net power generation within the system from chemical reactions or other sources, S_R		
Net power input by heat transfer, Q		

The terms P_1/ρ_1 and P_2/ρ_2 , which are parts of H_1 and H_2 , respectively, are often called the *flow work* or *PV work*. They are recognized as the work required to put a unit of mass into the system at "1" in Fig. 4.1 and the work done by the system on a unit mass leaving

¹For example, see G. J. Van Wylen and R. E. Sonntag, *Fundamentals of Classical Thermodynamics*, third edition, John Wiley, New York, NY, 1985, pages 113-121.

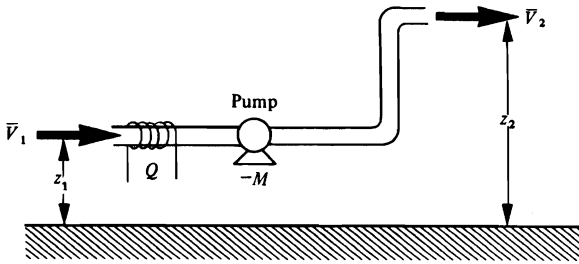


Fig. 4.1 Flow system for the application of the energy balance.

at "2," respectively. After this brief discussion explaining the basis of the problem at hand, namely, the flow of fluids, we now proceed to focus attention on some of the specific terms in Eq. (4.1) for steady-state conditions, namely,

$$\frac{d\Sigma}{dt} = 0, \quad W_1 = W_2 = W, \quad \text{and} \quad S_R = 0.$$

4.1.1 Evaluation of the kinetic energy terms

The rate of kinetic energy entering the system through area A_1 (normal to flow) is given by

$$W_1 E_{K1} = \frac{1}{2} \left[\int_0^{A_1} (\rho_1 v_1) v_1^2 dA_1 \right]. \quad (4.2)$$

Examine Eq. (4.2) for meaning; one may be tempted at this point to simply write $\frac{1}{2}(\rho A_1 \bar{V}_1) \bar{V}_1^2$ to represent the kinetic energy entering the system, where \bar{V}_1 is the average velocity ($= W_1 / \rho_1 A_1$). However, because the velocity varies in some manner across the cross-sectional area, the integration indicated by Eq. (4.2) is in order.

To account for the velocity distribution, the kinetic energy term can be written as:

$$W_1 E_{K1} = \frac{1}{2\beta_1} W_1 \bar{V}_1^2, \quad (4.3)$$

where β_1 is defined by

$$\frac{1}{\beta_1} = \frac{1}{A_1} \int_0^{A_1} \left[\frac{v_1}{\bar{V}_1} \right]^3 dA_1. \quad (4.4)$$

We can also use a similar expression for the rate at which kinetic energy leaves the system; so we write the difference between leaving and entering the system

$$W \Delta E_K = W \left[\frac{\bar{V}_2^2}{2\beta_2} - \frac{\bar{V}_1^2}{2\beta_1} \right]. \quad (4.5)$$

116 Energy Balance Applications in Fluid Flow

For laminar flow in a circular tube, $\beta = 0.5$, and for turbulent flow, β is nearly unity, and is usually approximated as such.

4.1.2 Evaluation of the potential energy terms

Potential energy is defined relative to some arbitrary reference plane for the fluid both leaving and entering the system. Therefore, the difference in potential energy of the fluid leaving and entering is simply

$$W\Delta E_p = Wg(z_2 - z_1),$$

or

$$W\Delta E_p = Wg\Delta z. \quad (4.6)$$

4.1.3 Mechanical energy equation, Bernoulli's equation

Substituting Eqs. (4.5) and (4.6) into Eq. (4.1) for steady-state conditions yields

$$\Delta H + \left[\frac{\bar{V}_2^2}{2\beta_2} - \frac{\bar{V}_1^2}{2\beta_1} \right] + g\Delta z + M^* - Q^* = 0. \quad (4.7)$$

Here $M^* = M/W$, and $Q^* = Q/W$. In this form, all the terms are now energies per unit mass of fluid flowing through the system. Further, if we express H by $U + P/\rho$, we obtain the overall energy balance:

$$\Delta U + \Delta \left[\frac{P}{\rho} \right] + \Delta \left[\frac{\bar{V}^2}{2\beta} \right] + g\Delta z + M^* - Q^* = 0. \quad (4.8)$$

The equation is also commonly found in its differential form for a differential segment of the system:

$$dU + d \left[\frac{P}{\rho} \right] + d \left[\frac{\bar{V}^2}{2\beta} \right] + g dz - \delta Q^* = 0. \quad (4.9)$$

Here δ prefacing Q^* emphasizes that it is not a true differential but that it merely represents the heat which is transferred across the system boundary.

A more common form of the energy balance for applications to fluid flow is a variation referred to as the *mechanical energy equation*. From Eq. (4.8), we see that the change in the internal energy for the unit mass of fluid as it passes through a short segment of the system is

$$dU = dQ^* - Pd(1/\rho) + \delta E_f, \quad (4.10)$$

where δE_f is the *mechanical energy per unit mass lost as frictional conversion into heat*. Substituting Eq. (4.10) into (4.9) and expanding $d(P/\rho)$ into

$$\left[(1/\rho)dP + Pd(1/\rho) \right]$$

yields

$$\frac{1}{\rho} dP + d \left[\frac{\bar{V}^2}{2\beta} \right] + g dz + \delta E_f = 0.$$

The integral of this equation, which applies to the whole system, finally yields (with M^* reinserted) the mechanical energy equation, which can be applied directly to many problems of fluid flow:

$$\int_{P_1}^{P_2} \frac{dP}{\rho} + \left[\frac{\bar{V}_2^2}{2\beta_2} - \frac{\bar{V}_1^2}{2\beta_1} \right] + g\Delta z + M^* + E_f = 0. \quad (4.11)$$

This equation is also called Bernoulli's equation. Actually, Bernoulli's equation only applies to the flow of ideal fluids, where $M^* = E_f = 0$, but Eq. (4.11), having been used so frequently in engineering, has taken on the connotation of Bernoulli's equation as well. Also note that it is written in terms of unit mass of material flowing.

4.2 FRICTION LOSSES IN STRAIGHT CONDUITS

Due to the utility of Eq. (4.11) in engineering calculations, considerable effort has been made to develop methods for estimating the friction loss E_f in various flow systems.

If we consider the friction loss in a straight conduit with steady flow of constant-density fluid, we can determine E_f in terms of the friction factor f . The control volume is a portion of a conduit with an arbitrary but constant cross-sectional area A and a length L . The fluid flows only due to a pressure difference of $P_2 - P_1$; then Eq. (3.3) gives us the force exerted by the fluid on the inside surface of the conduit.

$$F_K = (P_1 - P_2)A. \quad (4.12)$$

Since we are discussing a horizontal control volume with no mechanical work supplied or withdrawn, Eq. (4.11) reduces to

$$E_f = \frac{1}{\rho} (P_1 - P_2). \quad (4.13)$$

By comparing Eqs. (4.12) and (4.13), we see that

$$E_f = \frac{F_K}{\rho A}. \quad (4.14)$$

For circular tubes, $A = \pi R^2$ and $F_K = 2\pi RL(\frac{1}{2}\rho\bar{V}^2)f$. Thus,

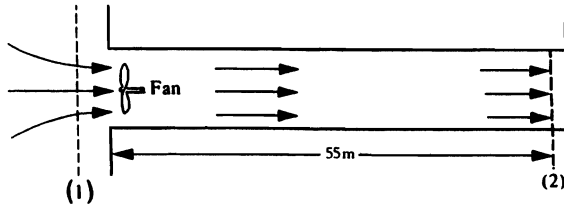
$$E_f = 2f \left[\frac{L}{D} \right] \bar{V}^2. \quad (4.15)$$

Again, for noncircular conduits, D may be replaced by the equivalent diameter D_e , which is discussed in Section 3.2. Equation (4.15) is a form of the well-known *Fanning equation*. Caution must be exercised by the reader in the exact definition of the friction factor; in much of the literature the friction factor is defined such that it is four times the friction factor employed here. Therefore, the Fanning equation may be found in a different form from that in Eq. (4.15).

118 Energy Balance Applications in Fluid Flow

Example 4.1 A fan draws air at rest and sends it through a horizontal rectangular duct, 200 mm × 300 mm and 55 m long. The air enters at 289 K and 750 mm Hg pressure at a rate of 0.472 m³ s⁻¹. What theoretical power is required of the fan if the air discharges at 750 mm Hg? (Pressure is commonly measured with manometers or barometers and given as column of Hg supported by the pressure. Normal atmospheric pressure is 760 mm Hg so that 760 mm Hg = 1.01325 × 10⁵ N m⁻².)

Solution. Consider the system below that is defined by placing planes 1 and 2 where shown. The mechanical equation includes M^* , because there is a fan in the system.



Because $P_1 \cong P_2 = 750$ mm Hg, then $\int_{P_1}^{P_2} dP = 0$. Also $\bar{V}_1 = 0$ and $\Delta z = 0$. Under these conditions, Eq. (4.11) reduces to

$$\frac{\bar{V}_2^2}{2\beta_2} + M^* + E_f = 0.$$

Now

$$D_e = \frac{2(0.2 \times 0.3) \text{ m}^2}{(0.2 + 0.3) \text{ m}} = 0.24 \text{ m}.$$

At normal atmospheric pressure and 289 K, the density of air is 1.22 kg m⁻³. Therefore,

$$\rho \cong \left(\frac{750}{760} \right) (1.22) = 1.20 \text{ kg m}^{-3}.$$

(Why is this an approximation? Just to the right of the fan do you think the pressure is equal to, greater than or less than 750 mm Hg?)

$$\bar{V}_2 = \frac{0.472 \text{ m}^3}{\text{s}} \bigg| \frac{1}{(0.2 \times 0.3) \text{ m}^2} = 7.87 \text{ m s}^{-1}.$$

The Reynolds number is now determined:

$$\text{Re} = \frac{D_e \bar{V}_2 \rho}{\eta} = \frac{(0.24)(7.87)(1.20)}{(1.78 \times 10^{-5})} = 1.27 \times 10^6.$$

*By stating that $P_2 = 750$ mm Hg, we ignore the *exit loss* which we shall discuss in Section 4.3.

From Fig. 3.2, $f = 0.0042$ (smooth). Because

$$E_f = 2 \left[\frac{L}{D_e} \right] \bar{V}_2^2 f,$$

the energy balance can be written as

$$M^* = - \left[\frac{1}{2\beta_2} + 2f \left[\frac{L}{D_e} \right] \right] \bar{V}_2^2.$$

For turbulent flows, $\beta_2 = 1$ so that

$$\begin{aligned} M^* &= - \left[\frac{1}{2} + (2)(0.0042) \left[\frac{55}{0.24} \right] \right] 7.87^2 \text{ m}^2 \text{ s}^{-2} \\ &= - \frac{150 \text{ m}^2}{\text{s}^2} \left| \frac{1 \text{ N s}^2}{1 \text{ kg m}} \right| \frac{1 \text{ W s}}{1 \text{ N m}} = -150 \text{ W s kg}^{-1}. \end{aligned}$$

Recall M^* is work done by the fluid, so that $-M^*$ is work done by the fan. Now we multiply M^* by the mass flow rate through the system to get the power.

$$\text{Power} = \frac{0.150 \text{ kW s}}{\text{kg}} \left| \frac{0.472 \text{ m}^3}{\text{s}} \right| \frac{1.20 \text{ kg}}{\text{m}^3} = 0.0850 \text{ kW}.$$

For straight conduits, Eq. (4.15) gives the friction loss E_f . However, in most flow systems there are fittings, bends, changes in cross sections, valves, etc. Therefore additional resistances must be included in E_f for the best application of Eq. (4.11). The following sections review some of the methods used to calculate such resistances.

4.3 ENLARGEMENT AND CONTRACTION

The friction loss associated with a *sudden enlargement* or a *sudden contraction* (Fig. 4.2) is calculated by using a *friction-loss factor* e_f . The friction loss for the particular geometry that upsets flow in conduits is evaluated in the following manner:

$$E_f = \frac{1}{2} \bar{V}^2 e_f, \quad (4.16)$$

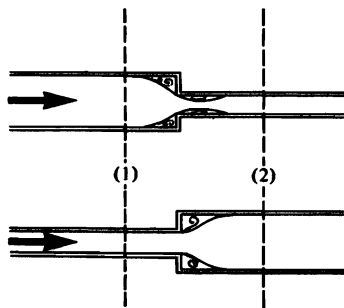


Fig. 4.2 Sudden contraction and enlargement.

where \bar{V} is the velocity of fluid in the *smaller* cross section. (Since other conventions are also used, the reader should always be certain of which velocity is chosen to define e_f .) By analogy with Eq. (4.15), e_f corresponds to a friction factor with *built-in* geometry effects. Hence, e_f depends on a Reynolds number and a geometric ratio of the system. We present values of e_f for enlargements and contractions in circular cross sections in Figs. 4.3 and 4.4, respectively. For both these figures, D is the smaller diameter, Re is calculated using the same D , and L is the length of the smaller pipe considered.

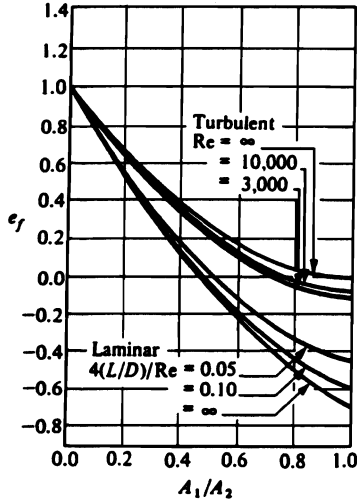


Fig. 4.3 Friction-loss factor for sudden expansion. (From W. M. Kays and A. L. London, *Trans. ASME* 74, 1179 (1952).)

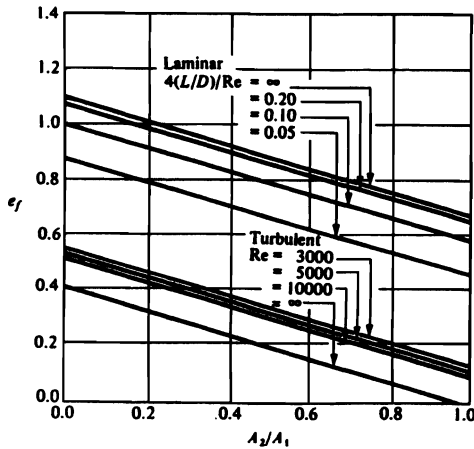


Fig. 4.4 Friction-loss factor for sudden contraction. (From Kays and London, *ibid.*)

The results for e_f in the case of enlargements apply equally well to all exit shapes (except for gradual expansions discussed in the following paragraphs), as can be seen by viewing the flow in Fig. 4.2. The extent of the region of vortices after the expansion does not depend on whether the corners are rounded. However, e_f for contraction (entrances) can be modified

significantly. Figure 4.5 shows the ratio of e_f for various inlet shapes to that for a sharp-edged entry.

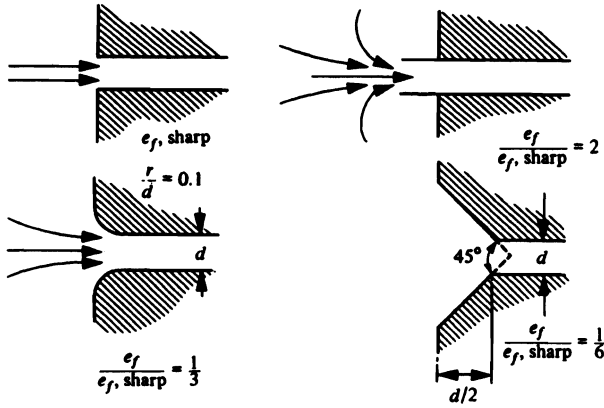


Fig. 4.5 Entrance-loss coefficients.

In flow through *gradual enlargements*, the energy losses are significantly reduced due to the elimination of the vortices shown in Fig. 4.2. Experiments on tapered enlargements show that the friction-loss factor e_f depends on both the taper angle β and the area ratio A_1/A_2 (Fig. 4.6). In reality, e_f should also depend on a Reynolds number, but this is not given in the figure, since, in turbulent flow, the dependence of e_f on the Reynolds number is small, as can be seen in Figs. 4.3 and 4.4. Consequently, data presented for e_f are usually assumed to apply to all Reynolds numbers in the regime of turbulent flow.

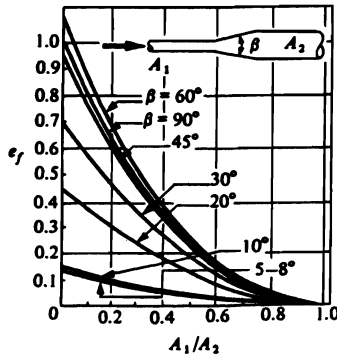


Fig. 4.6 Friction-loss factor for turbulent flow through gradual enlargements. (From *Steam—Its Generation and Use*, Babcock & Wilcox, New York, 1963, page 8-17.)

In *gradual contractions*, the converging boundaries have a tendency to steady the flow, and if the included angle of convergence is 30° or less, the energy loss factor can be approximated as 0.05-0.10. Again, when using these data, one must realize that they apply only to turbulent flow.

122 Energy Balance Applications in Fluid Flow

Example 4.2 In Example 4.1 the entrance and exit losses were ignored. This time we repeat the calculation and include these losses.

Solution. Refer to the figure included with Example 4.1. Keep plane 1 in place, but move plane 2 to the right so that it is just beyond the exit end of the duct. Now $P_1 = P_2 = 750$ mm Hg, and $\bar{V}_2^2 = \bar{V}_1^2 = 0$. The latter is true because the air flows at planes 1 and 2 are essentially within very large areas, which makes the average velocities small, and then these small velocities are squared. As before $\Delta z = 0$, then Eq. (4.11) reduces to

$$M^* + E_f = 0,$$

where

$$E_f = 2 \left[\frac{L}{D_e} \right] \bar{V}^2 f + \frac{1}{2} e_{f1} \bar{V}^2 + \frac{1}{2} e_{f2} \bar{V}^2,$$

with \bar{V} the velocity within the duct and e_{f1} and e_{f2} the energy loss coefficients for the entrance and the exit, respectively. Now, we solve for M^* :

$$M^* = - \left[\frac{1}{2} e_{f1} + \frac{1}{2} e_{f2} + 2 \left[\frac{L}{D_e} \right] f \right] \bar{V}^2.$$

Values of the Reynolds number, velocity, friction factor and L/D_e are all found in Example 4.1. With $Re = 1.27 \times 10^5$ and $A_2/A_1 = 0$, Fig. 4.4 gives $e_{f1} = 0.4$. With $A_1/A_2 = 0$, Fig. 4.3 gives $e_{f2} = 1.0$. Then

$$\begin{aligned} M^* &= - \left[\left[\frac{1}{2} \right] (0.4) + \left[\frac{1}{2} \right] (1.0) + (2)(0.0042) \left[\frac{55}{0.24} \right] \right] 7.87^2 \\ &= -163 \text{ W s kg}^{-1}. \end{aligned}$$

Also

$$\text{Power} = 0.0924 \text{ kW}.$$

By carefully accounting for the additional frictional losses in the system, our estimate of the power has increased by 8.7%.

4.4 FLOW THROUGH VALVES AND FITTINGS

To evaluate flow through valves and fittings, we usually assign an equivalent length to the fixture such that the pressure drop is given by Eq. (4.15), where L is replaced by L_e . Therefore

$$E_f = 2f \frac{L_e}{D} \bar{V}^2, \quad (4.17)$$

where f is evaluated for Re with the pipe diameter equal to the fitting diameter, and L_e/D for turbulent flow of various fittings is given in Table 4.2. Thus, when evaluating the friction loss through a system with fittings, the sum of the equivalent lengths of all the fittings is added to the length of the pipe; E_f is then determined by using Eq. (4.17).

Table 4.2 Equivalent length for various fixtures, turbulent flow*

Fitting	L_e/D	Fitting	L_e/D
45° elbow	15	Tee (as el, entering branch)	90
90° elbow, standard radius	31	Couplings, unions	Negligible
90° elbow, medium radius	26	Gate valve, open	7
90° elbow, long sweep	20	Gate valve, $\frac{1}{4}$ closed	40
90° square elbow	65	Gate valve, $\frac{1}{2}$ closed	190
180° close return bend	75	Gate valve, $\frac{3}{4}$ closed	840
Swing check-valve, open	77	Globe valve, open	340
Tee (as el, entering run)	65	Angle valve, open	170

*W. M. Rohsenow and H. Y. Choi, *Heat, Mass, and Momentum Transfer*, Prentice-Hall, Englewood Cliffs, New Jersey, 1961, p. 64. A more complete list is in R. H. Perry and C. H. Chilton (Eds.), *Chemical Engineers' Handbook*, fifth edition, McGraw-Hill, New York, NY, 1973, pages 5-35 to 5-38.

For example, if a pipe network contains 6 m of pipe with an inside diameter of 21 mm, two elbows (90°, medium radius), and a wide open gate valve, then the L/D ratio to be substituted into Eq. (4.15) would be

$$\begin{aligned} \left[\frac{L}{D} \right] &= \left[\frac{L}{D} \right]_{\text{pipe}} + 2 \left[\frac{L_e}{D} \right]_{\text{elbows}} + \left[\frac{L_e}{D} \right]_{\text{valve}} \\ &= \frac{6}{0.021} + (2)(26) + 7 = 345. \end{aligned}$$

4.5 FLOW THROUGH SMOOTH BENDS AND COILS

In curved pipes, the friction loss may rise considerably above the values for straight lengths of pipe, and the transition Reynolds number may be much higher than 2100. The maximum Reynolds number for laminar flow, or critical Reynolds number, Re_c , is given as a function of the coil diameter D_c and pipe diameter D :²

$$Re_c = 20,000 \left[\frac{D}{D_c} \right]^{0.32}, \quad 15 < \frac{D_c}{D} < 860. \quad (4.18)$$

The friction loss for laminar flow in a curved pipe can be expressed in terms of the ratio of the friction factor for the curved pipe to that for the same length of straight pipe. This

²H. Ito, *Trans. ASME* **82**, Series D, 123-34 (1959).

124 Energy Balance Applications in Fluid Flow

ratio is a function of $\text{Re}(D/D_c)^{1/2}$, which is given in a publication by Babcock and Wilcox.³ The effect of curvature on the friction factor for laminar flow is negligible for $\text{Re}(D/D_c)^{1/2} < 10$.

We can compute the friction loss for turbulent flow by using Eq. (4.15) and applying the ratio of curved-to-straight pipe friction factors, f_c/f_s , given by⁴

$$\frac{f_c}{f_s} = \left[\text{Re} \left[\frac{D}{D_c} \right]^2 \right]^{1/20} \quad (4.19)$$

for $\text{Re}(D/D_c)^2 > 6$.

4.6 FLOW MEASUREMENT

Efficient operation and control of engineering processes and experimental set-ups often require information concerning the quantities of flowing fluids. For measuring flow in closed conduits, there is a variety of measuring devices available; for example, velocity meters, head meters, or area meters. Although all of them can be used to determine the mass-flow rate, which is the information usually needed, none can measure the flow *directly*, so that, particularly in the case of compressible fluids, the meters require careful calibration. The devices described in this section are based on applying Eq. (4.11). Other devices for flow measurement and flow visualization are described in Appendix E.

4.6.1 Velocity meters

A commonly encountered velocity meter is the Pitot-static tube which measures local velocities. The Pitot tube consists essentially of a tube with an open end facing the stream, as shown in Fig. 4.7. The velocity of the fluid along the streamline x - y decreases to zero at y which corresponds to the tip of the Pitot-tube opening, and is called the stagnation point. Applying Eq. (4.11) between planes (1) and (2) along the streamline xy we have

$$\frac{P_2}{\rho} + 0 = \frac{P_1}{\rho} + \frac{v_1^2}{2}, \quad (4.20)$$

where P_1 denotes the upstream pressure, and v_1 the approach velocity. The pressure P_2 , which is called the stagnation pressure, is made up of two parts: (1) the pressure to be measured if the fluid were not moving—the static pressure, and (2) the pressure resulting from the sudden cessation of the streamline's kinetic energy—the velocity pressure. In other words,

$$P_2 = P_1 + \frac{\rho v_1^2}{2},$$

which is, in fact, a rearrangement of Eq. (4.20). The construction of the Pitot tube in Fig. 4.7 shows the static holes; at these locations, static pressure is measured, while the pressure differential $P_2 - P_1$ is measured by the complete assembly. Thus, after including a

³Steam—Its Generation and Use, Babcock & Wilcox, New York, NY, 1963, pages 8-17.

⁴H. Ito, *ibid.*

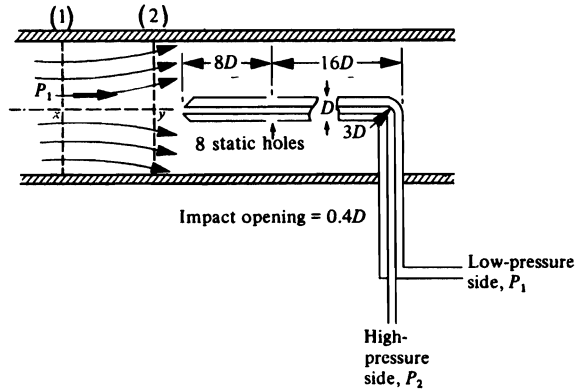


Fig. 4.7 Pitot-static tube and recommended dimensional relationships.

calibration constant C_p which takes care of nonideal behavior in the system, we rewrite Eq. (4.20) to yield the velocity of the fluid:

$$v_1 = C_p \left[\frac{2}{\rho} (P_2 - P_1) \right]^{1/2}; \quad (4.21)$$

C_p , which is sometimes called the Pitot-tube coefficient, usually has a value between 0.98 and 1.00.

Because the Pitot tube measures only local velocities, a traverse of the conduit must be made in order to obtain the complete profile, and from it the average velocity \bar{V} . To obtain the density ρ , we usually measure the temperature upstream from the probe tip. In the flow in a straight circular pipe at points preceded by a run of at least 50 diameters without obstructions, the ratio of V_{\max} (the velocity measured at the center line) to \bar{V} (the average velocity) can be found by relating the ratio to the Reynolds number. For laminar flow, of course,

$$\frac{\bar{V}}{V_{\max}} = \frac{1}{2}, \quad 0 < \text{Re} < 2.1 \times 10^3, \quad (4.22)$$

and for a large region of the turbulent range, namely, $10^4 < \text{Re} < 10^7$,

$$\frac{\bar{V}}{V_{\max}} = 0.62 + 0.04 \log \left[\frac{DV_{\max} \rho}{\eta} \right]. \quad (4.23)$$

In the range $2.1 \times 10^3 < \text{Re} < 10^4$, a traverse must be made because \bar{V}/V_{\max} is not predictable.

For gases at low flow rates ($< 60 \text{ m s}^{-1}$) and isothermal flow conditions, we may use Eq. (4.21) as it is. However, if there is a substantial temperature rise (high velocity), then an energy balance must be made between the upstream point, at which a temperature is measured, and the tip of the Pitot tube. For this case, Bernoulli's equation should be written

$$\int_{P_1}^{P_2} \frac{dP}{\rho} = \frac{v_1^2}{2}. \quad (4.24)$$

126 Energy Balance Applications in Fluid Flow

If the fluid is a compressible gas, we may assume that the flow is adiabatic and the gas ideal; thus the equation of state is

$$P \left[\frac{1}{\rho} \right]^\gamma = \text{constant}, \quad (4.25)$$

where γ is the ratio of the heat capacity at constant pressure to that at constant volume. Integrating Eq. (4.24) by using Eq. (4.25) yields

$$v_1 = C_p \sqrt{\left[\frac{2\gamma}{\gamma - 1} \right] \left[\frac{P_1}{\rho_1} \right] \left[1 - \left[\frac{P_1}{P_2} \right]^{(1-\gamma)/\gamma} \right]}. \quad (4.26)$$

Example 4.3 A Pitot-static tube is installed with its impact opening along the centerline of a long pipe with an inside diameter of 300 mm. Air at 339 K and $8.27 \times 10^4 \text{ N m}^{-2}$ (gauge pressure) passes through the pipe; the barometric pressure is 745 mm Hg ($9.93 \times 10^4 \text{ N m}^{-2}$). The pressure difference measured by the Pitot-static tube is 10.7 mm water. Calculate the mass flow rate in the pipe.

Solution. The absolute pressure in the pipe where P_1 is measured is

$$P_1 = 8.27 \times 10^4 + 9.93 \times 10^4 = 1.82 \times 10^5 \text{ N m}^{-2}.$$

At this pressure and 339 K, the gas density is

$$\begin{aligned} \rho_1 &= \frac{1 \text{ mol}}{0.0224 \text{ m}^3} \left| \frac{1.82 \times 10^5 \text{ N m}^{-2}}{1.0133 \times 10^5 \text{ N m}^{-2}} \right| \left| \frac{273 \text{ K}}{339 \text{ K}} \right| \left| \frac{28.8 \text{ g}}{1 \text{ mol}} \right| \left| \frac{1 \text{ kg}}{1000 \text{ g}} \right| \\ &= 1.86 \text{ kg m}^{-3} \end{aligned}$$

The manometer fluid used to measure the pressure drop is water so we need the conversion between height of water and pressure; it is $1 \text{ N m}^{-2} = 0.1020 \text{ mm water}$. Therefore

$$P_2 - P_1 = \frac{10.7 \text{ mm H}_2\text{O}}{0.1020 \text{ mm H}_2\text{O}} \left| \frac{1 \text{ N m}^{-2}}{1 \text{ N m}^{-2}} \right| = 1.049 \times 10^2 \text{ N m}^{-2}.$$

Now we utilize Eq. (4.21) to determine V_{\max} (assume $C_p = 1$):

$$v_1 = V_{\max} = \left[\frac{2 \text{ m}^3}{1.86 \text{ kg}} \left| \frac{1.049 \times 10^2 \text{ N}}{\text{m}^2} \right| \left| \frac{1 \text{ kg m}}{1 \text{ N s}^2} \right| \right]^{1/2} = 10.6 \text{ m s}^{-1}.$$

To find the average velocity, we utilize Eq. (4.23):

$$\frac{\bar{V}}{V_{\max}} = 0.62 + 0.04 \log \left[\frac{(0.3)(10.6)(1.86)}{2.03 \times 10^{-5}} \right] = 0.84$$

Therefore, the mass flow rate W can finally be determined:

$$W = \frac{(0.84)(10.6) \text{ m}}{\text{s}} \left| \frac{(\pi)(0.3)^2 \text{ m}^2}{4} \right| \left| \frac{1.86 \text{ kg}}{\text{m}^3} \right| = 1.17 \text{ kg s}^{-1}.$$

4.6.2 Head meters

There are essentially three types of head meters. They are so called because all of them place some sort of restriction in the flow line, causing a local increase in the velocity of the fluid and a corresponding decrease in the pressure *head*.^{*} The simplest is perhaps the *orifice plate* illustrated in Fig. 4.8; however, the *venturi meter* and *flow nozzle* (Figs. 4.9 and 4.10) are based on the same principle, and the same group of equations apply to all of them.

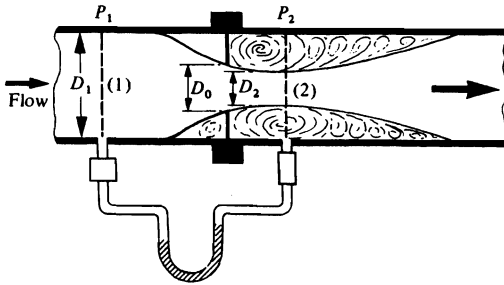


Fig. 4.8 Orifice meter.

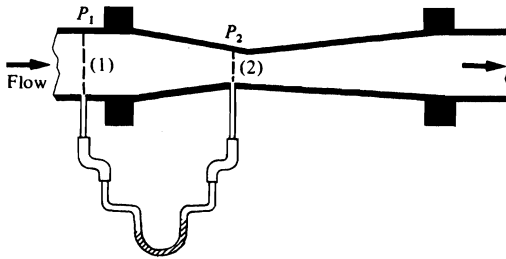


Fig. 4.9 Venturi meter.

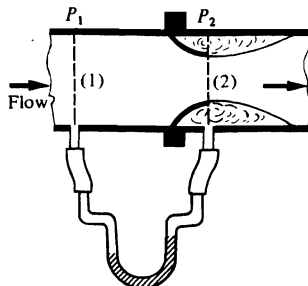


Fig. 4.10 Flow nozzle.

^{*}We discuss the term *head* in Chapter 5.

128 Energy Balance Applications in Fluid Flow

Specifically, consider the orifice meter in Fig. 4.8, which is of very simple construction. A thin plate with a centrally located circular hole is inserted into the duct, and, as indicated, the flow contracts before the hole, and continues to contract for a short distance downstream from the orifice to the location of the smallest flow section, known as the *vena contracta*. If we apply Eq. (4.11) to the system between (1) and (2), and neglect friction loss for the time being, then the mechanical energy balance (for incompressible fluids) with $\beta = 1$ is

$$\frac{P_2 - P_1}{\rho} + \frac{\bar{V}_2^2}{2} - \frac{\bar{V}_1^2}{2} = 0. \quad (4.27)$$

Also, for incompressible fluids (by continuity),

$$\bar{V}_1 = \left[\frac{D_2}{D_1} \right]^2 \bar{V}_2, \quad (4.28)$$

so that when Eq. (4.27) is solved for \bar{V}_2 in terms of the difference in pressure between the taps, we obtain

$$\bar{V}_2 = \left[\frac{2(P_1 - P_2)}{\rho \left[1 - \left(\frac{D_2}{D_1} \right)^4 \right]} \right]^{1/2}. \quad (4.29)$$

This is the theoretical velocity at the *vena contracta*, which disregards frictional energy losses and can never be achieved in practice. Therefore we utilize a *discharge coefficient* C_D which accounts for such losses and an additional geometric factor. The largest pressure drop is measured at the *vena contracta*, but it is more convenient to relate the velocity at the orifice plate \bar{V}_0 to the pressure drop, $(P_1 - P_2)$, and at the same time use the diameter of the plate opening D_0 instead of the diameter of the *vena contracta*. Thus we get the final form of the expression

$$\bar{V}_0 = C_D \left[\frac{2}{\rho} \frac{(P_1 - P_2)}{(1 - B^4)} \right]^{1/2}, \quad (4.30)$$

in which $B \equiv D_0/D_1$, or

$$\bar{V}_0 = K \left[\frac{2}{\rho} (P_1 - P_2) \right]^{1/2}, \quad (4.31)$$

where K is the *flow coefficient*, defined as $C_D/\sqrt{1 - B^4}$.

Equations (4.30) and (4.31) also apply to venturi and nozzle meters as well as to orifice plates, but, as will be discussed below, C_D and K are quite different. In addition, for both venturi and nozzle meters, as shown in Figs. 4.9 and 4.10, the minimum flow contraction corresponds to the position where P_2 is measured, hence $D_2 = D_0$, and $\bar{V}_2 = \bar{V}_0$.

For liquids (incompressible fluids), the mass flow rate is

$$W = KA_0 \sqrt{2\rho(P_1 - P_2)}. \quad (4.32)$$

For gases, we can modify this equation to a more general form, utilizing the *expansion factor Y*,

$$W = KYA_0 \sqrt{2\rho(P_1 - P_2)}. \tag{4.33}$$

Expansion factors for gases are different for each type of head meter; these are summarized in Table 4.3. For convenience, Fig. 4.11 shows values of *Y* for each of the above meter types. For liquids, *Y* is taken to be unity, as it is also for gases when the pressure difference is small compared with the total pressure.

Table 4.3 Expansion factors *Y* for flow meters*

Meter type	<i>Y</i>
Venturi and nozzle	$\left[\frac{\gamma(1 - r^{1-1/\gamma})(1 - B^4)}{(\gamma - 1)(1 - r)(r^{-2/\gamma} - B^4)} \right]^{1/2}$
Orifice (square-edged)	$1 - \left[\frac{1 - r}{\gamma} \right] (0.41 + 0.35B^4)$

*In these expressions for *Y*, $r = P_2/P_1$ and $\gamma = C_p/C_v$.

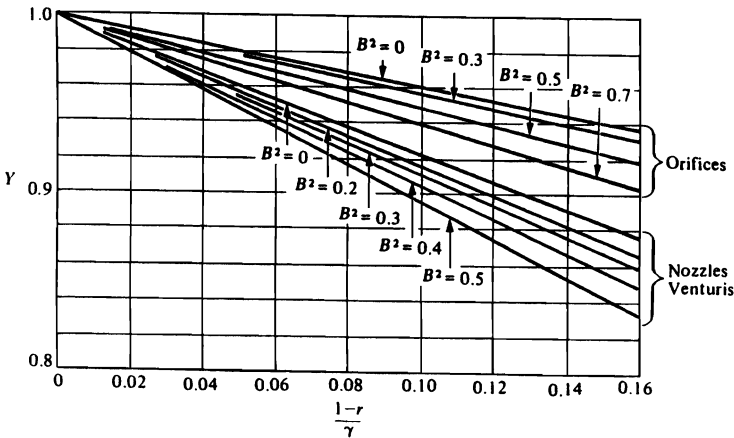


Fig. 4.11 Expansion factors for gases flowing through various head meters. (From Perry and Chilton, *ibid.*, page 5-11.)

For the orifice plate, we have to choose: (1) whether to use a square-edged hole, or one with a 45°-taper and a knife-edge inlet, and (2) where to locate the pressure taps with respect to the plate. Figure 4.12 illustrates the effect of various locations of taps on the flow coefficient, and shows how the stream is narrowed as it leaves the orifice plate, reaching a minimum at the *vena contracta*. In most cases, the upstream tap is located from one to two pipe diameters ahead of the plate, and the downstream tap either one-half of a pipe diameter downstream or exactly at the *vena contracta*, which would have to be found experimentally. As specified in the legend, the data of Fig. 4.12 apply specifically to square-edged circular orifices. Generally, such data depend to some extent on the exact design of the orifice plate

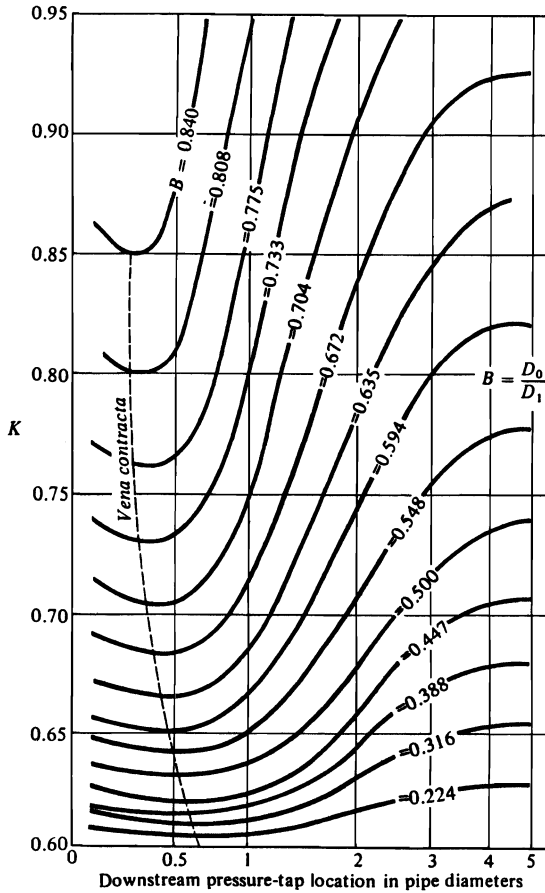


Fig. 4.12 Effect of tap locations on the flow coefficient. Applies to square-edged circular orifices with Re (at the orifice) greater than 30 000. (From Perry and Chilton, *ibid.*, page 5-12.)

and on the location of the pressure taps so that, to be safe, one should rely on manufacturer's information and/or self-calibration. However, there are data available in the general literature for various designs that may be consulted.^{5,6,7}

The square-edged orifice plate is most commonly used, but we use the sharp-edged plate to ensure reproducible coefficients when the plates must be often replaced, and recalibration is to be avoided each time. This is a problem, for example, in systems where the gas is dirty and the velocities high, which results in rapid erosion of the opening in the plate.

⁵G. F. Round and V. K. Gorg, *Applications of Fluid Dynamics*, Edward Arnold, London, 1986, page 394.

⁶*Fluid Meters: Their Theory and Application*, sixth edition, ASME, New York, 1971.

⁷R. H. Perry and C. H. Chilton (Eds.), *Chemical Engineers' Handbook*, fifth edition, McGraw-Hill, New York, NY, 1973, pages 5-12 to 5-15.

Orifice plates are the simplest and cheapest types of head meters, but they also cause the largest *permanent* pressure drop in the system. This refers to the fact that the pressure difference, $P_1 - P_2$, across the orifice is not entirely lost, and a partial pressure recovery is experienced downstream. The results of experiments indicate that the permanent loss of pressure for orifice plates is given by

$$\Delta P_{\text{loss}} = (1 - B^2)(P_1 - P_2). \quad (4.34)$$

The design of the venturi meter is such that a gradual restriction in flow area precedes the throat, which is a short, straight section; then the flow area gradually returns to the original area. On the upstream side, the included angle of convergence is about 25° , and on the downstream side, the angle of divergence is between 5 and 7° . A venturi tube is nearly frictionless under turbulent flow conditions, so that the typical values of C_D are between 0.98 and 1.0. However, in laminar flow, C_D drops rapidly with decreasing Reynolds number and calibration data should be consulted. For venturi meters, the permanent pressure drop is much lower than for orifices plates and may be approximated as ten percent of the measured differential.

Nozzles are similar to orifices in some respects, but are designed so that the discharge is preceded by a smooth contracting passage. As a result, nozzles have less eddying upstream and the measured pressure drop corresponds more closely to that for a venturi rather than an orifice meter. However, downstream from the nozzle discharge, the flow behavior is more similar to that of an orifice; thus the permanent pressure drop corresponds more closely to the orifice than to the venturi.

4.7 FLOW FROM LADLES

In metallurgical operations, molten metal is contained in refractory lined vessels (ladles). These ladles transport the metal to various points within a plant where molten metal is required. It is desirable to know the time required to completely or partially empty a ladle.

As a means of applying Bernoulli's equation, consider the vessel depicted in Fig. 4.13. The liquid level is obviously constant if the mass flow rates of the incoming and discharging streams are equal. For this steady-state system, $P_1 - P_2$, $M^* = 0$, and $\bar{V}_2^2 \gg \bar{V}_1^2$; thus Eq. (4.11) reduces to

$$\frac{\bar{V}_2^2}{2\beta_2} + g\Delta z + E_f = 0. \quad (4.35)$$

The friction loss E_f for this system is entirely due to the contraction nozzle, and we can evaluate it by the method applied in Section 4.3:

$$E_f = \frac{1}{2} e_f \bar{V}_2^2. \quad (4.36)$$

Combining Eqs. (4.35) and (4.36) yields

$$\frac{\bar{V}_2^2}{2} \left[\frac{1}{\beta_2} + e_f \right] + g\Delta z = 0. \quad (4.37)$$

Let h be the height of liquid; then

$$\bar{V}_2 = \left[\frac{1}{\beta_2} + e_f \right]^{-1/2} \sqrt{2gh}. \quad (4.38)$$

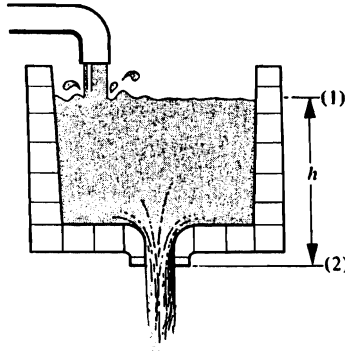


Fig. 4.13 Flow from a vessel in which h can be maintained constant.

For a given nozzle, we can evaluate the term in parentheses, which relates to the flow. As a vessel empties, β_2 may change as well as e_f which is a function of the Reynolds number. However, it is common engineering practice to recognize that $\bar{V}_2 = \sqrt{2gh}$ represents the maximum possible velocity of the exit stream, and then to assign a discharge coefficient C_D to a real situation:

$$\bar{V}_2 = C_D \sqrt{2gh} . \quad (4.39)$$

By comparing Eqs. (4.38) and (4.39), we can compute the discharge coefficient:

$$C_D = \left[\frac{1}{\beta_2} + e_f \right]^{-1/2} . \quad (4.40)$$

Now consider the case when the mass flow of the incoming stream is reduced so that the liquid level gradually diminishes. Then the velocity of the exit stream changes with time, but the velocity at any instant is still given by Eq. (4.39), where h is the liquid level at that instant. Finally, if the vessel contains a liquid and no liquid enters at the top, and then a bottom plug is removed, Eq. (4.39) still applies, but h becomes a function of time. This is the situation that applies to ladles; Fig. 4.14 shows a typical ladle design for molten steel.

The mass flow rate discharging from the ladle with a nozzle of area A_N is given by

$$\frac{dw}{dt} = A_N \rho \bar{V}_2 , \quad (4.41)$$

so that

$$\frac{dw}{dt} = A_N \rho C_D \sqrt{2gh} . \quad (4.42)$$

The integration limits at time $t = 0$, are $h = h_0$, and $w = w_0$.

$$\int_{w_0}^{w,h} \frac{dw}{\sqrt{2gh}} = A_N \rho \int_0^t C_D dt . \quad (4.43)$$

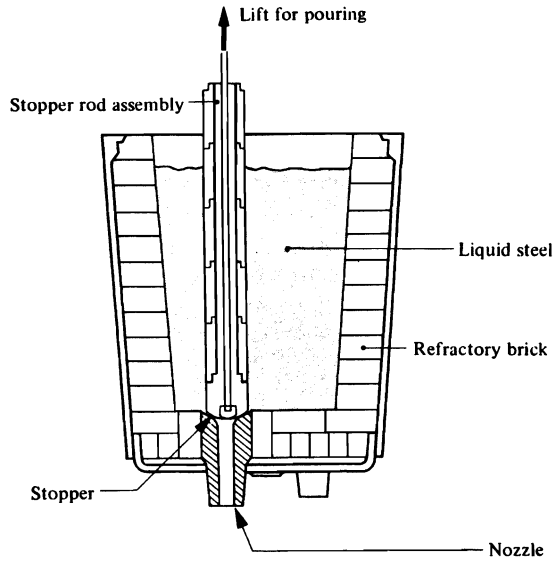


Fig. 4.14 Single-nozzle bottom-pour ladle for steel.

It is usually assumed that C_D is constant; also, many ladles have a constant circular cross section of $\pi D_L^2/4$, so that

$$dw = -\rho \frac{\pi D_L^2}{4} dh. \quad (4.44)$$

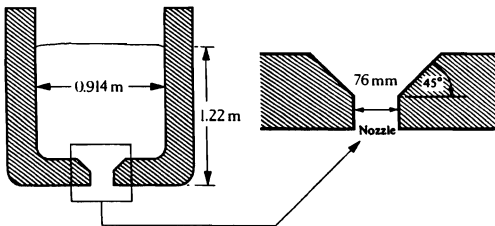
Thus we obtain the time t_f to completely empty the ladle by integrating Eq. (4.43):

$$t_f = \frac{\pi D_L^2}{2A_N C_D} \left(\frac{h_0}{2g} \right)^{1/2} \quad (4.45)$$

Example 4.4 A ladle with an inside diameter of 0.914 m and a capacity height of 1.22 m has a nozzle that tapers $\pi/4$ radians (45°) to a 76 mm exit diameter.

- Calculate the time to empty the ladle if it is filled with Al-7% Si alloy at 977 K.
- Calculate the discharge rate (kg s^{-1}) initially and when the ladle is 75% empty.

Data: $\eta = 2.75 \times 10^{-3} \text{ N s m}^{-1}$; $\rho = 2400 \text{ kg m}^{-3}$.



134 Energy Balance Applications in Fluid Flow

Solution. Equation (4.45) may be utilized if it is reasonable to treat C_D as a constant. Because e_f and β_2 both depend on the Reynolds number through the nozzle, C_D is actually a function of the depth of the melt. Let us first examine the manner in which C_D varies. This involves calculating the friction loss factor for flow through a contraction; hence we use Figs. 4.4 and 4.5.

Completely Full

Re is estimated by assuming $C_D = 1$.

$$\bar{V}_2 \approx \sqrt{2gh} = [(2)(9.8)(1.22)]^{1/2} = 4.89 \text{ m s}^{-1}$$

$$\text{Re} \approx \frac{D \bar{V}_2 \rho}{\eta} = \frac{(0.076)(4.89)(2400)}{2.75 \times 1.0^{-3}} = 3.24 \times 10^5$$

$$e_f = (0.4) \left[\frac{1}{6} \right] = 0.067$$

$$\beta_2 \approx 1 \text{ (flow is turbulent)}$$

$$C_D = (1 + 0.067)^{-1/2} = 0.97$$

Nearly empty (assume only 4 mm remain)

$$\bar{V}_2 \approx [(2)(9.8)(0.004)]^{1/2} = 0.28 \text{ m s}^{-1}$$

$$\text{Re} \approx \frac{(0.076)(0.28)(2400)}{2.75 \times 1.0^{-3}} = 1.86 \times 10^4$$

$$e_f = (0.5) \left[\frac{1}{6} \right] = 0.083$$

$$C_D = (1 + 0.083)^{-1/2} = 0.96$$

It is certainly reasonable to assume that C_D is constant, so we can use Eq. (4.45).

a) With $A_N = \pi D_N^2/4$, we can write:

$$t_f = \frac{2(D_L/D_N)^2}{C_D} \left[\frac{h_0}{2g} \right]^{1/2}$$

$$t_f = \frac{2(0.914/0.076)^2}{0.97} \left[\frac{1.22}{(2)(9.8)} \right]^{1/2}$$

$$t_f = 74.4 \text{ s}$$

b) The discharge rate is calculated with Eq. (4.41).

$$A_N = \frac{\pi D_N^2}{4} = \frac{(\pi)(0.076)^2}{4} = 4.54 \times 10^{-3} \text{ m}^2$$

Initial discharge rate (1.22 m level):

$$\begin{aligned}\frac{dw}{dt} &= A_N \rho \bar{V}_2 = (4.54 \times 10^{-3})(2400)(4.89)(0.97) \\ &= 51.7 \text{ kg s}^{-1}.\end{aligned}$$

Discharge rate at 75% empty (0.305 m level):

$$\frac{dw}{dt} = 51.6 \left(\frac{1}{4} \right)^2 = 25.8 \text{ kg s}^{-1}.$$

4.8 FLOW THROUGH PIPING NETWORKS

All of the effects of individual fittings, flow devices, pipe diameters, etc., on flow through fluid systems combine and must be considered when total systems involving pumps, valves and nozzles are put together. The goal of such systems is to provide fluid to particular locations at specified rates. In many cases, a single main supply line and pump are used to distribute fluid to a network of pipes that supply several outlets, such as spray cooling or internal cooling of process equipment or products. If the effects of variation of resistance to flow and therefore on flow quantity are not understood, unintended maldistribution of flow can occur.

Consider the system in Fig. 4.15. Let us assume that we want to deliver the same flow rate from each nozzle:

$$Q_1 = Q_2 = Q_3 = \frac{Q_0}{3}.$$

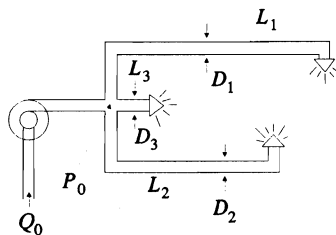


Fig. 4.15 Flow in network.

Since the pressure drop from the branch point, where $P = P_0$, to the atmosphere is the same,

$$\Delta P_1 = \Delta P_2 = \Delta P_3 = (P_0 - P_{\text{atm}}).$$

But the flow through a nozzle (Fig. 4.16) depends on the pressure of the nozzle entrance: see Table 4.4. For a given nozzle, as the pressure in the line behind it decreases, so does the flow. On the other hand, it can be seen that by picking a small orifice, the pressure drop across the nozzle can be very large for a similar flow, e.g., a hollow cone nozzle with a 0.218 in. orifice will deliver 1.25 gal/min at 10 psi pressure, whereas a 0.140 in. orifice will deliver 1.50 gal/min flow with a 100 psi pressure.

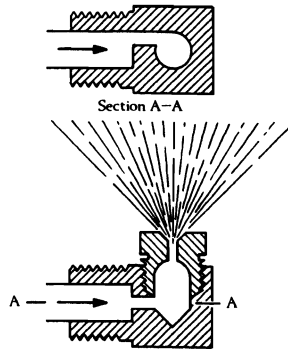


Fig. 4.16 A hollow-cone nozzle of the tangential type. (From R. H. Perry, C. H. Chilton, and S. D. Kirkpatrick, *Chemical Engineers' Handbook*, fourth edition, McGraw-Hill, New York, NY, 1963, page 18-63.)

Table 4.4 Discharge rates and included angle of spray from pressure nozzles. (From R. H. Perry, C. H. Chilton, and S. D. Kirkpatrick, *ibid.*, page 18-65.)

Nozzle type	Orifice diameter, in.	Discharge, gal/min, and included angle of spray							
		10 psi		25 psi		50 psi		100 psi	
		Discharge	Angle, deg.	Discharge	Angle, deg.	Discharge	Angle, deg.	Discharge	Angle, deg.
Hollow cone	0.046	—	—	0.10	65	0.135	68	0.183	75
	0.140	0.535	82	0.81	88	1.10	90	1.50	93
	0.218	1.25	83	1.88	86	2.55	89	3.45	92
	0.375	7.2	62	11.8	70	16.5	70		
Solid cone	0.047	—	—	0.167	65	0.235	70	0.34	70
	0.188	1.60	55	2.46	58	3.42	60	4.78	60
	0.250	3.35	65	5.40	70	7.50	70	10.4	75
	0.500	17.5	86	27.5	84	38.7	73		
Fan	0.031	0.085	40	0.132	90	0.182	110	0.252	110
	0.093	0.70	70	1.12	76	1.57	80	2.25	80
	0.187	2.25	50	3.70	59	5.35	65	7.70	65
	0.375	9.50	66	15.40	74	22.10	75	30.75	75

Note: 1 gal/min (gallon per minute) = $6.309 \times 10^{-5} \text{ m}^3 \text{ s}^{-1}$; 1 psi (lb_f/in²) = 6895 N m⁻².

If the nozzle pressure at the desired flow is high enough, the pressure drop down the length of feed pipe at that flow rate, ΔP_{pipe} , will be negligible by comparison to the drop across the nozzle. Then, although not exactly the same, the flows out of each nozzle will be close to each other. On the other hand, if the length of pipe is long, so that ΔP_{pipe} is on the same order as ΔP_{nozzle} , the flows will be different unless the pipe diameters are adjusted so that

$$\Delta P_{\text{pipe1}} = \Delta P_{\text{pipe2}} = \Delta P_{\text{pipe3}}$$

For this to be the case with $Q_1 = Q_2 = Q_3$ then

$$L_1 D_1^3 = L_2 D_2^3 = L_3 D_3^3 \tag{4.46}$$

because

$$\Delta P_{\text{pipe}} = \left[\frac{32 f \rho}{\pi^2} \right] L D^{-5} Q^2. \quad (4.47)$$

Given L_1 , L_2 and L_3 and the value of one of the pipe diameters to obtain the required Q , the remaining diameters can be calculated.

PROBLEMS

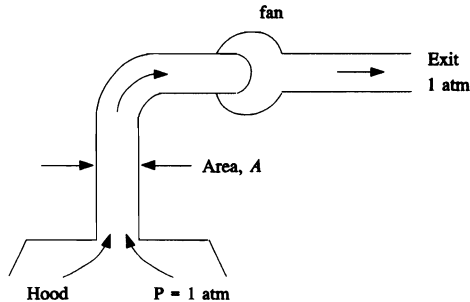
4.1 The reciprocal of β , as defined in Eq. (4.4) is called the kinetic energy correction factor. Derive the kinetic energy correction factors for the following flows:

- fully developed, laminar flow between infinite parallel plates;
- Hagen-Poiseuille flow in a circular tube;
- turbulent flow, in a tube of radius R , described by

$$\frac{\bar{V}}{V_{\text{max}}} = \left[\frac{r}{R} \right]^n$$

where $n = 1/7$.

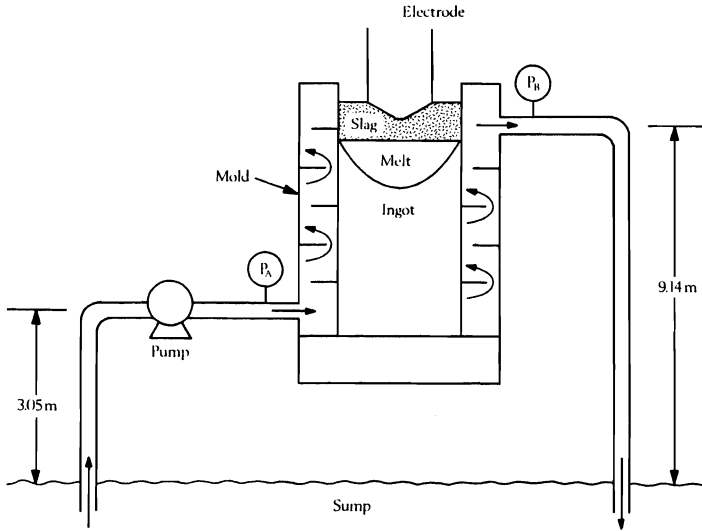
4.2 A fan is used to draw exhaust gases from a large hood. For highly turbulent flow, write an equation for the system which gives $-M^*\rho$ as a function of volume flow rate, Q . Neglect potential energy changes because a gas is being exhausted. For friction include only the contraction ($e_f = 0.4$), the expansion ($e_f = 1.0$) and the elbow ($L/D_e = 20, f = 0.001$). Note that $-M^*\rho$ has units of pressure and represents the "total pressure" against which the fan must operate.



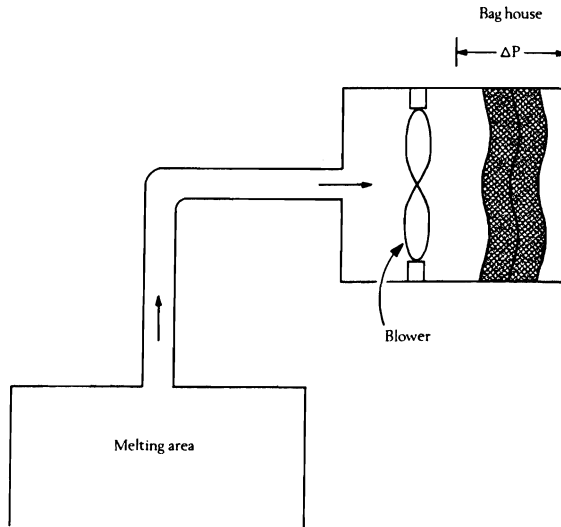
4.3 Cooling water is provided to the mold used in the electroslag remelting process depicted below. For flow through the mold,

$$E_f = K \bar{V}^2$$

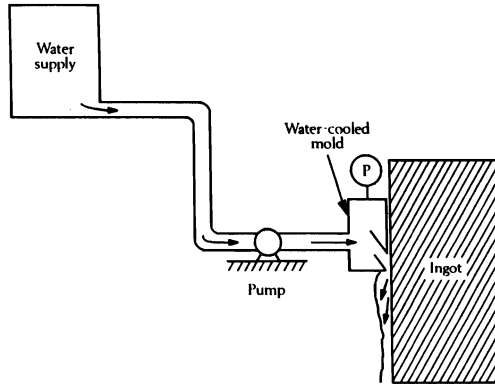
where \bar{V} is the average velocity of the water in the lines at the entrance and exit of the mold and K is a turbulent flow constant for the mold. When the pressure gauges read $P_A = 2.76 \times 10^5 \text{ N m}^{-2}$ and $P_B = 2.07 \times 10^5 \text{ N m}^{-2}$, the volume flow rate is $2.83 \times 10^{-3} \text{ m}^3 \text{ s}^{-1}$. Calculate $-M^*$ (in N m kg^{-1}) for the pump when the volume flow rate is $5.66 \times 10^{-3} \text{ m}^3 \text{ s}^{-1}$. Assume that friction losses through the straight lengths of pipes can be ignored. *Data:* D (pipes) = 15.4 mm; $f = 0.001$; $L_e/D = 26$ (elbows); e_f (entrance) = 0.8; e_f (exit) = 1.



4.4 A blower draws air from a melting area and directs the air to a "bag house" where particulates are filtered before the air is discharged to the environment. The melting area and the environment are at ambient temperature and pressure (289 K and $1.0133 \times 10^5\text{ N m}^{-2}$, respectively). When the pressure drop across the bag house (ΔP in the diagram) is $5.07 \times 10^3\text{ N m}^{-2}$, the volume flow rate is $0.944\text{ m}^3\text{ s}^{-1}$. Calculate the work done by the blower in N m per kg of air delivered by the blower. *Conduit Information:* length before elbow, 61 m ; length after elbow, 61 m ; diameter, 305 mm ; $L_e/D = 25$ (elbows); $f = 0.0043$; e_f (contraction) = 0.4 ; e_f (expansion) = 0.8 .



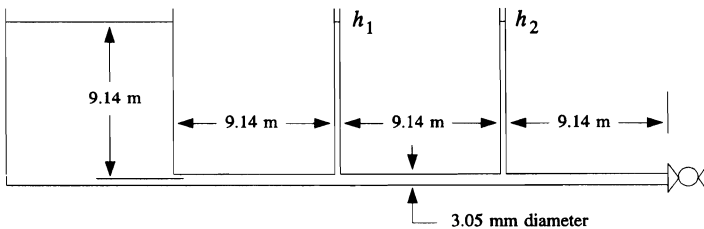
4.5 Water is pumped from a storage tank to a mold designed to produce nonferrous ingots by the "direct-chill" process. The water supply is at ambient pressure ($1.0133 \times 10^5 \text{ N m}^{-2}$), and the water leaving the mold impinges upon the surface of the ingot which is also at ambient pressure. A pressure gauge mounted in the manifold portion of the mold (pressure gauge P in the diagram) indicates an absolute pressure of $1.22 \times 10^5 \text{ N m}^{-2}$, when the volume flow rate is $3.93 \times 10^{-3} \text{ m}^3 \text{ s}^{-1}$. The water level in the tank is 3 m, and the vertical length of the pipe is 3 m. Calculate the theoretical power of the pump. Assume that the tank for the water supply has a very large diameter, and that the kinetic energy of the water within the manifold portion of the mold is negligible. *Piping Information:* total length of straight pipe, 9.14 m; diameter, 30.5 mm; $L_e/D = 25$ (elbows); $f = 0.004$; e_f (contraction) = 0.4; e_f (expansion) = 0.8.



4.6 Water, maintained at a constant level, is supplied to a long line from a filter tank filled with sand. There are two vertical branches attached to the main line as shown in the accompanying figure; these branches and the tank are open to ambient pressure (i.e., $1.0133 \times 10^5 \text{ N m}^{-2}$). At the end of the line there is a frictionless valve.

- When the valve is closed, what are the heights h_1 and h_2 in the vertical branches?
- When the valve is open, what is the mass flow rate?
- When the valve is open, what is the difference in height between h_1 and h_2 ?

Data: $\rho = 1,000 \text{ kg m}^{-3}$; $\eta = 1 \times 10^{-3} \text{ N s m}^{-2}$; ϵ/D (relative roughness) = 0.01; ω (sand) = 0.40; D_p (sand) = $152 \mu\text{m}$.



4.7 Liquid aluminum contains a small fraction of Al_2O_3 inclusions which are removed by filtering through a bed of ceramic spheres. The refined aluminum (i.e., filtered aluminum) is pumped to a holding vessel from which liquid metal is drawn to cast ingots. For the equipment arrangement shown below, calculate the theoretical power of the pump to process 2.52 kg s^{-1} . The important friction losses are in the filter bed, the transfer line which contains two 90° elbows (medium radius), and the entrance and exit.

140 Energy Balance Applications in Fluid Flow

Data: Aluminum:

$$\rho = 2644 \text{ kg m}^{-3}$$

$$\eta = 1.28 \times 10^{-3} \text{ N s m}^{-2}$$

Ceramic spheres:

$$\omega = 0.4$$

$$D_p = 0.61 \text{ mm}$$

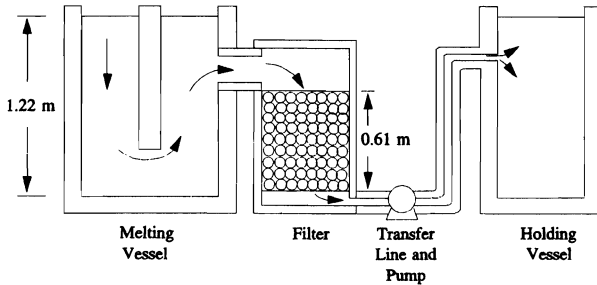
$$\text{Area (bed)} = 0.292 \text{ m}^2$$

Transfer line:

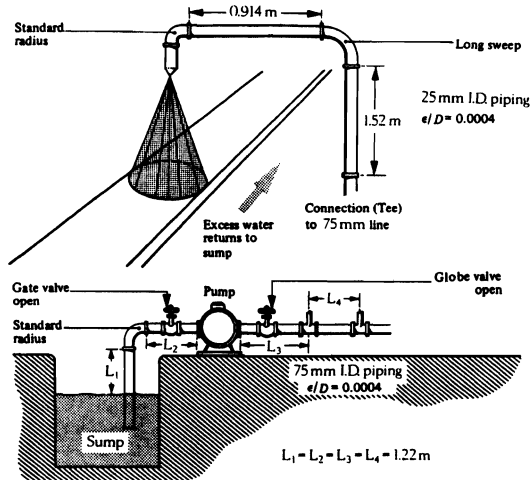
$$L \text{ (straight portions)} = 1.83 \text{ m}$$

$$D = 9.1 \text{ mm}$$

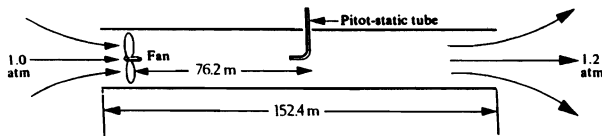
$$\epsilon \text{ (roughness)} = 9.1 \times 10^{-4} \text{ mm}$$



4.8 Hot-rolled steel sheet is quenched by passing under two water sprays as depicted below. Each spray requires $9.46 \times 10^{-4} \text{ m}^3 \text{ s}^{-1}$ of water at 294 K, and the pressure drop across each nozzle at this flow rate is 1.72×10^5 . Calculate the theoretical power required by the pump.



4.9 A fan draws air at rest and sends it through a straight duct 152 m long. The diam. of the duct is 0.61 m and a Pitot-static tube is installed with its impact opening along the center line. The air enters at 300 K and 1 atm and discharges at 1.2 atm. Calculate the theoretical work (in N m kg^{-1}) of the fan if the Pitot-static tube measures a pressure difference of 25.4 mm of water. (Note: $1 \text{ atm} = 1.0133 \text{ N m}^{-2}$.)



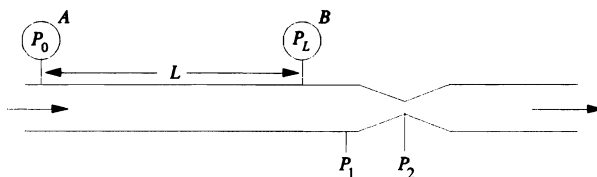
4.10 Compressed air at $6.9 \times 10^5 \text{ N m}^{-2}$ and 310 K flows through an orifice plate meter installed in a 75 mm I.D. pipe. The orifice has a 25 mm hole and the downstream pressure tap location is 38 mm from the plate. When the manometer reading is 358 mm Hg,

- What is the flow rate of air?
- What is the permanent pressure drop?

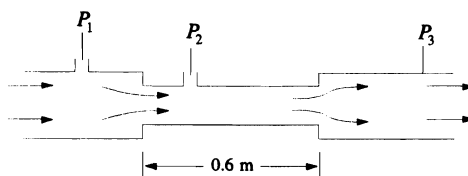
4.11 A venturi meter is installed in an air duct of circular cross-section 0.46 m in diameter which carries up to a maximum of $1.18 \text{ m}^3 \text{ s}^{-1}$ of air at 300 K and $1.1 \times 10^5 \text{ N m}^{-2}$. The throat diameter is 230 mm.

- Determine the maximum pressure drop that a manometer must be able to handle, i.e., what range of pressure drops will be encountered? Express the results in mm of water.
- Instead of the venturi meter, an orifice meter is proposed and the maximum pressure drop to be measured is 50 mm of water. Calculate what diameter of sharp-edged orifice should be installed in order to obtain the full scale reading at maximum flow.
- Estimate the permanent pressure drop for the devices in parts a) and b).
- If the air is supplied by a blower operating at 50% efficiency, what is the power consumption associated with each installation?

4.12 Liquid flows through a long straight tube and then through a Venturi meter. Pressure gauges *A* and *B* measure the pressure drop for a tube length *L*, and P_1 and P_2 are the pressures for the manometer used with the Venturi. Derive an equation for the ratio of the two pressure drops, $(P_0 - P_L)/(P_1 - P_2)$ in terms of *f*, *K*, *D*, and D_0 where *f* is friction factor for the tube, *K* is the flow coefficient of the Venturi, *D* is the diameter of the tube, and D_0 is the throat diameter.



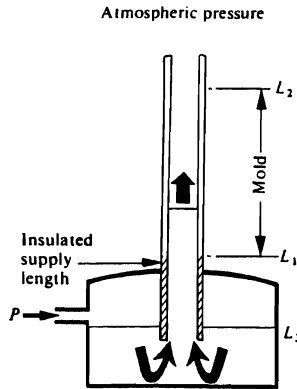
4.13 Lacking the funds to purchase a head meter, Mr. Make-do installed a 50 mm dia. tube in a 100 mm dia. line in order to measure flow rate. Pressure taps P_1 and P_2 are connected to a manometer.



- For flow which is highly turbulent ($Re \rightarrow \infty$), derive an equation which gives mass flow rate through the line in terms of the pressure difference $P_1 - P_2$.
- Develop an equation which could be used to calculate the permanent pressure drop (i.e., $P_1 - P_3$).

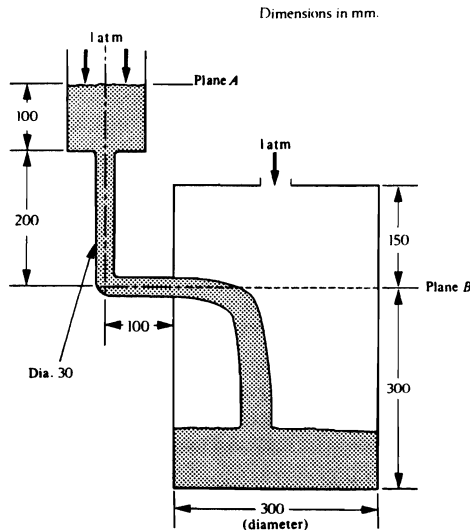
142 Energy Balance Applications in Fluid Flow

4.14 In order to *slush* cast seamless stainless-steel pipe, a *pressure pouring* technique is utilized, as depicted below.

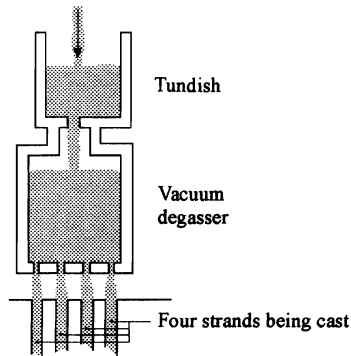


The mold must be filled rapidly up to level L_2 so that no solidification takes place until the entire mold is filled. Determine an expression that we can use to give the time it takes to fill the mold *only*. Consider the mold to be between L_1 and L_2 and open to atmospheric pressure at the top. Neglect the change of metal height L_3 in the ladle; you may also neglect the friction loss associated with the supply tube and mold tube walls, but the entrance loss may *not* be neglected.

4.15 Calculate the time to fill the mold, as depicted below, with molten metal if the metal level at plane A is maintained constant and the time to fill the runner system (entering *pipng*) is ignored. *Data* (all may be taken as constant): $\eta = 1.65 \times 10^{-3} \text{ N s m}^{-2}$; $\rho = 6410 \text{ kg m}^{-3}$; $f = 0.0025$ (runner); $e_f(\text{contraction}) = 0.1$; $e_f(\text{enlargement for liquid levels below } B) = 0$; $e_f(\text{enlargement for liquid levels above } B) = 1.0$; $L/D(90^\circ \text{ turn}) = 25$; $\beta = 1.0$.



4.16 In planning continuous casting, we use fluid flow analysis. Consider the illustrated configuration of the equipment, which includes in-line vacuum degassing.



- Determine the tundish and degasser nozzle sizes which are necessary to operate the system at a rate of 6.3 kg s^{-1} per strand. Suppose that for operational reasons it is desirable to maintain tundish and degasser bath depths of 0.76 and 1.83 m, respectively.
- If only 13 mm diameter degasser nozzles are available, how would their use affect the casting operation?

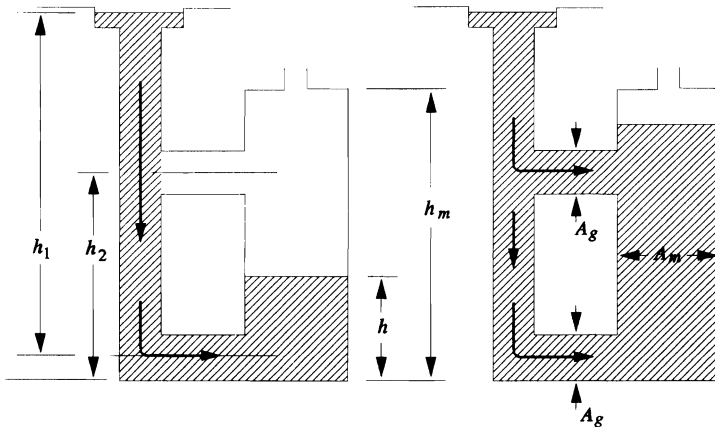
Inside dimensions: tundish, $2.4 \text{ m} \times 2.4 \text{ m} \times 1.2 \text{ m}$; degasser, $1.2 \text{ m} \times 1.2 \text{ m} \times 2.4 \text{ m}$.

Liquid-steel density = 7530 kg m^{-3} .

Discharge coefficients for tundish and vacuum degasser nozzles: $C_D = 0.8$.

Vacuum pressure = 10^{-3} atm (101 N m^{-2}).

4.17 Liquid metal flows into a permanent mold through a vertical gating-system. If the mold has a uniform area (A_m) and the metal flows through gates of equal areas (A_g), derive an equation which gives time to fill the mold. Assumptions: (i) no friction, and flow is turbulent; (ii) h_1 is constant; (iii) no flow through the upper gate until h equals h_2 .



4.18 If the pipes in Fig. 4.15 are of lengths $L_1 = 10 \text{ m}$, $L_2 = 5 \text{ m}$, and $L_3 = 1 \text{ m}$ and the nozzles are fan type with a 0.187 inch orifice, and D_1 is 3 cm, determine the diameter of pipes 2 and 3 needed to produce a flow of 3.70 gallons of water per minute through each nozzle. What pressure P_0 needs to be provided? What happens to the flow pattern if a small particle in the water clogs nozzle 1?

5

FLOW AND VACUUM PRODUCTION

The materials engineer must know not only how to measure flow, but also how to produce it. Some methods of producing flow and vacuum, such as gravity flow and suction lift, are well known, but there are many types of fans, pumps, and flow devices which are often required and used in materials laboratories and materials processing. Vacuum technology is a crucial part of materials processing and in materials science and engineering. Basic uses of vacuums include removal of gas molecules to permit travel of electrons, atoms, and ions through a required distance, removal of chemically active gases, decreasing the gas density to minimize heat transfer, refinement of melts, and controlled deposition of thin films on substrates. Keeping in mind that this is a textbook on transport phenomena, we have limited our presentation of vacuum technology to only several pages, and at that much of the presentation is qualitative and descriptive. We urge all readers involved in vacuum technology to immerse themselves in books devoted to this subject.^{1,2}

Unfortunately the jargon and units used in engineering associated with pumps, fans, blowers and vacuum-producing devices can be rather strange, particularly in the U.S.A. where the use of English units still prevails. Accordingly, along with the working equations, we explain the jargon and non-S.I. units.

5.1 PUMPS

In general, pumps may be classified as either positive-displacement pumps or centrifugal pumps. We may subdivide positive-displacement pumps into reciprocal or rotary types, and centrifugal pumps into tangential- or axial-flow types.

Positive-displacement pumps deliver a definite volume of liquid at every stroke or revolution, regardless of the pressure and friction against which they are working. There are two common types of reciprocating positive-displacement pumps—the double-acting piston

¹M. H. Hablani, *High-Vacuum Technology*, Marcel Dekker, Inc., New York, NY, 1990.

²J. F. O'Hanlon, *A User's Guide to Vacuum Technology*, Second edition, John Wiley & Sons, New York, NY, 1989, pages 35-42.

pump and the single-acting plunger pump—and a large number of different designs of rotary positive-displacement pumps, the gear pump perhaps being the best known.

In general, positive-displacement pumps are employed where delivery of a relatively small volume of liquid against high pressure is required. In reciprocating pumps, as the piston withdraws, the fluid discharge ceases, and so the delivery is in pulses. In double-acting pumps, this pulsating characteristic is lessened.

In centrifugal pumps, the fluid enters axially at the suction connection, accelerates radially out along the blades of the impeller, and leaves the pump tangentially at a high velocity. Centrifugal pumps can have various types of vane configurations, each with its own combination of power losses due to circulatory flow, fluid friction, shock, and mechanical friction.

When using a positive-displacement pump, the major factor to consider when specifying the pump is the power required. The power (as well as other factors) is also important when specifying a centrifugal pump. To determine the power, we apply Eq. (4.11) to a system.

Consider the system with a pump shown in Fig. 5.1, and write Eq. (4.11) from the plane at level (3) to the discharge plane (1).

$$\left[\frac{P_1}{\rho_1} - \frac{P_3}{\rho_3} \right] + \left[\frac{\bar{V}_1^2}{2\beta_1} - \frac{\bar{V}_3^2}{2\beta_3} \right] + g(z_1 - z_3) + E_f = -M^* \quad (5.1)$$

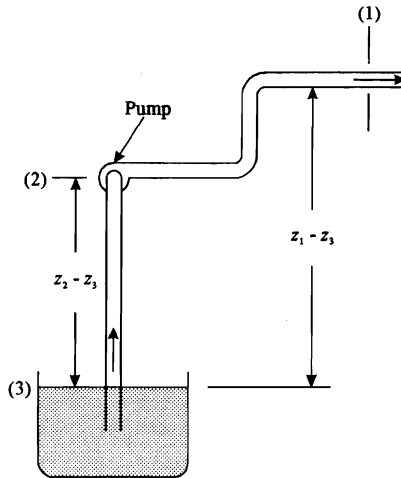


Fig. 5.1 Reference levels for the analysis of pump application.

If the frictional loss within the pump itself is accounted for by a mechanical efficiency Γ , then the work done by the pump is

$$\Gamma M_p^* = \left[\frac{P_1}{\rho_1} + \frac{\bar{V}_1^2}{2\beta_1} + gz_1 \right] - \left[\frac{P_3}{\rho_3} + \frac{\bar{V}_3^2}{2\beta_3} + gz_3 \right] + E_f \quad (5.2)$$

In the nomenclature associated with pumps, the quantities in the brackets are called *heads*, h , E_f is the *friction head*, and so

$$M_p^* = \frac{\Delta h}{\Gamma} \quad (5.3)$$

where Δh is the total head (i.e., the right side of Eq. (5.2)). Each head, as well as M_p^* , has the units of $J\text{ kg}^{-1}$ so that the power required by the pump from a motor (brake power) is given by

$$P_B = WM_p^* = \frac{W\Delta h}{\Gamma}, \quad (5.4)$$

where W is the mass flow rate in kg s^{-1} and P_B is in W . The power absorbed by the fluid (fluid power) is

$$P_f = W\Delta h \quad (5.5)$$

and, therefore,

$$\Gamma = \frac{P_f}{P_B}. \quad (5.6)$$

In the U.S.A., power ratings of pumps are given in *horsepower* (hp), whereas the ratings of the motors can be in either kW or hp. The conversion is $1\text{ kW} = 1.341\text{ hp}$. Often the flow rate is given in gallons per minute (gpm), so the reader should also be familiar with the following conversion:

$$1\text{ gallon (U.S.)} = 3.785 \times 10^{-3}\text{ m}^3.$$

In pumping liquids, there is a limit on the net positive *suction-head* that cannot be exceeded. This is set by the fact that if the dynamic pressure of the liquid ($P + \rho\bar{V}^2/2\beta$) falls below the vapor pressure of the liquid P_v , then the liquid vaporizes, and no liquid is drawn into the pump. This phenomenon is called *cavitation*. For example, consider the liquid just before it enters the pump at plane (2) in Fig. 5.1. In order to avoid cavitation,

$$\left[\frac{\bar{V}_2^2}{2\beta_2} + \frac{P_2}{\rho} \right] > \frac{P_v}{\rho}. \quad (5.7)$$

The pump lifts the liquid from the reservoir through a pipe, and Eq. (4.11), written between the reservoir surface (3), which is open to the atmosphere, and the suction entrance of the pump (2), assuming $\bar{V}_3 = 0$, is

$$\left[\frac{P_2}{\rho} - \frac{P_3}{\rho} \right] + \frac{\bar{V}_2^2}{2\beta_2} + g(z_2 - z_3) + E_f = 0. \quad (5.8)$$

From Eqs. (5.7) and (5.8), we obtain the following requirement in terms of the height of lift and the pressure at the reservoir:

$$\frac{P_3}{\rho} - g(z_2 - z_3) - E_f > \frac{P_v}{\rho}. \quad (5.9)$$

Therefore, the net positive suction-head defined below must indeed be positive:

$$h_{\text{nps}} = \left[\frac{P_3}{\rho} - \frac{P_v}{\rho} \right] - g(z_2 - z_3) - E_f > 0. \quad (5.10)$$

148 Flow and Vacuum Production

The efficiency of centrifugal pumps is a maximum at the design conditions, falling off on either side of them (Fig. 5.2). In selecting a centrifugal pump, one should consider its head-flow rate *characteristic curve*. The head is usually given in terms of feet of the fluid flowing through the pump, and indicates the height of a column of the liquid which could be pulled up through a frictionless pipe to the pump itself, assuming the limit imposed by cavitation, Eq. (5.10), is not exceeded. In practice, of course, the friction loss and any fitting or meter losses would have to be subtracted from this height.

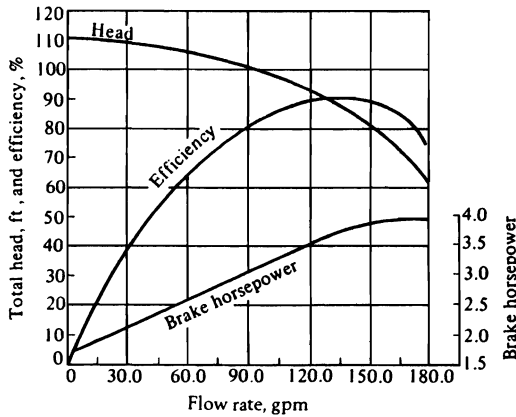
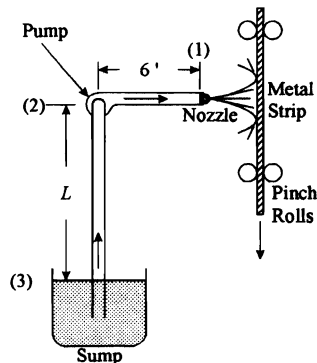


Fig. 5.2 Characteristic curves for a centrifugal pump.

When the head is expressed in feet, in reality the units are $\text{ft lb}_f \text{ lb}_m^{-1}$, where lb_f and lb_m are the units for pound force and pound mass from the English system of units. A pound force is the force required to accelerate one pound mass by the acceleration of gravity (32.2 ft s^{-2}). In the following example, the reader is exposed to these units, as well as conversions to SI units.

Example 5.1 A strip of metal emerging from a set of rolls is to be cooled by means of a spray of water. If 60 gpm are required, and the pressure drop across the spray nozzle is 15 psi at this flow rate, is it possible to install the pump, as depicted to the right, if the characteristic curves given in Fig. 5.2 apply? Assume 3-in. welded steel-piping up to the pump and 1-in. welded steel-piping to the nozzle. The problem is specified in units commonly encountered in engineering situations involving pumps in the U.S.A.



Solution. From Fig. 5.2, we obtain the total head delivered by the pump, $-M^*$, which is 107 ft at 60 gpm. In reality, the units of the head are $\text{ft lb}_f \text{ lb}_m^{-1}$.

Next we write Eq. (5.1) from planes (3) to (1). In this instance, $L = z_1 - z_3$, $\bar{V}_3 = 0$, $\beta_1 \approx 1$, and $\rho_1 = \rho_3 = \rho = 1000 \text{ kg m}^{-3}$; therefore the mechanical energy equation is

$$\left[\frac{P_1 - P_3}{\rho} \right] + \frac{\bar{V}_1^2}{2} + gL + E_f = -M^*$$

Starting with $-M^* = 107 \text{ ft lb}_f \text{ lb}_m^{-1}$, we convert to SI units:

$$-M^* = \frac{107 \text{ ft lb}_f}{\text{lb}_m} \left| \frac{1.356 \text{ N m}}{1 \text{ ft lb}_f} \right| \frac{1 \text{ lb}_m}{0.4536 \text{ kg}} = 320 \text{ N m kg}^{-1}.$$

Now we proceed to evaluate the terms on the left side of the mechanical energy equation. The pressure drop across the nozzle is given as 15 psi. This is equivalent to

$$P_1 - P_3 = \frac{15 \text{ lb}_f}{\text{in}^2} \left| \frac{1^2 \text{ in}^2}{(0.0254)^2 \text{ m}^2} \right| \frac{4.448 \text{ N}}{1 \text{ lb}_f} = 1.034 \times 10^5 \text{ N m}^{-2}.$$

Thus

$$\frac{P_1 - P_3}{\rho} = \frac{1.034 \times 10^5 \text{ N}}{\text{m}^2} \left| \frac{\text{m}^3}{1,000 \text{ kg}} \right| = 103.4 \text{ N m kg}^{-1}.$$

At 60 gpm, we calculate the velocity in the 1-in. pipe (diameter equals 25.4 mm) as follows:

$$\bar{V}_1 = \frac{60 \text{ gallon}}{\text{min}} \left| \frac{3.785 \times 10^{-3} \text{ m}^3}{1 \text{ gallon}} \right| \frac{1 \text{ min}}{60 \text{ s}} \left| \frac{4}{\pi} \right| \frac{1}{0.0254^2 \text{ m}^2}$$

$$\bar{V}_1 = 7.47 \text{ m s}^{-1}.$$

Similarly in the 3-in. pipe, we get

$$\bar{V} = 0.829 \text{ m s}^{-1}.$$

For now, we consider L (in m) to be an unknown. Therefore,

$$gL = \frac{9.807 \text{ m}}{\text{s}^2} \left| \frac{L \text{ m}}{1} \right| = 9.807L \text{ m}^2 \text{ s}^{-2} = 9.807L \text{ N m kg}^{-1}.$$

Next we formulate E_f :

$$E_f = \underbrace{\frac{1}{2} e_f \bar{V}^2}_{\text{entrance loss}} + 2f \underbrace{\left[\frac{L}{D} \right]}_{\text{3-in. pipe loss}} \bar{V}^2 + 2f \underbrace{\left[\frac{L}{D} \right]}_{\text{1-in. pipe loss}} \bar{V}_1^2.$$

From Figs. 4.4 and 4.5, we obtain:

$$e_f = (2)(0.4) = 0.8.$$

150 Flow and Vacuum Production

The Reynolds numbers are

$$\text{Re (1-in. pipe)} = \frac{D \bar{V}_1 \rho}{\eta} = \frac{(0.0254)(7.47)(1000)}{(0.001)} = 1.90 \times 10^5$$

and similarly

$$\text{Re (3-in. pipe)} = 6.32 \times 10^4.$$

Now we seek the respective friction factors:

	Re	ϵ/D	f
1-in. pipe	1.9×10^5	0.0018	0.0050
3-in. pipe	6.3×10^4	0.0006	0.0055

With these friction factors, we calculate E_f :

$$E_f = \left[\frac{1}{2} \right] (0.8)(0.829^2) + (2)(0.0055) \left[\frac{L}{0.0762} \right] (0.829^2) \\ + (2)(0.0050) \left[\frac{1.829}{0.0254} \right] (7.47^2)$$

$$E_f = 40.46 + 0.09921L, \text{ m}^2 \text{ s}^{-2} \text{ or N m kg}^{-1}.$$

Collecting terms in the mechanical energy equation we have:

$$103.4 + \frac{7.47^2}{2} + 9.807L + 40.46 + 0.09921L = 320.$$

Therefore, $L = 14.96$ m.

We should be suspect of this result. We know from our everyday experience that when pumps are situated more than 34 ft (10.4 m) above water, there is cavitation and the water cannot be pumped.

In a more formal manner, let's examine the net positive suction head. We use E_f only between (3) and (2). Also, $(P_3 - P_v)/\rho = P_3/\rho$ in this case. Therefore

$$h_{\text{nps}} = \frac{P_3}{\rho} - gL - E_f,$$

with

$$\frac{P_3}{\rho} = \frac{1 \text{ atm m}^3}{1000 \text{ kg}} \left| \frac{1.01325 \times 10^5 \text{ N}}{1 \text{ atm m}^2} \right. = 101.32 \text{ N m kg}^{-1}$$

$$gL = (9.807)(14.96) = 146.7 \text{ N m kg}^{-1}$$

and

$$E_f = (2)(0.0055) \left[\frac{14.96}{0.0762} \right] (0.829^2) = 1.48 \text{ N m kg}^{-1},$$

then

$$h_{\text{npss}} = -46.87 \text{ N m kg}^{-1}.$$

Cavitation will occur because $h_{\text{npss}} < 0$, and the installation will not work with $L = 14.96$ m. A solution is to decrease L to 6 m and to compensate for the reduction in friction loss, E_f , by adding a gate valve to the system between the pump and the nozzle.

With the gate valve, the friction losses are

$$E_f = \left[\frac{1}{2} \right] (0.8)(0.829^2) + (2)(0.0055) \left[\frac{6}{0.0762} \right] (0.829^2) + (2)(0.0050) \left[\frac{1.829}{0.0254} \right] (7.47^2) \\ + (2)(0.0050) \left[\frac{L_e}{D} \right]_v (7.47^2),$$

where $(L_e/D)_v$ is the equivalent length-to-diameter ratio for the gate valve. After collecting terms, we get

$$E_f = 41.05 + 0.558 \left[\frac{L_e}{D} \right]_v, \text{ N m kg}^{-1}.$$

Since the total head at the desired flow rate is 320 N m kg^{-1} , the system will perform as desired when $(L_e/D)_v$ is such that

$$320 = 103.4 + \frac{7.47^2}{2} + (9.807)(6) + 41.05 + 0.558 \left[\frac{L_e}{D} \right]_v$$

$$\left[\frac{L_e}{D} \right]_v = \frac{320 - 231.2}{0.558} = 159.$$

From Table 4.2 we see that the system will work with the gate valve closed about one-half. The reader can check to see whether the net positive suction head is positive.

5.2 FANS AND BLOWERS

Fans and blowers are used for moving gases. We employ fans when the pressure drop in the system to overcome is not larger than about 50 in. w.c.,* although volumes up to several hundred thousand cubic feet per minute (cfm) may be involved. Blowers and turboblowers, on the other hand, are used in situations where larger pressure drops occur.

As in the case of pumps, there are many different designs of fans—axial flow, propeller and cross-flow fans as well as centrifugal types with a variety of blade configurations. All manufacturers of gas-moving equipment supply characteristic curves describing the performance of their equipment under the specified operating conditions at the inlet, as, for example, in Fig. 5.3, which presents curves for both the static and total pressures and the

*The notation in. w.c., or inches water-column, is often used as the unit for pressure drop. Normal atmospheric pressure is 407.14 in. w.c.

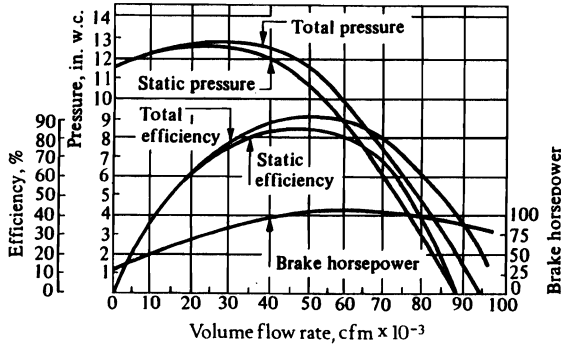


Fig. 5.3 Characteristic curves for a fan.

static and total efficiencies. If one wants to use a fan for moving a specified amount of gas against a given system resistance, it is necessary to know the static pressure developed by the fan at that flow rate.

Blowers are essentially constant-pressure machines with power consumption almost directly proportional to the volume delivered. Characteristic performance curves for a variable speed turboblower are given in Fig. 5.4. Pressure is in psig, which represents a gage pressure* in $\text{lb}_f \text{in}^{-2}$, and the speed of the blower is in revolutions per minute (rpm), and the volume flow rate is in cubic feet per minute (cfm). Blowers and turboblowers find their typical applications in large metallurgical processes, such as in producing the air blast for blast furnaces and smelting furnaces.

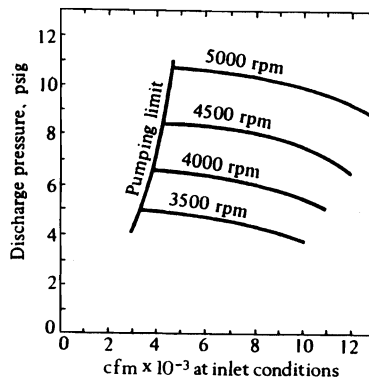


Fig. 5.4 Typical characteristic curves for a variable-speed blower.

Now, consider how the fan characteristics are measured. Figure 5.5(a) illustrates an appropriate system provided with a damper, so that the flow throughput may be varied. The Pitot tube measures the total pressure P_t , which is made up of the static pressure P_s (measured by the static pressure gage), and the dynamic pressure $\frac{1}{2}\rho V^2$. By adjusting the damper to various positions, the values of P_t and P_s corresponding to the various flow rates can be

*The gage pressure is the pressure in excess of the ambient pressure.

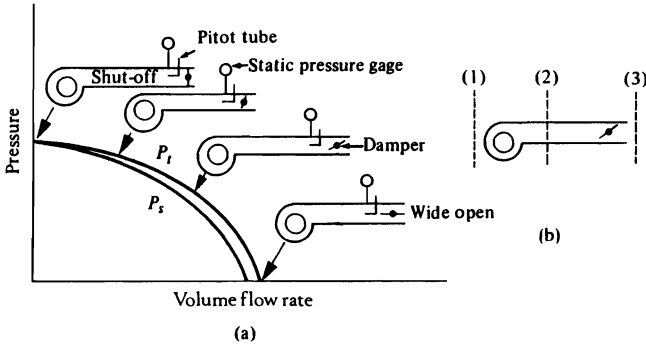


Fig. 5.5 Obtaining characteristic curves of a fan.

generated. Both of these values are relative to the inlet conditions, and are really pressure increases developed by the fan. At any flow rate, a theoretical horsepower may be calculated corresponding to either P_s or P_t , so that the definition of the *static efficiency*, Γ_s , as well as of the total efficiency, Γ , is based on the actual, or so-called brake horsepower.

The above statement can also be demonstrated by use of Bernoulli's equation applied to the system shown in Fig. 5.5(b). Between planes (1) and (3), the energy balance is simply

$$M^* + E_f = 0. \tag{5.11}$$

In this case, the system friction is composed of the resistance offered by the damper and the exit losses, that is, the friction between planes (2) and (3). The mechanical energy balance between planes (2) and (3) is then expressed

$$E_f = \left[\frac{P_2 - P_3}{\rho} \right] + \left[\frac{\bar{V}_2^2}{2} \right] \tag{5.12}$$

assuming $\beta = 1$.

Hence, by combining Eqs. (5.11) and (5.12), and noting $P_1 - P_3$, we arrive at

$$-M^* = \left[\frac{P_2 - P_1}{\rho} \right] + \left[\frac{\bar{V}_2^2}{2} \right], \tag{5.13}$$

or

$$-M^* \rho = (P_2 - P_1) + \left[\frac{\rho \bar{V}_2^2}{2} \right]. \tag{5.14}$$

Writing the above expression with the actual or brake horsepower P_B and the efficiency Γ , we obtain

$$\Gamma P_B = -M^* \rho Q = \left[(P_2 - P_1) + \frac{\rho \bar{V}_2^2}{2} \right] Q. \tag{5.15}$$

where Q is the volume flow rate.

Thus the total power delivered is based on the sum of the static pressure ($P_2 - P_1$) and the dynamic pressure ($\frac{1}{2}\rho\bar{V}_2^2$), or what we call the total pressure, as incorporated in brackets.

5.3 INTERACTIONS BETWEEN FANS OR PUMPS AND SYSTEMS

Because a fan is part of an overall system, the system as a whole determines the size of the fan required. For any system, there is a certain curve of volume flow rate versus system resistance or pressure drop (see Fig. 5.6). The reader should realize by now that the resistance usually increases as the square of the volume flow rate for a highly turbulent system. The system may contain any combination of duct work, beds of fluidized or packed solids, dust collectors, flues, etc. There is usually a specific volume throughput Q' , required for proper operation of the process; this fixes the pressure drop resistance of the system, which in turn must be overcome by the fan or blower. Essentially then, the fan characteristic curve must intersect the system curve at the desired $Q' - \Delta P$ coordinate (the so-called *operating point*). The efficiency and required horsepower are then fixed. Note that a different fan with a different characteristic curve would place the operating point at a different position on the system curve, resulting in a flow different from Q' .

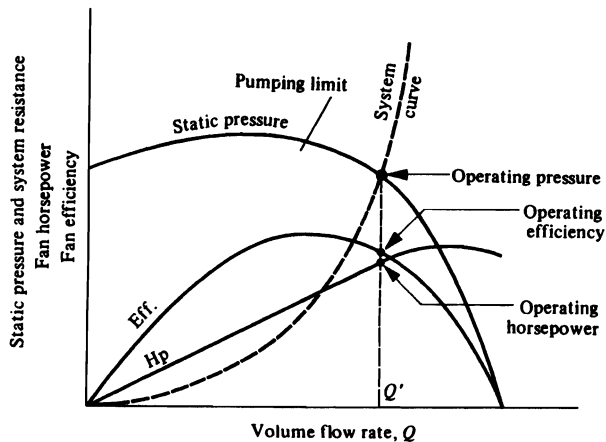


Fig. 5.6 Relationship between the fan curves and system curve. Often only the static pressure curve is supplied, so one assumes it is approximately the same as the total pressure curve.

The normal operating range for a fan is to the right of the peak of its pressure-volume curve. The so-called *pumping limit*, defines the furthest possible left-hand operating point. *Pumping* occurs when the fan is slowed down to the point where the static pressure created is less than the static pressure in the discharge line. At that point a flow reversal takes place. After this reversal, a momentary drop in the pressure in the discharge line occurs, and flow starts in a normal direction again. This pattern is repeated very rapidly and results in a pumping-type action, which may cause damage to the fan unless flow below this limit is avoided. It usually turns out that this point is reached at the maximum on the fan *total pressure* curve, which in turn is usually slightly to the right of the maximum of the static pressure curve.

It is not always possible to make desired changes in the operating point of a fan system. Changes in operating temperature or pressure drop require reevaluation of the system resistance curve, and if this changes, the operating point shifts, unless the fan is adjusted to keep Q' constant. Conversely, if it is desired to change Q' , then the operating point has to be changed, and consequently the fan characteristic curve must be changed.

In order to estimate the effect of deviations from the specified conditions, or the effect of a change in fan size or speed, on the behavior of the fan or the gas, the so-called *fan laws* are used to adjust from one set of operating variables to another. The variables are given in Table 5.1.

Table 5.1 Variables for fan laws

Speed of rotation	n
Impeller diameter	D
Gas density	ρ
Static pressure	P_s
Power	P_B
Volume flow	Q

The fan laws are:

$$Q = k_1 D^3 n, \quad (5.16)$$

$$P_s = k_2 D^2 n^2 \rho, \quad (5.17)$$

$$P_B = k_3 D^5 n^3 \rho. \quad (5.18)$$

As an example of the use of the fan laws, if the density of the gas varies, and the speed and volume flow remain constant, then Eqs. (5.17) and (5.18) tell us that both the horsepower and the static pressure would be expected to vary *directly* with the density. The proportionality constants k_1 , k_2 , and k_3 are constants over a limited range, which should not deviate too far from a given point on the curve of pressure versus flow rate.

Changes in the pattern of flow of the gases entering the fan will also change the characteristic curve, since the calibration is performed with gases entering smoothly at right angles to the rotor. If the gases enter otherwise, then their flow through the fan will affect the characteristic curves.

It is best, therefore, to overrate fans somewhat on both the pressure and volume specifications, but not too much, because severe damping, if necessary, decreases the efficiency and wastes the available power. The problems that can arise from errors in matching the system and fan curves are illustrated in the following example.

Example 5.2 Part of an iron-ore pelletizing plant consists of a moving chain grate (carrying a bed of pellets subjected to a hot gases) and associated gas cleaning and exhaust equipment, as shown schematically in Fig. 5.7. The total pressure drop due to duct work, at the required flow of 320 000 cfm at 394 K, is 3.5 in. w.c., and, when added to the *calculated* design bed-resistance of 9.5 in. w.c. at the design flow, gives a total system *design resistance* of 13.0 in. w.c. The fan to be used in this system is then specified to meet a 320 000 cfm flow with a 13.0 in. w.c. static pressure drop (point O in Fig. 5.8).

Suppose, however, that when the plant is built, the *actual* pressure drop across the bed of pellets at the required flow is 21.0 in. w.c. This means that the actual system curve (I)

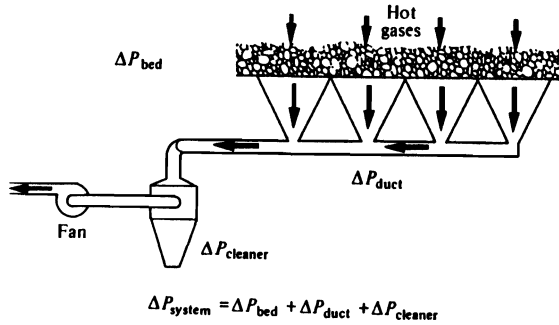


Fig. 5.7 Schematic diagram of an iron-ore pelletizing plant for Example 5.2.

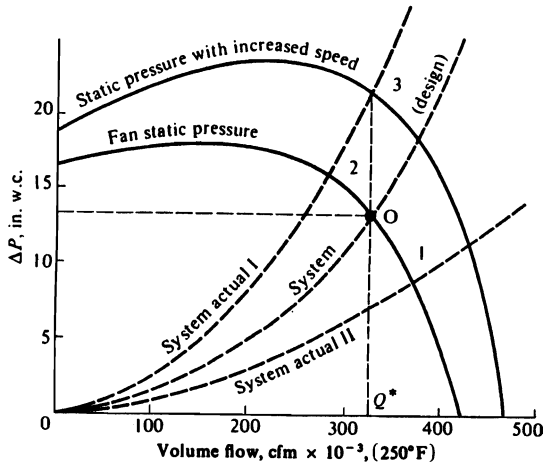


Fig. 5.8 Interaction between the system-resistance curves and fan curves for Example 5.2.

is different from the design system curve. Now the fan operates at point 2 (Fig. 5.8), and it pulls less than the required flow through the system (280 000 cfm). In this case, the only alternatives to regain a flow of 320 000 cfm are either to decrease the system resistance, or to change the characteristic curve by increasing the fan speed. In the first instance, one could decrease the system resistance by decreasing the bed height. If this is done, however, the lateral speed of the bed must be increased in order to keep the production rate at the design value. However, this may not be possible, because there is usually a minimum reaction time for the exposure of the solids to the hot gases, and the original design is usually close to that minimum. Changes in duct work may also be possible, but usually are not practical once the plant is built.

The other alternative—speeding up the fan until the operating condition is at point 3—is easier but may be very expensive. Reference to the fan laws shows us that the power required is proportional to the cube of the flow; that is, for constant fan size and gas density, $Q \propto n$, and $P_B \propto n^3$, so that $P_B \propto Q^3$. Therefore, for an increase of flow in the ratio

$320\,000/280\,000 = 1.14$, the ratio of the new horsepower required to the old will be $(1.14)^3 = 1.50$; in other words, a motor 50% more powerful is required. This may be quite expensive and could cause many problems in the electrical system. The ultimate solution is to buy a new fan.

If, on the other hand, the actual bed-resistance were, e.g., 7 in. w.c., then the fan would pull too much gas through the system, as at point 1 (Fig. 5.8). This can easily be corrected by increasing the system resistance through the use of dampers, until the system and fan curves coincide at the required flow and pressure drop, point O.

We have seen that the operating point of a system with a fan is given by the intersection of the system curve with the characteristic pressure curve of the fan. The same principle applies to the use of pumps where the operating curve is given by the intersection of the system curve with the characteristic head curve of the pump. In installations with more than one pump, this principle can lead to a rather surprising result; that the use of two equivalent pumps, rather than one, does not double the flow rate through the system. This is illustrated by the following example.

Example 5.3 Part of the process of regenerating spent hydrochloric acid from a continuous pickling line in a steel strip mill is shown in Fig. 5.9. When both pumps operate, the flow rate is 30 gpm ($1.89 \times 10^{-3} \text{ m}^3 \text{ s}^{-1}$). What is the flow rate when one pump operates? The pumps are identical with the same characteristic head curve, Fig. 5.10. Assume that the flow is highly turbulent and that the "head" in the system is primarily because of friction in the system.

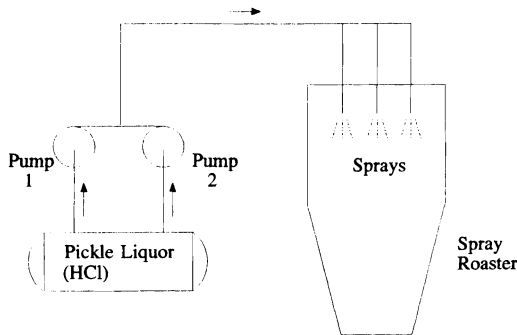


Fig. 5.9 System for Example 5.3.

Solution. With both operating, the pumps work against a head given by

$$h_{12} = E_f = KQ^2,$$

where h_{12} is the head overcome by both pumps 1 and 2, Q is the volume flow rate and K is a constant. We have assumed $E_f = KQ^2$ because the flow is turbulent. Therefore, the work done by one pump, when both are operating, must be

$$h_1 = \frac{h_{12}}{2} = \frac{KQ^2}{2},$$

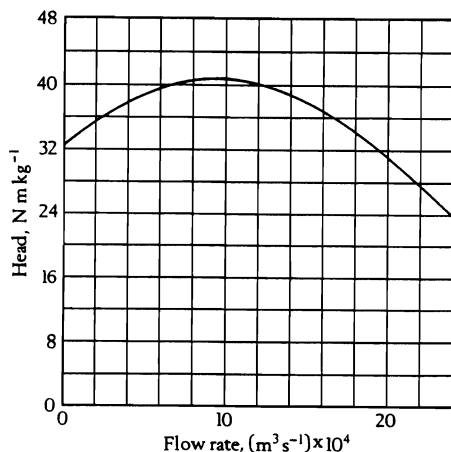


Fig. 5.10 Characteristic head curve for the pumps in Example 5.3.

with a flow rate of $Q/2$. Thus $Q/2 = 15 \text{ gpm}$ ($9.45 \times 10^{-4} \text{ m}^3 \text{ s}^{-1}$) which gives an operating point at $h_1 = 40.8 \text{ N m kg}^{-1}$ from Fig. 5.10. Therefore,

$$K = \frac{2}{\text{kg}} \left| \frac{40.8 \text{ N m}}{\text{kg}} \right| \frac{\text{s}^2}{(1.89 \times 10^{-3})^2 \text{ m}^6} = 2.28 \times 10^7 \text{ N s}^2 \text{ kg}^{-1} \text{ m}^{-5}.$$

With this value of K , we can plot the system curve on Fig. 5.10 and determine the operating point when one pump operates by itself.

$$h_1 = KQ^2.$$

$Q, \text{ m}^3 \text{ s}^{-1}$	$h_1, \text{ N m kg}^{-1}$
5×10^{-4}	5.7
10×10^{-4}	22.8
12.5×10^{-4}	35.6
15×10^{-4}	51.3

The curve generated by these calculated data intersects the characteristic head curve at $h = 39.2 \text{ N m kg}^{-1}$ and $Q = 13.2 \times 10^{-4} \text{ m}^3 \text{ s}^{-1}$ (21.0 gpm). Notice that with both pumps operating, the throughput is not doubled; in this example it increases by only 43%.

5.4 SUPERSONIC NOZZLES AND JET BEHAVIOR

During the past three decades, jets of gas have become important in several metallurgical processes; process engineers should therefore have a good understanding of the characteristics and behavior of jets, in order to make the best use of them. Applications of supersonic nozzles include injection of oxygen into molten steel baths for refining purposes, and inert gas jets used to atomize liquid metal streams into metal powders.

Consider the flow nozzle described in Fig. 5.11. If the area of the nozzle opening is considerably smaller than that of the approach pipe, then the velocity in the pipe is negligible (the gas is stagnant) with respect to the velocity at the nozzle opening, as long as the pressure in the pipe is at or above the *stagnation* pressure. The application of Bernoulli's equation to the adiabatic and frictionless flow of an ideal compressible gas under these conditions yields an equation for the velocity in the nozzle opening \bar{V}_t :

$$\bar{V}_t = \sqrt{\frac{2P_0}{\rho_0} \left[\frac{\gamma}{\gamma - 1} \right] \left[1 - \left(\frac{P_t}{P_0} \right)^{(\gamma - 1)/\gamma} \right]}, \tag{5.19}$$

where reference points are defined in Fig. 5.11 and $\gamma = C_p/C_v$. We may use this equation for a flow nozzle operating at subsonic velocities.

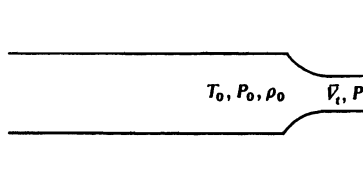


Fig. 5.11 Reference points for flow-nozzle equations.

Now the speed at which a compression-expansion wave passes through a medium, that is, the speed of sound V_s in that medium, is given by

$$V_s = \left(\frac{\partial P}{\partial \rho} \right)_s^{1/2}, \tag{5.20}$$

where the subscript on the partial derivative indicates constant entropy. For an ideal gas,

$$V_s = \left(\frac{\gamma P}{\rho} \right)^{1/2}. \tag{5.21}$$

The equation of momentum for one-dimensional flow is

$$\frac{dP}{\rho} + \bar{V} d\bar{V} = 0. \tag{5.22}$$

Substituting $dP = V_s^2 d\rho$ into Eq. (5.22), we get

$$V_s^2 \frac{d\rho}{\rho} + \bar{V} d\bar{V} = 0. \tag{5.23}$$

The continuity equation, which requires that the mass flow rate remain constant at all points in the nozzle

$$\frac{d\rho}{\rho} + \frac{d\bar{V}}{\bar{V}} + \frac{dA}{A} = 0, \tag{5.24}$$

160 Flow and Vacuum Production

must be satisfied along with Eq. (5.23), and so

$$\frac{d\bar{V}}{\bar{V}} \left[\frac{\bar{V}^2}{V_s^2} - 1 \right] = \frac{dA}{A}. \quad (5.25)$$

The Mach number, M , is defined as \bar{V}/V_s , so that finally

$$\frac{d\bar{V}}{\bar{V}} (M^2 - 1) = \frac{dA}{A}. \quad (5.26)$$

Now, if the velocity at any point in the nozzle is *less than* $M = 1$, and if the area of the nozzle decreases at that point (dA/A is negative), then the velocity increases at that point ($d\bar{V}/\bar{V}$ is positive).[†] At the throat $dA = 0$, so either $M = 1$ or $d\bar{V}/\bar{V} = 0$. If $M < 1$ at the throat, then $d\bar{V}/\bar{V}$ is zero and no further increase in velocity is possible, i.e., this is the maximum velocity which can be achieved.

If $M = 1$ at the throat, then we have reached the point at which supersonic flow can take place. By adding a diverging section on the end, and referring to Eq. (5.26), we see that if dA/A is positive, then either $d\bar{V}/\bar{V}$ will be positive, and a further increase to higher velocities is achieved in the diverging section, or the flow must come to a stop. The former case occurs as long as $P_t > P_{\text{exit}}$. A converging-diverging nozzle is shown in Fig. 5.12. It is usually called a *deLaval nozzle*.

For a converging nozzle, we obtain the conditions required to attain sonic velocity at the throat by using the energy relation for an ideal gas undergoing adiabatic flow:

$$\frac{T_0}{T} = 1 + \frac{\gamma - 1}{2} M^2. \quad (5.27)$$

When $M = 1$, sonic conditions exist denoted by an asterisk, and since the flow is also isentropic, substitution of the ideal gas relationship

$$\frac{P}{P_0} = \left[\frac{T}{T_0} \right]^{\gamma/(\gamma - 1)} = \left[\frac{\rho}{\rho_0} \right]^\gamma \quad (5.28)$$

gives the *critical pressure ratio*

$$\frac{P_t^*}{P_0} = \left[\frac{2}{\gamma + 1} \right]^{\gamma/(\gamma - 1)}. \quad (5.29)$$

This means that the ratio of throat pressure to reservoir pressure at the sonic flow condition is governed only by the value of γ . For air and oxygen, $P_t^*/P_0 = 0.528$. For pressure ratios between 1.00 and 0.528, the mass flow rate of the gas is $W_t = \rho_t \bar{V}_t A_t$, and using Eq. (5.28),

$$W_t = A_t \frac{2\rho_0 P_0 \gamma}{\gamma - 1} \left[1 - \left(\frac{P_t}{P_0} \right)^{(\gamma - 1)/\gamma} \right] \left[\frac{P_t}{P_0} \right]^{1/\gamma}. \quad (5.30)$$

[†]The reader should consider whether or not $M > 1$ can be achieved in the converging portion of a nozzle.

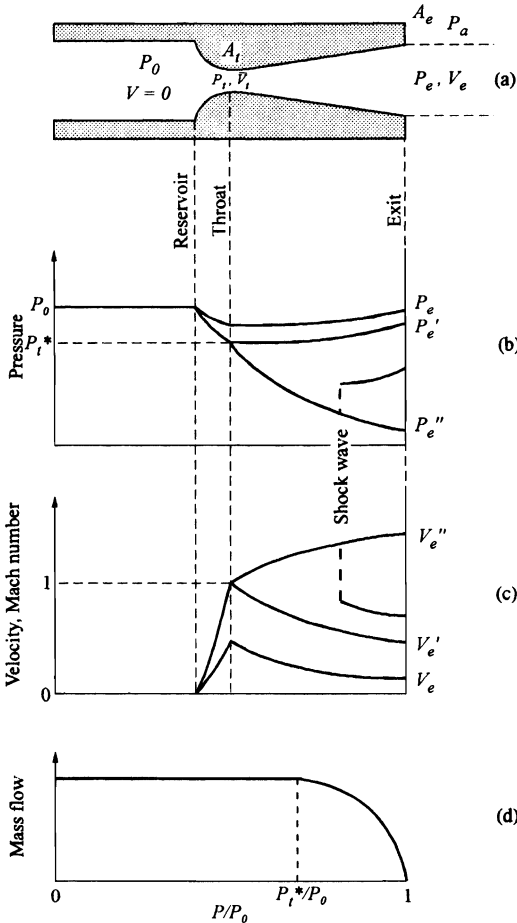


Fig. 5.12 Reference points and schematic internal conditions for various operating pressure ratios for converging-diverging nozzles.

Any further decrease in the ratio P_t/P_0 below that for the P_t^*/P_0 , caused, for example, by increasing the reservoir pressure P_0 , will not cause a further increase in the mass flow rate out of a converging nozzle, since the condition of isentropic flow is no longer satisfied beyond the nozzle. If $(P_t/P_0) \leq (P_t^*/P_0)$, then the nozzle is said to be *choked*, and the mass flow rate is

$$W_t^* = A_t \left[\rho_0 P_0 \gamma \left(\frac{2}{\gamma + 1} \right)^{(\gamma + 1)/(\gamma - 1)} \right]^{1/2} \quad (5.31)$$

For the nozzle with the additional diverging section, the mass flow at sonic or supersonic conditions is still given by Eq. (5.31). However, since the velocity increases along the length of the diverging portion, the pressure correspondingly decreases from that at the throat. The problem is to determine how long this portion of the nozzle should be made in order to

produce a jet with exit pressure P_e , equal to ambient pressure. Such a condition establishes the most effective condition for achieving the maximum supersonic jet length.

Up to this point, it has not been established what the absolute pressure at the throat, relative to the exit pressure, is. Several possible solutions arise, depending on the nozzle design. There are two values of P_t^*/P_e —and therefore two values of P_e , shown in Fig. 5.12(b), which result in isentropic shockless flow in the diverging portion of the nozzle for the conditions where $M = 1$ at the throat. The higher pressure P_e' will cause the flow to become subsonic again immediately at the throat, and will cause a decrease in velocity; the lower pressure P_e'' will allow supersonic flow throughout the nozzle. If the exit pressure is between P_e' and P_e'' , $P_t = P_t^*$, then somewhere in the nozzle, a discontinuous transition from a lower to higher pressure (and simultaneously from supersonic to subsonic flow) occurs, as shown schematically in Fig. 5.12. This produces a *shock wave*.

If the nozzle design is such that $P_e = P_e''$, then we may proceed to calculate the exit velocity, using the equation

$$V_e = \sqrt{\left[\left(\frac{2}{\gamma - 1} \right) \frac{\gamma P_0}{\rho_0} \left[1 - \left(\frac{P_e}{P_0} \right)^{(\gamma - 1)/\gamma} \right] \right]} \quad (5.32)$$

or

$$M_e^2 = \frac{2}{\gamma - 1} \left[\left(\frac{P_0}{P_e} \right)^{(\gamma - 1)/\gamma} - 1 \right]. \quad (5.33)$$

The mass flow rate and throat area are still given by Eq. (5.31).

Now that we have the mass flow rate, we may calculate the area of the exit by means of a mass balance, since $W_t^* = W_e$,

$$A_t \sqrt{\rho_0 P_0 \gamma \left(\frac{2}{\gamma + 1} \right)^{(\gamma + 1)/(\gamma - 1)}} = A_e \sqrt{\rho_0 P_0 \gamma \left(\frac{2}{\gamma - 1} \right) \left[1 - \left(\frac{P_e}{P_0} \right)^{(\gamma - 1)/\gamma} \right]} \cdot \left(\frac{P_e}{P_0} \right)^{1/\gamma}, \quad (5.34)$$

$$\left(\frac{A_t}{A_e} \right)^2 = \left(\frac{2}{\gamma - 1} \right) \left(\frac{\gamma + 1}{2} \right)^{(\gamma + 1)/(\gamma - 1)} \left(\frac{P_e}{P_0} \right)^{2/\gamma} \left[1 - \left(\frac{P_e}{P_0} \right)^{(\gamma - 1)/\gamma} \right]. \quad (5.35)$$

Ideally, we want $P_e = P_a$ (the ambient pressure), since then the ultimate adiabatic expansion is reached, and the jet issues from the nozzle at atmospheric pressure. If P_e is less than P_a , the ambient atmosphere compresses the flowing jet and collapses it in a series of shock waves. If $P_e > P_a$, the jet continues to expand beyond the nozzle tip. In both non-ideal situations, the efficiency of conversion of the nozzle velocity to jet momentum decreases.

The angle of divergence of the nozzle is usually about 7° in order to avoid separation of flow from the nozzle walls.

Example 5.4 In the basic oxygen steelmaking process, we decarburize a bath of molten iron-carbon alloy with gaseous oxygen which is blown into the bath from a lance held above the bath. Determine the dimensions of the converging-diverging nozzle which are required to achieve a velocity of Mach 2 at the exit with an oxygen flow rate of 15 000 scfm.* What is the required driving pressure?

Solution. From Eq. (5.33), we can obtain P_0 by assuming that $P_e = 1$ atm to achieve the best behavior of the jet, and noting that γ for O_2 is 1.4:

$$\left(\frac{P_0}{P_e}\right)^{0.286} = \frac{2^2}{\left(\frac{2}{0.4}\right)} + 1.0,$$

and thus

$$\frac{P_0}{P_e} = 7.85.$$

For $P_e = 1$ standard atmosphere, $P_0 = 7.95 \times 10^5 \text{ N m}^{-2}$ (7.84 atm). Now we can make use of Eq. (5.35) to find the ratio A_t/A_e :

$$\left(\frac{A_t}{A_e}\right)^2 = \left(\frac{2}{0.4}\right) \left(\frac{2.4}{2}\right)^{2.4/0.4} \left(\frac{1}{7.84}\right)^{2/1.4} \left[1 - \left(\frac{1}{7.84}\right)^{0.4/1.4}\right]$$

$$\left(\frac{A_t}{A_e}\right) = 0.595.$$

Finally, we can calculate A_t from Eq. (5.31), since the nozzle is choked, as otherwise supersonic velocities could not be reached.

The mass flow is

$$W_t^* = 15\,000 \text{ scfm} \times 0.089 \frac{\text{lb}_m}{\text{ft}^3} \times \frac{1 \text{ min}}{60 \text{ s}} = 22.2 \text{ lb}_m \text{ s}^{-1} = 10.1 \text{ kg s}^{-1}$$

$$10.1 = A_t \left\{ (10.41)(7.95 \times 10^5)(1.4) \left[\frac{2}{2.4} \right]^6 \right\}^{1/2} = 1.970 \times 10^3 A_t$$

$$A_t = 5.127 \times 10^{-3} \text{ m}^2$$

and

$$A_e = 8.617 \times 10^{-3} \text{ m}^2.$$

Thus, the throat diameter $d_t = 80.8$ mm, and the exit diameter $d_e = 105$ mm.

*Standard cubic feet per minute. $1 \text{ m}^3 \text{ s}^{-1} = 2.1189 \times 10^3 \text{ cfm}$.

As a jet exits from the nozzle, it entrains adjacent air, which in turn acts as a drag, creating turbulence. This slows some of the supersonically flowing gas to sonic and subsonic velocities and the supersonic core of the jet gradually decays, until at some distance from the nozzle the core disappears, and the entire jet is subsonic. Figure 5.13 shows the relationship between the exit velocity (in terms of Mach number) and the length of the supersonic core (in terms of either the ratio x/d_t , where x is the distance from the nozzle and d_t is the throat diameter, or the ratio x/d_e , where d_e is the exit diameter).

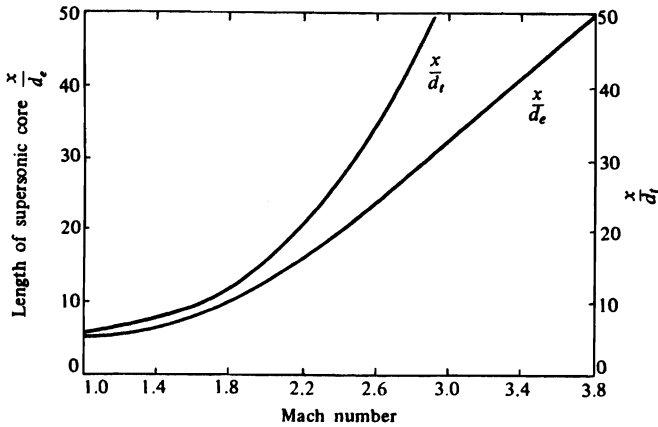


Fig. 5.13 Relationship between the length of supersonic core and exit Mach number.

We measure the overall spreading of the jet by the ratio r_0/r_i , where we define r_0 as the radius at which the velocity is one-half that at the center line. The typical velocity or impact pressure profile is that of a normal distribution about the center line. However, the spreading of the jet is minor until the supersonic core has decayed. Once this point has been reached, the jet expands at an included angle of about 18° . Figure 5.14 gives a dimensionless graph for determining the width of the jet as a function of the exit Mach number and the distance from the nozzle. We then take the *effective jet radius* r as $2r_0$, and can calculate it at any distance from the nozzle.

The increase in the mass flow of a subsonic jet due to the entrainment of the surrounding gas has been found to be directly proportional to the distance from the nozzle exit, according to the equation

$$W_x = W_e + k \sqrt{M_e \rho_e} \left[\frac{x}{d} \right], \tag{5.36}$$

where M_e = jet momentum at nozzle exit ($= W_e V_e$), x/d = distance from the nozzle exit, W_e = jet mass flow rate at nozzle exit, W_x = jet mass flow at x , ρ_e = density of the ambient gas.

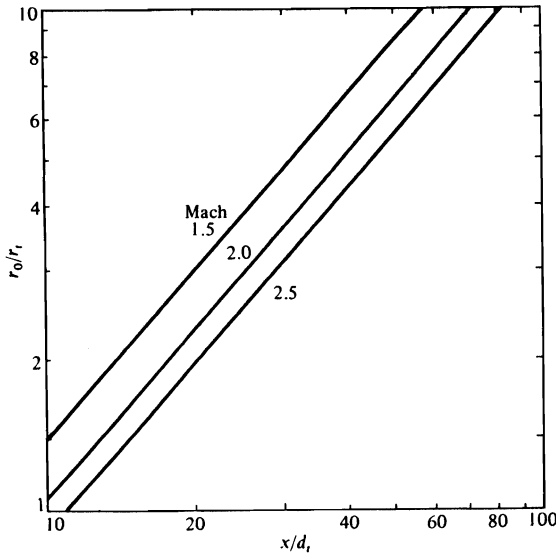


Fig. 5.14 Jet-spreading characteristics as a function of Mach number and distance from the nozzle. (Adapted from A. R. Anderson and F. R. Johns, *Jet Propulsion* 25, 13 (1955).)

In supersonic jets, the entrainment in the region where supersonic flow predominates is less than in the subsonic region, where Eq. (5.36) is satisfactory. A very satisfactory representation of the increased jet mass for supersonic jets with exit velocities between Mach 1 and 2 is given by*

$$\frac{W_x - W_e}{W_e} = 9 \times 10^{-3} \sqrt{\frac{T_0}{T_a A_e} \left[1 + \frac{(\gamma - 1)M^2}{2} \right]^{-1} \left[\left[\frac{x}{d_e} \right] - \left[\frac{x}{d_e} \right]_{\text{core}} \right]}, \quad (5.37)$$

where T_0 = stagnation temperature, °R, T_a = ambient temperature, °R, and $(x/d_e)_{\text{core}}$ = length of the supersonic core determined from Fig. 5.13. (Degrees Rankine, °R, is an absolute temperature scale equal to 9/5 K.) This equation does *not* describe the increasing entrainment in the region from the nozzle to a distance of about 10 nozzle diameters downstream, but since this is not the region of usual interest and also the rate of increase is not very strong in this region, the equation is still useful. Note that as the ambient temperature increases, the entrainment decreases.

We should point out that the entrainment of the surrounding gases dilutes the jet-gas concentration. For example, the concentration of oxygen in cold jets of pure oxygen issuing into cold air, at a distance of 6 ft (1.8 m) from the nozzle, is 90% in the case of a Mach 3 nozzle versus 80% in the case of a subsonic nozzle with 25 psig (1.7×10^5 Pa) driving pressure.

*This equation is derived from data presented in the report by J. D. Kapner and Kun Li, *Mixing Phenomena of Turbulent Supersonic Jets*, American Iron and Steel Inst., June 26, 1967.

5.5 VACUUM PRODUCTION

In materials processing, vacuum technology plays an important role in processes such as vacuum annealing, vacuum deposition of coatings, vacuum melting, and vacuum degassing. In addition, vacuum equipment is a standard item in almost every materials laboratory. For these reasons, it is important that materials engineers be acquainted with the principles and operation of vacuum-producing equipment.

The most important variable in the design and specification of equipment for a vacuum system is the pressure which the pumping system must be able to maintain in the work chamber. In the U.S.A., the most commonly used unit of vacuum measure is the torr,* which is equivalent to the old millimeters of mercury. In European usage, the pressure is commonly expressed in millibars (mbar), with 1 bar equal to normal atmospheric pressure. Therefore, $1000 \text{ mbar} = 760 \text{ torr} = 1.0133 \times 10^5 \text{ N m}^{-2}$. Figure 5.15 compares the various pressure scales, indicating the ranges of application of various types of vacuum gages and pumps.

Throughput (Q) is another term that is commonly used in vacuum technology. It is the quantity of gas, expressed as the volume of gas multiplied by its pressure, that passes a plane in a unit time. In SI units, throughput has units of $\text{Pa m}^3 \text{ s}^{-1}$. Coincidentally these units are equivalent to W , so throughput can also be pictured as energy flow. We should keep in mind that throughput is not a mass flow, but of course if the temperature is known then mass flow rate can be calculated from throughput.

Another variable is the speed at which the desired pressure is reached. We define the *speed* S_p , of any type of vacuum pump by

$$S_p = Q/P \quad (5.38)$$

where P is the pressure at the inlet to the pump, and Q is the throughput at that point. Typical units for S_p are $\text{m}^3 \text{ s}^{-1}$. We may use the same definition to express the pump-down speed of a system S_s , consisting of a working chamber, connecting duct work, and pumps, but the speed depends on the design of the rest of the system as well as on the pump itself.

A system, initially at atmospheric pressure, is first *roughed out* by either mechanical pumps or the first stage of an ejector system until a pressure is reached where vapor diffusion pumps, or further stages of an ejector system, become effective and can be used for final evacuation to the desired limiting pressure. During the initial roughing out, the gas density will be high enough, so that the mean free path of the gas is very small ($\sim 10^{-4} \text{ mm}$) compared with the dimensions of the conduit, and the flow rate of the gas is governed by the viscosity of the gas through the equations developed in previous chapters for turbulent and laminar flows. However, at low pressures, the density eventually reaches a value such that the mean free path is much greater than the conduit dimensions. At this point, viscosity is meaningless in determining the flow rate, and the gas flow becomes *molecular flow*. At an intermediate pressure, a transition flow regime is encountered when the mean free path is of the same order of magnitude as the equipment dimensions.

*The name torr comes from E. Torricelli, a student of Galileo, who devised the first single stroke pump by inverting a closed tube of mercury into a dish containing mercury, creating a vacuum in the tube.

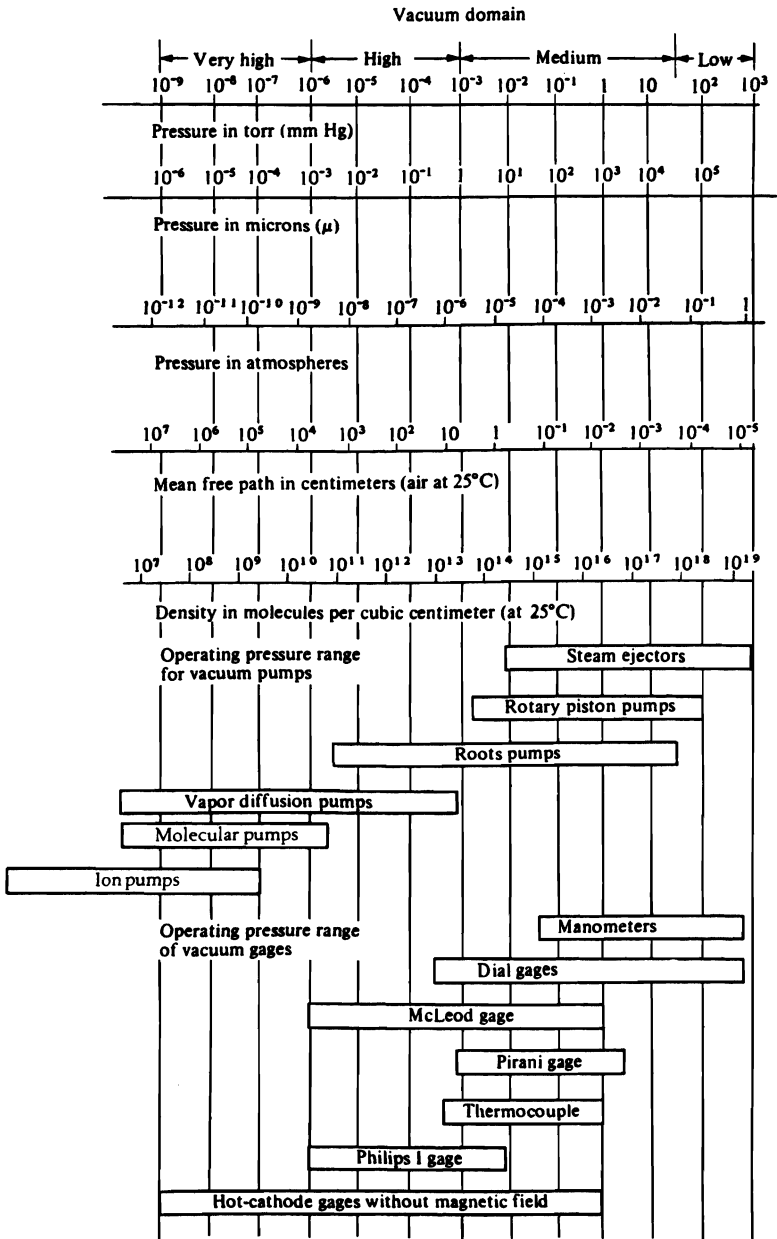


Fig. 5.15 Comparative pressure scales and ranges of application of various vacuum pumps and gages.

5.5.1 Molecular flow mechanics

In the *molecular flow* regime, the gas molecules move randomly, with a Maxwell-Boltzmann distribution of velocities, and collisions between molecules are rare compared to collisions with the walls. The only transfer of momentum is between molecules and the wall instead of from molecule to molecule. Net flow results from the statistical effect that the number of molecules leaving a given region is proportional to the number of molecules in the region, and the number reentering will be proportional to the number in the adjacent region. Knudsen developed the equations which govern the flow of gases through various geometries under molecular flow conditions. Consider a chamber with an aperture of area A , as in Fig. 5.16. The pressure on the downstream side of the aperture is P_2 and that in the chamber is P_1 . If the concentration of gas molecules is given by n (molecules mm^3), and the number hitting the wall is

$$Z = \frac{n\bar{V}}{4}, \text{ molecules mm}^{-2} \text{ s}^{-1}, \quad (5.39)$$

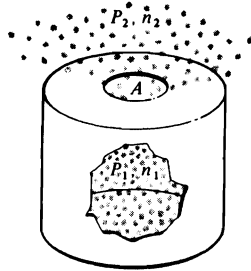


Fig. 5.16 Schematic chamber being evacuated from an internal pressure of P_1 to an external pressure of P_2 through an aperture of area A .

where \bar{V} is the average molecular speed given in Eq. (1.4), then the frequency Z of gas molecules per unit area passing from the high-pressure side of the aperture through it, is

$$Z_1 = \frac{n_1}{2\sqrt{\pi}} \left[\frac{2\kappa_B T}{m} \right]^{1/2}.$$

The frequency from the low-pressure side back through the opening

$$Z_2 = \frac{n_2}{2\sqrt{\pi}} \left[\frac{2\kappa_B T}{m} \right]^{1/2},$$

yields a net frequency

$$Z_{\text{net}} = Z_1 - Z_2 = \frac{1}{2\sqrt{\pi}} \left[\frac{2\kappa_B T}{m} \right]^{1/2} (n_1 - n_2). \quad (5.40)$$

For a circular opening, the net rate at which molecules leave the chamber is

$$\dot{n} = \frac{\pi D^2}{4} Z_{\text{net}} = \frac{\sqrt{\pi}}{8} \left[\frac{2\kappa_B T}{m} \right]^{1/2} D^2 (n_1 - n_2). \quad (5.41)$$

Because $n = P/\kappa_B T$,

$$\dot{n} = \left[\frac{2\pi}{m\kappa_B T} \right]^{1/2} \frac{D^2}{8} (P_1 - P_2), \text{ molecules s}^{-1} \quad (5.42)$$

or

$$\dot{n} = \left[\frac{2\pi}{MRT} \right]^{1/2} \frac{D^2}{8} (P_1 - P_2), \text{ kmol s}^{-1} \quad (5.43)$$

where M is the molecular weight, kg kmol^{-1} , and R is the gas constant ($R = 8.315 \text{ kJ kmol}^{-1} \text{ K}^{-1}$).

The throughput for flow of molecules across the aperture can be written as

$$Q = C(P_1 - P_2), \quad (5.44)$$

where C is the *conductance* of the aperture. By the definition of throughput and using the ideal gas law, we can also write

$$Q = \dot{n}RT, \quad (5.45)$$

so that

$$C = \frac{\dot{n}RT}{P_1 - P_2}. \quad (5.46)$$

By combining Eqs. (5.43) and (5.46), we arrive at the conductance of an aperture:

$$C = \left[\frac{2\pi RT}{M} \right]^{1/2} \frac{D^2}{8}. \quad (5.47)$$

We can write Eq. (5.47) in a simpler form:

$$C = \frac{\bar{V}}{4} A, \quad (5.48)$$

where \bar{V} is the Maxwellian speed of the molecules given by Eq. (1.4) and A is the area of the aperture. For other shapes (e.g., tubes), the conductance is usually given by Eq. (5.48) with a *transmission probability*, a , which is the probability that a molecule entering the tube will leave the tube at the other end. Thus, the conductance is found from

$$C = \frac{a\bar{V}}{4} A, \quad (5.49)$$

where A is the cross-sectional area of the tube. The conductance of an aperture of area A has a maximum value, and tubes and conduits of the same area will have a conductance less than the conductance of the aperture.

170 Flow and Vacuum Production

To describe molecular flow through long circular tubes, Knudsen derived

$$C = \frac{\pi \bar{V} D^3}{12L}, \quad (5.50)$$

or

$$a = \frac{4D}{3L}.$$

With this result, we can see that we must be careful in how we apply conductances. For example, Eq. (5.50) indicates that the conductance goes to infinity as L approaches zero, whereas the limit should be the value given by (5.48). In an attempt to deal with short tubes, it has been suggested that the aperture and the tube be considered as two flow resistors in series. When this is done

$$\frac{1}{C} = \frac{1}{C_1} + \frac{1}{C_2}, \quad (5.51)$$

where C is for the short tube, C_1 is for the aperture, and C_2 is for the "tube," itself, given by Eq. (5.50). As $L/D \rightarrow 0$ this result reduces to Eq. (5.48), and as $L/D \rightarrow \infty$, it reduces to Eq. (5.50). However, it is only approximate for intermediate values of L/D and can be in error by as much as 15%. Actually, the Monte Carlo method to track molecular motions through various configurations has been applied to calculate the transmission probabilities. Many of these results are reviewed and presented by O'Hanlon.³

The conductance of an entire vacuum system composed of several different components may be approximately calculated by analogy with electrical circuits. Specifically,

$$\frac{1}{C_{\text{system}}} = \frac{1}{C_1} + \frac{1}{C_2} + \frac{1}{C_3} + \dots \quad (5.52)$$

for a system with components 1, 2, 3, etc., in series, or, if the components are in parallel, then

$$C_{\text{system}} = C_1 + C_2 + C_3 + \dots \quad (5.53)$$

Table 5.2 presents the conductances of several shapes.

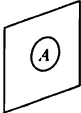
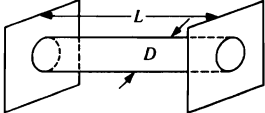

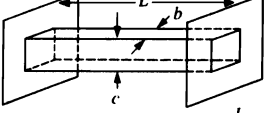
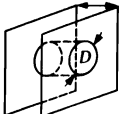
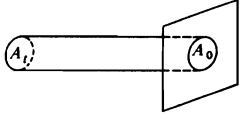
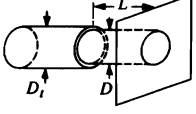
Example 5.4 A 150 mm diameter tube, with a length of 150 mm, connects a vacuum chamber and a vacuum pump. Which of the following modifications will give the greatest increase in conductance? (a) Decrease the length of the tube to 75 mm; (b) increase the diameter to 175 mm; (c) increase the length to 175 mm; (d) decrease the diameter to 125 mm.

Solution. We can immediately disregard modifications (c) and (d) because both result in an increase in L/D . The total conductance of the tube comprises the conductance of the aperture at the chamber-tube connection (C_1) and the tube itself (C_2). We combine Eqs. (5.48), (5.49) and (5.51):

$$\frac{1}{C} = \frac{4}{\bar{V}A} + \frac{4}{a\bar{V}A} = \frac{4}{\bar{V}A} \left[1 + \frac{1}{a} \right].$$

³J. F. O'Hanlon, *ibid.*

Table 5.2 Conductances of various geometric shapes for molecular flow*

Shape [†]	Conductance (L s ⁻¹) ^{††}	C, for air at 298 K
	$C = 3.64A \left(\frac{T}{M} \right)^{1/2}$	$= 11.7A$
	$C = 19.4 \frac{A^2}{BL} \left(\frac{T}{M} \right)^{1/2}$	$= 12.2 \frac{D^3}{L}$
	$C = 3.81 \frac{D^3}{L} \left(\frac{T}{M} \right)^{1/2}$	$= 12.2 \frac{(D_2 - D_1)^2 (D_2 + D_1)}{L}$
	$C = 9.70 \frac{b^2 c^2}{(b + c)L} \left(\frac{T}{M} \right)^{1/2}$	$= 31.1 \frac{b^2 c^2}{(b + c)L}$
	$C = 2.85D^2 \left(\frac{T}{M} \right)^{1/2} \left(\frac{1}{1 + 3L/4D} \right)$	$= 9.14 \frac{D^2}{1 + 3L/4D}$
	$C = 3.64 \left(\frac{T}{M} \right)^{1/2} \left(\frac{A}{1 - (A/A_1)} \right)$	$= \frac{11.7A_0}{1 - A_0/A_1}$
	$C = 3.81 \frac{D^3}{L} \left(\frac{T}{M} \right)^{1/2} \left(\frac{1}{1 + \frac{4D}{3L} \left(1 - \frac{D^2}{D_1^2} \right)} \right)$	$= \frac{12.2D^3}{L \left[1 + \frac{4D}{3L} \left(1 - \frac{D^2}{D_1^2} \right) \right]}$

*This table is taken from J. M. Lafferty, *Techniques of High Vacuum*, General Electric Report No. 64-RL-3791G, 1964.

[†]The variables and their respective dimensions are

- A = area, cm²,
- D = diameter, cm,
- L, b, c = length dimensions, cm,
- B = perimeter, cm,
- T = absolute temperature, K,
- M = molecular weight, g mol⁻¹

^{††}1 L s⁻¹ = 10⁻³ m³ s⁻¹. L is liter.

172 Flow and Vacuum Production

With the original dimensions of the tube, the transmission probability is

$$a = \frac{4D}{3L} = \frac{4 \times 150}{3 \times 150} = \frac{4}{3}$$

so that

$$C = 0.571 \left[\frac{\bar{V}A}{4} \right].$$

For modification (a):

$$a = \frac{4 \times 150}{3 \times 75} = \frac{8}{3}$$

and

$$C_{(a)} = 0.727 \left[\frac{\bar{V}A}{4} \right].$$

For modification (b):

$$a = \frac{4 \times 175}{3 \times 150} = \frac{14}{9}$$

and

$$C_{(b)} = 0.607 \left[\frac{\bar{V}A}{4} \right].$$

The greatest increase is achieved by modification (a).

Pumping speed has the same units as conductance, but it should be noted that conductance implies a pressure gradient across a specific geometry. Pumping speed is simply the volume of gas flowing across any plane in a system per second, which is measured at the pressure existing at that particular plane.

The pump-down speed of a system depends on both the pump speed and the conductance of the connections. Refer to the schematic diagram of a vacuum melting system in Fig. 5.17. Because $P = Q/S$ at the inlet to the duct, $P_p = Q/S_p$ at the inlet to the pump, and $(P - P_p) = Q/C$ over the duct length, then

$$\frac{1}{S} - \frac{1}{S_p} = \frac{1}{C}, \quad (5.54)$$

or

$$S = S_p \left[\frac{1}{1 + S_p/C} \right]. \quad (5.55)$$

This means that the effective pump speed S of a system being evacuated by a pump with rated speed S_p , cannot exceed S_p or C , whichever is smaller. If the conductance of the duct is the same as the pump speed, then $S = S_p/2$. This should emphasize why it is desirable to make connections between the working chamber and the pump as short and as wide as possible.

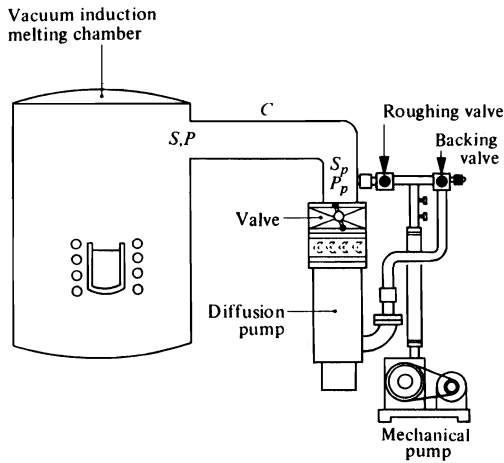


Fig. 5.17 A typical vacuum melting system.

5.5.2 Mechanical pumps

Most mechanical vacuum pumps are of the positive-displacement, rotary-piston type with sliding vanes, and sealed with oil. A small quantity of gas from the system is isolated, compressed, and discharged to the atmosphere with each rotation of the piston. These pumps have *intrinsic speeds*, S_0 , ranging in value from 5×10^4 to $0.35 \text{ m}^3 \text{ s}^{-1}$.

There is a lower limit to the pressure that a pump may produce, known as the ultimate pressure P_a , at which point the speed drops to zero. This limit is determined by the amount of back leakage of a very small quantity of gas Q_a , which is nearly independent of pressure. At the inlet to the pump,

$$S_p = \frac{Q - Q_a}{P_p} = S_0 \left[1 - \frac{Q_a}{Q} \right]. \tag{5.56}$$

At the ultimate pressure, $Q_a = Q$ and $S_0 = Q_a/P_a$. Therefore

$$S_p = S_0 \left[1 - \frac{P_a}{P_p} \right]. \tag{5.57}$$

Substitution of Eq. (5.57) into Eq. (5.55), and elimination of S_p and P_p by the use of $PS = Q = (P - P_p)C$, leads to a more realistic value for the speed of the system

$$S = S_0 \left[\frac{1 - P_a/P}{1 + S_0/C} \right], \tag{5.58}$$

or

$$S = S' \left[1 - \frac{P_a}{P} \right], \tag{5.59}$$

where

$$S' = S_0 \left[\frac{1}{1 + S_0/C} \right]$$

Single-stage pumps have ultimate pressures in the range from 10^{-2} - 10^{-3} torr. Two-stage mechanical pumps can reduce the ultimate pressure to 10^{-4} - 10^{-5} torr. In order to remove condensable gases (especially water vapor), a trap, either cold or chemical, should be placed ahead of the pump. If a slightly lower pressure is desired, and if the quantity of gas is large, a so-called Roots pump may be used in conjunction with an oil-sealed mechanical forepump. This combination may produce an ultimate pressure of 10^{-6} torr. Typical characteristic curves for various types of mechanical pumps are shown in Fig. 5.18.

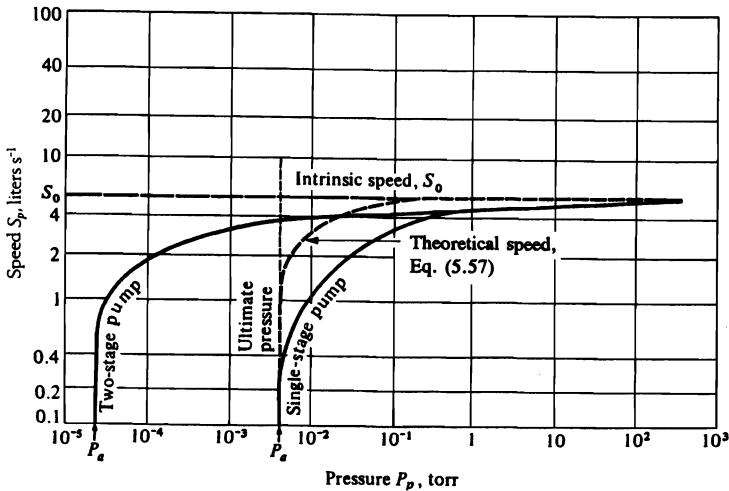


Fig. 5.18 The speed-pressure characteristics curves for a single- and two-stage rotary, oil-sealed, vane-type pump.

5.5.3 Diffusion pumps

We apply the term diffusion pump to a jet pump which utilizes the vapor from low vapor-pressure liquids to impart increased momentum to the gas molecules being removed from the system, eventually forcing them out of the mouth of the discharge into a mechanical forepump. Figure 5.19 illustrates a typical diffusion pump. The pump liquid is heated in the boiler until its vapor pressure reaches an optimum value of about 1 torr. This vapor is carried to a nozzle from which it is ejected as a high-velocity jet directed away from the incoming gas and towards the wall of the pump. The gas molecules flow into the annular space between the wall and column by molecular diffusion. Some fraction, H , of the molecules that encounter the jet in the first stage is entrained into the jet and driven downstream with higher velocities than the molecules would normally have. The jet expands and eventually strikes the water-cooled wall, the working fluid condenses, and flows down the walls back to the boiler. In multiple-jet pumps, the gas molecules being pumped are caught in a succession of jet spray stages, and eventually ejected from the diffusion pump into the foreline.

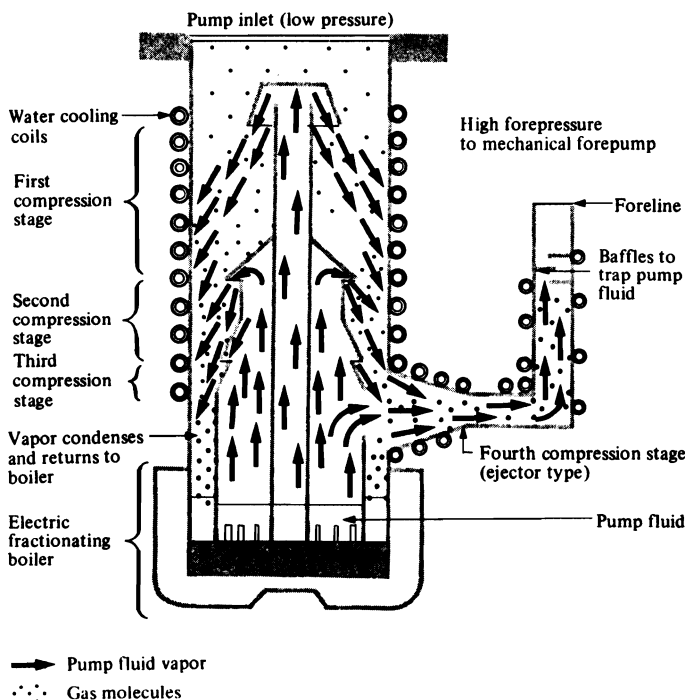


Fig. 5.19 Cross section of a typical vapor diffusion pump.

Since free molecular flow is needed for their successful operation, diffusion pumps usually operate at inlet pressures of 10^{-3} torr, or below. The compression ratios are not great enough to allow direct discharge to the atmosphere, so a relatively low forepressure must be maintained by a mechanical forepump, ultimately discharging to the atmosphere. For any diffusion pump there is a *limiting forepressure*, which is the pressure above which the boundary between the jet of pump vapor molecules and the randomly moving incoming gas molecules does not extend to the cold pump walls. In this situation, there is a direct connection between the high-vacuum and low-vacuum (forepump) sides of the jet, and effective pumping ceases. This pressure is typically of the order of 0.5 torr for multistage diffusion pumps and 0.05 torr for single-stage pumps.

We define the speed of diffusion pumps in the same way as for mechanical pumps. If A is the area of the pumping annulus, then the rate at which gas molecules are entrained by the jet is

$$HZA = \frac{HAn\bar{V}}{4}, \quad (5.60)$$

using the previously defined nomenclature. Then, the intrinsic pump speed S_0 is

$$S_0 = \frac{HZA}{n} = \frac{Q}{P_p} = \frac{HA\bar{V}}{4}, \quad (5.61)$$

and, substituting Eq. (1.4) for \bar{V} , we obtain

$$S_0 = \frac{H}{2\sqrt{\pi}} \left[\frac{2\kappa_B T}{m} \right]^{1/2} A, \quad (5.62)$$

or

$$S_0 = 3.64H \left[\frac{T}{M} \right]^{1/2} A, \text{ L s}^{-1}. \quad (5.63)$$

Specifically, for air at 293 K,

$$S_0 = 11.6(HA), \text{ L s}^{-1}, \quad (5.64)$$

where A is measured in cm^2 . The coefficient H is a measure of the collection efficiency of the pump and is called the *Ho coefficient* (named after T. L. Ho). For most diffusion pumps the Ho coefficient is about 0.5. These equations imply that S_0 is independent of the pressure for diffusion pumps, and this is nearly true, as shown in Fig. 5.20.

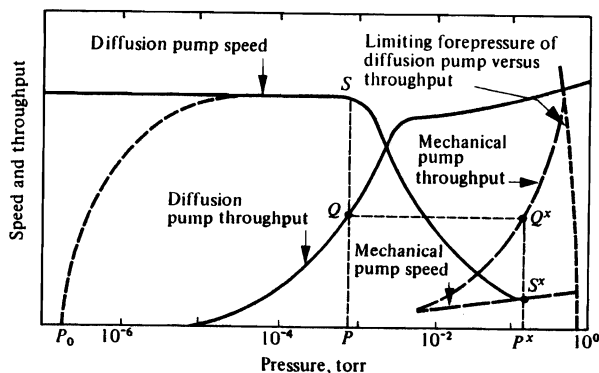


Fig. 5.20 Characteristic curve for a typical vacuum diffusion-pump, with the curves for a matching mechanical forepump included.

The ultimate pressures attainable with diffusion pumps depend on their design, including the number of stages, and also on the working fluid used. If we use mercury, a vapor trap, in the form of a baffle system externally cooled to low temperatures, must be placed between the diffusion pump and the system being evacuated in order to prevent back-diffusion of mercury vapor ($p_{\text{Hg}} = 1 \times 10^{-3}$ torr at 293 K). In this case, the effective speed of the pump is

$$S_p = S_0 \left[\frac{1}{1 + S_0/C_i} \right], \quad (5.65)$$

where C_i is the conductance of the trap. For well-designed traps, $S_p \approx S_0/2$. The ultimate pressures attainable with *well-trapped* mercury diffusion pumps are of the order of 10^6 - 10^7 torr. More commonly, low-vapor-pressure hydrocarbon oils or silicone oils are used as the working fluids. They are capable of producing vacuums of 10^6 torr without traps.

5.5.4 Pumpdown time

Returning to our vacuum melting unit, the basic equation relating the change in pressure in the tank to the pumping speed of the system, is

$$PS = -V \frac{dP}{dt} + Q_i, \quad (5.66)$$

where P = pressure measured at a specified point in the system, S = speed at that point, V = system volume, and Q_i = additional gas flow made up of the leak rate, interior surface outgassing, and any process gases. In well-maintained systems with no process gas evolution, Q_i is eventually brought to a negligible level.

Solving Eq. (5.66) for S and equating with Eq. (5.59), we obtain

$$\frac{dP}{(P - P_a)} = -\frac{S'}{V} dt. \quad (5.67)$$

We find the pumpdown time by integrating this equation from the initial tank pressure P_1 to the final pressure P_2

$$t = \frac{V}{S'} \ln \left[\frac{P_1 - P_a}{P_2 - P_a} \right]. \quad (5.68)$$

However, because S' is a function of the conductance, it is also a function of pressure at the higher pressures where viscous flow occurs. Therefore, in order to use Eq. (5.68), our approach will have to be to add several values of t obtained by incrementing S' until it is no longer a function of pressure. Equation (5.68) is not completely accurate, but it is a good approximation down to a pressure of the order of 1 torr.

Finally, we must consider the interaction and matching of the forepump and diffusion pump. Figure 5.20 includes the performance curves for a diffusion pump and a mechanical pump. In operation, the forepump is turned on, and run alone until a forepump inlet pressure less than the limiting forepressure of the diffusion pump is reached, at which point the lower stages of the diffusion pump become operative. If the pressure at the diffusion pump inlet is P , then the throughput is at point Q , and since the throughput is the same at any instant for both pumps, then the forepump inlet pressure is P^x , its speed is S^x , and its throughput Q^x .

Because the speed and throughput required of mechanical pumps when employed as forepumps are often rather low values, their use in large systems for roughing out would require excessively long pumpdown times. Therefore separate mechanical roughing pumps are often used, and then turned off when the diffusion pump-forepump combination can be applied.

5.5.5 Ejectors

For very large systems, other types of vapor pumps, called *steam ejectors*, are used. Figure 5.21 shows a schematic diagram of such an ejector. The steam is made to pass through a converging-diverging nozzle, designed to reach Mach 2 or higher at the nozzle exit and, correspondingly, a very low pressure P_e . The inlet port design pressure is then this P_e , and the steam jet entrains gas molecules at this pressure, as it leaves the nozzle. Flow into the port is again due to statistical molecular flow, at the lower pressures. Once entrained, the gas and steam slow down and are compressed in the diffuser so that they may exit at an

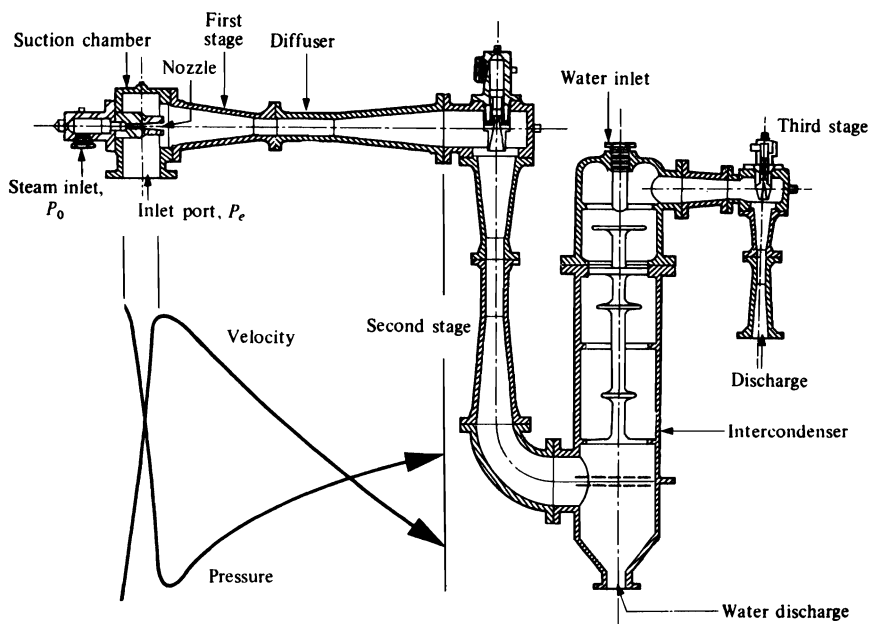


Fig. 5.21 Three-stage steam ejector with intercondenser. Schematic diagram of pressure-velocity relationships in the first-stage ejector is included.

exhaust pressure equal to the atmosphere, in the case of a single-stage pump, or at the design inlet pressure to the next stage in the case of a multiple-stage ejector. In order to lighten the load on the succeeding stages, condensers are often inserted between stages to remove the steam from the preceding stage.

The pumping capacity or throughput of a steam ejector is generally given in terms of pounds of dry air removed per hour. For comparison purposes

$$1 \text{ lb air at } 293 \text{ K hr}^{-1} \equiv 79.5 \text{ torr L s}^{-1}.$$

Figure 5.22 illustrates the range of pressures and throughputs obtainable with typical combinations of ejector stages and condensers.

5.5.6 Molecular pumps

We saw in Section 5.5.3 that diffusion pumps are often coupled with mechanical roughing pumps to achieve pressures that are typically 10^{-6} torr without traps. Molecular pumps can also be used to achieve similar pressures, although at somewhat more cost.

In molecular pumps, the gas molecules are imparted a velocity by momentum transfer from a fast-moving solid surface. In diffusion pumps, the gas molecules are entrapped and carried from the inlet to the discharge by the stream of vapor. In molecular pumps, collisions occur with the fast-moving surface. Pumps of this type can maintain pressures as low as 10^7 to 10^9 torr, while discharging at 10 to 40 torr (a considerably higher discharge pressure than tolerated by diffusion pumps).

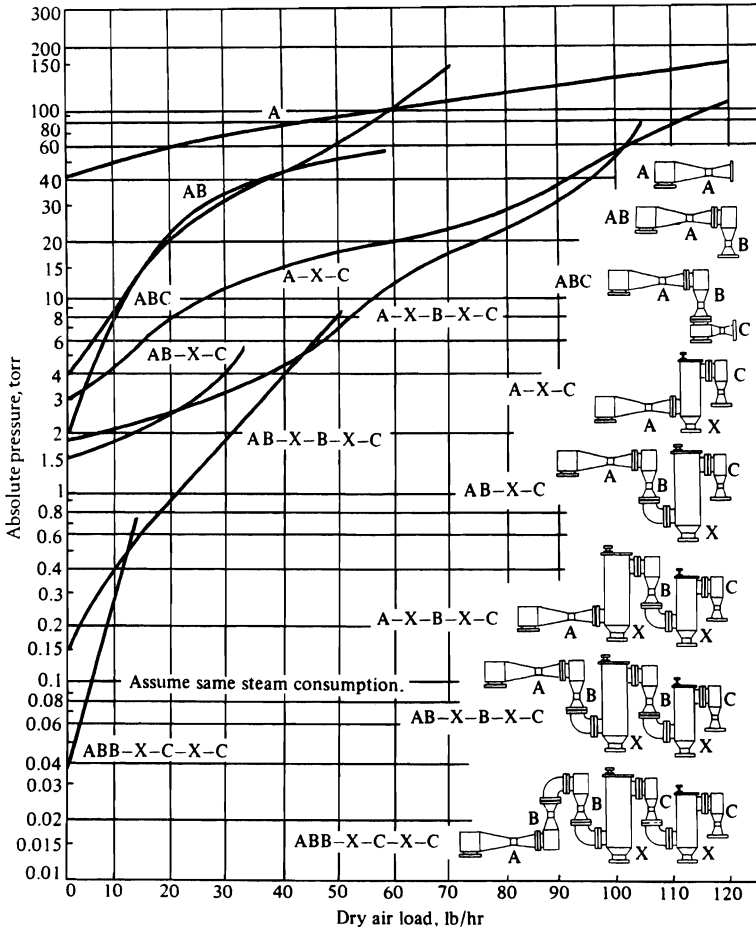


Fig. 5.22 Ranges of application of various steam-ejector (A, B, C)-intercondenser (X) combinations. (From an article by F. Berkeley, *Chem. Eng.* (April 1957), page 255.)

Advantages of molecular pumps include their installation in systems with smaller backing pumps than required when diffusion pumps are used. Backstreaming of oil molecules from the mechanical pump is lessened because the discharge pressure is relatively high. When large throughputs are needed, the turbomolecular pumps that are used are axial-flow turbines.

5.5.7 Gettering and ion pumps

The pressure region between 10^{-9} and 10^{-12} torr is often referred to as *ultrahigh vacuum*. At such low pressures, we start thinking about the number of molecules per unit volume rather than pressure as a force per unit area. Consequently, the amount of gas adsorbed on surfaces in the vacuum system is paramount, so maintaining a ultrahigh vacuum system requires the maintenance of ultraclean surfaces.

180 Flow and Vacuum Production

In an ultrahigh vacuum a surface can hold a large number of molecules compared to the number of molecules in the vacuum space. To effect a pumping action, a chemically active surface can be used to "get" molecules from the vacuum space by physisorption. The most commonly used material is titanium.

In the inset of Fig. 5.23, there is a titanium source that sublimates by electrical heating. The titanium atoms travel to the colder surrounding surface, where they condense and form a large surface of fresh titanium. In turn, the layer of fresh titanium forms stable compounds with chemically active gas molecules that strike the surface. The capture process is continuous so long as new layers are deposited.

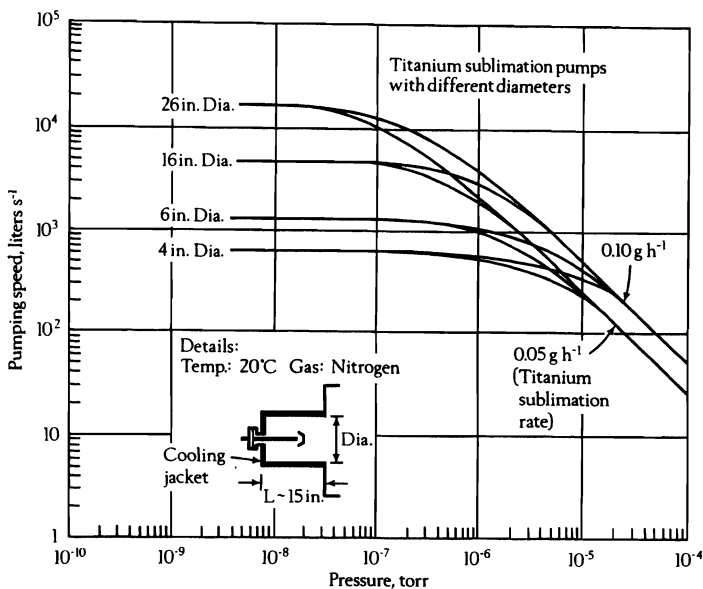


Fig. 5.23 Pumping speeds of gettering pumps of various sizes. (From M. H. Hablanian, *High Vacuum Technology*, Marcel Dekker, Inc., New York, N.Y., 1990.)

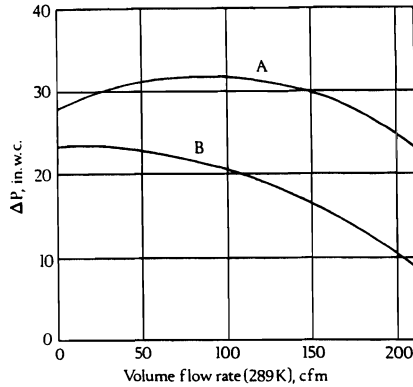
So-called sputter-ion pumps can also be used to supply the layer of fresh titanium. The device consists of a cylinder of stainless steel (the anode) and plates of titanium (the cathode) positioned near the open ends of the cylinder. Electrons are emitted from the cathode because 5 to 7 kV are applied between the electrodes. The trajectories of these electrons are controlled by a magnet which causes the electrons to move in very long helical paths in order to improve the chances of collisions between the electrons and gas molecules. These collisions produce positively charged ions that travel to the cathode (titanium). This collision ejects titanium atoms (i.e., sputtering) which deposit on other surfaces in the system and capture other molecules.

The pumping speed characteristics of a sputter-ion pump are qualitatively similar to that shown for the diffusion pump in Fig. 5.20, with the major advantage of having an ultimate pressure (P_u) that is less than 10⁻¹¹ torr. There is a range of intermediate pressures (10⁻⁷ to 10⁻⁵ torr), where the pumping speed is approximately constant. At lower pressures, the speed decreases to zero at P_u , and it decreases to very low values at higher pressures. Sputter-ion pumps have relatively low throughputs and should only be coupled with roughing pumps that

can achieve 10^{-3} torr. The cathodes are eroded by sputtering, and they must be replaced periodically, which is not a simple matter.

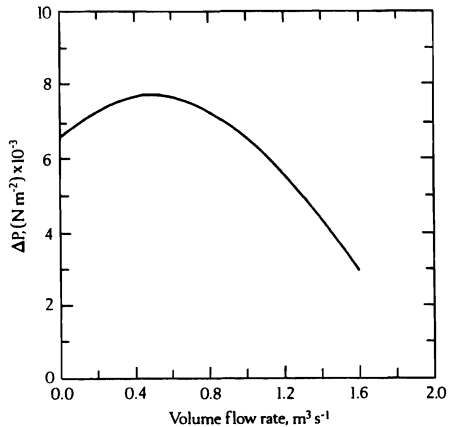
PROBLEMS

5.1 Refer to Example 3.5 for the system characteristics and the desired operating point for flow through a sinter bed. The bed has a cross-sectional area of 0.189 m^2 , and V_0 is a superficial velocity. You can select either fan A or fan B to blow the air. Their respective characteristic curves are given to the right.



- a) If you select fan A, what volume flow rate will be delivered through the sinter bed? Repeat for fan B. You may assume that the pressure drop through the sinter bed is proportional to the square of volume flow rate; i.e., $\Delta P = kQ^2$.
- b) Which fan, A or B, is better suited for the bed of ore and coal which is discussed? Explain why.
- c) What adaptation, if any, must be made to use the fan you have selected?

5.2 Refer to Problem 4.4. Suppose the characteristic curve of the fan is as shown to the right.



- a) Assume that $\Delta P = kQ^2$ for the entire system and determine the operating point.
- b) As particulates are collected, the pressure drop across the bag house increases. When the pressure drop increases by twenty percent, what will be the volume flow rate?

182 Flow and Vacuum Production

5.3 Two identical pumps are used to pump water from one reservoir to another whose level is 6.1 m higher than the first. When both pumps are operating the flow rate is $0.04 \text{ m}^3 \text{ s}^{-1}$. What is the flow rate when only one pump operates? Assume highly turbulent flow. The characteristic head curve for the pump is given by the following table.

Flow rate, $\text{m}^3 \text{ s}^{-1}$	Head, N m kg^{-1}
0	208
0.0057	211
0.0113	212
0.0170	211
0.0227	203
0.0340	178
0.0453	141
0.0566	99
0.0680	39
0.0736	15

5.4 Derive an equation for the conductance of a long straight tube. Assume viscous flow prevails and that the viscosity is given by Eq. (1.13).

- Write the conductance in terms of viscosity.
- Show that

$$\eta = \frac{m\bar{V}}{3\pi^{1/6}\sqrt{2}d^2},$$

where \bar{V} is the Maxwellian speed of the molecules.

- Write the conductance in terms of \bar{V} .

5.5 Compare the conductance for viscous flow in a long straight tube (from Problem 5.4c) to the conductance for molecular flow.

- How does each vary with \bar{V} ?
- How does each vary with temperature?
- For nitrogen at 300 K, what is the mean free path (see Eq. (1.5)) at normal atmospheric pressure (760 torr).

5.6 For nitrogen at 300 K, what is the minimum diameter of a long tube for viscous conduction at a) standard atmospheric pressure (760 torr). Repeat for b) 100 torr, c) 10 torr, d) 1 torr and e) 10^{-1} torr. [The criterion is $(\lambda/D) \geq 10$ where λ is the mean free path (see Eq. (1.5)).]

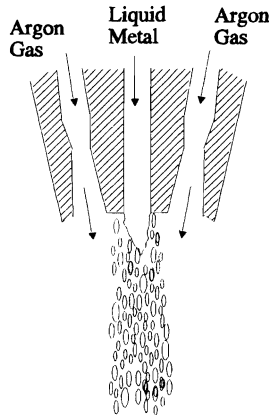
5.7 Consult Table 5.2 and obtain the conductance for two chambers connected by a tube with a diameter 250 mm and a length of 750 mm. Compare your result to the approximation given by Eq. (5.52). Assume that the gas is air at 298 K, with a molecular weight of $28.8 \text{ kg kmol}^{-1}$.

5.8 Consider the use of the two-stage pump of Fig. 5.18 that is connected to a chamber of 1 m^3 volume through a duct with an infinitely high conductance. Calculate the time to pumpdown to a) 10^{-2} torr and b) 10^{-4} torr.

5.9 A heat of steel (5×10^4 kg) is to be vacuum degassed from 5 ppm H_2 to 1 ppm H_2 and from 100 ppm N_2 to 75 ppm N_2 in 15 min. The steel is at 1873 K, and the chamber has 9 m^3 of space occupied by air after the top is closed with the ladle inside. At what pressure would you recommend operating the system? Calculate the throughputs of air, hydrogen and nitrogen that must be removed from the chamber. Consult Fig. 5.22 and specify a steam ejector to do the job.

5.10 An ultrahigh vacuum chamber (300 liters) is equipped with two pumping modes, one to achieve 10^{-4} torr and a titanium sublimation pump (Fig. 5.23) to achieve pressures below 10^{-4} torr. Assuming that nitrogen must be removed from the chamber, which pump(s) of Fig. 5.23 can be used if 10 minutes is an acceptable pumpdown time to go from 10^{-4} torr to 10^{-8} torr?

5.11 Supersonic nozzles are arranged circumferentially around a central orifice through which liquid metal is fed. The argon gas jets are focused on a point below the exit of the orifice, where they impinge on the metal stream to break it into fine droplets that solidify to microstructures of particular interest. It has been found that nozzle exit velocities on the order of Mach 3 are desirable. For a Mach 3 nozzle calculate the reservoir pressure P_0 needed, if the desired exit pressure is 1.0 atm and the flow rate of argon is 0.1 kg s^{-1} . What should the throat diameter, exit diameter and length of diverging section be? Assume $\gamma_{Ar} = 1.67$.



5.12 Derive Eq. (5.20).

PART TWO

ENERGY TRANSPORT

In the processing of materials, a situation almost invariably arises that necessitates a change in the temperature of a material, as, for example, in heat treating processes. We assume that the student is aware of the importance of being able to calculate the heat which is produced and used in such processes, by making heat balances. However, it is also desirable to have an understanding of how heat is transferred into, out of, and within materials processes, because many operations take place in such a way that the *rate* of energy transfer becomes the controlling factor in raising and lowering the temperature. Since we usually consider this energy to be virtually all thermal energy, we speak of *heat transfer* as the controlling factor.

There are two basic types of heat-transfer mechanisms: *conduction* and *radiation*. Quite frequently, however, three mechanisms are set forth, namely, conduction, radiation, and convection. To be more specific, convection is rather a process involving mass movement of fluids, than a real mechanism of heat transfer. In regard to this distinction it is better to speak of "heat transfer with convection" rather than of "heat transfer by convection." The term convection implies fluid motion, and mechanisms of heat transfer anywhere within the fluid are only conduction and radiation. We shall discuss conduction and radiation, and present the relationships used for describing heat transfer by each mechanism in the following chapters. Here, as an introduction, we shall consider them in brief.

Conduction is the transfer of heat by molecular motion which occurs between two parts of the same body, or between two bodies which are in physical contact with each other. In fluids, heat is conducted by molecular collisions; in solids, heat is conducted either by lattice waves in nonconductors or by a combination of lattice waves with the drift of the conduction electrons in conducting materials. The macroscopic theory of conduction is merely *Fourier's law*:

$$q_y = -k \frac{\partial T}{\partial y},$$

where q_y is the heat flux in the y -direction, $\partial T/\partial y$ is the temperature gradient in the y -direction, and k is the thermal conductivity. Note the analogy with Newton's law of viscosity (Eq. 1.3). In both cases, fluxes are proportional to gradients, and the relationships

also define the proportionality constants, namely, viscosity by Newton's law and thermal conductivity by Fourier's law.

The nature of heat transfer by radiation is quite different from that by conduction, and consequently the basic rate equation for heat transfer by radiation is in no way similar to Fourier's law. In Chapter 11, we shall analyze radiation problems in detail; here, we state briefly that thermal radiation is part of the electromagnetic spectrum. The energy flux emitted by an ideal radiator is proportional to the fourth power of its absolute temperature.

$$e_b = \sigma T^4,$$

where e_b is the emissive power (a special term for the thermal emission from an ideal radiator) and σ is the Stefan-Boltzmann constant. The processes of conduction and radiation frequently occur simultaneously, even within certain media. In many practical situations, however, one mode is negligible with respect to the other, and may be ignored.

When a moving fluid at one temperature is in contact with a solid at a different temperature, heat exchanges between the solid and the fluid by conduction at a rate given by Fourier's law where k is the conductivity of the fluid, and $\partial T/\partial y$ is the temperature gradient in the fluid normal to the wall at the fluid-solid interface. If the details of the convection are known in a given situation, then we can determine the distribution of temperature within the fluid, and calculate the heat flux at the wall. In many cases, such a detailed analysis is not available; then it is convenient to define the *heat-transfer coefficient*, h , by the equation

$$h = \frac{q_0}{T_s - T_f} = \frac{-k(\partial T/\partial y)_0}{T_s - T_f},$$

where T_s is the surface temperature, T_f is usually taken as some bulk fluid temperature, and q_0 is the heat flux at the wall. The units of h , which is a function of the fluid and the flow pattern of the system, are $\text{W m}^{-2} \text{K}^{-1}$. Much of the research on heat transfer has been devoted to the determination of h , since it enters into all problems of heat transfer with convection.

Convection is usually classified as either a *forced* convection or *free (natural)* convection. When a pump or other mechanical device causes the fluid to move, we call this process forced convection; when a fluid moves as a result of density difference, then we speak of a free or natural convection. Thus, when a radiator heats the air which rises, displacing colder air in the upper part of a room, the fluid motion is by natural convection.

In Part Two, we shall examine the thermal conductivity of materials and the various modes of heat transfer applied to situations in materials processing.

6

FOURIER'S LAW AND THERMAL CONDUCTIVITY OF MATERIALS

Thermal conductivity is an intrinsic property of materials. In this chapter we consider the thermal conductivity of various materials, such as gases, liquids, and solids, with the emphasis on solids, including porous solids.

6.1 FOURIER'S LAW AND THERMAL CONDUCTIVITY

Consider a slab of area A bounded by two large parallel surfaces a distance Y apart (Fig. 6.1). Initially, the slab is at a uniform temperature T_0 . At some instant, the lower surface is suddenly raised to a temperature T_1 , which is maintained. The material above the heated surface becomes heated, and the heat is gradually transferred across the slab toward the colder surface, which is kept at T_0 . A steady-state temperature distribution is attained when a constant rate of heat flow through the slab is required to maintain the temperature difference $T_1 - T_0$. It is found that for sufficiently small temperature differences, the rate of heat flow per unit area q is proportional to the temperature difference and inversely proportional to the distance between the surfaces; hence,

$$q = k \frac{(T_1 - T_0)}{Y}. \quad (6.1)$$

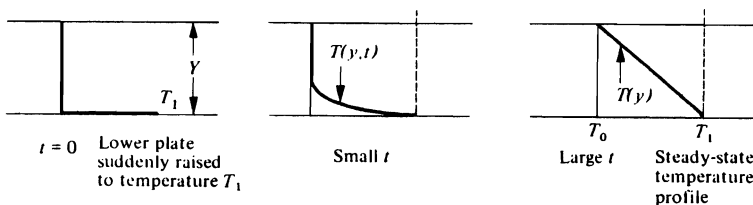


Fig. 6.1 Build-up to steady-state temperature profile for a solid slab.

188 Fourier's Law and Thermal Conductivity of Materials

Equation (6.1) also applies to liquids and gases, provided no convection or heat transfer by radiation is allowed to take place in the fluid. As stated, the temperature difference must be sufficiently small, because the thermal conductivity depends not only on the specific material, but also on the temperature. Equation (6.1) is therefore valid for fixed values of T_1 and T_0 for all values of Y .

As the temperature difference and the separation distance approach zero, the differential form of Fourier's law of heat conduction arises:

$$q_y = -k \frac{\partial T}{\partial y} \quad (6.2)$$

The flow of heat per unit area (heat flux) in the y -direction is proportional to the temperature gradient in the y -direction.

For a three-dimensional situation in which the temperature varies in all three directions in material with an isotropic thermal conductivity, we write

$$q_x = -k \frac{\partial T}{\partial x}; \quad q_y = -k \frac{\partial T}{\partial y}; \quad q_z = -k \frac{\partial T}{\partial z} \quad (6.3)$$

These three relations form the components of the single equation

$$\mathbf{q} = -k \nabla T \quad (6.4)$$

Note the similarity between Eq. (6.2) for one-dimensional heat flux and Eq. (1.2) for one-dimensional momentum flux. In each case, the flux is proportional to the gradient of a potential variable, temperature and velocity, respectively. The mathematical similarity ends, however, when we compare the three components for heat flux versus the nine components that express momentum transfer in three dimensions. This is because energy is a scalar quantity whereas momentum is a vector quantity.

The units involved in Fourier's law of heat conduction are

	SI units*	English units
q_x, q_y, q_z	W m ⁻²	Btu h ⁻¹ ft ⁻²
T	K	°F or °R
x, y, z	m	ft
k	W m ⁻¹ K ⁻¹	Btu h ⁻¹ ft ⁻¹ °F ⁻¹

The thermal conductivity of a material reflects the relative ease or difficulty of the transfer of energy through the material. This, in turn, depends on the bonding and structure of the material. When considering the thermal conductivity of most materials used in engineering, bear in mind that the effective thermal conductivity depends on the interaction between the intrinsic thermal conductivities of the phases present and the mode of energy transfer between them. In the following sections, we consider the thermal conductivity of various single phases, and then the effective thermal conductivity of some bulk materials.

*1 W m⁻¹ K⁻¹ = 0.57782 Btu h⁻¹ ft⁻¹ °F⁻¹.

Example 6.1 A flat slab of uniform thickness ($\delta = 0.02$ m) with an initial temperature of 300 K is placed in a furnace. At 900 s after being placed in the furnace, a series of thermocouples embedded in the slab gives a temperature distribution approximated by a second order polynomial:

$$T = a_0 + a_1 x + a_2 x^2$$

where T is temperature, K, x is distance from the centerline of the slab in mm, and the a_i s are constants. Assume that $T(x)$ is symmetrical. a) Solve for the constants in terms of the surface (T_s) and centerline (T_0) temperatures. b) Solve for the heat flux as a function of x in the slab if $T_s = 1000$ K and $T_0 = 400$ K. The thermal conductivity of the slab is $10 \text{ W m}^{-1} \text{ K}^{-1}$.

Solution. a) $T(x)$ is symmetrical. Therefore $\partial T/\partial x = 0$ at $x = 0$, and it is easy to show that $a_1 = 0$. The other two specifications give

$$T_s = a_0 + a_2 \left[\frac{\delta}{2} \right]^2$$

and

$$T_0 = a_0,$$

so that

$$a_2 = \frac{4(T_s - T_0)}{\delta^2}.$$

b) The flux is

$$q_x = -k \frac{\partial T}{\partial x}$$

and

$$\frac{\partial T}{\partial x} = 2a_2 x = \frac{8(T_s - T_0)}{\delta} \left[\frac{x}{\delta} \right].$$

Therefore,

$$q_x = - \frac{8k(T_s - T_0)}{\delta} \left[\frac{x}{\delta} \right].$$

Substituting values, we get

$$q_x = - \frac{(8)(600 \text{ K})}{0.02 \text{ m}} \left| \frac{10 \text{ W}}{\text{m K}} \right| \left[\frac{x}{0.02 \text{ m}} \right]$$

$$q_x = -2.4 \times 10^6 \left[\frac{x}{\delta} \right], \text{ W m}^{-2}.$$

The absolute value of the flux varies from its maximum of $2.4 \times 10^6 \text{ W m}^{-2}$ at the surface to zero at the centerline.

6.2 THERMAL CONDUCTIVITY OF GASES

Conduction of energy in a gas phase is primarily by transfer of translational energy from molecule to molecule as the faster moving (higher-energy) molecules collide with the slower ones.

For a simple, monatomic gas, we can develop an expression for the thermal conductivity in a similar manner as we did in Eq. (1.13) for viscosity. Assume that the gas in Fig. 1.5 is under the influence of a temperature gradient, $\partial T/\partial y$. The temperatures of the molecules at $y - \bar{y}$ and $y + \bar{y}$ are, respectively,

$$T \Big|_{y-\bar{y}} = T \Big|_y - \frac{2}{3} \lambda \frac{\partial T}{\partial y}, \quad (6.5)$$

and

$$T \Big|_{y+\bar{y}} = T \Big|_y + \frac{2}{3} \lambda \frac{\partial T}{\partial y}. \quad (6.6)$$

Here the average distance moved in the y -direction between collisions is \bar{y} , and $\bar{y} = \frac{2}{3}\lambda$, where λ is the mean free path as defined by Eq. (1.7).

If the heat capacity per molecule is c , then the net flux of thermal energy across the plane at y is given by the net difference between the energy of the molecules crossing the y -plane in the positive and in the negative directions:

$$q_y = ZcT|_{y-\bar{y}} - ZcT|_{y+\bar{y}} = Zc(T|_{y-\bar{y}} - T|_{y+\bar{y}}). \quad (6.7)$$

Equation (1.6) gives the expression for Z , the flux of molecules (number $m^{-2} s^{-1}$) crossing the y -plane in either the positive or the negative direction; Eqs. (6.5) and (6.6) give the expressions for the temperatures, so that ultimately

$$q_y = -\frac{nc\bar{V}\lambda}{3} \left[\frac{\partial T}{\partial y} \right]. \quad (6.8)$$

Denoting nc as C_v , the heat capacity per unit volume, and by comparing Eq. (6.8) to Eq. (6.2), we arrive at

$$k = \frac{C_v\bar{V}\lambda}{3}. \quad (6.9)$$

This equation is basic for an understanding of the thermal conductivity of gases. In some cases, it can be extended to aid in theorizing about the thermal conductivity of solids and liquids. For dilute gases with atoms assumed as rigid spheres, Eqs. (1.4) and (1.5) may be substituted for \bar{V} and λ in Eq. (6.9), with the result that

$$k = \frac{1}{d^2} \left[\frac{\kappa_B^3 T}{\pi^3 m} \right]^{1/2}. \quad (6.10)$$

This result suggests that the thermal conductivity of gases does not depend on pressure, but that it does depend on the square root of the temperature. For pressures to about 10 atm, this lack of dependence on pressure is essentially correct. The thermal conductivity, however, increases with temperature more than predicted by Eq. (6.10).

In the case of polyatomic gases, Eucken¹ developed an equation for the thermal conductivity of these gases at normal pressures:

$$k = \eta \left[C_p + \frac{1.25R}{M} \right], \quad (6.11)$$

where M is the molecular weight and C_p the heat capacity at constant pressure.

In the case of gas mixtures, we can estimate the thermal conductivity within a few percent by

$$k_{\text{mix}} = \frac{\sum_i X_i k_i M_i^{1/3}}{\sum_i X_i M_i^{1/3}}, \quad (6.12)$$

where X_i is the mole fraction of component i having molecular weight M_i and intrinsic thermal conductivity k_i . A comparison² of observed conductivities with calculated values, using Eq. (6.12), for binary gas mixtures involving air, CO, CO₂, H₂O, N₂, N₂O, NH₃, CH₄, C₂H₂, He, and Ar, indicates average discrepancies of only 2.7%, over the temperature range 273-353 K. Tests at elevated temperatures are not available, but the errors would probably be no larger. There are more complex equations, which reduce the errors to about 1%, but they are not as easy to use.

Figure 6.2 gives the thermal conductivities of several common gases as a function of temperature. The data are valid to at least 10⁶ Pa (approx. 10 atm).

Example 6.2 Calculate the thermal conductivity of a gas containing 40 mol% CH₄ and 60 mol% H₂, at 1.5×10^5 N m⁻² pressure and 1255 K.

Solution. From Fig. 6.2, $k_{\text{H}_2} = 0.51$ W m⁻¹ K⁻¹ and $k_{\text{CH}_4} = 0.22$ W m⁻¹ K⁻¹. Using Eq. (6.12) we get

$$k_{\text{mix}} = \frac{(0.6)(0.51)(2)^{1/3} + (0.4)(0.22)(16)^{1/3}}{(0.6)(2)^{1/3} + (0.4)(16)^{1/3}} = 0.34 \text{ W m}^{-1} \text{ K}^{-1}.$$

The fact that the pressure is 1.5×10^5 N m⁻² has no significance here, since the thermal conductivity is independent of pressure at this pressure level.

6.3 THERMAL CONDUCTIVITY OF SOLIDS

Solids transmit thermal energy by two modes, either one of which, or both, may operate. In all solids, energy may be transferred by means of elastic vibrations of the lattice moving through the crystal in the form of waves. In some solids, notably metals, free electrons moving through the lattice also carry energy in a manner similar to thermal conduction in a gas.

¹A. Eucken, *Physik Z.* **14**, 324 (1913).

²L. Friend and S. Adler, article in *Transport Properties in Gases*, Northwestern University Press, Evanston, IL, 1958.

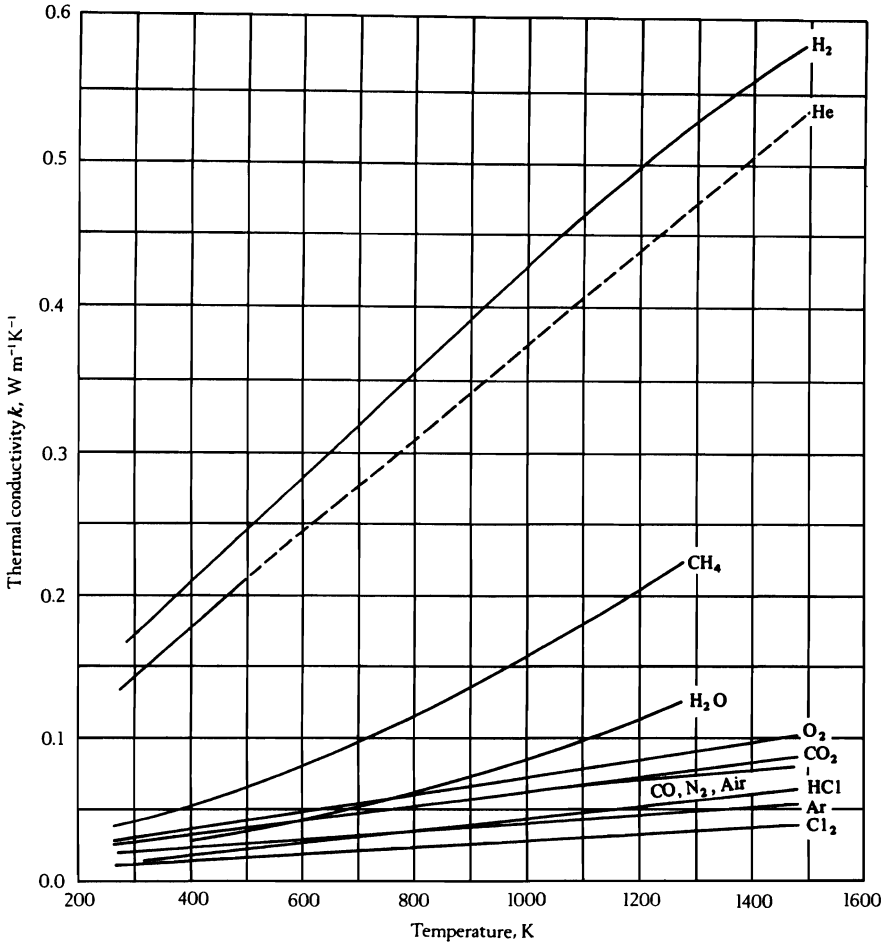


Fig. 6.2 Thermal conductivity of several gases. Data valid for up to 10^6 Pa (approx. 10 atm).

Recalling the fundamental treatments of bonding in solids, we remember that at ordinary temperatures all solids store thermal energy as vibratory motion of their atoms, and potential energy in the bonding between atoms. Einstein developed his theory for the heat capacity of solids by assuming that each atom vibrates independently of its neighbors. This, however, results in no conduction via lattice waves, which in fact exists because neighboring atoms do interact and therefore do not vibrate independently. Debye, in the process of improving Einstein's model of heat capacity, assumed that the lattice is made up of independent oscillators, and that these oscillators are simply considered to be elastic waves traveling in different directions with different polarizations and wavelengths, not necessarily associated with the atoms themselves. This led to his theory of specific heat ($C_v \propto T^3$ at low temperatures) which is more in agreement with experiments than Einstein's theory, and also gives a more satisfactory picture of thermal conductivity of insulating solids. Each lattice vibration (there is always a spectrum of vibrations) may be described as a traveling wave carrying energy and obeying the laws of quantum mechanics. By analogy with light theory, the waves in a crystal exhibit the attributes of particles and are called *phonons*.

If the forces between atoms were perfectly harmonic, two phonons moving through the crystal could collide and combine, with the resulting phonon having the same total energy and momentum; energy transport would continue in the direction of the resultant of the original phonons. If this were the only type of phonon-phonon interaction (Normal or N-type), then the only limit to the mean free-path of the phonons would be the dimensions of the piece of the material itself, since the resultant phonon acts in the same manner as the two original phonons as far as energy transport is concerned. Thermal conduction would thus be extremely easy. But the forces between atoms are not in perfect harmony, and there exists another type of collision between phonons, known as an Umklapp (U-process) collision. In this process, energy is conserved, while phonon momentum is not, and the result of such a collision is that a phonon moves in a direction opposite to the resultant of the original phonons. For these processes, the mean free-path of phonons is extremely short, being of the order of the distance between atoms. Since the number of phonons increases with temperature, the number of the U-processes also increases with temperature and the wavelength of the phonons λ_{ph} is proportional to $1/T$. At room temperature and above, \hat{C}_v for most materials is roughly constant, and if we use Eq. (6.9) to describe the thermal conductivity of a solid which conducts energy only by phonons, then k must decrease with increasing temperature. This is what happens in most electrically insulating substances, such as the oxides shown in Fig. 6.3 (but not in the form of porous, bulk materials).

When heat enters a crystal, the crystal expands, and this thermal expansion of the lattice is related to the bulk modulus B by a constant γ , known as Gruneisen's constant

$$\gamma = \frac{\hat{V}}{\hat{C}_v} \left[\frac{\partial P}{\partial T} \right]_v = \frac{3B\hat{V}\alpha}{\hat{C}_v}, \tag{6.13}$$

where \hat{V} = molar volume, α = linear thermal expansion coefficient, and \hat{C}_v = molar heat capacity. For most solids at ordinary temperatures, $\gamma \cong 2$. Combining this result with Lindeman's theory of the melting of solids, Debye showed that

$$\lambda_{ph} = \frac{20T_m d}{\gamma^2 T}, \tag{6.14}$$

where T_m = melting point, T = absolute temperature, and d = crystal-lattice dimension, resulting in the previously mentioned intuitive relation between phonon mean free path and temperature. Note that a high-melting-point material has a large value of λ at low temperatures, and therefore a large value of k at room temperature. We can observe this in the case of diamond, which has a thermal conductivity at room temperature comparable to that of copper, one of the best conductors known. However, the conductivity of diamond drops very rapidly to a small fraction of that of copper as the temperature increases.

At very low temperatures ($T < 10$ K), λ_{ph} approaches the dimensions of the crystal, since U-processes diminish rapidly as the temperature approaches absolute zero; consequently, the thermal conductivity rises rapidly. In this case, the larger the crystal, the higher the thermal conductivity, as illustrated in Fig. 6.4; this is an exception to Fourier's law.

Phonons are also scattered by differences in isotopic masses, chemical impurities, dislocations, and second phases. With these imperfections quantitative prediction of thermal conductivity is exceedingly difficult, but we can be sure that the less perfect the crystal is, the lower is the thermal conductivity.

The influence of structure and composition on the thermal conductivity of dielectric materials is difficult to predict. Qualitatively we know that materials with complex structures have a greater tendency toward thermal scattering of phonons (i.e., Umklapp collisions) and accordingly lower thermal conductivities. Mullite ($Al_2O_3 \cdot MgO$), for example, has a lower thermal conductivity than either pure Al_2O_3 or pure MgO . Comparisons between single

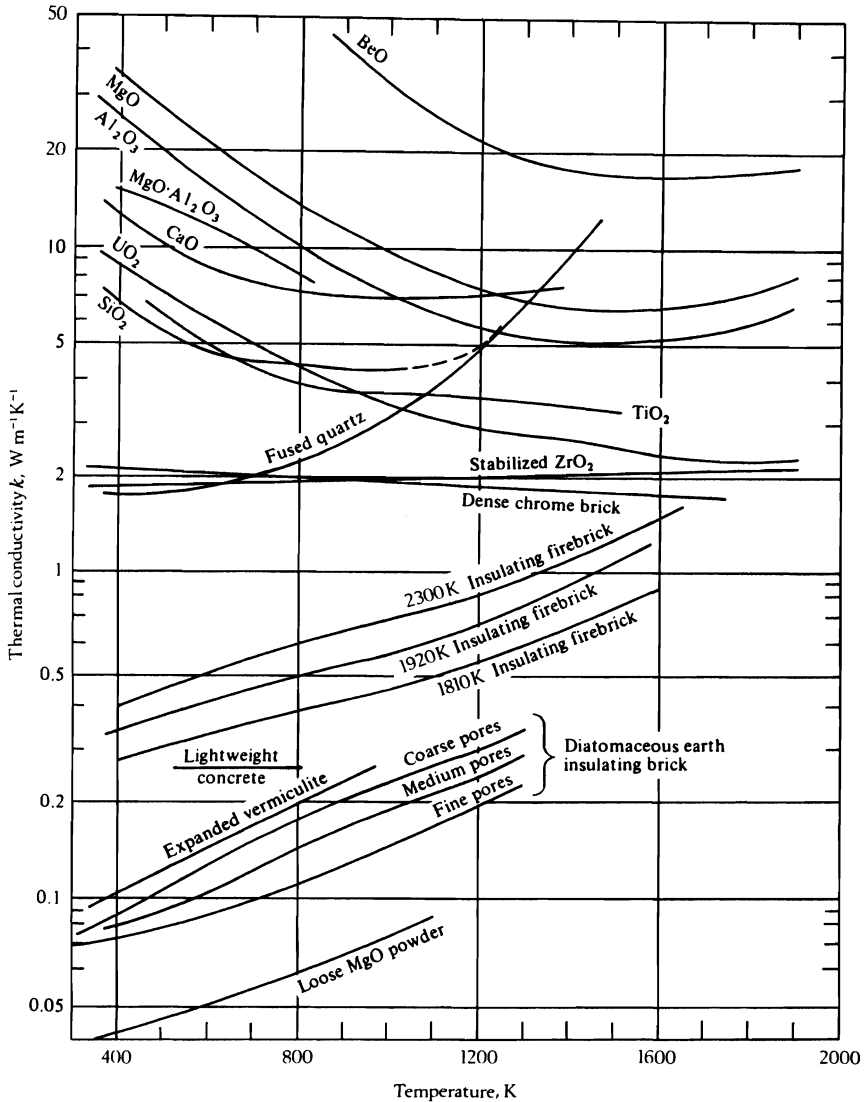


Fig. 6.3 Thermal conductivity of oxides and various insulating materials. (From A. Schack, *Industrial Heat Transfer*, Wiley, New York, NY, 1965, page 189.)

crystals and polycrystalline samples of Al_2O_3 , CaF_2 and TiO_2 show that the thermal conductivities are equal below 500 K (approx.), but at higher temperatures the polycrystalline samples are less conductive. The effect of composition in solid solutions of two oxides, MgO and NiO , is shown in Fig. 6.5. Numerous examples of the effects of structure and composition in dielectric materials are given by Kingery *et al.*³

³W. D. Kingery, H. K. Bowen and D. R. Uhlmann, *Introduction to Ceramics*, 2nd ed., John Wiley, New York, NY, 1976, pages 613-642.

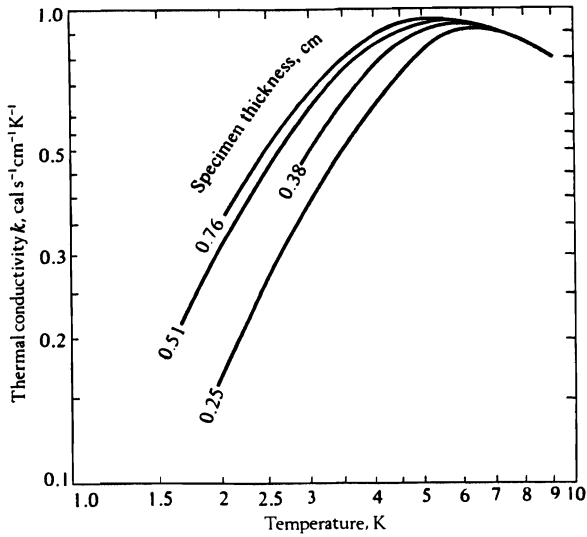


Fig. 6.4 Effect of specimen thickness on thermal conductivity of potassium chloride single crystals. (From W. J. deHaas and T. Biermasz, *Physica* 2, 673 (1935); 4, 752 (1937); 5, 47, 320, and 619 (1938).) Note: $1 \text{ cal s}^{-1} \text{ cm}^{-1} \text{ K}^{-1} = 418.4 \text{ W m}^{-1} \text{ K}^{-1}$.

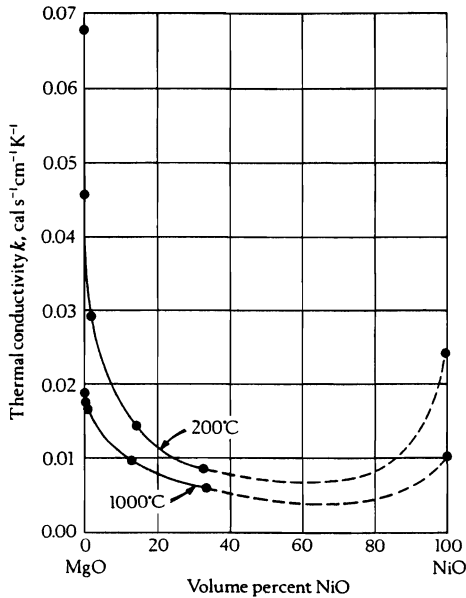


Fig. 6.5 Thermal conductivity in the solid-solution system MgO-NiO. (From Kingery *et al.*, *ibid.*, page 623.) Note: $1 \text{ cal s}^{-1} \text{ cm}^{-1} \text{ K}^{-1} = 418.4 \text{ W m}^{-1} \text{ K}^{-1}$.

196 Fourier's Law and Thermal Conductivity of Materials

As we proceed from electrical insulators to conductors, we deal with materials with increasing concentrations of conduction electrons. The conduction electrons in metals form an *electron gas* which obeys the laws of quantum mechanics. The electronic contribution to the volumetric heat capacity of a metal is given by

$$C_{V,el} = \frac{\pi^2 n_e k_B^2 T}{2\varepsilon_F}. \quad (6.15)$$

Here ε_F is the Fermi energy, and n_e is the number of free electrons per cm^3 . The Fermi energy is related to the average velocity of the electrons by

$$\bar{V}_F = \left[\frac{2\varepsilon_F}{m_e} \right]^{1/2}, \quad (6.16)$$

where \bar{V}_F = electron velocity at the Fermi surface, and m_e = electron mass. Using Eq. (6.15) for the heat capacity and Eq. (6.16) for the Fermi energy, Eq. (6.9) becomes

$$k_{el} = \frac{\pi^2 n_e k_B^2 T \lambda_{el}}{3m_e \bar{V}_F}, \quad (6.17)$$

where k_{el} is now the electronic contribution to the thermal conductivity. This predicts that the electronic contribution in metals *increases* with temperature, provided that λ_{el} does not decrease just as strongly with temperature.

To prove that the electrons in a metal carry the major portion of the thermal energy, the thermal and electrical conductivities should be proportionally related. This proportionality is known as the Wiedmann-Franz law and the constant of proportionality as the Lorentz number L :

$$L = \frac{k_{el}}{\sigma_e T} = \frac{\pi}{3} \left[\frac{\kappa_B}{e} \right]^2 = 2.45 \times 10^{-8} \text{ W ohm K}^{-2}, \quad (6.18)$$

where σ_e = the electrical conductivity, $\text{ohm}^{-1} \text{cm}^{-1}$, and e = the charge on an electron. When the experimental value of L is close to, or equal to, the theoretical value, then we assume that the electronic contribution to the thermal conductivity predominates. For pure metals near room temperature, experimental values of L range from $2.23 \times 10^{-8} \text{ W ohm K}^{-2}$ for copper to $3.04 \times 10^{-8} \text{ W ohm K}^{-2}$ for tungsten.

The thermal conductivities of pure metals are shown in Fig. 6.6. Since the thermal conductivity of all crystalline materials is made up of contributions from both k_{ph} and k_{el} , we can only crudely predict the temperature dependence. It is evident that the increase in k with temperature predicted by Eq. (6.17) does not operate in a strong fashion, and that most metals actually show a decrease in k with temperature. In the cases of pure nickel and pure iron, k decreases with temperature at low temperatures; at higher temperatures, the electronic contribution presumably overwhelms the phonon contribution, and k increases with temperature.

Qualitatively, at least, thermal conductivities in solids and alloys, in particular, can be explained *post facto* by Eq. (6.9) through the mean free path for phonons (λ_{ph}) and the mean free path for electrons (λ_e). In the case of phonons, λ_{ph} is governed by three interaction processes: the Umklapp collisions, scattering of phonons by crystal imperfections and solute atoms, and interactions between the phonons and the free electrons. Similarly, λ_e is limited

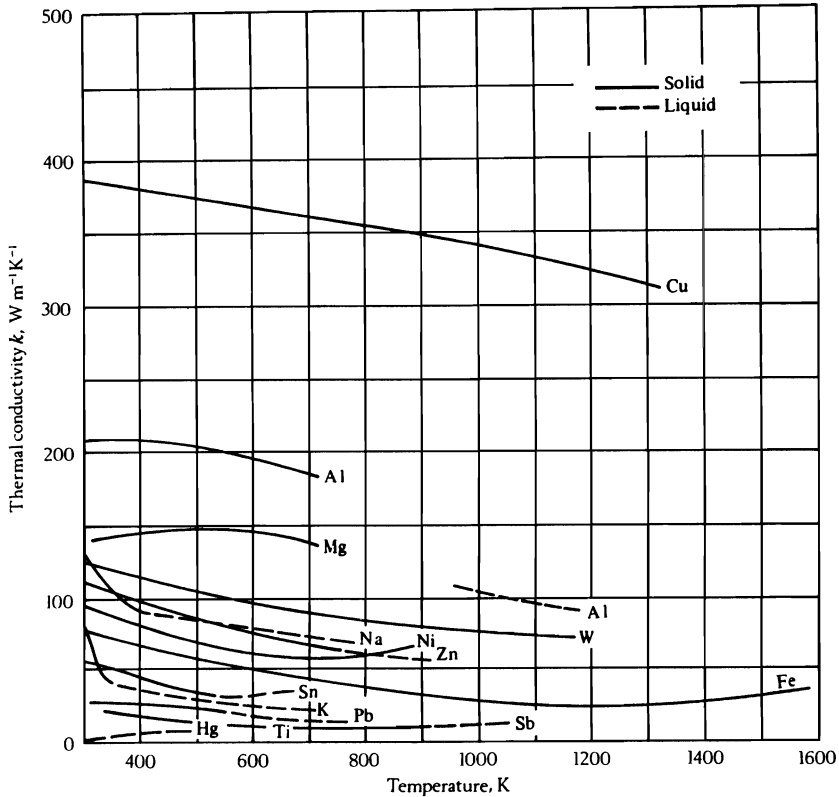


Fig. 6.6 Thermal conductivities of pure, solid, and liquid metals.

by scattering of electrons by crystal imperfections and solute atoms, electron-electron interactions, and the electron-phonon interactions. With the thermal conductivity comprising both λ_e and λ_{ph} , each involving several different mechanisms, it is not surprising that our ability to predict thermal conductivities in alloys is rather limited.

Figures 6.7 and 6.8 show the effect of alloying. Substitutional alloying and second phases both lower the conductivity from that of the pure metal, although a wide variety of ferrous alloys all reach the same limiting value at temperatures at or above the α - γ transition point. Note that the alloys in both Figs. 6.7 and 6.8 have absolute values of k that are about the same as those for the oxides in Fig. 6.3, which clearly are not metallic in nature. This indicates that a substantial portion of the thermal conduction is via phonons in alloys.

Klemens and Williams⁴ pointed out that the so-called Smith-Palmer equation has been used to describe experimental thermal conductivities in aluminum alloys (with the exception of high Si casting alloys) to within 5%. The Smith-Palmer equation is

$$k = AL\sigma_e T + B \quad (6.19)$$

⁴P. G. Klemens and R. K. Williams, *Int. Met. Rev.* **31**, 197 (1986).

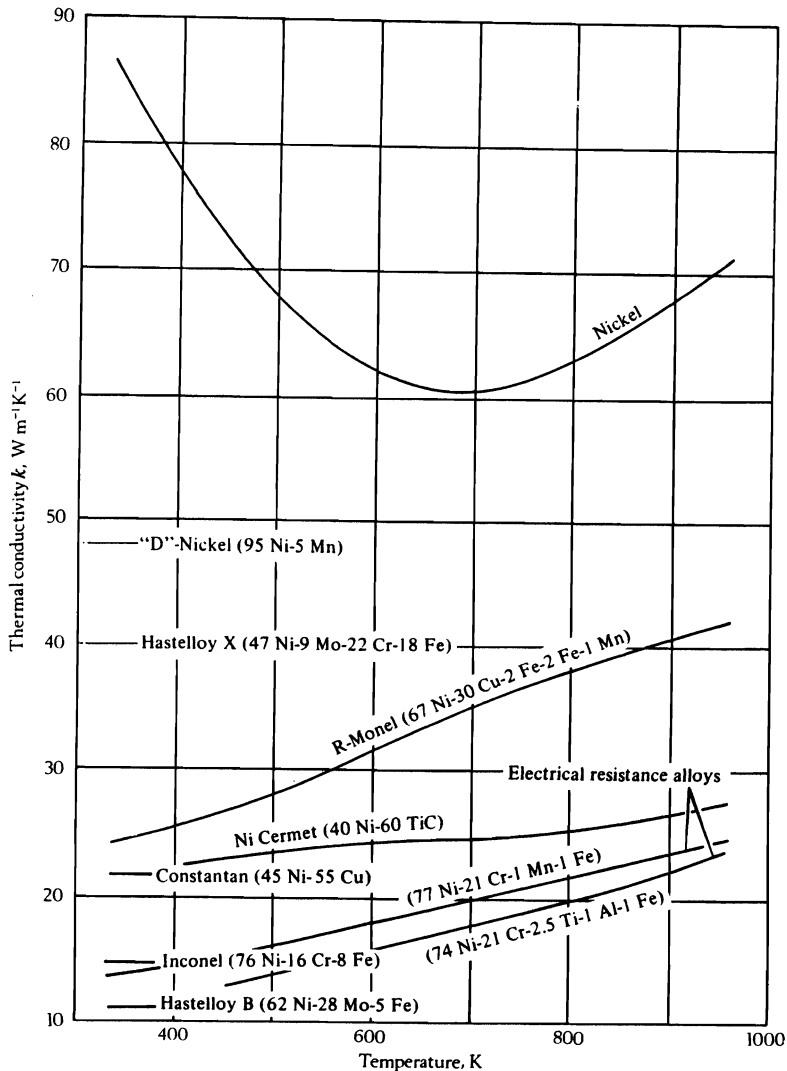


Fig. 6.7 Thermal conductivities of nickel and of nickel-base alloys.

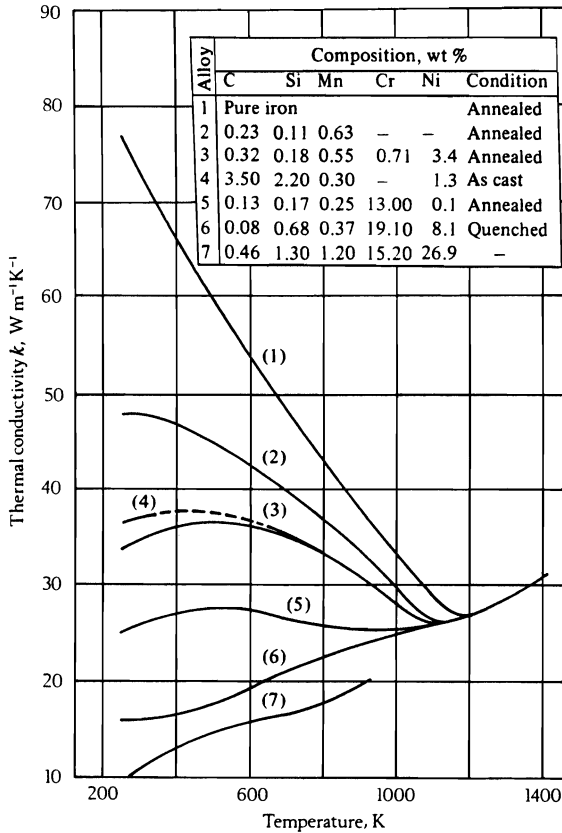


Fig. 6.8 Thermal conductivities of pure iron and iron-base alloys. (From Schack, *ibid.*)

where $A = 0.909$ and $B = 10.5 \text{ W m}^{-1} \text{ K}^{-1}$. Equation (6.19) has also been used for α and $\alpha + \beta$ Ti-alloys, with $A = 0.997$ and $B = 2.7 \text{ W m}^{-1} \text{ K}^{-1}$. Of course, in order to use Eq. (6.19), the electrical conductivity of the alloy, σ_e , must be known. This is advantageous, however, because it is relatively simple to measure electrical conductivity, whereas the thermal conductivity is a rather difficult measurement. Data on the electrical conductivity of metals and alloys are given in Brandes.⁵

Example 6.3 The electrical resistivity of magnesium is

$$\rho = a_0 + a_1 T, \text{ ohm m}$$

⁵E. A. Brandes (editor), *Smithells Metals Reference Book*, 6th ed., Butterworths, London, U.K., 1983, pages 19-1 to 19-7.

200 Fourier's Law and Thermal Conductivity of Materials

where T is temperature (K). The constants are $a_0 = 0.2 \times 10^{-8}$ ohm m and $a_1 = 1.68 \times 10^{-10}$ ohm m K⁻¹, which apply in the range $150 \leq T \leq 500$ K. Evaluate the Lorentz number for magnesium at 300 and 500 K.

Solution. Assume that $k_{el} = k$ so that Eq. (6.18) can be used. When we do this, the Lorentz number is

$$L = \frac{k\rho}{T} = k \left[\frac{a_0}{T} + a_1 \right].$$

From Fig. 6.6, $k(300 \text{ K}) = 140 \text{ W m}^{-1} \text{ K}^{-1}$; therefore

$$L(300 \text{ K}) = 140 \left[\frac{0.2 \times 10^{-8}}{300} + 1.68 \times 10^{-10} \right] = 2.44 \times 10^{-8} \text{ W ohm K}^{-2}.$$

In a similar manner, $k(500 \text{ K}) = 148 \text{ W m}^{-1} \text{ K}^{-1}$ and

$$L(500 \text{ K}) = 2.55 \times 10^{-8} \text{ W ohm K}^{-2}.$$

Notice that these values of L are within 4 pct. of the theoretical value given by Eq. (6.18).

In the case of semiconducting compounds, the thermal conductivity may be strongly influenced by phonon mechanisms at low or at moderate temperatures, but as more electrons are excited from valence to conduction states when the temperature is raised, the electron contribution increases, until k_{el} may predominate. In the intrinsic conduction range, the Lorentz number is given by

$$L = 2 \left[\frac{\kappa_B}{e} \right]^2 + \left[\frac{\kappa_B}{e} \right]^2 \frac{1}{(\sigma_n + \sigma_p)} \left[4 + \frac{E_g}{RT} \right]^2, \quad (6.20)$$

where σ_n = electrical conductivity via electrons in the conduction band, σ_p = electrical conductivity via holes in the valence band, and E_g = energy gap between bands. It has been shown,^{6,7} that this contribution is significant in the case of UO_2 , and is certainly significant for other semiconducting oxides, such as TiO_2 , ZrO_2 , and Nb_2O_5 . Since this contribution increases with temperature ($\sigma_n + \sigma_p$, σ_n , and σ_p all increase with temperature), it must be superimposed on the phonon contribution in order to totally explain the rise in the thermal conductivity at very high temperatures for semiconductors.

Conversely, other oxides, for example, SiO_2 , Al_2O_3 , and MgO , never show significant electronic conduction, and yet their thermal conductivities also increase with temperature at very high temperatures (see Fig. 6.3). This phenomenon has been explained on the basis of the ability of certain materials to transmit radiant energy (a *photon* contribution to thermal conductivity). This occurs when a material is no longer opaque, but translucent to incident radiation. Without going into the details of the interaction of radiation and solids, we can compute the radiant energy conductivity k_r from

$$k_r = \frac{16}{3} \frac{\sigma v^2 T^3}{a}, \quad (6.21)$$

⁶J. L. Bates, *Nucleonics* 19, 83 (1961).

⁷D. R. deHelar, *Nucleonics* 2, 92 (1963).

where σ = the Stefan-Boltzmann constant ($5.670 \times 10^{-8} \text{ W m}^{-2} \text{ K}^{-4}$), ν = the index of refraction, and a = the absorption coefficient equal to $1/\lambda_{ph}$, m^{-1} . When a is large (opaque material), the ability to absorb incident radiation is large; thus radiant energy is not transmitted through the solid as photons, but rather is absorbed at the surface and transferred to energy transmitted by the phonon or electron mechanisms.

When a is small (transparent material), k , may be quite significant. In general, the contribution of photon or radiant energy becomes significant for dense oxides at temperatures in the neighborhood of 1750 K.

Figure 6.9 presents thermal conductivity data for a variety of nonmetallic crystalline materials used for high-temperature applications. Some of these exhibit semiconducting electrical properties at elevated temperatures, and the transition in temperature dependence is probably caused by an increasing influence of the electronic conductance over the phonon contribution. The absolute value is again in the same range as that for the alloys in Figs. 6.7 and 6.8.

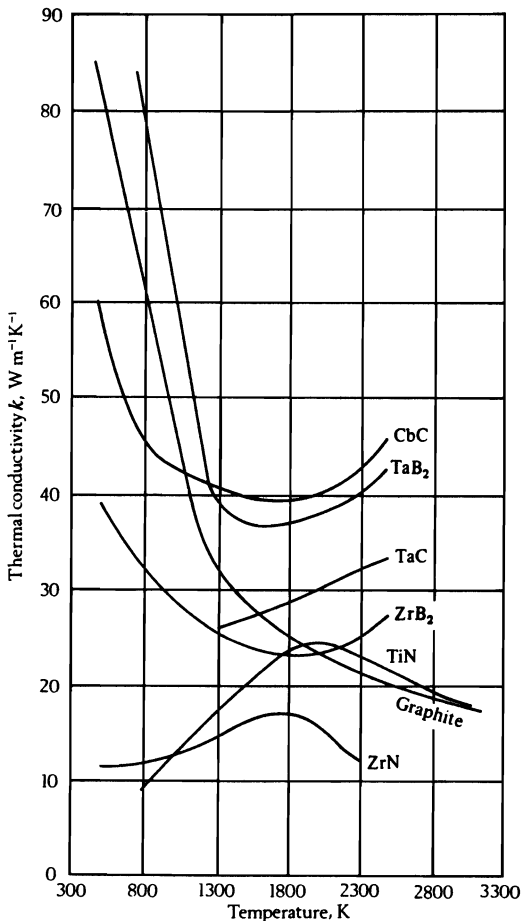


Fig. 6.9 Thermal conductivity of high-temperature materials.

202 Fourier's Law and Thermal Conductivity of Materials

Finally, for amorphous materials such as high polymers and glasses, thermal conduction is mainly via atomic or molecular migration (or radiation at high temperatures), because the material is too irregular in structure to support a phonon mechanism and the electron contribution is negligible. This results in very low values of conductivity, as indicated in Table 6.1.

Table 6.1 Thermal conductivities of amorphous or molecular solids

Substance	Temperature, K	k , $\text{W m}^{-1} \text{K}^{-1}$
Glass	373	0.76
Lead glass	273	0.87
Pyrex glass	373	1.16
Quartz glass	373	1.42
Asphalt	293	0.76
Polystyrene	293	0.12
Polyvinyl chloride	293	0.26

The thermal conductivity of glass can be explained on the basis of Eq. (6.9) and Eq. (6.21). In this context, λ is the phonon mean free path and \bar{V} is considered to be the speed of sound in the glass. The phonon mean free path is limited by the noncrystalline structure of the glass, so it is only on the order of interatomic distances and independent of temperature. Therefore, the thermal conductivity depends on temperature in the same way as C_v . Figure 6.10 shows this behavior for fused silica. The conductivity increases at low temperatures and then reaches a nearly constant value (excluding radiation) beyond approximately 600 K. High temperature conductivities show the expected increases because of the photon conductivity, i.e., Eq. (6.21).

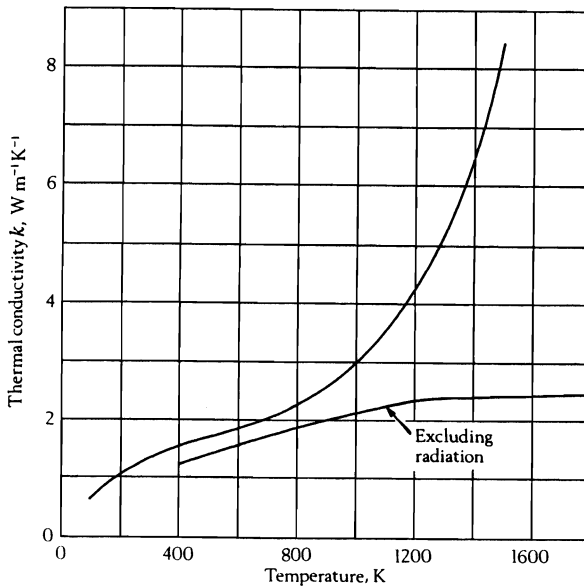


Fig. 6.10 Thermal conductivity of fused silica. (Adapted from Kingery *et al.*, *ibid.*, page 626.)

The effect of composition on the thermal conductivity of glass is shown in Fig. 6.11. The variation of thermal conductivity in glasses is not as pronounced as it is in crystalline materials because the mean free path for phonon conduction is not affected very much by composition.

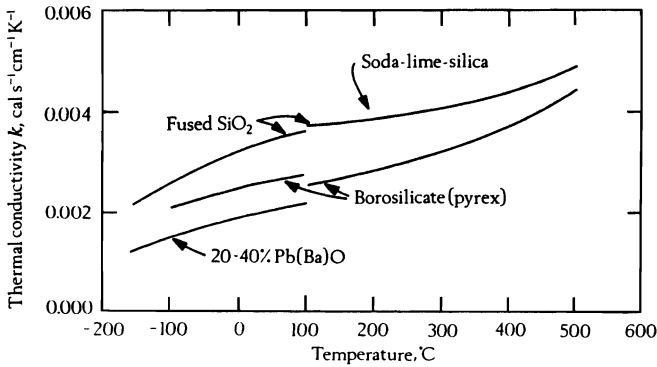


Fig. 6.11 The thermal conductivity in several glasses. (From Kingery *et al.*, page 626.)
 Note: $1 \text{ cal s}^{-1} \text{ cm}^{-1} \text{ K}^{-1} = 418.4 \text{ W m}^{-1} \text{ K}^{-1}$.

For polymeric materials the same thermal conduction mechanisms apply as in metallic and ceramic materials. There is no widely accepted quantitative theory to predict thermal conductivity in these materials. Their structure can vary from strongly crystalline to essentially amorphous, in which case the molecular chains are randomly arranged. In the amorphous state, the difficulty of propagating a lattice wave through the structure can be imagined, and since these are not electron-conducting materials, thermal energy has a difficult time being transmitted. Even when there are crystalline (ordered) regions within the polymer, they are usually surrounded by enough amorphous material that their improved conductivity does not significantly change their overall low conductivity. Table 6.2 gives some representative thermal data for polymeric materials.

To summarize, we should remember that the value of the thermal conductivity of solids is determined by the sum of several mechanisms, including those of phonons, electrons, photons, and atomic migration, regardless of the materials, and it is because of this fact that the prediction of this property is so difficult.

6.4 THERMAL CONDUCTIVITY OF LIQUIDS

As usual, when dealing with liquids, we are faced with a lack of knowledge of their structure. Using Eq. (6.9), Bird *et al.*⁸ modified a theory due to Bridgman which results in an expression for the thermal conductivity of liquids at densities away from the critical value:

$$k = 2.8\kappa_B V_s \left[\frac{N_0}{\bar{V}} \right]^{2/3}, \quad (6.22)$$

⁸R. Bird, W. Stewart and E. Lightfoot, *Transport Phenomena*, John Wiley, New York, N.Y., 1960, p. 260.

Table 6.2 Thermal conductivity and other thermal properties of polymeric materials

Material	Density (kg m ⁻³)	Specific heat (kJ kg ⁻¹ K ⁻¹)	Thermal conductivity (W m ⁻¹ K ⁻¹)	Coeff. of therm. exp. (μm K ⁻¹ m ⁻¹)	Thermal diffusivity (m ² s ⁻¹ × 10 ⁷)	Max. operating temp. (°C)
ABS (high impact)	1040	1.46	0.3	90	1.7	70
Acetal (homopolymer)	1420	1.46	0.2	80	0.7	85
Acetal (copolymer)	1410	1.46	0.2	95	0.72	90
Acrylic	1180	1.46	0.2	70	1.09	50
Cellulose acetate	1280	1.50	0.15	100	1.04	60
CAB	1190	1.46	0.14	100	1.27	60
Epoxy	1200	—	0.23	70	—	130
Modified PPO	1060	—	0.22	60	—	120
Nylon 66	1140	1.7	0.24	90	1.01	90
Nylon 66 (33% glass)	1380	1.2	0.52	30	1.33	100
PEEK	1300	—	—	48	—	204
PEEK (30% carbon)	1400	—	—	14	—	255
PET	1360	—	0.14	90	—	110
PET (36% glass)	1630	—	—	40	—	150
Phenolic (mineral filled)	1690	—	—	22	—	185
Polyamide-imide	1400	—	—	36	—	260
Polycarbonate	1150	1.2	0.2	65	1.47	125
Polyester	1200	—	0.2	100	—	—
Polyetherimide	1270	—	0.22	56	—	170
Polyethersulfane	1370	—	1.18	55	—	180
Polyimide	1420	—	—	45	—	260
Polyphenylene sulfide (30% carbon)	1460	—	—	16	—	200
Polypropylene	905	1.92	0.24	100	0.65	100
Polysulfane	1240	—	—	56	—	170
Polystyrene	1050	1.34	0.15	80	0.6	50
Polythene (LD)	920	2.30	0.33	200	1.17	50
Polythene (HD)	950	2.30	0.63	120	1.57	55
PTFE	2100	—	0.25	140	0.7	50
PVC (rigid)	1400	1.00	0.16	70	1.16	50
PVC (flexible)	1300	1.7	0.14	140	0.7	50
SAN	1080	1.38	0.17	70	0.81	60
DMC (polyester)	1800	—	0.2	20	—	130
SMC (polyester)	1800	—	0.2	20	—	130
Polystyrene foam	32	—	0.032	—	—	—
PV foam	32	—	0.032	—	—	—

(From R. J. Crawford, *Plastics Engineering*, second edition, Pergamon Press, Oxford, U.K., 1987, page 33.)

where \hat{V} = the molar volume, N_0 = Avogadro's number, and V_s = the speed of sound through the liquid, given by

$$V_s = \left[\frac{C_p}{C_v} \left(\frac{1}{\rho\beta} \right)_T \right]^{1/2},$$

where β = compressibility. This is based on the assumption that the molecules in the liquid are arranged in a cubic lattice and energy transfer is via collisions between molecules. The thermal conductivity of ordinary liquids near room temperature is considerably below that of crystalline solids, as indicated in Table 6.3, emphasizing the fact that energy transfer in ordinary liquids is difficult because of the lack of both phonon and electron conduction. However, liquid metals show much higher conductivities than other liquids, because electronic conduction is possible, and a survey of the Lorentz numbers for liquid metals indicates close agreement with the theoretical value. Data for liquid metals along with solid metals are included in Fig. 6.6 and Fig. 6.12.

Table 6.3 Thermal conductivities of various liquids

Substance	Temperature, K	k , $\text{W m}^{-1} \text{K}^{-1}$
Water	289	0.552
Water	311	0.415
Light oil	289	0.13
Light oil	311	0.14
Benzene	354	0.14
Fluoride salts	755	5.5
Slag	1865	4.0

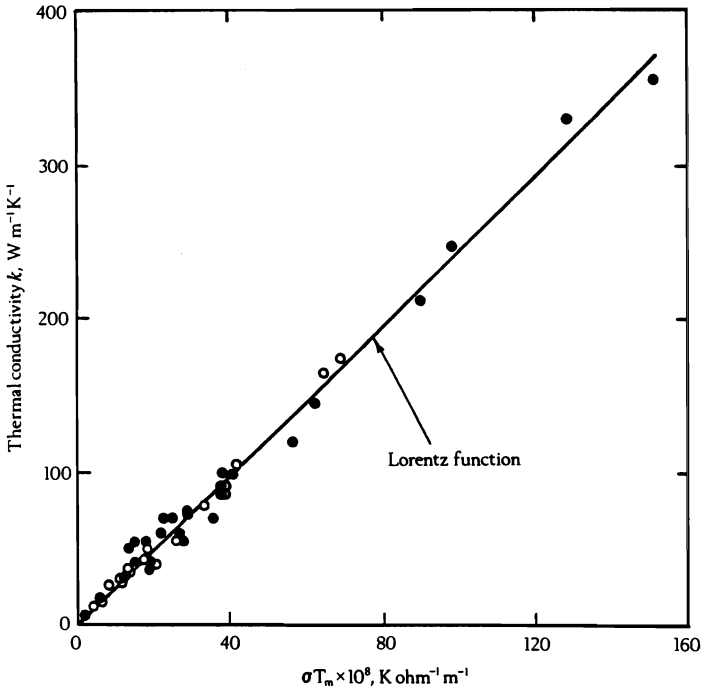


Fig. 6.12 Variation of thermal conductivity with the product of melting temperature and electrical conductivity of solid (●) and liquid (○) metals. (From E. T. Turkdogan, *Physical Chemistry of High Temperature Technology*, Academic Press, New York, N.Y., 1980, page 125.)

When dealing with molten salts, Iida and Guthrie⁹ correlated thermal conductivity at the melting point with the speed of sound; their equation is

$$k = 3.3 \times 10^{-7} U_s / \hat{V}^{2/3} \quad (6.23)$$

⁹T. Iida and R. I. L. Guthrie, *The Physical Properties of Liquid Metals*, Clarendon Press, Oxford, U.K., 1988, pages 248-250.

where U_s is the speed of sound in m s^{-1} and \hat{V} is the molar volume in $\text{m}^3 \text{mol}^{-1}$. If the speed of sound is not available, it can be estimated by

$$U_s = 16 \left[\frac{T_m}{M} \right]^{1/2} \quad (6.24)$$

where T_m = melting point, K, and M = formula weight, g mol^{-1} . Equation (6.23), by itself, gives values of k within 20 percent; however, U_s estimated by Eq. (6.24) is only within 40 percent so the overall error can be even greater than 20 percent.

The thermal conductivities of highly basic silicate melts, including some that are supercooled, are given as

$$k = a + bT \quad (6.25)$$

where a and b can be found in Table 6.4.

Table 6.4 Coefficients for Eq. (6.25)

System (mol %)	Temp., K	a W $\text{m}^{-1} \text{K}^{-1}$	b W $\text{m}^{-1} \text{K}^{-2}$
50SiO ₂ -50Na ₂ O	1400	1.03	—
60SiO ₂ -40Na ₂ O	900-1400	-0.063	5.2
70SiO ₂ -30Na ₂ O	800-1400	0.184	2.4
50SiO ₂ -50K ₂ O	1310	0.32	—
60SiO ₂ -40K ₂ O	950-1300	0.19	0.85
70SiO ₂ -30K ₂ O	900-1300	0.04	2.0

(From H. Ohta, Y. Waseda and Y. Shiraishi in H. A. Fine and D. R. Gaskell (eds.), *Second International Symposium on Metallurgical Slags and Fluxes*, The Metallurgical Society (AIME), Warrendale, PA, 1984, page 863.)

In these silicates, as well as in some metallurgical slags containing CaO-SiO₂-Al₂O₃, thermal conductivity increases with increasing temperature up to about 1000 K to 1300 K and then decreases with increasing temperature in both the solid glassy state and the liquid state. An exception is the silicate with the composition Na₂O·SiO₂, with a thermal conductivity that decreases with increasing temperature. Some data are given in Figs. 6.13 and 6.14. In these materials, the mean free path of the phonons is almost constant with temperature, so the changes in the thermal conductivity are attributed to the variation of the speed of sound with temperature. It is also important to note the "insulating" character of molten silicate slags. The low conductivity of these slags causes considerable difficulty in transferring heat from combustion gases above a slag to a metal phase below it.

From this discussion, we can see that to accurately predict the thermal conductivity of solids and liquids is difficult. One must be able to make intelligent estimates and extrapolations from known data. This in turn requires an understanding of the role of the various conduction mechanisms, and of the effects that structural and chemical variations may have on these mechanisms. Sometimes we can only make order-of-magnitude estimates if experimental data are not available. Figure 6.15 gives a summary of the typical ranges of thermal conductivities for various classes of materials.

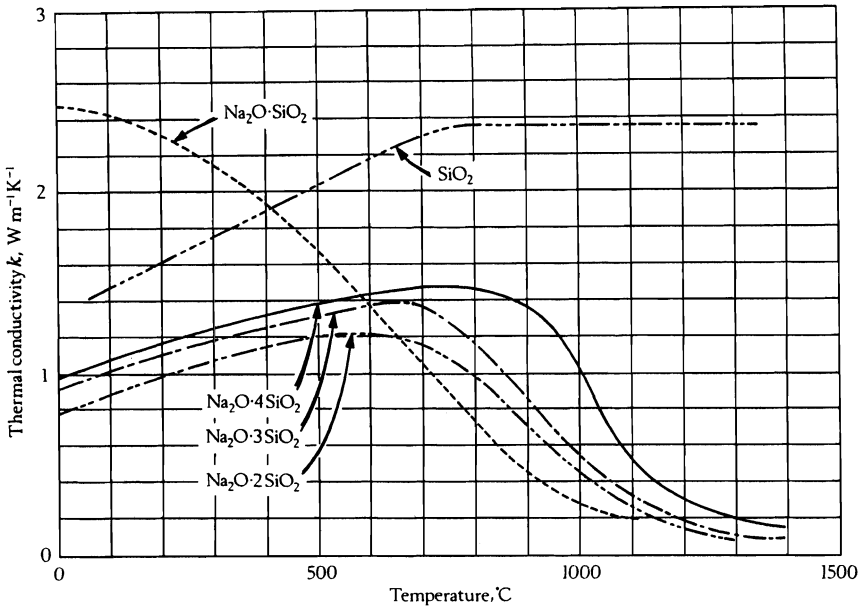


Fig. 6.13 Thermal conductivity of solid and molten $\text{Na}_2\text{O-SiO}_2$ silicates. (From K. Nagata and K. S. Goto in H. A. Fine and D. R. Gaskell (eds.), *ibid.*, pages 875-889.)

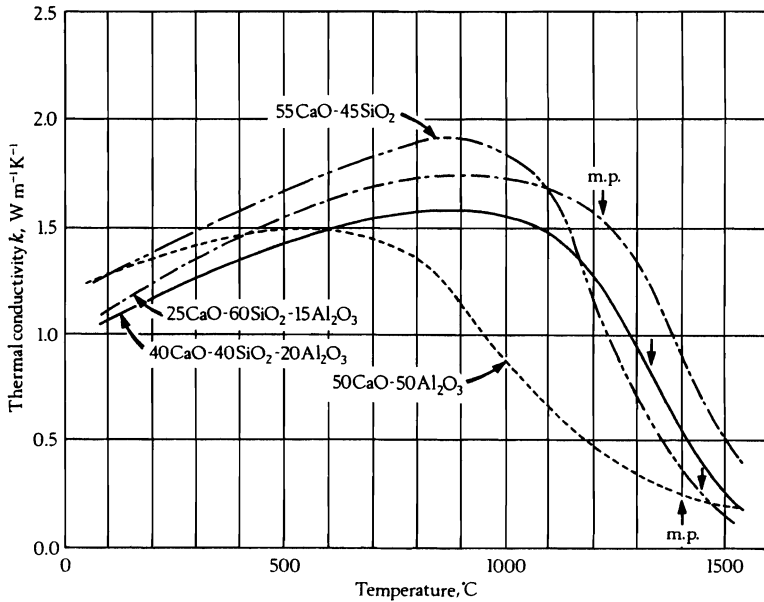


Fig. 6.14 Thermal conductivity of solid and molten $\text{CaO-SiO}_2\text{-Al}_2\text{O}_3$ slags. (From K. Nagata and K. S. Goto in H. A. Fine and D. R. Gaskell (eds.), *ibid.*, pages 875-889.)

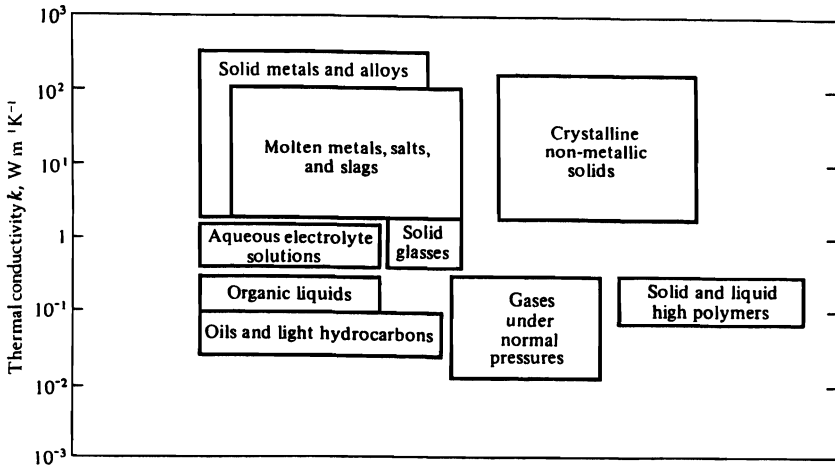


Fig. 6.15 Summary of the ranges of thermal conductivity for various classes of materials.

6.5 THERMAL CONDUCTIVITY OF BULK MATERIALS

So far, we have looked at the thermal conductivity of individual phases. We have seen the difficulties of arriving at exact predictions of thermal conductivity for most solids, particularly complex alloys. In most engineering situations, we are often faced with even more complex materials, for example, porous bulk materials. The thermal conductivity of such materials is certainly not equal to the intrinsic thermal conductivity of the solid involved. The question is: What value should be used?

6.5.1 Two-phase mixtures

Alloys known as cermets or metal-matrix composites have evolved. These are metallic alloys with a dispersion of a ceramic phase within the matrix. The thermal conductivity of such materials is a function of the volume fraction of each phase. For up to one-tenth volume fraction, V_d , of a dispersed phase of spherical particles with intrinsic thermal conductivity, k_d , it has been suggested that the thermal conductivity of the mixture, k_{mix} , may be found from the Maxwell equation,

$$\frac{k_{\text{mix}}}{k_c} = \frac{k_d/k_c + 2 - 2V_d(1 - k_d/k_c)}{k_d/k_c + 2 + V_d(1 - k_d/k_c)} \quad (6.26)$$

If the thermal conductivity of the continuous phase, k_c , is much larger than k_d , then

$$k_{\text{mix}} \cong k_c \left[\frac{1 - V_d}{1 + V_d/2} \right] \quad (6.27)$$

Data for the thermal conductivity of SAP Al-Al₂O₃ alloys¹⁰ are plotted in Fig. 6.16, along with k_{mix} calculated by using Eq. (6.27) and the data from Figs. 6.3 and 6.6. The agreement is less than satisfactory.

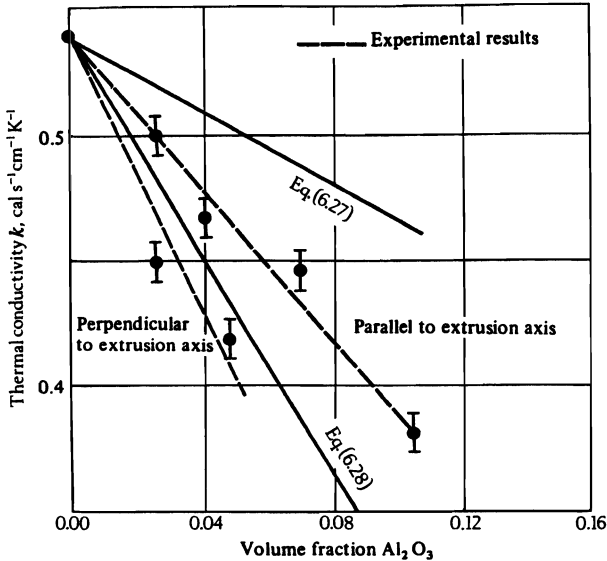


Fig. 6.16 Thermal conductivity of Al-Al₂O₃ (SAP) alloys at 100°C. Similar results are obtained on data available at 500°C. (Data from D. Nobili and M. A. DeBacci, *ibid.*) Note: 1 cal s⁻¹ cm⁻¹ K⁻¹ = 418.4 W m⁻¹ K⁻¹.

However, if we assume that the material behaves as if it were a series of plates of Al and Al₂O₃ normal to the direction of heat flow, then they would be equivalent to a series of resistors in an electric circuit, and

$$\frac{1}{k_{\text{mix}}} = \frac{V_c}{k_c} + \frac{V_d}{k_d} \quad (6.28)$$

Using this equation, we obtain better agreement with the experimental results. We should emphasize, however, that we lack the physical basis for this assumption, and that the purpose in including it at this point is only to stress the difficulty of predicting k for two-phase materials. Several models for the thermal conductivity of two-phase materials are summarized in Table 6.5.

6.5.2 Porous materials

Most ceramic materials and some powder metallurgy products have some low, internal porosity ω , as a result of having been sintered from powders. The pores are generally isolated from one another. At temperatures up to and slightly above the room temperature,

¹⁰D. Nobili and M. A. DeBacci, *J. Nuclear Materials* 18, 187 (1966).

Table 6.5 Thermal conductivities of two-phase mixtures based on models with various geometric arrangements.

Parallel	$\frac{k_{\text{mix}}}{k_c} = (1 - V_d) + V_d \frac{k_d}{k_c}$	(1)
Series	$\frac{k_{\text{mix}}}{k_c} = \frac{1}{(1 - V_d) + V_d \frac{k_c}{k_d}}$	(2)
Russell model: cubes in a cubic array; linear isotherms	$\frac{k_{\text{mix}}}{k_c} = \frac{1 - V_d^{2/3} + \frac{k_d}{k_c} V_d^{2/3}}{1 - V_d^{2/3} + V_d + \frac{k_d}{k_c} (V_d^{2/3} - V_d)}$	(3)
son Frey model: cubes in a cubic array; linear heat flow	$\frac{k_{\text{mix}}}{k_c} = \frac{1 - V_d^{1/3} + V_d + \frac{k_c}{k_d} (V_d^{1/3} - V_d)}{1 - V_d^{1/3} + \frac{k_c}{k_d} V_d^{1/3}}$	(4)
Rayleigh-Devries model: regular array of uniform spheres in contact. simple cubic array, $a = 1.31$ body-centered cubic, $a = 0.129$ face-centered cubic, $a = 0.0752$	$\frac{k_{\text{mix}}}{k_c} = 1 - \frac{3V_d}{\left[\frac{2 + k_d/k_c}{1 - k_d/k_c} \right] + V_d - a \left[\frac{1 - k_d/k_c}{4/3 + k_d/k_c} \right] V_d^{10/3} + \dots}$	(5)
Maxwell model: random distribution of spheres; no contact	$\frac{k_{\text{mix}}}{k_c} = \frac{\frac{k_d}{k_c} + 2 - 2V_d \left[1 - \frac{k_d}{k_c} \right]}{\frac{k_d}{k_c} + 2 + V_d \left[1 - \frac{k_d}{k_c} \right]}$	(6)
Bruggeman model: infinite range of bubble sizes in continuous phase	$1 - V_d = \frac{\frac{k_{\text{mix}}}{k_c} - \frac{k_d}{k_c}}{\left[\frac{k_{\text{mix}}}{k_c} \right]^{1/3} \left[1 - \frac{k_d}{k_c} \right]}$	(7)

k_d = thermal conductivity of discontinuous phase
 k_c = thermal conductivity of continuous phase
 V_d = volume fraction of discontinuous phase

Table provided by courtesy of A. Ortega, University of Arizona, Tucson, Arizona (1992). Also in W. D. Drotning, A. Ortega, and P. E. Havey, *Thermal Conductivity of Aqueous Foam*, Sandia Report SAND82-0742, Sandia National Laboratories, Albuquerque, New Mexico, 1982, pages 5 and 6.

the porosity has a thermal conductivity which is essentially zero. The effective thermal conductivity of the bulk materials is often estimated to be

$$k_{\text{eff}} = k_c(1 - \omega). \quad (6.29)$$

At larger porosities, the pores are not isolated and the porosity becomes continuous. Conductivity at room temperature is thus even lower than that predicted by Eq. (6.29). Figure 6.17 illustrates the effect of larger amounts of porosity on the thermal conductivity of partially sintered powder metal compacts.

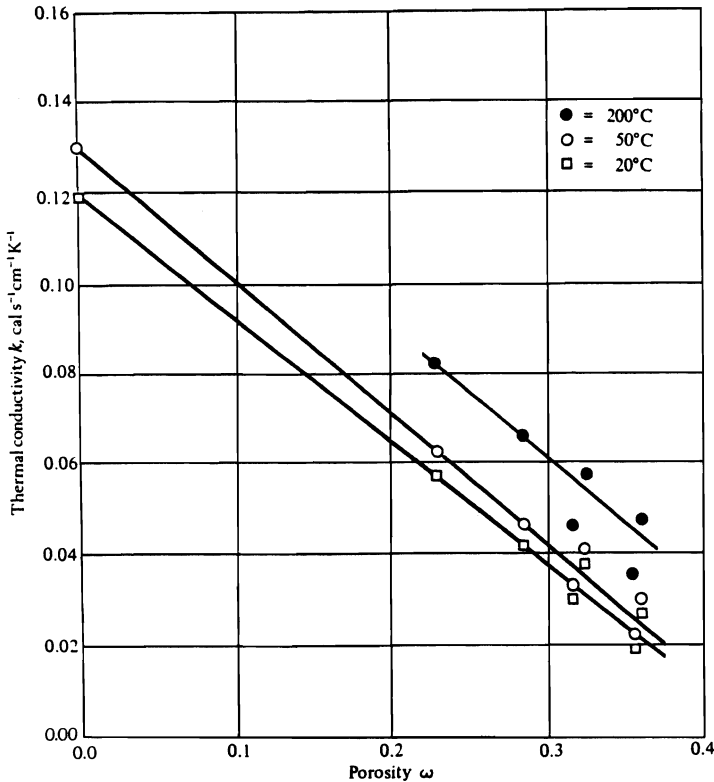


Fig. 6.17 Thermal conductivity of phosphor-bronze powder compacts as a function of porosity ω . (From P. Grootenhuis, R. W. Powell, and R. P. Tye, *Proc. Phys. Soc.* **65**, 502 (1952).)

In general, the conductivity of a loose packing, or packed bed, is a function of the thermal conductivity of the gas in the pores, the solid, the void fraction in the bed, and the temperature, because, as the temperature increases, the particle-to-particle thermal radiation also increases. Schotte¹¹ developed a technique for predicting the conductivity of packed beds, in which the gas phase is continuous; it is outlined below.

Taking the gas first, we can use the methods outlined in Section 6.2 to obtain k_g , except in the following instance. When the effective pore dimensions are of the same order of

¹¹W. Schotte, *A.I.Ch.E. Journal* **6**, 63 (1960).

212 Fourier's Law and Thermal Conductivity of Materials

magnitude as the mean free path of the gas, the true thermal conductivity of the gas decreases. This occurs when the particle diameter D_p is about 1000 times the mean free path of the gas. (The mean free path of air at room temperature and 1 atm is $\sim 10^{-5}$ cm. At 1810 K and 1 atm, it is $\sim 10^{-4}$ cm. Thus we are talking about situations where $D_p < 10^{-2}$ - 10^{-1} cm.) Deissler and Eian¹² developed a correlation for the *break-away* pressure P_b in $N\ m^{-2}$, above which no correction for this effect is required:

$$P_b = 4.32 \times 10^{-21} \frac{T}{D_p d^2}, \quad (6.30)$$

where T is temperature, K, D_p = the average particle diameter, m, and d = the mean diameter of the gas molecules, m. If the actual pressure is greater than P_b , no correction to the value of k_g read from Fig. 6.2 is needed, but if the actual pressure is less than P_b calculated by Eq. (6.30), then the thermal conductivity of the gas phase should then be calculated according to the equation

$$k_g = \frac{k_g^0}{1 + 4.95 \times 10^{-22} \left[\frac{C_p/C_v}{1 + C_p/C_v} \right] \left[\frac{1 - \omega}{\omega} \right] \left[\frac{TK_g^0}{PD_p d^2 C_p \eta} \right]}, \quad (6.31)$$

where k_g^0 is the uncorrected value obtained from Fig. 6.2; SI units are used for the variables. We see that k_g decreases, at any given temperature, as D_p decreases, and if the pores are small enough, then k_g is effectively zero. This effect is illustrated in Fig. 6.3 by the data for the thermal conductivity of porous brick.

Having obtained k_g , either directly or by using Eq. (6.31) if required, we use k_s , the intrinsic thermal conductivity of the solid phase, to calculate the ratio k_s/k_g . Then, using Fig. 6.18 we may find k_b , the *effective thermal conductivity* of the packed bed, from the ratio k_b/k_g . This correlation (Fig. 6.18) has been developed from data on many packed beds, and is accurate as given at temperatures less than 200°C.¹³ However, Fig. 6.18 should not be used outside the limit $1 < k_s/k_g < 6000$. If k_s/k_g is greater than 6000, then there may be appreciable contact conduction between particles which has not been accounted for in Fig. 6.18. However, this situation does not often arise, except possibly in compacts of powdered metals.

If the temperature is above 200°C we must add another term to k_b , found in the same manner as above, in order to obtain the true effective thermal conductivity of the bed. At higher temperatures, there is a contribution to the effective thermal conductivity of the bed by radiation heat-transfer from particle to particle. This contribution, for example, is important for 1-mm particles above 400°C and for 0.1-mm particles above 1500°C. Schotte considered the radiation from a plane on one side of a spherical particle to a plane on the other side. First, there is a direct radiation heat-transfer across the void space past the particle, with heat-transfer contribution:

$$Q_1 = -h_r \left[D_p^2 \frac{\pi}{4} \frac{\omega}{1 - \omega} \right] \left[D_p \frac{dT}{dx} \right], \quad (6.32)$$

¹²R. G. Deissler and C. S. Eian, NACA, RM E52CO5 (1952).

¹³For another review, see R. Krupiczka: Analysis of thermal conductivity of granular materials, *Intl. Chem. Engr.* 1, 122 (Jan. 1967). He arrives at a graph that is virtually the same as that of Deissler and Eian.

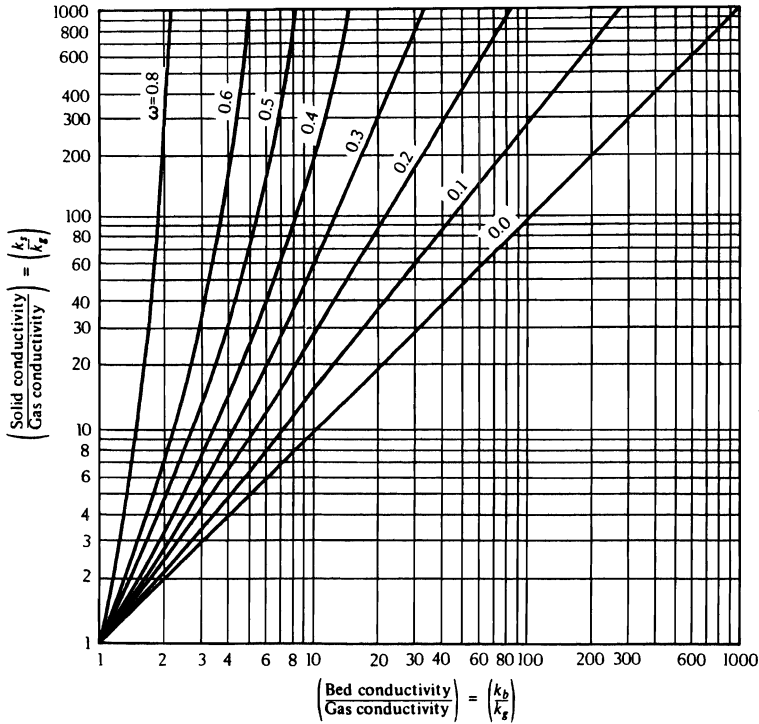


Fig. 6.18 Effect of porosity on packed bed thermal conductivity. (From Deissler and Eian, *ibid.*) Curves outside the range $0.2 \leq \omega \leq 0.6$ have not been tested as extensively as the others.

where h_r is the radiation heat-transfer coefficient between a particle and its neighbor, given by

$$h_r = 22.91\varepsilon \frac{T^3}{10^8}, \quad \text{W m}^{-2} \text{K}^{-1}.$$

Here ε is the emissivity of the solid, and T is the temperature, K. Secondly, there is radiation to and from the particle, in series with conduction through the particle. This is written

$$Q_2 = -D_p^2 \frac{\pi}{4} \left[\frac{k_s h_r D_p}{k_s + h_r D_p} \right] \left[\frac{dT}{dx} \right]. \quad (6.33)$$

When Q_1 and Q_2 are added, one obtains the total heat flow

$$Q = -k_r \left[D_p^2 \frac{\pi}{4} \frac{1}{1 - \omega} \right] \left[\frac{dT}{dx} \right],$$

where k_r is the radiation contribution to the effective thermal conductivity of the bed:

$$k_r = \frac{1 - \omega}{(1/k_s) + (1/k_r^0)} + \omega k_r^0, \quad (6.34)$$

and

$$k_r^0 = 22.91 \varepsilon D_p \left[\frac{T^3}{10^8} \right].$$

To evaluate the thermal conductivity of a packed bed, we use Fig. 6.18 (if necessary, use Eq. (6.31) to obtain k_g), then add k_r from Eq. (6.34) to obtain the effective thermal conductivity, as illustrated in Example 6.4. The reader will note that even at high temperatures, it is possible for porosity to contribute only slightly to k_r , provided the pore size is quite small. This is generally true of isolated pores as well as of pores in loose materials.

Example 6.4 Bearing in mind the importance of the effective thermal conductivity of molding sand in relation to the solidification rate of castings, let us see if we can predict the thermal conductivity of silica sand molds as a function of temperature, using the method described above.

Solution. Assume that the material is entirely quartz (SiO_2) with thermal conductivity given in Fig. 6.3, and that the atmosphere is dry air. If the bulk porosity is 40%, the grain size D_p is 3.81×10^{-4} m (AFS 43), and the emissivity of quartz is as given below, then we can proceed as outlined above.

1. Calculate P_b at 278 K

$$P_b = 4.32 \times 10^{-21} \frac{T}{D_p d^2}.$$

Assuming $d = 0.4$ nm

$$P_b = \frac{(4.32 \times 10^{-21})(278)}{(3.81 \times 10^{-4})(0.4 \times 10^{-9})^2} = 1.97 \times 10^4 \text{ N m}^{-2},$$

and we need to make no correction to the value read from Fig. 6.2. Subsequent calculations show that this condition holds true up to 1420 K. At 1555 K, k_g is calculated using Eq. (6.31).

2. Using the value of k_g in the table below, we calculate the ratio k_r/k_g at 278 K:

$$\frac{k_r}{k_g} = 384.$$

Then, from Fig. 6.18, we find that for $\omega = 0.4$, $k_b/k_g \approx 12$, or, because $k_g = 0.0225 \text{ W m}^{-1} \text{ K}^{-1}$, $k_b = 0.270 \text{ W m}^{-1} \text{ K}^{-1}$. This calculation is carried out at each temperature:

$T, \text{ K}$	$k_g, \text{ W m}^{-1} \text{ K}^{-1}$	k_r/k_g	k_b/k_g	$k_b, \text{ W m}^{-1} \text{ K}^{-1}$
278	0.022	384	12.0	0.26
500	0.036	167	9.5	0.34
722	0.050	90	7.9	0.40
944	0.062	79	7.5	0.46
1111	0.069	67	7.0	0.48
1389	0.076	136	9.0	0.68
1555	0.082	380	11.9	0.98

3. The radiation contribution to k_b is next calculated. At 278 K, $\varepsilon = 0.82$ and

$$k_r^0 = \frac{(22.91)(0.82)(3.81 \times 10^{-4})(278^3)}{10^8} = 1.54 \times 10^{-3} \text{ W m}^{-1} \text{ K}^{-1}.$$

Then

$$k_r = \frac{(1.0 - 0.4)}{\left[\frac{1}{8.65} \right] + \left[\frac{1}{0.00154} \right]} + (0.4)(0.00154) = 0.00154 \text{ W m}^{-1} \text{ K}^{-1}.$$

On the other hand, at 1555 K, $\varepsilon = 0.27$ and

$$k_r^0 = \frac{(22.91)(0.27)(3.81 \times 10^{-4})(1555^3)}{10^8} = 8.87 \times 10^{-2} \text{ W m}^{-1} \text{ K}^{-1}.$$

$$k_r = \frac{(1.0 - 0.4)}{\left[\frac{1}{26} \right] + \left[\frac{1}{0.0887} \right]} + (0.4)(0.0887) = 0.0885 \text{ W m}^{-1} \text{ K}^{-1}.$$

The values are added to the k_b values, given above, to obtain the final result.

Conductivities, W m ⁻¹ K ⁻¹							
$T, \text{ K}$	ε	k_r^0	k_r	+	k_b	=	k_{eff}
278	0.82	0.0015	0.0015		0.26		0.26
500	0.75	0.0081	0.0083		0.34		0.35
722	0.68	0.0225	0.0227		0.40		0.42
944	0.58	0.0429	0.0742		0.46		0.53
1111	0.49	0.0587	0.0583		0.48		0.54
1389	0.32	0.0692	0.0689		0.68		0.75
1555	0.27	0.0887	0.0885		0.98		1.07

When these calculated results are compared to experimental measurements, the agreement is surprisingly good.

We remind the reader that the previous calculation of the effective thermal conductivity applies to porous media with interconnected porosity. Mathematical models that predict the effective thermal conductivity with a measure of the degree of continuity of the solid phase are discussed by Marcussen.¹⁴

¹⁴L. Marcussen in T. Ashworth and D. R. Smith (eds.), *Thermal Conductivity 18*, Plenum Press, New York, N.Y., 1985, pages 585-598.

PROBLEMS

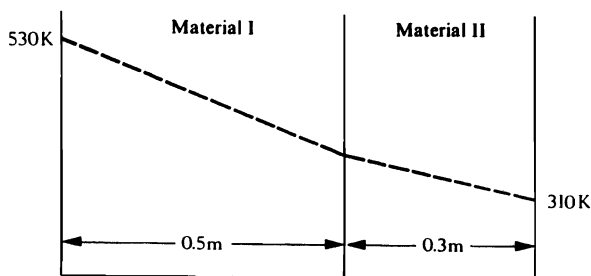
6.1 In the same system described in Problem 1.2, the temperature profile at $x = x_1$ is given by

$$T - T_0 = 6 \sin \left[\frac{\pi y}{2} \right], \quad 0 \leq y \leq 0.1 \text{ m},$$

where T is temperature (K) in the water, T_0 is temperature at $y = 0$, and y is distance from the flat plate in m. Find the heat flux to the wall at $x = x_1$. (The thermal conductivity of water is $0.62 \text{ W m}^{-1} \text{ K}^{-1}$, and the heat capacity is $4.19 \times 10^3 \text{ J kg}^{-1} \text{ K}^{-1}$.)

6.2 Determine the thermal conductivity of a test panel $150 \text{ mm} \times 150 \text{ mm}$ and 12 mm thick, if during a two-hour period $8.4 \times 10^4 \text{ J}$ are conducted through the panel when the two faces are at 290 K and 300 K .

6.3 At steady state, the temperature profile in a laminated system appears thus:



Determine the thermal conductivity of II if the steady-state heat flux is $12.6 \times 10^3 \text{ W m}^{-2}$ and the conductivity of I is $52 \text{ W m}^{-1} \text{ K}^{-1}$.

6.4 Show that Fourier's law can be written (for constant ρC_p) as

$$q_y = -\alpha \frac{d}{dy} (\rho C_p T)$$

for one-dimensional heat flow. In addition, show that Newton's law, for constant ρ , is

$$\tau_{yx} = -\nu \frac{d}{dy} (\rho v_x).$$

Discuss the analogies between the fluxes, constants, and gradients as they appear in these equations.

6.5 The thermal conductivity of helium at 400 K is $0.176 \text{ W m}^{-1} \text{ K}^{-1}$. Knowing only this datum, estimate the thermal conductivity of helium at 800 K . Compare your estimate to the value obtained from Fig. 6.2. What do you conclude about the equation that you used for your estimate?

6.6 Repeat Problem 6.5 but use the following equation to estimate the thermal conductivity of helium at 800 K:

$$k = \frac{15R}{4M} \eta$$

where R is the gas constant, M is the molecular weight, and η is the viscosity.

6.7 Calculate the thermal conductivity of carbon dioxide at 800 K and compare your result to that given in Fig. 6.2. The heat capacity of CO_2 at 800 K is $1.17 \text{ kJ kg}^{-1} \text{ K}^{-1}$.

6.8 a) Calculate the thermal conductivity of a gas containing 40 mol% He, 40 mol% H_2 , and 20 mol% N_2 at 1400 K.

b) Assume that the concentration of He is constant but that the concentrations of H_2 and N_2 vary as much as $\pm 5 \text{ mol\%}$ in a process. What is the variation in the thermal conductivity of the gas?

6.9 Refer to Fig. 6.3 and explain the variation of the thermal conductivity of MgO with temperature.

6.10 Refer to Fig. 6.5 and comment on the effect of impurity scattering of phonons in dielectric solid solutions. Assume that the inverse mean free path for different scattering processes are additive, so that

$$\frac{1}{\lambda_{\text{ph}}} = \frac{1}{\lambda_t} + \frac{1}{\lambda_i},$$

where λ_t is the thermal mean free path and λ_i is the impurity mean free path.

6.11 Electrical resistivities of Ti-Al alloys at 800 K are given in the table below. Aluminum is an " α -stabilizer."

At. pct. Al	Resistivity $\mu\text{ohm cm}$
0	112
3	140
6	165
11	190
33	210

Estimate the thermal conductivity for each alloy at 800 K.

6.12 The electrical conductivity of molten Pb-Sn alloys at 673 K is

$$\sigma = (100 - 48X)^{-1}$$

where σ is in $\mu\text{ohm}^{-1} \text{ cm}^{-1}$ and X is the atom fraction of Sn. Estimate the thermal conductivities of 90Pb-10Sn, 50Pb-50Sn and 10Pb-90Sn alloys (compositions in mol pct).

6.13 Use the Maxwell-Eucken equation and predict the thermal conductivity of a two-phase solid (A plus B) as a function of composition (wt.pct.). A and B are insoluble in each other, and the following data apply: $k_A = 13 \text{ W m}^{-1} \text{ K}^{-1}$; $k_B = 7 \text{ W m}^{-1} \text{ K}^{-1}$, $\rho_A = 4 \times 10^3 \text{ kg m}^{-3}$; $\rho_B = 3 \times 10^3 \text{ kg m}^{-3}$.

218 Fourier's Law and Thermal Conductivity of Materials

6.14 A flat heater is sandwiched between two solids of equal areas (0.1 m^2) with different thermal conductivities and thicknesses. The heater operates at a uniform temperature and provides a constant power of 290 W. The external surface temperature of each solid is 300 K, and there is perfect thermal contact at each internal interface.

- Calculate the heat flux through each solid.
- What is the operating temperature of the heater?

Solid	Thermal Conductivity, $\text{W m}^{-1} \text{K}^{-1}$	Thickness, mm
<i>A</i>	35	60
<i>B</i>	9	30

HEAT TRANSFER AND THE ENERGY EQUATION

We have designed this chapter to introduce the reader to three interwoven topics. First, we develop differential equations in terms of temperature in space (and with time if transient conditions apply) for several simple problems, by writing energy balances for unit volumes. In order to obtain solutions, we integrate the differential equations to ascertain the temperature and arbitrary constants, and then apply boundary and initial conditions to obtain the particular solution. The general procedure is similar to that followed in Chapter 2 for obtaining the velocity profiles.

Second, several of the examples are concerned with heat transfer to and from moving fluids. We deal only with laminar convection, but this enables the reader to become involved in the fundamentals of heat transfer with convection.

Third, we bring to the reader's attention more general forms of the equation of energy, leading to Tables 7.3-7.5 which may be used in a manner similar to the general momentum equations given in Chapter 2.

7.1 HEAT TRANSFER WITH FORCED CONVECTION IN A TUBE

Consider laminar flow in a circular tube of radius R , as depicted in Fig. 7.1. If the tube and the fluid exchange heat, then clearly the fluid's temperature is a function of both the r - and z -directions. A suitable unit volume is a ring-shaped element, Δr thick and Δz high. Energy enters and leaves this ring by thermal conduction; also, a unit mass of fluid, which enters with an enthalpy, must leave with a different enthalpy. Let us now develop the energy balance for the unit volume.

Rate of energy in by conduction across surface at r	$2\pi r \Delta z q_r _r$
Rate of energy out by conduction across surface at $r + \Delta r$	$2\pi(r + \Delta r)\Delta z q_r _{r + \Delta r}$
Rate of energy in by conduction across surface at z	$2\pi r \Delta r q_z _z$

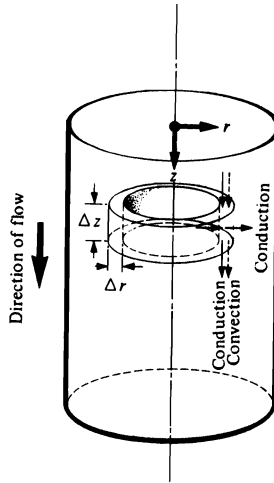


Fig 7.1 Elemental circular ring used to develop the differential energy balance for laminar tube flow.

Energy out by conduction across surface at $z + \Delta z$	$2\pi r \Delta r q_z _{z + \Delta z}$
Energy in due to fluid flow (enthalpy) across surface at z	$\rho v_z 2\pi r \Delta r H _z$
Energy out due to fluid flow across surface at $z + \Delta z$	$\rho v_z 2\pi r \Delta r H _{z + \Delta z}$

Here H is the enthalpy per unit mass, and v_z is the velocity in the z -direction. At steady state, the energy balance requires equal inputs and outputs. If we divide all terms by $2\pi \Delta r \Delta z$, we obtain

$$\frac{r q_r|_{r + \Delta r} - r q_r|_r}{\Delta r} + r \frac{q_z|_{z + \Delta z} - q_z|_z}{\Delta z} + r \rho v_z \frac{H|_{z + \Delta z} - H|_z}{\Delta z} = 0. \quad (7.1)$$

Now Δr and Δz are allowed to approach zero.

$$\frac{\partial(r q_r)}{\partial r} + r \frac{\partial q_z}{\partial z} + r \rho v_z \frac{\partial H}{\partial z} = 0. \quad (7.2)$$

If C_p is the heat capacity, then

$$\frac{\partial H}{\partial z} = C_p \frac{\partial T}{\partial z}. \quad (7.3)$$

Also

$$q_r = -k(\partial T/\partial r) \quad \text{and} \quad q_z = -k(\partial T/\partial z). \quad (7.4a, b)$$

Substituting Eqs. (7.3) and (7.4) into Eq. (7.2) yields an energy equation written in terms of temperature:

$$v_z \frac{\partial T}{\partial z} = \frac{k}{\rho C_p} \left[\frac{1}{r} \frac{\partial}{\partial r} \left[r \frac{\partial T}{\partial r} \right] + \frac{\partial^2 T}{\partial z^2} \right]. \quad (7.5)$$

We can further simplify the energy balance (Eq. (7.5)), since, except for the very slow flow of liquid metals, the term $(k/\rho C_p)\partial^2 T/\partial z^2$ is negligible even though $v_z(\partial T/\partial z)$ is not. With this assumption, Eq. (7.5) reduces to

$$v_z \frac{\partial T}{\partial z} = \frac{k}{\rho C_p} \left[\frac{1}{r} \frac{\partial}{\partial r} \left[r \frac{\partial T}{\partial r} \right] \right]. \quad (7.6)$$

Equation (7.6) contains v_z , the factor that ties together heat transfer and convection. Here we consider fully developed laminar flow; the velocity distribution is therefore parabolic, and is given by Eqs. (2.31) and (2.33):

$$v_z = 2\bar{V}_z \left[1 - \left(\frac{r}{R} \right)^2 \right].$$

By including this velocity distribution, Eq. (7.6) becomes

$$2\bar{V}_z \left[1 - \left(\frac{r}{R} \right)^2 \right] \frac{\partial T}{\partial z} = \frac{k}{\rho C_p} \left[\frac{1}{r} \frac{\partial}{\partial r} \left[r \frac{\partial T}{\partial r} \right] \right]. \quad (7.7)$$

We consider the special case where a *fully developed temperature profile* exists. For any set of boundary conditions, a fully developed temperature profile exists when $(T_R - T)/(T_R - T_m)$ is a unique function of r/R , *independent of z* . Then

$$\frac{T_R - T}{T_R - T_m} = f(r/R), \quad (7.8)$$

or

$$\frac{\partial}{\partial z} \left(\frac{T_R - T}{T_R - T_m} \right) = 0, \quad (7.9)$$

where T_R = temperature of fluid at the wall, and T_m = mean temperature of the fluid. A fully developed temperature profile is analogous to fully developed flow. This is exemplified by Fig. 7.2, where the liquid flowing in the z -direction encounters the heated section of the tube. Over a finite interval downstream from this point, the temperature profile changes from uniform to fully developed.

For a fully developed temperature profile, an important corollary arises; namely, the heat transfer coefficient is uniform along the pipe. We realize this by employing the definition of the heat transfer coefficient based on the mean temperature of the fluid:

$$h \equiv \frac{q_R}{T_R - T_m} = -\frac{k}{R} \frac{\partial}{\partial(r/R)} \left(\frac{T_R - T}{T_R - T_m} \right)_{r=R}, \quad (7.10)$$

where q_R is the flux evaluated at the wall ($r = R$). Because the derivative in Eq. (7.10) has a unique value at the wall, independent of z , h is therefore uniform along the pipe under the fully developed temperature conditions.

Now consider the case where q_R is uniform. This represents a uniform heat flux at the wall, and could be physically obtained by using an electric heater, depicted in Fig. 7.2. Further, since h and q_R are constant, Eq. (7.10) specifies that $T_R - T_m$ is constant, and

$$\frac{\partial T_R}{\partial z} = \frac{\partial T_m}{\partial z}. \quad (7.11)$$

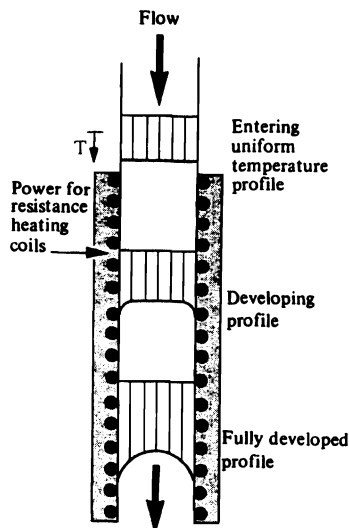


Fig. 7.2 Heating a fluid in a tube showing the development of the temperature profile.

(Note that T_R and T_m themselves are not constants.) Now expand Eq. (7.9) in a general sense where each quantity varies as follows:

$$\left[\frac{\partial T_R}{\partial z} - \frac{\partial T}{\partial z} \right] - \left[\frac{T_R - T}{T_R - T_m} \right] \left[\frac{\partial T_R}{\partial z} - \frac{\partial T_m}{\partial z} \right] = 0. \quad (7.12)$$

Then Eq. (7.11) shows that

$$\frac{\partial T_R}{\partial z} = \frac{\partial T}{\partial z} = \frac{\partial T_m}{\partial z}. \quad (7.13)$$

Equation (7.13) is important because it allows Eq. (7.7) to be integrated directly using $\partial T/\partial z = \partial T_m/\partial z$:

$$2\bar{V}_z \left[\frac{\partial T_m}{\partial z} \right] \int_{r=0}^r r \left[1 - \left(\frac{r}{R} \right)^2 \right] dr = \frac{k}{\rho C_p} \int_{\partial T/\partial r = 0}^{\partial T/\partial r} d \left[r \frac{\partial T}{\partial r} \right]. \quad (7.14)$$

Integrating, we get

$$2\bar{V}_z \left[\frac{\partial T_m}{\partial z} \right] \frac{r}{2} \left[1 - \frac{1}{2} \left(\frac{r}{R} \right)^2 \right] = \frac{k}{\rho C_p} \frac{\partial T}{\partial r}. \quad (7.15)$$

A second integration with $T = T_R$ at $r = R$ finally results in

$$T_R - T = \left[\frac{\bar{V}_z \rho C_p}{8R^2 k} \right] \left[\frac{\partial T_m}{\partial z} \right] (3R^4 - 4r^2 R^2 + r^4). \quad (7.16)$$

Having obtained the temperature profile, we can evaluate h . From Eq. (7.10), $(T_R - T_m)$ and q_R must then be evaluated. First, we find $(T_R - T_m)$ by performing the integration:

$$T_R - T_m = \frac{\int_0^R v_z(T_R - T)2\pi r dr}{\int_0^R v_z 2\pi r dr} \quad (7.17)$$

Second, we determine q_R by evaluating the gradient at the wall using Eq. (7.16):

$$q_R = -k \left(\frac{\partial T}{\partial r} \right)_{r=R} \quad (7.18)$$

When these operations have been carried out, we can determine the heat transfer coefficient. The final result, with D as the diameter, is

$$\frac{hD}{k} = 4.36. \quad (7.19)$$

The dimensionless number resulting from this analysis is the *Nusselt number*. This important dimensionless number for heat flow with *forced* convection reappears as we examine other solutions and correlations. For emphasis, then, the Nusselt number is

$$\text{Nu}_\infty \equiv \frac{hD}{k} \quad (7.20)$$

This Nusselt number is for fully developed flow and uniform heat flux with parabolic velocity profile. It is subscripted with ∞ because it represents the limiting case of a fully developed temperature profile. Many situations have been analyzed, some of which are given in Table 7.1 and others in Holman.¹

Table 7.1 Nusselt numbers for fully developed laminar flow*

Geometry	Velocity distribution [†]	Condition at wall	$\text{Nu}_\infty = \frac{hD_e}{k}$
Circular tube	Parabolic	Uniform q_R	4.36
Circular tube	Parabolic	Uniform T_R	3.66
Circular tube	Slug flow	Uniform q_R	8.00
Circular tube	Slug flow	Uniform T_R	5.75
Parallel plates	Parabolic	Uniform q_R	8.23
Parallel plates	Parabolic	Uniform T_R	7.60
Triangular duct	Parabolic	Uniform q_R	3.00
Triangular duct	Parabolic	Uniform T_R	2.35

*From W. M. Rohsenow and H. Y. Choi, *Heat, Mass and Momentum Transfer*, Prentice-Hall, Englewood Cliffs, New Jersey, 1961, page 141.

[†]Slug flow refers to a flat velocity profile.

[‡] D_e is the equivalent diameter, as defined in Chapter 3.

¹J. P. Holman, *Heat Transfer*, sixth edition, McGraw-Hill, New York, N.Y., 1986, page 281.

7.2 HEAT TRANSFER WITH LAMINAR FORCED CONVECTION OVER A FLAT PLATE

In Chapter 2, the velocity distribution, within the boundary layer over a flat plate, was determined. Here we consider the case of a plate at a different temperature than the fluid, with the plate serving to heat or cool the fluid. Just as a velocity profile continually changes with distance from the leading edge, and results in a *momentum boundary layer* which increases in thickness, there is also a changing temperature profile and development of a *thermal boundary layer* when heat transfer is involved. We depict this situation along with a unit element in Fig. 7.3. With a depth of unity perpendicular to the page, the contributions to the energy balance are:

Energy in by conduction across surface at x	$q_x _x \Delta y \cdot 1$
Energy out by conduction across surface at $x + \Delta x$	$q_x _{x + \Delta x} \Delta y \cdot 1$
Energy in by conduction across surface at y	$q_y _y \Delta x \cdot 1$
Energy out by conduction across surface at $y + \Delta y$	$q_y _{y + \Delta y} \Delta x \cdot 1$
Energy in due to fluid flow (sensible heat) across surface at x	$\rho v_x \Delta y \cdot 1 \cdot H _x$
Energy out due to fluid flow (sensible heat) across surface at $x + \Delta x$	$\rho v_x \Delta y \cdot 1 \cdot H _{x + \Delta x}$
Energy in due to fluid flow (sensible heat) across surface at y	$\rho v_y \Delta x \cdot 1 \cdot H _y$
Energy out due to fluid flow (sensible heat) across surface at $y + \Delta y$	$\rho v_y \Delta x \cdot 1 \cdot H _{y + \Delta y}$

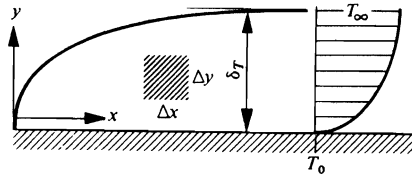


Fig. 7.3 Development of the thermal boundary layer and the temperature distribution over a flat plate.

Adding all these quantities, dividing through by $\Delta x \Delta y$, and taking the limits as $\Delta x \rightarrow 0$ and $\Delta y \rightarrow 0$, we obtain

$$\frac{\partial q_x}{\partial x} + \frac{\partial q_y}{\partial y} + \frac{\partial(\rho v_x H)}{\partial x} + \frac{\partial(\rho v_y H)}{\partial y} = 0. \quad (7.21)$$

For constant density and conductivity, Eq. (7.21) becomes

$$\rho H \left[\frac{\partial v_x}{\partial x} + \frac{\partial v_y}{\partial y} \right] + \rho \left[v_x \frac{\partial H}{\partial x} + v_y \frac{\partial H}{\partial y} \right] = k \left[\frac{\partial^2 T}{\partial x^2} + \frac{\partial^2 T}{\partial y^2} \right]. \quad (7.22)$$

Since continuity requires that $(\partial v_x / \partial x) + (\partial v_y / \partial y) = 0$ and $dH = C_p dT$, we finally obtain

$$\rho C_p \left[v_x \frac{\partial T}{\partial x} + v_y \frac{\partial T}{\partial y} \right] = k \left[\frac{\partial^2 T}{\partial x^2} + \frac{\partial^2 T}{\partial y^2} \right]. \quad (7.23)$$

The temperature gradient in the y -direction is much steeper than that in the x -direction; therefore the x -directed second derivative term may be neglected. Then Eq. (7.23) simplifies to

$$v_x \frac{\partial T}{\partial x} + v_y \frac{\partial T}{\partial y} = \alpha \frac{\partial^2 T}{\partial y^2}. \quad (7.24)$$

Here $\alpha = k/\rho C_p$, which is called the *thermal diffusivity*. It has the same units of kinematic viscosity, which is sometimes called *momentum diffusivity*. In addition, the momentum boundary layer equation, developed in Chapter 2, is

$$v_x \frac{\partial v_x}{\partial x} + v_y \frac{\partial v_x}{\partial y} = \nu \frac{\partial^2 v_x}{\partial y^2}. \quad (2.87)$$

Equations (7.24) and (2.87) are analogous. If $\nu = \alpha$, and if the velocity and thermal boundary conditions are similar, then the temperature and velocity profiles are exactly identical, and the thermal boundary layer δ_T equals the momentum boundary layer δ .

The method of solution for Eq. (7.24) parallels that for the velocity distribution, as given in Section 2.7.1. For the case of a uniform-temperature plate, the following boundary conditions apply

$$\text{B.C.1} \quad \text{at } y = 0, \quad T = T_0;$$

$$\text{B.C.2} \quad \text{at } y = \infty, \quad T = T_\infty;$$

$$\text{B.C.3} \quad \text{at } x \leq 0, \quad T = T_\infty.$$

We do not present the method of solution here, but Fig. 7.4 gives the temperature T as a function of y and x . The temperature is a part of the dimensionless temperature Θ on the ordinate, which includes the wall temperature T_0 and the bulk fluid temperature T_∞ . Space dimensions x and y appear together on the abscissa in exactly the same way, as shown in Fig. 2.7 for describing the velocity profiles. Several curves are shown in Fig. 7.4, each for a different value of the *Prandtl number*, Pr . This number is the ratio of ν/α , and for Pr equal to unity, the Θ curve in Fig. 7.4 is exactly the same as v_x/V_∞ in Fig. 2.7. Therefore, the Prandtl number controls the similarity between the velocity profiles and the temperature profiles.

Knowing the temperature profile, we can determine the heat-transfer coefficient. From the results given in Fig. 7.4, the *local* heat transfer coefficient is

$$h_x = \frac{-k \left[\frac{\partial T}{\partial y} \right]_{y=0}}{T_0 - T_\infty} = 0.332k \text{Pr}^{0.343} \left[\frac{V_\infty}{\nu x} \right]^{1/2}, \quad \text{Pr} \geq 0.6, \quad (7.25)$$

or, in terms of dimensionless numbers,

$$\text{Nu}_x = 0.332 \text{Pr}^{0.343} \text{Re}_x^{0.5}, \quad (7.26)$$

where $\text{Nu}_x \equiv h_x x/k$, which is called the *local* Nusselt number. If we wish to know the *average* heat-transfer coefficient, then we can find it by averaging h_x from $x = 0$ to $x = L$:

$$h = \frac{1}{L} \int_0^L h_x dx = 0.664k \text{Pr}^{0.343} \left[\frac{V_\infty}{\nu L} \right]^{1/2},$$

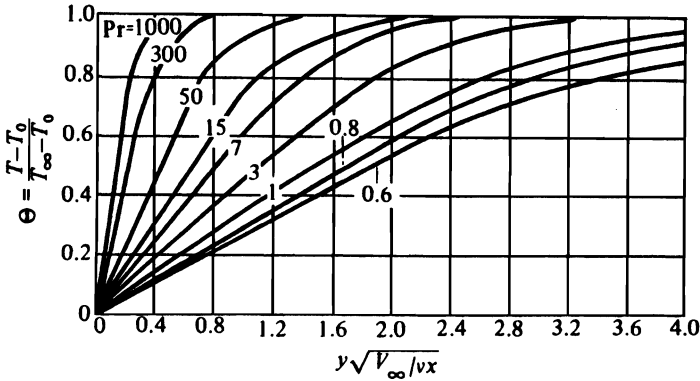


Fig. 7.4 Dimensionless temperature profiles in the laminar boundary layer over a flat plate for various Pr. (From E. Z. Pohlhausen, *Z. Angew. Math. Mech.* 1, 115 (1921).)

or

$$Nu_L = 0.664 Pr^{0.343} Re_L^{0.5} \tag{7.27}$$

Note the general form of either Eq. (7.26) or (7.27). We shall find in Chapter 8 that the Nusselt number is generally a function of the Reynolds and Prandtl numbers in problems of forced convection.

For the case of $Pr = 1$ ($\nu = \alpha$), the thermal boundary layer is given by

$$\frac{\delta_T}{x} = \frac{5.0}{\sqrt{V_\infty x / \nu}} \tag{7.28}$$

which is the same as the momentum boundary layer.

At this point it is instructive to examine Prandtl numbers for various fluids; approximate values are given in Table 7.2. These numbers represent values that include several substances, and cover substantial temperature ranges. The Prandtl numbers of liquids vary significantly with temperature; however, gases show almost no variation in Pr with temperature. From Table 7.2, we see that for gases $\delta_T \cong \delta$, for common liquids $\delta_T < \delta$, and for liquid metals—due to their high thermal conductivity— $\delta_T \gg \delta$. To a close approximation, the ratio of the boundary layer thicknesses is

$$\frac{\delta_T}{\delta} = 0.975 Pr^{-1/3}, \quad Pr > 0.5. \tag{7.29}$$

Table 7.2. Typical Prandtl numbers

Substance	Range of Prandtl number (ν/α)
Common liquids (water, alcohol, etc.)	2-50
Liquid metals	0.001-0.03
Gases	0.7-1.0

Equations (7.27)-(7.29) are valid only for $Pr > 0.5$, and thus do not apply to liquid metals. For liquid metals with uniform wall temperatures as a boundary condition, the results are approximated by²

$$Nu_x = \sqrt{Re_x Pr} \left[\frac{0.564}{1 + 0.90 \sqrt{Pr}} \right]. \quad (7.30)$$

For a uniform heat flux at the wall, we present these results.³

$$Pr > 0.5, \quad Nu_x = 0.458 Pr^{0.343} \sqrt{Re_x}; \quad (7.31)$$

$$0.006 \leq Pr \leq 0.03, \quad Nu_x = \sqrt{Re_x Pr} \left[\frac{0.880}{1 + 1.317 \sqrt{Pr}} \right]. \quad (7.32)$$

Example 7.1 Air at 1 atm ($1.013 \times 10^5 \text{ N m}^{-2}$) and 290 K flows parallel to a plate's surface at 15 m s^{-1} . The plate, 0.3 m long, is at 360 K. Assume that laminar flow is stable along the entire length.

- Calculate the thicknesses of the velocity and thermal boundary layers 0.15 m from the leading edge of the plate.
- Calculate the rate of heat transfer from the entire plate per 0.1 m of plate width.

Solution.

- We calculate the thickness of the momentum boundary layer using Eq. (2.101),

$$\frac{\delta}{x} = \frac{5.0}{\sqrt{V_\infty x / \nu}}.$$

For air, evaluating ν at an average boundary-layer temperature of $\frac{1}{2}(290 + 360) = 325 \text{ K}$, the kinematic viscosity is $18.4 \times 10^{-6} \text{ m}^2 \text{ s}^{-1}$. Then,

$$\frac{V_\infty x}{\nu} = \frac{15 \text{ m}}{\text{s}} \left| \frac{0.15 \text{ m}}{\text{s}} \right| \frac{\text{s}}{18.4 \times 10^{-6} \text{ m}^2} = 1.22 \times 10^5,$$

and

$$\delta = \frac{(0.15)(5.0)}{\sqrt{1.22 \times 10^5}} = 2.15 \times 10^{-3} \text{ m} = 2.15 \text{ mm}.$$

Next, we use Eq. (7.29)

$$\frac{\delta_T}{\delta} = 0.975 Pr^{-1/3}.$$

²E. M. Sparrow and J. L. Gregg, *J. Aero. Sc.* **24**, 852 (1957).

³R. J. Nickerson and H. P. Smith, as reported in Rohsenow and Choi, *ibid.*, page 149.

228 Heat Transfer and the Energy Equation

The Prandtl number for air, evaluated at 325 K, is 0.703. Then

$$\delta_T = (2.15)(0.975)(0.703)^{-1/3} = 2.36 \text{ mm}.$$

b) Equation (7.27) is used for the average heat-transfer coefficient, which applies to the whole plate.

$$\text{Nu}_L = (0.664)(0.703^{0.343}) \sqrt{2.44 \times 10^5} = 291.$$

The thermal conductivity for air at 325 K is $28.1 \times 10^{-3} \text{ W m}^{-1} \text{ K}^{-1}$. Then

$$h = \frac{k}{L} \text{Nu}_L = \frac{(28.1 \times 10^{-3})(291)}{(0.3)} = 27.2 \text{ W m}^{-2} \text{ K}^{-1},$$

and finally

$$Q = hA(T_\infty - T) = (27.2)(0.3 \times 0.1)(360 - 290) = 57.1 \text{ W}.$$

7.3 HEAT TRANSFER WITH NATURAL CONVECTION

In Sections 7.1 and 7.2 we considered heat transfer with forced convection. In forced convection, the known velocity distribution can be entered into the energy equation. The situation is more complex in problems of heat transfer with natural convection because the velocities are not known *a priori* to solving the energy equation. Hence, the velocity and temperature distributions cannot be treated as separate problems; the temperature distribution, in effect, produces the velocity distribution by causing density differences within the fluid.

Consider the vertical surface in Fig. 7.5; the surface is at T_0 , and it heats the neighboring fluid whose bulk temperature is T_∞ . In this situation, the velocity component v_y is quite small; the fluid moves almost entirely upward, and therefore we write the momentum equation for the x -component only. For steady forced convection over a flat plate, we ignored the gravity force, and no pressure gradient was involved. We cannot ignore these forces in free convection, and therefore the momentum equation for the present case contains these terms

$$v_x \frac{\partial v_x}{\partial x} + v_y \frac{\partial v_x}{\partial y} = -\frac{1}{\rho} \frac{\partial P}{\partial x} + \nu \frac{\partial^2 v_x}{\partial y^2} + g_x. \quad (7.33)$$

We apply the so-called *Boussinesq approximation* in which variations in the density of the fluid are neglected except in the buoyancy force term that drives the natural convection. Thus, in Eq. (7.33) the density is a reference density at the reference temperature, T_∞ . Therefore, the inertial terms become

$$\rho_\infty \left[v_x \frac{\partial v_x}{\partial x} + v_y \frac{\partial v_x}{\partial y} \right],$$

and the pressure gradient is approximated as

$$\frac{\partial P}{\partial x} \approx \frac{dP}{dx} = -\rho_\infty g.$$

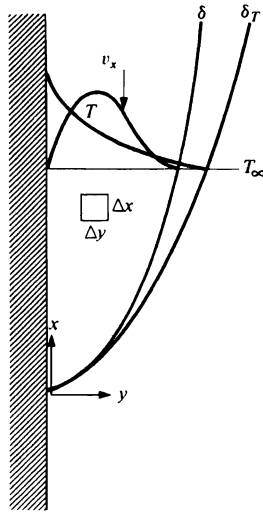


Fig. 7.5 Thermal and momentum boundary layers for vertical plate natural convection.

With $g_x = -g$, the buoyancy term is simply

$$\rho g_x = -\rho_\infty g \left[1 + \beta(T_\infty - T) \right],$$

where the volume expansion coefficient β is defined as

$$\beta = -\frac{1}{\rho} \left[\frac{\partial \rho}{\partial T} \right]_p.$$

The momentum balance in the x -direction then becomes

$$v_x \frac{\partial v_x}{\partial x} + v_y \frac{\partial v_x}{\partial y} = \nu \frac{\partial^2 v_x}{\partial y^2} + g\beta(T - T_\infty), \quad (7.34)$$

which is identical with Eq. (2.87), except for the addition of the buoyancy term. Equation (7.34) shows that the momentum equation must be coupled to an appropriate energy equation, in order to treat the buoyancy term.

The energy equation applied to the control volume $\Delta x \Delta y$ in this case is identical to that for flow over a flat plate:

$$v_x \frac{\partial T}{\partial x} + v_y \frac{\partial T}{\partial y} = \alpha \frac{\partial^2 T}{\partial y^2}. \quad (7.35)$$

This equation is coupled to Eq. (7.34) by the presence of the velocity terms. The mathematical task at hand is, therefore, to solve the coupled equations with the boundary conditions:

$$\text{B.C.1} \quad \text{at } y = 0, \quad v_x = v_y = 0, \quad T = T_0;$$

$$\text{B.C.2} \quad \text{at } y = \infty, \quad v_x = v_y = 0, \quad T = T_\infty.$$

230 Heat Transfer and the Energy Equation

Analytical solutions of such coupled differential equations are beyond the scope of this text; we simply present the results. First, however, let us examine a dimensional analysis approach in order to bring forth pertinent dimensionless numbers.

The problem is to determine the conditions for which the velocity profile in a natural convection situation is similar to the velocity profile in another natural convection situation. Both systems have the same boundary conditions, i.e., velocity is zero at the surface and within the bulk fluid removed from the surface. Now employ the dynamic similarity argument introduced in Section 3.1.1.

First, Eq. (7.34) is written for system 1:

$$v_{x1} \frac{\partial v_{x1}}{\partial x_1} + v_{y1} \frac{\partial v_{x1}}{\partial y_1} = \nu_1 \frac{\partial^2 v_{x1}}{\partial y_1^2} + g_1 \beta_1 (T - T_\infty)_1. \quad (7.36)$$

System 2 is related to system 1 by geometrical and dynamic similarities expressed by the ratios:

$$\begin{aligned} K_L &\equiv \frac{x_1}{x_2} = \frac{y_1}{y_2} = \frac{L_1}{L_2} & K_v &= \frac{\nu_1}{\nu_2} \\ K_v &\equiv \frac{v_{x1}}{v_{x2}} = \frac{v_{y1}}{v_{y2}} = \frac{v_1}{v_2} & K_g &= \frac{g_1}{g_2} \\ K_\beta &\equiv \frac{\beta_1}{\beta_2} & K_T &= \frac{(T - T_\infty)_1}{(T - T_\infty)_2} = \frac{(T_0 - T_\infty)_1}{(T_0 - T_\infty)_2}. \end{aligned} \quad (7.37)$$

Now, we replace v_{x1} , x_1 , ν_1 , v_{y1} , g_1 , etc. in Eq. (7.36) by their equivalents in Eq. (7.37); then we write Eq. (7.34) for system 2:

$$\frac{K_v^2}{K_L} v_{x2} \frac{\partial v_{x2}}{\partial x_2} + \frac{K_v^2}{K_L} v_{y2} \frac{\partial v_{x2}}{\partial y_2} = \frac{K_v K_v}{K_L^2} \nu_2 \frac{\partial^2 v_{x2}}{\partial y_2^2} + K_g K_\beta K_T g_2 \beta_2 (T - T_\infty)_2. \quad (7.38)$$

Equation (7.38) if rewritten without all the K s would of course be valid, because it would transform back to Eq. (7.34). Hence,

$$\frac{K_v^2}{K_L} = \frac{K_v K_v}{K_L^2} = K_g K_\beta K_T = 1, \quad (7.39)$$

and therefore

$$\frac{v_1^2}{L_1} = \frac{v_2^2}{L_2}, \quad \frac{v_1 v_1}{L_1^2} = \frac{v_2 v_2}{L_2^2}.$$

Thus,

(7.40a,b,c)

$$g_1 \beta_1 (T_0 - T_\infty)_1 = g_2 \beta_2 (T_0 - T_\infty)_2.$$

If we combine Eqs. (7.40a) and (7.40b) we get

$$\frac{v_1 L_1}{\nu_1} = \frac{v_2 L_2}{\nu_2}, \quad (7.41)$$

which are Reynolds numbers. The combination of Eqs. (7.40b) and (7.40c), yields

$$\frac{g_1 \beta_1 (T_0 - T_\infty)_1 L_1^2}{v_1 v_2} = \frac{g_2 \beta_2 (T_0 - T_\infty)_2 L_2^2}{v_2 v_2}. \quad (7.42)$$

The group of variables represented in Eq. (7.42) could be considered a dimensionless number, but by reflecting on the physical aspects, we realize that the velocity of the fluid is not an independent quantity, but that it rather depends on the buoyant force. Hence, the v 's are eliminated from Eq. (7.42), and substituting their equivalents from Eq. (7.41), we obtain

$$\frac{g_1 \beta_1 (T_0 - T_\infty)_1 L_1^3}{v_1^2} = \frac{g_2 \beta_2 (T_0 - T_\infty)_2 L_2^3}{v_2^2}. \quad (7.43)$$

This dimensionless number is important in natural convection problems and is called the *Grashof number*, Gr. When buoyancy is the only driving force for convection, the velocity profile is determined entirely by the quantities in the Grashof number, and the Reynolds number is superfluous.

Recall that for forced convection, as discussed in Section 7.2, the Nusselt number is correlated in the general form

$$\text{Nu} = f(\text{Pr}, \text{Re}), \quad \text{forced convection.}$$

Correspondingly then, for natural convection, the Nusselt number is correlated as

$$\text{Nu} = f(\text{Pr}, \text{Gr}), \quad \text{natural convection.}$$

Returning to the complete solution of Eqs. (7.34), (7.35) and the appropriate boundary conditions, we present the velocity and temperature distributions (see Fig. 7.6). The curves show that for $\text{Pr} \leq 1$, $\delta_T \cong \delta$, but for $\text{Pr} > 1$, $\delta_T < \delta$. For liquid metals, therefore, δ_T is about equal to δ in free convection as contrasted to forced convection in which $\delta_T \gg \delta$. Corresponding to the temperature profile, shown in Fig. 7.6b, the local Nusselt number is

$$\frac{\text{Nu}_x}{\sqrt[4]{\text{Gr}_x/4}} = \frac{0.676 \text{Pr}^{1/2}}{(0.861 + \text{Pr})^{1/4}}. \quad (7.44)$$

Equation (7.44) applies for a wide range of Pr numbers ($0.00835 \leq \text{Pr} \leq 1000$) for laminar flow conditions, with $10^8 < \text{Gr}_x \cdot \text{Pr} < 10^{10}$.

Example 7.2 Calculate the initial heat transfer rate from a plate at 360 K, 0.3 m long \times 0.1 m wide hung vertically in air at 290 K. Contrast the results with those of Example 7.1.

Solution. Equation (7.44) should be integrated to obtain the average heat transfer coefficient which can be applied to the whole plate.

In Eq. (7.44), because h_x varies as $x^{-1/4}$, then the average h equals $\frac{4}{3}h_x$. Hence Nu_L defined as hL/k is

$$\frac{\text{Nu}_L}{\sqrt[4]{\text{Gr}_L/4}} = \frac{0.902 \text{Pr}^{1/2}}{(0.861 + \text{Pr})^{1/4}}. \quad (7.45)$$

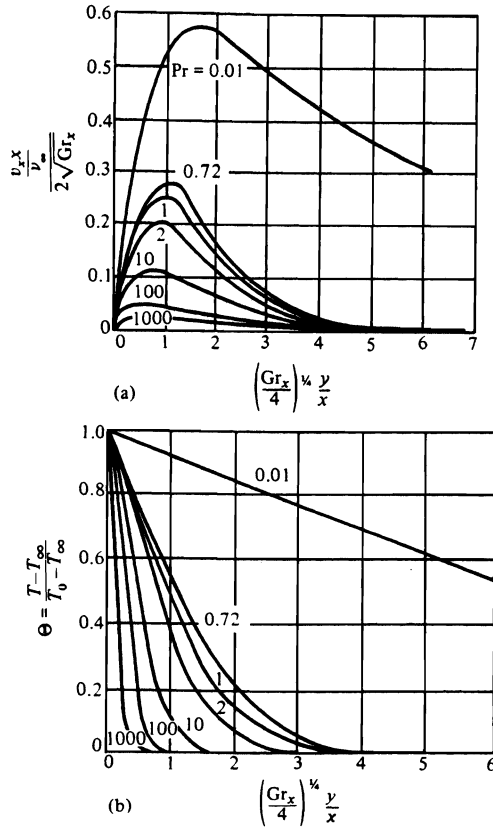


Fig. 7.6 Laminar natural convection for a vertical plate. (a) Dimensionless velocity profiles. (b) Dimensionless temperature profiles. (Calculated by S. Ostrach, *Nat. Advisory Comm. Aeronaut. Tech. Note 2635*, Feb. 1952, as presented in W. M. Rohsenow and H. Y. Choi, *Heat, Mass, and Momentum Transfer*, Prentice-Hall, Englewood Cliffs, New Jersey, 1961, pages 155-159.)

or

$$Nu_L = 0.902 \sqrt[4]{\frac{Gr_L \cdot Pr^2}{4(0.861 + Pr)}} \quad (7.45a)$$

We evaluate the properties at the average boundary temperature of 325 K. For air at 325 K

$$Pr = 0.703 \quad \text{and} \quad g\beta/v^2 = 9.85 \times 10^7 \text{ K}^{-1} \text{ m}^{-3}.$$

The Grashof number is

$$Gr_L = \frac{g\beta}{v^2} (T_0 - T_\infty)L^3 = (9.85 \times 10^7)(360 - 290)(0.3^3) = 1.86 \times 10^8.$$

Next, we calculate the product $Gr_L \cdot Pr$ to test for laminar flow conditions

$$Gr_L \cdot Pr = (1.86 \times 10^8)(0.703) = 1.31 \times 10^8.$$

Since it is between 10^4 and 10^{10} , Eq. (7.45a) is valid. When we substitute values of Gr_L and Pr into Eq. (7.45a),

$$Nu_L = 55.8,$$

from which,

$$h = Nu_L \frac{k}{L} = (55.8) \left[\frac{28.1 \times 10^{-3}}{0.3} \right] = 5.23 \text{ W m}^{-2} \text{ K}^{-1}.$$

Finally, we evaluate the rate of heat transfer Q .

$$Q = h(T_\infty - T_0)A = (5.23)(360 - 290)(0.1 \times 0.3) = 11.0 \text{ W}.$$

For Example 7.1, Q was 57.1 W; that is, the rate of heat transfer for forced convection is considerably higher. This is the usual case.

It is instructive to look at special forms of Eq. (7.45a). First, if $Pr = 0.7$, then it reduces to

$$Nu_L = 0.477 Gr_L^{1/4}. \quad (7.45b)$$

It so happens that for many gases, including air, O_2 , CO , He (and other inert gases), H_2 and CO_2 , Pr is very close to 0.7 and practically constant for temperatures even as high as 1900 K. Thus, we can apply Eq. (7.45b) directly to gases.

Second, if $Pr \rightarrow 0$ (liquid metals), then Eq. (7.59a) reduces to

$$Nu_L = 0.936 \sqrt[4]{\frac{Gr_L \cdot Pr^2}{4}}. \quad (7.45c)$$

7.4 HEAT CONDUCTION

We consider heat conduction through the wall of a hollow solid cylinder. Figure 7.7 depicts the situation, and also locates a suitable unit volume with a thickness Δr . From a practical point of view, we may visualize a long cylindrical shaped furnace, and it is desirable to calculate the heat loss to the surroundings. Suppose the cylinder is long enough so that end effects are negligible; in addition, the system is at steady state, so that both the inside and outside surfaces of the wall are at some fixed temperatures, T_1 and T_2 , respectively. For such a system, we develop the energy equation.

$$\text{Rate of energy in by conduction across surface at } r \quad 2\pi r l q_r|_r$$

$$\text{Rate of energy out by conduction across surface at } r + \Delta r \quad 2\pi r l q_r|_{r + \Delta r}$$

At steady state, these are the only terms that contribute to the energy balance. Thus

$$2\pi r l q_r|_{r + \Delta r} - 2\pi r l q_r|_r = 0.$$

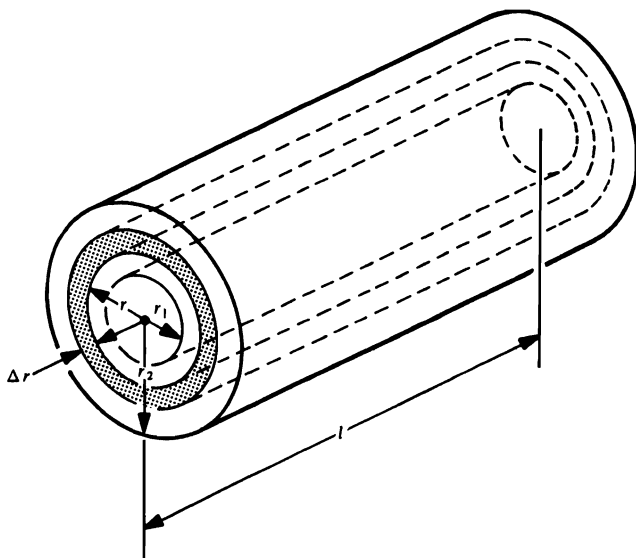


Fig. 7.7 Heat conduction through a solid cylindrical wall. The shaded area depicts the unit volume.

If we divide all terms by $2\pi l\Delta r$, and take the limit as Δr approaches zero, we obtain

$$\frac{d(rq_r)}{dr} = 0. \quad (7.46)$$

Equation (7.46) requires that

$$rq_r = C_1. \quad (7.47)$$

Note that q_r , the heat flux, is not constant in itself. Since $q_r = -k(dT/dr)$, Eq. (7.47) yields

$$-k \frac{dT}{dr} = \frac{C_1}{r}. \quad (7.48)$$

Integrating once again, we find for constant thermal conductivity that

$$T = -\frac{C_1}{k} \ln r - \frac{C_2}{k}. \quad (7.49)$$

By absorbing k in new constants, Eq. (7.49) simplifies even more to

$$T = C_3 \ln r + C_4. \quad (7.50)$$

The boundary conditions under consideration are

$$\text{B.C.1} \quad \text{at } r = r_1, \quad T = T_1;$$

$$\text{B.C.2} \quad \text{at } r = r_2, \quad T = T_2.$$

Determination of the constants using the boundary conditions yields the temperature distribution

$$\frac{T - T_2}{T_1 - T_2} = \frac{\ln(r/r_2)}{\ln(r_1/r_2)}, \quad (7.51)$$

and the heat flux

$$q_r = -k \frac{dT}{dr} = \frac{k}{r} \left[\frac{T_1 - T_2}{\ln(r_1/r_2)} \right]. \quad (7.52)$$

As the heat flows through the wall, it encounters larger areas, so that the flux itself decreases. The heat flow Q , however, is constant (as it must be for steady state), and is given by

$$Q = q_r(2\pi rL) = \frac{2\pi kL}{\ln(r_1/r_2)} (T_1 - T_2). \quad (7.53)$$

This problem, elementary as it is, demonstrates an interesting engineering characteristic. Suppose we use the cylindrical wall as the insulation of a furnace wall. As increasing thicknesses of insulation are added, the outside layer, because of its greater area, offers less resistance to heat flow than an inner layer of the same thickness. Thus, from a cost point of view, the expense of additional insulation can become greater than the savings associated with reduction in heat losses.

Example 7.3 As part of a proposed continuous annealing process, a rod passes through a cylindrical furnace chamber 101 mm inside diameter and 15.2 m long. The inside surface temperature of the furnace wall under operating conditions is predicted to be about 920 K and the outside surface about 310 K. If it is decided that a heat loss of 73 kW is an acceptable figure, then which of the following insulations would you use?

	$k, \text{ W m}^{-1} \text{ K}^{-1}$	Cost, \$ per m^3
Insulation A	0.70	350
Insulation B	0.35	880

Solution. Equation (7.53) can be written

$$\ln \left[\frac{r_2}{r_1} \right] = \frac{2\pi kL}{Q} (T_1 - T_2).$$

For A, then

$$\ln \left[\frac{r_2}{r_1} \right] = \frac{(2\pi)(0.70)(15.2)(920 - 310)}{(73 \times 10^3)} = 0.559,$$

so that with $r_1 = 50.5$ mm, we have $r_2 = 88.3$ mm. Similarly for B, using the ratio of conductivities, we get

$$\ln \left[\frac{r_2}{r_1} \right] = \left[\frac{0.35}{0.70} \right] (0.559) = 0.280.$$

236 Heat Transfer and the Energy Equation

so that $r_2 = 66.8$ mm. We calculate the volume of insulation and the corresponding cost.

$$\text{Cost } A = \frac{\pi(88.3^2 - 50.5^2) \text{ mm}^2}{1000^2 \text{ mm}^2} \left| \frac{1 \text{ m}^2}{\text{m}^2} \right| \frac{15.2 \text{ m}}{\text{m}^3} \left| \frac{350 \$}{\text{m}^3} \right| = \$87.69.$$

In the same manner, $\text{Cost } B = \$80.34$. The obvious choice is B .

7.5 THE GENERAL ENERGY EQUATION

In Sections 7.1-7.4, we determined temperature distributions and heat fluxes for some simple systems, by developing pertinent energy balances in differential form. In this section we develop the general energy equation, which can be reduced to solve specific problems.

Consider the stationary unit volume $\Delta x \Delta y \Delta z$ in Figs. 2.4 and 2.5; we apply the law of conservation of energy to the fluid contained within this volume at any given time

$$\left[\begin{array}{c} \text{rate of accumulation} \\ \text{of internal and} \\ \text{kinetic energy} \end{array} \right] = \left[\begin{array}{c} \text{net rate of internal} \\ \text{and kinetic energies} \\ \text{in by convection} \end{array} \right] + \left[\begin{array}{c} \text{net rate of} \\ \text{heat in by} \\ \text{conduction} \end{array} \right] - \left[\begin{array}{c} \text{net rate of} \\ \text{work done} \\ \text{by fluid} \end{array} \right]. \quad (7.54)$$

This statement of the law of energy conservation is not completely general, because other forms of energy transport, e.g., radiation, and sources such as electrical Joule heating, are not included.

The rate of accumulation of internal and kinetic energy within the unit volume is simply

$$\Delta x \Delta y \Delta z \frac{\partial}{\partial t} \left(\rho U + \frac{1}{2} \rho v^2 \right), \quad (7.55)$$

where U is the internal energy per unit mass of fluid and v is the *magnitude* of the local fluid velocity.

The *net* rate of internal and kinetic energies in by convection is

$$\begin{aligned} & \Delta y \Delta z \left\{ v_x \left(\rho U + \frac{1}{2} \rho v^2 \right) \Big|_x - v_x \left(\rho U + \frac{1}{2} \rho v^2 \right) \Big|_{x + \Delta x} \right\} \\ & + \Delta x \Delta z \left\{ v_y \left(\rho U + \frac{1}{2} \rho v^2 \right) \Big|_y - v_y \left(\rho U + \frac{1}{2} \rho v^2 \right) \Big|_{y + \Delta y} \right\} \\ & + \Delta x \Delta y \left\{ v_z \left(\rho U + \frac{1}{2} \rho v^2 \right) \Big|_z - v_z \left(\rho U + \frac{1}{2} \rho v^2 \right) \Big|_{z + \Delta z} \right\}. \end{aligned} \quad (7.56)$$

In a similar manner, the net rate of energy in by conduction is

$$\Delta y \Delta z \{ q_x|_x - q_x|_{x + \Delta x} \} + \Delta x \Delta z \{ q_y|_y - q_y|_{y + \Delta y} \} + \Delta x \Delta y \{ q_z|_z - q_z|_{z + \Delta z} \}. \quad (7.57)$$

The work done by the fluid consists of work against gravity, work against pressure, and work against viscous forces. The rate of doing work against the three components of gravity is

$$-\rho \Delta x \Delta y \Delta z (v_x g_x + v_y g_y + v_z g_z). \quad (7.58)$$

The rate of doing work against the pressure at the six faces of the unit volume is

$$\begin{aligned} \Delta y \Delta z \left\{ (Pv_x)|_{x+\Delta x} - (Pv_x)|_x \right\} + \Delta x \Delta z \left\{ (Pv_y)|_{y+\Delta y} - (Pv_y)|_y \right\} \\ + \Delta x \Delta y \left\{ (Pv_z)|_{z+\Delta z} - (Pv_z)|_z \right\}. \end{aligned} \quad (7.59)$$

The rate of doing work against the x -directed viscous forces is

$$\begin{aligned} \Delta y \Delta z \left\{ \tau_{xx}v_x|_{x+\Delta x} - \tau_{xx}v_x|_x \right\} + \Delta x \Delta z \left\{ \tau_{yx}v_x|_{y+\Delta y} - \tau_{yx}v_x|_y \right\} \\ + \Delta x \Delta y \left\{ \tau_{zx}v_x|_{z+\Delta z} - \tau_{zx}v_x|_z \right\}. \end{aligned} \quad (7.60)$$

Similar expressions may be written for the work against the y - and z -directed viscous forces

$$\begin{aligned} \Delta y \Delta z \left\{ \tau_{xy}v_y|_{x+\Delta x} - \tau_{xy}v_y|_x \right\} + \Delta x \Delta z \left\{ \tau_{yy}v_y|_{y+\Delta y} - \tau_{yy}v_y|_y \right\} \\ + \Delta x \Delta y \left\{ \tau_{zy}v_y|_{z+\Delta z} - \tau_{zy}v_y|_z \right\}, \end{aligned} \quad (7.61)$$

and

$$\begin{aligned} \Delta y \Delta z \left\{ \tau_{xz}v_z|_{x+\Delta x} - \tau_{xz}v_z|_x \right\} + \Delta x \Delta z \left\{ \tau_{yz}v_z|_{y+\Delta y} - \tau_{yz}v_z|_y \right\} \\ + \Delta x \Delta y \left\{ \tau_{zz}v_z|_{z+\Delta z} - \tau_{zz}v_z|_z \right\}. \end{aligned} \quad (7.62)$$

Substituting all these expressions into Eq. (7.54), dividing by $\Delta x \Delta y \Delta z$, and taking the limit as Δx , Δy , and Δz approach zero, we obtain one form of the energy equation

$$\begin{aligned} \frac{\partial}{\partial t} \left(\rho U + \frac{1}{2} \rho v^2 \right) = - \left[\frac{\partial}{\partial x} v_x \left(\rho U + \frac{1}{2} \rho v^2 \right) + \frac{\partial}{\partial y} v_y \left(\rho U + \frac{1}{2} \rho v^2 \right) + \frac{\partial}{\partial z} v_z \left(\rho U + \frac{1}{2} \rho v^2 \right) \right] \\ - \left[\frac{\partial q_x}{\partial x} + \frac{\partial q_y}{\partial y} + \frac{\partial q_z}{\partial z} \right] + \rho (v_x g_x + v_y g_y + v_z g_z) \\ - \left[\frac{\partial}{\partial x} P v_x + \frac{\partial}{\partial y} P v_y + \frac{\partial}{\partial z} P v_z \right] \\ - \left[\frac{\partial}{\partial x} (\tau_{xx}v_x + \tau_{xy}v_y + \tau_{xz}v_z) + \frac{\partial}{\partial y} (\tau_{yx}v_x + \tau_{yy}v_y + \tau_{yz}v_z) \right. \\ \left. + \frac{\partial}{\partial z} (\tau_{zx}v_x + \tau_{zy}v_y + \tau_{zz}v_z) \right]. \end{aligned} \quad (7.63)$$

If all the terms involving $(\rho U + \frac{1}{2}\rho v^2)$ are expanded and combined, we can obtain

$$\rho \left[\frac{\partial}{\partial t} \left(U + \frac{1}{2}v^2 \right) + v_x \frac{\partial}{\partial x} \left(U + \frac{1}{2}v^2 \right) + v_y \frac{\partial}{\partial y} \left(U + \frac{1}{2}v^2 \right) + v_z \frac{\partial}{\partial z} \left(U + \frac{1}{2}v^2 \right) \right] + \left(U + \frac{1}{2}v^2 \right) \left[\frac{\partial \rho}{\partial t} + \frac{\partial}{\partial x} \rho v_x + \frac{\partial}{\partial y} \rho v_y + \frac{\partial}{\partial z} \rho v_z \right]. \quad (7.64)$$

Continuity (Eq. A, Table 2.1) requires that the second term in the above expression is zero; the remaining term in the expression is the substantial derivative of $(U + \frac{1}{2}v^2)$, so that we may write Eq. (7.63) as

$$\begin{aligned} \rho \frac{D}{Dt} \left(U + \frac{1}{2}v^2 \right) &= \left[\frac{\partial q_x}{\partial x} + \frac{\partial q_y}{\partial y} + \frac{\partial q_z}{\partial z} \right] + \rho (v_x g_x + v_y g_y + v_z g_z) \\ &\quad - \left[\frac{\partial}{\partial x} P v_x + \frac{\partial}{\partial y} P v_y + \frac{\partial}{\partial z} P v_z \right] \\ &\quad - \left[\frac{\partial}{\partial x} (\tau_{xx} v_x + \tau_{xy} v_y + \tau_{xz} v_z) + \frac{\partial}{\partial y} (\tau_{yx} v_x + \tau_{yy} v_y + \tau_{yz} v_z) \right. \\ &\quad \left. + \frac{\partial}{\partial z} (\tau_{zx} v_x + \tau_{zy} v_y + \tau_{zz} v_z) \right]. \end{aligned} \quad (7.65)$$

For most heat flow problems, it is convenient to eliminate internal energy from Eq. (7.65). The manipulation that leads to the following equation is rather lengthy, and is not given here, except to say that with the aid of the conservation of momentum, we can write Eq. (7.65) as

$$\rho \frac{DU}{Dt} = - \left[\frac{\partial}{\partial x} q_x + \frac{\partial}{\partial y} q_y + \frac{\partial}{\partial z} q_z \right] - P \left[\frac{\partial v_x}{\partial x} + \frac{\partial v_y}{\partial y} + \frac{\partial v_z}{\partial z} \right] + \eta \Phi, \quad (7.66)$$

where the quantity Φ is known as the *dissipation function*,

$$\begin{aligned} \Phi &= 2 \left[\left[\left(\frac{\partial v_x}{\partial x} \right)^2 + \left(\frac{\partial v_y}{\partial y} \right)^2 + \left(\frac{\partial v_z}{\partial z} \right)^2 \right] + \left[\left(\frac{\partial v_x}{\partial y} + \frac{\partial v_y}{\partial x} \right)^2 + \left(\frac{\partial v_y}{\partial z} + \frac{\partial v_z}{\partial y} \right)^2 + \left(\frac{\partial v_z}{\partial x} + \frac{\partial v_x}{\partial z} \right)^2 \right] \right. \\ &\quad \left. - \frac{2}{3} \left[\frac{\partial v_x}{\partial x} + \frac{\partial v_y}{\partial y} + \frac{\partial v_z}{\partial z} \right]^2 \right]. \end{aligned} \quad (7.67)$$

From the definition of enthalpy, $H = U + P/\rho$, we write

$$\frac{DU}{Dt} = \frac{DH}{Dt} - \frac{1}{\rho} \frac{DP}{Dt} + \frac{P}{\rho^2} \frac{D\rho}{Dt}, \quad (7.68)$$

but from continuity,

$$\frac{1}{\rho} \frac{D\rho}{Dt} + \frac{\partial v_x}{\partial x} + \frac{\partial v_y}{\partial y} + \frac{\partial v_z}{\partial z} = 0,$$

so that

$$\rho \frac{DU}{Dt} = \rho \frac{DH}{Dt} - \frac{DP}{Dt} - P \left[\frac{\partial v_x}{\partial x} + \frac{\partial v_y}{\partial y} + \frac{\partial v_z}{\partial z} \right] = 0. \quad (7.69)$$

Substitution of Eq. (7.69) into Eq. (7.66) leads to

$$\rho \frac{DH}{Dt} = - \left[\frac{\partial}{\partial x} q_x + \frac{\partial}{\partial y} q_y + \frac{\partial}{\partial z} q_z \right] + \frac{DP}{Dt} + \eta \Phi. \quad (7.70)$$

From the thermodynamic relations of properties, we can write

$$dH = C_p dT + \frac{1}{\rho} (1 - T\beta) dP, \quad (7.71)$$

where C_p is the heat capacity, and $\beta \equiv -(1/\rho)(\partial\rho/\partial T)_P$.

From Eq. (7.71), it follows that

$$\rho \frac{DH}{Dt} = \rho C_p \frac{DT}{Dt} + (1 - T\beta) \frac{DP}{Dt}, \quad (7.72)$$

and from the Fourier rate equations, that

$$q_x = -k \frac{\partial T}{\partial x}, \quad q_y = -k \frac{\partial T}{\partial y}, \quad q_z = -k \frac{\partial T}{\partial z}.$$

Substituting Eq. (7.72) and the rate equations into Eq. (7.70) finally gives the energy equation in terms of temperature:

$$\rho C_p \frac{DT}{Dt} = \frac{\partial}{\partial x} \left[k \frac{\partial T}{\partial x} \right] + \frac{\partial}{\partial y} \left[k \frac{\partial T}{\partial y} \right] + \frac{\partial}{\partial z} \left[k \frac{\partial T}{\partial z} \right] + T\beta \frac{DP}{Dt} + \eta \Phi. \quad (7.73)$$

We usually simplify Eq. (7.73). For example, if k is independent of the space coordinates, we write

$$\rho C_p \frac{DT}{Dt} = k \nabla^2 T + T\beta \frac{DP}{Dt} + \eta \Phi. \quad (7.74)$$

Further, if the system is an *ideal* gas, $\beta = 1/T$:

$$\rho C_p \frac{DT}{Dt} = k \nabla^2 T + \frac{DP}{Dt} + \eta \Phi. \quad (7.75)$$

Many problems involve incompressible fluids where the viscous dissipation term is negligible. In this instance, $\beta = \Phi = 0$, and

$$\rho C_p \frac{DT}{Dt} = k \nabla^2 T. \quad (7.76)$$

240 Heat Transfer and the Energy Equation

In the conduction of heat through *solids*, the velocity is zero; the compressibility term is ignored, so that

$$\rho C_p \frac{\partial T}{\partial t} = k \nabla^2 T. \tag{7.77}$$

7.6 THE ENERGY EQUATION IN RECTANGULAR AND CURVILINEAR COORDINATES

In this section, we give the fluxes and the energy equation—already developed in rectangular coordinates—in cylindrical and spherical coordinates. Tables 7.3, 7.4, and 7.5 may be used for the problems of heat flow by discarding unnecessary terms, rather than setting up problems by means of shell balances.

Table 7.3 Components of the energy flux, q^*

Rectangular	Cylindrical	Spherical
$q_x = -k \frac{\partial T}{\partial x}$ (A)	$q_r = -k \frac{\partial T}{\partial r}$ (D)	$q_r = -k \frac{\partial T}{\partial r}$ (G)
$q_y = -k \frac{\partial T}{\partial y}$ (B)	$q_\theta = -k \frac{1}{r} \frac{\partial T}{\partial \theta}$ (E)	$q_\theta = -k \frac{1}{r} \frac{\partial T}{\partial \theta}$ (H)
$q_z = -k \frac{\partial T}{\partial z}$ (C)	$q_z = -k \frac{\partial T}{\partial z}$ (F)	$q_\phi = -k \frac{1}{r \sin \theta} \frac{\partial T}{\partial \phi}$ (I)

*This table and the following two tables are from R. B. Bird, W. E. Stewart, and E. N. Lightfoot, *Transport Phenomena*, Wiley, New York, 1960, pages 317-319.

Table 7.4 The equation of energy in terms of energy and momentum fluxes

Rectangular coordinates

$$\begin{aligned} \rho C_v \left(\frac{\partial T}{\partial t} + v_x \frac{\partial T}{\partial x} + v_y \frac{\partial T}{\partial y} + v_z \frac{\partial T}{\partial z} \right) &= - \left[\frac{\partial q_x}{\partial x} + \frac{\partial q_y}{\partial y} + \frac{\partial q_z}{\partial z} \right] \\ &- T \left(\frac{\partial P}{\partial T} \right)_\rho \left(\frac{\partial v_x}{\partial x} + \frac{\partial v_y}{\partial y} + \frac{\partial v_z}{\partial z} \right) - \left\{ \tau_{xx} \frac{\partial v_x}{\partial x} + \tau_{yy} \frac{\partial v_y}{\partial y} + \tau_{zz} \frac{\partial v_z}{\partial z} \right\} \\ &- \left\{ \tau_{xy} \left(\frac{\partial v_x}{\partial y} + \frac{\partial v_y}{\partial x} \right) + \tau_{xz} \left(\frac{\partial v_x}{\partial z} + \frac{\partial v_z}{\partial x} \right) + \tau_{yz} \left(\frac{\partial v_y}{\partial z} + \frac{\partial v_z}{\partial y} \right) \right\}. \end{aligned} \quad (\text{A})$$

Cylindrical coordinates

$$\begin{aligned} \rho C_v \left(\frac{\partial T}{\partial t} + v_r \frac{\partial T}{\partial r} + \frac{v_\theta}{r} \frac{\partial T}{\partial \theta} + v_z \frac{\partial T}{\partial z} \right) &= - \left[\frac{1}{r} \frac{\partial}{\partial r} (r q_r) + \frac{1}{r} \frac{\partial q_\theta}{\partial \theta} + \frac{\partial q_z}{\partial z} \right] \\ &- T \left(\frac{\partial P}{\partial T} \right)_\rho \left(\frac{1}{r} \frac{\partial}{\partial r} (r v_r) + \frac{1}{r} \frac{\partial v_\theta}{\partial \theta} + \frac{\partial v_z}{\partial z} \right) - \left\{ \tau_{rr} \frac{\partial v_r}{\partial r} + \tau_{\theta\theta} \frac{1}{r} \left(\frac{\partial v_\theta}{\partial \theta} + v_r \right) \right. \\ &+ \left. \tau_{zz} \frac{\partial v_z}{\partial z} \right\} - \left\{ \tau_{r\theta} \left[r \frac{\partial}{\partial r} \left(\frac{v_\theta}{r} \right) + \frac{1}{r} \frac{\partial v_r}{\partial \theta} \right] + \tau_{rz} \left(\frac{\partial v_z}{\partial r} + \frac{\partial v_r}{\partial z} \right) \right. \\ &+ \left. \tau_{\theta z} \left(\frac{1}{r} \frac{\partial v_z}{\partial \theta} + \frac{\partial v_\theta}{\partial z} \right) \right\}. \end{aligned} \quad (\text{B})$$

Spherical coordinates

$$\begin{aligned} \rho C_v \left(\frac{\partial T}{\partial t} + v_r \frac{\partial T}{\partial r} + \frac{v_\theta}{r} \frac{\partial T}{\partial \theta} + \frac{v_\phi}{r \sin \theta} \frac{\partial T}{\partial \phi} \right) &= - \left[\frac{1}{r^2} \frac{\partial}{\partial r} (r^2 q_r) \right. \\ &+ \left. \frac{1}{r \sin \theta} \frac{\partial}{\partial \theta} (q_\theta \sin \theta) + \frac{1}{r \sin \theta} \frac{\partial q_\phi}{\partial \phi} \right] - T \left(\frac{\partial P}{\partial T} \right)_\rho \left(\frac{1}{r^2} \frac{\partial}{\partial r} (r^2 v_r) \right. \\ &+ \left. \frac{1}{r \sin \theta} \frac{\partial}{\partial \theta} (v_\theta \sin \theta) + \frac{1}{r \sin \theta} \frac{\partial v_\phi}{\partial \phi} \right) - \left\{ \tau_{rr} \frac{\partial v_r}{\partial r} + \tau_{\theta\theta} \left(\frac{1}{r} \frac{\partial v_\theta}{\partial \theta} + \frac{v_r}{r} \right) \right. \\ &+ \left. \tau_{\phi\phi} \left(\frac{1}{r \sin \theta} \frac{\partial v_\phi}{\partial \phi} + \frac{v_r}{r} + \frac{v_\theta \cot \theta}{r} \right) \right\} - \left\{ \tau_{r\theta} \left(\frac{\partial v_\theta}{\partial r} + \frac{1}{r} \frac{\partial v_r}{\partial \theta} - \frac{v_\theta}{r} \right) \right. \\ &+ \left. \tau_{r\phi} \left(\frac{\partial v_\phi}{\partial r} + \frac{1}{r \sin \theta} \frac{\partial v_r}{\partial \phi} - \frac{v_\phi}{r} \right) + \tau_{\theta\phi} \left(\frac{1}{r} \frac{\partial v_\phi}{\partial \theta} + \frac{1}{r \sin \theta} \frac{\partial v_\theta}{\partial \phi} - \frac{\cot \theta}{r} v_\phi \right) \right\}. \end{aligned} \quad (\text{C})$$

Note: The terms contained in braces { } are associated with viscous dissipation and may usually be neglected, except for systems with large velocity gradients.

Table 7.5 The equation of energy in terms of the transport properties (for Newtonian fluids of constant ρ , η , and k ; note that the constancy of ρ implies that $C_v = C_p$)

Rectangular coordinates

$$\begin{aligned} \rho C_v \left(\frac{\partial T}{\partial t} + v_x \frac{\partial T}{\partial x} + v_y \frac{\partial T}{\partial y} + v_z \frac{\partial T}{\partial z} \right) &= k \left[\frac{\partial^2 T}{\partial x^2} + \frac{\partial^2 T}{\partial y^2} + \frac{\partial^2 T}{\partial z^2} \right] \\ &+ 2\eta \left\{ \left(\frac{\partial v_x}{\partial x} \right)^2 + \left(\frac{\partial v_y}{\partial y} \right)^2 + \left(\frac{\partial v_z}{\partial z} \right)^2 \right\} + \eta \left\{ \left(\frac{\partial v_x}{\partial y} + \frac{\partial v_y}{\partial x} \right)^2 \right. \\ &\left. + \left(\frac{\partial v_x}{\partial z} + \frac{\partial v_z}{\partial x} \right)^2 + \left(\frac{\partial v_y}{\partial z} + \frac{\partial v_z}{\partial y} \right)^2 \right\}. \end{aligned} \quad (\text{A})$$

Cylindrical coordinates

$$\begin{aligned} \rho C_v \left(\frac{\partial T}{\partial t} + v_r \frac{\partial T}{\partial r} + \frac{v_\theta}{r} \frac{\partial T}{\partial \theta} + v_z \frac{\partial T}{\partial z} \right) &= k \left[\frac{1}{r} \frac{\partial}{\partial r} \left(r \frac{\partial T}{\partial r} \right) + \frac{1}{r^2} \frac{\partial^2 T}{\partial \theta^2} + \frac{\partial^2 T}{\partial z^2} \right] \\ &+ 2\eta \left\{ \left(\frac{\partial v_r}{\partial r} \right)^2 + \left[\frac{1}{r} \left(\frac{\partial v_\theta}{\partial \theta} + v_r \right) \right]^2 + \left(\frac{\partial v_z}{\partial z} \right)^2 \right\} + \eta \left\{ \left(\frac{\partial v_\theta}{\partial z} + \frac{1}{r} \frac{\partial v_z}{\partial \theta} \right)^2 \right. \\ &\left. + \left(\frac{\partial v_z}{\partial r} + \frac{\partial v_r}{\partial z} \right)^2 + \left[\frac{1}{r} \frac{\partial v_r}{\partial \theta} + r \frac{\partial}{\partial r} \left(\frac{v_\theta}{r} \right) \right]^2 \right\}. \end{aligned} \quad (\text{B})$$

Spherical coordinates

$$\begin{aligned} \rho C_v \left(\frac{\partial T}{\partial t} + v_r \frac{\partial T}{\partial r} + \frac{v_\theta}{r} \frac{\partial T}{\partial \theta} + \frac{v_\phi}{r \sin \theta} \frac{\partial T}{\partial \phi} \right) &= k \left[\frac{1}{r^2} \frac{\partial}{\partial r} \left(r^2 \frac{\partial T}{\partial r} \right) \right. \\ &+ \frac{1}{r^2 \sin \theta} \frac{\partial}{\partial \theta} \left(\sin \theta \frac{\partial T}{\partial \theta} \right) + \frac{1}{r^2 \sin^2 \theta} \frac{\partial^2 T}{\partial \phi^2} \left. \right] + 2\eta \left\{ \left(\frac{\partial v_r}{\partial r} \right)^2 \right. \\ &+ \left(\frac{1}{r} \frac{\partial v_\theta}{\partial \theta} + \frac{v_r}{r} \right)^2 + \left(\frac{1}{r \sin \theta} \frac{\partial v_\phi}{\partial \phi} + \frac{v_r}{r} + \frac{v_\theta \cot \theta}{r} \right)^2 \left. \right\} \\ &+ \eta \left\{ \left[r \frac{\partial}{\partial r} \left(\frac{v_\theta}{r} \right) + \frac{1}{r} \frac{\partial v_r}{\partial \theta} \right]^2 + \left[\frac{1}{r \sin \theta} \frac{\partial v_r}{\partial \phi} + r \frac{\partial}{\partial r} \left(\frac{v_\phi}{r} \right) \right]^2 \right. \\ &\left. + \left[\frac{\sin \theta}{r} \frac{\partial}{\partial \theta} \left(\frac{v_\phi}{\sin \theta} \right) + \frac{1}{r \sin \theta} \frac{\partial v_\theta}{\partial \phi} \right]^2 \right\}. \end{aligned} \quad (\text{C})$$

Note: The terms contained in braces { } are associated with viscous dissipation and may usually be neglected, except for systems with large velocity gradients.

Example 7.4 Refer back to Fig. 7.3 and the system described in Section 7.2. Using Table 7.4 or 7.5 derive the energy equation.

Solution. Table 7.5 is selected because the fluid has constant properties. Flow is two-dimensional in rectangular coordinates so Eq. (A) is the best choice. Before proceeding, recall that there are two velocity components v_x and v_y . Also, it is a good idea to qualitatively sketch the temperature field. Having done so, you should recognize that $T = T(x, y)$. Now, we can proceed to simplify Eq. (A) in Table 7.5. Notice that $C_v = C_p$.

$$\frac{\partial T}{\partial t} = 0 \quad \text{because there is steady state.}$$

$$v_z \frac{\partial T}{\partial z} = 0 \quad \text{because } v_z = 0 \text{ and } T = T(x, y).$$

$$\frac{\partial^2 T}{\partial z^2} = 0 \quad \text{because } T = T(x, y).$$

All terms in { } are zero because we neglect viscous heating. We are left with

$$\rho C_p \left[v_x \frac{\partial T}{\partial x} + v_y \frac{\partial T}{\partial y} \right] = k \left[\frac{\partial^2 T}{\partial x^2} + \frac{\partial^2 T}{\partial y^2} \right].$$

Except for fluids with very low Pr numbers, we can ignore conduction in the direction of flow; hence

$$\frac{\partial^2 T}{\partial x^2} \approx 0$$

and we finally write:

$$v_x \frac{\partial T}{\partial x} + v_y \frac{\partial T}{\partial y} = \alpha \frac{\partial^2 T}{\partial y^2}.$$

PROBLEMS

7.1 For laminar flow, calculate the results given in Table 7.1 for Nu_∞ for slug flow ($v_x = \text{uniform}$) and uniform heat flux in a circular tube.

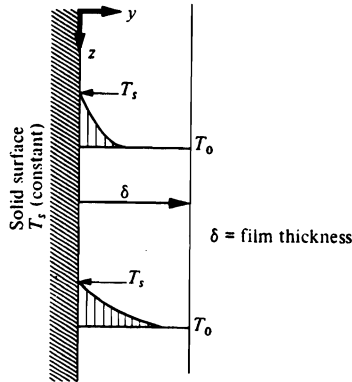
7.2 A liquid film at T_0 flows down a vertical wall at a higher temperature T_s . Consider heat transfer from the wall to the liquid for such contact times that the liquid temperature changes appreciably only in the immediate vicinity of the wall. (See figure on next page.)

a) Show that the energy equation can be written (state assumptions):

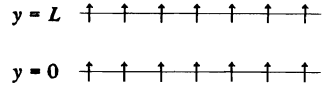
$$\rho C_p v_z \frac{\partial T}{\partial z} = k \frac{\partial^2 T}{\partial y^2}.$$

- b) The energy equation contains v_z . What would you use for v_z ?
 c) Write appropriate boundary conditions.

7.2 (cont.)

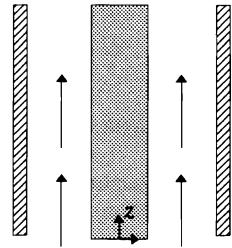


7.3 A gap of thickness L exists between two parallel plates of porous solids. Fluid is forced to flow through the bottom plate, across the gap, and then through the upper plate. Assume that the fluid flows with a constant velocity V in laminar flow with straight streamlines across the gap. The system is at steady state with the upper and lower plates at T_L and T_0 , respectively.



- a) Write an appropriate energy equation and boundary conditions for the fluid in the gap.
- b) Solve for the temperature in the gap.
- c) Derive an equation for the heat flux across the gap.

7.4 A liquid of constant density and viscosity flows upward in the annulus ($R_1 \leq r \leq R_2$) between two very long and concentric cylinders. Assume that both the flow and the temperature are fully developed. The inner cylinder is electrically heated and supplies a constant and uniform flux, q_r , to the liquid. The outer cylinder is maintained at a constant temperature, T_0 .

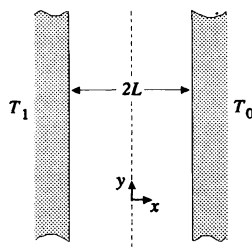


- a) Solve for v_z .
- b) Write the energy equation and state your assumptions.
- c) Write appropriate boundary conditions.

Fluid enters at T_0

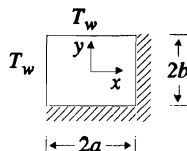
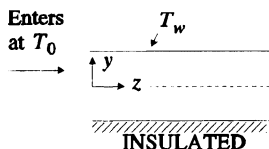
7.5 Air at 0.3 m s^{-1} and 365 K flows parallel to a flat plate at 310 K . a) Calculate the distance from the leading edge to where the momentum boundary layer thickness is 6 mm . b) At the same distance from the leading edge, what is the thermal boundary layer thickness? c) Up to the same distance from the leading edge, how much heat is transferred to the plate (one side) in 600 s , if the plate is 100 mm wide?

7.6 Consider natural convection between parallel vertical plates maintained at T_1 and T_0 , respectively. Assume that the plates are very long and the convection is fully developed. For constant properties: a) Write the energy equation and boundary conditions for temperature. b) Write the momentum equation with the Boussinesq approximation and boundary conditions for velocity.



7.7 The surface temperature of a vertical plate is maintained at 390 K. At 0.24 m from the bottom of the plate, calculate the heat transfer coefficient to: a) air at 290 K; b) helium at 290 K.

7.8 Liquid metal flows through a channel with a rectangular cross-section. Two walls are perfectly insulated and two are at a constant temperature of T_w . The metal has temperature T_0 as it enters the channel, and $T_w > T_0$. Assume steady state, fully developed flow and no solidification.

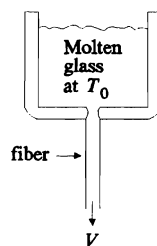


- Write the energy equation in terms of temperature for constant thermal properties.
- Write the boundary conditions.

7.9 Consider the creeping flow of a fluid about a rigid sphere as illustrated by Fig. 2.9. The sphere is maintained at T_0 and the fluid approaches from below with a temperature T_∞ and velocity V_∞ . a) Write the energy equation which applies to the fluid in the vicinity of the sphere. Assume steady-state conditions. b) Write appropriate boundary conditions for part a). c) What other equations or results would you use in order to solve the system described by parts a) and b)?

7.10 A very long fiber of glass (radius = R) is extracted from a hole in the bottom of a crucible. It is extracted with a constant velocity V into a gas at T_∞ ; assume slug flow.

- For uniform properties write the energy equation for temperature in the fiber. Do not ignore conduction in the direction of flow.
- Write boundary conditions. [Hint: At $r = R$, the flux to the surface must equal the flux to the surrounding gas "via h ."]]



7.11 Starting with Eq. (7.44), derive Eq. (7.45) and define the dimensionless numbers in Eq. (7.45).

7.12

- Determine an expression that gives the heat flow Q (W) through a solid spherical shell with inside and outside radii of r_1 and r_2 , respectively.
- Examine the results regarding what happens as the shell thickness becomes larger compared with the inside radius.

7.13 A sphere of radius R is in a motionless fluid (no forced or natural convection). The surface temperature of the sphere is maintained at T_R and the bulk fluid temperature is T_∞ .

- Develop an expression for the temperature in the fluid surrounding the sphere.
- Determine the Nusselt number for this situation. Such a value would be the limiting value for the actual system with convection as the forces causing convection become very small.

7.14 For the system in Fig. 2.1 develop an expression for the temperature distribution in the falling film. Assume fully developed flow, constant properties, and fully developed temperature profile. The free liquid surface is maintained at $T = T_0$ and the solid surface at $T = T_s$, where T_0 and T_s are constants. a) Ignore viscous heating effects. b) Include viscous heating effects.

Answer b)

$$\frac{T - T_0}{T_s - T_0} = \frac{x}{\delta} \left\{ 1 + \frac{3}{4} \text{Br} \left[1 - \left(\frac{x}{\delta} \right)^3 \right] \right\},$$

where $\text{Br} = \frac{\eta \bar{V}^2}{k(T_s - T_0)}$, Brinkman number.

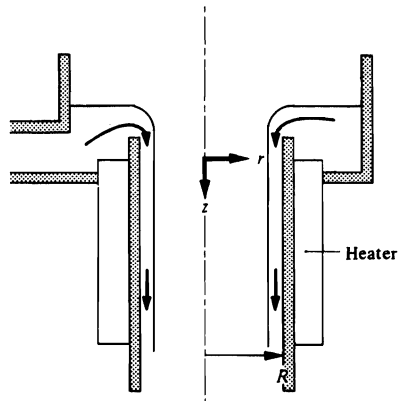
7.15 Consider heat conduction through a plane wall of thickness Δx , and T_1 and T_2 are the surface temperatures. Derive the steady-state heat flux in terms of T_1 , T_2 and Δx if the thermal conductivity varies according to

$$k = k_0(1 + aT)$$

where k_0 and a are constants.

7.16 A liquid at a temperature T_0 continuously enters the bottom of a small tank, overflows into a tube, and then flows downward as a film on the inside. At some position down the tube ($z = 0$) when the flow is fully developed, the pipe heats the fluid with a uniform flux q_R . The heat loss from the liquid's surface is sufficiently small so that it may be neglected.

- For steady-state laminar flow with constant properties, develop by shell balance or show by reducing an equation in Table 7.5 the pertinent differential energy equation that applies to the falling film.
- Write the boundary conditions for the heat flow.
- What other information must complement parts a) and b) in order to solve the energy equation?



8

CORRELATIONS AND DATA FOR HEAT TRANSFER COEFFICIENTS

The problems of heat flow with convection, discussed in the preceding chapter, pertain to simple systems with laminar flow. Despite the simplicity of laminar flow problems, they should not be underestimated. Many simple solutions have been applied to real systems with approximating assumptions and, besides, the simpler systems provide models for interpretation of complex systems. The more complex nature of turbulent flow and its limited accessibility to mathematical treatment requires, however, an empirical approach to heat transfer. On the other hand, the study of turbulent flow is not entirely empirical; it is possible to establish certain theoretical bases for the analyses of turbulent transfer processes and an introduction to this complex area is given in Chapter 16.

Figure 8.1 illustrates heat transfer in a bounded fluid. The fluid is artificially subdivided into three regions: the turbulent core, the transition zone, and the laminar sublayer near the surface. In the turbulent core, thermal energy is transferred rapidly due to the eddy (mixing) action of turbulent flow. Conversely, within the laminar sublayer, energy is transferred by conduction alone—a much slower process than the eddy process. In the transition zone, energy transport by both conduction and by eddies is appreciable. Hence, most of the total temperature drop between the fluid and the surface is across the laminar sublayer and the transition zone. Within the turbulent core, the temperature gradients are quite shallow.

In Chapter 3, it was convenient to define a friction factor to deal with momentum transport in fluids in contact with surfaces. Similarly, for energy transport between fluids and surfaces, it is convenient to define a heat transfer coefficient by

$$h = \frac{q_0}{T_0 - T_f} = \frac{-k(\partial T/\partial y)_0}{T_0 - T_f}, \quad (8.1)$$

where the subscript "0" refers to the respective quantities evaluated at the wall, and T_f is some temperature of the fluid. If the fluid is infinite in extent, we take T_f as the fluid temperature far removed from the surface, and designate it T_∞ . If the fluid flows in a confined space, such as inside a tube, T_f is usually the *mixed mean temperature*, denoted by T_m ; it is a temperature that would exist if the fluid at a particular cross section were removed and allowed to mix adiabatically.

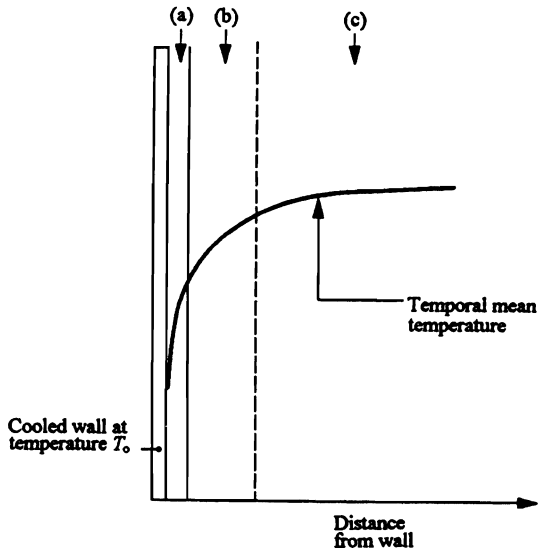


Fig. 8.1 Temperature profile of a flowing fluid bounded by a cooler wall; (a) laminar sublayer, (b) transition zone, and (c) turbulent core.

As explained in Chapter 7, h is a function of the fluid's properties (k , η , ρ , C_p), the system geometry, the flow velocity, and the value of the defining temperature difference. We deal in the remainder of this chapter with predicting the dependence of h on these quantities, by presenting experimental data for various systems in the form of correlations based on dimensional analysis.

8.1 HEAT TRANSFER COEFFICIENTS FOR FORCED CONVECTION IN TUBES

In Section 3.1, we presented a method of dimensional analysis utilizing a rearrangement of differential equations in order to show that the friction factor was a function of the Reynolds number. We used the same method in Section 7.3 for natural convection. Here we bring the reader's attention to a different technique of dimensional analysis, while deriving those dimensionless numbers which are pertinent to the heat transfer system of forced convection within a tube.

8.1.1 Dimensional analysis—Buckingham's pi theorem

We may obtain pertinent dimensionless numbers without reference to the basic differential equations, if we can identify the variables sufficient to specify a given situation. A systematic way of determining the groups is known as *Buckingham's pi theorem*.¹ Simply stated, it reads: *The functional relationship among q quantities, whose units may be given in terms of u fundamental units, may be written as a function of $q - u$ dimensionless groups (the π 's).*

¹E. Buckingham, *Trans. ASME* 35, 262 (1915).

In the application of the pi theorem, these rules are helpful:

- a) Compile a list of the q significant quantities and their respective fundamental units. The fundamental units are L (length), M (mass), Θ (time), and T (temperature).
- b) Select the primary quantities or primary q 's. The number of primary q 's should equal u , the number of fundamental units.
- c) Form each π term by expressing the ratio of the remaining q 's (one at a time) to the product of the primary q 's, each raised to an unknown power determined as shown below.

We now illustrate the method for heat transfer in forced convection. We presume that the heat transfer coefficient for fully developed forced convection in a tube is a function of the variables

$$h = f(\bar{V}, \rho, k, \eta, C_p, D). \tag{8.2}$$

We can express all these quantities in terms of the four fundamental dimensions $M, L, \Theta,$ and T . Specifically,

$\bar{V}, L\Theta^{-1},$	$\eta, ML^{-1}\Theta^{-1},$	$D, L.$
$\rho, ML^{-3},$	$C_p, L^2\Theta^{-2}T^{-1},$	
$k, ML\Theta^{-3}T^{-1},$	$h, M\Theta^{-3}T^{-1},$	

Note that energy is given the units of work (force \times distance), namely, $ML^3\Theta^{-1}$.

The number of fundamental units in this case is four. Thus, since $u = 4$, select as the four primary q 's, $\bar{V}, D, \rho,$ and k , leaving $h, \eta,$ and C_p . Proceed to form the first π term.

$$\pi_1 = \frac{h}{\bar{V}^a D^b \rho^c k^d} = \frac{M\Theta^{-3}T^{-1}}{(L\Theta^{-1})^a (L)^b (ML^{-3})^c (ML\Theta^{-3}T^{-1})^d}.$$

Equating the exponents of each dimension to zero, so that the π group is dimensionless, we obtain

$$\begin{aligned} M: & 1 = c + d, \\ L: & 0 = a + b - 3c + d, \\ \Theta: & -3 = -a - 3d, \\ T: & -1 = -d. \end{aligned}$$

Solving these four equations simultaneously, we obtain $a = 0, b = -1, c = 0,$ and $d = 1$. Thus

$$\pi_1 = \frac{hD}{k} \equiv Nu \quad (\text{Nusselt number}).$$

Similarly, the following π groups can be obtained:

$$\pi_2 = \eta/\rho\bar{V}D \equiv \frac{1}{Re},$$

$$\pi_3 = C_p\eta/k \equiv Pr \quad (\text{Prandtl number}).$$

Thus, heat transfer data in forced convection can be correlated in terms of these three groups or dimensionless numbers:

$$Nu = Nu(Re, Pr). \tag{8.3}$$

250 Correlations and Data for Heat Transfer Coefficients

Equation (8.3) is not complete enough in some situations. If fully developed flow is not assumed, then the length to diameter ratio L/D must be included. In addition, for large temperature differences, the temperature dependence of the fluid viscosity may be handled approximately by including the group η_m/η_0 , where η_m is the viscosity at the mixed mean temperature T_m , and η_0 is the viscosity at the temperature of the solid surface. Hence, a complete correlation is written in the form

$$\text{Nu} = \text{Nu}(\text{Re}, \text{Pr}, L/D, \eta_m/\eta_0). \quad (8.4)$$

This dimensional analysis is of great use in experimental work involving heat transfer. For example, h depends on eight physical quantities: D , \bar{V} , ρ , η_m , η_0 , C_p , k , and L . To study all combinations of eight independent variables for ten values of each would require 10^8 tests, whereas, by giving Nu as a function of only four groups $(\text{Re}, \text{Pr}, L/D, \eta_m/\eta_0)$, 10^4 tests would suffice. Thus, a graduate student would require only five years of research instead of 50,000 years!

8.1.2 Correlations for forced convection in tubes

For fully developed flow in tubes, a correlation for flow in smooth tubes with nearly constant wall temperature is presented in Fig. 8.2. The Reynolds number used here, $\text{Re}_m = D\bar{V}\rho/\eta_m$, is convenient because the laminar-to-turbulent transition is at about 2100 (the same as in Fig. 3.2), even when η_0 differs appreciably from η_m .

For highly turbulent flow ($\text{Re}_m > 10,000$), the equation

$$\text{Nu}_m = 0.026 \text{Re}_m^{0.8} \text{Pr}_m^{1/3} \left(\frac{\eta_m}{\eta_0} \right)^{0.14} \quad (8.5)$$

reproduces experimental data to within about $\pm 20\%$ in the range $10^4 < \text{Re}_m < 10^5$, $0.6 < \text{Pr} < 100$, and $L/D > 10$. As we discuss later, the data need not be restricted to the situations of constant wall temperature.

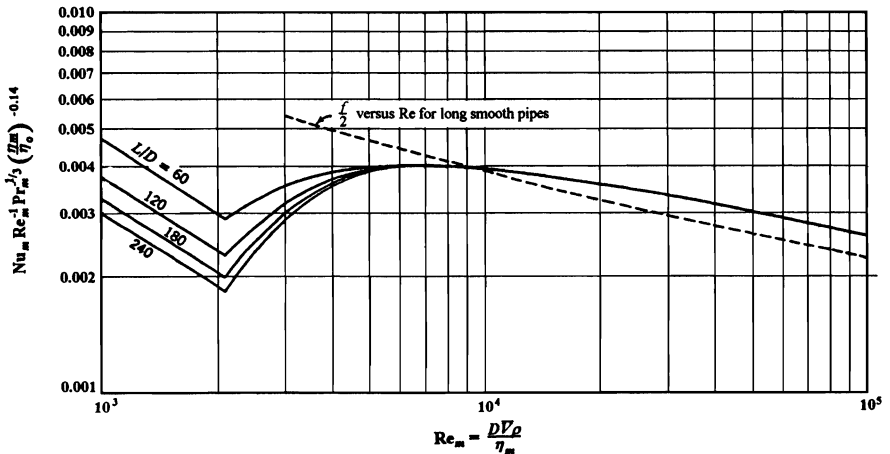


Fig. 8.2 Heat transfer coefficients for fully developed flow in smooth tubes. (From E. N. Seider and G. E. Tate, *Ind. Eng. Chem.* **28**, 1429 (1936).)

We superimpose the plot of $f/2$ on Fig. 8.2 for long, hydraulically smooth tubes, where

$$j_H = St_m \left[\frac{C_{p,m} \eta_f}{k_m} \right]^{2/3} = \frac{f}{2}. \tag{8.6}$$

St_m is the Stanton number, and j_H is often referred to as a *j-factor*. The Stanton number is defined

$$St \equiv \frac{Nu}{Re \cdot Pr} = \frac{h}{C_p \rho V}.$$

Equation (8.6) is Colburn’s analogy between heat transfer and fluid friction. The analogy breaks down for $Re_m < 10,000$, and also for rough tubes because f is affected more by roughness than its counterpart j_H . The effect of wall roughness was studied for air and Fig. 8.3 relates the heat transfer coefficient to the ratio of the friction factor f in the rough pipe to the friction factor f_s in a smooth pipe of the same diameter. The results have not been tested extensively, and should probably be restricted to use with gases.

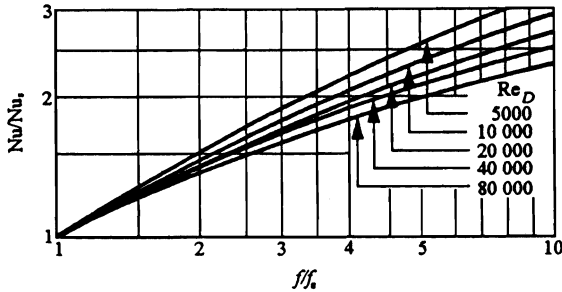


Fig. 8.3 Effect of roughness on heat transfer in turbulent flow. (From W. Nunner, VDI—Forschungsheft No. 455/1956 (VID-Verlag GmbH-Dusseldorf).)

For liquid metals, where $0.005 < Pr < 0.05$, the following equation represents available experimental data with $Re > 10,000$ and for a uniform heat flux:²

$$Nu_q = 6.7 + 0.0041(Re \cdot Pr)^{0.793} \exp(41.8 Pr). \tag{8.7}$$

Because of the very high values of h in liquid metals, $(T_0 - T_m)$ is not very large, so that the mixed mean temperature properties can be used without significant error.

Equation (8.7) for liquid metals applies to uniform heat flux along the tube. For uniform wall temperature, the difference between Nu_w (uniform wall temperature) and Nu_q (uniform heat flux) is significant for liquid metals (Fig. 8.4); for $Pr > 0.5$ the difference between Nu_w and Nu_q is small, and hence Eq. (8.5) is also approximately valid for constant heat flux boundary conditions.

²W. M. Rohsenow and H. Y. Choi, *Heat, Mass, and Momentum Transfer*, Prentice-Hall, Englewood Cliffs, NJ, 1961, page 193.

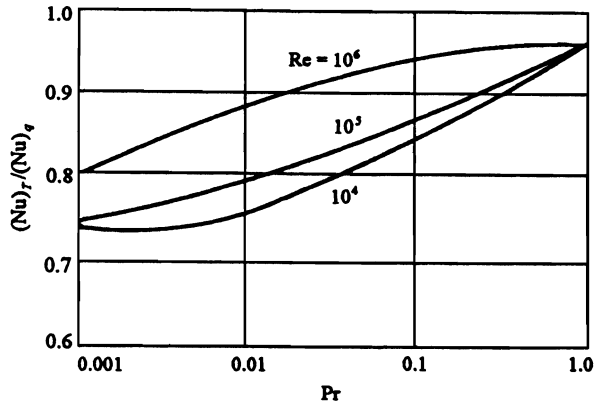
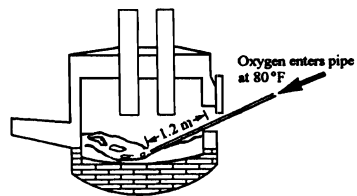


Fig. 8.4 Comparison of uniform wall temperature and uniform heat flux in tubes. (From R. A. Seban and T. T. Shimazaki, *Trans. ASME* 73, 803 (1951).)

Example 8.1 A 5 ton (4536 kg) heat of steel must be decarburized from 0.40 to 0.20% C in 5 min. A convenient method for accomplishing this is to blow oxygen through a submerged lance. A low carbon steel pipe of 12.7 mm I.D. is used as the lance, despite the fact that the end of the pipe gradually melts. If we estimate the portion of the lance within the furnace to be at 1744 K, calculate the temperature at which the oxygen enters the liquid steel. Neglect the pressure drop through the pipe and assume that the pressure in the pipe equals $1.22 \times 10^5 \text{ N m}^{-2}$ (1.2 atm).



Solution. The oxygen requirement, for $\text{C} + \frac{1}{2}\text{O}_2(\text{g}) \rightarrow \text{CO}(\text{g})$, is

$$\begin{aligned} \bar{V}_p &= \frac{(4536)(0.20) \text{ kg C}}{(100)(300) \text{ s}} \left| \frac{1 \text{ kmol C}}{12.011 \text{ kg C}} \right| \left| \frac{0.5 \text{ kmol O}_2}{1 \text{ kmol C}} \right| \left| \frac{32 \text{ kg O}_2}{1 \text{ kmol O}_2} \right| \left| \frac{4}{\pi(12.7)^2 \text{ mm}^2} \right| \left| \frac{1000^2 \text{ mm}^2}{1 \text{ m}^2} \right| \\ &= 318 \text{ kg m}^{-2} \text{ s}^{-1}. \end{aligned}$$

The oxygen enters the tube at 300 K, and as it proceeds through the pipe its temperature rises. Consequently, the properties of the oxygen vary with distance down the tube. A commonly employed estimation is to evaluate the properties of the fluid at its average temperature along the heated pipe. The heat transfer coefficient corresponding to these properties is then calculated, assumed to be constant along the pipe, and used to determine the heat transferred to the gas.

First, arbitrarily assume that the gas leaves the pipe at 820 K. Then take the average T_m as $(820 + 300)/2 = 560 \text{ K}$ for the last 1.2 m of pipe. At 560 K, the properties of O_2 are $\eta = 32.4 \times 10^{-6} \text{ kg m}^{-1} \text{ s}^{-1}$; $k = 45.8 \times 10^{-3} \text{ W m}^{-1} \text{ K}^{-1}$; $C_p = 991 \text{ J kg}^{-1} \text{ K}^{-1}$; $\text{Pr} = 0.701$.

At 820 K, $\eta = 41.5 \times 10^{-6} \text{ kg m}^{-1} \text{ s}^{-1}$, which we use for η_0 . Now calculate Re_m :

$$\text{Re}_m = \frac{D \bar{V} \rho}{\eta_m} = \frac{(12.7 \times 10^{-3})(318)}{(32.4 \times 10^{-6})} = 1.25 \times 10^5.$$

Thus, Eq. (8.5) applies, so that

$$\begin{aligned} \text{Nu}_m &= 0.026 \text{Re}_m^{0.8} \text{Pr}_m^{1/3} \left(\frac{\eta_m}{\eta_0} \right)^{0.14} = (0.026)(1.25 \times 10^5)^{0.8} (0.701)^{1/3} \left(\frac{32.4 \times 10^{-6}}{41.5 \times 10^{-6}} \right)^{0.14} \\ &= 267. \end{aligned}$$

Therefore

$$h = \frac{k_m \text{Nu}_m}{D} = \frac{(45.8 \times 10^{-3})(267)}{12.7 \times 10^{-3}} = 963 \text{ W m}^{-2} \text{ K}^{-1}.$$

An energy balance applied to the fluid over a differential length of pipe, dx , can be written

$$WC_p dT_m = h(T_0 - T_m)(\pi D dx),$$

where W = mass flow rate, kg s^{-1} , and T_0 = temperature of pipe wall. Integrating for a length of pipe L , with h , C_p , and T_0 taken as constants, yields

$$h \int_0^L dx = - \frac{WC_p}{\pi D} \int_{\Delta T_0}^{\Delta T_L} d \ln (T_m - T_0),$$

or

$$\ln \frac{\Delta T_L}{\Delta T_0} = - \frac{hL\pi D}{WC_p} = - \frac{4hL}{\rho \bar{V} C_p D}.$$

Substituting numerical values yields

$$\ln \frac{\Delta T_L}{(820 - 300)} = - \frac{(4)(963)(1.2)}{(318)(991)(12.7 \times 10^{-3})},$$

from which

$$\Delta T_L = 164 \text{ K} \quad \text{or} \quad T_m = 984 \text{ K (at } x = L = 1.2 \text{ m)}.$$

Recalling our initial guess of 820 K, we see that in terms of estimating properties we have selected reasonably good values.

As a second guess, assume that the gas leaves the pipe is 940 K. Then, we take the average T_m as $(940 + 300)/2 = 620 \text{ K}$. At 620 K, the properties of O_2 are $\eta = 35.1 \times 10^{-6} \text{ kg m}^{-1} \text{ s}^{-1}$; $k = 48.4 \times 10^{-3} \text{ W m}^{-1} \text{ K}^{-1}$; $C_p = 1010 \text{ J kg}^{-1} \text{ K}^{-1}$; $\text{Pr} = 0.732$.

When we repeat the method of calculation using these new values, we get $\text{Re}_m = 1.15 \times 10^5$, $\text{Nu}_m = 256$, and $h = 976 \text{ W m}^{-2} \text{ K}^{-1}$. The difference between the first and the second estimates of h is only 1.3%. Finally, $\Delta T_L = 165 \text{ K}$, or $T_m = 985 \text{ K}$ (at $x = L = 1.2 \text{ m}$). We could repeat the process, but of course our second result is practically the same as the first. Hence, it is not necessary to do so.

254 Correlations and Data for Heat Transfer Coefficients

The conclusion that the gas temperature is lower than the metal temperature when it exits from the lance becomes significant when the bubble size is calculated in order to obtain the surface area and residence time for calculations of mass transfer. Since the gas is not fully expanded when it exits from the pipe, the bubble size, calculated on the basis of the pipe size, is smaller than the ultimately expanded bubble size, and the rate of rise is faster than anticipated on the basis of the pipe size.

8.2 HEAT TRANSFER COEFFICIENTS FOR FORCED CONVECTION PAST SUBMERGED OBJECTS

In the following correlations, the heat transfer coefficient h is defined for the total surface area of the submerged object, and the defining fluid temperature is that far removed from the surface. We evaluate all the properties, however, at the *film temperature*, $T_f = (T_0 + T_\infty)/2$.

In Fig. 8.5, $j_H = Nu_f Re_f^{-1} Pr_f^{1/3}$ is plotted versus Re for a long cylinder perpendicular to the fluid. The figure also shows a plot of $f/2$ versus Re to illustrate that $j_H < f/2$, which is usually the case in flows with curved streamlines. Colburn's analogy breaks down here because of the form drag which has no counterpart in heat transfer.

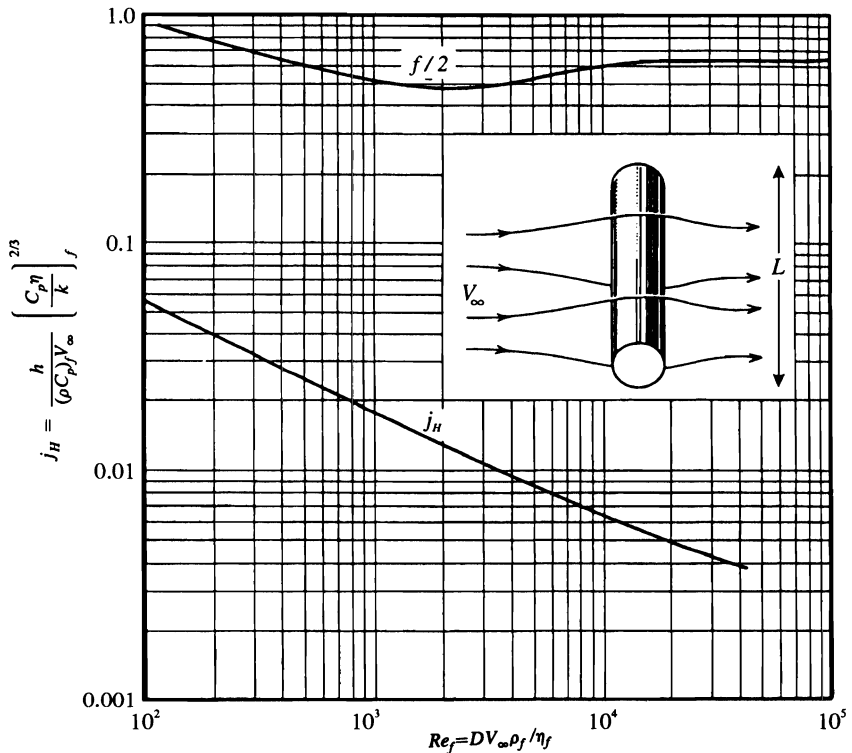


Fig. 8.5 Heat and momentum transfer for a cylinder perpendicularly oriented to flow. (j_H from T. K. Sherwood and R. L. Pigford, *Absorption and Extraction*, second edition, McGraw-Hill, New York, 1952, page 70; f from F. Eisner, see Fig. 3.9.)

These results agree closely with McAdams' correlation³ which is based on experiments with water, oils, and air. Over the range $1 < Re_f < 10^3$, McAdams specifies

$$Nu_f Pr_f^{-0.3} = 0.35 + 56 Re_f^{0.52}. \quad (8.8)$$

For higher Reynolds numbers, $10^3 < Re < 5 \times 10^4$, data collected for air are correlated by

$$Nu_f Pr_f^{-0.3} = 0.26 Re_f^{0.60}. \quad (8.9)$$

More recent correlations are summarized by Holman,⁴ among which the most comprehensive is that given by Churchill and Bernstein:⁵

$$Nu_f = 0.3 + \frac{0.62 Re_f^{1/2} Pr_f^{1/3}}{\left[1 + (0.4/Pr_f)^{2/3}\right]^{3/4}} \left[1 + \left(\frac{Re_f}{2.82 \times 10^5}\right)^{5/8}\right]^{4/5} \quad (8.10)$$

for $10^2 < Re_f < 10^7$ and $Re_f Pr_f > 0.2$. Equation (8.10) was tested against data for air, water, and liquid sodium so it has a wide range of applicability. Notice, however, that it is not useful for very small Reynolds numbers ($Re_f < 100$); furthermore it underestimates data somewhat in the range $2 \times 10^4 < Re_f < 4 \times 10^5$. For this range, the second brackets on the right-hand-side of Eq. (8.10) should be replaced with

$$1 + \left(\frac{Re_f}{2.82 \times 10^5}\right)^{1/2}.$$

Holman⁴ also gives correlations, based on empirical data, for heat transfer between fluids and noncircular cylinders.

Figure 8.6 gives Nu_f for the flow past a sphere. The relationship plotted is

$$hD/k_f = 2.0 + 0.60(DV_\infty \rho_f / \eta_f)^{1/2} (C_p \eta / k)^{1/3}. \quad (8.11)$$

This equation predicts that Nu approaches 2 as Re approaches zero; we can calculate this result for pure conduction, from a sphere at a uniform temperature in an infinite stagnant medium. Another correlation for heat transfer between fluids and spheres is that given by Whitaker:⁶

$$Nu_\infty = 2 + \left(0.4 Re_\infty^{1/2} + 0.06 Re_\infty^{2/3}\right) Pr_\infty^{0.4} \left(\frac{\eta_\infty}{\eta_s}\right)^{1/4}, \quad (8.12)$$

where the properties are evaluated at the temperature of the free stream, except η_s , which is the viscosity at the temperature of the sphere. The ranges for Eq. (8.12) are $0.71 < Pr_\infty < 380$, $3.5 < Re_\infty < 7.6 \times 10^4$, and $1.0 < (\eta_\infty / \eta_s) < 3.2$. Neither Eq. (8.11) nor (8.12) should be used for liquid metals.

³W. H. McAdams, *Heat Transmission*, third edition, McGraw-Hill, New York, 1954, page 268.

⁴J. P. Holman, *Heat Transfer*, sixth edition, McGraw-Hill, New York, 1986, pages 292-296.

⁵S. W. Churchill and M. Bernstein, *J. Heat Transfer* **99**, 300 (1977).

⁶S. Whitaker, *AIChE J.* **18**, 361 (1972).

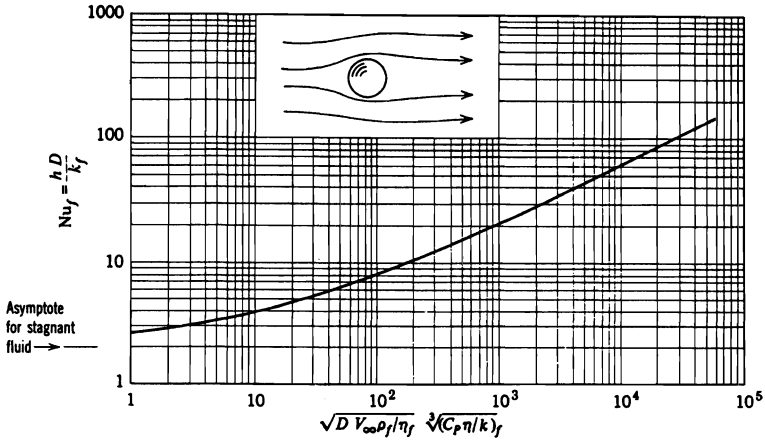


Fig. 8.6 Heat transfer from a sphere to a flowing fluid. (From W. E. Ranz and W. R. Marshall, Jr., *Chem. Eng. Prog.* **48**, 141-146, 173-180 (1952).)

Figure 8.7 shows results for the flow parallel to an isothermal semi-infinite flat plate. For this flow system, the Colburn analogy holds very well because there is no form drag; therefore, the local heat transfer coefficient is related to the friction factor by

$$\frac{h_x}{C_p \rho V_\infty} \text{Pr}^{2/3} = \frac{f_x}{2}. \tag{8.13}$$

For turbulent flow (from Fig. 3.5), $f_x = 0.0592 \text{Re}_x^{-1/5}$; then Eq. (8.13) is

$$\frac{h_x}{C_p \rho V_\infty} \text{Pr}^{2/3} = 0.0296 \text{Re}_x^{-1/5}, \tag{8.14}$$

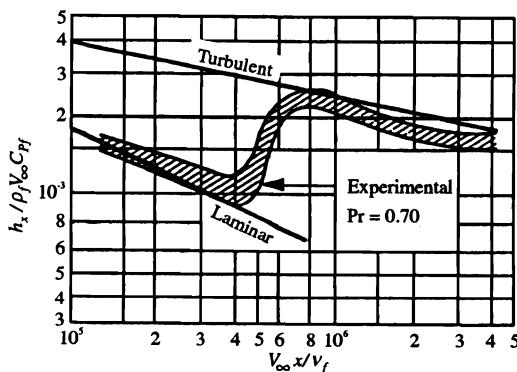


Fig. 8.7 Heat transfer coefficient for flow over flat plate with turbulent boundary layer and uniform heat flux. Experimental data collected for air, and compared to the analysis for turbulent flow (Eq. (8.12)), and laminar flow (Eq. (7.27)). (From R. A. Seban and D. L. Doughty, *Trans. ASME* **78**, 217 (1956).)

or

$$\frac{h_x x}{k} = \text{Nu}_x = 0.0296 \text{Re}_x^{0.8} \text{Pr}^{1/3}. \quad (8.15)$$

The average coefficient h between $x = 0$ and $x = L$ is

$$hL/k = \text{Nu}_L = 0.037 \text{Re}_L^{0.8} \text{Pr}^{1/3}. \quad (8.16)$$

(Here the initial part of the plate where laminar flow could exist has been ignored.)

Equation (8.15) overestimates the experimental data by approximately 4 to 19 pct. The agreement can be improved simply by modifying Eq. (8.15), so it becomes

$$\text{Nu}_x = 0.026 \text{Re}_x^{0.8} \text{Pr}^{1/3}. \quad (8.17)$$

The data agree with the laminar boundary layer result (Eq. (7.27)). Note that Eqs. (8.13)-(8.17) are valid for $\text{Pr} > 0.5$, but not for liquid metals; the equations are valid for either uniform wall temperature or uniform heat flux.

Example 8.2 A hot-wire anemometer is a device which indirectly measures the velocity of a moving fluid. It is usually a platinum wire which is heated electrically and positioned normal to the motion of the fluid. At a steady power input to the wire, its temperature reaches a steady value which can be related to the fluid velocity. The temperature of the wire is determined by measuring current, voltage drop, and hence electrical resistance, and by knowing how the resistance varies with the temperature. Thus, both the heat flux—from the wire to the fluid—and the wire temperature are measured electrically. Given air at 290 K flowing normal to the wire (3 mm in diameter) at 330 K, with a heat flux of 6300 W m^{-2} , determine the velocity of the air.

Solution. Assume that Eq. (8.9) applies:

$$\text{Nu}_f \text{Pr}_f^{-0.3} = 0.26 \text{Re}_f^{0.60},$$

$$h = \frac{q_0}{\Delta T} = \frac{6300}{(330 - 290)} = 157.5 \text{ W m}^{-2} \text{ K}^{-1}.$$

Use the properties of air at $T_f = 310 \text{ K}$: $\rho = 1.13 \text{ kg m}^{-3}$; $C_p = 1.01 \times 10^3 \text{ J kg}^{-1} \text{ K}^{-1}$; $k = 27.0 \times 10^{-3} \text{ W m}^{-1} \text{ K}^{-1}$; $\eta = 1.89 \times 10^{-5} \text{ kg m}^{-1} \text{ s}^{-1}$; $\text{Pr}_f = 0.705$.

$$\text{Nu}_f = \frac{hD}{k_f} = \frac{(157.5)(0.003)}{(27.0 \times 10^{-3})} = 17.5,$$

$$\text{Re}_f^{0.60} = \frac{(17.5)}{(0.705)^{0.3}(0.26)} = 74.75,$$

$$\text{Re}_f = 1326.$$

Thus, Eq. (8.9) applies as assumed, and

$$V_\infty = \left[\frac{\eta_f}{\rho_f} \right] \left[\frac{\text{Re}_f}{D} \right] = \left[\frac{1.89 \times 10^{-5}}{1.13} \right] \left[\frac{1326}{0.003} \right] = 7.40 \text{ m s}^{-1}.$$

8.3 HEAT TRANSFER COEFFICIENTS FOR NATURAL CONVECTION

In Chapter 7, the discussion of natural convection in laminar flow led to a dimensionless equation of the form

$$\text{Nu} = \text{Nu}(\text{Gr}, \text{Pr}).$$

This corresponds to the results of dimensional analysis in this chapter if the Reynolds number, the important number for forced convection, is replaced by the Grashof number, the important number for natural convection.

Figure 8.8 shows the results of correlating experimental data for free convection from vertical plates and horizontal cylinders to gases and liquids with Prandtl numbers ranging from about 0.5 to 10. The effect of the variation of properties with temperature is included by evaluating properties at $T_f = \frac{1}{2}(T_0 + T_\infty)$. The dimensionless numbers are then defined as $\text{Nu}_L \equiv \frac{hL}{k_f}$, $\text{Pr} \equiv \frac{\nu_f}{\alpha_f} = \frac{C_p \eta_f}{k_f}$, and $\text{Gr}_L \equiv g \frac{L^3 \rho_f^2 \beta_f (T_0 - T_\infty)}{\eta_f^2}$.

The characteristic dimension L is the plate length. For cylinders, the characteristic dimension is one-half the circumference, that is, $\pi D/2$; by defining L as such, note how closely the curves for the two different correlations lie. In fact, very often no distinction is made between these two cases, and a third case, namely, that of vertical cylinders with characteristic dimension taken as length, is included in the correlations.*

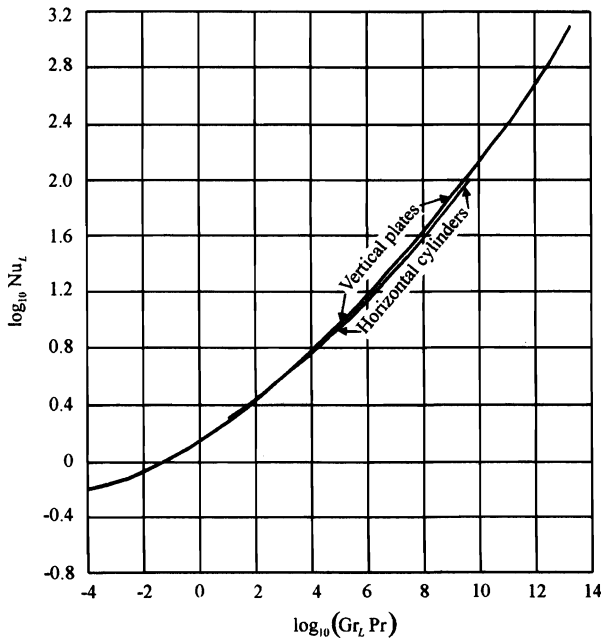


Fig. 8.8 Heat transfer coefficients for natural convection. (From W. H. McAdams, *ibid.*, pages 173-176.)

*This procedure can be followed when $(D/L) \geq 35/(\text{Gr}_L^{1/4})$ and L is vertical length.

In Chapter 7, Ostrach's analysis of laminar natural convection past vertical plates led to Eq. (7.45). This relationship holds in the laminar flow region $10^4 < Gr Pr < 10^9$ for a wide range of Prandtl numbers ($0.00835 \leq Pr \leq 1000$). For the sake of completeness, let us repeat it:

$$\frac{Nu_L}{\sqrt[4]{Gr_L/4}} = \frac{0.902 Pr^{1/2}}{(0.861 + Pr)^{1/4}} \quad (7.45)$$

In the range of $0.6 < Pr < 10$, the data can be represented by a much simpler equation (still for laminar flow):*

$$Nu_L = 0.56(Gr_L Pr)^{1/4} \quad (8.18)$$

For liquid metals, the data in the laminar range for horizontal cylinders were correlated by⁷

$$Nu_D = 0.53 \left[\frac{Pr}{0.952 + Pr} \right]^{1/4} (Gr_D Pr)^{1/4} \quad (8.19)$$

The expression is of the same form as Eq. (7.45), and also closely corresponds numerically if the characteristic dimension D (diameter) is replaced by L taken as $\pi D/2$.

In the turbulent range of $10^9 < Gr Pr < 10^{12}$, the following equation has been proposed as possibly valid for a wide range of Pr for vertical plates⁸ and horizontal cylinders with L replaced by $\pi D/2$:

$$Nu_L = 0.0246 Gr_L^{2/5} Pr^{7/15} (1 + 0.494 Pr^{2/3})^{-2/5} \quad (8.20)$$

We use a much simpler form of Eq. (8.20) for $0.6 < Pr < 10$:

$$Nu_L = 0.13 (Gr_L Pr)^{1/3} \quad (8.21)$$

Perhaps the most encompassing correlation for natural convection heat transfer from long horizontal cylinders is that of Churchill and Chu⁹; it is

$$Nu_D = \left\{ 0.60 + \frac{0.387 (Gr_D Pr)^{1/6}}{[1 + (0.559/Pr)^{9/16}]^{8/27}} \right\}^2 \quad (8.22)$$

which applies for $10^{-5} < Gr_D Pr < 10^{12}$. In situations involving natural convection and mixed convection (forced convection plus natural convection) from very small diameter (< 0.01 mm) cylinders, the results of Gebhart *et al.*¹⁰ can be consulted.

*To make a distinction between plates and cylinders in Fig. 8.8, the coefficient 0.56 in Eq. (8.18) should be replaced by 0.59 and 0.53, respectively.

⁷Reactor Handbook 2; Engineering, AEC-3646 (May, 1955), page 283.

⁸W. M. Rohsenow and H. Y. Choi, *ibid.*, page 204.

⁹S. W. Churchill and H. H. S. Chu, *Int. J. Heat Mass Transfer* **18**, 1049 (1975).

¹⁰B. Gebhart, T. Andunson and L. Pera, in *Heat Transfer 1970*, U. Grigull and E. Hahne (editors), Elsevier Publishing, Amsterdam, 1970, Session NC3.2.

260 Correlations and Data for Heat Transfer Coefficients

For a single *sphere* of diameter D in a body of fluid, the relationship

$$\text{Nu}_D = 2 + 0.060 \text{Gr}_D^{1/4} \text{Pr}^{1/3}. \quad (8.23)$$

agrees with available data for $\text{Gr}_D^{1/4} \text{Pr}^{1/3} < 200$. In most instances, if the fluid is a gas, this restriction means that the equation applies to small particles. Note that the relationship yields $\text{Nu}_D = 2$ when the fluid is motionless, as in Problem 7.14 where free convection is neglected.

Churchill¹¹ gives the following correlation for spheres in fluids with $\text{Pr} \geq 0.7$ and $\text{Gr}_D \text{Pr} \leq 10^{11}$:

$$\text{Nu}_D = 2 + \frac{0.589 \text{Gr}_D^{1/4} \text{Pr}^{1/4}}{\left[1 + (0.469/\text{Pr})^{9/16}\right]^{4/9}}. \quad (8.24)$$

Example 8.3 Write an expression to relate the growth rate of a single spherical nucleus of solid as it develops in a pure supercooled liquid. Express the result in terms of dR/dt as a function of supercooling ΔT and the properties of the metal. The thermal profile is depicted below; the temperature of the solid may be assumed as the freezing point T_M .

Solution. The rate at which latent heat of fusion evolves is equal to the rate at which heat flows from the interface into the bulk liquid

$$4\pi\rho_s H_f R^2 \frac{dR}{dt} = 4\pi R^2 h \Delta T,$$

where ρ_s = density of the solid, H_f = latent heat of fusion, and $\Delta T = T_M - T_\infty$ = amount of undercooling;

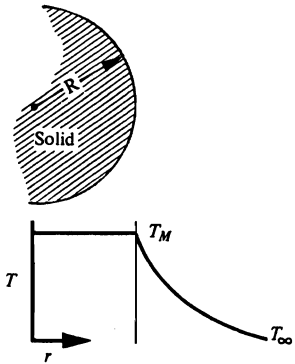
$$\frac{dR}{dt} = \frac{h}{\rho_s H_f} \Delta T.$$

From Eq. (8.23),

$$\frac{hD}{k} = 2 + 0.060 \left[\frac{D^3 \rho^2 g \beta \Delta T}{\eta^2} \right]^{1/4} \left[\frac{\eta C_p}{k} \right]^{1/3}.$$

When this is substituted into the expression for dR/dt , we obtain

$$\frac{dR}{dt} = \frac{k\Delta T}{\rho_s H_f} \left[\frac{1}{R} + 0.0504 \left[\frac{\rho^2 g \beta \Delta T}{R \eta^2} \right]^{1/4} \left[\frac{\eta C_p}{k} \right]^{1/3} \right].$$



¹¹S. W. Churchill, "Free Convection Around Immersed Bodies," in E. U. Schlünder, Ed.-in-Chief, *Heat Exchanger Design Handbook*, Section 2.5.7, Hemisphere Publishing Corp., New York, 1983.

Students of phase transformations are invited to use this as a basis for further discussion and/or refinement.

In the previous discussion of this section, heat transfer took place in the presence of convection mostly in the vertical direction. The convection behavior in the vicinity of horizontal surfaces is quite different, as shown in Fig. 8.9, and the correlations of Eqs. (8.18)-(8.21) do not apply. McAdams¹² recommends the following equations for some situations of natural convection from *horizontal* surfaces:

1. For a square plate with a surface warmer than the fluid facing upward, or cooler surface facing downward:

$$Nu_L = 0.14(Gr_L Pr)^{1/3}, \quad (8.25)$$

in the turbulent range, $2 \times 10^7 < Gr_L < 3 \times 10^{10}$, and

$$Nu_L = 0.54(Gr_L Pr)^{1/4}, \quad (8.26)$$

in the laminar range, $10^5 < Gr_L < 2 \times 10^7$.

2. For a square plate with a surface warmer than the fluid and facing downward, or cooler surface facing upward:

$$Nu_L = 0.27(Gr_L Pr)^{1/4}, \quad (8.27)$$

for $10^6 < Gr_L Pr < 10^{11}$.

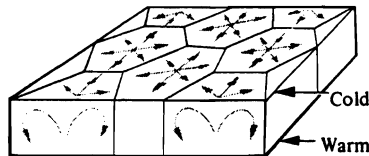


Fig. 8.9 The convection pattern over a horizontal surface which is warmer than the fluid.

In Eqs. (8.25)-(8.27), L is the length of the side of the square. As approximations, we can also apply the equations to horizontal circular disks with L defined as $0.9 D$ (D being the disk diameter). The characteristic length, for a surface other than a square or a circle, should be taken as $L = A/P$ where A is the surface area and P is the perimeter.

In this very brief exposition of correlations used to estimate heat transfer coefficients, we have omitted many different geometrical and flow configurations. We recommend that

¹²W. H. McAdams, *ibid.*, page 180.

262 Correlations and Data for Heat Transfer Coefficients

interested readers consult heat transfer texts, such as Holman,¹³ Incropera and DeWitt,¹⁴ Azbel,¹⁵ and Karlekar and Desmond.¹⁶

8.4 QUENCHING HEAT TRANSFER COEFFICIENTS

In the next chapter, we present analytical expressions which describe the temperature during heating or cooling as a function of time and position within a solid. The most difficult variable to ascribe to such unsteady-state situations is probably the heat transfer coefficient governing the energy transport between the solid's surface and the surroundings. The methods of estimating h for some convection systems, which were presented in previous sections of this chapter, can be applied satisfactorily to certain problems of unsteady-state heat flow. For the most part, however, correlations of h -values applicable to quenching operations have not been obtained because of the complexity of the convection systems.

Despite the importance of quenching operations in the heat treatment of alloys, materials engineers have not considered nearly enough of the quantitative aspects of quenching heat transfer, which is strongly linked to boiling heat transfer. Historically, the primary purpose of boiling heat transfer has been simply the conversion of liquid into vapor, and perhaps this is the reason why it has not been studied enough by materials engineers. On the other hand, engineers who are involved with the development of nuclear reactors, rocket nozzles, and spacecraft have conducted considerable research into the boiling process.

Although boiling is a familiar phenomenon, from the point of view of energy transport it is a complicated process. Figure 8.10 illustrates the complexities of boiling in which several regimes exist. If a heated metal surface is submerged in a pool of liquid at its saturation temperature, T_{sat} , the following events take place. As the surface temperature T_w is raised above T_{sat} , convection currents circulate within the superheated liquid. Heat transfer with convection takes place, and the correlations discussed for natural convection in Section 8.3 apply. However, the liquid cannot be indefinitely superheated so that further increases of $(T_w - T_{sat})$ above approximately 2 K are accompanied by vapor bubbles forming at preferred sites on the surface. This is regime II, in which most of the bubbles do not exceed a certain size necessary for their escape. In regime III, $(T_w - T_{sat})$ is large enough so that larger and more stable bubbles grow, and at the same time more bubbles form because more nucleation sites become active on the solid's surface. This mechanism, which is called nucleate boiling, can generate very high heat fluxes. As the bubbles rapidly form and detach themselves from the surface, fresh liquid rushes to the former bubble site, and the very rapid process of bubble formation and detachment repeats itself over and over again. The net result is that all the bubble sites act as micropumps and create a large degree of convection at the surface.

If $(T_w - T_{sat})$ is raised to even higher values, for example, 40 K in water, then the nucleation sites on the surface become so numerous that the bubbles coalesce, and tend to

¹³J. P. Holman, *ibid.*, Chapters 6 and 7.

¹⁴F. P. Incropera and D. P. DeWitt, *Fundamentals of Heat and Mass Transfer*, third edition, John Wiley, New York, NY, Chapters 7, 8, and 9, 1990.

¹⁵D. Azbel, *Fundamentals of Heat Transfer for Process Engineering*, Noyes Publications, Park Ridge, NJ, Chapter 3, 1984.

¹⁶B. V. Karlekar and R. M. Desmond, *Engineering Heat Transfer*, West Publishing, St. Paul, MN, Chapters 8 and 9, 1977.

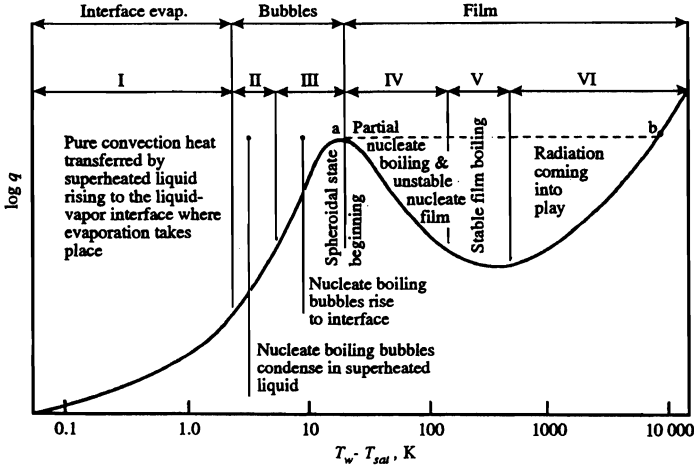


Fig. 8.10 Characteristic boiling curve. (From W. M. Rohsenow, *Developments in Heat Transfer*, MIT Press, Cambridge, MA, 1964, Chapter 8.)

form a vapor blanketing layer. Beyond this point, the heat flux decreases with increasing $(T_w - T_{sat})$ because of the vapor's insulating nature.* Regime IV encompasses this effect wherein an unstable vapor film forms but collapses and reforms rapidly. For values of $(T_w - T_{sat})$ greater than about 480 K (for water), a stable film exists (regime V). This is called *film boiling*, with which rather low heat fluxes are associated (contrasted to nucleate boiling); for values of $(T_w - T_{sat})$ greater than 920 K, radiation across the vapor blanket becomes important, and the rate of heat transfer increases accordingly.

Returning to quenching, we see that Fig. 8.11 shows a typical cooling curve of a metal part plunged into water. Note the three distinct stages during the cooling process. Stage A, called the vapor cooling stage, occurs immediately upon immersing the part in the water. Liquid vaporizes adjacent to the surface and forms a continuous vapor film. Cooling during this stage proceeds by film boiling and, if the part is at a sufficiently high temperature (i.e., steel), also by radiation. The second stage, B, is often denoted as the "vapor transport stage." This term is not really appropriate because during this stage there is a transition from

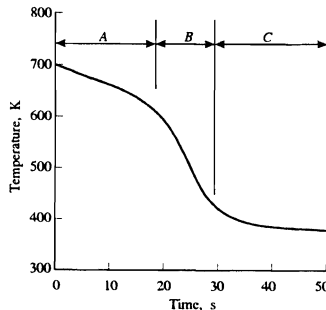


Fig. 8.11 Cooling curve of a metal part quenched in water.

*Heated solid surfaces are subjected to *burnout*, unless the heating is reduced, because the operating point of the system will jump from point a to point b on the boiling curve.

264 Correlations and Data for Heat Transfer Coefficients

partial nucleate boiling and unstable film boiling to entirely nucleate boiling. During stage *C*, referred to as the liquid cooling stage, there is less vapor formation, and eventually cooling occurs by only natural convection. Thus we see that as the metal cools from its initial elevated temperature to the fluid's temperature, it passes through all the regimes of the boiling curve (Fig. 8.10).

For these and other reasons, no comprehensive body of engineering correlations has evolved and been applied to quenching problems. Rather, most of the literature give some average values of h which apply to specific cases.

For example, we can find the values of a parameter H , known as the *severity of quench*, and defined as h/k , which represent quenching practices for steel. Table 8.1 gives some typical values of H .

Table 8.1 Severity of quench values and heat transfer coefficients for steel^a

Quench media	H -value, m^{-1}	h , $W\ m^{-2}\ K^{-1}$
Oil, no agitation	7.9	270
Oil, moderate agitation	13.8	480
Oil, good agitation	19.7	680
Oil, violent agitation	27.6	970
Water, no agitation	39.4	1400
Water, strong agitation	59.0	2000
Brine, no agitation	78.7	2700
Brine, violent agitation	196	6800

^aValues of H from M. A. Grossman, *Elements of Hardenability*, ASM, Cleveland, 1952; values of h calculated using $k = 35\ W\ m^{-1}\ K^{-1}$.

Data from this table should be applied only to conditions for which the values are derived. For example, h can depend strongly on the temperature of the liquid media alone. The values shown above are for quenchants at room temperature. In addition, during quenching h varies with the temperature of the solid itself. The values in Table 8.1 are derived specifically to predict the time to cool steel from its austenizing temperature to a temperature midway between the austenizing and original quench temperatures. Therefore all that we can say about the above h -values is that they are average and apply during cooling from about 1090 K to 690 K. It is left to the reader to comprehend the "political" terms—moderate agitation, good agitation, and violent agitation—given in Table 8.1.

For precipitation-hardenable aluminum alloys, an important step in their heat treatment is the cooling rate during quenching from the homogenization temperature. If the cooling rate is too low through a critical range of about 700 to 530 K, then precipitation occurs, and subsequent aging cannot be controlled. On the other hand, if the cooling rate during quenching is too great, then intolerable distortion in many parts occurs. In practice, therefore, heat treaters usually quench aluminum alloys in heated water to slow cooling and minimize distortion.

Brines, quenching oils, polymer solutions, and emulsions are used for quenching, in addition to water. Technological aspects, as well as heat transfer characteristics, of various quenchants are discussed in *Metals Handbook*¹⁷ and in Sinha.¹⁸ Usually, one of these

¹⁷*Metals Handbook*, Ninth edition, vol. 4, American Society for Metals, Metals Park, OH, 1981, pages 31-68 and 688-695.

¹⁸A. K. Sinha, *Ferrous Physical Metallurgy*, Butterworths Publ., Boston, MA, 1989, pages 442-460.

alternatives to water is selected when lower cooling rates are needed, except for brine, which causes a faster quench.

Figure 8.12 gives heat transfer coefficients measured for as-casts billets of copper immersed vertically in water. Figure 8.13 gives some values of h for water/PAG (polyalkylene glycol) solutions based on experimentally measured cooling rates through the range 700-530 K. When solutions of PAG and water are used, h is dependent on concentration. In these instances, an immiscible PAG-rich liquid phase forms at about 350 K (the exact temperature depends on the concentration). Thus, near the hot solid, the liquid separates into two immiscible liquid phases, and the surface becomes coated with the very viscous PAG-rich phase. Therefore, the rate of heat transfer is not controlled by a water vapor film whose thickness is dependent on the bulk water temperature to a large extent, but rather by the layer of the PAG-rich phase whose thickness and properties are presumably more predictable and not so much dependent on the bulk liquid temperature. Hence, more uniform cooling and reduction of distortion are achieved.

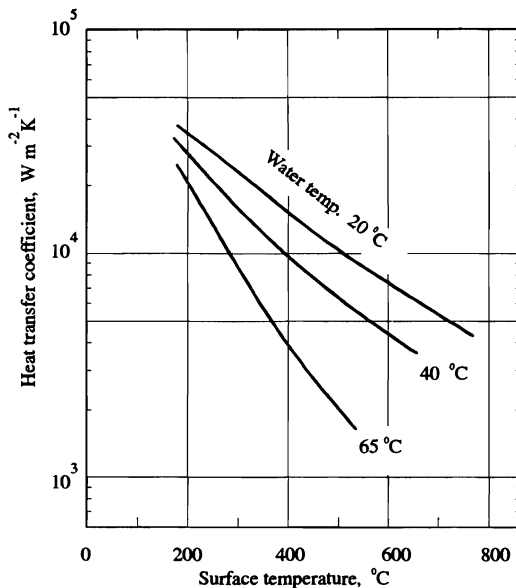


Fig. 8.12 Heat transfer coefficients for immersion of copper billets in water. (From M. Bamberger and B. Prinz, *Mat. Sci. Tech.* 2, 410-415 (1986).)

Stolz¹⁹ devised a numerical technique for obtaining heat transfer coefficients during quenching from measurements of interior temperatures of a solid sphere. By means of this technique heat transfer coefficients for quenching oils were evaluated as a function of the surface temperature of the solid. Figure 8.14 shows these data for oils designated as slow, intermediate, and fast. The figure also shows that between 1140 K and 895 K the heat transfer coefficients of all three types of oils are similar; over this range all three oils form a continuous vapor film on the solid's surface, and h is only about $570 \text{ W m}^{-2} \text{ K}^{-1}$. From 645 K to 325 K, similar heat transfer coefficients are found for all three oils. The main differences among these oils lie in the regions where the heat transfer coefficients are greater

¹⁹G. Stolz, Jr., *J. Heat Transfer* 82, 20-26 (1960).

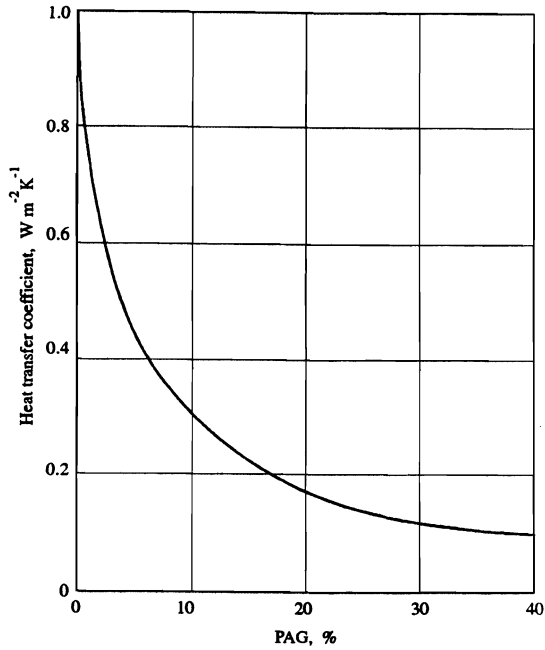


Fig. 8.13 Heat transfer coefficients for cooling aluminum through the critical range of 700-530 K in water and water-polyalkylene glycol (PAG) solutions. (Reproduced by permission of Progressive Metallurgical Industries, Gardena, CA.)

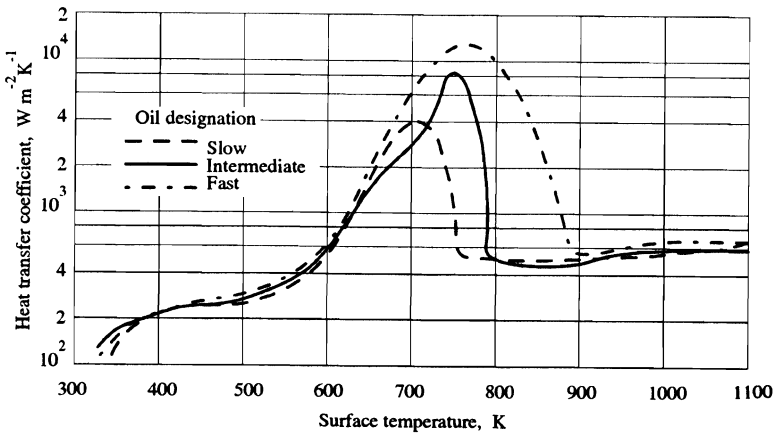


Fig. 8.14 Heat transfer coefficients in quenching oils. (From G. Stolz, V. Paschkis, C. F. Bonilla, and G. Acevedo, *JISI* 193, 116-123 (1959).)

than $570 \text{ W m}^{-2} \text{ K}^{-1}$, showing that the stable vapor film breaks down first (at a higher surface temperature) for the fast oil, and last for the slow oil.

The results for water and aqueous solutions of 1% NaOH and 5% NaOH are given in Fig. 8.15; all three solutions have a bulk temperature of 316 K. For these aqueous solutions, h is initially between 1700 and $5100 \text{ W m}^{-2} \text{ K}^{-1}$. In a quench, these initial values of h represent the rapid vaporization of water as the solid plunges into the water. This period is only a fraction of a second, after which h drops to values indicative of the vapor film stage, but this is short-lived, especially for the 5% NaOH solution. The marked increase in heat transfer in the presence of NaOH over the range 1050 K-500 K is due to exploding salt crystals that make the vapor film unstable. All three solutions, however, reach the same peak value of h at approximately 480 K.

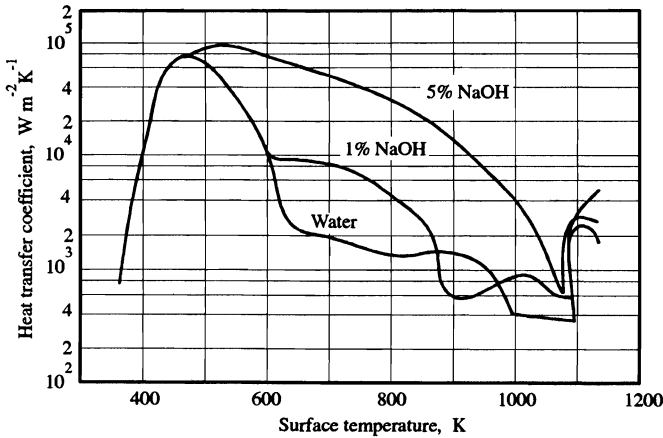


Fig. 8.15 Heat transfer coefficients in aqueous quenching media. (From V. Paschakis and G. Stolz, Heat and Mass Flow Analyzer Laboratory, Columbia University, New York.)

In order to quench very long metal shapes, such as the strip from a hot strip mill or a continuously cast slab, we often use a multiplicity of water sprays. Figure 8.16 shows cooling data with a fan-type spray of water at 294 K which impinges on a hot horizontal surface from above. There is a sharp increase in the heat flux at about 900-750 K, which represents a transition from boiling with a vapor film to nucleate boiling.

When the vapor film is present during spray cooling, the rate of heat transfer depends on the degree to which the steam film can be broken down by the impinging droplets. With sprays, the droplets approaching the hot metal surface encounter the vapor film, and their success in penetrating this film depends on their kinetic energy. If the sprays are placed closer to the metal surface or the water velocity is increased, thereby increasing the droplets' kinetic energy, then the probability that the droplets will penetrate the film increases and so does the rate of heat removal.

With this in mind, it has been argued that a continuous stream of water, because of its high kinetic energy associated with its large mass, should penetrate the vapor film and bring about an increase in heat transfer rates.²⁰ For this reason, large nozzles in combination with low water pressure have been utilized to produce a falling stream, or jet, of water which does not break into droplets. For such a jet, an increase in the flow rate of water increases

²⁰E. R. Morgan, T. E. Dancy, and M. Korchynsky, *J. Metals* 17, No. 8, 829-831 (1965).

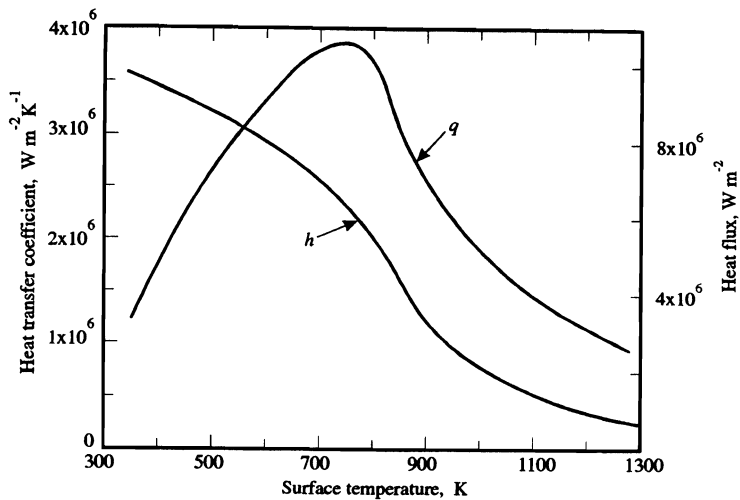


Fig. 8.16 Heat flux and heat transfer coefficients for cooling a horizontal surface from above with a fan-type spray of water at 294 K. (Adapted from P. M. Auman, D. K. Griffiths, and D. R. Hill, *Iron Steel Engineer*, Sept., 1967.)

the rate of heat transfer up to a point. If the jet-flow rate passes a critical value, then the falling jet breaks up into less effective droplets, and the rate of heat transfer decreases.

In addition to water sprays, oil sprays have been used for quenching. It was found in a study,²¹ that the cooling rate due to properly applied oil sprays was three to five times the cooling rate by immersing in oil in the conventional manner. Figure 8.17 shows some of these data.

Heat transfer coefficients for water spray cooling with slight overlapping of the spray cones are given in Fig. 8.18. Notice that results for immersion in water are also shown and that only the lines for the two highest spray intensities lie above the line for immersion in water.

8.5 HEAT TRANSFER COEFFICIENTS IN FLUIDIZED BEDS

Heat transfer in fluidized beds is of interest mainly because of a relatively new technology pertaining to combustion and gasification of solid fuels. Fluidized beds also are used extensively as dryers and chemical reactors. Here, however, we consider the fluidized bed as a possible medium for effecting the heating or cooling of immersed solids, as in heat treatment or quenching of metallic alloys.

Heat transfer between a fluidized bed and a solid surface immersed in the bed involves the convective heat transfer associated with the gas and the heat transfer associated with the contact between the fluidized particles and the immersed surface. The contact, itself, results in very little conduction and most of this heat transfer is associated with the complex

²¹N. V. Zimin, UDC 621.784.06, pages 854-858, Plenum Press, New York, 1968. Translated from *Metallovedenie i Termicheskaya Obrabotka Metallov*, No. 11, 62-68 (Nov., 1967).

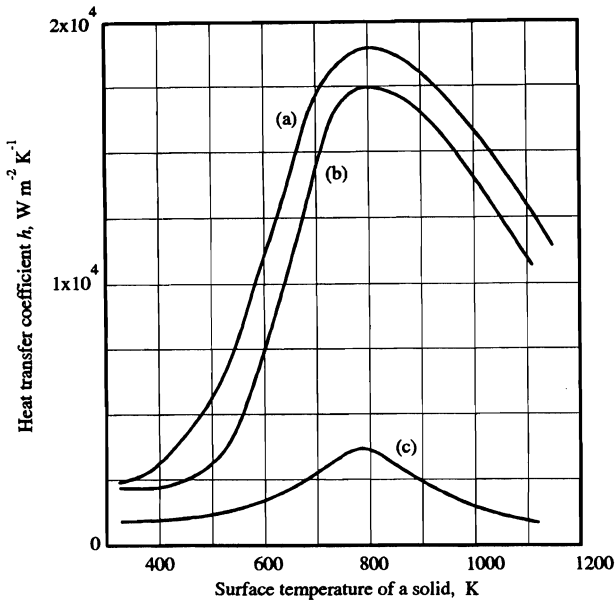


Fig. 8.17 Heat transfer coefficients for oil-spray quenching and immersion in oil. (a) Very strong spray; flow rate $> 0.70 \text{ m}^3 \text{ s}^{-1} \text{ m}^2$. (b) Strong spray; flow rate $= 0.60 \text{ m}^3 \text{ s}^{-1} \text{ m}^2$. (c) Still oil. (From Zimin, *ibid.*)

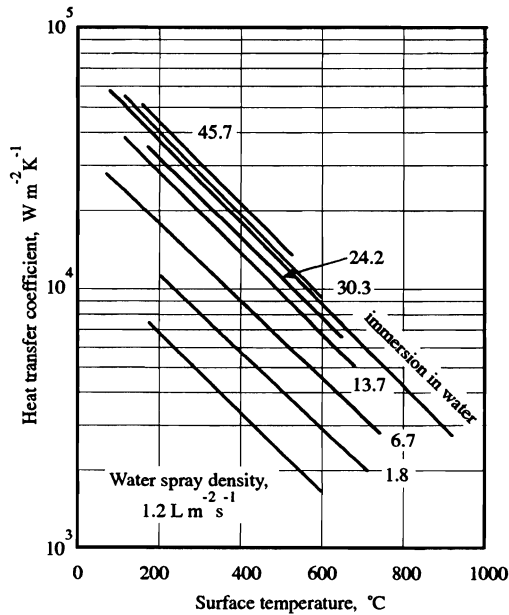


Fig. 8.18 Heat transfer coefficient as function of surface temperature during spray cooling with various spray intensities. (From M. Bamberger and B. Prinz, *ibid.*)

270 Correlations and Data for Heat Transfer Coefficients

convection between the contacting solids. In addition, heat transfer by radiation can be significant, so that correlations for heat transfer coefficients can be quite complicated. One such equation is the following:²²

$$\text{Nu} = 0.85 \text{Ar}^{0.1} \left[\frac{\rho_p}{\rho_g} \right]^{0.14} \left[\frac{C_p}{C_g} \right]^{0.24} (1 - \omega)^{2/3} + 0.046 \text{RePr} \frac{(1 - \omega)^{2/3}}{\omega} + \frac{\bar{D}}{k_g} \sigma^* (T_\infty^2 + T_s^2)(T_\infty + T_s). \quad (8.28)$$

Thermophysical properties are evaluated at $(T_\infty + T_s)/2$, and Nu has an error of ± 16 percent.

Equation (8.28) contains the usual Nusselt, Reynolds and Prandtl numbers for the fluid, as well as the Archimedes number, Ar, which is defined as

$$\text{Ar} = \frac{g \bar{D}^3 \rho_g (\rho_p - \rho_g)}{\eta_g^2}, \quad (8.29)$$

where g is gravitational acceleration, the subscripts g and p are for the gas and particles making up the bed, and \bar{D} is the mean diameter of the particles. \bar{D} is defined as

$$\bar{D} = \left[\sum_i \frac{\phi_i}{D_i} \right]^{-1}, \quad (8.30)$$

where ϕ_i is the mass fraction of particles with diameter of D_i . The Nusselt and Reynolds numbers are

$$\text{Nu} = \frac{h \bar{D}}{k_g},$$

and

$$\text{Re} = \frac{\bar{D} V_0}{\nu_g}.$$

Finally, the last term in Eq. (8.28) accounts for radiation with T_∞ taken as the temperature of the fluidized bed core (analogous to a free stream temperature in a single phase fluid) and T_s is the temperature of the surface of the immersed solid. The factor σ^* depends on the emissivities of the immersed solid, ϵ_s , and the effective emissivity of the bed, ϵ_e , according to

$$\sigma^* = \frac{\sigma}{\left[\frac{1}{\epsilon_s} + \frac{1}{\epsilon_e} - 1 \right]}, \quad (8.31)$$

²²V. A. Borodulya, Y. S. Teplitsky, I. I. Markevich, A. F. Hassan and T. P. Yeryomenko, *Int. J. Heat Mass Transfer* **34**, 47-53 (1991).

where $\sigma = 5.670 \times 10^{-8} \text{ W m}^{-2} \text{ K}^{-4}$,

$$\frac{\varepsilon_e}{\varepsilon_b} = A + (1 - A) \left[\frac{T_s}{T_\infty} \right]^4 \quad (8.32)$$

and

$$A = 1 - \exp \left(-0.16 \text{ Ar}_\infty^{0.26} \right), \quad (8.33)$$

where ε_b is calculated below and Ar_∞ is evaluated at T_∞ .

As if all of the above has not yet buried us completely, we must finally evaluate ε_b as follows:

$$\varepsilon_b = 1.63 \frac{\omega - \omega_{mf}}{1 - \omega_{mf}} \varepsilon_p^{0.310} + \left[1 - 1.63 \frac{\omega - \omega_{mf}}{1 - \omega_{mf}} \right] \varepsilon_p^{0.485}. \quad (8.34)$$

where ε_p is the intrinsic emissivity of the particles. Equation (8.28) is valid within the ranges: $0.1 \leq \bar{D} \leq 6 \text{ mm}$; $0.1 \leq P \leq 10 \text{ MPa}$; $293 \leq T_\infty \leq 1473 \text{ K}$; $293 \leq T_s \leq 1373 \text{ K}$; $1.4 \times 10^2 \leq \text{Ar} \leq 1.1 \times 10^7$.

Example 8.6 A bed of alumina particles (1 mm) is fluidized ($\omega = 0.6$) with air at 700 K and a superficial velocity of 3.5 m s^{-1} . Assume that the emissivity of the bed is 0.8 and the following data for the alumina particles apply: $C_p = 830 \text{ J kg}^{-1} \text{ K}^{-1}$, $\rho_p = 3900 \text{ kg m}^{-3}$. Calculate the heat transfer coefficient for heating nickel alloy parts ($\varepsilon_s = 0.5$) in the bed when $T_s = 300 \text{ K}$ and $T_\infty = 600 \text{ K}$.

Solution. First let's collect properties for air, with the bed operating at 1 standard atmosphere.

$T, \text{ K}$	$\rho_g, \text{ kg m}^{-3}$	$C_p, \text{ J kg}^{-1} \text{ K}^{-1}$	$k_g, \text{ W m}^{-1} \text{ K}^{-1}$	$\eta_g, \text{ N s m}^{-2}$
500	0.696	1030	40.7×10^{-3}	270×10^{-7}
600	0.584	1051	46.9×10^{-3}	306×10^{-7}
700	0.498	1075	52.4×10^{-3}	339×10^{-7}

With $T_\infty = 700 \text{ K}$,

$$\text{Ar}_\infty = \frac{g \bar{D}^3 \rho_g (\rho_p - \rho_g)}{\eta_g^2} = \frac{(9.81)(1 \times 10^{-3})^3 (0.498)(3900)}{(3.39 \times 10^{-5})^2} = 16\,580$$

and from Eq. (8.33)

$$A = 1 - \exp \left[-(0.16)(16\,580)^{0.26} \right] \approx 0.865.$$

The effective emissivity is calculated with Eq. (8.32); this gives

$$\frac{\varepsilon_e}{\varepsilon_b} = 0.865 + (1 - 0.865) \left[\frac{300}{700} \right]^4 = 0.870$$

*This is the Stefan-Boltzmann constant. Radiation heat transfer is the subject of Chapter 11, where this constant is discussed and used repeatedly.

272 Correlations and Data for Heat Transfer Coefficients

and

$$\varepsilon_e = 0.870 \varepsilon_b = (0.870)(0.8) = 0.696.$$

With Eq. (8.31), we have

$$\sigma^* = \frac{5.670 \times 10^{-8}}{\left[\frac{1}{0.5} + \frac{1}{0.696} - 1 \right]} = 2.33 \times 10^{-8} \text{ W m}^{-2} \text{ K}^{-4}.$$

Now we can evaluate the last term of Eq. (8.28); with $k_g(500 \text{ K}) = 0.0407 \text{ W m}^{-1} \text{ K}^{-1}$:

$$\begin{aligned} \frac{\bar{D}}{k_g} \sigma^* (T_\infty^2 + T_s^2)(T_\infty + T_s) &= \frac{(1 \times 10^{-3})(2.33 \times 10^{-8})(700^2 + 300^2)(700 + 300)}{0.0407} \\ &= 0.33. \end{aligned}$$

This calculation tells us that radiation heat transfer cannot be neglected at these temperatures.

With $T_s = 300 \text{ K}$, the properties of the gas are evaluated at $(700 + 300)/2 = 500 \text{ K}$:

$$\text{Ar} = \frac{(9.81)(1 \times 10^{-3})^3(0.696)(3900)}{(2.70 \times 10^{-3})^2} = 3.65 \times 10^4; \quad \frac{\rho_p}{\rho_g} = \frac{3900}{0.696} = 5600;$$

$$\frac{C_p}{C_g} = \frac{830}{1030} = 0.806; \quad \text{Re} = \frac{(1 \times 10^{-3})(3.5)(0.696)}{2.70 \times 10^{-5}} = 90.2;$$

$$\text{Pr} = 0.684 \quad \text{and} \quad \omega = 0.6.$$

We substitute these values into Eq. (8.28):

$$\begin{aligned} \text{Nu} &= (0.85)(3.65 \times 10^4)^{0.1} (5600)^{0.14} (0.806)^{0.24} (1 - 0.6)^{2/3} \\ &\quad + (0.046)(90.2)(0.684) \frac{(1 - 0.6)^{2/3}}{0.6} + 0.33 \\ &= 4.19 + 2.57 + 0.33 = 7.09. \end{aligned}$$

Therefore,

$$h = \frac{k_g \text{Nu}}{\bar{D}} = \frac{(0.0407)(7.09)}{(1 \times 10^{-3})} = 289 \text{ W m}^{-1} \text{ K}^{-1}.$$

When $T_s = 600 \text{ K}$, the properties are evaluated at 650 K ; otherwise the same procedure is followed. The results are $\text{Nu} = 6.07$ and $h = 301 \text{ W m}^{-1} \text{ K}^{-1}$. The heat transfer coefficient changes by only 4.3 percent.

8.6 HEAT-TRANSFER COEFFICIENTS IN PACKED BEDS

The heat transfer coefficient for flow through packed beds could be given by an expression of the form $\text{Nu} = A \text{Re}^n \text{Pr}^m$. Here we are dealing exclusively with gases as the fluid phase, and since the Prandtl numbers of gases are all about equal over a wide range of temperatures, there is not any strong dependence of Nu or Pr for gas-solid heat transfer. So we are left with finding the relationship between Nu and Re. However, this is much easier said than

done, as most of the experimental work on this subject has been confined to much lower temperatures than those of most metallurgical processes.

The highest temperatures—1100°C—were employed by Furnas²³ in 1932. Kitaev and coworkers²⁴ summarized the results of the pertinent studies at elevated temperatures, and also some at lower temperatures. Their review includes a complete reanalysis of Furnas' data. They present the results with the volumetric heat-transfer coefficient, h_v , in a dimensional equation

$$h_v = \frac{AV_{0g}^{0.9}T^{0.3}f(\omega)}{D_p^{0.75}}, \quad (8.35)$$

where $h_v = hS =$ volumetric heat transfer coefficient, kcal m⁻³ h⁻¹ K⁻¹

$A =$ a coefficient dependent on bed material,

$T =$ temperature, °C,

$D_p =$ particle diameter, mm,

$V_{0g} =$ superficial gas velocity, m s⁻¹

$f(\omega) =$ function of void fraction.

For natural, lump materials, $A = 160$ and $f(\omega) = 0.5$, so that

$$h_v = \frac{80V_{0g}^{0.9}T^{0.3}}{D_p^{0.75}}.$$

A nomogram was developed, Fig. 8.19, which facilitates the determination of h_v . Pape *et al.*²⁵ experimentally confirmed the predictions of Fig. 8.19 up to 1100°C for 10 mm pellets.

For spheres, the equation

$$h_v = \frac{12V_{0g}T^{0.3}}{D_p^{1.35}} \quad (8.36)$$

agrees with Furnas' results and those of Saunders and Ford,²⁶ when D_p is in meters.

Example 8.7 Estimate the volumetric heat transfer coefficient in a shaft furnace in which hot gases (1200°C) are used to heat iron oxide pellets, 25 mm in diameter. The gas velocity is 1.0 m s⁻¹.

Solution. Entering the nomograph at 1.0 m s⁻¹, going up to 1200°C, across to 25 mm, and down, we find that $h_v = 12\,500$ kcal m⁻³ h⁻¹°C⁻¹. This becomes

$$h_v = \frac{12\,500 \text{ kcal}}{\text{m}^3 \text{ h } ^\circ\text{C}} \quad \left| \quad \frac{4.184 \times 10^3 \text{ J}}{1 \text{ kcal}} \quad \right| \quad \left| \quad \frac{1 \text{ h}}{3600 \text{ s}} \quad \right| \quad \left| \quad \frac{1^\circ\text{C}}{1 \text{ K}} \right|$$

²³C. C. Furnas, *U.S. Bureau Mines Bull.*, No. 261 (1932).

²⁴B. I. Kitaev, Y. G. Yaroshenko, and V. D. Suchkov, *Heat Exchange in Shaft Furnaces*, Pergamon Press, New York, 1968.

²⁵P. O. Pape, R. Frans and G. H. Geiger, *Ironmaking and Steelmaking*, 138 (1976).

²⁶O. H. Saunders and H. Ford, *JISI I*, 292 (1940).

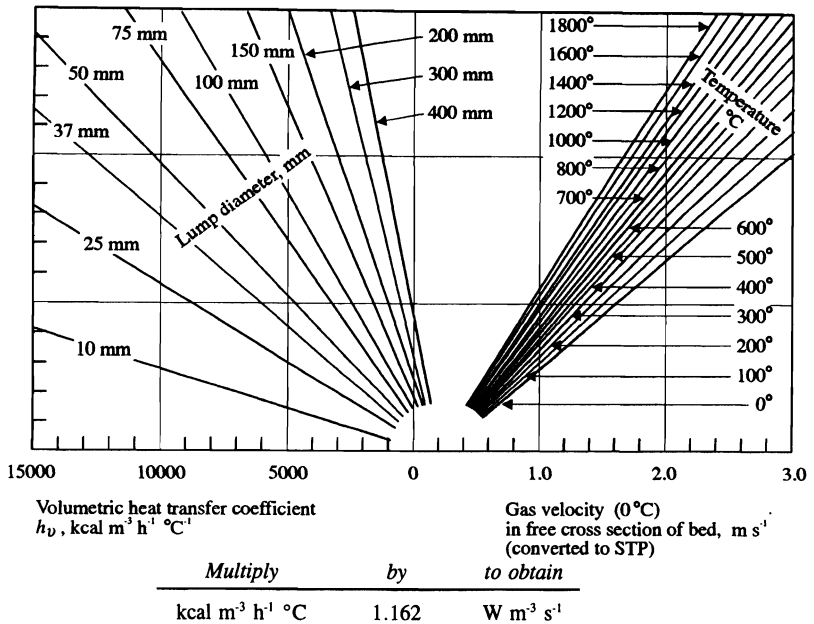


Fig. 8.19 Nomograph for the volumetric heat transfer coefficient hS or h_v , based on knowledge of the superficial gas velocity, V_{0g} , the gas temperature, and the particle diameter D_p . (Adapted from B. I. Kitaev *et al.*, *ibid.*)

8.7 HEAT TRANSFER COEFFICIENTS IN FORGING

Forging involves deformation of alloys at a temperature where the stresses to strain the material are relatively low. As an alloy is forged it loses heat to the forging die, which causes a decrease in the workpiece temperature and an increase in the deformation stresses. Thus, it is important to predict the heat transfer from the workpiece to the die because this has a direct bearing on the power required to carry out the forging operation and on the ability of the metal to plastically deform and fill the die cavity. We must also realize that the heat loss from the workpiece represents a heat gain by the die. For one thing, there is a softening of the surface of the die making it more subject to plastic deformation and wear. The die is also subject to thermal fatigue because the temperature at the die surface fluctuates cyclically. Knowledge of the heat transfer between the workpiece and the die is, therefore, important, and in order to model the forging process we should have data on the so-called *contact heat transfer coefficient*.

It is the rule rather than the exception that, when two solids of a different temperature are brought into contact, there is a discontinuity of temperature at the contact interface. At the microscopic level some of the asperities on the two surfaces touch each other to form paths for energy conduction, but otherwise the energy is transferred by radiation across the tiny depressions and by conduction through fragmented oxide layers and lubrication films.

The actual heat transfer process is so complex that we normally rely on empirical measurements of the contact heat transfer coefficient, which is defined as

$$h = \frac{q}{\Delta T} \quad (8.37)$$

where q is the flux ($W m^{-2}$) and ΔT is the temperature difference at the interface of the two pieces in contact. Figure 8.20 gives some data for the contact heat transfer coefficient of an aluminum alloy (Al 6061-O) at various temperatures of the die (H-12 tool steel). The contact heat transfer coefficient varies with both forging pressure (i.e., the normal stress at the surface) and temperature of the workpiece, as well as the surface roughness, the type of lubricant, and the temperature of the die material. These factors should be considered in using contact heat transfer coefficients for estimating temperature distributions during forging.

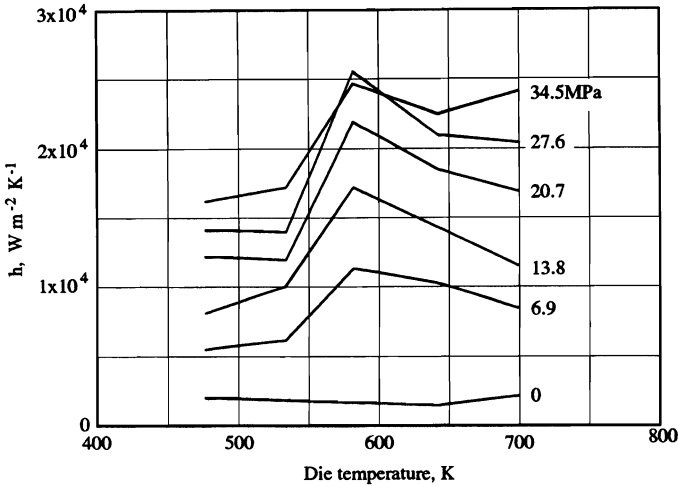
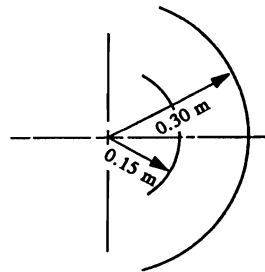


Fig. 8.20 Contact heat transfer coefficient as a function of die temperature and the forging pressure. Test conditions: workpiece Al 6061-O; lubricant MoS₂; surface roughness of workpiece = 0.74 μm; surface roughness of die = 0.93 μm. (From V. K. Jain, *J. Mater. Shaping Technol.* 8, 193 (1990).)

PROBLEMS

8.1 Hot gases flow inside an insulated horizontal tube with dimensions shown to the right. Determine the heat transfer coefficients for both the inside and outside surfaces. The gas at 1370 K flows with an average velocity of 4 m s⁻¹. The environment surrounding the tube is air at 300 K, and the outside surface temperature is 330 K. The gas is ideal so that $\beta = 1/T$, and at these high temperatures η for the gas does not change appreciably with temperature. *Data for gas inside tube:*



T, K	$\rho, kg m^{-3}$	$\eta, kg s^{-1} m^{-1}$	$k, W m^{-1} K^{-1}$	$C_p, J kg^{-1} K^{-1}$
1370	0.30	4.1×10^{-5}	0.086	1.0×10^3

276 Correlations and Data for Heat Transfer Coefficients

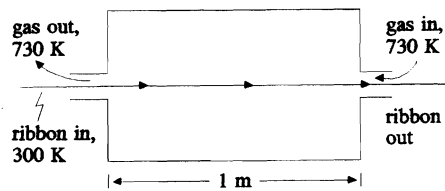
8.2 Molten aluminum is preheated while being transferred from a melting furnace to a casting tundish by pumping through a heated tube, 50 mm in diameter, at a flow rate of 1.3 kg s^{-1} . The tube wall is kept at a constant temperature at 1030 K. a) Calculate the heat transfer coefficient between the tube wall and the aluminum. b) Using this value of the heat transfer coefficient, how long would the tube have to be to heat the aluminum from 950 K to 1025 K? *Data for aluminum:* $k = 86 \text{ W m}^{-1} \text{ K}^{-1}$; $\rho = 2560 \text{ kg m}^{-3}$; $C_p = 1050 \text{ J kg}^{-1} \text{ K}^{-1}$; $\eta = 1.2 \times 10^{-3} \text{ kg s}^{-1} \text{ m}^{-1}$.

8.3 A sheet of glass (1 m length) is cooled from an initial temperature of 1250 K by blowing air at 300 K parallel to the surface of the glass. The free stream velocity of the air is 30 m s^{-1} . Calculate the initial heat transfer coefficient and when the glass has cooled to 400 K.

8.4 A long cylindrical bar of steel (30 mm diameter) is heated in a tempering furnace to 810 K. It is then cooled in a cross-stream of moving air at 300 K with a free stream velocity of 30 m s^{-1} . Calculate the heat transfer coefficient that applies when the bar begins to cool.

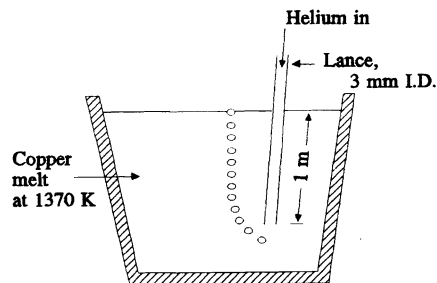
8.5 Refer to Example 8.1, in which a tube with a uniform surface temperature was considered. Now consider flow through a tube which is electrically heated so that the heat flux along the length of the tube is uniform. The fluid has a mixed mean temperature of T_0 as it enters the heated length of the tube. Assume constant and uniform thermal properties and steady state. a) For a small length of tube, Δx , write an energy balance on the fluid (see Example 8.1). b) Take the limit as $\Delta x \rightarrow 0$. c) Integrate part b) and obtain an equation which gives the mixed mean temperature of the fluid as it leaves the heated section of the tube.

8.6 A rapidly solidified ribbon is annealed by continuously passing it through a tube with countercurrent hot gas, which flows at 30 m s^{-1} and 730 K. Estimate the heat transfer coefficient, and calculate the temperature of the ribbon leaving the tube. *Data and thermal properties:* Ribbon thickness, 1 mm; ribbon width, 150 mm; ribbon velocity, 0.17 m s^{-1} .



	$\rho, \text{ kg m}^{-3}$	$C_p, \text{ J kg}^{-1} \text{ K}^{-1}$	$k, \text{ W m}^{-1} \text{ K}^{-1}$
Gas	0.64	2000	0.04
Ribbon	6400	500	30

8.7 In order to reduce the amount of dissolved hydrogen, dry helium is bubbled through molten copper. In order to prevent clogging of the submerged end of the lance, the helium must enter the melt at a temperature greater than the freezing point of copper (1356 K). What is the maximum mass flow rate of helium which can be employed if the supply of helium is at 300 K?



8.8 Calculate the initial rate of losing energy (W) of an aluminum plate ($1.2 \text{ m} \times 1.2 \text{ m} \times 10 \text{ mm}$) and heated uniformly to 370 K when it is a) cooled in a horizontal position by a stream of air at 290 K with a velocity of 2 m s^{-1} ; b) suspended vertically in stagnant air at the same temperature.

8.9 Oil flows in a long horizontal 50 mm I.D. copper tube at an average velocity of 3 m s^{-1} . If the oil has a bulk temperature of 370 K and the air surrounding the tube is at 290 K, calculate a) the "liquid-side" heat transfer coefficient; b) the "vapor-side" heat transfer coefficient; c) the temperature of the copper tube; d) the rate of heat transfer to the air.

Data for oil:

T (K)	ρ (kg m^{-3})	C_p ($\text{kJ kg}^{-1} \text{K}^{-1}$)	$\eta \cdot 10^2$ (N s m^{-2})	$\nu \cdot 10^6$ ($\text{m}^2 \text{s}^{-1}$)	$k \cdot 10^3$ ($\text{W m}^{-1} \text{K}^{-1}$)	$\alpha \cdot 10^7$ ($\text{m}^2 \text{s}^{-1}$)	Pr	$\beta \cdot 10^3$ (K^{-1})
290	890.0	1.868	99.9	1120	145	0.872	12 900	0.70
300	884.1	1.909	48.6	550	145	0.859	6400	0.70
320	871.8	1.993	14.1	161	143	0.823	1965	0.70
340	859.9	2.076	5.31	61.7	139	0.779	793	0.70
360	847.8	2.161	2.52	29.7	138	0.753	395	0.70
370	841.8	2.206	1.86	22.0	137	0.738	300	0.70

8.10 Replace the oil with sodium and repeat Problem 8.5. Compare or contrast the results of the two problems.

8.11 A heat treating furnace is 6 m long, 3 m wide and 6 m high. If a check with thermocouples indicates that the average wall temperature is 340 K and the top is 365 K, calculate the heat loss from the furnace in W. A quick estimate can be made by using the simplified equations given in Problem 8.14.

8.12 In flow past a flat plate, a laminar boundary layer exists over the forward portion between 0 and L_{tr} , and the turbulent boundary layer exists beyond L_{tr} . With this model, the average h over a plate of length L (with $L > L_{tr}$) can be determined as indicated

$$h = \frac{1}{L} \left[\int_0^{L_{tr}} h_{x(\text{lam})} dx + \int_{L_{tr}}^L h_{x(\text{turb})} dx \right].$$

Take $\text{Re}_{tr} = 3.2 \times 10^5$ and show that

$$\frac{hL}{k} = 0.037 \text{Pr}^{1/3} (\text{Re}^{0.8} - 15\,500).$$

[Hint: $L_{tr}/L = \text{Re}_{tr}/\text{Re}_L$.]

8.13 A steel plate, 2.5 m by 2.5 m by 2.5 mm, is removed from an oven at 430 K and hung horizontally in a laboratory at 295 K. a) Calculate the initial heat loss (W) from the steel. b) Repeat if the plate is hung vertically.

8.14 Repeat Problem 8.13 using one of the following simplified equations, which apply reasonably well to air, CO, N_2 , and O_2 in the range 310-1090 K. L and D are in m, ΔT in K, and h in $\text{W m}^{-2} \text{K}^{-1}$. $L = A/P$ with A = surface area and P = perimeter of the surface.

278 Correlations and Data for Heat Transfer Coefficients

Vertical plates of length L :

$$h = 1.42 (\Delta T/L)^{1/4}, \quad 5 \times 10^{-6} < L^3 \Delta T < 50$$

$$h = 1.45 (\Delta T)^{1/3}, \quad 50 < L^3 \Delta T < 5 \times 10^4.$$

Horizontal pipes of diameter D :

$$h = 1.22 (\Delta T/D)^{1/4}, \quad 5 \times 10^{-6} < D^3 \Delta T < 50$$

$$h = 1.24 (\Delta T)^{1/3}, \quad 50 < D^3 \Delta T < 5 \times 10^4.$$

Horizontal plate,* hot surface up or cold surface down:

$$h = 1.32 (\Delta T/L)^{1/4}, \quad 5 \times 10^{-5} < L^3 \Delta T < 0.30$$

$$h = 1.52 (\Delta T)^{1/3}, \quad 0.30 < L^3 \Delta T < 470.$$

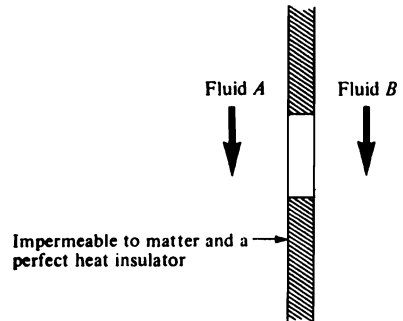
Horizontal plate,* hot surface down or cold surface up:

$$h = 0.59 (\Delta T/L)^{1/4}, \quad 0.005 < L^3 \Delta T < 470.$$

Are the results for the heat transfer coefficients within 20 pct of the results using the more complete correlations (as in Problem 8.13)?

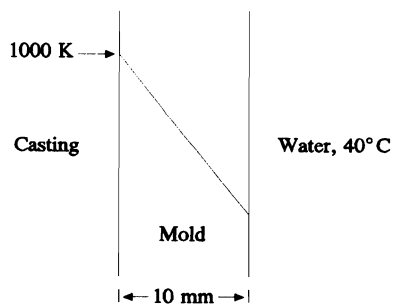
8.15 Two fluids are separated by a solid with a thickness of 10 mm and a thermal conductivity of $22 \text{ W m}^{-1} \text{ K}^{-1}$. For each of the following scenarios, estimate the heat transfer coefficient on each side of the solid and the surface temperatures of the solid.

	Fluid	Free stream velocity, m s^{-1}	Free stream temperature, K
a)	A air	15.2	300
	B air	0	650
b)	A air	0	300
	B sodium	0	650
c)	A air	15.2	300
	B sodium	0	650
d)	A sodium	15.2	365
	B sodium	0	650



8.16 A wire with a diameter of 0.03 mm and 0.3 m in length is heated by an electrical current and placed in helium at 280 K. a) If the surface temperature of the wire is 600 K, calculate the electric power. b) Calculate the electric power, for the same wire temperature, if there is a cross flow of helium with a free stream velocity of 20 m s^{-1} .

8.17 A copper mold is used to make a casting of a nickel-base alloy. During most of the solidification period, the temperature profile in the copper is linear, with the surface on the casting side maintained constant at 1000 K. The other side of the mold contacts the water at 40°C (313 K). What is the surface temperature on the water side of the mold?



8.18 Glass plate can be made stronger by inducing compressive residual surface stresses. This is done by a process called thermal tempering. The glass is heated to a temperature between the softening point (~ 750 K) and the glass transition temperature (~ 600 K). It is then cooled to room temperature in a stream of air, or in some cases immersed in an oil bath. Compare the heat transfer coefficients, as the glass cools from 700 K to 300 K, in air ($V_\infty = 30$ m s⁻¹) and in "fast" oil.

8.19 Polymeric fibers are formed by heating the polymer to its viscous liquid state and then pumping it through small, round orifices. From each orifice, a single fiber is formed which solidifies almost immediately upon passing into air. Compare the heat transfer coefficients that can be obtained by forming the fibers (0.1 mm diameter) in air and in helium. The fibers are formed at 50 m s⁻¹.

8.20 A steel rod (25 mm diameter and 0.6 m length) is heated vertically in a large bath of molten salt at 920 K. Calculate the heat transfer coefficient when the bar is at 640 K.
Data for molten salt: $k = 86$ W m⁻¹ K⁻¹; $C_p = 870$ J kg⁻¹ K⁻¹; $\rho = 3200$ kg m⁻³; $\beta = 2 \times 10^{-5}$ K⁻¹; $\eta(920$ K) = 1.03×10^{-3} N s m⁻²; $\eta(780$ K) = 1.24×10^{-3} N s m⁻²; $\eta(640$ K) = 1.65×10^{-3} N s m⁻².

8.21 Consider a vertical surface (1.5 m) at 600 K that loses heat by natural convection to nitrogen at 300 K. Using the simplified equations given in Problem 8.14, calculate and plot the heat transfer coefficient as the surface temperature decreases from 600 K to 300 K.

8.22 We can maximize the heat transfer coefficient in a fluidized bed by selecting the optimum superficial velocity. Start with Eq. (8.28), neglect the term for radiation, and assume that the thermophysical properties are constant. With these assumptions, the correlation is of the form:

$$Nu = Nu(Re, \omega)$$

Re and ω are interrelated, so Nu can be optimized with respect to Re. Carry out the optimization with

$$\omega^{4.7} Ar = 18 Re + 2.70 Re^{1.687}.$$

(This equation is from C. Y. Wen and Y. H. Yu, *Fluid Particle Technology*, Chem. Eng. Prog. Symposium Series, No. 62, AIChE, New York, 1966.)

8.23 Bars (50 mm diameter) of steel, on cooling beds, cool from a rolling temperature (1150 K) to a shearing temperature (650 K) in a horizontal position with all surfaces exposed to ambient air. The air temperature can vary from 250 K to 310 K. Calculate the convective heat transfer coefficients that apply to the two extremes of ambient conditions.

CONDUCTION OF HEAT IN SOLIDS

Materials engineers easily recognize that the conduction of heat within solids is fundamental to understanding and controlling many processes. We could cite numerous examples to emphasize the importance of this topic. Some important applications that fall in this category include estimating heat losses from process equipment, quenching, or cooling operations where the cooling rate of a part actually controls its microstructure and hence its application, and solidification.

9.1 THE ENERGY EQUATION FOR CONDUCTION

The general equation for the conduction of heat in a solid free of heat sources or sinks can be written

$$\nabla \cdot k \nabla T = \rho \frac{\partial(C_p T)}{\partial t} \quad (9.1)$$

The more common form of this equation is written for conductivity independent of position in space and heat capacity independent of temperature:

$$\frac{\partial T}{\partial t} = \alpha \nabla^2 T = \alpha \left[\frac{\partial^2 T}{\partial x^2} + \frac{\partial^2 T}{\partial y^2} + \frac{\partial^2 T}{\partial z^2} \right], \quad (9.2)$$

where the thermal diffusivity, as defined in Chapter 7, is $\alpha = k/\rho C_p$. Equation (9.2), although not as rigorous as Eq. (9.1), is used when analytical solutions are sought.

When the temperature is not a function of time but only depends upon position in space, then Eq. (9.2) becomes

$$\nabla^2 T = \frac{\partial^2 T}{\partial x^2} + \frac{\partial^2 T}{\partial y^2} + \frac{\partial^2 T}{\partial z^2} = 0. \quad (9.3)$$

Equation (9.3) therefore applies to *steady-state* conduction in systems free of heat sources and sinks. It is often referred to as the *Laplace equation*.

9.2 STEADY-STATE ONE-DIMENSIONAL SYSTEMS

9.2.1 Infinite flat plate

Equation (9.3) for an infinite flat plate, such as that in Fig. 9.1, reduces to

$$d^2T/dx^2 = 0. \quad (9.4)$$

Boundary conditions are

$$\text{B.C. 1} \quad \text{at } x = 0, \quad T = T_1; \quad (9.5)$$

$$\text{B.C. 2} \quad \text{at } x = L, \quad T = T_2. \quad (9.6)$$

We can solve Eq. (9.4) quite simply, in accordance with the boundary conditions, to yield the temperature profile:

$$\frac{T - T_1}{T_2 - T_1} = \frac{x}{L}. \quad (9.7)$$

In addition, the heat flux through the slab may be described as follows:

$$q = -k \frac{dT}{dx} = \frac{k}{L} (T_1 - T_2). \quad (9.8)$$

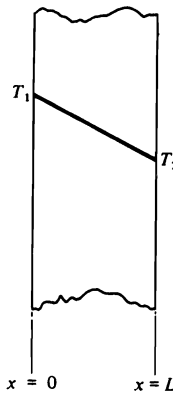


Fig. 9.1 Steady-state temperature distribution in a plate.

9.2.2 Series composite wall

Consider a simple series wall made up of two different materials whose thermal conductivities are k_1 and k_2 (Fig. 9.2). There is a flow of heat from the gas at temperature T_i through its boundary layer, the composite wall, and the boundary layer of the gas at T_0 .

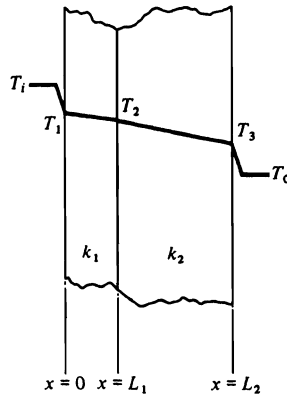


Fig. 9.2 Steady-state temperature distribution in a composite wall.

The unidirectional heat flux through the four parts of the entire circuit is constant because steady state prevails. Thus

$$Q = Ah_i(T_i - T_1) = \frac{k_1 A}{L_1} (T_1 - T_2) = \frac{k_2 A}{L_2} (T_2 - T_3) = Ah_o(T_3 - T_o). \quad (9.9)$$

We can build up a solution based on the four equalities in Eq. (9.9). However, this procedure is rather tedious, and it is much easier to make use of the *resistance concept*.

The flow of heat Q through material, subject to a temperature difference $T_j - T_k$, is analogous to the flow of current I , as a result of a potential difference $E_j - E_k$ through an electrical conductor. From Ohm's law for electricity, the thermal resistance R_t for heat flow is visualized:

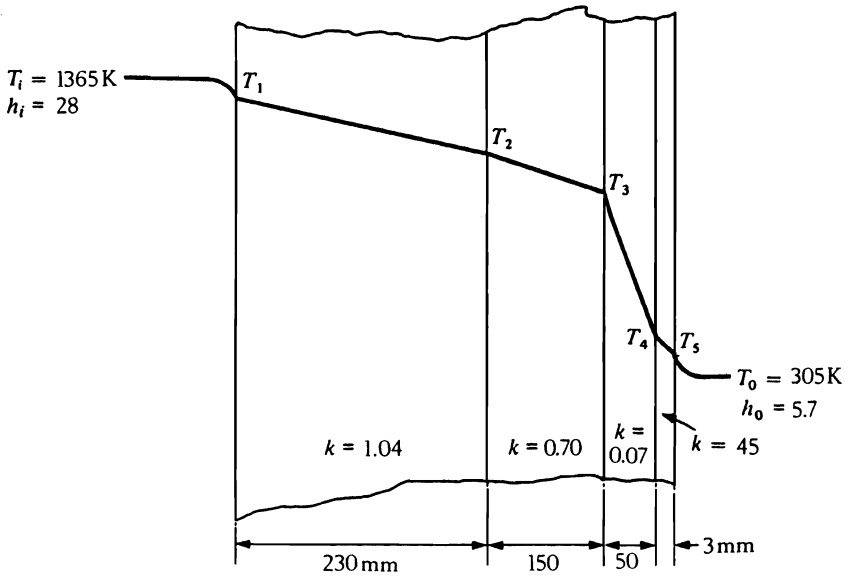
$$R_t = \frac{T_j - T_k}{Q}. \quad (9.10)$$

Thus for the composite wall, the four thermal resistances are $1/Ah_i$, L_1/k_1A , L_2/k_2A , and $1/Ah_o$. The total resistance for the whole circuit is simply their sum, so that the heat flow is

$$Q = \frac{T_i - T_o}{1/h_iA + L_1/k_1A + L_2/k_2A + 1/h_oA}. \quad (9.11)$$

With Eq. (9.11), we only need to know the total temperature drop across the system to calculate the heat flux, which we can use to determine the temperature at any position within the composite wall.

Example 9.1 A furnace wall is constructed of 230 mm of fire brick ($k = 1.04 \text{ W m}^{-1} \text{ K}^{-1}$), 150 mm of insulating brick ($k = 0.70 \text{ W m}^{-1} \text{ K}^{-1}$), 50 mm of glass-wool insulation ($k = 0.07 \text{ W m}^{-1} \text{ K}^{-1}$), and 3 mm thick steel plate ($k = 45 \text{ W m}^{-1} \text{ K}^{-1}$) on the outside. The heat transfer coefficients on the inside and outside surfaces are 28 and $5.7 \text{ W m}^{-2} \text{ K}^{-1}$, respectively. The gas temperature inside the furnace is 1365 K and the outside air temperature is 305 K. a) Calculate the heat flux through the wall. b) Determine the temperatures at all interfaces.



Solution.

$$a) \quad q = \frac{T_i - T_o}{AR_t}$$

and

$$AR_t = \frac{1}{28} + \frac{0.230}{1.04} + \frac{0.150}{0.70} + \frac{0.050}{0.07} + \frac{0.003}{45} + \frac{1}{5.7} = 1.361 \text{ W}^{-1} \text{ m}^2 \text{ K}.$$

Therefore,

$$q = \frac{(1365 - 305)}{1.361} = 778.8 \text{ W m}^{-2}.$$

$$b) \quad T_i - T_1 = \frac{q}{h_i} = \frac{778.8}{28} = 27.8 \text{ K}$$

$$T_1 = 1337.2 \text{ K}.$$

Similarly,

$$T_1 - T_2 = \frac{q}{(k_1/L_1)} = \frac{(778.8)(0.230)}{1.04} = 172.2 \text{ K}$$

$$T_2 = 1165.0 \text{ K}.$$

The remaining temperatures are determined in the same manner, yielding $T_3 = 998.2 \text{ K}$ and $T_4 = T_5 = 441.8 \text{ K}$.

In addition to the resistances discussed in this section, composite walls often have another type of thermal resistance. When two elements of the composite are in contact, a resistance occurs which depends on the roughness of the two surfaces, the fluid between the surfaces, and the contact pressure. For furnace walls, it is customary to ignore the additional resistance because of the very high thermal resistance of the refractories; for metallic composite walls, however, it is wise to include it. Unfortunately, each individual situation is different, and so experimental information must be obtained.

9.2.3 Infinite cylinder

For steady radial flow of heat through the wall of the hollow cylinder depicted in Fig. 9.3, the Laplace equation still applies. The Laplace equation written in cylindrical coordinates can be deduced from Eq. (B), Table 7.5.

$$\frac{1}{r} \frac{\partial}{\partial r} \left[r \frac{\partial T}{\partial r} \right] + \frac{1}{r^2} \frac{\partial^2 T}{\partial \theta^2} + \frac{\partial^2 T}{\partial z^2} = 0. \quad (9.12)$$

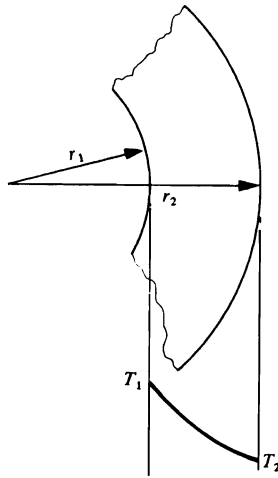


Fig. 9.3 Steady-state temperature distribution in a hollow cylinder.

For the case at hand, temperature depends only on the radial coordinate; therefore, Eq. (9.12) reduces to:

$$\frac{1}{r} \frac{d}{dr} \left[r \frac{dT}{dr} \right] = 0. \quad (9.13)$$

The boundary conditions under consideration are

$$\text{B.C. 1} \quad \text{at } r = r_1, \quad T = T_1, \quad (9.14)$$

$$\text{B.C. 2} \quad \text{at } r = r_2, \quad T = T_2. \quad (9.15)$$

At this point, the reader should note that this problem and the one discussed in Section 7.4 are identical. By way of illustration, we have used a different starting point here. In any event, the temperature profile is given by

$$\frac{T - T_2}{T_1 - T_2} = \frac{\ln(r/r_2)}{\ln(r_1/r_2)}. \quad (7.51)$$

It then follows that the heat flux q , (W m^{-2}) and the heat flow Q (W) are given by Eqs. (7.52) and (7.53), respectively.

9.2.4 Composite cylindrical wall

Consider the cylindrical composite wall shown in Fig. 9.4. By referring to Eq. (7.53), we can see for steady-state conditions, that Q is constant. For a length L , we have

$$\begin{aligned} Q &= h_i(2\pi r_1 L)(T_i - T_1) = \frac{2\pi k_1 L}{\ln(r_2/r_1)}(T_1 - T_2) = \frac{2\pi k_2 L}{\ln(r_3/r_2)}(T_2 - T_3) \\ &= h_o(2\pi r_3 L)(T_3 - T_o). \end{aligned}$$

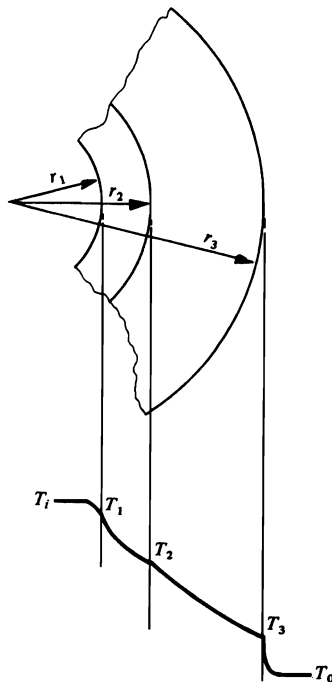


Fig. 9.4 Steady-state temperature distribution in a composite cylindrical wall.

Again, the series concept is the most convenient method to relate the heat flow to the overall temperature drop:

$$Q = \frac{T_i - T_0}{\frac{1}{2\pi L r_1 h_i} + \frac{\ln(r_2/r_1)}{2\pi L k_1} + \frac{\ln(r_3/r_2)}{2\pi L k_2} + \frac{1}{2\pi L r_3 h_o}} \quad (9.16)$$

Note that the form of the thermal resistance attributed to the cylindrical wall differs from that of the slab. By comparing Eq. (9.16) to Eq. (9.11), we can contrast the thermal resistances as follows:

$$\begin{aligned} \text{Infinite slab: } R_t &= \frac{L}{kA}, \\ \text{Infinite cylinder: } R_t &= \frac{\ln(r_2/r_1)}{2\pi L k}, \\ \text{Surface to fluid: } R_t &= \frac{1}{Ah}. \end{aligned} \quad (9.17)$$

As an application of Eq. (9.16), consider the design of a single-wall tube furnace to operate at T_1 internally while placed in some environment at T_0 . The radial heat flow through the furnace wall is then given by Eq. (9.16) written for a tube composed of a single layer with conductivity k :

$$Q = \frac{2\pi L(T_i - T_0)}{\frac{1}{h_i r_1} + \frac{1}{k} \ln \frac{r_2}{r_1} + \frac{1}{h_o r_2}} \quad (9.18)$$

If we examine Eq. (9.18), then we see that as r_2 (the outer radius) increases, there is an increasing resistance to radial heat conduction as embodied in the \ln term. Simultaneously, however, as r_2 increases, the outer cooling surface area increases as well. This dual effect suggests that there exists a particular outer radius for which the heat loss (or gain) is a maximum. To examine this proposed effect, fix r_1 , and determine that particular value of r_2 for which $dQ/dr_2 = 0$:

$$\frac{dQ}{dr_2} = \frac{-2\pi L(T_i - T_0)(1/kr_2 - 1/h_o r_2^2)}{\left[\frac{1}{h_i r_1} + \frac{1}{k} \ln \frac{r_2}{r_1} + \frac{1}{h_o r_2} \right]^2} = 0.$$

From this, we obtain the critical outer radius

$$r_{2c} = k/h_o. \quad (9.19)$$

The existence of a critical radius shows that under some conditions, and contrary to common expectations, the heat loss through a tube furnace can actually be decreased by decreasing the insulating wall thickness.

9.3 TRANSIENT SYSTEMS, FINITE DIMENSIONS

In this section, we consider conduction heat transfer in solids, in which the temperature varies not only with position in space, but also undergoes a continuous change with time at any position.

9.3.1 Newtonian heating or cooling

When a solid such as a flat plate, initially at a uniform temperature T_i , is cooled by a fluid at temperature T_f , the temperature distribution varies with time, as shown in Fig. 9.5(a). If the plate is thin (Fig. 9.5(b)), and/or its thermal conductivity high, then the temperature gradients within the plate are negligible, and we may consider the temperature only as a function of time. In the next section, we examine the conditions under which this criterion is met; we find that if $hL/k \leq 0.1$, then the analysis that follows is valid.

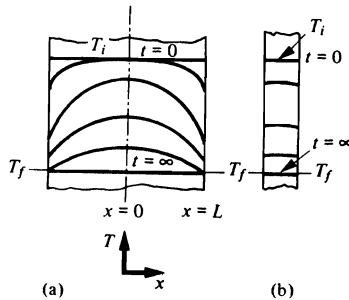


Fig. 9.5 Transient temperature distributions during cooling of (a) a thick plate, and (b) a thin plate.

For this situation, we equate the rate of heat lost by the plate to the rate of heat transfer to the fluid:

$$-V\rho C_p \frac{dT}{dt} = hA(T - T_f), \quad (9.20)$$

where V = volume of the plate, and A = area of the plate exposed to the fluid. Rearranging for integration and taking $T = T_i$ at $t = 0$, we have

$$\frac{T - T_f}{T_i - T_f} = \exp \left[\frac{-hAt}{\rho C_p V} \right]. \quad (9.21)$$

The analysis applies only to the cases in which internal gradients are negligible. If this requirement is met, we speak of Newtonian cooling. Note that no geometric restrictions are imposed, since Eq. (9.21) just specifies A and V ; also note that the solution does not contain the conductivity.

The temperature history of such objects during cooling is illustrated in Fig. 9.6, which shows that for the same surface radius, R , or semithickness, L , the time it takes an infinite cylinder (or infinite square rod) to cool within 1% of thermal equilibrium with its surrounding fluid is almost 50% longer than for a sphere (or cube) of the same material. On the other hand, an infinite plate of the same material and semithickness equal to the cylinder radius requires 100% more time.

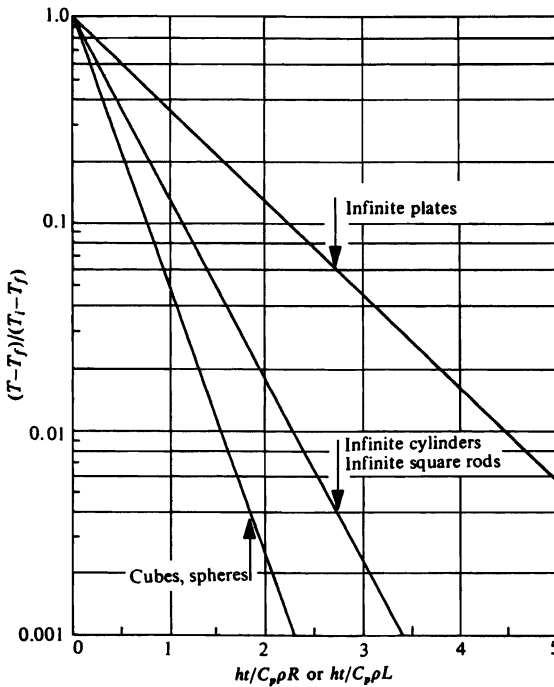


Fig. 9.6 Cooling (or heating) of bodies with negligible temperature gradients. R is radius, and L is semithickness.

Example 9.2 A plate of aluminum alloy with dimensions $6 \text{ mm} \times 300 \text{ mm} \times 300 \text{ mm}$ is solutionized at 810 K , and then quenched into water at 365 K . Over the temperature range $810\text{--}530 \text{ K}$, the heat transfer coefficient for quenching may be assumed constant as $510 \text{ W m}^{-2} \text{ K}^{-1}$. In the range $530\text{--}365 \text{ K}$, the heat transfer coefficient may be approximated as $2550 \text{ W m}^{-2} \text{ K}^{-1}$. a) Calculate the cooling rate during quenching at that instant when the plate is at 590 K . b) Repeat, when the plate is at 420 K . c) Determine the time it takes the plate to cool to 390 K . The properties of the aluminum are: $k = 78 \text{ W m}^{-1} \text{ K}^{-1}$, $C_p = 1000 \text{ J kg}^{-1} \text{ K}^{-1}$, $\rho = 2880 \text{ kg m}^{-3}$.

Solution. We can write an expression for the cooling rate by simply rearranging Eq. (9.20):

$$\frac{dT}{dt} = -\frac{h}{\rho C_p} \frac{A}{V} (T - T_f).$$

For a plate or slab whose thickness is much less than its width and length, A/V may be assumed equal to A/V for an infinite plate. Therefore

$$\frac{A}{V} = \frac{1}{L} = \frac{1}{0.003 \text{ m}} = 333.3 \text{ m}^{-1}.$$

$$\text{a) } \frac{dT}{dt} = -\frac{510 \text{ W}}{\text{m}^2 \text{ K}} \left| \frac{333.3}{\text{m}} \right| \left| \frac{\text{m}^3}{2880 \text{ kg}} \right| \left| \frac{\text{kg K}}{1000 \text{ J}} \right| (590 - 365) \text{ K} \left| \frac{1 \text{ J}}{1 \text{ W s}} \right|$$

$$\frac{dT}{dt} = -13.3 \text{ K s}^{-1} \text{ at } 590 \text{ K}.$$

$$\text{b) } \frac{dT}{dt} = - \frac{(2550)(333.3)(420 - 365)}{(2880)(1000)} = -16.4 \text{ K s}^{-1} \text{ at } 420 \text{ K.}$$

c) First we calculate time t_1 to cool to 530 K. Use Eq. (9.21):

$$\frac{T - T_f}{T_i - T_f} = \exp \left[- \frac{h}{\rho C_p} \frac{A}{V} t_1 \right],$$

$$\frac{530 - 365}{810 - 365} = \exp \left[- \frac{(510)(333.3)t_1}{(2880)(1000)} \right].$$

Solving for t_1 , we have $t_1 = 16.81$ s. Second we calculate time t_2 to cool from 530 to 390 K; during this period T_i is interpreted as 530 K.

$$\frac{390 - 365}{530 - 365} = \exp \left[- \frac{(2550)(333.3)t_2}{(2880)(1000)} \right].$$

Solving for t_2 , we get $t_2 = 6.39$ s. Therefore, total time to cool to 390 K is $t = t_1 + t_2 = 23.2$ s. The reader is assured that the assumption that the internal temperature gradients are non-existent, as applied to this particular example, is valid.

9.3.2 Bodies with internal temperature gradients

For the flat plate of Fig. 9.5(a), the applicable differential equation by reference to Eq. (9.2) is

$$\frac{\partial T}{\partial t} = \alpha \frac{\partial^2 T}{\partial x^2}. \quad (9.22)$$

We find the solution $T(x,t)$ of this equation for the boundary conditions

$$T(x,0) = T_i \quad (\text{uniform}), \quad (9.23)$$

$$\frac{\partial T(0,t)}{\partial x} = 0, \quad (9.24)$$

$$\frac{\partial T(L,t)}{\partial x} + \frac{h}{k} [T(L,t) - T_f] = 0, \quad (9.25)$$

by employing the method of separation of variables.

The boundary condition in time (Eq. (9.23)) is usually referred to as the initial condition. For this case, the initial condition is a uniform temperature; we could, however, consider some arbitrary temperature distribution, $f(x)$, existing at time zero. Equation (9.24) results from the symmetry of the problem, and we develop the final boundary condition (Eq. (9.25)) by equating the heat flux at the surface to the rate of heat transfer to the fluid. Before proceeding, we give some attention to the boundary conditions.

When applying the method of separation of variables, there are three basic types of boundary conditions that can be treated analytically. They are:

$$T(\text{boundary}) = 0, \tag{9.26a}$$

$$\frac{\partial T}{\partial x}(\text{boundary}) = 0, \tag{9.26b}$$

and

$$\frac{\partial T}{\partial x}(\text{boundary}) \pm \frac{h}{k} T(\text{boundary}) = 0. \tag{9.26c}$$

Comparing Eqs. (9.24) and (9.25) to Eqs. (9.26b) and (9.26c), respectively, we see that we must make a modification because T_f is not necessarily zero. The modification, however, is easily recognized; specifically, let $\theta = T - T_f$, so that the differential equation and boundary conditions become

$$\frac{\partial \theta}{\partial t} = \alpha \frac{\partial^2 \theta}{\partial x^2}, \tag{9.27}$$

$$\theta(x,0) = T_i - T_f = \theta_i, \tag{9.28}$$

$$\frac{\partial \theta}{\partial x}(0,t) = 0, \tag{9.29}$$

$$\frac{\partial \theta(L,t)}{\partial x} + \frac{h}{k} \theta(L,t) = 0. \tag{9.30}$$

The method of separation of variables consists of seeking a product solution of the form $\theta(x,t) = X(x) \cdot G(t)$. Then Eq. (9.27) becomes

$$\frac{1}{X} \frac{d^2 X}{dx^2} = \frac{1}{\alpha G} \frac{dG}{dt} = -\lambda^2, \tag{9.31}$$

from which

$$\frac{d^2 X}{dx^2} + \lambda^2 X = 0, \tag{9.32}$$

and

$$\frac{dG}{dt} + \alpha \lambda^2 G = 0. \tag{9.33}$$

We write the solution for Eq. (9.32)

$$X = c_1 \cos \lambda x + c_2 \sin \lambda x, \tag{9.34}$$

* λ^2 is called the separation constant. Consider the possibilities of using either $+\lambda^2$ or $\lambda = 0$ in Eq. (9.31).

and for Eq. (9.33), the solution is

$$G = \exp(-\lambda^2 \alpha t). \tag{9.35}$$

Boundary condition (9.29) requires that $c_2 = 0$, and Eq. (9.30) can be shown to require that

$$\cot \lambda_n L = \frac{1}{(h/k)L} (\lambda_n L), \tag{9.36}$$

where λ_n takes on an infinite number of *eigenvalues*. Figure 9.7 indicates this for the first three *eigenvalues*.

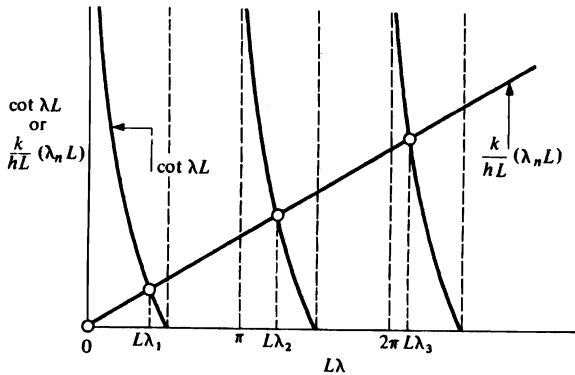


Fig. 9.7 Solutions of λ_n roots of Eq. (9.36).

Taking the product of Eqs. (9.34) and (9.35) with $c_2 = 0$, and realizing that all values of λ_n satisfying Eq. (9.36) are suitable, we have

$$\theta = \sum_{n=1}^{\infty} A_n \exp(-\lambda_n^2 \alpha t) \cos \lambda_n x, \tag{9.37}$$

where the A_n s have absorbed the constants involved. The initial condition (9.28) still remains to be satisfied. When Eq. (9.28) is substituted into Eq. (9.37), we get

$$\theta_i = \sum_{n=1}^{\infty} A_n \cos \lambda_n x. \tag{9.38}$$

Multiplying both sides of this equation by $\cos \lambda_m x \, dx$, and integrating from $x = 0$ to $x = L$, we obtain

$$\theta_i \int_0^L \cos \lambda_m x \, dx = \int_0^L \sum_{n=1}^{\infty} A_n \cos \lambda_n x \cos \lambda_m x \, dx. \tag{9.39}$$

When $m \neq n$, all integrals on the right-hand side of Eq. (9.39) are zero, and when $m = n$ the integral has the nonzero value

$$A_n \left[\frac{L}{2} + \frac{1}{2\lambda_n} \sin \lambda_n L \cos \lambda_n L \right].$$

The integral on the left-hand side of Eq. (9.39) is $(1/\lambda_n) \sin \lambda_n L$. Therefore

$$A_n = \frac{2\theta_i \sin \lambda_n L}{\lambda_n L + \sin \lambda_n L \cos \lambda_n L}. \tag{9.40}$$

The final solution is then

$$\frac{\theta}{\theta_i} = \frac{T - T_f}{T_i - T_f} = 2 \sum_{n=1}^{\infty} \frac{\sin \lambda_n L}{\lambda_n L + \sin(\lambda_n L) \cos(\lambda_n L)} \exp(-\lambda_n^2 \alpha t) \cos(\lambda_n x), \tag{9.41}$$

where the λ_n s are the roots of Eq. (9.36), given in Table 9.1.

Table 9.1 The first four roots of Eq. (9.36)*

Bi	k/hL	$\lambda_1 L$	$\lambda_2 L$	$\lambda_3 L$	$\lambda_4 L$
100	0.01	1.5552	4.6658	7.7764	10.8871
10	0.10	1.4289	4.3058	7.2281	10.2003
1	1.0	0.8603	3.4256	6.4373	9.5293
0.1	10.0	0.3111	3.1731	6.2991	9.4354

*A more comprehensive table can be found in H. S. Carslaw and J. C. Jaeger, *Conduction of Heat in Solids*, second edition, Oxford University Press, Oxford, UK, 1959, page 491.

Evaluations of Eq. (9.41) and the analogous solutions for infinitely long cylinders and spheres have been presented in many graphical forms for practical use. They are in terms of a *relative temperature* as a function of the *Fourier number*, *Biot number*, and *relative position*. These four dimensionless variables are defined as follows:

1. relative temperature $\equiv \frac{T - T_f}{T_i - T_f}$,
2. Fourier number (Fo) $\equiv \frac{\alpha t}{L^2} = \frac{kt}{\rho C_p L^2}$,
3. Biot number (Bi) $\equiv \frac{hL}{k}$,
4. relative position $\equiv \frac{x}{L}$.

For plates, L is the semithickness, and x is the distance from the center. For cylinders and spheres, the radius R replaces L , and r replaces x in the above definitions.

Among the earliest graphs prepared were the so-called Gurney-Lurie charts.¹ These charts are still referred to in engineering. However, the charts are limited to a small range of Fo and Bi values. Other diagrams commonly used are the Heisler charts² for $0.01 \leq Bi < \infty$ and $Fo > 0.2$. For more convenience, Figs. 9.8, 9.9 and 9.10 have been constructed for the temperature response of infinite plates, infinite cylinders, and spheres, respectively.

¹H. P. Gurney and J. Lurie, *Ind. Eng. Chem.* 15, 1170-1172 (1923).

²M. P. Heisler, *Trans ASME* 69, 227-236 (1947).

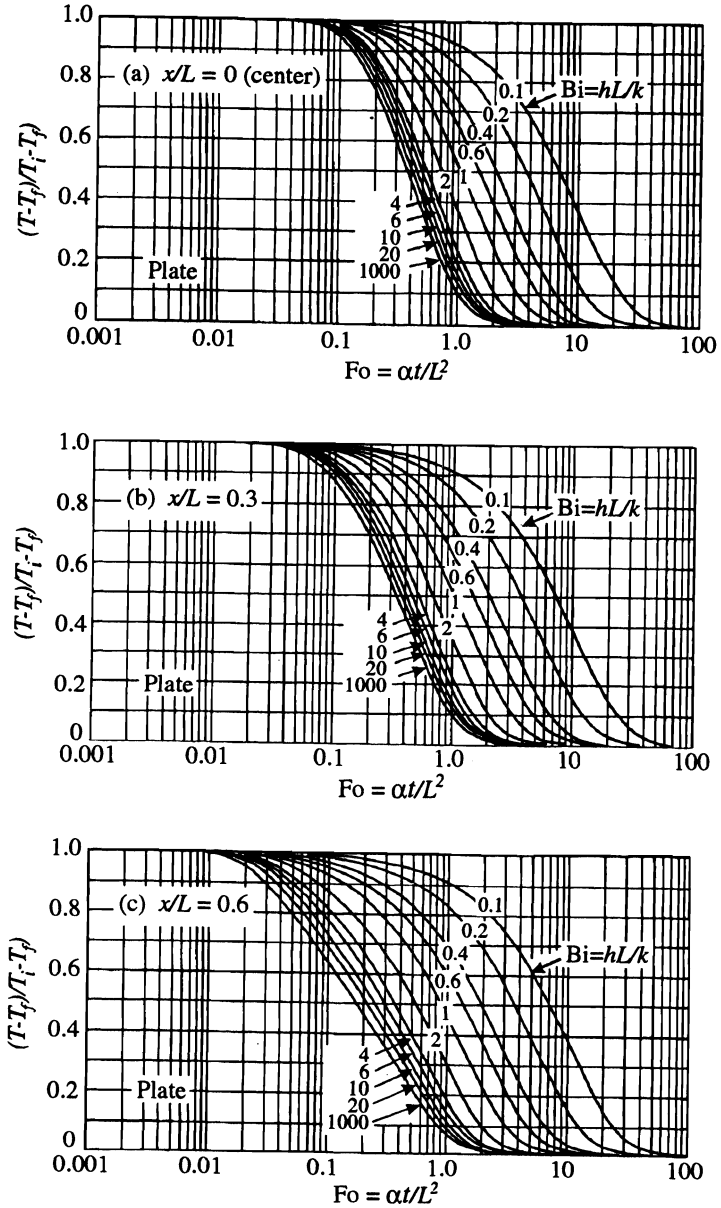


Fig. 9.8 Temperature response of an infinite plate initially at a uniform temperature T_i , and then subjected to a convective environment at T_p .

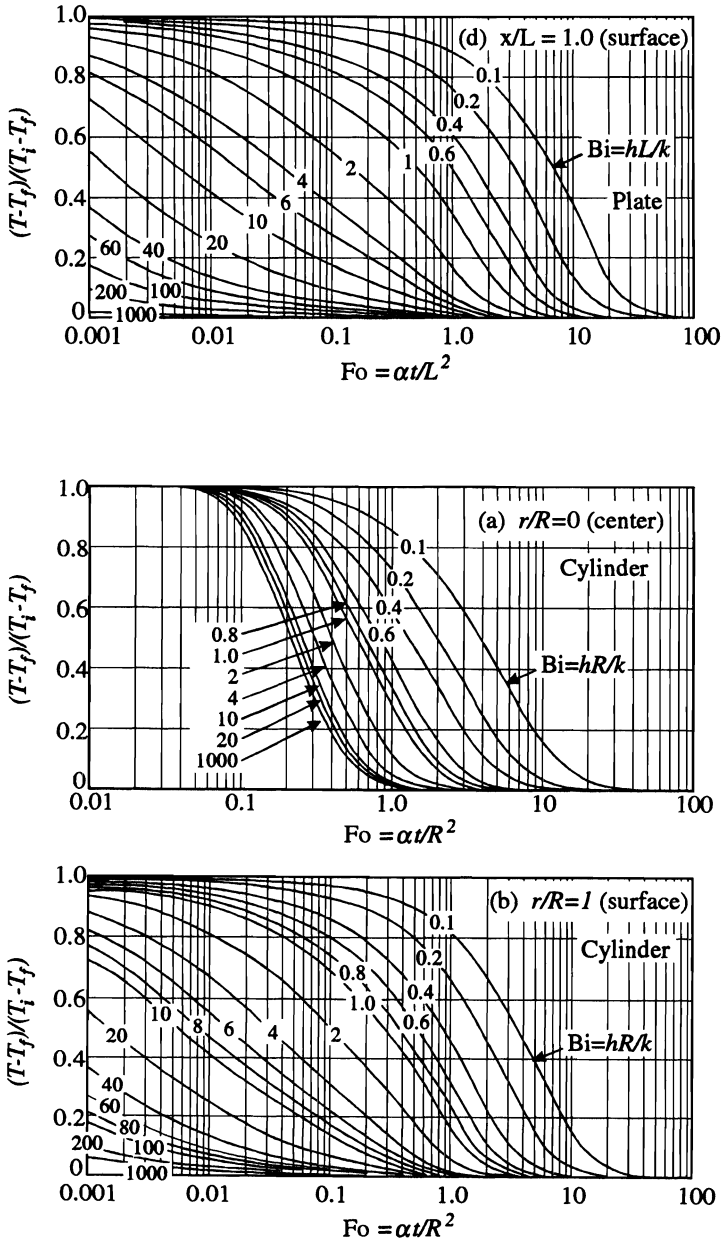


Fig. 9.9 Temperature response of an infinite cylinder initially at a uniform temperature T_i , and then subjected to a convective environment at T_f .

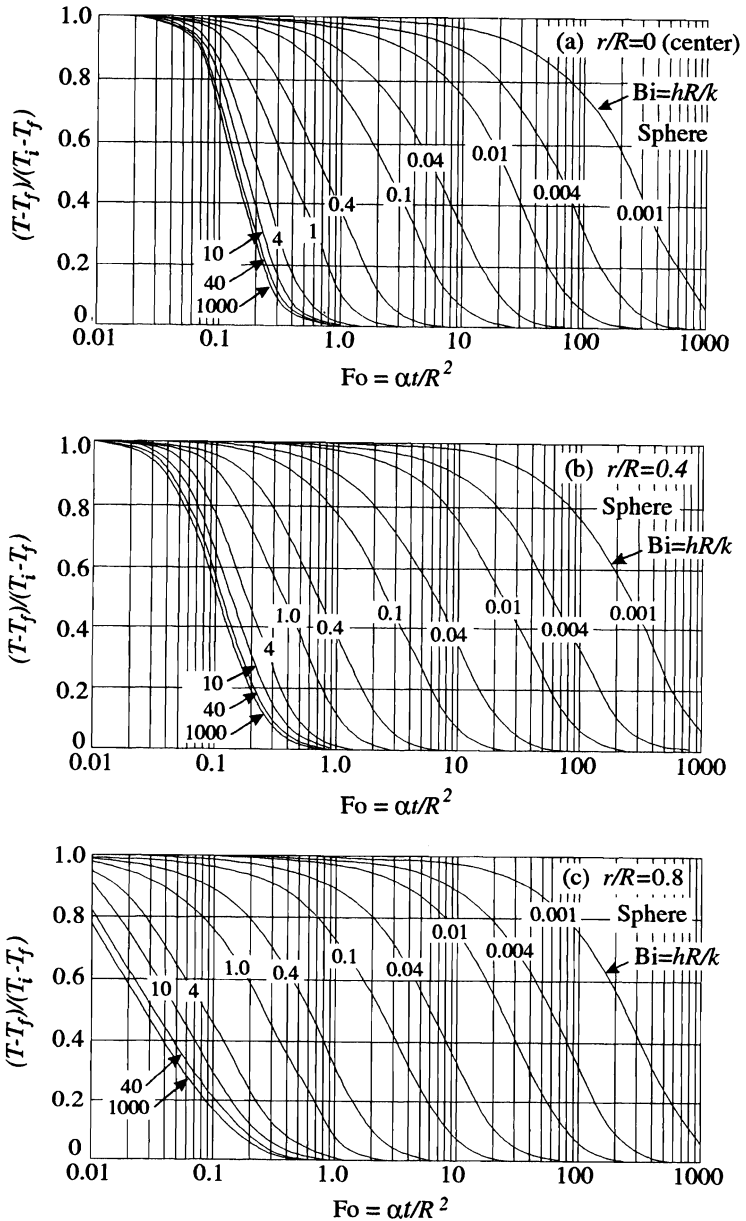


Fig. 9.10 Temperature response of a sphere initially at a uniform temperature T_i , and then subjected to a convective environment at T_f .

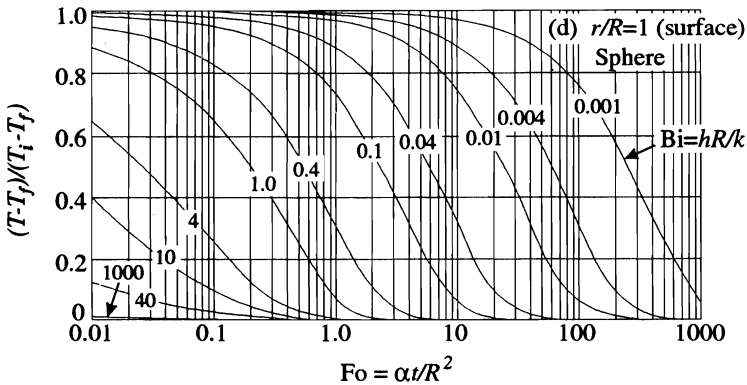


Fig. 9.10 (continued)

Example 9.3 As an example of the use of Fig. 9.9, consider a very long cylindrical stainless steel bar, 127 mm in diameter, which is heated to 478 K uniformly across its diameter. The bar is then cooled in a blast of fan forced air at 300 K with $h = 142 \text{ W m}^{-2} \text{ K}^{-1}$. a) Find the time it takes for the center to reach 310 K. b) When the center reaches 310 K, what is the surface temperature? c) What would be the minimum possible time for the center of the bar to reach 310 K if it were cooled in an ideal quenchant ($H = \infty$) at 300 K. The thermal properties of the stainless steel are $k = 16 \text{ W m}^{-1} \text{ K}^{-1}$ and $\alpha = 4.08 \times 10^{-6} \text{ m}^2 \text{ s}^{-1}$.

Solution.

a) When $T = 310 \text{ K}$ at the center, we have

$$\frac{T - T_f}{T_i - T_f} = \frac{310 - 300}{478 - 300} = 0.056.$$

Also

$$\text{Bi} = \frac{hR}{k} = \frac{(142)(0.0635)}{(16)} = 0.563.$$

From Fig. 9.9(a), $\alpha t/R^2 \approx 3.2$. Then

$$t = \frac{(3.2)(0.0635)^2}{4.08 \times 10^{-6}} = 3.16 \times 10^3 \text{ s}.$$

b) For the surface temperature, we refer to Fig. 9.9(b). When $\text{Fo} = 3.2$ and $\text{Bi} = 0.563$, we find that

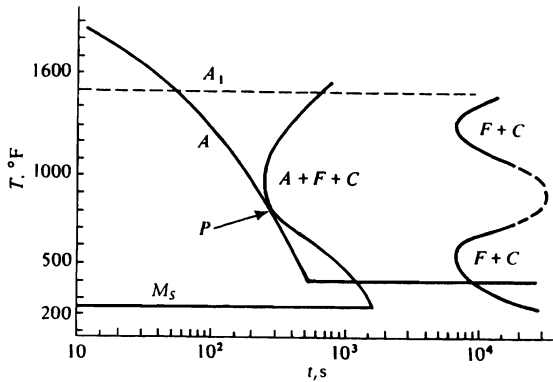
$$\frac{T - T_f}{T_i - T_f} \approx 0.040.$$

Therefore, $T = 0.040(478 - 300) + 300 = 303 \text{ K}$.

- c) The minimum possible time would correspond to the situation in which the surface temperature is equal to the temperature of the cooling medium; that is, $Bi \rightarrow \infty$. It is sufficient to use Fig. 9.9(a) with $Bi = 1000$. Thus, $\alpha t/R^2 = 0.60$, and

$$t = \frac{(0.60)(0.0635)^2}{4.08 \times 10^{-6}} = 593 \text{ s.}$$

Example 9.4 The process of austempering requires that a steel be quenched to just above its M_s temperature, and then isothermally transformed to a lower bainite structure that resembles tempered martensite. For a steel with the continuous cooling diagram below, estimate the maximum thickness of plate that can be completely austempered by quenching into molten salt at 400°F from a 1600°F austenitizing temperature with $h = 50 \text{ Btu h}^{-1} \text{ ft}^{-2} \text{ }^\circ\text{F}^{-1}$. For the steel, assume $\alpha = 0.46 \text{ ft}^2 \text{ h}^{-1}$ and $k = 20 \text{ Btu h}^{-1} \text{ ft}^{-1} \text{ }^\circ\text{F}^{-1}$. English units are commonly used in the metal processing industry in the U.S.A., so let's work this example with them.



Solution. Since we must cool at such a rate as to bring the center of the plate past the "nose" of the curve without undergoing any transformation, we start by assuming that point P is the critical point. Since point P is at 800°F , then

$$\frac{T - T_f}{T_i - T_f} = \frac{800 - 400}{1600 - 400} = 0.333.$$

Figure 9.8(a) is used for the calculation. What is needed is the value of the semithickness L that will result in agreement among Bi , Fo , and reduced temperature. Point P is at $t \approx 400 \text{ s}$, or 0.111 hr , then

$$Fo = (0.46)(0.111)/L^2 = 0.0511/L^2$$

and

$$Bi = \frac{50}{20} L = 2.5L,$$

with L in ft.

Try $L = 0.1$ ft. In this case, $Bi = 0.25$ and, from Fig. 9.8(a), Fo should be 5.3. However, with $L = 0.1$ ft, $Fo = 5.11$, so that this value of L does not satisfy Fo and Bi simultaneously.

Try $L = 0.05$ ft. Now $Bi = 0.125$, and Fo from Fig. 9.8(a) is 10. With $L = 0.05$ ft, Fo is calculated as 20.4.

We have bracketed the actual value, and after more trial and error, the value of $L = 0.095$ ft leads to agreement between $Bi = 0.24$ and $Fo = 5.6$. Thus we can say that a plate 2.28 in. thick can be fully austempered.

It is important to indicate when limiting cases are valid, such as Newtonian cooling. This, of course, simplifies our work, as Fig. 9.11 demonstrates.

Figure 9.11 presents the solution for the infinite plate in the form of temperature distributions for different times during cooling in media of various Biot numbers. Examination of Fig. 9.11 shows that the temperature gradients within the slab decrease as Bi decreases. A low value of Bi , physically interpreted, reflects low resistance to heat flow

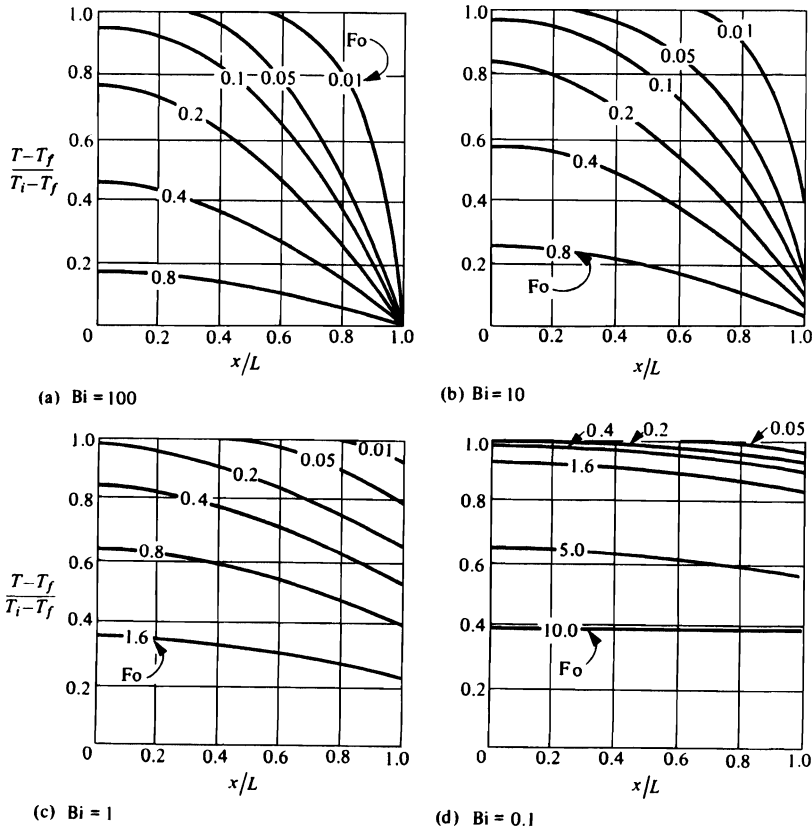


Fig. 9.11 Temperature profiles for infinite plates when cooled under conditions of various Biot numbers.

within the body, L/k , relative to the resistance of the cooling media h^{-1} . In practice, when $Bi \leq 0.1$, the temperature is nearly uniform within the plate. For such cases, we approximate the cooling or heating processes as being controlled solely by surface resistance, and we can apply the Newtonian relationship, Eq. (9.21), as a very close approximation. We may also apply the same approximation to the heating or cooling of cylinders and spheres, with the criterion $Bi \leq 0.1$ still being in effect.

At the other extreme, when the cooling or heating process can be considered to be completely controlled by the internal resistance of the body, then the surface temperature, in effect, immediately changes to T_f , the temperature of the fluid, and remains constant at this temperature. This situation can be considered as a special case with $Bi \rightarrow \infty$. Alternatively, a new solution to Eq. (9.22) could be developed for the same boundary conditions as those of Eqs. (9.23) and (9.24), with $T(L,t) = T_f$ replacing Eq. (9.25). The solution to this problem is given by

$$\frac{T - T_f}{T_i - T_f} = \frac{4}{\pi} \sum_{n=0}^{\infty} \frac{(-1)^n}{2n+1} \exp \left[-\frac{(2n+1)^2 \pi^2}{4} \frac{\alpha t}{L^2} \right] \cos \frac{(2n+1)\pi}{2} \frac{x}{L}. \quad (9.42)$$

Examination of Fig. 9.11 shows that the criterion, $T(L,t) = T_f$, is closely approximated when $Bi = 100$. Thus when $Bi \geq 100$, Eq. (9.41) can be very closely approximated by Eq. (9.42).

9.3.3 Long-time and short-time solutions

The solutions to many problems of unsteady-state heat conduction are in the form of infinite series, such as Eqs. (9.41) and (9.42). This type of series converges rapidly for large Fourier numbers. For short times (small $\alpha t/L^2$), however, the convergence is very slow, requiring an expansion of a great number of terms in the series to obtain sufficiently accurate answers. If we require a solution for short times, alternative series that evolve by the method of Laplace transforms when solving Eq. (9.22) are more convenient. These alternative series have the advantage of converging rapidly for small $\alpha t/L^2$, but the disadvantage of converging very slowly for large $\alpha t/L^2$. Thus the two kinds of solutions complement each other, depending on what value of $\alpha t/L^2$ is of interest. These considerations are important when we wish to use the actual equations, rather than the graphical solutions, as might be the case in computer programming, for example.

If we desire a long-time solution, rather than the complete series of Eq. (9.41), it is convenient to use only the first one or two terms of the series. For this case, we write

$$\frac{T - T_f}{T_i - T_f} = 2 \sum_{n=1}^2 \xi_n \exp [-(\lambda_n L)^2 Fo] \cos \left[(\lambda_n L) \left(\frac{x}{L} \right) \right]. \quad (9.43)$$

Here

$$\xi_n = \frac{\sin(\lambda_n L)}{\lambda_n L + \sin(\lambda_n L) \cos(\lambda_n L)}.$$

The value of $\lambda_n L$ depends on the value of the index n and the Biot number; hence ξ_n is also a function of the same. Values of $(\lambda_n L)$ and ξ_n for $n = 1$ and $n = 2$ are given in Table 9.2.

Table 9.2 Coefficients for the first two terms in Eq. (9.41).

Bi	$\lambda_1 L$	$\lambda_2 L$	ξ_1	ξ_2
0.01	0.0998	3.1448	0.5008	-0.001019
0.02	0.1410	3.1479	0.5017	-0.002000
0.04	0.1987	3.1543	0.5033	-0.004012
0.06	0.2425	3.1606	0.5049	-0.005978
0.08	0.2791	3.1668	0.5065	-0.007862
0.1	0.3111	3.1731	0.5080	-0.009830
0.2	0.4328	3.2039	0.5155	-0.01906
0.4	0.5932	3.2636	0.5290	-0.03596
0.6	0.7051	3.3204	0.5407	-0.05088
0.8	0.7910	3.3744	0.5508	-0.06411
1.0	0.8603	3.4256	0.5596	-0.07584
1.5	0.9882	3.5422	0.5768	-0.09996
2.0	1.0769	3.6436	0.5892	-0.1184
4.0	1.2646	3.9352	0.6144	-0.1607
6.0	1.3496	4.1116	0.6239	-0.1802
8.0	1.3978	4.2264	0.6285	-0.1906
10.0	1.4289	4.3058	0.6310	-0.1967
15	1.4729	4.4255	0.6338	-0.2042
20	1.4961	4.4915	0.6350	-0.2074
40	1.5325	4.5979	0.6362	-0.2109
60	1.5451	4.6353	0.6364	-0.2116
80	1.5514	4.6543	0.6365	-0.2119
100	1.5552	4.6658	0.6365	-0.2120
∞	1.5708	4.7124	0.6366	-0.2122

Example 9.5 A slab of aluminum, 100 mm thick, is quenched from 800 K in a bath of water at 300 K. The heat transfer coefficient is estimated to be 11 000 W m⁻² K⁻¹.

- a) Calculate the temperature at the center of the slab 30 s after being plunged into the water. Use the first two terms of Eq. (9.41).
- b) Repeat, using Fig. 9.8.

The properties of the aluminum are the same as those listed in Example 9.2.

Solution.

$$a) \quad Bi = \frac{hL}{k} = \frac{(11\ 000)(0.050)}{78} = 7.05.$$

$$Fo = \frac{\alpha t}{L^2} = \frac{(2.71 \times 10^{-5})(30)}{(0.050)^2} = 0.325.$$

The first two terms in the infinite series are probably adequate because $Fo > 0.25$. From Table 9.2, $\lambda_1 L = 1.375$, $\xi_1 = 0.6263$ and $\lambda_2 L = 4.1719$, $\xi_2 = -0.1856$. Substituting values into Eq. (9.43) with $x/L = 0$:

$$\frac{T - T_f}{T_i - T_f} = 2 \left\{ 0.6263 \exp \left[-(1.375^2)(0.325) \right] - 0.1856 \exp \left[-(4.1719^2)(0.325) \right] \right\}$$

$$\frac{T - T_f}{T_i - T_f} = 2 \{ 0.3388 - 0.00064 \}.$$

302 Conduction of Heat in Solids

The absolute value of the first term is much larger than the second; this indicates that Eq. (9.41) is converging rapidly, and therefore a good answer results by the use of Eq. (9.43). Solving, we have

$$\frac{T - T_f}{T_i - T_f} = 0.6764,$$

and

$$T = 0.6764(800 - 300) + 300 = 638 \text{ K}.$$

b) By reading Fig. 9.8(a), the result is

$$\frac{T - T_f}{T_i - T_f} \approx 0.68,$$

which is very close to the result by calculation. This difference would have been smaller if we had considered longer times, but would have been larger for shorter times. Usually, Eq. (9.43) suffices for problems of this type if $Fo > 0.25$; it is wise, however, to compare results with those obtained by using Figs. 9.8-9.10.

When the long-time solution is not appropriate, we may utilize the alternative series mentioned above. Here we only present the first several terms of the series without going through the analysis of solving the differential equation. We may deduce the following expression from an equation given by Carslaw and Jaeger³

$$\begin{aligned} \frac{T - T_f}{T_i - T_f} = 1 - & \left[\operatorname{erfc} \frac{(1 - x/L)}{2\sqrt{Fo}} + \operatorname{erfc} \frac{(1 + x/L)}{2\sqrt{Fo}} \right] \\ & + \exp [\operatorname{Bi}(1 - x/L) + \operatorname{Bi}^2 Fo] \cdot \operatorname{erfc} \left[\operatorname{Bi}\sqrt{Fo} + \frac{1 - x/L}{2\sqrt{Fo}} \right] \\ & + \exp [\operatorname{Bi}(1 + x/L) + \operatorname{Bi}^2 Fo] \cdot \operatorname{erfc} \left[\operatorname{Bi}\sqrt{Fo} + \frac{1 + x/L}{2\sqrt{Fo}} \right]. \quad (9.44) \end{aligned}$$

Equation (9.44) contains the *complementary error function*, erfc . The $\operatorname{erfc} N$ is related to the $\operatorname{erf} N$ (the error function) simply by

$$\operatorname{erfc} N = 1 - \operatorname{erf} N,$$

and the $\operatorname{erf} N$ is defined as the value of a definite integral. The definite integral is

$$\operatorname{erf} N = \frac{2}{\sqrt{\pi}} \int_0^N e^{-\beta^2} d\beta.$$

³H. S. Carslaw and J. C. Jaeger, *Conduction of Heat in Solids*, second edition, Oxford University Press, Oxford, UK, 1959, page 310.

The error function is commonly encountered, and hence it has been tabulated. An abbreviated compilation is given in Table 9.3.

Table 9.3 Tabulation of the error function

<i>N</i>	erf <i>N</i>	<i>N</i>	erf <i>N</i>	<i>N</i>	erf <i>N</i>	<i>N</i>	erf <i>N</i>
0.00	0.00000	0.40	0.4284	0.80	0.7421	1.40	0.9523
0.05	0.05637	0.45	0.4755	0.85	0.7707	1.50	0.9661
0.10	0.1125	0.50	0.5205	0.90	0.7969	1.60	0.9763
0.15	0.1680	0.55	0.5633	0.95	0.8209	1.70	0.9838
0.20	0.2227	0.60	0.6039	1.00	0.8427	1.80	0.9891
0.25	0.2763	0.65	0.6420	1.10	0.8802	1.90	0.9928
0.30	0.3286	0.70	0.6778	1.20	0.9103	2.00	0.9953
0.35	0.3794	0.75	0.7112	1.30	0.9340		

Notes

a) erf 0 = 0; erf ∞ = 1,

c) $N > 2.0, \text{erfc } N \cong \frac{e^{-N^2}}{\sqrt{\pi N}},$

b) $N < 0.2, \text{erf } N \cong \frac{2N}{\sqrt{\pi}},$

d) erf (-*N*) = - erf (*N*).

As the reader probably suspects, long-time and short-time solutions are also available for cylinders and spheres. These solutions can be deduced by reference to Carslaw and Jaeger.⁴

In materials processing, the rates of heating and/or cooling are often more important than the determination of the temperature itself. For cases where Newtonian cooling applies, the determination of cooling rates is not too difficult; we discussed this in Section 9.3.1, and illustrated it in Example 9.2. However, when Newtonian cooling does not apply, it is necessary to resort to other means. If analytical expressions are desired, then solutions such as those discussed in Section 9.3.2 and this section may be used to determine $\partial T/\partial t$. If approximate and graphical solutions are needed, then charts given by Paschkis⁵ may be consulted. Surprisingly enough, cooling or heating rates at the surfaces of cylinders and spheres are only 3-4% higher than for plates, when the cooling rates are compared at the same Fourier number. In the internal positions, however, the cooling or heating rates of plates, cylinders and spheres do differ greatly.

Example 9.6 Continuous anneal and continuous quench and temper processes for steel have been installed worldwide over the last decade. In order to achieve the same properties in the commercial product as in the laboratory, the cooling rates in a continuous line must be the same as for the specimens processed in the laboratory. This scale-up is not always understood by materials engineers who are accustomed to working with very thin specimens in the laboratory. Consider a steel that must be cooled from austenitizing temperature (1200 K) to 810 K at an average cooling rate of 3600 K s⁻¹ to achieve the required microstructure. Various thicknesses in the range of 1.0 mm to 2.0 mm are to be processed. Determine whether the desired cooling rate can be achieved throughout the thicknesses if the quenchant has a heat transfer coefficient of $3 \times 10^4 \text{ W m}^{-2} \text{ K}^{-1}$. In order to obtain the necessary production rate in the process, the strip must be in the quenchant (at 285 K) for no more than 0.5 s, and the strip should be no hotter than 400 K when it leaves the quench tank.

⁴H. S. Carslaw and J. C. Jaeger, *ibid*.

⁵V. Paschkis, *Welding Research Supplement*, Sept. 1946, pages 497-502.

304 Conduction of Heat in Solids

Solution. The thermal properties are $C_p = 600 \text{ J kg}^{-1} \text{ K}^{-1}$, $k = 21.5 \text{ W m}^{-1} \text{ K}^{-1}$ and $\rho = 7700 \text{ kg m}^{-3}$. For the thinner section, we calculate the Biot number.

$$\text{Bi} = \frac{hL}{k} = \frac{(3 \times 10^4)(0.5 \times 10^{-3})}{(21.5)} = 0.698.$$

We refer to Fig. 9.8(a) to determine the Fo and the time to achieve 810 K.

$$\frac{T - T_f}{T_i - T_f} = \frac{810 - 285}{1200 - 285} = 0.574.$$

This gives Fo = 1.2, which happens at

$$t = \frac{L^2 \text{Fo}}{\alpha} = \frac{\rho C_p L^2 \text{Fo}}{k} = \frac{(7700)(600)(0.5 \times 10^{-3})^2 (1.2)}{(21.5)} = 6.45 \times 10^{-2} \text{ s},$$

so the average cooling rate from 1200 to 810 K is

$$\frac{\Delta T}{\Delta t} = \frac{1200 - 810}{6.45 \times 10^{-2}} = 6050 \text{ K s}^{-1}.$$

We should also estimate the time required to cool the strip to 400 K.

$$\frac{T - T_f}{T_i - T_f} = \frac{400 - 285}{1200 - 285} = 0.126.$$

This corresponds to Fo = 4, which happens at $t = 0.215 \text{ s}$. Therefore, strip of 1 mm thickness can be successfully processed.

We now repeat the calculations for the thicker strip.

$$\text{Bi} = \frac{(3 \times 10^4)(1 \times 10^{-3})}{(21.5)} = 1.40.$$

$$\frac{T - T_f}{T_i - T_f} = 0.574.$$

From Fig. 9.8(a), Fo = 0.75 and

$$t = \frac{(7700)(600)(1 \times 10^{-3})^2 (0.75)}{(21.5)} = 0.161 \text{ s}.$$

Therefore, the average cooling rate to cool from 1200 to 810 K is

$$\frac{\Delta T}{\Delta t} = \frac{1200 - 810}{0.161} = 2.42 \times 10^3 \text{ K s}^{-1},$$

which is much less than the specified cooling rate of 3600 K s^{-1} . The thicker strip cannot be quenched rapidly enough in this process.

9.4 TRANSIENT CONDITIONS, INFINITE AND SEMI-INFINITE SOLIDS

In Section 9.3, all the solids we considered had at least one dimension of finite extent. In this section, we consider the so-called infinite and semi-infinite solids. The solutions for the

semi-infinite solids can be applied when the time involved in transient situations is very short, or during the time of interest the depth of material affected by the boundary condition is less than the thickness of material itself. There are many applications of these solutions, such as heat transfer in certain solidification problems, and also in diffusion problems which are discussed in Part III, Mass Transport. We start by looking at a stationary source in an infinite solid. A moving source with steady power will be considered in Section 9.6; this has application in materials processes such as laser heating and welding.

9.4.1 Infinite solid

Consider the infinite solid in Fig. 9.12(a) where at time zero a thin slice of material $\Delta x'$ thick at $x = x'$ is at some temperature T_i . This temperature peak decays with time, as shown in Fig. 9.12(b). Again for transient heat conduction, Eq. (9.22) applies, and the solution is

$$T(x,t) = \frac{T_i}{2\sqrt{\pi\alpha t}} \exp \left[-\frac{(x - x')^2}{4\alpha t} \right] \Delta x'. \tag{9.45}$$

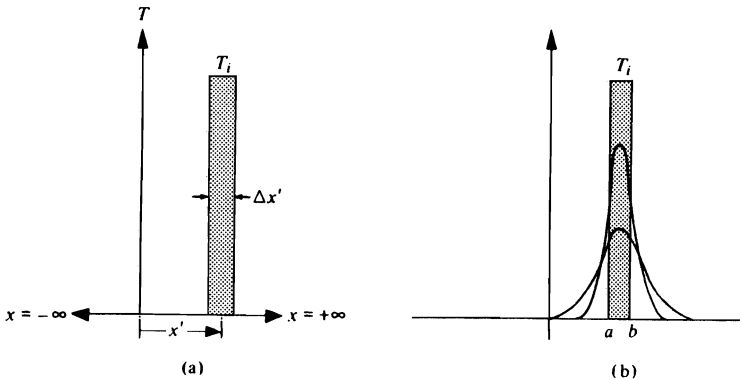


Fig. 9.12 Temperature distribution in an infinite solid showing (a) an initial temperature peak, and (b) the decay of the peak with time.

If another slice of the same thickness exists at time zero with a different temperature T_i , then the temperature at x and t is the sum of contributions from both peaks. For this case then, Eq. (9.45) is applied to the peaks at x'_1 and x'_2 and the temperature is

$$T(x,t) = \sum_{n=1}^2 \frac{T_{i_n}}{2\sqrt{\pi\alpha t}} \exp \left[-\frac{(x - x'_n)^2}{4\alpha t} \right] \Delta x'. \tag{9.46}$$

Now think of many such slices side by side occupying the whole space. If the thicknesses of the individual slices are allowed to approach zero, then all the various T_{i_n} s can be considered to form a function $f(x')$. In this case, examine the series in the limit as the slices all approach zero thickness

$$T(x,t) = \lim_{\Delta x' \rightarrow 0} \sum_{n=1}^{\infty} \frac{f(x'_n)}{2\sqrt{\pi\alpha t}} \exp \left[-\frac{(x - x'_n)^2}{4\alpha t} \right] \Delta x'. \tag{9.47}$$

As $\Delta x' \rightarrow 0$, the infinite summation becomes an integral

$$T(x,t) = \int_{x'=-\infty}^{\infty} \frac{f(x')}{2\sqrt{\pi\alpha t}} \exp\left[-\frac{(x-x')^2}{4\alpha t}\right] dx'. \quad (9.48)$$

As an example consider an initial distribution (Fig. 9.13). For this case, we develop the solution by recognizing that $f(x') = 0$ for all x except $a < x < b$ where $f(x') = T_i$. Substituting this information into Eq. (9.48) yields

$$T = \int_{-\infty}^a 0 dx + \int_a^b \frac{T_i}{2\sqrt{\pi\alpha t}} \exp\left[-\frac{(x-x')^2}{4\alpha t}\right] dx' + \int_b^{\infty} 0 dx. \quad (9.49)$$

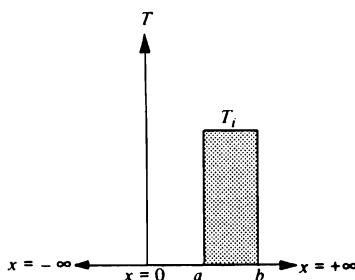


Fig. 9.13 The initial distribution of uniform temperature T_i between $x = a$ and $x = b$.

Let $\beta = (x' - x)/2\sqrt{\alpha t}$; this transforms Eq. (9.49) into

$$T = \frac{T_i}{\sqrt{\pi}} \int_{\beta = (a-x)/2\sqrt{\alpha t}}^{(b-x)/2\sqrt{\alpha t}} e^{-\beta^2} d\beta = \frac{T_i}{2} \left[\frac{2}{\sqrt{\pi}} \int_0^{(b-x)/2\sqrt{\alpha t}} e^{-\beta^2} d\beta - \frac{2}{\sqrt{\pi}} \int_0^{(a-x)/2\sqrt{\alpha t}} e^{-\beta^2} d\beta \right]. \quad (9.50)$$

Therefore we write Eq. (9.50) as

$$T = \frac{T_i}{2} \left[\operatorname{erf} \left[\frac{b-x}{2\sqrt{\alpha t}} \right] - \operatorname{erf} \left[\frac{a-x}{2\sqrt{\alpha t}} \right] \right]. \quad (9.51)$$

9.4.2 Semi-infinite solid

A semi-infinite solid has an extent of $0 \leq x < \infty$, that is, a very thick solid with a surface at $x = 0$. At this surface the transient is put into effect. For example, we solve the problem with the following conditions for the region $0 \leq x < \infty$:

$$T(x,0) = f(x), \quad (9.52)$$

$$T(0,t) = 0. \tag{9.53}$$

We develop the solution to this problem by referring to an infinite solid with the initial condition depicted in Fig. 9.14(a). For the *odd function* where $f(-x') = -f(x')$, the boundary condition (9.53) is automatically satisfied; therefore we use Eq. (9.48) as follows to satisfy this boundary condition:

$$T = \int_{-\infty}^0 \frac{-f(-x')}{2\sqrt{\pi\alpha t}} \exp\left[\frac{-(x-x')^2}{4\alpha t}\right] dx' + \int_0^{\infty} \frac{f(x')}{2\sqrt{\pi\alpha t}} \exp\left[\frac{-(x-x')^2}{4\alpha t}\right] dx'. \tag{9.54}$$

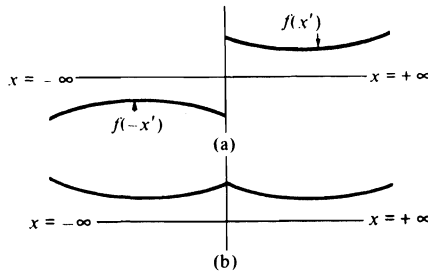


Fig. 9.14 Temperature distribution in infinite solids that satisfy boundary conditions for semi-infinite solids. (a) Odd function, $T(0,t) = 0$. (b) Even function, $\partial T(0,t)/\partial x = 0$.

The problem with the flux equal to zero at the surface is set up in a similar manner. For this case, the conditions for the region $0 \leq x < \infty$ become

$$T(x,0) = f(x), \tag{9.55}$$

$$\frac{\partial T}{\partial x}(0,t) = 0. \tag{9.56}$$

We indicate the method of setting up this situation in Fig. 9.14(b), where an *even function*, $f(x') = f(-x')$, gives symmetry to the temperature field about $x = 0$, so that condition (9.56) is automatically satisfied. Thus we use Eq. (9.48) in the following form

$$T = \int_{-\infty}^0 \frac{f(-x')}{2\sqrt{\pi\alpha t}} \exp\left[\frac{-(x-x')^2}{4\alpha t}\right] dx' + \int_0^{\infty} \frac{f(x')}{2\sqrt{\pi\alpha t}} \exp\left[\frac{-(x-x')^2}{4\alpha t}\right] dx'. \tag{9.57}$$

Finally as an application of Eq. (9.54), consider the important and often encountered problem of the semi-infinite solid with the conditions

$$T(x,0) = T_i, \tag{9.58}$$

$$T(0,t) = T_s. \tag{9.59}$$

This situation is depicted in Fig. 9.15. Initially the semi-infinite solid is at a uniform temperature T_i , and its surface is abruptly brought to a temperature that is maintained at T_s . Thus, we can think of the temperature field in the vicinity of the surface of a thick solid, even a solid with a finite thickness, provided certain conditions are met, as will be discussed.

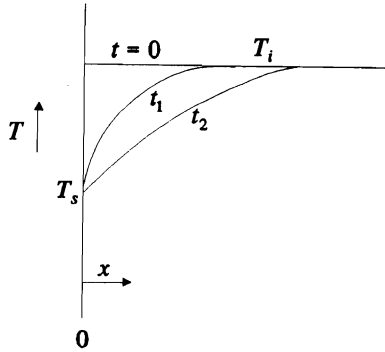


Fig. 9.15 Temperature in a semi-infinite solid with its surface temperature constant for $t > 0$.

If we define $\theta = T - T_s$, the conditions become

$$\theta(x,0) = T_i - T_s = \theta_i, \quad (9.60)$$

$$\theta(0,t) = 0. \quad (9.61)$$

Thus Eq. (9.54) applies for θ , where $f(x') = \theta_i$ (uniform initial distribution). Even so, after we look at Eq. (9.54) we might hesitate to use it because it involves integrating to $x = \infty$. This is done in Appendix F. Here, we give the final equation, which is

$$\frac{T - T_s}{T_i - T_s} = \operatorname{erfc} \left[\frac{x}{2\sqrt{\alpha t}} \right]. \quad (9.62)$$

To summarize, Eq. (9.62) describes the temperature as a function of position and time in a semi-infinite solid initially at a uniform temperature T_i , with its surface temperature suddenly raised or lowered to T_s at $t = 0$ and maintained for $t > 0$. In practice, we consider a solid to be semi-infinite until such time as all of the solid differs appreciably from T_i .

Equation (9.62) is applied to many problems in materials processing. Another important problem of heat flow for a semi-infinite solid remains to be discussed. For the cooling (or heating) of slabs, Eq. (9.41) was developed; however, as mentioned previously, this equation is unwieldy for "short times." For short times we found that Eq. (9.44) was more appropriate. Here, we present a solution that is a slightly simplified version of Eq. (9.44), which applies for the very short times when the center of the slab has not yet felt the effects of the changing temperature field. For such a situation, we may consider the solid to be semi-infinite, and the following initial and boundary conditions must be satisfied:

$$T(x,0) = T_i, \quad (9.63)$$

$$k \frac{\partial T(0,t)}{\partial x} = h[T(0,t) - T_f]. \quad (9.64)$$

We present only the final solution:

$$\frac{T - T_i}{T_f - T_i} = \operatorname{erfc} \left[\frac{x}{2\sqrt{\alpha t}} \right] - e^{\gamma} \operatorname{erfc} \left[\frac{x}{2\sqrt{\alpha t}} + \frac{h}{k} \sqrt{\alpha t} \right], \quad (9.65)$$

where

$$\gamma = \frac{h}{k} \sqrt{\alpha t} \left[\frac{x}{\sqrt{\alpha t}} + \frac{h}{k} \sqrt{\alpha t} \right]$$

The solution given by Eq. (9.65) is also shown in Fig. 9.16.

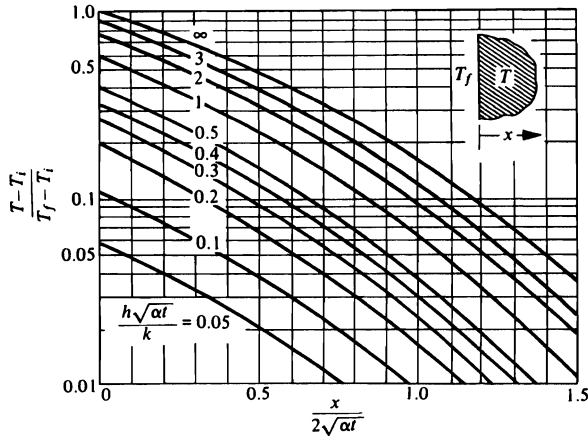
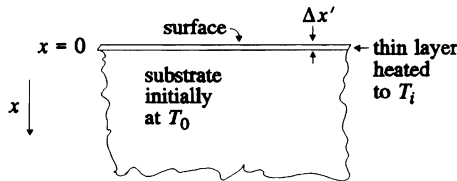


Fig. 9.16 Temperature history in a semi-infinite solid with surface resistance. (From P. J. Schneider, *Conduction Heat Transfer*, Addison-Wesley, Reading, MA, 1955, page 266.)

Example 9.7 Lasers can be used in several materials processing schemes including the rapid heating and subsequent quenching of surface layers. Suppose a laser is pulsed once at the surface and heats a very thin layer of thickness $\Delta x'$ to temperature T_i . Derive an equation that gives cooling rate, $\partial T / \partial t$, versus distance from the surface and time after the single pulse of energy from the laser.



Solution. If we neglect the small heat loss from the surface, then the solution is twice the relative temperature (also called dimensionless temperature) given by Eq. (9.45) with $x' = 0$.

$$\frac{T - T_0}{T_i - T_0} = \frac{2\Delta x'}{2\sqrt{\pi\alpha t}} \exp \left[-\frac{x^2}{4\alpha t} \right],$$

$$\frac{\partial T}{\partial t} = (T_i - T_0) \Delta x' \left\{ \frac{1}{\sqrt{\pi\alpha t}} \frac{\partial}{\partial t} \left[\exp \left[-\frac{x^2}{4\alpha t} \right] \right] + \exp \left[-\frac{x^2}{4\alpha t} \right] \frac{\partial}{\partial t} \left[\frac{1}{\sqrt{\pi\alpha t}} \right] \right\}$$

This simplifies to

$$\frac{\partial T}{\partial t} = \left(\frac{T - T_0}{t} \right) \left[\frac{x^2}{4\alpha t} - \frac{1}{2} \right].$$

Example 9.8 Aluminum oxide at 300 K is pulsed with a laser such that $0.1 \mu\text{m}$ of its surface is raised to 3600 K. Calculate the cooling rate at a depth of $0.3 \mu\text{m}$ as a function of temperature. The thermal diffusivity of the aluminum oxide is $1.6 \times 10^{-6} \text{ m}^2 \text{ s}^{-1}$.

Solution. The equation derived in Example 9.7 applies. We need temperature versus time first. This is found from

$$T - T_0 = (T_i - T_0) \frac{\Delta x'}{\sqrt{\pi\alpha t}} \exp \left[-\frac{x^2}{4\alpha t} \right],$$

with $(T_i - T_0) = 3300 \text{ K}$, $\Delta x' = 1 \times 10^{-7} \text{ m}$, and $x = 3 \times 10^{-7} \text{ m}$. Temperature and time are tabulated below in the first two columns. The corresponding heating and cooling rates are in the third column.

Time, s	$(T - T_0)$, K	$\partial T/\partial t$, K s ⁻¹
1×10^{-9}	0.004	4.93×10^7
5×10^{-9}	125.0	5.78×10^{10}
1×10^{-8}	360.7	3.27×10^{10}
2×10^{-8}	515.2	5.23×10^9
3×10^{-8}	531.8	-5.54×10^8
5×10^{-8}	496.9	-2.17×10^9
1×10^{-7}	404.4	-1.45×10^9
5×10^{-7}	202.4	-1.91×10^8
1×10^{-6}	145.1	-7.05×10^7
5×10^{-6}	65.6	-6.53×10^6
1×10^{-5}	46.5	-2.32×10^6

Before leaving this example, it is instructive to point out some features of the temperature field. At a depth of $0.3 \mu\text{m}$, there is a heating period of somewhat less than $3 \times 10^{-8} \text{ s}$, during which a maximum temperature of more than 832 K is achieved. Heating is followed by cooling at rates less than the heating rates, and the material returns to within 50 K of the base temperature in only $1 \times 10^{-5} \text{ s}$. This example demonstrates that extremely high heating and cooling rates are achievable in the surface layers of solids when they are pulsed with lasers.

Example 9.9 The *Jominy end-quench* test is commonly used to assess the hardenability of steels. The temperature near the quenched end can be approximated as that in a semi-infinite solid with its surface (i.e., the end of the Jominy bar) quenched by a spray of 295 K water with $h \rightarrow \infty$.

In an eutectoid steel, a microstructure of 50% martensite-50% pearlite is achieved at a distance of 9 mm from the end-quench when the steel is initially heated to 1090 K before the quench. Assume that the achievable microstructure depends on the time to cool to 840 K. Knowing this, predict the maximum thickness of a plate in which a 50% martensite-50% pearlite microstructure can be achieved when the plate is quenched in brine with no agitation

($h = 2700 \text{ W m}^{-2} \text{ K}^{-1}$). The thermal properties of the steel are $k = 21.5 \text{ W m}^{-1} \text{ K}^{-1}$, $C_p = 600 \text{ J kg}^{-1} \text{ K}^{-1}$, and $\rho = 7700 \text{ kg m}^{-3}$.

Solution. Starting with our knowledge of the Jominy end-quench, we calculate the time to achieve 840 K at $x = 9 \text{ mm}$.

$$\frac{T - T_s}{T_i - T_s} = \text{erf} \left[\frac{x}{2\sqrt{\alpha t}} \right]$$

$$\frac{840 - 295}{1090 - 295} = 0.6855 = \text{erf} \left[\frac{x}{2\sqrt{\alpha t}} \right].$$

From Table 9.3 and $\alpha = 4.65 \times 10^{-6} \text{ m}^2 \text{ s}^{-1}$:

$$\frac{x}{2\sqrt{\alpha t}} = 0.7115,$$

and

$$t = \frac{x^2}{(0.7115^2)(4\alpha)} = \frac{(0.009^2)}{(0.7115^2)(4)(4.65 \times 10^{-6})} = 8.60 \text{ s}.$$

In order to deal with the plate, we make use of Fig. 9.8(a). The semithickness of the plate, however, appears in both Fo and Bi so that a trial-and-error solution is sought. We fix the relative temperature at 0.6855 and read corresponding values of Fo and Bi from the curves in Fig. 9.8(a). The length derivable from Fo is L_1 :

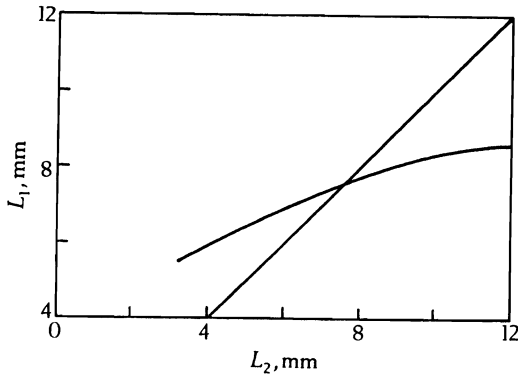
$$L_1 = \left[\frac{\alpha t}{\text{Fo}} \right]^{1/2} = \left[\frac{4.65 \times 10^{-6} \times 8.60}{\text{Fo}} \right]^{1/2},$$

and the length from Bi is L_2 :

$$L_2 = \frac{k \text{ Bi}}{h} = \left[\frac{21.5 \text{ Bi}}{2700} \right].$$

The solution is when $L = L_1 = L_2$. By some trial-and-error, we find that the solution is in the region $0.4 \leq \text{Bi} \leq 1.5$; so we plot several values in this range.

Fo	Bi	L_1 , mm	L_2 , mm
1.3	0.4	5.55	3.18
1	0.6	6.32	4.78
0.65	1.0	7.84	7.96
0.52	1.5	8.77	11.94



The solution is $L = 7.7$ mm so that the thickness of the plate is 15.4 mm.

9.5 SIMPLE MULTIDIMENSIONAL PROBLEMS

In this section we present methods of obtaining solutions for solid shapes such as cubes, rectangular bars, and short cylinders. These solutions can be obtained directly by simply combining solutions for the semi-infinite solid, the infinitely long cylinder, and the infinite slab, which are given in Sections 9.3 and 9.4.

As an example, consider an infinitely long bar with a rectangular cross-section $2L$ by $2l$, using coordinates as illustrated by Fig. 9.17. The bar is initially at the uniform temperature T_i , and then it is suddenly exposed to a convective environment at T_f . In such a bar, $T(x, y, t)$ must satisfy the partial differential equation

$$\frac{\partial T}{\partial t} = \alpha \left[\frac{\partial^2 T}{\partial x^2} + \frac{\partial^2 T}{\partial y^2} \right]. \quad (9.66)$$

Recall that the temperature in solids is best represented by the relative temperature; here, we assign Θ so that

$$\Theta = \frac{T - T_f}{T_i - T_f}.$$

We can prove that the solution $\Theta(x, y, t)$ is the product

$$\Theta(x, y, t) = X(x, t) \cdot Y(y, t). \quad (9.67)$$

Here, $X(x, t)$ is the solution for the temperature response in the infinite slab of thickness $2L$, and $Y(y, t)$ is the solution for the infinite slab of thickness $2l$. The reader is invited to pursue Problem 9.22 at the end of this chapter to satisfy himself of the validity of Eq. (9.67).

We may also make use of the solution for the semi-infinite solid in combination with solutions to solids such as the infinite plate or semi-infinite cylinder. For example, consider the semi-infinite cylinder for which we seek the solution of $\Theta(r, y, t)$. If $S(y, t)$ represents the solution to the semi-infinite solid in the regime $0 \leq y < \infty$, and $C(r, t)$ is the solution for the infinitely long cylinder, then the solution we seek is simply their product, that is,

$$\Theta(r, y, t) = S(y, t) \cdot C(r, t). \quad (9.68)$$

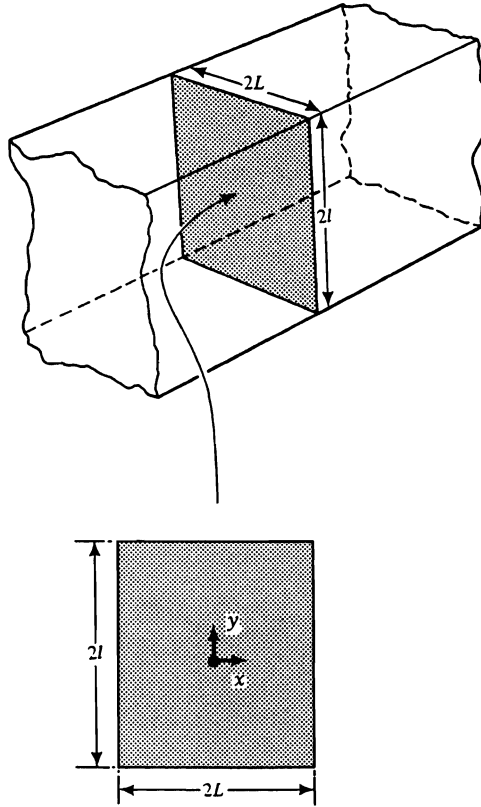


Fig. 9.17 Rectangular bar showing the system of coordinates.

By means of this method, many so-called *product solutions* can be developed for a large number of solid shapes, some of which are depicted in Fig. 9.18, with their respective solutions indicated.

Example 9.10 A cylindrical polyethylene preform (at 300 K) is to be preheated for 100 s in a bath of hot oil at 500 K with $h = 200 \text{ W m}^{-1} \text{ K}^{-1}$. The polyethylene has a thermal diffusivity of $1 \times 10^{-7} \text{ m}^2 \text{ s}^{-1}$ and a thermal conductivity of $0.34 \text{ W m}^{-1} \text{ K}^{-1}$. The preform has a diameter of 10 mm and a length of 8 mm. a) Calculate the temperature at its geometrical center. b) What is the surface temperature at one-half of the distance between the ends?

Solution.

$$\text{a) } \text{Bi}_R = \frac{hR}{k} = \frac{(200)(0.005)}{0.34} = 2.94,$$

$$\text{Fo}_R = \frac{\alpha t}{R^2} = \frac{(1 \times 10^{-7})(100)}{(0.005)^2} = 0.400.$$

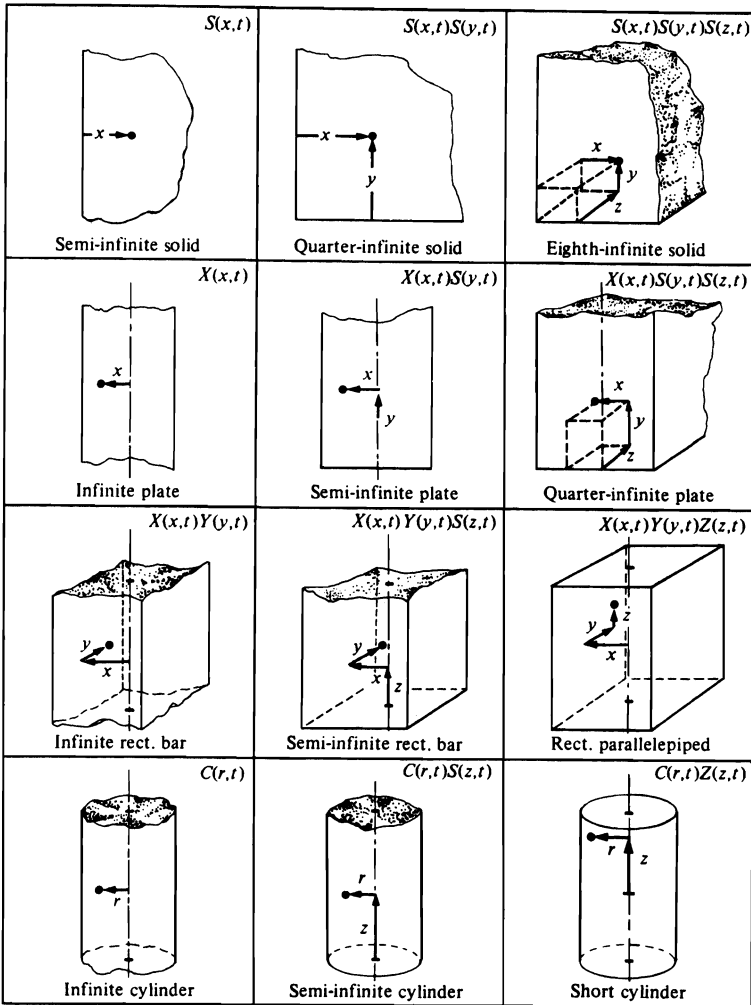


Fig. 9.18 The composition of product solutions.

From Fig. 9.9(a),

$$C(0,t) = \left[\frac{T_0 - T_f}{T_i - T_f} \right]_{\infty \text{ cyl.}} = 0.407.$$

Additionally,

$$Bi_L = \frac{hL}{k} = \frac{(200)(0.004)}{0.34} = 2.35,$$

$$Fo_L = \frac{\alpha t}{L^2} = \frac{(1 \times 10^{-7})(100)}{(0.004)^2} = 0.625.$$

From Fig. 9.8(a),

$$X(0, t) = \left[\frac{T_0 - T_f}{T_i - T_f} \right]_{\infty \text{ plate}} = 0.552.$$

To get the solution, we take the product

$$\frac{T - T_f}{T_i - T_f} = C(0, t) \cdot X(0, t) = (0.407)(0.552) = 0.225,$$

and

$$T = (0.225)(300 - 500) + 500 = 455 \text{ K}.$$

b) For this case we use Fig. 9.9(b):

$$C(R, t) \approx 0.545.$$

Now the product is

$$\frac{T - T_f}{T_i - T_f} = C(R, t) \cdot X(0, t) = (0.545)(0.552) = 0.300,$$

and

$$T = (0.300)(300 - 500) + 500 = 440 \text{ K}.$$

In Example 9.10, we were given the time and asked to determine the temperature so that the method of solution was direct. Given a specified temperature to be achieved and asked to determine the time, however, is not so simple and requires trial-and-error iterations. Some of the problems at the end of this chapter are posed in the latter scenario.

9.6 MOVING SOURCES

Processes that utilize concentrated power sources in materials processing include processes for surface modification, cutting, and joining. Power sources include laser beams, electron beams, and electric arcs. Here we present and discuss analytical solutions to two types of mathematical sources that are used to estimate the temperature field in processes involving moving sources. The solutions are presented again in the next chapter where they are applied to thermal aspects of welding.

9.6.1 Moving point source

A power source that is approximated as a point source moves with a constant velocity on the surface of a thick plate. The situation is depicted in Fig. 9.19, where an isotherm is shown. In front of the source, the thermal gradients are steeper than the gradients behind

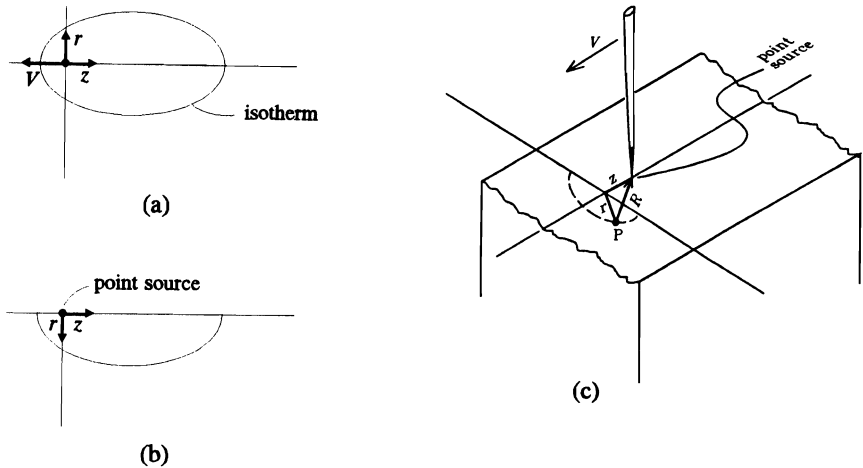


Fig. 9.19 Moving point source and an isotherm on the surface of a thick plate. The point source is moving to the left with velocity V . (a) View from the top; (b) view of transverse section; (c) perspective showing coordinates of point P on an isotherm in terms of the cylindrical coordinates r and z or in terms of the spherical coordinate $R = (z^2 + r^2)^{1/2}$.

the source. Therefore, the front of any isotherm is closer to the source than it is behind the source.

In cylindrical coordinates, the energy equation can be deduced from Eq. (B) in Table 7.5. For constant and uniform thermal properties, we have

$$\frac{\partial T}{\partial t} = \alpha \left[\frac{1}{r} \frac{\partial}{\partial r} \left(r \frac{\partial T}{\partial r} \right) + \frac{\partial^2 T}{\partial z^2} \right]. \quad (9.69)$$

This equation gives $\partial T/\partial t$ experienced by any stationary unit element in the solid. Suppose, however, that we choose an element that moves with the same constant velocity, V , of the source. If we do this, it becomes convenient to work with a moving coordinate system with the origin at the source, as depicted in Fig. 9.19. With respect to the moving coordinate system, Eq. (9.69) transforms to

$$V \frac{\partial T}{\partial z} = \alpha \left[\frac{1}{r} \frac{\partial}{\partial r} \left(r \frac{\partial T}{\partial r} \right) + \frac{\partial^2 T}{\partial z^2} \right]. \quad (9.70)$$

Furthermore, it is convenient to also think in terms of a spherical distance from the moving origin. This spherical coordinate is denoted R to avoid confusion with the cylindrical coordinate r . The spherical coordinate is related to z and r by

$$R^2 = z^2 + r^2. \quad (9.71)$$

With source strength given as power, Q , in W , the temperature must satisfy two boundary conditions:

$$\text{B.C. 1: } T = T_{\infty} \quad \text{at } R = \infty, \quad (9.72)$$

$$\text{B.C. 2: } Q = \left[(2\pi R^2) \left[-k \frac{\partial T}{\partial R} \right] \right]_{R=0}. \quad (9.73)$$

Equation (9.72) can be satisfied by assuming

$$T = T_{\infty} + \theta(z, r) \exp \left[\frac{Vz}{2\alpha} \right], \quad (9.74)$$

then Eq. (9.70) becomes

$$\frac{\partial^2 \theta}{\partial z^2} + \frac{\partial}{\partial r} \left[r \frac{\partial \theta}{\partial r} \right] + \frac{V^2}{4\alpha^2} \theta = 0. \quad (9.75)$$

A solution to Eq. (9.75) is

$$\theta = \frac{A}{R} \exp \left[-\frac{VR}{2\alpha} \right], \quad (9.76)$$

in which A is an arbitrary constant. (Remember R is single variable that represents both r and z , Eq. (9.71).) With the solution in this form, Eq. (9.73) requires

$$A = \frac{Q}{2\pi k};$$

therefore, the temperature in the thick plate is

$$T - T_{\infty} = \frac{Q}{2\pi kR} \exp \left[\frac{Vz}{2\alpha} \right] \exp \left[-\frac{VR}{2\alpha} \right]. \quad (9.77)$$

This result was originally given by Rosenthal.⁶

Equation (9.77) can also be written

$$T - T_{\infty} = \frac{QV}{4\pi k\alpha} \left(\text{Pe}_z^2 + \text{Pe}_r^2 \right)^{-1/2} \exp \left[\text{Pe}_z - \left(\text{Pe}_z^2 + \text{Pe}_r^2 \right)^{1/2} \right], \quad (9.78)$$

where Pe_z and Pe_r are Peclet numbers defined as

$$\text{Pe}_z = \frac{Vz}{2\alpha} \quad \text{and} \quad \text{Pe}_r = \frac{Vr}{2\alpha}.$$

Notice that in Eq. (9.78) we have resorted to cylindrical coordinates, z and r . With cylindrical coordinates, it is more convenient to derive an equation for the so-called *peak temperature*. Suppose we insert a thermocouple into the plate and measure temperature versus time. Of course, the thermocouple is fixed so it experiences the temperature of a stationary observer. Temperature increases as the source moves toward the vicinity of the thermocouple but then decreases as the source passes by. Hence, at a given distance r from the path of the source, a unique peak temperature is achieved. In materials processing,

⁶D. Rosenthal, *Weld. J.* **20**, 220s (1941).

knowledge of the peak temperature is important because it pertains to the likelihood of a transformation occurring during the heating and cooling cycle.

The peak temperature can be found by finding the following extremum in Eq. (9.78):

$$\frac{\partial Pe_r}{\partial Pe_z} = 0.$$

The result of this operation is

$$Pe_z^2 + Pe_r^2 = Pe_z \left[1 + (Pe_z^2 + Pe_r^2)^{1/2} \right]. \quad (9.79)$$

Except in the immediate vicinity of the point source, Eq. (9.79) is closely approximated with

$$Pe_r^2 \approx 2Pe_z. \quad (9.80)$$

Equation (9.80) is a good approximation only if $Pe_r > 5$; otherwise the following approximations can be consulted to obtain values of Pe_z and Pe_r that satisfy Eq. (9.79):

$$\log_{10} Pe_r = 0.505 \log_{10} Pe_z + 0.02, \quad 10^{-2} \leq Pe_r \leq 10^{-1}$$

and

$$\log_{10} Pe_r = 0.547 \log_{10} Pe_z + 0.100, \quad 10^{-1} \leq Pe_r \leq 5.$$

If $Pe_r > 5$ applies, then the peak temperature, T_p , can be obtained by substituting $T_p = T$ and Eq. (9.80) into Eq. (9.78). The final result is

$$T_p - T_\infty = \left[\frac{QV}{2\pi k\alpha e} \right] \left[\frac{1}{2 + Pe_r^2} \right], \quad Pe_r > 5. \quad (9.81)$$

where $e = 2.7183$. Equation (9.81) was first derived by Adams.⁷

If Eq. (9.81) cannot be used, then a set of values of Pe_z and Pe_r that satisfy Eq. (9.79) should be obtained and then substituted into Eq. (9.78) with $T = T_p$, the peak temperature. This procedure is illustrated in the following example.

Example 9.11 Estimate the peak temperature as a function of r , the radial distance from the path of a moving laser. Aluminum oxide at 300 K is subjected to a 1 kW laser beam, moving at 1 mm s⁻¹. Assume that the efficiency of the laser energy is 30 percent. The thermal diffusivity of the aluminum oxide is 1.6×10^{-6} m² s⁻¹, and its thermal conductivity is 6 W m⁻¹ K⁻¹.

Solution. Let us start with $r = 0.05$ mm.

$$Pe_r = \frac{Vr}{2\alpha} = \frac{(1 \times 10^{-3})(5 \times 10^{-5})}{(2)(1.6 \times 10^{-6})} = 1.562 \times 10^{-2}.$$

⁷C. M. Adams, *Weld J.* 37, 210s (1958).

Then

$$\log_{10} Pe_r = 0.505 \log_{10} Pe_z + 0.02,$$

and with $Pe_r = 1.562 \times 10^{-2}$, we calculate $Pe_z = 2.42 \times 10^{-4}$. These values give

$$[Pe_z^2 + Pe_r^2]^{1/2} = 1.562 \times 10^{-2},$$

so that Eq. (9.78) with $T = T_p$ can be used:

$$T_p - 300 = \frac{(300)(0.001) \exp [2.42 \times 10^{-4} - 1.562 \times 10^{-2}]}{(4\pi)(6)(1.6 \times 10^{-6})(1.562 \times 10^{-2})} = 1.57 \times 10^5 \text{ K.}$$

Obviously any real material melts at this temperature.

The peak temperatures at other values of r are determined in the same way, provided the appropriate estimates for Pe_z are used. The results are tabulated below.

r , mm	Pe_r	T_p , K
0.05	1.562×10^{-2}	1.57×10^5
0.10	3.125×10^{-2}	7.75×10^4
0.5	1.562×10^{-1}	1.41×10^4
1	3.125×10^{-1}	6349
2	0.625	2722
3	0.938	1638
4	1.25	1152
6	1.875	732
8	2.5	559
10	3.125	472

Notice that the peak temperatures are above the melting point for approximately the first two millimeters.

9.6.2 Moving Line Source

When the plate is thin enough, it is better to assume that the power source is a *line source*, Fig. 9.20. Equation (9.70) applies; the solution⁸ is

$$T - T_\infty = \frac{Q}{2\pi k\delta} \exp (Pe_z) K_0 \left(\sqrt{Pe_z^2 + Pe_r^2} \right), \tag{9.82}$$

where δ is the thickness of the plate and K_0 is the modified Bessel function of the second kind and order zero. An approximation⁹ is

$$K_0 \left(\sqrt{Pe_z^2 + Pe_r^2} \right) \approx \left(\frac{\pi}{2} \right)^{1/2} \frac{\exp \left(-\sqrt{Pe_z^2 + Pe_r^2} \right)}{\sqrt[4]{Pe_z^2 + Pe_r^2}}, \tag{9.83}$$

⁸D. Rosenthal, *ibid.*

⁹C. M. Adams, *ibid.*

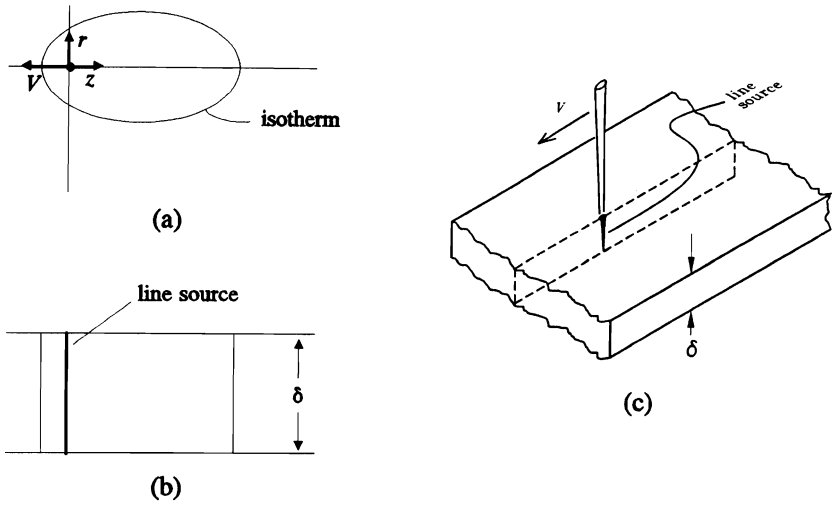


Fig. 9.20 Moving line source and an isotherm in a thin plate. (a) View from top; (b) view of transverse section along the path of the source ($r = 0$); (c) perspective showing the line source.

so that

$$T - T_{\infty} = \frac{Q}{\sqrt{8\pi} k\delta} \frac{\exp(\text{Pe}_z) - \sqrt{\text{Pe}_z^2 + \text{Pe}_r^2}}{\sqrt[4]{\text{Pe}_z^2 + \text{Pe}_r^2}}. \quad (9.84)$$

As before, the peak temperature is derived by finding the extremum

$$\frac{\partial \text{Pe}_r}{\partial \text{Pe}_z} = 0.$$

The final result, based on the approximation of Eq. (9.83), is

$$T_p - T_{\infty} \approx \frac{Q}{\sqrt{8\pi e} k\delta \text{Pe}_r}. \quad (9.85)$$

Example 9.12 Select $r = 1$ mm, use the conditions specified in Example 9.11 and determine peak temperature versus the thickness of the plate.

$$\text{Pe}_r = \frac{Vr}{2\alpha} = \frac{(0.001)(0.001)}{(2)(1.6 \times 10^{-6})} = 0.3125.$$

$$T_p - 300 = \frac{(300)}{(\sqrt{8\pi e})(6)(0.3125)\delta} = \frac{19.36}{\delta}.$$

The results are tabulated below.

δ , mm	T_p , K
5	4172 (melts)
10	2236
20	1268
30	945
40	784

PROBLEMS

(For practice in manipulating units, some of the problems are in English units.)

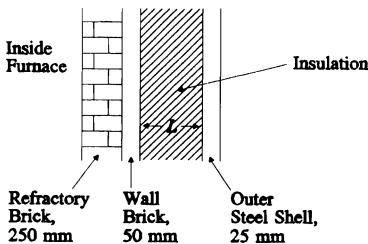
9.1 A furnace wall is constructed of 7 in. of fire brick ($k = 0.60 \text{ Btu h}^{-1} \text{ ft}^{-1} \text{ }^\circ\text{F}^{-1}$), 4 in. of red brick ($k = 0.40$), 1 in. of glass-wool insulation ($k = 0.04$), and $\frac{1}{8}$ in. steel plate ($k = 26$) on the outside. The heat transfer coefficients on the inside and outside surfaces are 9 and $3 \text{ Btu h}^{-1} \text{ ft}^{-2} \text{ }^\circ\text{F}^{-1}$, respectively. The gas temperature inside the furnace is 2500°F , and the outside air temperature is 90°F .

- Calculate the heat-transfer rate through the wall ($\text{Btu h}^{-1} \text{ ft}^2$).
- Determine the temperatures at all interfaces.

9.2 Consider the flow of heat through a spherical shell. For steady-state conditions, the inside surface ($r = R_1$) is at temperature T_1 , and the outside surface ($r = R_2$) is at T_2 .

- Write the pertinent differential energy equation that applies.
- Write the boundary conditions and develop an expression for the temperature distribution in the shell.
- Develop an expression for the heat flow (Q , W) through the shell.
- Determine the thermal resistance of the spherical shell.

9.3 In order to reduce the heat loss through a large furnace wall, the decision has been made to add external insulation. Calculate the thickness of insulation required to reduce the heat loss by 75%. Before the change is made, no outer steel shell is used.



Data: Refractory brick and wall brick:

$$k = 0.87 \text{ W m}^{-1} \text{ K}^{-1}.$$

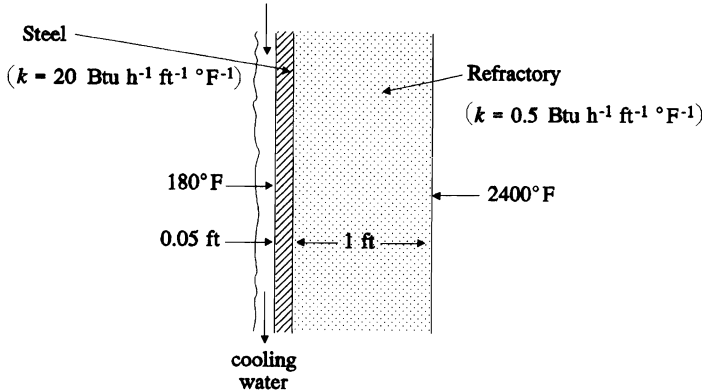
$$\text{Insulation: } k = 0.090 \text{ W m}^{-1} \text{ K}^{-1}.$$

$$\text{Steel: } k = 43 \text{ W m}^{-1} \text{ K}^{-1}.$$

$$h = 55 \text{ W m}^{-1} \text{ K}^{-1} \text{ (inside furnace).}$$

$$h = 11 \text{ W m}^{-1} \text{ K}^{-1} \text{ (outside furnace).}$$

9.4 The wall of a blast furnace is water-cooled. Given the inside- and outside-surface temperatures (2400°F and 180°F), what is the heat transfer coefficient for the water? The water, itself, is at 80°F . Assume steady-state conditions.



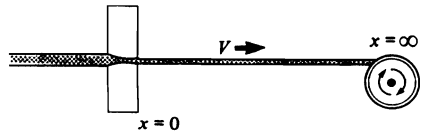
9.5 Consider steady-state heat conduction through a cylindrical wall. The fluid on the inside is at 590 K with a heat transfer coefficient of $23 \text{ W m}^{-2} \text{ K}^{-1}$. The temperature on the outside surface of the wall is known and maintained at 420 K. The heat flow rate through the cylindrical wall is 200 W per 1 m length of the cylinder. If the wall has a thermal conductivity of $0.17 \text{ W m}^{-1} \text{ K}^{-1}$, what are the inside and outside radii of the cylindrical wall? The ratio of the outside radius to inside radius is 2.

9.6 Small droplets of a molten glass maintain their amorphicity if they cool at a rate of at least 10 K s^{-1} , measured at 1070 K. For a spherical droplet with 0.1 mm diameter, what is the required heat transfer coefficient to achieve the minimum cooling rate? The quench environment is maintained at 293 K. *Data for the glass:* $\rho = 3000 \text{ kg m}^{-3}$; $C_p = 840 \text{ J kg}^{-1} \text{ K}^{-1}$; $k = 17 \text{ W m}^{-1} \text{ K}^{-1}$.

9.7 A small sphere (diameter = 0.30 mm), initially at 1365 K, drops through a gas layer of 150 mm with an average velocity of 3 m s^{-1} and then through a liquid layer of 30 mm with an average velocity of 3 mm s^{-1} . *Data for the sphere:* $\rho = 2560 \text{ kg m}^{-3}$; $C_p = 840 \text{ J kg}^{-1} \text{ K}^{-1}$; $k = 0.86 \text{ W m}^{-1} \text{ K}^{-1}$. *Heat transfer coefficients:* h (gas) = $40 \text{ W m}^{-2} \text{ K}^{-1}$; h (liquid) = $280 \text{ W m}^{-2} \text{ K}^{-1}$.

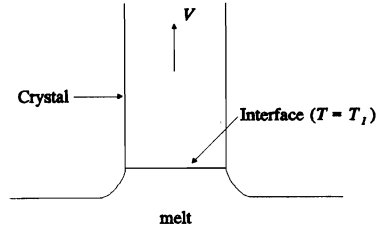
- What is the temperature of the droplet just before it impacts the liquid?
- What is the temperature of the droplet when it reaches the bottom of the liquid layer?

9.8 A thin wire is extruded at a fixed velocity through dies, and the wire temperature at the die is a fixed value T_0 . The wire then passes through the air for a long distance before it is rolled onto large spools. It is desired to investigate the relationship between wire velocity and the distance from the extrusion nozzle for specific values of T_0 .



- Derive the differential equation for determining wire temperature as a function of distance from the nozzle. [*Hint:* Since temperature gradients across the wire are certainly negligible, a slice between x and $x + \Delta x$ may be chosen that includes the wire surface. The heat balance then includes heat lost to the surroundings at T_∞ .]
- State boundary conditions and solve for the temperature in the extended wire.

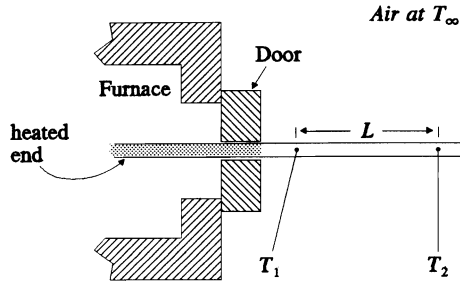
9.9 A very long crystal (dia. = D) is slowly withdrawn with a velocity V from a melt maintained at only a few degrees above the freezing point. The diameter of the crystal is small enough so that radial temperature gradients can be ignored. There is heat loss from the crystal to the surroundings, maintained at T_∞ ; the heat transfer coefficient is h . Assume steady-state conditions.



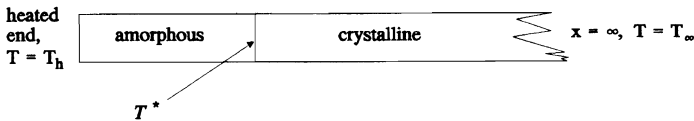
- a) Distance in the crystal and measured from the interface is z . Derive the energy equation in terms of temperature.
- b) Write appropriate boundary conditions and solve for temperature in the crystal.
- c) If $h = 110 \text{ W m}^{-2} \text{ K}^{-1}$, what is the maximum diameter of the crystal so that the radial temperature gradient can be ignored?

[Note: If you have solved Problem 9.8, then you can write the equation for temperature by inspection.]

9.10 One end of a long thin rod is inserted into a furnace through a hole in the furnace door. Two thermocouples are inserted along the length of the bar and indicate steady-state temperatures of T_1 and T_2 , respectively. Assume that the temperature in the bar only varies along its length and derive an equation which can be used to calculate h of the surrounding air as a function of T_1 , T_2 , P (perimeter), A (area), L , T_∞ , and k (thermal conductivity of the bar).



9.11 One end of an amorphous rod is heated so that a portion crystallizes. Derive an equation that can be used for finding the position of the interface after steady state is achieved. The interface temperature is T^* . Assume one-directional conduction along the length of the rod and heat loss to the surroundings at T_∞ with a uniform heat transfer coefficient.



- a) Assume equal thermal properties in the amorphous and crystalline states.
- b) Assume k (crystal) = $4k$ (amorphous).

9.12 Consider the Newtonian cooling of a thin plate (15 mm thick) with a length and width of 1.2 m each. Initially the plate is at 530 K, and then it is cooled by natural convection as it is suspended vertically in air at 300 K. Use the simplified equations given in Problem 8.14 and answer the following questions.

- a) Early in the cooling process, does h vary with $(\Delta T)^{1/4}$ or $(\Delta T)^{1/3}$?

324 Conduction of Heat in Solids

- b) Near the end of the cooling process, does h vary with $(\Delta T)^{1/4}$ or $(\Delta T)^{1/3}$? Determine the temperature at which the transition occurs.
- c) Derive (an) equation(s) which give(s) the temperature of the bar consistent with the assumption of Newtonian cooling and h varying with $(\Delta T)^{1/3}$ and/or $(\Delta T)^{1/4}$.

9.13 In some alloys, grain refinement can be achieved by cycling the alloy above and below a transformation temperature.

Suppose an alloy sphere, initially at a uniform temperature T_0 , is immersed in a bath of heated oil. The electric heaters are controlled so that the temperature of the oil (T_f) follows a cyclic variation given by

$$T_f - T_m = A \sin \omega t$$

where

T_m = time average mean oil temperature (constant),

A = amplitude of variation, and

ω = frequency.

Derive an expression for the temperature of the sphere as a function of time and the heat transfer coefficient. Assume that the temperature of the sphere is uniform.

9.14 Ball bearings (12 mm diameter spheres) are austenitized at 1145 K and then quenched into a large tank of oil at 310 K. Calculate:

- The time to cool the center of a bearing to 480 K.
- The surface temperature when the center is at 480 K.
- The space-mean temperature when the center is at 480 K.
- If 10,000 balls are quenched per hour, calculate the rate of heat removal from the oil that is needed to maintain its temperature at 310 K.

Data for ball bearings: $h = 1700 \text{ W m}^{-2} \text{ K}^{-1}$; $\rho = 7210 \text{ kg m}^{-3}$; $C_p = 630 \text{ J kg}^{-1} \text{ K}^{-1}$; $k = 43 \text{ W m}^{-1} \text{ K}^{-1}$.

9.15 Rapid solidification of Cu is effected by dropping molten droplets into water at 310 K. The droplets may be approximated as spheres with a diameter of 5 mm. Calculate the time for the droplets to cool to 365 K if they enter the water at 1450 K.

Data for Cu in S.I. units: Freezing point = 1358, C_p (solid) = 377; C_p (liquid) = 502; heat of fusion = $2.07 \times 10^5 \text{ J kg}^{-1}$; ρ (solid) = 8970; ρ (liquid) = 8490; k (solid) = 346; k (liquid) = 311.

Data for water quench:

Temperature range	$h, \text{ W m}^{-2} \text{ K}^{-1}$
1450-920 K	450
920-360 K	2270

9.16 Steel ball bearings (60 mm in diameter) are austenitized at 1089 K and then quenched in fluid X at 310 K. It is known by utilizing a thermocouple that a continuous vapor film surrounds the bearings for 72 s until the surface temperature drops to 530 K and at the same time the center temperature is 645 K. Knowing these results, determine the time it takes for the center of smaller bearings (6 mm in diameter) of the same steel to reach 920 K when quenched from 1089 K into fluid X at 310 K.

9.17 An open-ended cylindrical section of a steel pressure vessel 10 ft in diameter with 8-in. thick walls is being heat-treated. The wall temperature is brought to a uniform value of 1750°F. Then the vessel is quenched into slow oil at 70°F. Gather the data and work the problem in English units.

- How long does it take for the surface to reach 1000°F?
- What is the temperature at the center of the wall at that time?

9.18 A cylindrical piece of steel, 50 mm in diameter and initially at 1145 K, is quenched in water at 295 K ($H = 59 \text{ m}^{-1}$). Calculate the temperature at the surface of the piece after 60 s, 120 s, and 300 s. Compare your results with the temperature at the same location if the piece had been quenched in oil ($H = 20 \text{ m}^{-1}$). *Data:* $\alpha = 6.4 \times 10^{-6} \text{ m}^2 \text{ s}^{-1}$.

9.19 Compute the temperature, as a function of time, across a slab of steel 100 mm thick, cooled from 1145 K by water sprays from both sides. *Data:* $\alpha = 6.2 \times 10^{-6} \text{ m}^2 \text{ s}^{-1}$.

9.20 Consider a short cylinder 150 mm high and with a diameter of 150 mm. The cylinder is initially at a uniform temperature of 530 K and cools in ambient air at 300 K. Assume steel with $\alpha = 6.2 \times 10^{-6} \text{ m}^2 \text{ s}^{-1}$ and $k = 35 \text{ W m}^{-1} \text{ K}^{-1}$.

- Write the differential equation that describes the temperature within the cylinder.
- Calculate the temperature at the geometric center after 3600 s of cooling.
- Calculate the temperature on the cylindrical surface midway between the end faces after 3600 s of cooling. Estimate heat transfer coefficients by consulting Problem 8.14.
- In answering parts b) and c), show why your calculation procedure was justified, that is, demonstrate that the differential equation in part a) is satisfied.

9.21 A steel blank, 300 mm in diameter and 600 mm long, is heated in a preheating furnace maintained at 1410 K as the first step in a forging operation.

- Calculate the temperature in the center of the blank after the blank has been heated for 5400 s from an initial temperature of 295 K.
- Calculate the time required to heat a smaller blank, 150 mm in diameter and 300 mm long, to the same center temperature as the larger blank in part a).

Data: $h = 110 \text{ W m}^{-2} \text{ K}^{-1}$; $k = 35 \text{ W m}^{-1} \text{ K}^{-1}$; $\rho = 7690 \text{ kg m}^{-3}$; $C_p = 500 \text{ J kg}^{-1} \text{ K}^{-1}$.

9.22 The temperature field $T(x,y,t)$ in an infinitely long rectangular ($2L \times 2l$) bar must satisfy the partial differential equation

$$\frac{\partial^2 T}{\partial x^2} + \frac{\partial^2 T}{\partial y^2} = \frac{1}{\alpha} \frac{\partial T}{\partial t}$$

Prove that $T(x,y,t)$ can be found by the product

$$T(x,y,t) = T_l(x,t) \cdot T_L(y,t),$$

where $T_l(x,t)$ is the solution for the temperature history in the semi-infinite plate bounded by $l < x < +l$, and $T_L(y,t)$ is the solution for the temperature history in the semi-infinite plate bounded by $-L < y < L$.

9.23 A strip of spring steel (0.5 mm thick) is heated to 1090 K and quenched in "slow oil" maintained at 310 K. Using Fig. 8.14, calculate the cooling rate at 1090 K, 755 K, and 590 K. *Data:* k (1090 K) = $26 \text{ W m}^{-1} \text{ K}^{-1}$; k (755 K) = $35 \text{ W m}^{-1} \text{ K}^{-1}$; k (590 K) = $38 \text{ W m}^{-1} \text{ K}^{-1}$; $\rho = 7840 \text{ kg m}^{-3}$; $C_p = 628 \text{ J kg}^{-1} \text{ K}^{-1}$.

9.24 A thermoplastic (polypropylene) at 500 K is injected into a mold at 300 K to form a plate that is 4 mm thick. The plastic may not be ejected until the center-line temperature is 360 K. Estimate the time required so that the plastic can be ejected (this is called the "freeze-off" time).

9.25 A very long cylinder is cooled in a fluid in which the heat transfer coefficient is constant but its value is unknown. At the center, the temperature does not noticeably decrease until the relative temperature at the surface cools to 0.5. Based on this information, deduce the heat transfer coefficient. *Data for solid:* radius = 80 mm; $\rho = 2000 \text{ kg m}^{-3}$; $C_p = 480 \text{ J kg}^{-1} \text{ K}^{-1}$; $k = 0.246 \text{ W m}^{-1} \text{ K}^{-1}$.

9.26 The end ($z = 0$) of very long cylindrical bar is heated uniformly with a constant flux of q_0 . The side of the bar loses heat to the surroundings at T_∞ with a uniform and constant value of h . Before heating, the bar is at a uniform temperature of T_i .



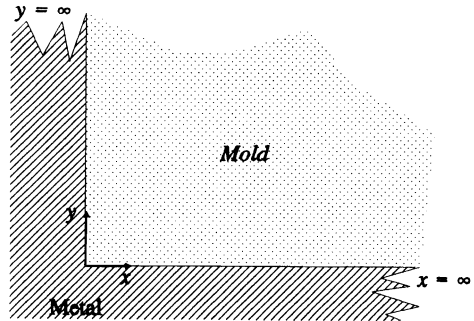
- For constant thermal properties, write an appropriate form of the equation of energy for temperature within the bar during the transient period.
- Give appropriate boundary conditions and an initial condition for part a).
- Is it possible to reach a steady state? Give a reason for your answer.

9.27 A very large and thick slab of copper is initially at a uniform temperature of 600°F . The surface temperature is suddenly lowered to 100°F by a water spray.

- What is the temperature at a depth of 3 in., 4 min. after the surface temperature has changed?
- If it is necessary to predict the temperature in the slab for a period of 5 minutes, what must be the thickness of the slab so that it can be approximated as a semi-infinite solid?

Data for copper: $\rho = 552 \text{ lb}_m \text{ ft}^{-3}$; $C_p = 0.100 \text{ Btu lb}_m^{-1} \text{ }^\circ\text{F}^{-1}$; $k = 215 \text{ Btu h}^{-1} \text{ ft}^{-1} \text{ }^\circ\text{F}^{-1}$.
Work this out in English units.

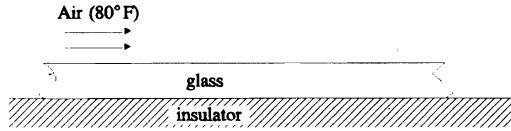
9.28 Initially the mold for a junction-shaped casting is at a uniform temperature, T_0 . Then liquid metal at its freezing point, T_s , is poured into the mold. During the period of time it takes for the metal to solidify, the surface of the mold is maintained at T_s . Assume constant thermal properties of the mold. For the upper right quadrant of the mold which extends to ∞ for both x and y , write a solution that yields temperature as a function of coordinates in the mold and time.



9.29 A ceramic brick, with dimensions $150 \text{ mm} \times 75 \text{ mm} \times 75 \text{ mm}$ and initially at 310 K, is heated in a salt bath maintained at 865 K. The heat transfer coefficient is uniform for all faces and equals $280 \text{ W m}^{-2} \text{ K}^{-1}$. Thermal properties of the brick are as follows: $k = 1.7 \text{ W m}^{-1} \text{ K}^{-1}$; $\rho = 3200 \text{ kg m}^{-3}$; $C_p = 840 \text{ J kg}^{-1} \text{ K}^{-1}$. a) How long will it take for the center of the brick to reach 810 K? b) When the center is at 810 K, what is the maximum temperature difference in the brick?

9.30 A solid circular cylinder of steel, with a diameter of 240 mm and a length of 183 mm, is initially at 300 K. A treatment to transform retained austenite requires cooling in liquid nitrogen (78 K). For a cooling time of 2520 s, it is known (by measurement) that a point in the center of a circular face is at 100 K. What is the temperature at the geometric center of the cylinder. *Data:* $\rho = 7690 \text{ kg m}^{-3}$; $C_p = 795 \text{ J kg}^{-1} \text{ K}^{-1}$; $k = 35 \text{ W m}^{-1} \text{ K}^{-1}$; $h = 230 \text{ W m}^{-2} \text{ K}^{-1}$.

9.31 A sheet of glass, 0.02 ft thick, is cooled from an initial temperature of 1800°F by air flowing over the top surface of the glass. The convective heat transfer coefficient for the air is $8 \text{ Btu h}^{-1} \text{ ft}^{-2} \text{ }^\circ\text{F}^{-1}$, and the glass rests on a perfect insulator.



- a) What time is required for the bottom surface of the glass to cool to 400°F?
- b) When the bottom surface is at 400°F, what is the temperature of the top surface?

Do this problem in English units.

Thermal properties of the glass are $k = 0.32 \text{ Btu h}^{-1} \text{ ft}^{-1} \text{ }^\circ\text{F}^{-1}$, $\rho = 200 \text{ lb}_m \text{ ft}^{-3}$ and $C_p = 0.2 \text{ Btu lb}_m^{-1} \text{ }^\circ\text{F}^{-1}$.

9.32 A cylinder, initially at 300°F, is plunged into a large melt of a low melting point metal maintained at 810 K; the heat transfer coefficient may be taken to be infinity. The dimensions of the cylinder are 230 mm diameter and 150 mm length.

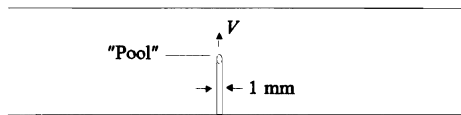
- a) After 100 s of heating in the melt, what is the temperature in the geometric center of the cylinder?
- b) After 5 s, what is the temperature at the centers of the circular surfaces?

Data: $k = 5.2 \text{ W m}^{-1} \text{ K}^{-1}$; $\rho = 4810 \text{ kg m}^{-3}$; $C_p = 420 \text{ J kg}^{-1} \text{ K}^{-1}$.

9.33 A laser beam is used as a moving point source to harden the surface of a thick piece of steel by multiple passes (i.e., rapid scanning) across the surface; no melting occurs. To what depth is it possible to produce martensite with one pass if the critical cooling rate for the steel is 280 K s^{-1} at 810 K. For this steel it is known that austenite exists at $T \geq 1090 \text{ K}$. *Data for steel:* $\alpha = 7.2 \times 10^{-6} \text{ m}^2 \text{ s}^{-1}$; $k = 35 \text{ W m}^{-1} \text{ K}^{-1}$; initial temperature = 300 K.

Laser conditions: Power = 4 kW at 50 percent efficiency; speed = 420 mm s⁻¹.

9.34 A laser beam is used to remelt silicon in a process to produce material for solar cells. The silicon is 100 mm wide and 2 mm thick. The molten pool passes across the width of the silicon, as shown in the diagram, with a velocity



$V = 400 \text{ m s}^{-1}$. The bulk of the silicon is at 293 K. Assume that the pool can be treated as a moving source.

- a) Calculate the maximum cooling rate in the silicon. At what location is this cooling rate achieved?
- b) At what distances from the centerline of the path left by the laser beam, is a peak temperature of 1280 K achieved?

Data: Beam conditions, 5 kW at 50% efficiency. Silicon: melting temperature is 1700 K; heat of fusion is $1.41 \times 10^3 \text{ kJ kg}^{-1}$; thermal conductivity is $100 \text{ W m}^{-1} \text{ K}^{-1}$; thermal diffusivity is $5.2 \times 10^{-5} \text{ m}^2 \text{ s}^{-1}$.

SOLIDIFICATION OF METALS

The production of most metal parts, including articles produced by powder-metallurgy techniques, involves solidification. Castings obviously entail solidification; forgings and wrought products are also castings that have been hot worked, and their behavior in many cases can be traced back to the method of solidification. In particular, the solidification rate of alloys is an extremely important processing variable. The solidification rate relates directly to the coarseness—or fineness—of dendritic structures and hence controls the spacing and distribution of microsegregates, such as coring, second phases, and inclusions. Thermal gradients during freezing are also of great significance, being related to the formation of macrosegregation and porosity in alloys. For these metallurgical reasons and from a process engineering viewpoint, solidification heat transfer should be recognized as an important topic.

10.1 SOLIDIFICATION IN SAND MOLDS

The following analysis applies when the metal solidifies in sand molds, or more generally, when the predominant resistance to heat flow is within the mold itself, e.g., the mold is made of plaster, granulated zircon, mullite, or various other materials that are poor conductors of heat, such as ceramic shell-molds in investment casting processes.

Consider pure liquid metal with no superheat poured against a flat mold wall of a poor conductor. Figure 10.1 shows the temperature distribution in the metal and the mold at some time during solidification. Because all the resistance to heat flow is almost entirely within the mold, the surface temperature T_s nearly equals the melting temperature of the metal T_M . This means that during freezing the temperature drop through the solidified metal is small, and at the metal-mold interface a constant temperature of $T_s \cong T_M$ is maintained. Under these conditions, the temperature history in the mold is given by Eq. (9.64) (i.e., the solution for a semi-infinite body):

$$\frac{T - T_M}{T_0 - T_M} = \operatorname{erf} \frac{x}{2\sqrt{\alpha t}}, \quad (10.1)$$

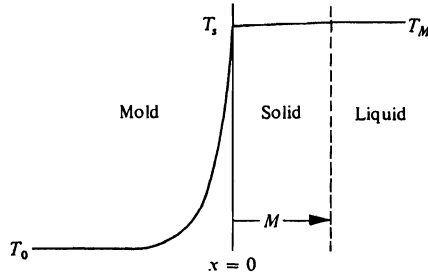


Fig. 10.1 The temperature distribution during solidification of a metal in a sand mold.

where x is the distance into the mold, α is its thermal diffusivity, and T_0 is the initial uniform temperature (usually T_0 is room temperature). The use of this equation implies that the mold is sufficiently thick to satisfy the boundary condition $T(\infty, t) = T_0$; in practice, this requirement is often met.

Of primary interest is the rate at which heat is extracted from the solidifying metal, which ultimately leads to a determination of the total solidification time. Equation (10.1) is used to obtain the amount of heat which flows into the mold, and this quantity of heat must equal the latent heat evolved during solidification.

The heat flux into the mold follows from Eq. (10.1):

$$q|_{x=0} = -k \left[\frac{\partial T}{\partial x} \right]_{x=0} = \frac{k(T_M - T_0)}{\sqrt{\pi\alpha t}}. \quad (10.2)$$

Remembering that $\alpha = k/\rho C_p$, we rewrite Eq. (10.2) as

$$q|_{x=0} = \frac{\sqrt{k\rho C_p}}{\sqrt{\pi t}} (T_M - T_0). \quad (10.3)$$

The product $k\rho C_p$ represents the ability of the mold to absorb heat at a certain rate and is called the *heat diffusivity*.*

The rate at which latent heat is evolved per unit area can be written

$$q|_{x=0} = \rho' H_f \frac{dM}{dt}, \quad (10.4)$$

where ρ' = density of solidifying metal, H_f = latent heat of fusion of the metal, J kg^{-1} , and M = thickness of metal solidified.

Equating Eq. (10.3) to Eq. (10.4) yields the rate at which the interface advances into the liquid:

$$\frac{dM}{dt} = \frac{(T_M - T_0)\sqrt{k\rho C_p}}{\rho' H_f \sqrt{\pi t}}. \quad (10.5)$$

Integration follows, with the limit

$$M = 0 \quad \text{at } t = 0, \quad (10.6)$$

*The heat diffusivity has units of $\text{J}^2 \text{m}^{-4} \text{K}^{-2} \text{s}^{-1}$ and should not be confused with thermal diffusivity.

which gives

$$M = \frac{2}{\sqrt{\pi}} \left[\frac{T_M - T_0}{\rho' H_f} \right] \sqrt{k\rho C_p} \sqrt{t}. \quad (10.7)$$

Thus, we see that the amount of solidification depends on certain metal characteristics, $(T_M - T_0)/\rho' H_f$, and the mold's heat diffusivity, $k\rho C_p$.

10.1.1 Effect of contour on solidification time

Freezing from a planar mold wall, as discussed above, is not the usual problem engineers encounter in practice. It is often important to evaluate the freezing times of complex shapes, in which the contour of the mold wall has some influence on solidification time. For example, contrast heat flow into the convex and concave walls to the plane mold wall situation shown in Fig. 10.2. Heat flow into the convex surface is divergent and, therefore, more rapid than into the plane mold. In contrast, heat flow into the concave surface is convergent and less rapid than into the plane mold wall.

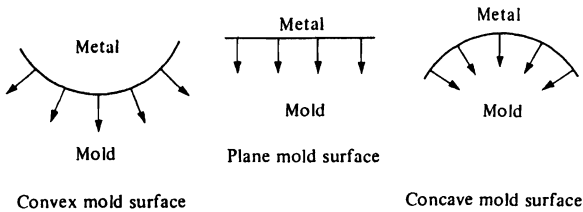


Fig. 10.2 Effect of contour on the heat flux into molds.

As a first approximation, such effects are sometimes neglected because the heated zone in the mold is shallow, and the difference in heat flow between a plane mold wall and a contoured wall is small. As such, we visualize that a given mold surface area has the ability to absorb a certain amount of heat in a given time regardless of its contour. Thus, we generalize Eq. (10.3) for all contours, and for a given surface area A , the mold absorbs an amount of heat Q in time t :

$$Q = \int_0^t Aq|_{x=0} dt = \frac{Ak(T_M - T_0)}{\sqrt{\pi\alpha}} \int_0^t \frac{dt}{\sqrt{t}} = \frac{2Ak(T_M - T_0)}{\sqrt{\pi\alpha}} \sqrt{t}. \quad (10.8)$$

For a casting of volume V to completely solidify, all its latent heat must be removed; hence, the total latent heat Q evolved is

$$Q = \rho' V H_f. \quad (10.9)$$

Equations (10.8) and (10.9) are then combined to yield the solidification time of a casting in terms of its volume-to-surface area ratio:

$$t = C \left[\frac{V}{A} \right]^2. \quad (10.10)$$

where

$$C \equiv \frac{\pi}{4} \left[\frac{\rho' H_f}{T_M - T_0} \right]^2 \left[\frac{1}{k \rho C_p} \right].$$

Equation (10.10) is often referred to as Chvorinov's rule, and C , as Chvorinov's constant. It permits comparison of freezing times of castings with different shapes and sizes. The relationship works best for casting geometries in which none of the mold material becomes saturated with heat, such as in internal corners or internal cores. The success of this relationship hinges on the mold material absorbing the same amount of heat per unit area exposed to the metal. This is strictly true only for castings which have similar shapes but different sizes.

In applications when more precision is required, it is necessary to account for the effect of mold contour on solidification. To quantify some contour effects, let us examine differences among castings of three basic shapes, namely, the infinite plate, the infinitely long cylinder, and the sphere. First, we define two dimensionless parameters, β and γ :

$$\beta \equiv \frac{V/A}{\sqrt{\alpha t}},$$

and

$$\gamma \equiv \left[\frac{T_M - T_0}{\rho' H_f} \right] \rho C_p.$$

With these parameters, the freezing times for the three basic shapes are calculated by

$$\beta = \gamma \left[\frac{2}{\sqrt{\pi}} + \frac{1}{a\beta} \right], \quad (10.11)$$

where $a = \infty$ for infinite plates, $a \approx 4$ for infinite circular cylinders and $a = 3$ for spheres.

We can deduce Eq. (10.11) from Eq. (10.10) by a rearrangement. The values of a for the cylinder and spheres have resulted by rearranging expressions presented by Adams and Taylor;¹ their expression for the cylinder is approximate while that for the sphere is exact.

Equation (10.11) shows the error of using Chvorinov's rule without regard to the mold contours. For example, let us calculate the value of β for $\gamma \approx 1$, which is typical of metal-silica sand combinations.

$$\beta \text{ (plate)} = 1.13,$$

$$\beta \text{ (cylinder)} = 1.32,$$

$$\beta \text{ (sphere)} = 1.37.$$

We see that if we treat the three cases all as plates (i.e., neglecting the contour), then we would make an error of as much as 40-50% in freezing time for equivalent values of V/A .

¹C. M. Adams and H. F. Taylor, *Trans. AFS* **65**, 170-176 (1957).

The value of a for spheres may be used for other chunky shapes such as cubes. Similarly, the expression for solidification time of a cylinder may be used to approximate the freezing time of bars of square cross section.

Example 10.1 Determine the solidification time of the following iron castings, both poured with no superheat into sand molds:

- a slab-shaped casting 100 mm thick;
- a spherically shaped casting 100 mm in diameter.

Iron Data: $T_M = 1808$ K; $H_f = 2.27 \times 10^5$ J kg⁻¹; $\rho' = 7210$ kg m⁻³.

Sand Data: $k = 0.865$ W m⁻¹ K⁻¹; $\rho = 1600$ kg m⁻³; $C_p = 1170$ J kg⁻¹ K⁻¹.

Solution. Assume the mold is initially at 300 K.

$$\gamma = \frac{(1808 - 300)(1600)(1170)}{(7210)(2.72 \times 10^5)} = 1.44.$$

$$\alpha = \frac{0.865}{(1600)(1170)} = 4.62 \times 10^{-7} \text{ m}^2 \text{ s}^{-1}.$$

- a) For the slab, with thickness $\delta = 100$ mm, $a = \infty$ and

$$\frac{V}{A} = \frac{\delta}{2} = \frac{0.100}{2} = 0.050 \text{ m}.$$

Equation (10.11) gives:

$$\beta = \frac{2}{\sqrt{\pi}} \gamma = \frac{(2)(1.44)}{\sqrt{\pi}} = 1.62,$$

so that

$$\frac{V/A}{\sqrt{\alpha t}} = 1.62.$$

Therefore,

$$t = \frac{(V/A)^2}{1.62^2 \alpha} = \frac{(0.050)^2}{(1.62^2)(4.62 \times 10^{-7})} = 2060 \text{ s}.$$

- b) For the sphere, D (diameter) = 100 mm, $a = 3$ and

$$\frac{V}{A} = \frac{D}{6} = \frac{0.100}{6} = 0.0167 \text{ m}.$$

Equation (10.11) becomes:

$$\beta = 1.44 \left[\frac{2}{\sqrt{\pi}} + \frac{1}{3\beta} \right],$$

334 Solidification of Metals

from which $\beta = 1.88$. Therefore,

$$t = \frac{(0.0167^2)}{(1.88^2)(4.62 \times 10^{-7})} = 171 \text{ s.}$$

The sphere solidifies in less than one-tenth the time required for the slab to solidify.

10.1.2 Effect of superheat on solidification time

We can assess the effect of superheat on the solidification time by realizing that, in addition to absorbing latent heat, the sand must also absorb the superheat. Again, we assume that the temperature gradients within the casting are negligible, and at the time solidification is complete, the entire casting is close to its freezing point. In this case, the total quantity of heat to be removed from the casting is

$$Q = \rho'VH_f + \rho'_l VC_{p,l}\Delta T_s. \quad (10.12)$$

The subscript l denotes liquid phase properties, and ΔT_s is the amount of superheat in degrees.

We now consider infinite plate castings, and in order to make the analysis simple, yet sufficiently accurate, we assume that Eq. (10.8) is valid even though the interface temperature of the mold is not constant while the liquid phase loses its superheat. In view of this approximation, it is certainly acceptable not to distinguish differences in the density of the liquid and solid phases. Thus $\rho'_l \cong \rho'$, and when Eq. (10.12) is set equal to Eq. (10.8), we obtain

$$t = \frac{\pi}{4} \frac{1}{k\rho C_p} \left[\frac{\rho' H'_f}{T_M - T_0} \right]^2 \left[\frac{V}{A} \right]^2. \quad (10.13)$$

In this expression, H'_f is the *effective heat of fusion*, and represents the sum of the latent heat of fusion and the liquid's superheat, that is,

$$H'_f = H_f + C_{p,l}\Delta T_s. \quad (10.14)$$

Note that the solidification time is still proportional to $(V/A)^2$.

10.2 SOLIDIFICATION IN METAL MOLDS

When poured into metal molds, castings freeze rapidly, and temperatures change drastically in both the mold and the casting. An understanding of the variables affecting solidification in metal molds is important because most ingots, all permanent mold castings, and all die castings are made in metal molds. Also many sand castings are made in molds that incorporate metal inserts called chills at strategic positions to increase the rate of solidification.

The analysis of heat transfer when metal is poured against a chill wall is more complicated than that when metal is poured into a sand mold; this is due to the fact that metal molds are much better heat conductors than sand molds. The added complexities are illustrated by the casting-mold situation shown in Fig. 10.3. At the solidified metal-mold interface, a temperature drop exists, due to thermal contact resistance. The condition of no contact resistance would exist only if the mold-casting contact were so intimate that wetting would occur, that is, the casting would become soldered to the mold.

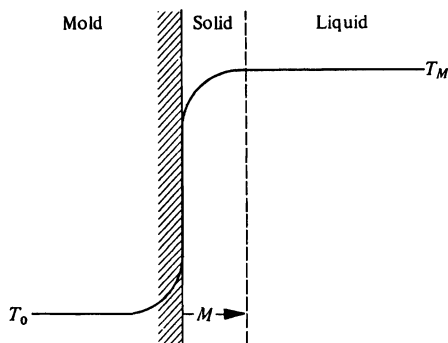


Fig. 10.3 The temperature distribution during the solidification of a metal from a chill wall.

In addition to the contact resistance, there are other differences between solidification in sand and in chill molds:

- The thermal conductivity of the metal being cast forms an important portion of the overall resistance to heat flow. This results in the surface temperature being well below the melting point, while appreciable thermal gradients exist within the solidifying metal.
- More total heat is removed during solidification because of the solidified metal which is subcooled. Thus, the heat capacity of the solidifying metal is important.

In the following sections, we discuss selected problems of solidification, each of practical importance.

10.2.1 Constant casting surface temperature

Consider a mass of pure liquid metal, initially at its freezing temperature, which has its surface suddenly cooled to a constant temperature, T_s . After some solidification has occurred, the temperature profile in the solidifying metal will appear as the solid profile (Fig. 10.4(a)). The temperature profile is identical to the temperature profile in the semi-infinite solid depicted in Fig. 10.4(b), except that the temperature field in the solidifying metal is between T_M and T_s rather than actually extending to T_∞ . However, the temperature "reaches" for T_∞ just as in the semi-infinite solid, and the temperature distribution within the solidified metal takes the form

$$\frac{T - T_s}{T_\infty - T_s} = \operatorname{erf} \frac{x}{2\sqrt{\alpha't}} \quad (10.15)$$

In Fig. 10.4(a), T_∞ is not known *a priori*. It is an imaginary temperature which makes the temperature distribution analogous to the case of the semi-infinite solid, or it may be thought of as an integration constant. To distinguish the thermal transport properties of the solidifying metal, primes are used. The thermal transport properties of the mold have no primes.

We now develop an expression for the rate of solidification by applying the boundary condition

$$T(M,t) = T_M, \quad (10.16)$$

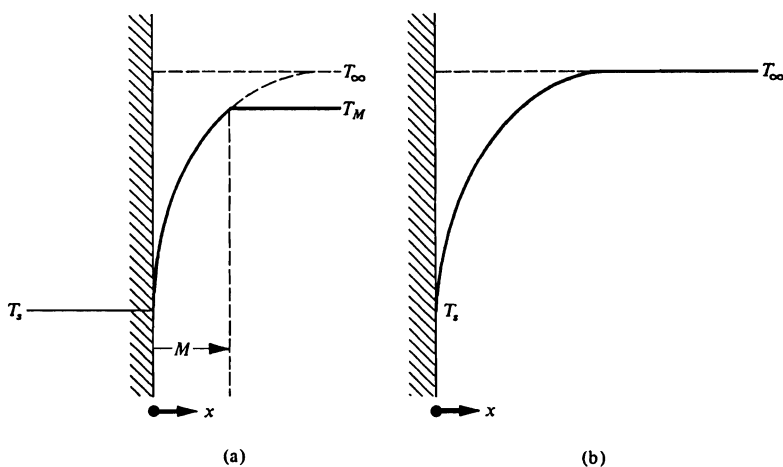


Fig. 10.4 Analogous temperature distributions in (a) solidifying metal, and (b) a semi-infinite solid.

i.e., the temperature at the solid-liquid interface is the freezing point. In addition, we recognize that the rate of evolution of latent heat of fusion equals the heat flux into the solid at the interface; that is

$$k' \frac{\partial T}{\partial x}(M, t) = H_f \rho' \frac{dM}{dt}. \quad (10.17)$$

When applied to the temperature distribution, Eq. (10.16) yields

$$\frac{T_M - T_s}{T_\infty - T_s} = \operatorname{erf} \frac{M}{2\sqrt{\alpha' t}}. \quad (10.18)$$

Since the left-hand side of this equation is constant, the argument of the error function must also be constant. Hence

$$M = 2\beta\sqrt{\alpha' t}. \quad (10.19)$$

Once again the thickness solidified is proportional to \sqrt{t} .

To evaluate the constant β , we evaluate the heat flux at the solid-liquid interface which we obtain from Eq. (10.17):

$$\begin{aligned} k' \frac{\partial T}{\partial x}(M, t) &= \frac{(T_\infty - T_s) \sqrt{k' \rho' C'_p}}{\sqrt{\pi} \sqrt{t}} \exp \left[-\frac{M^2}{4\alpha' t} \right] \\ &= \frac{(T_M - T_s) \sqrt{k' \rho' C'_p}}{\sqrt{\pi} \sqrt{t} \operatorname{erf} \beta} \exp(-\beta^2). \end{aligned} \quad (10.20)$$

The latent heat evolved at the interface is written

$$H_f \rho' \frac{dM}{dt} = H_f \rho' \beta \frac{\sqrt{\alpha'}}{\sqrt{t}}. \quad (10.21)$$

Substituting Eqs. (10.20) and (10.21) into Eq. (10.17), and simplifying, we have

$$\beta e^{\beta^2} \operatorname{erf} \beta = (T_M - T_s) \frac{C_p'}{H_f \sqrt{\pi}}. \quad (10.22)$$

We now have an expression to calculate β . We may use Fig. 10.5 to evaluate β , rather than using Eq. (10.22) which entails trial and error.

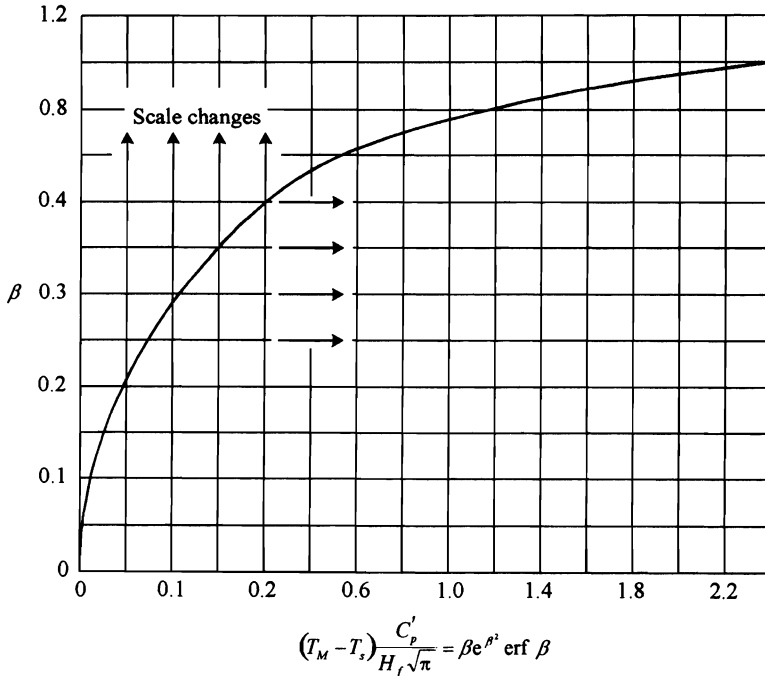


Fig. 10.5 Evaluation of β for Eq. (10.22).

To summarize, β can be determined from Fig. 10.5. Thus the thickness solidified is known (Eq. (10.19)), T_∞ can be determined (Eq. (10.18)), and the temperature distribution can be computed (Eq. (10.15)), if so desired.

This analysis is, of course, valid for unidirectional heat flow; its results can be applied to slab-shaped castings. If the solidification time is sought, then evaluate β and use Eq. (10.19) with $M = L$, the semithickness of the slab.

The above method of solution is not systematic and cannot be extended to the solidification of other shapes. However, Adams² presented a method utilizing a power series that can be extended to the freezing of spheres and cylinders. His results for solidification

²C. M. Adams, "Thermal Considerations in Freezing," *Liquid Metals and Solidification*, ASM, Cleveland, OH, 1958.

times of spheres and cylinders freezing with a constant surface temperature, T_s , are given in Fig. 10.6.

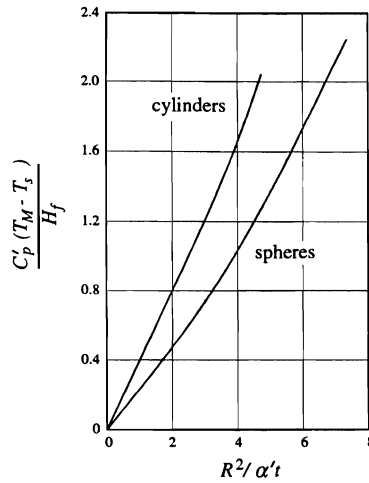


Fig. 10.6 Solidification times for spheres and cylinders with constant surface temperature. (From C. M. Adams, "Thermal Considerations in Freezing," *Liquid Metals and Solidification*, ASM, Cleveland, OH, 1958.)

While application of the foregoing is limited because it is difficult to imagine practical situations in which a constant surface temperature is maintained, an example of a case of practical importance is the determination of the solidification rate in a large steel ingot poured against a copper, water-cooled mold wall,* except for the initial stage of solidification. The solutions are also useful for indicating the maximum freezing rate that can be obtained by direct cooling, since the boundary condition of constant surface temperature corresponds to a case of $h \rightarrow \infty$ at the surface.

10.2.2 Gradients within mold and casting, no interface resistance

We depict this case in Fig. 10.7. Both mold and metal form barriers to heat flow. The mold is initially at room temperature, and the liquid metal is at its melting point. The mold is thick enough so that no temperature rise occurs on its exterior surface, and we can consider it to be semi-infinite. This case is applicable, for example, in determining the solidification rate of a large ingot in a thick metal mold; it applies after sufficient material has frozen so that interface resistance is no longer important. This analysis is also useful in deciding if a particular metal-sand mold combination is such that T_s does, or does not, approximate T_M .

In the previous problem, T_s was fixed as the boundary condition of the situation. In the case at hand, T_s is established at a particular level, depending upon the thermal properties of both the mold and the solidifying metal.

We now proceed to develop the solution which satisfies the requirements

$$\lim_{\xi \rightarrow 0} \left[k \left(\frac{\partial T}{\partial x} \right)_{x=0-\xi} - k' \left(\frac{\partial T}{\partial x} \right)_{x=0+\xi} \right] = 0; \quad (10.23)$$

*Such processes would include electroslag remelting and vacuum arc melting.

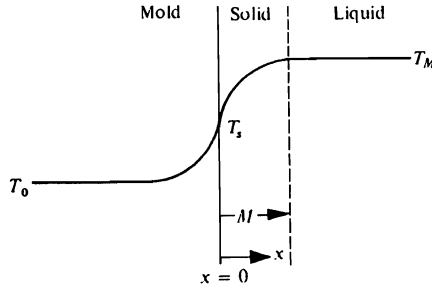


Fig. 10.7 Temperature distribution during solidification with no interface resistance.

that is, the heat flux into the casting-mold interface from the solidifying metal must equal the flux away from the interface into the mold. We repeat the two additional boundary conditions that must be satisfied at the freezing interface:

$$T(M,t) = T_M, \quad (10.16)$$

$$k' \frac{\partial T}{\partial x}(M,t) = \rho' H_f \frac{dM}{dt}. \quad (10.17)$$

The mold is semi-infinite in the negative x -domain with some unknown surface temperature T_s . Thus

$$\frac{T - T_s}{T_0 - T_s} = \operatorname{erf} \frac{-x}{2\sqrt{\alpha t}}, \quad (10.24)$$

where T_0 is the initial uniform temperature of the mold. For the solidifying metal, Eq. (10.15) applies again; however, note at this point that T_∞ and T_s are both unknown,

$$\frac{T - T_s}{T_\infty - T_s} = \operatorname{erf} \frac{x}{2\sqrt{\alpha' t}}. \quad (10.15)$$

When we apply Eq. (10.16) to Eq. (10.15), we realize that the argument of the error function is constant, and again defined as β , so that Eq. (10.19) applies.

On differentiating Eqs. (10.24) and (10.15), and applying Eqs. (10.23), (10.16), and (10.17), we obtain

$$\frac{(T_M - T_s)C_p'}{H_f\sqrt{\pi}} = \beta e^{\beta^2} \operatorname{erf} \beta, \quad (10.22)$$

$$\frac{(T_M - T_0)C_p'}{H_f\sqrt{\pi}} = \beta e^{\beta^2} \left[\sqrt{\frac{k' \rho' C_p'}{k \rho C_p}} + \operatorname{erf} \beta \right], \quad (10.25)$$

$$\frac{(T_\infty - T_s)C_p'}{H_f\sqrt{\pi}} = \beta e^{\beta^2}, \quad (10.26)$$

$$\frac{T_s - T_0}{T_\infty - T_s} = \sqrt{\frac{k'\rho'C'_p}{k\rho C_p}} \quad (10.27)$$

To summarize the results of this section, we calculate the temperature profiles in both the mold and the solidifying metal; we also determine the thickness solidified. As a reminder, remember that the thermal transport properties with primes are for the solidifying metal.

We calculate the temperature profile in the mold by completing the following steps:

- 1) Calculate the mold-casting interface temperature T_s from the known thermal properties

$$(T_M - T_0) \left[\frac{C'_p}{H_f} \right] \quad \text{and} \quad \sqrt{\frac{k'\rho'C'_p}{k\rho C_p}}$$

and Fig. 10.8, which was derived by calculating β on a trial-and-error solution of Eq. (10.25), and then determining T_s from Eq. (10.22).

- 2) The value of T_s thus obtained can be used in Eq. (10.24) for the temperature profile in the mold.

We calculate the temperature profile in the solidifying metal by performing these steps:

- 1) Calculate T_s from Fig. 10.8.
- 2) Determine T_∞ using either Eq. (10.26) or Eq. (10.27).
- 3) The values of T_∞ and T_s thus obtained can be used in Eq. (10.15) for the temperature profile in the metal.

If we wish to calculate the thickness of the solidified metal, then we determine T_s from Fig. 10.8 and use Fig. 10.5 for a value of β . With this value of β , Eq. (10.19) can be applied.

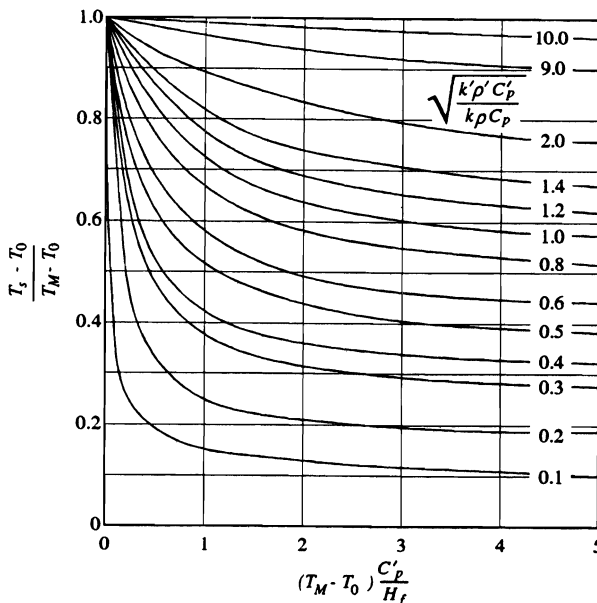


Fig. 10.8 Relative mold-casting interface temperatures for unidirectional freezing with no interface resistance. (From C. C. Reynolds, *Trans. AFS* 72, 343 (1964).)

Example 10.2 Determine the freezing time of an iron slab-shaped casting which is 100 mm thick. Assume no interface resistance, and consider the cases of pure iron poured at its freezing point into a) a sand mold, and b) a very thick copper mold with no resistance to heat transfer at the casting-mold interface.

Mold Data:

Material	$k, \text{W m}^{-1} \text{K}^{-1}$	$\rho, \text{kg m}^{-3}$	$C_p, \text{J kg}^{-1} \text{K}^{-1}$
Sand	0.865	1600	1170
Copper	398	8970	380

Iron Data: $T_M = 1808 \text{ K}$; $H_f = 2.72 \times 10^5 \text{ J kg}^{-1}$; $\rho' = 7210 \text{ kg m}^{-3}$; $k' = 83 \text{ W m}^{-1} \text{K}^{-1}$; $C'_p = 670 \text{ J kg}^{-1} \text{K}^{-1}$; $T_0 = 300 \text{ K}$.

Solution.

$$\text{a) } (T_M - T_0) \frac{C'_p}{H_f} = (1808 - 300) \frac{670}{2.72 \times 10^5} = 3.71,$$

$$\sqrt{\frac{k' \rho' C'_p}{k \rho C_p}} = \sqrt{\frac{(83)(7210)(670)}{(0.865)(1600)(1170)}} = 15.7.$$

From Fig. 10.8, we obtain T_s :

$$\frac{T_s - T_0}{T_M - T_0} = 1.$$

Therefore, $T_s = T_M$, and the analysis used in Example 10.1 is valid, so that $t(\text{sand}) = 2060 \text{ s}$.

$$\text{b) } (T_M - T_0) \frac{C'_p}{H_f} = 3.71, \text{ as in part a),}$$

$$\sqrt{\frac{k' \rho' C'_p}{k \rho C_p}} = \sqrt{\frac{(83)(7210)(670)}{(398)(8970)(380)}} = 0.544.$$

From Fig. 10.8, we get

$$\frac{T_s - T_0}{T_M - T_0} \approx 0.42$$

$$T_s = (0.42)(1808 - 300) + 300 = 933 \text{ K}.$$

Now we resort to Fig. 10.5 to obtain the value of β :

$$(T_M - T_s) \frac{C'_p}{H_f \sqrt{\pi}} = (1808 - 933) \left[\frac{670}{2.72 \times 10^5 \sqrt{\pi}} \right] = 1.22,$$

342 Solidification of Metals

and $\beta \approx 0.87$. Finally, we use Eq. (10.19), with $M = 0.050$ m and $\alpha' = 1.72 \times 10^{-5}$ m² s⁻¹.

$$t = \frac{M^2}{4\beta^2\alpha'} = \frac{(0.050)^2}{(4)(0.87^2)(1.72 \times 10^{-5})}$$

$$t \text{ (copper mold)} = 48 \text{ s.}$$

10.2.3 Interface resistance

In the previous sections, we depicted situations in which the surface temperature T_s remained constant. When we examine the more likely situation of some interface resistance, then the surface temperature of the casting varies with time, and the analysis becomes more complex. Before analyzing the temperature history in the mold and casting in a general case (Fig. 10.3), let us first consider a simpler case (Fig. 10.9).

In Fig. 10.9, the mold is kept at a constant and uniform temperature, T_0 , by internal water cooling. The interface resistance to heat transfer is much greater than the resistance of the solidifying metal. It applies in continuous casting in lower portions of the mold where the solidified shell pulls away from the mold wall and an air gap forms a significant resistance to heat transfer. Practical importance is also attached to this case for estimating the thickness solidified in small thin-section parts cast in conductive metal molds, when the solidification time is small.

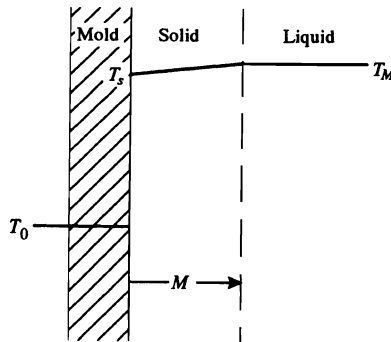


Fig. 10.9 Temperature distribution during solidification with a predominant interface resistance.

Notice $T_s \neq T_M$, and the heat leaves the casting via h at the surface to a water-cooled mold maintained at T_0 . Here we simplify the analysis by approximating the temperature profile within the solidifying metal as a linear function. Then we write the heat flux at the casting-mold interface as

$$q|_{x=0} = k' \frac{T_M - T_s}{M}. \quad (10.28)$$

Also

$$q|_{x=0} = h(T_s - T_0). \quad (10.29)$$

We then eliminate the surface temperature T_s , which varies, by combining Eqs. (10.28) and (10.29); because of the linear temperature profile, we express the flux at the solid-liquid interface simply as

$$q|_{x=0} = q|_{x=M} = \frac{T_M - T_0}{1/h + M/k'}. \quad (10.30)$$

In addition, at $x = M$, the latent heat is evolved so that

$$q|_{x=M} = \rho'H_f \frac{dM}{dt}. \quad (10.31)$$

By combining Eqs. (10.30) and (10.31) and integrating with $M = 0$ at $t = 0$, we obtain

$$M = \frac{h(T_M - T_0)}{\rho'H_f} t - \frac{h}{2k'} M^2. \quad (10.32)$$

Adams³ solved the problem approximately but in a more rigorous manner in which the temperature profile is not assumed to be linear as above. The more refined analysis is similar to Eq. (10.32) with an additional factor a :

$$M = \frac{h(T_M - T_0)}{\rho'H_f a} t - \frac{h}{2k'} M^2. \quad (10.33)$$

In this expression

$$a \equiv \frac{1}{2} + \sqrt{\frac{1}{4} + \frac{C'_p(T_M - T_0)}{3H_f}}.$$

Equation (10.33) is almost exact for $hM/k \geq 1/2$. For $hM/k < 1/2$, the thickness solidified is overestimated by approximately 10-15%.

Example 10.3 When Eq. (10.33) applies show that M varies linearly with time for small times and parabolically with time for large times.

Solution. Small times: $t \rightarrow 0$, $M^2 \rightarrow 0$ and Eq. (10.33) gives

$$M \approx \frac{h(T_M - T_0)}{\rho'H_f a} t.$$

The result is linear because the heat transfer is limited by the resistance across $x = 0$.

Large times: $t \rightarrow \infty$, $T_s \rightarrow T_0$ and the system behaves as though $h \rightarrow \infty$. In this case Eq. (10.33) reduces to

$$M \approx \left[\frac{2k'(T_M - T_s)}{\rho'H_f a} \right]^{1/2} t^{1/2}.$$

³C. M. Adams, *ibid.*

344 Solidification of Metals

The result is parabolic because the heat transfer is limited by the conduction through the increasing thickness of solidified metal.

Example 10.4 Estimate thickness solidified versus time when iron freezes against a mold maintained at 300 K. For iron use the data in Example 10.2. a) Assume $h = 10^3 \text{ W m}^{-2} \text{ K}^{-1}$. b) Assume $h = 10^4 \text{ W m}^{-2} \text{ K}^{-1}$.

Solution. It is easier to rearrange Eq. (10.33), so we can calculate t as a function of M ; then

$$t = \frac{\rho' H_f a}{h(T_M - T_0)} \left[M + \frac{h}{2k'} M^2 \right].$$

$$\text{a) } a = \frac{1}{2} + \sqrt{\frac{1}{4} + \frac{(670)(1808 - 300)}{(3)(2.72 \times 10^5)}} = 1.72$$

$$\frac{\rho' H_f a}{h(T_M - T_0)} = \frac{(7210)(2.72 \times 10^5)(1.72)}{(1000)(1808 - 300)} = 2237$$

$$\frac{h}{2k'} = \frac{1000}{2(83)} = 6.02.$$

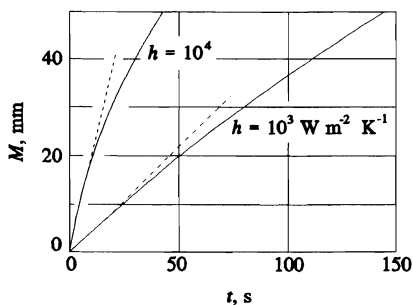
Therefore,

$$t = 2237 M + 1.347 \times 10^4 M^2 \quad (t \text{ in s; } M \text{ in m}).$$

b) With $h = 10^4 \text{ W m}^{-2} \text{ K}^{-1}$, the relationship is

$$t = 223.7 M + 1.347 \times 10^4 M^2.$$

The results for both cases are shown in the following figure. As expected solidification is faster with the greater heat transfer coefficient; in addition the linearity of $M(t)$ extends to about twice the thickness solidified.



Now we consider a case that differs somewhat from Fig. 10.9. In addition to the resistance to heat transfer at the mold-metal interface, the mold also offers a comparable resistance to heat transfer. The temperature distribution is shown in Fig. 10.10. At the mold-metal interface, the temperature on the casting side is T_{sC} , and on the mold-side it is T_{sM} .

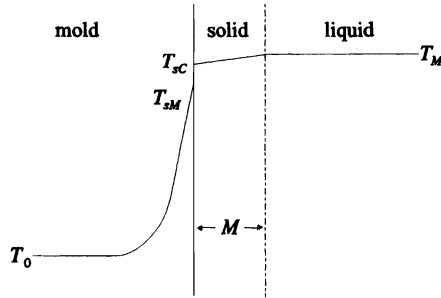


Fig. 10.10 Temperature distribution during solidification with interface resistance to heat transfer.

To start this *approximate analysis*, we deduce a time-dependent thermal resistance, R , for heat transfer into the very thick mold of an insulating material. Thus, from Eq. (10.3):

$$R = \frac{\sqrt{\pi t}}{\sqrt{k\rho C_p}}.$$

With the thermal resistance across the interface taken as $1/h$, we get the total thermal resistance

$$R_T = \frac{M}{k'} + \frac{1}{h} + \frac{\sqrt{\pi t}}{\sqrt{k\rho C_p}}, \quad (10.34)$$

and Eq. (10.30) can be replaced with

$$q|_{x=0} = \frac{T_M - T_0}{\frac{1}{h} + \frac{M}{k'} + \sqrt{\frac{\pi t}{k\rho C_p}}}. \quad (10.35)$$

To keep the problem tractable, we ignore the sensible heat extracted from the solidifying metal. Further, we neglect M/k' and thereby restrict this approximate analysis to solidification in relatively insulating molds. With these restrictions in mind, we equate Eqs. (10.31) and (10.35) and arrive at

$$\frac{dM}{dt} = \left[\frac{T_M - T_0}{\rho'H_f} \right] \left[\frac{1}{h} + \sqrt{\frac{\pi t}{k\rho C_p}} \right]^{-1}. \quad (10.36)$$

Equation (10.36) is integrated with $M = 0$ at $t = 0$; the result is Eq. (10.7) corrected by a factor of ϕ :

$$M = \frac{2\phi}{\sqrt{\pi}} \left[\frac{T_M - T_0}{\rho'H_f} \right] \sqrt{k\rho C_p} \sqrt{t}, \quad (10.37)$$

where

$$\phi = 1 - \frac{\sqrt{k\rho C_p}}{h\sqrt{\pi t}} \ln \left[1 + \frac{h\sqrt{\pi t}}{\sqrt{k\rho C_p}} \right].$$

This factor accounts for resistance to heat transfer across the metal-mold interface. For small times (i.e., thin section castings), the interface resistance retards solidification significantly. The retarding effect is greater in less insulating molds (i.e., an increased heat diffusivity).

Before we leave discussion of this type of problem, we repeat that the analysis is approximate. An exact solution could be obtained by determining the flux at the surface of the mold on the basis of the temperature distribution given by Eq. (9.67).

Example 10.5 Recalculate the solidification time of the iron casting, 100 mm thick, in Example 10.1. Assume that $h = 2800 \text{ W m}^{-2} \text{ K}^{-1}$.

Solution. A trial-and-error solution is required because ϕ depends upon solidification time. From Example 10.1, $t = 2060 \text{ s}$. Let's assume, for our first estimate, that $t = 2300 \text{ s}$.

$$\begin{aligned} \phi &= 1 - \frac{\sqrt{(0.865)(1600)(1170)}}{(2800) \sqrt{2300 \pi}} \ln \left[1 + \frac{(2800) \sqrt{2300 \pi}}{\sqrt{(0.865)(1600)(1170)}} \right] \\ &= 1 - 5.346 \times 10^{-3} \ln [1 + 187.0] = 0.972. \end{aligned}$$

Notice that $\phi \sim 1$; typically $0.8 < \phi \leq 1$, unless $t < 100 \text{ s}$ when $0.5 < \phi < 0.9$.

From the result of Example 10.1, we can write

$$t = \left[\frac{1}{0.972} \right]^2 (2060) = 2180 \text{ s}.$$

We overestimated the solidification time, so that ϕ , itself, is closer to unity. One or more iterations could be done, but in view of the approximations involved, it might not be worth the added effort. Go ahead and do it anyway!

10.2.4 Gradients within mold and casting with interface resistance

In tackling this situation, we extend the concept of the mold-metal interface temperature introduced in Section 10.2.2. However, in this case there is no constant temperature at the casting-mold interface; rather, there are two surface temperatures, neither of which is constant. To handle this problem, consider an imaginary reference plane between the mold and casting which is at T_s , where T_s is constant and determined by the method of Section 10.2.2 using Eq. (10.27). The contact resistance is then apportioned on both sides of the imaginary plane in accordance with the equations

$$h_M = \left[1 + \sqrt{\frac{k\rho C_p}{k'\rho'C'_p}} \right] h, \quad (10.38)$$

$$h_c = \left[1 + \sqrt{\frac{k' \rho' C'_p}{k \rho C_p}} \right] h. \quad (10.39)$$

In these expressions, h is the total heat transfer coefficient across the interface, h_M is the coefficient on the mold side of the plane, and h_c is the coefficient on the casting side of the plane.

Figure 10.11 depicts the entire situation, showing the surface temperatures, T_{sC} and T_{sM} , of the casting and the mold, respectively. We handle the problem as follows:

- 1) We first solve for T_s as if there were no interface resistance.
- 2) Using T_s obtained in (1) and applying Eq. (10.39), we isolate the casting half and study it by using the analysis given in Section 10.2.3. For the casting side, heat is transferred from T_{sC} to T_s via h_c .
- 3) If we wish to study the mold half, we resort to the results of Section 9.4.2 and use Eq. (9.65) or Fig. 9.16. For the mold side, heat is supplied to the mold from a source at T_s to the surface at T_{sM} via h_M .

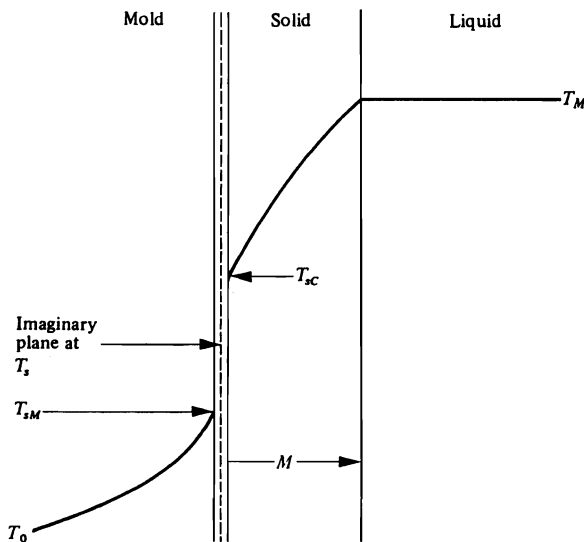


Fig. 10.11 Temperature distribution in the casting and mold when the interface resistance does not predominate.

We present Fig. 10.12 to illustrate the effect of the contact thermal resistance. First, in order to solidify the same amount of metal, it takes more time with some resistance. Note, also, that the two curves become parallel after the early stages of solidification, and M varies linearly with \sqrt{t} for both cases. For the early stage of solidification, M does not vary linearly with \sqrt{t} when there is some contact resistance.

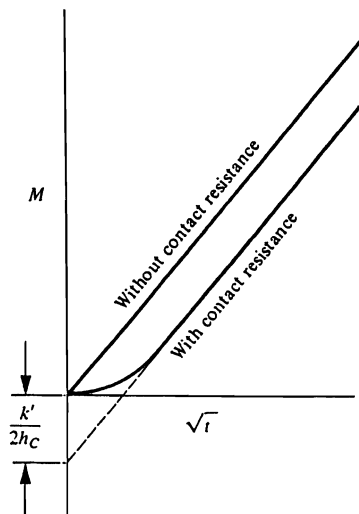


Fig. 10.12 Rate of solidification in metal molds with and without contact resistance.

Example 10.6 a) Determine the freezing time of the 100 mm thick slab of iron discussed in Example 10.2 when it is cast in a very thick copper mold. The total heat transfer coefficient across the casting-mold interface may be taken as $1400 \text{ W m}^{-2} \text{ K}^{-1}$. b) When the casting has completely solidified, what is the surface temperature of the mold?

Solution.

- a) First solve the problem as if there were no interface resistance, and obtain T_i . This was done in Example 10.2(b), with the result $T_i = 933 \text{ K}$. Using Eq. (10.39), determine the coefficient on the casting side of the interface:

$$h_c = \left[1 + \sqrt{\frac{(83)(7210)(670)}{(398)(8970)(380)}} \right] (1400) = 2161 \text{ W m}^{-2} \text{ K}^{-1}.$$

Now use Eq. (10.33), but be sure to substitute h_c for h and $(T_M - T_i)$ for $(T_M - T_0)$. Substituting properties and $M = 0.050 \text{ m}$, we have

$$0.050 = \frac{(2161)(1808 - 933)}{(7210)(2.72 \times 10^5) a} t - \frac{(2161)(0.050^2)}{(2)(83)},$$

in which

$$a = \frac{1}{2} + \sqrt{\frac{1}{4} + \frac{(670)(1808 - 933)}{(3)(2.72 \times 10^5)}} = 1.484.$$

Solving for t yields $t = 127 \text{ s}$.

- b) To solve for the surface temperature of the mold, we may use Eq. (9.65) or Fig. 9.16 with h replaced by h_M , T_f replaced by T_s , and T_i replaced by T_0 . We obtain h_M by using Eq. (10.38):

$$h_M = \left[1 + \sqrt{\frac{(398)(8970)(380)}{(83)(7210)(670)}} \right] (1400) = 3975 \text{ W m}^{-2} \text{ K}^{-1}.$$

Then

$$\frac{h_M}{k} \sqrt{\alpha t} = \frac{3975}{398} \sqrt{\frac{(398)(91.9)}{(8970)(380)}} = 1.035.$$

From Fig. 9.16, for the surface we have

$$\frac{T_{sM} - T_0}{T_s - T_0} \approx 0.60,$$

so that

$$T_{sM} = (0.60)(933 - 300) + 300 = 680 \text{ K}.$$

Up to this point, we have recognized that a thermal resistance exists at the mold-casting interface in all cases unless soldering occurs. Since no bonding takes place at the interface, the casting and the mold are free to move due to thermal-physical effects. In fact, it is well known that when a metal is cast against a metal mold, a gap forms at the interface. This gap is formed as a result of the mold expanding due to its absorption of heat, and to the solid skin of metal shrinking due to its lowering temperature. Usually, the prediction of the rate of heat transfer across the gap is not reliable, and so we rely upon empirical measurements of surface temperatures and the heat absorbed by the mold to deduce appropriate heat transfer coefficients. Some heat transfer coefficients for various casting situations are given in Table 10.1. Such values are strongly dependent on specific processes and geometrical situations, so the data in Table 10.1 should serve only as general guidelines.

Reference to Table 10.1 indicates that the heat transfer coefficients can be time dependent in static castings and position dependent in continuous castings. Nishida *et al.*⁴ give time-temperature solutions for cylindrical and slab castings in molds where the air gap forms during solidification, and methods to calculate the resulting heat transfer coefficients. Kelly *et al.*⁵ show how the heat transfer coefficient (or the surface heat flux) may be calculated for continuous casting in a round billet mold. Kim *et al.*⁶ give an inverse method for estimating the heat transfer coefficient as a function of time from temperature measurements inside the casting.

⁴Y. Nishida, W. Droste, and S. Engler, *Metall. Trans. B* **17B**, 833 (1986).

⁵J. E. Kelly, K. P. Michalek, T. G. O'Connor, B. G. Thomas and J. A. Dantzig, *Metall. Trans. A* **19A**, 2589 (1987).

⁶W. S. Kim, M. N. Ozisik, and L. G. Hector, "Inverse Problem of Solidification for Determining Air-Gap Resistance to Heat Flow during Metal Casting," in *Proceedings of XXII ICHMT Conference on Heat and Mass Transfer in Manufacturing Processes*, Dubrovnik, Yugoslavia, August 27-31, 1990.

350 Solidification of Metals

Table 10.1 Heat transfer coefficients across casting-mold interfaces

Casting situation	Heat transfer coefficient $W\ m^{-2}\ K^{-1}$	Reference listed below
Steel in continuous casting mold	280-2300	(a)
Steel in continuous casting mold, 4×4 in. withdrawal rate of 20 in./min	480	(b)
withdrawal rate of 100 in./min	790	
withdrawal rate of 175 in./min	1080	
Ductile iron in gray iron mold (coated with amorphous carbon)	1700	(c)
Steel in static cast iron mold	1020	(c)
Copper in centrifugal steel mold	230-340	(d)
Aluminum alloy in small permanent copper molds	1700-2600	(e)
Steel against chill mold in vacuum (decreases with time)	400-130	(f)
Steel in continuous casting meniscus	2800	(g)
below meniscus	2800-1000	
Uranium in graphite molds	2000	(h)

- a) A. W. D. Hills and M. R. Moore, *Heat and Mass Transfer in Process Metallurgy*, Inst. Min. and Met., London, 1967.
 b) E. Y. Kung and J. C. Pollock, *Simulation* 29-36 (Jan. 1968).
 c) C. C. Reynolds, *ibid.*
 d) R. W. Ruddle, *The Solidification of Castings*, second edition, The Institute of Metals, London, 1957.
 e) B. Bardes and M. C. Flemings, *Trans. AFS* 74, 406 (1966).
 f) H. Jacobi, *Proceedings Fifth International Conference on Vacuum Metallurgy and ESR*, Munich, 1976.
 g) K. P. Michalek, J. E. Kelley and J. A. Dantzig, in *Modeling and Control of Casting and Welding Processes*, S. Kou and R. Mehrabian (editors), The Metallurgical Society-AIME, Warrendale, PA, 1986, pages 497-516.
 h) A. D. Rollett, H. D. Lewis and P. S. Dunn, in S. Kou and R. Mehrabian (editors), *ibid.*, pages 565-575.

10.3 CONTINUOUS CASTING

The basic features of a continuous casting machine are depicted in Fig. 10.13. The metal passes through a water-cooled metal mold forming a thin solidified skin (6 to 18 mm), and is then subjected to a water spray for the remainder of solidification. Figure 10.14 schematically shows the temperature distribution within the partially frozen casting as it moves downward with a velocity u in the y -direction. While in the mold, the conduction of heat in the thin shell of solid is much greater in the x -direction than in the y -direction. Therefore the conduction of heat in the withdrawal direction may be ignored. Under these

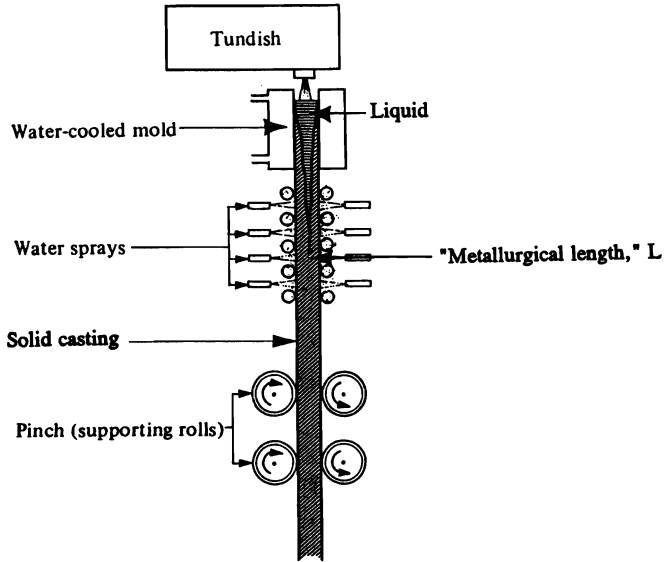


Fig. 10.13 A strand casting machine.

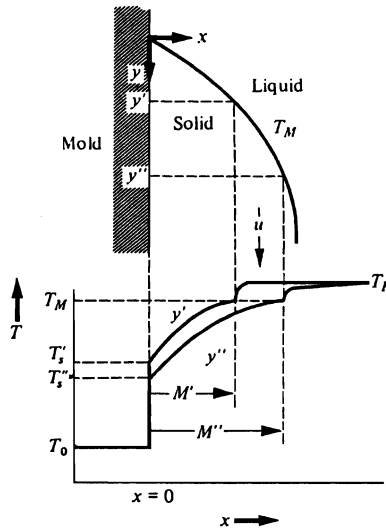


Fig. 10.14 The partially frozen portion of a continuous casting and the temperature profile as a function of the distance down the mold.

circumstances, the analysis used for static casting as presented in Section 10.2.3 may be applied with only minor modifications.

As the metal passes through the mold, we assume that a constant heat transfer coefficient applies at the mold-casting interface, while the heat is removed by the water-cooled mold maintained at T_0 . Equation (10.33) applies if the time t is recast as the distance down the

352 Solidification of Metals

mold wall y , divided by the casting velocity u . We account for the effect of liquid superheat by realizing that on passing down from the tundish, enough turbulence prevails in the liquid core, at least between the mold walls, so that we may assume that the liquid temperature is constant in the y -direction, at T_p . Then, at the solid-liquid interface, latent heat plus the liquid superheat is conducted toward the mold wall through the solid skin, and in the formulation the effective latent heat of fusion H'_f applies in which

$$H'_f = H_f + C_{p,l}(T_p - T_M).$$

The results are convenient when presented in dimensionless variables. From Eq. (10.33), we deduce the variables

$$\frac{h^2 y}{uk' \rho' c'_p}, \quad \frac{C'_p(T_M - T_0)}{H'_f}, \quad \text{and} \quad \frac{hM}{k'}.$$

These variables and others are used in Figs. 10.15-10.17 to present the results. We can determine the thickness of solid metal at various positions down the mold from Fig. 10.15. Figure 10.16 shows how the surface temperature T_s of the cast metal varies with the mold position, and we use Fig. 10.17 to calculate the total rate of heat removal entering the mold of length L . Skin thickness and surface temperature are important parameters, since the solid skin on exit from the mold must be of some minimum strength. The rate of heat removal is useful when computing cooling water requirements.

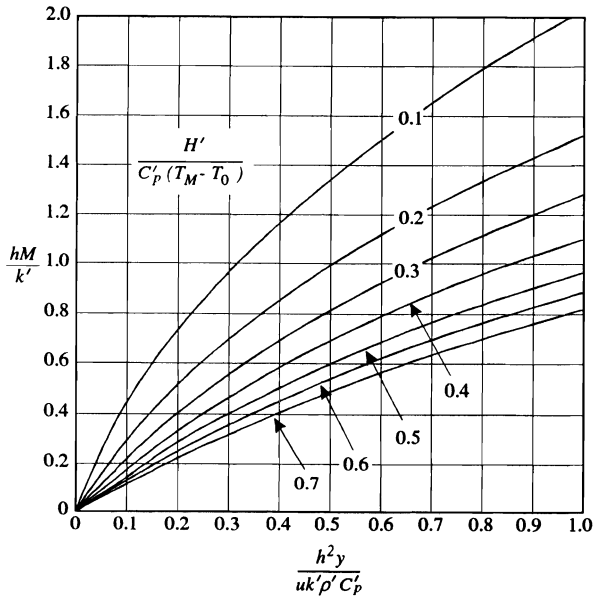


Fig. 10.15 Thickness solidified, M , versus distance down the mold. (Figures 10.15-10.17 are from A. W. D. Hills and M. R. Moore, *ibid.*)

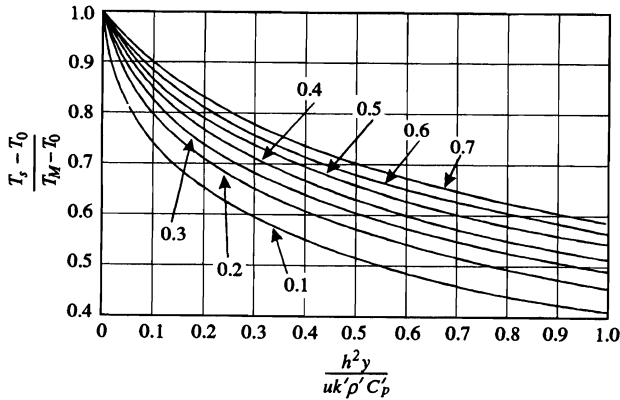


Fig. 10.16 Surface temperature versus distance down the mold. Numbers on the curves are the same as in Fig. 10.15.

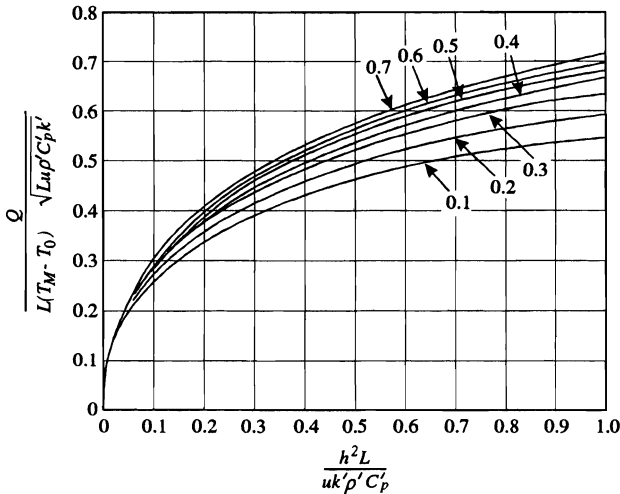


Fig. 10.17 Rate of heat removal by mold cooling water Q versus mold length L . Numbers on the curves are the same as in Fig. 10.15.

Example 10.7 Determine a) the mold length, and b) the cooling water requirements to produce steel slab (0.61 m wide by 75 mm thick) at a withdrawal rate of 50 mm s⁻¹. The solid skin on exit from the mold should be 13 mm thick, and a heat transfer coefficient of 2000 W m⁻² K⁻¹ may be assumed. To minimize the cooling of the recirculated water, only a 6 K temperature rise of the water is allowed.

Data for steel:

- Freezing temperature = 1770 K,
- Pouring temperature (from tundish) = 1800 K,
- Latent heat of fusion = 2.67 × 10⁵ J kg⁻¹,

354 Solidification of Metals

$$\begin{aligned} \text{Solid density} &= 7690 \text{ kg m}^{-3}, \\ \text{Solid heat capacity} &= 670 \text{ J kg}^{-1} \text{ K}^{-1}, \\ \text{Liquid heat capacity} &= 596 \text{ J kg}^{-1} \text{ K}^{-1}, \\ \text{Solid thermal conductivity} &= 60 \text{ W m}^{-1} \text{ K}^{-1}. \end{aligned}$$

Solution.

$$\text{a) } \quad \frac{hM}{k'} = \frac{(2000)(0.013)}{60} = 0.433,$$

$$\begin{aligned} H'_f &= H_f + C_{p,l}(T_p - T_M) = 2.67 \times 10^5 + 596(1800 - 1770) \\ &= 2.85 \times 10^5 \text{ J kg}^{-1}, \end{aligned}$$

and

$$\frac{H'_f}{C'_p(T_M - T_0)} = \frac{2.85 \times 10^5}{670(1770 - 294)} = 0.288.$$

From Fig. 10.15, we get

$$\frac{h^2 y}{uk' \rho' C'_p} \approx 0.20.$$

Therefore,

$$y = L = \frac{(0.20)(0.050)(60)(7690)(670)}{2000^2} = 0.77 \text{ m}.$$

b) From Fig. 10.17,

$$\frac{Q}{L(T_M - T_0) \sqrt{Lu\rho' C'_p k'}} \approx 0.38,$$

$$Q = (0.38)(0.77)(1770 - 294) \sqrt{(0.77)(0.050)(7690)(670)(60)} = 1.49 \times 10^6 \text{ W}.$$

Now we calculate the flow rate of water (the specific heat of water is $4184 \text{ J kg}^{-1} \text{ K}^{-1}$).

$$\text{Flow rate} = \frac{1.49 \times 10^6 \text{ J}}{\text{s}} \left| \frac{\text{kg K}}{4184 \text{ J}} \right| \left| \frac{1}{6 \text{ K}} \right| = 59.4 \text{ kg s}^{-1},$$

or

$$= \frac{59.4 \text{ kg}}{\text{s}} \left| \frac{\text{m}^3}{1000 \text{ kg}} \right| \left| \frac{264.2 \text{ gal}}{1 \text{ m}^3} \right| \left| \frac{60 \text{ s}}{1 \text{ min}} \right|$$

$$= 942 \text{ gallons per minute (gpm)}.$$

Below the mold in a continuous casting, heat extraction is continued by means of water sprays. Under these conditions, the heat flux at the surface of the solidified metal is

$$q_{x=0} = h_{\text{spray}}(T_{\text{surf}} - T_{\text{wat}}).$$

Finally, below the spray zone, heat extraction continues by radiation, so that

$$q_{x=0} = \varepsilon\sigma(T_{\text{surf}}^4 - T_{\text{amb}}^4),$$

where ε = emissivity of the scale on the surface, and σ = Stefan-Boltzmann constant, which are both defined in the next chapter. The overall result is that the position of the solidified front moves at varying rates, depending on the heat flux at the surface, but as M increases, the rate becomes less and less influenced by the surface condition and is instead influenced by the rate of conduction of energy through the solidified shell.

A severe problem can arise when the cooling flux provided by water sprays is not high enough compared to the flux in the mold. As the solid skin moves from the mold to the spray zone, the temperature gradient in the solid may be quite steep, providing a strong flux of energy to the surface. If the spray heat transfer coefficient is not high enough, or the sprays do not properly cover the surface, this energy will not be extracted from the metal as fast as it arrives and the temperature at the surface of the metal will therefore increase. If this increase is too large (100 K is considered the allowable maximum), the strength of the metal degrades to the point where it might crack, causing surface quality problems during subsequent rolling. Computations to illustrate this problem are not easily done analytically, but are best handled numerically, using techniques discussed in Chapter 16.

Because of these complications, the reader is cautioned against using the often-quoted "metallurgical length" equation

$$L = k'uD^2,$$

(where k' is a constant for a given metal and casting shape, u is the casting speed and D is the outer dimension of the cast section), except for qualitative estimates of where the final solidification occurs. This equation does, however, point out that the final solidification point does increase directly with casting speed.

10.4 CRYSTAL GROWTH

It is possible to obtain crystals of several hundreds of materials for applications as electronic, optical or magnetic materials, dielectrics, piezoelectrics, etc. The crystal growth processes are probably more numerous than the applications, themselves, and so here we restrict our discussion to melt-grown crystals. An excellent perspective on crystal growth technology is given by Brice.⁷

Actually, heat transfer during crystal growth is only one part of the transport phenomena which should be considered. In fact, it is the mass transfer that is most consequential in determining the success or failure in achieving suitable crystals.

Clearly, semiconductor crystals constitute the greatest portion of crystals produced in the world, and silicon dominates this portion. A sketch of a Czochralski-type crystal grower, which is the most common technique for growing silicon, is shown in Fig. 10.18(a). Another technique makes use of the floating-zone process, which is shown in Fig. 10.18(b).

⁷J. C. Brice, *Crystal Growth Processes*, Blackie & Son Ltd., Bishopbriggs, Glasgow, 1986.

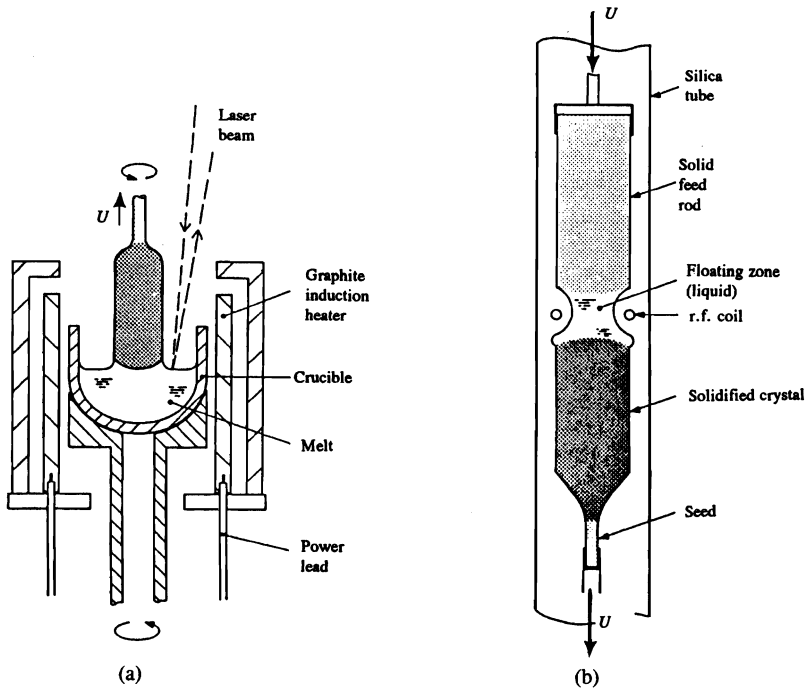


Fig. 10.18 Crystal growing processes: (a) Czochralski grower; (b) floating-zone.

In a Czochralski grower, the charge material is placed in a crucible and melted. A seed crystal is attached to a vertical *pull* rod, lowered until it touches the melt, allowed to melt back slightly, and then raised slowly so that crystallization proceeds from the seed crystal. The crystal is rotated slowly as it is pulled, and the crystal diameter is controlled by adjusting pull-rate and/or heat input to the melt. The reflected laser beam senses the exact position of the surface of the melt for the control of the pull-rates.

The floating-zone is used in zone melting, in which only a portion of the charge is melted, and this zone is slowly moved through the charge. Many types of heat sources are used for zone melting, including induction, resistance, electron beam, and laser beam. The zone is moved either by mechanically moving the power source with respect to the crystal or vice versa. Zone melting is usually done without a crucible (i.e., *floating zone* melting) for reactive and high-melting-point materials. The molten zone is held in place by surface tension forces sometimes aided by a magnetic field.

The conduction heat transfer in the solidified crystal is described by the energy equation, written in cylindrical coordinates:

$$\frac{\partial T}{\partial t} - U \frac{\partial T}{\partial z} = \alpha \left[\frac{\partial^2 T}{\partial z^2} + \frac{1}{r} \frac{\partial}{\partial r} \left(r \frac{\partial T}{\partial r} \right) \right], \quad (10.40)$$

where U = velocity of the crystal. For simplicity, we assume that conduction is one-dimensional, and the solid-liquid interface is flat. Also, the crystal is long enough that

steady state is achieved with respect to coordinates that also move with velocity U . With these assumptions, Eq. (10.40) reduces to

$$\frac{d^2T}{dz^2} + \frac{U}{\alpha} \frac{dT}{dz} = 0. \quad (10.41)$$

We write the same equation for the liquid using the subscript L :

$$\frac{d^2T_L}{dz^2} + \frac{U}{\alpha_L} \frac{dT_L}{dz} = 0. \quad (10.42)$$

The interface is at $z = 0$, the solid is in the region $z \leq 0$, and the liquid is in $z \geq 0$. We can solve these equations with the following boundary conditions:

$$T = T_L = T_M \quad \text{at} \quad z = 0, \quad (10.43)$$

and

$$\frac{dT}{dz} = G_S \quad \text{at} \quad z = 0, \quad (10.44)$$

$$\frac{dT_L}{dz} = G_L \quad \text{at} \quad z = 0, \quad (10.45)$$

where G_S and G_L are the thermal gradients in the solid and liquid, respectively, at the interface. The results are

$$T = T_M + \frac{\alpha G_S}{U} \left[1 - \exp \left(-\frac{zU}{\alpha} \right) \right], \quad (10.46)$$

and

$$T_L = T_M + \frac{\alpha_L G_L}{U} \left[1 - \exp \left(-\frac{zU}{\alpha_L} \right) \right]. \quad (10.47)$$

Keep in mind that the utility of Eqs. (10.46) and (10.47) is that they represent the steady-state temperature profiles in the vicinity of the interface. Actually, Eqs. (10.46) and (10.47) give unrealistic results for the far-field conditions. Specifically,

$$T_L \rightarrow T_M + \frac{\alpha_L G_L}{U} \quad \text{as} \quad z \rightarrow \infty,$$

and

$$T \rightarrow -\infty \quad \text{as} \quad z \rightarrow -\infty.$$

It is understood, therefore, that Eqs. (10.46) and (10.47) provide asymptotic solutions for $z = 0$, which are approximately true at finite values of z .

Finally, we point out that G_S , G_L and U are not all independent variables because at the interface, the heat carried by the solid comprises the heat conducted to the interface in the liquid plus the heat of fusion generated at the moving interface. Therefore,

$$kG_S = k_L G_L + \rho U H_f, \quad (10.48)$$

358 Solidification of Metals

and by fixing any two among G_s , G_L and U , then the third variable is established. Normally, G_L and U are taken to be the process variables, so G_s follows.

Example 10.8 In the growth of silicon, the maximum gradient in the solid that can be tolerated is 0.5 K mm^{-1} (so that the dislocation number density is not excessive).

- If the crystal must be grown with $G_L \geq 0$, what is the maximum growth rate that can be used?
- What happens to the growth velocity if G_s does not change, but G_L is increased abruptly by 10 pct? This could happen by a fluctuation in the power source or by spurious convection in the liquid.

Data for silicon: $k = 31 \text{ W m}^{-1} \text{ K}^{-1}$; $k_L = 50 \text{ W m}^{-1} \text{ K}^{-1}$; $\alpha = 1.32 \times 10^{-5} \text{ m}^2 \text{ s}^{-1}$; $\alpha_L = 1.94 \times 10^{-5} \text{ m}^2 \text{ s}^{-1}$; $T_M = 1683 \text{ K}$; $H_f = 1.80 \times 10^6 \text{ J kg}^{-1}$; $\rho = 2300 \text{ kg m}^{-3}$.

Solution. a) We use Eq. (10.48) and solve for U .

$$U = \frac{kG_s - k_L G_L}{\rho H_f}.$$

In order that U be positive (i.e., there is solidification and not melting), then $kG_s > k_L G_L$ or $G_L < (k/k_L)G_s$. Therefore,

$$G_L < \left[\frac{31}{50} \right] 500$$

$$G_L < 310 \text{ K m}^{-1}.$$

To be safe, let's select $G_L = 200 \text{ K m}^{-1}$. Then,

$$U = \frac{(31)(500) - (50)(200)}{(2300)(1.80 \times 10^6)} = 1.33 \times 10^{-6} \text{ m s}^{-1} = 1.33 \mu\text{m s}^{-1}.$$

This is an extremely small velocity, which resulted because we specified such a very low value of G_s , resulting in a low number of dislocations. Commercial silicon crystals are grown at an order of magnitude higher rate (approximately 1.4×10^{-5} to $2 \times 10^{-5} \text{ m s}^{-1}$).

$$\text{b) } U = \frac{(31)(50) - (50)(200 \times 1.1)}{(2300)(1.80 \times 10^6)} = 1.09 \times 10^{-6} \text{ m s}^{-1} = 1.09 \mu\text{m s}^{-1}.$$

The 10 pct. increase in G_L causes a decrease of 11 pct. in U . If the silicon melt was doped, this change in U would be reflected as a decrease in the concentration of dopant in the crystal as the system adjusts to the new growth velocity.

Equations (10.41)-(10.47) were presented so that we could study the dynamics of the interface. Suppose our interest is to take a more global approach, so that we want the temperature distribution in the crystal while taking into account the power loss from the crystal to the surroundings. The case of a uniform heat transfer coefficient along the length of the crystal was presented as Problem 9.9. If you did not solve this problem, we invite you to do so now. Here, we present a more realistic case in which the heat loss from a floating-

zone crystal and its feed rod is by radiation. Our presentation is based on the work of Donald.⁸

The information we seek comprises the temperature distribution and the power loss from the crystal. The crystal is grown at a high temperature so that the radiant heat flux is

$$q_r = \sigma \varepsilon T^4. \quad (10.49)$$

Equation (10.49) is introduced and utilized extensively in Chapter 11. The variable σ is the Stefan-Boltzmann constant ($\sigma = 5.670 \times 10^{-8} \text{ W m}^{-2} \text{ K}^{-4}$), and ε is a material-surface property called emissivity. Typically, in this process the growth rate is so small that it can be neglected, insofar as the temperature distribution in the solid is hardly affected and in the overall power distribution, its contribution is negligible. We make the additional simplification that the temperature is only a function of z , where z is the distance coordinate along the length of the crystal. The steady-state energy balance on a length Δz in a crystal with a uniform radius R is

$$\frac{d^2 T}{dz^2} = \frac{2\varepsilon\sigma T^4}{kR}. \quad (10.50)$$

As the solution to Eq. (10.50), Donald gives

$$\frac{T}{T_M} = \frac{1}{\left[1 + \frac{z}{\lambda_0}\right]^{2/3}}, \quad (10.51)$$

where

$$\lambda_0 = \left[\frac{5kR}{9\varepsilon\sigma T_M^3}\right]^{1/2},$$

and T_M is the melting temperature of the crystal.

The power radiated from the crystal and the feed rod is obtained by an integration over the entire length,

$$Q = 2\pi R \int_{-\infty}^{\infty} \varepsilon\sigma T^4 dz = 2\pi R \varepsilon\sigma T_M^4 \left[\frac{6}{5} \lambda_0\right]. \quad (10.52)$$

This integration does not include the power loss from the zone, itself. When this is included, Donald recommends

$$Q = 2\pi \varepsilon\sigma T_M^4 \lambda_0 \left[\frac{6}{5} + \frac{L}{\lambda_0}\right], \quad (10.53)$$

where L is the length of the floating zone. Calculated and experimentally measured power requirements for many elements are shown in Fig. 10.19.

⁸D. K. Donald, *Rev. Scient. Instr.* **32**, 811 (1961)

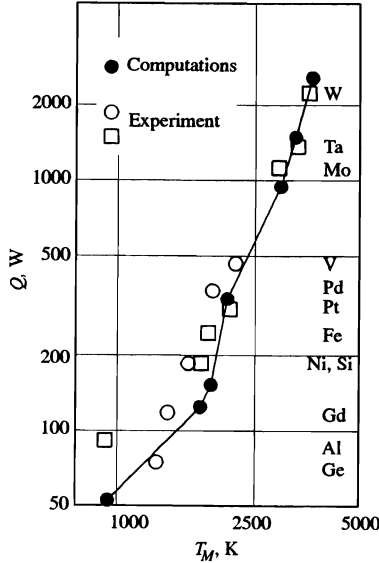


Fig. 10.19 Power required for floating zones in rods of several elements (radius = 12.7 mm). (From D. K. Donald, *ibid.*)

Example 10.9 Estimate the thermal gradients in silicon at the solid-liquid interface in the floating-zone process. The crystal (10 mm dia.) is grown at $5 \times 10^{-5} \text{ m s}^{-1}$. Assume that the emissivity of silicon is 0.2. Other properties of silicon are given in Example 10.5.

Solution.

$$\lambda_0 = \left[\frac{5kR}{9\epsilon\sigma T_M^3} \right]^{1/2} = \left[\frac{(5)(31)(0.005)}{(9)(0.2)(5.670 \times 10^{-8})(1683^3)} \right]^{1/2} = 0.0399 \text{ m.}$$

The temperature gradient is obtained by differentiating Eq. (10.51):

$$\frac{dT}{dz} = -\frac{2T_M}{3\lambda_0} \left[1 + \frac{z}{\lambda_0} \right]^{-5/3},$$

$$G_s = \left| \left[\frac{\partial T}{\partial z} \right]_{z=0} \right| = \frac{2T_M}{3\lambda_0} = \frac{(2)(1683)}{(3)(0.0399)} = 2.81 \times 10^4 \text{ K m}^{-1}.$$

G_L is obtained from Eq. (10.48):

$$G_L = \frac{k}{k_L} G_s - \frac{\rho U H_f}{k_L} = \frac{(31)(2.81 \times 10^4)}{(50)} - \frac{(2300)(5 \times 10^{-5})(1.80 \times 10^6)}{(50)}$$

$$= 1.328 \times 10^4 \text{ K m}^{-1}.$$

In recent years, the mathematical modeling and computer simulation of Czochralski crystal growth (and related processes) have received much attention because of the enormous technological importance of single crystal materials. A good start in understanding the many complexities involved can be gained by reading a short paper by Derby.⁹

PROBLEMS

Data for Problems 10.1-10.8 and Problems 10.27 and 10.28.

Mold material*	k , W m ⁻¹ K ⁻¹	ρ , kg m ⁻³	C_p , J kg ⁻¹ K ⁻¹
Silica sand	0.52	1600	1170
Mullite	0.38	1600	750
Plaster	0.35	1120	840
Zircon sand	1.0	2720	840
Ceramic shell	0.70	1800	1100
Copper	390	9000	380

Casting material	T_M , K	H_f , J kg ⁻¹	ρ' , kg m ⁻³	C_p' , J kg ⁻¹ K ⁻¹	k' , W m ⁻¹ K ⁻¹
Iron	1808	2.72×10^5	7210	750	40
Nickel	1728	2.91×10^5	7850	670	35
Aluminum	933	3.91×10^5	2400	1050	260

*Note: Only typical values can be given here. Actual properties depend on temperature, particle size, binders, porosity, etc.

10.1 Plot distance solidified versus the square root of time for the following metals (in each case the pure metal is poured at its melting point against a flat mold wall): a) iron in a silica sand mold, b) aluminum in a silica sand mold, c) iron in a mullite mold heated to 1260 K.

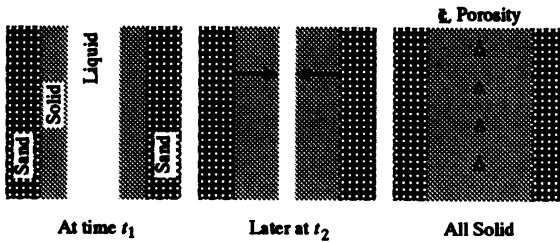
10.2 How long does it take to freeze a 100 mm diameter sphere of pure iron in a silica sand mold, assuming: a) no superheat and neglecting the heat flow divergence? b) no superheat and realizing that a sphere is being cast? c) 110 K superheat and realizing that a sphere is being cast?

10.3 Plot distance solidified versus time for iron poured at its melting point into a heavy copper mold, assuming that a) there is a large flat mold wall and no resistance exists to heat flow at the mold-metal interface; b) interface resistance to heat flow is finite ($h = 570 \text{ W m}^{-2} \text{ K}^{-1}$).

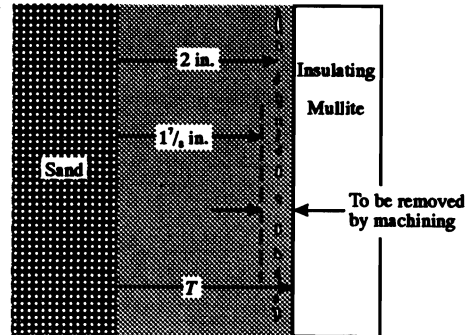
10.4 Show whether iron can be cast against a very thick aluminum mold wall without causing the aluminum to melt.

10.5 Slab-shaped steel castings are prone to center-line porosity, which—for our purposes—is simply an alignment of defects along the plane of last solidification. The sketch on the next page shows the solidification of a slab cast in silica sand and the location of the centerline porosity.

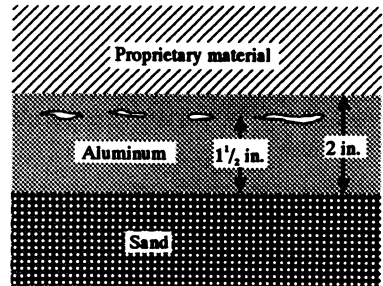
⁹J. J. Derby, *MRS Bulletin XIII*, 29 (October 1988).



The solidification time for the 2-in. slab cast in sand is known to be 6 min; when cast in an insulating mullite mold, the time is 60 min. If a casting is made in the composite mold depicted to the right, determine the thickness T the casting should have to yield $1\frac{7}{8}$ in. of sound metal after machining.



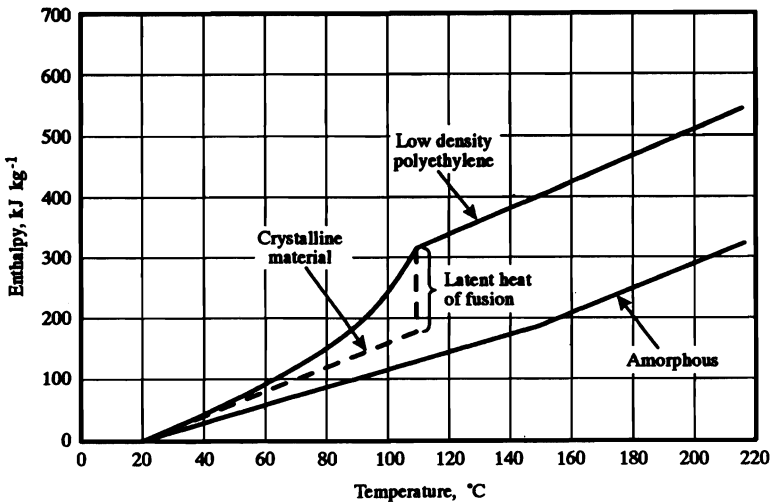
10.6 A 2-in. thick slab of aluminum is cast in a mold made of silica sand (forming one face) and a proprietary material (forming the other face). The aluminum is poured with no superheat, and the as-cast structure of the slab is examined after solidification and cooling. The examination shows that the plane of last solidification (i.e., the plane where the two solidification fronts meet) is located $1\frac{1}{2}$ in. from the sand side. Knowing this, calculate the *heat diffusivity* (not the thermal diffusivity) of the proprietary material.



10.7 Consider solidification in a flat ceramic shell mold with a thickness L . There is heat loss from the outside surface to the surroundings with a constant heat transfer coefficient ($h = 150 \text{ W m}^{-2} \text{ K}^{-1}$). Except for very early times, the temperature in the mold is at steady state. a) Derive an equation for thickness solidified versus time. b) A plate of nickel (38 mm thick) is cast in a ceramic shell mold (10 mm thick). Calculate the solidification time.

10.8 Repeat Problem 10.7, but replace the flat mold with a cylindrical shell of thickness L . A cylinder of nickel (38 mm diameter) is cast into the mold with a thickness of 10 mm.

10.9 Low density polyethylene is injected into a water-cooled copper mold. The temperature of the melt entering the mold is 465 K. The polyethylene is molded to form a plate that is 10 mm thick. Estimate the time required for all of the polyethylene reach less than 335 K, when it can be safely ejected from the mold. Assume that the heat transfer coefficient at the polyethylene-copper interface is relatively high ($h = 4000 \text{ W m}^{-2} \text{ K}^{-1}$) because cooling occurs while the molding is under pressure. The enthalpy of polyethylene is given below. Other properties of low density polyethylene are $k = 0.26 \text{ W m}^{-1} \text{ K}^{-1}$ and $\rho = 920 \text{ kg m}^{-3}$.



10.10 Repeat Problem 10.9 for amorphous polyethylene ($\rho = 970 \text{ kg m}^{-3}$). This polymer can be safely ejected at 315 K. Compare the achievable production rates of the two forms of polyethylene.

10.11 Aluminum oxide is solidified in a water-cooled molybdenum mold to form continuous fibers with a diameter of $200 \mu\text{m}$. Estimate the length of the mold required to completely solidify the aluminum oxide as it exits from the mold, as a function of the fiber velocity. Assume that $h = 4000 \text{ W m}^{-2} \text{ K}^{-1}$ in the mold. Data for Al_2O_3 : $k = 11 \text{ W m}^{-1} \text{ K}^{-1}$; $C_p = 1230 \text{ J kg}^{-1} \text{ K}^{-1}$; $\rho = 3016 \text{ kg m}^{-3}$; $T_M = 2327 \text{ K}$; $H_f = 1.07 \times 10^6 \text{ J kg}^{-1}$.

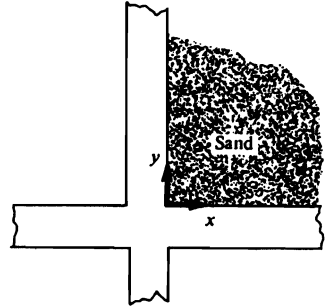
10.12 A continuous casting machine forms molten steel into a slab, 1.93 m wide and 229 mm thick, at a production rate of 52.5 kg s^{-1} . Assume that $h = 1135 \text{ W m}^{-2} \text{ K}^{-1}$. a) Determine the vertical length of the mold if the solid shell must be 12 mm thick at the mold exit. b) Calculate the cooling water requirement (kg s^{-1}) if its temperature rise is from 300 to 307 K. Data for low carbon steel: $k = 35 \text{ W m}^{-1} \text{ K}^{-1}$; $C_p = C_{p,l} = 670 \text{ J kg}^{-1} \text{ K}^{-1}$; $\rho = 7690 \text{ kg m}^{-3}$; $H_f = 2.79 \times 10^5 \text{ J kg}^{-1}$; $T_M = 1790 \text{ K}$.

10.13 The dwell time in the mold of a continuous casting machine is defined as the period which the metal spends in the mold during solidification; that is, $t = L/u$, in which t = dwell time, L = length of mold over which solidification is occurring, and u = velocity of metal through the mold. Since the skin solidified in the mold is thin, a simple analysis might be expected to apply. a) Neglect conduction in the withdrawal direction and write an expression

364 Solidification of Metals

for thickness solidified versus time. b) Compare the results for dwell time in Problem 10.12 and the dwell time calculated from part a) for the same conditions.

10.14 A junction-shaped casting, as depicted to the right, is made in a sand mold. The junction may be considered infinitely long in the z -direction. For the upper right quadrant of sand:



- Write a differential equation for temperature.
- Write the boundary conditions (for time and space) that apply.
- Write the solution yielding temperature as a function of position in the sand and time.
- Derive an equation for the heat absorbed by the sand as a function of time and the lengths of the junction legs.

10.15 Equations (10.32) and (10.33) are approximations for the case depicted in Fig. 10.9. The exact solution for the temperature in the solidified skin is

$$\frac{T - T_0}{T_M - T_0} = \left[\frac{1}{\operatorname{erf} \beta} \right] \operatorname{erf} \left[\beta \frac{M_0 + x}{M_0 + M} \right],$$

where β satisfies

$$\beta e^{\beta^2} \operatorname{erf} \beta = (T_M - T_0) \frac{C'_p}{H_f \sqrt{\pi}}$$

and M_0 satisfies

$$\frac{2k'\beta^2}{hM_0} = (T_M - T_0) \frac{C'_p}{H_f}.$$

- Show that the above relationships are exact.
- If t_0 is a time defined as

$$t_0 = \frac{M_0^2}{4\beta^2\alpha'},$$

show that the thickness solidified is

$$M = 2\beta \sqrt{\alpha'} \left[(t_0 + t)^{1/2} - t_0^{1/2} \right].$$

10.16 Usually when Eq. (10.48) is invoked, the solid-liquid interface is considered to be at the freezing temperature (i.e., at the equilibrium temperature). In *rapid solidification processing*, however, the interface can be significantly undercooled. If H_f is the latent heat at the equilibrium temperature: a) rewrite Eq. (10.48) in a more precise manner, taking into account that C_p of the solid and liquid phases are not necessarily equal; b) rewrite Eq. (10.48) in accordance with part a) and also account for the densities not being equal.

10.17 Is it possible that $G_L < 0$ during crystal growth? Can there be solidification? Do you think the planar interface will be stable?

10.18 A single crystal in the form of a long thin rod is grown by the Czochralski method (Fig. 10.18(a)). Assume that the heat conduction is one dimensional and that the heat transfer coefficient is uniform along the length of rod. a) Write the energy equation for temperature along the length of the crystal and obtain the solution for the temperature distribution. b) Use the properties given in Example 10.8 for silicon and assume that $h = 100 \text{ W m}^{-2} \text{ K}^{-1}$ (uniform). Calculate G_S for growth rates of 10^{-6} , 10^{-5} and 10^{-4} m s^{-1} . c) Calculate the corresponding values of G_L and briefly discuss your results.

10.19 The properties of aluminum near the melting point are given: $T_M = 933 \text{ K}$; $k = 210 \text{ W m}^{-1} \text{ K}^{-1}$. Consult Chapter 11 for emissivity. Calculate the power loss to maintain a floating zone in aluminum. Compare your results to Fig. 10.19 and discuss.

10.20 Welding of a "thin plate" can be analyzed by starting with Eq. (9.85) for the peak temperature around a moving line source. With r as the cylindrical radius from the line source, we can set $T_p = T_M$ (the melting point of the base metal) at $r = r_M$; then

$$T_M - T_0 = \frac{Q}{\rho C_p \delta V r_M \sqrt{2\pi e}}$$

Show that

$$\frac{1}{T_p - T_0} = \frac{V r' \delta \rho C_p \sqrt{2\pi e}}{Q} + \frac{1}{T_M - T_0}$$

where $r' = r - r_M$. For $r' \geq 0$ this gives the peak temperature in the base metal next to the weld.

10.21 Welding of a "thick plate" can be analyzed by starting with Eq. (9.81) for the peak temperature around a moving point source. As in Problem 10.20, set $T_p = T_M$ at $r = r_M$ and show that

$$\frac{1}{T_p - T_0} = \frac{2\pi k \alpha e}{QV} \left[\frac{V r'}{2\alpha} \right]^2 + \frac{1}{T_M - T_0}$$

where $r' = (r^2 - r_M^2)^{1/2}$, provided $r' \geq 0$.

Problems 10.22-10.26 should be attempted after Problems 10.20 and 10.21 have been solved.

10.22 Sketch temperature versus time at $r = 0$, $r = r_M$ and $r > r_M$ in a thin plate that is welded.

10.23 A very thick steel plate is welded with 5 kW and 75 pct. efficiency at a welding speed of 4.2 mm s^{-1} . Prior to welding the plate is preheated to 480 K. Assume that the fusion zone (i.e., the edge of the molten weld metal) corresponds to the 1644 K isotherm. a) Calculate the peak temperature at a distance of 1 mm from the fusion zone. b) What is the cooling rate at that location when the temperature is 1070 K? *Data for steel:* $k = 35 \text{ W m}^{-1} \text{ K}^{-1}$; $\rho = 7690 \text{ kg m}^{-3}$; $C_p = 754 \text{ J kg}^{-1} \text{ K}^{-1}$.

366 Solidification of Metals

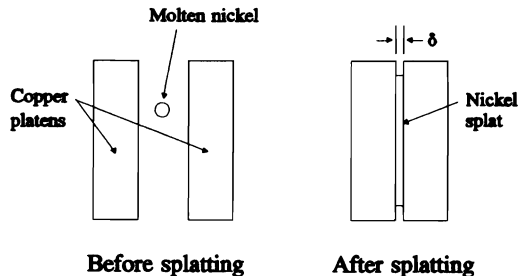
10.24 Derive an equation for the thermal gradient, $\partial T/\partial r$, at the edge of a weld pool ($r = r_M$) of a material with a freezing point of T_M . The plate is steel and very thick. Thermal properties are given in Problem 10.23.

10.25 The surface of damaged silicon can be annealed by passing a laser beam over the surface in order to effect melting to a depth below the damaged layer. When the silicon resolidifies, it does so epitaxially so that the crystal structure of the underlying single crystal is maintained.

Assume that the silicon is at 293 K and is "thick." The molten pool is 1 mm thick, and the laser beam moves at a velocity of 20 cm s^{-1} with a power of 8 kW at 75% efficiency. a) Calculate the distance from the edge of the molten pool where a peak temperature of 1273 K is achieved. b) Calculate the maximum cooling rate directly behind the molten pool. [Hint: Start with the steady-state temperature associated with a moving point source (Chapter 9) and make a transformation from moving to stationary coordinates.] Consult Example 10.8 for properties of silicon.

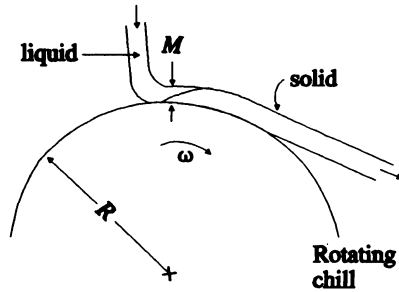
10.26 Steel plate, 19 mm thick, is welded with 4 kW at 80 pct. efficiency with a welding speed of 2.5 mm s^{-1} . Assume that the edge of the molten pool corresponds to the isotherm of 1700 K. For this steel it is known that some martensite is found in the vicinity of the weld when the cooling rate exceeds 4.6 K s^{-1} at 866 K. a) If the plate is not preheated, would you expect to produce a weld with martensite? b) What is the peak temperature at 0.3 mm from the edge of the weld metal? Problem 10.24 gives properties of the steel.

10.27 Nickel is "splat cooled" between two platens of copper which are rapidly accelerated toward each other. The process is sketched below.



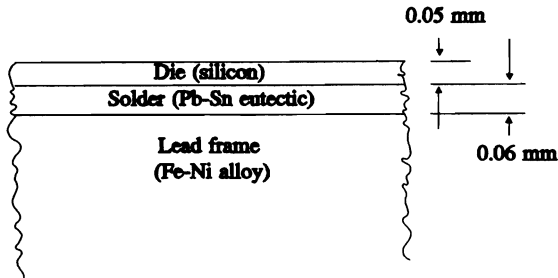
The splat thickness (δ) is 0.1 mm. Neglect superheat in the nickel droplet. a) Calculate the minimum freezing time of the splat by assuming no interfacial resistance to heat flow. b) Calculate the freezing time assuming that $h = 2000 \text{ W m}^{-2} \text{ K}^{-1}$, and the temperature of the copper platens is 293 K. Properties are listed at the beginning of this section.

10.28 In melt spinning, a jet of molten metal is directed to the surface of a rotating chill. Solidification takes place very rapidly, and a very thin ribbon of metal with thickness δ is produced. The process is shown on the next page.



Calculate the rate of solidification (dM/dt in mm s^{-1}) when M is one-half of δ . Assume one-dimensional heat flow in the solidified metal and in the rotating chill, with $h = 1.7 \times 10^4 \text{ W m}^{-2} \text{ K}^{-1}$. The metal ribbon is aluminum with a thickness of $50 \mu\text{m}$, and the rotating chill is copper. Properties are listed at the beginning of this section.

10.29 Silicon dies are attached to the lead frames in microelectronic devices by soldering (see sketch below).



Assume that initially the die and the lead frame are at 423 K and that the solder is molten with no superheat ($T_M = 456 \text{ K}$). The ambient above the die is at 293 K . a) What is the temperature at the solder/lead frame interface during solidification of the solder? b) What is the temperature at the solder/die interface early during the solidification of the solder? c) Estimate the time required for the top surface of the die to achieve 428 K . d) Has the solder completely solidified in the time calculated for part c)?

Data:

	$T_M, \text{ K}$	$H_f, \text{ J kg}^{-1}$	$k, \text{ W m}^{-1} \text{ K}^{-1}$	$\rho, \text{ kg m}^{-3}$	$C_p, \text{ J kg}^{-1} \text{ K}^{-1}$
Fe-Ni alloy	—	—	12.6	8700	670
Pb-Sn eutectic	456	54×10^3	33.6	9200	209
Si		(See Example 10.8)			

RADIATION HEAT TRANSFER

In Chapter 6, we alluded to energy transfer by radiation as a mechanism for heat flow, but due to the entirely different natures of conduction and radiation, only a limited discussion of radiation appeared prior to this chapter. Energy transport by conduction depends on the existence of a conducting material. On the other hand, radiation is electromagnetic energy in transport; therefore, energy travels through space via radiation. The rate equations for conduction and radiation reflect their very different characters, and show no similarity. The energy flux by conduction is proportional to the thermal gradient, that is, $q_x = -k(\partial T/\partial x)$. In radiant heat transfer, the energy flux—so-called emissive power—is proportional to the fourth power of the absolute temperature; that is, $e \propto T^4$.

Solids, liquids, and some gases emit radiant energy composed of many wavelengths in the spectrum of electromagnetic radiation. The excitation process causing radiation may vary and can be classified as fluorescence, x-radiation, radio waves, etc. The thermal radiation is of primary interest here, and its range of wavelengths is taken to be 0.1-100 μm .

11.1 BASIC CHARACTERISTICS

Thermal radiation is defined as the energy transferred by electromagnetic waves that originate from a body because of its molecular motion which characterizes temperature. The rate at which energy is emitted depends on the substance itself, its surface condition, and its surface temperature.

Figure 11.1 depicts a surface emitting and receiving thermal radiation. The total emissive power e is the flux of thermal radiation energy *emitted* into the entire volume above the surface. In terms of electromagnetic waves, the total emissive power is the sum of all the energy carried by all wavelengths emitted from the surface per unit area per unit time. The quantity e is also called *emissive power*, *emittance*,* *total hemispherical radiation intensity*, *radiance*, or *radiant-flux density*. We use the terminology of emissive power.

*To add to the confusion, emittance is also used as a synonym for *emissivity*, which is a surface property presented in Section 11.2.

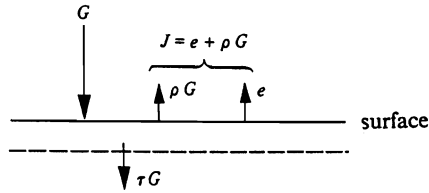


Fig. 11.1 The distribution of thermal radiation at a surface.

We define the *total irradiation*, G , of a body as the flux of thermal radiant energy incoming to the surface, and the *total radiosity*, J , as the total flux of radiant energy leaving the surface of a body. The total radiosity includes both the energy emitted and the energy reflected by the surface. As fluxes, the units of G and J are in W m^{-2} .

The incoming energy (total irradiation) can be absorbed, reflected, or transmitted, so that

$$G = \alpha G + \rho G + \tau G,$$

or

$$\alpha + \rho + \tau = 1, \quad (11.1)$$

where α = absorptivity (fraction of G absorbed), ρ = reflectivity (fraction of G reflected), and τ = transmissivity (fraction of G transmitted). Most liquids and solids are opaque to thermal radiation, so that $\tau = 0$, and

$$\alpha + \rho = 1. \quad (11.2)$$

The principal exceptions to this are glasses and silicate melts.

11.2 THE BLACK RADIATOR AND EMISSIVITY

In the study of real surfaces, it is convenient to define a hypothetical ideal surface called a black radiator. A black radiator is a surface which absorbs all incoming radiation; thus $\alpha = 1$, and $\rho = 0$. Another important characteristic of the black radiator is that it is a perfect emitter, since it emits radiation of all wavelengths, and its total emissive power is theoretically the highest that can be achieved at a given temperature. It follows that any real body emitting thermal radiation has a total emissive power of some fraction of the emissive power of a black radiator, which is often called a black body. This fraction is defined as the emissivity ϵ . Therefore,

$$e = \epsilon e_b. \quad (11.3)$$

Imagine a region in a space completely filled with black body radiation. A real body 1 emitting radiation at a rate of e_1 is placed in this region; the net rate of energy transferred from the body is

$$q_{1,\text{net}} = \underbrace{e_1}_{\text{energy emitted}} - \underbrace{\alpha_1 e_b}_{\text{energy absorbed}} \quad (11.4)$$

By utilizing Eq. (11.3), we can also write

$$q_{1,\text{net}} = \varepsilon_1 e_b - \alpha_1 e_b. \tag{11.5}$$

If the body is in thermal equilibrium with the black body radiation, then $q_{\text{net}} = 0$, and $\alpha_1 = \varepsilon_1$. The same result can be obtained for any other body placed in this space, and thus *the absorptivity and emissivity of any body at thermal equilibrium are equal*.

It is important to note that although black body radiation is hypothetical, radiation very closely approximating that of a black radiator can be realized. Figure 11.2 depicts radiation emanating from a hollow space having nonblack walls at a uniform temperature. Since the hole is small, only a very small fraction of the radiation entering the hole and diffusely reflecting off the nonblack walls escapes; hence the escaping energy is entirely representative of the radiation within the cavity.

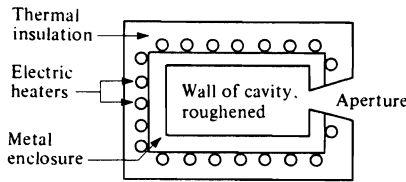


Fig. 11.2 Laboratory black body.

The energy emitted from any point on the walls of the enclosure is εe_b ; when this radiation strikes other parts of the enclosure, a certain fraction is reflected, namely, $\rho \varepsilon e_b$. Similarly, a second reflection equals $\rho(\rho \varepsilon e_b)$, and the third one is $\rho^3 \varepsilon e_b$. Since the hole is small, probability favors radiation that ultimately passes through the hole to be made up of an infinite number of such reflections. Therefore

$$e(\text{hole}) = \varepsilon e_b (1 + \rho + \rho^2 + \rho^3 + \dots), \tag{11.6}$$

or

$$e(\text{hole}) = \varepsilon e_b \frac{1}{1 - \rho}, \tag{11.7}$$

and since $\alpha = 1 - \rho$, and thermal equilibrium exists within the cavity, then $\varepsilon = 1 - \rho$ for the isothermal cavity. Therefore Eq. (11.7) reduces to

$$e(\text{hole}) = e_b. \tag{11.8}$$

Since radiation from a cavity is very nearly black, the *hohlraum* (heated cavity), shown in Fig. 11.2, is normally used as a radiation standard. Such an enclosure may be constructed with heavy metal internal walls that are roughened and oxidized to provide a surface of high emissive power. The walls are heated electrically, and the exterior is well insulated.

11.3 THE ENERGY DISTRIBUTION AND THE EMISSIVE POWER

The thermal radiation from a solid body is composed of a continuous spectrum of wavelengths forming an energy distribution. Figure 11.3 depicts the spectrum of a black body at various temperatures. For most engineering calculations, the total emissive power of a black body at a particular temperature is an important quantity, which is given by the area under the curve applied at that temperature. Therefore

$$e_b = \int_0^{\infty} e_{b,\lambda} d\lambda, \quad (11.9)$$

where λ is the wavelength, and $e_{b,\lambda}$ is the *monochromatic emissive power*. *Planck's equation* or *Planck's distribution law* relates $e_{b,\lambda}$ to the wavelength and the absolute temperature:

$$e_{b,\lambda} = \frac{2\pi hc^2 \lambda^{-5}}{\exp\left[\frac{ch}{\kappa_B \lambda T}\right] - 1}, \quad (11.10)$$

where h = Planck's constant, c = velocity of light, and κ_B = Boltzmann's constant. Substituting Eq. (11.10) into Eq. (11.9) and integrating for all wavelengths results in the *Stefan-Boltzmann* equation for black body radiation, which is

$$e_b = \sigma T^4, \quad (11.11)$$

where the constant σ is

$$\sigma = \frac{2\pi^5 \kappa_B^4}{15c^2 h^3} = 5.669 \times 10^{-8} \text{ W m}^{-2} \text{ K}^{-4}. \quad (11.12)$$

In view of the Stefan-Boltzmann equation, the total emissive power e of a real surface is

$$e = \varepsilon \sigma T^4. \quad (11.13)$$

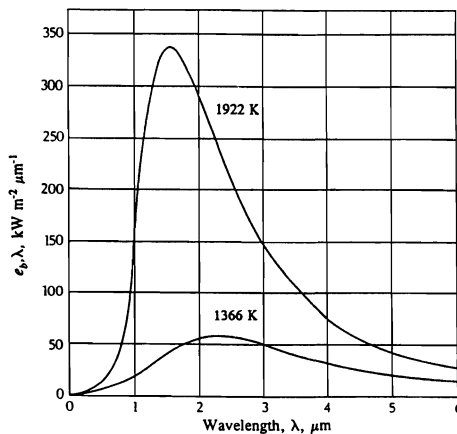


Fig. 11.3 Black body spectral emissive power.

According to Fig. 11.4, the ratio e/e_b of a real surface varies with wavelength; thus the quantity ϵ used in Eq. (11.13) is in fact the mean value of ϵ_λ , the spectral emissivity.* Qualitatively, the spectral emissivity for metals decreases with increasing wavelength. In contrast, the spectral emissivity of electric nonconductors has a tendency to increase with increasing wavelength, but the variation of e_λ with λ can be quite irregular. Figure 11.5 depicts experimental results showing these trends for aluminum having three different surface finishes. For the bare metal surface (commercial finish), the emissivity decreases almost steadily with increasing wavelength. The anodized aluminum behaves as a nonmetal, since the anodizing process produces a thick† oxide coating on the surface. Furthermore, by comparing the commercial surface finish with the polished surface, we see that roughness increases emissivity. But since the descriptions such as polished, rough, or commercial finish are rather vague, emissivity data should be used judiciously with regard to the surface description.

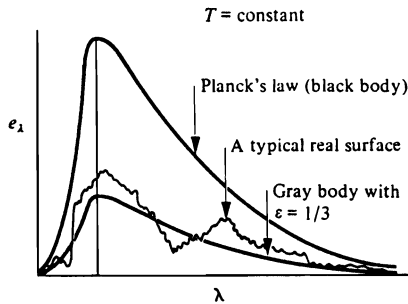


Fig. 11.4 Comparison of black, gray, and real surfaces.

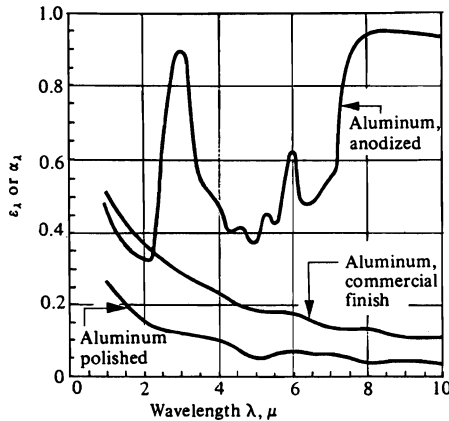


Fig. 11.5 Typical wavelength dependence of ϵ_λ and α_λ for metals.

*Spectral emissivity is sometimes called monochromatic emissivity.

†Relative to the depth of participating material which is only a fraction of a micron for metals.

Not only does emissivity vary with wavelength, but in the case of well-polished surfaces, it is also a function of the view angle from the normal to the surface (Fig. 11.6). Therefore, a directional emissivity ϵ_ϕ exists, but for our purposes the ϵ used for calculations is the average value for a substance emitting radiation in all directions as well as all wavelengths. In this sense, ϵ used for most calculations is properly called the *total hemispherical emissivity*; usually, however, it is simply called emissivity.

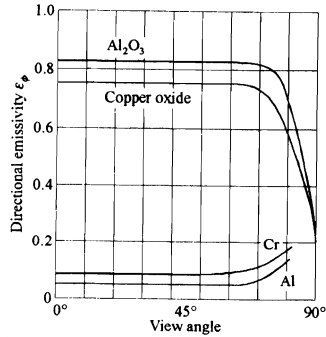


Fig. 11.6 Variation of directional emissivity. The surfaces are well polished.

The curves in Fig. 11.6 illustrate the characteristics of electrical conductors and electrical insulators. Conductors emit somewhat more energy at high angles with respect to the observer, whereas the insulators have an opposite behavior. As a result, two different spheres, heated to the same incandescent temperature, appear as sketched in Fig. 11.7. Keep in mind that Fig. 11.7 is for highly polished surfaces, called *specular* surfaces; the differences are not so great for rough surfaces (*diffuse* surfaces).



Fig. 11.7 Effect of directional emissivity on the appearance of radiating spheres: (a) electrical conductor with brighter periphery; (b) electrical insulator with dimmer periphery.

Figures 11.8 and 11.9 give the emissivity of several substances including polished metals. Additional data are given in Table 11.1; several oxides and some refractory materials are listed. More extensive listings of emissivity data are available in texts on radiation heat transfer,¹⁻⁵ as well as in compilations such as used for Figs. 11.8 and 11.9 and by Wood

¹H. C. Hottel and A. F. Sarofim, *Radiative Transfer*, McGraw-Hill, New York, NY, 1967.

²E. M. Sparrow and R. D. Cess, *Radiation Heat Transfer*, Brooks/Cole, Belmont, CA, 1966.

³T. J. Love, *Radiative Heat Transfer*, Merrill, Columbus, OH, 1968.

⁴R. Siegel and J. Howell, *Thermal Radiation Heat Transfer*, second edition, McGraw-Hill, New York, NY, 1980.

⁵M. Q. Brewster, *Thermal Radiative Transfer and Properties*, John Wiley, New York, NY, 1991.

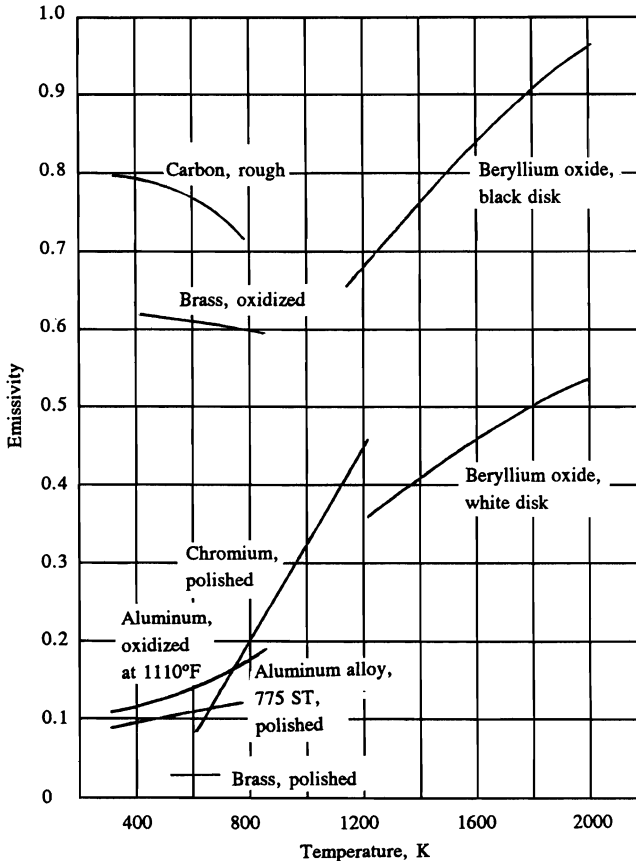


Fig. 11.8 The emissivity of several materials. (From G. G. Gubareff, J. E. Janssen, and R. H. Torborg, *Thermal Radiation Properties Survey*, Honeywell Research Center, Minneapolis, MN, 1960.)

*et al.*⁶ and Touloukian and DeWitt.⁷ In metals, emissivity increases with electrical resistance, and, correspondingly, with temperature. For electric nonconductors, the emissivities are much higher than for *clean* metal surfaces, and they often, but not always, decrease with temperature.

When searching for emissivity data, the reader should be cognizant that many ceramic materials and coatings transmit considerable amounts of the incident radiation and must be

⁶W. D. Wood, H. W. Deem and C. F. Lucks, *Thermal Radiative Properties of Selected Materials*, DMIC Report 177, Volumes 1 and 2, Defense Metals Information Center, Battelle, Columbus, OH, 1962.

⁷Y. S. Touloukian and D. P. DeWitt, *Thermal Radiative Properties*, IFI/Plenum, New York, NY, 1970.

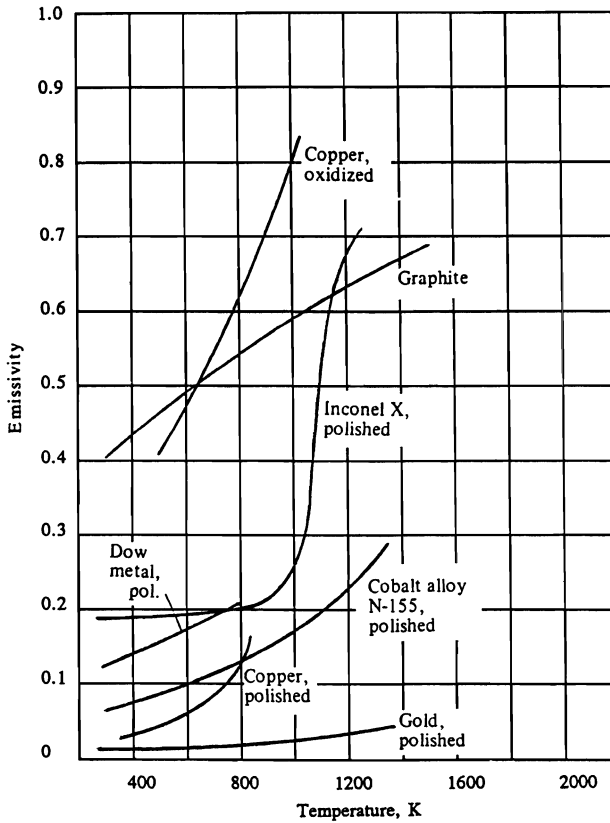


Fig. 11.8 (continued).

Table 11.1 The emissivity of some ceramic materials. (From H. C. Hottel and A. F. Sarofim, *ibid.*)

Material	Temperature, K	Emissivity
Cuprous oxide	1070-1370	0.66-0.54
Magnesium oxide	550-1100	0.55-0.20
	1170-1980	0.20
Nickel oxide	920-1530	0.59-0.86
Thorium oxide	550-770	0.58-0.36
	770-1100	0.36-0.21
Alumina-silica-iron oxide		
58-80% Al ₂ O ₃ , 16-38% SiO ₂ , 0.4% Fe ₂ O ₃	1280-1840	0.61-0.43
26-36% Al ₂ O ₃ , 50-60% SiO ₂ , 1.7% Fe ₂ O ₃	1280-1840	0.73-0.62
61% Al ₂ O ₃ , 35% SiO ₂ , 3% Fe ₂ O ₃	1280-1840	0.78-0.68
Fireclay brick	1273	0.75
Magnesite refractory brick	1273	0.38
Quartz (opaque)	570-1110	0.92-0.80
Zirconium silicate	510-770	0.92-0.80
	770-1105	0.80-0.52

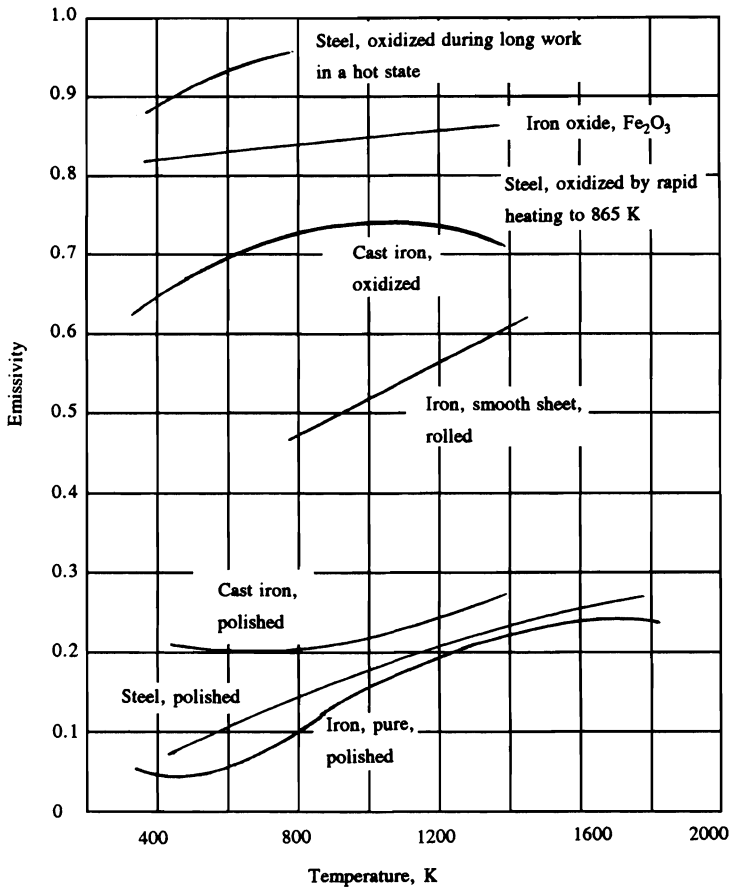


Fig. 11.9 Variation of emissivity with temperature and conditions of ferrous materials. (From G. G. Gubareff *et al.*, *ibid.*)

relatively thick to be effectively opaque. The emissivity of a coating, or thick film, therefore, reported by one investigator might vary considerably from that for the same coating material reported by another. Reasons for such a variance are differences in the surface conditions (including the underlying material) and in the thicknesses of the coatings.

Absorption coefficients (not α) can vary strongly with wavelength. For example, many glasses of 3 mm thickness are effectively infinitely thick to thermal radiation emanating at room temperature. At elevated temperatures, however, a large fraction of the energy of the total spectrum has wavelengths less than $2.5 \mu\text{m}$ (see Fig. 11.3) and in this range the absorption coefficient of glass is so low that the energy can be transmitted up to 300 to 400 mm through the glass. Nevertheless, even if transparent thick films are applied to opaque substrates, the surfaces are treated as though they have emissivities. Usually the emissivity of a metal substrate coated with a nonmetallic is significantly greater than the emissivity of the substrate, itself, but somewhat less than the inherent emissivity of the coating. In Section 11.12, we discuss briefly the combined roles of phonon conduction and photon transmission in semitransparent materials at elevated temperatures.

11.4 GRAY BODIES AND ABSORPTIVITY

The absorptivity of a real surface is even more difficult to evaluate with precision than its emissivity. In addition to the factors which affect emissivity, the absorptivity depends on the character of the incoming radiation; therefore, in general, we cannot regard the absorptivity as dependent on the surface alone. Hence, we assign two subscripts to α , the first to represent the temperature of the absorbing surface, and the second—the source temperature of the incoming radiation. We have already seen in Section 11.2 that the emissivity ϵ_1 of a surface at T_1 is equal to the absorptivity α_1 which the surface exhibits for black radiation from a source at the same temperature T_1 ; for this reason, it is customary in a wide variety of engineering problems to assume that $\alpha = \epsilon$. We shall now discuss the conditions for which it is permissible to deduce α -values from ϵ -values.

If α_λ is independent of λ , the surface is said to be *gray*, and its total absorptivity is independent of the incoming spectral energy distribution; then for a surface at T_1 receiving radiation from an emitter at T_2 , $\alpha_{12} = \alpha_{11}$. Since $\alpha_{11} = \epsilon_1$, we see that the emissivity may be substituted for α , even though the temperatures of the source radiation and the receiver are not the same. There are very few substances with α_λ independent of λ , but many real surfaces may be considered gray. For example, look at the emissivity of polished Inconel X in Fig. 11.8. The emissivity is almost constant in the range 300 to 900 K, and if this surface were in an enclosure with temperatures in this range, then the gray assumption would be good. However, if either the enclosure temperature or the Inconel surface temperature was between 900 and 1300 K, where the emissivity of the Inconel varies rapidly with temperature, the material would be very much nongray. Thus, when available, a convenient criterion for grayness versus nongrayness is the emissivity versus temperature curve.

Under conditions of radiation from a source at T_1 incident on a *metallic* surface at a lower temperature T_2 , we prefer to evaluate the absorptivity of the metallic surface as

$$\alpha_{21} = \epsilon_2(T^*), \quad (11.14)$$

in which $T^* = \sqrt{T_1 T_2}$. We illustrate the use of these approximations in the following section.

11.5 EXCHANGE BETWEEN INFINITE PARALLEL PLATES

When a system is of simple geometry such as infinite parallel plates, concentric cylinders, or concentric spheres, the evaluation of radiant heat transfer is simplified because all of the radiation leaving one of the surfaces is completely intercepted by the other surface. We shall treat more complex geometrical aspects in the next section, but here we consider a case of simple geometry to show the utilization of the system properties. Specifically, consider the two parallel surfaces of infinite extent in Fig. 11.10. In this schematic representation, the energy is viewed as two parts: the radiation originating from surface 2 is shown in Fig. 11.10(a); radiation originating from surface 1 is shown in Fig. 11.10(b).

The irradiation of surface 1 from surface 2 consists of all the upward pointing arrows in Fig. 11.10(a), or

$$e_2 + \rho_{12}\rho_{22}e_2 + \rho_{12}^2\rho_{22}^2e_2 + \dots + \rho_{12}^n\rho_{22}^ne_2. \quad (11.15)$$

We write this infinite series as

$$\frac{e_2}{1 - \rho_{12}\rho_{22}}. \quad (11.16)$$

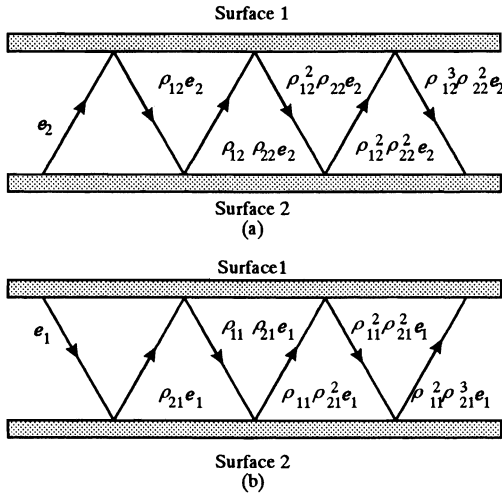


Fig. 11.10 Radiation exchange between parallel surfaces. (a) Irradiation originating from surface (1). (b) Irradiation originating from surface (2).

In a similar manner, the summation of the upward pointing arrows in Fig. 11.10(b) is

$$\frac{\rho_{21} e_1}{1 - \rho_{11} \rho_{21}} \tag{11.17}$$

The sum of these two terms is the total irradiation of surface 1; thus

$$G_1 = \frac{e_2}{1 - \rho_{12} \rho_{22}} + \frac{\rho_{21} e_1}{1 - \rho_{11} \rho_{21}} \tag{11.18}$$

The net heat flux from surface 1 is

$$q_{1,net} = J_1 - G_1, \tag{11.19}$$

but the radiosity J_1 comprises the radiation emitted at surface 1 plus that reflected,

$$J_1 = e_1 + \rho_{1x} G_1. \tag{11.20}$$

(The second subscript of ρ is not denoted at this point.) By combining Eqs. (11.18)-(11.20), we find that the net heat flux from surface 1 is

$$q_{1,net} = e_1 - (1 - \rho_{1x}) G_1 = e_1 - \alpha_{1x} G_1$$

or

$$q_{1,net} = e_1 - \left[\frac{\alpha_{12} e_2}{1 - \rho_{12} \rho_{22}} + \frac{\alpha_{11} \rho_{21} e_1}{1 - \rho_{11} \rho_{21}} \right] \tag{11.21}$$

Here α_{1x} is denoted α_{12} and α_{11} for the first and second terms on the right side of Eq. (11.21) because it is associated with the radiations originating at surfaces 2 and 1, respectively.

380 Radiation Heat Transfer

The basic practical difficulty in the analysis of systems with nonblack surfaces is what absorptivity value should be used. In the light of this problem, discussed in Section 11.4, let us analyze the various forms that Eq. (11.21) takes depending on the manner in which we evaluate α_{11} . The gray assumption which would apply for Inconel-X plates, if both were between 300 and 900 K, makes $\alpha_{12} = \alpha_{11} = \epsilon_1$, $\alpha_{21} = \alpha_{22} = \epsilon_2$, and $\rho_{12} = \rho_{11} = 1 - \epsilon_1$, and $\rho_{21} = \rho_{22} = 1 - \epsilon_2$. In this case, Eq. (11.21) simplifies to

$$q_{1,\text{net}} = (e_{b1} - e_{b2}) \frac{1}{1/\epsilon_1 + 1/\epsilon_2 - 1}. \quad (11.22)$$

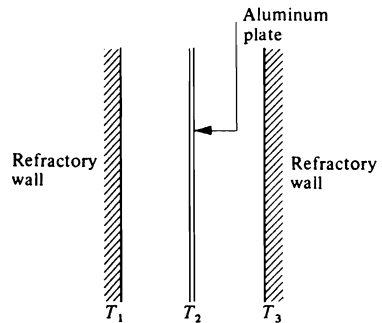
For metal plates, we can improve Eq. (11.22) by the approximation of Eq. (11.14); we evaluate the emissivity of the cooler surface at $T^* = \sqrt{T_1 T_2}$. For example, if surface 2 is hotter than 1, we write Eq. (11.22) as

$$q_{1,\text{net}} = (e_{b1} - e_{b2}) \frac{1}{1/\epsilon_1(T^*) + 1/\epsilon_2 - 1}. \quad (11.23)$$

We accomplish the evaluation of radiant heat transfer between nongray surfaces with the most precision only by considering the best approximation for their absorptivities, and, also the variation in properties with direction. Fortunately, many industrial materials, especially refractories used in furnaces, behave as gray diffuse radiators so that these details may be omitted from analysis. We shall consider nonblack surfaces as gray in this chapter. More details regarding nongray surfaces and directional properties can be found in the more advanced treatments of radiation heat transfer listed in Section 11.3. The presentations of radiation heat transfer in Holman⁸ and Incropera and DeWitt⁹ are also more comprehensive and should be consulted when it is apparent that the surfaces under consideration cannot be assumed gray and diffuse.

Example 11.1 We can use the above results to illustrate the principle of *radiation shields*. Multiple shields are very effective when used as high-temperature insulation against thermal radiation. To illustrate the principle, develop an expression for the reduction in radiant heat transfer between two infinite and parallel refractory walls, when a thin plate of aluminum is placed between them. Assume that all surfaces are gray; the emissivity of the walls is 0.8 and the emissivity of the aluminum is 0.2.

The system with appropriate subscripts is shown to the right.



⁸J. P. Holman, *Heat Transfer*, sixth edition, McGraw-Hill, New York, NY, 1986, Chapter 8.

⁹F. P. Incropera and D. P. DeWitt, *Fundamentals of Heat and Mass Transfer*, third edition, John Wiley, New York, NY, 1990, Chapters 12 and 13.

Solution. First, we examine the case in the absence of the aluminum sheet, that is, direct radiant transfer from surface 1 to surface 3. Equation (11.22) applies with appropriate change of subscripts. Therefore

$$q_{1,\text{net}} \text{ (no shield)} = (e_{b1} - e_{b3}) \frac{1}{1/\varepsilon_1 + 1/\varepsilon_3 - 1}.$$

Now in the presence of the shield, we apply Eq. (11.22) to the net radiant flux from surface 1 to surface 2. Hence

$$q_{1,\text{net}} = (e_{b1} - e_{b2}) \frac{1}{1/\varepsilon_1 + 1/\varepsilon_2 - 1}.$$

Similarly, we write the radiant flux from surface 2 to surface 3 as

$$q_{2,\text{net}} = (e_{b2} - e_{b3}) \frac{1}{1/\varepsilon_2 + 1/\varepsilon_3 - 1}.$$

Since $q_{2,\text{net}} = q_{1,\text{net}}$ (steady state), we eliminate e_{b2} from these equations:

$$q_{1,\text{net}} = \frac{(e_{b1} - e_{b3})}{(1/\varepsilon_1 + 1/\varepsilon_2 - 1) + (1/\varepsilon_2 + 1/\varepsilon_3 - 1)}.$$

The ratio of radiant flux with the shield to that without the shield is

$$\frac{q_{1,\text{net}} \text{ (with shield)}}{q_{1,\text{net}} \text{ (no shield)}} = \frac{(1/\varepsilon_1 + 1/\varepsilon_3 - 1)}{(1/\varepsilon_1 + 1/\varepsilon_2 - 1) + (1/\varepsilon_2 + 1/\varepsilon_3 - 1)}.$$

With $\varepsilon_1 = \varepsilon_3 = 0.8$, and $\varepsilon_2 = 0.2$, this ratio equals 0.143. Insertion of more shields would lower the ratio even more considerably.

11.6 VIEW FACTORS

Having discussed the complexities of property evaluation, we now consider geometric arrangements in radiation heat transfer. In this connection, we introduce the *view factor*. In the engineering literature different terms are used for this factor, such as *configuration factor*, *direct-exchange factor*, *angle factor*, or simply *factor*, and perhaps others which are unknown to us.

The simplest case for calculating the net loss of energy from a body due to radiation is to visualize a body at temperature T_1 which is completely surrounded by an environment at T_2 . Since the environment completely surrounds the body, the radiation impinging on surface 1 is black (as in a cavity). The thermal flux (or emissive power) from the body is $e_1 = \varepsilon_1 \sigma T_1^4$, and that absorbed by the body from the large isothermal cavity is $\alpha_{12} e_{b2} = \alpha_{12} \sigma T_2^4$. Then

$$q_{1,\text{net}} = \sigma [\varepsilon_1 T_1^4 - \alpha_{12} T_2^4], \quad (11.24)$$

and when we assume that the body is gray, $\alpha_{12} = \varepsilon_1$, and we write Eq. (11.24) as

$$q_{1,\text{net}} = \sigma \varepsilon_1 (T_1^4 - T_2^4). \quad (11.25)$$

The more general case of radiation exchange is a system composed of several surfaces at different temperatures and of different emissivities. Such a situation involves the use of the

382 Radiation Heat Transfer

view factor, F_{ij} . We define it as the fraction of the radiation which leaves surface i in all directions and is intercepted by surface j .

To evaluate F_{12} , imagine the two black surfaces, of areas A_1 and A_2 , shown in Fig. 11.11. A small surface element dA_1 emits radiation in all directions (from one side), and a small surface element dA_2 on the other surface intercepts some of this radiation. Let r be the distance between the surface elements, and ϕ_1 and ϕ_2 the angles that r makes with the two normals, as depicted in the figure. The intensity of the radiation transferred from dA_1 to dA_2 , called E_{12} , is proportional to:

1. The apparent area of dA_1 viewed from dA_2 , $\cos \phi_1 dA_1$.
2. The apparent area of dA_2 viewed from dA_1 , $\cos \phi_2 dA_2$.
3. The reciprocal of the distance squared, $1/r^2$, between the two surface elements, as in all radiation problems.

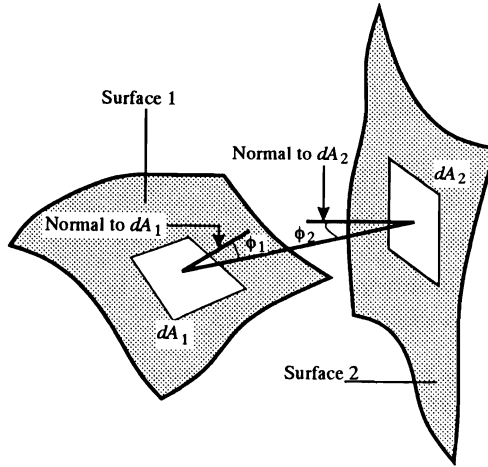


Fig. 11.11 Exchange of radiation between elemental areas.

Thus

$$dE_{12} = I \frac{\cos \phi_1 dA_1 \cos \phi_2 dA_2}{r^2}, \quad (11.26)$$

where I is a proportionality constant. By inspecting Eq. (11.26), I must be the intensity leaving dA_1 in a particular direction; it has units of W m^{-2} per steradian.

At this point, it may appear that I and e_b (the emissive power of a black body) are identical. This is *not* the case, and here we digress from the major argument. Consider the radiation received from the entire field of view to dA_1 , that is, the hemisphere in Fig. 11.12. Visualize dA_2 as the unit surface described by the ring on the hemisphere. Since the normals to a spherical surface are coincident to the radii, ϕ_2 in Eq. (11.26) must be 0, so that $\cos \phi_2 = 1$. The elemental area dA_2 is given by the product of $r d\phi_1$ and its length, $2\pi \sin \phi_1 r$. If we integrate over the entire hemisphere, Eq. (11.26) yields (for isotropic I) per unit area dA_1 :

$$dE_{12} (\text{hemisphere}) = 2\pi I \int_0^{\pi/2} \frac{\cos \phi_1 \sin \phi_1 r^2 d\phi_1}{r^2},$$

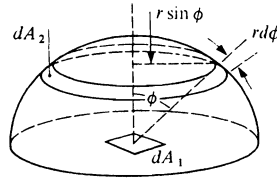


Fig. 11.12 Hemispherical radiation intensity.

or

$$dE_{12} \text{ (hemisphere)} = \pi I. \tag{11.27}$$

Note that

$$dE_{12} \text{ (hemisphere)} = \frac{dE_{12}}{dA_1} = e_1. \tag{11.28}$$

Since we have been discussing a black body, the result states that the emissive power of a black body e_b is the product of π and the intensity of the emitted black body radiation per steradian:

$$e_b = \pi I. \tag{11.29}$$

Thus, by combining Eqs. (11.26) and (11.29), we return to the major argument, and express the general equation for the transfer of radiant energy from one black body to another as

$$E_{12} = \int_{A_1} dE_{12} = \frac{e_b}{\pi} \int_{A_1} \int_{A_2} \frac{\cos \phi_1 \cos \phi_2}{r^2} dA_2 dA_1. \tag{11.30}$$

For convenience, the view factor F_{12} , which is dimensionless, is introduced here; it is defined by the equation

$$A_1 F_{12} = \frac{1}{\pi} \int_{A_1} \int_{A_2} \frac{\cos \phi_1 \cos \phi_2}{r^2} dA_2 dA_1. \tag{11.31}$$

This integral contains nothing but geometrical aspects of radiant exchange, and has fortunately been evaluated for many geometries. Usually, one does not have to perform the integration oneself. Now we can write a simple equation to express the energy emitted by a black surface 1 and intercepted by surface 2, using the definition of F_{12} ,

$$E_{12} = e_{b1} A_1 F_{12}. \tag{11.32}$$

In exactly the same manner, we could have developed an analogous expression for the energy originating at 2 and arriving at 1.

$$E_{21} = e_{b2} A_2 F_{21}. \tag{11.33}$$

384 Radiation Heat Transfer

Then, the net exchange of energy from 1 to 2 is $A_1 q_{1,\text{net}}$ or $Q_{1,\text{net}}$:

$$Q_{1,\text{net}} = E_{12} - E_{21}. \quad (11.34)$$

At thermal equilibrium $Q_{1,\text{net}} = 0$, and from Eqs. (11.32) and (11.33) and the fact that the emissive power of a black body depends only upon temperature, we see that $A_2 F_{21} = A_1 F_{12}$. In general, we can say that

$$A_i F_{ij} = A_j F_{ji}. \quad (11.35)$$

Equation (11.35), though simple, is very useful, and the reader should keep it in mind.

Values of F_{12} have been calculated for various geometric arrangements of two surfaces. Figures 11.13-11.15 provide such view factor charts. More extensive listings can be found in texts on radiation heat transfer. Although we have restricted the discussion leading up to the view factor charts to black surfaces, it is apparent that for nonblack surfaces, with emissivities independent of emission angles, F_{12} can be calculated by the method discussed above and again represents the fractional radiation from A_1 intercepted by A_2 . Thus such a calculation is exact for black surfaces, and very useful for most nonmetallic, oxidized or rough metal surfaces which exhibit nearly isotropic surface properties.

Since the view factor is the fraction of radiation emitted by a surface and intercepted by another surface, then all the radiation from any surface must be ultimately intercepted when there are many surfaces involved. For example, if surface 1 is *seen* by surfaces 2, 3, 4 . . . n , then

$$F_{12} + F_{13} + F_{14} + \dots + F_{1n} = 1. \quad (11.36)$$

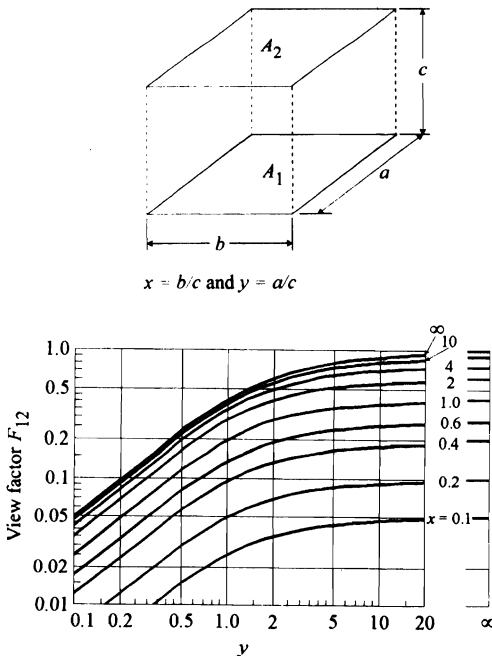


Fig. 11.13 View factors for identical, parallel, directly opposed rectangles. (From T. J. Love, *ibid.*)

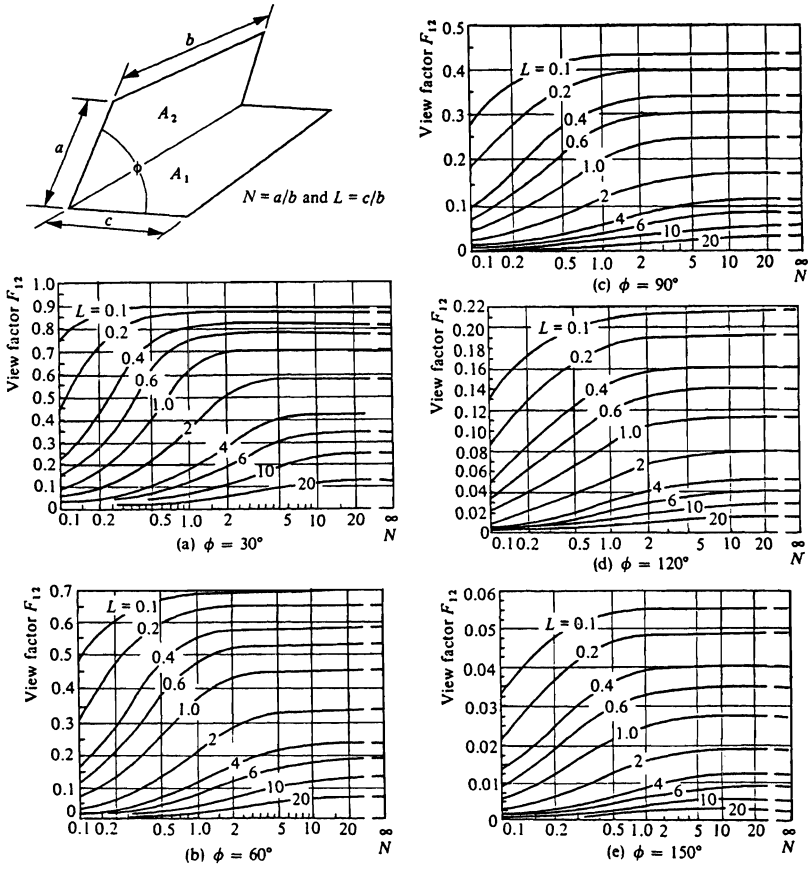


Fig. 11.14 View factors for two rectangles with a common edge. (From T. J. Love, *ibid.*)

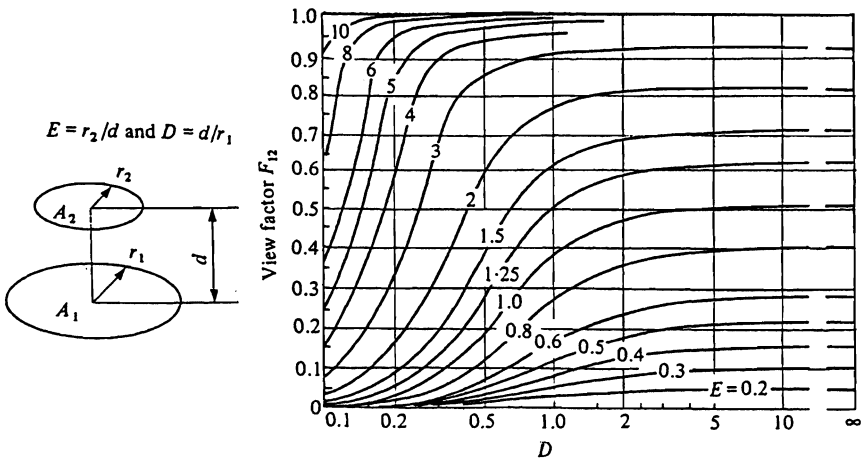
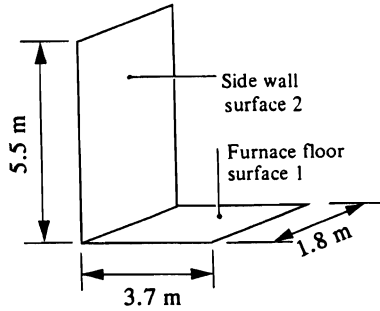


Fig. 11.15 View factors for parallel, directly opposed disks. (From T. J. Love, *ibid.*)

386 Radiation Heat Transfer

Example 11.2 Calculate the net heat flow by radiation to the furnace wall at 530 K from the furnace floor at 810 K. Both surfaces can be considered to be black radiators.



Solution. The energy emitted by the black surface 1 and intercepted by 2 is $E_{12} = e_{b1}A_1F_{12}$. Similarly, the energy emitted by surface 2 and intercepted by surface 1 is $E_{21} = e_{b2}A_2F_{21}$. The net exchange of energy from surface 1 to surface 2 is $Q_{1,net} = E_{12} - E_{21}$, and, since $A_2F_{21} = A_1F_{12}$, we can finally write the net exchange of energy from surface 1 to surface 2 as

$$Q_{1,net} = A_1F_{12}(e_{b1} - e_{b2}) = A_1F_{12}\sigma[T_1^4 - T_2^4].$$

Figure 11.14(c) is used to evaluate F_{12} with $N = 5.5/1.8 = 3.06$, $L = 3.7/1.8 = 2.06$, and $\phi = 90^\circ$. The view factor F_{12} is approximately 0.16. Recalling that $\sigma = 5.699 \times 10^{-8} \text{ W m}^{-2} \text{ K}^{-4}$, we determine that

$$Q_{1,net} = (1.8 \times 3.7)(0.16)(5.669) \left[\left(\frac{810}{100} \right)^4 - \left(\frac{530}{100} \right)^4 \right] = 21\,240 \text{ W}.$$

11.7 ELECTRIC CIRCUIT ANALOG

Consider an all-black surface enclosure (Fig. 11.16(a)) in which

$$F_{12} + F_{13} + F_{14} = 1. \quad (11.37)$$

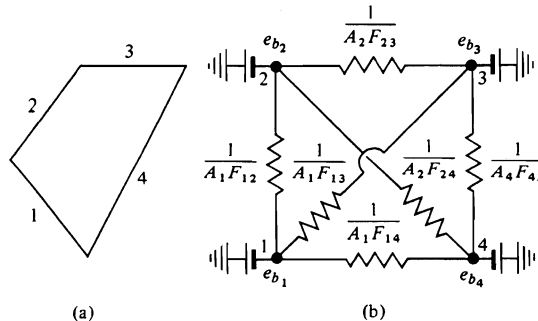


Fig. 11.16 (a) A black enclosure. (b) Its electrical analog.

The net power (W) from surface 1 is

$$\begin{aligned} Q_{1,\text{net}} &= (E_{12} - E_{21}) + (E_{13} - E_{31}) + (E_{14} - E_{41}) \\ &= A_1 F_{12}(e_{b1} - e_{b2}) + A_1 F_{13}(e_{b1} - e_{b3}) + A_1 F_{14}(e_{b1} - e_{b4}). \end{aligned} \quad (11.38)$$

We can also develop Eq. (11.38) by analyzing the situation with an electric analog. We think of each surface as a node in the electric analog (Fig. 11.16(b)) and represent the potential at each node by e_{bi} , the current by the heat flow, and the resistance between two potential nodes i and j by $1/A_i F_{ij}$. We draw the circuit, and connect each node by resistors to all the other nodes. We can then easily recognize the net heat flow from any surface. For example, we obtain the net heat flow from surface 4 by simply summing the analog currents through the three resistors connected to node 4:

$$Q_{4,\text{net}} = A_1 F_{14}(e_{b4} - e_{b1}) + A_2 F_{24}(e_{b4} - e_{b2}) + A_4 F_{43}(e_{b4} - e_{b3}).$$

It may be desirable to express the net heat flow only in terms of A_4 . In this case, we utilize Eq. (11.35) to yield

$$Q_{4,\text{net}} = A_4 F_{41}(e_{b4} - e_{b1}) + A_4 F_{42}(e_{b4} - e_{b2}) + A_4 F_{43}(e_{b4} - e_{b3}). \quad (11.39)$$

The electric analog for a gray surface is also very useful in solving many problems. The total energy flux radiating from a surface is its radiosity, or

$$J = \rho G + \varepsilon e_b, \quad (11.40)$$

where G is the irradiation. The net heat flux transferred from the surface is

$$q_{\text{net}} = J - G, \quad (11.41)$$

and by eliminating G from these last two equations, we get

$$q_{\text{net}} = \frac{\varepsilon}{1 - \varepsilon} (e_b - J).$$

Therefore, for the net heat flow from a surface of area A , we can write

$$Q_{\text{net}} = \frac{\varepsilon}{1 - \varepsilon} A(e_b - J). \quad (11.42)$$

Thus, we can represent a gray surface with a potential of a black surface reduced by a resistance $(1 - \varepsilon)/A\varepsilon$, as in Fig. 11.17. The use of an electric analog is particularly useful when dealing with gray surfaces. We illustrate this in Example 11.3.

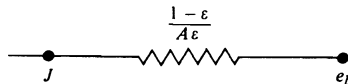
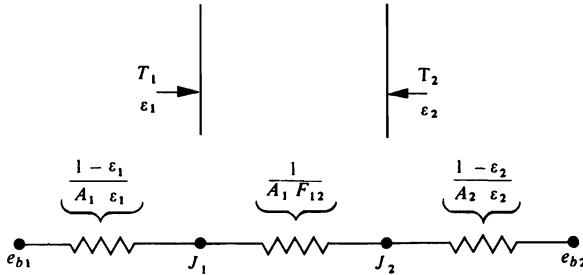


Fig. 11.17 Electric analog of a gray surface.

388 Radiation Heat Transfer

Example 11.3 Consider the exchange of energy between two parallel and gray plates. For infinitely long plates, 1 and 2, use the method of electric analogs and develop an expression for the heat flux if the plates are at T_1 and T_2 , and have emissivities of ε_1 and ε_2 , respectively.

Solution. The system and the appropriate analog are shown below.



By examining the analog circuit, the reader can see that each surface is represented by the nodes shown in Fig. 11.17. The analog circuit is completed by connecting the radiosity nodes with the resistance between the surfaces. Therefore, when dealing with gray surfaces, connect the radiosities; when dealing with black surfaces, connect the black body emissive powers, as shown in Fig. 11.16(b).

To solve the problem, simply determine the total resistance between e_{b1} and e_{b2} . The total resistance is

$$\frac{1 - \varepsilon_1}{A_1 \varepsilon_1} + \frac{1}{A_1 F_{12}} + \frac{1 - \varepsilon_2}{A_2 \varepsilon_2}.$$

Then by using Ohm's law, we can immediately write an expression for the net heat flow from 1 to 2:

$$Q_{1,\text{net}} = \frac{(e_{b1} - e_{b2})}{\frac{1 - \varepsilon_1}{A_1 \varepsilon_1} + \frac{1}{A_1 F_{12}} + \frac{1 - \varepsilon_2}{A_2 \varepsilon_2}}.$$

In this case, $A_1 = A_2$, and $F_{12} = 1$. Therefore

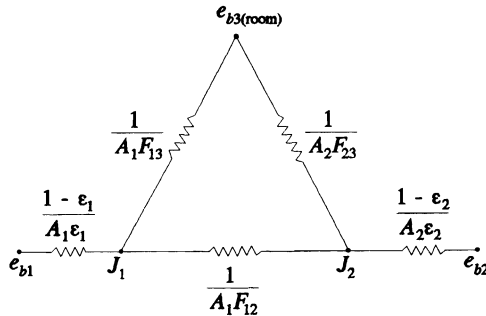
$$q_{1,\text{net}} = \frac{Q_{1,\text{net}}}{A_1} = \frac{(e_{b1} - e_{b2})}{1/\varepsilon_1 - 1 + 1/\varepsilon_2}.$$

This expression is the same as Eq. (11.22). After having treated a few situations by using electric analogs, the reader will become quite apt at developing expressions involving radiation exchange between gray and/or black surfaces.

Example 11.4 In Example 11.2, we were very careful to say that the calculation was "the net exchange of energy from surface 1 to surface 2." But with other surfaces in the radiation circuit, the result we obtained would not have been the total power delivered to surface 2. With this in mind, let us consider the two surfaces in Example 11.2 to be plates with gray surfaces, while insulating the bottom side of plate 1 and the left side of plate 2. The plates are placed in a large room at 300 K. Calculate the net power gain or loss to each plate.

Data: $\varepsilon_1 = \varepsilon_2 = 0.5$.

Solution. The room is a black radiator and each plate is gray. The radiation circuit, therefore, has three nodes.



Let's take care of the view factors first. From Example 11.2, $F_{12} = 0.16$. Thus, $F_{13} = 1 - F_{12} = 0.84$. Also,

$$F_{21} = \frac{A_1 F_{12}}{A_2} = \frac{(3.7 \times 1.8)(0.16)}{(5.5 \times 1.8)} = 0.108,$$

so that $F_{23} = 1 - F_{21} = 0.892$.

The resistances in the circuit are calculated as

$$\frac{1 - \epsilon_1}{A_1 \epsilon_1} = \frac{(1 - 0.5)}{(3.7 \times 1.8)(0.5)} = 0.150 \text{ m}^{-2},$$

$$\frac{1 - \epsilon_2}{A_2 \epsilon_2} = \frac{(1 - 0.5)}{(5.5 \times 1.8)(0.5)} = 0.101 \text{ m}^{-2},$$

$$\frac{1}{A_1 F_{13}} = \frac{1}{(3.7 \times 1.8)(0.84)} = 0.179 \text{ m}^{-2},$$

$$\frac{1}{A_2 F_{23}} = \frac{1}{(5.5 \times 1.8)(0.892)} = 0.113 \text{ m}^{-2},$$

$$\frac{1}{A_1 F_{12}} = \frac{1}{(3.7 \times 1.8)(0.16)} = 0.938 \text{ m}^{-2}.$$

Now we apply Kirchoff's law at nodes J_1 and J_2 ,

$$\frac{e_{b1} - J_1}{0.150} + \frac{J_2 - J_1}{0.938} + \frac{e_{b3} - J_1}{0.179} = 0,$$

$$\frac{e_{b2} - J_2}{0.101} + \frac{J_1 - J_2}{0.938} + \frac{e_{b3} - J_2}{0.113} = 0.$$

390 Radiation Heat Transfer

After substituting the values of e_{b1} , e_{b2} and e_{b3} , we have two equations, with two unknowns J_1 and J_2 , which are solved to give

$$e_{b1} = \sigma T_1^4 = (5.669)(8.10)^4 = 24\,400 \text{ W m}^{-2},$$

$$e_{b2} = (5.669)(5.30)^4 = 4470 \text{ W m}^{-2},$$

$$e_{b3} = (5.669)(3.0)^4 = 459 \text{ W m}^{-2},$$

$$J_1 = 12\,600 \text{ W m}^{-2},$$

$$J_2 = 3120 \text{ W m}^{-2}.$$

The power losses of plates 1 and 2 are

$$E_{1,\text{net}} = \frac{e_{b1} - J_1}{(1 - \varepsilon_1)/\varepsilon_1 A_1} = \frac{24\,400 - 12\,600}{0.150} = 78\,300 \text{ W},$$

and

$$E_{2,\text{net}} = \frac{e_{b2} - J_2}{(1 - \varepsilon_2)/\varepsilon_2 A_2} = \frac{4470 - 3120}{0.101} = 13\,400 \text{ W}.$$

As a check, we calculate the power received by the room.

$$E_{3,\text{net}} = \frac{J_2 - e_{b3}}{1/A_2 F_{23}} + \frac{J_1 - e_{b3}}{1/A_1 F_{13}} = \frac{3120 - 459}{0.113} + \frac{12\,600 - 459}{0.179} = 91\,700 \text{ W}.$$

The overall energy balance must satisfy

$$E_{3,\text{net}} = E_{1,\text{net}} + E_{2,\text{net}},$$

and we are within 0.01%.

11.8 FURNACE ENCLOSURES

As an application of radiant heat transfer, consider furnace design. We often encounter a situation in which energy is transferred from a *heat source* to a *heat sink* with intermediate refractory walls. For example, the heat source might be a row of electric resistors to heat a metal part placed in a furnace. In normal furnaces, the radiation incident on the refractory walls is so large compared to the heat conduction through the walls that we may approximate the conduction as zero when calculating radiant fluxes. Such walls are examples of *no-net-flux surfaces*. This assumption greatly simplifies the problem of transferring radiant heat from a source to a sink.

As an example, consider the transfer from face 1 (the source) to the opposite face 2 (the sink) with intermediate refractory walls (Fig. 11.18(a)). All surfaces are assumed to be gray, and the electric analog is given in Fig. 11.18(b). First, simplify the circuit by combining all the resistances between J_1 and J_2 , remembering that in parallel circuits conductances are

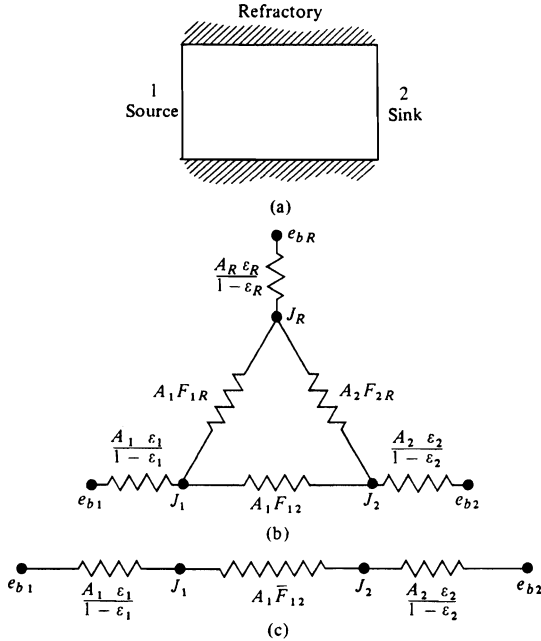


Fig. 11.18 (a) Furnace enclosure. (b) and (c) Its electric analogs. (In this case, conductances rather than resistances are indicated.)

directly additive, and in series circuits the sample applies to resistances. The equivalent conductance between J_1 and J_2 is

$$A_1 \bar{F}_{12} = A_1 F_{12} + \frac{1}{1/A_1 F_{1R} + 1/A_2 F_{2R}}, \tag{11.43}$$

and the circuit reduces to Fig. 11.18(c). The symbol \bar{F}_{12} is often used when the several view factors in a system are all combined, as illustrated here. Finally, the equivalent resistance for the entire circuit is

$$\frac{1}{A_1 \mathcal{F}_{12}} = \frac{1}{A_1} \frac{1 - \epsilon_1}{\epsilon_1} + \frac{1}{A_1 \bar{F}_{12}} + \frac{1}{A_2} \frac{1 - \epsilon_2}{\epsilon_2}. \tag{11.44}$$

The symbol \mathcal{F}_{12} is used when the entire circuit has been reduced to one equivalent resistance; thus \mathcal{F}_{12} depends not only on the individual view factors of the elements in the system but also on the individual emissivities. Since we are approximating the refractory walls as *no-net-flux* surfaces, then the current from J_R to e_{bR} is zero, and the current that goes from e_{b1} to e_{b2} in the equivalent circuit of Fig. 11.18(c) represents the net flow of energy from the source to the sink. In this sense, we refer to \bar{F}_{12} as the *total exchange factor* because it takes into account reradiating surfaces between the two surfaces (source and sink) of primary interest.

In this case, then

$$Q_{1,net} = A_1 \mathcal{F}_{12} (e_{b1} - e_{b2}) = A_1 \mathcal{F}_{12} \sigma (T_1^4 - T_2^4), \tag{11.45}$$

in which $A_1 \mathcal{F}_{12}$ is given by Eq. (11.44).

In furnaces, electric resistors very often provide the source of heat, and can be mounted on a back-insulated refractory wall in a parallel array, as shown in Fig. 11.19. It is convenient to replace such a system by an equivalent continuous gray plane, having an effective emissivity ϵ_p and a temperature equal to that of the resistors. The gray plane is imaginary, and we show it by the dotted line in Fig. 11.19. To calculate ϵ_p , we make use of Fig. 11.20 to determine \bar{F}_{PE} , this is equivalent to \bar{F}_{12} in Eq. (11.43). Then, by rearranging Eq. (11.44) with $\epsilon_p = 1$, we can determine \mathcal{F}_{PE} from the expression

$$\mathcal{F}_{PE} = \frac{1}{\frac{1}{\bar{F}_{PE}} + \frac{C}{\pi D} \left[\frac{1}{\epsilon_E} - 1 \right]} \tag{11.46}$$

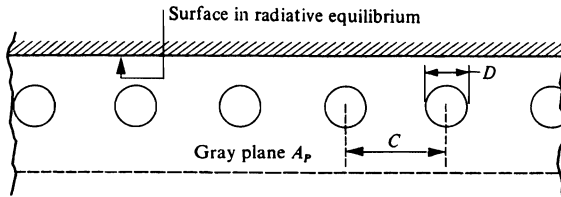


Fig. 11.19 A refractory-backed row of cylindrical elements.

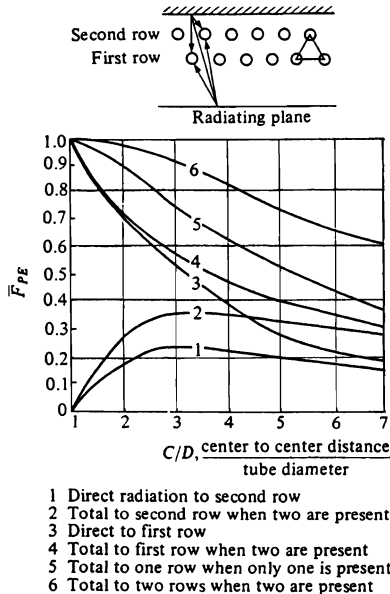


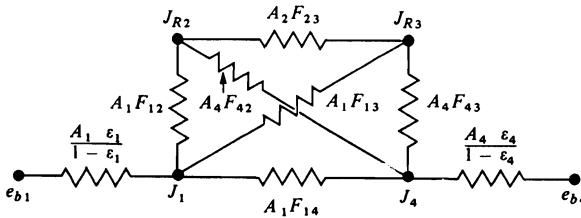
Fig. 11.20 Total exchange factors \bar{F}_{PE} between a black plane (P) and one or two rows of cylindrical elements (E) backed by a no-net-flux refractory wall. Direct view factors F_{PE} are also shown for comparison. Note that the elements form an array of equilateral triangles. (From H. C. Hottel and A. F. Sarofim, *ibid.*, page 114.)

where C/D is defined in Fig. 11.20. If no reradiating surface (no back-insulated refractory wall) exists, then $\mathcal{F}_{PE} = \bar{F}_{PE}$ in this expression. Finally, we can consider the elements equivalent to the plane A_p with an emissivity $\epsilon_p = \mathcal{F}_{PE}$ at the operating temperature of the elements.

Example 11.5 A furnace has a floor $1\text{ m} \times 2\text{ m}$, and located at the top, 1.5 m away, are heating elements, 50 mm in diameter, 1 m long on 100 mm centers backed by a well-insulated refractory roof. The heating elements are Nichrome IV ($\epsilon = 0.74$), which operate at a surface temperature of 1370 K . The side walls are insulated refractory (no-net-flux) surfaces. Find the rate at which heat can be transferred to a sheet of aluminum at 300 K ($1\text{ m} \times 2\text{ m}$, $\epsilon = 0.15$) placed on the floor of the preheated furnace.

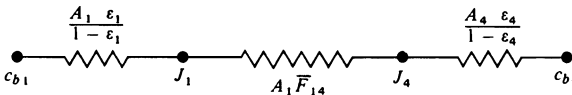
Solution. To demonstrate only the aspects of radiant heating, we shall ignore convective heating on the upper surface of the aluminum sheet and heat transfer that might occur by conduction across minute contact points between the sheet and the furnace floor.

To calculate the rate at which heat is transferred by radiation to the upper surface of the sheet, we divide the system into four zones: (1) an equivalent gray plane to represent the elements, (2) the side walls of dimensions $1.5\text{ m} \times 2\text{ m}$, (3) the side walls of dimensions $1.5\text{ m} \times 1\text{ m}$, and (4) the upper surface of the aluminum sheet. The analog circuit (showing conductances) is shown below.



In this particular example, to solve for $A_1\bar{F}_{14}$, the equivalent conductance for the entire circuit between J_1 (source) and J_4 (sink), would be a messy task if done by algebraic means. A 4×4 matrix could be set up and solved on a computer rather easily, or one could set up an actual analog circuit. For our purposes, we refer the reader to Fig. 11.21, from which \bar{F}_{14} can be found directly. In Fig. 11.21, the *total exchange factor* is presented for several geometries of source-sink combinations connected by perfect radiating walls (i.e., no-net-flux surfaces). Naturally, we have selected a geometry represented on the figure!

By using Fig. 11.21, we can represent the circuit very simply as shown here.



Using Fig. 11.21, we find, for the geometry of a 2:1 rectangular opening with $D = 1\text{ m}$ and $X = 1.5\text{ m}$, that

$$\bar{F}_{14} = 0.51.$$

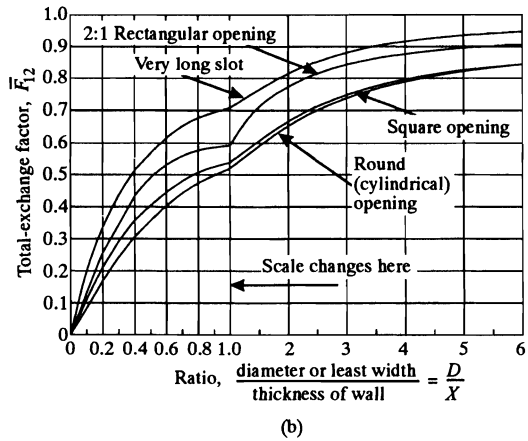
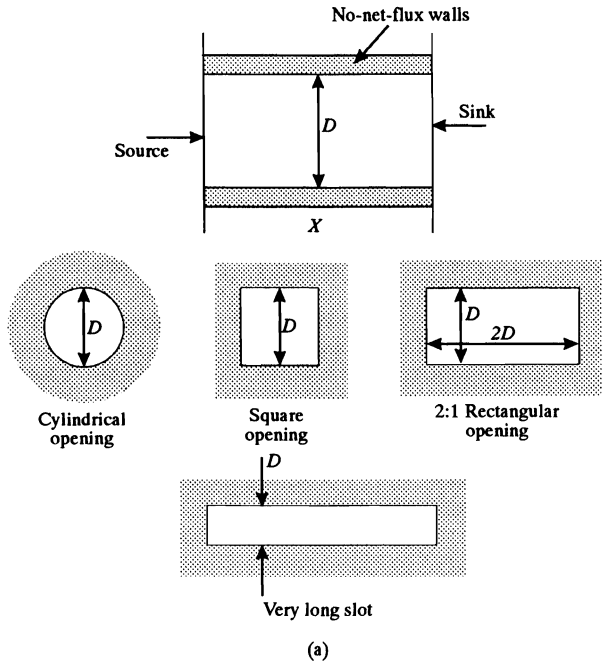


Fig. 11.21 Total exchange factors between parallel source and sink connected by no-net-flux walls. (a) Various geometries included, and (b) values of the total exchange factor. (From H. C. Hottel and A. F. Sarofim, *ibid.*, page 110.)

Next we proceed to determine ε_1 . From Fig. 11.20 (curve 5) with $C/D = 2$, we obtain $\overline{F}_{PE} = 0.88$. Then, from Eq. (11.46),

$$\varepsilon_1 = \varepsilon_p = \mathcal{F}_{PE} = \frac{1}{\frac{1}{0.88} + \frac{2}{\pi} \left[\frac{1}{0.74} - 1 \right]} = 0.735.$$

Now using Eq. (11.44) with $A_1 = A_4$, we get

$$\frac{1}{\mathcal{F}_{14}} = \frac{1 - \varepsilon_1}{\varepsilon_1} + \frac{1}{\overline{F}_{14}} + \frac{1 - \varepsilon_4}{\varepsilon_4} = \frac{1 - 0.735}{0.735} + \frac{1}{0.51} + \frac{1 - 0.15}{0.15}$$

$$\mathcal{F}_{14} = 0.125.$$

Therefore,

$$Q_{1,\text{net}} = A_1 \mathcal{F}_{14} \sigma (T_1^4 - T_4^4) = (1 \times 2)(0.125)(5.669) \left[\left(\frac{1370}{100} \right)^4 - \left(\frac{300}{100} \right)^4 \right]$$

$$= 49\,800 \text{ W}.$$

To this, we could add the heat transferred to the bottom of the plate; assume that the furnace floor had been preheated to 1370 K prior to the insertion of the aluminum plate, and that all the heat transferred across the furnace floor-aluminum sheet interface is via radiation across a gap of two infinitely long parallel plates. Using Eq. (11.22), and assuming that the emissivity of the refractory floor is 0.8, we obtain

$$Q = \frac{(2 \times 1)(5.669) \left[\left(\frac{1370}{100} \right)^4 - \left(\frac{300}{100} \right)^4 \right]}{1/0.8 + 1/0.15 - 1} = 57\,600 \text{ W}.$$

$$Q (\text{total}) = 49\,800 + 57\,600 = 107\,400 \text{ W}.$$

The heat flow rates calculated above are the initial values, and apply only when the cold sheet has been inserted in the oven. We deal with the more general problem of describing the transient heating of a sheet in Section 11.12.

11.9 RADIATION COMBINED WITH CONVECTION

In the preceding sections of this chapter we considered energy transfer by radiation as an isolated phenomenon. Indeed, in many high-temperature applications, problems should be tackled in this manner because, at high temperatures, radiation can completely dominate since radiant heat flow depends on the fourth power of the absolute temperature. In many practical situations, however, we cannot neglect convective heat transfer, and it is necessary to consider both modes of energy transport.

When we include radiation in a calculation of a situation which also involves convection, we realize that the total heat flow is the sum of the convective heat flow and the radiant heat

flow. Thus, we conveniently use the total heat transfer coefficient h_r , which comprises the heat transfer coefficient h , in the usual sense, and the radiant heat transfer coefficient h_r :

$$h_r = h + h_r. \quad (11.47)$$

We define the radiant heat transfer coefficient as

$$h_r = \frac{q_{1,\text{net}}}{(T_1 - T_2)} = \mathcal{F}_{12} \left[\frac{\sigma(T_1^4 - T_2^4)}{T_1 - T_2} \right], \quad (11.48)$$

in which $T_1 - T_2$ is a temperature difference and T_2 is chosen as a convenient temperature in the system.

We often encounter the situation in which surface 1 is completely surrounded by or exposed only to some fluid whose bulk temperature is at T_f . In this case, it is convenient to select T_2 as T_f , and since $\mathcal{F}_{12} = \varepsilon_1$, we write

$$h_r = \varepsilon_1 \left[\frac{\sigma(T_1^4 - T_2^4)}{T_1 - T_2} \right]. \quad (11.49)$$

The square-bracketed part of Eqs. (11.48) and (11.49) is sometimes called the temperature factor, F_T .

Example 11.6 A thermocouple with an emissivity of 0.7 measures the temperature of a gas flowing in a long duct whose internal wall surfaces are at 533 K. The temperature indicated by the thermocouple is 811 K, and the convective heat transfer coefficient between the gas and the surface of the thermocouple is $110 \text{ W m}^{-2} \text{ K}^{-1}$. Determine the true temperature of the gas.

Solution. The temperature of the thermocouple is less than that of the gas because the thermocouple radiates to the wall. We can write an energy balance for the steady state in which the radiant heat flow from the thermocouple to the wall equals the convective heat flow from the gas to the couple. Assuming that the thermocouple can be approximated as a gray surface, we write

$$hA_1(T_f - T_1) = A_1F_{12}\varepsilon_1\sigma(T_1^4 - T_2^4),$$

where A_1 is the thermocouple surface area; T_f , T_1 , and T_2 are the temperatures of the fluid, thermocouple, and duct walls, respectively. Since the thermocouple is completely surrounded by the duct walls, $F_{12} = 1$. The gas temperature is then found by

$$T_f - T_1 = \frac{\varepsilon_1\sigma}{h} (T_1^4 - T_2^4) = \frac{(0.7)(5.669)}{110} \left[\left(\frac{811}{100} \right)^4 - \left(\frac{533}{100} \right)^4 \right] = 127 \text{ K},$$

and $T_f = 938 \text{ K}$.

Errors such as those indicated by the above example have induced engineers to pursue thermocouple designs which incorporate radiation shields and/or means of increasing h between the fluid and the thermocouple. Some devices are illustrated in Fig. 11.22.

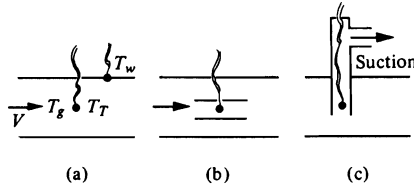
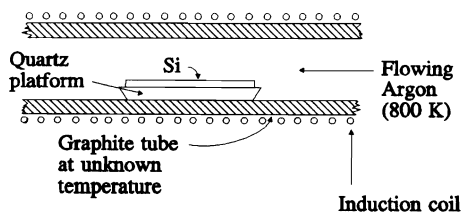


Fig. 11.22 Measurement of flowing gas temperatures. (a) Simplest device most liable to errors. (b) Incorporation of a radiation shield. (c) Incorporation of a radiation shield and use of the increased fluid velocity past the thermocouple's surface.

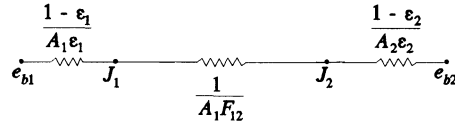
Process engineers should recognize that the gas temperature in an oven or furnace might not be equal to the temperature of a major source of radiation. If this is overlooked, serious problems of overheating in materials processing can develop. The source of the heat for the process can be a combustion flame, an electric arc, or a resistance-heating element; consequently, the source is often at a very high temperature, where radiation from the source to any surface at a lower temperature is significant. For example, it may be that a gas-fired combustion chamber for a tempering furnace produces a gas that is not too hot by adding excess air to the combustion gases, but if the piece to be tempered "sees" the flame, the radiation from the flame at its temperature will tend to raise the temperature of the piece above that of the gas alone. This can result in "burned" material. Sometimes material can be accidentally melted in this way, as in annealing lines for aluminum. Failed water-cooling jackets, whose surfaces are subjected to radiation from an arc, are not uncommon.

Example 11.7 Ribbon silicon, $25 \text{ mm} \times 150 \text{ mm}$, intended for a photovoltaic application, is to be stress-relieved at 800 K by heating in flowing argon. The set-up shown below is used. The graphite tube is heated by an induction coil. Before the ribbon is introduced, care is taken to measure the true gas temperature, and it is found to be 800 K at a given flow rate. During a few trial runs, the temperature of the ribbon is found to be 850 K , even though the argon is maintained at 800 K . Estimate the temperature of a graphite tube. The convective heat transfer coefficient is $50 \text{ W m}^{-2} \text{ K}^{-1}$.



398 Radiation Heat Transfer

Solution. We make a radiation circuit to get started. Assume that the area of the graphite tube (node J_2) is infinitely larger than that of the silicon ribbon (node J_1).



The total equivalent resistance is

$$\frac{1}{A_1 \mathcal{F}_{12}} = \frac{1 - \epsilon_1}{A_1 \epsilon_1} + \frac{1}{A_1 F_{12}} + \frac{1 - \epsilon_2}{A_2 \epsilon_2}$$

or

$$\frac{1}{\mathcal{F}_{12}} = \frac{1 - \epsilon_1}{\epsilon_1} + \frac{1}{F_{12}} + 0.$$

But $F_{12} = 1$ so that $\mathcal{F}_{12} = \epsilon_1$ and

$$q_{1,net} = \frac{Q_{1,net}}{A_1} = \sigma \epsilon_1 (T_1^4 - T_2^4).$$

We could have recognized this immediately because the silicon "sees" only graphite by the assumption that $A_1/A_2 = 0$. As written, $q_{1,net} < 0$ because $T_1 < T_2$. For convenience, let $q_{rad} = -q_{1,net}$. For simplicity, we ignore the energy conducted through the quartz, which supports the silicon; then at steady state:

$$q_{rad} = q_{conv},$$

$$\sigma \epsilon_1 (T_2^4 - T_1^4) = h_{conv} (T_1 - T_f).$$

With $\epsilon_1 = 0.15$, we have

$$T_2^4 = \frac{h_{conv}(T_1 - T_f)}{\sigma \epsilon_1} + T_1^4 = \frac{50(850 - 800)}{(5.669 \times 10^{-8})(0.15)} + 850^4 = 8.16 \times 10^{11} \text{ K}^4.$$

Therefore, $T_2 = 950 \text{ K}$.

11.10 RADIATION FROM GASES

The methods given in the preceding sections are applicable only to systems involving gases which are transparent to radiation. Gases with simple symmetrical molecules, such as H_2 , He , O_2 , and N_2 , are essentially transparent to radiation, but heteropolar gases (CO , CO_2 , H_2O , SO_2 , NH_3 , HCl), which interact with radiation sufficiently, must sometimes be made part of the system for calculations.

Solids emit radiation at all wavelengths, whereas gases emit and absorb radiation only between narrow regions of wavelengths called bands. Analysis of radiation participation should be made for each band, and the total effect can be obtained by summation. However,

it is more convenient to solve the problems in terms of the total radiation and emission characteristics of the gases.

As a first approximation, the total number of radiating gas molecules present in a space determines the emissivity and absorptivity of the gas. This approximation works best at lower pressures with corresponding large mean free paths permitting each molecule to radiate as though it is alone, with a minimal shielding effect by the other molecules present in space. Gas radiation differs from the radiation of solids whose emission and absorption are surface phenomena, because when calculating emission and absorption for a gas layer at a particular temperature, its thickness and pressure must be taken into account. In fact, the emissivity and absorptivity of a gas are functions of the active gas species, temperature, thickness and shape, total pressure, and the partial pressure of the gas. To handle all these complexities, a series of charts based on experimental data has been developed for evaluating the emissivities and absorptivities of various gases.

Consider a hemisphere of radius L , containing a heteropolar gas of a given partial pressure; the problem is to determine the radiant heat exchange between the gas at temperature T_g and a unit element at the center of the base of the hemisphere. The emission of the gas to the surface is $\varepsilon_g \sigma T_g^4$ per unit surface area, where ε_g denotes gas emissivity. Specifically, the *reduced* emissivity ε'_g for CO_2 is presented as a function of the absolute temperature and the product of L and partial pressure in Fig. 11.23. These values are called reduced emissivities because they are plotted for a reduced pressure; that is, all data are at near-zero partial pressure and at a total pressure of 1 standard atm. The graphs apply strictly to the hemispherical body of gas defined above; we discuss briefly how to treat other shapes.

The effect of total pressure on ε_g for CO_2 is given in Fig. 11.24, where the ratio of the actual emissivity, at the state being considered, to the reduced emissivity is presented as C_c . For shapes other than hemispheres, we take L as the *effective beam length*, and calculate it for use with Figs. 11.23 and 11.24. Table 11.2 lists L for shapes other than hemispheres. For approximate calculations of shapes which are not listed, we can take L as $3.4 \times$ volume/surface area.

For a presentation and discussion of radiation data for other gas species and interactions between species that account for radiation in overlapping wavelength bands, the reader should consult the text by Hottel and Sarofim.¹⁰ The charts were originally developed in the 1940s and 1950s when English units were the preferred system. To convert from absolute temperature in degrees Rankine ($^{\circ}\text{R}$) to kelvins, simply use $9^{\circ}\text{R} = 5 \text{ K}$. The pressure-length units on the curves are converted according to

$$1 \text{ atm ft} = 3.0886 \times 10^4 \text{ Pa m} = 3.0886 \times 10^4 \text{ N m}^{-1}.$$

¹⁰H. C. Hottel and A. F. Sarofim, *ibid.*, Chapter 6.

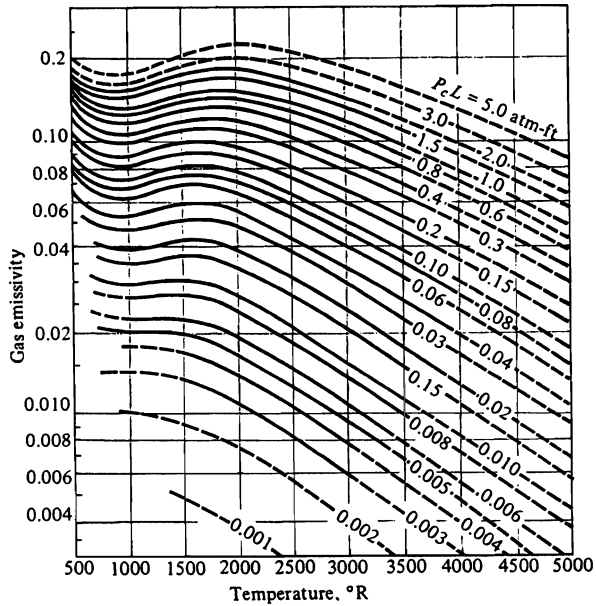


Fig. 11.23 Reduced emissivity of carbon dioxide. (From H. C. Hottel and A. F. Sarofim, *ibid.*, Chapter 6.)

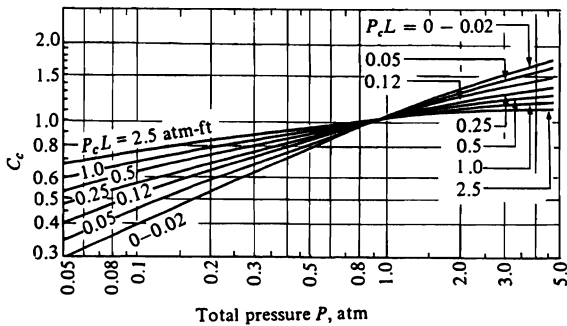


Fig. 11.24 Correction factor for CO₂ emissivity. (From F. Kreith, *Principles of Heat Transfer*, second edition, International Textbook Co., 1965, page 231.)
 1 standard atm = 1.0133×10^5 Pa.

Table 11.2 Beam lengths for gas radiation. (From H. C. Hottel, Chapter IV in *Heat Transmission*, by W. H. McAdams, McGraw-Hill, 1954.)

Shape	Characterizing dimension, X	Factor by which X is multiplied to obtain mean beam length, L	
		When $p_g L = 0$	For average values of $p_g L$
Sphere	Diameter	2/3	0.60
Infinite cylinder	Diameter	1	0.90
Semi-infinite cylinder, radiating to center of base	Diameter	—	0.90
Right-circular cylinder, height = diameter, radiating to center of base	Diameter	—	0.77
Same, radiating to whole surface	Diameter	2/3	0.60
Infinite cylinder of half-circular cross section, radiating to spot on middle of flat side	Radius	—	1.26
<i>Rectangular parallelepipeds</i>			
1:1:1 (cube)	Edge	2/3	—
1:1:4, radiating to 1×4 face } radiating to 1×1 face } radiating to all faces }	Shortest edge	0.90	—
		0.86	—
		0.89	—
1:2:6, radiating to 2×6 face } radiating to 1×6 face } radiating to 1×2 face } radiating to all faces }	Shortest edge	1.18	—
		1.24	—
		1.18	—
		1.20	—
1:∞:∞ (infinite parallel planes)	Distance between planes	2	—
<i>Space outside</i>			
Space outside infinite bank of tubes with centers on equilateral triangles; tube diameter = clearance	Clearance	3.4	2.8
Same as preceding, except tube diameter = one-half clearance	Clearance	4.45	3.8
Same, except tube centers on squares, diameter = clearance	Clearance	4.1	3.5

Example 11.8 Determine the emissivity of a gas containing 50% N_2 and 50% CO_2 at a total pressure of 2 atm with $T_g = 1110$ K. The gas is contained in a very long cylindrical space having a 0.6 m diameter.

Solution. From Table 11.2, assuming radiation to its base:

$$L = (0.90)(0.6) = 0.54 \text{ m (1.77 ft)},$$

and

$$P_g L = (0.50)(2)(1.77) = 1.77 \text{ atm ft.}$$

From Fig. 11.23, the reduced emissivity of CO_2 , with $T = 1110$ K = 1998 °R, is $\epsilon'_c = 0.17$. Fig. 11.24 gives $C_c = 1.10$. Finally, $\epsilon_g = C_c \epsilon'_c = (1.10)(0.17) = 0.19$.

11.11 ENCLOSURES FILLED WITH RADIATING GAS

By evaluating the emissivity and absorptivity of a gas by the method outlined in Section 11.10, we now evaluate the interchange of radiant energy between a gas and the surface of its enclosure. First, consider a black bounding surface. The gas emits energy which is entirely absorbed by the black surface, but, on the other hand, the gas absorbs only a fraction of the radiation from the surface. Thus we write the flux of energy from the gas to the surface 1 as

$$q_{g \rightarrow 1} = e_g - \alpha_{g1} e_{b1} = \epsilon_g e_{bg} - \alpha_{g1} e_{b1} = \sigma (\epsilon_g T_g^4 - \alpha_{g1} T_1^4). \quad (11.50)$$

When the bounding surface is gray, it reflects part of the energy emitted by the gas which is partially absorbed in successive passes back through the gas. In this case, we give the flux of energy by the right side of Eq. (11.50) multiplied by a factor between ϵ_1 and 1. For surfaces with ϵ_1 of 0.7 or greater, it is sufficient to use the following equation:

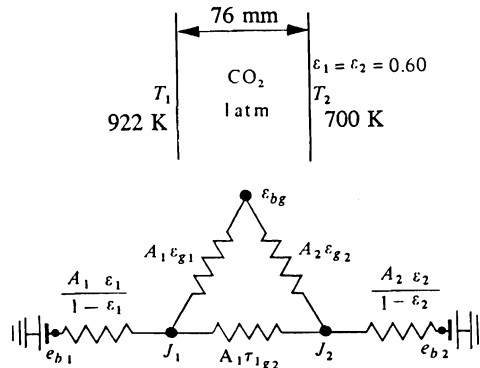
$$q_{g \rightarrow 1} = \sigma \left(\frac{\epsilon_1 + 1}{2} \right) (\epsilon_g T_g^4 - \alpha_{g1} T_1^4), \quad (11.51)$$

where the factor is simply $(\epsilon_1 + 1)/2$.

In order to incorporate participating gases into a system containing surfaces, the gas is a floating node of potential e_{bg} and there is a conductance $A_i \epsilon_{gi}$ between the gas node and the surface i . Due to the presence of the gas which absorbs some of the radiation between surface nodes, the conductances between the surfaces themselves are multiplied by the gas transmissivity; for example, the conductance between surfaces i and j is $A_i F_{ij} \tau_{ij}$. The following example demonstrates the use of such an electric analog for a system with a participating gas.

Example 11.9 Two large parallel plates (with emissivity of 0.6) at temperatures of 922 K and 700 K, transfer radiation across a 76 mm gap filled with CO_2 at 1 atm pressure. Calculate the rate of heat transfer from the hot plate to the cold plate.

Solution. We show the system and its electrical analog below.



In order to evaluate the emissivities and transmissivities of the gas, we must know its temperature. Assume the gas temperature is 810 K (this can be checked later). From Table 11.2, $L = (2)(0.076) = 0.152$ m (0.499 ft). Next, Figs. 11.23 and 11.24, with $P_c L = 0.499$ atm ft, give $\varepsilon'_c = 0.125$ and $C_c = 1.05$, respectively. Thus

$$\varepsilon_{g1} = \varepsilon_{g2} = (0.125)(1.05) = 0.131,$$

and

$$\tau_{1g2} = 1 - \varepsilon_{g1} = 1 - 0.131 = 0.869.$$

The network can be reduced to a single equivalent resistance between 1 and 2. Here, $A_1 = A_2 = A$ and $F_{12} = 1$, so that

$$\begin{aligned} \frac{1}{\mathcal{F}_{12}} &= \frac{1 - \varepsilon_1}{\varepsilon_1} + \frac{1}{F_{12}\tau_{1g2} + \frac{1}{1/\varepsilon_{g1} + 1/\varepsilon_{g2}}} + \frac{1 - \varepsilon_2}{\varepsilon_2} \\ &= \frac{0.4}{0.6} + \frac{1}{(1)(0.869) + \frac{1}{1/0.131 + 1/0.131}} + \frac{0.4}{0.6} \\ &= 2.40. \end{aligned}$$

Then,

$$q_{1-2} = \mathcal{F}_{12}\sigma(T_1^4 - T_2^4) = \frac{(5.669)}{(2.40)} \left[\left(\frac{922}{100} \right)^4 - \left(\frac{700}{100} \right)^4 \right] = 11\,400 \text{ W m}^{-2}.$$

Now we check the assumption that $T_g = 810$ K. $e_{b1} = (5.669)(9.22^4) = 40\,967 \text{ W m}^{-2}$; similarly, $e_{b2} = 13\,611 \text{ W m}^{-2}$.

$$J_1 = e_{b1} - \frac{q_{1-2}}{\varepsilon_1/(1 - \varepsilon_1)} = 40\,967 - \frac{11\,400}{0.6/0.4} = 33\,400 \text{ W m}^{-2},$$

and

$$J_2 = 13\,611 - \frac{11\,400}{0.6/0.4} = 6\,010 \text{ W m}^{-2}.$$

Since $A_1\varepsilon_{g1} = A_2\varepsilon_{g2}$, e_{bg} must be the average of J_1 and J_2 , so that

$$e_{bg} = \frac{33\,400 + 6\,010}{2} = 19\,700 \text{ W m}^{-2},$$

and

$$T_g = \left(\frac{e_{bg}}{\sigma} \right)^{1/4} = \left(\frac{19\,700}{5.669 \times 10^{-8}} \right)^{1/4} = 767 \text{ K}.$$

The problem could be solved again with this as the gas temperature; in this case, however, 767 K is sufficiently close to the assumed 810 K, so that no significant improvement in the result would be gained.

404 Radiation Heat Transfer

It is instructive to extend the above example, by comparing it to the case of no participating gas (see Example 11.3). In this case

$$\frac{1}{\mathcal{F}_{12}} = \frac{1}{\varepsilon_1} + \frac{1}{\varepsilon_2} - 1 = \frac{1}{0.6} + \frac{1}{0.6} - 1 = 2.33.$$

This is hardly different from the factor (2.40) determined in Example 11.9. Therefore, even though we have selected an example involving an atmosphere of 100% CO₂, we could still consider the atmosphere to be transparent for many calculations. Only at partial pressures greater than about 4 atm of the participating species and/or with very large enclosure dimensions, would the effect of the gas be more evident.

The likely application of these principles to processes, which might involve combustion gases at 1 atm total pressure, requires only small corrections to heat fluxes. For example, a typical combustion gas at 1670 K could contain 12% CO₂. From Fig. 11.23, the reduced emissivity for a rather large L (e.g., 1 m) is only 0.08.

11.12 RADIATION IN TRANSPARENT SOLIDS

In Chapter 6 we saw that an important contribution to the effective thermal conductivity in transparent ceramics and glasses at high temperatures is the radiation heat transfer. Now we examine the transfer of radiant energy through such a medium.

Consider two surfaces with the space between them occupied by a solid that is transmitting and absorbing. For the solid we use the subscript s and assume that $\alpha_s = \varepsilon_s$, so that

$$\alpha_s + \tau_s = \varepsilon_s + \tau_s = 1. \quad (11.52)$$

The power leaving surface 1 is $J_1 A_1 F_{12} \tau_s$, and that leaving surface 2 is $J_2 A_2 F_{21} \tau_s$; therefore, the net power from 1 to 2 is

$$Q_{1,2} = A_1 F_{12} \tau_s (J_1 - J_2), \quad (11.53)$$

or

$$Q_{1,2} = A_1 F_{12} (1 - \varepsilon_s) (J_1 - J_2). \quad (11.54)$$

Inspection of Eq. (11.54) reveals that $A_1 F_{12} (1 - \varepsilon_s)$ is the *conductance* or $[A_1 F_{12} (1 - \varepsilon_s)]^{-1}$ is the *resistance* between J_1 and J_2 , as indicated by Fig. 11.25.

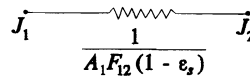


Fig. 11.25 Resistance for partially transmitted radiation between nodes J_1 and J_2 .

Now at the surface itself, there is an exchange process with the partially transmitting solid, which we assume is nonreflecting. A power balance at surface 1 is

$$Q_{1,s} = A_s F_{s1} \varepsilon_s e_{bs} - J_1 A_1 F_{1s} \varepsilon_s,$$

where the first term on the right hand side is the power emitted by the solid and the second is the radiation emanating from surface 1 that is absorbed by the solid (recall $\alpha_s = \epsilon_s$). With $A_1 F_{1s} = A_s F_{s1}$ we have

$$Q_{1,s} = \frac{e_{bs} - J_1}{1/A_1 F_{1s} \epsilon_s} \tag{11.55}$$

This exchange between the partially transmitting solid and surface 1 is represented by Fig. 11.26.

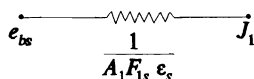
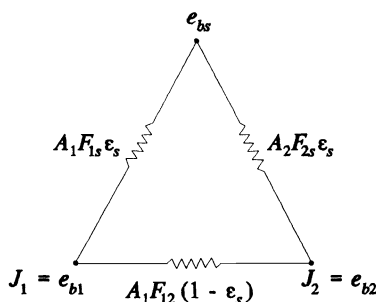


Fig. 11.26 Resistance between a partially transmitting solid and a surface with a radiosity of J_1 .

Example 11.10 Two large plates with emissivity of 1 are at 1001 K and 999 K, respectively. They are separated by 1 mm of glass with an absorption coefficient of 0.1 mm^{-1} . Calculate the "radiation" thermal conductivity of the glass.

Solution. The radiation circuit, with conductances, is constructed:



The *absorption coefficient* is not the same as the absorptivity, α_s , but it is used to estimate α_s . From basic optics, the fraction of energy absorbed by a solid of thickness δ with an absorption coefficient λ is $\exp(-\lambda\delta)$. Therefore,

$$\alpha_s = \exp(-\lambda\delta) = \exp(-0.1 \times 1) = 0.905.$$

We assume $\epsilon_s = \alpha_s$. The equivalent resistance for the circuit is

$$A_1 \mathcal{F}_{12} = A_1 F_{12} (1 - \epsilon_s) + \left[\frac{1}{A_1 F_{1s} \epsilon_s} + \frac{1}{A_2 F_{2s} \epsilon_s} \right]^{-1},$$

or

$$\mathcal{F}_{12} = 1 - \frac{\epsilon_s}{2},$$

406 Radiation Heat Transfer

because $A_1 = A_2$ and $F_{12} = F_{1s} = F_{2s} = 1$. The radiant flux is

$$q = \frac{Q_{1,2}}{A_1} = \mathcal{F}_{12}\sigma(T_1^4 - T_2^4),$$

but also

$$q = k_{\text{rad}} \frac{(T_1 - T_2)}{\delta}.$$

By comparing the two equations, we get

$$k_{\text{rad}} = \frac{\mathcal{F}_{12}\sigma(T_1^4 - T_2^4)\delta}{T_1 - T_2} = \frac{\left[1 - \frac{0.905}{2}\right](5.669)(10.01^4 - 9.99^4)(1)}{(1001 - 999)} = 125 \text{ W m}^{-1} \text{ K}^{-1}.$$

Before you leave this example, you should also show that, if $T_1 \rightarrow T_2$, then

$$k_{\text{rad}} \rightarrow 4\sigma \left[1 - \frac{\varepsilon_s}{2}\right] T^3.$$

The spectral absorptivity of several glasses can be found in Hottel and Sarofim.¹¹ From these data the total hemispherical emissivity of glass of different thicknesses over a wide temperature range has been obtained (Fig. 11.27). As the glass thickness goes to infinity, the limiting value of ε is 0.91 (and not 1.0), because some of the energy emitted within the glass is reflected internally at the glass surface.

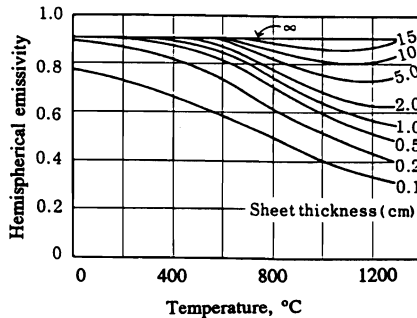


Fig. 11.27 Total hemispherical emissivity of window glass as a function of thickness and temperature. (From H. C. Hottel and A. F. Sarofim, *ibid.*, page 243.)

¹¹H. C. Hottel and A. F. Sarofim, *ibid.*, pages 240-241.

11.13 TRANSIENT CONDUCTION WITH RADIATION AT THE SURFACE

In Chapter 9, we discussed some solutions to transient problems involving solids with heat applied to, or withdrawn from, the surface via convective h . In several operations, notably heat treating processes, stock is heated with radiation. The condition of heat input at the receiver (stock) surface from a heat source at constant temperature T_s is

$$\mathcal{F}_{s1}\sigma[T_s^4 - T^4(0,t)] = -k \frac{\partial T(0,t)}{\partial x} \tag{11.56}$$

We determine \mathcal{F}_{s1} according to the methods discussed in previous sections, depending on the spatial relationship between the source and stock and their respective emissivities. We can put Eq. (11.56) in a dimensionless form

$$M[\theta_s^4 - \theta^4(0, Fo)] = - \frac{\partial \theta(0, Fo)}{\partial (x/l)} \tag{11.57}$$

where

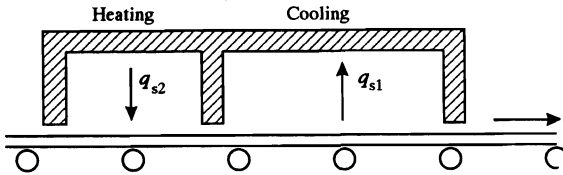
$$M = \frac{\mathcal{F}_{s1}\sigma T_0^3 l}{k}, \quad Fo = \frac{\alpha t}{l^2},$$

$$\theta = \frac{T}{T_0}, \quad \theta_s = \frac{T_s}{T_0}.$$

T_0 is the initial temperature of the stock, and l is its characteristic dimension.

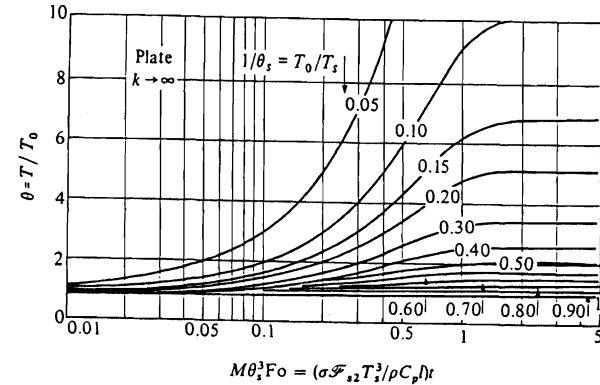
Consider specifically the temperature response of a sheet, $0 \leq x \leq l$, thin enough for Newtonian conditions (no internal gradients) to apply, which is heated at $x = 0$ by a radiation heat source at constant temperature. The back face ($x = l$) loses a negligible amount of heat so that $[\partial T(l,t)/\partial x] = 0$. We give the solution to this problem in Figs. 11.28(a) and (b) for heating and cooling, respectively. For other closely related situations we refer the reader to Schneider.^{12,13}

Example 11.11 (from Schneider) We heat treat a continuous sheet of steel (1 mm thick) by passing it through a radiant furnace designed to provide a heat and cool cycle. The furnace consists of 3.05 m long ceiling heat-source section ($\mathcal{F}_{s1} = 0.72$) at 1478 K followed by a ceiling heat-sink section ($\mathcal{F}_{s1} = 0.86$) at 144 K. If the sheet enters the furnace at 294 K, must be heated to 1367 K, and then cooled to 533 K before leaving the oven, calculate a) the required feed velocity, and b) the length of the cooling section. *Data:* density of steel = 7788 kg m⁻³; heat capacity = 460 J kg K⁻¹.

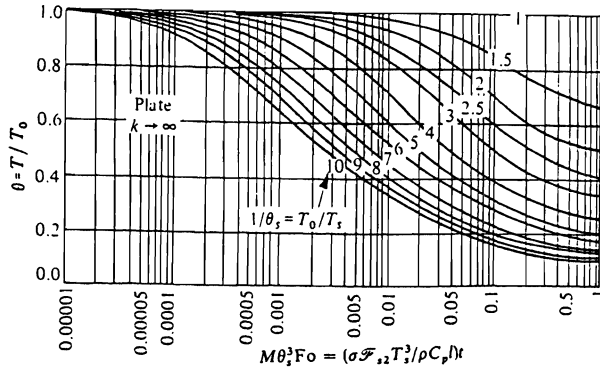


¹²P. J. Schneider, *Temperature Response Charts*, Wiley, New York, NY, 1963, pages 143-149.

¹³P. J. Schneider, *J. Aero/Space Sciences* 27, No. 7, 546-548 (1960).



(a) Heating, $\theta_s = T_s / T_0 > 1$



(b) Cooling, $\theta_s = T_s / T_0 < 1$

Fig. 11.28 Temperature of a plate, $0 \leq x \leq l$, with no internal thermal gradients and an insulated back face, at $x = l$, after sudden exposure to (a) a radiation heat source (heating) or (b) a radiation heat sink (cooling). (From P. J. Schneider, *Temperature Response Charts*, John Wiley, New York, NY, 1963, pages 147 and 148.)

Solution.

a) For the heating section, we apply Fig. 11.28(a) with

$$\frac{1}{\theta_s} = \frac{T_0}{T_s} = \frac{294}{1478} = 0.199$$

$$\theta = \frac{T \text{ (leaving)}}{T_0} = \frac{1367}{294} = 4.65.$$

From Fig. 11.28(a)

$$M\theta_s^3 F_0 = \frac{\mathcal{F}_{s1} \sigma T_0^3 l}{k} \left(\frac{T_s}{T_0} \right)^3 \frac{kt}{\rho C_p l^2} = \frac{\mathcal{F}_{s1} \sigma T_s^3 t}{\rho C_p l} = 0.980.$$

Then the heating exposure time is

$$t = \frac{0.980 \rho C_p l}{\mathcal{F}_{s1} \sigma T_s^3} = \frac{(0.980)(7788)(460)(0.001)}{(0.72)(5.669 \times 10^{-8})(1478^3)} = 26.6 \text{ s.}$$

Thus, the feed velocity is $(3.05/26.6) = 0.115 \text{ m s}^{-1}$.

b) Figure 11.28(b) is used for the cooling section with

$$\frac{1}{\theta_s} = \frac{T_0}{T_s} = \frac{1367}{144} = 9.49$$

$$\theta = \frac{T \text{ (leaving)}}{T_0} = \frac{533}{1367} = 0.390.$$

Then from Fig. 11.28(b)

$$M\theta_s^3 F_0 = 0.0072,$$

from which we determine the cooling exposure time:

$$t = \frac{(0.0072)(7788)(460)(0.001)}{(0.86)(5.669 \times 10^{-8})(144^3)} = 177 \text{ s.}$$

Thus, the required length of the cooling section is

$$(0.115)(177) = 20.4 \text{ m.}$$

11.14 TRANSIENT HEATING WITH THERMAL STRESSES

In the case of heating material with large cross-sections for subsequent hot-working, such as forging, extrusion, piercing, etc., blooms or ingots are heated in large furnaces, which are usually gas-fired by radiant burners. If placed cold into a hot furnace enclosure, the surface of the piece is immediately subjected to intense radiant heat and increases in temperature rapidly, governed by Eqs. (9.43) and (11.49). As the surface is heated, it expands. During the period when the interior is still at a low temperature, this causes a constraint on the expansion of the hot surface region, and a compressive stress develops at and near the surface, while a tensile stress develops in the interior.

Sun¹⁴ calculated the principal stresses and determined that the maximum tensile stresses were found to be at the center after 4.2 hours of heating an ingot with a diameter of 100 cm. The calculated principal stress in the axial direction (σ_z) is shown in Fig. 11.29, where it can be seen that the tensile stress is a maximum at the center of the ingot, neutral near the surface, and compressive at the surface.

Sun hypothesized that if σ_z at the center exceeds 90 percent of the yield strength of the material, then internal cracks result. To avoid reaching these stress levels, the heating must be controlled so that thermal stresses are limited to below the yield strength of the material.

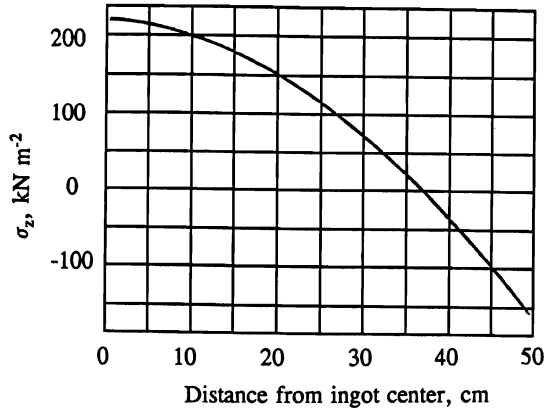


Fig. 11.29 Distribution of σ_z in 100 cm diameter ingot of Hastelloy X placed cold into furnace at 1500 K, after 4.2 hours in the furnace. (From R. C. Sun, *Metall. Trans.* 1, 1881-1887, 1970.)

The point of this discussion is to make the reader aware of this problem, which usually occurs when radiation is the predominant heat transfer mechanism. Radiative heating can also cause thermal shock in ceramic materials very easily, because of their relatively low thermal conductivities.

PROBLEMS

11.1 A radiation heat transfer coefficient is often defined as $q = h_r(T_1 - T_2)$.

- a) For a gray solid at T_1 , completely surrounded by an environment at T_2 , show that h_r is given by

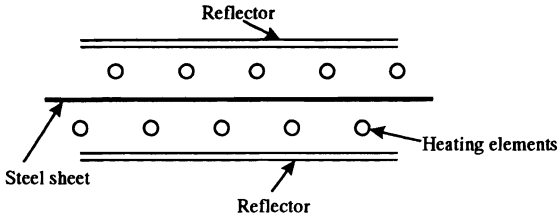
$$h_r = \sigma \varepsilon_1 (T_1^2 + T_2^2) / (T_1 + T_2).$$

- b) Calculate the rate of heat transfer (by radiation and convection) from a vertical surface, 1.5 m high, and the percentage by radiation for the following cases:

Surface ($\varepsilon = 0.8$) at:	Air at:
500 K	300 K
800 K	300 K
1100 K	300 K

11.2 A metal sphere at 1255 K is suddenly placed in a vacuum space whose walls are at 355 K. The sphere is 50 mm in diameter, and we may assume that its surface is perfectly black. a) Calculate the time it takes to cool the sphere to 420 K. Assume that a uniform temperature exists in the sphere at each instant. *Data for sphere:* $\rho = 7000 \text{ kg m}^{-3}$; $C_p = 1000 \text{ J kg}^{-1} \text{ K}^{-1}$. b) Discuss the validity of the assumption in part a) with quantitative reasoning using a conductivity of $50 \text{ W m}^{-1} \text{ K}^{-1}$.

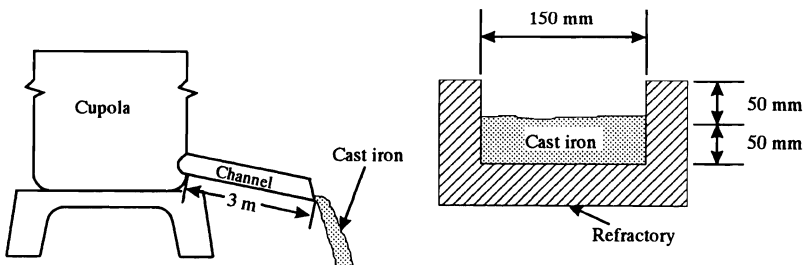
11.3 Steel sheet is preheated in vacuum for subsequent vapor deposition. The steel sheet is placed between two sets of cylindrical heating elements (25 mm in diameter). The heating efficiency is kept high by utilizing radiation reflectors of polished brass. The steel sheet and radiation reflectors may be considered to be infinite parallel plates. a) Calculate the rate of heat transfer from the heating elements (maintained at 1810 K) to the steel when the steel is at 300, 390, 530, 670 and 810 K. The reflectors may be assumed to be at 310 K. b) Plot the results of part a) and determine by graphical integration the average value of the heat transfer rate as the steel is heated from 300 to 810 K. c) From part b) determine the time it takes to heat a steel sheet 6 mm thick from 300 to 810 K.



- Data:
- ϵ (heating elements) = 0.9
 - ϵ (steel sheet) = 0.3
 - ϵ (reflectors) = 0.03
 - ρ of steel = 7690 kg m⁻³
 - C_p of steel = 628 J kg⁻¹ K⁻¹
 - Area of steel to area of elements = 10/1.

11.4 A large furnace cavity has an inside surface temperature of 1090 K. The walls of the furnace are 0.3 m thick. A hole 150 mm × 150 mm is open through the furnace wall to the room at 295 K. a) Calculate the power loss by radiation through the open hole. b) Calculate the power loss if a sheet of nickel covers the hole on the outside surface. Data: emissivity of furnace refractories = 0.9; emissivity of nickel sheet = 0.4.

11.5 Cast iron is continually tapped from the bottom of a cupola into an open refractory channel. The metal enters at 1810 K and runs down the channel at a rate of 0.50 kg s⁻¹. The dimensions of the channel are shown below. Neglect the heat loss by conduction through the refractory and estimate the metal discharge temperature. Data for molten cast iron: $C_p = 830$ J kg⁻¹ K⁻¹; $\rho = 6890$ kg m⁻³; $\epsilon = 0.30$.



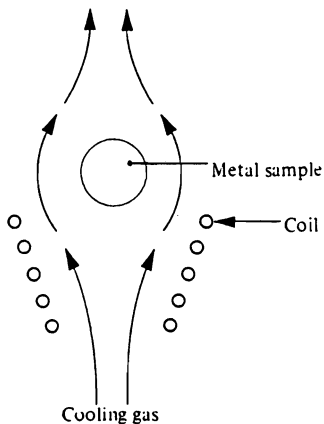
412 Radiation Heat Transfer

11.6 A method of melting metal so as to avoid crucible contamination is levitation. A metal sample is placed in an electromagnetic field from a coil wound as a cone. The field not only supplies power to melt the metal but also to levitate it. But with this setup, the strength of field necessary to keep the sample levitated is sometimes such that the metal is overheated. A means of preventing this is to flow cooling gas past the sample.

Develop an expression that relates the steady-state temperature of the metal to the heating power supplied by the field (Q_p), the gas temperature T_0 , the gas velocity V , and any other parameters which you think are essential. Metal temperatures of interest are 1360-1920 K, and the convection heat transfer coefficient can be expressed as

$$h_c = KV^{0.7},$$

in which K is a known constant.

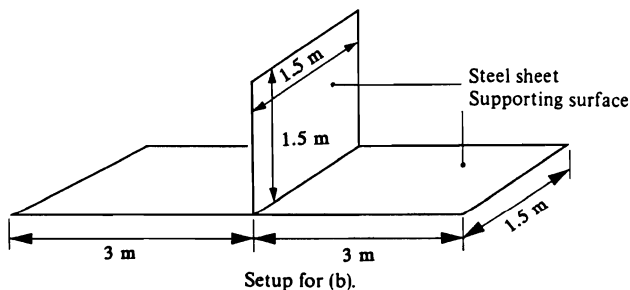


11.7 A steel sheet, 12.5 mm thick and having the shape of a square 1.5 m \times 1.5 m, comes out of a heat-treating furnace at 1090 K. During heat treatment its surface was oxidized so that its emissivity is 0.8.

- Calculate its initial cooling rate ($K s^{-1}$) if it is suspended freely by a wire in a room at 300 K. Neglect all heat transfer with convection, i.e., deal only with radiation heat transfer.
- Calculate its initial cooling rate if it is supported vertically on a horizontal surface (also at 300 K) which has an emissivity of 0.2. Again deal only with radiation heat transfer.

Data (all units in SI):

	Supporting surface	Steel sheet
Thermal conductivity	50	20
Density	600	8010
Heat capacity	630	600
Emissivity	0.2	0.8

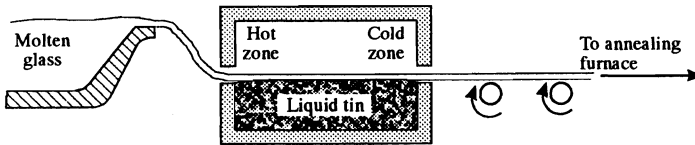


11.8 Brass sheet, 1.6 mm thick, passes through a continuous tempering surface. The first portion of the furnace is filled with gases at 920 K, moving against the strip direction at a speed of 0.3 m s⁻¹. The strip itself moves at a speed of 0.05 m s⁻¹. The walls are of SiO₂ brick, each 0.3 m from the brass sheet as it moves vertically, and the gases are 40% H₂O, 10% CO₂, and 50% N₂. How many meters of strip would have to be in the first portion of the furnace so that the strip could exit into the second section at a temperature of 700 K?

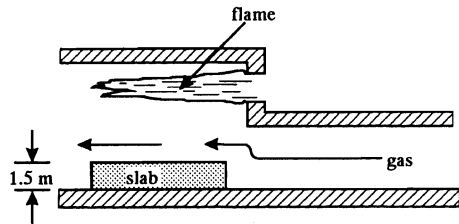
Data:

$$\begin{aligned}
 C_{p_{\text{brass}}} &= 428 \text{ J kg}^{-1} \text{ K}^{-1} & C_{p_{\text{gas}}} &= 1110 \text{ J kg}^{-1} \text{ K}^{-1} & \eta_{\text{gas}} &= 4 \times 10^{-5} \text{ N s m}^{-2} \\
 \rho_{\text{brass}} &= 9200 \text{ kg m}^{-3} & \rho_{\text{gas}} &= 0.48 \text{ kg m}^{-3} \\
 k_{\text{brass}} &= 170 \text{ W m}^{-1} \text{ K}^{-1} & k_{\text{gas}} &= 0.086 \text{ W m}^{-1} \text{ K}^{-1}
 \end{aligned}$$

11.9 Estimate the length of the furnace, shown below, that is used for forming sheet glass (3 mm thick). The glass enters the furnace at 1500 K, and it should leave at 1100 K. The liquid tin and the furnace are kept at 1000 K. Assume that the heat transfer coefficient at the tin-glass interface is infinite. The emissivity of the glass is shown in Fig. 11.27. Other properties of the glass are $k = 4.2 \text{ W m}^{-1} \text{ K}^{-1}$; $C_p = 420 \text{ J kg}^{-1} \text{ K}^{-1}$; $\rho = 3320 \text{ kg m}^{-3}$. The emissivity of the molten tin is 0.1.



11.10 A slab of steel is placed into a reheat furnace so that it can be heated to 1500 K and subsequently hot-rolled to plate. The gas temperature in the furnace has been carefully measured and found to be 1520 K. Energy to the furnace is by burning gas, and its flame behaves as though it is a gray surface ($\epsilon = 0.9$) at 2000 K. The convective heat transfer coefficient is 85 W m⁻² K⁻¹ and the emissivity of the steel is 0.8. Estimate the temperature of the slab after the system comes to thermal equilibrium. For simplicity assume that the flame and slab surface are parallel planes that are 5 m × 5 m, and the gas is transparent. Consider only heat exchange among the slab, flame and gas.

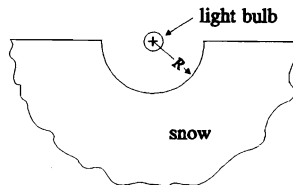


11.11 One side of a flat ceramic shell mold (30 mm thick) is maintained at 1500 K while the opposite side radiates into a large room at 300 K. The emissivity of the radiating surface is 0.5, and the thermal conductivity of the ceramic mold material is 0.7 W m⁻¹ K⁻¹. Calculate the steady-state flux and the surface temperature of the mold.

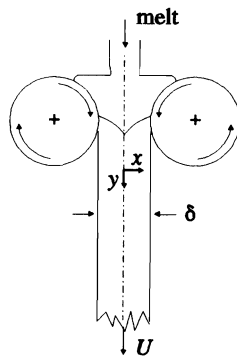
11.12 A plate is heated uniformly to 810 K, and then it is suspended vertically next to and parallel to a cooler plate in a large room. Both plates are 1.3 m × 1.3 m × 12.5 mm thick, and they are separated by 0.3 m. The cooler plate and the room are at 300 K. What is the initial cooling rate (K s⁻¹) of the hotter plate? Data: $\epsilon = 0.7$ and $\rho C_p = 8 \times 10^6 \text{ J m}^{-3} \text{ K}^{-1}$ for both plates.

414 Radiation Heat Transfer

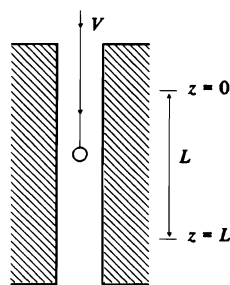
11.13 A light bulb (100 watts) can be approximated to be a sphere. It is held at the top level of a large amount of snow; after steady state is achieved, a hole with the form of a hemisphere of radius R is made in the snow. Consider only radiation heat transfer from the bulb to the snow and to the surroundings. Within the snow, however, there is conduction heat transfer. The snow and the surroundings are at 0°F . The surface of the snow forming the hole is at 32°F . *Thermal properties of snow:* $k = 0.2 \text{ Btu h}^{-1} \text{ ft}^{-1} \text{ }^\circ\text{F}^{-1}$; $\rho C_p = 10 \text{ Btu ft}^{-3} \text{ }^\circ\text{F}^{-1}$; $\varepsilon = 0.7$. a) Calculate the radius of the hole. b) Calculate the surface temperature of the light bulb. Assume that this surface is black and that the radius of the spherical bulb is 0.2 ft .



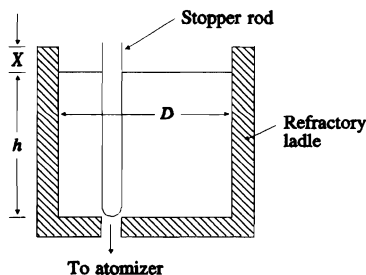
11.14 Thin sheet of alloy is prepared by "roller casting." In this process, a melt solidifies between two rolls that are water-cooled to produce sheet of thickness δ . *Assume:* (1) that temperature in the sheet is independent of x ; (2) that conduction in the y -direction *cannot* be ignored; (3) heat loss from the surface is *only* by radiation; (4) the sheet temperature at $y = 0$ is T_0 and the room temperature is T_R , and (5) sheet velocity is U . a) Give a differential equation for the temperature, T , in the sheet that applies for $x \geq 0$. Be sure that your equation is consistent with the assumptions. b) Write appropriate boundary conditions for T . c) If this had been presented as a numerical problem, how would you solve it?



11.15 A sphere is suspended by a wire and is lowered at a constant velocity into a very long cylindrical tube as indicated in the sketch. Assume that, over the length L , the view factor is constant, the tube wall has a constant temperature T_w , and the rate of descent (V) is constant. If the sphere has an emissivity ε and enters the length L with a temperature T_0 , derive an equation which gives its temperature as it leaves the length L . $T_w \gg T_0$ and the sphere radius is R ; consider only radiation heat transfer.



11.16 A ladle of hot metal is used to feed an atomizer to produce metal powder. By means of a controlled stopper rod, the metal slowly leaves the ladle at a constant mass flow rate, W . Assume that the ladle refractory can be treated as a "no-net-flux surface" and that the only heat loss from the ladle is by radiant heat transfer.

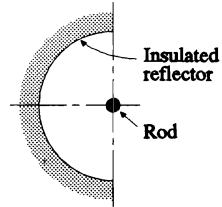


- a) When the ladle is full (i.e., $X = 0$), write an equation that gives the radiant heat loss (Q , energy/time) from the top surface of the melt.

- b) When the ladle is 3/4 empty and $D/X = 4$, write an equation for Q . Use the following variables: T_1 = temperature of metal; T_2 = temperature of surroundings; h = depth of melt; D = inside diameter of ladle; $A = \pi D^2/4$ = area of top surface of melt; ϵ_1 = emissivity of melt surface; and X = distance from top of ladle to top of melt (see diagram).

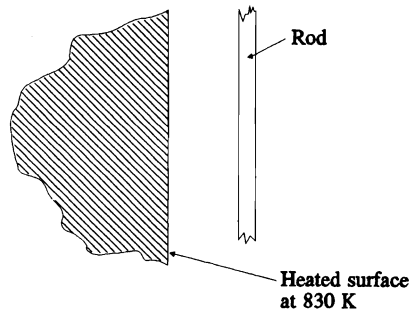
In your answers give numerical values for view factors and total exchange factors.

- 11.17 A long rod ($\epsilon = 0.8$) is heated to 1255 K and is placed near a well insulated reflector ($\epsilon = 0.01$) as shown. The purpose of the reflector is to retard the cooling of the rod. The diameter of the rod is 75 mm, and the diameter of the reflector is 500 mm. The room surrounding the reflector and the rod are at 300 K. a) Calculate the radiant power loss per unit length of the rod when its temperature is 1255 K. b) Repeat if there is no reflector.



- 11.18 Two parallel plates, 0.3×0.6 m, are spaced 0.3 m apart in a large heat treating furnace and heated uniformly to 810 K. They are then removed from the furnace and cooled in a room maintained at 300 K. The emissivities of the plates are 0.4 and 0.8, respectively. Other thermal properties are equal. Calculate the ratio of the initial cooling rates ($K s^{-1}$) of the plates. Consider only radiation heat transfer.

- 11.19 A long rod, with a diameter of 3 mm, is placed in a vacuum parallel to a large and flat heated surface. The other side of the rod is exposed to vacuum chamber walls at 300 K. Assume that the heated surface and the surface of the rod are both gray with equal emissivities of 0.7. The rod has a volumetric heat capacity of $\rho C_p = 6.7 \times 10^6 J m^{-3} K^{-1}$. Calculate the heating rate of the rod at 335 K, 500 K, 700 K, and 800 K.



- 11.20 For a cylindrical ingot of steel, 1 m diameter by 2 m long, placed in a refractory-lined furnace at 1500 K, calculate the radiation heat transfer coefficient to the steel surfaces. Repeat when the surface of the steel has reached 500 K and 1000 K.

PART THREE

MASS TRANSPORT

The rate at which many processes occur is determined by diffusion, and it is most desirable to treat these processes in a quantitative manner when possible. The carburizing of steel, the oxidation of silicon, and solid-state sintering are just a few examples of diffusion-controlled processes.

On the other hand, there are processes whose rate is determined by the rate of reaction at an interface between two phases. Kinetics describes the rates of reactions in contrast to Fick's law of diffusion. As you may suspect, many processes are of mixed control, that is, neither the reaction rate nor the diffusional transport process alone controls the overall transfer of material.

In general, most processes involve a variety of different steps occurring in gaseous, solid, or liquid phases, and at different phase boundaries. When one step is much slower than the others, a limiting condition is reached and this *rate determining step* determines the overall reaction rate; if none of the steps is much slower than the others, a more general condition—*mixed control*—is achieved. This parallels heat flow problems in that the overall diffusion of heat into or out of a body may be controlled entirely by its thermal diffusivity or by the heat transfer coefficient at its surface, depending on their relative magnitudes. A good example of this is the cooling of solids which, as limiting conditions, either obey Newton's law of cooling, or, if the heat transfer coefficient approaches infinity, cool at a rate entirely controlled by the solid's ability to diffuse heat.

In this part, we introduce the materials engineer to basic equations and analyses that describe the various mechanisms of mass transport through and between phases. Materials engineers constantly deal with these phenomena, and learning these basics is critical to understanding, controlling, and developing processes to produce materials.

12

FICK'S LAW AND DIFFUSIVITY OF MATERIALS

In Chapter 1, we introduced Newton's law of viscosity describing momentum transport due to a velocity gradient, and in Chapter 6 Fourier's law of heat conduction was described as energy transfer due to a temperature gradient. In Chapter 12, we present Fick's law of diffusion which describes the transport of a chemical species through a phase due to the concentration gradient of the species.

12.1 DEFINITION OF FLUXES—FICK'S FIRST LAW

Diffusion is the movement of a species from a region of high concentration to a region of low concentration. Consider Fig. 12.1, which depicts a plate of iron of thickness L . Initially, both sides of the plate are exposed to the same pressure of hydrogen, which means that the concentration of hydrogen dissolved in the iron is uniform across the plate. At some instant, $t = 0$, the upper surface is subjected to a much higher pressure of the gas, which establishes a new hydrogen concentration at that surface. The material beneath this surface is gradually enriched as the hydrogen diffuses from the high concentration at the upper surface into the low concentration region. A steady-state concentration profile is eventually reached when a constant rate of hydrogen mass is required from the gas phase at $x = 0$, in order to maintain the concentration difference across the plate.

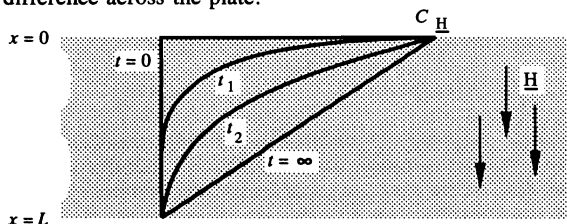


Fig. 12.1 Establishment of steady-state concentration gradient; Fick's first law.

420 Fick's Law and Diffusivity of Materials

If the concentration of component A (hydrogen in this example) is given in mass units, then the rate equation for diffusion may be written

$$W_{Ax} = -D_A \left[\frac{\partial \rho_A}{\partial x} \right], \quad (12.1)$$

where W_{Ax} = mass flux of A in the x -direction, $\text{kg (of } A) \text{ m}^{-2} \text{ s}^{-1}$, ρ_A = mass concentration of A , $\text{kg (of } A) \text{ m}^{-3}$ (of total material), and D_A = diffusion coefficient, or diffusivity of A , $\text{m}^2 \text{ s}^{-1}$.

In the materials field, the rate equation is usually written in terms of molar concentrations:

$$j_{Ax} = -D_A \left[\frac{\partial C_A}{\partial x} \right], \quad (12.2)$$

where j_{Ax} = molar flux of A in the x -direction, $\text{mol (of } A) \text{ m}^{-2} \text{ s}^{-1}$, and C_A = molar concentration of A , $\text{mol (of } A) \text{ m}^{-3}$ (of total material).

Equations (12.1), (12.2), and other alternative statements of the rate equation are all referred to as *Fick's first law of diffusion* which states that species A diffuses in the direction of decreasing concentration of A , similarly as heat flows by conduction in the direction of decreasing temperature, and momentum is transferred in viscous flow in the direction of decreasing velocity.

Equations (12.1) and (12.2) are convenient forms of the rate equation when the density of the total solution is uniform, that is, in solid or liquid solutions, or in a dilute gaseous mixture. When the density is not uniform, other forms of Fick's first law may be preferable. For example, the mass flux may be given by

$$W_{Ax} = -\rho D_A \left[\frac{\partial \rho_A^*}{\partial x} \right], \quad (12.3)$$

where ρ is the density of the entire solution, kg m^{-3} , and ρ_A^* is the mass fraction of A . Similarly, the molar flux may take the form

$$j_{Ax} = -CD_A \left[\frac{\partial X_A}{\partial x} \right], \quad (12.4)$$

in which C is the local molar concentration in the solution at the point where the gradient is measured, $\text{mol (of all components) m}^{-3}$ (of total solution), and X_A is the mole fraction of A (C_A/C) in the solution.

The diffusivities D_A , appearing in Eqs. (12.1)-(12.4), are of a particular type, known as the *intrinsic diffusion coefficient*, since they are defined in the presence of a concentration gradient of A .

12.2 DIFFUSION IN SOLIDS

It behooves materials engineers to understand diffusion mechanisms, and especially the implications of the terms self-diffusion, intrinsic diffusion, interdiffusion, interstitial diffusion, vacancy diffusion, etc., so that they can make intelligent estimates of diffusivities for practical uses. In the following sections, we consider the various types of diffusion coefficients and mechanisms of diffusion.

12.2.1 Self-diffusion

If we could stand inside the lattice of a solid, we would see a continual motion of the atoms, each vibrating about its normal lattice point. Furthermore, we would see occasional unoccupied sites called vacancies. If we focus on a vacancy, we will eventually see the site suddenly become occupied and one of its neighboring sites become vacant. In this way, a particular atom can slowly progress through the lattice. Alternatively, the vacancy wanders randomly through the lattice. Either way, the net effect is a random motion of the atoms themselves.

The rate at which an atom meanders through the lattice of a pure metal is the *self-diffusion rate*. We can measure it using radioactive atoms (tracers), as illustrated in Fig. 12.2, which depicts self-diffusion between a central region initially with a uniform concentration C_A^T of radioactive atoms and two adjoining regions initially containing only normal atoms. It is assumed that the diffusion behavior of normal and of radioactive atoms is virtually the same, and by using a scheme as in Fig. 12.2 we can measure the rate at which the atoms diffuse among themselves, that is, self-diffusion.

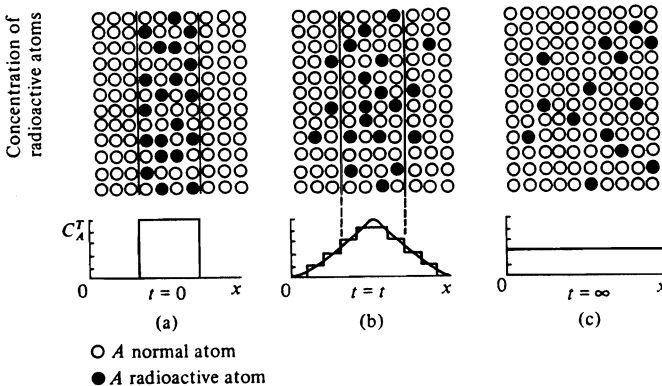


Fig. 12.2 Self-diffusion in materials. (a) Condition before diffusion. (b) Condition after some diffusion. (c) Uniform condition after prolonged diffusion.

We can also speak of self-diffusion rates in homogeneous materials in the same manner as we do for pure metals. In an alloy of gold and nickel, for example, we can determine the self-diffusion coefficient of gold atoms D_{Au}^* , if the central layer of the homogeneous alloy initially contains radioactive gold atoms in the same proportion to Ni atoms as in the outer layers (Fig. 12.3). Similarly, if radioactive nickel atoms are initially present in the central layer, then we can determine its self-diffusion coefficient, D_{Ni}^* . Figure 12.4 gives self-diffusion data for the entire range of compositions in the gold-nickel system. It should be emphasized that *self-diffusion data apply to homogeneous alloys in which there is no gradient in chemical composition*. Also, D_i^* values depend on the composition of the material and the temperature.

You may recall from Chapter 1 that Einstein proposed the equation

$$D^* = B^* \kappa_B T \tag{1.17}$$

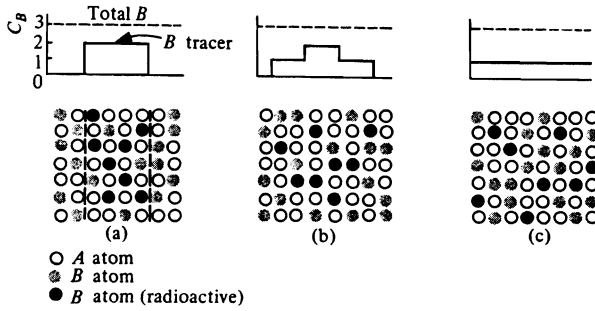


Fig. 12.3 Self-diffusion in an alloy.

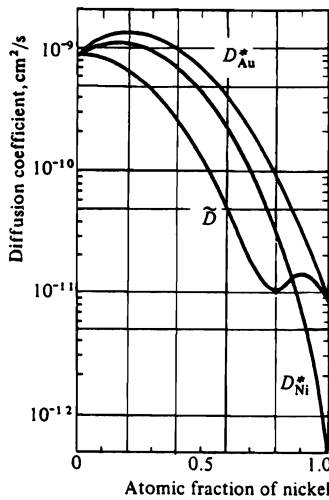


Fig. 12.4 Diffusion coefficients in gold-nickel alloys. \bar{D} is the interdiffusion coefficient and D^* the self-diffusion coefficient. (From J. E. Reynolds, B. L. Averbach, and M. Cohen, *Acta Met.* 5, 29 (1957).)

to describe self-diffusion, where B^* is the self-diffusion "mobility," a measure of the ability of an atom to migrate within the structure without any external field or chemical free energy gradient providing a driving force.

The probabilistic approach has shown that the self-diffusion coefficient in a simple cubic lattice may be expressed as¹

$$D^* = \frac{1}{6} \delta^2 \nu, \tag{12.5}$$

where δ is the interatomic spacing, and ν is the jump frequency. From measurements of D^* and δ , the jump frequency appears to be approximately 10^8 - 10^{10} s^{-1} , which is 1 in every 10^4 or 10^5 vibrations per atom. Most studies of self-diffusion are concerned with this sort of information, that is, with the structure and motion within the lattice of a solid. Some data for pure solid metals are given in Fig. 12.5 and for dilute solid alloys, in Fig. 12.6.

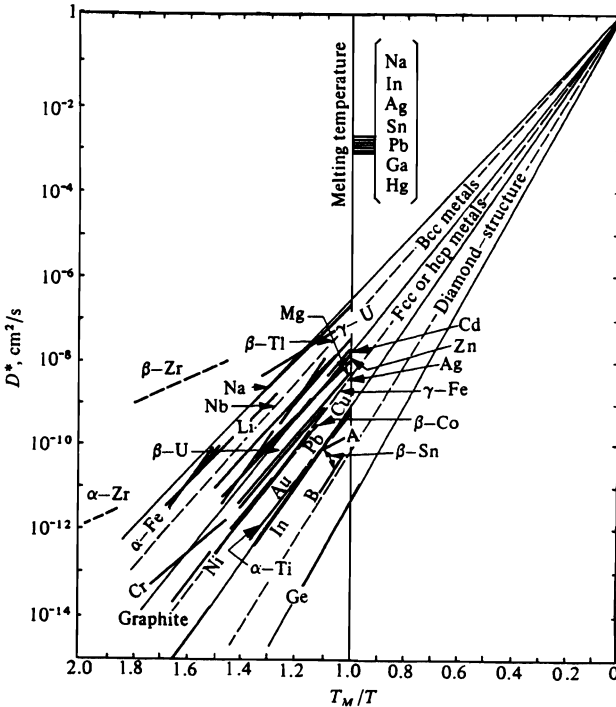


Fig. 12.5 Self-diffusion coefficients for pure metals, plotted as $\log D$ versus T_M/T , where T_M is the melting temperature. (From O. D. Sherby and M. T. Simnad, *Trans. ASM* 54, 227 (1961).)

In the development leading to Eq. (12.5), we assume that the atom jumps are completely random and uncorrelated, meaning that any of the atoms surrounding a vacancy may exchange places with the vacancy. However, if we follow the motion of tracer atoms moving via vacancies, we must realize that the tracer atom is only one of the many atoms around a vacancy and that the tendency for that particular atom (the tracer) to exchange places with the vacancy is not as great as for any atom in general to exchange. This means that the vacancy is often likely to move away from the tagged atom, with diffusion then actually

¹See, for example, P. G. Shewmon, *Diffusion in Solids*, second edition, The Minerals, Metals & Materials Soc., Warrendale, PA, 1989, pages 53-68, or R. E. Reed-Hill and R. Abbaschian, *Physical Metallurgy Principles*, third edition, PWS-Kent, Boston, 1992, pages 360-364.

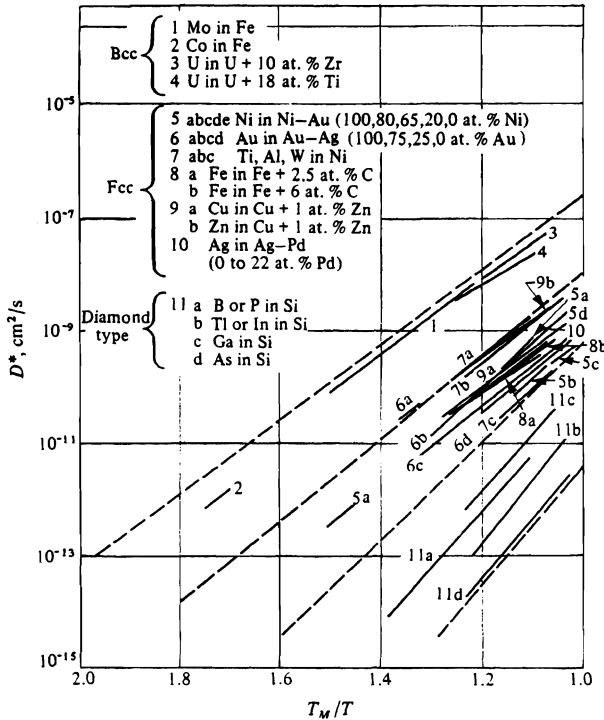


Fig. 12.6 Effect of dilute alloying on self-diffusion and rate of solute substitutional diffusion for a number of metallic systems. T_M is the temperature halfway between the liquidus and solidus of the alloy. (From O. D. Sherby and M. T. Simnad, *ibid.*)

occurring by exchange of an untagged atom with the vacancy, but remaining undetected as long as we only follow the tagged atom displacement. The self-diffusion coefficient, D_i^T , calculated from the results of tracer studies, is thus slightly lower than the true self-diffusion coefficient D_i^* . They are related by means of the *correlation coefficient*, f :

$$D_i^T = f D_i^* \tag{12.6}$$

Table 12.1 gives f calculated for several different crystal structures. For interstitial diffusion, f is equal to 1.0, since the host lattice is not involved in the mechanism.

Table 12.1 Correlation coefficients for various structures*

Structure	f
Diamond	0.500
Simple cubic	0.655
Body-centered cubic	0.721
Face-centered cubic	0.781

*From K. Compaan and Y. Haven, *Trans. Faraday Soc.* **52**, 786 (1956).

12.2.2 Diffusion under the influence of a composition gradient

In most materials processing situations, diffusion occurs because a concentration gradient or driving force is provided. When this force is present, the diffusion coefficient used to calculate the flux of atoms is *not* the self-diffusion coefficient, except under special circumstances.

Consider the diffusion of interstitial atoms through a lattice via interstitial sites, for example, the diffusion of carbon through iron. In this instance, carbon is in dilute concentration, and it diffuses through the stationary iron lattice without displacing the iron atoms from their own sites. Thus, if we treat a problem involving the diffusion of carbon in iron, we can safely use a value for carbon's diffusivity in iron from a handbook, even though it is not clearly specified what type of diffusion coefficient is given. We presume that the interstitial mechanism dominates if the solute atoms are considerably smaller in size than the solvent atoms. If the solute radius begins to approach that of the solvent, this mechanism no longer operates, and movement of the solvent atoms as well as motion of the solute atoms takes place. In this case, then, diffusion involves interchange of solute and solvent atoms on sites in the alloy. In substitutional alloys, the influence of a chemical gradient is such that we must clearly recognize the right type of diffusion coefficient: either the *intrinsic diffusion coefficient* or *interdiffusion coefficient*. Both types are discussed below, but first it seems appropriate to discuss briefly the various mechanisms by which substitutional alloy elements are thought to diffuse. More detailed discussions of diffusion mechanisms in solids are available in many sources on materials science or physical metallurgy.²

Vacancy mechanism. This is a mechanism by which an atom on a site adjacent to a vacancy jumps into the vacancy. While some distortion of the lattice is required for the atom to pass between neighboring atoms, the energy associated with this distortion is not prohibitive, and this mechanism is well established as the predominant one in many metals and ionic compounds.

Ring mechanism. In some bcc metals, it is thought there might exist a mechanism of diffusion in which a ring of three atoms may rotate, resulting in diffusion. This possibility is considered to be more plausible than an exchange of two atoms, since it involves less strain energy than a two-atom exchange. However, direct evidence of either of these mechanisms operating in metals is lacking.

Interstitialcy mechanism. This mechanism involves the addition of an extra solute atom to the lattice, by pushing an adjacent atom out of its normal site and into an interstitial site. The motion continues as the new, oversized interstitial atom pushes a further atom out of its normal site in a chain-reaction type of process. This mechanism is believed to operate in some compounds in which one atom is smaller than the other, for example, in AgBr, where silver diffuses via this mechanism. In most metals, however, this mechanism seems unlikely to operate. We find a possible exception in materials subjected to bombardment by radiation, in which case high energy particles may knock atoms out of their normal sites and into interstitial positions.

Thinking of diffusion in general, we can see now the basic difference between diffusion and heat flow quite clearly. Heat flow in a medium does not cause the medium to move while diffusion, in itself, involves the movement of the medium, and thus contributes to the velocity of the medium. Refer to Fig. 12.7 and consider a diffusion couple made by joining a gold and a nickel bar together so that there is diffusion across the marked interface. The inert markers may be pieces of fine tungsten wire (insoluble in the alloy) which are located

²See, for example, S. Mrowec, *Defects and Diffusion in Solids—An Introduction*, Elsevier Scientific Publ., Amsterdam, 1980, pages 174-196, or R. J. Borg and G. J. Dienes, *An Introduction to Solid State Diffusion*, Academic Press, Boston, 1988, pages 53-60.

in the plane of joining. During a diffusion anneal of many hours, interdiffusion of the gold and nickel occurs and changes the concentration distribution as shown. But, because gold diffuses more rapidly than nickel, more gold atoms than nickel atoms diffuse past the inert markers. Figure 12.7(b) shows in an exaggerated form the transfer of gold atoms across the plane of markers without any nickel atoms crossing over. If the vacancy concentration remains uniform, that is, the volume is constant, this transfer of gold atoms requires that the bar of pure gold must shorten while the nickel bar (now containing the transferred gold atoms) lengthens by the same amount. In the same manner, the transfer of nickel atoms across the plane of markers without any gold atoms crossing over is shown, producing the shift due to Ni. The net result of these two simultaneous processes is shown, producing the shift due to Au. The net result of these two simultaneous processes is that the side that was originally pure gold is somewhat shorter, and the other side is correspondingly longer. An alternative description is that the inert markers have moved from their original position toward the gold end of the specimen. This is the viewpoint taken if one end of the specimen is the reference plane, and the movement is called the Kirkendall shift or the *Kirkendall effect*. The differences between the various "types" of diffusion coefficients mentioned above are related to the Kirkendall effect, and are pointed out below.

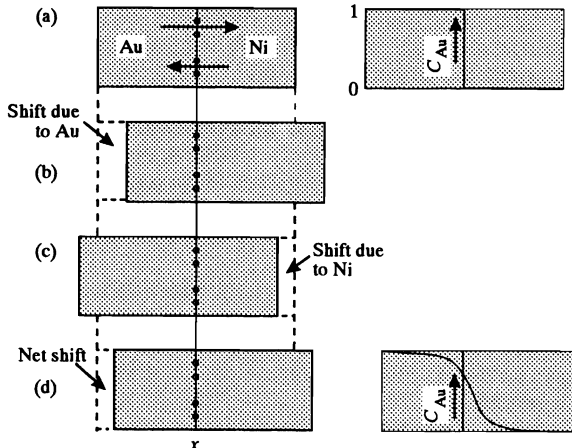


Fig. 12.7 The interdiffusion of gold and nickel, and the resulting bulk flow and composition profiles.

Due to bulk motion in the gold-nickel diffusion couple, we note that the solid bar moves with a velocity depending on the difference between the rates of diffusion of gold and nickel. An observer sitting on a lattice plane moving with the solid's velocity would notice a flux of gold atoms past that plane given by

$$j_{\text{Au}} = -D_{\text{Au}} \frac{\partial C_{\text{Au}}}{\partial x}.$$

However, an observer sitting on an unattached plane in space, would see the total flux of gold atoms passing by as

$$N_{\text{Au}} = -D_{\text{Au}} \frac{\partial C_{\text{Au}}}{\partial x} + v_x C_{\text{Au}}, \quad (12.7)$$

where the flux is expressed by N_{Au} , rather than by j_{Au} , to emphasize that it is relative to the stationary plane. The accumulation of gold as a function of time within a unit volume (Δx

thick) that straddles the stationary plane is given by the net difference between the gold entering and leaving. Thus, we may write:

$$\Delta x \left[\frac{\partial C_{\text{Au}}}{\partial t} \right] = N_{\text{Au}|x} - N_{\text{Au}|x+\Delta x}. \quad (12.8)$$

When the $\lim_{\Delta x \rightarrow 0}$ is taken, we obtain

$$\frac{\partial C_{\text{Au}}}{\partial t} = - \frac{\partial N_{\text{Au}}}{\partial x}, \quad (12.9)$$

which, on substituting Eq. (12.7), becomes

$$\frac{\partial C_{\text{Au}}}{\partial t} = \frac{\partial}{\partial x} \left[D_{\text{Au}} \frac{\partial C_{\text{Au}}}{\partial x} - v_x C_{\text{Au}} \right]. \quad (12.10)$$

Similarly, we can obtain the accumulation of nickel in the same unit volume:

$$\frac{\partial C_{\text{Ni}}}{\partial t} = - \frac{\partial}{\partial x} \left[D_{\text{Ni}} \frac{\partial C_{\text{Ni}}}{\partial x} - v_x C_{\text{Ni}} \right]. \quad (12.11)$$

If the vacancy concentration within the unit volume is constant, then the volume is approximately constant and

$$\frac{\partial C}{\partial t} = \frac{\partial C_{\text{Ni}}}{\partial t} + \frac{\partial C_{\text{Au}}}{\partial t} = 0, \quad (12.12)$$

which requires, by Eqs. (12.10) and (12.11), that

$$v_x = \frac{1}{(C_{\text{Au}} + C_{\text{Ni}})} \left[D_{\text{Au}} \left[\frac{\partial C_{\text{Au}}}{\partial x} \right] + D_{\text{Ni}} \left[\frac{\partial C_{\text{Ni}}}{\partial x} \right] \right]. \quad (12.13)$$

Only in terms of the gold concentration gradient, this takes the form

$$v_x = \frac{1}{C} [D_{\text{Au}} - D_{\text{Ni}}] \left[\frac{\partial C_{\text{Au}}}{\partial x} \right]. \quad (12.14)$$

Having obtained an expression for v_x , we can now write the rate of accumulation of gold solely in terms of diffusion coefficients and concentration gradients, by substituting Eq. (12.14) into (12.10):

$$\frac{\partial C_{\text{Au}}}{\partial t} = \frac{\partial}{\partial x} \left[(X_{\text{Ni}} D_{\text{Au}} + X_{\text{Au}} D_{\text{Ni}}) \frac{\partial C_{\text{Au}}}{\partial x} \right]. \quad (12.15)$$

We developed Eq. (12.15) from the viewpoint of a stationary observer. However, this requires that the position of a reference plane fixed in space can be determined. In the experimental set-up of Fig. 12.7, the inert markers could provide such a reference plane. But

428 Fick's Law and Diffusivity of Materials

in applying diffusion data to a commercial process, we cannot expect to be provided with inert markers. In addition, Eq. (12.15) is useful for determining D_{Au} and D_{Ni} , but is of no value in the sense that analytical solutions to practical diffusion problems cannot be conveniently developed from it. Instead, the basic complexity that arises from the bulk motion is avoided by merely using Fick's first law in its simplest form, that is, for gold

$$j_{Au} = -\tilde{D} \left[\frac{\partial C_{Au}}{\partial x} \right]. \quad (12.16)$$

Note that the diffusion coefficient is written differently; \tilde{D} includes the basic concept that the flux is proportional to the concentration gradient but side-steps the issue of bulk flow. With \tilde{D} defined in this way, the accumulation of gold within the unit volume is

$$\Delta x \left[\frac{\partial C_{Au}}{\partial t} \right] = [j_{Au}|_x - j_{Au}|_{x+\Delta x}]. \quad (12.17)$$

When taking the $\lim_{\Delta x \rightarrow 0}$, we obtain the unsteady-state equation for unidirectional diffusion in solids:

$$\frac{\partial C_{Au}}{\partial t} = \frac{\partial}{\partial x} \left[\tilde{D} \frac{\partial C_{Au}}{\partial x} \right]. \quad (12.18)$$

We use this equation, which is often called *Fick's second law*, to obtain analytical solutions for diffusion problems. By comparing Eqs. (12.15) and (12.18), the relation between the more fundamental quantities, D_{Au} and D_{Ni} —called *intrinsic* diffusion coefficients—and the more useful quantity, \tilde{D} —called the *interdiffusion*, *mutual diffusion*, or *chemical diffusion* coefficient—is evident

$$\tilde{D} = X_{Ni}D_{Au} + X_{Au}D_{Ni}. \quad (12.19)$$

Figure 12.4 shows \tilde{D} for the gold-nickel system.

12.2.3 Darken's equations

Fick's laws contain the implicit assumption that the driving force for diffusion is the concentration gradient. A more fundamental viewpoint assumes that the driving force is a chemical free energy gradient. There is usually a direct correspondence between the two gradients, but occasionally the relationship becomes inverted and so-called "up-hill" diffusion, that is, diffusion against a concentration gradient, occurs. Darken³ provided an analysis of this situation.

The flux of A atoms passing through an unit area in the x -direction is \dot{n}_{Ax} , defined by

$$\dot{n}_{Ax} = \frac{-n_A B_A}{N_0} \left[\frac{\partial \bar{G}_A}{\partial x} \right], \quad (12.20)$$

³ \tilde{D} as the quantity used in diffusion calculations is often called simply the diffusion coefficient and denoted D .

³L. S. Darken, *Trans. AIME* **180**, 430 (1949).

where n_A is the number of A atoms per unit volume, B_A is the mobility of A atoms in the presence of the energy gradient, N_0 is Avogadro's number, and \bar{G}_A is the partial molar free energy of A (also called the chemical potential of A). Recalling from thermodynamics that

$$\bar{G}_A = G_A^0 + RT \ln a_A,$$

then Eq. (12.20) can be written as

$$\dot{n}_{Ax} = \frac{-n_A B_A RT}{N_0} \left[\frac{\partial \ln a_A}{\partial x} \right], \quad (12.21)$$

where a_A is the activity of A . Now comparing Eq. (12.21) to Fick's first law (Eq. (12.2)), we find that

$$D_A = B_A \kappa_B T \left[\frac{\partial \ln a_A}{\partial \ln X_A} \right], \quad (12.22)$$

where κ_B (Boltzmann's constant) = R/N_0 , and X_A is the mole fraction of A . Examine this expression as applied to a thermodynamically ideal solution with $a_A = X_A$. It reduces to

$$D_A = B_A \kappa_B T, \quad (12.23)$$

which is known as the *Nernst-Einstein* equation. If the mobility B_A , in the presence of a driving force, is independent of composition, then D_A in an ideal solution alloy is independent of composition. However, it is reasonable to expect B_A to be a function of composition in alloys and non-stoichiometric compounds and so, even if the solutions are thermodynamically ideal, D_A may still be a function of composition. In addition, due to the fact that $D_A^* = B_A^* \kappa_B T$ for self-diffusion, it is often stated that Eq. (12.23) may be written as $D_A^* = B_A \kappa_B T$ for an ideal solution. However, this is *not* true, unless fortuitously $B_A^* = B_A$, for there is no reason to think that B_A under the influence of an energy gradient should be the same as B_A^* with no energy gradient present. Figure 12.4 shows clearly that D_A^* is not a constant with composition; at best, one would have to know B_A^* as a function of composition, and since mobilities are usually computed *from* diffusion coefficient measurements, this becomes an exercise in rhetoric.

Only in one instance—in nonmetallic stoichiometric compounds—may B_A^* and B_A be the same, and D_A^* be calculated from an independent measurement (such as ionic electrical conductivity) of B_A . We shall learn more about this subject in Section 12.3.

Returning to Eq. (12.19), we can modify the expression. From the Gibbs-Duhem equation, we know that

$$\left[\frac{\partial \ln a_B}{\partial \ln X_B} \right] = \left[\frac{\partial \ln a_A}{\partial \ln X_A} \right], \quad (12.24)$$

and only if $B_A = B_A^*$ and $B_B = B_B^*$, then Eq. (12.19) can be written as

$$\tilde{D} = (X_A D_B^* + X_B D_A^*) \left[\frac{\partial \ln a_A}{\partial \ln X_A} \right]. \quad (12.25)$$

430 Fick's Law and Diffusivity of Materials

If we know the self-diffusion coefficients and the way in which the activity of A varies with composition, then we can calculate the interdiffusion coefficient, which is the useful value for engineering calculations. If the system is ideal, only then does Eq. (12.25) become

$$\tilde{D} = X_A D_B^* + X_B D_A^* \tag{12.26}$$

But since the restrictions that B_A equals B_A^* and B_B equals B_B^* apply, Eqs. (12.25) and (12.26) are of limited application.

Equation (12.25) does give insight into the conditions where diffusion may occur from the point of view of an uphill concentration gradient. The best-known example is the experiment carried out by Darken.⁴ He welded two pieces of carbon steel together and studied the diffusion of carbon, as schematically shown in Fig. 12.8. One of the bars contained 3.80% Si and 0.48% C, while the other contained only 0.44% C. Figure 12.8(a) shows the initial carbon distribution and we might expect that the carbon distribution would simply have evened out at 0.46% C. However, because silicon greatly increases the activity

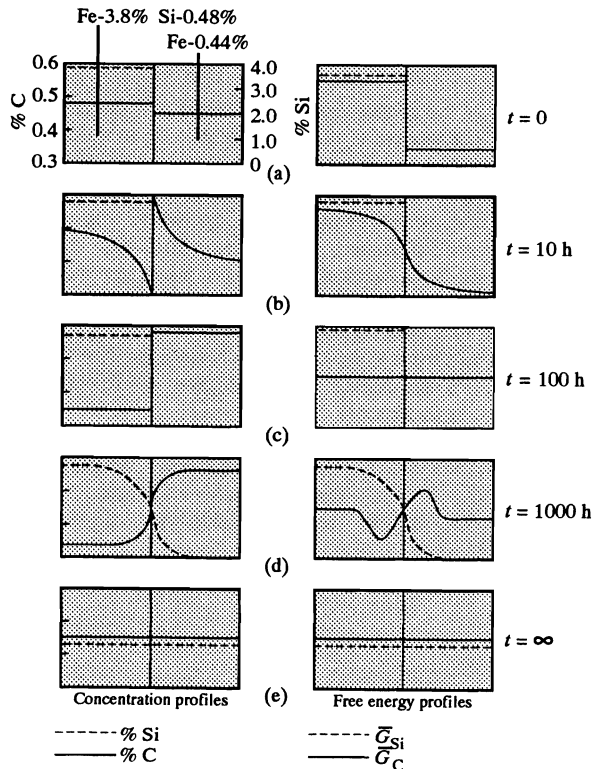


Fig. 12.8 Concentration and partial molar free-energy curves at various times for Fe-C and Fe-C-Si alloys welded together and annealed.

⁴L. S. Darken, *Trans. AIME*, Inst. Met. Div., Tech. Pub. 2443 (1948).

of carbon in iron, the carbon in the left-hand bar was at a much higher chemical potential than it would have been at if no silicon had been present. The result was that a sizeable amount of carbon diffused from left to right, and after a short time, the carbon gradient was as shown in Fig. 12.8(b). If the silicon did not diffuse, the final profile would look as in Fig. 12.8(c). If diffusion continues until both chemical potential curves are flat, not only for carbon but also for silicon, then the silicon will eventually diffuse to the right-hand side. The diffusion of silicon will be much slower than that of carbon, since it involves substitutional diffusion rather than the interstitial mechanism by which carbon diffuses. This means that the higher carbon concentration (created on the right-hand side before appreciable silicon diffusion occurred) will then decrease until ultimately both the silicon and carbon gradients become flat (Fig. 12.8(e)).

A formalism for treating diffusion in multicomponent solids can be found in Kirkaldy and Young⁵; they also discuss many examples of diffusion in ternary metallic solids.⁶

12.2.4 Temperature dependence of diffusion in solids

Temperature has a tremendous influence on diffusion in solids. Specifically, the Arrhenius equation adequately describes the relationship between any type of diffusion coefficient and temperature:

$$D = D_0 e^{-Q/RT}, \quad (12.27)$$

in which Q is the activation energy, and D_0 is sometimes called the frequency factor, both essentially constant over a wide temperature range.

Much effort has gone into the development of theoretical expressions for D_0 . Recall Eq. (12.5), in which the self-diffusion coefficient D^* is expressed in terms of the jump frequency ν and the interatomic distance δ . According to Zener,⁷ if the jump process is an activated one, then ν can be described by

$$\nu = \nu_0 Z e^{-\Delta G^\ddagger/RT}, \quad (12.28)$$

where ν_0 = vibrational frequency of the atom in the lattice, Z = coordination number, and ΔG^\ddagger = free energy of activation required for the atom to jump from one site into the next.

Since

$$\Delta G^\ddagger = \Delta H^\ddagger - T\Delta S^\ddagger,$$

then

$$D^* = D_0 e^{-(\Delta H^\ddagger/RT)}, \quad (12.29)$$

in which

$$D_0 = \frac{\delta^2 \nu_0 Z}{6} e^{(\Delta S^\ddagger/R)}.$$

⁵J. S. Kirkaldy and D. J. Young, *Diffusion in the Condensed State*, The Institute of Metals, London, 1986, pages 140-148.

⁶J. S. Kirkaldy and D. J. Young, *ibid.*, Chapter 7.

⁷C. Zener, *J. Applied Physics* **22**, 372 (1951).

ΔH^\ddagger is synonymous with Q , the activation energy for diffusion; δ , v_0 , and ΔS^\ddagger do not vary significantly with temperature, so the result is that D_0 varies with temperature only slightly. This is somewhat different from saying that D_0 is a constant, but for practical purposes it is a close approximation.

There are many data available on metallic systems, and some of these are presented in Figs. 12.9, 12.10, and 12.11. In addition, there are several rules that may be used to estimate Q and D_0 if data are completely missing. Sherry and Simnad⁸ developed a correlation equation for predicting self-diffusion data in pure metals:

$$D^* = D_0 e^{-(K_0 + v)(T_m/T)}, \quad (12.30)$$

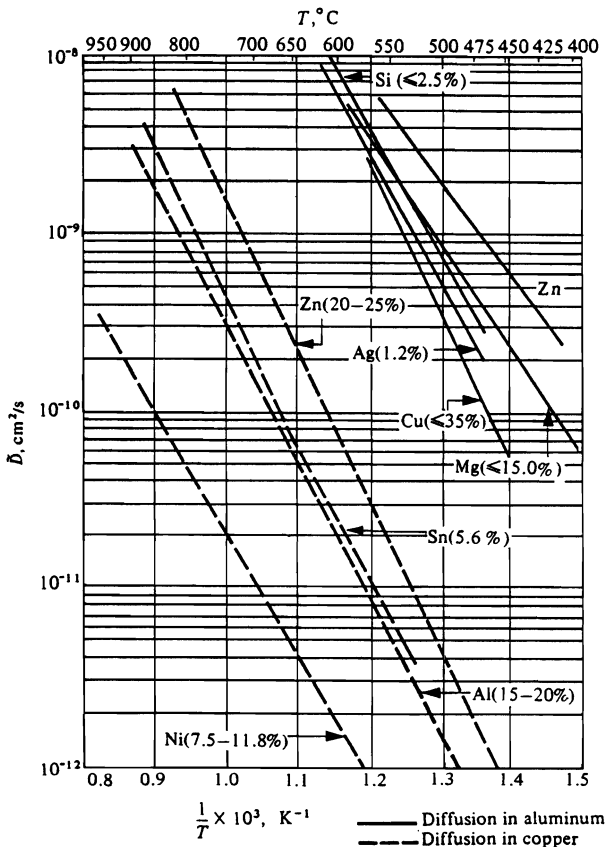


Fig. 12.9 Interdiffusion coefficients in nonferrous metals.

⁸O. D. Sherry and M. T. Simnad, *Trans. ASM* 54, 227 (1961).

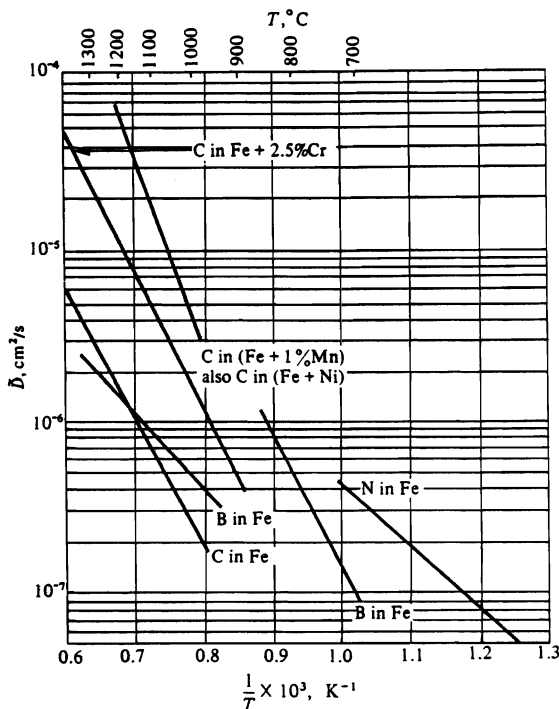


Fig. 12.10 Interdiffusion coefficients of interstitial elements through ferrous materials.

where K_0 depends only on the crystal structure, V is the normal valence of the metal, and T_M is the absolute melting point. The values of K_0 are

Crystal structure	K_0
bcc	14
fcc	17
hcp	17
Diamond	21

For estimation purposes, D_0 is approximated as $1 \times 10^{-4} \text{ m}^2 \text{ s}^{-1}$, as shown for most metals in Fig. 12.5. Furthermore, Q is predicted by

$$Q = RT_M(K_0 + V). \quad (12.31)$$

This correlation has been tested for self-diffusion in alloys, in which case T_M is taken as the temperature halfway between the liquidus and solidus for the alloy; it also applies to intrinsic diffusivities of solutes in dilute concentrations in a variety of solvent hosts, with reasonably satisfactory results.

By now the reader has surely surmised that diffusion in metals and alloys is of substantial scientific interest and engineering importance. In the limited space herein, we have only discussed *volume* diffusion effects, but we would be remiss not to at least alert the readers that *grain boundary* diffusion and *surface* diffusion are also very important. In most circumstances, volume diffusion dominates, but grain boundary diffusion (and hence the effect

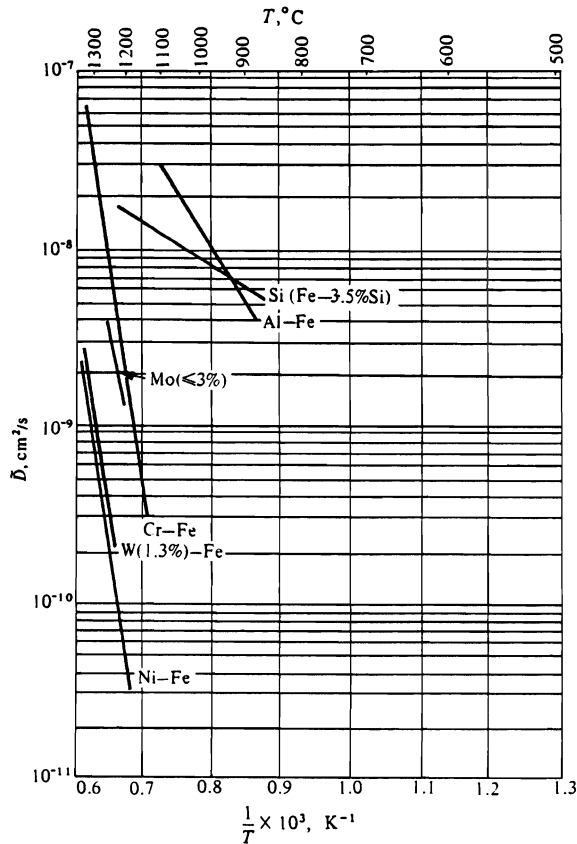


Fig. 12.11 Interdiffusion coefficients in ferrous materials.

of grain size) can be important in polycrystalline metals at relatively low temperatures and in thin films. Surface diffusion is important in sintering and in the growth of some thin films. Many of the references devoted to diffusion phenomena discuss grain boundary diffusion and surface diffusion.^{9,10,11,12}

⁹S. Mrowec, *ibid.*, pages 275-283.

¹⁰R. W. Baluffi in *Diffusion in Crystalline Solids*, G. E. Murch and A. S. Nowick, Editors, Academic Press, Orlando, 1984, Chapter 6.

¹¹J. S. Kirkaldy and D. J. Young, *ibid.*, pages 27-34.

¹²R. J. Borg and G. J. Dienes, *ibid.*, pages 139-144, 151-156.

12.3 DIFFUSION IN CERAMIC MATERIALS

The distinction between diffusion in metals and ceramics is mainly that ceramics have bonds with a significant component of ionic character. Even so, diffusion in these materials takes place via the same atomic mechanisms as in metals, but because of the electrical structure of the crystals, there is an additional strong relation between electrical conductivity and diffusion mechanisms. Their diffusion mechanisms, like those of metals, are closely related to atomic defects such as vacancies in the crystals, because these point defects provide the paths by which diffusion usually occurs. To discuss defects in nonmetals and their relationships to conduction and diffusion in any detail would consume at least an entire chapter, and would not serve the purpose of this text; we give, however, a short introduction to the subject. For more details we refer the reader to the several books available on this subject.* Diffusivities of ions in some crystals are given in Table 12.2.

Table 12.2 Diffusivities in nonmetallic crystals

Diffusing ion	Crystal in which diffusion takes place	D_0 , $\text{m}^2 \text{s}^{-1}$	Q , J mol^{-1}
Ag^+	$\alpha\text{-Cu}_2\text{S}$	38×10^{-9}	19 100
Cu^+	$\alpha\text{-Ag}_2\text{S}$	12×10^{-9}	13 300
Ag^+	$\alpha\text{-Cu}_2\text{Te}$	2.4×10^{-4}	87 300
Cu^+	$\alpha\text{-AgI}$	16×10^{-9}	9420
Li^+	$\alpha\text{-AgI}$	50×10^{-9}	19 100
Se^-	$\alpha\text{-Ag}_2\text{S}$	17×10^{-9}	83 850
Pb^{++}	PbCl_2	7.8×10^{-4}	150 000
Pb^{++}	PbI_2	10.6×10^{-4}	126 000
O^-	Fe_2O_3	$1 \times 10^{+7}$	611 000
Fe^{+++}	Fe_2O_3	$4 \times 10^{+1}$	469 000
Co^{++}	CoO	2.15×10^{-7}	144 000
Ni^{++}	NiO	1.83×10^{-7}	192 000
O^-	NiO	1.0×10^{-9}	226 000
Cr^{+++}	Cr_2O_3	1.37×10^{-5}	256 000

Stoichiometric AB crystals may contain several different types of point defects. The *Schottky defect* refers to equal numbers of cation and anion vacancies, that is, $[V_A] = [V_B]$.[†] The *Frenkel defect* may occur on either the cation or anion sublattice, when equal numbers of vacancies are balanced by interstitials of the same species, that is, $[V_A] = [A_i]$. An example of a material that exhibits Schottky defects is NaCl , in which $[V_{\text{Na}}] = [V_{\text{Cl}}]$. Frenkel

*W. Jost, *Diffusion in Solids, Liquids, Gases*, Academic Press, New York, 1960.

K. Hauffe, *Oxidation of Metals*, Plenum Press, New York, 1965.

O. Kubaschewski and B. E. Hopkins, *Oxidation of Metals and Alloys*, Plenum Press, New York, 1962.

P. Kofstad, *High Temperature Oxidation of Metals*, Wiley, New York, 1966.

F. A. Kroger, *Imperfections in Crystals*, North-Holland, New Amsterdam, 1964.

R. J. Borg and G. J. Dienes, *ibid.*

J. S. Kirkaldy and D. J. Young, *ibid.*

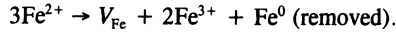
G. E. Murch and A. S. Nowick, Editors, *ibid.*

[†]In this discussion, the notation $[V_A]$ refers to the concentration, m^{-3} , of vacant A sites, $[A_i]$ refers to the concentration of A atoms on interstitial sites, and $[A_B]$ to the concentration of A atoms on sites normally occupied by B atoms. We alert the reader, however, that many use the bracket, $[\]$, for defect concentrations expressed on a fractional basis.

436 Fick's Law and Diffusivity of Materials

defects predominate in AgBr, in which $[V_{Ag}] = [Ag_i]$. If diffusion is via vacancies, any chemical additions that increase the concentration of vacancies will tend to increase the diffusion coefficient. For example, if $CdCl_2$ is added to NaCl, then, since the cadmium cation has a +2 charge, electrical balance in the crystal can only be maintained if one cation site is left vacant for every cadmium atom added, thus increasing $[V_{Na}]$.

Many ceramic materials show deviations from stoichiometry, which may be due to unequal concentrations of cation and anion defects. This is particularly true of transition metal oxides, such as TiO_2 , Nb_2O_5 , NiO, CoO, and wustite, Fe_xO . In the latter case, the defects are predominantly cation vacancies $[V_{Fe}]$, with charge neutrality maintained by the creation of Fe^{3+} ions according to the equation



Some of the trivalent iron ions may be ionized according to*



which results in an increase in electronic conduction via electron holes as further deviations from stoichiometry occur.

Because of the electrical nature of the defects and of the diffusing species (ions), ionic electrical conduction and diffusion are inseparable processes. Consider an ionic material in which one ionic species makes the predominant contribution to electrical conduction (for example, Na^+ cations in NaCl). The general equation for the transport of the species in the x -direction under the influence of an electric field and a concentration gradient in the x -direction is:

$$\dot{n}_{ix} = -D_i \left(\frac{\partial n_i}{\partial x} \right) - B_i n_i z_i e \left(\frac{\partial \phi}{\partial x} \right), \quad i \text{ ions m}^{-2} \text{ s}^{-1}, \quad (12.32)$$

where z_i = number of charges on the diffusing species,
 n_i = concentration of diffusing species, ions m^{-3} ,
 B_i = mobility of species i (steady-state velocity of the particle under the influence of a unit force), $m^2 s^{-1} V^{-1} C^{-1}$,
 D_i = the diffusion coefficient of species i , $m^2 s^{-1}$
 $e = 1.6 \times 10^{-19} C \text{ charge}^{-1}$,
 ϕ = electrical potential, V.

In the absence of a concentration gradient, the flux is

$$\dot{n}_{ix} = -B_i n_i z_i e \left(\frac{\partial \phi}{\partial x} \right), \quad i \text{ ions m}^{-2} \text{ s}^{-1}. \quad (12.33)$$

Note that in the physics and electrical engineering literature, $\sigma = ne\mu$, where μ is called the mobility. Since this is applied to electron or electron-hole conduction, $z = -1$ or $+1$, and therefore, $\mu = Be$. In this case, the units of σ are $ohm^{-1} m^{-1}$, n are m^{-3} , $e = 1.6 \times 10^{-19} C$, and $\mu = m^2 s^{-1} V^{-1}$.

Since the current density I is given by

$$I = \dot{n}_{ix} z_i e, \quad A m^{-2}, \quad (12.34)$$

The notation h^ is used to represent an electron hole in the valence band, contributing to p -type, or hole conduction; similarly, e' is the symbol for electrons in the conduction band.

then

$$I = -B_i n_i (z_i e)^2 \left[\frac{\partial \phi}{\partial x} \right]. \quad (12.35)$$

The electrical conductivity σ is defined by

$$\sigma_i = \frac{1}{-\left[\frac{\partial \phi}{\partial x} \right]} = -B_i n_i (z_i e)^2, \quad \text{ohm}^{-1} \text{ m}^{-1}. \quad (12.36)$$

Now by recalling Eq. (12.23), we can relate the electrical conductivity and diffusivity by the expression:

$$\frac{\sigma_i}{D_i} = \frac{n_i (z_i e)^2}{\kappa_B T}. \quad (12.37)$$

This equation is known as the "extended" Nernst-Einstein equation.

In order to predict D_i from conductivity measurements, we must know the fraction of the total conductivity due to species i ; this fraction is called the transference number of species i , denoted t_i . This number, obtained from electrolysis experiments, gives the fraction of the total current carried by a particular species, and the total of all transference numbers must equal one. Therefore

$$\sum_{\text{cation species}} t_{\text{cation } i} + \sum_{\text{anion species}} t_{\text{anion } i} + t_{\text{electron}} = 1. \quad (12.38)$$

Thus

$$\sigma_i = t_i \sigma_{\text{total}}, \quad \text{ohm}^{-1} \text{ m}^{-1}. \quad (12.39)$$

Equation (12.37) has been tested for several compounds. For example, in NaCl, $t_{\text{Na}^+} \cong 1$, so that $\sigma_{\text{measured}} \cong \sigma_{\text{Na}^+}$. Therefore, if we assume that all of the sodium ions in the crystal participate in the conduction process, then

$$D_{\text{Na}} = \frac{\sigma_{\text{total}} \kappa_B T}{n_{\text{Na}^+} e^2}, \quad (12.40)$$

where n_{Na^+} is the number of sodium ions per cubic meter. In order to test this, Mapother *et al.*¹³ measured the conductivity of NaCl and then, using radioactive sodium, measured diffusion coefficients of sodium, D_{Na}^T , both as functions of temperature. The values of D_{Na} calculated by means of Eq. (12.37) and the D_{Na}^T values are compared in Fig. 12.12. The agreement between the two values is excellent at the higher temperatures. The discrepancy at the lower temperatures points out the effect of CdCl₂ present as an impurity in NaCl in dilute concentration. By adding CdCl₂, $[V_{\text{Na}}]$ increases, thereby increasing D_{Na} over that in the pure material. However, the conductivity expression does not include this added effect, and the values differ when the concentration of vacancies due to CdCl₂ is significant, compared to the intrinsic concentration of vacancies.

¹³D. Mapother, H. N. Crooks, and R. Mauer, *J. Chem. Phys.* **18**, 1231 (1950).

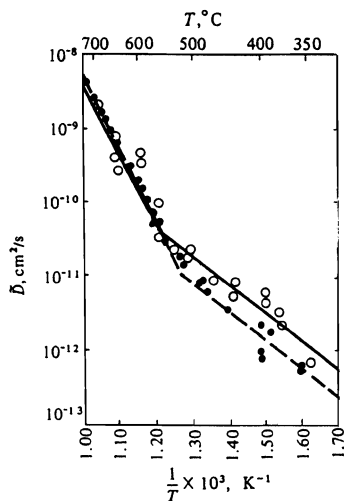
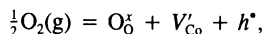


Fig. 12.12 Log D versus $1/T$ for sodium in NaCl as determined with radioactive sodium (\circ), and as calculated from the conductivity (\bullet). (From D. Mapother, H. N. Crooks, and R. Mauer, *J. Chem. Phys.* **18**, 1231 (1950).)

Non-stoichiometry, resulting in vacancies on the cation sublattice, can also have an effect on D_i^* (and through Eq. (12.25) or (12.26) on \bar{D}) in the same manner as impurities. For example, CoO exists as a non-stoichiometric oxide with defects on the cation sublattice in the form of vacancies.¹⁴ This amounts to the addition of an oxygen anion without addition of a cation, according to the reaction



where O_0^x indicates an excess oxygen ion on a regular oxygen site, V_{Co}' a singly-ionized cation vacancy, and h^* a free electron hole. The notation for building the superscripts is x means neutral (for example, Na^+ substituting for Li^+), \bullet means positive (and multiple dots means multiple positive), and $'$ means negative (and again, multiple $'$ define multiple negative).

Presumably, diffusion of Co^{++} ions should be via a vacancy mechanism on the cation sublattice, with diffusivity increasing as the concentration of cation vacancies increases. The phase diagram (Fig. 12.13) shows the Co-CoO equilibrium. When P_{O_2} is increased above that existing at this lower boundary of the CoO phase field, the molar concentration of Co decreases as oxygen is added to the oxide, until finally an oxygen pressure is reached at which $X_{\text{Co}} = 0.492$ (corresponding to $\text{Co}_{0.969}\text{O}$) beyond which Co_3O_4 forms. This occurs at $P_{\text{O}_2} = 0.53$ atm at 1000°C . Price and Wagner measured chemical diffusion coefficients in CoO by equilibrating a single crystal of CoO with an atmosphere at low P_{O_2} (4.7×10^{-2} atm); then, at time zero, they changed the oxygen potential to a higher level, near the CoO- Co_3O_4 boundary. The change in X_{Co} ($= -X_{\text{Co}}$) is measured as a function of time by following the change in electrical conductivity, since the conductivity in this material is proportional to the concentration of electron holes, which is dependent, in turn, on the oxygen content through the equilibrium constant for the reaction shown above:

$$K = \frac{[h^*][V_{\text{Co}}']}{P_{\text{O}_2}^{1/2}}$$

¹⁴J. B. Price and J. B. Wagner, Jr., *Zeit. f. physik. Chemie, Neue Folge* **49**, 3-4 (1966).

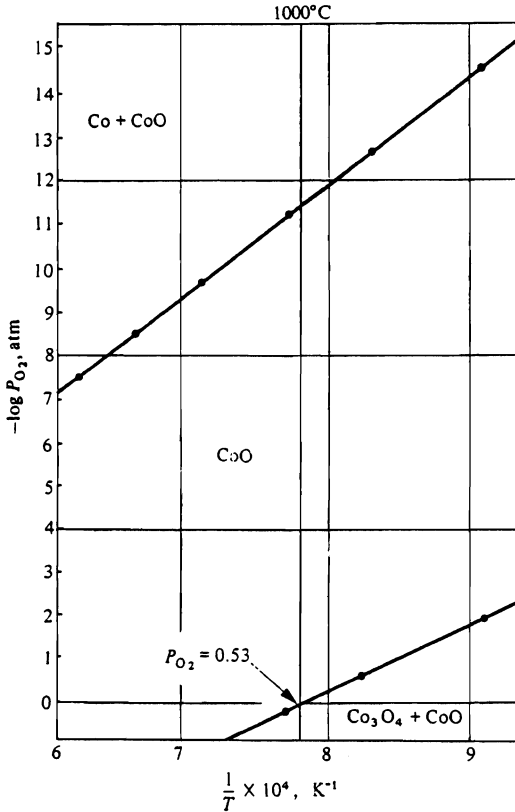


Fig. 12.13 The stable phase field of cobaltous oxide with respect to oxygen pressure and temperature.

Although \tilde{D} is generally composition-dependent in non-stoichiometric crystals, in this case the deviations from non-stoichiometry are small, and \tilde{D} is found to be essentially constant with composition:

$$\tilde{D} = 4.33 \times 10^{-7} \exp (-24\,000/RT), \text{ m}^2 \text{ s}^{-1}.$$

Since the cobalt cation is much smaller than the oxygen anion, D_{Co} is very much greater than D_O in CoO. Then we may use Eq. (12.25), neglecting the term $D_O^* X_{Co}$, if we further assume that $B_{Co} = B_{Co}^*$ in order to calculate D_{Co}^* from the \tilde{D} data:

$$\tilde{D} \cong D_{Co}^* X_O \left[\frac{\partial \ln a_{Co}}{\partial \ln X_{Co}} \right].$$

We may calculate the thermodynamic factor by noting that

$$\left(\frac{\partial \ln a_{\text{Co}}}{\partial \ln X_{\text{Co}}} \right) = - \left(\frac{\partial \ln a_{\text{O}}}{\partial \ln X_{\text{Co}}} \right),$$

and that

$$a_{\text{O}} = \left(\frac{P_{\text{O}_2}}{P_{\text{O}_2}^0} \right)^{1/2},$$

where $P_{\text{O}_2}^0$ is the standard oxygen pressure, 1 atm. We obtain the slope of the $\log a_{\text{O}}$ versus $\log X_{\text{O}}$ plot from the data of Error and Wagner,¹⁵ who measured $[V_{\text{Co}}]$ as a function of P_{O_2} across the CoO phase field:

$$\begin{aligned} - \left(\frac{\partial \ln a_{\text{O}}}{\partial \ln X_{\text{Co}}} \right) &\cong - \left(\frac{\Delta \log a_{\text{O}}}{\Delta \log X_{\text{Co}}} \right) = - \left[\frac{\frac{1}{2} (\log P_{\text{O}_2, \text{initial}} - \log P_{\text{O}_2, \text{final}})}{\log X_{\text{Co, initial}} - \log X_{\text{Co, final}}} \right] \\ &= - \left[\frac{\frac{1}{2} (\log 4.7 \times 10^{-2} - \log 5.1 \times 10^{-1})}{\log (0.4963) - \log (0.4936)} \right] = +1.45 \times 10^2. \end{aligned}$$

At 1000°C, $\tilde{D} = 2.16 \times 10^{-11} \text{ m}^2 \text{ s}^{-1}$, and $X_{\text{O}} \cong 0.50$. Substituting into Eq. (12.25) as simplified above, we find D_{Co}^* to be $2.98 \times 10^{-13} \text{ m}^2 \text{ s}^{-1}$. Applying the correlation coefficient, $f = 0.78$ for the fcc cation sublattice, then

$$D_{\text{Co}}^T = 0.78 D_{\text{Co}}^* = 2.33 \times 10^{-13} \text{ m}^2 \text{ s}^{-1} \quad (\text{calculated}),$$

which is in good agreement with Carter and Richardson's¹⁶ measured value

$$D_{\text{Co}}^T = 2.60 \times 10^{-13} \text{ m}^2 \text{ s}^{-1} \quad (\text{measured}).$$

In some oxides, ionic conduction is unusually high; these are called *super ionic conductors*. These oxides have unusually high concentrations of charge carriers and vacancies or interstitial ions. One example is β -alumina, which is a sodium aluminate of variable composition between $(\text{Al}_2\text{O}_3)_{5.33}\text{Na}_2\text{O}$ and $(\text{Al}_2\text{O}_3)_{8.5}\text{Na}_2\text{O}$. The sodium atoms are the fast-diffusing species, because they occupy sites in a crystal plane that is sparsely populated and can therefore diffuse easily via the large number of vacant sites in that plane. Another material that exhibits fast ionic transport is zirconia, which is stabilized with either calcia (CaO) or yttria (Y_2O_3). In this case, the oxygen anions diffuse six orders of magnitude faster than the cations because there is a very large concentration of O^{2-} vacancies, which is controlled by the concentration of Ca^{2+} or Y^{3+} .

When molten silicate is cooled to form a rigid glass, there remain spaces, where the monovalent and divalent metallic ions reside amongst the network structure. This is discussed in more detail in Chapter 1. The silicon ions are integral to the covalently bonded network so their mobility is extremely limited. On the other hand, the ions in the spaces diffuse readily.

¹⁵N. Error and J. B. Wagner, Jr., *J. Phys. Chem. Solids* **29**, 1597 (1968).

¹⁶R. E. Carter and F. D. Richardson, *J. Metals* **200**, 1244 (1954).

The diffusion coefficient of sodium ions in a silicate glass is shown in Fig. 12.14. In the range of 870 to 910 K, there is a transition in the diffusion coefficient. At temperatures above the transition, the silicate can be regarded as supercooled liquid, whereas below the transition the silicate is a rigid glass, which affords considerably less mobility of the sodium ions.

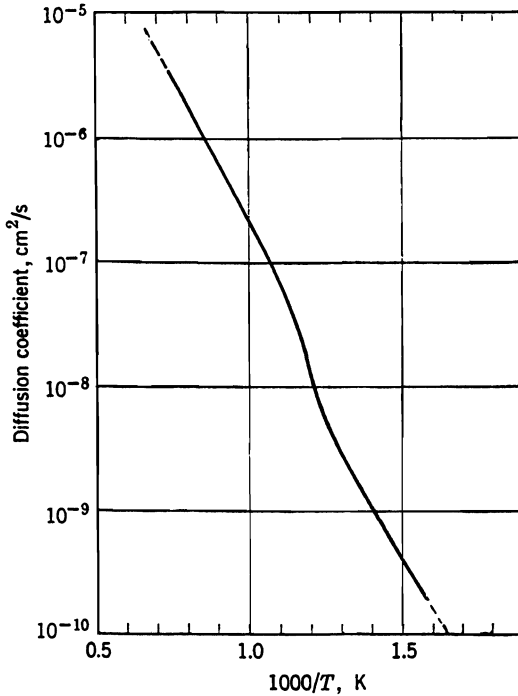


Fig. 12.14 Diffusion of Na^+ in a sodium silicate glass. (From W. D. Kingery, *Introduction to Ceramics*, John Wiley, New York, 1960, page 239.)

The spaces in the silicate structure also allow for diffusion of many other ions and small atoms; notable are hydrogen and water vapor. Depending on the composition of the glass, diffusion of molecular H_2 can be accompanied by OH^- ions, which result from the formation of $(\text{Si}^{4+}\text{O}^{2-}\text{OH}^-)^{-1}$ groups. Water vapor probably diffuses as both H_2O and OH^- ions, which are part of $(\text{SiOH})^{3+}$ groups.

Typically diffusion coefficients in glasses are several orders of magnitude greater than they are in crystalline solids. This has the consequence that the presence of a small amount of a glassy phase in a ceramic has a very strong effect on diffusion-controlled processes in a multiphase system.

A good review of the mechanisms of diffusion in oxide glasses and extensive listings of diffusion data are given by Frischat.¹⁷

¹⁷G. H. Frischat, *Ionic Diffusion in Oxide Glasses*, Trans Tech Publications, Aedermannsdorf, Switzerland, 1975.

12.4 DIFFUSION IN ELEMENTAL SEMICONDUCTORS

Because of their technological importance, and the sophistication of their processing, almost all of which involves diffusion treatments, it is important to know something about the diffusion of alloying elements (dopants) and impurities in silicon and germanium. Both of these elements are intrinsic semiconductors; that is, they have energy band gaps that are small enough that thermal excitation of electrons into a conduction band occurs. Their intrinsic conductivities increase with increasing temperature.

Germanium is tetravalent; the four outer electrons form covalent bonds with four neighboring Ge atoms. If a pentavalent impurity, such as phosphorous, is substituted for germanium, the extra outer electron associated with phosphorous is easily activated into the conduction band, increasing the material's electronic, or n -type conductivity. Conversely, if a trivalent impurity, such as boron, is substituted for a germanium atom, the band is short of one electron, which may be provided from the electrons in the valence band, leaving behind a hole or positive conduction charge and contributing to p -type conductivity, when the number of such atoms is greater than the number of intrinsic conduction electrons.

Diffusion in germanium is primarily by a vacancy mechanism. Table 12.3 gives the constants that can be used with Eq. (12.27) to calculate diffusion coefficients for various elements in Ge, and Fig. 12.15 shows that the diffusion of pentavalent elements is faster than for Ge self-diffusion, leading to the conclusion that vacancies are electron acceptors, stimulating the diffusion of the n -type dopants. The converse appears to be true of Group III elements.

Silicon, on the other hand, exhibits more complex mechanistic behavior. At temperatures below 1440 K, self-diffusion is thought to take place via the vacancy mechanism; above that temperature interstitial motion dominates. Table 12.4 and Fig. 12.16 give diffusion coefficients for impurities in silicon. In this case, all of the elements diffuse faster than the silicon itself.*

Table 12.3 Diffusion constants in Ge

Element	$D_0, \text{m}^2 \text{s}^{-1}$	$Q, \text{kJ mol}^{-1}$
Ge	1.85×10^{-3}	296
B	1.1×10^{-3}	438
Al	1.6×10^{-2}	313
Ga	4.0×10^{-3}	304
In	3.3×10^{-3}	292
P	2.5×10^{-4}	240
As	1.03×10^{-3}	242
Sb	3.2×10^{-4}	234
Li	3.1×10^{-7}	49
Cu	4.0×10^{-7}	32

(From R. J. Borg and G. J. Dienes, *ibid.*, page 197.)

The elements Li and Cu diffuse as interstitials so their activation energies are much lower than the energies of the other elements, which are substitutional. This relates to a potential processing problem in microelectronics. That is, extraneous interstitial impurities that diffuse very quickly can poison or modify intentionally doped regions in semiconductors and kill devices. This emphasizes one reason that microelectronic processing must be done in a very clean environment.

*For a more detailed discussion of the mechanism, refer to R. J. Borg and G. J. Dienes, *ibid.*, pages 198-202.

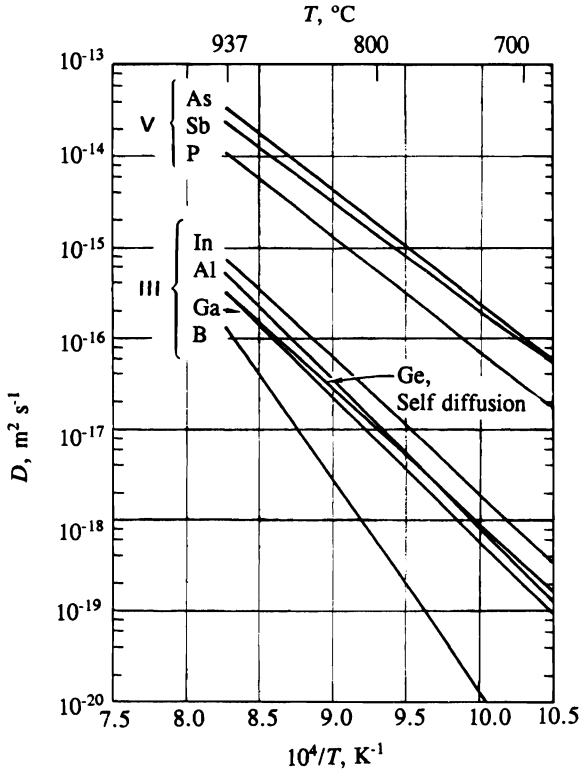


Fig. 12.15 Diffusion coefficients for Group III and Group V elements in Ge. (From R. J. Borg and G. J. Dienes, *ibid.*, page 196.)

Table 12.4 Diffusion constants in Si

Element	$D_0, \text{m}^2 \text{s}^{-1}$	$Q, \text{kJ mol}^{-1}$
B	5.1×10^{-4}	357
Al	8.0×10^{-4}	335
Ga	3.6×10^{-4}	339
In	16.5×10^{-4}	377
P	10.5×10^{-4}	356
As	60.0×10^{-4}	405
Sb	12.9×10^{-4}	384
Bi	1.03×10^{-1}	447

(From R. J. Borg and G. J. Dienes, *ibid.*, page 201.)

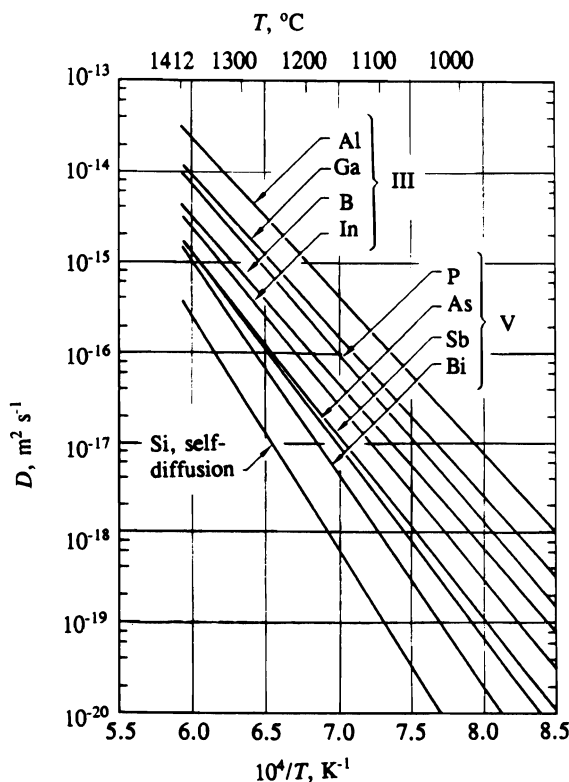


Fig. 12.16 Diffusion coefficients for Group III and Group V elements in Si. (From R. J. Borg and G. J. Dienes, *ibid.*, page 201.)

12.5 DIFFUSION IN LIQUIDS

As in the previous chapters, in which the transport properties of liquids were discussed, the predicting, correlating, and extrapolating of diffusion data in liquids are difficult because of our lack of understanding of the structure of liquids. The difficulties of making accurate experimental determinations of diffusion coefficients in liquids due to natural convection, and the problems of sampling, further complicate the diffusion problem. In the following sections, we discuss various theories of the liquid state as they relate to diffusion, and then present data for a variety of liquids.

12.5.1 Liquid state diffusion theories

Hydrodynamical theory. The earliest theoretical equation for prediction of self-diffusion in a liquid is that of Einstein.¹⁸ In this theory, the diffusing species are non-reacting spherical particles of radius R moving through a continuous medium of viscosity η with

¹⁸A. Einstein, *Ann. Phys. (Leipzig)* 17, 549 (1905).

steady-state velocity V_∞ . According to Eq. (2.119), the force on a sphere moving at steady-state in laminar flow is

$$F = 6\pi R\eta V_\infty, \quad (2.119)$$

and since the definition of the mobility B is V_∞/F , we have

$$B = \frac{1}{6\pi R\eta}.$$

Combining this result with Eq. (12.23), we get

$$D = \frac{\kappa_B T}{6\pi R\eta}, \quad (12.41)$$

which is known as the Stokes-Einstein equation. This was then modified by Sutherland,¹⁹ who adopted a slightly different form of the drag force, with the result that

$$D = \frac{\kappa_B T}{4\pi R\eta}. \quad (12.42)$$

This equation is known as the Sutherland-Einstein equation.

Although the use of Stokes' law for this purpose may seem unjustified, since it neglects interatomic forces and considers only form drag, the results, in terms of predicted data, are remarkable. For example, in liquid metals, if we substitute the measured values of D^* and η into Eq. (12.42) and then calculate the radii of the diffusing species, we obtain very good agreement between these predicted radii and the radii of ions, as shown in Table 12.5.

Table 12.5 Comparison of calculated and Pauling radii for self-diffusion in liquid metals

Element	Temperature range, °C	Sutherland model, nm	Pauling radii, * nm
Na	110-630	0.151-0.453	0.157
Hg	274-364	0.120-0.124	0.139
In	448-1013	0.136-0.306	0.142
Ag	977-1397	0.137-0.137	0.134
Zn	394-837	0.129-0.075	0.121
Sn	575-956	0.130-0.222	0.142

^{*}The radii used for comparison are those reported by Pauling for single-bond metallic situations. See L. Pauling, *Nature of the Chemical Bond*, Cornell University Press, Ithaca, NY, 1960, page 403.

In the comparisons shown in Table 12.5, self-diffusion data of pure elements were used to calculate the radii in the third column. Equations (12.41) and (12.42) have also been used to explain diffusing particles that differ in size from the host.²⁰ When the radius of the diffusing particle is large compared to the host, Eq. (12.41) is the better choice. When the radius of the diffusing particle is approximately equal to that of the host, then Eq. (12.42) is better. In spite of the shortcomings of the hydrodynamic assumptions leading to Eqs. (12.41)

¹⁹W. Sutherland, *Philosophical Magazine* **9**, 781 (1905).

²⁰T. Iida and R. I. L. Guthrie, *The Physical Properties of Liquid Metals*, Clarendon Press, Oxford, 1988, pages 214-215.

446 Fick's Law and Diffusivity of Materials

and (12.42), they have proven to be useful in that they have been used as the basis for semiempirical equations of the form

$$D^* = A \left(\frac{T_M}{M} \right)^{1/2} V_M^{1/3}, \quad (12.43)$$

where A is a constant, M is the atomic weight or molecular weight, T_M is the melting point, and D^* and V_M are self-diffusion coefficient and molar (or atomic) volume, respectively, each evaluated at T_M . For liquid metals, Turkdogan²¹ recommends $A = 3.27 \times 10^{-6}$ and Iida and Guthrie²² recommend 3.5×10^{-6} , when the variables in Eq. (12.43) are in c.g.s. units.

The Sutherland-Einstein equation is useful in predicting self-diffusion data for a wide variety of other substances, including molten semiconductors, polar liquids, associated liquids, and molten sulfur. If we assume that the atoms in the liquid are in a cubic array, then for materials generally the simple theory predicts that

$$2R = (\hat{V}/N_0)^{1/3},$$

and

$$D^* = \frac{\kappa_B T}{2\pi} \left(\frac{N_0}{\hat{V}} \right)^{1/3}, \quad (12.44)$$

where \hat{V} is the molar volume and N_0 is Avogadro's number.

Hole theory. The oldest *structural* picture of a liquid is the hole theory which presumes the existence of holes or vacancies randomly distributed throughout the liquid and providing ready diffusion paths for atoms or ions. The concentration of these holes would have to be very great in order to account for the volume increase upon melting, thus resulting in much higher diffusion rates in liquids than in solids just below the melting point. This jump in D on melting is obvious in Fig. 12.5. The hole theory, however, does not result in a prediction of diffusion coefficients by itself, although it has been used to estimate the activation energy for self-diffusion in a liquid, by assuming that this energy is equal to that required to form a hollow sphere (hole) of a diameter on the order of a fraction of a nanometer.

Eyring theory. Eyring *et al.*²³ applied their activated state theory of diffusion, which works reasonably well in solids, to liquid diffusion, assuming that the migrating atoms move from hole to hole in the liquid by a process of discrete jumps. If the liquid is considered quasi-crystalline, and the atoms are in a cubic configuration, then an expression relating D^* and η results:

$$D^* = \frac{\kappa_B T}{2R\eta}. \quad (12.45)$$

²¹E. T. Turkdogan, *Physical Chemistry of High Temperature Technology*, Academic Press, New York, 1980, page 115.

²²T. Iida and R. I. L. Guthrie, *ibid.*, page 212.

²³H. Eyring, S. Glasstone, and K. Laidler, *Theory of Rate Processes*, McGraw-Hill, New York, 1941.

This expression obviously predicts D^* values six times larger than that given by the Sutherland-Stokes equation. Subsequent revisions of this equation by Li and Chang,²⁴ and by Eyring *et al.*²⁵ improved the agreement with the Sutherland-Stokes equation, but do not shed any more light on the structure of liquids, nor are they any more useful from a prediction standpoint.

Fluctuation theory. Because the ideas of a well-defined "activated state" as well as of discrete "holes" in the liquid have been difficult to accept, Cohen and Turnbull,²⁶ and later, Swalin²⁷ and Reynik²⁸ developed the fluctuation theory. In this theory, the "extra" volume in the liquid (over that of the solid) is distributed evenly throughout the liquid, making the *average* nearest neighbor distance increase. One may imagine a diffusing atom contained in a cage whose dimensions are constantly fluctuating. Local fluctuations in density then occasionally open up holes or openings in the cage large enough to allow the atom to diffuse out of the cage. In their approach, Cohen and Turnbull consider that a critical fluctuation must occur before diffusion occurs, whereas Swalin and Reynik both think that a spectrum of fluctuations occurs, with cooperative motion of the neighboring atoms resulting in diffusive motion of an atom. No activation energy is required, since there is virtually no difference between an atom moving forward as a result of cooperative movements and an atom not moving. The result of Swalin's theory^{29,30} is that D^* exhibits a linear dependence on temperature.

Reynik proposed a small fluctuation model which also predicts a linear temperature dependence of D^* on T (K):

$$D^* = a + bT, \quad \text{cm}^2 \text{ s}^{-1}, \quad (12.46)$$

where $a = 1.72 \times 10^{24} ZX_0^4 K$, $b = 2.08 \times 10^9 ZX_0$, Z = number of nearest neighbors, X_0 = maximum diffusive displacement due to normal vibrations, \AA , and K = a force constant.

Since

$$X_0 = \bar{d} - 2R, \quad (12.47)$$

where \bar{d} = average interatomic distance in the liquid, \AA , and R = ion radius, \AA , the evaluation of this theory relies on the use of x-ray data for \bar{d} and Z , and b -values obtained from correlations to fit an equation of the form of Eq. (12.46). From the calculated values of X_0 and Eq. (12.47), R -values are obtained which agree quite closely with Pauling's neutral atom radii, suggesting that in liquid metals the diffusing ion core carries its valence electrons with it.

The problem of all the theoretical approaches is that the tests of the theories rely on the functional relationship between D and T . For example, while Reynik can reasonably fit liquid

²⁴J. C. M. Li and P. Chang, *J. Chem. Physics* **23**, 518 (1955).

²⁵H. Eyring, T. Ree, D. Grant, and R. Hirst, *Z. Elektrochem.* **64**, 146-152 (1962).

²⁶M. H. Cohen and D. Turnbull, *J. Chem. Physics* **31**, 1164 (1959).

²⁷R. A. Swalin, *Acta Met.* **7**, 736 (1959).

²⁸R. J. Reynik, *Trans. AIME* **245**, 75 (1969).

²⁹R. J. Reynik, *Applied Physics Letters* **9**, 239 (1966).

³⁰R. Swalin and V. G. Leak, *Acta Met.* **13**, 471 (1965).

metal diffusion data to a linear relationship, Saxton and Sherby³¹ concluded that diffusion in liquid metals is a thermally activated process, obeying an Arrhenius relationship (Eq. (12.27)), which is clearly at odds with a linear relationship with T . The activation energies Q are apparently not large, and so, when the RT term is on the same order of magnitude as Q , D is not a strong function of temperature. Thus critical tests of these models is difficult.

It should also be stated that the methods of molecular dynamics and computer simulations have recently shown that the concepts of "holes" and activated rate theory do not physically represent diffusion in non-ionic liquids.³² The reason becomes quite clear if we look at the results of simulations of trajectories of molecules in a solid, liquid, and gas, which are shown in Fig. 12.17.

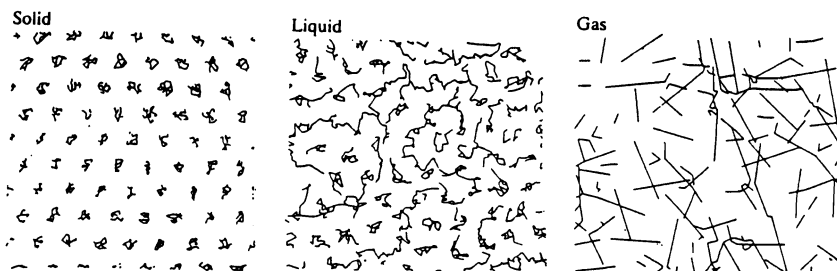


Fig. 12.17 Simulations of trajectories of molecules in solid, liquid, and gas. (Reproduced from T. Iida and R. I. L. Guthrie, *ibid.*, page 5.)

In the solid, the molecules are constrained to highly localized positions in the crystal, whereas the molecules in the liquid and the gas are free to wander. The major differences between the two fluids are the mean free path between collisions and the average velocity of the particles. Therefore, activated rate theory, which has proven to be quite useful in understanding diffusion in solids, does not appear to be applicable for diffusion in liquids.

12.5.2 Liquid diffusion data

The remarkable characteristic of diffusion in liquid metals, and in liquids in general, is the fact that the values of D are almost all approximately the same order of magnitude, 10^{-8} - 10^{-9} $\text{m}^2 \text{s}^{-1}$, even though their solid-state properties differ widely. Furthermore, the activation energies are also approximately equal, usually in the range 4 to 16 kJ mol^{-1} . Because the data are still presented in the Arrhenius form, we present the data in this section in the same way.

Diffusion in liquid metals. Figure 12.18 gives some data for self-diffusion in pure liquid metals, Fig. 12.19 for interdiffusion in common nonferrous binary alloys, and Fig. 12.20 for

³¹H. Saxton and O. Sherby, *Trans. ASM* 55, 826 (1962).

³²J. S. Kirkaldy and D. J. Young, *ibid.*, page 90.

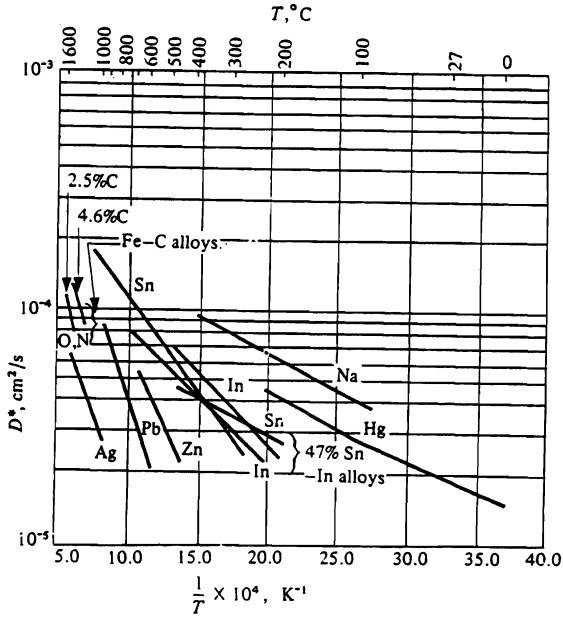


Fig. 12.18 Self-diffusion data in liquid metals.

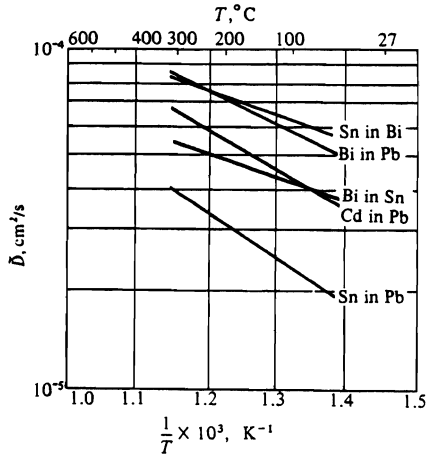


Fig. 12.19 Interdiffusion coefficients in liquid nonferrous alloys.

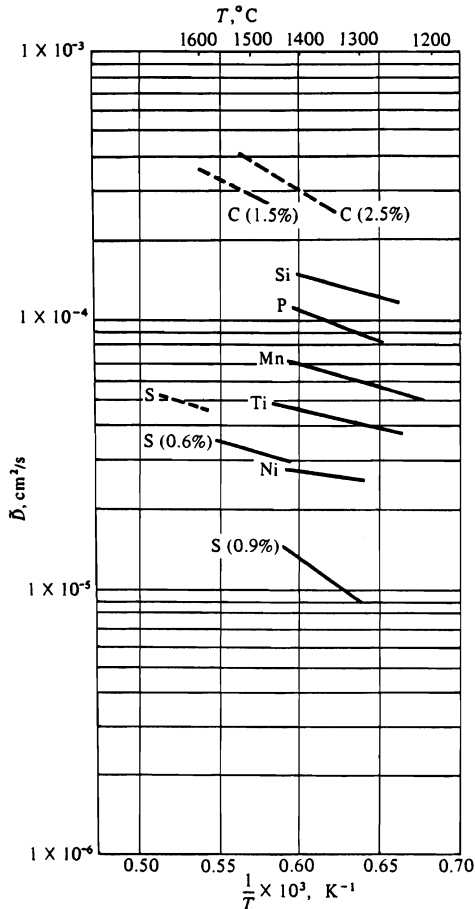


Fig. 12.20 Interdiffusion coefficients in ferrous liquid alloys
(——— carbon-saturated; - - - pure Fe).

ferrous alloys. We refer the reader to Edwards *et al.*,³³ Yang and Derge,³⁴ Elliott *et al.*,³⁵ or Brandes³⁶ for listings of data.

Diffusion in molten salts and silicates. Again, we know so little of the detailed structure of molten halides, sulfides, oxides, and silicates, that no really satisfactory quantitative expression is available for predicting diffusivities in these materials. However, if we refer

³³J. B. Edwards, E. E. Huccke, and J. J. Martin, *Metallurgical Reviews* **13**, No. 120, 1 (1968).

³⁴L. Yang and G. Derge, paper in *Physical Chemistry of Process Metallurgy*, AIME **7**, 195 (1961).

³⁵J. F. Elliott, M. Gleiser, and V. Ramachrishna, *Thermochemistry for Steelmaking II*, Addison-Wesley, 1963.

³⁶E. A. Brandes (Editor), *Smithells Metals Reference Book*, Sixth Edition, Butterworths, London, 1983, Chapter 13.

to Chapter 1 in which we discussed the relationship between bonding and viscosity, we realize that the same semiquantitative arguments can be used with regard to diffusion in these materials, particularly in light of the Stokes-Einstein model of diffusion.

Consider first the molten salts. We may describe their structure as holes within a molecular assembly that has density fluctuations and short-range order, but with the added restriction of electroneutrality, so that the cation and anion charge densities must remain equal in any region of the melt. Diffusion coefficients measured in molten salts are remarkably close to values observed in liquid metals, even though there is an obvious difference in bonding. Molten salts have highly polarized ionic bonds, in contrast to the metallic bond. Table 12.6 gives some typical data for self-diffusion in molten salts. Note that the activation energies for the salts are, however, larger than the activation energies for self-diffusion in metals.

Table 12.6 Self-diffusivities in molten salts[†]

Diffusate	Melt	Temp. range, °C	$D_0 \times 10^8$, $\text{m}^2 \text{s}^{-1}$	Q , kJ mol^{-1}	Typical D^* value, $\text{m}^2 \text{s}^{-1}$	°C
Na	NaCl	845-916	8	16.7	14.2×10^{-9}	906
Cl	NaCl	825-942	23	29.7	8.8×10^{-9}	933
Na	NaNO ₃	315-375	12.88	20.8	2.00×10^{-9}	328
NO ₃	NaNO ₃	315-375	8.97	21.2	1.26×10^{-9}	328
Tl	TlCl	487-577	7.4	19.2	3.89×10^{-9}	502
Zn	ZnBr ₂	394-650	790	67.2	0.22×10^{-9}	500

[†]Data from L. Yang and G. Derge, *ibid.*

In molten silicates, the picture is more complicated; from the relation between the degree of polymerization of the silicates and their viscosity, we can postulate that the diffusivity of oxygen, for example, is lower in the more acid silicates, and increases rapidly as the concentration of free oxygen ions increases near the orthosilicate composition. On the other hand, the diffusivity of basic cations should not depend on the slag composition to such an extent.

There are relatively few diffusion data available for molten silicates; some, which are relevant to metallurgical slags and mattes, are presented in Table 12.7. The curious result, which has not yet been satisfactorily explained, is that the tracer self-diffusion coefficient of oxygen in a basic slag is greater than the self-diffusion coefficients of calcium in the same slag. It is also greater than that of silicon and aluminum, but we may explain this on the basis that silicon is tied up in SiO_4^{4-} ions, which clearly do not diffuse as easily as the smaller O^{2-} ions; aluminum is probably tied up in AlO_3^{3-} ions, which diffuse only a fraction more easily than the SiO_4^{4-} ions. Note also that the activation energies are now quite large, in correspondence to the increased difficulty of movement of these complex molecules, presumably requiring much more complicated relative movements of nearest neighbor ions in order to affect any net movement of a molecule. Diffusion data for slags and liquid glasses are also reviewed and presented by Turkdogan.³⁷

³⁷T. T. Turkdogan, *Physicochemical Properties of Molten Slags and Glasses*, The Metals Society, London, England, 1983, pages 40-51.

Table 12.7 Self-diffusivities in molten silicates and sulfides[†]

System	Temp. range, °C	$D_0 \times 10^8$, $\text{m}^2 \text{s}^{-1}$	Q , kJ mol^{-1}	D^* , $\text{m}^2 \text{s}^{-1}$
Ca in CaO-Al ₂ O ₃ -SiO ₂ (39/21/40)	1350-1540	—	290	6.7×10^{-11} (1673 K)
Ca in CaO-Al ₂ O ₃ -SiO ₂ (40/20/40)	1350-1450	—	290	$6.2\text{-}6.7 \times 10^{-11}$ (1673 K)
Si in CaO-Al ₂ O ₃ -SiO ₂ (40/20/40)	1350-1460	—	290	1×10^{-11} (1703 K)
O in CaO-Al ₂ O ₃ -SiO ₂ (40/20/40)	1370-1520	—	40	4×10^{-10} (1703 K)
Fe in CaO-Al ₂ O ₃ -SiO ₂ (30/15/55)	1500	—	—	$2.4\text{-}3.1 \times 10^{-10}$
Fe in CaO-Al ₂ O ₃ -SiO ₂ (43/22/35)	1500	—	—	$2.1\text{-}5.0 \times 10^{-10}$
Fe in FeO-SiO ₂ (61/39)	1250-1305	—	170	9.6×10^{-9} (1548 K)
P in CaO-Al ₂ O ₃ -SiO ₂ (40/21/39)	1300-1500	—	195	2×10^{-10} (1673 K)
Fe in Fe-S (33.5%)	1150-1238	65.7	56.9	
Fe in Fe-S (31.0%)	1164-1234	298	71	
Fe in Fe-S (29.0%)	1158-1254	20 200	116	
Fe in Fe (48.1%)-Cu (20.5%)-S (31.9%)	1160-1250	1440	90.0	
Fe in Fe (32.0%)-Cu (40.0%)-S (28.0%)	1168-1244	35.7	57.3	
Cu in Cu-S (19.8%)	1160-1256	69.3	53.6	
Cu in Fe (32.0%)-Cu (40.0%)-S (28.0%)	1160-1245	564	82.4	

[†]Data from L. Yang and G. Derge, *ibid.*

Table 12.8 Diffusivities in common liquids at 298 K

Solute	Solvent	Concentration	D , $\text{m}^2 \text{s}^{-1}$
HCl	Water	0.1 M	3.05×10^{-9}
NaCl	Water	0.1 M	1.48×10^{-9}
CaCl ₂	Water	0.1 M	1.10×10^{-9}
H ₂	Water	Dilute	5.0×10^{-9}
O ₂	Water	Dilute	2.5×10^{-9}
SO ₂	Water	Dilute	1.7×10^{-9}
NH ₃	Water	Dilute	2.0×10^{-9}
Cl ₂	Water	Dilute	1.44×10^{-9}
H ₂ SO ₄	Water	Dilute	1.97×10^{-9}
Na ₂ SO ₄	Water	0.01 M	1.12×10^{-9}
K ₄ Fe(CN) ₆	Water	0.01 M	1.18×10^{-9}
Ethanol	Water	$X = 0.05$	1.13×10^{-9}
Glucose	Water	0.39%	0.67×10^{-9}
Benzene	CCl ₄	Dilute	1.53×10^{-9}
CCl ₄	Benzene	Dilute	2.04×10^{-9}
Br ₂	Benzene	Dilute	2.7×10^{-9}
CCl ₄	Kerosene	Dilute	0.96×10^{-9}
CO ₂	Ethanol	Dilute	4.0×10^{-9}
CCl ₄	Ethanol	Dilute	1.50×10^{-9}
Phenol	Ethanol	Dilute	0.89×10^{-9}

Diffusion in common liquids. Table 12.8 gives some data for diffusivities in aqueous and organic solvents. Again, note that they are all on the order of $10^{-9} \text{ m}^2 \text{ s}^{-1}$, even though there are obvious differences in bonding between these liquids and liquid metals or slags.

12.6 DIFFUSION IN GASES

In gases, we are not faced with the problem of Kirkendall shift phenomena, since any tendency for more A molecules to go in one direction than B molecules in the opposite direction is immediately counteracted by the fact that a pressure gradient cannot build up; thus in gases, $D_A = D_B = D_{AB} = \bar{D}$.[†] Of course, one must still superimpose the bulk flow term in Eq. (12.7) onto Fick's first law to obtain the total flux if there is convection.

Chemists and chemical engineers have spent a great deal of time and effort in developing equations which predict diffusion coefficients in gases. For example, based on the kinetic theory of gases, the following equation applies to prediction of self-diffusivity of spherical A atoms diffusing in pure A :

$$D_{AA}^* = \frac{2}{3} \left[\frac{\kappa_B^3}{\pi^3 m_A} \right]^{1/2} \frac{T^{3/2}}{Pd^2} \quad (12.48)$$

For the interdiffusivity of two unequal size spherical atoms A and B , kinetic theory predicts

$$D_{AB} = \frac{2}{3} \left[\frac{\kappa_B^3}{\pi^3} \right]^{1/2} \left[\frac{1}{2m_A} + \frac{1}{2m_B} \right]^{1/2} \left[\frac{T^{3/2}}{P \left(\frac{d_A + d_B}{2} \right)^2} \right] \quad (12.49)$$

where $\kappa_B = \text{Boltzmann's constant}$, $1.38 \times 10^{-16} \text{ ergs molecule}^{-1} \text{ K}^{-1}$, $d = \text{molecular diameter, cm}$, $m = \text{molecular mass, g molecule}^{-1}$, $P = \text{pressure, dyn cm}^{-2}$, and $T = \text{temperature, K}$.

Equations (12.48) and (12.49) give the proper pressure dependence up to about 10 atm; the predicted temperature dependency is only qualitatively correct in that D_{AB} actually varies more with temperature.³⁸

To predict D_{AB} more accurately, it is better to apply the Chapman-Enskog theory than the above equations. For monoatomic gases, which act ideally, we have

$$D_{AB} = \frac{0.0018583T^{3/2}}{P(\sigma_{AB})^2 \Omega_{D,AB}} \left[\frac{1}{M_A} + \frac{1}{M_B} \right]^{1/2} \quad (12.50)$$

where $\sigma_{AB} = \frac{1}{2}(\sigma_A + \sigma_B) = \text{collision diameter, \AA}$,
 $\Omega_{D,AB} = \text{collision integral for } A\text{-}B \text{ mixture at dimensionless temperature, } T_{AB}^*$, for the Lennard-Jones potential,

[†]Chemical engineers often use the notation D_{AB} to refer to the diffusion of A in an A - B mixture. This is the same as \bar{D} , which, if $D_A = D_B$, is also equal to D_A and to D_B .

³⁸R. B. Bird, W. E. Stewart, and E. N. Lightfoot, *ibid.*

$$T_{AB}^* = \left[\frac{\kappa_B}{\varepsilon} \right]_{AB} T,$$

$$\left[\frac{\varepsilon}{\kappa_B} \right]_{AB} = \left[\left[\frac{\varepsilon}{\kappa_B} \right]_A \left[\frac{\varepsilon}{\kappa_B} \right]_B \right]^{1/2} = \text{average intermolecular force parameter, K,}$$

M_A, M_B = molecular weights of species A and B ,
 T = temperature, K,
 P = pressure, atm.

The values of the force parameters and the collision diameters for common gases are given in Table 1.1, and the collision integral can be calculated³⁹:

$$\Omega_{D,AB} = \frac{A}{T_{AB}^{*B}} + \frac{C}{\exp DT_{AB}^*} + \frac{E}{\exp FT_{AB}^*} + \frac{G}{\exp HT_{AB}^*}, \quad (12.51)$$

where $A = 1.06036$, $B = 0.15610$, $C = 0.19300$, $D = 0.47635$, $E = 1.03587$, $F = 1.52996$, $G = 1.76474$, and $H = 3.89411$. Note that the collision integral values for diffusion are only slightly different from those for gas viscosity calculations.

The force parameters for metal vapors are not well known, but Turkdogan⁴⁰ has estimated many of them. For ε/κ_B , he recommends

$$\varepsilon/\kappa_B = 1.15 T_b, \text{ K,} \quad (12.52)$$

and

$$\varepsilon/\kappa_B = 1.92 T_M, \text{ K,} \quad (12.53)$$

where T_b and T_M are the boiling and melting temperatures, respectively. Although Eqs. (12.52) and (12.53) give somewhat different values of ε/κ_B , the errors in D_{AB} , particularly at temperatures greater than T_M , are not great. Melting points, boiling points, molar volumes, and Turkdogan's estimates of collision diameters are given in Table 12.9.

Example 12.1 Calculate the diffusion coefficient for iron vapor diffusing through argon, at 1600°C, assuming that pure iron is the source of the vapor.

Solution. Using the Chapman-Enskog equation, we obtain

$$D_{\text{Fe-Ar}} = \frac{0.001858(1873)^{3/2}}{(1)(\sigma_{\text{Fe-Ar}})^2 \Omega_{D,\text{Fe-Ar}}} \left[\frac{1}{55.85} + \frac{1}{39.54} \right]^{1/2}.$$

We evaluate $\sigma_{\text{Fe-Ar}}$ from the data in Tables 1.1 and 12.9:

$$\sigma_{\text{Fe-Ar}} = \frac{\sigma_{\text{Fe}} + \sigma_{\text{Ar}}}{2} = \frac{2.43 + 3.42}{2} = 2.92 \text{ \AA}.$$

³⁹R. C. Reid, J. M. Prausnitz, and T. K. Sherwood, *The Properties of Gases and Liquids*, third edition, McGraw-Hill, New York, NY, 1977, pages 549 and 550.

⁴⁰E. T. Turkdogan, paper in *Steelmaking, The Chipman Conference*, J. F. Elliott (ed.), Addison-Wesley, Reading, Massachusetts, 1962.

Table 12.9 Estimated collision diameters for metal vapors*

Metal	Melting point, °C	Boiling point, °C	Molar volume, cm ³ mol ⁻¹			σ, Å	
			\hat{V} (sol.)	\hat{V} (liq.)	\hat{V}_b (liq.)	From \hat{V} (sol.)	From \hat{V}_b (liq.)
Ag	960.8	2163	11.02	11.60	13.06	2.72	2.74
Al	660	2057	10.49	11.36	13.26	2.67	2.76
Bi	271	1477	—	20.76	24.07	—	3.37
Cd	321	765	13.34	14.01	14.89	2.90	2.97
Co	1493	2877	7.14	7.68	8.98	2.36	2.43
Cu	1083	2570	7.58	8.01	9.15	2.39	2.44
Fe	1535	2833	7.60	7.94	9.55	2.40	2.47
Ga	29.8	1983	—	11.43	13.87	—	2.80
Hg	-38.9	357	14.09	14.65	15.71	2.95	2.92
In	156.4	2087	15.94	16.33	19.98	3.07	3.16
K	63.7	760	46.0	47.10	59.36	4.37	4.54
Li	186	1317	13.27	13.40	16.76	2.89	2.98
Mg	651	1103	14.66	15.47	20.30	3.00	3.18
Na	97.9	883	24.04	24.79	31.07	3.52	3.66
Ni	1453	2816	7.11	7.57	9.02	2.34	2.43
Pb	327.4	1717	18.35	19.39	22.47	3.22	3.29
Pu	637	3300	14.20	14.49	18.78	2.95	3.11
Sb	630.5	1440	18.59	18.74	20.29	3.23	3.18
Sn	231.9	2770	16.41	17.04	21.63	3.11	3.25
Tl	303	1457	—	18.10	20.64	—	3.19
Zn	419.5	906	9.56	9.45	10.19	2.59	2.51

*From E. T. Turkdogan, *ibid.*

In order to evaluate the collision integral, we need to calculate $(\epsilon/\kappa_B)_{Fe-Ar}$

$$\left(\frac{\epsilon}{\kappa_B} \right)_{Fe-Ar} = \left(\frac{\epsilon}{\kappa_B} \right)_{Fe}^{1/2} \left(\frac{\epsilon}{\kappa_B} \right)_{Ar}^{1/2} = \sqrt{(3521)(124)} = 655 \text{ K.}$$

Then

$$T^* = \left(\frac{\kappa_B}{\epsilon} \right)_{Fe-Ar} T = \frac{1873}{655} = 2.86,$$

which gives $\Omega_{D,Fe-Ar} = 0.92$. Finally,

$$\begin{aligned} D_{Fe-Ar} &= \frac{0.001858(1873)^{3/2}}{(1)(2.92)^2(0.92)} \left[\frac{1}{55.85} + \frac{1}{39.54} \right]^{1/2} = 4.00 \text{ cm}^2 \text{ s}^{-1} \\ &= 4.00 \times 10^{-4} \text{ m}^2 \text{ s}^{-1}. \end{aligned}$$

Many other correlations have been developed for nonmetallic gases. The most successful correlation, which makes the prediction of D_{AB} over a wide range of binary gas systems and

456 **Fick's Law and Diffusivity of Materials**

temperatures possible, is that of Fuller *et al.*⁴¹ They correlated 340 data points in a theoretically justified form, predicted D_{AB} to within 10% of the measured values 92.6% of the time, and had an average error of only 4.3% and a standard deviation of 6.17%. Their equation is

$$D_{AB} = \frac{(1 \times 10^{-3})T^{1.75}}{P(v_B^{1/3} + v_A^{1/3})^2} \left[\frac{1}{M_A} + \frac{1}{M_B} \right]^{1/2}, \quad \text{cm}^2 \text{ s}^{-1}, \quad (12.54)$$

where T = temperature, K, P = pressure, atm, M_A, M_B = molecular weight of species A and B , g mol⁻¹, and v_A, v_B = diffusion volumes, given for simple molecules in Table 12.10. This approach is relatively simple and avoids the necessity to evaluate the collision integral.

Table 12.10 Diffusion volumes for simple molecules*

Molecule	ν	Molecule	ν	Molecule	ν
H ₂	7.07	Ne	5.59	NH ₃	14.9
D ₂	6.70	Ar	16.1	H ₂ O	12.7
He	2.88	Kr	22.8	Cl ₂	37.7
N ₂	17.9	CO	18.9	Br ₂	67.2
O ₂	16.6	CO ₂	26.9	SO ₂	41.1
Air	20.1	N ₂ O	35.9		

*From E. N. Fuller, P. D. Schettler, and J. C. Giddings, *ibid.*

Values of D_{AB} in gas phases are usually in the range 10⁻⁵ to 10⁻³ m² s⁻¹. Figure 12.21 gives some representative data.

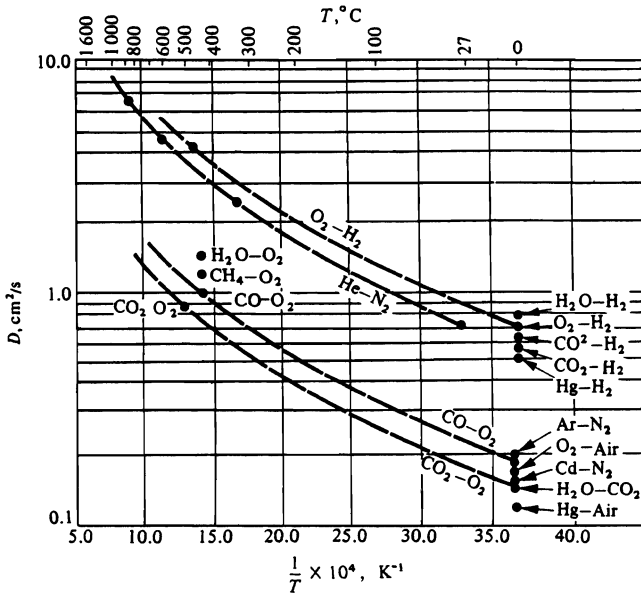


Fig. 12.21 Diffusion coefficients in gas mixtures.

⁴¹E. N. Fuller, P. D. Schettler, and J. C. Giddings, *Indust. and Eng. Chem.* **58**, 19 (May 1966).

12.7 DIFFUSION THROUGH POROUS MEDIA

As we have pointed out in previous chapters, materials engineers often encounter situations where they must deal with the properties of solids containing some degree of porosity. Gas diffusion through porous media is important in such fields as ore reduction or roasting, vapor penetration into foundry sands, outgassing of powder metallurgy and ceramic compacts, gas phase alloying of powders, and catalysis.

In general, gas phase diffusion through porous media occurs by one of two mechanisms: ordinary diffusion or Knudsen diffusion. (A third mechanism, surface diffusion, may be important at low temperatures, but for most elevated temperature processes, it is negligible.) The size of the pores through which diffusion is taking place determines whether ordinary or Knudsen diffusion predominates. With ordinary diffusion, the pores are large *relative to the mean free path* of the gas molecules. Knudsen diffusion is important when the pores are small in relation to the mean free path.

When ordinary diffusion prevails, the total diffusion path, from one plane in the porous media to a parallel plane, is longer than when no aggregate is present, because of the irregularity of the porosity. Even after correcting for the decrease in cross-sectional area available for diffusion, using the void fraction, ω , we must make a further decrease in the D_{AB} value, in order to yield the *effective interdiffusivity*. We accomplish this by introducing a new factor, the *tortuosity*, τ , so that

$$D_{AB,\text{eff}} = \frac{D_{AB}\omega}{\tau}. \quad (12.55)$$

The tortuosity is a number greater than one, ranging from values of 1.5-2.0 for unconsolidated particles, to as high as 7 or 8 for compacted particles. It is not a function of the void fraction, but does depend on the particle size, particle size distribution, and particle shape. Estimates of the tortuosity may be made by comparisons with previous results using similar materials, such as presented in Fig. 12.22.

When the gas density is low, or the pore size small, then the molecules have a higher probability of collision with the pore walls than with each other, similarly as in the flow of molecules in a vacuum system. An analysis of the flow of molecules through a cylindrical pore of radius r under a concentration gradient yields

$$j_A = \frac{2}{3} r \bar{V} \left[\frac{dC_A}{dx} \right].$$

By using Eq. (1.4) for \bar{V} , the average speed of the molecules, and comparing it with Fick's first law, we obtain the Knudsen diffusion coefficient:

$$D_K = 9700r \sqrt{T/M}, \quad \text{cm}^2 \text{ s}^{-1}, \quad (12.56)$$

where r = pore radius, cm, T = temperature, K, and M = molecular weight of the diffusing species, g mol⁻¹. Since collisions between species are negligible at low pressures, this equation applies equally to any component present.

There are two tests that we may use to determine when ordinary diffusion no longer predominates and Knudsen diffusion becomes important. In the first test, we may estimate the pore radius and compare it to the mean free path of the gas λ , given by

$$\lambda = \left(\sqrt{2} \pi d^2 n \right)^{-1}, \quad (1.5)$$

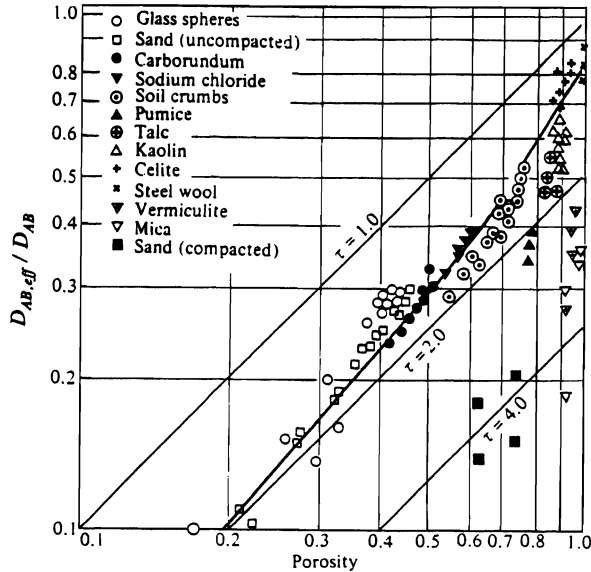


Fig. 12.22 Hydrogen-air diffusion in various unconsolidated porous media. (Adapted from L. N. Satterfield and T. K. Sherwood, *The Role of Diffusion in Catalysts*, Addison-Wesley, Reading, MA, 1963.)

where d = collision diameter of the molecule, cm, and n = concentration of the molecules, cm^{-3} . If r and λ are of the same order of magnitude, or if the pore diameter is only one order larger, then Knudsen diffusion is presumably important. At elevated temperatures, this may occur when pore diameters are on the order of $10 \mu\text{m}$ or less.

The other test involves comparing the calculated values of D_{AB} and D_K . If the ratio D_{AB}/D_K is small, then we take ordinary diffusion as the rate determining step. Conversely, if D_{AB}/D_K is large, then we presume that Knudsen diffusion controls.

Since even the micropores are not straight and smooth, we must also define tortuosity for those systems where Knudsen diffusion predominates:

$$D_{K,\text{eff}} = \frac{D_K \omega}{\tau} \quad (12.57)$$

The results of a large number of tests at relatively low temperatures where tortuosity has been calculated for systems in which Knudsen diffusion predominates are shown in Table 12.11.

Example 12.2 Consider the diffusion of metal vapors into molding sand when steel is cast. Calculate the diffusion coefficient for manganese vapor through silica sand at 1600°C , assuming that the only other gas present is argon. The pore radius is 0.005 cm , and the porosity is 0.45 .

Solution. The first step is to test for the importance of Knudsen diffusion. Calculating $D_{\text{Mn-Arg}}$, as in Example 12.1, we obtain $3.4 \text{ cm}^2 \text{ s}^{-1}$ for Mn at 1600°C . Then we calculate D_K , using Eq. (12.56).

$$D_K = (9700)(0.005) \left(\frac{1873}{55} \right)^{1/2} = 283 \text{ cm}^2 \text{ s}^{-1}.$$

Table 12.11 Knudsen diffusion and flow in porous media*

Material	Gases	T, K	$r, \text{\AA}$	τ
Alumina pellets	N_2, He, CO_2	303	96	0.85
Fresh and regenerated silica-alumina cracking catalyst	H_2, N_2	298	31-50	2.1
Water-gas shift catalyst	O_2, N_2	298	177	2.7
Ammonia synthesis catalyst	O_2, N_2	298	203	3.8
Vycor glass	$He, Ne, H_2, A, N_2, O_2, Kr, CH_4, C_2H_6$	292-298	30-50	5.9
Silica-alumina cracking catalyst	He, Ne, A, N_2	273-323	16	0.725
Silica-alumina cracking catalyst	He, Ne, N_2	273-323	24	0.285
Silica-alumina cracking catalyst	Cumene	420	(24)	5.6

*From L. N. Satterfield and T. K. Sherwood, *ibid.*

Then

$$\frac{D_{Mn-Ar}}{D_K} = \frac{3.4}{2.83} = 0.0119,$$

which implies that in this situation ordinary diffusion controls.

As a further check, we calculate the mean free path of Mn vapor where $n = 4.48 \times 10^4$ atoms/ \AA^3 , $d = 2.4 \text{\AA}$, and $\lambda = 1/\sqrt{2} \pi(4.48 \times 10^4)(5.76) = 87 \text{\AA}$. Based on the fact that the pore size is on the order of 10^5\AA , and λ_{Mn} is much less than that, we conclude that Knudsen diffusion is unimportant in this instance, and that we may analyze the problem in terms of ordinary diffusion.

The tortuosity τ for metal vapor diffusion through porous compacts has a range 3-6, with 4 considered to be an average value.⁴² Therefore, for a sand mold with a void fraction of 0.45, we have

$$D_{Mn-Ar,eff} = \frac{D_{Mn-Ar}\omega}{\tau} = \frac{(3.4)(0.45)}{(4.0)} = 0.383 \text{ cm}^2 \text{ s}^{-1},$$

or

$$D_{Mn-Ar,eff} = 3.83 \times 10^{-5} \text{ m}^2 \text{ s}^{-1},$$

which is approximately one-tenth the value in the gas phase alone.

PROBLEMS

12.1 Show that the units in Eq. (12.1) are as indicated. Do the same for Eqs. (12.2) and (12.3).

12.2 Discuss the reasons why self-diffusion data must apply to homogeneous materials only.

12.3 Read one of the references of Footnote 1 and derive Eq. (12.5).

⁴²J. M. Svoboda and G. H. Geiger, *Trans. AIME* **245**, 2363 (1969).

460 Fick's Law and Diffusivity of Materials

12.4 Look up the article by Compaan and Haven (Table 12.1) and summarize the method used to derive the correlation coefficients in Table 12.1.

12.5 Work out the units in Eq. (12.20).

12.6 Derive Eq. (12.28), after reading Zener's article.

12.7 Using the method of Fuller, Schettler, and Giddings, estimate the diffusion coefficient for a CO₂-O₂ gas mixture at 1-atm pressure and 700 K and compare the result to the data in Fig. 12.21.

12.8 Given a tortuosity of 2.0, a void fraction of 0.25, and $r = 5 \times 10^{-3}$ cm, calculate the effective diffusion coefficient for CO-CO₂ in a reduced iron oxide pellet at 800 K.

12.9 PbS has a NaCl-type structure. Would you expect the self-diffusion coefficient of Pb or S to be higher? How would you expect the addition of Ag₂S to affect the diffusion coefficient of Pb, knowing that the defects in PbS are predominantly Frenkel defects on the Pb sublattice, and that the undoped PbS is an *n*-type semiconductor? How would Bi₂S₃ additions affect it? [Ref.: G. Simovich and J. B. Wagner, Jr., *J. Chem. Phys.* **38**, 1368 (1963).]

12.10 Describe the conditions under which the following terms are applicable: (1) self-diffusion, (2) tracer diffusion, (3) chemical diffusion, (4) interstitial diffusion, (5) substitutional diffusion, (6) interdiffusion coefficient, and (7) intrinsic diffusion.

12.11 Calculate the self-diffusion coefficient in liquid lead using the Sutherland hydrodynamical model, and the Eyring activated state model. Data for viscosity of liquid metals is given in Fig. 1.9. Calculate D^* at 873 K, 1073 K, and 1273 K. a) Do the calculated diffusion coefficients vary linearly with temperature according to the fluctuation model of Reynik? according to the Arrhenius relation (Eq. (12.27))? b) What is the error in the calculated values? Experimental results for liquid lead are given in Fig. 12.18.

12.12 The self-diffusion coefficients of gold and nickel in Au-Ni alloys are shown in Fig. 12.4. Show that the alloys of Au and Ni are not ideal solutions.

12.13 The diffusion coefficient of acetone vapor in air is 1.1×10^{-5} m² s⁻¹ at 273 K and 1 atm. What is the diffusion coefficient at 500 K and 0.5 atm?

12.14 The diffusion coefficient of He in Pyrex* is 2.6×10^{-16} m² s⁻¹ at 373 K and 1.6×10^{-14} m² s⁻¹ at 873 K. What is it at 1000 K? *Pyrex® is a type of glass commonly used in laboratories.

12.15 The diffusion coefficient of oxygen in liquid copper is not linear with temperature. The following data are available:

$$\text{at } 1150^\circ\text{C}, D = 7 \times 10^{-9} \text{ m}^2 \text{ s}^{-1}$$

$$\text{at } 1250^\circ\text{C}, D = 10^{-8} \text{ m}^2 \text{ s}^{-1}.$$

Predict the diffusion coefficient at 1350°C.

12.16 What is the diffusivity of Mg vapor in helium gas at 1200 K? The gas has a composition of 90 He and 10 Mg (by volume).

12.17 At 1500°C, the diffusivity of Cr in molten nickel is $5 \times 10^{-9} \text{ m}^2 \text{ s}^{-1}$. At 1600°C, it is $7 \times 10^{-9} \text{ m}^2 \text{ s}^{-1}$. Estimate the diffusivity at 1700°C.

12.18 Calculate the diffusion coefficient D_{AB} for zinc vapor diffusing through helium at 773 K.

12.19 At 1 atm. pressure and 1900 K, the diffusion coefficient for a gaseous suboxide (Al_2O) in argon is $5 \times 10^{-4} \text{ m}^2 \text{ s}^{-1}$. Predict the diffusion coefficient for Al_2O in argon at 1900 K and 10^{-6} atm.

12.20 At 273 K and 1 atm. the diffusion coefficient for cadmium vapor in nitrogen is $1.5 \times 10^{-5} \text{ m}^2 \text{ s}^{-1}$. Calculate the diffusion coefficient for cadmium vapor in helium at 1500 K and 0.5 atm.

12.21 To quantify the nucleation theory of the liquid to solid transformation, it is necessary to have a value of the self-diffusion coefficient for the liquid at temperatures significantly less than the freezing point. Given that D^* of liquid metal A is $5 \times 10^{-9} \text{ m}^2 \text{ s}^{-1}$ at 1200 K and $10^{-8} \text{ m}^2 \text{ s}^{-1}$ at 1500 K, estimate D^* at 900 K. Use two distinctly different methods and compare the two estimates.

12.22 At 1500°C the diffusion coefficient of Mo in an Fe melt is $3 \times 10^{-9} \text{ m}^2 \text{ s}^{-1}$ and at 1600°C it is $3.5 \times 10^{-9} \text{ m}^2 \text{ s}^{-1}$. Predict the diffusion coefficient of Mo in an Fe melt which has been supercooled to 1200°C.

12.23 A binary gas of A and B molecules has a diffusion coefficient of $10 \text{ cm}^2 \text{ s}^{-1}$ at 0°C and 1 atm. Predict the diffusion coefficient in the same gas at 500°C and 10 atm.

12.24 A chamber containing $\text{O}_2(\text{g})$ and $\text{N}_2(\text{g})$ is divided by a porous solid, 1 cm thick. On one side of the porous solid, there is continuous flow keeping the composition at 80 mole percent O_2 . On the other side, there is also continuous flow which maintains the composition of O_2 at 40 mole percent. The pressures and temperatures in both parts of the chamber are uniform and constant at 1 atm. and 1000 K, respectively. The porous solid has pores with an average radius of $1 \mu\text{m}$, a porosity of 0.2 and a tortuosity of 5. Calculate the flux of oxygen which diffuses through the porous solid.

DIFFUSION IN SOLIDS

This chapter, in which the primary aim is to obtain solutions to Fick's laws of diffusion, is similar to Chapter 9 where we presented solutions to heat conduction problems. Therefore, much of the groundwork laid in Chapter 9 reappears in the following discussions. We begin by presenting some classical approaches used for determining diffusion coefficients in solids, and then consider some applied problems involving diffusion in solids as the rate-limiting step.

13.1 STEADY-STATE DIFFUSION EXPERIMENTS

As an example of the application of Fick's first law, consider an iron tube held in the isothermal part of a furnace. A carburizing gas is passed through the inside of the tube, and a gas of a different composition is passed over the outside. The carbon activity, thus has a gradient from the inside surface to the outside surface. Steady state is reached when the carbon concentration at each point in the tube wall no longer changes with time. By this time, the appropriate differential equation for steady-state diffusion through a cylinder can be derived from shell balances. If the diffusion coefficient of carbon in iron is a constant, independent of composition, then by analogy with Eq. (9.13),

$$\frac{1}{r} \frac{d}{dr} \left[r \frac{dC}{dr} \right] = 0. \quad (13.1)$$

The solution to this equation is given by its heat transfer analog from Eq. (7.51):

$$\frac{C - C_2}{C_1 - C_2} = \frac{\ln (r/r_2)}{\ln (r_1/r_2)}, \quad (13.2)$$

464 Diffusion in Solids

where r_1 and r_2 are the inside and outside radii of the tube, and C_1 and C_2 are the corresponding concentrations of carbon at these surfaces. Thus a plot of C versus $\ln r$ should be a straight line. However, for carbon diffusing in γ -iron, the slope of such a plot, as shown in Fig. 13.1, becomes smaller on passing from the low-carbon side to the high-carbon side. Therefore, the diffusion coefficient must be a function of composition, Eqs. (13.1) and (13.2) do not apply, and we must approach the problem somewhat differently.

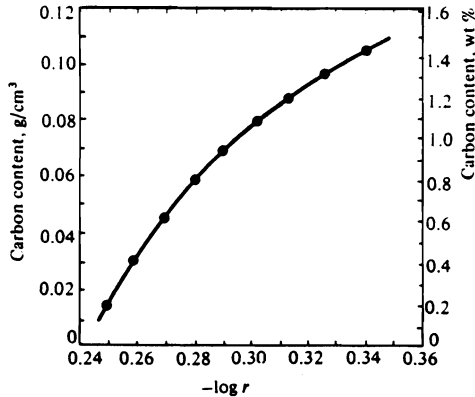


Fig. 13.1 Steady-state carbon concentration profile through a hollow cylinder of iron at 1000°C. (From R. P. Smith, *Acta Met.* 1, 578 (1953).)

In addition to the fact that $\partial C/\partial t = 0$, steady state also means that the quantity of carbon passing through the tube per unit time is constant and independent of r . Thus

$$J = 2\pi r l j_r, \quad (13.3)$$

where l = length of the cylinder, j_r = local flux, and J = quantity of carbon passing through the tube wall per unit time. Since

$$j_r = -D \frac{dC}{dr}, \quad (13.4)$$

we may express Eq. (13.3) as

$$r \left[-D \frac{dC}{dr} \right] = \frac{J}{2\pi l},$$

or

$$\frac{dC}{d \ln r} = \frac{-J}{2\pi l D}. \quad (13.5)$$

For a given experiment, we can measure J and l , and if the carbon concentrations within the tube wall are determined by chemical analyses, then we can determine D from the slope of the plot of C versus $\ln r$.

Similar experiments have also been performed for determining the diffusion coefficient of gases through metals such as, for example, the diffusion of hydrogen through a metal foil in Fig. 13.2. According to Fick's first law, the flux of hydrogen through the metal is

$$j_x = -D \frac{dC}{dx} \quad (13.6)$$

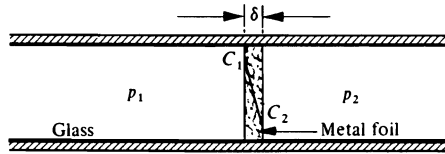


Fig. 13.2 Experiment for diffusion of hydrogen through metal foils.

The foils are very thin, and so it is extremely difficult to determine the concentration as a function of distance through the foil. The experimental results therefore consist of a measured steady-state flux, the hydrogen pressure drop across the foil, and the foil's thickness. To obtain D from the data, we take the value of C in the metal at each gas-metal interface as the solubility S that would exist in equilibrium with the gas.* From Sievert's law, we know that for equilibrium between gas and the metal

$$S_1 = Kp_1^{1/2}, \quad (13.7a)$$

and

$$S_2 = Kp_2^{1/2}, \quad (13.7b)$$

in which K is the equilibrium constant for the reaction



and p_1 and p_2 are the partial pressures of hydrogen on both sides of the foil with a thickness δ , as shown in Fig. 13.2.

The gradient dC/dx can then be expressed in terms of the pressures:

$$\frac{dC}{dx} = \frac{S_1 - S_2}{\delta} = \frac{K}{\delta} \left(\sqrt{p_1} - \sqrt{p_2} \right). \quad (13.9)$$

Combining Eqs. (13.6) and (13.9), we obtain the flux:

$$j_x = \frac{-DK}{\delta} \left(\sqrt{p_1} - \sqrt{p_2} \right). \quad (13.10)$$

*This is true under the conditions when the solution of gas in the surface of the metal occurs much more rapidly than the rate at which the diffusing species leaves the surface and enters the bulk metal. Experimentally, we check this assumption by determining the fluxes for two thicknesses of foil under the same pressure drop and temperature. If equilibrium does exist at the interface, then ΔC is the same for both cases, and the flux is inversely proportional to the thickness.

466 Diffusion in Solids

In relation to the diffusion of gases through solids, the term *permeability*, P , is often used and defined by

$$P = DS = DK\sqrt{p}, \tag{13.11}$$

so that

$$j_x = \frac{-(P_1 - P_2)}{\delta}, \tag{13.12}$$

and permeability is then given by an equation of the form

$$P = Ap^{1/2}e^{-Q_p/RT}, \tag{13.13}$$

which includes the temperature dependence of both S and D , with A and Q_p as constants. Unfortunately, there are also other ways to define permeability, which is rather confusing. For example, using a different definition, we obtain the flux:

$$j_x = -\frac{P^*}{\delta} \left(\sqrt{p_1} - \sqrt{p_2} \right), \tag{13.14}$$

so that $P^* = P = DS$ only at 1 atm pressure, or 0.1013 MPa:

$$P^* = DK. \tag{13.15}$$

In this case, we have

$$P^* = P_0^* e^{-Q_p/RT}. \tag{13.16}$$

The units given to P^* and P_0^* are not typically S.I. units; rather $P_0^* = \text{cm}^3(\text{STP}) \text{ s}^{-1} \text{ cm}^{-2}$ measured for 1 cm thickness and at 1 atm pressure, and $Q_p = \text{cal mol}^{-1}$ (activation energy for permeation).

There are other sets of units which apply to P_0^* as well, and therefore one should be extremely careful of the term *permeability* because different definitions and units are used. Table 13.1 gives some representative data for various systems, using Eqs. (13.15) and (13.16) to define permeability. For data on permeability of gases through polymers, refer to Pauly.¹

Table 13.1 Permeability data for gas-metal systems

Gas	Metal	P_0^* , $\text{cm}^3(\text{STP}) \text{ s}^{-1} \text{ cm}^{-1} \text{ atm}^{-1/2}$	Q_p , cal mol^{-1}
H ₂	Ni	1.2×10^{-3}	13 850
H ₂	Cu	$1.5\text{-}2.3 \times 10^{-4}$	16 000-18 700
H ₂	α -Fe	2.9×10^{-3}	8400
H ₂	Al	$3.3\text{-}4.2 \times 10^{-1}$	30 800
N ₂	Fe	4.5×10^{-3}	23 800
O ₂	Ag	2.9×10^{-3}	22 550

¹The units in Eq. (13.14) are: $\delta = \text{cm}$, $p = \text{atm}$, and $j_x = \text{cm}^3(\text{STP}) \text{ s}^{-1} \text{ cm}^{-2}$.

¹S. Pauly, "Permeability and Diffusion Data," in J. Brandrup and E. H. Immergut, editors, *Polymer Handbook*, third edition, John Wiley & Sons, New York, NY, 1989, pages VI/435 to VI/449.

Example 13.1 The solubility of hydrogen dissolved in aluminum at 873 K is $2.5 \times 10^{-4} \text{ cm}^3(\text{STP}) \text{ g}^{-1}$. Assume that Sievert's law holds. a) Calculate the equilibrium constant, b) the solubility in g cm^{-3} , and c) the diffusion coefficient for hydrogen in aluminum at 873 K.

Solution. a) When solubility data are given in this manner, it is assumed that the condensed phase has been equilibrated with the gas at 1 standard atm of pressure. Then, according to Eq. (13.8), the equilibrium constant is

$$K = \frac{S}{p^{1/2}}.$$

Therefore, K is simply

$$K = \frac{2.5 \times 10^{-4} \text{ cm}^3(\text{STP})}{1 \text{ atm}^{1/2} \text{ g}} = 2.5 \times 10^{-4} \text{ cm}^3(\text{STP}) \text{ atm}^{-1/2} \text{ g}^{-1}.$$

b) Notice the curious units for the *atomic* hydrogen dissolved in the aluminum (i.e., the solubility). The solubility is the mass of *molecular* hydrogen, expressed as a volume at standard temperature and pressure (STP). We did not invent these units, but they are the units most often given. Let's calculate a concentration in more familiar units. The density of Al at 873 K is 2.55 g cm^{-3} .

$$S = \frac{2.5 \times 10^{-4} \text{ cm}^3(\text{STP})}{\text{g (Al)}} \left| \frac{1 \text{ mol (H}_2\text{)}}{22\,400 \text{ cm}^3(\text{STP})} \right| \left| \frac{2 \text{ g (H)}}{1 \text{ mol (H}_2\text{)}} \right| \left| \frac{2.55 \text{ g (Al)}}{\text{cm}^3 \text{ (Al)}} \right|$$

$$= 5.69 \times 10^{-8} \text{ g cm}^{-3}.$$

c) From Table 13.1, $P_0^* \approx 0.37 \text{ cm}^3(\text{STP}) \text{ s}^{-1} \text{ cm}^{-1} \text{ atm}^{-1/2}$ and $Q_p = 30\,800 \text{ cal mol}^{-1}$. Then with Eq. (3.16) we calculate

$$P^* = 0.37 \exp \left[-\frac{30\,800}{(1.987)(873)} \right] = 7.19 \times 10^{-9} \text{ cm}^3(\text{STP}) \text{ s}^{-1} \text{ cm}^{-1} \text{ atm}^{-1/2},$$

and

$$D = \frac{P^*}{K} = \frac{7.19 \times 10^{-9} \text{ cm}^3(\text{STP})}{\text{s cm atm}^{1/2}} \left| \frac{\text{g(Al) atm}^{1/2}}{2.5 \times 10^{-4} \text{ cm}^3(\text{STP})} \right| \left| \frac{\text{cm}^3}{2.55 \text{ g(Al)}} \right|$$

$$= 1.13 \times 10^{-5} \text{ cm}^2 \text{ s}^{-1},$$

or $D = 1.13 \times 10^{-9} \text{ m}^2 \text{ s}^{-1}$.

Example 13.2 A pilot plant for hydrogenation of hydrocarbon vapor is to be constructed of a low-alloy steel. In designing, the question of the effect of wall thickness on the rate of hydrogen loss through the wall is raised. If the inside diameter of a vessel 1 m long is 10 cm, calculate the rate of hydrogen loss as a function of wall thickness at 723 K and a pressure of 75 atm hydrogen, assuming that the gas diffusing through the wall is collected and removed at 1 atm.

468 Diffusion in Solids

Solution. Combining Eqs. (13.2), (13.3), and (13.4), and assuming that D is constant, we have

$$J = -2\pi l D \frac{C_1 - C_2}{\ln(r_1/r_2)}$$

In terms of permeability

$$j = \frac{-2\pi l D K (\sqrt{p_1} - \sqrt{p_2})}{\ln(r_1/r_2)} = \frac{-2\pi l P^* (\sqrt{p_1} - \sqrt{p_2})}{\ln(r_1/r_2)}$$

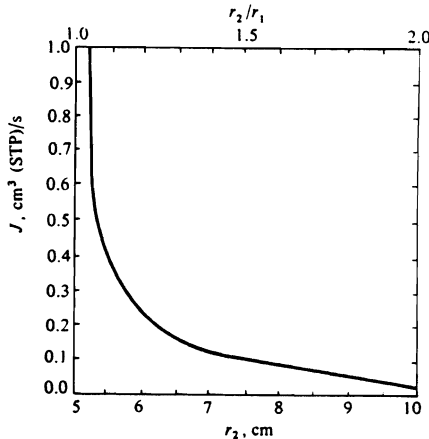
From Table 13.1 and Eq. (13.16), $P^* = 8.4 \times 10^{-6} \text{ cm}^3(\text{STP}) \text{ s}^{-1} \text{ cm}^{-1} \text{ atm}^{-1/2}$. Therefore

$$J = \frac{-2\pi(100)(8.4 \times 10^{-6})(\sqrt{75} - \sqrt{1})}{\ln r_1 - \ln r_2} = \frac{-0.0404}{1.609 - \ln r_2},$$

with the outside radius given in cm. In more general terms, where r_1 is not specified, but l is still 1 m,

$$J = \frac{-0.0404}{\ln(r_1/r_2)}, \text{ cm}^3(\text{STP}) \text{ s}^{-1}.$$

Both results are shown below:



It probably makes sense to design the vessel with a 6 or 7 cm wall thickness.

13.2 TRANSIENT DIFFUSION EXPERIMENTS

Under many circumstances it is not possible to carry out steady-state experiments in order to determine diffusion coefficients in solids. This means that we must use the results of transient experiments and solve Eq. (12.18) in its general form

$$\frac{\partial C}{\partial t} = \nabla(D\nabla C) \quad (13.17)$$

for various boundary conditions. In correspondence with heat conduction, a solution to Eq. (13.17) is usually either a series of error functions, which converge rapidly for short times, or a trigonometric series which converges rapidly for long times. In the following sections, we examine several solutions to Eq. (13.17) and their applications.*

13.2.1 Thin film source: infinite and semi-infinite sink

The solution and procedure that follow have been used in self-diffusion studies of substitutional atoms. Radioactive tracers are used as solutes since their concentration can be determined quite accurately, even at low concentrations. A small quantity β of the tracer is plated as a thin film $\Delta x'$ thick on one end of a long rod of tracer-free material. The rod is then annealed at the diffusion temperature of interest. Since D^* is a self-diffusion coefficient and does not depend on position for such an application, Fick's second law is

$$\frac{\partial C}{\partial t} = D^* \frac{\partial^2 C}{\partial x^2} \tag{13.18}$$

Suppose we take a second tracer-free rod and butt-weld it to the plated end (without any diffusion occurring), and then carry out the diffusion anneal. According to Eq. (9.45), we see that the solution is

$$C(x,t) = \frac{C_i}{2\sqrt{\pi D^* t}} \exp\left[\frac{-x^2}{4D^* t}\right] \Delta x' \tag{13.19}$$

Here C_i is the concentration of the tracer in the plated material whose thickness is $\Delta x'$.

Since $C_i \Delta x'$ is the quantity of tracer material plated as the thin film, we write the solution

$$C(x,t) = \frac{\beta}{2\sqrt{\pi D^* t}} \exp\left[\frac{-x^2}{4D^* t}\right], \tag{13.20}$$

which describes the spreading by diffusion of a thin plate source into an infinite sink. This is illustrated in Fig. 13.3.

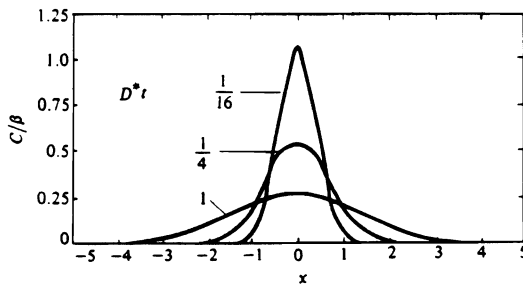


Fig. 13.3 Spreading of concentration from a plane source at $x = 0$.

*Extensive compilations of solutions are presented in J. Crank, *The Mathematics of Diffusion*, Oxford University Press, London, 1956, and W. Jost, *Diffusion in Solids, Liquids, and Gases*, Academic Press, 1960. With appropriate change of variables, one can also refer to H. S. Carslaw and J. C. Jaeger, *Conduction of Heat in Solids*, second edition, Oxford University Press, 1959.

Note that we may determine D^* without measurement or control of β , since a plot of $\log C$ versus x^2 at time t yields D^* directly.

Now suppose that the second bar has not been welded to the first. Then a *semi-infinite* bar would extend over the region $x > 0$ with an impermeable barrier at $x = 0$. In either case, infinite or semi-infinite,

$$\frac{\partial C}{\partial x} = 0 \quad \text{at } x = 0. \quad (13.21)$$

If diffusion is allowed, the material that would normally diffuse in the negative x -direction is *reflected* at the $x = 0$ plane, and moves in the positive x -direction. The concentration at any x in the $+x$ domain is then given by the superposition of the original solution for $x > 0$ and the reflected solution for $x < 0$, or

$$C(x,t) = \frac{\beta}{\sqrt{\pi D^* t}} \exp \left[\frac{-x^2}{4D^* t} \right]. \quad (13.22)$$

13.2.2 Diffusion couple with constant \tilde{D}

This case is exemplified in Fig. 13.4(a) by butt-welding two bars of A - B alloy of concentrations C_1 and C_2 . If \tilde{D} is independent of composition, and the bars extend far enough in the positive and negative domains to be considered infinite, then Eq. (13.18) applies with the boundary conditions:

$$C(x,0) = C_1 \quad \text{at } x < 0, \quad (13.23a)$$

$$C(x,0) = C_2 \quad \text{at } x > 0, \quad (13.23b)$$

$$C(-\infty, t) = C_1, \quad (13.23c)$$

$$C(\infty, t) = C_2. \quad (13.23d)$$

Due to symmetry, the concentration at $x = 0$ immediately takes on the average value of C_1 and C_2 . Let this average be C_s ; then it is easy to see that in the positive x -domain, the solution is directly analogous to the temperature distribution of the semi-infinite solid, as discussed in Section 9.4.2 culminating in Eq. (9.62). Appropriately changing the symbols, we can write the solution:

$$\frac{C - C_s}{C_2 - C_s} = \text{erf} \frac{x}{2\sqrt{\tilde{D}t}}. \quad (13.24)$$

Figure 13.4(b) illustrates this result in a general form, from which one may obtain \tilde{D} -values from measurements of C , x , and t . Since $\text{erf } x = -\text{erf}(-x)$, the concentration profile given by Eq. (13.24) is symmetrical about $x = 0$. This is known as the *Grube solution*, and applies when \tilde{D} is not a function of concentration. Since \tilde{D} is usually a function of composition, the use of Eq. (13.24) is restricted to small differences between C_1 and C_2 . For example, a good value for the diffusion coefficient of A in 50A-50B alloy could be determined from a couple of 45% A alloy welded to a 55% A alloy.

Apart from application to diffusion couples, we can use Eq. (13.24) to predict concentration-time curves for situations where the part in which diffusion occurs is thick enough so that, within the time for diffusion, there is still a region of the part unchanged in composition.

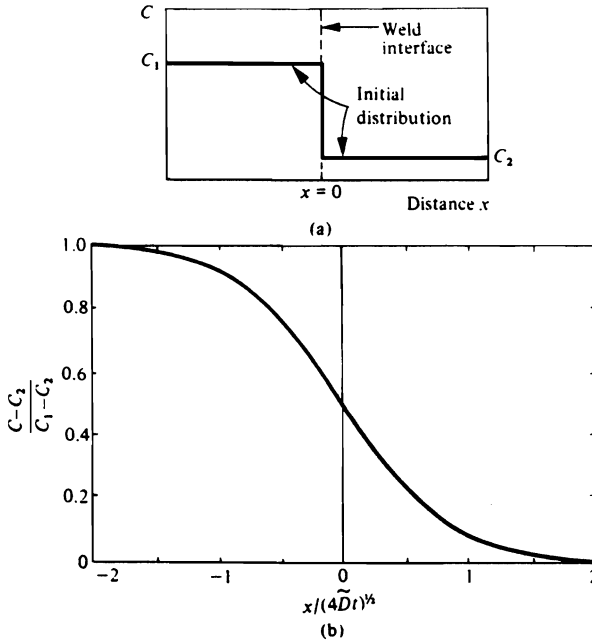
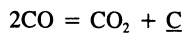


Fig. 13.4 Interdiffusion between an alloy of composition C_1 and an alloy of composition C_2 . a) Initial distribution. b) Diffusion profile when the initial distribution is as in a).

Example 13.3 A piece of AISI 1020 steel is heated to 1255 K (in the austenite region) and subjected to a carburizing atmosphere such that the reaction



is in equilibrium with 1.0% C in solution at the surface. Calculate the carbon profile after 1, 3, and 10 hours, assuming that diffusion within the solid is the rate-limiting step.

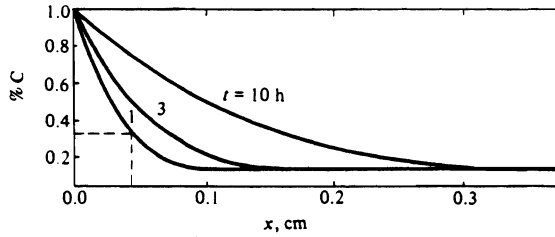
Solution. The initial condition is $C_2 = 0.2\%$ C, and the boundary condition at the surface is $C_s = 1.0\%$ C.

At 1255 K, $D_c = 2.0 \times 10^{-11} \text{ m}^2 \text{ s}^{-1}$. Therefore, Eq. (13.24) for the distribution after 1 hour is

$$C(x,3600) = 1.0 + (0.2 - 1.0) \operatorname{erf} \frac{x}{2\sqrt{(2 \times 10^{-11})(3.6 \times 10^3)}}.$$

472 Diffusion in Solids

Specifically at $x = 5 \times 10^{-4}$ m, $C = 0.35\%$ C. The results for various locations as well as for the longer times are:



13.2.3 Diffusion couple with variable \tilde{D}

The analysis in Section 13.2.2 is valid only for \tilde{D} independent of concentration. In general, however, the diffusion coefficient varies with composition, and since there is a concentration gradient, this means that \tilde{D} changes with position. This variation in \tilde{D} is particularly evident in diffusion couple experiments in which pure A is joined to pure B , and a continuous solid solution is formed. Fick's second law must be written over all compositions between A and B , and for such situations this is

$$\frac{\partial C}{\partial t} = \frac{\partial}{\partial x} \left[\tilde{D} \frac{\partial C}{\partial x} \right]. \quad (13.25)$$

The solution to Eq. (13.25) that follows is useful for obtaining \tilde{D} over a range of compositions, but not for the *a priori* task of predicting a concentration profile for a diffusion anneal. In other words, it does not give a solution $C(x,t)$, which is usually sought, but rather allows $\tilde{D}(C)$ to be calculated from an experimental plot of $C(x)$. This method of analyzing experimental data is called the *Boltzmann-Matano* technique.

We combine the position variable x and the time variable t into one variable $\lambda = x/\sqrt{t}$, so that we consider C to be a function of only the one variable, λ . Using this definition of λ , we transform Eq. (13.25) into an ordinary differential equation:

$$\frac{\partial C}{\partial t} = \frac{\partial \lambda}{\partial t} \left[\frac{dC}{d\lambda} \right] = -\frac{1}{2} \frac{x}{t^{3/2}} \left[\frac{dC}{d\lambda} \right] = -\frac{\lambda}{2t} \left[\frac{dC}{d\lambda} \right], \quad (13.26a)$$

and

$$\frac{\partial C}{\partial x} = \frac{\partial \lambda}{\partial x} \left[\frac{dC}{d\lambda} \right] = \frac{1}{t^{1/2}} \left[\frac{dC}{d\lambda} \right]. \quad (13.26b)$$

Substituting into Eq. (13.25), we obtain

$$-\frac{\lambda}{2t} \left[\frac{dC}{d\lambda} \right] = \frac{\partial}{\partial x} \left[\frac{\tilde{D}}{t^{1/2}} \left[\frac{dC}{d\lambda} \right] \right] = \frac{1}{t} \frac{d}{d\lambda} \left[\tilde{D} \frac{dC}{d\lambda} \right],$$

or finally we can get

$$-\frac{\lambda}{2} \frac{dC}{d\lambda} = \frac{d}{d\lambda} \left[\tilde{D} \frac{dC}{d\lambda} \right]. \quad (13.27)$$

Consider the diffusion couple depicted in Fig. 13.5(a). Then for $C(\lambda)$, we recognize that

$$C = C_1, \quad \text{for } \lambda = -\infty, \quad (13.28a)$$

and

$$C = C_2, \quad \text{for } \lambda = +\infty. \quad (13.28b)$$

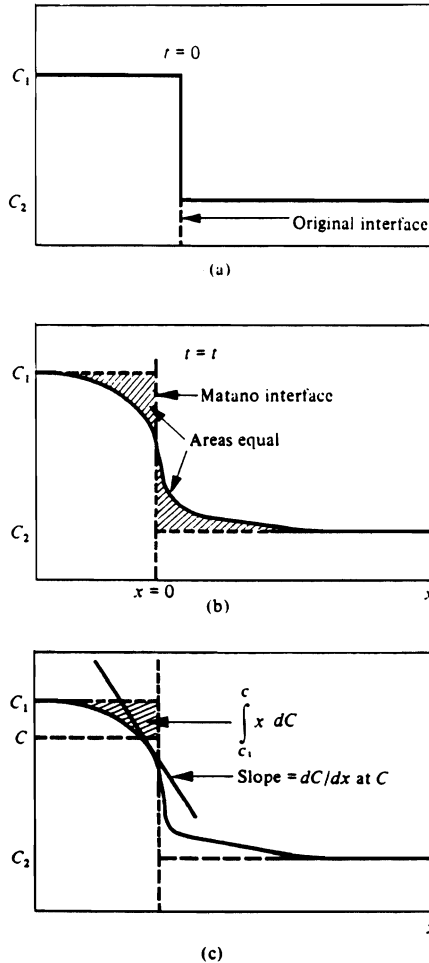


Fig. 13.5 a) Initial conditions. b) Definition of location of Matano interface after diffusion has taken place for a time t . c) The integral and the slope obtained in order to calculate \bar{D} at composition C .

We then solve Eq. (13.27) by integrating between $C = C_1$ and $C = C_2$:

$$-\frac{1}{2} \int_{C_1}^{C_2} \lambda dC = \tilde{D} \left. \frac{dC}{d\lambda} \right|_{C_1}^{C_2}. \quad (13.29)$$

Since the concentration gradient goes to zero as C approaches C_1 , the right-hand side of Eq. (13.29) is simply $\tilde{D}(dC/d\lambda)$. Then

$$\tilde{D} = -\frac{1}{2 \left[\frac{dC}{d\lambda} \right]} \int_{C_1}^{C_2} \lambda dC. \quad (13.30)$$

From Eq. (13.29), we obtain the definition of the *Matano interface*; since the concentration gradient also goes to zero as C approaches C_2 , Eq. (13.29) gives us the additional condition that

$$\int_{C_1}^{C_2} \lambda dC = 0. \quad (13.31)$$

Since experimental data are available only at some constant time t , Eqs. (13.30) and (13.31) can be written in terms of x and t , and the relationships used for calculating \tilde{D} from the measured concentration profile are

$$\tilde{D} = -\frac{1}{2t} \frac{1}{\left[\frac{dC}{dx} \right]} \int_{C_1}^{C_2} x dC, \quad (13.32)$$

and we choose the plane defining $x = 0$ such that

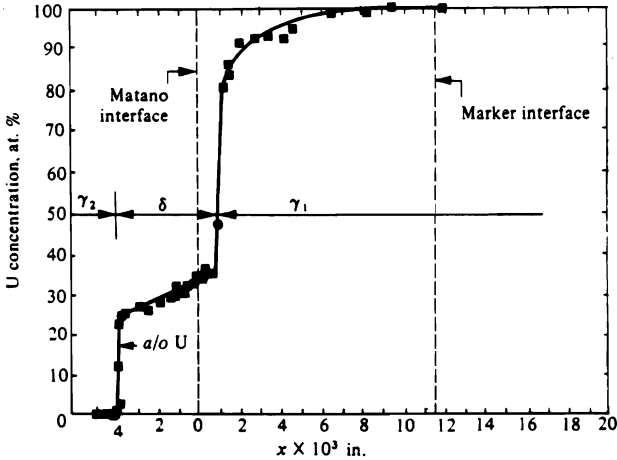
$$\int_{C_1}^{C_2} x dC = 0. \quad (13.33)$$

In Fig. 13.5(b), the plane $x = 0$ is given by the line that makes the two hatched areas equal. We calculate the value of \tilde{D} at a given C by measuring the cross-hatched area, which is the integral in Eq. (13.32), and the reciprocal slope at that point, dx/dC . The diffusion coefficient \tilde{D} , found by applying Eq. (13.32) in this manner, is the interdiffusion coefficient discussed in Section 13.2.3.

In addition, if we place inert markers at the original plane of welding, we can also determine the intrinsic diffusion coefficients. This is left for the reader to do in Problem 13.9. Furthermore, Jost² pointed out that it is not necessary for a single phase to exist over the entire range of the diffusion region. A discontinuity in $C(x)$ and $\tilde{D}(C)$ exists where an intermediate phase is formed. The only condition required when applying the Boltzmann-Matano technique is that the concentrations in both phases on either side of the interface between the phases are independent of time.

²W. Jost, *Diffusion in Solids, Liquids, and Gases*, Academic Press, New York, 1960, page 76, and also W. Jost, *Z. Physik* **127**, 163 (1950).

Example 13.4 A diffusion couple made of pure Nb welded to pure U is held at 800°C for 49 days. The resulting concentration profile, shown below, is obtained with a microprobe analyzer. Note that an intermediate phase δ is formed between the two solid solution, γ_1 and γ_2 . Calculate \bar{D} at 90 at. % U.



(From N. L. Peterson and R. F. Ogilvie, *Trans. AIME* **218**, 439 (1960).)

Solution. Let C represent the composition of U. First, the Matano interface is chosen, such that

$$\int_{-\infty}^0 x dC = \int_0^{\infty} x dC.$$

This is found by trial and error, and placed on the figure as shown.

At 90% U, dC/dx is evaluated:

$$dC/dx = 4.60 \times 10^3 \text{ at. \% in}^{-1} = 1.81 \times 10^5 \text{ at. \% m}^{-1}.$$

Also

$$\int_{c=100}^{c=90} x dC = -1.32 \times 10^{-3} \text{ m at. \%}, \text{ by graphical means;}$$

$$t = \frac{49 \text{ days}}{1} \left| \frac{3600 \text{ s}}{\text{h}} \right| \left| \frac{24 \text{ h}}{\text{day}} \right| = 4.23 \times 10^6 \text{ s}.$$

Thus

$$\bar{D} (90\% \text{ U}) = \frac{-(-1.32 \times 10^{-3})}{2(4.23 \times 10^6)(1.810 \times 10^5)} = 8.6 \times 10^{-16} \text{ m}^2 \text{ s}^{-1}.$$

13.3 FINITE SYSTEM SOLUTIONS

The solutions to Fick's laws presented thus far represent useful cases in many situations when the sink cannot be considered infinite or semi-infinite. On the other hand, there are many situations in which the effect of the diffusion process on the composition is felt at the furthest point in the material prior to the end of the diffusion treatment. This condition can arise quite often when small parts are exposed to a gaseous environment, and there is diffusion of the gas species into the part. Conversely, metal and ceramic parts must often be degassed. When dealing with these situations, it is usually safe to assume that the rate-limiting step of the overall mass transfer is the diffusion of the gas species into the solid. Hence, we seek solutions of Fick's second law with a surface concentration imposed at time zero and maintained constant.

To illustrate this case, consider the diffusion into or out of a slab of infinite length and thickness $2L$. Initially the slab has a uniform concentration C_i , and then its surfaces are raised or lowered to C_s and maintained constant. Hence, we are seeking a solution to Fick's second law with constant \tilde{D} (or simply D):

$$\frac{\partial C}{\partial t} = D \frac{\partial^2 C}{\partial x^2}. \quad (13.34)$$

The initial and boundary conditions of interest are

$$C(x,0) = C_i, \quad (13.35a)$$

and at the slab center,

$$\frac{\partial C}{\partial x}(0,t) = 0, \quad (13.35b)$$

and at the surface,

$$C(L,t) = C_s. \quad (13.35c)$$

The solution to this problem can be determined in the same manner as the solution of the heat conduction equation in Section 9.4.2. By separation of variables it has the form:

$$\theta = X(x)G(t),$$

where θ is $(C - C_s)$, and all the boundary conditions can be written in a homogeneous form. According to Eqs. (9.34) and (9.35), we see that

$$X = c_1 \cos \lambda x + c_2 \sin \lambda x, \quad (13.36)$$

and

$$G = \exp(-\lambda^2 Dt). \quad (13.37)$$

Boundary condition (13.35b) requires that $c_2 = 0$, and when we apply (13.35c) $c_1 \cos \lambda L = 0$ results. This is satisfied by $\lambda = (2n + 1)\pi/2L$, where n is any integer from 0 to ∞ . Hence

$$\theta = \sum_{n=0}^{\infty} A_n \exp\left[\frac{-(2n+1)^2\pi^2}{4} \frac{Dt}{L^2}\right] \cos\left[\frac{(2n+1)\pi}{2} \frac{x}{L}\right], \quad (13.38)$$

where the A_n s are now the constants involved. The initial condition, $\theta(x,0) = \theta_i = C_i - C_s$, remains to be satisfied and when substituted into Eq. (13.38), it yields:

$$\theta_i = \sum_{n=1, \text{odd}}^{\infty} A_n \cos \frac{(2n+1)\pi}{2} \frac{x}{L}. \quad (13.39)$$

If we apply Fourier's analysis to Eq. (13.39) as we demonstrated previously for Eq. (9.38), then we obtain

$$A_n = \frac{(-1)^n}{(2n+1)} \frac{4}{\pi} \theta_i. \quad (13.40)$$

Thus the solution we seek is

$$\frac{\theta}{\theta_i} = \frac{C - C_s}{C_i - C_s} = \frac{4}{\pi} \sum_{n=0}^{\infty} \frac{(-1)^n}{2n+1} \exp \left[\frac{-(2n+1)^2 \pi^2}{4} \frac{Dt}{L^2} \right] \cos \frac{(2n+1)\pi}{2} \frac{x}{L}. \quad (13.41)$$

Equation (13.41) is useful for describing concentration profiles as a function of time. However, the total amount of material that diffuses into or out of the slab is often of more interest, particularly when this is the only measurable quantity. So, the average concentration \bar{C} is required:

$$\bar{C} = \frac{1}{L} \int_0^L C \, dx. \quad (13.42)$$

Carrying out this operation, using Eq. (13.41) for C , we obtain the relative change in average composition for diffusion into a slab:

$$\frac{\bar{C} - C_s}{C_i - C_s} = \frac{8}{\pi^2} \sum_{n=0}^{\infty} \frac{1}{(2n+1)^2} \exp \left[\frac{-(2n+1)^2 \pi^2}{4} \frac{Dt}{L^2} \right]. \quad (13.43)$$

This expression is good for diffusion into or out of a slab. If we take the first term in the series, then

$$\frac{\bar{C} - C_s}{C_i - C_s} = \frac{8}{\pi^2} \exp(-t/\tau), \quad (13.44)$$

where τ is the time constant for the diffusion process ($\tau = 4L^2/\pi^2 D$). It is apparent that a graph of $\log \bar{\theta}$ versus (t/τ) is a straight line and that we can obtain D from the slope. We plot Eq. (13.43) in Fig. 13.6, along with diffusion into or out of cylinders and spheres (see Table 13.2). For long times ($Dt/L^2 > 0.05$), the first term of the series is sufficient, and a straight line relationship is obeyed.

For diffusion into or out of simple multidimensional shapes other than the infinite plate, infinite cylinder, or sphere, we handle the problem in the same manner as we treated heat transfer to or from these shapes in Section 9.5. We can combine product solutions to yield the solution for the shape of interest.

Table 13.2 The relative change in average composition for the basic shapes*Diffusion in a slab of semithickness, L*

I.C.: $C(x,0) = C_i$,

B.C.: $C(L,t) = C_s$,

$$\frac{\partial C}{\partial x}(0,t) = 0.$$

Solution:

$$\frac{\bar{C} - C_s}{C_i - C_s} = \frac{8}{\pi^2} \sum_{n=0}^{\infty} \frac{1}{(2n+1)^2} \exp \left[\frac{-(2n+1)^2 \pi^2}{4} \frac{Dt}{L^2} \right]. \quad (13.43)$$

Diffusion in solid circular cylinder of radius, R

I.C.: $C(r,0) = C_i$,

B.C.: $C(R,t) = C_s$,

$$\frac{\partial C}{\partial r}(0,t) = 0.$$

Solution:

$$\frac{\bar{C} - C_s}{C_i - C_s} = \sum_{n=1}^{\infty} \frac{4}{\xi_n^2} \exp \left[\frac{-\xi_n^2 Dt}{R^2} \right], \quad (13.45)$$

where $\xi_n = 2.405, 5.520, 8.654, 11.792, 14.931$, when $n = 1, 2, 3, 4, 5$, etc.**Diffusion in spheres of radius, R*

The same set of initial and boundary conditions as for the cylinder above:

$$\frac{\bar{C} - C_s}{C_i - C_s} = \frac{6}{\pi^2} \sum_{n=1}^{\infty} \frac{1}{n^2} \exp \left[\frac{-n^2 \pi^2 Dt}{R^2} \right]. \quad (13.46)$$

* ξ_n are roots of the equation $J_0(x) = 0$, where $J_0(x)$ is the Bessel function of zero order.

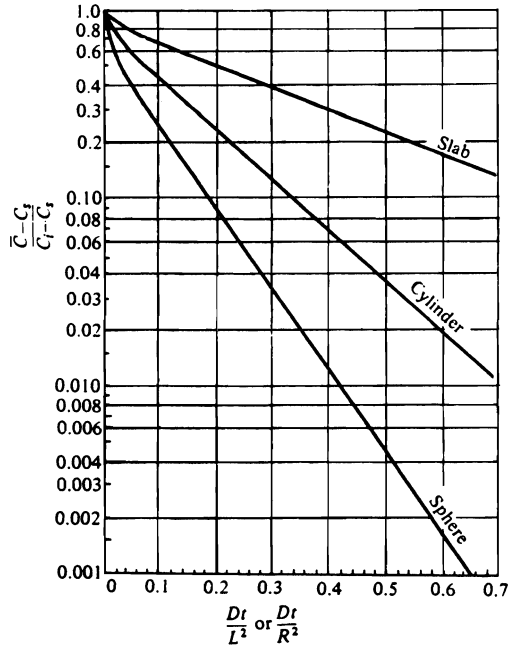


Fig. 13.6 The relative change in average composition for the basic shapes. R = radius, and L = semithickness.

Example 13.5 Calculate the fraction of hydrogen remaining in a) a 100 mm thick slab of steel, 3 m long \times 1.2 m wide, b) a 100 mm square billet of steel, 4 m long, and c) a 100 mm square billet of steel, 200 mm long, after 40 hours of vacuum outgassing treatment at a temperature where $D_H = 1.0 \times 10^{-9} \text{ m}^2 \text{ s}^{-1}$, assuming an initially uniform distribution.

Solution. a) Consider this to be an infinite plate. Then

$$\frac{Dt}{L^2} = \frac{(1 \times 10^{-9})(40 \times 3600)}{(5 \times 10^{-2})^2} = 5.76 \times 10^{-2}.$$

From Fig. 13.6, we have

$$\frac{\bar{C} - C_s}{C_i - C_s} = 0.74.$$

480 Diffusion in Solids

b) The desired solution can be obtained as the product of the infinite plate solutions for the two 100 mm dimensions:

$$\frac{\bar{C} - C_s}{C_i - C_s} = (0.74)(0.74) = 0.55.$$

c) In this case, first evaluate Dt/L^2 for the 200 mm dimension:

$$\frac{Dt}{L^2} = \frac{(1 \times 10^{-9})(40 \times 3600)}{0.1^2} = 1.44 \times 10^{-2}.$$

From Fig. 13.6, we get

$$\left[\frac{\bar{C} - C_s}{C_i - C_s} \right]_{200 \text{ mm}} = 0.90.$$

Therefore,

$$\frac{\bar{C} - C_s}{C_i - C_s} = (0.90)(0.74)(0.74) = 0.49.$$

13.4 MICROELECTRONIC DIFFUSION PROCESSING

Some materials result from processes in which alloying elements or *dopants* are diffused into a hot matrix to change electronic or magnetic properties. This is particularly true of silicon processed into devices. Frequently, a junction is fabricated by using two steps, each involving diffusion. The two steps are *predeposition* and *drive-in* diffusion.

In predeposition, a silicon wafer is placed in a high-temperature furnace and exposed to a gas that contains the dopant. Depending on the gas and the temperature, a constant concentration of the dopant is established at the surface. The goal of the predeposit step is to diffuse a small amount of the dopant into a fraction of a micrometer at the surface. Obviously, the silicon matrix is semi-infinite so the concentration profile of the dopant is

$$\frac{C - C_s}{C_0 - C_s} = \operatorname{erf} \left[\frac{x}{2\sqrt{Dt}} \right], \quad (13.47)$$

where C_s is the constant surface concentration, C_0 is the initial concentration (assumed to be uniform), x is distance measured from the surface at $x = 0$, D is the diffusion coefficient of the dopant in the silicon, and t is time. The situation is depicted in Fig. 13.7.

The amount of dopant predeposited, usually expressed in terms of the number of dopant atoms, is

$$J = A \int_0^t j_{x=0} dt, \quad (13.48)$$

where A is the surface area of the silicon wafer and $j_{x=0}$ is the flux of dopant atoms at the surface ($x = 0$). It can be shown that the flux at the surface is

$$j_{x=0} = (C_s - C_0) \left(\frac{D}{\pi t} \right)^{1/2}; \quad (13.49)$$

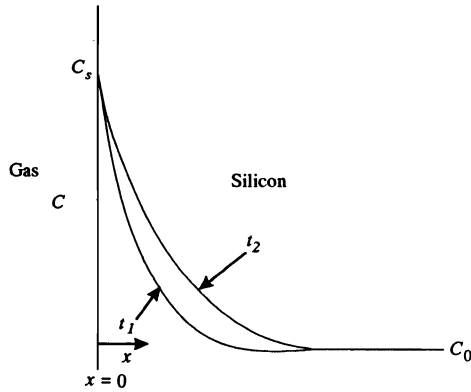


Fig. 13.7 The concentration of dopant at the surface of a silicon wafer during the predeposition step; $t_2 > t_1$.

then by combining Eqs. (13.48) and (13.49) and carrying out the integration, we get the amount predeposited. It is

$$J = \frac{2A}{\pi^{1/2}} (C_s - C_0)(Dt)^{1/2}. \tag{13.50}$$

During predeposition, we also calculate the diffusion depth of the dopant profile; it is

$$\ell = (Dt)^{1/2}. \tag{13.51}$$

Values of diffusion coefficients and approximate surface concentrations for two dopants, boron and phosphorus, are given in Table 13.3. The units are those most likely to be encountered in device fabrication technology.

Table 13.3 Surface concentrations and diffusion coefficients for boron and phosphorus

T, K	Boron		Phosphorus	
	C_s , atoms cm^{-3}	D , $\mu\text{m}^2 \text{h}^{-1}$	C_s , atoms cm^{-3}	D , $\mu\text{m}^2 \text{h}^{-1}$
1223	4.5×10^{20}	1.6×10^{-3}	9×10^{20}	1.7×10^{-3}
1273	4.8×10^{20}	5.2×10^{-3}	1.0×10^{21}	6.4×10^{-3}
1323	5.0×10^{20}	1.7×10^{-2}	1.1×10^{21}	2.0×10^{-2}
1373	5.1×10^{20}	5.8×10^{-2}	1.2×10^{21}	7.3×10^{-2}
1423	5.2×10^{20}	1.6×10^{-1}	1.2×10^{21}	1.8×10^{-1}

Example 13.6 Boron is predeposited on a silicon wafer with an initial concentration of 5×10^{15} atoms cm^{-3} . Conditions are 30 minutes at 1223 K. Calculate a) the amount deposited; b) the diffusion length; c) the concentration at the diffusion length.

482 Diffusion in Solids

Solution. a) From Table 13.3, $C_s = 4.5 \times 10^{20}$ atoms cm^{-3} and $D = 1.6 \times 10^{-3} \mu\text{m}^2 \text{h}^{-1}$. Equation (13.50) applies, so that

$$\begin{aligned} \frac{J}{A} &= \frac{2}{\pi^{1/2}} (C_s - C_0)(Dt)^{1/2} = \frac{2}{\pi^{1/2}} (4.5 \times 10^{20} - 5 \times 10^{15})(1.6 \times 10^{-3})^{1/2} (0.5)^{1/2} \\ &= \frac{1.44 \times 10^{19} \text{ atoms } \mu\text{m}}{\text{cm}^3} \left| \frac{1 \text{ cm}}{10^4 \mu\text{m}} \right. = 1.44 \times 10^{15} \text{ atoms cm}^{-2}. \end{aligned}$$

b) Equation (13.51) is used.

$$\ell = (1.6 \times 10^{-3} \times 0.5)^{1/2} = 2.83 \times 10^{-2} \mu\text{m} = 2.83 \times 10^{-6} \text{ cm}.$$

Notice how small ℓ is; this is typical.

c) Equation (13.47) applies with $x = \ell = (Dt)^{1/2}$. Thus, with Table 9.3 we get

$$\frac{C - C_s}{C_0 - C_s} = \text{erf} \left[\frac{1}{2} \right] = 0.5205,$$

and

$$\begin{aligned} C &= (0.5205)(5 \times 10^{15} - 4.5 \times 10^{20}) + 4.5 \times 10^{20} \\ &= 2.16 \times 10^{20} \text{ atoms cm}^{-3}. \end{aligned}$$

From the above example we see that a very thin layer of the dopant is deposited on to the surface of the silicon matrix. This was done by the chemical reaction with the gas and allowing a small amount of diffusion to occur. Another method of producing a high concentration of dopant at the surface is *ion implantation*. In this method a beam of ions is accelerated into a mass-separating magnetic field, which selects the dopant ions from unwanted ions, similar to the separation in a mass spectrometer. The beam of dopant ions is aimed at the silicon target, where the ions come to rest after colliding with the nuclei and electrons in the surface layer of the target, which also tends to create vacancies in the host lattice. Ion implantation can be controlled better than predeposition through the gas, both in terms of minimizing lateral spread and in establishing a very sharp definition of the dopant at the surface. A very high density of crystalline defects, especially vacancies, however, is a disadvantage because they can reduce the electronic performance of the device.

After the predeposition step, drive-in diffusion is done to allow diffusion from the surface further into the silicon. This is illustrated by Fig. 13.8. To prevent escape of the dopant, a very thin layer of silica (SiO_2) is made on the surface. During the drive-in, the boundary conditions and the initial condition for $C(x,t)$ are

$$\frac{\partial C(0,t)}{\partial x} = 0, \tag{13.52a}$$

$$C(\infty,t) = C_0, \tag{13.52b}$$

and

$$C(x,0) = f(x'). \tag{13.52c}$$

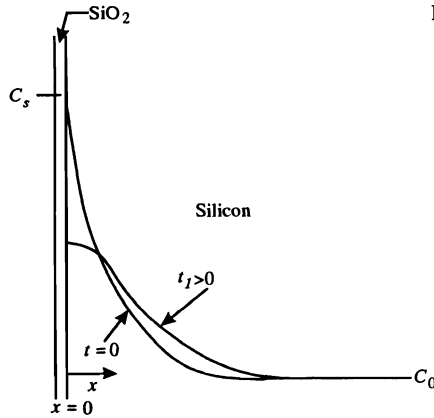


Fig. 13.8 The concentration of dopant near the surface of a silicon wafer during the drive-in step. The distribution at $t = 0$ is that from the predeposition step.

Equation (13.52a) applies at the surface, Eq. (13.52b) simply gives the concentration in the interior, and Eq. (13.52c) represents the distribution of dopant that results from the predeposition.

The solution which satisfies Fick's second law of diffusion and Eqs. (13.52a,b,c) can be deduced from Appendix G. Then

$$C - C_0 = \int_{x'=0}^{\infty} \frac{f(x') - C_0}{2\sqrt{\pi Dt}} \left\{ \exp \left[\frac{-(x - x')^2}{4Dt} \right] - \exp \left[\frac{-(x + x')^2}{4Dt} \right] \right\} dx', \quad (13.53)$$

where $f(x')$ is the distribution of the solute from the predeposition step and given by Eq. (13.47). By combining Eqs. (13.47) and (13.53), we get

$$\frac{C - C_0}{C_s - C_0} = \int_{x'=0}^{\infty} \frac{\text{erfc}(x'/2\ell)}{2\sqrt{\pi Dt}} \left\{ \exp \left[\frac{-(x - x')^2}{4Dt} \right] - \exp \left[\frac{-(x + x')^2}{4Dt} \right] \right\} dx'. \quad (13.54)$$

Equation (13.54) is the solution, but, unfortunately, it is cumbersome and requires a numerical integration. Therefore, an approximate solution is often invoked.

The dopant taken up by the silicon in the predeposit step is approximated to be a thin source on the surface of the silicon. The strength of the source is given by the amount deposited per unit area. Thus, Eq. (13.22) applies with C relative to C_0 and the source strength (β) given by J/A , Eq. (13.50).

$$\frac{C - C_0}{C_s - C_0} = \frac{2}{\pi} \left[\frac{\ell^2}{Dt} \right]^{1/2} \exp \left[-\frac{x^2}{4Dt} \right]. \quad (13.55)$$

Notice that C_s and ℓ are from the predeposit step, but D and t are for the drive-in step.

The so-called "junction depth" (x_j) is important because it is a measure of the depth of diffusion after drive-in diffusion. The junction depth is defined as follows.

Since $C_s \gg C_0$, Eq. (13.55) is approximated by

$$\frac{C}{C_s} \cong \frac{2}{\pi} \left[\frac{\ell}{Dt} \right]^{1/2} \exp \left[-\frac{x^2}{4Dt} \right], \quad (13.56)$$

and x_j is that value of x where $C = C_0$. Then

$$x_j = \left\{ 4Dt \ln \left[\left[\frac{2}{\pi} \right] \left[\frac{C_s}{C_0} \right] \left[\left(\frac{\ell^2}{Dt} \right)^{1/2} \right] \right] \right\}^{1/2} \quad (13.57)$$

Example 13.7 After the predeposit step, the wafer of Example 13.6 is subjected to drive-in at 1423 K for 2 h. Calculate: a) the junction depth; b) the concentration at that depth; and c) the surface concentration.

Solution. a) Equation (13.57) applies with ℓ , C_s and C_0 given in Example 13.6. From Table 13.3 $D = 1.6 \times 10^{-1} \mu\text{m}^2 \text{h}^{-1} = 4.44 \times 10^{-13} \text{cm}^2 \text{s}^{-1}$; also $t = 7200 \text{s}$.

$$x_j = \left\{ 4 \times 4.44 \times 10^{-13} \times 7200 \ln \left[\left[\frac{2}{\pi} \right] \left[\frac{4.5 \times 10^{20}}{5 \times 10^{15}} \right] \left[\frac{2.83^2 \times 10^{-12}}{4.44 \times 10^{-13} \times 7200} \right]^{1/2} \right] \right\}^{1/2}$$

$$x_j = 3.19 \times 10^{-4} \text{cm} = 3.19 \mu\text{m}.$$

b) $C = C_0 = 5 \times 10^{15} \text{atoms cm}^{-3}$. We obtain an exact result by using Eq. (13.55).

$$\frac{C - C_0}{C_s - C_0} = \frac{2}{\pi} \left[\frac{2.83^2 \times 10^{-12}}{4.44 \times 10^{-13} \times 7200} \right]^{1/2} \exp \left[- \frac{3.19^2 \times 10^{-8}}{4 \times 4.44 \times 10^{-13} \times 7200} \right]$$

$$= 1.115 \times 10^{-5}.$$

Therefore,

$$C = (1.115 \times 10^{-5})(4.5 \times 10^{20} - 5 \times 10^{15}) + 5 \times 10^{15}$$

$$= 1.00 \times 10^{16} \text{atoms cm}^{-3}.$$

c) We use Eq. (13.55) with $x = 0$.

$$\frac{C - 5 \times 10^{15}}{4.5 \times 10^{20} - 5 \times 10^{15}} = \frac{2}{\pi} \left[\frac{2.83^2 \times 10^{-12}}{4.44 \times 10^{-13} \times 7200} \right]^{1/2} = 0.0319.$$

$$C = 1.43 \times 10^{19} \text{atoms cm}^{-3}.$$

13.5 HOMOGENIZATION OF ALLOYS

During solidification of alloys, *coring* occurs, because the rate of diffusion for most alloying elements in the solid state is too slow to maintain a solid of uniform concentration in equilibrium with the liquid. A cast structure is exemplified in Fig. 13.9 showing the repetitive pattern of microsegregation. In the case at hand we presume the alloy to be a single phase.

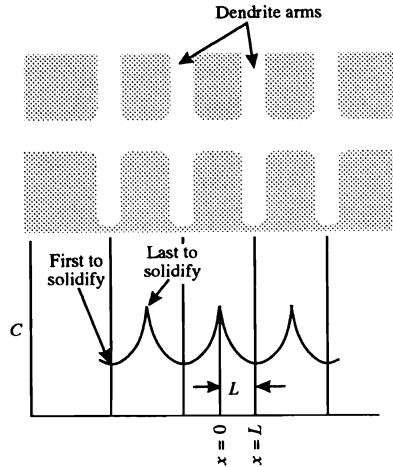


Fig. 13.9 A dendritic structure showing the *coring* or microsegregation of the alloying element. L is one-half of the dendrite arm spacing.

The dendrite arms develop during solidification and their spacing depends upon the alloy and the rate of cooling from the liquidus temperature to the nonequilibrium solidus temperature. Depending on the cooling rate, the *dendritic arm spacing* can be between $5 \mu\text{m}$ and $400 \mu\text{m}$, with typical values ranging from $50 \mu\text{m}$ to $200 \mu\text{m}$.

Dendritic structures occur in cast products that encompass ingots, shaped castings, continuous castings, and weldments. The *coring*, or microsegregation, is coincidental with the growth of the dendrites. Imagine a local region in a solidifying casting that comprises several to many dendrite arms. As solidification proceeds within the local region, solute is rejected to the *interdendritic* liquid, when the concentration of solute in the solid is less than that of the interdendritic liquid. The microsegregation can be closely approximated by a simple solute balance.³ That is, the solute rejected from the dendritic solid equals the increase of solute in the interdendritic liquid. Therefore, within a local region undergoing solidification we have

$$(C_L - C_s^*) df_s = (1 - f_s) dC_L, \tag{13.58}$$

where

C_L = weight percent of solute in the interdendritic liquid;

C_s^* = weight percent of solute in the dendritic solid at the solid-liquid interface;

and

f_s = local weight fraction of solid.

³M. C. Flemings, *Solidification Processing*, McGraw-Hill, New York, NY, 1974, pages 34-36, 142.

486 Diffusion in Solids

When we use Eq. (13.58), it is assumed that there is sufficient diffusion of solute in the liquid so that it is uniform. This is usually valid because the diffusion length in the liquid is many times greater than the dendrite arm spacing. On the other hand, the diffusion coefficient of the solute in the solid is typically 5 or 6 orders of magnitude less than in the liquid, so we assume no diffusion in the solid. Consequently, as a layer of solid with a concentration C_s^* forms, its concentration never changes as subsequent solid of different C_s^* grows from the interdendritic liquid.

To get a quantitative picture of the microsegregation, we integrate Eq. (13.58). Then

$$\int_{C_L=C_0}^{C_L} \frac{dC_L}{C_L - C_s^*} = \int_{f_s=0}^{f_s} \frac{df_s}{1 - f_s},$$

or

$$1 - f_s = \exp \left[- \int_{C_L=C_0}^{C_L} (C_L - C_s^*)^{-1} dC_L \right], \quad (13.59)$$

where C_0 is the concentration of solute in the unsolidified melt (i.e., the alloy composition). In dendritically freezing alloys, the solid-liquid interface is very close to equilibrium so that C_s^* can be taken as the solid in equilibrium with the liquid. Many binary alloys have phase diagrams in which the ratio $C_s^*/C_L = k$ can be approximated as a constant, called the equilibrium partition ratio. With a constant k , we can substitute $C_s^* = kC_L$ into Eq. (13.59) and carry out the integration. The result is

$$\frac{C_L}{C_0} = (1 - f_s)^{k-1},$$

or

$$\frac{C_s^*}{C_0} = k(1 - f_s)^{k-1}. \quad (13.60)$$

As an example, suppose $k = 0.3$; then the microsegregation according to Eq. (13.60) is shown in Fig. 13.10. The first solid that forms has a concentration $C_s^* = kC_0$ and then succeeding solid has progressively higher values of C_s^* . But with no diffusion in the solid, the microsegregation, which develops, remains.

As $f_s \rightarrow 1$, Eq. (13.60) predicts $C_s^* \rightarrow \infty$. In reality, a reaction, such as a eutectic reaction, takes place near the end of solidification when the interdendritic liquid becomes sufficiently enriched in solute. In any event, after solidification is complete there is microsegregation, and in many applications it is necessary to subsequently heat treat the alloy to reduce the microsegregation by diffusion. This process is called homogenization.

During homogenization, the alloy naturally tends toward a uniform concentration (Fig. 13.11). We need only examine what happens within one dendritic element since the profile is periodic, and there is no net flow of solute from any dendritic region to the next.

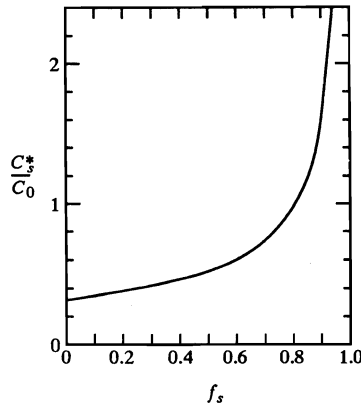


Fig. 13.10 Microsegregation in a dendritic solid with $k = 0.3$.

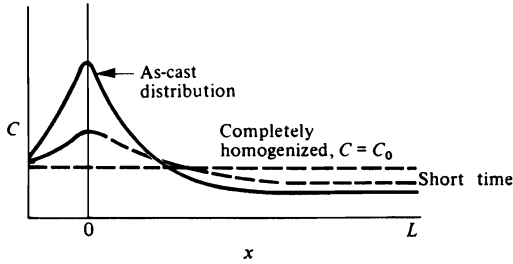


Fig. 13.11 Dendritic element, $0 < x < L$, used for describing homogenization kinetics.

To describe the homogenization kinetics, a solution to Fick’s second law is needed that satisfies

$$\text{I.C.: } C(x,0) = f(x), \tag{13.61a}$$

$$\text{B.C.: } \frac{\partial C}{\partial x} (0,t) = 0, \tag{13.61b}$$

$$\frac{\partial C}{\partial x} (L,t) = 0, \quad t > 0. \tag{13.61c}$$

The solution can be obtained by applying the method of separation of variables. Here we simply present the solution as given by Crank⁴:

$$C(x,t) = C_0 + \sum_{n=1}^{\infty} A_n \exp \left[-n^2 \pi^2 \frac{Dt}{L^2} \right] \cos \frac{n\pi x}{L}, \tag{13.62}$$

⁴J. Crank, *The Mathematics of Diffusion*, Oxford University Press, London, 1957, page 58.

with

$$A_n = \frac{2}{L} \int_0^L f(x) \cos \frac{n\pi x}{L} dx. \quad (13.63)$$

In Eq. (13.62), C_0 is the overall or average alloy content, and we evaluate the A_n s by Eq. (13.63) using $f(x)$ as the initial solute distribution.

A useful parameter to describe the homogenization kinetics is the *residual segregation index* δ , which is defined as

$$\delta \equiv \frac{C_M - C_m}{C_M^0 - C_m^0}, \quad (13.64)$$

where C_M = maximum concentration, that is, $C_M = C(0,t)$; C_M^0 = initial maximum concentration, that is, $C_M^0 = C(0,0)$; C_m = minimum concentration, that is, $C_m = C(L,t)$; and C_m^0 = initial minimum concentration, that is, $C_m^0 = C(L,0)$. For no homogenization, $\delta = 1$, and after complete homogenization, $\delta = 0$.

We can find $C_M - C_m$ by applying Eq. (13.62) to $x = 0$ and $x = L$, and performing the indicated subtraction. The residual segregation index can then be written as

$$\delta = \frac{2 \sum_{n=1,3,\dots,\infty} A_n \exp \left[-n^2 \pi^2 \frac{Dt}{L^2} \right]}{C_M^0 - C_m^0}. \quad (13.65)$$

Equation (13.65) has been used to analyze the homogenization of chromium in cast 52100 steel (1%C-1.5%Cr). Figure 13.12 shows the results. The practical conclusions of such studies show that:

1. In commercial material, with relatively large dendrite arm spacing (200-400 μm), substitutional elements do not homogenize unless excessively high temperatures and long diffusion times are employed. For example, in laboratory-cast 52100 ingots the dendrite arm spacing could typically be 300 μm , which would have to be held at 1450 K for about 20 hours to reduce δ to 0.2 for chromium. In large commercial ingots, dendrite arm spacings are larger and homogenization is even more difficult to achieve.
2. Significant homogenization of substitutional elements is possible at reasonable temperatures and times only if the material has fine dendrite arm spacings (<50 μm), which result from rapid solidification.
3. Interstitial elements (such as carbon in steel) diffuse very rapidly at austenizing temperatures.

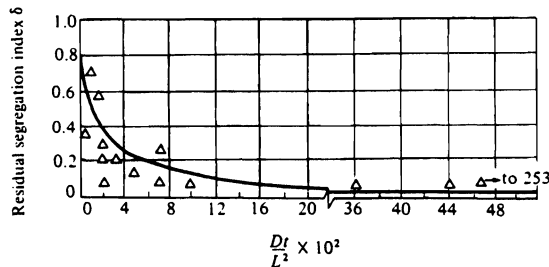
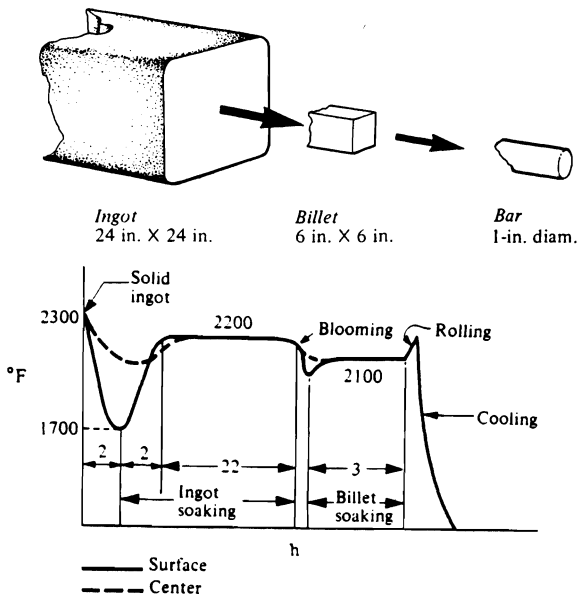


Fig. 13.12 The residual segregation index for chromium in cast 52100 steel. (From M. C. Flemings, D. R. Poirier, R. V. Barone, and H. D. Brody, *JISI*, 371, April 1970.)

Homogenization studies have also been carried out for 4340 low-alloy steel⁵ and 7075 aluminum alloy.⁶ In Reference 6, the analysis and discussion of homogenization emphasizes the dissolution of a nonequilibrium second phase during solutionizing.

Example 13.7 An ingot of 52100 steel goes through the processing schedule indicated below. Estimate the residual segregation index of chromium for the material in the center and the outside surface of the finished bar. Neglect the small amount of diffusion that occurs during blooming, rolling, and final cooling. Near the surface of the original cast ingot, the dendrite arm spacing is 40 μm, and in the center, it is 800 μm. The diffusion coefficient of chromium in this steel at these temperatures is given by

$$D = 2.35 \times 10^{-5} \exp [-17\,300/T(K)], \text{ cm}^2 \text{ s}^{-1}.$$



Reduction schedule for 52100 alloy steel bars.

Solution. Before proceeding directly to the solution of this problem, we should recognize that, although the basis for Eq. (13.65) assumes a constant diffusion coefficient (hence isothermal treatment), we can apply it to non-isothermal conditions.

For example, if a part is subjected to n heat treatment steps, each at a different temperature and for different times, we can compute the total magnitude of Dt/L^2 as

$$\frac{Dt}{L^2} = \frac{1}{L^2} \sum_{i=1}^n D_i t_i.$$

⁵T. F. Kattamis and M. C. Flemings, *Trans. TMS-AIME* **233**, 992 (1965).

⁶S. N. Singh and M. C. Flemings, *Trans. TMS-AIME* **245**, 1803 (1969).

490 Diffusion in Solids

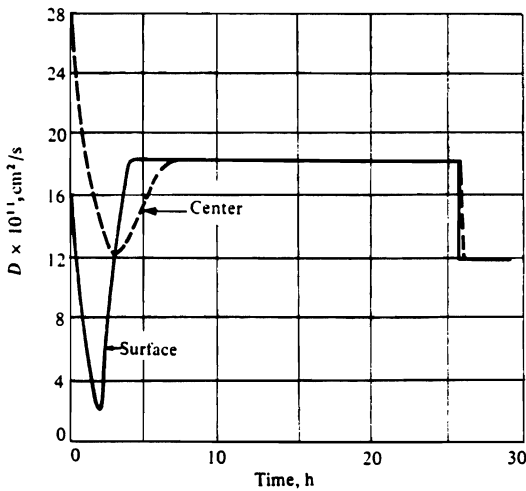
We can then use this value of Dt/L^2 in Eq. (13.65). For a continuous nonisothermal situation, we compute the total magnitude of Dt/L^2 to be used as

$$\frac{Dt}{L^2} = \frac{1}{L^2} \int_0^t D(t) dt.$$

For hot-working in which D and L are both time dependent, Dt/L^2 should be evaluated as

$$\frac{Dt}{L^2} = \int_0^t \frac{D(t)}{[L(t)]^2} dt.$$

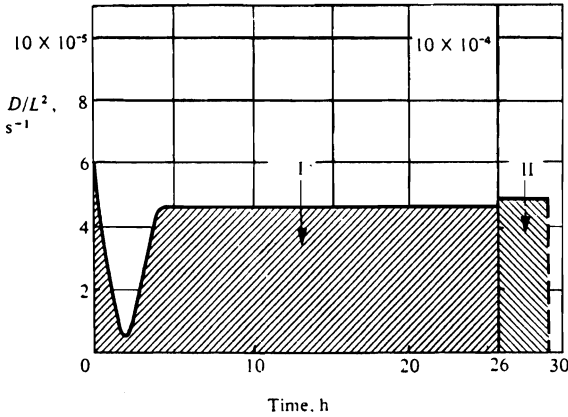
Now we determine $D(t)$, given the thermal process schedule and $D(T)$.



During the processing, assume that the dendrite spacing decreases in proportion to the changes of linear dimensions. Based on this, $L(t)$ is given in the table below.

Time	Center of ingot, L , cm	Surface of ingot L , cm
0-26 h	0.040	0.0020
26-29 h	0.010	0.0005

Now Dt/L^2 for the "surface" material can be evaluated by determining the area under the curve in the figure below.



Under area I	$112 \times 10^{-5} \text{ h s}^{-1}$
Under area II	$141 \times 10^{-5} \text{ h s}^{-1}$
Total	$253 \times 10^{-5} \text{ h s}^{-1}$

$$\frac{Dt}{L^2} (\text{surface}) = 253 \times 10^{-5} \times 3600 = 9.10.$$

According to Fig. 13.12, this value of Dt/L^2 indicates that the surface material would be homogeneous since $\delta \cong 0$.

In the center of the ingot, since the dendrite spacing is 20 times the spacing of the surface, then (neglecting small differences in the thermal history)

$$\frac{Dt}{L^2} (\text{center}) \cong \frac{Dt}{L^2} (\text{surface}) \times \frac{1}{20^2} = \frac{9.10}{400} = 0.0228.$$

From Fig. 13.12, we see that $\delta \cong 0.27$, and a significant amount of microsegregation remains in the material.

13.6 FORMATION OF SURFACE LAYERS

The rate of formation of oxide (sulfide) layers on metals and alloys exposed to oxidizing (sulfidizing) conditions is a matter of considerable technological importance. In general, it is not possible to say *a priori* that the rate of formation of a nonmetallic layer will be controlled by diffusion. For example, the initial rate of formation of the layer is often determined by the rate of an interface reaction between the gas and solid. As growth proceeds, if the specific volume of the oxide is much larger than that of the metal substrate, separation of the two phases may occur, causing an interruption in the growth of the oxide layer. However, in many cases this separation does not occur, and growth continues by diffusion of either the metal out through the oxide layer, or diffusion of oxygen into the metal-oxide interface, or a combination of both. In the case of adherent oxides, eventually

the diffusion flux slows down to the point where it is considerably slower than the interface reaction, and diffusion controls the rate of growth of the layer from then on.

If we consider the situation in Fig. 13.13, we can derive an expression for the rate of increase in the oxide thickness M . In this example, the metal is divalent, and the oxygen anions, having a large ionic radius, diffuse only at a negligible rate through the oxide layer so that $j_{O^{2-}} = 0$. Thus the oxide thickens because the metal cations diffuse through the oxide so that the oxidation reaction can proceed. At any instant, the flux of cations through the oxide is given by Fick's law (Eq. (12.2)):

$$j = (j_{A^{2+}}) = -D \left[\frac{\partial C}{\partial x} \right].$$

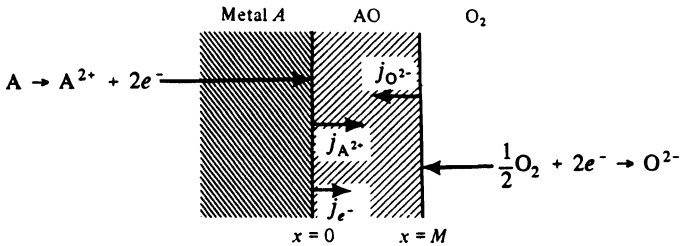


Fig. 13.13 The oxide layer on a metal showing the direction of flow of ions and electrons.

Here D is the diffusivity of the cation, and C is the cation concentration. If the oxide layer is thin, then we approximate the concentration profile of the cation as linear, and can integrate Fick's law as

$$j \int_0^M dx = - \int_{C_0}^{C_M} D dC.$$

Here, C_0 is the cation concentration at $x = 0$, and C_M is that at $x = M$. If the boundary conditions C_M and C_0 are unchanged with time (that is, with M), then the instantaneous flux at any thickness M is

$$j = \frac{1}{M} \int_{C_M}^{C_0} D dC, \quad (13.66)$$

or

$$j = \frac{k}{M},$$

where k is a constant, and has the units of $\text{mol m}^{-1} \text{s}^{-1}$.

The flux is proportional to the rate of growth of the thickness of the oxide layer:

$$j \propto \frac{dM}{dt},$$

or

$$\frac{k}{M} \propto \frac{dM}{dt}, \quad (13.67)$$

so that

$$\int_0^M M \, dM = \int_0^t k' \, dt,$$

or

$$M^2 = 2k't, \quad (13.68)$$

where k' is a constant with units $\text{m}^2 \text{s}^{-1}$, known as the *Tammann scaling constant*⁷ or the *Pilling and Bedworth constant*.⁸ The parabolic nature of the rate of change of the oxide thickness with time is apparent.

Experimentally, it is usually more convenient to measure mass gain rather than the oxide thickness. Then

$$\frac{\Delta m}{A} = M\rho_0, \quad (13.69)$$

where $\Delta m/A = \text{kg (mass gained)} \text{ m}^{-2}$ (surface area), and $\rho_0 = \text{concentration of oxygen in the oxide, kg of oxygen m}^{-3}$ of oxide.

If we substitute Eq. (13.69) into Eq. (13.68), we obtain

$$\left(\frac{\Delta m}{A} \right)^2 = \frac{2k'}{\rho_0^2} t,$$

or

$$\left(\frac{\Delta m}{A} \right)^2 = k_p t, \quad (13.70)$$

where k_p is the *practical parabolic scaling constant*, $(\text{kg O}_2)^2 \text{ m}^{-4} \text{ s}^{-1}$. Usually, we obtain experimental data by mass gain measurements, and take straight-line behavior when we plot $(\Delta m/A)^2$ versus t as an indication of diffusion-controlled oxidation.

Such data alone, however, do not indicate which *species* is responsible for the major material flow, that is, whether the metal is diffusing out from the oxide-metal interface or the oxygen is diffusing in. Wagner⁹ has extended this simple expression to express k_p in terms of diffusion coefficients of the migrating species.

Combining Eqs. (12.23), (12.37), and (12.39), we obtain the relation

$$n_i B_i = \frac{t_i \sigma}{(z_i e)^2}, \quad (13.71)$$

⁷G. Tammann, *Z. Anorg. u. Allgem. Chem.* **111**, 78 (1920).

⁸N. B. Pilling and R. E. Bedworth, *J. Inst. Metals* **29**, 529 (1923).

⁹C. Wagner, *Atom Movements*, Amer. Soc. for Metals, Cleveland, OH, 1951, page 153.

494 Diffusion in Solids

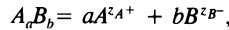
where n_i = concentration of the migrating species, B_i = mobility of the species, σ = total electrical conductivity of the compound, t_i = transference number of species i , z_i = valence, and e = electronic charge. Now, using Eq. (12.32) and substituting Eqs. (12.37) and (13.71), we obtain the flux \dot{n}_i :

$$\dot{n}_i = - \frac{t_i \sigma}{(z_i e)^2} \left[\kappa_B T \left[\frac{\partial \ln n_i}{\partial x} \right] + z_i e \left[\frac{\partial \phi}{\partial x} \right] \right], \quad (13.72)$$

or in terms of the free energy for an ideal solution

$$\dot{n}_i = - \frac{t_i \sigma}{(z_i e)^2} \left[\frac{\partial \mu_i}{\partial x} + z_i e \frac{\partial \phi}{\partial x} \right], \quad (13.73)$$

where μ_i is the chemical potential (per atom) of species i . If the compound formed has the stoichiometric composition $A_a B_b$, where A is the cation, then the scale consists of ions according to the dissociation reaction:



where the z s are the respective valences. Since the scale cannot have a net charge, the fluxes of individual species are related by

$$z_a \dot{n}_{A^+} = z_b \dot{n}_{B^-} + \dot{n}_e. \quad (13.74)$$

Using Eq. (13.73) for each flux and recalling Eq. (12.38), we obtain an expression for $\partial \phi / \partial x$:

$$\frac{\partial \phi}{\partial x} = \frac{1}{e} \left[- \frac{t_A}{z_A} \frac{\partial \mu_{A^+}}{\partial x} + \frac{t_B}{z_B} \frac{\partial \mu_{B^-}}{\partial x} + t_e \frac{\partial \mu_e}{\partial x} \right]. \quad (13.75)$$

In order to obtain an expression for the total flux in terms that we can measure, we must replace the expressions involving μ_{A^+} , μ_{B^-} , and μ_e . We first consider the equilibria

$$A = A^{z_A+} + z_A e, \quad (13.76a)$$

and

$$B + z_B e = B^{z_B-}. \quad (13.76b)$$

At equilibrium

$$\mu_A = \mu_{A^+} + z_A \mu_e, \quad (13.76c)$$

and

$$\mu_B = \mu_{B^-} - z_B \mu_e. \quad (13.76d)$$

For the compound in general, we get

$$d\mu_A = - \left| \frac{z_A}{z_B} \right| d\mu_B, \quad (13.77)$$

from the Gibbs-Duhem relationship. Then, eliminating μ_{A^+} , μ_{B^-} , and μ_e from Eqs. (13.75) and (13.73) and using Eqs. (13.76a,b) and (13.77), we obtain expressions for the particle fluxes:

$$\dot{n}_{A^+} = \frac{z_B t_A t_e \sigma}{z_A e^2 z_B^2} \left[\frac{\partial \mu_B}{\partial x} \right], \quad A \text{ ions } m^{-2} s^{-1} \quad (13.78)$$

and

$$\dot{n}_{B^-} = - \frac{t_B t_e \sigma}{e^2 z_B^2} \left[\frac{\partial \mu_B}{\partial x} \right], \quad B \text{ ions } m^{-2} s^{-1}. \quad (13.79)$$

Since the growth rate of the compound is the sum of the particle fluxes (although either may go to zero), we obtain

$$\dot{n}_{A_a B_b} = \frac{n_{A^+}}{a} - \frac{n_{B^-}}{b} = \frac{\sigma(t_A + t_B)t_e}{e^2 z_B^2 b} \left[\frac{\partial \mu_B}{\partial x} \right], \quad \text{molecules } A_a B_b \text{ } m^{-2} s^{-1}. \quad (13.80)$$

If we use, for some reason, Eq. (13.80), we usually convert the units to give the flux in g-equivalents $m^{-2} s^{-1}$. Denoting the number of equivalents per mole by the symbol r ,* we obtain the growth rate:

$$\dot{n}_{A_a B_b} = \frac{r\sigma(t_A + t_B)t_e}{e^2 z_B^2 N_0} \left[\frac{\partial \mu_B}{\partial x} \right], \quad \text{g-equivalents } A_a B_b \text{ } m^{-2} s^{-1}. \quad (13.81)$$

We define the *rational rate constant*, k_r , as $\int_0^x \dot{n}_{A_a B_b} dx$; then

$$k_r = \frac{r}{e^2 N_0 z_B^2} \int_{\mu_B^i}^{\mu_B^0} \sigma(t_A + t_B)t_e d\mu_B, \quad (13.82)$$

where μ_B^i and μ_B^0 are the chemical potentials of B at the inside and outside (metal and gas) interfaces of the oxide, respectively; k_r has the units of g-equivalents $m^{-1} s^{-1}$ and is related to the parabolic rate constant k_p by

$$k_p = \frac{2\rho_0(\text{at. wt } B)^2}{r(\text{mol. wt } A_a B_b)} k_r. \quad (13.83)$$

The Tammann scaling constant is related to k_r by

$$k' = \frac{2(\text{at. wt } B)}{\rho_0 b z_B} k_r. \quad (13.84)$$

*Note that *numerically* $r = z_B$, but that their *units* differ.

496 Diffusion in Solids

If we assume that the anion exists as B_2 in the gaseous state, and there is ideal gas behavior, we can substitute

$$d\mu_B = \frac{1}{2} \kappa_B T d \ln p_{B_2}$$

into Eq. (13.82) and obtain

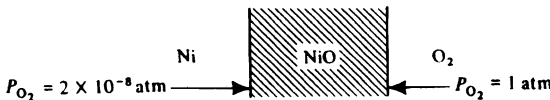
$$k_r = \frac{r\kappa_B T}{2e^2 N_0 z_B^2} \int_{p_{B_2}^i}^{p_{B_2}^o} t_e(t_A + t_B) \sigma d \ln p_{B_2}. \quad (13.85)$$

We note that although t_e may approach 1.0, and $(t_A + t_B)$ may approach zero, the expression $(t_A + t_B)$ cannot equal zero even for an electronic oxide conductor because it would cause a charge imbalance. In an electronic semiconductor, the product $t_e(t_A + t_B)$ is a very small number, and k_r is small. In this case, where $t_e = 1.0$, if we assume that mobilities B_A and B_B are equal to B_A^* and B_B^* , respectively, we can substitute Eq. (12.37) into Eq. (13.85) and obtain

$$k_r = \frac{n_B r}{2N_0} \int_{p_{B_2}^i}^{p_{B_2}^o} \left[\left| \frac{z_A}{z_B} \right|^2 \frac{n_A}{n_B} D_A^* + D_B^* \right] d \ln p_{B_2}. \quad (13.86)$$

When D_A^* or D_B^* are very different in magnitude, we may further simplify this expression as shown in the following example.

Example 13.8 Given the diffusion data for self-diffusion of Ni^{2+} and O^{2-} ions in NiO at $1190^\circ C$, calculate the rational rate constant and the parabolic rate constant for the oxidation of Ni in pure oxygen. It is known that $D_O^* \ll D_{Ni}^*$.



Solution. Since D_O^* is much less than D_{Ni}^* , we simplify Eq. (13.86) to

$$k_r = \frac{n_B r}{2N_0} \int_{p_{O_2}^i}^{p_{O_2}^o} D_{Ni}^* d \ln p_{O_2}.$$

The term $n_B r / N_0$ has the units of equivalents m^{-3} . In this case, we have

$$\frac{n_B r}{N_0} = \frac{2\rho_{NiO}}{\text{mol. wt}_{NiO}} = \frac{2(7.44 \times 10^3)}{74.69} = 1.99 \times 10^2 \text{ equivalents } m^{-3}.$$

Alternatively, if we take z_B as electronic charges per B atom, and n_B is the concentration of B atoms m^{-3} , then we must divide by Faraday's constant, 96 487 coulombs/equivalent, and multiply by the charge on an electron, 1.602×10^{-19} coulombs per charge. In this case, we get

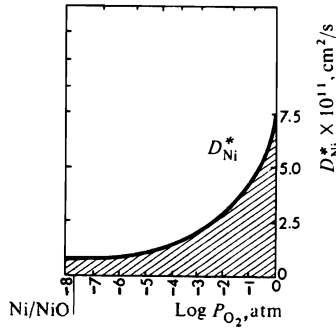
$$k_r = \frac{n_B z_B e}{F^2} \int_{p_{O_2}^i}^{p_{O_2}^o} D_{Ni}^* 2.3 d \ln p_{O_2}$$

$$= \frac{(6.00 \times 10^{28})(2)(1.602 \times 10^{-19})}{2 \times 96\,487} \int_{p_{B_2}^o}^{p_{B_2}^o} D_{Ni}^* d \ln p_{O_2}$$

Thus either way

$$k_r = \frac{1.99 \times 10^2}{2} \int_{p_{B_2}^o}^{p_{B_2}^o} (D_{Ni}^*) d \ln p_{O_2}$$

We evaluate the integral graphically. The figure below gives D_{Ni}^* as a function of p_{O_2} in NiO. The area under the curve is equal to the integral/2.303. The area is



equal to $16 \times 10^{-15} m^2 s^{-1}$. Therefore

$$k_r = \left[\frac{1.99 \times 10^2}{2} \right] (2.303)(16 \times 10^{-15}) = 3.66 \times 10^{-12} \text{ equivalents } m^{-1} s^{-1}$$

From Eq. (13.83), the parabolic rate constant is

$$k_p = \frac{2\rho_0(\text{mol. wt}_O)^2}{r(\text{mol. wt}_{NiO})} k_r = \frac{(2)(7.44 \times 10^3)(16^2)}{(2)(74.69)} (3.66 \times 10^{-12})$$

$$= 9.33 \times 10^{-8} (\text{kg } O_2)^2 m^{-4} s^{-1}$$

498 Diffusion in Solids

Many metals exhibit parabolic oxidation kinetics, among them iron, nickel, cobalt, manganese, copper, and aluminum. Table 13.4 lists some typical values of k_p . Some, however, do not form compact, adherent oxides, and the kinetics of their oxidation are governed by either gas-solid reaction rates or gas-phase transport. For example, both molybdenum and tungsten form oxides that volatilize immediately upon reaction, and continually expose fresh metal to further oxidation, with no limit by solid-state diffusion on the rate.

Table 13.4 Parabolic oxidation constants for various metals

Metal	Oxide	$k_p, (\text{kg O}_2)^2 \text{ m}^{-4} \text{ s}^{-1}$	Conditions	
			Temp., °C	$p_{\text{O}_2}, \text{ atm}$
Co	CoO	2.43×10^{-6}	1000	1.0
Cu	Cu ₂ O	6.3×10^{-7}	1000	0.083
Ni	NiO	3.8×10^{-8}	1000	1.0
Fe	FeO	1.6×10^{-5}	1000	3×10^{-14}
Fe	FeO/Fe ₃ O ₄ /Fe ₂ O ₃	1.4×10^{-4}	1000	1.0
Ni-10%Cr	Complex	5.0×10^{-8}	1000	1.0
Cr	Cr ₂ O ₃	1.3×10^{-9}	900	0.1
Fe-1%Ti	Complex	1.6×10^{-5}	1000	1.0
Al	Al ₂ O ₃	8.5×10^{-14}	600	1.0

*There is a considerable variation in this number, since the surface condition appears to have a strong effect.

Certain metals absorb a significant amount of oxygen in solid solution during the process of oxidation; zirconium, for example, can dissolve up to 29 at. % oxygen in solid solution prior to the formation of ZrO₂. Once the oxide layer has formed, its thickness increases in proportion to $\sqrt{k't}$, according to Eq. (13.79), and the thickness of the oxide as measured from the original surface is

$$M = \frac{2\hat{V}_{\text{Zr}}}{\hat{V}_{\text{ZrO}_2}} \sqrt{k't}, \quad (13.87)$$

where \hat{V}_{Zr} is the molar volume of Zr and \hat{V}_{ZrO_2} is the molar volume of ZrO₂. The diffusing species in the oxide is the oxygen anion moving in from the gas phase to the ZrO₂-Zr interface. At the interface, some of the oxygen dissolves in the metal, and some reacts to form more ZrO₂. Beyond the interface and into the metallic phase, for $x > M$, we have

$$\frac{\partial T}{\partial t} = D_o \frac{\partial^2 C}{\partial x^2}, \quad (13.88)$$

where C is the oxygen concentration, mol m⁻³. If equilibrium is established at all times at the interface, and C_e is the oxygen content of the metal in equilibrium with ZrO₂, then

$$C(M, T) = C_e, \quad (13.89a)$$

$$C(\infty, t) = 0, \quad (13.89b)$$

$$C(x, 0) = 0. \quad (13.89c)$$

The solution to Eq. (13.88) subject to Eqs. (13.87) and (13.89a,b,c) is

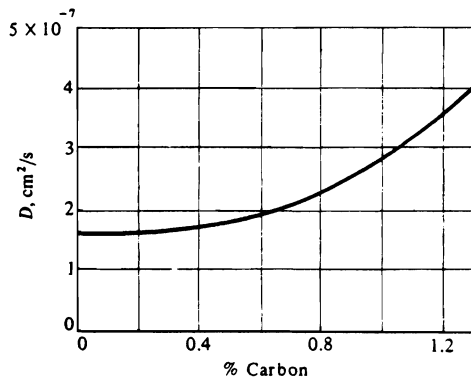
$$C = C_e \frac{\operatorname{erfc} \left[\frac{x}{2\sqrt{D_0 t}} \right]}{\operatorname{erfc} \left[\frac{\hat{V}_{Zr}}{\hat{V}_{ZrO_2}} \sqrt{k'/D_0} \right]}, \tag{13.90}$$

where x is the distance from the original interface, and $x' = x - M$, where x' is the distance from the oxide-metal interface. Thus

$$C = C_e \frac{\operatorname{erfc} \left[\frac{x'}{2\sqrt{D_0 t}} + \frac{\hat{V}_{Zr}}{\hat{V}_{ZrO_2}} \sqrt{k'/D_0} \right]}{\operatorname{erfc} \left[\frac{\hat{V}_{Zr}}{\hat{V}_{ZrO_2}} \sqrt{k'/D_0} \right]}. \tag{13.91}$$

PROBLEMS

13.1 One side of an iron sheet, 0.01 cm thick, is subjected to a carburizing atmosphere at 1200 K such that a surface concentration of 1.2% carbon is maintained. The opposite face is maintained at 0.1% carbon. At steady state, determine the flux ($\text{mol cm}^{-2} \text{s}^{-1}$) of carbon through the sheet: a) if the diffusion coefficient is assumed to be independent of concentration ($D = 2 \times 10^{-7} \text{ cm}^2 \text{ s}^{-1}$); b) if the diffusion coefficient varies as shown to the right.



13.2 A composite foil made of metal A bonded to metal B , each 0.01 cm thick, is subjected to 0.5 atm of pure hydrogen on metal A 's face; the other side, metal B 's face, is subjected to a perfect vacuum. At the temperature of interest and 1 atm of hydrogen, the solubility of hydrogen in metal A is $4 \times 10^{-4} \text{ g per cm}^3$ of A and in B it is $1 \times 10^{-4} \text{ g per cm}^3$ of B . It is also known that hydrogen diffuses four times faster in A than B and that A and B do not diffuse in each other. Draw the concentration profile of hydrogen across the composite foil at steady state.

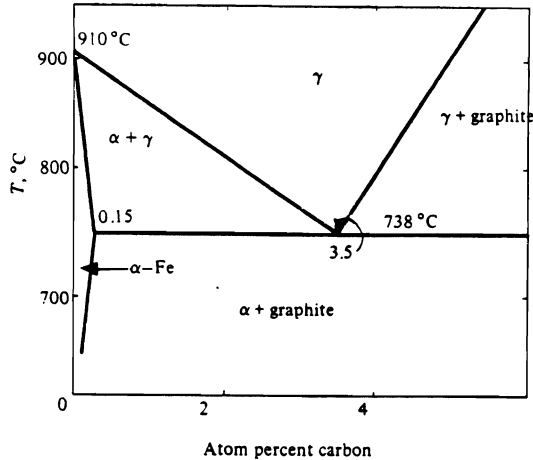
500 Diffusion in Solids

13.3 A thin sheet of iron at 800°C is subjected to different gaseous atmospheres on both of its surfaces such that the composition of one face is at 4 atom percent carbon and the other is at zero atom fraction carbon. At steady state, make a plot of the composition profile in the sample indicating *clearly* compositions and respective distances.

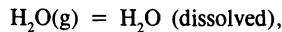
The thickness is 1 mm and density changes during the experiment may be neglected. At 800°C, it is known that the diffusion coefficient of carbon in iron is given by:

$$D = 10^{-6} \text{ cm}^2 \text{ s}^{-1} \text{ in ferrite } (\alpha),$$

$$D = 10^{-8} \text{ cm}^2 \text{ s}^{-1} \text{ in austenite } (\gamma).$$



13.4 Often electronic packages are hermetically sealed with polymers, but after being put in service corrosion is sometimes observed. This happens because H₂O molecules can diffuse through polymers. Assume that the equilibrium between water vapor and water dissolved (or absorbed) by the polymer is simply represented by the reaction:

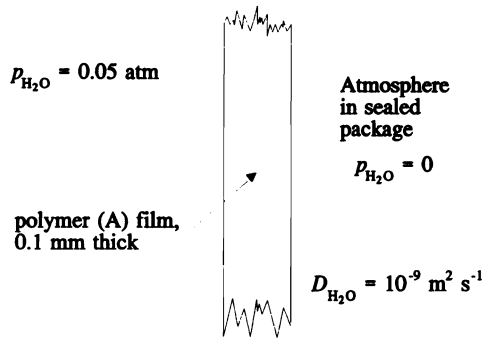


with the equilibrium constant

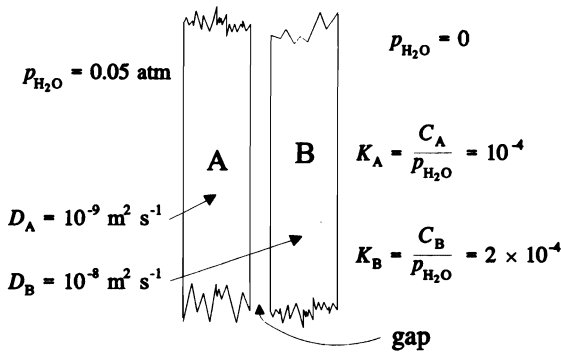
$$K = \frac{C}{p_{\text{H}_2\text{O}}} = 10^{-4}.$$

where C is the concentration of H₂O in the polymer (moles cm⁻³) and $p_{\text{H}_2\text{O}}$ is the pressure of H₂O(g) in atm.

- a) Assume equilibrium at the surfaces and calculate the flux of H₂O through the polymer (in moles cm⁻² s⁻¹); assume steady state.



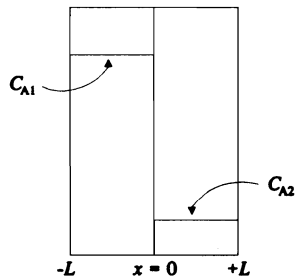
b) Now two films, polymer A and B, are used. Each is 0.1 mm thick.



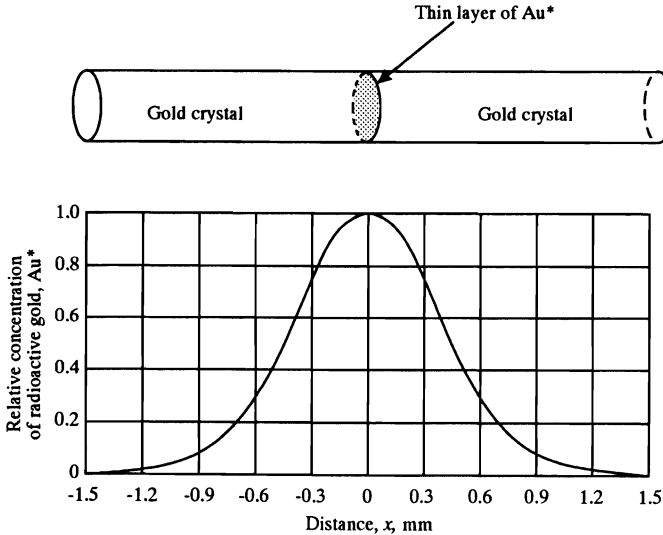
Assume steady state and equilibrium at all interfaces. What is the pressure of $\text{H}_2\text{O}(\text{g})$ in the gap?

13.5 Hydrogen gas is maintained at 3 bar and 1 bar on opposite sides of a plastic membrane which is 0.3 mm thick. The temperature is 25°C , and the diffusion coefficient of hydrogen in the plastic is $8.7 \times 10^{-10} \text{ m}^2 \text{ s}^{-1}$. The solubility of hydrogen in the membrane is $1.5 \times 10^{-3} \text{ kmol m}^{-3} \text{ bar}^{-1}$. What is the mass diffusion flux of hydrogen through the membrane? Give your result in $\text{kmol s}^{-1} \text{ m}^{-2}$.

13.6 The Grube solution is used to analyze diffusion data for a diffusion couple in which the solid is semi-infinite on both sides and when the chemical diffusion coefficient is uniform. Now consider a diffusion couple made from two thin solids so that the Grube solution for semi-infinite solids is not applicable. Such a couple is shown to the right with the initial condition for C_A shown. a) Assume that \bar{D} is uniform. Write a partial differential equation for $C_A(x, t)$ where x is the space coordinate and t is time. b) For $0 \leq x \leq L$, write appropriate boundary conditions and an appropriate initial condition for C_A . You may assume that component A is not volatile; i.e., no A is lost from the diffusion couple.



13.7 An unknown amount of radioactive gold is deposited as a thin layer on the ends of two rods of gold. The two rods are then joined to form a specimen having a planar source of radioactive gold (Au^*) atoms at the origin $x = 0$. After diffusion for 100 hours at 920°C , the distribution of Au^* is as shown below. Calculate the self-diffusion coefficient of gold in pure gold, based on the data at 0.3 mm and 0.6 mm as indicated in the plot of the relative concentration of gold.



13.8 Silicon is exposed to a gas that establishes a concentration of 10^{18} atoms (Al) cm^{-3} on the surface of the silicon. The process is carried out at 1473 K . a) After 30 min, at what depth below the surface of the Si will the concentration be 10^{16} atoms cm^{-3} ? b) Calculate the amount of Al (in atoms cm^{-2}) that diffuses into the Si after 30 min of treatment at 1473 K .

13.9 The Matano-Boltzmann analysis is used to calculate the interdiffusion coefficient, \bar{D} , from diffusion couple data. It can also be used to determine the intrinsic diffusion coefficients in a binary by inserting inert markers at the original interface.

- a) The distance moved by the markers is proportional to the square root of time. Show that v_x in Eq. (12.14) is given by

$$v_x = \frac{S}{2t},$$

where S is the distance moved by the markers and t is the diffusion time.

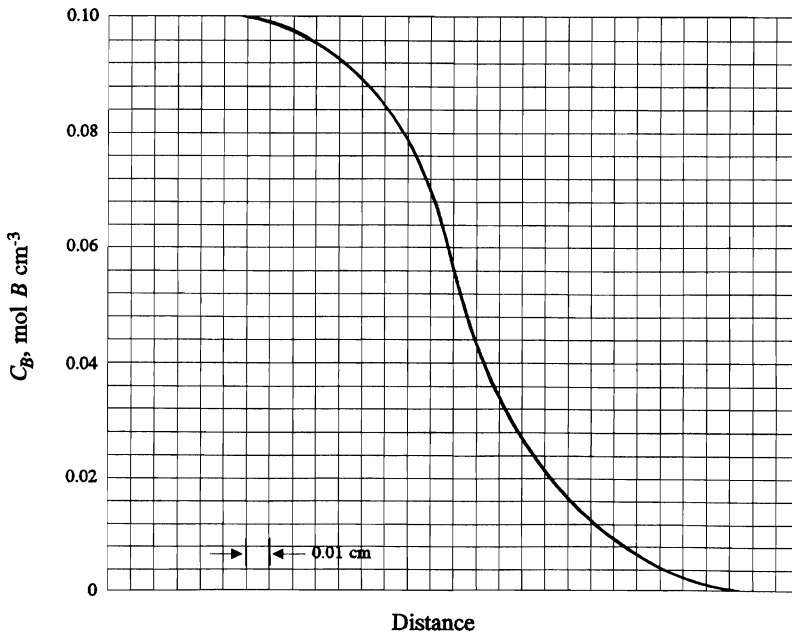
- b) Assuming that \bar{D} and S are determined in a diffusion-couple, what two equations are needed to simultaneously solve for the intrinsic diffusion coefficients in the binary. [Hint: Review Section 12.2.2.]

13.10 A gold-nickel diffusion couple of limiting compositions $X_{\text{Ni}} = 0.0974$ and $X_{\text{Ni}} = 0.4978$ is heated at 925°C for 2.07×10^6 s. Layers 0.003 in. (0.0762 mm) thick and parallel to the original interface are machined off and analyzed. a) Using the data tabulated

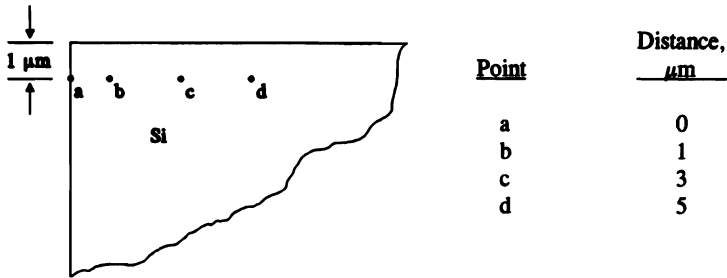
below, calculate the diffusion coefficient at 20, 30, and 40 at. % nickel. b) Suppose that markers are inserted at the original interface and move along during the diffusion process at a composition of 0.30 atom fraction nickel. From this, determine the intrinsic coefficients of gold and nickel at 0.30 atom fraction nickel.

Slice No.	at% Ni	Slice No.	at% Ni	Slice No.	at% Ni	Slice No.	at% Ni
11	49.78	21	35.10	29	21.38	38	13.26
12	49.59	22	33.17	30	20.51	39	12.55
14	47.45	23	31.40	31	19.12	41	11.41
16	44.49	24	29.74	32	17.92	43	10.48
18	40.58	26	25.87	33	16.86	45	9.99
19	38.01	27	24.11	35	15.49	47	9.74
20	37.01	28	22.49	37	13.90		

13.11 Metals A and B form alloys of fcc structure at 1200°C. They are allowed to interdiffuse as a diffusion couple for 10^3 s, and the concentration profile obtained is given in the accompanying figure. Determine the value of the interdiffusion coefficient, \bar{D} , at a concentration $C_B = 0.02 \text{ mol cm}^{-3}$.

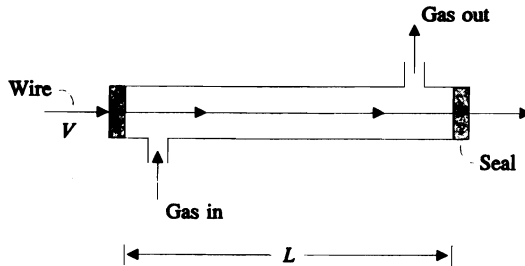


13.12 Intrinsic silicon (i.e., pure Si) is processed in a gas which establishes a concentration of 10 ppm (1 ppm = 10^{-4} wt. %) of boron at the surface of the silicon. Distances from the left vertical face are given in the following table.



After 10 h exposure to the gas, what are the concentrations of boron at points a, b, c and d? At the process temperature, the diffusion coefficient for B in Si is $D = 10^{-12} \text{ cm}^2 \text{ s}^{-1} = 10^{-4} \mu\text{m}^2 \text{ s}^{-1}$.

13.13 A fine steel wire of 0.2 wt.% C is passed through a tube furnace at 1200°C which contains a carburizing gas. The composition of the carburizing gas is adjusted so that it fixes 0.8 wt.% C on the surface of the wire. By neglecting diffusion in the axial direction of the wire, calculate the average composition of the wire after it passes through the tube. At this temperature the steel is a single phase (austenite). *Data:* diameter of wire, 0.01 cm; length of furnace, L , 1.5 m; velocity of wire, V , 15 cm s^{-1} .



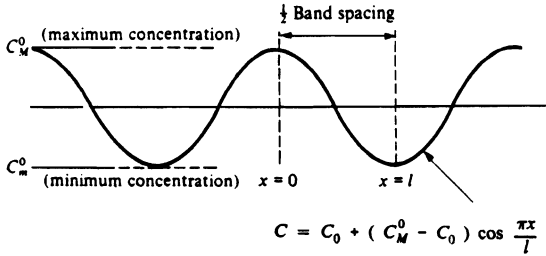
13.14 A thin layer of Au is plated on to the end of a Ni bar. The bar is annealed at 900°C for 10 h; at 900°C the interdiffusion coefficient of Au in Ni is $10^{-11} \text{ cm}^2 \text{ s}^{-1}$. It is known that Au and Ni are completely soluble at 900°C . After the treatment, the concentration of Au at a distance of 0.05 cm from the end is 0.1 atom fraction of Au. At what distance from the end is the atom fraction of Au equal to 0.05?

13.15 A long cylindrical bar of steel which contains 3 ppm of hydrogen is dehydrogenated by a two-step vacuum process. The first step is treatment at 150°C for time period t_1 , followed by the second step at 300°C for time period t_2 . If $t_1 = 2t_2$, calculate: a) the total time ($t = t_1 + t_2$) to reduce the average composition to 1.5 ppm of hydrogen, and b) the center composition after the two-step treatment. *Data:* $D_H = 1.0 \exp(-4000/T)$ with D_H in $\text{cm}^2 \text{ s}^{-1}$ and T in K. The diameter of the bar is 2 cm.

13.16 The solubility of hydrogen in solid copper at 1000°C is 1.4 ppm (by mass) under a pressure of hydrogen of 1 atm. At 1000°C , $D_H = 10^{-6} \text{ cm}^2 \text{ s}^{-1}$. a) Determine the time for hydrogen to reach a concentration of 1.0 ppm at a depth of 0.1 mm in a large chunk of copper initially with null hydrogen if the copper is subjected to 2 atm pressure of H_2 at

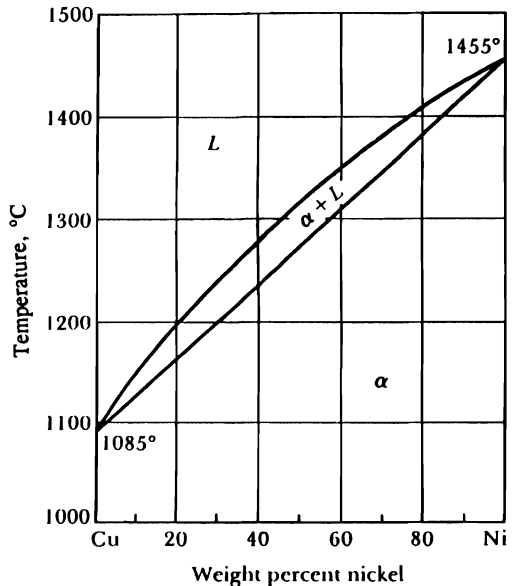
1000°C. b) Copper foil, 0.2 mm thick, is equilibrated with hydrogen at a pressure of 4 atm at 1000°C. The same foil is then placed in a perfect vacuum at 1000°C and held for 60 s. Calculate the concentration of hydrogen at the center of the foil after the 60 s period.

13.17 The term "banding" is used to describe chemical heterogeneity in rolled alloys that shows up as closely spaced light and dark bands in the microstructure of steel. These bands represent areas of segregation of alloying elements that formed during freezing of the ingot. During rolling the segregated areas are elongated and compressed into narrow bands. Assume that the alloy concentration varies sinusoidally with distance after rolling according to the sketch below.



If the steel is now heated to the austenite range and held at some constant temperature, then a) schematically sketch the concentration profile as time passes; b) write a differential equation for concentration (state assumptions) and c) write the boundary conditions (for time and space) that apply; d) solve for the concentration as a function of time and x; e) derive an equation for the residual segregation index.

13.18 Assume that the banding in a wrought cupronickel alloy (single phase) is described by the cosine function in Problem 13.17. The average composition of the alloy is 10% Ni-90% Cu, and the segregation ratio before homogenization is 1.4. Segregation ratio is defined as $S = C_M^0/C_m^0$. a) What are the maximum and minimum compositions of nickel? b) In order to homogenize the alloy in the shortest time possible, what temperature would you select? c) If the average distance between maximum compositions is 10^{-2} cm, determine the time to achieve a residual segregation ratio of 0.1 at 950°C. A diffusion coefficient can be obtained from Fig. 12.9. d) The alloy is given a "step" homogenization treatment which consists of 10 hours at 700°C, 10 hours at 800°C and 10 hours at 900°C. What is the residual segregation index after this treatment?



506 Diffusion in Solids

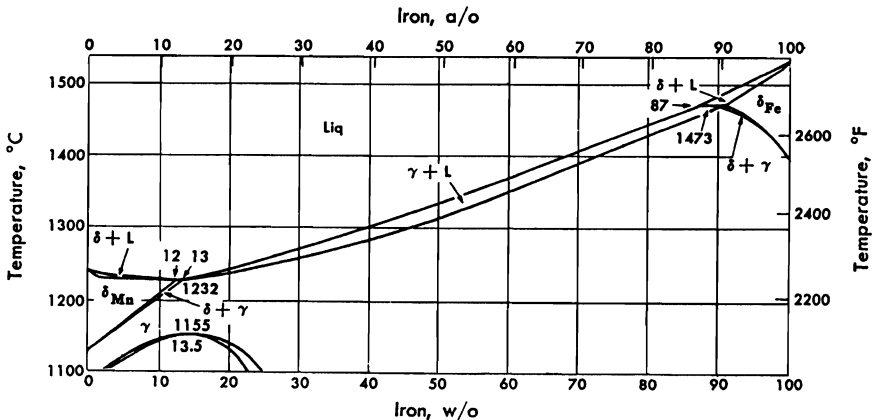
13.19 A junction in silicon is made by doping with boron using predeposition followed by drive-in diffusion. a) Five minutes at 1100°C are required to deposit the dopant. At what distance from the surface is the concentration of boron raised to 3×10^{18} atoms cm^{-3} . Assume that the silicon is initially pure. b) How much boron (per cm^2 of silicon surface) will have been taken up by the silicon during the deposition step? c) To prevent loss of boron during the drive-in step, the surface is masked with silica (SiO_2). Now calculate the time required to achieve a concentration of boron equal to 3×10^{18} atoms cm^3 at a depth of 6×10^{-4} cm if the drive-in treatment is carried out at 1150°C.

13.20 By ion implantation, lithium can be concentrated in a very thin surface layer (10^{-6} cm) on a nickel substrate. After implanting the surface layer, it has a lithium concentration of 10^{20} atoms cm^{-3} . Determine the time at 1000 K for reducing the surface concentration to 10^{19} atoms cm^3 . At 1000 K, the interdiffusion diffusion coefficient of lithium in nickel is 5×10^{-8} $\text{cm}^2 \text{s}^{-1}$.

13.21 A cylindrical bar of Fe (dia. of 1 cm) is suspended in a well mixed and small melt of Mn maintained at 1300°C. Assume that there is local equilibrium at the solid-liquid interface and calculate the time required to raise the manganese composition at the center of the bar to 1 wt.%. The interdiffusion coefficient of Mn in Fe is given by

$$D = 0.49 \exp \left[-\frac{33\,200}{T} \right]$$

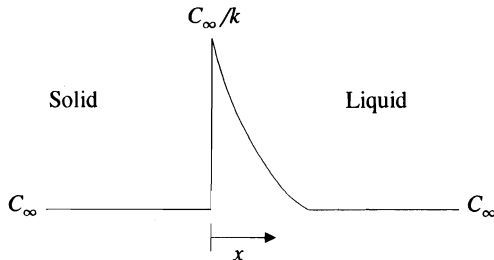
with T in K and D in $\text{cm}^2 \text{s}^{-1}$.



13.22 A very thin sheet of Fe-0.2 atom fraction B is "sandwiched" between two large pieces of iron, and then the entire assembly is heated to 1000°C. The sheet is only 5×10^{-3} cm thick and at 1000°C diffusion bonding occurs as the boron diffuses into the iron. Assume that the boron is completely soluble and that there is only a single phase. a) Calculate the time required for the concentration of B to achieve its maximum at a distance of 1 mm from the original joint. b) What is the maximum concentration at 1 mm? c) At the time corresponding to part a), what is the atom fraction of B at the original joint?

13.23 A batch of steel exhibits "banding," which is a form of microsegregation in the wrought condition. The spacing between the bands is $50\ \mu\text{m}$. After 10 h of a high temperature homogenization treatment, the residual segregation index is 0.2 (determined by electron beam microanalysis). A second batch of the same type of steel has a band spacing of $100\ \mu\text{m}$. How long must this batch be maintained at the high temperature to achieve the same residual segregation index of 0.2?

13.24 A melt with uniform concentration of solute, C_∞ , is solidified with a planar interface. Chemical equilibrium is maintained at the interface, which moves with a constant velocity V . The concentration profile at steady state, with no convection in the liquid, is as depicted:



- Use a moving coordinate system with the origin ($x = 0$) at the solid-liquid interface and derive the differential equation for the concentration profile in the liquid.
- Write appropriate boundary conditions and solve for $C(x)$.
- Determine the concentration gradient in the liquid at $x = 0$. How does the concentration gradient relate to the velocity of the interface?
- The characteristic length, δ , defined by

$$j_0 = \frac{D}{\delta} \left[\frac{C_\infty}{k} - C_\infty \right],$$

where j_0 is the diffusional flux at the interface ($x = 0$). Determine δ in terms of the solidification velocity and the concentration gradient at the interface.

13.25 A powder-ceramic compact is outgassed at 500°C in a chamber filled with pure argon in order to remove air before sintering. The tortuosity of the compact is 4, its porosity is 0.2, and the average pore radius is $200\ \text{\AA}$. The compacts are $50\ \text{mm}$ long \times $25\ \text{mm}$ diameter. Calculate the fraction of air remaining after 1 h of outgassing treatment.

13.26 In order to make a transformer steel with the proper hysteresis loop, a low silicon steel sheet (2 mm thick) is to be exposed on both sides to an atmosphere of SiCl_4 which dissociates to Si(g) and $\text{Cl}_2(\text{g})$. The Si(g) dissolves in the steel up to 3 wt. % at equilibrium.

- Indicate what partial differential equation and what boundary and initial conditions would apply in order to calculate the diffusion of Si into the sheet.
- Using the data in Fig. 12.11, calculate the time to achieve an average concentration of 2.85 wt. % Si at 1255 K.

MASS TRANSFER IN FLUID SYSTEMS

In Chapters 2 and 7, we demonstrated the development of differential equations pertinent to momentum and energy transport in simple fluid systems. In this chapter, we consider how to formulate and describe elementary diffusion and mass transfer problems in fluid systems. We use practically the same procedure in this situation as we did previously; we develop a differential equation, and a solution containing arbitrary constants evolves. These constants are evaluated by applying boundary conditions that specify the concentration or the mass flux at the bounding surfaces. Again, we demonstrate the principles involved by considering specific examples, but first let us reconsider the general situation.

Species A in a gas stream moving in the x -direction is under the influence of a concentration gradient, also in the x -direction. The molar flux of A relative to stationary coordinates is then made up of two parts: $C_A v_x^*$ which is the molar flux of A resulting from the bulk motion, and $j_{Ax} = -CD_A(\partial X_A/\partial x)$ which is the diffusive contribution. Thus

$$N_{Ax} = -CD_A \frac{\partial X_A}{\partial x} + C_A v_x^* = C_A v_{Ax}. \quad (14.1)$$

Here v_x^* is the local *molar average velocity* in the x -direction, and v_{Ax} is the velocity of A in the x -direction with respect to stationary coordinates, and C is the total molar concentration in the solution. Thus, we define v_x^* so that the *total molar flux* of all components in the x -direction is made up of the sum of the n component fluxes in the same direction:

$$C v_x^* = \sum_{i=1}^n C_i v_{ix}. \quad (14.2)$$

For a binary A - B system, we write

$$v_x^* = \frac{1}{C} (C_A v_{Ax} + C_B v_{Bx}) = \frac{1}{C} (N_{Ax} + N_{Bx}). \quad (14.3)$$

510 Mass Transfer in Fluid Systems

When we combine Eq. (14.3) with Eq. (14.1), we obtain a form of Fick's first law for a binary solution:

$$N_{Ax} = X_A(N_{Ax} + N_{Bx}) - CD_A \frac{\partial X_A}{\partial x}. \quad (14.4)$$

14.1 DIFFUSION THROUGH A STAGNANT GAS FILM

Consider the system shown in Fig. 14.1 where liquid A is evaporating into gas B , and a constant liquid level at $x = 0$ is maintained. At the liquid-gas phase interface ($x = 0$), the gas phase concentration of A is that corresponding to the vapor pressure of A at that temperature.* For simplicity, also assume that the solubility of B in liquid A is negligible and that the entire system is maintained at a constant temperature and pressure. At the top of the tube, a stream of A - B gas flows past slowly, thereby maintaining a constant concentration of A at $x = l$ which is less than the liquid-gas interface concentration. Therefore, a concentration difference of A exists between $x = 0$ and $x = l$, which causes diffusion. When the system attains a steady state, there is a net motion of A away from the evaporating surface and the vapor B in the tube is stationary.

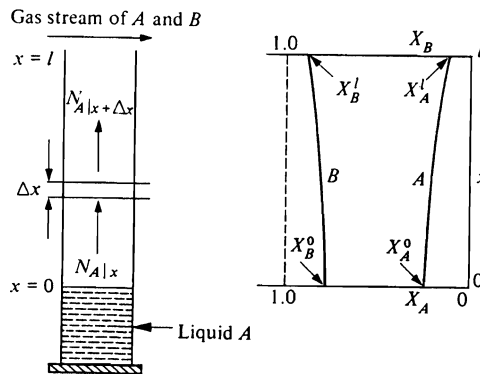


Fig. 14.1 Diffusion of A and B at steady state. B is not in motion, but note that the graph shows how its concentration profile is not linear because of the motion of A .

*This implies that equilibrium is maintained at the interface. From a simplified mechanistic viewpoint, atoms (or molecules) can readily leave the liquid state and enter the gas phase. This assumption is valid except at very high diffusion rates where the rate of transfer of atoms across the liquid-gas interface is not able to keep pace with the exhaustion of the atoms away from the interface.

Under these conditions, despite the fact that gas B is stationary, there is bulk motion of fluid since A itself is moving, and its motion contributes to the average velocity. Thus we refer to Eq. (14.4) for the flux of A with $N_{Bx} = 0$. Solving for N_{Ax} , we obtain

$$N_{Ax} = -\frac{CD_A}{1 - X_A} \frac{dX_A}{dx}. \quad (14.5)$$

A mass balance on a unit volume Δx of column height (see Fig. 14.1) for steady state is

$$SN_{Ax|x} - SN_{Ax|x+\Delta x} = 0, \quad (14.6)$$

in which S is the cross-sectional area. In the expected manner, we divide by Δx and take the limit as $\Delta x \rightarrow 0$:

$$\frac{dN_{Ax}}{dx} = 0. \quad (14.7)$$

Substitution of Eq. (14.6) for N_{Ax} yields

$$\frac{d}{dx} \left(\frac{CD_A}{1 - X_A} \frac{dX_A}{dx} \right) = 0. \quad (14.8)$$

As pointed out in Chapter 12, diffusion coefficients for isothermal gas solutions are very nearly independent of concentration; also, C is constant for an ideal gas mixture at constant temperature and pressure. Hence we simplify the derivative further:

$$\frac{d}{dx} \left(\frac{1}{1 - X_A} \frac{dX_A}{dx} \right) = 0. \quad (14.9)$$

Two successive integrations can be made directly, resulting in

$$-\ln(1 - X_A) = c_1x + c_2, \quad (14.10)$$

and we determine the constants by use of the boundary conditions:

$$\text{B.C.1:} \quad \text{at } x = 0, \quad X_A = X_A^0; \quad (14.11a)$$

$$\text{B.C.2:} \quad \text{at } x = l, \quad X_A = X_A^l. \quad (14.11b)$$

When we evaluate the constants and substitute them into Eq. (14.10), we obtain the concentration profile:

$$\ln \left(\frac{1 - X_A}{1 - X_A^0} \right) = \frac{x}{l} \ln \left(\frac{1 - X_A^l}{1 - X_A^0} \right), \quad (14.12)$$

or

$$\ln \left(\frac{X_B}{X_B^0} \right) = \frac{x}{l} \ln \left(\frac{X_B^l}{X_B^0} \right). \quad (14.13)$$

Figure 14.1 shows these solutions, where the slope of dX_A/dx is not uniform with x although the flux N_{Ax} is. A gradient of A in the gas must be accompanied by a gradient of B . Consequently, B has a tendency to diffuse down the column, but this diffusive tendency is

exactly compensated by the opposing bulk motion of the gas in the direction of diffusion of gas A .

The information that is most often sought is the rate of mass transfer at the liquid-gas interface. We obtain this by using Eq. (14.5):

$$N_{Ax|x=0} = -\frac{CD_A}{1 - X_A^0} \left[\frac{dX_A}{dx} \right]_{x=0} = \frac{CD_A}{l} \ln \left[\frac{1 - X_A^l}{1 - X_A^0} \right], \quad (14.14)$$

or

$$N_{Ax|x=0} = -\frac{CD_A}{(X_B)_{\ln}} \left[\frac{X_A^0 - X_A^l}{l} \right], \quad (14.15)$$

where $(X_B)_{\ln}$ is the *log mean* of the terminal values of X_B , defined as

$$(X_B)_{\ln} = \frac{X_B^l - X_B^0}{\ln (X_B^l/X_B^0)}. \quad (14.16)$$

Equation (14.15) is somewhat more appealing than Eq. (14.14) because a characteristic concentration difference $X_A^0 - X_A^l$ over a distance l is evident. For a gas in which species A is dilute, Eq. (14.15) reduces to

$$N_{Ax|x=0} = D_A \left[\frac{C_A^0 - C_A^l}{l} \right], \quad (14.17)$$

which could have resulted from originally ignoring bulk motion and expressing the flux of A simply as

$$j_{Ax} = -D_A \frac{dC_A}{dx}. \quad (14.18)$$

Typical applications of Eqs. (14.14) and (14.15) are evaporation and sublimation processes which involve diffusion of the vapor being created (gas A) through a stationary gas (gas B). Also, a method for measuring diffusion coefficients is to measure the rate of fall of liquid A in a small glass tube as gas B passes by the top. Furthermore, these results find use in the "film theories" of mass transfer.

Example 14.1 In order to determine the diffusivity of Mn in the gas phase, a melt of pure Mn is held in a chamber at 1600°C through which pure Ar flows. The level of the Mn is 2.0 cm below the edge of the crucible. The weight of the crucible is monitored continuously, and when the rate of weight loss is steady with time, that rate is found to be 2.65×10^{-7} mol cm⁻² s⁻¹. Calculate $D_{\text{Mn-Ar}}$.

Solution. At 1600°C, $P_{\text{Mn}}^0 = 0.03$ atm, which may be taken as the pressure just above the liquid surface.

The pressure of manganese may be taken as zero at the crucible edge, as the argon flowing across the opening removes it immediately.

Since the concentration of manganese is clearly dilute, $D_{\text{Mn-Ar}}$ is obtained directly from Eq. (14.17). The concentration is expressed in mol cm⁻³.

$$C_A^0 = \frac{P_A^0}{RT} = \frac{0.03 \text{ atm}}{0.082051 \text{ atm} \cdot \frac{\text{mol K}}{10^3 \text{ cm}^3} \cdot 1873 \text{ K}}$$

$$= 1.61 \times 10^{-7} \text{ mol cm}^{-3},$$

and

$$D_{\text{Mn-Ar}} = \frac{2.65 \times 10^{-7} \times 2.0}{1.61 \times 10^{-7}} = 3.3 \text{ cm}^2 \text{ s}^{-1}.$$

14.2 DIFFUSION IN A MOVING GAS STREAM

Figure 14.2 illustrates one technique used to determine the vapor pressure of a metal (liquid or solid). Argon, as a carrier gas, passes over the sample which is at the temperature corresponding to the vapor pressure being determined. This gas, containing the saturation concentration of the metal vapor, enters the exit tube at $z = 0$, and at the cool end of the exit tube the metal condenses, so we can collect it for a mass determination.

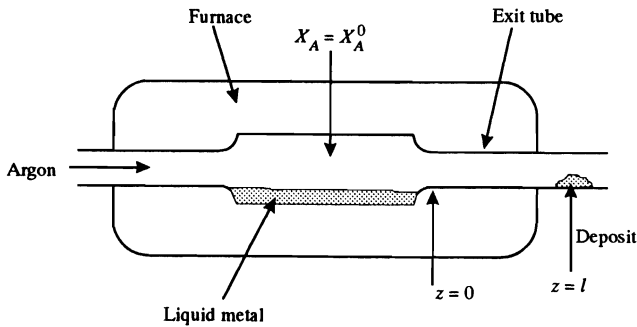


Fig. 14.2 Diffusion in a moving gas stream.

A mass balance applied to a section Δz long for steady state yields

$$\frac{dN_{Az}}{dz} = 0. \quad (14.19)$$

We may choose either Eq. (14.1) or Eq. (14.4) to represent N_{Az} ; here we select Eq. (14.1) from which we write

$$v_z^* \frac{dC_A}{dz} - \frac{d}{dz} \left[CD_A \frac{dX_A}{dz} \right] = 0. \quad (14.20)$$

We can certainly consider that the argon-metal gas solution is ideal, and if the temperature between $z = 0$ and $z = l$ is uniform, then C and D_A are constants, and Eq. (14.20) takes the form

$$\frac{d^2 X_A}{dz^2} - \frac{v_z^*}{D_A} \frac{dX_A}{dz} = 0. \quad (14.21)$$

The boundary conditions can be represented as:

$$\text{B.C.1: at } z = 0, \quad X_A = X_A^0 \text{ (saturation value);} \quad (14.21a)$$

$$\text{B.C.2: at } z = l, \quad X_A = 0. \quad (14.21b)$$

The second boundary condition implies that the temperature at l is low enough so that the vapor pressure of A is negligible. We can obtain the solution to Eq. (14.21) directly by integrating twice, or by treating it as a linear homogeneous differential equation with constant coefficients. Applying the latter method, the solution is

$$X_A = c_1 e^{r_1 z} + c_2 e^{r_2 z}, \quad (14.22)$$

where r_1 and r_2 are the roots of

$$r^2 - \frac{v_z^*}{D_A} r = 0. \quad (14.23)$$

Thus, $r_1 = 0$ and $r_2 = v_z^*/D_A$, and the solution is

$$X_A = c_1 + c_2 \exp \left[\frac{v_z^*}{D_A} z \right]. \quad (14.24)$$

We evaluate the arbitrary constants by using Eqs. (14.24) and (14.21a and b):

$$c_2 = - \frac{X_A^0}{\left[\exp \left[\frac{v_z^* l}{D_A} \right] - 1 \right]}, \quad (14.25)$$

and

$$c_1 = X_A^0 \left[1 + \frac{1}{\exp \left[\frac{v_z^* l}{D_A} \right] - 1} \right]. \quad (14.26)$$

The concentration profile can then be written:

$$\frac{X_A}{X_A^0} = \frac{\exp \left[\frac{v_z^* l}{D_A} \right] - \exp \left[\frac{v_z^* z}{D_A} \right]}{\exp \left[\frac{v_z^* l}{D_A} \right] - 1}. \quad (14.27)$$

We evaluate the flux at which the metal vapor enters the exiting gas stream at $z = 0$. It is

$$N_{Az}|_{z=0} = C \left[-D_A \left[\frac{\partial X_A}{\partial z} \right]_{z=0} + X_A^0 v_z^* \right],$$

or

$$N_{Az|z=0} = C v_z^* X_A^0 \left[1 - \frac{1}{1 - \exp\left[\frac{v_z^* l}{D_A}\right]} \right] \tag{14.28}$$

If S is the cross-sectional area of the tube, then $SN_{Az|z=0}$ represents the amount of A passing through the tube; experimentally, we determine this quantity by weighing the condensate formed at $z = l$ over a measured period of time. The product SCv_z^* is the total molar flow down the tube, and simply represents the number of moles of argon passed per unit time plus the moles of condensate collected per unit time. The vapor pressure of A is related to these experimental quantities by

$$\frac{P_A^0}{P} = X_A^0 = \frac{SN_{Az|z=0}}{SCv_z^*} \frac{\left[\exp\left[\frac{v_z^* l}{D_A}\right] - 1 \right]}{\exp\left[\frac{v_z^* l}{D_A}\right]} \tag{14.29}$$

where P_A^0 is the vapor pressure of A , and P is the total pressure. Preferably, the effect of diffusion should be negligible for best experimental results due to the uncertainty of the diffusion coefficient and because we would have to assume an experimental set up that corresponds to the mathematical formulation.

The real value of the analysis lies in the group v_z^*l/D_A which indicates how to set up the experiment, so that the effects of diffusion may be ignored. If $v_z^*l/D_A \geq 5$, the effect of diffusion may be ignored because the last term in Eq. (14.29) is ≥ 0.993 and < 1.0 . To insure sufficiently high values of v_z^*l/D_A , the experimentalist should provide a small diameter tube between $z = 0$ and $z = l$, and use argon or nitrogen as the carrier gas, rather than hydrogen or helium, since D in the lighter gases is larger than in the heavier gases.

Example 14.2 An experimental apparatus is being constructed to study the thermodynamics of Mn-Cu alloys by measuring the Mn vapor pressure over the molten alloys at 1400 K. In order to use the transport technique, what exit tube dimensions and argon gas flow rates should be used?

Solution. The criterion that provides the most direct experimental measurement of P_{Mn}^0 (the equilibrium pressure over the alloy) is

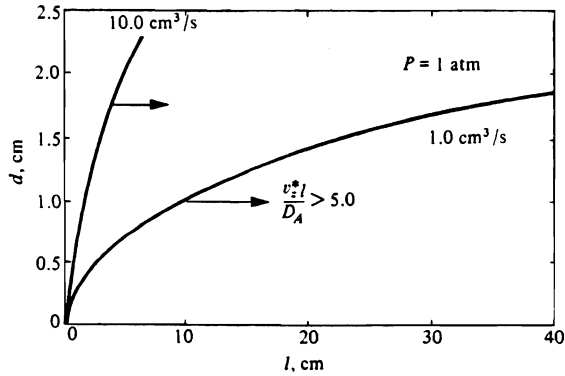
$$P_{Mn}^0 = P \frac{N_{Mn}}{N}$$

where N_{Mn} is the number of moles of Mn condensed and $N = N_{Mn} + N_{Ar} =$ total moles of gas passing through the exit tube over some period of time. This is essentially true when $v^*l/D_{Mn-Ar} \geq 5.0$.

We evaluate D_{Mn-Ar} at 1400 K as $2.6 \times 10^{-4} \text{ m}^2 \text{ s}^{-1}$. Therefore, v^*l must be greater than $13.0 \times 10^{-4} \text{ m}^2 \text{ s}^{-1}$. Since $v^* \cong 4n_{Ar}RT/\pi d^2P$, and $\dot{n} \cong \dot{n}_{Ar}$ (mol Ar s^{-1}), then

$$\frac{4\dot{n}_{Ar}RTl}{\pi P} \geq 13.0 d^2,$$

where d is the tube diameter. The figure below shows the results, with the preferred designs to the right of each curve.



At temperatures where P_{Mn}^0 is greater than negligible values, and $n > n_{Ar}$, the curves should be shifted even further to the right for better results.

14.3 DIFFUSION INTO A FALLING LIQUID FILM

In this section, we consider a fluid system moving in such a way that the velocity distribution is unaffected by diffusion into the fluid. Figure 14.3 shows a film of liquid B falling in laminar flow down a wall. Gas A is absorbed at the liquid-gas interface; we restrict the situation to that where the penetration distance of A into B is small relative to the film thickness. We wish to calculate the amount of gas absorbed after the film travels a distance L .

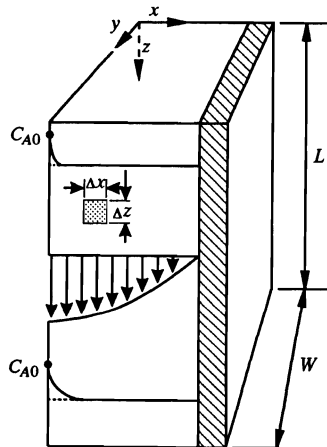


Fig. 14.3 Absorption into a falling film.

First, we develop a mass balance on component A . The gas-liquid interface concentration of A , at all values of z , is the saturation concentration C_A^0 , thus A diffuses into the liquid which initially contains less than the saturation amount of A . As the film drops, the liquid is exposed to C_A^0 for a longer time, and more penetration of A into the film results. We see, therefore, that C_A changes both with x and z , and we select as the unit volume Δx by Δz by unity in the y -direction.

Then the mass balance for A is simply

$$N_{Az|z} \Delta x - N_{Az|z+\Delta z} \Delta x + N_{Ax|x} \Delta z - N_{Ax|x+\Delta x} \Delta z = 0. \quad (14.30)$$

Dividing by $\Delta x \Delta z$, and performing the usual limiting process, we get

$$\frac{\partial N_{Az}}{\partial z} + \frac{\partial N_{Ax}}{\partial x} = 0. \quad (14.31)$$

We now have to insert into this equation the expressions for N_{Az} and N_{Ax} . For the molar flux in the z -direction, we write

$$N_{Az} = -CD_A \frac{\partial X_A}{\partial z} + C_A v_z^*, \quad (14.32)$$

and neglect the diffusive contribution, realizing that A moves in the z -direction primarily due to bulk flow. In addition, for a small increase in the concentration of A , $v_z^* \cong v_z$. Finally, we give N_{Az} by the simplified expression

$$N_{Az} = C_A v_z. \quad (14.33)$$

For the molar flux in the x -direction, we write

$$N_{Ax} = -D_A \frac{\partial C_A}{\partial x} + C_A v_x^*. \quad (14.34)$$

That is, in the x -direction, A is transported primarily by diffusion, there being almost no bulk flow in the x -direction due to the small solubility of A in B . Substitution of Eqs. (14.32) and (14.34) into Eq. (14.31) yields the differential equation for $C_A(x,z)$:

$$v_z \frac{\partial C_A}{\partial z} = D_A \frac{\partial^2 C_A}{\partial x^2}. \quad (14.35)$$

When dealing with energy transport in a convective system, it is necessary to obtain the velocity profile $v_z(x)$; similarly, we need to describe the velocity for the analogous situation of mass transfer in a convective system. For a falling film, we have already worked this out in Chapter 2, and we know that the result for fully developed flow is

$$v_z = v_{\max} \left[1 - \left(\frac{x}{\delta} \right)^2 \right],$$

where δ is the film thickness, and x is the distance into the film from the gas-liquid surface.

If, as indicated in Fig. 14.3, A has penetrated only a slight distance into the film, then for the most part species A sees only v_{\max} . Further, since it does not penetrate very far, we can consider that the liquid is semi-infinite. These conditions would hold, for example, for short

contact times. With these approximations we write the differential equation and the boundary conditions as follows:

$$v_{\max} \frac{\partial C_A}{\partial z} \cong D_A \frac{\partial^2 C_A}{\partial x^2}; \quad (14.36)$$

$$\text{at } z = 0, \quad C_A = C_A^i, \quad x \geq 0; \quad (14.37a)$$

$$\text{at } x = 0, \quad C_A = C_A^0, \quad L \geq z \geq 0; \quad (14.37b)$$

$$\text{at } x = \infty, \quad C_A = C_A^i, \quad L \geq z \geq 0. \quad (14.37c)$$

Note that we may alternatively view z/v_{\max} as the time t over which a moving slice of liquid has been subjected to the surface concentration C_A^0 . Thus, we recognize the solution to Eq. (14.36), subject to Eqs. (14.37a), (14.37b), and (14.37c), as the solution for the temperature distribution in a semi-infinite solid, initially at a uniform temperature, which is suddenly subjected to a new constant surface temperature. Then, referring to Eq. (9.62), we have

$$\frac{C_A - C_A^0}{C_A^i - C_A^0} = \text{erf} \frac{x}{2\sqrt{D_A z/v_{\max}}}. \quad (14.38)$$

Now knowing the concentration profile, we proceed to determine the local diffusion mass flux at the surface, $x = 0$:

$$N_{Ax}|_{x=0} = -D_A \left[\frac{\partial C_A}{\partial x} \right]_{x=0} = (C_A^0 - C_A^i) \frac{D_A v_{\max}}{\pi z}, \quad (14.39)$$

which gives the average rate of A transferred per unit across the entire surface between $z = 0$ and $z = L$ as

$$\bar{N}_{Ax}|_{x=0} = \frac{1}{L} \int_0^L N_{Ax}|_{x=0} dz = 2(C_A^0 - C_A^i) \frac{D_A v_{\max}}{\pi L}. \quad (14.40)$$

Pigford¹ solved the complete equation

$$v_{\max} \left[1 - \left(\frac{x}{\delta} \right)^2 \right] \frac{\partial C_A}{\partial z} = D_A \frac{\partial^2 C_A}{\partial x^2}, \quad (14.41)$$

and obtained the result:

$$\frac{\bar{C}_A^L - C_A^0}{C_A^i - C_A^0} = 0.7857e^{-5.1213\eta} + 0.1001e^{-39.318\eta} + \dots, \quad (14.42)$$

where $\eta = D_A L / \delta^2 v_{\max}$, and \bar{C}_A^L = bulk average composition of the liquid at L .

¹R. L. Pigford, *Ph.D. Thesis*, University of Illinois, 1941.

For small values of η , corresponding to short contact times or very thick films, we obtain

$$\frac{\bar{C}_A^L - C_A^0}{C_A^i - C_A^0} = \frac{6D_A L}{\pi \delta^2 \bar{V}}, \quad (14.43)$$

and for long times, we have

$$\frac{\bar{C}_A^L - C_A^0}{C_A^i - C_A^0} = 0.7857 e^{-5.1213\eta}. \quad (14.44)$$

14.4 THE MASS TRANSFER COEFFICIENT

In Chapter 7, we analyzed simple problems of heat transfer with laminar convection, and formulated the temperature distribution from which we calculated heat transfer rates by evaluating the heat fluxes at the fluid-solid boundary. With the fluxes, we wrote expressions for the heat transfer coefficients, and we saw that $Nu = f(Re, Pr)$, and gained insight into what was to follow in Chapter 8, where we presented the correlations for heat transfer in convective systems.

Having considered diffusion in the presence of forced convection in Section 14.3, it is convenient to introduce the *mass transfer coefficient*. As we mentioned, we may treat the movement of a species as the sum of a diffusional contribution and a bulk flow contribution (see Eq. (14.1)). To be analogous with heat transfer, a mass transfer coefficient for transfer of A into or out of a phase is defined in terms of the *diffusive* contribution normal to the interface:

$$k_M = \frac{j_A^0}{C_A^0 - C_{A\infty}} = - \frac{D_A (\partial C_A / \partial x)_{x=0}}{C_A^0 - C_{A\infty}}. \quad (14.45)$$

Here, the superscript 0 refers to quantities evaluated at the interface, and $C_{A\infty}$ to some concentration of A within the fluid, usually the bulk concentration. Note that, while k_M in Eq. (14.45) is defined in terms of the diffusion flux at the surface, in general, at interfaces involving a fluid phase, there is the additional contribution to mass transfer caused by bulk flow. We define the mass transfer coefficient here only in terms of the diffusive contribution, rather than of the total flux N_A^0 . This is because the coefficient so defined is somewhat more fundamental, since we might expect the diffusion flux to be approximately proportional to a characteristic concentration difference as indicated by Eq. (14.45), whereas the bulk flow contribution can be relatively independent of any concentration difference. Similarly, when both heat and mass transfer occur, it is advantageous to retain the definition of the heat transfer coefficient given by Eq. (8.1), which considers only the conduction flux.

In the limit of low mass transfer rates, as is often the case, we may neglect the distortion of the velocity and concentration profiles by mass transfer, and the bulk flow term is negligible. Then

$$k_M = \frac{N_A^0}{C_A^0 - C_{A\infty}}. \quad (14.46)$$

This equation is definitional only, and we must evaluate it by means of various analytical expressions for the flux. As the first example of applying Eq. (14.46), consider the results of diffusion into a falling film in Section 14.3. We evaluate the *local* mass transfer coefficient relating the rate of mass transfer of A into the liquid when the time of contact is short, by substituting Eq. (14.39) into Eq. (14.46).

$$k_{M,z} = \frac{N_{Ax}|x=0}{C_A^0 - C_{A\infty}} = \frac{D_A v_{\max}}{\pi z}, \quad (14.47)$$

or in terms of dimensionless groups, and recalling that $v_{\max} = \frac{3}{2}\bar{V}$,

$$\frac{k_{M,z} z}{D_A} = \frac{3\bar{V}z\nu}{2\pi\nu D_A}. \quad (14.48)$$

The group $k_{M,z}z/D_A$ is called the *Sherwood number*, Sh , or alternatively the *mass transfer Nusselt number*, Nu_M . The Reynolds number should be easily recognized. The Schmidt number, Sc , which is defined by

$$Sc = \frac{\nu}{D}, \quad (14.49)$$

is the analog of the Prandtl number encountered in heat transfer.

Most available forced-convection mass transfer correlations are in the form:

$$Sh = f(Re, Sc, \text{geometry}),^* \quad (14.50)$$

as, for example, in the situation above. Specifically, we could write Eq. (14.48) as

$$Sh_z = \frac{3}{2\pi} Re_z^{1/2} Sc^{1/2}. \quad (14.51)$$

In this case, by subscripting with z , we emphasize that local values are being considered. If we used Eq. (14.40) instead of Eq. (14.39), we would define an *average* mass transfer coefficient over the film length L .

$$k_M = \frac{(C_A^0 - C_A^i) \left[\frac{4D_A v_{\max}}{\pi L} \right]^{1/2}}{(C_A^0 - C_A^i)} = \frac{6D_A \bar{V}}{\pi L}. \quad (14.52)$$

We can then write this in dimensionless form as

$$Sh_L = \frac{6}{\pi} Re_L^{1/2} Sc^{1/2}, \quad (14.53)$$

where the subscript L indicates that the quantities are averaged over the entire film length.

*The product $ReSc$, which we often encounter in mass transfer, is sometimes called the Peclet number, Pe .

In the case of long contact times, where Eq. (14.44) applies, the rate at which A is absorbed in the distance dz is

$$\bar{V}\delta d\bar{C}_A = k_M(C_A^0 - \bar{C}_A) dz.$$

Over the entire length of the film, the absorption rate of A is

$$\bar{V}\delta \int_{C_A^i}^{\bar{C}_A^L} \frac{d\bar{C}_A}{C_A^0 - \bar{C}_A} = k_M \int_0^L dz.$$

The integration yields

$$k_M = \frac{\bar{V}\delta}{L} \ln \frac{C_A^0 - C_A^i}{C_A^0 - \bar{C}_A^L}. \quad (14.54)$$

Substituting Eq. (14.44), we obtain

$$k_M = \frac{\bar{V}\delta}{L} [\ln(e^{5.1213\eta}) - \ln 0.7857] = \frac{\bar{V}\delta}{L} [5.1213\eta + 0.241] \cong 3.42 \frac{D_A}{\delta}. \quad (14.55)$$

By rearranging this expression, we get

$$\frac{k_M \delta}{D_A} = \text{Sh} \cong 3.42, \quad (14.56)$$

which is similar to the results given in Table 7.1, where the Nusselt number was found to be a constant for fully developed laminar flow. This equation is applicable when $\text{Re}(=\Gamma/\eta) \leq 25$, where Γ is the mass flow rate per unit width of film.

Having been tested for absorption of gases into liquids flowing down wall columns, Eq. (14.56) sometimes underestimates the actual mass transfer coefficient. At low Reynolds numbers, this is now understood to be partly due to the so-called *Marangoni effect*, in which upward-directed surface tension forces counteract the downward-directed gravitational forces, causing rippling and turbulence on the surface and an increase in mass transfer, which is not anticipated in the simplified development described above.

Example 14.3 A method for degassing molten metals involves exposing a thin film of metal to vacuum by allowing it to flow continuously over an inclined plate. Calculate the average hydrogen concentration of an alloy, with an initial concentration of $1 \text{ m}^3 \text{ H}_2(\text{STP})$ per m^3 of alloy, flowing down a plate 1 m long and 0.15 m wide, which is inclined at an angle of 10 deg from the horizontal. The concentration of hydrogen at the surface exposed to the vacuum may be taken as zero. The desired film thickness is $1 \times 10^{-3} \text{ m}$. Data are as follows: $\rho = 8.32 \times 10^3 \text{ kg m}^{-3}$, $\eta = 6 \times 10^{-3} \text{ N s m}^{-2}$, $D_H = 1.3 \times 10^{-8} \text{ m}^2 \text{ s}^{-1}$.

Solution. Using Eq. (2.14), we find the average velocity:

$$\bar{V} = \frac{(8.32 \times 10^3 \text{ kg m}^{-3})(9.8 \text{ m s}^{-1})(1 \times 10^{-3} \text{ m})^2 (\cos 80^\circ)}{3(6 \times 10^{-3} \text{ N s m}^{-2})} = 7.86 \times 10^{-1} \text{ m s}^{-1}.$$

The contact time is

$$\frac{L}{\bar{V}} = \frac{1}{0.786 \text{ m s}^{-1}} = 1.27 \text{ s.}$$

Since this is very short, we make use of Eq. (14.52) to calculate an average k_M :

$$k_M = \frac{6D_H \bar{V}}{\pi L} = \frac{6(1.3 \times 10^{-8})(0.786)}{(3.14)(1)} = 1.4 \times 10^{-4} \text{ m s}^{-1}.$$

Then

$$j_{H_2} = 1.4 \times 10^{-4} \text{ m s}^{-1} (1 \text{ m}^3 \text{ H}_2 \text{ m}^{-3} \text{ alloy}) = 1.4 \times 10^{-4} \text{ m}^3 \text{ H}_2 \text{ m}^{-2} \text{ s}^{-1}.$$

Total content removed per m^2 of exposed surface is $= j_{H_2}$ (contact time)

$$= 1.78 \times 10^{-4} \text{ m}^3 \text{ H}_2 \text{ m}^{-2} \text{ film.}$$

Initial total content $= (1 \text{ m}^3 \text{ H}_2 \text{ m}^{-3} \text{ alloy})(1.0 \times 10^{-3} \text{ m}^3 \text{ alloy m}^{-2} \text{ film})$

$$= 1.0 \times 10^{-3} \text{ m}^3 \text{ H}_2 \text{ m}^{-2} \text{ film.}$$

Final total content $= 0.0010 - 0.000178 = 0.000822 \text{ m}^3 \text{ H}_2 \text{ m}^{-2} \text{ film}$, or the average content of the metal is reduced to $0.822 \text{ m}^3 \text{ H}_2 \text{ m}^{-3} \text{ alloy}$.

Under many circumstances encountered in interphase mass transfer, the bulk flow term is not important, and the diffusive contribution in the mass flux equation is all that we need to consider. On the other hand, there may be occasions, particularly where transfer to and from gas phases is involved, in which this contribution is not negligible. In this case, we write

$$N_A = \theta k_M (C_A^0 - C_A^i), \quad (14.57)$$

where N_A is the total interphase flux, and θ is a correction factor that depends on N_A , N_B , and k_M according to

$$\theta = \frac{N_A + N_B}{k_M \left[\exp \left(\frac{N_A + N_B}{k_M} \right) + 1 \right]}. \quad (14.58)$$

Figure 14.4 gives a graph of θ as a function of $(N_A + N_B)/k_M = \phi$. A limiting case is equimolar counterdiffusion, in which $N_A = -N_B$ and $\phi = 0$, so that $\theta = 1.0$ and no correction is involved.

In case we do not know N_A , and $N_B = 0$, the expression

$$1 + \frac{C_A^0 - C_A^i}{\frac{N_A}{N_A + N_B} - C_A^0} = \exp \left(\frac{N_A + N_B}{k_M} \right) \quad (14.59)$$

may be used to evaluate N_A at high mass transfer rates.

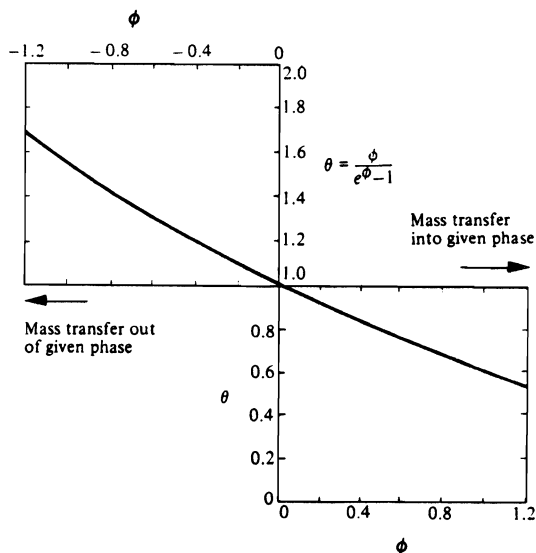


Fig. 14.4 The variation of coefficients with mass transfer rate. (From R. B. Bird, W. E. Stewart, and E. N. Lightfoot, *Transport Phenomena*, Wiley, New York, 1960, page 664.)

Thus, forced convection mass transfer at high mass transfer rates (large N_A and/or N_B) is generally correlated by

$$\text{Sh} = f(\text{Re}, \text{Sc}, N_A, \text{ and geometry}). \quad (14.60)$$

For the most part, we do not make use of this form in materials processing.

14.5 GENERAL EQUATION OF DIFFUSION WITH CONVECTION

In this section, we summarize the general approach to the law of mass conservation in the volume element $\Delta x \Delta y \Delta z$, depicted in Fig. 2.4, through which a fluid containing A in solution is flowing. In the following expressions, ρ_A is the mass *concentration* (for example, kg of $A \text{ m}^{-3}$ of total solution) as defined by Eq. (12.3); W_{Ax} is the total *mass flux* of A in the x -direction and is composed of a diffusive term and a convective term. Specifically

$$W_{Ax} = -\rho D_A \left[\frac{\partial \rho_A^*}{\partial x} \right] + \rho_A v_x = \rho_A v_{Ax}, \quad (14.61)$$

where ρ is the density of the entire solution, ρ_A^* is the mass *fraction* of A , and v_x is the local *mass average velocity* in the x -direction; thus, we define v_x such that the total mass flux of all components in the x -direction is made up of the sum of the n component fluxes in the same direction:

$$\rho v_x = \sum_{i=1}^n \rho_i v_{ix}. \quad (14.62)$$

524 Mass Transfer in Fluid Systems

For a binary, in order to illustrate, we write

$$v_x = \frac{1}{\rho} (\rho_A v_{Ax} + \rho_B v_{Bx}) = \frac{1}{\rho} (W_{Ax} + W_{Bx}).$$

Now we can proceed to develop a mass balance for the volume element. The various contributions to the mass balance of component A are

Accumulation of mass of A in the volume element	$\Delta x \Delta y \Delta z \frac{\partial \rho_A}{\partial t}$,
Input of A across face at x	$\Delta y \Delta z W_{Ax} _x$,
Output of A across face at $x + \Delta x$	$\Delta y \Delta z W_{Ax} _{x+\Delta x}$.

There are also input and output terms in the y - and z -directions. When we write the entire mass balance for species A , divide through by $\Delta x \Delta y \Delta z$, and take the limits in the usual manner, we obtain the *general equation of continuity for component A*:

$$\frac{\partial \rho_A}{\partial t} + \frac{\partial W_{Ax}}{\partial x} + \frac{\partial W_{Ay}}{\partial y} + \frac{\partial W_{Az}}{\partial z} = 0. \quad (14.63)$$

The quantities W_{Ax} , W_{Ay} , W_{Az} are the rectangular components of the *mass flux vector*, $W_A = \rho_A v_A$, which includes motion of A due to diffusion and bulk flow:

$$W_A = -\rho D_A \nabla \rho_A^* + \rho_A v = \rho_A v_A. \quad (14.64)$$

Finally, by combining Eqs. (14.63) and (14.64), we develop the *diffusion equation for component A*:

$$\frac{\partial \rho_A}{\partial t} + \nabla \cdot \rho_A v = \nabla \cdot \rho D_A \nabla \rho_A^*. \quad (14.65)$$

As is usually the case, simplifications are utilized more frequently than general equations. Often, one can assume constant mass density and D_A , and make some simplification. For *constant ρ and D_A* , Eq. (14.65) becomes

$$\frac{\partial \rho_A}{\partial t} + v \nabla \rho_A = D_A \nabla^2 \rho_A, \quad (14.66)$$

or if divided by M_A (molecular weight of A), we get

$$\frac{\partial C_A}{\partial t} + v \nabla C_A = D_A \nabla^2 C_A. \quad (14.67)$$

The left side of this equation is DC_A/Dt , showing direct similarity with Eq. (7.76) which is the basis for the numerous analogies between heat and mass transport in fluids with constant ρ .

The above analysis could have been made equally well in terms of molar fluxes such as we have used previously. Then the equation of continuity for component A becomes:

$$\frac{\partial C_A}{\partial t} + \nabla N_A = 0, \quad (14.68)$$

and the diffusion equation for A in solution becomes:

$$\frac{\partial C_A}{\partial t} + \nabla \cdot C_A v^* = \nabla \cdot CD_A \nabla X_A. \quad (14.69)$$

For constant C and D_A , Eq. (14.69) takes the form

$$\frac{\partial C_A}{\partial t} v^* \nabla C_A = D_A \nabla^2 C_A. \quad (14.70)$$

This equation is usually applied to low-density gases at constant temperature and pressure. The left side of this equation cannot be written as DC_A/Dt because of the appearance of v^* rather than of v . A more simplified form of the above equations, which is used for diffusion in solids or stationary liquids ($v = 0$ in Eq. (14.67)), or for equimolar counterdiffusion in gases ($v^* = 0$ in Eq. (14.70)), is *Fick's second law of diffusion*:

$$\frac{\partial C_A}{\partial t} = D_A \nabla^2 C_A. \quad (14.71)$$

In Tables 14.1 and 14.2, we summarize the most important equations of this discussion in rectangular, cylindrical, and spherical coordinates. Fick's second law of diffusion can be obtained by setting the velocity components in Table 14.2 equal to zero.

Table 14.1 The equation of continuity of A in various coordinate systems

Rectangular coordinates:

$$\frac{\partial C_A}{\partial t} + \left[\frac{\partial N_{Ax}}{\partial x} + \frac{\partial N_{Ay}}{\partial y} + \frac{\partial N_{Az}}{\partial z} \right] = 0 \quad (A)$$

Cylindrical coordinates:

$$\frac{\partial C_A}{\partial t} + \left[\frac{1}{r} \frac{\partial}{\partial r} (r N_{Ar}) + \frac{1}{r} \frac{\partial N_{A\theta}}{\partial \theta} + \frac{\partial N_{Az}}{\partial z} \right] = 0 \quad (B)$$

Spherical coordinates:

$$\frac{\partial C_A}{\partial t} + \left[\frac{1}{r^2} \frac{\partial}{\partial r} (r^2 N_{Ar}) + \frac{1}{r \sin \theta} \frac{\partial}{\partial \theta} (N_{A\theta} \sin \theta) + \frac{1}{r \sin \theta} \frac{\partial N_{A\phi}}{\partial \phi} \right] = 0 \quad (C)$$

Table 14.2 The equation of diffusion of A for constant ρ and D_A

Rectangular coordinates:

$$\frac{\partial C_A}{\partial t} + \left[v_x \frac{\partial C_A}{\partial x} + v_y \frac{\partial C_A}{\partial y} + v_z \frac{\partial C_A}{\partial z} \right] = D_A \left[\frac{\partial^2 C_A}{\partial x^2} + \frac{\partial^2 C_A}{\partial y^2} + \frac{\partial^2 C_A}{\partial z^2} \right] \quad (\text{A})$$

Cylindrical coordinates:

$$\begin{aligned} \frac{\partial C_A}{\partial t} + \left[v_r \frac{\partial C_A}{\partial r} + v_\theta \frac{1}{r} \frac{\partial C_A}{\partial \theta} + v_z \frac{\partial C_A}{\partial z} \right] \\ = D_A \left[\frac{1}{r} \frac{\partial}{\partial r} \left[r \frac{\partial C_A}{\partial r} \right] + \frac{1}{r^2} \frac{\partial^2 C_A}{\partial \theta^2} + \frac{\partial^2 C_A}{\partial z^2} \right] \end{aligned} \quad (\text{B})$$

Spherical coordinates:

$$\begin{aligned} \frac{\partial C_A}{\partial t} + \left[v_r \frac{\partial C_A}{\partial r} + v_\theta \frac{1}{r} \frac{\partial C_A}{\partial \theta} + v_\phi \frac{1}{r \sin \theta} \frac{\partial C_A}{\partial \phi} \right] \\ = D_A \left[\frac{1}{r^2} \frac{\partial}{\partial r} \left[r^2 \frac{\partial C_A}{\partial r} \right] + \frac{1}{r^2 \sin \theta} \frac{\partial}{\partial \theta} \left[\sin \theta \frac{\partial C_A}{\partial \theta} \right] + \frac{1}{r^2 \sin^2 \theta} \frac{\partial^2 C_A}{\partial \phi^2} \right] \end{aligned} \quad (\text{C})$$

14.6 MASS TRANSFER WITH FORCED CONVECTION OVER A FLAT PLATE

As an application of the above equations, consider the flow system in which a thin, semi-infinite plate of solid A dissolves very slowly under steady-state conditions, into an unbounded fluid of stream of A and B . The flow is initially at uniform velocity, concentration, and temperature. For constant properties of the fluid, we may write the boundary layer equations of momentum, energy, mass, and continuity as follows:

$$\text{Continuity, } \frac{\partial v_x}{\partial x} + \frac{\partial v_y}{\partial y} = 0, \quad (14.72)$$

$$\text{Momentum, } v_x \frac{\partial v_x}{\partial x} + v_y \frac{\partial v_x}{\partial y} = \nu \frac{\partial^2 v_x}{\partial y^2}, \quad (14.73)$$

$$\text{Energy, } v_x \frac{\partial T}{\partial x} + v_y \frac{\partial T}{\partial y} = \alpha \frac{\partial^2 T}{\partial y^2}, \quad (14.74)$$

$$\text{Mass, } v_x \frac{\partial C_A}{\partial x} + v_y \frac{\partial C_A}{\partial y} = D_A \frac{\partial^2 C_A}{\partial y^2}. \quad (14.75)$$

Equations (14.72)-(14.74) were obtained in Chapter 7 for zero mass transfer. The assumption that the same equations are valid in the presence of mass transfer means that any additional momentum and energy fluxes associated with mass transfer are negligible. Equation (14.75) is derived from Eq. (A) in Table 14.2 with $\partial C_A/\partial t = 0$, $\partial^2 C_A/\partial x^2 = 0$, $v_z = 0$, and by neglecting the negligible amount of diffusion in the x -direction.

A typical set of boundary conditions that may be specified is:

$$\begin{aligned} \text{B.C.1: } x \leq 0, \quad v_x = V_\infty, \quad v_y = 0, \quad T = T_\infty, \\ C_A = C_{A\infty} \quad \text{for all } y, \end{aligned} \tag{14.76a}$$

$$\begin{aligned} \text{B.C.2: } y = \infty, \quad v_x = V_\infty, \quad v_y = 0, \quad T = T_\infty, \\ C_A = C_{A\infty} \quad \text{for } x > 0, \end{aligned} \tag{14.76b}$$

$$\begin{aligned} \text{B.C.3: } y = 0, \quad v_x = 0, \quad v_y = v_0, \quad T = T_0, \\ C_A = C_A^0 \quad \text{for } x > 0. \end{aligned} \tag{14.76c}$$

The fact that $v_y = v_0$ at the wall accounts for the bulk motion accompanying diffusion from the wall. The method of solving Eqs. (14.72)-(14.75) subject to the conditions (Eqs. (14.76a, b, and c)) is not given here, but Fig. 14.5 presents the results for certain values of Pr and Sc. Note that the differential equations and boundary conditions for temperature and concentration are analogous; therefore, when Pr = Sc = 1, the velocity, temperature, and concentration profiles within the boundary layer must coincide. Figure 14.5 shows these results, along with the results for Pr = Sc = 0.7; velocity profiles remain unchanged.

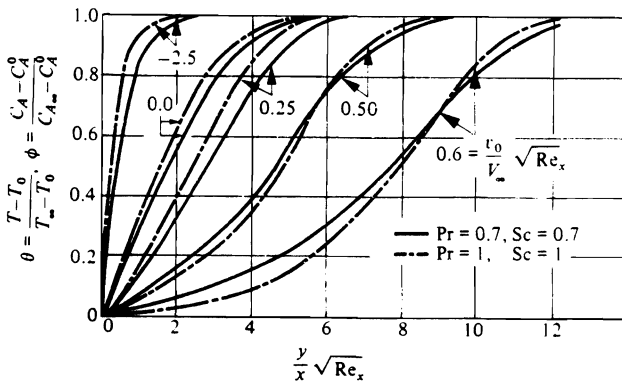


Fig. 14.5 Temperature and concentration profiles in a laminar boundary layer on a flat plate for Pr = Sc = 0.7, and Pr = Sc = 1. Curves for Pr = Sc = 1 also represent velocity profiles. (From J. P. Hartnett and E. R. G. Eckert, *Trans. ASME* 79, 247 (1957).)

These profiles show a dependency on the mass flux $(v_0 \sqrt{Re_x} / V_\infty)$. Mass transfer away from the plate (positive v_0) gives flatter profiles as would be true if the solid surface were porous and a gas diffused upward through the plate, or if a liquid passed through the porous plate and evaporated. On the other hand, mass transfer toward the plate (negative v_0) gives

528 Mass Transfer in Fluid Systems

steeper profiles; this situation can be obtained if condensation occurs at the surface, or suction is applied to a porous membrane. Figure 14.6 shows the local heat and mass transfer coefficients plotted against the parameter $v_0 \sqrt{\text{Re}_x} / V_\infty$. For $v_0 = 0$ (no mass transfer, or, more realistically, at low mass transfer rates), the local mass transfer coefficient is given by Eq. (7.26) with simple changes of notations, namely: $h_x \rightarrow k_{M,x}$, $k \rightarrow D_A$, and $\text{Pr} \rightarrow \text{Sc}$. Then, the local Sherwood number is

$$\text{Sh}_x = 0.332 \text{Sc}^{0.343} \text{Re}_x^{1/2}, \quad (14.77)$$

and the average Sherwood number is

$$\text{Sh}_L = 0.664 \text{Sc}^{0.343} \text{Re}_L^{1/2}. \quad (14.78)$$

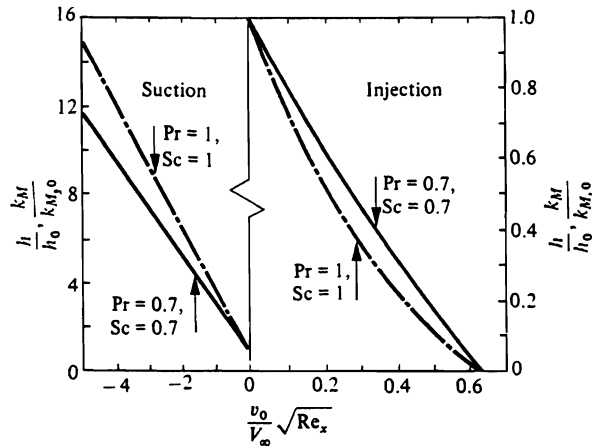


Fig. 14.6 Heat and mass transfer coefficients for laminar flow over a flat plate. Subscript zero indicates the respective coefficients for zero bulk flow normal to wall. (From J. P. Hartnett and E. R. G. Eckert, *ibid.*)

These solutions are valid for most fluids, including liquid metals. Table 14.3 gives typical magnitudes of Prandtl and Schmidt numbers for fluids.

Table 14.3 Typical magnitudes of Prandtl numbers and Schmidt numbers

	Pr	Sc
Gases	0.6-1.0	0.1-2.0
Liquids	1-10	10^2 - 10^3
Liquid metals	10^{-2}	10^3

It can be shown that the expression for the ratio of the concentration boundary layer to the momentum boundary layer is:

$$\frac{\delta_c}{\delta} = \frac{1}{1.026 \sqrt[3]{\text{Sc}}}. \quad (14.79)$$

According to Eq. (14.79), the concentration boundary layer and the velocity layers for gases are about the same as in heat transfer, where δ_T and δ were similar because Pr was about unity. For liquid metals, however, while we found that in the case of heat transfer $\delta_T \gg \delta$, now we see that $\delta_c \ll \delta$. This means that we can use temperature profiles to predict mass transfer profiles and rates, or vice versa, for gas phase transfer, but we cannot do likewise for liquid metals, because their concentration and temperature boundary layer profiles differ widely.

14.7 CORRELATIONS OF MASS TRANSFER COEFFICIENTS FOR TURBULENT FLOW

We have seen in the previous sections that many forced-convection mass transfer situations are analogous to heat transfer situations, and the appropriate heat transfer solutions apply with simple changes of notations, namely: $\alpha \rightarrow D_A$, $T \rightarrow C_A$, $\text{Pr} \rightarrow \text{Sc}$, and $\text{Nu} \rightarrow \text{Sh}$. In addition, we may assume that the results for natural convection resulting from density differences caused by mass transfer may be correlated by a mass transfer Grashof number,

$$\text{Gr}_M = g\xi(X_A - X_{A\infty})L^3/\nu^2,$$

where ξ is the concentration coefficient of volumetric expansion defined as:

$$\xi = \frac{1}{\rho} \left[\frac{\partial \rho}{\partial X_A} \right]_T.$$

In this case, we may use correlations for heat transfer to yield mass transfer data if the substitution $\text{Gr} \rightarrow \text{Gr}_M$ is made. The flow parameters such as Re and position parameters such as L/D remain the same.

We noted in Chapter 8 that in turbulent flow there is an analogy between the friction factor f for turbulent flow in tubes and heat transfer, which is given as the Chilton-Colburn " j -factor," j_H :

$$j_H = \frac{\text{Nu}}{\text{RePr}} (\text{Pr})^{2/3} = \frac{f}{2}. \quad (8.6)$$

Continuing the analogy, we define a mass transfer j -factor, j_M , for fully developed flow in round tubes:

$$j_M = \frac{\text{Sh}}{\text{ReSc}} (\text{Sc})^{2/3} = \frac{f}{2}. \quad (14.80)$$

If the temperature profile is not fully developed, then we use Fig. 8.2 where we take L/D into account, and substitute j_M for j_H .

In the case of flow parallel to a flat surface, from the results of Chapter 8, we write for average values in *laminar* flow:

$$j_H = j_M = \frac{f}{2} = \frac{0.664}{\sqrt{\text{Re}_L}}, \quad (14.81)$$

and in *turbulent* flow:

$$j_H = j_M = \frac{f}{2} = \frac{0.037}{\text{Re}_L^{0.2}}. \quad (14.82)$$

This relationship has been found to adequately describe the rate of deposition of metallic solutes from liquid to solid,² and the rate of dissolution of carbon into iron melts.³

In flow around curved surfaces, such as spheres and cylinders, $f/2$ greatly exceeds j_H and j_M . However, the analogy still holds between heat and mass transfer, so that j_H and j_M should be equivalent. To illustrate this, consider the heat transfer correlation given in Chapter 8 for forced convection around a sphere of radius R :

$$2hR/k_f = 2.0 + 0.60 \operatorname{Re}_f^{1/2} \operatorname{Pr}_f^{1/3}. \quad (8.11)$$

Translated into the j_H form it becomes

$$j_H = \frac{2.0}{\operatorname{RePr}^{1/3}} + \frac{0.60}{\operatorname{Re}^{1/2}}.$$

By analogy we get

$$j_M = \frac{2.0}{\operatorname{ReSc}^{1/3}} + \frac{0.6}{\operatorname{Re}^{1/2}}. \quad (14.83)$$

Figure 14.7 illustrates the results of experiments where j_M is plotted as a function of Re for dissolution of uranium spheres in flowing cadmium,⁴ cinnamic acid spheres in flowing water, 2-naphthol spheres in flowing water,⁵ and for comparison purposes, j_H ,⁶ and $f/2$.⁷ Note that the data from the liquid metal experiments show lower values of j_M at low Re values than those observed in the organic system experiments. This may be partially corrected for by the presence of the Schmidt number in the expression given in Eq. (14.83), which is not plotted in Fig. 14.7. No equation accounts for the peak in j_M near Reynolds numbers of 10^5 , so usually the graph is preferred rather than an equation in this range.

For natural convection, the mass transfer analog of

$$\operatorname{Nu}_L = 0.13 (\operatorname{Gr}_L \operatorname{Pr})^{1/3} \quad (8.18)$$

has been applied to both the rate of dissolution of carbon in molten iron⁸ and the rate of dissolution of steel in molten iron-carbon alloys,⁹ and found to be quite reasonable as an approximation, with the best fit of the data yielding the equation

$$\operatorname{Sh}_L = 0.11 (\operatorname{Gr}_{M,L} \operatorname{Sc})^{1/3}. \quad (14.84)$$

²W. N. Gill, R. P. Vanek, R. V. Jelinek, and C. S. Grove, *AIChEJ* **6**, 139 (1960).

³M. Kosaka and S. Minowa, *Trans. Japan Iron and Steel Inst.* **8**, 393 (1968).

⁴F. D. Taylor, L. Burris, and C. J. Geankoplis, *I. & E. C. Fundamentals* **4**, 119 (1965).

⁵L. R. Steele and C. K. Geankoplis, *AIChEJ* **5**, 178 (1959).

⁶T. K. Sherwood, *Ind. Engr. Chem.* **42**, 2077 (1950).

⁷F. H. Garner and R. D. Suckling, *AIChEJ* **4**, 114 (1958).

⁸M. Kosaka and S. Minowa, *ibid.*

⁹M. Kosaka and S. Minowa, *Tetsu-to-Hagane* **53**, 983 (1967).

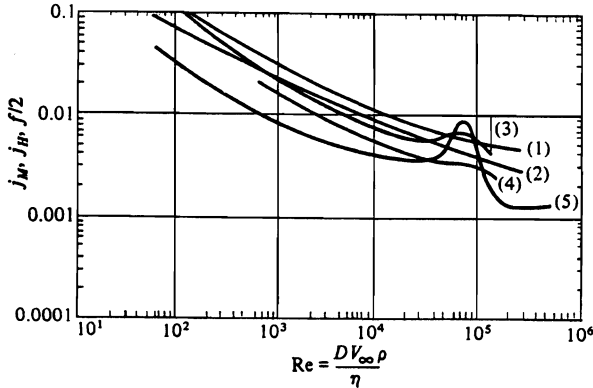


Fig. 14.7 Comparison of mass, heat, and momentum transfer to spheres. (1) $f/2$; (2) Chilton-Colburn factor j_H ; (3) j_M for cinnamic acid-water system; (4) j_M for 2-naphthol-water system; (5) j_M for uranium dissolving in cadmium.

Many processes depend on gas-liquid contact and mass transfer between the phases. Although this is a very complex area,¹⁰ several relationships have been found that describe the process of mass transfer *on the liquid side* of a gas bubble-liquid interface. One of the most useful is that of Hughmark.¹¹ His expression is

$$\frac{k_M d}{D} = 2.0 + a \left[\left[\frac{V_t d}{\nu} \right]^{0.48} \left[\frac{\nu}{D} \right]^{0.339} \left[\frac{g^{1/3} d}{D^{2/3}} \right]^{0.072} \right]^b, \quad (14.85)$$

where d is the bubble diameter, V_t is the terminal velocity of the rising bubble, and a and b are constants that depend on whether the bubbles act singly or in swarms. For single bubbles, $a = 0.061$ and $b = 1.61$. This relationship has been tested in molten copper-carbon monoxide systems, and was found satisfactory for describing the rate of transfer of oxygen in the copper to the interface.¹²

Equation (14.85) is of the form

$$\text{Sh} = f \left[\text{Re}, \text{Sc}, \left[\frac{g^{1/3} d}{D^{2/3}} \right] \right].$$

The velocity in the Reynolds number is the velocity of the gas bubble relative to the liquid velocity. When an expression for the velocity in terms of the density difference, $\rho_l - \rho_g$, is substituted, the final result depends on the Grashof number, Gr_M , instead. Without the third group that shows up in Hughmark's correlation, the result is

$$\text{Sh} = f \left[\text{Gr}'_M, \text{Sc} \right].$$

¹⁰For reviews, see P. H. Calderbank, *Trans. Inst. Chem. Engrs.* **212**, 209 (1967); F. H. H. Valentin, *Absorption in Gas-Liquid Dispersions*, Spon Ltd., London, 1967.

¹¹G. A. Hughmark, *I. & E. C. Process Design and Development* **6**, 218 (1967).

¹²C. R. Nanda and G. H. Geiger, *Metall. Trans.* **2**, 1101 (1971).

532 Mass Transfer in Fluid Systems

Accordingly, some mass transfer correlations involving gas bubbles in liquid are presented in this way. In bubble swarms, we can use¹³

$$\text{Sh} = 0.31 \text{Gr}'_M{}^{1/3} \text{Sc}^{1/3} \quad (14.86)$$

for $d < d_c$, and

$$\text{Sh} = 0.42 \text{Gr}'_M{}^{1/3} \text{Sc}^{1/2} \quad (14.87)$$

for $d > d_c$. Equations (14.86) and (14.87) apply to two distinct regimes, which are divided by a critical bubble diameter, $d_c \approx 2.5$ mm. The Grashof number is defined as

$$\text{Gr}'_M = \frac{gd^3\rho_\ell(\rho_\ell - \rho_g)}{\eta_\ell^2}, \quad (14.88)$$

where the subscripts ℓ and g refer to the liquid and gas, respectively.

In applying Eqs. (14.85)-(14.87), one must have a way to estimate the surface area of the bubbles in the swarm. For bubble swarms, this is problematic; furthermore, the ultimate goal is to quantify the relationship between the mass transfer and the flow rate of the gas. With this attitude, Fruehan and Martonik¹⁴ recommend combining Ak_M , when dealing with bubble swarms, where A is the surface area. Their result is

$$Ak_M = 0.008 Q^{0.75} H^{0.69}, \quad (14.89)$$

where Ak_M has units of $\text{cm}^3 \text{s}^{-1}$, Q is the flow rate of the gas in $\text{cm}^3 \text{s}^{-1}$, and H is the depth of the liquid above the injection nozzle (called a tuyere) in cm.

Example 14.4 Small individual bubbles of diameter d are often approximated as nonrotating spheres rising in liquids. Starting with the mass transfer form of Eq. (8.11), show that the correlation can be put in the form

$$\text{Sh} = f(\text{Gr}'_M, \text{Sc}).$$

Solution. Equation (8.11) in mass transfer form is

$$\text{Sh} = \frac{k_M d}{D} = 2.0 + 0.60 \text{Re}^{1/2} \text{Sc}^{1/3},$$

where

$$\text{Re} = \frac{dV_t \rho_\ell}{\eta_\ell}.$$

The terminal velocity can be found from Section 3.3.2, from which it can be shown that

$$V_t = \left[\frac{4dg(\rho_\ell - \rho_g)}{3f\rho_g} \right]^{1/2},$$

¹³P. H. Calderbank and M. Yoo-Young, *Chem. Eng. Sci.* **16**, 39 (1961).

¹⁴R. J. Fruehan and L. J. Martonik, in *Proceedings of the Third International Iron and Steel Congress*, American Society for Metals, Metals Park, OH, 1978, pp. 229-238.

where f is the friction factor. Using this terminal velocity, the Reynolds number can be written as

$$\text{Re} = \frac{2d\rho_t}{\eta_t} \left[\frac{dg(\rho_t - \rho_g)}{3f\rho_t} \right]^{1/2},$$

or, with the definition of the Grashof number, Eq. (14.88), as

$$\text{Re} = 2 \left[\frac{\text{Gr}'_M}{3f} \right]^{1/2}.$$

If f is constant, which is approximately valid for $2 \times 10^2 \leq \text{Re} \leq 2 \times 10^5$, then we get the result

$$\text{Sh} \cong 2.0 + 0.77 (\text{Gr}'_M)^{1/4} \text{Sc}^{1/3}.$$

In the Stokes' law regime ($\text{Re} \leq 1.0$), $f = 24/\text{Re}$; thus

$$\text{Re} = \frac{\text{Gr}'_M}{18},$$

and

$$\text{Sh} = 2.0 + 0.14 \text{Gr}'_M^{1/2} \text{Sc}^{1/3}.$$

Note that the Chilton-Colburn analogy is applicable only at relatively low mass transfer rates, and that the best results are obtained when similar materials are utilized in both the heat and analogous mass transfer situations. Turbulent flow mass transfer correlations based on studies using common liquids appear to be directly translatable into liquid metal systems, but heat transfer data are not quite as accurate in predicting mass transfer, although usually satisfactory to within an order of magnitude.

Also, many of the tests of applicability of heat transfer correlations to mass transfer involving the gas phase have not been made at conditions likely to be of interest to materials engineers, particularly at elevated temperatures and high rates of transfer, so they should be used with caution.

Example 14.5 Graphite particles are often added to molten cast iron in order to increase the carbon content when scrap steel is used as starting material. The time required to dissolve the particles is of interest. Determine the time to dissolve particles of graphite as a function of the bath's carbon content.

The particles have a shape factor λ of 1.5, and a characteristic dimension \bar{D}_p of 0.14 cm. The particles float, and are swept to the side of the surface of the melt by the magnetically induced stirring action, where the metal velocity relative to the graphite is approximately 25 cm s^{-1} . Due to the displacement of metal by graphite, the surface area of an individual particle in contact with the metal is calculated as $\frac{3}{8}$ of the total particle surface area. In addition, a portion of the particle exposed to the atmosphere is burned to CO due to the air circulating over the bath surface. Thus, the recovery of carbon in the melt is less than 100%, and experience shows that, in fact, the recovery is only 50%. Therefore, the mass of an individual particle (of density ρ_s) that dissolves in the melt is

$$m = \frac{1}{2} \left[\frac{\pi}{6} \bar{D}_p^3 \rho_s \right],$$

534 Mass Transfer in Fluid Systems

and its surface area exposed to the melt is

$$A = \frac{3}{8} \pi \bar{D}_p^2 \lambda.$$

Solution. The mass flow, in terms of g (carbon) s^{-1} is

$$\frac{dm}{dt} = -k_M A \rho_L (C_0 - C_\infty),$$

where ρ_L is liquid density, $g\ cm^{-3}$, C_0 is weight fraction of carbon at the particle-melt interface, and C_∞ = weight fraction of carbon in the bulk melt.

We evaluate the mass transfer coefficient from Fig. 14.8, which has been developed by several investigators for the dissolution of rotating carbon rods in Fe-C melts. For a velocity of $25\ cm\ s^{-1}$, k_M for graphite is $0.02\ cm\ s^{-1}$. Now, since

$$\frac{dm}{dt} = -\frac{1}{4} \pi \bar{D}_p^2 \rho_s \frac{d\bar{D}_p}{dt},$$

and the area is as given above, we can determine the time to dissolve a particle:

$$\int_0^{\bar{D}_p} d\bar{D}_p = \frac{3}{2} k_M \lambda \frac{\rho_L}{\rho_s} (C_0 - C_\infty) \int_0^t dt,$$

or

$$t = \frac{2\rho_s \bar{D}_p}{3\rho_L \lambda k_M (C_0 - C_\infty)},\ s.$$

The results are plotted on the next page.

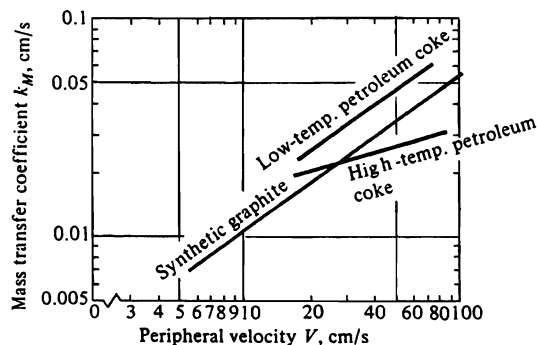
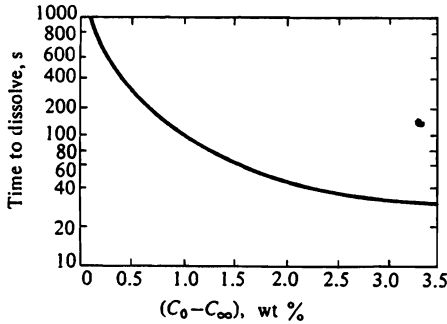


Fig. 14.8 Mass transfer coefficients for carbon dissolution in Fe-C melts. (From R. G. Olsson, V. Koump, and T. F. Perzak, *Trans. AIME* **236**, 426 (1965); O. Angeles, G. H. Geiger, and C. R. Loper, *Trans. AFS* **76**, 629 (1968); and M. Kosaka and S. Minowa, *Trans. Japan Iron Steel Inst.* **8**, 393 (1968).)



14.8 MODELS OF THE MASS TRANSFER COEFFICIENT

Since most conditions in which mass transfer is important involve fluids undergoing turbulent motion, we must usually rely on the preceding correlations, with experimental studies giving the necessary empirical coefficients. However, there are situations when test data are outside the experimental scope of variables, and it is desirable to know whether and how the experimental data can be extended to the new situation. Several theories of the process of mass transfer have been developed, which attempt to present models of what actually happens at the interface between two fluids or between a fluid and solid from a fundamental viewpoint, in order to aid in intelligent extrapolation of data.

The oldest theory is the film theory of Lewis and Whitman¹⁵ who suggested that there is an unmixed layer or film in the fluid next to the actual interface, continuously exposed to the completely mixed bulk fluid on one side and to the other phase on the other. This layer, devoid of any fluid motion, is supposed to offer all the resistance to the transfer of component A from the interface into the bulk solution, as depicted in Fig. 14.9. The transfer takes place purely by atomic or molecular diffusion through the film. Figure 14.9 indicates the concentration profile assumed in the model. Since the entire concentration change from $C_{A\infty}$ to C_A^0 is assumed to take place within the film in a steady-state manner, and since the mass-transfer coefficient is defined by

$$j_A = k_M(C_A - C_{A\infty}),$$

we can compare this to

$$j_A = -D \frac{dC_A}{dx} = +D \frac{(C_A^0 - C_{A\infty})}{\delta_{\text{eff}}},$$

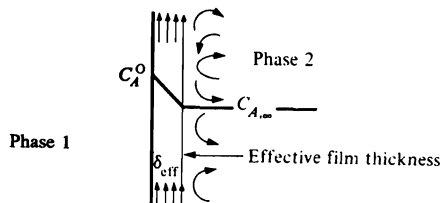


Fig. 14.9 The "effective film thickness" model.

¹⁵W. K. Lewis and W. Whitman, *Ind. Engr. Chem.* **16**, 1215 (1924).

with the result that $k_M = D/\delta_{\text{eff}}$, where δ_{eff} is the effective film thickness. This result often appears in cases where the flux is measured and the overall concentration change ($C_A^0 - C_{A\infty}$) is known, and then either the diffusivity is known (or more often assumed) and δ_{eff} is calculated, or *vice versa*. As noted below, the significance of δ_{eff} is dubious, at best.

From a fluid mechanics standpoint, it was recognized at an early stage that interfaces between fluids are bound to be unstable with time, and that any given element of fluid at the interface does not remain there for long. Thus, the film theory is much too crude to be really meaningful. Higbie¹⁶ proposed a model to describe the contact between two fluids, in which he assumed that one fluid exposes a "packet" of fluid to the other phase for an average time θ , which is taken to be extremely short, such that the packet is subject only to unsteady-state diffusion or "penetration" by the transferred species during its contact time with the other phase. The packet is assumed to be stagnant internally during this time, and well mixed before and after. Figure 14.10 gives a schematic picture of the situation. This theory results in a prediction that

$$k_M = 2\sqrt{D/\pi\theta} \quad (14.90)$$

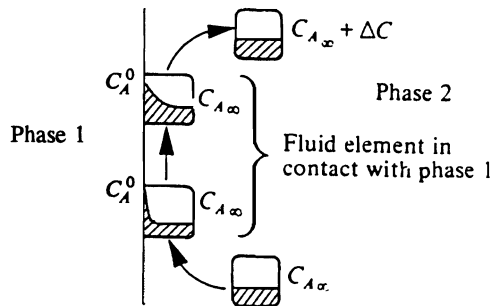


Fig. 14.10 Schematic diagram of fluid motion in penetration theory.

The logical extension of this theory was performed by Danckwerts¹⁷ who suggested that the idea of a constant time of exposure θ ought to be replaced by an average time of exposure calculated from an assumed distribution of residence times of the packets at the surface. The result of this "surface renewal" theory is again a relationship of the form

$$k_M \propto \sqrt{D} \quad (14.91)$$

The constants in his equation, like the constant θ in Higbie's equation, are not readily obtainable with the exception of bubbles rising through a liquid, in which case we may estimate θ to be the time required for a bubble to rise a distance equal to its diameter.

When considering the three theories, it is apparent that the dependence of k_M on D is different. Experimentally, it has been found that k_M is proportional to D^n where n varies from 0.5 to 1.0, depending on the fluids and the circumstances. In order to resolve this

¹⁶R. Higbie, *Trans. AIChEJ* **31**, 365 (1935).

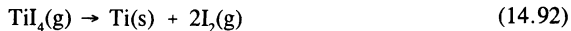
¹⁷P. U. Danckwerts, *Ind. Engr. Chem.* **43**, 1460 (1951).

discrepancy, Dobbins¹⁸ and Toor and Marchello¹⁹ proposed a combined *film penetration theory* in which the residence time of the surface elements (Higbie model) is long enough to allow the concentration gradient to approach a steady state across the finite thickness of the element (film model). This theory approaches each of the other theories as limiting cases. When D is large or the rate of surface renewal is small (θ is large), then n approaches 1.0 and so the film theory is applicable. When D is small or θ is small (rapid surface renewal rate), n approaches 0.5, and the penetration theory results. In any case, there are still parameters that must be specified in order to use the theory for predictive purposes, and they are not readily obtainable.*

14.9 MASS TRANSFER IN CHEMICAL VAPOR DEPOSITION

If we want to consider chemical vapor deposition, we should be prepared to deal with complex phenomena involving thermodynamics, reaction rates, convection patterns, and mass transfer in systems that are nonisothermal and far from equilibrium. The reactions involved can be extremely complex and multifold. All of this aside, we present a relatively simple scenario in order to illustrate the role of mass transfer in the kinetics of forming a film via chemical vapor deposition.

Titanium tetraiodide (TiI_4) is used as a feed gas to a reactor which contains a suitable substrate. The substrate is heated and the TiI_4 decomposes according to



and the titanium film is deposited. Excess $\text{TiI}_4(\text{g})$ and $\text{I}_2(\text{g})$ leave the reactor.

At the gas-solid interface, we assume that reaction (14.92) is at equilibrium. The standard free energy change of the reaction is

$$\Delta G^\circ = 402\,000 - 118\,T, \text{ kJ kmol}^{-1}$$

for $653 \leq T \leq 1943$ K. The equilibrium constant is

$$\ln K = -\frac{\Delta G^\circ}{RT},$$

or

$$\ln K = -\frac{48\,300}{T} + 14.2. \quad (14.93)$$

We use the equilibrium constant to determine the concentrations of the gas species at the gas-solid interface. Assuming an ideal gas mixture, the equilibrium constant gives

$$K = \frac{X_1^2}{X_2}, \quad (14.94)$$

¹⁸W. E. Dobbins, *Int. Conference on Water Pollution Research*, London, 1962, Pergamon Press, New York, 1964, page 61.

¹⁹H. L. Toor and J. M. Marchello, *AIChEJ* **4**, 97 (1958).

*For another discussion of the various models of mass transfer refer to E. L. Cussler, *Diffusion: Mass Transfer in Fluid Systems*, Cambridge University Press, Cambridge, UK, 1984, pages 281-296.

538 Mass Transfer in Fluid Systems

where X_1 and X_2 are the mole fractions of I_2 and TiI_4 , respectively. For mass transfer calculations, it is convenient to express the concentrations in kmol m^{-3} , so with P as the reactor pressure we write

$$C_1 = \frac{X_1 P}{RT}, \text{ kmol } I_2 \text{ m}^{-3} \text{ gas}, \quad (14.95)$$

$$C_2 = \frac{X_2 P}{RT}, \text{ kmol } TiI_4 \text{ m}^{-3} \text{ gas}. \quad (14.96)$$

After substituting Eqs. (14.95) and (14.96) into Eq. (14.94), we get the equilibrium concentrations at the gas-solid interface; namely

$$\frac{C_1^2}{C_2} = \frac{PK}{RT}. \quad (14.97)$$

Example 14.6 Calculate (a) the concentration of gas molecules in the TiI_4 -Ti reactor and (b) the equilibrium concentrations of TiI_4 and I_2 at the solid-gas interface. The reactor operates at 1 standard atmosphere of pressure and 1500 K.

Solution. a) The total concentration of gas molecules is

$$C = \frac{P}{RT} = \frac{1 \text{ atm}}{8.205 \times 10^{-2} \text{ m}^3 \text{ atm}} \left| \frac{\text{kmol K}}{1500 \text{ K}} \right|$$

$$= 8.125 \times 10^{-3} \text{ kmol m}^{-3}.$$

b) At 1500 K, Eq. (14.93) gives

$$K = \exp \left[-\frac{43,800}{T} + 14.2 \right] = 3.059 \times 10^{-7},$$

and then from Eq. (14.97), we compute

$$\frac{C_1^2}{C_2} = \frac{PK}{RT} = \frac{(1)(3.059 \times 10^{-7})}{(8.205 \times 10^{-2})(1500)} = 2.485 \times 10^{-9}.$$

Also, $C = C_1 + C_2$; therefore

$$\frac{C_1^2}{C - C_1} = 2.485 \times 10^{-9}.$$

With $C = 8.125 \times 10^{-3} \text{ kmol m}^{-3}$, we get $C_1 = 4.492 \times 10^{-6} \text{ kmol } I_2 \text{ m}^{-3}$ and $C_2 = 8.121 \times 10^{-3} \text{ kmol } TiI_4 \text{ m}^{-3}$.

The above example is a quick review of using thermodynamics to calculate the equilibrium interface concentrations. We proceed to analyze the mass transfer, which

controls the overall kinetics of the growth of the titanium film. The flux of TiI_4 from the bulk gas to the interface is

$$j_2 = k_{M2}(C_{\infty 2} - C_2),$$

and the flux of I_2 from the interface to the bulk gas is

$$j_1 = k_{M1}(C_1 - C_{\infty 1}).$$

In these equations, concentrations in the bulk gas are $C_{\infty 2}$ and $C_{\infty 1}$, the interfacial concentrations are C_1 and C_2 , and the fluxes are in $\text{kmol m}^{-2} \text{s}^{-1}$. If we proceed to evaluate the mass transfer coefficients, we will quickly realize that $D_{AB} = D_1 = D_2$ and $k_{M1} = k_{M2} = k_M$. Hence,

$$j_2 = k_M(C_{\infty 2} - C_2) \quad (14.98)$$

and

$$j_1 = k_M(C_1 - C_{\infty 1}). \quad (14.99)$$

Notice now the problem is over-specified, because the fluxes calculated by Eqs. (14.98) and (14.99) may not satisfy the stoichiometry of reaction (14.92) (specifically $j_1 = 2j_2$). We must decide, therefore, whether the flux of the reactant (TiI_4) to the surface or the flux of the product (I_2) away from the surface controls the overall mass transfer. The slower of the two is called the *rate limiting step*.

Example 14.7 For the conditions of Example 14.6, determine the *rate limiting step*.

Solution.

$$j_2 = k_M(8.125 - 8.121) \times 10^{-3} = 4 \times 10^{-6} k_M,$$

$$j_1 = k_M(4.492 - 0) \times 10^{-6} = 4.492 \times 10^{-6} k_M.$$

It is obvious that $j_1 \ll j_2$, so the flux of I_2 away from the surface is the rate limiting step.

We are ready to make use of the mass transfer coefficient to estimate the growth kinetics of the titanium film. According to reaction (14.92) for every 2 kmol of I_2 formed, we deposit 1 kmol of Ti. Therefore,

$$2j_1 = j_{\text{Ti}} = \frac{\rho}{M} \frac{d\delta}{dt}, \quad (14.100)$$

where ρ is the density of the film, δ is the thickness, M is the atomic weight (kg kmol^{-1}), and t is time. After combining Eqs. (14.99) and (14.100), the growth rate is obtained; it is

$$\frac{d\delta}{dt} = 2M\rho^{-1} k_M(C_1 - C_{\infty 1}). \quad (14.101)$$

With $\delta = 0$ and $t = 0$, we get

$$\delta = 2M\rho^{-1} k_M(C_1 - C_{\infty 1})t. \quad (14.102)$$

540 Mass Transfer in Fluid Systems

Example 14.8 Estimate the mass transfer coefficient for the film growth of Ti from TiI_4 at 1 atm, and compute the growth rate at 1500 K. The gas flows parallel to the substrate (3 cm long) with a speed of 5 m s^{-1} .

Solution. We consult Bird *et al.*²⁰ for the Lennard-Jones parameters of I_2 : $\sigma_1 = 4.982 \text{ \AA}$ and $(\varepsilon/\kappa_B)_1 = 550 \text{ K}$. The Lennard-Jones parameters of TiI_4 are estimated, again from Bird *et al.*,²¹ from the boiling point (653 K) and molar volume. These two estimates are $(\varepsilon/\kappa_B)_2 = 751 \text{ K}$ and $\sigma = 5.805 \text{ \AA}$. Therefore,

$$\sigma_{12} = \frac{\sigma_1 + \sigma_2}{2} = \frac{4.982 + 5.805}{2} = 5.394 \text{ \AA};$$

$$\left(\frac{\varepsilon}{\kappa_B} \right)_{12} = \left[\left(\frac{\varepsilon}{\kappa_B} \right)_1 \left(\frac{\varepsilon}{\kappa_B} \right)_2 \right]^{1/2} = \sqrt{(550)(751)} = 643 \text{ K}.$$

Then

$$T^* = \left[\frac{\kappa_B}{\varepsilon} \right]_{12} T = \frac{1500 \text{ K}}{643 \text{ K}} = 2.33$$

and Eq. (12.51) gives $\Omega_{D,12} = 1.022$. By making use of Eq. (12.50), we finally estimate D_{12} .

$$\begin{aligned} D_{12} &= \frac{(1.858 \times 10^{-3})(1500^{3/2})}{(1)(5.394^2)(1.02^2)} \left(\frac{1}{253.8} + \frac{1}{555.5} \right) \\ &= 0.270 \text{ cm}^2 \text{ s}^{-1} = 2.70 \times 10^{-5} \text{ m}^2 \text{ s}^{-1}. \end{aligned}$$

We must also estimate the viscosity of the gas, which is practically all TiI_4 . For this we use Eq. (1.14).

$$T^* = \left[\frac{\kappa_B}{\varepsilon} \right]_2 T = \frac{1500}{751} = 1.997.$$

Table 1.2 gives $\Omega_\eta = 1.175$, and with $\sigma = \sigma_2 = 5.805 \text{ \AA}$ we have

$$\begin{aligned} \eta_2 &= 2.67 \times 10^{-5} \frac{\sqrt{(555.5)(1500)}}{(5.805)^2(1.175)} = 6.16 \times 10^{-4} \text{ Poise} \\ &= 6.16 \times 10^{-7} \text{ N s m}^{-2}. \end{aligned}$$

²⁰R. B. Bird, W. E. Stewart and E. N. Lightfoot, *Transport Phenomena*, John Wiley & Sons, New York, NY, 1960, page 744.

²¹R. B. Bird *et al.*, *ibid.*, page 22.

The Reynolds number ($\rho_2 = 1.50 \text{ kg m}^{-3}$) is

$$\text{Re}_L = \frac{LV_\infty \rho_2}{\eta_2} = \frac{(0.03)(5)(1.50)}{(6.16 \times 10^{-7})} = 3.65 \times 10^5.$$

For flow parallel to a flat plate, this is laminar so we can use Eq. (14.78). Therefore

$$\begin{aligned} \text{Sh} &= 0.664 \text{ Sc}^{0.343} \text{ Re}_L^{1/2} = 0.664 \left[\frac{6.16 \times 10^{-7}}{1.50 \times 2.70 \times 10^{-5}} \right]^{0.343} (3.65 \times 10^5)^{1/2} \\ &= 94.45, \end{aligned}$$

and

$$k_M = 94.45 \frac{D_{12}}{L} = \frac{(94.45)(2.70 \times 10^{-5})}{0.03} = 0.0875 \text{ m s}^{-1}.$$

The growth rate is given by Eq. (14.101):

$$\begin{aligned} \frac{d\delta}{dt} &= 2M\rho^{-1} k_M (C_1 - C_\infty) \\ &= \frac{2}{\text{kmol}} \left| \frac{47.90 \text{ kg}}{\text{kmol}} \right| \left| \frac{\text{m}^3}{4400 \text{ kg}} \right| \left| \frac{0.0875 \text{ m}}{\text{s}} \right| \left| \frac{4.492 \times 10^{-6} \text{ kmol}}{\text{m}^3} \right| \\ &= 8.558 \times 10^{-9} \text{ m s}^{-1} = 30.81 \mu\text{m h}^{-1}. \end{aligned}$$

Before leaving this section, we remind the reader that a rather simple case was considered. Only one reaction was considered, and we analyzed the mass transfer. Reaction rate kinetics were not included. The gas flow was isothermal, and simple flow parallel to a flat plate was used to estimate the mass transfer coefficient. In most chemical vapor deposition processes, the conditions in the reactor are not so simple. Modern day simulations rely on simultaneously solving the momentum, energy, and species conservation equations along with realistic boundary conditions. A review that discusses the complexities involved is that of Jensen.²²

PROBLEMS

14.1 A solute is being desorbed from the surface of a melt. The concentration of the solute varies according to

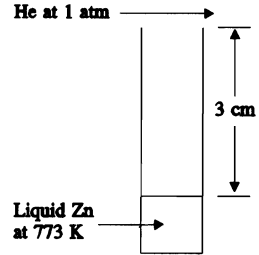
$$\frac{C - C_s}{C_\infty - C_s} = a \left[\frac{x}{\delta_c} \right] + b \left[\frac{x}{\delta_c} \right]^2,$$

where C = concentration, moles cm^{-3} ; C_s = concentration at the surface; C_∞ = bulk concentration; a, b = constants; x = distance from the surface; and δ_c = thickness of the concentration boundary layer. What is the mass transfer coefficient?

²²K. F. Jensen, *Chem. Eng. Sci.* **42**, 923 (1987).

542 Mass Transfer in Fluid Systems

14.2 a) Calculate the diffusion coefficient D_{AB} for zinc vapor diffusing through helium at 773 K. The atomic weight of Zn is 65.4 g mol⁻¹.
 b) Calculate the flux of Zn evaporation if the vapor pressure of Zn at 773 K is 0.1 atm. Express the flux in mol s⁻¹ cm⁻².



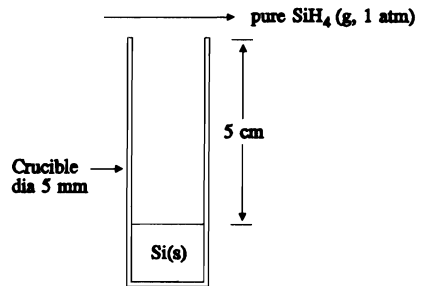
14.3 Silicon can be grown by the chemical vapor deposition of silane (SiH₄). Given a system in which silicon grows from the bottom of an inert crucible as shown adjacent, predict the growth rate of silicon. Assume that at the gas/silicon interface equilibrium is established according to the reaction



with the equilibrium constant given by

$$K = \frac{P_{\text{H}_2}^2}{P_{\text{SiH}_4}} = 10^{-4}.$$

It is also known that $D_{\text{H}_2-\text{SiH}_4} = 1 \text{ cm}^2 \text{ s}^{-1}$.



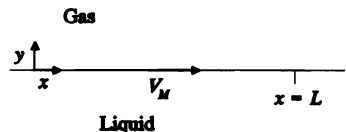
14.4 Consider diffusion through a stagnant gas as in Section 14.1; however, in this case the gas is not isothermal, but rather temperature varies according to

$$\frac{T - T_0}{T_\ell - T_0} = \frac{x}{\ell},$$

where x and ℓ are indicated in Fig. 14.1, T is temperature, T_0 is the temperature at $x = 0$, and T_ℓ is the temperature at $x = \ell$. Assume that D_{AB} varies with temperature according to Eq. (12.49); i.e., $D_{AB} = AT^{3/2}$ and A is constant. Obtain the concentration profile which gives the mole fraction of A (X_A) as a function of distance up the tube (x).

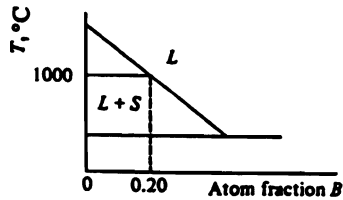
14.5 Derive expressions for diffusion through a spherical shell that are analogous to Eq. (14.12) (concentration profile) and Eq. (14.14) (molar flux).

14.6 Liquid flows in one direction, from $x = 0$ to $x = L$, with a velocity V_M . Because of the "no-slip" condition, the velocity of the gas along the surface $y = 0$ is also V_M . When the gas crosses the plane at $x = 0$, its concentration of A is uniform and constant, $C_{A\infty}$. However, at $y = 0$ and $0 \leq x \leq L$, its concentration is C_A° .



Assume steady state. a) Write a partial differential equation for $C_A(x, y)$ in the gas. b) Write boundary conditions for C_A that are needed to solve part a). c) Solve for $C_A(x, y)$.

14.7 At 1000°C metal *A* is soluble in liquid *B* but *B* is not soluble in solid *A* as shown in the pertinent part of the phase diagram. A 5 cm diameter cylinder of *A* is rotated at 1000 revolutions per minute (rpm) in a large melt of 0.5 atom fraction *B* at 1000°C, and it is noted that after 15 minutes the bar diameter is 4.8 cm. For the same temperature, estimate the bar diameter after 15 minutes if another 5 cm diameter cylinder of *A* is rotated in a large melt of the same composition, but now it is rotated at 4000 rpm. By analogy with Eq. (14.78) assume that



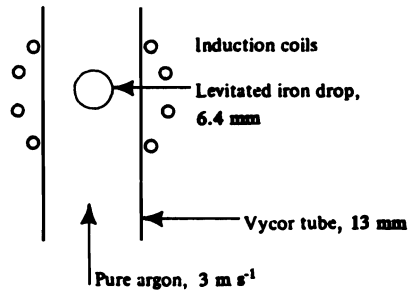
$$Sh_R = (\text{constant}) Sc^{0.343} Re_R^{1/2}$$

where *R* is the radius of the bar, and the velocity in the Reynolds number is the tangential velocity of the rotating bar.

14.8 Use dimensional analysis to show:

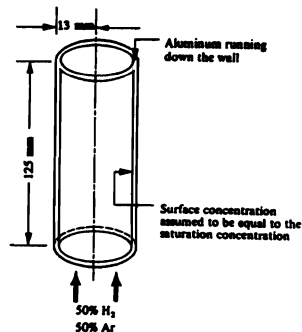
- a) $Sh = f(Re, Sc)$ for forced convection;
- b) $Sh = f(Gr, Sc)$ for natural convection.

14.9 Levitation melting is a means of supporting a metallic melt by an electromagnetic field. No impurities are added in melting and operation under an inert atmosphere removes dissolved gases. At 1920 K and 1 atm hydrogen pressure, the solubility of hydrogen in iron is 31 cm³ per 100 g of iron. Estimate the rate at which hydrogen can be removed from a levitated drop of iron that initially contains 10 ppm in the set-up shown to the right. Assume that vigorous convection occurs within the iron drop, the gas temperature is 1920 K, and Eq. (8.11), in mass transfer form, applies.



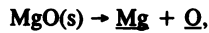
14.10 Hydrogen gas is being absorbed from a gas in an experimental set-up shown in the figure to the right. The absorbing liquid is aluminum at 1030 K, which is falling in laminar flow with an average velocity of 2.5 mm s⁻¹.

What is the hydrogen content of the aluminum leaving the tube if it enters with no hydrogen? At *T* = 1030 K and 1 atm hydrogen pressure, the solubility of hydrogen is 1 cm³ per 100 g of aluminum, the density of Al = 2.5 g cm⁻³, and *D_H* = 1 × 10⁻⁹ m² s⁻¹.



544 Mass Transfer in Fluid Systems

14.11 When ceramic oxides are used to contain molten metals, they can dissolve and add undesirable impurities to the melt. This is especially true when melting is done under vacuum. For example, magnesium oxide decomposes (slowly) according to

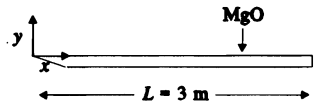


where the underlines indicate that the elements are dissolved in the melt. The equilibrium constant for the reaction is

$$K = C_{\text{Mg}} C_{\text{O}} = 10^{-6},$$

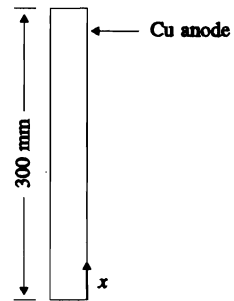
where C_{Mg} and C_{O} are the concentrations (moles per cm^3 of melt) of $\underline{\text{Mg}}$ and $\underline{\text{O}}$, respectively.

- a) For flow parallel to a plate of MgO, calculate the average mass transfer coefficient for Mg dissolving in the melt. Assume that $C_{\text{Mg}} = C_{\text{O}}$. For $x < 0$, $C_{\text{Mg}} = 0$ in the melt and $V_{\infty} = 3 \text{ m s}^{-1}$.
- b) What is the average flux of MgO dissolving in the melt? *Melt properties:* $\rho = 8000 \text{ kg m}^{-3}$; $k = 50 \text{ W m}^{-1} \text{ K}^{-1}$; $C_p = 840 \text{ J kg}^{-1} \text{ K}^{-1}$; $\eta = 1.24 \times 10^{-3} \text{ N s m}^{-2}$; and $D_{\text{O}} = D_{\text{Mg}} = 5 \times 10^{-9} \text{ m}^2 \text{ s}^{-1}$.

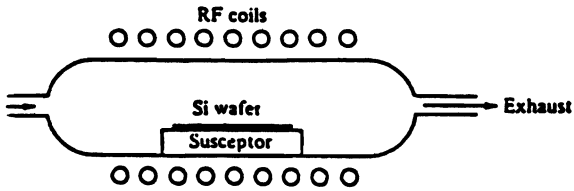


14.12 A common procedure for decreasing the hydrogen content of a melt is to allow bubbles of an inert gas (*viz.*, He) to rise through the melt. Assume that Eq. (8.11), in a form suitable for mass transfer, applies. a) Estimate the mass transfer coefficient from the melt to a single bubble for the removal of dissolved hydrogen. b) Will the overall kinetics of hydrogen removal from the melt depend on mass transfer in the liquid, in the bubble, or both? Justify your answer. c) Derive an equation that can be used to calculate the concentration of dissolved hydrogen as a function of time. *Data:* bubble diameter, 2 mm; melt density, 7000 kg m^{-3} ; melt viscosity, $2 \times 10^{-3} \text{ N s m}^{-2}$; diffusivity (hydrogen in melt), $5 \times 10^{-9} \text{ m}^2 \text{ s}^{-1}$; and diffusivity (hydrogen in gas bubble), $10^{-4} \text{ m}^2 \text{ s}^{-1}$.

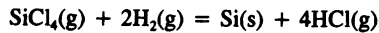
14.13 Consider an electrodeposition process that is controlled by mass transfer at the anode. Calculate the average mass transfer coefficient for the dissolution of the copper anode assuming that the process is controlled by the flux of cupric ions. Assume natural convection and an isothermal solution. *Data:* Mole fraction of Cu^{2+} ions at surface is 0.05; in the bulk it is 0.01. Properties of solution: $\rho = 1200 \text{ kg m}^{-3}$, $\eta = 2 \times 10^{-3} \text{ N s m}^{-2}$, $D = 5 \times 10^{-9} \text{ m}^2 \text{ s}^{-1}$, and $\xi = 4$.



14.14 A schematic diagram of a vapor-phase epitaxial growth system is shown.

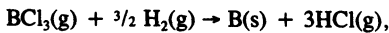


A gas mixture of SiCl_4 and H_2 enters the reactor; assume that the reaction at the surface is



a) Sketch the concentration of each gas species as a function of the vertical distance from the silicon surface. b) Assume two dimensional flow (rectangular coordinates) and constant ρ and D for all species in the gas phase. Give an appropriate equation of diffusion for $\text{HCl}(\text{g})$ in an isothermal system. Also give the momentum equation. c) Select an origin and write boundary conditions that are appropriate for the equation of diffusion, with the intent of predicting the growth rate of the epitaxial silicon.

14.15 Boron fibers for composites can be made by running a very fine tungsten wire (12.5 μm dia.) through a reactor tube that is continuously fed with a gas comprising 20% BCl_3 and 80% H_2 . The substrate wire is heated electrically and causes the gases to react and deposit boron. Assume that the reaction is

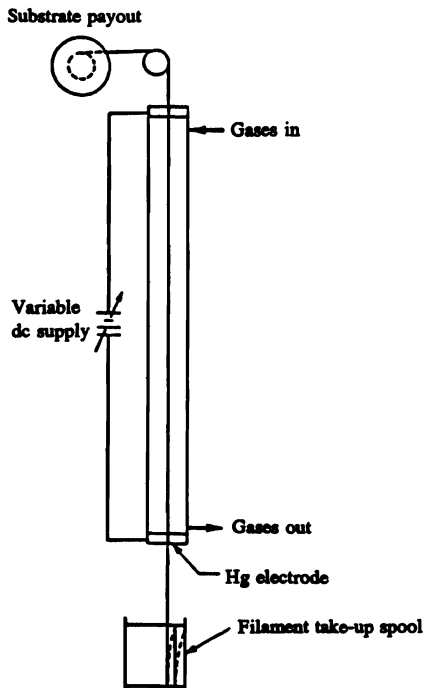


and is controlled solely by mass transfer. The standard free energies of formation are

$$\Delta G^\circ (\text{HCl}) = -22\,240 + 1.53 T, \text{ cal gmol}^{-1};$$

$$\Delta G^\circ (\text{BCl}_3) = -96\,560 - 12.35 T, \text{ cal gmol}^{-1}.$$

a) Pick a substrate temperature for depositing the boron. b) Estimate the mass transfer coefficients for the reactants and products. Which species will control the overall deposition rate? (For a discussion of the technology and applications of these fibers see M. E. Buck, *Advanced Materials and Progress In Metal Processes*, 9/87, pp. 61-65.)



INTERPHASE MASS TRANSFER

In Chapter 14 we undertook much of the analytical presentation to familiarize ourselves with mass transfer coefficients as they arise from considerations of diffusion with convection in a single phase only. There are many situations, however, in which two fluids or a solid and fluid are in contact, and interphase transfer by diffusion with convection takes place in one or both phases. In some cases, convective mass transfer may be important in controlling the overall rate; in others it is not important. If there is a reaction at the interface, it may very well be the controlling step.

Experimentally, it is difficult to study interphase transfer, and at the same time separate the individual phase resistances; so an *overall transfer coefficient* is usually measured. Having determined this coefficient, we then attempt, via a mathematical model, to *deduce* the individual phase coefficients, such as those presented in Chapter 14. In some cases the results are clear cut, and we are then able to adjust process conditions to optimize the process. In other cases, however, we cannot differentiate between models even though they may be based on important differences in basic assumptions, because their predictions can be numerically similar within experimental error. Then we deal with the overall coefficients and utilize them, but only if the fluid conditions are similar in both the prototype and model cases.

The objective of this chapter is to indicate the relationships between the individual phase transfer coefficients and the overall coefficients, and to examine several cases in detail, showing how different fluid conditions can influence the overall coefficient through their effects on the individual coefficients.

15.1 TWO-RESISTANCE MASS TRANSFER THEORY

Let us investigate the situation as it might exist in a gas-liquid physical reaction. Figure 15.1 depicts the phases in contact and the concentration profiles in each phase. The mole fraction of A in the bulk gas phase is $Y_{A\infty}$, and it decreases to Y_A^* at the interface. In the liquid, the mole fraction drops from X_A^* at the interface to $X_{A\infty}$ in the bulk liquid. The bulk

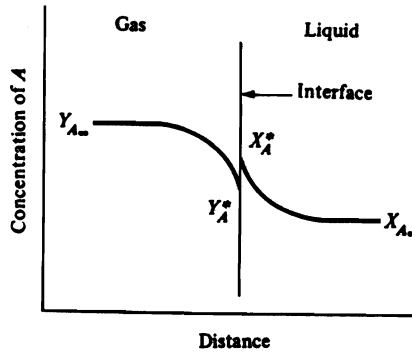


Fig. 15.1 The two-resistance mass transfer concept.

concentrations $X_{A\infty}$ and $Y_{A\infty}$ are obviously not in equilibrium, otherwise diffusion of the solute would not occur. To determine the rate of mass transfer between the phases, it is necessary to consider the sequential "steps" in the process.

For example, assume that the only resistances to the overall process are diffusional resistances within the fluids themselves, and that there is no resistance to the transfer of A across the interface. Consequently, the interface concentrations, X_A^* and Y_A^* , are equilibrium values. In some instances, of course, the atoms or molecules cannot be accommodated into the new phase as rapidly as they might jump from their original phase across the interface. If the accommodation process is slow relative to the diffusional processes, then X_A^* and Y_A^* would not represent equilibrium concentrations. In most situations, X_A^* and Y_A^* are the equilibrium values, and we proceed with the "two-resistance" theory.

For steady-state transfer, the rate at which A reaches the interface from the gas must equal the rate at which it diffuses into the bulk liquid. Thus, if $\kappa_{M,g}$ and $\kappa_{M,l}$ are the local coefficients, then the flux of A is

$$N_A = \kappa_{M,g}(Y_{A\infty} - Y_A^*) = \kappa_{M,l}(X_A^* - X_{A\infty}). \quad (15.1)$$

In this instance, since N_A is given in $\text{mol m}^{-2} \text{s}^{-1}$, and the concentrations are expressed as mole fractions, the mass transfer coefficients ($\kappa_{M,g}$ and $\kappa_{M,l}$) have the units of $\text{mol m}^{-2} \text{s}^{-1}$. The units of the mass transfer coefficients, as presented in Chapter 14 and found within the Sherwood number, are m s^{-1} . Of course, κ s are derivable from k s; specifically, we have $\kappa_A = k_A C$, recalling that C is the total molar concentration (mol m^{-3}) of the solution in question.

In experimental determinations of the rate of mass transfer, it is usually possible to determine solute concentrations in the bulk fluids by sampling. But, because the concentration boundary layers are usually extremely thin, it is physically impossible to approach the interface sufficiently closely to measure X_A^* and Y_A^* . Under these circumstances, only the overall effect in terms of either $X_{A\infty}$ or $Y_{A\infty}$ can be determined.

Consider the equilibrium of solute A as partitioned between the gas phase and a solvent, depicted in Fig. 15.2. The curve for the system is unique at fixed temperature and partial pressure of A in the gas phase. On the curve, we identify the four concentrations referred to in Eq. (15.1), specifically X_A^* , Y_A^* , $X_{A\infty}$, and $Y_{A\infty}$. In addition, we show X_{AY} and Y_{AX} which represent equilibrium concentrations corresponding to $Y_{A\infty}$ and $X_{A\infty}$, respectively. Y_{AX} , in

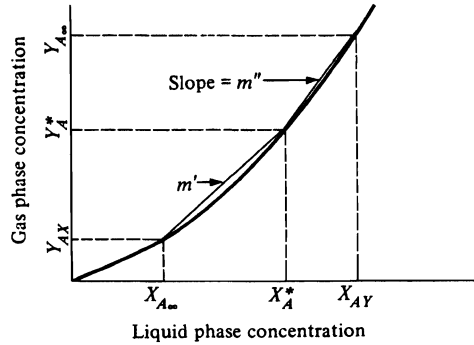


Fig. 15.2 The equilibrium curve for solute A partitioned between gas and liquid phases.

equilibrium with $X_{A\infty}$, is as good a measure of $X_{A\infty}$ as $X_{A\infty}$ itself, and moreover it is on the same basis as $Y_{A\infty}$. We may then measure the entire two-phase mass transfer effect in terms of an overall mass transfer coefficient, K_g :

$$N_A = K_g(Y_{A\infty} - Y_{AX}). \quad (15.2)$$

From the geometry of the figure, we can show that the relationship among the individual phase coefficients and the overall coefficient is

$$N_A/K_g = N_A/\kappa_{M,g} + m'N_A/\kappa_{M,l},$$

or

$$1/K_g = 1/\kappa_{M,g} + m'/\kappa_{M,l}. \quad (15.3)$$

In a similar manner, X_{AY} is a measure of $Y_{A\infty}$, and we may use it to define another overall coefficient K_l :

$$N_A = K_l(X_{AY} - X_{A\infty}). \quad (15.4)$$

It readily follows that

$$1/K_l = 1/m''\kappa_{M,g} + 1/\kappa_{M,l}. \quad (15.5)$$

Equations (15.3) and (15.5) lead to the following relationships among the mass-transfer resistances:

$$\frac{\text{gas phase resistance}}{\text{total resistance}} = \frac{1/\kappa_{M,g}}{1/K_g}, \quad (15.6)$$

and

$$\frac{\text{liquid phase resistance}}{\text{total resistance}} = \frac{1/\kappa_{M,l}}{1/K_l}. \quad (15.7)$$

550 Interphase Mass Transfer

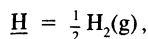
If the individual phase coefficients, $\kappa_{M,g}$ and $\kappa_{M,l}$, have roughly the same values, then we can demonstrate the importance of the shape of the equilibrium partition curve. If m' is small (equilibrium partition curve is fairly flat and solute A is very soluble in the liquid), then Eq. (15.3) shows that the major resistance is really $1/\kappa_{M,g}$, and the rate of mass transfer is gas-phase controlled.

Under such circumstances, even large increases in $\kappa_{M,l}$ do not significantly change K_g , and efforts to increase the mass transfer rate are best directed toward decreasing the gas-phase resistance. Conversely, when m'' is large (solute A is relatively insoluble in the liquid) and $\kappa_{M,g}$ and $\kappa_{M,l}$ are nearly equal, the major resistance is in the liquid. In these instances, efforts to bring about substantial increases in the rate of mass transfer are best directed toward increasing the liquid coefficient $\kappa_{M,l}$.

When overall coefficients are used in calculations, they are frequently synthesized through the correlations developed (such as those in Chapter 14) for the individual coefficients of the phases in contact. It is important to recognize the limitations in this procedure. For example, the hydrodynamic circumstances must be the same as those for which the correlations were developed. This is especially true in the case of two fluids, where motion in one may influence motion in the other. In other situations, absorption of surface-active substances at the interface may slow down reactions (chemical or physical) to such an extent that the estimated overall coefficient in no way reflects the magnitudes of the individual phase coefficients.

On the other hand, most experimental studies of reaction rates measure overall coefficients, from which attempts are often made to deduce individual phase resistances. Again, if experimentally measured *overall* coefficients are to be used in practice, the conditions with respect to fluid motion and reactant supply must also be similar, unless it is clear that the controlling resistance of the overall transfer lies in a nonfluid phase.

Example 15.1 In order to remove hydrogen from molten copper at 1150°C, the copper is brought in contact with pure argon at 1 atm pressure. Hydrogen diffuses to the argon, and undergoes the reaction



in which \underline{H} represents hydrogen dissolved in liquid copper. At 1150°C and 1 atm hydrogen pressure, the solubility of hydrogen in molten copper is 7.0 cm³ H₂(STP)/100 g of copper. Assuming that the mass transfer coefficients (κ s) within the individual phases are roughly equal in any process involving contact of argon and the copper, determine whether the rate of mass transfer would be gas-phase or liquid-phase controlled.

Solution. We proceed by examining the equilibrium of hydrogen between the gas phase (Ar-H₂) and the liquid (Cu- \underline{H}). We ignore the presence of Cu in the gas phase because its vapor pressure is very low at this temperature. To examine the relative values of the mass transfer rates, we need to express the concentrations in mole fractions. In the liquid phase, we convert the solubility to the mole fraction of \underline{H} in the liquid as follows

$$X_H = \frac{7.0 \text{ cm}^3 \text{ H}_2(\text{STP})}{0.1 \text{ kg Cu}} \left| \frac{1 \text{ mol H}_2}{22\,400 \text{ cm}^3 \text{ H}_2(\text{STP})} \right| \left| \frac{1 \text{ kmol H}_2}{1000 \text{ mol H}_2} \right| \left| \frac{1 \text{ kmol } \underline{H}}{0.5 \text{ kmol H}_2} \right| \left| \frac{63.5 \text{ kg Cu}}{1 \text{ kmol Cu}} \right|$$

$$= 3.97 \times 10^{-4}.$$

We can express the equilibrium constant for the reaction as

$$K_{\text{eq}} = \frac{X_H}{\sqrt{Y_{H_2}}},$$

where Y_{H_2} is the mole fraction of hydrogen in the gas; it follows that $K_{cq} = 3.97 \times 10^{-4}$ at 1150°C . Therefore, we can express the equilibrium partition of hydrogen between the phases as

$$X_H = 3.96 \times 10^{-4} \sqrt{Y_{H_2}}.$$

By referring to Fig. 15.2, we can estimate m' and m'' with $Y_{H\infty} = 0$ and $X_{H\infty} = 3.97 \times 10^{-4}$. In addition, because we are assuming $\kappa_{M,R} = \kappa_{M,l}$, Eq. (15.1) indicates that

$$Y_{H\infty} - Y_H^* \cong X_H^* - X_{H\infty}.$$

Therefore

$$Y_H^* \cong X_{H\infty} - X_H^* \cong 10^{-4},$$

$$m' = \frac{Y_{H_2}^* - Y_{HX}}{X_H^* - X_{H\infty}} \cong \frac{10^{-4} - 1}{0 - 4 \times 10^{-4}} \cong 2.5 \times 10^3,$$

$$m'' = \frac{Y_{H\infty} - Y_H^*}{X_{HY} - X_H^*} = \frac{0 - Y_H^*}{0 - X_H^*} = \frac{\sqrt{Y_H^*}}{K_{cq}} = \frac{10^{-2}}{4 \times 10^{-4}} \cong 25.$$

If we now examine Eq. (15.3) or Eq. (15.5), with these values of m' and m'' , it is easy to see that major resistance to mass transfer is in the liquid phase and the overall rate of mass transfer is liquid-phase controlled.

15.2 MIXED CONTROL IN GAS-SOLID REACTIONS

In Chapter 13 we examined several solutions for diffusion within solids; we found that some of these solutions were appropriate to situations involving gas-solid reactions at surfaces. Specifically, we examined those cases in which the solute surface concentration in the solid could be considered to be in equilibrium with the gas-phase environment. In many processes, this is indeed the case, because most reactions do proceed readily at the high temperatures. There are situations, however, in which exceptions to this generalization should be made, as the next two subsections demonstrate.

15.2.1 Carburization of iron with surface reaction and diffusion as controlling factors

If an iron plate is exposed to a $\text{CH}_4\text{-H}_2$ atmosphere, then carburization occurs at the surface according to



and consequently carbon diffuses into the plate. The objective is to describe the kinetics of the carburization.

It has been proposed¹ that the surface reaction proceeds at a rate given by

$$\frac{1}{A} \frac{dn_C}{dt} = r_1 \frac{P_{\text{CH}_4}}{P_{\text{H}_2}^v} - r_2 P_{\text{H}_2}^{2-v} C_s, \quad (15.9)$$

¹C. Wagner, *Notes from Course 3.63*, MIT, Cambridge, MA, 1955.

552 Interphase Mass Transfer

where dn_C/dt is the amount of carbon in mol taken up by the surface area A per unit time, r_1 and r_2 are reaction rate constants, P_{CH_4} and P_{H_2} are the partial pressures in the gas phase, presumed to be constants, C_s is the surface concentration of carbon in mol m^{-3} , and ν is a number between zero and two, depending on the details of the reaction mechanism.

At equilibrium, $dn_C/dt = 0$; therefore, from Eq. (15.9) we can obtain the equilibrium concentration of carbon

$$C_e = \frac{r_1 P_{CH_4}}{r_2 P_{H_2}^{\nu}} \quad (15.10)$$

Substitution of Eq. (15.10) into Eq. (15.9) gives

$$\frac{1}{A} \frac{dn_C}{dt} = r(C_e - C_s), \quad (15.11)$$

where

$$r \equiv r_2 P_{H_2}^{2-\nu}.$$

We can incorporate Eq. (15.11) into one of the boundary conditions for the diffusion of carbon in the plate. Consider the region $0 \leq x \leq L$ in which $x = 0$ is the center of the plate, and $x = L$ is the semithickness of the plate. The appropriate differential equation is

$$\frac{\partial C}{\partial t} = D \frac{\partial^2 C}{\partial x^2}, \quad (15.12)$$

where C is the carbon concentration and D is the diffusion coefficient of carbon in iron. We assume that only a single phase of iron exists. Therefore, the initial and boundary conditions are

$$C(x,0) = C_i \text{ (uniform)}, \quad (15.13a)$$

$$\frac{\partial C}{\partial x}(0,t) = 0, \quad (15.13b)$$

and

$$\frac{\partial C}{\partial x}(L,t) + \frac{r}{D}(C_s - C_e) = 0. \quad (15.13c)$$

Condition (15.13c) states that the amount of carbon furnished by the surface reaction must equal the amount diffusing into the interior. Note that Eq. (15.13c) is exactly the same condition existing at the surface of a solid losing heat to a surrounding environment at T_f , at a rate dependent on the heat transfer coefficient. In fact, Eq. (15.12) and its boundary conditions, Eqs. (15.13a), (15.13b), and (15.13c), are exactly the same as Eq. (9.22) and its boundary conditions, Eqs. (9.23)-(9.25). Hence, Eq. (9.43) and Fig. 9.9 are proper solutions to the problem at hand if we merely replace

$$\frac{T - T_f}{T_i - T_f} \quad \text{by} \quad \frac{C - C_e}{C_i - C_e},$$

$$\alpha t/L^2 \quad \text{by} \quad Dt/L^2,$$

and

$$hL/k \quad \text{by} \quad rL/D.$$

15.2.2 Transport in the gas phase and diffusion as controlling factors

In this section, we examine a situation in which the gas phase composition does not remain constant, because the reaction rate at the surface of the solid is so rapid that the gas cannot be replenished instantaneously by the incoming fresh gas. As an example, suppose we wish to carburize the surface of low-carbon sheet steel with a $\text{CH}_4\text{-H}_2$ atmosphere. The steel is in the form of an open coil so that the gas can flow between parallel layers as depicted in Fig. 15.3. We assume that the thickness of the sheet in the y -direction is sufficiently large so that diffusion into a semi-infinite solid holds. However, there is a depletion of methane with increasing x because it is consumed by reaction. Hence, the concentration of carbon in the steel varies with x as well as with t (time).

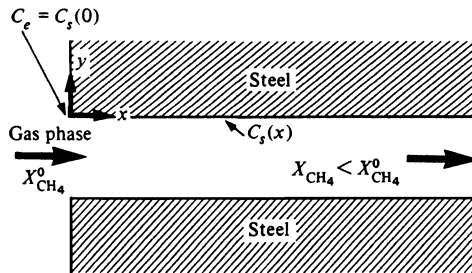


Fig. 15.3 Carburization of steel by gas flowing between parallel sheets.

To simplify the problem considerably, we may disregard the variation of the methane concentration normal to the flow direction; in the solid, the diffusion of carbon in the x -direction is ignored since the diffusive component in the y -direction is so much greater.

Therefore, Fick's second law for diffusion in the steel applies, and is written

$$\frac{\partial C}{\partial t} = D \frac{\partial^2 C}{\partial y^2}, \quad (15.14)$$

where C is the carbon concentration, and D is its diffusion coefficient in the steel. Initially, the steel contains C_i of carbon; hence

$$C(x, y, 0) = C_i. \quad (15.15)$$

Along the plane $y = 0$, we presume that equilibrium exists between the surface carbon and the atmosphere according to

$$K_{\text{eq}} = \frac{C_s P_{\text{H}_2}^2}{P_{\text{CH}_4}},$$

where K_{eq} is the thermodynamic equilibrium constant for the reaction (15.8). Thus, we can represent the relationship between the local methane mole fraction, X_{CH_4} , and the local surface concentration as

$$C(x, 0, t) = X_{\text{CH}_4}(x, t) \frac{K_{\text{eq}}}{P} = C_s, \quad (15.16)$$

554 Interphase Mass Transfer

where X_{CH_4} is the mole fraction of methane, P is the total pressure, and $X_{\text{CH}_4} \ll 1$. At the entrance, we have the original mole fraction, $X_{\text{CH}_4}^0$; thus

$$C(0,0,t) = X_{\text{CH}_4}^0 \frac{K_{\text{eq}}}{P} = C_e, \quad (15.17)$$

where C_e equals the equilibrium concentration for the original gas composition.

As the gas flows between the parallel plates from x to $x + dx$, the loss of methane per unit time equals

$$-n \left[\frac{\partial X_{\text{CH}_4}}{\partial x} \right] dx,$$

where $\partial X_{\text{CH}_4}/\partial x$ is negative, and n is the flow rate of the gas in mol s^{-1} . The amount of carbon diffusing from the surface, $b dx$, per unit time into the two surfaces equals

$$-2b dx D \left[\frac{\partial C}{\partial y} \right]_{y=0},$$

where b is the sheet width normal to the plane of Fig. 15.3, and C is given in mol m^{-3} . Equating this value to the loss of methane per unit time, and substituting Eq. (15.16), we get

$$\left[\frac{\partial C}{\partial y} \right]_{y=0} = \frac{nP}{2bDK_{\text{eq}}} \left[\frac{\partial C}{\partial x} \right]_{y=0} \quad (15.18)$$

for $x > 0$. To summarize, we wish to solve Eq. (15.14), subject to Eqs. (15.15), (15.17), and (15.18). A method of accomplishing this was presented by Wagner,² and is as follows.

Assuming that C depends only on x/\sqrt{t} and y/\sqrt{t} , we define the dimensionless variables:

$$\xi = \frac{2bDK_{\text{eq}}}{nP} \frac{x}{2\sqrt{Dt}}; \quad \eta = \frac{y}{2\sqrt{Dt}}.$$

Substitution of ξ and η into Eq. (15.14) gives

$$\frac{\partial^2 C}{\partial \eta^2} + 2 \left[\xi \frac{\partial C}{\partial \xi} + \eta \frac{\partial C}{\partial \eta} \right] = 0. \quad (15.19)$$

Substitution of ξ and η into Eqs. (15.17), (15.15), and (15.18), respectively, yields

$$C = C_e \quad \text{for } \xi = 0, \eta = 0; \quad (15.20a)$$

$$C = C_i \quad \text{for } \xi = \infty, \eta = \infty; \quad (15.20b)$$

$$\left[\frac{\partial C}{\partial \xi} \right]_{\eta=0} = \left[\frac{\partial C}{\partial \eta} \right]_{\eta=0}. \quad (15.20c)$$

We can transform Eq. (15.19) into an ordinary differential equation if we consider C a function of the sum $\sigma = \xi + \eta$:

$$\frac{d^2 C}{d\sigma^2} + 2\sigma \frac{dC}{d\sigma} = 0. \quad (15.21)$$

²C. Wagner, *ibid.*, and *Zeitsch. f. physik. Chem.* **192**, 157 (1943).

The solution to Eq. (15.21), subject to Eqs. (15.20a, b, and c), is

$$\frac{C - C_i}{C_e - C_i} = \operatorname{erfc} \left[\frac{\frac{2bDK_{\text{eq}}}{\dot{n}P} x + y}{2\sqrt{Dt}} \right]. \quad (15.22)$$

Example 15.2 Calculate the distance x over which the surface concentration C_s does not vary excessively after carburizing. Specifically, it is required that the ratio $(C_s - C_i)/(C_e - C_i) \geq 0.75$. Surface carburization is carried out with dilute methane/argon-hydrogen at 1000°C and 1 atm, and the appropriate equilibrium constant is $0.7 \text{ atm mol cm}^{-3}$. The gas flows at a linear velocity of 0.1 m s^{-1} through a separation of 2 cm between steel sheets for 5 h. At 1000°C , the diffusion coefficient of carbon in γ -iron is $3 \times 10^{-11} \text{ m}^2 \text{ s}^{-1}$.

Solution. Seeking the surface concentration C_s , we obtain from Eq. (15.22) with $y = 0$:

$$\frac{C_s - C_i}{C_e - C_i} = 1 - \operatorname{erf} \left[\frac{\frac{2bDK_{\text{eq}}}{\dot{n}P} x}{2\sqrt{Dt}} \right].$$

We require the left-hand side of the equation to be 0.75. Hence

$$0.25 = \operatorname{erf} \left[\frac{\frac{2bDK_{\text{eq}}}{\dot{n}P} x}{2\sqrt{Dt}} \right].$$

We find the argument of the error function to be 0.225 (Table 9.3), so that

$$x = 0.450 \sqrt{t/D} \frac{\dot{n}}{2b} \frac{P}{K_{\text{eq}}}.$$

Next we evaluate $\dot{n}/2b$ and K_{eq} .

$$\dot{n} = \frac{0.1 \text{ m}}{\text{s}} \left| \frac{0.02b \text{ m}^2}{\text{s}} \right| \left| \frac{1 \text{ kmol}}{22.4 \text{ m}^3(\text{STP})} \right| \left| \frac{273 \text{ K}}{1273 \text{ K}} \right| = 1.915b \times 10^{-5} \text{ kmol s}^{-1};$$

therefore

$$\frac{\dot{n}}{2b} = \frac{1.915b \times 10^{-5} \text{ kmol}}{\text{s}} \left| \frac{\text{m}}{2b \text{ m}} \right| = 9.574 \times 10^{-6} \text{ kmol s}^{-1} \text{ m}^{-1}.$$

Also,

$$K_{\text{eq}} = \frac{0.7 \text{ atm mol}}{\text{cm}^3} \left| \frac{10^6 \text{ cm}^3}{1 \text{ m}^3} \right| \left| \frac{1 \text{ kmol}}{10^3 \text{ mol}} \right| = 700 \text{ atm kmol m}^{-3}.$$

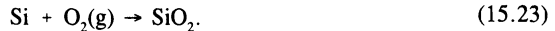
Then, by substituting $t = 18\,000 \text{ s}$, $D = 3 \times 10^{-11} \text{ m}^2 \text{ s}^{-1}$, and $P = 1 \text{ atm}$, we calculate x to be 0.15 m .

Of practical significance, this section shows that excessive nonuniformity of the surface concentration can only be prevented by a sufficient concentration of the reactant species in the exit gas phase. For example, we saw in the above problem that there was a limit to the distance that could be properly carburized for the specifications put forth. If the specifications had been more severe, for example, $[C_s - C_i / C_e - C_i] \geq 0.90$, then a higher velocity of carburizing gas would have had to be supplied to achieve the same value of x , thus raising the concentration of the reactant species in the exit gas. If the active species is valuable, recovery of this component or recirculation of the exit gas must be used. This is an important economic consideration in chromizing steel with $\text{CrCl}_2(\text{g})$.

15.2.2 Oxidation of silicon

Silicon dioxide (SiO_2) is used to protect the surface of silicon against unwanted reactions and diffusion. Specifically, the diffusivities of boron and phosphorus in SiO_2 are much smaller than they are in silicon. So if a region of a silicon substrate is covered with SiO_2 , the SiO_2 effectively serves as a mask when the substrate is placed in a furnace for diffusion processing. The SiO_2 mask is also used for selective diffusion in conjunction with photolithography.

Consider first the oxidation of silicon by dry oxygen. The reaction is



The overall mass transfer of oxygen is shown in Fig. 15.4, where there is mass transfer in the gas, diffusion through the SiO_2 , and finally the reaction at the SiO_2 -Si interface. We assume that the concentration of the diffusing species in the oxide is linear.

The oxidation rate is low enough that the flux through the gas, the flux through the oxide, and the reaction flux are all equal.

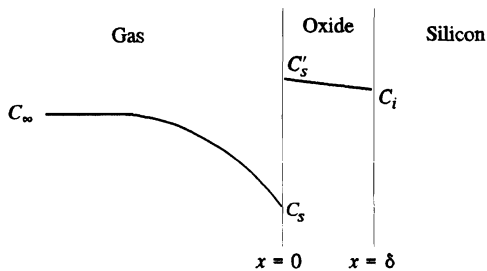


Fig. 15.4 Model for oxidation of silicon.

Hence, $j_G = j_O = r$ with

$$j_G = k_M(C_\infty - C_s), \quad (15.24)$$

$$j_O = \frac{D}{\delta}(C_s' - C_i), \quad (15.25)$$

and

$$r = k_r C_i. \quad (15.26)$$

The subscripts G and O are for gas and oxide, respectively. At $x = \delta$, the reaction flux, r , is first order with the reaction rate constant k_r , and k_M is the mass transfer coefficient in the gas.

The concentrations in the gas are

$$C_\infty = \frac{P_{O_2}^\infty}{\kappa_B T},$$

and

$$C_s = \frac{P_{O_2}^s}{\kappa_B T},$$

where κ_B , the Boltzmann's constant, is used rather than the customary gas constant because the concentrations of O_2 in the gas have units of molecules m^{-3} . At the gas-oxide interface, C_s and C'_s are at equilibrium; hence

$$C'_s = KP_{O_2}^s,$$

where K is the equilibrium constant. It is also convenient to express C_i in terms of its equivalent partial pressure of oxygen; hence

$$C_i = KP'_{O_2}.$$

Now we can express the fluxes given by Eqs. (15.24)-(15.26) in terms of pressure gradients, as follows:

$$j_G = \frac{k_M}{\kappa_B T} (P_{O_2}^\infty - P_{O_2}^s), \quad (15.27)$$

$$j_O = \frac{DK}{\delta} (P_{O_2}^s - P'_{O_2}), \quad (15.28)$$

and

$$r = k_r K (P'_{O_2} - 0). \quad (15.29)$$

It is convenient to use an analog with three resistances in series and an overall potential of $P_{O_2}^\infty - 0$. We get

$$j = \frac{P_{O_2}^\infty}{\frac{\kappa_B T}{k_M} + \frac{1}{k_r K} + \frac{\delta}{DK}}. \quad (15.30a)$$

If we prefer to use concentrations, rather than pressures, the equivalent result is

$$j = \frac{k_r K' C_\infty}{\frac{k_r K'}{k_M} + 1 + \frac{k_r \delta}{D}}, \quad (15.30b)$$

where $K' = K\kappa_B T$. Keep in mind that this flux has units of O_2 molecules $m^{-2} s^{-1}$.

558 Interphase Mass Transfer

The film thickens by reaction (15.23), so the mass per unit area is $\rho d\delta/dt$, with ρ the density of the oxide. Therefore, the flux of adding oxygen molecules to the film is

$$j = \frac{\rho}{M} \frac{d\delta}{dt}, \quad (15.31)$$

where m is the mass per molecule (O_2). We equate Eqs. (15.30b) and (15.31); this results in

$$\frac{k_r K' C_\infty}{\frac{k_r K'}{k_M} + 1 + \frac{D}{k_r \delta}} = \frac{\rho}{M} \frac{d\delta}{dt}. \quad (15.32)$$

With $\delta = \delta_i$ at $t = 0$, the integrated result (in dimensionless form) is

$$\frac{\delta^2 - \delta_i^2}{2Dt} + \left[\frac{1}{k_r} + \frac{K'}{k_M} \right] \frac{(\delta - \delta_i)}{t} - \frac{mK'C_\infty}{\rho} = 0. \quad (15.33)$$

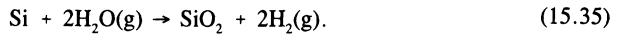
If *dry oxidation* is done, then the gas is pure O_2 and $C_s = C_\infty$ (see Fig. 15.4). Effectively, this is the same as making $k_M \rightarrow \infty$, and Eq. (15.33) reduces to

$$\delta = \frac{A}{2} \left[\left\{ 1 + \frac{4B(t + \tau)}{A^2} \right\}^{1/2} - 1 \right], \quad (15.34)$$

where

$$A \equiv \frac{2D}{k_r}, \quad B \equiv \frac{2DC'_s m}{\rho}, \quad \tau = \frac{\delta_i^2 + A\delta_i}{B}.$$

Oxidation in *steam* is by the reaction:



Consequently, H_2O diffuses from the gas and through the film to the reaction site at the oxide-silicon interface, and H_2 leaves the reaction site by diffusing through the film in the opposite direction. At 1273 K, the diffusivity of hydrogen through SiO_2 is more than 1000 times that of steam, so the oxidation rate is controlled by the diffusion of steam.

The oxidation rate is much faster in steam than it is in dry oxygen, largely because C'_s in steam is much greater than it is in dry oxygen. At 1273 K, $C'_s(\text{steam}) = 3 \times 10^{19}$ molecules cm^{-3} whereas $C'_s(\text{oxygen}) = 5 \times 10^{16}$ molecules cm^{-3} .

Equation (15.34) also applies for oxidation in either dry oxygen or steam. The oxidation constants depend on temperature according to the following equations:

dry oxygen

$$A = 1.18 \times 10^{-10} \exp \left[\frac{8840}{T} \right], \text{ m}$$

$$B = 1.81 \times 10^{-13} \exp \left[-\frac{14\,050}{T} \right], \text{ m}^2 \text{ s}^{-1}$$

steam

$$A = 3.32 \times 10^{-12} \exp \left(\frac{14\,170}{T} \right), \text{ m}$$

$$B = 4.95 \times 10^{-14} \exp \left(-\frac{7926}{T} \right), \text{ m}^2 \text{ s}^{-1}.$$

The equations for the oxidation constants were derived from a figure given by Yang,³ who also gives more discussion on the oxidation of silicon and oxide and nitride masks.

Example 15.3 Assume $\delta_i = 20$ nm. a) Calculate the time required to grow a 150 nm-thick oxide on silicon in dry oxygen at 1300 K. b) Suppose you want to achieve the same thickness of oxide in less time. Using dry oxygen again, determine the required time at 1400 K. c) For the same thickness and time as part b), determine the temperature if the oxidation is carried out in steam.

Solution. a) $A = 1.18 \times 10^{-10} \exp \left(\frac{8840}{1300} \right) = 1.06 \times 10^{-7} \text{ m};$

$$B = 1.81 \times 10^{-13} \exp \left(-\frac{14\,050}{1300} \right) = 3.66 \times 10^{-18} \text{ m}^2 \text{ s}^{-1};$$

$$\tau = \frac{\delta_i^2 + A\delta_i}{B} = \frac{(20 \times 10^{-9})^2 + (1.06 \times 10^{-7})(20 \times 10^{-9})}{3.66 \times 10^{-18}} = 688 \text{ s}.$$

Next, we calculate t from Eq. (15.34):

$$\begin{aligned} t + \tau &= \frac{A^2}{4B} \left\{ \left[1 + \frac{2\delta}{A} \right]^2 - 1 \right\} \\ &= \frac{(1.06 \times 10^{-7})^2}{(4)(3.66 \times 10^{-18})} \left\{ \left[1 + \frac{(2)(150 \times 10^{-9})}{(1.06 \times 10^{-7})} \right]^2 - 1 \right\} \\ &= 10\,491 \text{ s} \end{aligned}$$

and

$$t = 10\,491 - 688 = 9803 \text{ s}.$$

b) For less time, a higher temperature is required. With $T = 1400$ K, we follow the same procedure of part a) and calculate: $A = 6.52 \times 10^{-8} \text{ m}$; $B = 7.93 \times 10^{-18} \text{ m}^2 \text{ s}^{-1}$; $\tau = 215 \text{ s}$; and $t = 3856 \text{ s}$. We see that raising the temperature by 100 K decreases the time by 63%.

³E. S. Yang, *Fundamentals of Semiconductor Devices*, McGraw-Hill, New York, NY, 1978, pages 66-73.

560 Interphase Mass Transfer

c) For the same time as part b), $t = 3856$ s, we expect a lower temperature in steam. For the first trial, we try 1200 K. Then

$$A = 3.32 \times 10^{-12} \exp \left(\frac{14\,170}{1200} \right) = 4.46 \times 10^{-7} \text{ m},$$

$$B = 4.95 \times 10^{-14} \exp \left(-\frac{7926}{1200} \right) = 6.70 \times 10^{-17} \text{ m}^2 \text{ s}^{-1},$$

and

$$\tau = \frac{(20 \times 10^{-9})^2 + (4.46 \times 10^{-7})(20 \times 10^{-9})}{6.70 \times 10^{-17}} = 139 \text{ s}.$$

From these values, we get $t = 1195$ s. This time is much less than the 3856 s found in part b), so we can select a lower temperature. After a few more trials, we get $T = 1118$ K.

Wen⁴ discussed in detail the mathematical solutions to the kinetic equations for many different models of gas-solid reactions; he showed how similar some of the results are in terms of experimental weight loss versus time data for models differing widely in terms of assumptions made. His theme is that misleading conclusions concerning rate-controlling mechanisms can easily be made, unless much care is taken to ensure that experimental conditions eliminate control by steps being ignored in the analysis. However, it should be kept in mind that overall coefficients can be useful information from the design engineering standpoint.

15.3 MASS TRANSFER WITH VAPORIZATION

As pointed out in Chapter 5, there are many processes that involve heating materials in a vacuum. In vacuum melting or heat treating of ferrous alloys, valuable elements, such as manganese or chromium, may be lost, or undesirable impurities, such as zinc or lead, may be removed. In Knudsen effusion cells, use is made of the measured rate of vaporization of an element to determine thermodynamic properties of the material.

In all of these cases, there are several steps involved in the overall mass transfer process: 1. transport of the volatile species to the surface of the condensed phase; 2. formation of volatile compounds at the surface; 3. evaporation from the surface into the gas or vacuum; and 4. transport away from the surface into the gas or vacuum. Depending on conditions, any one of these steps may be rate limiting, or several may make a mixed-control process.

15.3.1 Knudsen effusion cells

The Knudsen cell is used to study thermodynamic properties of alloys by taking advantage of the high volatility of one component relative to the others, and determining the vapor pressure of this species as a function of alloy content. The vapor pressure is determined by measuring the force exerted by a molecular stream emanating into a vacuum from a very

⁴C. Y. Wen, *I. & E. C.* **60**, No. 9, 34 (1968).

small hole in the end of a hollow cell containing the alloy. Under these conditions, free molecular diffusion occurs; then, by referring to Section 5.5.1, we have

$$Z_{\text{net}} = \left[\frac{\kappa_B T}{2\pi m} \right]^{1/2} (n_1 - n_2), \text{ molecules m}^{-2} \text{ s}^{-1},$$

or

$$J = \frac{A_e(P_1 - P_2)}{\sqrt{2\pi MRT}}, \text{ mol s}^{-1},$$

where P_1 and P_2 are in N m^{-2} , and R has units of $\text{N m mol}^{-1} \text{K}^{-1}$.

These expressions give the net rate at which atoms or molecules leave the cell through an infinitely thin orifice opening. Because of the difficulty of constructing an infinitely thin opening, that is with no walls, there is a correction to the theoretical flux accounting for the small probability of molecules rebounding and not passing through the opening. The Clausing factor, W_e , gives the probability of passing and is a function of the ratio of the orifice thickness to radius, l/r , as given in Table 15.1. When this factor is included, then

$$J = \frac{A_e W_e (P_1 - P_2)}{\sqrt{2\pi MRT}}. \tag{15.36}$$

Table 15.1 Clausing factors for effusion cells*

l/r	W_e
0	1.00
0.1	0.9524
0.2	0.9092
0.3	0.8699
0.4	0.8341

*From P. Clausing, *Annalen der Physik* **12**, 976 (1932).

At the same time as vapor leaves through the orifice, the solid within the cell loses alloy from its surface initially having an alloy concentration of C_A^0 . If the area of the orifice, A_e , is small relative to the exposed surface area of the alloy, A_s , then we may take the partial pressure within the cell, P_1 , as uniform. Furthermore, P_1 is the pressure of the volatile component in equilibrium with its concentration on the surface of the solid, C_A^s . Therefore, Fig. 15.5 gives the situation, and the diffusive flux within the solid to the surface equals the effusive flux

$$J = +DA_s \left[\frac{\partial C_A}{\partial x} \right]_{x=0} = \frac{A_e W_e (P_1 - P_2)}{\sqrt{2\pi MRT}}, \tag{15.37}$$

where C_A is in mol m^{-3} .

In order for free molecular diffusion to occur, P_2 must be very low ($< 10^{-6}$ atm). In fact, a gradient at the surface is obtained more quickly if the cell is placed in a vacuum, especially since P_1 is on the order of only 10^{-3} - 10^{-6} atm; P_1 is related to the surface mole fraction X_A by

$$P_1 = \gamma_A X_A P_A^0,$$

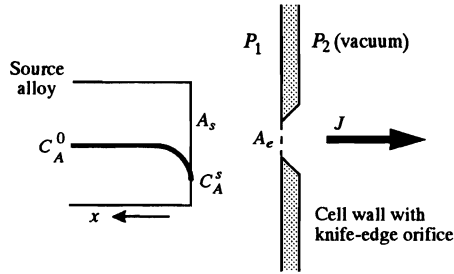


Fig. 15.5 The conditions in a Knudsen effusion cell.

where γ_A is the activity coefficient relative to the pure component, and P_A^0 is the vapor pressure of the pure component at the temperature in question. Thus, with $P_2 = 0$ in a vacuum,

$$DA_s \left[\frac{\partial C_A}{\partial x} \right]_{x=0} = \frac{A_e W_e \gamma_A P_A^0 C_A^s}{\rho \sqrt{2\pi MRT}}, \quad (15.38)$$

where $\rho = \text{mol alloy m}^{-3}$, the molar density of the alloy. Fick's second law describes diffusion within the solid; the boundary condition at the surface of the solid is Eq. (15.38).

If we consider the alloy as a semi-infinite solid, then we seek a solution to

$$\frac{\partial C_A}{\partial t} = D \frac{\partial^2 C_A}{\partial x^2}, \quad (15.39)$$

with

$$C_A(x, 0) = C_A^0, \quad (15.40a)$$

$$\frac{\partial C_A(0, t)}{\partial x} - Y C_A(0, t) = 0, \quad (15.40b)$$

and

$$C(\infty, t) = C_A^0, \quad (15.40c)$$

where

$$Y \equiv A_e W_e \gamma_A P_A^0 / A_s D \rho \sqrt{2\pi MRT}, \text{ m}^{-1}.$$

Carslaw and Jaeger⁵ give the solution to Eq. (15.39) satisfying Eqs. (15.40a, b, and c):

$$\frac{C_A}{C_A^0} = \text{erf} \frac{x}{2\sqrt{Dt}} + \exp(Yx + Y^2 Dt) \text{erfc} \left[\frac{x}{2\sqrt{Dt}} + Y\sqrt{Dt} \right]. \quad (15.41)$$

⁵H. S. Carslaw and J. C. Jaeger, *Conduction of Heat in Solids*, second edition, Oxford University Press, New York, NY, 1959, page 71.

The surface concentration of the solid C_A^s , obtained by letting $x = 0$ in Eq. (15.41), is

$$C_A^s/C_A^0 = \exp(Y^2Dt) \operatorname{erfc}(Y\sqrt{Dt}). \quad (15.42)$$

Figure 15.6 gives times allowable in order to limit the surface depletion to 5% in Fe-Mn alloys, based on Eq. (15.42).

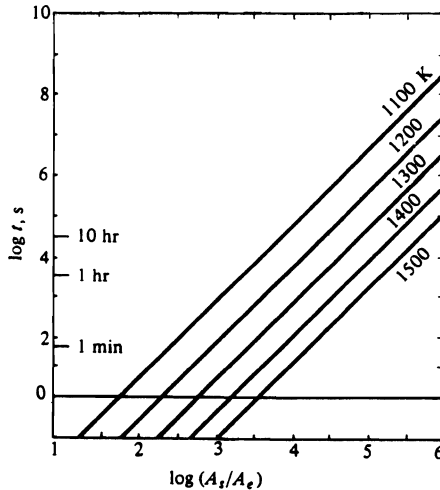


Fig. 15.6 Calculated times for 5% depletion of the surface of 5 wt% Mn-Fe alloys. (Adapted from D. L. Shroeder and J. F. Elliott, *Trans. AIME* **236**, 1091 (1967).)

15.3.2 Alloy vaporization during melting

In general, vaporization from liquid metals is not very different than that from solid metals. If the melting is carried out under a vacuum, there are again two steps: mass transfer to the free surface, and vaporization from the surface into the vacuum. If there is an inert gas pressure above the surface, there is an additional resistance to mass transfer, and as the gas density increases (or vacuum decreases), this may become significant relative to the resistance of the other transport steps.

Consider the first step. Mass transfer within the liquid to the surface could be calculated from a correlation of the form $Sh = f(Re, Sc)$ if this were available for the particular physical arrangement and stirring conditions involved. In the case of induction melting, there is no general correlation available, so we shall make use of an hypothesis by Machlin,⁶ which states that flow across the surface of an inductively stirred melt may be considered to be slug flow without any velocity gradients within the surface layer. The volatile solute is supplied to the surface solely by diffusion from within this surface layer. This hypothesis is exactly the same as Higbie's "penetration theory" discussed in Section 14.8. The only new assumption is that the "lifetime" θ of a surface element is equal to the average distance from the center of the melt to the edge of the crucible, divided by the average velocity of the melt at the surface. In the induction stirring case, θ is of the order of 1 s or less.

⁶E. S. Machlin, *Trans. AIME* **218**, 314 (1960).

564 Interphase Mass Transfer

For this step in the process then, the average mass-transfer coefficient is

$$k_{M,l} = 2\sqrt{D/\pi\theta} \quad , \text{ m s}^{-1}, \quad (14.90)$$

and the flux to the surface from the bulk liquid is

$$j_A = k_{M,l}(C_{A\infty} - C_A^s), \text{ mol m}^{-2} \text{ s}^{-1}, \quad (15.43)$$

where $C_{A\infty}$ is the bulk concentration and C_A^s is the surface concentration.

The second step is the evaporation itself. Returning to Section 15.3.1 and assuming that no chemical reactions are involved,* we have

$$j_A = \frac{\gamma_A P_A^0 C_A^s}{\rho\sqrt{2\pi MRT}}, \quad (15.44)$$

or

$$k_{M,e} = \frac{\gamma_A P_A^0}{\rho\sqrt{2\pi MRT}}, \quad (15.45)$$

where $k_{M,e}$ is the evaporation mass transfer coefficient.

The final step in the sequence involves mass transfer within the vapor phase, as influenced either by convection (when the gas pressure is $> 10^{-2}$ atm), or by molecular flow mechanics, as in a vacuum. In the former case, since $k_{M,g} \propto D$, and since Eqs. (12.49) and (12.50) indicate that D increases directly with reciprocal pressure, it is apparent that with a good vacuum, $k_{M,g}$ becomes very large.

Now consider the overall process in a good vacuum where the gas phase resistance is negligible. The fluxes due to liquid phase mass transfer (Eq. (15.43)), and evaporation (Eqs. (15.44) and (15.45)) are equal:

$$j_A = k_{M,l}(C_{A\infty} - C_A^s) = k_{M,e}C_A^s.$$

Solving for C_A^s , we get

$$C_A^s = \frac{k_{M,l}}{k_{M,l} + k_{M,e}} C_{A\infty}.$$

Substituting, we obtain

$$j_A = \left[\frac{k_{M,e}k_{M,l}}{k_{M,l} + k_{M,e}} \right] C_{A\infty} = KC_{A\infty}, \quad (15.46)$$

*We often see an additional multiplier on the right-hand side of Eq. (15.44). This is the *condensation coefficient* α , which is a measure of the proportion of atoms leaving a surface that do not return to it. If α is unity, then all of the atoms leaving that surface do not return to the surface, but are condensed instead on cool surfaces away from the melt. Typically, α is taken as unity for high temperature vaporization.

where K is the overall rate constant,* defined as

$$1/K = 1/k_{M,l} + 1/k_{M,e}.$$

By evaluating $k_{M,l}^{-1}$ and $k_{M,e}^{-1}$, we can either determine the greater resistance, or calculate changes by using $k_{M,l}$ and $k_{M,e}$ to calculate K . In the latter case,

$$-V \frac{dC_{A\infty}}{dt} = A_s K C_{A\infty},$$

where the left side is the rate of decrease of solute A and the right side is the mass flow of A from the surface, and where A_s and V are the surface area of the melt exposed to vacuum and the volume of the melt, respectively. Integrating, with $C_{A\infty} = C_A^0$ at $t = 0$, we have

$$\ln \frac{C_A^0}{C_{A\infty}} = \frac{A_s}{V} K t. \quad (15.47)$$

These effects are illustrated in the following example.

Example 15.4 We wish to test for the rate-controlling step in the loss of manganese from iron, induction melted under vacuum, given that $D_{Mn} = 9 \times 10^{-9} \text{ m}^2 \text{ s}^{-1}$, $T = 1600^\circ\text{C}$, $\gamma_{Mn} = 1.0$, $P_{Mn}^0 = 4.665 \times 10^3 \text{ N m}^{-2}$, and $M = 54.9 \text{ kg kmol}^{-1}$.

Solution. If the lifetime θ is taken as 1 s, then

$$k_{M,l} = 2\sqrt{D/\pi\theta} = 1.07 \times 10^{-4} \text{ m s}^{-1}.$$

Next

$$\begin{aligned} k_{M,e} &= \frac{\gamma_{Mn} P_{Mn}^0}{\rho \sqrt{2\pi MRT}} = \frac{(1)(4.665 \times 10^3)}{(128)\sqrt{(2\pi)(54.9)(8.314 \times 10^3)(1873)}} \\ &= 4.97 \times 10^{-4} \text{ m s}^{-1}. \end{aligned}$$

Thus,

$$\frac{1}{K} = (1.07 \times 10^{-4})^{-1} + (4.97 \times 10^{-4})^{-1} = 1.14 \times 10^4 \text{ m}^{-1} \text{ s},$$

or

$$K = 8.8 \times 10^{-5} \text{ m s}^{-1}.$$

It is apparent that when there is a good vacuum, liquid-phase mass transfer offers 82% of the total resistance; thus we may say that it essentially controls the rate.

This changes, however, if the stirring is increased to decrease θ . For example, if θ decreases to 0.1 s, then

$$k_{M,l} = 3.39 \times 10^{-4} \text{ m s}^{-1},$$

*The constant K is sometimes called the *specific evaporation constant*.

and

$$\frac{1}{k_{M,l}} = 2.95 \times 10^3 \text{ m}^{-1} \text{ s}.$$

Now the liquid-phase mass transfer and the evaporation process are almost equivalent in their contribution to K , and there is mixed control. Furthermore, K has increased to $1.97 \times 10^{-4} \text{ m s}^{-1}$.

Since neither $k_{M,l}$ nor $k_{M,e}$ depend on the external pressure, K is independent of vacuum pressure as long as $k_{M,g}$ remains very large. When $k_{M,g}$ becomes about an order of magnitude smaller than $k_{M,l}$ or $k_{M,e}$, it is rate controlling. Since $k_{M,g}$ is proportional to P^{-1} , then K decreases with P , as long as δ_{eff} in the gas phase remains constant. When the gas phase is dense, then $k_{M,g}$ is controlled by natural or forced convection. Figure 15.7 illustrates the effect of system pressure on K for vaporization of manganese from steel. Figure 15.8 gives the results of the application of Eq. (15.47) to calculate the rate of loss of manganese at 1580°C for various (A_s/V) and K values. One apparent result is that the use of an argon atmosphere to increase pressure decreases K to the point where the loss of manganese is negligible.

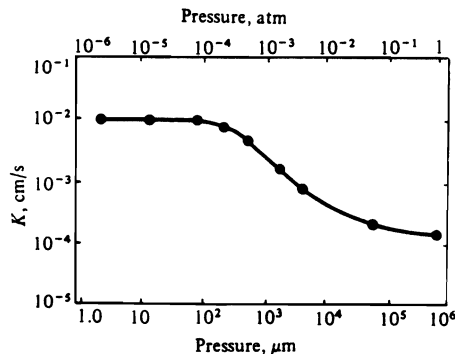


Fig. 15.7 Overall mass transfer coefficients for Mn vaporization from 0.25% C steel at 1580°C as a function of the pressure of Ar over the melt. (From R. G. Ward, *JISI* **201**, 11 (1963).)

Some other experimental values of K for the loss of various elements from iron-base melts into good vacuums are given in Table 15.2.

Laser welding, using high power beams focused on small areas, has introduced new problems of composition control in the weld zone. Volatile elements can be lost and the integrity of the weld can be compromised. Collur *et al.*⁷ analyzed the problem and demonstrated the role of Knudsen vaporization in controlling the rate of compositional changes.

⁷M. M. Collur, A. Paul and T. Debroy, *Metall. Trans. B* **18B**, 733-740 (1987).

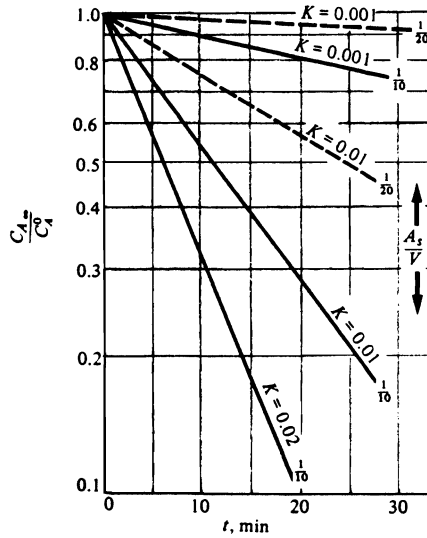


Fig. 15.8 Decrease in concentration of alloying element as a function of mass transfer coefficient and A_s/V ratio. Units of K are cm s^{-1} , and units of A_s/V are ft^{-1} .

Table 15.2 Overall evaporation constants for iron-base melts at 1600°C

Element	$K, \text{m s}^{-1}$
Mn	8.4×10^{-5}
Cu	4.8×10^{-5}
Sn	2.3×10^{-5}
Cr	2.1×10^{-6}
S	7.0×10^{-6}

*From R. Ohno and T. Ishida, *JISI, London* 206, 904 (1968).

PROBLEMS

15.1 Argon containing 2 volume percent of hydrogen is bubbled through a melt of aluminum at 970 K. The bubbling is continued to equilibrium with this gas at 1 atm. Initially the melt contains $5 \times 10^{-6} \text{ m}^3$ (STP) of hydrogen per kg of aluminum. It is known that the solubility of hydrogen is $10 \times 10^{-6} \text{ m}^3$ (STP) kg^{-1} . Determine whether the rate of mass transfer is gas-phase or liquid-phase controlled, a) at the beginning of degassing and b) near the end of degassing.

15.2 Iron wire (4 mm dia.) is boronized at 1200°C in a gas that establishes an equilibrium concentration of 15×10^{-3} wt.pct. boron. The transfer of boron is partly controlled by the reaction kinetics between the gas and the iron, as given by Eq. (15.11) with $r = 5 \times 10^{-8} \text{ m s}^{-1}$ at the surface. a) Make a plot of the concentration of boron (in wt.pct.) at the surface. b) When the concentration at the surface is 90% of the equilibrium value, what is the concentration in the center of the wire?

568 Interphase Mass Transfer

15.3 Refer to Example 15.2. a) Plot the distance x that satisfies the specification in Example 15.2 as a function of the gas velocity up to 1 m s^{-1} . b) Repeat if the separation between the sheets is reduced to 5 mm.

15.4 Assume that the initial thickness of an oxide layer on silicon is 10 nm. Determine the thickness of the oxide after oxidation in dry oxygen at 1350 K for 7000 s.

15.5 The standard free energy of formation of $\text{SiO}_2(\text{s})$ is

$$\Delta G^\circ = -215\,600 + 41.5 T, \text{ cal mol}^{-1},$$

for $700 \leq T \leq 1700 \text{ K}$. Suppose the pure oxygen in Problem 15.4 is replaced with 90% Ar-10% O_2 . Would this appreciably change the oxidation kinetics?

15.6 The vapor pressure of $\text{Zn}(\text{s})$ is

$$\log_{10} P(\text{mm Hg}) = -\frac{6850}{T} - 0.755 \log_{10} T + 11.24.$$

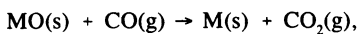
(Note: $760 \text{ mm Hg} = 1 \text{ standard atm} = 1.0133 \times 10^5 \text{ N m}^{-2}$.) Thermodynamic data at 1200 K give

$$\frac{\ln \gamma_{\text{Zn}}}{(1 - X_{\text{Zn}})} = 3.875 X_{\text{Zn}} - 3.425.$$

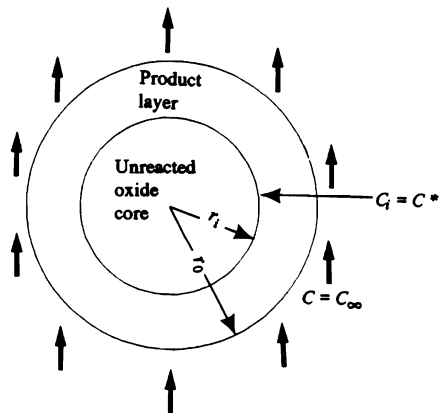
For other temperatures, assume that the regular solution model applies so that $T \ln \gamma_{\text{Zn}} = \text{constant}$. a) Calculate the initial flux of Zn from 70-40 brass by sublimation into a vacuum as a function of temperature. b) Calculate the surface concentration as a function of time with sublimation into the vacuum at 1200 K.

15.7 Ferritic stainless steel parts are vacuum heat-treated in order to maintain a shiny surface finish. If AISI 410 (12% Cr) parts are heat treated in a vacuum of $10 \mu\text{m}$ of Hg at 1140 K for 2 hours, what will the concentration of chromium on the surface of the parts be? At 1140 K, the vapor pressure of pure Cr is $1.33 \times 10^{-5} \text{ Pa}$, and D_{Cr} in iron is approximately $10^{-16} \text{ m}^2 \text{ s}^{-1}$.

15.8 A model for the reduction of a spherical oxide is illustrated to the right. Assume mixed control, with mass transfer in the gas and diffusion through the porous product layer controlling the overall kinetics. A reducing gas flows past the sphere with a concentration C_∞ , and at the product-oxide interface its concentration is C^* . Derive an equation that gives the rate at which the oxide is reduced in kmol s^{-1} . The overall reaction is

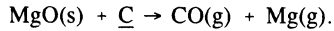


where MO is the metal oxide.



15.9 Using data in Table 15.2, plot the change in concentration with time (up to 3600 s) of a melt of iron containing 1% Mn, 1% Cr, and 0.05% S. The melt is contained in a nonreacting crucible, which has the dimensions 0.5 m dia. by 1 m height.

15.10 The melt of Problem 15.9 also contains carbon, which reacts with the magnesia crucible according to the overall reaction:



Assume that evaporation can only occur at the surface of the well-mixed melt. a) Hypothesize the reduction reaction at the melt-crucible interface. b) Hypothesize vaporization reactions at the melt surface. c) What are the mass transfer steps for oxygen? for magnesium? for carbon? For each mass transfer step, make a schematic concentration profile.

15.11 In vacuum laser welding, it is difficult to measure the temperature of the molten pool. One estimate of the temperature can be made from collecting a sample of vapor evaporated from the weld pool. The ratio of elements in the sample is the ratio of vaporization rates of the elements. If 201 stainless steel is welded and the ratio of Cr/Mn in the condensed vapor sample is 0.56, estimate the pool temperature, assuming that the pool is an ideal thermodynamic solution.

NUMERICAL METHODS AND MODELS

Our major goal in this introductory text is to present fundamentals. We hope that has been accomplished in Chapters 1-15. We also tried to orient our pedagogy to materials science and engineering, by including many examples and problems in order to instill the necessity of applying transport phenomena in designing and operating processes, intelligently and economically.

Very often, however, materials processing is so complex that transport phenomena can only be applied if materials engineers resort to numerical methods and models. In this chapter, an introduction is given to a numerical method and some models.

16.1 FINITE DIFFERENCE APPROXIMATIONS

Finite difference approximations are indispensable in solving problems involving multidimensional transport, nonhomogeneous or nonlinear boundary conditions, or variable properties. Although the majority of practical problems entail such complexities, it is still important to be familiar with at least the analytical solutions found in this text. In setting up the more complex problems using finite difference approximations, the analytical solutions often provide a convenient check on the computations. We start by considering two problems with simple geometry and constant transport properties.

16.1.1 Euler method

The first problem, often encountered in metal casting, is that of a thermally insulating material that forms the internal mold (called a core) that is surrounded on both sides by a solidifying metal. The situation is depicted in Fig. 16.1.

The semithickness of the core is L , and it is thin enough that after a relatively short time into the solidification period, the region $0 \leq x \leq 2L$ can become saturated with heat and lose its ability to further extract energy from the solidifying metal. This could lead to a "hot spot" in the solidifying metal near the core resulting in a porous casting. The problem to be solved, therefore, is the computation of the time-temperature history of the core to determine its adequacy to absorb heat.

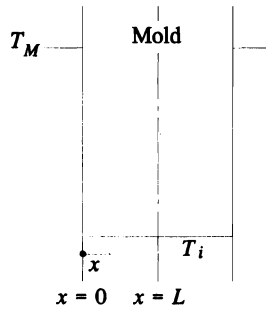


Fig. 16.1 Mold material surrounded by solidifying metal.

Formally presented, the situation is described by

$$\frac{\partial T}{\partial t} = \alpha \frac{\partial^2 T}{\partial x^2}; \tag{16.1}$$

the boundary conditions are

$$\frac{\partial T}{\partial x}(L, t) = 0 \quad t \geq 0, \tag{16.2}$$

and

$$T(0, t) = T_M \quad t \geq 0, \tag{16.3}$$

and the initial condition is

$$T(x, 0) = T_i. \tag{16.4}$$

To determine the temperature as a function of location and time, the domain $0 \leq x \leq L$ is subdivided into small segments of length Δx , as shown in Fig. 16.2. Nodes are numbered consecutively 0 to N from left to right.

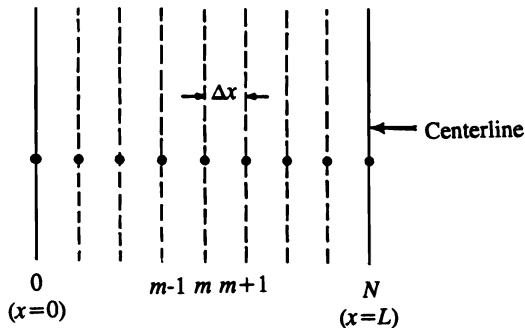


Fig. 16.2 The domain $0 \leq x \leq L$ subdivided into segments.*

*In Chapter 9, $x = 0$ was at the centerline. The two different coordinate systems can be reconciled with a simple coordinate transformation.

At any particular time, the gradient between nodes m and $m+1$ is

$$\left(\frac{\partial T}{\partial x}\right)_{m+1/2} \approx \frac{T_{m+1} - T_m}{\Delta x}.$$

Similarly,

$$\left(\frac{\partial T}{\partial x}\right)_{m-1/2} \approx \frac{T_m - T_{m-1}}{\Delta x}.$$

For the conduction equation, the second derivative is required; this is

$$\frac{\partial}{\partial x} \left(\frac{\partial T}{\partial x}\right)_m \approx \frac{1}{\Delta x} \left[\left(\frac{\partial T}{\partial x}\right)_{m+1/2} - \left(\frac{\partial T}{\partial x}\right)_{m-1/2} \right].$$

Therefore,

$$\left(\frac{\partial^2 T}{\partial x^2}\right)_m \approx \frac{1}{(\Delta x)^2} [T_{m-1} - 2T_m + T_{m+1}], \tag{16.5}$$

and Eq. (16.1) for an interior node becomes

$$\frac{\partial T_m}{\partial t} = \frac{\alpha}{(\Delta x)^2} [T_{m-1} - 2T_m + T_{m+1}]. \tag{16.6}$$

At the centerline ($m = N$), the finite difference equation is derived in a different manner. The flux to the centerline is

$$- \frac{k}{\Delta x} [T_N - T_{N-1}],$$

and the accumulation of energy is

$$\frac{\Delta x}{2} \rho C_p \frac{\partial T_N}{\partial t},$$

where $\Delta x/2$ is the volume associated with node N . Then at this *insulated surface*, the finite difference equation is written as

$$\frac{\partial T_N}{\partial t} = \frac{2\alpha}{(\Delta x)^2} [T_{N-1} - T_N]. \tag{16.7}$$

For convenience, *normalized variables* are introduced. The normalized temperature (u), time (θ) and position (x') are defined as follows:

$$u = \frac{T - T_i}{T_M - T_i}, \quad \theta = \text{Fo} = \frac{\alpha t}{L^2}, \quad \text{and} \quad x' = \frac{x}{L}.$$

With the normalized coordinates, Eqs. (16.1)-(16.4) are replaced by

$$\frac{\partial u}{\partial \theta} = \frac{\partial^2 u}{\partial x'^2}, \tag{16.8}$$

$$\frac{\partial u}{\partial x'}(1, \theta) = 0,$$

$$u(0, \theta) = 1, \quad (16.10)$$

and

$$u(x', 0) = 0. \quad (16.11)$$

For the interior nodes the finite difference equation, Eq. (16.6), becomes

$$\frac{\partial u_m}{\partial \theta} \approx \frac{1}{(\Delta x')^2} [u_{m-1} - 2u_m + u_{m+1}], \quad (16.12)$$

and at the insulated surface ($m = N$) Eq. (16.7) becomes

$$\frac{\partial u_N}{\partial \theta} \approx \frac{2}{(\Delta x')^2} [u_{N-1} - u_N]. \quad (16.13)$$

In an actual application the number of nodes should be large, but in order to illustrate the calculation process we take $N = 4$. Equation (16.10) requires $u_0 = 1$; then the difference equations for nodes 1, . . . N are as follows:

$$\frac{\partial u_1}{\partial \theta} \approx \frac{1}{(\Delta x')^2} [u_0 - 2u_1 + u_2] = \frac{1}{(\Delta x')^2} [1 - 2u_1 + u_2], \quad (16.14a)$$

$$\frac{\partial u_2}{\partial \theta} \approx \frac{1}{(\Delta x')^2} [u_1 - 2u_2 + u_3], \quad (16.14b)$$

$$\frac{\partial u_3}{\partial \theta} \approx \frac{1}{(\Delta x')^2} [u_2 - 2u_3 + u_4], \quad (16.14c)$$

$$\frac{\partial u_4}{\partial \theta} \approx \frac{1}{(\Delta x')^2} [2u_3 - 2u_4]. \quad (16.14d)$$

The initial temperatures are $u_1 = u_2 = u_3 = u_4 = 0$.

There are several methods for proceeding; here the so-called *Euler* method is used, in which

$$u_m^{v+1} = u_m^v + \frac{\partial u_m}{\partial \theta} \Delta \theta. \quad (16.15)$$

It is necessary to add superscripts to indicate time; e.g., u_m^v is the present temperature and u_m^{v+1} is the future temperature after one time step of duration $\Delta \theta$.

By combining Eqs. (16.14) through (16.15) for $m = 1, \dots, N$ with the appropriate superscripts, we get

$$u_1^{v+1} = P + (1 - 2P) u_1^v + P u_2^v \quad (16.16a)$$

$$u_2^{v+1} = P u_1^v + (1 - 2P) u_2^v + P u_3^v \quad (16.16b)$$

$$u_3^{v+1} = P u_2^v + (1 - 2P) u_3^v + P u_4^v \quad (16.16c)$$

$$u_4^{v+1} = 2P u_3^v + (1 - 2P) u_4^v \quad (16.16d)$$

where $P = \Delta\theta/(\Delta x')^2$. Initially each u_m^v is known (starting with $u_m^0 = 0$), so that Eqs. (16.16a,b,c,d) comprise four equations with the four unknowns, u_m^{v+1} . After the simultaneous equations are solved, the temperatures at $m = 1, \dots, 4$ are known for time step $v+1$ ($\theta = \Delta\theta$) and then the process is repeated for as many time steps ($\theta = v\Delta\theta$) as desired.

Table 16.1 gives calculated temperatures at the insulated surface for $N = 5$ ($\Delta x' = 0.2$) and $N = 10$ ($\Delta x' = 0.1$) with $P = 0.25$. Also shown are the temperatures based on the exact solution (Eq. (9.42)). With more nodes the results are closer to the exact solution. With even more nodes, the agreement between the approximated temperatures and the exact temperatures would be even closer. However, with smaller values of $\Delta x'$, we must be careful because the Euler method can result in unstable numerical oscillations in the solution if either $\Delta\theta$ is too large or $\Delta x'$ is too small. Specifically, the Euler method requires that $P = \Delta\theta/(\Delta x')^2 \leq 0.5$, in order to prevent unstable numerical oscillations. Thus, if we choose to reduce $\Delta x'$, $\Delta\theta$ has to be correspondingly reduced in order to meet the criterion of $P \leq 0.5$. Accordingly, more computer time would be required to execute the calculations.

Table 16.1 Normalized temperature, u , at the center (insulated surface) with $P = 0.25$ (Euler method)

θ	With $\Delta x' = 0.2$	With $\Delta x' = 0.1$	Exact Solution, Eq. (9.42)
0.2	0.225	0.229	0.235
0.4	0.525	0.527	0.531
0.6	0.710	0.711	0.714
0.8	0.822	0.824	0.826
1.0	0.892	0.893	0.894

The numerical results can also be used to estimate the amount of energy taken up by the core as a function of time. There are two methods for carrying out this estimate.

The first method is to track the gradient at the core surface in contact with the metal. This surface is at $x = 0$ in Fig. 16.2. For each time step the energy absorbed by the core can be approximated as the product of the flux and the duration of the time step. By summing these products for all of the time steps, the integrated or total energy absorbed by the core can be estimated. The accuracy of this method depends on the accuracy of the estimate of the gradient at $x = 0$.

The second method is based upon calculations of the average temperature in the core. For this particular problem, this method is more accurate than the first because the estimates of temperature are more exact than the estimates of the gradient at $x = 0$. We can show this by attacking the problem both ways.

In the first method the estimated gradient, in terms of normalized variables, is $(u_1^v - u_0^v)/\Delta x'$. In terms of the original dimensional variables, this is

$$\left[\frac{\Delta u}{\Delta x'} \right]_0^v = \frac{L}{T_M - T_i} \frac{T_1^v - T_0^v}{\Delta x}$$

Therefore, the flux at the metal/core interface is approximated as

$$q_0^v \approx -k \frac{T_1^v - T_0^v}{\Delta x} = -k \left[\frac{T_M - T_i}{L} \right] \left[\frac{\Delta u}{\Delta x'} \right]_0^v$$

and the energy absorbed by the area A of the core for one time step is $q_0^v A \Delta t$. Therefore,

$$\begin{aligned}\hat{Q}_m &= \left| A \sum_1^v q_0^v \Delta t \right| = Ak \left[\frac{T_M - T_i}{L} \right] \frac{L^2}{\alpha} \sum_1^v \left| \left[\frac{\Delta u}{\Delta x'} \right]_0^v \right| \Delta \theta \\ &= AL\rho C_p (T_M - T_i) \sum_1^v \left| \left[\frac{\Delta u}{\Delta x'} \right]_0^v \right| \Delta \theta.\end{aligned}\quad (16.17)$$

As before, the energy given up by the solidified portion of the casting (assumed to be pure metal) is

$$\hat{Q}_c = V \rho' H_f, \quad (16.18)$$

where V is the volume solidified next to the casting-core surface. With $\hat{Q}_c = \hat{Q}_m$, Eqs. (16.17) and (16.18) finally give

$$\frac{(V/A)}{L\gamma} = \sum_1^v \left| \left[\frac{\Delta u}{\Delta x'} \right]_0^v \right| \Delta \theta, \quad (16.19)$$

where γ , as defined in Chapter 10, is

$$\gamma = \left[\frac{T_M - T_i}{\rho' H_f} \right] \rho C_p.$$

In the second method, the average normalized temperature at a given time is calculated. The volume of material associated with the nodes $m = 0$ and $m = N$ is $0.5 \Delta x'$, so the average normalized temperature is

$$\bar{u}^v = \frac{1}{N} \left[\frac{1}{2} (u_0^v + u_N^v) + \sum_{m=1}^{N-1} u_m^v \right]. \quad (16.20)$$

The average dimensional temperature is

$$\bar{T}^v = \bar{u}^v (T_M - T_i) + T_i,$$

so that the energy absorbed by one-half of the core must be

$$\hat{Q}_m = AL\rho C_p (\bar{T}^v - T_i) = AL\rho C_p (T_M - T_i) \bar{u}^v. \quad (16.21)$$

With $\hat{Q}_m = \hat{Q}_c$, we combine Eqs. (16.18) and (16.21); the result is

$$\frac{(V/A)}{L\gamma} = \bar{u}^v. \quad (16.22)$$

Of course, Eq. (16.22) is another approximate counterpart to the exact solution of Eqs. (16.8)-(16.11).

Approximations of $V/AL\gamma$ based on Eqs. (16.19) and (16.22), with $P = 0.25$ and $N = 10$, are given in Table 16.2. Also shown are exact values of $V/AL\gamma$. The table shows that the estimates based on calculating the average temperature are more accurate than are those based on estimating the gradient at the core-casting interface.

Table 16.2 Amount of solidification as $V/AL\gamma$ versus θ with $P = 0.25$ and $N = 10$

θ	Finite Difference Approximations		
	Therm. Grad., Eq. (16.19)	Avg. Temp., Eq. (16.22)	Exact Solution
0.04	0.163	0.231	0.229
0.2	0.434	0.506	0.505
0.4	0.626	0.699	0.698
0.6	0.742	0.817	0.817
0.8	0.814	0.888	0.886
1.0	0.857	0.932	0.930

Another casting problem involves conduction through a thin shell mold, from solidifying metal with energy loss at the outside surface. The shell mold has a thickness L . In this case, the surface in contact with the metal is located at $x = 0$, and the outer surface of the mold is at $x = L$ (see Fig. 16.3).

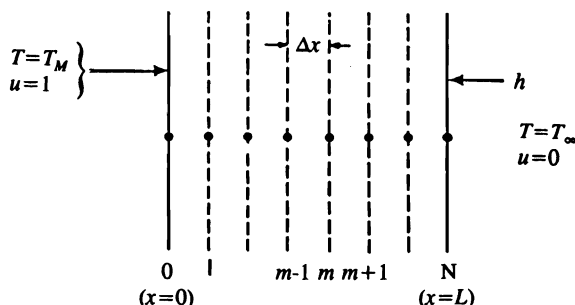


Fig. 16.3 Shell mold of thickness L subdivided into segments for estimating temperature during heat conduction.

Also, the normalized temperature is selected so that $u = 1$ and $u = 0$ correspond to $T = T_M$ and $T = T_\infty$, respectively; thus

$$u = \frac{T - T_\infty}{T_M - T_\infty}.$$

By selecting $\theta = \alpha t/L^2$ and $x' = x/L$, then the heat conduction equation is Eq. (16.8). The boundary conditions and initial condition are as follows:

$$u(0, \theta) = 1, \tag{16.23a}$$

$$\frac{\partial u}{\partial x'}(1, \theta) + \text{Bi } u(1, \theta) = 0, \tag{16.23b}$$

$$u(x', 0) = \frac{T_i - T_\infty}{T_M - T_\infty} = u_i, \tag{16.23c}$$

where T_i is the initial temperature of the shell mold. Since the mold is often preheated, the effect of the preheat temperature on the solidification time is of particular interest.

The temperatures at nodes 1 through $N-1$ are approximated by Eq. (16.12). By writing an energy balance for node N (with a volume of $\Delta x'/2$), we get

$$\frac{\partial u_N}{\partial \theta} = \frac{1}{(\Delta x')^2} [-2(1 + \text{Bi } \Delta x') u_N + 2u_{N-1}], \quad (16.24)$$

with $\text{Bi} = hL/k$.

In order to advance the solution in time, we again utilize the Euler method and combine Eq. (16.15) with Eqs. (16.12) and (16.24). For nodes 1 through $N-1$, we get

$$u_m^{v+1} = P u_{m-1}^v + (1 - 2P) u_m^v + P u_{m+1}^v, \quad (16.25)$$

and for node N

$$u_N^{v+1} = 2P u_{N-1}^v + [1 - 2P(1 + \text{Bi } \Delta x')] u_N^v. \quad (16.26)$$

As before $P = \Delta\theta/(\Delta x')^2$, and the superscripts v and $v+1$ represent the present and next time, respectively.

By selecting $P = 0.25$ and $\Delta x' = 0.1$, then $\Delta\theta = 0.0025$; with $u_0 = 1$ the set of equations becomes:

$$\begin{aligned} u_1^{v+1} &= 0.25 + 0.5 u_1^v + 0.25 u_2^v, & m = 1 \\ u_m^{v+1} &= 0.25 u_{m-1}^v + 0.5 u_m^v + 0.25 u_{m+1}^v, & m = 2, 3, \dots, 9 \\ u_{10}^{v+1} &= 0.5 u_9^v + (0.5 - 0.125 \text{Bi}) u_{10}^v, & m = N = 10. \end{aligned} \quad (16.27)$$

Some calculated temperature distributions are shown in Fig. 16.4 for two mold preheat temperatures and two Biot numbers. Notice that steady state is achieved in a relatively short period of $\theta = 1$, which corresponds to a real time of only a few or several minutes. Notice, too, that the temperature of the exterior surface of the mold can decrease and then increase to its steady state value in some circumstances (e.g., Fig. 16.4a).

The thermal gradients at $x' = 0$, derived from the temperature distributions, can be used to calculate the total energy extracted from the casting. Hence to estimate the thickness solidified from the mold wall, Eq. (16.19) applies. These estimates are shown in Fig. 16.5.

The previous examples were selected with the intention of introducing the numerical method; hence, the examples were kept simple. The thermal properties of the mold and the heat transfer coefficient at the exterior surface of the mold were constants. In practice, however, these properties depend on temperature.

It should be noted that variable properties can be included in the finite difference approximation (FDA) method by updating the properties with the current temperatures as the calculation proceeds from one time step to the next. The FDA method can also be extended to two-dimensional and three-dimensional heat conduction problems so that complex casting geometries can be analyzed.

Alloys solidify over a temperature range; in such cases, nodes are assigned in the solidifying casting as well as in the mold. Sophisticated computer codes can be used to show the positions of isotherms in both the mold and casting, to assist the casting engineer in locating "hot spots," designing and locating risers, estimating solidification times, and in predicting microstructural features and physical properties that depend upon the temperature history during solidification.

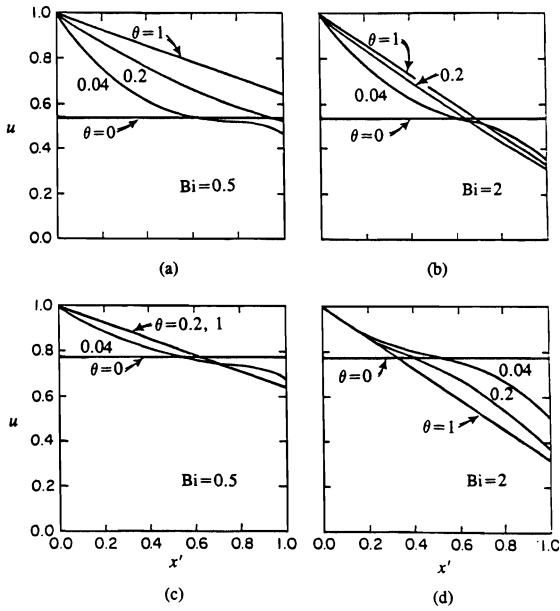


Fig. 16.4 Calculated temperature profiles in a shell mold of finite thickness with heat loss from the surface. (a) Preheat temperature $u_m^0 = 0.536$ and $Bi = 0.5$; (b) $u_m^0 = 0.536$ and $Bi = 2$; (c) $u_m^0 = 0.778$ and $Bi = 0.5$; (d) $u_m^0 = 0.778$ and $Bi = 2$.

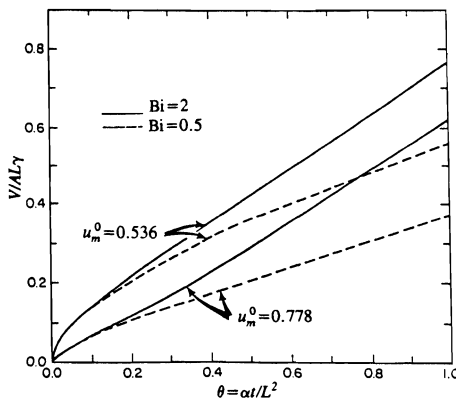


Fig. 16.5 Estimate of thickness solidified (V/A) versus time in shell mold of finite thickness with heat loss from the exterior surface.

16.1.2 The Crank-Nicolson method

In the Euler method, the time derivative at the beginning of the time step is used to estimate the temperature at the next time. The Euler method is said to be *explicit* for this reason. A method with better accuracy is the Crank-Nicolson method, which is *implicit*.

In the Crank-Nicolson method an average of the time derivative is used. That is, instead of using Eq. (16.15), we use

$$u_m^{v+1} = u_m^v + \frac{1}{2} \left[\left. \frac{\partial u}{\partial \theta} \right|_m^v + \left. \frac{\partial u}{\partial \theta} \right|_m^{v+1} \right] \Delta \theta. \quad (16.28)$$

But, Eq. (16.12) tells us that

$$\left. \frac{\partial u}{\partial \theta} \right|_m^v = \frac{1}{(\Delta x')^2} [u_{m-1}^v - 2u_m^v + u_{m+1}^v],$$

and

$$\left. \frac{\partial u}{\partial \theta} \right|_m^{v+1} = -\frac{1}{(\Delta x')^2} [u_{m-1}^{v+1} - 2u_m^{v+1} + u_{m+1}^{v+1}],$$

so that ultimately we can write Eq. (16.28) as follows:

$$u_m^{v+1} = u_m^v + \frac{P}{2} \left[(u_{m-1}^v - 2u_m^v + u_{m+1}^v) + (u_{m-1}^{v+1} - 2u_m^{v+1} + u_{m+1}^{v+1}) \right], \quad (16.29)$$

where $P = \Delta \theta / (\Delta x')^2$ as before. Notice that the unknown values of u^{v+1} now appear on both sides of the equation, so this method is implicit. We find it necessary to deal with simultaneous equations in order to get a solution.

To see how this is applied, let's return to the problem pertaining to Figs. 16.1 and 16.2. The temperature at $m = 0$ is fixed by the boundary condition of Eq. (16.10). At $m = N$, we use Eq. (16.13) again. Therefore,

$$u_N^{v+1} = u_N^v + P \left[(u_{N-1}^v - u_N^v) + (u_{N-1}^{v+1} - u_N^{v+1}) \right]$$

or

$$-P u_{N-1}^{v+1} + (1 + P) u_N^{v+1} = P u_{N-1}^v + (1 - P) u_N^v. \quad (16.30)$$

We set up the system as matrices for $N = 4$; remember $u_0^v = u_0^{v+1} = 1$.

$$\begin{bmatrix} (1+P) & -P/2 & & & \\ -P/2 & (1+P) & -P/2 & & \\ & -P/2 & (1+P) & -P/2 & \\ & & -P & (1+P) & \end{bmatrix} \begin{bmatrix} u_1 \\ u_2 \\ u_3 \\ u_4 \end{bmatrix}^{v+1} = \begin{bmatrix} (1-P) & P/2 & & & \\ P/2 & (1-P) & P/2 & & \\ & P/2 & (1-P) & P/2 & \\ & & P & (1-P) & \end{bmatrix} \begin{bmatrix} u_1 \\ u_2 \\ u_3 \\ u_4 \end{bmatrix}^v \quad (16.31)$$

The right hand side can be computed directly because all of the components are known. Of course, we simply get a column matrix of constants. To the first element in the column matrix of constants, we must remember to add P because $u_0^v = u_0^{v+1} = 1$ in this example.

The left side contains the unknowns, which must be solved as a system of algebraic equations. The process is repeated for each time step.

The computational effort appears to be greater with the Crank-Nicolson method than it appears with the Euler method. Keep in mind, however, that the accuracy of the estimate for the time derivative is improved so that larger time steps can be taken. Furthermore, unstable numerical oscillations are avoided so we are not restricted to $P \leq 0.5$.

With the explicit method, we used $P = 0.25$ for the problem at hand (Table 16.1), so that for the case of $\Delta x' = 0.2$, the time steps were of duration $\Delta\theta = P(\Delta x')^2 = 0.01$. In order to achieve the normalized temperature at $\theta = 1$, 100 time steps were required. Now to demonstrate the advantage of the Crank-Nicolson method, let's double P ($P = 0.5$) with $\Delta x'$ kept at 0.2. Then $\Delta\theta = 0.02$, and 50 time steps are required to arrive at $\theta = 1$. These results are given in Table 16.3, which compare favorably with Table 16.1. Although we have used larger time steps, the accuracy of the results is better than found in Table 16.1 for $\theta = 0.2$ and comparable for larger values of θ .

Table 16.3 Normalized temperature, u , at the center (insulated surface) with $P = 0.5$ and $\Delta x' = 0.2$ (Crank-Nicolson method)

θ	Numerical Solution	Exact Solution
0.2	0.232	0.235
0.4	0.526	0.531
0.6	0.709	0.714
0.8	0.822	0.826
1.0	0.891	0.894

The code used for the results is given below. It is written in BASIC so that a matrix inversion (statement 180) could be used. For very large matrices as encountered in practice, this cannot be done. With tridiagonal matrices, a very efficient algorithm can be devised (e.g., see Carnahan *et al.*¹ or Guthrie²). Commonly employed algorithms to solve matrices are based upon the Gauss-Siedel method.³

```

11      REM ***          VAX-BASIC PROGRAM          ***
12      REM ***          FOR                        ***
13      REM ***          SOLVING EQUATION(16.31)    ***
14      REM ***          (P = 0.5, delta x' = 0.2)  ***

20      DIM A(5,5),B(5,1),C(5,5),D(5,1)
30      DIM E(5,1),F(5,5)

40      REM --- read the matrices
50      MAT READ A(5,5)
60      MAT READ C(5,5)
70      MAT READ D(5,1)

80      MAT B = ZER(5,1)

```

¹B. Carnahan, H. A. Luther and J. O. Wilkes, *Applied Numerical Methods*, John Wiley & Sons, New York, 1969, pages 441-442.

²R. I. L. Guthrie, *Engineering in Process Metallurgy*, Clarendon Press, Oxford, UK, 1989, page 382.

³R. E. Scraton, *Basic Numerical Methods*, Edward Arnold, London, UK, 1984, pages 50-51.

582 Numerical Methods and Models

```

90     SUBT = 0
100    FOR I = 1 TO 50

110    REM --- compute the time step
120    T = I * 0.02
130    SUBT = SUBT + 1

140    REM --- compute the right hand side
150    MAT E = C * D
160    E(1,1) = E(1,1) + 0.5

170    REM --- compute the inverse matrix of A
180    MAT F = INV(A)

190    REM --- compute the temperature
200    REM --- for next time step
210    MAT B = F * E

220    REM --- print out the results
230    IF SUBT = 10 THEN PRINT "Time = "; T &
                        \ MAT PRINT B \ SUBT = 0

240    MAT D = B

250    NEXT I

410    REM MATRIX ---- A (for P = 0.5)
420    DATA 1.5 , -0.25, 0, 0, 0
430    DATA -0.25, 1.5 , -0.25, 0, 0
440    DATA 0, -0.25, 1.5 , -0.25, 0
450    DATA 0, 0, -0.25, 1.5 , -0.25
460    DATA 0, 0, 0, -0.5 , 1.5

470    REM MATRIX ---- C (for P = 0.5)
480    DATA 0.5 , 0.25, 0, 0, 0
490    DATA 0.25, 0.5 , 0.25, 0, 0
500    DATA 0, 0.25, 0.5 , 0.25, 0
510    DATA 0, 0, 0.25, 0.5 , 0.25
520    DATA 0, 0, 0, 0.5 , 0.5

530    DATA MATRIX ---- D (temperature)
540    DATA 0
550    DATA 0
560    DATA 0
570    DATA 0
580    DATA 0

999    END

```

16.1.3 Two-dimensional formulation

For the sake of some variety, let us consider the mass diffusion of solute in a single-phase material. Suppose we want to study the homogenization kinetics in an as-cast alloy with microsegregation. The microstructure is shown in Fig. 16.6 as a transverse section through a columnar dendritic alloy with a primary dendrite arm spacing of $180 \mu\text{m}$. The microstructure is periodic so we can study the domain of the smaller square with sides of $90 \mu\text{m}$. This problem is an extension of the one-dimensional case of homogenization in Section 13.5. Formally presented we have

$$\frac{\partial C}{\partial t} = D \left[\frac{\partial^2 C}{\partial x^2} + \frac{\partial^2 C}{\partial y^2} \right]. \quad (16.32)$$

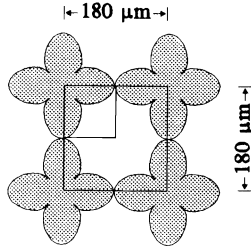


Fig. 16.6 Transverse section through columnar dendritic structure.

Let L and ℓ be the dimensions of the smaller domain in Fig. 16.6; then the boundary conditions are

$$\frac{\partial C}{\partial x}(L, y, t) = 0 \quad t \geq 0, \tag{16.33}$$

$$\frac{\partial C}{\partial x}(0, y, t) = 0 \quad t \geq 0, \tag{16.34}$$

$$\frac{\partial C}{\partial y}(x, \ell, t) = 0 \quad t \geq 0, \tag{16.35}$$

and

$$\frac{\partial C}{\partial y}(x, 0, t) = 0 \quad t \geq 0, \tag{16.36}$$

and the initial condition is

$$C(x, y, 0) = f(x, y). \tag{16.37}$$

Equations (16.32) through (16.37) represent a mathematical formulation of the problem. Before we proceed, let's think about the situation in a less formal manner. We have an inhomogeneous single-phase solid with the initial concentration of the solute arbitrarily disposed in the rectangular region $L \times \ell$. If the solid is heated, then diffusion takes place so we must also satisfy some boundary conditions. In this case we require no mass flux of the solute across the system boundaries. Hence, we write the four boundary conditions as Eqs. (16.33) through (16.36).

Following the reasoning that led us to Eq. (16.5), we divide the domain into nine rectangles shown in Fig. 16.7. We select a relatively small number of nodes for the sake of illustrating the method. With two-dimensional transport, double indexing of the nodes is often done, but here we simply number the nodes consecutively in order to simplify the notation. It is also somewhat easier to see the development of the resulting matrices when each node has a single index.

First we write approximations for the second derivatives at an internal node. In this example, we only have four internal nodes (5, 6, 9 and 10), but typically the internal nodes form the largest proportion of the total. At internal node n , we have

$$\left[\frac{\partial^2 C}{\partial x^2} \right]_n \approx \frac{1}{(\Delta x)^2} (C_{n-1} - 2C_n + C_{n+1}) \tag{16.38}$$

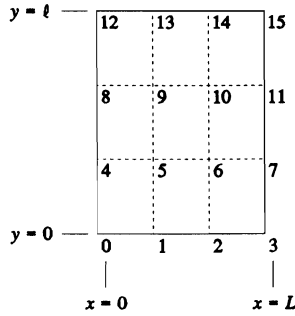


Fig. 16.7 The domain $L \times l$ subdivided into areas of $(\Delta x) \times (\Delta y)$.

and

$$\left[\frac{\partial^2 C}{\partial y^2} \right]_n \approx \frac{1}{(\Delta y)^2} (C_{n-4} - 2C_n + C_{n+4}). \tag{16.39}$$

To be more general, the subscripts $(n-4)$ and $(n+4)$ could be replaced by $(n-I)$ and $(n+I)$, respectively, where I is the number of vertical columns. With these approximations, Eq. (16.32) becomes

$$\left[\frac{\partial C}{\partial t} \right]_n \approx \frac{D}{(\Delta x)^2} (C_{n-1} - 2C_n + C_{n+1}) + \frac{D}{(\Delta y)^2} [C_{n-4} - 2C_n + C_{n+4}]. \tag{16.40}$$

As before we must now decide how to treat the time derivative. Usually, the Crank-Nicolson method is used because, after the added work in setting up the problem is invested, the resulting algorithms are generally more useful than if we had used the simpler Euler method. Proceeding with the Crank-Nicolson method, the time derivative is

$$\left[\frac{\partial C}{\partial t} \right]_n = \frac{1}{2} \left[\frac{\partial C}{\partial t} \right]_n^{\nu+1} + \frac{1}{2} \left[\frac{\partial C}{\partial t} \right]_n^\nu, \tag{16.41}$$

where now we have added the superscript ν for the present time and $\nu+1$ for the next time.

You can see that we are proceeding with the method of Section 16.1.2, except now the bookkeeping is a little more tedious.

The concentration at time $\nu+1$ is

$$C_n^{\nu+1} = C_n^\nu + \left[\frac{\partial C}{\partial t} \right]_n \Delta t, \tag{16.42}$$

and after Eqs. (16.40)-(16.42) are combined, we get

$$\begin{aligned} C_n^{\nu+1} = C_n^\nu + \frac{\Delta\theta_x}{2} [C_{n-1}^{\nu+1} - 2C_n^{\nu+1} + C_{n+1}^{\nu+1}] + \frac{\Delta\theta_y}{2} [C_{n-4}^{\nu+1} - 2C_n^{\nu+1} + C_{n+4}^{\nu+1}] \\ + \frac{\Delta\theta_x}{2} [C_{n-1}^\nu - 2C_n^\nu + C_{n+1}^\nu] + \frac{\Delta\theta_y}{2} [C_{n-4}^\nu - 2C_n^\nu + C_{n+4}^\nu], \end{aligned} \tag{16.43}$$

where $\Delta\theta_x = D\Delta t/(\Delta x)^2$ and $\Delta\theta_y = D\Delta t/(\Delta y)^2$.

Ultimately we must deal with simultaneous equations and solve for the unknowns C_n^{v+1} . With this in mind, Eq. (16.43) is rearranged into the following form for setting up the matrices:

$$\begin{aligned}
 -\frac{\Delta\theta_y}{2} C_{n-4}^{v+1} - \frac{\Delta\theta_x}{2} C_{n-1}^{v+1} + (1 + \Delta\theta_x + \Delta\theta_y) C_n^{v+1} - \frac{\Delta\theta_x}{2} C_{n+1}^{v+1} - \frac{\Delta\theta_y}{2} C_{n+4}^{v+1} &= \frac{\Delta\theta_y}{2} C_{n-4}^v \\
 + \frac{\Delta\theta_x}{2} C_{n-1}^v + (1 - \Delta\theta_x - \Delta\theta_y) C_n^v + \frac{\Delta\theta_x}{2} C_{n+1}^v + \frac{\Delta\theta_y}{2} C_{n+4}^v, & \quad (16.44)
 \end{aligned}$$

where $n = 5, 6, 9, 10$.

Nodes along the boundaries are considered next; e.g., a solute balance at either node 1 or 2 gives

$$\begin{aligned}
 \frac{\Delta y}{2} \left[-D \frac{C_n - C_{n-1}}{\Delta x} \right] &= \frac{\Delta y}{2} \left[-D \frac{C_{n+1} - C_n}{\Delta x} \right] + \Delta x \left[-D \frac{C_{n+4} - C_n}{\Delta y} \right] \\
 + \frac{1}{2} \Delta x \Delta y \left[\frac{\partial C}{\partial t} \right]_n, & \quad (16.45)
 \end{aligned}$$

where the area associated with the node is Δx by $\Delta y/2$. Again, we take the Crank-Nicolson average for the time derivative. The result is

$$\begin{aligned}
 -\frac{\Delta\theta_x}{2} C_{n-1}^{v+1} + (1 + \Delta\theta_x + \Delta\theta_y) C_n^{v+1} - \frac{\Delta\theta_x}{2} C_{n+1}^{v+1} - \Delta\theta_y C_{n+4}^{v+1} &= \frac{\Delta\theta_x}{2} C_{n-1}^v \\
 + (1 - \Delta\theta_x - \Delta\theta_y) C_n^v + \frac{\Delta\theta_x}{2} C_{n+1}^v + \Delta\theta_y C_{n+4}^v, & \quad (16.46)
 \end{aligned}$$

where $n = 1, 2$.

Along the top boundary, Eq. (16.46) does not apply because in place of diffusion from node n to node $n+4$, there is instead diffusion from $n-4$ to n . This results in

$$\begin{aligned}
 -\Delta\theta_y C_{n-4}^{v+1} - \frac{\Delta\theta_x}{2} C_{n-1}^{v+1} + (1 + \Delta\theta_x + \Delta\theta_y) C_n^{v+1} - \frac{\Delta\theta_x}{2} C_{n+1}^{v+1} &= \Delta\theta_y C_{n-4}^v \\
 + \frac{\Delta\theta_x}{2} C_{n-1}^v + (1 - \Delta\theta_x - \Delta\theta_y) C_n^v + \frac{\Delta\theta_x}{2} C_{n+1}^v, & \quad (16.47)
 \end{aligned}$$

where $n = 13, 14$.

For the left and right boundaries, the procedure gives

$$\begin{aligned}
 -\frac{\Delta\theta_y}{2} C_{n-4}^{v+1} + (1 + \Delta\theta_y + \Delta\theta_x) C_n^{v+1} - \Delta\theta_x C_{n+1}^{v+1} - \frac{\Delta\theta_y}{2} C_{n+4}^{v+1} &= \frac{\Delta\theta_y}{2} C_{n-4}^v \\
 + (1 - \Delta\theta_y - \Delta\theta_x) C_n^v + \Delta\theta_x C_{n+1}^v + \frac{\Delta\theta_y}{2} C_{n+4}^v, & \quad (16.48)
 \end{aligned}$$

for the left boundary where $n = 4, 8$, and

$$\begin{aligned}
 -\frac{\Delta\theta_y}{2} C_{n-4}^{v+1} - \Delta\theta_x C_{n-1}^{v+1} + (1 + \Delta\theta_y + \Delta\theta_x) C_n^{v+1} - \frac{\Delta\theta_y}{2} C_{n+4}^{v+1} &= \frac{\Delta\theta_y}{2} C_{n-4}^v \\
 + \Delta\theta_x C_{n-1}^v + (1 - \Delta\theta_y - \Delta\theta_x) C_n^v + \frac{\Delta\theta_y}{2} C_{n+4}^v, & \quad (16.49)
 \end{aligned}$$

for the right boundary where $n = 7, 11$.

586 Numerical Methods and Models

Each corner node has an area of $(\Delta x/2) \times (\Delta y/2)$. Then a solute mass balance at node $n = 0$ is

$$\theta = \frac{\Delta y}{2} \left[-D \frac{C_{n+1} - C_n}{\Delta x} \right] + \frac{\Delta x}{2} \left[-D \frac{C_{n+4} - C_n}{\Delta y} \right] + \frac{\Delta x \Delta y}{4} \left[\frac{\partial C}{\partial t} \right]_n. \quad (16.50)$$

After the Crank-Nicolson average for the time derivative is set up, the resulting equation is substituted into Eq. (16.50) and rearranged. The result is

$$(1 + \Delta\theta_x + \Delta\theta_y) C_n^{v+1} - \Delta\theta_x C_{n+1}^{v+1} - \Delta\theta_y C_{n+4}^{v+1} = (1 - \Delta\theta_x - \Delta\theta_y) C_n^v + \Delta\theta_x C_{n+1}^v + \Delta\theta_y C_{n+4}^v, \quad (16.51)$$

with $n = 0$. Similarly at $n = 3$:

$$-\Delta\theta_x C_{n-1}^{v+1} + (1 + \Delta\theta_x + \Delta\theta_y) C_n^{v+1} - \Delta\theta_y C_{n+4}^{v+1} = \Delta\theta_x C_{n-1}^v + (1 - \Delta\theta_x - \Delta\theta_y) C_n^v + \Delta\theta_y C_{n+4}^v. \quad (16.52)$$

At $n = 12$:

$$-\Delta\theta_y C_{n-4}^{v+1} + (1 + \Delta\theta_x + \Delta\theta_y) C_n^{v+1} - \Delta\theta_x C_{n+1}^{v+1} = \Delta\theta_y C_{n-4}^v + (1 - \Delta\theta_x - \Delta\theta_y) C_n^v + \Delta\theta_x C_{n+1}^v. \quad (16.53)$$

At $n = 15$:

$$-\Delta\theta_y C_{n-4}^{v+1} - \Delta\theta_x C_{n-1}^{v+1} + (1 + \Delta\theta_x + \Delta\theta_y) C_n^{v+1} = \Delta\theta_y C_{n-4}^v + \Delta\theta_x C_{n-1}^v + (1 - \Delta\theta_x - \Delta\theta_y) C_n^v. \quad (16.54)$$

We finally have an equation for each of the 16 nodes in our system, so the matrices can be written. We take $\Delta x = \Delta y = 30 \mu\text{m}$ and assume that $D = 10^{-14} \text{ m}^2 \text{ s}^{-1} = 10^{-2} \mu\text{m}^2 \text{ s}^{-1}$. With $\Delta\theta_x = \Delta\theta_y = 0.01$, the time steps are $\Delta t = 0.01(\Delta x)^2/D = 900 \text{ s}$. In one day (not an unreasonable time for homogenization), there are 96 time steps. In reality, it would be better to have more spatial resolution so $\Delta\theta_x$ and $\Delta\theta_y$ could be greater than 0.01. We continue with our rather coarse grid, however, for illustrative purposes in setting up the matrices that result in Eq. (16.55) on the next page.

Examination of Eq. (16.55) reveals that a pattern has emerged. The coefficients for the concentrations all fall on the diagonals in the coefficient matrices, and they are equal. In this example, the coefficient matrix on the left side of Eq. (16.55) has all diagonal elements equal to 1.02.

Figure 16.8 illustrates other aspects of the matrices. Each internal node has four neighbors, and the concentrations of the four neighbors are weighted evenly by their respective coefficients of $-\Delta\theta/2$, when $\Delta\theta = \Delta\theta_x = \Delta\theta_y$. At a boundary, where one of the four neighbors is missing, the coefficient of its opposite counterpart is doubled. Where two of the four neighbors are missing, as at a corner, then each coefficient of the two neighboring concentrations is doubled.

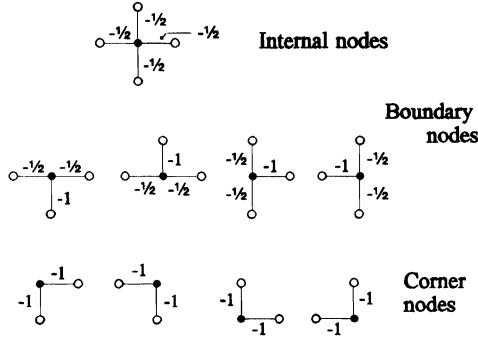
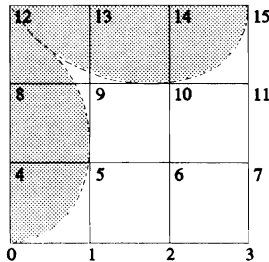


Fig. 16.8 Coefficients for neighboring concentrations surrounding the unknown concentrations, C_n^{n+1} , in Eq. (16.55). The coefficients are multiples of $\Delta\theta_x$ and $\Delta\theta_y$.

As an example of applying this to a homogenization calculation, let's assume that we measure the initial distribution of solute with an electron beam microprobe analyzer (EBMA). In the area of $90 \mu\text{m} \times 90 \mu\text{m}$ outlined in Fig. 16.6, we determine that the initial concentrations of solute "B" at the 16 nodal points are those shown in Fig. 16.9.

The code that is based on this model follows. Calculated results at selected times are given in Table 16.4. Notice that solute is not exactly conserved as shown by the small decrease in the average concentration with time (Table 16.4). This is a numerical artifact because the domain has been divided into only nine subregions. Better accuracy could be obtained by using more nodes.



Nodes	C, %B
0, 15	1.1
1, 11	1.4
2, 7	2.0
3	2.5**
4, 14	1.06
5, 10	1.2
6	1.8
8, 13	1.03
9	1.10
12	1.0*
<hr/>	
Avg.	1.374

*minimum
**maximum

Fig. 16.9 Initial distribution of solute for homogenization calculation.

```

11  REM ***      VAX-BASIC PROGRAM      ***
12  REM ***      FOR                      ***
13  REM ***      SOLVING EQUATION(16.55) ***

20  DIM A(16,16),B(16,1),C(16,16),D(16,1)
30  DIM E(16,1),F(16,16)

40  REM --- read the matrices
50  MAT READ A(16,16)
60  MAT READ C(16,16)
    
```

```

70  MAT READ D(16,1)
80  MAT B = ZER(16,1)

90  SUBT = 0
100 FOR I = 1 TO 96

110  REM --- compute the time step
120  T = I * 0.25
130  SUBT = SUBT + 1

140  REM --- compute the right hand side
150  MAT E = C * D

160  REM -- compute the inverse matrix of A
170  MAT F = INV(A)

180  REM --- compute the concentration
190  REM --- for next time step
200  MAT B = F * E

210  REM --- print out the results
220  IF SUBT = 4 THEN PRINT "Time = "; T; "Hours" &
      \ MAT PRINT B \ SUBT = 0

230  MAT D = B

240  NEXT I

400  REM MATRIX ---- A
410  DATA 1.02, -0.01, 0,0, -0.01, 0,0,0,0,0,0,0,0,0,0,0,0
420  DATA -0.005, 1.02, -0.005, 0,0, -0.01, 0,0,0,0,0,0,0,0,0,0,0,0
430  DATA 0,-0.005, 1.02, -0.005, 0,0, -0.01, 0,0,0,0,0,0,0,0,0,0,0,0
440  DATA 0,0,-0.01, 1.02, 0,0,0, -0.01, 0,0,0,0,0,0,0,0,0,0,0,0
450  DATA -0.005, 0,0, 0, 1.02, -0.01, 0,0,-0.005,0,0,0,0,0,0,0,0,0
460  DATA 0,-0.005, 0,0, -0.005, 1.02, -0.005, 0,0,-0.005,0,0,0,0,0,0,0,0,0
470  DATA 0,0,-0.005, 0,0, -0.005, 1.02, -0.005, 0,0,-0.005,0,0,0,0,0,0,0,0,0
480  DATA 0,0,0,-0.005, 0,0, -0.01, 1.02, 0,0,0,0,-0.005,0,0,0,0,0,0,0,0
490  DATA 0,0,0,0,-0.005, 0,0, 0, 1.02, -0.01,0,0,-0.005,0,0,0,0,0,0,0,0
500  DATA 0,0,0,0,0,-0.005, 0,0, -0.005, 1.02, -0.005,0,0,-0.005,0,0,0,0,0,0,0
510  DATA 0,0,0,0,0,0,-0.005, 0,0, -0.005, 1.02, -0.005,0,0,-0.005,0,0,0,0,0,0,0
520  DATA 0,0,0,0,0,0,0,-0.005, 0,0, -0.01, 1.02, 0,0,0,0,0,-0.005,0,0,0,0
530  DATA 0,0,0,0,0,0,0,0,-0.01, 0,0, 0, 1.02, -0.01,0,0,0,0,0,0,0,0
540  DATA 0,0,0,0,0,0,0,0,0,-0.01, 0,0, -0.005, 1.02, -0.005,0,0,0,0,0,0,0,0
550  DATA 0,0,0,0,0,0,0,0,0,0,-0.01, 0,0, -0.005, 1.02, -0.005,0,0,0,0,0,0,0,0
560  DATA 0,0,0,0,0,0,0,0,0,0,0,-0.01, 0,0, -0.01, 1.02

600  REM MATRIX ---- C
610  DATA 0.98, 0.01, 0,0, 0.01, 0,0,0,0,0,0,0,0,0,0,0,0,0,0,0,0
620  DATA 0.005, 0.98, 0.005, 0,0, 0.01, 0,0,0,0,0,0,0,0,0,0,0,0,0,0,0,0
630  DATA 0, 0.005, 0.98, 0.005, 0,0, 0.01, 0,0,0,0,0,0,0,0,0,0,0,0,0,0,0,0
640  DATA 0,0, 0.01, 0.98, 0, 0,0, 0.01, 0,0,0,0,0,0,0,0,0,0,0,0,0,0,0,0
650  DATA 0.005, 0,0, 0, 0.98, 0.01, 0,0, 0.005, 0,0,0,0,0,0,0,0,0,0,0,0,0,0,0,0
660  DATA 0, 0.005, 0,0, 0.005, 0.98, 0.005, 0,0, 0.005, 0,0,0,0,0,0,0,0,0,0,0,0,0,0,0,0
670  DATA 0,0, 0.005, 0,0, 0.005, 0.98, 0.005, 0,0, 0.005, 0,0,0,0,0,0,0,0,0,0,0,0,0,0,0,0
680  DATA 0,0,0, 0.005, 0,0, 0.01, 0.98, 0, 0,0, 0.005, 0,0,0,0,0,0,0,0,0,0,0,0,0,0,0,0
690  DATA 0,0,0,0, 0.005, 0,0, 0, 0.98, 0.01, 0,0, 0.005, 0,0, 0.005, 0,0,0,0,0,0,0,0,0,0,0,0
700  DATA 0,0,0,0,0, 0.005, 0,0, 0.005, 0.98, 0.005, 0,0, 0.005, 0,0, 0.005, 0,0,0,0,0,0,0,0,0,0,0,0
710  DATA 0,0,0,0,0,0, 0.005, 0,0, 0.005, 0.98, 0.005, 0,0, 0.005, 0,0, 0.005, 0,0,0,0,0,0,0,0,0,0,0,0
720  DATA 0,0,0,0,0,0,0, 0.005, 0,0, 0.01, 0.98, 0, 0,0, 0,0,0,0,0,0,0,0,0,0,0,0,0,0,0,0
730  DATA 0,0,0,0,0,0,0,0, 0.01, 0,0, 0, 0.98, 0.01, 0,0,0,0,0,0,0,0,0,0,0,0,0,0,0,0,0,0
740  DATA 0,0,0,0,0,0,0,0,0, 0.01, 0,0, 0.005, 0.98, 0.005, 0,0,0,0,0,0,0,0,0,0,0,0,0,0,0,0,0,0
750  DATA 0,0,0,0,0,0,0,0,0,0, 0.01, 0,0, 0.005, 0.98, 0.005, 0,0,0,0,0,0,0,0,0,0,0,0,0,0,0,0,0,0
760  DATA 0,0,0,0,0,0,0,0,0,0,0, 0.01, 0,0, 0.01, 0.98

800  REM MATRIX ---- D (Initial compositions, %B)
810  DATA 1.1
820  DATA 1.4
830  DATA 2.0
840  DATA 2.5
850  DATA 1.06
860  DATA 1.2
870  DATA 1.8
880  DATA 2.0
890  DATA 1.03
900  DATA 1.10

```

```

910     DATA 1.2
920     DATA 1.4
930     DATA 1.0
940     DATA 1.03
950     DATA 1.06
960     DATA 1.1
999     END

```

Table 16.4 Concentrations during homogenization

	Initial	8 hours	16 hours	24 hours	
C_0	1.1	1.214	1.277	1.313	
C_1	1.4	1.400	1.403	1.399	
C_2	2	1.818	1.675	1.578	
C_3	2.5	2.059	1.820	1.671	Maximum
C_4	1.06	1.156	1.225	1.269	
C_5	1.2	1.296	1.329	1.343	
C_6	1.8	1.640	1.556	1.498	
C_7	2	1.818	1.675	1.578	
C_8	1.03	1.080	1.135	1.186	
C_9	1.1	1.146	1.196	1.237	
C_{10}	1.2	1.296	1.329	1.343	
C_{11}	1.4	1.400	1.403	1.399	
C_{12}	1	1.043	1.094	1.146	Minimum
C_{13}	1.03	1.080	1.135	1.186	
C_{14}	1.06	1.156	1.225	1.269	
C_{15}	1.1	1.214	1.277	1.313	
Avg.	1.374	1.363	1.360	1.358	

A figure of merit of the process is the residual segregation index, δ , defined in Eq. (13.64). The calculated values of δ versus dimensionless time are plotted in Fig. 16.10. Even after 24 hours, complete homogenization is not effected.

As mentioned before, a code such as given here may not be capable of solving the problem except for a rather limited number of nodes. In order to treat a larger multi-nodal situation, the reader might consider an algorithm based on the *alternating direction implicit (ADI)* method,⁴ which involves taking a half-time step at nodes in the vertical direction followed by a half-time step at the nodes in the horizontal direction. The resulting matrices for the half-time steps are tridiagonal, which can be solved very efficiently. With full-time steps as done here, the implicit method leads to a banded matrix that is not tridiagonal (e.g., Eq. (16.55)).

In Sections 16.1.1-16.1.3 the coefficient matrices remained constant as time marched forward because the heat transfer coefficient and transport properties were constant. The finite difference approximation, however, enables us to use heat transfer coefficients or transport properties that vary. Here we illustrate the use of radiation heat transfer at the surface, which must be treated accordingly because of its T^4 behavior.

⁴B. Carnahan, H. A. Luther and J. O. Wilkes, *ibid.*, pages 452-461.

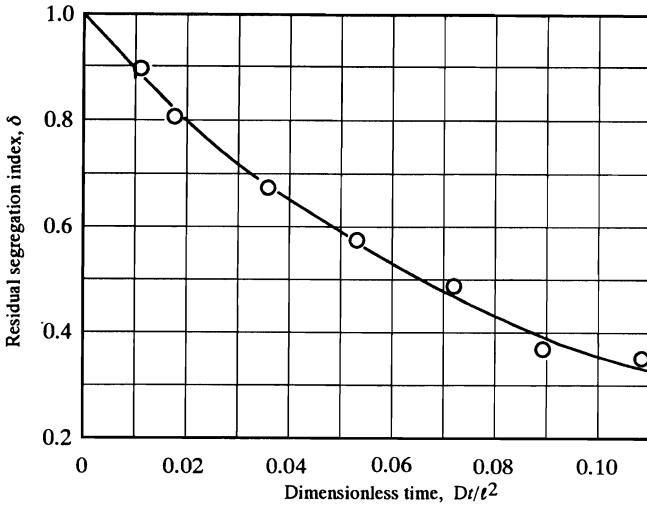


Fig. 16.10 Homogenization kinetics for two-dimensional diffusion.

16.1.4 Radiation heat transfer at a surface

Consider a green ceramic slab that is placed into a high temperature furnace for sintering at 2000 K. Our goal is to estimate the temperature distribution within the green slab as it is heated by radiation emanating from the walls of the furnace. The thermal conductivity of the porous ceramic varies with temperature, but the volumetric heat capacity is constant. Both surfaces of the slab are equally heated by radiation so that the temperature is symmetrical on both sides of $x = 0$.

The energy equation is

$$\frac{\partial T}{\partial t} = \frac{\partial}{\partial x} \left[\alpha \frac{\partial T}{\partial x} \right]. \quad (16.56)$$

At the surface exchanging radiant energy ($x = L$), the power balance is

$$-k \frac{\partial T}{\partial x} (L, t) = \mathcal{F} \sigma (T^4(L, t) - T_w^4)$$

or

$$\frac{\partial T}{\partial x} (L, t) = \frac{\mathcal{F} \sigma}{k} (T_w^4 - T^4(L, t)), \quad (16.57)$$

where T_w is the temperature of the radiating furnace walls. At the plane of symmetry, we have

$$\frac{\partial T}{\partial t} (0, t) = 0, \quad (16.58)$$

and the initial condition is

$$T(x,0) = T_i \text{ (uniform)}. \quad (16.59)$$

For the sake of minimizing the algebra involved, let's formulate the finite difference approximation with the Euler method. The internal points will have to be treated differently than they were in Section 16.1.1 because the thermal diffusivity varies with temperature. At a node m , the energy balance in finite difference form is

$$-k_- \frac{T_m - T_{m-1}}{\Delta x} = -k_+ \frac{T_{m+1} - T_m}{\Delta x} + \Delta x \rho C_p \left[\frac{\partial T}{\partial t} \right]_m,$$

where k_- is the average thermal conductivity between nodes m and $m-1$ and k_+ is the average between nodes $m+1$ and m . After rearranging, we get

$$\left[\frac{\partial T}{\partial t} \right]_m = \frac{\alpha_+}{(\Delta x)^2} (T_{m+1} - T_m) - \frac{\alpha_-}{(\Delta x)^2} (T_m - T_{m-1}).$$

With the Euler method,

$$T_m^{v+1} = T_m^v + \left[\frac{\partial T}{\partial t} \right]_m \Delta t$$

or

$$T_m^{v+1} = T_m^v + \Delta\theta_+ (T_{m+1}^v - T_m^v) - \Delta\theta_- (T_m^v - T_{m-1}^v),$$

where $\Delta\theta_+ = \alpha_+ \Delta t / (\Delta x)^2$ and $\Delta\theta_- = \alpha_- \Delta t / (\Delta x)^2$. The form suitable for setting up the matrix is

$$T_m^{v+1} = +\Delta\theta_- T_{m-1}^v + (1 - \Delta\theta_+ - \Delta\theta_-) T_m^v + \Delta\theta_+ T_{m+1}^v, \quad (16.60)$$

for $0 < m < N$.

An energy balance at $m = 0$ can be written as follows:

$$0 = -k_+ \left[\frac{T_1 - T_0}{\Delta x} \right] + \frac{\Delta x}{2} \rho C_p \left[\frac{\partial T}{\partial t} \right]_0$$

or

$$\left[\frac{\partial T}{\partial t} \right]_0 = \frac{2\alpha_+}{(\Delta x)^2} (T_1 - T_0). \quad (16.61)$$

The Euler method gives

$$T_0^{v+1} = T_0^v + 2\Delta\theta_+ (T_1^v - T_0^v)$$

or

$$T_0^{v+1} = (1 - 2\Delta\theta_+) T_0^v + 2\Delta\theta_+ T_1^v. \quad (16.62)$$

At the surface exchanging radiant energy, the energy balance is

$$-k_- \left[\frac{T_N - T_{N-1}}{\Delta x} \right] + \mathcal{F} \sigma [T_w^4 - T_N^4] = \frac{\Delta x}{2} \rho C_p \left[\frac{\partial T}{\partial t} \right]_N$$

or

$$\left[\frac{\partial T}{\partial t} \right]_N = \frac{2\alpha_-}{(\Delta x)^2} (T_{N-1} - T_N) + \frac{2\mathcal{F}\sigma}{\rho C_p \Delta x} (T_w^4 - T_N^4). \quad (16.63)$$

With the Euler method this gives

$$T_N^{v+1} = T_N^v + 2\Delta\theta_- (T_{N-1}^v - T_N^v) + A$$

or

$$T_N^{v+1} = 2\Delta\theta_- (T_{N-1}^v) + (1 - 2\Delta\theta_-) T_N^v + A, \quad (16.64)$$

where

$$A = \frac{2\mathcal{F}\sigma\Delta t}{\rho C_p \Delta x} (T_w^4 - (T_N^v)^4).$$

We cannot include T_N^4 in the matrices for the variables because the elements can only be linear terms. Therefore, A in the right side of Eq. (16.64) must be evaluated at every time step v and treated as a constant.

For illustrative purposes, we consider a green ceramic slab that has a thickness of 60 mm and a thermal conductivity that varies with temperature according to

$$k = 5 \times 10^{-4} T + 0.40,$$

with T in K and k in $\text{W m}^{-1} \text{K}^{-1}$. The volumetric heat capacity of the ceramic, ρC_p , is $2.3 \times 10^6 \text{ J m}^{-3} \text{K}^{-1}$, and its emissivity is 0.5. The ceramic slab has been preheated uniformly to 1000 K, before we insert it into the high temperature furnace with its walls at 2020 K.

We set up the matrices for the first three time steps. To keep the problem relatively simple, let $N = 4$ so that $\Delta x = 1.5 \times 10^{-2} \text{ m}$. Recall $\Delta\theta \leq 0.5$ because we are using the Euler method. The radiation boundary condition is highly nonlinear so we should take small time steps to get reasonably good values of A . Suppose, $\Delta\theta_- = 0.025$ at $m = N$ then each time step will be of a different duration. Notice too that $\Delta\theta_+$ will not be exactly 0.025 except at the beginning.

Initially $v = 0$ and $t = 0$. We have the following properties and coefficients:

$$k_+ = k_- = k(1000 \text{ K}) = 0.90 \text{ W m}^{-1} \text{K}^{-1};$$

$$\alpha_+ = \alpha_- = \alpha(1000 \text{ K}) = 3.91 \times 10^{-7} \text{ m}^2 \text{s}^{-1};$$

$$\Delta\theta_+ = \Delta\theta_- = 0.025;$$

$$\Delta t = \frac{\Delta\theta_-(\Delta x)^2}{\alpha_-} = \frac{(0.025)(1.5 \times 10^{-2})^2}{3.91 \times 10^{-7}} = 14.39 \text{ s}.$$

594 Numerical Methods and Models

The view factor for the radiating surface is unity, so that $\mathcal{F} = \varepsilon = 0.5$; therefore

$$A = \frac{2 \cdot \mathcal{F} \sigma \Delta t}{\rho C_p \Delta x} \left(T_w^4 - (T_N^v)^4 \right) = \frac{(2)(0.5)(5.669 \times 10^{-8})(14.39)}{(2.3 \times 10^6)(1.5 \times 10^{-2})} (2020^4 - 1000^4) = 370 \text{ K}.$$

Now, we set up the matrix to solve for the temperatures at time step $v+1$ when $t = 14.39$ s:

$$\begin{bmatrix} T_0^1 \\ T_1^1 \\ T_2^1 \\ T_3^1 \\ T_4^1 - 370 \end{bmatrix} = \begin{bmatrix} 0.95 & 0.05 & & & \\ 0.025 & 0.95 & 0.025 & & \\ & 0.025 & 0.95 & 0.025 & \\ & & 0.025 & 0.95 & 0.025 \\ & & & 0.05 & 0.95 \end{bmatrix} \begin{bmatrix} 1000 \\ 1000 \\ 1000 \\ 1000 \\ 1000 \end{bmatrix}.$$

The solution is tabulated, along with new values of k_+ , k_- , α_+ and α_- (all in SI units) for next time step.

		k_+	k_-	$\alpha_+ \times 10^7$	$\alpha_- \times 10^7$
T_0^1	1000	0.90	—	3.91	—
T_1^1	1000	0.90	0.90	3.91	3.91
T_2^1	1000	0.90	0.90	3.91	3.91
T_3^1	1000	0.992	0.90	4.31	3.91
T_4^1	1370	—	0.992	—	4.31

Remember we decided to fix $\Delta\theta_-$ at $m = N = 4$, so that for the second time step

$$\Delta t = \frac{(0.025)(1.5 \times 10^{-2})^2}{4.31 \times 10^{-7}} = 13.05 \text{ s},$$

and $t_2 = 14.39 + 13.05 = 27.44$ s.

$$A = \frac{(2)(0.5)(5.669 \times 10^{-8})(13.05)}{(2.3 \times 10^6)(1.5 \times 10^{-2})} (2020^4 - 1370^4) = 281 \text{ K}.$$

Now we calculate and tabulate $\Delta\theta_-$ and $\Delta\theta_+$ for each node.

	$\Delta\theta_-$	$\Delta\theta_+$
T_0^1	—	0.02267
T_1^1	0.02267	0.02267
T_2^1	0.02267	0.02267
T_3^1	0.02267	0.0250
T_4^1	0.0250	—

With these values we can set up the matrix for the next time step:

$$\begin{bmatrix} T_0^2 \\ T_1^2 \\ T_2^2 \\ T_3^2 \\ T_4^2 - 281 \end{bmatrix} = \begin{bmatrix} 0.9547 & 0.0453 & & & \\ 0.02267 & 0.9547 & 0.02267 & & \\ & 0.02267 & 0.9547 & 0.02267 & \\ & & 0.02267 & 0.9523 & 0.0250 \\ & & & 0.05 & 0.95 \end{bmatrix} \begin{bmatrix} 1000 \\ 1000 \\ 1000 \\ 1000 \\ 1370 \end{bmatrix}.$$

The new temperatures and values of thermal conductivities and diffusivities are tabulated below.

		k_+	k_-	$\alpha_+ \times 10^7$	$\alpha_- \times 10^7$
T_0^2	1000	0.90	—	3.91	—
T_1^2	1000	0.90	0.90	3.91	3.91
T_2^2	1000	0.902	0.90	3.92	3.91
T_3^2	1009	1.060	0.902	4.60	3.92
T_4^2	1633	—	1.060	—	4.60

For the third time step

$$\Delta t = \frac{(0.025)(1.5 \times 10^{-2})^2}{4.58 \times 10^{-7}} = 12.28 \text{ s},$$

and $t_3 = 27.44 + 12.28 = 39.72 \text{ s}$.

$$A = \frac{(2)(0.5)(5.669 \times 10^{-8})(12.28)}{(2.3 \times 10^6)(1.5 \times 10^{-2})} (2020^4 - 1653^4) = 192.$$

Again we calculate and tabulate $\Delta\theta_-$ and $\Delta\theta_+$ for each node.

	$\Delta\theta_+$	$\Delta\theta_-$
T_0^2	—	0.02134
T_1^2	0.02134	0.02134
T_2^2	0.02134	0.02139
T_3^2	0.02139	0.0250
T_4^2	0.0250	—

Now the matrices for the next time step are set up:

$$\begin{bmatrix} T_0^3 \\ T_1^3 \\ T_2^3 \\ T_3^3 \\ T_4^3 - 192 \end{bmatrix} = \begin{bmatrix} 0.9573 & 0.0427 & & & \\ 0.02134 & 0.9573 & 0.02134 & & \\ & 0.02134 & 0.9573 & 0.02139 & \\ & & 0.02139 & 0.9536 & 0.0250 \\ & & & 0.05 & 0.95 \end{bmatrix} \begin{bmatrix} 1000 \\ 1000 \\ 1000 \\ 1009 \\ 1633 \end{bmatrix} .$$

The new temperatures at $t = 39.72$ s are 1000, 1000, 1000, 1024 and 1794 K. Having gone through three time steps, we stop here. After almost 40 s the surface is at 1794 K, but very little of the slab has heated. Very steep thermal gradients have developed near the surface, yet the center has not begun to heat.

A computer code to simulate complete heating of the slab, defined as heating the center to 2000 K, is given. Output includes the spatially dependent thermal properties and the coefficient matrix for the unknowns at each time step. Calculated temperatures are plotted in Fig. 16.11. The surface attains 2000 K in 30 minutes, but at that time the center is only at 1300 K. It requires 184 minutes for the center to reach 2000 K.

```

11      REM ***          VAX-BASIC PROGRAM          ***
12      REM ***          FOR                        ***
13      REM ***          SOLVING RADIATION PROBLEM  ***

20      DIM C(5,5),T(5,1),NewT(5,1)
30      DIM KP(5),KN(5),AlphaP(5),AlphaN(5)
40      DIM ThetaP(5),ThetaN(5)

50      REM --- read the initial temperatures
60      MAT READ T(5,1)
70      PRINT "Initial Temperatures"
80      MAT PRINT T

90      dx = 1.5E-2
100     SumTime = 0
105     SubSumTime = 0
110     FurTemp = 2020
120     ITER = 0

130     WHILE (T(1,1) <= 2000)
140         ITER = ITER + 1
150         REM --- compute the thermal conductivities
160         FOR I = 1 TO 4
170             KP(I) = (0.5*(5E-4)*(T(I,1) + T(I+1,1))) + 0.4

```

```

180     AlphaP(I) = KP(I) / (2.3E6)
190     KN(I+1) = (0.5*(5E-4)*(T(I,1) + T(I+1,1))) + 0.4
200     AlphaN(I+1) = KN(I+1) / (2.3E6)
210     NEXT I

220     REM --- compute the time step
230     ThetaP(4) = 0.025
240     ThetaN(5) = 0.025
250     dT = ThetaP(4) * (dX**2) / AlphaN(5)
260     SumTime = SumTime + dT
265     SubSumTime = SubSumTime + dT

270     REM --- compute 'A'
280     A = (2*(0.5)*(5.669E-8)*dT)*((FurTemp**4) - (T(5,1)**4)) &
        / ((2.36E6)*dX)

290     REM --- compute 'Theta'
300     FOR I = 1 TO 3
310         ThetaP(I) = AlphaP(I) * dT / (dX**2)
320         ThetaN(I+1) = AlphaN(I+1) * dT / (dX**2)
330     NEXT I

340     REM --- obtain the matrix
350     MAT C = ZER(5,5)
360     C(1,1) = 1 - (2*ThetaP(1))
370     C(1,2) = 2*ThetaP(1)
380     FOR I = 2 TO 4
390         C(I,I-1) = ThetaN(I)
400         C(I,I) = 1 - ThetaN(I) - ThetaP(I)
410         C(I,I+1) = ThetaP(I)
420     NEXT I
430     C(5,4) = 2*ThetaN(5)
440     C(5,5) = 1 - (2*ThetaN(5))
450     REM --- compute the temperatures for next step
460     MAT NewT = C * T
470     NewT(5,1) = NewT(5,1) + A
480     MAT T = NewT

490     IF (SubSumTime >= 600) THEN GOSUB 800
500     NEXT

510     GOSUB 800

700     REM MATRIX ---- T (Initial Temperatures)
710     DATA 1000
720     DATA 1000
730     DATA 1000
740     DATA 1000
750     DATA 1000

790     STOP

800     PRINT "K+", "K-", "Alpha+", "Alpha-"
810     FOR I = 1 TO 5
820         PRINT KP(I), KN(I), AlphaP(I), AlphaN(I)
830     NEXT I
840     PRINT "Theta+", "Theta-"
850     FOR I = 1 TO 5
860         PRINT ThetaP(I), ThetaN(I)
870     NEXT I
880     PRINT "delta T is ";dT; " (s)"
890     SumTime1 = SumTime / 60
900     PRINT "Total time is ";SumTime1; " (min)"
910     PRINT "Iteration : ";ITER
920     PRINT "A : "; A
930     PRINT "MATRIX is "
940     MAT PRINT C,
950     PRINT "Temperatures for next step"
960     MAT PRINT T
970     SubSumTime = SubSumTime - 600
980     RETURN

999     END

```

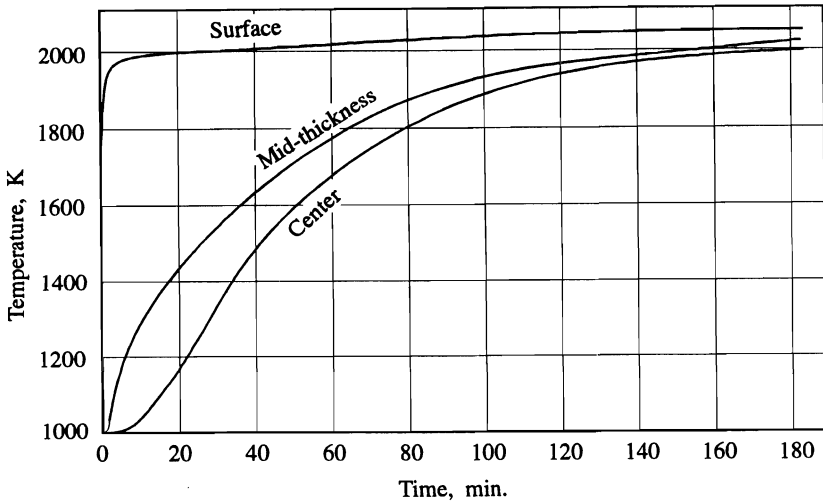


Fig. 16.11 Calculated temperatures in green ceramic slab (60 mm thick).

16.2 TURBULENT FLOW

Turbulent conditions, rather than laminar, usually prevail in materials processing. Accordingly, we make use of empirically based correlations for friction factors, heat transfer coefficients and mass transfer coefficients, such as presented in Chapters 3, 8 and 15. Even if those respective chapters were complete in summarizing all that has been studied and categorized, materials engineers encounter situations not previously analyzed and presented in such neat packages. For example, many processes involve recirculating flows: flows driven by electromagnetic forces; flows associated with the filling of vessels, ladles and molds; and flows driven by the injection of gas jets or large bubble swarms to effect reactions and mixing.

We know that sometimes even small disturbances of the fluid streamlines in laminar flow can cause turbulence. In forced convection, flows with small Reynolds numbers involve fluids in which the inertial forces are small relative to the viscous forces. For large Reynolds numbers, however, the inertial forces overcome the viscous forces (which tend to dissipate the inertial forces to neighboring streamlines), and the disturbances amplify or at least persist.

Turbulent flow can be advantageous in that it enhances heat and mass transfer rates. In some processes, however, its fluctuating and rather unpredictable nature is deleterious. For example, crystals grown in turbulently convecting melts exhibit segregation in the form of striations that are approximately parallel to the overall interface. Whether turbulence is to be desired or avoided depends upon the specific process under consideration, but for certain it can be said that the convection is complicated and difficult to describe and predict.

16.2.1 Fluctuation nature of turbulence

The dependent variables (v_x , v_y , v_z , T and C_i) have *instantaneous* values in turbulent flow; it is impossible to predict their exact values at any instant. Fortunately, the *time-averaged* quantities are by far more important and used in analyzing turbulence. The two are simply related; e.g., the x -component of velocity at a point in the flow field is

$$v_x = \bar{v}_x + v'_x, \quad (16.65)$$

where v_x = instantaneous velocity component, \bar{v}_x = time-averaged quantity* (see Fig. 1.2), and v'_x = fluctuation. Likewise, instantaneous pressure, temperature and concentrations can be expressed in the same manner; e.g., the pressure is

$$P = \bar{P} + P' \tag{16.66}$$

Consider the continuity equation for an incompressible fluid in a two-dimensional flow field; specifically Eq. (A) in Table 2.1 reduces to

$$\frac{\partial v_x}{\partial x} + \frac{\partial v_y}{\partial y} = 0 \tag{16.67}$$

When Eq. (16.67) is combined with Eq. (16.65) and a similar equation for v_y , the result is

$$\left[\frac{\partial \bar{v}_x}{\partial x} + \frac{\partial \bar{v}_y}{\partial y} \right] + \left[\frac{\partial v'_x}{\partial x} + \frac{\partial v'_y}{\partial y} \right] = 0 \tag{16.68}$$

The x-component of the momentum equation (Eq. (D) in Table 2.2) is

$$\frac{\partial v_x}{\partial t} + v_x \frac{\partial v_x}{\partial x} + v_y \frac{\partial v_x}{\partial y} = -\frac{1}{\rho} \frac{\partial P}{\partial x} + \nu \left[\frac{\partial^2 v_x}{\partial x^2} + \frac{\partial^2 v_x}{\partial y^2} \right] + g_x \tag{16.69}$$

In order to simplify our presentation somewhat, we assume that $\partial^2 v_x / \partial x^2$ can be neglected. We also rewrite Eq. (16.69) in the following equivalent form by adding v_x times Eq. (16.67) to it:

$$\frac{\partial v_x}{\partial t} + \frac{\partial}{\partial x} (v_x v_x) + \frac{\partial}{\partial y} (v_x v_y) = -\frac{1}{\rho} \frac{\partial P}{\partial x} + \frac{1}{\rho} \frac{\partial}{\partial y} \left[\eta \frac{\partial v_x}{\partial y} \right] + g_x \tag{16.70}$$

Our goal is to rewrite Eq. (16.70) in terms of the time-averaged variables, \bar{v}_x , \bar{v}_y , and \bar{P} . For two-dimensional flow, the quantities \bar{v}_x , \bar{v}_y , and \bar{P} vary as (x, y, t) , but the fluctuating quantities v'_x , v'_y and P' vary as (x, y, z, t) . Even though the time-averaged flow is two-dimensional, the turbulent fluctuations are still three-dimensional.

The substitution of Eqs. (16.65) and (16.66) into Eq. (16.70) yields

$$\begin{aligned} \frac{\partial}{\partial t} (\bar{v}_x + v'_x) + \frac{\partial}{\partial x} [(\bar{v}_x + v'_x)(\bar{v}_x + v'_x)] + \frac{\partial}{\partial y} [(\bar{v}_x + v'_x)(\bar{v}_y + v'_y)] = \\ -\frac{1}{\rho} \frac{\partial}{\partial x} (\bar{P} + P') + \frac{1}{\rho} \frac{\partial}{\partial y} \left[\eta \frac{\partial}{\partial y} (\bar{v}_x + v'_x) \right] + g_x \end{aligned} \tag{16.71}$$

We want to use Eq. (16.71) in the time-average sense, and the time averages of the fluctuations, themselves, are zero. Thus, $\bar{v}'_x = 0$, $\bar{v}'_y = 0$, and $\bar{P}' = 0$. With this in mind, we now examine the time averaging of the product of the factors involving v_x :

$$\overline{(\bar{v}_x + v'_x)(\bar{v}_x + v'_x)} = \bar{v}_x \bar{v}_x + 2\bar{v}_x \bar{v}'_x + \overline{v'_x v'_x} = \bar{v}_x \bar{v}_x + 0 + 0 = \bar{v}_x \bar{v}_x$$

*Also called the temporal mean velocity or mean velocity.

$$\begin{aligned}\overline{(\bar{v}_x + v'_x)(\bar{v}_y + v'_y)} &= \overline{\bar{v}_x \bar{v}_y} + \overline{\bar{v}_x v'_y} + \overline{v'_x \bar{v}_y} + \overline{v'_x v'_y} = \bar{v}_x \bar{v}_y + 0 + 0 + \overline{v'_x v'_y} \\ &= \bar{v}_x \bar{v}_y + \overline{v'_x v'_y}.\end{aligned}$$

Even though $\overline{v'_x}$ and $\overline{v'_y}$ are each zero, we can use continuity and show that the time average of their product ($\overline{v'_x v'_y}$) must always be negative and never zero in a turbulent flow. Suppose v'_y is positive, then v'_x must be negative to compensate for the fluid leaving the unit element in the positive y -direction. On the other hand, if v'_y is negative, then v'_x must be positive. Hence, $v'_x v'_y$ is always negative and its time average can never be zero.

The instantaneous continuity equation is Eq. (16.68), and when the equation is time averaged we get

$$\left[\frac{\partial \bar{v}_x}{\partial x} + \frac{\partial \bar{v}_y}{\partial y} \right] = 0. \quad (16.72)$$

When we time average Eq. (16.71) and combine it with Eq. (16.72), the result is

$$\frac{\partial \bar{v}_x}{\partial t} + \bar{v}_x \frac{\partial \bar{v}_x}{\partial x} + \bar{v}_y \frac{\partial \bar{v}_x}{\partial y} = -\frac{1}{\rho} \frac{\partial \bar{P}}{\partial x} + \frac{1}{\rho} \frac{\partial}{\partial y} \left[\eta \frac{\partial \bar{v}_x}{\partial y} - \overline{\rho v'_y v'_x} \right] + g_x. \quad (16.73)$$

The form of Eq. (16.73) is exactly the same as our original equation for v_x , Eq. (16.70), with the exception of the term $\overline{v'_y v'_x}$, and it is this term that is at the heart of turbulent flow models.

If at the same time we had considered the temperature field of the flow, then the derived energy equation for the turbulent flow would be

$$\frac{\partial \bar{T}}{\partial t} + \bar{v}_x \frac{\partial \bar{T}}{\partial x} + \bar{v}_y \frac{\partial \bar{T}}{\partial y} = \frac{1}{\rho C_p} \frac{\partial}{\partial y} \left[k \frac{\partial \bar{T}}{\partial y} - \rho C_p \overline{v'_y T'} \right]. \quad (16.74)$$

Added to the familiar form of the energy equation is the term containing $\overline{v'_y T'}$. This term and the previous $\overline{v'_y v'_x}$ account for the effect of the turbulence on the energy and momentum transport, respectively.

We can add species conservation to the presentation by simply referring to Eq. (A) in Table 15.3. The equation of diffusion that goes with the two-dimensional flow of Eq. (16.73) is

$$\frac{\partial \bar{C}_A}{\partial t} + \bar{v}_x \frac{\partial \bar{C}_A}{\partial x} + \bar{v}_y \frac{\partial \bar{C}_A}{\partial y} = \frac{\partial}{\partial y} \left[D_A \frac{\partial \bar{C}_A}{\partial y} - \overline{v'_y C'_A} \right], \quad (16.75)$$

where we simply replaced C_A with \bar{C}_A and added $\overline{v'_y C'_A}$ to account for the effect of turbulence on the transport of species A .

Equations (16.73)-(16.75) are for those two-dimensional flow fields in which the *diffusional** terms in the x -direction are negligible and can be neglected. This was done to keep the presentation short, but at the same time show the essential connection between the equations used for laminar flow and those used for turbulent flow. The full three-dimensional

*For the instantaneous variables, these terms are $\eta(\partial^2 v_x / \partial x^2)$, $\alpha(\partial^2 T / \partial x^2)$, and $D_A(\partial^2 C_A / \partial x^2)$. They are often referred to as diffusional terms because they are momentum diffusion, heat diffusion and mass diffusion, respectively.

turbulent flow equation for the x -component of momentum, that compares to Eq. (D) in Table 2.2, is

$$\begin{aligned} \frac{\partial \bar{v}_x}{\partial t} + \bar{v}_x \frac{\partial \bar{v}_x}{\partial x} + \bar{v}_y \frac{\partial \bar{v}_x}{\partial y} + \bar{v}_z \frac{\partial \bar{v}_x}{\partial z} = & -\frac{1}{\rho} \frac{\partial \bar{P}}{\partial x} + \frac{1}{\rho} \left\{ \frac{\partial}{\partial x} \left[\eta \frac{\partial \bar{v}_x}{\partial x} - \rho \overline{v'_x v'_x} \right] \right. \\ & \left. + \frac{\partial}{\partial y} \left[\eta \frac{\partial \bar{v}_x}{\partial y} - \rho \overline{v'_y v'_x} \right] + \frac{\partial}{\partial z} \left[\eta \frac{\partial \bar{v}_x}{\partial z} - \rho \overline{v'_z v'_x} \right] \right\} + g_x. \end{aligned} \quad (16.76)$$

16.2.2 Eddy diffusivities

Again for brevity, consider transport in the y -direction. The *total* fluxes are

$$\tau_{xy} = - \left[\eta \frac{\partial \bar{v}_x}{\partial y} - \rho \overline{v'_y v'_x} \right], \quad (16.77)$$

$$q_y = - \left[k \frac{\partial \bar{T}}{\partial y} - \rho C_p \overline{v'_y T'} \right], \quad (16.78)$$

and

$$j_{Ay} = - \left[D_A \frac{\partial \bar{C}_A}{\partial y} - \overline{v'_y C'_A} \right]. \quad (16.79)$$

The total fluxes are usually written with eddy diffusivities; then they appear as

$$\tau_{xy} = -\rho (\nu + \varepsilon_M) \frac{\partial \bar{v}_x}{\partial y}, \quad (16.80)$$

$$q_y = -\rho C_p (\alpha + \varepsilon_H) \frac{\partial \bar{T}}{\partial y}, \quad (16.81)$$

and

$$j_{Ay} = -(D_A + \varepsilon_C) \frac{\partial \bar{C}_A}{\partial y}, \quad (16.82)$$

where ε_M , ε_H and ε_C are the momentum, heat, and species eddy diffusivities, respectively. We see that the diffusivities are defined such that

$$\overline{v'_y v'_x} = -\varepsilon_M \frac{\partial \bar{v}_x}{\partial y}, \quad (16.83)$$

$$\overline{v'_y T'} = -\varepsilon_H \frac{\partial \bar{T}}{\partial y}, \quad (16.84)$$

and

$$\overline{v'_x C'_A} = -\varepsilon_c \frac{\partial \overline{C_A}}{\partial y}. \quad (16.85)$$

Life would be simpler if the eddy diffusivities were only fluid properties, but they are properties of both the fluid and the fluid motion. Herein lies the difficulty in modelling turbulent flow.

16.2.3 Prandtl mixing length

In this model small packets of the fluid fluctuate normal to the direction of the mean flow. The Prandtl mixing length, ℓ , is the average distance traveled by these packets normal to the mean flow. According to the model, the fluctuations are

$$v'_x = v'_y = -\ell \frac{\partial \overline{v_x}}{\partial y},$$

so the turbulent component of the total momentum is

$$-\rho \overline{v'_x v'_y} = \rho \varepsilon_M \frac{\partial \overline{v_x}}{\partial y} = \rho \ell^2 \left[\frac{\partial \overline{v_x}}{\partial y} \right]^2.$$

Thus, the eddy momentum diffusivity becomes

$$\varepsilon_M = \ell^2 \frac{\partial \overline{v_x}}{\partial y}. \quad (16.86)$$

With only Eq. (16.86) nothing is gained because all we have done is to replace our ignorance of the behavior of ε_M with the behavior of ℓ .

For boundary layer flow, Prandtl made a second hypothesis that ℓ is proportional to distance from the wall:

$$\ell = Ky, \quad (16.87)$$

where K is a constant. In addition near the wall (but beyond the laminar sublayer), the shear stress is approximately constant ($\tau_{xy} = \tau_w$) and $\varepsilon_M \gg \nu$ so that

$$\tau_w = \rho \ell^2 \left[\frac{\partial \overline{v_x}}{\partial y} \right]^2 = \rho K^2 y^2 \left[\frac{\partial \overline{v_x}}{\partial y} \right]^2,$$

or, after integration,

$$\overline{v_x} = \frac{\tau_w^{1/2}}{\rho^{1/2} K} \ln y + C, \quad (16.88)$$

where C is an integration constant. So far we have an equation of the form that compares to experimental measurements except in the region extremely close to the wall where the laminar sublayer persists.

In the laminar sublayer, $v_x = \bar{v}_x$, and

$$\tau_{xy} = -\tau_w = \eta \frac{\partial \bar{v}_x}{\partial y},$$

so with $\bar{v}_x = 0$ at $y = 0$, we get

$$\bar{v}_x = \frac{\tau_w}{\eta} y. \tag{16.89}$$

We have characterized two regions: the laminar sublayer where $\nu \gg \varepsilon_M$ and Eq. (16.89) applies, and the turbulent layer where $\varepsilon_M \gg \nu$ and Eq. (16.88) applies. There is also a buffer layer (sometimes called the transitional layer) where $\varepsilon_M \sim \nu$.

The so-called *universal velocity profile* is a three-part equation for these three layers that is based upon the forms of Eqs. (16.88) and (16.89). Before giving the universal velocity profile, we define a dimensionless velocity u^+ and a dimensionless coordinate y^+ . They are

$$u^+ = \frac{\rho^{1/2}}{\tau_w^{1/2}} \bar{v}_x$$

and

$$y^+ = \frac{\tau_w^{1/2}}{\rho^{1/2} \nu} y.$$

With these definitions, Eq. (16.89) becomes

$$u^+ = y^+, \tag{16.90}$$

and Eq. (16.88) becomes

$$u^+ = \frac{1}{K} \ln y^+ + C. \tag{16.91}$$

The buffer layer has an equation of the same form as Eq. (16.88). By comparing these equations with empirical data, the set of equations that describe the universal velocity profile is as follows:

laminar sublayer:	$0 < y^+ < 5$	$u^+ = y^+$,
buffer layer:	$5 < y^+ < 30$	$u^+ = 5.0 \ln y^+ - 3.05$,
turbulent layer:	$30 < y^+ < 400$	$u^+ = 2.5 \ln y^+ + 5.5$.

We emphasize that the final result was determined from experimental data. The Prandtl mixing length model gave the form of the equation for fitting the data.

Prandtl's mixing length model has been found to be quite useful for analyzing two-dimensional boundary layer flows. Here we used the model to show how it forms the basis for the universal velocity profile. Launder and Spalding⁵ review the model and include empirical estimates of the mixing length, ℓ , for various applications.

⁵B. E. Launder and D. B. Spalding, *Lectures in Mathematical Models of Turbulence*, Academic Press, London, 1972, pages 23-45.

16.2.4 Two-equation model

Within at least the materials processing community, the two-equation models of Spalding and Launder⁶ have been extensively applied to assist in analyzing a variety of flows, including recirculating flows.

Equation (16.80) can be written

$$\tau_{xy} = -(\eta + \eta_t) \frac{\partial \bar{v}_x}{\partial y}, \quad (16.92)$$

where $\eta_t = \rho \varepsilon_M$ = the turbulent viscosity. In the so-called $K \sim \varepsilon$ model,* the dependent variables are the *turbulence energy*, K , and the *dissipation rate of turbulence energy*, ε . The quantities K and ε are determined by transport equations, which are differential equations to be described below. After K and ε are determined, the turbulent viscosity is calculated by

$$\eta_t = \frac{C_\eta \rho K^2}{\varepsilon}, \quad (16.93)$$

where C_η is an empirical constant.

The transport equation for K is

$$\rho \frac{DK}{Dt} = \frac{1}{\sigma_K} \left\{ \frac{\partial}{\partial x} \left[\eta_t \frac{\partial K}{\partial x} \right] + \frac{\partial}{\partial y} \left[\eta_t \frac{\partial K}{\partial y} \right] + \frac{\partial}{\partial z} \left[\eta_t \frac{\partial K}{\partial z} \right] \right\} + \eta_t G_K - \varepsilon, \quad (16.94)$$

where σ_K is another empirical constant and $\eta_t G_K$ is the turbulent counterpart to the viscous dissipation given in Eq. (A) of Table 7.5; i.e.,

$$\begin{aligned} \eta_t G_K = 2\eta_t & \left\{ \left[\frac{\partial \bar{v}_x}{\partial x} \right]^2 + \left[\frac{\partial \bar{v}_y}{\partial y} \right]^2 + \left[\frac{\partial \bar{v}_z}{\partial z} \right]^2 \right\} \\ & + \eta_t \left\{ \left[\frac{\partial \bar{v}_x}{\partial y} + \frac{\partial \bar{v}_y}{\partial x} \right]^2 + \left[\frac{\partial \bar{v}_x}{\partial z} + \frac{\partial \bar{v}_z}{\partial x} \right]^2 + \left[\frac{\partial \bar{v}_y}{\partial z} + \frac{\partial \bar{v}_z}{\partial y} \right]^2 \right\}. \end{aligned}$$

For laminar flows, we normally ignore viscous dissipation. With turbulent flows, however, η_t can be as much as 1000 η so that the turbulent dissipation is kept in Eq. (16.94).

The transport equation for ε is

$$\begin{aligned} \rho \frac{D\varepsilon}{Dt} = \frac{1}{\sigma_\varepsilon} & \left\{ \frac{\partial}{\partial x} \left[\eta_t \frac{\partial \varepsilon}{\partial x} \right] + \frac{\partial}{\partial y} \left[\eta_t \frac{\partial \varepsilon}{\partial y} \right] + \frac{\partial}{\partial z} \left[\eta_t \frac{\partial \varepsilon}{\partial z} \right] \right\} \\ & + \frac{\varepsilon}{K} (C_1 G_K - C_2 \rho \varepsilon), \end{aligned} \quad (16.95)$$

where σ_ε , C_1 and C_2 are yet more empirical constants. For most turbulent flows Launder and Spalding recommend $C_\eta = 0.09$, $\sigma_K = 1.0$, $\sigma_\varepsilon = 1.3$, $C_1 = 1.44$ and $C_2 = 1.92$. These values are normally selected or used as a starting point when calculated results are to be

⁶B. E. Launder and D. B. Spalding, *Comp. Meth. in Appl. Mech. Eng.* **3**, 269-289 (1974).

*We use K to avoid confusion with thermal conductivity, k .

compared to experiment. Equations (16.94) and (16.95), in conjunction with the components of the turbulent momentum equation, must all be solved simultaneously. The procedure is complex and requires an efficient computational scheme, such as that described by Gosman *et al.*⁷ Furthermore, modifications to some of the constants used in determining K and ε are required if axisymmetric jets or wakes are to be studied.⁸

Energy and mass transport can also be included by rewriting Eqs. (16.78) and (16.79) in the following forms:

$$q_y = -(k + k_t) \frac{\partial T}{\partial y} \quad (16.96)$$

and

$$j_{Ay} = -(D_A + D_{At}) \frac{\partial C_A}{\partial y}, \quad (16.97)$$

where we show the fluxes in the y -direction as examples to introduce the *turbulent thermal conductivity*, k_t , and the *turbulent mass diffusivity*, D_{At} . After the turbulent viscosity is known, these quantities may be estimated⁹ from

$$k_t \approx C_p \eta_t \quad (16.98)$$

and

$$D_{At} \approx \frac{\eta_t}{\rho}, \quad (16.99)$$

where C_p is the heat capacity of the fluid.

Fortunately there are software packages for solution of fluid flow problems that include options for turbulence. Some of these are PHOENICS, FLUENT, TEACH-2E, and FIDAP. Numerous examples involving materials processing can be found in Szekely *et al.*¹⁰ Here, we give Fig. 16.12 as an example of applying the $K \sim \varepsilon$ model to simulations of the temperature and velocity fields in the direct chill (DC) casting process for producing aluminum alloy ingots. The simulations were for a cylindrical ingot (550 mm diameter) of Al-4 wt.pct. Cu cast at a rate of 0.833 mm s⁻¹. In Fig. 16.12a, the simulation was based upon using the conservation equations for laminar flow with no added terms to account for the effect of turbulence. In Fig. 16.12b, the $K \sim \varepsilon$ model was employed. Turbulence enhances thermal conduction so that the thermal gradients in the melt are lessened and the melt pool ("liquid sump") is less deep with a smoother profile. The latter is thought to be more realistic of the actual process.

⁷A. D. Gosman, W. M. Pun, A. K. Runchal, D. B. Spalding, and M. Wolfshtein, *Heat and Mass Transfer in Recirculating Flows*, Academic Press, New York, 1969, pages 18-112.

⁸B. E. Launder and D. B. Spalding, *ibid.*

⁹J. Szekely, J. W. Evans and J. K. Brimacombe, *The Mathematical and Physical Modeling of Primary Metals Processing Operations*, John Wiley & Sons, New York, 1988, pages 166-167.

¹⁰J. Szekely, J. W. Evans and J. K. Brimacombe, *ibid.*

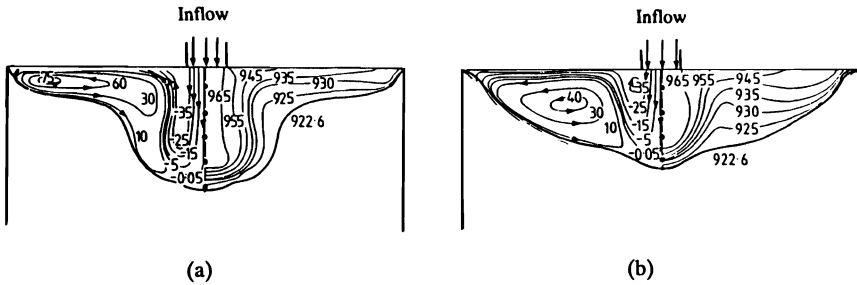


Fig. 16.12 Simulations of the temperature (right side) and streamlines (left side) in the liquid pool of a DC ingot: (a) modeled with laminar flow; (b) modeled with turbulent flow. (Adapted from S. C. Flood, L. Katgerman, A. H. Langille, S. Rogers and C. M. Read in *Light Metals 1989*, P. G. Campbell (editor), The Minerals, Metals and Materials Society, Warrendale, PA, pages 943-947.)

16.3 DISCRETIZATION IN CONVECTIVE FLOWS

In Section 16.1 we dealt exclusively with finite difference approximations of diffusive fluxes. It is worthwhile to also be acquainted with approximations of the convective terms in the conservation equations because there are some potential pitfalls. To keep our discussion simple we start with only two terms from the energy equation. From Eq. (A) in Table 7.4, we select one of the convective terms and one of the diffusive terms:

$$\rho C_p v_x \frac{dT}{dx} = \frac{d}{dx} \left[k \frac{dT}{dx} \right], \quad (16.100)$$

where we have substituted the usual Fourier's rate law for the flux.

Consider three internal nodes shown in Fig. 16.13 for discretizing the temperature. An energy balance at steady state takes on the following terms:

$$(\rho C_p v_x)_L T_L + \left[-k_L \frac{T_m - T_{m-1}}{\Delta x} \right] = (\rho C_p v_x)_R T_R + \left[-k_R \frac{T_{m+1} - T_m}{\Delta x} \right], \quad (16.101)$$

where the subscripts L and R refer to properties and variables that are evaluated at the intermediate left (L) and right (R) positions shown in Fig. 16.13. Therefore,

$$T_L = \frac{T_m}{2} + \frac{T_{m-1}}{2},$$

and

$$T_R = \frac{T_{m+1}}{2} + \frac{T_m}{2},$$

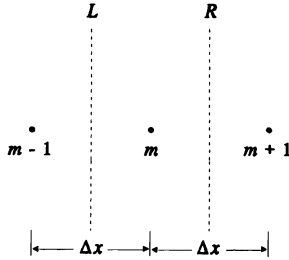


Fig. 16.13 Three internal nodes with left (*L*) and right (*R*) intermediate positions for averaging.

which give

$$\begin{aligned} \frac{(\rho C_p v_x)_L}{2} (T_m + T_{m-1}) - \frac{(\rho C_p v_x)_R}{2} (T_{m+1} + T_m) = \\ k_L \frac{(T_m - T_{m-1})}{\Delta x} - k_R \frac{(T_{m+1} - T_m)}{\Delta x}. \end{aligned} \tag{16.102}$$

Next we collect terms for each of the three temperatures and get

$$a_m T_m = a_R T_{m+1} + a_L T_{m-1}, \tag{16.103}$$

where the coefficients are defined as

$$a_m = \frac{(\rho C_p v_x)_L}{2} - \frac{(\rho C_p v_x)_R}{2} - \frac{k_L}{\Delta x} - \frac{k_R}{\Delta x},$$

$$a_R = \frac{(\rho C_p v_x)_R}{2} - \frac{k_R}{\Delta x},$$

and

$$a_L = -\frac{(\rho C_p v_x)_L}{2} - \frac{k_L}{\Delta x}.$$

Equation (16.103) is perfectly adequate provided we realize that there are severe limitations on the grid spacing Δx in order to guarantee numerical stability. This is the potential pitfall because we have discretized a differential equation with an advective term by *central differencing*.

To illustrate the pitfall, remember that continuity requires

$$(\rho v_x)_R = (\rho v_x)_L.$$

608 Numerical Methods and Models

Also let us assume $k_L = k_R = k$ and $(C_p)_R = (C_p)_L = C_p$, then Eq. (16.103) becomes

$$-\frac{2k}{\Delta x} T_m = \left[\frac{\rho C_p v_x}{2} - \frac{k}{\Delta x} \right] T_{m+1} + \left[-\frac{\rho C_p v_x}{2} - \frac{k}{\Delta x} \right] T_{m-1}$$

or

$$4T_m = (2 - P)T_{m+1} + (2 + P)T_{m-1}, \tag{16.104}$$

where $P \equiv \rho C_p v_x \Delta x / k$. The instability is associated with the coefficient $(2 - P)$. If we allow $P > 2$, we get a nonsensible result. This can be seen by a simple example. Suppose $P = 4$, $T_{m+1} = 100$ K, and $T_{m-1} = 200$ K. A sensible result would give $100 < T_m < 200$ K, but Eq. (16.103) gives $T_m = 250$ K, which is clearly nonsensible. Suppose $P = 1$, and T_{m+1} and T_{m-1} are 100 K and 200 K, as before. Now Eq. (16.104) gives $T_m = 175$ K, which is sensible. If we are willing to accept that P must be less than two, then our calculations will be stable, but this can severely restrict us because $(v_x \Delta x) < 2\alpha$. So either we restrict ourselves to situations with convective speeds that are rather small, or we must select Δx to be small and thereby sacrifice computational efficiency. This disadvantage in discretizing the equation with the central differencing scheme has led to the *upwind finite difference* method.

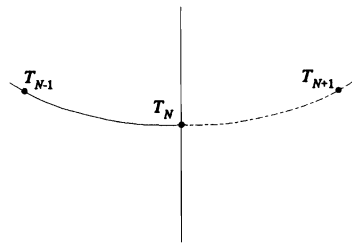
In the upwind method, we focus on the advection terms which form the left side (L.S.) of Eq. (16.102). To simplify our notation somewhat, let $u = \rho C_p v_x$. Then the L.S. is replaced¹¹ with

$$\begin{aligned} \text{L.S.} = \frac{1}{2} \{ & (u_L + |u_L|)T_{m-1} - (u_r - |u_r|)T_{m+1} \\ & - (u_R + |u_R| - u_L + |u_L|)T_m \}. \end{aligned} \tag{16.105}$$

The diffusion terms in Eq. (16.102) are evaluated with the usual central differencing so no change in the right side is needed. Equation (16.105) is based upon always evaluating the advected energy into or out of the unit element at the *upstream* node.

PROBLEMS

16.1 Derive an alternative to Eq. (16.7) for an insulated surface, in a way which is different than that in the text. The insulated surface is at node N , and there is an imaginary node at $N+1$ with the same temperature as T_{N-1} .



¹¹Equation (16.105) is from D. Poulidakos and S. Kimura in A. Bejan, *Convection Heat Transfer*, John Wiley & Sons, New York, 1984, pages 440-446.

16.2 Use finite difference approximations and set up the one-dimensional heat conduction problem that is specified as follows:

$$\frac{\partial T}{\partial t} = \alpha \frac{\partial^2 T}{\partial x^2},$$

with

$$T(L, t) = T_L \quad t > 0,$$

$$T(0, t) = T_0 \quad t > 0,$$

and

$$T(x, 0) = T_i.$$

Divide the domain $0 \leq x \leq L$ into four segments so that $\Delta x = L/4$. a) Write the set of algebraic equations in matrix form using the Euler method. b) Repeat using the Crank-Nicolson method.

16.3 Write a computer program that can be used to solve for $T(x, t)$ in Problem 16.2a.

16.4 Write a computer program that can be used to solve for $T(x, t)$ in Problem 16.2b.

16.5 Consider the problem in Fig. 16.1 and the VAX-BASIC program for solving Eq. (16.31). Modify and use the program to solve for the time required for the center of the core to heat to 873 K, when molten aluminum encapsulates a plaster core. Thermal data can be found with the problems of Chapter 10.

16.6 Consider one-dimensional homogenization as in Section 13.5. The following microsegregation data in an Fe-Ni alloy are reported.

$x, \mu\text{m}$	% Ni	$x, \mu\text{m}$	% Ni	$x, \mu\text{m}$	% Ni
0	12	30	16	60	29
10	13	40	18.5	70	37
20	14	50	23	80	45

- Plot the data and determine the average concentration of nickel.
- Set up the set of algebraic equations that result from making finite difference approximations. For simplicity, use $\Delta x = 20 \mu\text{m}$ and the Euler method.

16.7 Extend the one-dimensional homogenization model of Problem 16.6 to the two-dimensional model considered in Section 16.1.3. For $L = \ell = 80 \mu\text{m}$, the following microsegregation data are given (see Fig. 16.7 for identification of the nodes).

Nodes	% Ni	Nodes	% Ni
0,15	14	5,10	16
1,11	23	6	29
2,7	37	8,13	13
3	45	9	14
4,14	13	12	12
		Average	20.25

610 Numerical Methods and Models

- a) The diffusion coefficient for nickel in γ -iron at $1273 \leq T \leq 1560$ K is

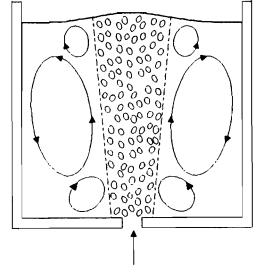
$$D = \exp(0.0519 X_{Ni} + 1.51) \exp\left[-\frac{38,380 + 5.85 X_{Ni}}{T}\right],$$

where D = diffusion coefficient, $\text{cm}^2 \text{s}^{-1}$; X_{Ni} = atom percent Ni; T = temperature, K. Calculate an appropriate diffusion coefficient for homogenizing the alloy at 1350 K.

- b) Determine the residual segregation index as a function of time for homogenization at 1350 K.

16.8 Consider radiant heating of a poorly conducting slab as described in Section 16.1.4. Using the same thermal properties and furnace temperature (2020 K), determine the time to heat the center to 2000 K as a function of the thickness of the slab, in the range of 30 mm to 90 mm.

16.9 Gas is injected into the bottom of a melt contained in a large cylindrical vessel; the recirculating flow is turbulent. Assume axisymmetric flow and write an appropriate momentum equation for the liquid.



APPENDIX A

Physical Constants

Quantity	Symbol	Value
Gas constant	R	$8.31441 \text{ J K}^{-1} \text{ mol}^{-1}$ $1.985857 \text{ Btu lbmol}^{-1} \text{ }^\circ\text{R}^{-1}$ $8.205 \times 10^{-2} \text{ m}^3 \text{ atm kmol}^{-1} \text{ K}^{-1}$
Boltzmann constant	k_B	$1.3807 \times 10^{-23} \text{ J K}^{-1} \text{ molecule}^{-1}$
Avogadro's number	N_0	$6.02204 \times 10^{23} \text{ molecules mol}^{-1}$ $6.02204 \times 10^{26} \text{ molecules kmol}^{-1}$
Planck constant	h	$6.62618 \times 10^{-34} \text{ J s molecule}^{-1}$
Stefan-Boltzmann constant	σ	$5.6703 \times 10^{-8} \text{ W m}^{-2} \text{ K}^{-4}$ $0.1714 \times 10^{-8} \text{ Btu h}^{-1} \text{ ft}^{-2} \text{ }^\circ\text{R}^{-4}$
Gravitational acceleration at sea level	g	9.80665 m s^{-2} 32.174 ft s^{-2}
Standard atmospheric pressure	P	$1.01325 \times 10^5 \text{ N m}^{-2}$ $14.69595 \text{ lb}_f \text{ in}^{-2} \text{ (psi)}$ $2116.22 \text{ lb}_f \text{ ft}^{-2}$

APPENDIX B

Thermal Properties

The compilations given in Tables B.1-B.3 are only samplings of thermal data. More comprehensive sources for data are listed here.

1. Y. S. Touloukian and C. Y. Ho (eds.), *Thermophysical Properties of Matter*, IFI/Plenum, New York, NY.
 - Volume 1. Thermal Conductivity-Metallic Elements and Alloys (1970).
 - Volume 2. Thermal Conductivity-Nonmetallic Solids (1970).
 - Volume 3. Thermal Conductivity-Nonmetallic Liquids and Gases (1970).
 - Volume 4. Specific Heat-Metallic Elements and Alloys (1970).
 - Volume 5. Specific Heat-Nonmetallic Solids (1970).
 - Volume 6. Specific Heat-Nonmetallic Liquids and Gases (1970).
 - Volume 7. Thermal Radiative Properties-Metallic Elements and Alloys (1970).
 - Volume 8. Thermal Radiative Properties-Nonmetallic Solids (1972).
 - Volume 9. Thermal Radiative Properties-Coatings (1972).
 - Volume 10. Thermal Diffusivity (1973).
 - Volume 11. Viscosity (1975).
 - Volume 12. Thermal Expansion-Metallic Elements and Alloys (1975).
 - Volume 13. Thermal Expansion-Nonmetallic Solids (1977).
2. J. Brandrup and E. H. Immergut (eds.), *Polymer Handbook*, third edition, John Wiley, New York, NY (1989).
3. V. Shah, *Handbook of Plastics Testing Technology*, John Wiley, New York, NY (1984).
4. ASM International Handbook Committee, *Engineered Materials Handbook*, Metals Park, OH.
 - Volume 1. Composites (1987).
 - Volume 2. Engineering Plastics (1988).

614 Appendix B

5. E. A. Brandes and G. B. Brook (eds.), *Smithells Metals Reference Book*, seventh edition, Butterworths-Heinemann, Oxford (1992).
6. R. D. Pehlke, A. Jeyarajan and H. Wada, *Summary of Thermal Properties for Casting Alloys and Mold Materials*, National Science Foundation, Applied Research Division, Grant No. DAR78-26171, 1982.
7. P. D. Desai, R. K. Chu, R. H. Bogaard, M. W. Ackermann and C. Y. Ho, Part I: *Thermophysical Properties of Carbon Steels*; Part II: *Thermophysical Properties of Low Chromium Steels*; Part III: *Thermophysical Properties of Nickel Steels*; Part IV: *Thermophysical Properties of Stainless Steels*, CINDAS Special Report, Purdue University, West Lafayette, IN, September 1976.
8. N. B. Vargaftik, *Tables of Thermophysical Properties of Liquids and Gases*, 2nd edition, Hemisphere Publishing Corp., New York, 1975.
9. L. M. Sheppard and G. Geiger (eds.), *Ceramic Source*, vol. 6, The American Ceramic Society, Westerville, OH (1991).

Table B.1 Thermal Properties of Selected Metallic Materials

Material	Composition wt.pct.	T K	ρ kg m ⁻³	C_p kJ kg ⁻¹ K ⁻¹	k W m ⁻¹ K ⁻¹	H_f kJ kg ⁻¹
Aluminum	Al	300	2698	0.90	237	398
		600	2636	1.04	232	
		933 (s)	2555	1.19	211	
		933 (ℓ)	2368	1.09	91	
		1200	2296	1.09	99	
	Al-4.5Cu	300	2830	0.88	188	
		600	2750	1.02	192	
Copper	Cu	300	8920	0.38	398	205
		800	8690	0.44	371	
		1356 (s)	8400	0.49	330	
		1356 (ℓ)	8000	0.49	166	
		1600	7800	0.49	174	
Brass	Cu-40Zn	300	8400	0.39	127	
		600	8240	0.42	158	
		900	8080	0.45	150	
Iron	Fe	300	7860	0.43	79.6	277
		600	7780	0.58	54.6	
		900	7670	0.76	37.4	
		1033	7620	1.26 (max)	—	
		1040	7620	1.16	—	
		1184 (α)	7570	0.72	28.2	
		1184 (γ)	7660	0.61	28.2	
		1400	7515	0.64	30.6	
		1673 (γ)	7397	0.68	33.7	
		1673 (δ)	7344	0.73	33.4	
		1809 (δ)	7257	0.76	34.6	
		1809 (ℓ)	7022	0.79	40.3	
		2000	6866	0.79	42.6	
AISI 1026	Fe-0.23C-0.63Mn	300	7860	0.48	52.4	
		700	7730	0.61	41.2	
		1000	7645	0.84	29.7	
		1023	7640	1.44 (max)	28.6	
		1100 (γ)	7620	0.64	25.9	
		1300	7550	0.64	27.8	
AISI 304	Fe-19Cr-10Ni	300	8260	0.50	15.2	
		600	8150	0.56	19.7	
		900	8030	0.65	24.0	
		1200	7890	0.65	27.9	
		1500	—	0.67	31.9	
Nickel	Ni	300	8900	0.44	89.2	297
		600	8780	0.60	65.3	
		631	8770	0.67 (max)	63.8	
		702	8740	0.52	65.3	
		1728 (s)	(8280)	0.65	87.5	
		1728 (ℓ)	7905	0.66	—	
		1900	7700	0.66	—	
MAR-M200	Ni-0.15C-9Cr-10Co- 12.5W-1.8Cb-2Ti-5Al	300	8520	0.40	12.7	
		600	8430	0.42	14.0	
		900	8330	0.46	16.8	
		1200	8180	0.52	22.8	

*Data collected from several sources.

Table B.2 Thermal Properties of Selected Ceramic Materials*

Material	Crystal Structure	ρ (kg m ⁻³)	β Thermal Expansion (10 ⁻⁶ K ⁻¹)	k Thermal Conductivity (W m ⁻¹ K ⁻¹)	C_p Specific Heat (kJ kg ⁻¹ K ⁻¹)	ϵ Emissivity**
Pyrex glass	Amorphous	2520	4.6	1.3 at 400 K 1.7 at 800 K	0.335 at 100 K 0.117 at 700 K	0.85 at 100 K (N) 0.85 at 900 K (N) 0.75 at 1100 K (N)
TiO ₂	Rutile tetragonal	4250	9.4	8.8 at 400 K	0.799 at 400 K	0.83 at 450 K (T) 0.89 at 1300 K (T)
	Anatase tetragonal	3840		3.3 at 1400 K	0.920 at 1700K	
	Brookite orthorhombic	4170				
Al ₂ O ₃	Hexagonal	3970	7.2-8.6	27.2 at 400 K	0.1088	0.75 at 100 K (N) 0.53 at 1000 K (N) 0.41 at 1600 K (N)
				5.8 at 1400 K	0.20 at 1273 K	
Cr ₂ O ₃	Hexagonal	5210	7.5	10-33	0.670 at 300 K 0.837 at 1000 K 0.879 at 1600 K	0.69 (N) 0.91 (N)
Mullite	Orthorhombic	2800	5.7	5.2 at 400 K	0.1046	0.5 at 1200 K (N) 0.65 at 1500 K (N)
				3.3 at 1400 K	0.20 at 1273 K	
Partially stabilized ZrO ₂	Cubic, monoclinic, tetragonal	5700-5750	8.0-10.6	1.8-2.2	0.400	
Fully stabilized ZrO ₂	Cubic	5560-6100	13.5	1.7 at 400 K	0.502 at 400 K	0.82 at 0 K (N) 0.4 at 1200 K 0.5 at 2000 K (N)
				1.9 at 1600 K	0.669 at 2400 K	
Plasma-sprayed ZrO ₂	Cubic, monoclinic, tetragonal	5600-5700	7.6-10.5	0.69-2.4		0.61-0.68 at 700 K (T) 0.25-0.4 at 2800 K (T)
CeO ₂	Cubic	7280	13	9.6 at 400 K	0.370 at 300 K	0.65 at 1300 K (T) 0.45 at 1550 K (T) 0.40 at 1800 K (T)
				1.2 at 1400 K	0.520 at 1200 K	

Table B.2 Thermal Properties of Selected Ceramic Materials* (continued)

Material	Crystal Structure	Density (kg m^{-3})	β Thermal Expansion (10^{-6}K^{-1})	k Thermal Conductivity ($\text{W m}^{-1} \text{K}^{-1}$)	C_p Specific Heat ($\text{kJ kg}^{-1} \text{K}^{-1}$)	ϵ Emissivity**
TiB ₂	Hexagonal	4500-4620	8.1	65-120 at 300 K 54-122 at 2300 K	0.632 at 300 K 0.1155 at 1400 K	0.8 at 1000 K (N) 0.85 at 1400 K (N) 0.4 at 2800 K (N)
TiC	Cubic	4920	7.4-8.6	33 at 400 K 43 at 1400 K	0.544 at 293 K 0.1046 at 1366 K	0.5 at 800 K (N) 0.85 at 1500 K 0.38 at 2800 K (N)
TaC	Cubic	1440-1450	6.7	32 at 400 K 40 at 1400 K	0.167 at 273 K 0.293 at 1366 K	0.2 at 1600 K (N) 0.33 at 3000 K (N)
C ₁₅ C ₂	Orthorhombic	6700	9.8	19	0.502 at 273 K 0.837 at 811 K	
SiC	α hexagonal β cubic	3210 3210	4.3-5.6	63-155 at 400 K 21-33 at 1400 K	0.628-0.1046	0.85 at 400 K (N) 0.80 at 1800 K (N)
SiC (CVD)	β cubic	3210	5.5	121 at 400 K 34.6 at 1600 K	0.837 at 400 K 0.1464 at 2000 K	
Si ₃ N ₄	α hexagonal β hexagonal	3180 3190	3.0	9-30 at 400 K	0.400-1.600	0.9 at 600 K (N) 0.8 at 1300 K (N)
TiN	Cubic	5430-5440	8.0	24 at 400 K 67.8 at 1773 K 56.9 at 2573 K	0.628 at 273 K 0.1046 at 1366 K	0.4 at 800 K (N) 0.8 at 1400 K (N) 0.5 at 2100 K (N) 0.33 at 3000 K (N)
Graphites (with grain)	Hexagonal	2210	0.1-19.4	1.67-518.8	0.711-1.423	0.8 at 1366 K (T)

*From L. M. Sheppard and G. Geiger (eds.), *Ceramic Source*, vol. 6, The American Ceramic Society, Westerville, OH, 1991, p. 345.

**N is for normal, and T is for total hemispherical emissivity.

Table B.3 Thermal Properties of Selected Polymers Used for Molding and Extrusion

Material	ρ kg m ⁻³	C_p kJ kg ⁻¹ K ⁻¹	k W m ⁻¹ K ⁻¹	β^* 10 ⁻⁵ K ⁻¹
Polyethylene				
low density	910-925	2.3	0.33	10-22
high density	940-965	2.3	0.46-0.50	11-13
Polypropylene	900-910	1.9	0.12	8.1-10
Polystyrene				
general purpose	1040-1050	1.3	0.10-0.14	6-8
impact resistant	1030-1060	1.3-1.5	0.042-0.13	3.4-21
Polymethylmethacrylate	1170-1200	1.5	0.17-0.25	5-9
Polyvinylchloride				
rigid	1300-1580	0.84-1.2	0.15-0.21	5-10
plasticized	1160-1350	1.3-2.1	0.13-0.17	7-25
ABS**	1030-1060	1.3-1.7	0.19-0.33	8-10
Cellulose acetate	1220-1340		0.17-0.33	8-18
Fluoropolymers				
-CF ₂ -CF ₂ - (teflon)	2140-2200	1.0	0.25	10
-CF ₂ -CFCl-	2100-2200	0.92	0.20-0.22	4.5-7.0
Nylon-6,6	1130-1150	1.7	0.24	8
Polycarbonate	1200	2.2	0.20	6.8
Polysulfone	1240	1.3	0.12	5.2-5.6
Epoxy-glass composite	1600-2000	3.3	0.17-0.42	1-5

* β is linear expansion coefficient

**Acrylonitrile-butadiene-styrene

Data selected from M. Chanda and S. K. Roy, *Plastics Technology Handbook*, Marcel Dekker, New York, NY, 1987, Appendix 3.

Table B.4 Thermophysical Properties of Gases at Atmospheric Pressure*

T (K)	ρ (kg m ⁻³)	C_p (kJ kg ⁻¹ K ⁻¹)	$\eta \times 10^7$ (N s m ⁻²)	$\nu \times 10^6$ (m ² s ⁻¹)	$k \times 10^3$ (W m ⁻¹ K ⁻¹)	$\alpha \times 10^6$ (m ² s ⁻¹)	Pr
Air							
300	1.1614	1.007	184.6	15.89	26.3	22.5	0.707
400	0.8711	1.014	230.1	26.41	33.8	38.3	0.690
500	0.6964	1.030	270.1	38.79	40.7	56.7	0.684
600	0.5804	1.051	305.8	52.69	46.9	76.9	0.685
700	0.4975	1.075	338.8	68.10	52.4	98.0	0.695
800	0.4354	1.099	369.8	84.93	57.3	120	0.709
900	0.3868	1.121	398.1	102.9	62.0	143	0.720
1000	0.3482	1.141	424.4	121.9	66.7	168	0.726
1200	0.2902	1.175	473.0	162.9	76.3	224	0.728
1400	0.2488	1.207	530	213	91	303	0.703
1600	0.2177	1.248	584	268	106	390	0.688
1800	0.1935	1.286	637	329	120	482	0.683
2000	0.1741	1.337	689	396	137	589	0.672
Carbon Dioxide (CO ₂)							
300	1.7730	0.851	149	8.40	16.55	11.0	0.766
400	1.3257	0.942	190	14.3	24.3	19.5	0.737
500	1.0594	1.02	231	21.8	32.5	30.1	0.725
600	0.8826	1.08	270	30.6	40.7	42.7	0.717
700	0.7564	1.13	305	40.3	48.1	56.3	0.717
800	0.6614	1.17	337	51.0	55.1	71.2	0.716
Carbon Monoxide (CO)							
300	1.1233	1.043	175	15.6	25.0	21.3	0.730
400	0.8421	1.049	218	25.9	31.8	36.0	0.719
500	0.67352	1.065	254	37.7	38.1	53.1	0.710
600	0.56126	1.088	286	51.0	44.0	72.1	0.707
700	0.48102	1.114	315	65.5	50.0	93.3	0.702
800	0.42095	1.140	343	81.5	55.5	116	0.705
Helium (He)							
300	0.1625	5.193	199	122	152	180	0.680
400	0.1219	5.193	243	199	187	295	0.675
500	0.09754	5.193	283	290	220	434	0.668
600	-	5.193	320	-	252	-	-
700	0.06969	5.193	350	502	278	768	0.654
800	-	5.193	382	-	304	-	-
900	-	5.193	414	-	330	-	-
1000	0.04879	5.193	446	914	354	1400	0.654
Water Vapor (steam)							
380	0.5863	2.060	127.1	21.68	24.6	20.4	1.06
400	0.5542	2.014	134.4	24.25	26.1	23.4	1.04
500	0.4405	1.985	170.4	38.68	33.9	38.8	0.998
600	0.3652	2.026	206.7	56.60	42.2	57.0	0.993
700	0.3140	2.085	242.6	77.26	50.5	77.1	1.00
800	0.2739	2.152	278.6	101.7	59.2	100	1.01

Table B.4 Thermophysical Properties of Gases at Atmospheric Pressure* (continued)

T (K)	ρ (kg m ⁻³)	C_p (kJ kg ⁻¹ K ⁻¹)	$\eta \times 10^7$ (N s m ⁻²)	$\nu \times 10^6$ (m ² s ⁻¹)	$k \times 10^3$ (W m ⁻¹ K ⁻¹)	$\alpha \times 10^6$ (m ² s ⁻¹)	Pr
Hydrogen (H ₂)							
300	0.08078	14.31	89.6	111	183	158	0.701
400	0.06059	14.48	108.2	179	226	258	0.695
500	0.04848	14.52	126.4	261	266	378	0.691
600	0.04040	14.55	142.4	352	305	519	0.678
700	0.03643	14.61	157.8	456	342	676	0.675
800	0.03030	14.70	172.4	569	378	849	0.670
900	0.02694	14.83	186.5	692	412	1030	0.671
1000	0.02424	14.99	201.3	830	448	1230	0.673
1100	0.02204	15.17	213.0	966	488	1460	0.662
1200	0.02020	15.37	226.2	1120	528	1700	0.659
1300	0.01865	15.59	238.5	1279	568	1955	0.655
1400	0.01732	15.81	250.7	1447	610	2230	0.650
1500	0.01616	16.02	262.7	1626	655	2530	0.643
1600	0.0152	16.28	273.7	1801	697	2815	0.639
1700	0.0143	16.58	284.9	1992	742	3130	0.637
1800	0.0135	16.96	296.1	2193	786	3435	0.639
1900	0.0128	17.49	307.2	2400	835	3730	0.643
2000	0.0121	18.25	318.2	2630	878	3975	0.661
Nitrogen (N ₂)							
300	1.1233	1.041	178.2	15.86	25.9	22.1	0.716
400	0.8425	1.045	220.4	26.16	32.7	37.1	0.704
500	0.6739	1.056	257.7	38.24	38.9	54.7	0.700
600	0.5615	1.075	290.8	51.79	44.6	73.9	0.701
700	0.4812	1.098	321.0	66.71	49.9	94.4	0.706
800	0.4211	1.122	349.1	82.90	54.8	116	0.715
900	0.3743	1.146	375.3	100.3	59.7	139	0.721
1000	0.3368	1.167	399.9	118.7	64.7	165	0.721
1100	0.3062	1.187	423.2	138.2	70.0	193	0.718
1200	0.2807	1.204	445.3	158.6	75.8	224	0.707
1300	0.2591	1.219	466.2	179.9	81.0	256	0.701
Oxygen (O ₂)							
300	1.284	0.920	207.2	16.14	26.8	22.7	0.711
400	0.9620	0.942	258.2	26.84	33.0	36.4	0.737
500	0.7698	0.972	303.3	39.40	41.2	55.1	0.716
600	0.6414	1.003	343.7	53.59	47.3	73.5	0.729
700	0.5498	1.031	380.8	69.26	52.8	93.1	0.744
800	0.4810	1.054	415.2	86.32	58.9	116	0.743
900	0.4275	1.074	447.2	104.6	64.9	141	0.740
1000	0.3848	1.090	477.0	124.0	71.0	169	0.733
1100	0.3498	1.103	505.5	144.5	75.8	196	0.736
1200	0.3206	1.115	532.5	166.1	81.9	229	0.725
1300	0.2960	1.125	588.4	188.6	87.1	262	0.721

*Condensation of Table A.4 in F. P. Incropera and D. P. DeWitt, *Fundamentals of Heat and Mass Transfer*, 3rd edition, John Wiley, New York, NY, 1990.

APPENDIX C

Conversion Factors

Table C.1 Linear measure equivalents

Multiply by value in table to obtain these units →		kilometer (km)	meter (m)	centimeter (cm)	millimeter (mm)	micrometer (μm)	angstrom (\AA)	foot (ft)	inch (in)
Given in these units ↓									
kilometer (km)	1	10^3	10^5	10^6	10^9	10^{13}	3.2808×10^3	3.937×10^4	
meter (m)	10^{-3}	1	10^2	10^3	10^6	10^{10}	3.2808	3.937×10^1	
centimeter (cm)	10^{-5}	10^{-2}	1	10	10^4	10^8	3.2808×10^{-2}	3.937×10^{-1}	
millimeter (mm)	10^{-6}	10^{-3}	10^{-1}	1	10^3	10^7	3.2808×10^{-3}	3.937×10^{-2}	
micrometer (μm)	10^{-9}	10^{-6}	10^{-4}	10^{-3}	1	10^4	3.2808×10^{-6}	3.937×10^{-5}	
angstrom (\AA)	10^{-13}	10^{-10}	10^{-8}	10^{-7}	10^{-4}	1	3.2808×10^{-10}	3.937×10^{-9}	
foot (ft)	3.048×10^{-4}	3.048×10^{-1}	30.48	3.048×10^2	3.048×10^5	3.048×10^9	1	12	
inch (in)	2.54×10^{-5}	2.54×10^{-2}	2.54	25.4	2.54×10^4	2.54×10^8	8.333×10^{-2}	1	

Table C.2 Volume equivalents

Multiply by value in table to obtain these units →		cubic centimeter (cm ³)	cubic feet (ft ³)	cubic inch (in ³)	cubic meter (m ³)	gallons (U.S.) (gal)	liters* (L)
Given in these units ↓							
cubic centimeter (cm ³)	1		3.531×10^{-5}	6.102×10^{-2}	10^{-6}	2.642×10^{-4}	10^{-3}
cubic feet (ft ³)	2.832×10^4		1	1.728×10^3	2.832×10^{-2}	7.481	28.32
cubic inch (in ³)	16.39		5.787×10^{-4}	1	1.639×10^{-5}	4.329×10^{-3}	1.639×10^{-2}
cubic meter (m ³)	10^6		35.31	6.102×10^4	1	2.642×10^2	10^3
gallons (U.S.) (gal)	3.785×10^3		1.337×10^{-1}	2.31×10^2	3.785×10^{-3}	1	3.785
liters (L)	10^3		3.531×10^{-2}	6.102×10^1	10^{-3}	2.642×10^{-1}	1

Table C.3 Mass equivalents

Multiply by value in table to obtain these units →	Given in these units ↓						
	gram (g)	kilogram (kg)	pound (lb _m)	ton, long	ton, short	ounces (oz)	tonne* (t)
gram (g)	1	10^{-3}	2.205×10^{-3}	9.84×10^{-7}	1.102×10^{-6}	3.527×10^{-2}	10^{-6}
kilogram (kg)	10^3	1	2.205	9.842×10^{-4}	1.102×10^{-3}	35.27	10^{-3}
pound (lb _m)	4.536×10^2	0.4536	1	4.464×10^{-4}	5.0×10^{-4}	16	4.938×10^{-4}
ton, long	1.016×10^6	1.016×10^3	2.24×10^3	1	1.12	3.584×10^4	1.016
ton, short	9.072×10^5	9.072×10^2	2.00×10^3	8.929×10^{-1}	1	3.20×10^4	0.9074
ounces (oz)	28.35	2.835×10^{-2}	6.25×10^{-2}	2.79×10^{-5}	3.125×10^{-5}	1	1.877×10^{-5}
tonne* (t)	10^6	10^3	2.205×10^3	9.842×10^{-1}	1.102	5.327×10^4	1

*metric

Table C.4 Density equivalents

Multiply by value in table to obtain these units →	g cm ⁻³					lb _m in ⁻³
	Given in these units ↓	g L ⁻¹	kg m ⁻³	lb _m ft ⁻³	kg m ⁻³	
g cm ⁻³	1	10 ³	10 ³	62.43	62.43	3.613 × 10 ⁻²
g L ⁻¹	10 ⁻³	1	1	6.243 × 10 ⁻²	6.243 × 10 ⁻²	3.613 × 10 ⁻⁵
kg m ⁻³	10 ⁻³	1	1	6.243 × 10 ⁻²	6.243 × 10 ⁻²	3.613 × 10 ⁻⁵
lb _m ft ⁻³	1.602 × 10 ⁻²	16.02	16.02	1	1	5.787 × 10 ⁻⁴
lb _m in ⁻³	27.68	2.768 × 10 ⁴	2.768 × 10 ⁴	1.728 × 10 ³	1.728 × 10 ³	1

Table C.5 Force equivalents

Multiply by value in table to obtain these units →	dyne (g cm s ⁻²)				poundal (lb _m ft s ⁻²)	pound force (lb _f)
	Given in these units ↓	Newton, N (kg m s ⁻²)	Newton, N (kg m s ⁻²)	Newton, N (kg m s ⁻²)		
dyne (g cm s ⁻²)	1	10 ⁻⁵	10 ⁻⁵	7.233 × 10 ⁻⁵	7.233 × 10 ⁻⁵	2.248 × 10 ⁻⁶
Newton, N (kg m s ⁻²)	10 ⁵	1	1	7.233	7.233	2.248 × 10 ⁻¹
poundal (lb _m ft s ⁻²)	1.3826 × 10 ⁴	1.3826 × 10 ⁻¹	1.3826 × 10 ⁻¹	1	1	3.108 × 10 ⁻²
pound force (lb _f)	4.448 × 10 ⁵	4.448	4.448	32.17	32.17	1

Table C.6 Energy equivalents

	Multiply by value in table to obtain these units →		Given in these units ↓							
	Btu	cal	erg	ft lb _f	hp h [*]	joule, J	kcal	kW h	L atm	
Btu	1	2.52×10^2	1.055×10^{10}	7.7816×10^2	3.93×10^{-4}	1.055×10^3	2.520×10^{-1}	2.93×10^{-4}	10.41	
cal	3.97×10^{-3}	1	4.184×10^7	3.086	1.558×10^{-6}	4.184	10^{-3}	1.162×10^{-6}	4.129×10^{-2}	
erg	9.478×10^{-11}	2.39×10^{-8}	1	4.376×10^{-8}	3.725×10^{-14}	10^{-7}	2.39×10^{-11}	2.773×10^{-14}	9.869×10^{-10}	
ft lb _f	1.285×10^{-3}	3.241×10^{-1}	1.356×10^7	1	5.0505×10^{-7}	1.356	3.241×10^{-4}	3.766×10^{-7}	1.338×10^{-2}	
hp h [*]	2.545×10^3	6.4162×10^5	2.6845×10^{13}	1.98×10^6	1	2.6845×10^6	6.4162×10^2	7.455×10^{-1}	2.6494×10^4	
joule, J	9.478×10^{-4}	2.39×10^{-1}	10^7	7.376×10^{-1}	3.725×10^{-7}	1	2.39×10^{-4}	2.773×10^{-7}	9.869×10^{-3}	
kcal	3.9657	10^3	4.184×10^{10}	3.086×10^3	1.558×10^{-3}	4.184×10^3	1	1.162×10^{-3}	41.29	
kW h	3.4128×10^3	8.6057×10^5	3.6×10^9	2.655×10^6	1.341	3.6×10^6	8.6057×10^2	1	3.5534×10^4	
L atm	9.604×10^{-2}	24.218	1.0133×10^5	74.73	3.774×10^{-5}	1.0133×10^2	2.422×10^{-2}	2.815×10^{-5}	1	

*hp h is horsepower hour.

Table C.7 Pressure equivalents

Multiple by value in table to obtain these units →	atmosphere (atm)	bar	lb _f ft ⁻²	lb _f in ⁻²	N m ⁻² (Pascal, Pa)	Column of Hg at 0°C		Column of H ₂ O at 15°C	
						in	mm	ft	mm
Given in these units ↓									
atmosphere (atm)	1	1.0133	2.1162×10^3	14.696	1.0133×10^5	2.992×10^1	7.60×10^2	33.93	1.0342×10^4
bar	0.9869	1	2.0886×10^3	14.503	1×10^5	2.9529×10^1	7.5002×10^2	33.48	1.0206×10^4
lb _f ft ⁻²	4.7252×10^{-4}	4.7879×10^{-4}	1	6.9444×10^{-3}	4.7879×10^1	1.414×10^{-2}	3.591×10^{-1}	1.603×10^{-2}	4.887
lb _f in ⁻²	6.8043×10^{-2}	6.8946×10^{-2}	144	1	6.8944×10^3	2.036	5.171×10^1	2.309	7.0378×10^2
N m ⁻² (Pascal, Pa)	9.8687×10^{-5}	1×10^{-5}	2.0886×10^{-2}	1.4504×10^{-4}	1	2.9529×10^{-4}	7.5002×10^{-3}	3.3458×10^{-4}	1.0198×10^{-1}
Hg column, in	3.3421×10^{-2}	3.3866×10^{-2}	7.0726×10^1	4.9124×10^{-1}	3.3864×10^3	1	2.54×10^1	1.134	3.456×10^2
Hg column, mm	1.3158×10^{-3}	1.3333×10^{-3}	2.7845	1.934×10^{-2}	1.3332×10^2	3.937×10^{-2}	1	4.464×10^{-2}	13.61
H ₂ O column, ft	2.947×10^{-2}	2.986×10^{-2}	62.372	4.3314×10^{-1}	2.9888×10^3	8.819×10^{-1}	22.4	1	3.048×10^2
H ₂ O column, mm	9.669×10^{-5}	9.797×10^{-5}	2.046×10^{-1}	1.421×10^{-3}	9.806	2.893×10^{-3}	7.349×10^{-2}	3.281×10^{-3}	1

Table C.8 Viscosity equivalents

Given in these units ↓	Multiply by value in table to obtain these units →					
	centipoise (cP)	$\text{g cm}^{-1} \text{s}^{-1}$ (poise, P)	$\text{lb}_m \text{ft}^{-1} \text{s}^{-1}$	$\text{lb}_m \text{ft}^{-1} \text{hr}^{-1}$	$\text{lb}_y \text{s ft}^{-2}$	N s m^{-2}
centipoise (cP)	1	10^{-2}	6.7197×10^{-4}	2.4191	2.0886×10^{-5}	10^{-3}
$\text{g cm}^{-1} \text{s}^{-1}$ (poise, P)	10^2	1	6.7197×10^{-2}	2.4191×10^2	2.0886×10^{-3}	0.1
$\text{lb}_m \text{ft}^{-1} \text{s}^{-1}$	1.4882×10^3	14.882	1	3.6×10^3	3.1081×10^{-2}	1.4882
$\text{lb}_m \text{ft}^{-1} \text{hr}^{-1}$	4.1338×10^{-1}	4.1338×10^{-3}	2.7778×10^{-4}	1	8.6336×10^{-6}	4.1338×10^{-4}
$\text{lb}_y \text{s ft}^{-2}$	4.788×10^4	4.788×10^2	32.174	1.1583×10^5	1	4.7879×10^1
N s m^{-2}	10^3	10	6.7197×10^{-1}	2419.1	2.0886×10^{-2}	1

Table C.9 Thermal conductivity equivalents

Multiply by value in table to obtain these units →	Btu h ⁻¹ ft ⁻¹ °F ⁻¹	cal s ⁻¹ cm ⁻¹ K ⁻¹	erg s ⁻¹ cm ⁻¹ K ⁻¹	W m ⁻¹ K ⁻¹
Btu h ⁻¹ ft ⁻¹ °F ⁻¹	1	4.1365×10^{-3}	1.7307×10^5	1.7307
cal s ⁻¹ cm ⁻¹ K ⁻¹	2.4175×10^2	1	4.1840×10^7	4.1840×10^2
erg s ⁻¹ cm ⁻¹ K ⁻¹	5.7780×10^{-6}	2.3901×10^{-8}	1	10^{-5}
W m ⁻¹ K ⁻¹	5.7780×10^{-1}	2.3901×10^{-3}	10^5	1

Table C.10 Diffusivity equivalents

Multiply by value in table to obtain these units →	cm ² s ⁻¹	ft ² h ⁻¹	m ² s ⁻¹
cm ² s ⁻¹	1	3.8750	10^{-4}
ft ² h ⁻¹	2.5807×10^{-1}	1	2.5807×10^{-5}
m ² s ⁻¹	10^4	3.8750×10^4	1

APPENDIX D

Description of Particulate Materials

In materials processing there are instances when the material is present as a collection of particles. Properties of the individual particles and more often the properties of the aggregate of all the particles must be measured and ultimately related to the transport of momentum, energy and mass. Metals, ceramics and polymers may all be produced in particulate form by crushing, grinding, precipitation, attrition, spraying, or atomization. The correlation of particulate behavior, either alone or in fluid-solid situations, has not been easy to accomplish because of the difficulty in establishing meaningful parameters describing size, size distribution, shape, and surface characterization. For most engineering purposes, the use of the mean particle diameter has sufficed, but first the particle sizes in a powder have to be measured.

Measurement Methods

Sieving: The use of sieves is widely used and is the most reliable method for particles greater than 30 μm . Various sequences of screen apertures are available; most screen apertures are square. The sequence of openings is usually a geometric progression. If the edge length of a square opening is increased by $\sqrt{2}$, the area of the opening is doubled. This is the basis for the U.S. Sieve Series, for which the base is a 1 mm opening (no. 18 screen). The Tyler Series is based on the opening in a 200 mesh sieve, 74 μm , or 0.0029 inch. The openings and corresponding screen designations for those and four other common screen series are given in Table D.1.

Elutriation: By passing air through a bed of particles at various velocities, material of various sizes can be elutriated from the bed and collected separately.¹ The result is separations by weight fraction of the original sample carried off at various air velocities. Then, using Stokes' law for spherical particles, and solving for diameter, the weight fraction

¹P. S. Roller, *ASTM Bull.* 37, 607 (1932).

632 Appendix D

Table D.1 Wire mesh sieve series

Mesh number	Aperture dimension, in					
	U.S. Std.	Tyler Std.	British Std.	IMM	DIN	AFNOR
1					0.197	0.197
1½					0.1575	0.1575
2					0.118	0.124
2½	0.315	0.312			0.0985	0.0985
3	0.265	0.263			0.0786	0.0786
3½	0.223	0.221				
4	0.187	0.185			0.059	0.063
5	0.157	0.156	0.1320	0.100	0.0472	0.0492
6	0.132	0.131	0.1107		0.0394	0.0394
7	0.111	0.110	0.0949			
8	0.0937	0.093	0.0810	0.062	0.0295	0.0315
9		0.078				
10	0.0787	0.065	0.0660	0.050	0.0236	0.0248
12	0.0661	0.055	0.0553	0.0416	0.0197	0.0197
14	0.0555	0.046	0.0474		0.01695	
16	0.0469	0.039	0.0395	0.0312	0.01575	0.01575
18	0.0394		0.0336			
20	0.0331	0.0328		0.025	0.0118	0.0124
22			0.0275			
24		0.0276			0.00985	0.00985
25	0.0280		0.0236	0.020		
28		0.0232				
30	0.0232		0.0197	0.0166		
32		0.0195				
35	0.0197	0.0164		0.0142		
36			0.0166			
40	0.0165			0.0125	0.0059	0.0063
42		0.0138				
44			0.0136			
45	0.0138					
48		0.0116				
50	0.0117			0.01	0.00472	0.00492
52			0.0116			
60	0.0098	0.0097	0.0099	0.0083	0.00394	0.00394
65		0.0082				
70	0.0083			0.0071	0.00354	
72			0.0083			
80	0.0070	0.0069		0.0062	0.00295	0.00315
85			0.0070			
90				0.0055		
100	0.0059	0.0058	0.0060	0.0050	0.00236	0.00248
115		0.0049				
120	0.0049		0.0049	0.0042		0.00197
140	0.0041					
150		0.0041	0.0041	0.0033		
170	0.0035	0.0035	0.0035			
200	0.0029	0.0029	0.0030	0.0025		
230	0.0024					
240			0.0026			
250		0.0024				
270	0.0021	0.0021				
300			0.0021			
325	0.0017	0.0017				
400		0.0015				

Notes: IMM is Institution of Mining and Metallurgy (British), DIN is the German standard, and AFNOR is the French standard.

represents that quantity with diameter less than that of spheres with an equal free-fall velocity. This method is good down to particles of 2 or 3 μm in diameter, and up to about 100 μm .

The void fraction

An important parameter in characterizing flow through porous media is the voidage ω , which is often difficult to know or predict under industrial conditions. We define the voidage, or void fraction, by

$$\omega = \frac{\text{volume of voids}}{\text{volume of voids} + \text{volume of solids}},$$

or

$$\omega = 1 - \frac{\text{bulk density of the porous medium}}{\text{true density of the solid material}}. \quad (\text{D.1})$$

The closest possible packing of equal-size spheres gives $\omega = 0.259$. This is rarely achieved in practice, since most materials are at least somewhat irregular in shape and exhibit a relatively high degree of friction between particles. Typical values of ω lie between 0.35 and 0.5 in a loosely packed medium. In most instances, we must measure ω *in situ*, using Eq. (D.1).

Since there are voids in the packing of equal-size spheres, small particles may enter without changing the overall volume of the bed, so clearly, the size distribution of the particles has an effect on the bulk density of the bed. Furnas² made some classical studies on the void fractions in packed beds, using binary mixtures of particles (two different sizes) in various proportions. He started, in each case, with materials with the same initial (single component) voidages ω^0 , mixed them, and measured ω for the mixture. Figure D.1 shows his results for $\omega^0 = 0.5$. It is clear that, as the difference in the particle size increases, lower and lower ω values are obtainable, with minimum voidages occurring in the range 55-67 wt% of the larger-size material. Essentially, the same range for minimum voidages is found when $\omega^0 = 0.6$ and 0.4.

Furnas also made calculations of the *minimum* void fractions for three- and four-component mixtures of particles in which each component *alone* exhibits the same voidage. If the coarse and fine particles in a binary mixture are of *equal particle density* and *equal initial voidage*, then when the voids, ω , in the coarse material are saturated with fines, the volume fraction of coarse material is $1/(1 + \omega)$, and the amount of fine material is $1 - [1/(1 + \omega)]$. A third, still smaller, component can then be added to the binary mixture, filling the interstices of the second component, etc. The *total volume fraction* of solids in the mixture is then

$$(1 - \omega_m) = \frac{1}{1 + \omega} + \left[1 - \frac{1}{1 + \omega}\right] + \left[1 - \frac{1}{1 + \omega}\right] \frac{\left[1 - \frac{1}{1 + \omega}\right]}{\left[\frac{1}{1 + \omega}\right]} + \dots$$

²C. C. Furnas, *Ind. & Eng. Chem.* 23, 1052 (1931).

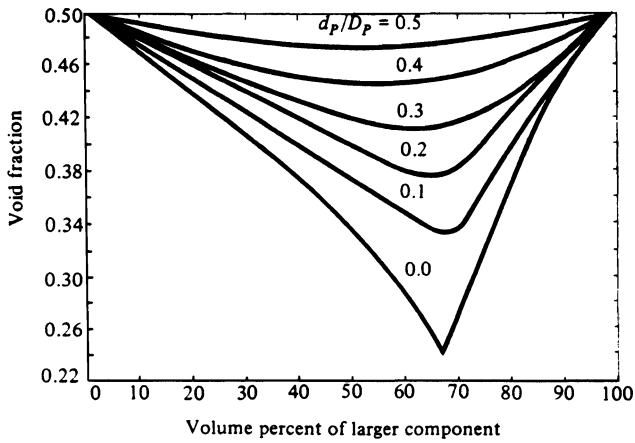


Fig. D.1 Experimental voidage of two-component particle mixtures, both having initial void fractions of 0.5. The numbers on the curves refer to the ratio of the particle diameters. (From Furnas, *ibid.*)

which simplifies to

$$(1 - \omega_m) = \frac{1}{1 + \omega} + \frac{\omega}{1 + \omega} + \frac{\omega^2}{1 + \omega} + \dots + \frac{\omega^n}{1 + \omega}. \quad (D.2)$$

When each term in Eq. (D.2) is multiplied by $100/(1 - \omega_m)$, the result is the percentage of each component in a mixture which will produce the minimum voids. Figure D.2 illustrates the results obtained by Furnas for two samples of mixtures with all initial components having $\omega = 0.4$ and 0.6 , respectively. It should be emphasized that Figs. D.1 and D.2 refer only to minimum voids.

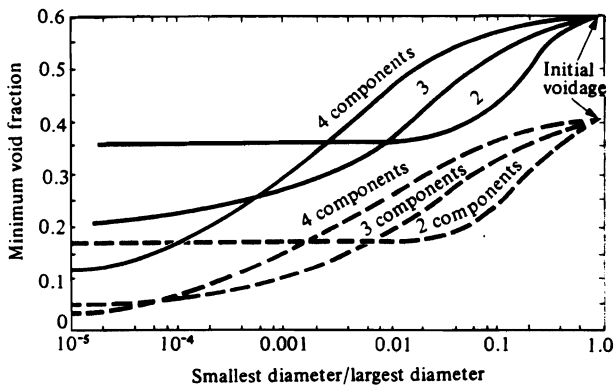


Fig. D.2 Calculated minimum voidage in two-, three-, and four-component particle mixtures. (From Furnas, *ibid.*)

White and Walton,³ who used geometric considerations and *assumed close packing of spheres*, computed the number and size of particles needed to fill interstices in the packing with each addition of a smaller component. This led to a reduction in the overall void fraction as smaller particles are added. With an ideal five-component mixture, the voidage is 0.149, decreased from the initial 0.259. Table D.2 indicates some of the results of their calculations. Experience with foundry sands indicates that this approach, although idealized, is useful.

Table D.2 Effect of size gradations on properties of a rhombohedral packing. (From White and Walton, *ibid.*)

Property	Mixture with:				
	Primary	Secondary	Tertiary	Quaternary	Quinary
Diameter	d	$0.414d$	$0.225d$	$0.177d$	$0.116d$
Relative number	1	1	2	8	8
Volume of space	$0.524d^3$	$0.037d^3$	$0.006d^3$	$0.0026d^3$	$0.0008d^3$
Volume of spheres added	$0.524d^3$	$0.037d^3$	$0.012d^3$	$0.021d^3$	$0.0064d^3$
Total solid volume of spheres added	$0.524d^3$	$0.561d^3$	$0.573d^3$	$0.595d^3$	$0.602d^3$
Fractional voids in mixtures	0.2595	0.207	0.190	0.158	0.149
Weight of spheres in final mixture, %	77.08	5.47	1.75	3.31	0.97
Total surface area of spheres in mixture	$3.14d^2$	$3.68d^2$	$4.00d^2$	$4.77d^2$	$5.11d^2$

³H. White and S. Walton, *J. Am. Ceramic Soc.* **20**, 155 (1937).

APPENDIX E

Flow Measurement Instruments

Area meters

The flow meters discussed in Chapter 4 are based on the principle of placing a restriction on the flowing stream, creating a pressure drop and a corresponding change in flow velocity through the restricted flow area. However, in area meters the pressure drop stays constant and the flow area changes as the velocity changes, rather than *vice versa*. The most common type of area meter—called a rotameter—is illustrated in Fig. E.1. The flow is read by measuring the height of a float in the *slightly tapered* column.

A force balance applied to the float determines the equilibrium position. When a fluid of density ρ moves past the float and maintains it in suspension, we can use the same force balance that was used several times in Chapters 2 and 3 for particle dynamics. The net buoyant weight of the float is balanced by the upward force created by the moving fluid. This is expressed as

$$(\rho_f - \rho) \frac{m_f}{\rho_f} g = F_K, \quad (\text{E.1})$$

where m_f is the mass of the float, and ρ_f is the float density.

For a given meter through which a given fluid flows, the left side of Eq. (E.1) is constant and independent of flow rate. Accordingly, F_K is constant when the float is at equilibrium, and, if the flow rate changes, then the float counters the effect of this change by taking on a new equilibrium position. For example, if the float is at some equilibrium position corresponding to some mass flow rate and then the mass flow rate increases, F_K becomes larger, and the float rises. However, as the float rises, the tapered tube presents a larger cross-sectional area for flow, and the velocity of the fluid between the float and the tube wall decreases, so that a new equilibrium position is eventually reached, where F_K returns to the value expressed by Eq. (E.1).

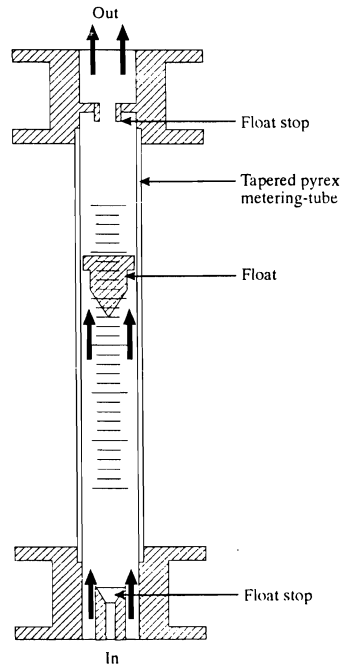


Fig. E.1 Rotameter.

The variety in designs of rotameters is so great that there does not exist one relationship valid for all types of rotameters to describe how the mass flow rate varies with height. The manufacturers usually supply calibration data for their devices, each set of data being appropriate for a specific fluid. Thus, if a gas mixture such as He plus 10% O₂ is being passed through a rotameter calibrated for He alone, then the user is fooling himself unless the rotameter is recalibrated for the He plus 10% O₂ mixture. One can also make use of a dimensional analysis of the system that would indicate how the physical parameters interact.¹

When we apply a dimensional analysis to a float of a given geometry, the following functional relationship between dimensionless groups evolves

$$\frac{W}{D_f \sqrt{m_f g \rho (1 - \rho/\rho_f)}} = f \left[\frac{\sqrt{m_f g \rho (1 - \rho/\rho_f)}}{\eta}, \frac{D_t}{D_f} \right], \quad (\text{E.2})$$

¹W. L. McCabe, J. C. Smith, and P. Harriott *Unit Operations of Chemical Engineering*, fourth edition, McGraw-Hill, New York, NY, 1985, pages 202-205.

where W = mass flow rate, D_f = characteristic diameter of float, and D_t = diameter of the tube.

The ratio D/D_f , of course, is directly related to the meter reading h , so that Eq. (E.2) does show the general form $W = W(h)$. Equation (E.2) is important because it indicates how the same set of curves generated to fit its functional relationship can be used for all fluids. Thus, if one intends to utilize a rotameter for many different fluids (for example, as a laboratory item), one should know enough characteristics of the rotameter to be able to make it completely versatile.

Flow totalizers

In some cases, for example, in pilot or bench-scale research work, the total flow through a line is required. There are many flow totalizers available, depending on the magnitude of the flow being studied. A common type is a volumetric meter, called the *rotary vane meter* (see Fig. E.2a), which is applicable for either liquids or gases. Such meters measure flows from approximately $10^{-3} \text{ m}^3 \text{ s}^{-1}$ to $2 \text{ m}^3 \text{ s}^{-1}$ with an accuracy of better than half of a percent.

For metering and totalizing liquids, the *rotating disk meter* is used (Fig. E.2b). It operates over a range from 6×10^{-5} to $6 \times 10^3 \text{ m}^3 \text{ s}^{-1}$ with an accuracy of one percent.

For totalizing gas flow, the *liquid-sealed gas meter* is employed (Fig. E.2c). This type is designed for the range from $10^{-4} \text{ m}^3 \text{ s}^{-1}$ to $2 \text{ m}^3 \text{ s}^{-1}$ and has an accuracy of about half of a percent.

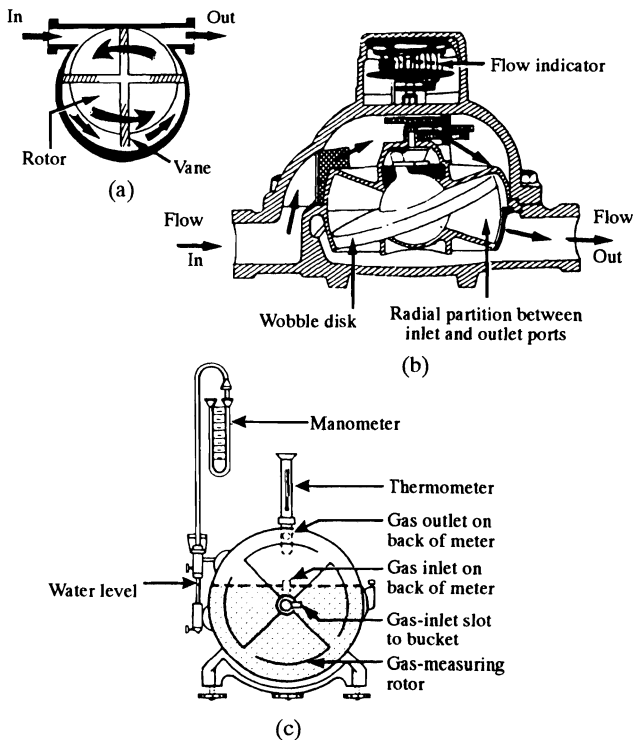


Fig. E.2 Various flow totalizers. (a) Rotary vane meter, (b) rotating disk meter, and (c) liquid-sealed gas meter. In each case, the shaft feeds a mechanical counter.

APPENDIX F

Derivation of Eq. (9.62) for Semi-infinite Solids

From Chapter 9, we recognized that Eq. (9.54) satisfies the boundary conditions of Eqs. (9.60) and (9.61) along with the initial condition of $f(x') = \theta_i$ (uniform). First, we put Eq. (9.54) in a more convenient form:

$$\theta = \frac{1}{2\sqrt{\pi\alpha t}} \int_0^{\infty} f(x') \left\{ \exp \left[\frac{-(x-x')^2}{4\alpha t} \right] - \exp \left[\frac{-(x+x')^2}{4\alpha t} \right] \right\} dx'. \quad (\text{F.1})$$

Next we change variables, $\beta = (x' - x)/2\sqrt{\alpha t}$ and $\beta' = (x' + x)/2\sqrt{\alpha t}$, and substitute $f(x') = \theta_i$:

$$\frac{\theta}{\theta_i} = \frac{1}{\sqrt{\pi}} \int_{\beta = -x/2\sqrt{\alpha t}}^{\infty} e^{-\beta^2} d\beta - \frac{1}{\sqrt{\pi}} \int_{\beta' = +x/2\sqrt{\alpha t}}^{\infty} e^{-\beta'^2} d\beta', \quad (\text{F.2})$$

or noting that primes are no longer necessary, we have

$$\frac{\theta}{\theta_i} = \frac{1}{\sqrt{\pi}} \left[\int_{\beta = -x/2\sqrt{\alpha t}}^{\infty} e^{-\beta^2} d\beta + \int_{\beta = \infty}^{+x/2\sqrt{\alpha t}} e^{-\beta^2} d\beta \right]. \quad (\text{F.3})$$

Figure F.1 schematically indicates these integrals, and shows that their sum results in

$$\frac{\theta}{\theta_i} = \frac{1}{\sqrt{\pi}} \int_{-x/2\sqrt{\alpha t}}^{+x/2\sqrt{\alpha t}} e^{-\beta^2} d\beta = \frac{2}{\pi} \int_0^{x/2\sqrt{\alpha t}} e^{-\beta^2} d\beta. \quad (\text{F.4})$$

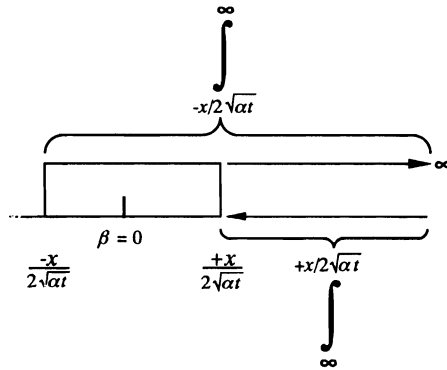


Fig. F.1 Schematic representation of the integral in Eq. (F.3).

The solution in its final form is

$$\frac{T - T_s}{T_i - T_s} = \operatorname{erf} \frac{x}{2\sqrt{\alpha t}}. \quad (9.62)$$

APPENDIX G

Derivation of Eq. (13.53) for Drive-in Diffusion

After predeposition the concentration of the dopant is given by the curve marked $t = 0$ in Fig. 13.8. This becomes the initial distribution for the silicon wafer when it is subjected to drive-in diffusion. Assuming no loss of dopant from the surface, the boundary conditions and the initial condition for $C(x,t)$ are given by Eqs. (13.52a,b,c). Now if we change the concentration to one that is relative to C_0 , then Eqs. (13.52a,b,c) become

$$\frac{\partial}{\partial x} [C(0,t) - C_0] = 0, \quad (\text{G.1})$$

$$C(\infty, t) - C_0 = 0, \quad (\text{G.2})$$

and

$$C(x,0) - C_0 = f(x') - C_0. \quad (\text{G.3})$$

If we make $f(x')$ in Fig. 13.8 into an even function (e.g., as in Fig. 9.14b), then Eq. (9.48) applies with $C - C_0$ substituted for T and D substituted for α . For an even function, $f(-x') = f(x')$ so Eq. (9.48) is written

$$C - C_0 = \int_{x'=0}^{\infty} \frac{f(x') - C_0}{2\sqrt{\pi Dt}} \left\{ \exp \left[-\frac{(x - x')^2}{4Dt} \right] - \exp \left[-\frac{(x + x')^2}{4Dt} \right] \right\} dx'. \quad (13.53)$$

- Abbaschian, R., 423
 Absorptivity
 definition, 370
 of gases, 402
 Absorption coefficient, 405
 Activation energy, 431
 for viscous flow, 14
 Adams, C.M., 318, 332, 337, 338, 340, 343
 Aggregative fluidization, 104
 Alternating direction implicit method, 590
 Aluminum quenching, 301
 Analog, electric, 386–390
 Anderson, A.R., 165
 Angeles, O.F., 534
 Archimedes number, 270
 Area meters, 124, 637
 Arrhenius equation, 431
 Auman, P.M., 268
 Austempering, 298
 Average velocity, 42
 Averbach, B.L., 422
 Azbel, D., 262

 β -alumina, 440
 Bag house, 138
 Ball bearings, 324
 Bamberger, M., 269
 Banding, 505
 Bardes, B., 350
 Barone, R.V., 488
 Basic oxygen steelmaking, 163
 Beam lengths for gas radiation, 401
 Bed, 101
 Bedworth, R.E., 493
 Bernoulli's equation, 113, 116–117, 153
 application to flow from ladles, 131
 application to pitot tube, 125
 Bernstein, M., 255
 Biesenberger, J.A., 34
 Bills, P.M., 24, 25
 Bingham plastics, 29
 Biot number, 293, 299
 Bird, R.B., 1, 203, 240, 523
 Black body, 370
 Black radiator
 approximation of, 370–371
 definition, 370
 Blake-Kozeny equation, 94
 Blasius, H., 65
 Blowers, 151
 Boiling heat transfer, 262
 Boltzmann-Matano technique, 472
 Boltzmann's constant, 372

 Bonilla, C.F., 266
 Boiret, M., 26, 27
 Borg, R.J., 425
 Boundary layer, 62
 mass transfer, 528–529
 momentum, 224
 thermal, 224
 Brake horsepower, 153
 Brewster, M.Q., 374
 Brice, J.C., 355
 Bridgman, 203
 Brimacombe, J.K., 605
 Brines used for quenching, 264
 Brody, H.D., 488
 Bromley, L., 10
 Buckingham's Pi theorem, 248
 Buffer layer, 603
 Buoyant force, 70
 Burnout, 263

 Calderbank, P.H., 532
 Carburization, 504
 of iron, 551
 Carburizing, 473, 490–497, 552–556
 example of, 481–482
 Carnahan, B., 581, 590
 Carslaw, H.S., 293, 303, 469, 562
 Carter, R.E., 440
 Cast iron, 411
 Cavitation, 147
 Centipoise, 6
 Central differencing, 607
 Centrifugal pump, 145–146
 axial flow, 145
 tangential, 145
 Ceramic materials, 209, 507, 544, 591, 631
 brick, 326
 Cess, R.D., 374
 Chang, P., 447
 Chapman, T., 16, 18
 Chapman-Enskog theory, 11, 13, 453
 Characteristic boiling curve, 263
 Characteristic energy parameter, 9
 table of, 11
 Chemical diffusion coefficient, 428
 Chemical vapor deposition, 537
 Cheremisinoff, N.P., 106
 Chill, solidification against, 334–335
 Chilton-Colburn theory, 531–533
 Churchill, S.W., 255
 Chvorinov's rule, 332
 Clausing factor, 561
 Cohen, M., 422
 Cohen, M.H., 447

- Colburn's analogy
 heat transfer, 251
- Collision cross section, 7
- Collision integral
 definition, 10
 graph, 455
 table, 12
- Collur, M.M., 566
- Complementary error function, 302
- Composite cylindrical wall, 286
- Concentration boundary layer, 528
- Condensation coefficient, 564
- Conductance, 169
- Conductance of vacuum system
 components, 170
 definition, 170
 table, 171
- Conduction heat transfer
 through cylindrical walls, 233–235
- Configuration factor, 381
 (see View factor)
- Conservation of energy, 114
- Contact heat-transfer coefficient, 274
- Contact resistance, during solidification,
 347–348
- Continuous annealing process, 235, 303
- Continuous casting, 342, 350–355
 example problem, 353–354
 fluid flow in, 143
 heat removal by mold, 353
 heat transfer in, 355
 machine, 363
 surface temperature during, 355
 thickness solidified, graph, 354
- Continuous quench and temper process, 303
- Continuity equation
 cylindrical coordinates, 57
 rectangular coordinates, 57
 spherical coordinates, 57
 vector notation, 55
- Convection, natural, 258
- Convective flows, 606
- Convective momentum, 52
- Converging-diverging nozzles, 161
- Cooling rates
 chart for determination of, 310
- Cooling water requirements, 353
- Core, 571
- Coring, 485
- Correlation coefficient, f , 424
- Crank, J., 469, 487
- Crank-Nicolson method, 580
- Crawford, R.J., 34
- Creeping flow around a solid sphere, 68–74
- Critical radius, 287
- Crystal growth, 355
 heat transfer during, 355
- Curved pipes, friction loss in, 123–124
- Cylinders, solidification times for, 331–332
- Czochralski-type crystal grower, 355
- Damper, 152
- Danckwerts, P.U., 536
- Dancy, T.E., 267
- Darcy, 91
- Darcy's law, 90, 93
- Darken, L.S., 428, 430
- Darken's equation, 428
- Davison, J.F., 104
- Debroy, T., 566
- Debye, P., 188
- Deem, H.W., 375
- Deissler, R.B., 212
- De Laval nozzle, 160–162
- Dendrite arms, 485
- Dendritic arm spacing, 485
- Dendritic structures, 329, 485
- Derge, G., 450–451
- Desmond, R.M., 262
- DeWitt, D.P., 262, 375, 380
- Die castings, 334
- Diens, G.J., 425
- Diffuse surfaces, 374
- Diffusion
 in a moving gas stream, 513–516
 in a slab, 478
 in ceramic materials, 435
 in common liquids, 453
 in gases, 453–456
 in liquid metals, 448
 in liquids, 444
 in molten salts and silicates, 450
 in porous media, 457–459
 in solid circular cylinder, 478
 in spheres, 478
 into a falling liquid film, 516–519
 Knudsen, 457
 through a stagnant gas film, 510–513
- Diffusion anneal, 469
- Diffusion coefficient
 chemical, 428
 interdiffusion, 428
 intrinsic, 420
 Knudsen, 457
 mutual, 428
 ordinary, 457
 self-, 421–423

- Diffusion coefficient data
 - in porous media, 457–459
 - in solid ferrous alloys, 433–434
 - inter-, in common liquids, 452
 - inter-, in gases, 453
 - inter-, in liquid ferrous alloys, 450
 - inter-, in liquid nonferrous alloys, 449
 - self-, in dilute solid alloys, 424
 - self-, in liquid metals, 445, 449
 - self-, in molten salts, 451
 - self-, in pure solid metals, 423, 432
- Diffusion constants in Si, 443
- Diffusion couple, 470–480
- Diffusion equation, 524
 - general, 523–526
- Diffusion in solids
 - finite systems, 476–480
 - interstitial alloys, 425
 - steady-state, 463
 - through cylinders, 464
 - transient, 468
- Diffusion into a falling liquid film, 516–519
- Diffusion pump
 - Ho coefficient, 176
 - limiting forepressure, 175
 - multi-stage, 175
 - speed of, 175–176
 - ultimate pressure of, 176
 - vapor trap, 176
- Diffusion through gases
 - moving gas, 513–516
 - stagnant gas, 510–513
- Diffusion through porous media, 457
- Diffusion volume, 456
- Diffusivity
 - heat, 330
 - momentum, 6
- Dilatant fluids, 29
- Dimensional analysis, 77
 - Buckingham's Pi theorem, 248
 - similarity technique, 77, 230
- Direct-exchange factor, 381
 - (see View factor)
- Discharge coefficient, 128
- Dissipation function, 238
- Dissipation rate of turbulence energy, 604
- Dobbins, W.E., 537
- Donald, D.K., 359
- Drag coefficient, 83
- Drag force, 67
- Drag form, 70
- Dopants, 480
- Doughty, D.L., 256
- Drive-in diffusion, 480, 643
- Dynamic similarity, 230
- Eddy diffusivities, 601
- Effective beam length
 - definition, 399
 - of hemispheres, 399
 - of shapes, other than hemispheres, 399–400
- Effective heat of fusion, 334
- Effective interdiffusivity, 457
- Effective jet radius, 164
- Effective thermal conductivity of packed bed, 212
- Effect of mold contour on solidification, 332
- Effect of superheat on solidification time, 334
- Efficiency
 - of fans, 152
 - of pumps, 146–147
- Effusion cells, 561
- Eian, C.S., 212
- Eigenvalues, 292
- Einstein, A., 14, 192, 421, 445
- Ejectors, 166
- Ejector system, 166
- Electric analogs, 386–388
- Electric arcs, 315
- Electrical conduction, 436
- Electron beams, 315, 356
- Electron conduction, 436
- Electron-hole conduction, 436
- Electroslag remelting, 137, 338
- Elliott, J.F., 450, 563
- Elutriation, 108, 631
- Emissive power
 - definition, 369
- Emissivity
 - as function of view angle, 374
 - as function of wavelength, 373
 - of ferrous materials, 377
 - of gases, 399
 - of metal surfaces, 374–377
 - of oxides, 376–377
 - of several materials, 375
 - of some ceramic materials, 376
 - reduced, 399–400
- Emittance
 - definition, 369
- Emulsions
 - used for quenching, 264
- Energy equation, 236–242
 - (see General energy equation)
 - for conduction, 281

- Energy transfer by radiation, 369
- Epitaxial growth, 545
- Equation of continuity, 50, 51
 - in cylindrical coordinates, 57
 - in rectangular coordinates, 57
 - in spherical coordinates, 57
 - of A in various coordinate systems, table, 525
- Equation of energy in terms of energy and momentum fluxes, 241
- Equation of motion, 50
 - (see Navier-Stokes' equation)
 - in cylindrical coordinates, 59
 - in rectangular coordinates, 58
 - in spherical coordinates, 60
- Equivalent diameter for noncircular conduits, 117
- Equivalent length for various fixtures, 123
- Ergun's equation, 93, 97
 - friction factor associated with, 96
- Error, N., 440
- Error function
 - complementary, 302
 - definition, 308
 - table, 303
- Eucken, A., 191
- Euler method, 571, 574
- Evans, J.W., 605
- Evaporation, 512
- Evaporation constants, 565
 - table, 567
- Exchange between infinite parallel plates, 378
- Expansion factor, 129
 - figure, 129
 - for flow meters, 129
 - table, 129
- Extended Nernst-Einstein equation, 437
- Eyring, H., 15
- Eyring theory, 446
- Eyring's theory of viscosity, 15
- Falling film flow, 39–41
 - average velocity in, 42
 - maximum velocity in, 42
 - velocity distribution in, 43
 - volume flow rate in, 43
- Falling-sphere viscometer, 71
- Fan laws, 155
- Fanning equation, 117
- Fan, 118, 137, 151–158
- Fan characteristics, 152
- Fan laws, 155
- Fans
 - characteristic curve, 152
 - horsepower of, 153
 - interaction with system, 154–158
 - pumping limit of, 154
 - static efficiency, 153
 - total efficiency, 153
- Fermi energy, 196
- Fick's first law, 419
 - of diffusion, 420
- Fick's second law, 428, 469
 - of diffusion, 525
- FIDAP software, 605
- Film boiling, 263, 267
- Film penetration theory, 537
- Film theory, 535
- Finite difference approximation, 571
 - method, 578
- First law of thermodynamics, 113
- Flemings, M.C., 350, 485, 488–489
- Floating-zone process, 355
- Flood, S.C., 606
- Flow
 - laminar, 3
 - streamline, 3
 - turbulent, 3
- Flow, creeping, around a sphere, 68
 - momentum-flux distribution in, 69
 - normal forces in, 70
 - pressure distribution in, 69
 - velocity components, 69
- Flow between parallel plates, 44
 - average velocity in, 45
 - maximum velocity in, 45
 - shear stress distribution in, 45
 - velocity distribution in, 45
 - volume flow rate in, 45
- Flow coefficient, for meters, 128
- Flow in noncircular conduits, 81–82
- Flow measurement, 124–131
 - area meters, 637
 - (see Velocity meters, Head meters, and Area meters)
- Flow nozzle, 127
- Flow of a falling film, 41
- Flow over a flat plate, 62
 - boundary layer in, 62–66
 - drag force in, 67
 - Reynolds number for, 63, 66
- Flow past a sphere, 85–90
- Flow past submerged bodies, 82–90
- Flow through a circular tube, 46
 - average velocity in, 48
 - example problem, 48

- maximum velocity in, 47
 - Newtonian fluids, 46
 - Power law non-Newtonian fluids, 49
 - velocity distribution in, 47
 - volume flow rate in, 48
- Flow through fluidized beds, 101
- Flow through piping networks, 135
- Flow through valves and fittings, 122–123
- Flow totalizers, 639
- Fluctuation theory, 447
- FLUENT* software, 605
- Fluidity, 15
- Fluidized, 101
- Fluidized beds, 101–112
 - applications of, 106–107
 - elutriation in, 108
 - particulate fluidization, 101, 105
 - Reynolds number in, 103
- Fluids
 - Newtonian, 29, 42
 - Non-Newtonian, 29
 - Rheopectic, 31
- Flux
 - heat, 188
 - mass, 420
 - molar, 420
 - momentum, 188
 - units, 420
- Forced-convection mass transfer correlations, 520
- Ford, H., 273
- Forging, 274
- Form drag, 85
 - (see Friction factor for flow past a sphere)
- Foundry molding sands
 - effect of contour on solidification rates, 331
 - permeability of, 91
 - thermal conductivity of, 214
- Fourier number, 293
- Fourier's law, 185, 187–188
 - in three dimensions, 188
 - of heat conduction, 188
- Frantz, J.F. 103
- Frenkel defect, 435
- Frenkel, J., 13
- Frequency factor, 431
- Freuhan, R.J., 532
- Friction drag, 85
- Friction factor, 76
 - dimensional analysis for, 77–79
 - experimental results, 79
 - for flow in rectangular ducts, 82
 - for flow in tubes, 76, 80
 - for flow parallel to flat plates, 83, 84
 - for flow past flat plates, 83, 84
 - for flow past a sphere, 88
 - for flow past submerged objects, 87
 - for flow through packed beds, 94, 95
 - for laminar flow past a sphere, 87
- Friction head, 146
- Friction loss
 - in straight conduit, 117–119
 - through valves and fittings, 119
- Friction loss factor
 - gradual contractions, 121
 - gradual enlargements, 121
 - sudden contraction, 119
 - sudden enlargement, 119
- Froude number, 63
- Fully developed temperature profile, 221
- Furnace design, 390
- Furnas, C.C., 273, 633
- Galileo number, 104
- Ganesan, S. 100
- Gas phase transport control, 553
- Gas-solid reactions, 551
 - models of, 560
- Gas temperature, 397
- Gases
 - absorptivity, 399
 - collision diameters in, 455
 - diffusion coefficients in, 454
 - diffusion in, 453–456
 - diffusion in binary gases, 464
 - emissivity, 399
 - reduced emissivity, 399–400
 - thermal conductivity of, 190–192
 - transmissivity, 403
 - viscosity of, 7–13
- Geiger, G.H., 531
- General energy equation
 - components of, 236–240
 - in curvilinear coordinates, 240
 - in cylindrical coordinates, 240, 242
 - in rectangular coordinates, 240, 242
 - in spherical coordinates, 240, 242
- General equation of continuity, 524
- General equation of diffusion with convection, 523
- General momentum equation, 50
- Generalized Newtonian fluids (GNF), 30
- Germanium, 442
- Gettering pumps, 180
- Glass, thermal conductivity of, 203
- Glasses, 370

- Gosman, A.D., 605
 Grain-boundary diffusion, 433
 Graphite, 533
 Grashof number
 for heat transfer, 231
 for mass transfer, 531–532
 for natural convection, 258
 Gray bodies, 373, 378
 Green, H.S., 16
 Griffiths, D.K., 268
 Grossmann, M.A., 264
 Grube solution, 470
 Gruneisen's constant, 193
 Gupta, R., 106
 Gurney-Lurie charts, 293
 Guthrie, R.I.L., 20, 205, 446, 581
- Hagen-Poiseuille law, 48
 Harrison, D., 104
 Hauffe, K., 435
 Head
 friction, 146
 net positive suction, 147
 pressure, 127
 total, 146
 Head meters, 124, 127–131
 Heat conduction through a hollow solid cylinder, 233
 Heat diffusivity, 330
 Heat flow for a semi-infinite solid, 308
 Heat flux
 through cylinders, 285–286
 through flat walls, 282–283
 through the slab, 282
 Heat of fusion, effective, 334
 Heat transfer, boiling, 262
 Heat transfer between fluids and spheres, 255
 Heat-transfer coefficient, 221, 223
 across casting-mold interfaces, 350
 definition, 247
 effect of roughness on, 251
 for forced convection, 254
 for fully developed forced convection in tubes, 249–250
 for natural convection, 258–262
 for oil-spray quenching and immersion in oil, 269
 for quenching oils, 265
 for water-spray cooling, 268
 in aqueous quenching media, 267
 liquid metals, 251
 of natural convection from horizontal surfaces, 261
 on the casting side of interface, 347
 on the mold side of interface, 347
 over a flat plate, 224–228
 average, 225
 local, 225
 radiant, 396
 total, 396
 total, across metal-mold interface, 347–349
 volumetric, 274
 Heat-transfer coefficients for
 flow in tubes, 250
 flow over a flat plate, 256
 flow past a sphere, 255
 flow through packed beds, 272
 Heat-transfer coefficients for natural convection for
 horizontal cylinders, 259
 horizontal surfaces, 261
 vertical plates, 259
 Heat transfer during crystal growth, 355
 Heat transfer for natural convection, 228–233, 258
 Heat transfer from a sphere to a flowing fluid, 256
 Heat transfer in fluidized beds, 268
 Heat treatment, 262, 407, 486, 560
 of a continuous sheet of steel, 407
 Heisler charts, 293
 Higbie, R., 536
 Hill, D.R., 268
 Hills, A.W.D., 350, 352,
 Ho coefficient, 176
 Hohlraum, 371
 Hole theory of liquids, 13, 446
 Holman, J.P., 255, 262, 380
 Homogenization, 486–491
 of alloys, 485
 kinetics, 582
 Hopkins, B.E., 435
 Horsepower, 147
 Hottel, H.C., 374, 376, 392, 400
 Hot-wire anemometer, 257
 Howell, J., 374
 Hughmark, G.a., 531
 Hydraulic radius, 93
 Hydrodynamical theory, 444
 Hydrogen, 544
 removal from metal, 550
- Iida, T., 20, 205, 446
 Incropera, F.P., 262, 380
 Induction, 356
 Infinite solid

- transient heat conduction, 305
- Ingot, 334
- Insulation, 287, 321
 - critical radius of, 287
 - effect of, 283
- Interatomic spacing, 18, 423
 - table, 19
- Interdendritic liquid, 485
- Interdiffusion, 448, 450,
- Interdiffusion coefficient, 428
 - in ferrous materials, 434
 - in nonferrous metals, 432
 - of interstitial elements through ferrous materials, 433
- Interface resistance, 342–346
- Intermolecular force parameter, 454
- Internal temperature gradients, 290
- Interstitialcy mechanism, 425
- Intrinsic diffusion coefficient, 420, 425
- Intrinsic speed of vacuum pumps, 173
- Ion implantation, 482, 507
- Iron ore sinter plant
 - pressure drop across, 98–100
- Iron oxide
 - effect on slag viscosity, 22, 24–25
- Isentropic shockless flow, 162
- Ishida, T., 567
- j*-factor
 - heat transfer, 251
 - mass transfer, 529
- Jacobi, H., 350
- Jaeger, J.C., 293, 303, 469, 562
- Jain, V.K., 275
- Jensen, K.F., 541
- Jets, supersonic
 - area of interaction with bath, 158
 - impact pressure, 159–165
 - length of core, 164
 - momentum of, 164
 - spreading of jet, 165
- Johns, F.R., 165
- Jominy end-quench test, 310
- Jost, W., 435, 469, 474, 485
- Jump frequency, 423
- K*– ϵ model, 604
- Kapner, J.D. 165
- Karlekar, B.V., 262
- Katgerman, L., 606
- Kattamis, T.F., 489
- Kinematic viscosity, 6
- Kinetic energy terms, 115–117
- Kinetic theory of gases, 7, 453
- Kirchoff's law, 389
- Kirkaldy, J.S., 431, 513
- Kirdendall effect, 426
- Kirkwood, J.G., 16
- Kitaev, B.I., 273
- Knudsen, 168, 170
- Knudsen diffusion, 457
 - coefficient, 457
- Knudsen effusion cells, 560–562
- Kofstad, P., 435
- Kreith, F., 400
- Kubaschewski, O., 435
- Kucharski, M., 21
- Kunii, D., 106
- Kroger, F.A., 435
- Kwauk, M., 103
- Ladles
 - discharge coefficient for, 132
 - flow from, 131
 - time to empty, 133
- Laminar flow, 3
- Laminar sublayer, 603
- Langhaar, H., 68
- Langille, A.H., 606
- Laplace equation, 282
 - written in cylindrical coordinates, 285
- Lasers, 309–310, 318
 - beams, 315, 356
- Laser welding, 566, 569
- Latent heat, 330
- Lauder, B.E., 603, 605
- Law of conservation of momentum, 54
- Lead, diffusion in, 460
- Lennard-Jones potential, 9, 11, 18, 464
- Leva, M., 103
- Levenspiel, O., 106
- Levitation melting, 412
 - mass transfer during, 543
- Lewis, W.K., 535
- Li, J.C.M., 447
- Li, Kun, 165
- Lightfoot, E.N., 203, 240, 523
- Liquid metals, 259
 - diffusion in, 445
 - structure of, 456
 - thermal conductivity in, 197
- Liquid phase control, example of, 565–566
- Liquid-sealed gas meter, 639
- Local mass transfer coefficients, 520
- Log mean, 512
- Long horizontal cylinders, 259
- Long-time solutions, 300

- Lorenz number, 196
 Love, T.J., 374
 Lucks, L.F., 375
 Luther, H.A., 581, 590
- Mach number, 160, 164–165
 Machlin, E.S., 563
 Manganese
 vaporization from molten steel, 566
 Mapother, D., 437
 Marangoni effect, 521
 Marchello, J.M., 537
 Marcussen, L., 215
 Marshall, W.R., Jr., 256
 Martonik, L.J., 532
 Mass flux vector, 524
 Mass transfer, 509
 correlations involving gas bubbles, 532
 gas-liquid, 531
 to spheres, 531
 Mass transfer coefficient
 average, 520
 definition, 519
 for laminar flow over a flat plate, 528
 local, 520
 models, 535–537
 Mass transfer, interphase
 film penetration theory, 537
 two-resistance theory, 547–551
 Mass transfer j -factor, 529–530
 Mass transfer Nusselt number, Nu_M , 520
 Mass transfer resistances, 548
 Matano interface, 474–475
 Maximum velocity, 42
 Maxwell-Boltzmann distribution of
 velocities, 168
 McAdams, W.H., 255, 258, 261
 Mean free path, 8
 Mechanical energy equation, 113
 Mechanical vacuum pumps
 intrinsic speeds, 173
 positive displacement, 173
 rotary piston, 173
 Melt spinning, 366
 Metallurgical length, 355
 Method of separation of variables, 291
 Microsegregation, 485, 582
 Microsegregates, 329
 Minimum fluidization, 102
 Minimum void fractions, 633
 Mixed control of reactions
 gas-liquid, 547–551
 gas-solid, 551–560
- Mixed mean temperature, 247
 Mobility, 15, 429
 in an electrical field, 436, 496
 in an energy gradient, 429
 self-diffusion, 422
 Models of gas-solid reactions, 560
 Molar average velocity, 509
 Mold length, 353
 Mold material, 361
 Molecular flow, 166, 168
 Molecular flow mechanics, 168–173
 Molecular liquids, viscosity of, 15
 Molecular pumps, 178
 Molten plastics, 29
 Momentum
 conservation, law of, 54
 convective, 52
 flux, 42
 general equations, 50–56
 viscous, 53
 Momentum balance, 39
 for flow between parallel plates, 44
 for flow in a tube, 46
 in a falling film, 40, 41
 Momentum boundary layer, 226, 229
 Momentum diffusivity, 225
 Momentum equation
 cylindrical coordinates, 59
 rectangular coordinates, 58
 spherical coordinates, 60
 Momentum transport, 5
 Monochromatic emissive power, 372
 Moore, M.R., 350, 352
 Morgan, E.R., 267
 Moving line source, 319
 Moving point source, 315
 Mrowec, S., 425
 Mutual diffusion coefficient, 428
- Nanda, C.R., 531
 Nandapurkar, P.J., 100
 Natural convection
 heat transfer, 259, 261
 mass transfer, 529
 Navier-Stokes' equation, 50, 55, 56
 Nernst-Einstein equation, 429
 extended, 437
 Net positive suction head, 147
 Newtonian fluid, 5
 Newtonian heating or cooling, 288
 conditions for validity, 288, 299
 example problem, 289
 Newton's law of viscosity, 6, 55
 No-net-flux surfaces, 390

- figure, 392
- Noncircular conduits, 81–82
- Nonmetallic stoichiometric compounds, 429
- Non-Newtonian fluids, 29–34
- Normalized variables, 573
- Nozzle
 - converging, 158–165
 - conditions for sonic flow, 161–162
 - mass flow rate from, 161–162
 - spray, 136
- Nucleate boiling, 262–263, 267
- Nusselt number
 - definition, 223
 - for laminar flow, 223
 - local, 225
- Ω -integral for viscosity, 11
- Ohno, R., 567
- Oil, thermal conductivity of, 205
- Oils, heat transfer in, 264–266
- Operating point, 154
- Orifice plate, 127–131
- Ostwald power law, 29
- Overall evaporation constants, 567
- Overall mass transfer coefficients, 547
- Overall rate constant, 565
- Oxidation
 - parabolic, 497–498
 - parabolic rate constants, 498
- Oxide layers, 491
- Oxides
 - defect structures in, 438
 - thermal conductivity of, 193–194, 200
 - data, 194
- Packed beds, heat-transfer coefficient in, 272
- Pape, P.O., 273
- Parabolic scaling constant, 493
- Parabolic oxidation constants for various metals, 498
- Particulate materials, 631
- Paul, A., 566
- Pauling, L., 445
- Pauly, S., 466
- Paschkis, V., 266–267, 303
- Peak temperature, 317
- Peclet number, 317, 520
- Pelletizing, 155
- Penetration theory, 536
- Permanent mold castings, 334
- Permeability, 90, 92, 466
 - data, 466
 - specific permeability, 91
- Peterson, N.L., 485, 513
- PHOENICS* software, 605
- Phonons, 192
 - mean free path of, 193
- Photon contribution to thermal conductivity, 200
- Pickling, 157
- Pigford, R.L., 254, 518
- Pilling and Bedworth constant, 493
- Pilling, N., 493
- Pitot static tubes, 124–126
- Planck's constant, 372
- Planck's distribution law, 372
- Planck's equation, 372
- Poirier, D.R., 100, 488
- Poise
 - definition, 6
 - units, 6
- Polyalkylene-glycol, 265
- Polyethylene, 313, 363
- Polymer solutions
 - used for quenching, 264
- Polymers, 30, 466, 500, 631
 - glass transition temperature of, 33
 - rheology of, 31
 - viscosity of, 31
- Polymeric materials
 - thermal conductivity and other thermal properties of, 204
- Polypropylene, 326
- Porous materials, thermal conductivity of, 211
- Porous media
 - flow through, 101
- Positive displacement pumps, 146
 - power, 146
 - reciprocal, 145
 - rotary, 145
- Powders, 88
- Powder metallurgy, 98, 209
 - particle sizing, 88, 89
 - powder rolling, 112
 - pressure drop for flow through compacts, 100
 - thermal conductivity of compacts, 211
- Power required for floating zones, 360
- Practical parabolic scaling constant, 493
- Prandtl mixing length, 602
- Prandtl number
 - definition, 225
 - of liquids, 226
 - table, 226
- Praysnitz, J.M., 454

- Precipitation-hardenable aluminum alloys, 264
- Predisposition, 480
- Pressure drop
 - for flow across a packed bed, 94, 95
 - for flow through fittings, 122–123
 - for flow through a pipe, 80
 - for flow through a piping system, 135
- Pressure pouring, 142
- Price, J.B., 438
- Prinz, B., 269
- Product solutions, 313–315
 - example of, 313
 - figure illustrating, 314
- Pseudoplastics fluids, 29
- Pumpdown time, 177
- Pumping limit, of fans, 154
- Pumping speed
 - definition, 172
 - effective, 172
 - of vacuum pumps, 172–173
 - of vacuum systems, 172–173
 - units, 173
- Pumps (*see* Vacuum pumps)
 - centrifugal, 145–146, 148
 - characteristic curve, 148
 - diffusion, 175
 - efficiency of, 148
 - positive displacement, 145–146
 - reciprocating, 145
 - rotary, 145
- Quenchants, 264
- Quenching
 - aluminum, 266, 289
 - heat transfer coefficients in, 264–269
 - heat transfer in, 262–268
 - of steel sheet, 140, 264
 - oils, 264–268
 - salt solutions, 264
- Radiance, 369
- Radiant heat transfer, 369
 - between infinite parallel plates, 378–381
 - electrical analog of, 387
 - within furnaces, 383, 384
- Radiant furnace, 407
- Radiant thermal conductivity, 195
- Radiant-flux density, 369
- Radiation from gases, 398–404
- Radiation heat transfer
 - ceramics, 404
 - glasses, 404
- Radiation heat-transfer coefficient, 396
- Radiation shields, 380
- Radioactive tracers, 469
- Radiosity, total, 370
- Ranz, W.E., 256
- Rate-determining step, 417
- Rational rate constant, 495
- Read, C.M., 606
- Recirculating flows, 598
- Reduced emissivity, 399
 - of carbon dioxide, 400
- Reduced temperature, 16
- Reduced viscosity, 16
- Reduced volume, 16
- Reed-Hill, R.E., 423
- Reflectivity, 370
- Refractory walls, 391
- Reheat furnace, 413
- Reid, R.C., 454
- Relative interface temperature during
 - freezing, graph, 340
- Relative position, 293
- Relative roughness, 79
- Relative temperature, 293
- Residual segregation index, 488
- Resistance concept, 283
- Reynik, R.J., 447
- Reynolds, 4
- Reynolds, J.E., 422
- Reynolds number, 4, 63, 78, 446
 - for flow over a flat plate, 63, 66
 - for flow past submerged objects, 87
 - for flow through fluidized beds, 103
 - for flow through packed beds, 95, 96
 - for flow through a pipe, 48
 - local, 66
 - transition from laminar to turbulent flow, 75, 79
- Rheology, 29
- Rheopectic fluids, 31
- Richardson, F.D., 440
- Ring mechanism, 425
- Rodriguez, F., 34
- Rogers, S., 606
- Rohsenow, W.M., 251, 259, 263
- Roots pump, 174
- Rosenthal, D., 317
- Rotary vane meter, 639
- Rotameter, 131–132, 637
- Rotating disk meter, 639
- Roughness
 - effect on heat transfer, 251
 - table, 80
 - values, 80

- Ruddle, R.W., 350
- Salt solutions, heat transfer in, 264
- Salts, molten
diffusion in, 450
thermal conductivity of, 207
- Sand
solidification in, 329–334
thermal conductivity of, 214–215
- Sarofim, A.F., 374, 376, 394, 400
- Satterfield, L.N., 458
- Saunders, O.H., 273, 413
- Saxton, H., 448
- Schack, A., 194, 199
- Schmidt number
definition, 520
- Schneider, P.J., 309, 407
- Schotte, W., 211
- Schottky defect, 435
- Schroeder, D.L., 562, 563
- Scruton, R.E., 581
- Seban, R.A., 256
- Sebastian, D.H., 34
- Seed crystal, 356
- Segregation index, 488
- Self-diffusion, 421–424
in liquid metals, 445
- Self-diffusion coefficients for pure metals, 423
- Self-diffusion mobility, 422
- Semiconductor crystals, 355
- Semiconductors, thermal conductivity of, 200
- Semi-infinite bar, 470
- Semi-infinite body, solution of heat flow equation for, 341
- Semi-infinite plate, steady-state, conduction through, 282
- Semithickness, 293
- Separation constant, 291
- Separation of variables, 291
- Severity of quench, 264
- Shape factor λ , 96
- Shape factor, 96, 97
table, 97
- Shape factor for screened particles, 97
- Shape factor for solidification in sand molds, 332–333
- Shear stress, 5
- Sheet glass, 413
- Sheet, heating of with radiation, 407–409
- Shell mold, 413, 577
- Sherby, O.D., 432, 448
- Sherwood number
definition, 520
prediction in gas-liquid transfer, 527
- Sherwood, T.K., 250, 454, 458
- Shewmon, P.G., 423
- Shock wave, 162
- Short-time solutions, 300
- Siegel, R., 374
- Sievert's law, 465
- Sieving, 631
- Silica equivalence of aluminum oxide, 23
- Silicate glass, 441
- Silicate melts, 370
- Silicon, 358, 366, 397, 441, 480–481, 502, 507, 542, 643
oxidation of, 556
- Similarity technique, 77–79
- Simnad, M.T., 432
- Singh, S.N., 489
- Sinha, A.K., 264
- Sintering, iron ore, 98
- Slags
structure of, 22–24
thermal conductivity of, 206–208
viscosity of, 22–29
- Slurries, 29
- Soldering, 367
- Solidification
against a chill, 334–338
convection during, 100
effect of mold contour on, 332
in a sand mold, 329–331
interface resistance during, 342–346
rate, 329, 335
time of a casting, 331
- Spalding, D.B., 603, 605
- Sparrow, E.M., 374
- Specific permeability, 91
- Specular surfaces, 374
- Speed, 166
- Sphere (*see* Flow around a sphere)
buoyant forces on, 70
form drag on, 70
friction drag on, 70
solidification time for, 337–339
- Splat cooling, 366
- Spray heat-transfer coefficient, 355
- Sprays, heat transfer with, 268–269
- Sputter-ion pumps, 180
- Stagnation temperature, 165
- Stanton number, 251
- Static efficiency, 153
- Steady-state conduction through

- composite cylinder, 286–285
 - in a composite wall, 283
 - in a flat plate, 282
 - in a hollow cylinder, 285
 - in an infinite cylinder, 295
 - in an infinite plate, 294
- Steam ejectors, 177–179
 - pumping capacity, 178
- Stefan-Boltzmann
 - constant, 186
 - equation, 372
- Stewart, W., 203, 240
- Stewart, W.E., 523
- Stoke, 6
- Stokes-Einstein equation, 445
- Stokes' law, 71, 445, 631
- Stolz, G., 265–267
- Stream function, 65
- Streamline flow, 3
- Streeter, V.L., 54, 69
- Sun, R.C., 409–410
- Superficial velocity, 91, 93, 102
- Superheat, effect of on solidification time, 324
- Super ionic conductors, 440
- Supersonic core, 164
- Supersonic nozzles
 - design of, 158–165
 - exit velocity, 162
 - mass flow rate from, 159–165
- Surface area of particles
 - for irregular particles, 96–97
 - per unit volume of bed, 96
 - per unit volume of particles, 95
- Surface condition, effect on nucleate boiling, 267
- Surface depletion, 560–563
- Surface diffusion, 433
- Surface renewal theory, 536
- Surface resistance, effect of on temperature distribution in semi-infinite solid, 306–310
- Sutherland-Einstein equation, 445
- Swalin, R., 447
- Szekely, J., 605
- Tammann, G., 493
- Tammann scalling constant, 493
- Taylor, H.F., 332
- TEACH 2-E software, 605
- Temperature distribution
 - in infinite solids, 307
 - in semi-infinite solids, 308–310
- Temperature history in a semi-infinite solid
 - with surface resistance, 309
- Temperature profile, fully developed, 221
- Temperature response for
 - infinite cylinders, 293, 295
 - infinite plates, 293–294
 - spheres, 293, 296–297
- Tempering furnace, 397
- Temporal mean velocity, 4
- Terminal velocity, 71, 89 103
- Thermal boundary layer, 226, 229
- Thermal conductivity, 187–218
 - in aluminum alloys, 197
 - of amorphous or molecular solids, 202
 - of bulk materials, 208
 - carbides, 201
 - of cermets, 208
 - of common gases, 191
 - of dielectric materials, 193
 - of gases, 190–191
 - of gas mixtures, 191
 - in glasses, 203
 - of graphite, 201
 - of highly basic silicate melts, 206
 - of insulating materials, 194
 - of liquid metals, 197
 - of liquids, 203–208
 - of materials, 188
 - of metal-matrix composites, 208
 - of molding sands, 203–205
 - of nickel and nickel-base alloys, 198
 - of nitrides, 201
 - of oxides, 194, 200
 - of packed beds, 211–214
 - of polyatomic gases, 191
 - of polymers, 203
 - of powder metal compacts, 211
 - of pure iron and iron-base alloys, 199
 - of pure metals, 196
 - of semiconducting compounds, 200
 - of silica sand molds, 214
 - of slag, 205, 208
 - in solids and alloys, 196
 - of solid and molten CaO-SiO₂-Al₂O₃ slags, 207
 - of solid and molten Na₂O-SiO₂ silicates, 207
 - of solid metals, 205
 - of solids, 191
 - of steels, 199
 - of two-phase mixtures, 210, 212
 - of various liquids, 205
- Thermal diffusivity, 225
- Thermal gradients, 357

- Thermal radiation
 - definition, 369
- Thermal resistance, 283, 287
 - fluid-solid interface, 285
 - infinite cylinder, 285
 - infinite slab, 283
- Thermal shock, 410
- Thermal stresses, 409
- Thermocouple, 396
 - effect of radiation on indicated temperature, 396
- Thickness of solidified layer
 - in chill molds, 334–338
 - in sand molds, 330
- Thixotropic fluids, 31
- Throughput
 - in vacuum technology, 166
- Toor, H.L., 537
- Torr, 166
- Tortuosity, 457
- Total exchange factor, 391–394
- Total head, 147
- Total heat-transfer coefficient, 396
- Total hemispherical emissivity, 374
 - of window glass, 406
- Total hemispherical radiation intensity, 369
- Total irradiation, 370
- Total molar flux, 509
- Total radiosity, 370
- Total solidification time, 330
- Touloukian, Y.S., 375
- Tracer atom, 423
- Tracer, diffusion coefficient with, 424
- Tracers, 469–480
- Transference number, 437, 494
- Transient conduction with radiation, 407–409
- Transient diffusion, 468
- Transition metal oxides, 436
- Transmission probability, 169
- Transmissivity
 - definition, 370
 - of gases, 402–404
- Tube-bundle theory, 93
- Turbulence, 598
- Turbulence layer, 604
- Turbulent flow, 3
 - in pipes, transition value of Re , 75
- Turbulent layer, 603
- Turbulent mass diffusivity, 605
- Turbulent thermal conductivity, 605
- Turkdogan, E.T., 25, 446, 454, 455
- Tumbull, D., 447
- Tuyeres, 106
- Two-resistance mass transfer concept, 547–548
- Umklapp collision, 193
- Units
 - diffusion coefficient, 420
 - heat flux, 188
 - heat-transfer coefficient, 186
 - kinematic viscosity, 6
 - mass flux, 420
 - mass transfer coefficient, 519–523
 - molar flux, 420
 - thermal conductivity, 188–189
 - viscosity, 6
- Universal velocity profile, 603
- Unsteady-state heat conduction, 300
- Up-hill diffusion, 428
- Upwind finite difference method, 608
- Urban, G., 26, 27
- Vacancies, 421
- Vacancy mechanism, 425
- Vacuum arc melting, 338
- Vacuum
 - annealing, 166
 - arc melting, 338
 - degassing, 166, 183
 - deposition, 166
 - gauges, 167
 - melting, 166
 - processes, 166
 - pumps, 167
 - units of, 166
- Vacuum melting system
 - pump-down speed, 172
- Vacuum melting, 560
 - vaporization during, 560, 563–567
- Vacuum pumps
 - characteristic curve, 174, 176
 - diffusion, 175
 - intrinsic speed of, 173
 - limiting forepressure, 175
 - mechanical, 173
 - ultimate pressure, 174
- Valves
 - equivalent length of, 123
 - table, 123
- Vapor deposition, 411
- Vapor diffusion pumps, 166
- Vaporization (*see* Evaporation constants)
 - during melting, 563–567
 - from liquid metals, 563
 - Knudsen cell, 560

- mass transfer coefficient, 564
- Vector notation, 55
- Velocity
 - average in gas, 7–8
 - temporal mean, 3
 - time averaged, 3
- Velocity distributions, for turbulent flow in tubes, 77
- Velocity meters, 124–126
- Velocity of light, 372
- Velocity profile
 - in laminar flow, 4
 - in turbulent flow, 5
- Vena contracta, 128–129
- Venturi meter, 127, 131
- View factor
 - charts, 384–385
 - definition, 381–384
 - for identical, parallel, directly opposed rectangles, 384
 - for parallel, directly opposed disks, 385
 - for two rectangles with a common edge, 385
 - hemispherical, 382–383
- Viscoelastic fluids, 29
- Viscosity
 - activation energy of, 21
 - of alloys, 22
 - of common liquids, 17
 - definition, 6
 - of gas mixtures, 12
 - of gases, 7–14
 - graph, 14
 - iron-carbon system, 21–22
 - kinematic, 6
 - of liquid metals, 18–20
 - of liquid metals and alloys, 16
 - of liquid metals at 1 atm, 17
 - of liquids, 13
 - of liquid salts, 28–29
 - of liquid slags, 26
 - of molten slags, silicates, and salts, 22
 - of non-Newtonian fluids, 29
 - temperature dependence of, 9, 13, 15
 - units, 6
- Viscosity function $f(\kappa_B T/\epsilon)$, 11
- Viscous momentum, 53
- Void fraction, 633
 - in packed beds, 633
 - minimum, 633
- Volume flow rate, Q , 43
- Void fraction, 93
 - effect of packing on, 101
- Volume-surface mean diameter, 96
- Wake formation, 86
- Wagner, C., 493, 504, 551, 554
- Wagner, J.B., 438, 440
- Wall effect, 98
- Ward, R.G., 566
- Water
 - diffusion in, 452
 - heat transfer in, 263–268
 - thermal conductivity of, 205
- Water column, 151
- Water cooling jackets, 397
- Water sprays, 355
- Weidmann-Franz law, 197
- Welding, 315
 - of thick plate, 365
 - of thin plate, 365
- Wen, C.Y., 104, 560
- Wetted perimeter, 81, 93
- Whitaker, S., 255
- Whitman, W., 535
- Wilhelm, R.H., 103
- Wilke, C.R., 12
- Wilkes, J.O., 581, 590
- Wood, W.D., 375

- Yang, E.S., 559
- Young, D.J., 431
- Yu, Y.H., 104

- Zener, C., 431
- Zenz, F.A., 102
- Zimin, N.V., 269
- Zirconia, 440

SUMMARY OF DIMENSIONLESS NUMBERS

$Bi = \frac{hL}{k}$	Biot number
$f = \frac{\Delta P}{(L/d)(\rho v^2/2)}$	Friction factor
$Fo = \frac{\alpha t}{L^2}$	Fourier number for heat conduction
$Fo_D = \frac{Dt}{L^2}$	Fourier number for diffusion
$Gr = \frac{g\beta(T - T_R)L^3}{\nu^2}$	Grashof number for heat transfer
$Gr_M = \frac{g\xi(X - X_R)L^3}{\nu^2}$	Grashof number for mass transfer
$Nu = \frac{hL}{k}$	Nusselt number
$Pe = ReSc$	Peclet number
$Pr = \frac{\nu}{\alpha}$	Prandtl number
$Sc = \frac{\nu}{D}$	Schmidt number
$Sh = \frac{k_m L}{D}$	Sherwood number

Parameters for dimensionless numbers:

<p>C_p = specific heat, J kg⁻¹ K⁻¹ D = diffusion coefficient, m² s⁻¹ d = characteristic dimension (diameter), m g = gravitational acceleration, m s⁻² h = heat transfer coefficient, W m⁻² K⁻¹ k = thermal conductivity, W m⁻¹ K⁻¹ k_M = mass transfer coefficient, m s⁻¹ L = characteristic length, m ΔP = pressure difference, N m⁻² T = temperature, K T_R = reference temperature, K</p>	<p>t = time, s V = characteristic velocity, m s⁻¹ X = concentration (mole fraction) X_R = reference concentration (mole fraction) $\alpha = k/\rho C_p$ = thermal diffusivity, m² s⁻¹ β = thermal volumetric expansivity (see p. 229) ξ = mass volumetric expansivity (see p. 529) η = viscosity, N s m⁻² ρ = density of fluid, kg m⁻³ $\nu = \eta/\rho$ = kinematic viscosity, m² s⁻¹</p>
--	--